LAND SUBSIDENCE

Edited by

A. I. JOHNSON
A. Ivan Johnson, Inc., 7474 Upham Court, Arvada, Colorado 80003, USA

A contribution to the International Hydrological Program of UNESCO (IHP-IV; Project M-3.5c)

Proceedings of the Fourth International Symposium on Land Subsidence, held at Houston, Texas, 12–17 May 1991.
The symposium was convened by the International Association of Hydrological Sciences (IAHS) and the United Nations Educational, Scientific and Cultural Organization (UNESCO), as part of the International Hydrological Program (IHP), with cosponsorship by the United Nations Environment Program, US Geological Survey, US Bureau of Mines, Harris-Galveston Coastal Subsidence District, US National Committee for Scientific Hydrology.
Cooperators included the Association of Geoscientists for International Development, the International Association of Hydrogeologists, the International Society for Mine Surveying, the International Society of Soil Mechanics and Foundation Engineers, and the International Mine Water Association.

IAHS Publication No. 200

Published by the International Association of Hydrological Sciences 1991.
IAHS Press, Institute of Hydrology, Wallingford, Oxfordshire OX10 8BB, UK.

IAHS Publication No. 200.

ISBN 0-947571-92-2

The photograph opposite is reproduced with the approval of the American Geophysical Union; AGU published the photograph on the cover of the November 16, 1982, issue of EOS.

Previous Land Subsidence titles in the same series:

LAND SUBSIDENCE. Tokyo Symposium 1969
Vols 1 and 2
Publs no. 88 and no. 89 (1970), price $8 each

LAND SUBSIDENCE. Proceedings of the Anaheim Symposium, December 1976
Publ. no. 121 (1977), price $30

LAND SUBSIDENCE *edited by A. I. Johnson, Laura Carbognin & L. Ubertini.* Proceedings of the Venice Symposium, March 1984
Publ. no.151 (1986), price $45
ISBN 0-947571-40-X

These publications may be ordered from the IAHS Wallingford or Washington addresses

The camera-ready copy for the papers was prepared by the authors and assembled/finished at IAHS Press by Penny Kisby and Sarah Cage. Some papers were retyped by Betty Johnson.

Printed in The Netherlands by Krips Repro Meppel.

In honor of Dr Poland's 40 years of research on land subsidence, this proceedings volume is dedicated to him

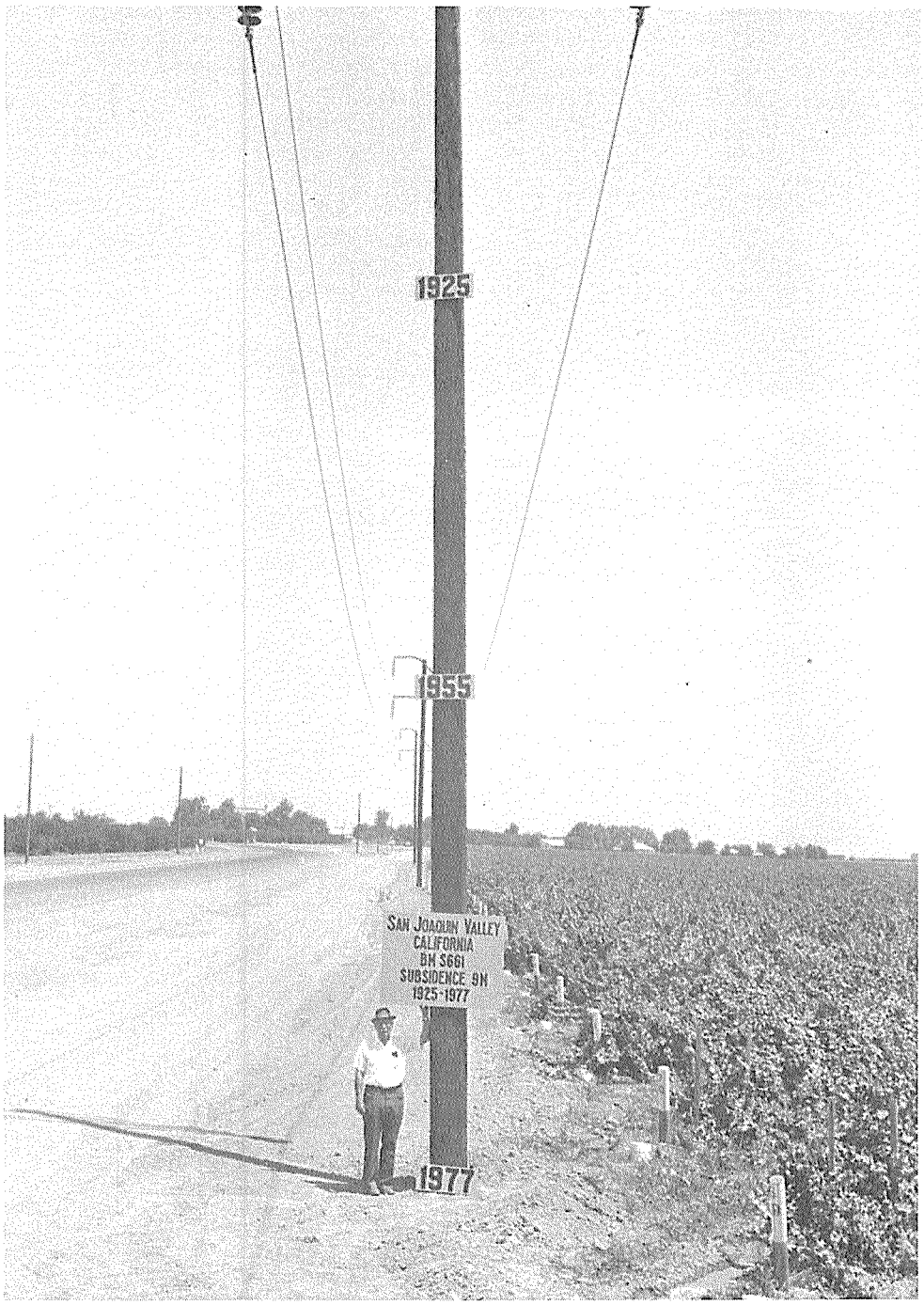

Dr Joseph F. Poland (Sacramento, California, USA) retired US Geological Survey Senior Scientist for land subsidence research, stands at a site near benchmark S661 in the San Joaquin Valley southwest of Mendota, California. The benchmark subsided 8.93 m (29.3 ft) between 1925 and 1974 as a result of heavy pumping of ground water. Signs on the telephone post were used to show the respective heights of the land surface in 1925, 1955 and 1977 for a subsidence field trip. *Photograph by Richard L. Ireand, US Geological Survey, Sacramento, California, USA.*

PREFACE

Subsidence (land surface sinking) is a phenomenon that occurs in many parts of the world. The subsidence results from the heavy withdrawal of ground water, geothermal fluids, oil, and gas; the extraction of coal, sulphur, and other solids through mining; the hydro-compaction of sediments; oxidation and shrinkage of organic deposits; the catastrophic development of sinkholes in karst terrain, and other phenomena. Over 50 areas of contemporary subsidence are known, some with as much as 10 meters (33 feet) in countries such as Mexico, Japan and the United States for example. Many more areas are likely to develop in the next few decades as a result of accelerated exploitation of natural resources---especially ground water---in order to meet the demands of increasing population and industrial development throughout the world.

Developers, and the engineers and scientists making the studies and plans, of industrial complexes, urban developments, water supply systems, and natural resource extractions need to know about the potential hazards, costs, and socio-environmental impacts that can result from land subsidence. To provide a forum for exchange of such information from international and interdisciplinary specialists who have had to solve the problems related to land subsidence, a series of international symposia on land subsidence have been organized by the International Association of Hydrological Sciences (IAHS) and the United Nations Educational, Scientific, and Cultural Organization (UNESCO) starting in 1969.

The Fourth International Symposium on Land Subsidence (FISOLS) was held 12-17 May 1991 in Houston, Texas, USA---a site of major subsidence-induced problems. The symposium was convened by the IAHS Ground Water Commission and UNESCO. At the time of going to print with this volume, the Symposium was cosponsored by the United Nations Environmental Program (UNEP), U.S. Geological Survey (USGS), U.S. Bureau of Mines (USBM), Harris-Galveston Coastal Subsidence District (HGCSD), and U.S. National Committee for Scientific Hydrology (USNC/SH). Cooperators included the Association of Geoscientists for International Development (AGID), International Association of Hydrogeologists (IAH), the International Society for Mine Surveying (ISMS), International Society of Soil Mechanics and Foundation Engineers (ISSMFE), and International Mine Water Association (IMWA). Other cosponsors and cooperators from international and national organizations were to be announced during the symposium.

The problems of land subsidence were among those included in the list of research projects recommended by UNESCO's International Hydrological Decade, which began in 1965, and the International Hydrological Program---a continuing UNESCO program beginning in 1975. The continuing UNESCO Working Group for IHP-IV project M-3.5(c): "Ground Water Assessment and Environmental Impact due to Over-Development---Land Subsidence" presently consists of A. Ivan Johnson, Chairman (USA), Laura Carbognin (Italy), Joseph F. Poland (USA), Soki Yamamoto (Japan), and German Figueroa Vega (Mexico). The land subsidence research needs stated in the IHD/IHP project documents have resulted in IAHS/UNESCO sponsorship of the International Symposium on Land Subsidence in 1969 in Tokyo, Japan; the Second International Symposium on Land Subsidence in 1976 in Anaheim, California, USA; the Third International Symposium in 1984 in Venice, Italy; and the present (1991) Fourth International

Symposium in Houston, Texas, USA. All four symposia have been held in locations of major subsidence problems. Papers presented in the three earlier symposia were published as IAHS Publications No. 88 and 89, 121, and 151, respectively. The papers published in this volume represent selected papers presented at the Fourth Symposium.

Because of man's continuing heavy impact on the surface and subsurface environment, the problems of land subsidence have become increasingly critical over the years since 1969. Therefore, the purpose of the Fourth Symposium was to bring together international interdisciplinary specialists on the problems of land subsidence and to present results of research and practice in the subject; to exchange with all participants the experiences related to cause, effect, control and remediation of subsidence; promote technology transfer between the various disciplines and countries represented at the meeting; and to evaluate the advance of knowledge taking place on this subject since 1984 and thus chart a path for future research on land subsidence. This symposium was somewhat different from the others in several aspects. One is that it was even broader and more interdisciplinary in coverage. A second aspect was the discussion of a number of mathematical analyses and modeling techniques useful in predicting the amount of subsidence that may result from certain actions. The program also showed the potential inter-relationships of subsidence characteristics, methods of study, and means of remedial work, whether due to withdrawal of fluids or solid matter (mining). The need for a broad interdisciplinary approach to any study of subsidence and to correction of resultant problems was another aspect adequately demonstrated by the program and by the wide range of sponsors and cosponsors that worked together to develop the program.

The symposium was held at the beautiful Doubletree Hotel at Post Oak Road in Houston, Texas, USA. Attendees from about 30 countries received useful and interesting information from the approximately 110 papers presented at the symposium. Because of time constraints, nearly 50 of those papers were presented as posters during the refreshment breaks. Most of the oral and poster authors submitted full length papers for publication. Papers were submitted to three specialists for peer review, after which any needed revision was made and camera ready copy was prepared. Because of interest in having good international coverage of land subsidence research and occurrence, editing of papers by authors from countries in which English is not the primary language was kept to the minimum needed to assure the papers would be technically understandable. Of the over 100 papers presented at the symposium, 62 are published in this volume. Of these papers eight discussed subsidence problems related to ground water withdrawal, four to oil and gas withdrawal, ten to mining, six to earth fissures, three to sinkholes and organic deposits, five on environmental factors, three on coastal and inland flooding, five on instrumentation and measurement, five on remedial measures, and thirteen on theory and modeling.

General Chairman for the FISOLS symposium was Ivan Johnson, Consulting Engineer, Arvada, Colorado, USA. Ronald Neighbors, Harris-Galveston Coastal Subsidence District, Friendswood, Texas, was Chairman of the Local Arrangements Committee and was assisted by his staff members Bill Holzchuh and Carole Baker, as well as by Neil Bishop, Turner, Collie, & Braden; Bob Gabrysch, U.S. Geological Survey; Frank Marshall, McClelland Engineers; Jerry Rogers,

University of Houston; and John Seifert, William F. Guyton Associates, Inc.; all of Houston, Texas. The Technical Program Committee was chaired by Ivan Johnson, Honorary President of IAHS; and other members were Joseph F. Poland, U.S. Geological Survey (Retired), Sacramento, California, USA; Alice Aureli, UNESCO Representative, Paris, France; Laura Carbognin, National Research Council's Institute for Study of Dynamics of Large Masses, Venice, Italy; and Soki Yamamoto, Professor Emeritus, University of Tsukuba, Japan; German Figueroa Vega, ISSMFE Representative, Consultant, Mexico City, Mexico; and Adam Chrzanowski, ISMS Representative, University of New Brunswick, Fredericton, NB, Canada. In addition to assisting with development of the program, members of the Program Committee also served as reviewers of the authors' papers.

On behalf of the International Association of Hydrological Sciences, appreciation is expressed to the cosponsors and cooperating organizations for their financial or service support to the symposium. Also acknowledged with appreciation are the contributions of members of the FISOLS Local Arrangements and Program Committees, session chairmen, authors, reviewers, and many other people who gave of their time, effort, and knowledge to produce the successful program and field trips. A special thanks goes to IAHS Secretary General Henny Colenbrander (Netherlands) who was always available when administrative problems arose, and Betty Johnson, who provided the very heavy secretarial assistance needed for the symposium. Finally, this volume would not have been possible without the excellent publication assistance of Penny Kisby and her assistants at the IAHS Publication Office in Wallingford, UK.

The Organizing Committee hopes all readers find this publication interesting and informative. The interdisciplinary nature of the program and of the sponsorship of this symposium and its proceedings should encourage new multidisciplinary research and study to solve the many problems related to land subsidence.

Ivan Johnson
Symposium General Chairman
A. Ivan Johnson, Inc.
7474 Upham Court
Arvada, Colorado 80003, USA

CONTENTS

10 THEORY AND MODELING

PREFACE

Subsidence (land surface sinking) is a phenomenon that occurs in many parts of the world. The subsidence results from the heavy withdrawal of ground water, geothermal fluids, oil, and gas; the extraction of coal, sulphur, and other solids through mining; the hydro-compaction of sediments; oxidation and shrinkage of organic deposits; the catastrophic development of sinkholes in karst terrain, and other phenomena. Over 50 areas of contemporary subsidence are known, some with as much as 10 meters (33 feet) in countries such as Mexico, Japan and the United States for example. Many more areas are likely to develop in the next few decades as a result of accelerated exploitation of natural resources---especially ground water---in order to meet the demands of increasing population and industrial development throughout the world.

Developers, and the engineers and scientists making the studies and plans, of industrial complexes, urban developments, water supply systems, and natural resource extractions need to know about the potential hazards, costs, and socio-environmental impacts that can result from land subsidence. To provide a forum for exchange of such information from international and interdisciplinary specialists who have had to solve the problems related to land subsidence, a series of international symposia on land subsidence have been organized by the International Association of Hydrological Sciences (IAHS) and the United Nations Educational, Scientific, and Cultural Organization (UNESCO) starting in 1969.

The Fourth International Symposium on Land Subsidence (FISOLS) was held 12-17 May 1991 in Houston, Texas, USA---a site of major subsidence-induced problems. The symposium was convened by the IAHS Ground Water Commission and UNESCO. At the time of going to print with this volume, the Symposium was cosponsored by the United Nations Environmental Program (UNEP), U.S. Geological Survey (USGS), U.S. Bureau of Mines (USBM), Harris-Galveston Coastal Subsidence District (HGCSD), and U.S. National Committee for Scientific Hydrology (USNC/SH). Cooperators included the Association of Geoscientists for International Development (AGID), International Association of Hydrogeologists (IAH), the International Society for Mine Surveying (ISMS), International Society of Soil Mechanics and Foundation Engineers (ISSMFE), and International Mine Water Association (IMWA). Other cosponsors and cooperators from international and national organizations were to be announced during the symposium.

The problems of land subsidence were among those included in the list of research projects recommended by UNESCO's International Hydrological Decade, which began in 1965, and the International Hydrological Program---a continuing UNESCO program beginning in 1975. The continuing UNESCO Working Group for IHP-IV project M-3.5(c): "Ground Water Assessment and Environmental Impact due to Over-Development---Land Subsidence" presently consists of A. Ivan Johnson, Chairman (USA), Laura Carbognin (Italy), Joseph F. Poland (USA), Soki Yamamoto (Japan), and German Figueroa Vega (Mexico). The land subsidence research needs stated in the IHD/IHP project documents have resulted in IAHS/UNESCO sponsorship of the International Symposium on Land Subsidence in 1969 in Tokyo, Japan; the Second International Symposium on Land Subsidence in 1976 in Anaheim, California, USA; the Third International Symposium in 1984 in Venice, Italy; and the present (1991) Fourth International

Symposium in Houston, Texas, USA. All four symposia have been held in locations of major subsidence problems. Papers presented in the three earlier symposia were published as IAHS Publications No. 88 and 89, 121, and 151, respectively. The papers published in this volume represent selected papers presented at the Fourth Symposium.

Because of man's continuing heavy impact on the surface and subsurface environment, the problems of land subsidence have become increasingly critical over the years since 1969. Therefore, the purpose of the Fourth Symposium was to bring together international interdisciplinary specialists on the problems of land subsidence and to present results of research and practice in the subject; to exchange with all participants the experiences related to cause, effect, control and remediation of subsidence; promote technology transfer between the various disciplines and countries represented at the meeting; and to evaluate the advance of knowledge taking place on this subject since 1984 and thus chart a path for future research on land subsidence. This symposium was somewhat different from the others in several aspects. One is that it was even broader and more interdisciplinary in coverage. A second aspect was the discussion of a number of mathematical analyses and modeling techniques useful in predicting the amount of subsidence that may result from certain actions. The program also showed the potential inter-relationships of subsidence characteristics, methods of study, and means of remedial work, whether due to withdrawal of fluids or solid matter (mining). The need for a broad interdisciplinary approach to any study of subsidence and to correction of resultant problems was another aspect adequately demonstrated by the program and by the wide range of sponsors and cosponsors that worked together to develop the program.

The symposium was held at the beautiful Doubletree Hotel at Post Oak Road in Houston, Texas, USA. Attendees from about 30 countries received useful and interesting information from the approximately 110 papers presented at the symposium. Because of time constraints, nearly 50 of those papers were presented as posters during the refreshment breaks. Most of the oral and poster authors submitted full length papers for publication. Papers were submitted to three specialists for peer review, after which any needed revision was made and camera ready copy was prepared. Because of interest in having good international coverage of land subsidence research and occurrence, editing of papers by authors from countries in which English is not the primary language was kept to the minimum needed to assure the papers would be technically understandable. Of the over 100 papers presented at the symposium, 62 are published in this volume. Of these papers eight discussed subsidence problems related to ground water withdrawal, four to oil and gas withdrawal, ten to mining, six to earth fissures, three to sinkholes and organic deposits, five on environmental factors, three on coastal and inland flooding, five on instrumentation and measurement, five on remedial measures, and thirteen on theory and modeling.

General Chairman for the FISOLS symposium was Ivan Johnson, Consulting Engineer, Arvada, Colorado, USA. Ronald Neighbors, Harris-Galveston Coastal Subsidence District, Friendswood, Texas, was Chairman of the Local Arrangements Committee and was assisted by his staff members Bill Holzchuh and Carole Baker, as well as by Neil Bishop, Turner, Collie, & Braden; Bob Gabrysch, U.S. Geological Survey; Frank Marshall, McClelland Engineers; Jerry Rogers,

University of Houston; and John Seifert, William F. Guyton Associates, Inc.; all of Houston, Texas. The Technical Program Committee was chaired by Ivan Johnson, Honorary President of IAHS; and other members were Joseph F. Poland, U.S. Geological Survey (Retired), Sacramento, California, USA; Alice Aureli, UNESCO Representative, Paris, France; Laura Carbognin, National Research Council's Institute for Study of Dynamics of Large Masses, Venice, Italy; and Soki Yamamoto, Professor Emeritus, University of Tsukuba, Japan; German Figueroa Vega, ISSMFE Representative, Consultant, Mexico City, Mexico; and Adam Chrzanowski, ISMS Representative, University of New Brunswick, Fredericton, NB, Canada. In addition to assisting with development of the program, members of the Program Committee also served as reviewers of the authors' papers.

On behalf of the International Association of Hydrological Sciences, appreciation is expressed to the cosponsors and cooperating organizations for their financial or service support to the symposium. Also acknowledged with appreciation are the contributions of members of the FISOLS Local Arrangements and Program Committees, session chairmen, authors, reviewers, and many other people who gave of their time, effort, and knowledge to produce the successful program and field trips. A special thanks goes to IAHS Secretary General Henny Colenbrander (Netherlands) who was always available when administrative problems arose, and Betty Johnson, who provided the very heavy secretarial assistance needed for the symposium. Finally, this volume would not have been possible without the excellent publication assistance of Penny Kisby and her assistants at the IAHS Publication Office in Wallingford, UK.

The Organizing Committee hopes all readers find this publication interesting and informative. The interdisciplinary nature of the program and of the sponsorship of this symposium and its proceedings should encourage new multidisciplinary research and study to solve the many problems related to land subsidence.

Ivan Johnson
Symposium General Chairman
A. Ivan Johnson, Inc.
7474 Upham Court
Arvada, Colorado 80003, USA

Land Subsidence (Proceedings of the Fourth International Symposium on Land Subsidence, May 1991). IAHS Publ. no. 200, 1991.

Subsidence at Houston, Texas, 1973-1987

S. R. HOLDAHL & D. B. ZILKOSKI
National Geodetic Survey, Charting and Geodetic Services
National Ocean Service, NOAA, Rockville, Maryland 20852, USA
J. C. HOLZSCHUH
Harris-Galveston Coastal Subsidence District, Houston, Texas 77058, USA

ABSTRACT Models of vertical deformation are needed for calculation of vertical motion corrections to leveling data in areas like Houston, TX, where significant subsidence results from withdrawal of groundwater. The repeated levelings at Houston have been used as test data to refine and evaluate surface-fitting methods used in scientific studies to quantify and interpolate crustal motion and subsidence. Now the same modeling procedures are used to create a data base of coefficients for correcting old leveling measurements forward in time, to allow simultaneous adjustment with recent measurements.
The regional subsidence pattern at Houston, TX, has been derived from repeated levelings and extensometer data. The leveling surveys were performed in distinct epochs: 1973, 1978, 1983, and 1987. The earliest extensometer records date from 1973. The Houston region was divided into two zones according to whether water levels in artesian wells had recently risen (east zone) or fallen (west zone). The west zone shows mildly nonlinear and increasing subsidence rates ranging up to -72 mm/yr in 1987, just 7 miles west of downtown Houston. The east zone was characterized by rates of up to -70 mm/yr from 1973 to 1978, followed by 60-90 percent decreases in these rates by 1987. The sharp decrease has been caused by regulated declines (44-84 percent) in pumping of groundwater, as well as importation of surface water from Lake Houston. The subsidence model for Houston was derived at the same time its level network was adjusted, using multiquadric (MQ) analysis for spatial interpolation of subsidence velocities. A quadratic height function was used for west Houston, with one set of unknown coefficients to describe regional variation of subsidence velocity and another to describe acceleration. Subsidence in east Houston was modeled as a sequence of regionally variable velocities; one set of MQ coefficients describes the velocity pattern between 1973 and 1978, and a second set describes the subsidence from 1978 to 1987. The coefficients that define the Houston subsidence model were placed in a data base, and then accessed to successfully calculate corrections for old leveling data.

INTRODUCTION

The National Geodetic Survey is presently developing improved methods for modeling vertical motion. This development must precede readjustment of the national level network which extends into many areas of crustal motion and subsidence. The geodetic objective of these models is to allow old leveling data in vertically deforming areas to be

corrected to the rough equivalent of recent measurements. This improves the reliability of the leveling and allows use of the traditional static adjustment model in the adjustment of the national net. The nonlinear subsidence at Houston is a good example to illustrate some of the new techniques that may be applied in the national project.

The phenomenon of land surface subsidence has long been recognized as a serious problem in the area near Houston. (See fig. 1.) As early as 1926, a meter of subsidence was reported at Goose Creek oil field at the north end of Galveston Bay. The subsidence at Goose Creek was due to the withdrawal of oil from shallow reservoirs and was confined to the small area of the oil field itself.

Since that time, the nearby cities of Houston and Galveston, as well as a large petrochemical industry, have all seen dramatic growth. This growth was supported exclusively by large withdrawals of groundwater from vast aquifers which underlie most of this Gulf Coast region. These withdrawals lowered water pressures in the aquifers allowing the many clay beds to compress, resulting in the lowering of the land surface (subsidence) up to 3 m in some areas. Thousands of acres of valuable land have been submerged due to subsidence and even larger areas are now subject to flooding from hurricane storm surge or overflow of freshwater streams and bayous during periods of heavy rainfall.

Land subsidence continues to the present at Houston and is being studied intensively by the Harris-Galveston Coastal Subsidence District, an organization whose task is to

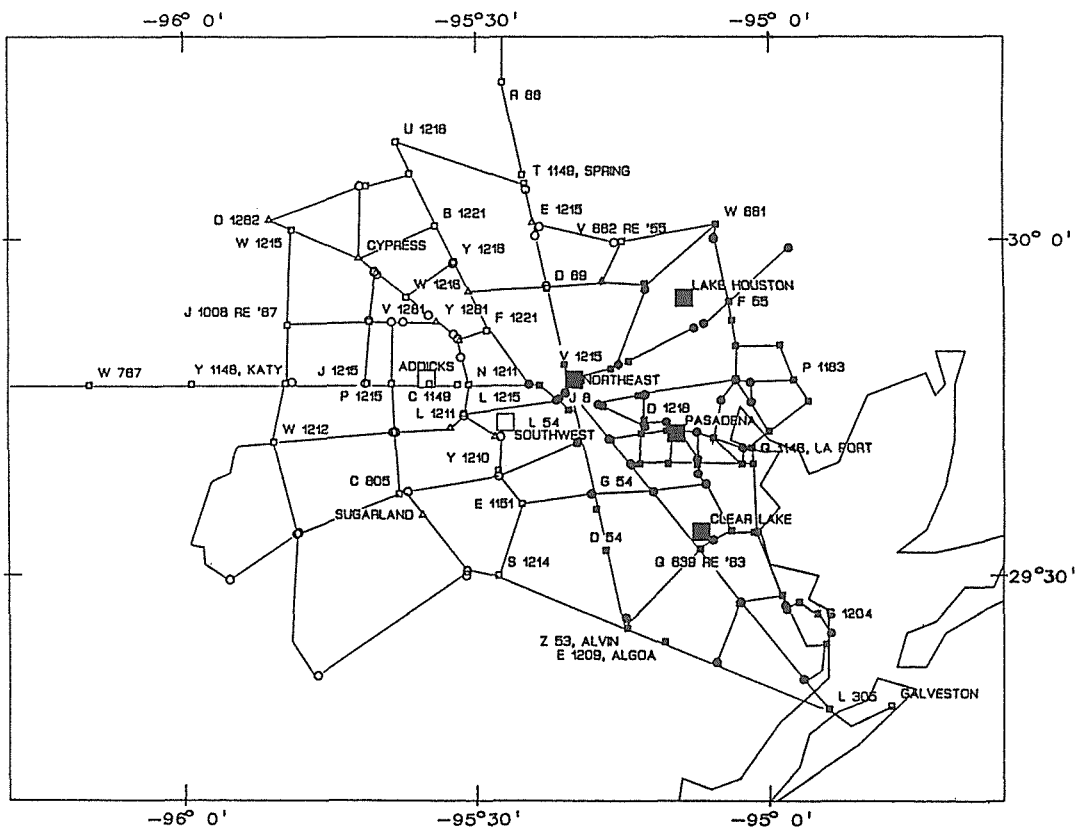

FIG. 1 Locations of level lines and extensometers - Houston, TX. Solid symbols are used to distinguish east Houston modeling district.

balance the sometimes conflicting requirements for water resources and a stable land surface.

Between 1963 and 1978, all of the region within 20 miles of Houston had subsided at least 3 dm. A maximum change, exceeding 1.5 m for that time interval, was centered east of Houston about halfway to Baytown (Balazs, 1980). This is the area in which the heaviest groundwater withdrawals were occurring for Houston's growing petrochemical industry.

Balazs (1980) compared level survey results from 1963, 1973, 1976, and 1978. A significant conclusion in that report was that subsidence rates between 1973 and 1978 had slowed by 25 percent on the east side of Houston where maximum change had occurred for the prior period 1963-73. The lowering of subsidence rates in that region was attributed to reduced withdrawal of water for industrial use. Increasing amounts of surface water brought in by newly constructed canal systems have continued to replace water previously taken from underground.

During the period from 1978 to present, groundwater withdrawals continued to decrease on the east side of Houston due to the continued regulation of groundwater and the availability of surface water to replace it. The area to the west of Houston, however, was continuing a period of rapid growth which was supported solely by groundwater withdrawals. The means to supply surface water to west Houston have not yet been implemented. After a partial releveling of the Houston network in 1983, Zilkoski (1984) also calculated a decrease in subsidence east of Houston and noted continued rapid subsidence on the west side of Houston (328.6 mm between Houston and Addicks) since 1978. This result seemed to conform well with the pumping patterns.

The present analysis of the 1987 leveling survey is aimed at determining the most recent subsidence velocities as well as to quantify and document how the subsidence pattern has shifted during the period from 1973 to 1987. The leveling measurements made in 1973, 1978, 1983, and 1987 were the basis of the investigation. The 1973 and 1978 surveys were undoubtedly biased by magnetic errors that were not known to exist in 1978. All of the Zeiss Ni-1 leveling measurements used in the present analysis have been corrected for magnetic error using a procedure based on empirical calibrations (Holdahl et al., 1987).

The computation of Houston's elevations has become complicated because subsidence rates are changing with time. Most computer programs for calculating motion utilize simple models which assume that motion is constant in time. In this study, more advanced techniques are used to model accelerations in the subsidence rates. This report documents significant aspects of this mathematical model, and gives the results of the investigation to determine the recent character of subsidence at Houston. The model established for Houston can be used to interpolate subsidence rates to points where no repeat leveling data exist, and allows short term predictions of future subsidence. The Subsidence District has used a geotechnical model to predict subsidence with good results, but data are available for only 20 widely spaced locations in the area. The model described herein can be used to fill in the "holes" between those locations.

MATHEMATICAL DEVELOPMENT

In the usual adjustment of a static level network, where the land surface is assumed to be stable, it is only necessary to solve for heights considered constant in time. All historical level measurements in the network are collected and a least squares adjustment is performed to remove any inconsistencies caused by random errors or small

residual systematic errors. This is not done at Houston because subsidence causes large inconsistencies, and such an adjustment would only result in average heights that would be difficult to associate with any particular date.

The Quadratic Height Function

Furthermore, acceleration of Houston's subsidence with time must be allowed by the selected mathematical model for height. One acceptable height function is given below:

$$H_i = H_0 + H'(t_i - t_0) + H''(t_i - t_0)^2 \tag{1}$$

The height H_i corresponds to time t_i. H_0 is the height at a specified reference time t_0. H' is the velocity at time t_0, and H'' is half the acceleration. Modeling of the subsidence is a surface fitting exercise in which

$$H' = \sum_{j=1}^{n_v} v_j[(x - x_j)^2 + (y - y_j)^2]^{1/2} \tag{2}$$

and

$$H'' = \sum_{k=1}^{n_a} a_k[(x - x_k)^2 + (y - y_k)^2]^{1/2} \tag{3}$$

The (x_j, y_j) and (x_k, y_k) are coordinates of "nodal points," in the terminology of multiquadric (MQ) analysis. The nodal points are located at bench marks which, after review of profiles, are known to indicate maximums and minimums of motion or are otherwise critical to the description of the movement pattern. Expressions (2) and (3) are used to calculate the velocity and acceleration at location (x,y). The coefficients v_j (corresponding to velocity) and a_j (corresponding to acceleration) are unknowns to be solved for in the adjustment of a mixed-age network of repeated levelings. The reference-time heights for all stations, H_0, are also unknowns.

Expression (2) gives the velocity at the reference time, t_0. The more general expression for velocity, for any time t_i is

$$\text{velocity} = H' + 2H''(t_i - t_0) \tag{4}$$

and the expression for acceleration is

$$\text{acceleration} = 2H'' \tag{5}$$

Leveling measures differences in height between two points, for example P_1 and P_2. In our model, this measurement is expressed mathematically as

$$\Delta H_{2\text{-}1} = H_{2,0} - H_{1,0} + (H_2' - H_1')(t_i - t_0) + (H_2'' - H_1'')(t_i - t_0)^2 \tag{6}$$

In expression (6), $H_{1,0}$ denotes the height at P_1 at time t_0, and H_1' denotes the velocity at P_1 at time t_0, etc. West Houston can be reliably modeled with the quadratic height function, i.e., expression (1).

Extensometer records show that subsidence east of Houston has slowed to almost

zero in some locations. The Pasadena extensometer record indicates a sharp decrease in 1978, at about the time when significant amounts of imported surface water from Lake Houston allowed pressure in aquifers to be maintained or rise. The sharp change in subsidence velocity in 1978 motivated the use of a different modeling technique for east Houston.

Time Partitioning

East Houston is defined to be the zone that encompasses the solid symbols in figure 1. The part of this boundary separating east and west Houston corresponds to the line of zero net change in the Chico and Evangeline aquifer levels. Within the east zone, water levels have rebounded or remained unchanged. In the west zone, water levels continue to be lowered.

This spatial districting of Houston allows use of a different height function for the east zone. However, the east zone data also required a modeling strategy we will call "time partitioning" which is similar to the technique used by Vanicek et al. (1979), to model vertical motions in southern California. The motion in the east zone was assumed to be rapid and linear prior to 1978, followed by slower linear motion after 1978. Separate sets of MQ coefficients were used to describe the vertical motion before and after 1978.

The expression for height, when using time districting, is as follows:

$$H_i = H_0 + \sum_{k=1}^{n_t} H_k' T_k \tag{7}$$

where each T_k is some fraction of the time interval t_{k+1}-t_k. For simplicity, assume $t_0 = t_n$, and $t_i < t_n$, where t_n is the latest time boundary, then

$$t_k = \begin{cases} 0, & \text{if } t_i > t_{k+1} \\ t_i - t_{k+1}, & \text{if } t_k < t_i < t_{k+1} \\ t_k - t_{k+1}, & \text{if } t_i < t_k \end{cases} \tag{8}$$

For east Houston, the two time partitions are defined to be 1972-1978, and 1978-1987.3. The reference time, t_0, was taken to be 1987.3.

APPLICATION TO THE HOUSTON LEVEL NETWORK

Figure 1 shows the Houston level network that was leveled all or in part in 1973, 1978, 1983, and 1987. An initial height for the network is obtained from the tide gauge at Galveston. Mean sea level (MSL) is equated with zero height and MSL is related to the nearby tide gauge bench mark by leveling. An initial velocity was obtained by fitting a straight line through the plot of mean sea level with time. Mean sea level has been rising at Galveston by an average rate of 6.3 mm/yr. The eustatic (global) rise of sea level can account for 1.0 mm/yr; therefore, the remainder is attributed to coastal subsidence of the land. Thus, an initial estimate for velocity of -5.3 ± 0.3 mm/yr and an acceleration of 0.0 ±0.1 mm/yr^2 were assigned to the tide gauge at Galveston.

Well outside of Houston, bench marks K 87 (RIVERSIDE) and Z 6 (SEALY) were constrained to be stable (zero velocity and acceleration). These two points, too far to the north and west of Houston to be shown in figure 1, were concluded to be outside the zone of significant subsidence. This conclusion was arrived at after reviewing profiles of relative elevation change made from comparisons of the unadjusted repeated levelings. Closer in, bench marks U 1216, and D 1282 in the northwest sector of figure 1 were also constrained to have zero velocity in 1987.

Compaction data from six extensometer locations (see large square symbols in fig. 1) were also used to control the adjustment to determine the reference-time heights and motion coefficients which constitute the subsidence model. The compaction records from the Clear Lake, Addicks, Pasadena, Northeast, Southwest, and Lake Houston installations were considered deep enough to provide good estimates of subsidence, meaning that no compaction is believed to occur below the base of the well. The Clear Lake, Pasadena, and Addicks installations have been in existence for several relevelings and are known to provide accurate indications of subsidence. The Northeast, Southwest, and Lake Houston installations were more recently constructed to the same standards, and their reliability is still being investigated.

The compaction data from the Clear Lake, Addicks, and Pasadena recorders showed nonlinear subsidence, and accordingly were input to the level net adjustment as a sequence of monthly observed heights. But first, a free adjustment of only the 1987 leveling survey provided heights for the inner pipes at these gauges. The compaction data then were used to compute heights of a second point (at the same location) which is moving vertically by the amount of the compaction, but has the identical 1987.3 height as the top of the non-moving inner pipe. The inner pipe should not move because it presumably extends below the lowest compacting layers. However, the ground around the site is subsiding because of compaction. The observed heights correspond to the subsiding ground surface.

The compaction records at Northeast, Southwest, and Lake Houston show linear subsidence, and accordingly, were input to the Houston level net adjustment as velocities with zero accelerations. The velocities and weights were derived from a straight line fit to those compaction records. Compaction recorders at Baytown, East End, NASA, Seabrook, and Texas City (not shown in fig. 1) all show nonlinear and decreasing rates of compaction, but these installations are not considered deep enough to reveal total subsidence.

The above-described boundary and interior controls, together with two additional zero-velocity constraints to the extreme southwest, were used to determine the subsidence model.

RESULTS AND MODEL VALIDATION

The velocity surfaces for 1973 and 1987.3 are shown in figures 2a and 2b. Figure 2b shows more rapid subsidence west of Houston for 1987, while at the same time subsidence has slowed or terminated for areas to the east. The eastern locality that showed the greatest reduction is near La Porte. Between 1973 and 1978, this area was subsiding at a rate of 65 mm/yr or more. By 1987, these rates had been reduced by at least 90 percent near the coast and lesser percentages near central Houston. To the west of Houston, the 1973 velocities for bench marks Y 1281, C 1149, and C 805 were respectively -52, -32, and 4 mm/yr. By 1987, these same velocities had increased to -76, -61, and -31 mm/yr. The dramatic reduction of subsidence east of Houston and the significant increase of subsidence west of Houston become graphically evident by

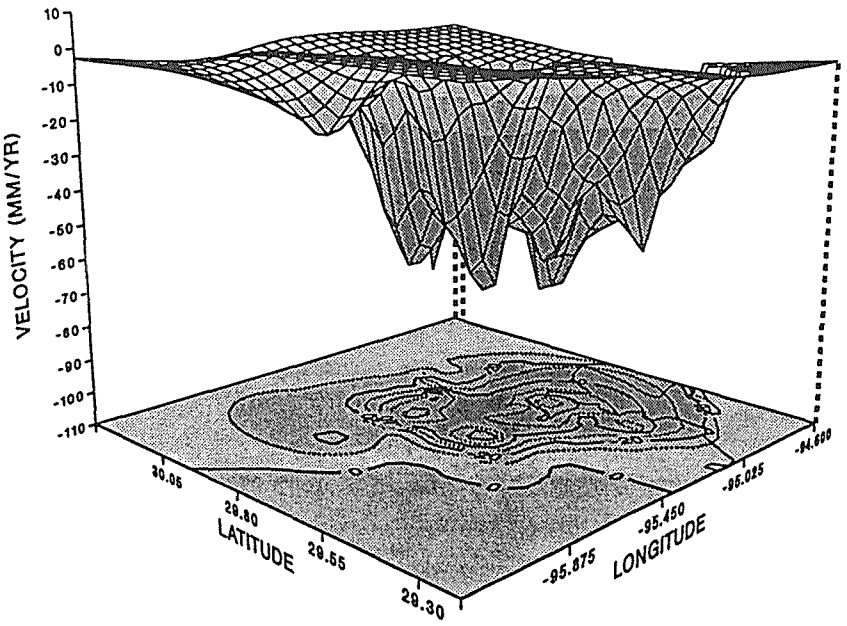

FIG. 2a Upper subsidence velocity surface corresponds to 1973.

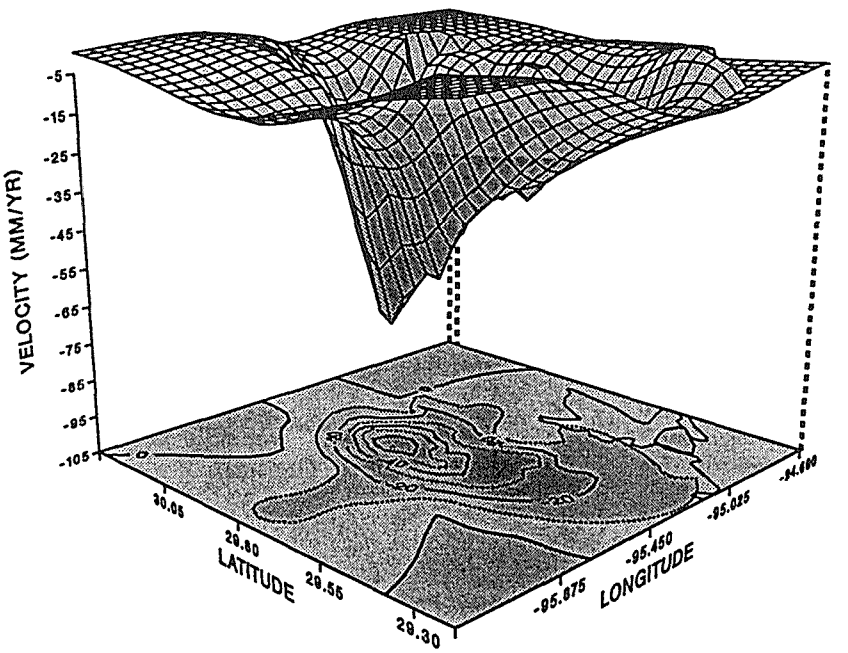

FIG. 2b Lower velocity surface corresponds to subsidence in 1987. Subsidence is greatly reduced near the coastline on the east side of the region. View is from southwest.

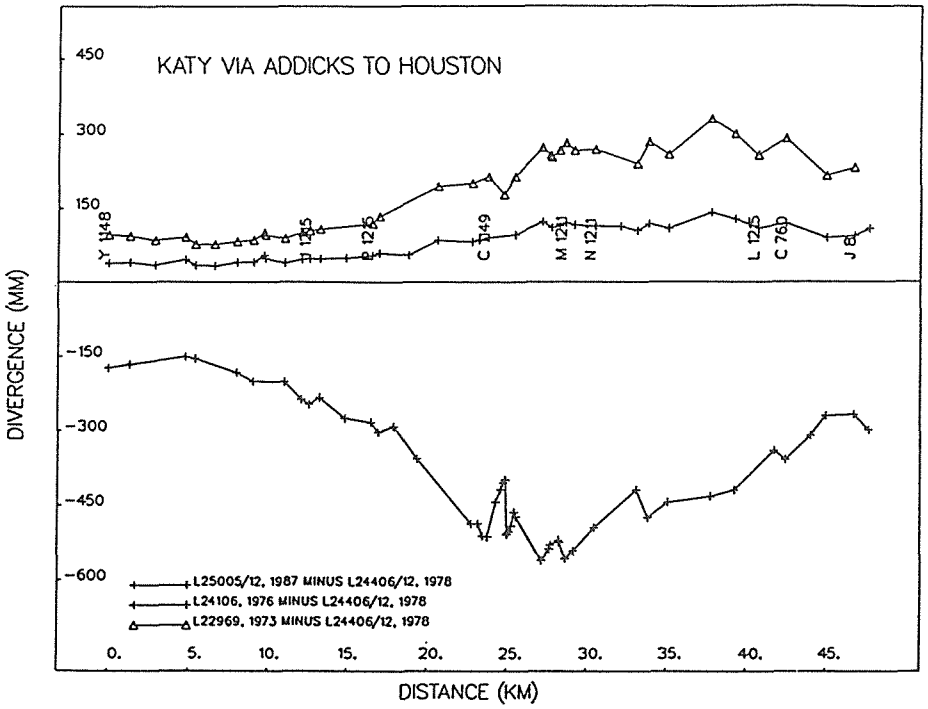

FIG. 3a Profile of subsidence along a route of leveling between Katy and Houston, TX.

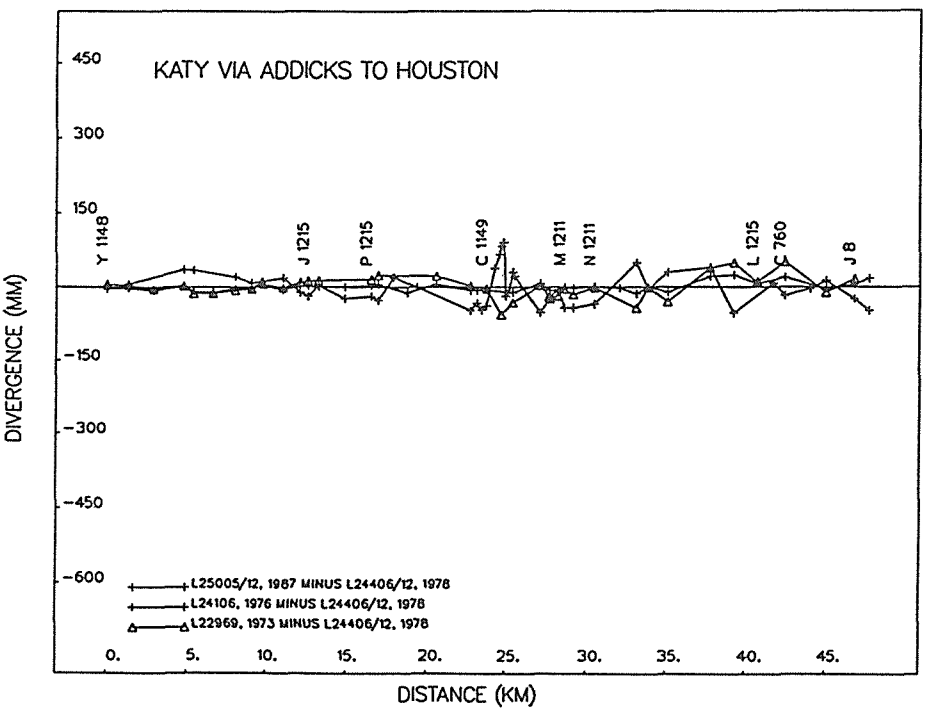

FIG. 3b Same profile as 3a but plotted after application of subsidence corrections.

comparing figures 2a and 2b. Table 1 contains the subsidence velocities and standard deviations for specific points shown in figure 1.

The modeled vertical motions should accurately reflect the observed subsidence along a path. Figure 3a is a subsidence profile which compares 1973, 1976, and 1987 surveys to the 1978 survey between Katy (bench mark Y 1148) and central Houston (bench mark J 8). There is approximately 200 mm of subsidence between 1973 and 1978, and additional subsidence of 500 mm between 1978 and 1987.

It is interesting to see if the subsidence model can be used to remove the motions seen in profiles like figure 3a. After storing the velocity and acceleration coefficients in a proper data structure, along with other pertinent parameters, the coefficients were accessed to evaluate subsidence for any point in the Houston region. The date, t_i, and point position (x,y) were provided to a subroutine which calculated the elevation change since time t_0. Using this procedure for pairs of bench marks, it is possible to formulate subsidence corrections for leveling measurements. For example, the 1973.3 measurements in figure 3a can be reduced to 1978.3. After applying subsidence corrections, a new profile can be made where all levelings are reduced to the same point in time. In Figure 3b, the 1973, 1976, and 1987 levelings have all been reduced to t_0 = 1978. The regional trend of motion is removed from the profile. Notice, however, that only the regional trend of motion is removed. It would be possible to remove all minor localized motion by adding more MQ nodal points, but this is not done in order to keep the model compact and meaningful. In the region surrounding Houston, there is motion at the 1-3 cm level caused by alternate wetting (rain) and drying of clay beds near the surface. The rms (root mean square) scatter of heights reduced to 1978, relative to the observed heights of 1978, are 2.4, 1.0, and 3.8 cm for the 1973, 1976, and 1987 surveys, respectively.

After application of subsidence corrections, which removes the 50-60 cm of subsidence seen in "before-corrections" profiles, it was evident that corrected height differences between adjacent bench marks will be in error at the 1-3 cm level in the Houston region because of the small random local motion associated with seasonal rainfall. Discrepancies may occasionally be as large as 10 cm. Consequently, the modeling process cannot completely restore old levelings to their original precision of 1 mm per kilometer. In Houston, any leveling which is several years old and between adjacent bench marks about 1 km apart should have an assigned uncertainty of 1-3 cm, even if water is not being pumped nearby.

Figure 4 shows how east Houston's 1978 time boundary permits a sequence of velocities that fit the data at the Pasadena extensometer. The later velocity value should be good for predicting height changes into the near future. A previous solution using a parabolic fit for the same locality did not predict well. The first of the two velocities in figure 4 underpredicts slightly, but this slight misfit may occur because other monitored points in the vicinity of the Pasadena extensometer were experiencing somewhat less subsidence prior to 1978.

SUMMARY

The techniques for modeling nonlinear vertical motion described here adapt well to the subsidence problem in Houston. Houston's subsidence model enables the production of a variety of computer generated graphics such as the subsidence contour maps shown in figures 2a and 2b. Predictions of subsidence into the near future can be accomplished using velocities calculated for 1987.

Regulated reductions of pumping east of Houston are responsible for the dramatic decrease in subsidence there since 1978. The Coastal Water Authority Canal System has

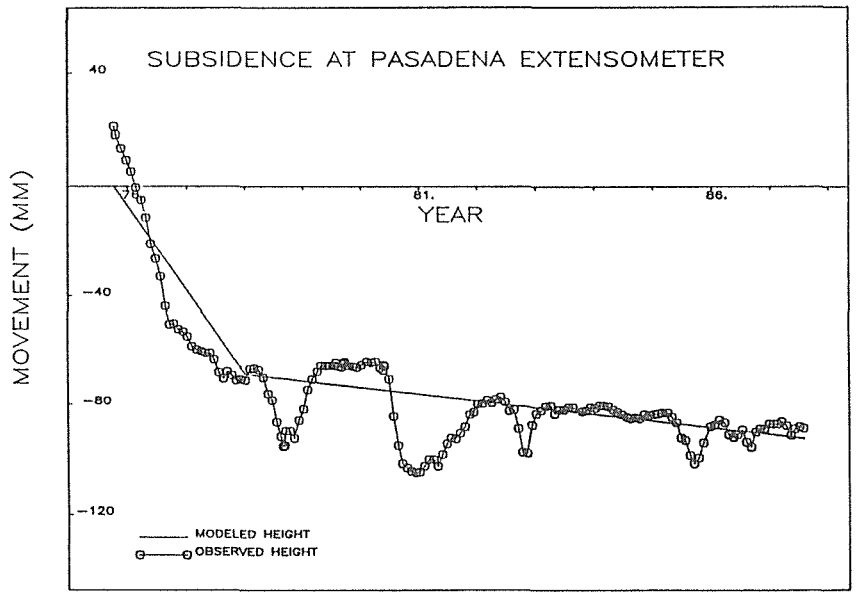

FIG. 4 Extensometer record showing subsidence at Pasadena, TX. Slopes of straight line segments correspond to modeled rates of motion before and after 1978.

provided alternative surface water since 1978. No alternative source of water is available for the area west of Houston, which has experienced rapid residential and commercial growth. All water comes from deep aquifers and pumping has increased significantly due to expansion and growth since 1973. Table 1 contrasts velocities calculated for 1973 and 1987 at selected points in Houston. The changes in velocity have a direct correspondence with regional changes in water level.

A good model for height change can be very useful. The Harris-Galveston area is so large that it has become increasingly difficult to organize a rapid survey campaign to relevel the entire subsiding region. Because the dynamic model accounts for height change, it is not necessary to level all parts of the network at exactly the same time. The model determination process permits observations of any dates. This facilitates the management of monitoring activities by allowing more flexibility in planning. Slow-moving areas or zones of low economic importance can be measured less frequently.

The model can be used to interpolate or predict height at locations which are not on a line of releveling, while recognizing that interpolation reliability decreases as distance from surrounding levelings increases. Such information may be necessary to resolve legal or engineering problems. The calculations can be made economically for any desired time.

From the geodetic point of view, it is necessary that a first- and second-order level network be useful for control of large engineering projects, mapping, and related survey activities. But in a subsiding area, most levelings may be biased by motion soon after the adjusted heights are determined. Consequently, a mechanism such as Houston's subsidence model must be available to correct for motion so old measurements can be made useful. Figure 4 shows that corrected old measurements in the Houston area can be incorporated in a national or broad regional adjustment of the area without biasing newer survey results, provided the corrected measurements are given a realistic weight.

TABLE 1 Subsidence velocities, Houston, Texas
(See figure 1 for locations of benchmarks.)

WEST ZONE

Benchmark name	1987 velocity (mm/yr)		acceleration (mm/yr^2)	
Tidal 19, Galveston	- 5.5	0.4*	0.02	±0.14*
S 1214	-29.6	4.9	-2.14	0.83
C 805	-31.1	4.2	-1.88	0.71
W 1212	-16.6	4.6	-1.43	0.75
Y 1148	-19.2	3.6	-0.67	0.60
Y 1210	-29.8	4.2	3.30	0.69
E 1151	-32.5	4.5	0.55	0.75
SOUTHWEST **	-47.2	0.8	-0.01	0.16
ADDICKS **	-54.6	1.2	-1.65	0.18
N 1211	-51.4	3.0	-0.53	0.52
J 1215	-31.5	3.7	-1.78	0.63
W 767	-12.7	3.8	-1.40	0.89
B 1221	-18.8	3.5	-0.06	0.62
F 1221	-64.8	4.0	0.30	0.66
CYPRESS	-16.5	2.2	-0.37	0.41
Y 1281	-76.1	2.8	-1.73	0.45
T 1149	-17.9	4.1	-0.19	0.67
R 88	- 4.1	5.5	0.05	0.88
V 1281	-53.6	2.8	-2.31	0.47
Y 1216	-58.3	3.8	-1.71	0.64

EAST ZONE

Benchmark name	Pre-1978 velocity (mm/yr)		Post-1978 velocity (mm/yr)	
L 305	- 2.5	± 3.7*	- 3.1	± 1.3*
P 1183	-43.0	5.1	- 3.6	2.3
Q 1146	-66.8	5.0	- 7.1	1.6
Z 53	-14.1	4.8	-14.1	1.6
Q 639 RE '63	-41.5	4.6	-15.1	1.5
CLEAR LAKE **	-26.7	4.3	-13.2	0.4
J 8	-34.8	4.3	-24.1	1.4
W 661	- 5.8	5.8	- 5.1	1.9
V 1215	-41.7	5.0	-26.4	1.4
F 55	-19.3	5.5	- 8.0	1.7
D 1218	-50.2	5.3	- 9.8	1.6
PASADENA **	-31.5	2.9	- 2.5	0.5
D 54	-32.2	5.3	-18.1	1.8
NORTHEAST **	-42.0	4.4	-21.0	0.3
G 54	-47.6	4.7	-34.6	1.6
LAKE HOUSTON **	-22.2	5.5	-11.3	0.3

* Standard deviation
** Extensometer

To properly serve geodetic purposes, the subsidence velocity surface should be made to taper down to zero velocity near a well defined outer boundary of the region. Outside that boundary, terrain height can be considered unchanging. The outer boundary for Houston is adequately defined on the east by Galveston Bay, and to the north it can pass through bench mark R 88. But to the southwest, it is unclear where the line of zero velocity should be placed. Further study is required. For completeness, the model should also be extended backward in time to account for motion prior to 1973.

Future subsidence computations at Houston will utilize the Global Positioning System (GPS) data. Simultaneous with the 1987 leveling project, many points in Houston were positioned three-dimensionally by GPS measurements. Further monitoring of those points is anticipated, and planned combinations of leveling and GPS measurements will allow subsidence to be monitored even more efficiently.

ACKNOWLEDGMENT John Chase and Janice Bengston of NGS assisted with organization and profiling of the leveling data.

REFERENCES

Balazs, E.I. (1980) The 1978 Houston-Galveston and Texas Gulf Coast vertical control surveys. NOAA Technical Memorandum NOS NGS 27, National Geodetic Information Branch, NOAA, Rockville, MD.

Gabrysch, R.K. (1982) Groundwater withdrawals and land-surface subsidence in the Houston-Galveston region, Texas, 1906-80. Open-File Report 82-571, United States Geological Survey.

Holdahl, S.R., Strange, W.E., & Harris, R.J. (1987) Empirical calibration of Zeiss Ni-1 level instruments to account for magnetic errors. Manuscripta Geodaetica, 12:28-39.

Neighbors, R.J. & Thompson, R.E. (1984) Subsidence in the Houston-Galveston area of Texas. Proceedings of the Third International Symposium on Land Subsidence, Venice, Italy, March 18-25.

Vanicek, P., Elliott, M.R., & Castle, R.O. (1979) Four-dimensional modelling of recent vertical movements in the area of the Southern California uplift. In: C.A. Whitten, R. Green and B.K. Meade (Editors) Recent Crustal Movements, 1977. Tectonophysics, 52; 287-300.

Zilkoski, D.B. (1984) The 1983 Houston-Galveston Subsidence Network. Proceedings of 1984 ASP-ASCM Fall Convention, San Antonio, TX, pp 147-156.

Land Subsidence (Proceedings of the Fourth International Symposium on Land Subsidence, May 1991). IAHS Publ. no. 200, 1991.

A New Three Dimensional Finite Difference Model of Ground Water Flow and Land Subsidence in the Houston Area

ROLANDO BRAVO, JERRY R. ROGERS &
THEODORE G. CLEVELAND
Department of Civil and Environmental Engineering, University of Houston, Houston, Texas 77204, USA

ABSTRACT This paper presents a methodology to analyze the subsidence problem in the Houston area using a modified version of the Three Dimensional Finite Difference Ground Water Flow Model developed by the U.S. Geological Survey (USGS). The program simulates the hydrological conditions of the Chicot and Evangeline Aquifers, which underlie Houston, and couples the ground water storage changes in the compressible beds with the aquifer system compaction. The subsidence analysis uses a methodology that is independent of the time interval used in solving the ground water flow governing equation. The regional model is calibrated using actual data from extensometers and piezometers operated by the U.S. Geological Survey in many places throughout Houston. The model uses flux boundary conditions that were estimated using a radial flow analog and Darcy's law. Some head data were generated using the regional variable theory called kriging to supply head estimates in areas where data were unavailable. A one year simulation was made, and a rough estimate of prediction error indicates that the model performs well for locations where data were available.

INTRODUCTION

In the Houston area, land subsidence has occurred for many years. One recognized cause of subsidence in Houston is withdrawal of ground water for municipal, industrial, and agricultural water supply (Williams and Ranzau, 1987). This withdrawal has lowered the static head distribution in the aquifers beneath Houston, and the lowered heads have in turn caused critical subsidence in certain areas. Some land surface has subsided nearly 3 meters since 1906. The U.S. Geological Survey (since the mid 1950's), the Houston-Galveston Coastal Subsidence District (since its creation in 1975), and the City of Houston are all interested in subsidence in the area because parts of the Houston-Galveston area are subject to flood damage which can be intensified by subsidence.

Bravo, et al., (1991) developed a new methodology to predict the compaction and rebound of the soil column given hydraulic heads in the soil. This paper presents a flow and subsidence model to determine the head distributions in the underlying aquifers and to predict regional subsidence.

BACKGROUND

The Houston-Galveston region includes all of Harris and Galveston Counties, and parts of six adjoining counties. Houston is the fifth most populous city in the United States, and third largest in port tonnage. The downtown is 15 meters above sea level; the Johnson Space Center to the south is 5.2 meters above sea level. The region is subject to hurricanes

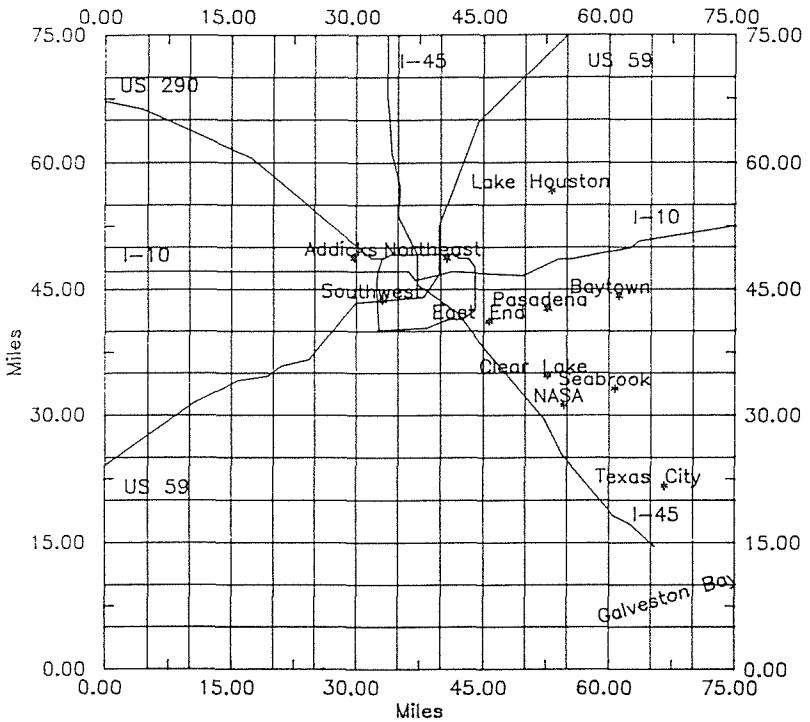

FIG. 1 Location of borehole extensometers of the USGS (Open File Report 89-057). Boundary and grid of the model.

and storms that historically have caused storm surges of 4 to 6 meters and daily rainfall depths up to 107 centimeters. Sections of the region are prone to storm surge flooding and land subsidence compounds the flooding. This problem is the motivation behind the studies of subsidence and ground water flow by Bravo (1990) and earlier researchers.

The major water bearing units in the Houston-Galveston area are the Chicot and Evangeline aquifers. The Chicot aquifer overlies the Evangeline aquifer that overlies the Burkeville confining layer. The relationship of the Chicot aquifer, the Evangeline aquifer, and the Burkeville layer is shown in Figure 2. The Chicot and Evangeline aquifers consist of unconsolidated and discontinuous layers of sand and clay that dip toward the Gulf of Mexico. A detailed description of the subsurface geology is given by Ryder (1988).

PREVIOUS MODELS

The first hydrological model of subsurface flow in the Houston area was the electrical analog model of Wood and Gabrysch (1965). Their model covered about 129.50 km^2 and was used to predict water levels under various conditions of pumping. Its weaknesses were that the aquifers were simulated independently of each other, the western area pumping schedules could not be simulated, the aquifer designation was somewhat fuzzy, and the transmissivities of the aquifers and vertical leakage between the aquifers were not well modeled. In spite of these problems, prior to the 1965 model, predicting aquifer response to various pumping schedules would have been very laborious.

Another early ground water flow model was the electrical analog model by Jorgensen (1975). The model covered about 235.70 km^2 and simulated two layers with vertical leakage. The area modeled was made larger than the Wood and Gabrysch model to

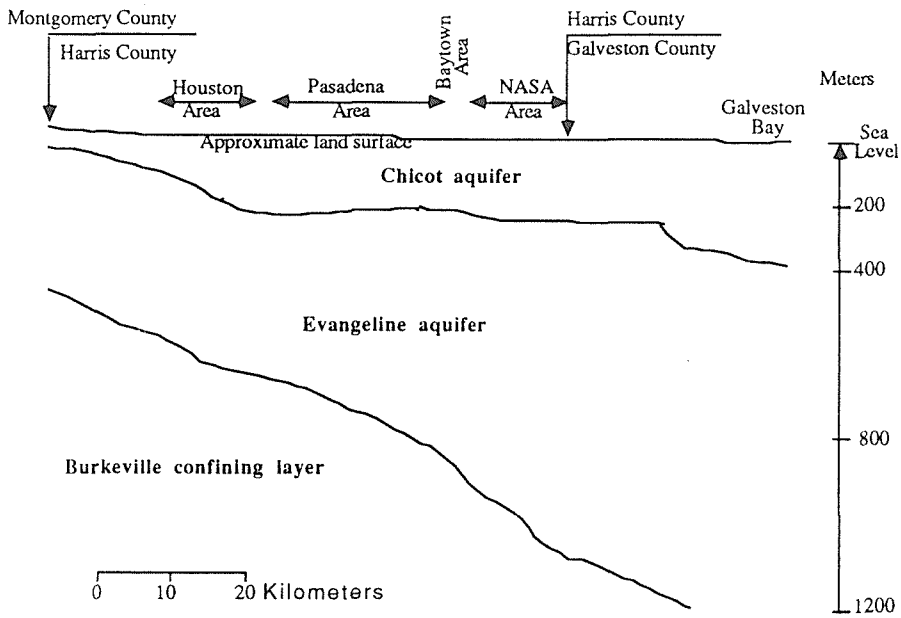

FIG. 2 Hydrologic profile from the Houston area (from Gabrysch, 1976).

minimize boundary effects. Aquifer transmissivities and storage coefficients were estimated from data for many aquifer tests in the Houston area. The model incorporated clay compaction but was not designed to predict subsidence. Jorgensen incorporated more advanced hydrologic concepts but noted that the observed cones of depression in the 1970's extended beyond the model's fixed head boundary. He stated that the model is sensitive to boundary conditions for all simulations beyond 1970.

Meyer and Carr (1979) developed and calibrated a five layer flow and consolidation model of the Chicot and Evangeline aquifers. Their model covered 699.30 km^2 and extended far beyond the Houston area. The model used the USGS-2D Trescott code to solve the flow equations (Trescott et al., 1975). The model had a fine mesh grid in the Houston area and a coarse mesh at its extremities. The arbitrary fixed head boundaries were extended to areas of minimal pumping to reduce boundary effects and eliminate the necessity of imposing flux boundary conditions.

CONCEPTUAL HYDROLOGICAL MODEL

This work describes a methodology to incorporate flux boundary conditions, uses regional variable theory to estimate initial conditions for locations where there are no data, and uses a consolidation theory that is relatively independent of the simulation time steps.

The subsurface lithology of the Houston area is composed of sand and clay layers of varying thickness. Bravo (1990) studied sonic, spontaneous-potential, and conductivity logs for five of the eleven borings shown in Figure 1 (Baytown, Clear Lake, Johnson Space Center, Southwest and Addicks). The logs were manually interpreted to generate geologic profiles of the subsurface at the five sites (Keys, 1971). Interpreted geologic profiles for the Baytown, Clear Lake and Johnson Space Center boring are show in Bravo et al., (1991).

The representation of the subsurface geology was further simplified by concentrating the sand and clay layers in a manner consistent with the stratigraphy in the East-West direction and developing the eight layer conceptual model shown in Figure 3. The North-

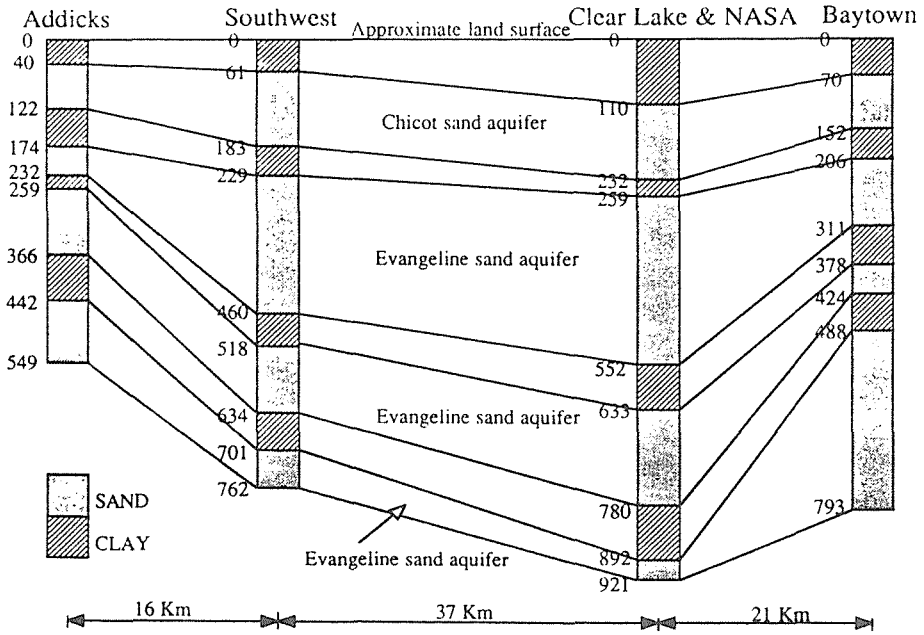

FIG. 3 Conceptual model of the ground water hydrology of the Houston area. The numbers indicate meters below land surface.

South subsurface geology was modeled using the conceptual model and adjusting the thickness of each layer so that the overall aquifer thickness follows the transect shown in Figure 2. The East-West subsurface model was extrapolated horizontally beyond the limits shown in Figure. 3 because there was no further stratigraphic information.

CONCEPTUAL AQUIFER FLOW MODEL

The Chicot Aquifer was modeled as an isotropic aquifer with the potential for either confined or unconfined horizontal flow. The Evangeline Aquifer sand layers were modeled as confined leaky isotropic aquifers. The intervening clay layers were modeled as semi-pervious formations. The effects of delayed storage in the clay layers were modeled as a source term in the flow model but were computed in the consolidation model.

The conceptual hydrogeologic model and flow model are described mathematically by (Bear and Verruijt, 1987)

$$\nabla\cdot(T_i\nabla\phi_i) + \frac{\phi_i - \phi_{i-1}}{\sigma_i} + R_i - P_i = S\frac{\partial\phi_i}{\partial t} + S_{sk}\frac{\partial\phi_i}{\partial t} \qquad (1)$$

subject to the boundary conditions

$$\phi_i(x,y,t) = \text{known on } d\Gamma_1 \text{ (Dirichlet condition)} \qquad (2)$$

$$T_i\frac{\partial\phi_i}{\partial x}\frac{\partial x}{\partial n} = \text{known on } d\Gamma_2 \text{ (Neuman condition)} \qquad (3)$$

and the initial conditions

$$\phi_i(x,y,0) = \text{known on } \Gamma \qquad (4)$$

where $\phi_i(x,y,t)$ is the piezometric head in sand layer i,

$T_i(x,y)$ is the transmissivity in sand layer i,

$\sigma_i(x,y)$ is the conductance of the clay layer between sand layer i-1 and i,

$R_i(x,y)$ is the recharge in sand layer i,

$P_i(x,y)$ is the pumping from layer i,

n is the outward unit normal vector along the boundary of the flow domain,

$d\Gamma$ is the boundary of the flow domain ($d\Gamma_1 \cup d\Gamma_2 = d\Gamma$),

Γ is the flow domain,

S is the storage coefficient of the aquifer,

S_{sk} is the specific storage of the semi-pervious clay layers.

Unconfined flow in the Chicot Aquifer, when it occurs, was modeled using the Dupuit assumptions and a backwards time linearization. The transmissivity was calculated as the product of saturated thickness and hydraulic conductivity.

A prescribed piezometric head boundary condition (Dirichlet) was applied along the edge of the model that intersects Galveston Bay, while a prescribed flux boundary condition (Neuman) was applied along the rest of the boundary. The previous regional models of ground water flow in the Houston area used prescribed head everywhere along the boundary. The present work used a flux boundary condition because there were not sufficient data to determine a prescribed head boundary condition for the area studied.

Piezometric contour maps from 1980 to 1989 were observed to have the same appearance as contour maps that would be expected for radial steady flow to a well. This fact suggested that one test the relationship between radial distances from a hypothetical origin and the piezometric head. In most directions the relationship between the piezometric head and the logarithm of the radial distance was found to be linear and the slopes of the regression lines were almost the same for the ten years studied (Bravo, 1990; Bravo et al., 1990). These slopes can be used to estimate the hydraulic gradient at the boundary.

The extent of the region studied was chosen to cover the withdrawal areas (pumping areas) for the same decade. The boundary is shown in Figure 2. The radial flow analog and Darcy's law were used to estimate the flux into the domain of interest. The pumping rates for the ten years studied varied from 440 million m^3 $year^{-1}$ to 741 million m^3 $year^{-1}$; yet the values for the fluxes were relatively constant. Because of this behavior, it was assumed that the fluxes remain constant for prediction horizons of several years. A ground water budget that assumes the clay layers contribute an amount of water equal to 25% of pumping (the proportion concluded by Meyer and Carr, 1979) was satisfied using this flux boundary condition, further strengthening confidence in the flux boundary methodology.

INITIAL CONDITIONS

Initial piezometric heads for all the cells in the model were unavailable. A regional variable theory (kriging) was used to estimate the initial piezometric heads in the cells for which there was no data (Marsily, 1986). A circular search pattern for kriging the data assumed the variation of the heads in the North-South direction were statistically independent for the variation of the heads in the East-West direction (Davis, 1986). This assumption was consistent with the methodology used to determine the flux boundary conditions.

AQUIFER HYDRAULIC CHARACTERICTICS

The transmissivities and storage coefficients for the sand layers were taken from previous studies (Jorgensen, 1975; Meyer and Carr, 1979). The vertical hydraulic conductivities and storage coefficients of the semi-pervious layers were determined independently using the methods developed by Bravo (1990).

CONCEPTUAL SUBSIDENCE MODEL

The principle of effective stress was used to model the relationship of soil compaction and ground water piezometric head (Bear and Verruijt, 1987). In an unconfined aquifer the change in effective stress was expressed as

$$\Delta\sigma' = -\gamma_w (1 - n_e + \theta_w) \Delta h \tag{5}$$

where $\Delta\sigma'$ is the change in effective stress,

γ_w is the specific weight of water,

n_e is the effective porosity of the porous medium,

θ_w is the moisture content above the water table as a fraction of total volume,

Δh is the change in the water table elevation.

In a confined aquifer the change in effective stress was given by

$$\Delta\sigma' = -\gamma_w \Delta\phi \tag{6}$$

where $\Delta\phi$ is the change in the piezometric head.

Studies of the change in effective stress and the elastic compaction or expansion of soil indicate that the change in the thickness of an aquifer is proportional to the change in the effective stress. This relationship is expressed as

$$\Delta b = \frac{\Delta\sigma'}{\gamma_w} S_{ske}\, b_o \tag{7}$$

where Δb is the change in aquifer thickness,

S_{ske} is the skeletal component of elastic storage,

b_o is the initial thickness of the aquifer.

The elastic storage coefficient S_{ke} is defined as the product of S_{ske} and b_o. Studies have also shown that when compressible fine grained soils are subjected to stresses greater than a maximum value, the compaction is permanent. This kind of compaction is called inelastic compaction.

The compaction per unit increase in effective stress in the inelastic range is considerably greater than in the elastic range. When the increased effective stress is reduced below the inelastic range the soil resumes its elastic characteristics (with a new initial thickness) unless the effective stress increases beyond the new maximum elastic range. A relation between the inelastic compaction and effective stress similar to the relation for the elastic range was used as a first approximation.

The specific storage coefficient S_{sk} of the semi-pervious clay layers in Equation 1 is

determined by both the elastic and inelastic behavior of the soil. The coefficient takes the value of the elastic specific storage whenever the piezometric head is greater than the preconsolidation head. The coefficient takes the value of the inelastic specific storage coefficient when the piezometric head is less than the preconsolidation head.

An implicit approach was used to rewrite the right most term of Equation 1 for modeling the loss or gain of water in the clay layers (Leake and Prudic,1988). This approach allowed the use of much larger time steps in the simulation model than in previous studies which used explicit formulations of the elastic and inelastic storage coefficients (Meyer and Carr, 1979). The implicit formulation is written as

$$\frac{S'_{sk}}{\Delta t} = \frac{S^{m}_{sk}}{\Delta t}\left[\phi^{m} - \Phi^{m-1}\right] + \frac{S_{ske}}{\Delta t}\left[\Phi^{m-1} - \phi^{m-1}\right] \qquad (8)$$

subject to

$$S^{m}_{sk} = \begin{cases} S_{ske}, & \phi^{m} > \Phi^{m-1} \\ S_{skv}, & \phi^{m} < \Phi^{m-1} \end{cases}$$

where ϕ^{m} is the piezometric head at time step m,

Φ^{m-1} is the preconsolidation piezometric head at time step m-1.

This formulation was used in the flow model and once heads were computed for the entire aquifer system, the consolidation was computed using Equations 5 through 7. The values of S_{ske} and S_{skv} were obtained using the methodology described by Bravo (1990).

FLOW AND SUBSIDENCE MODEL SOLUTION

The flow model described by Equations 1 through 3, and Equation 8 was solved using the Modular Three-Dimensional Finite Difference Ground Water Flow Model (MODFLOW) developed by the U.S. Geological Survey (McDonald and Harbaugh, 1988). Transient flow for the geometry defined by the boundary shown in Fig. 4 was modeled using injection wells to simulate the fluxes along the boundary. The subsidence model described by Equations 5 through 7 was solved using the code developed by Leake and Prudic (1988). Their solution code was attached to the MODFLOW code for this research. The subsidence module solved Equations 5 through 7 using the flow solution from Equations 1 through 3 and Equation 8. Because the module also tracked the preconsolidation heads it was an intimate part of the flow model.

RESULTS

The flow model was operated for a simulation period of one year, using initial data from 1983. Figure 4 shows the observed 1984 head distribution in the Chicot Aquifer. Contours are head in feet. The vertical and horizontal scales are in miles. Figure 5 is the simulated head distribution (missing data are estimated by kriging). Figures 6 and 7 are the observed and simulated head distributions in 1984 for the Evangeline Aquifer system. To measure the performance of the model the relative prediction error for the Chicot and Evangeline Aquifers were calculated. The formula used was

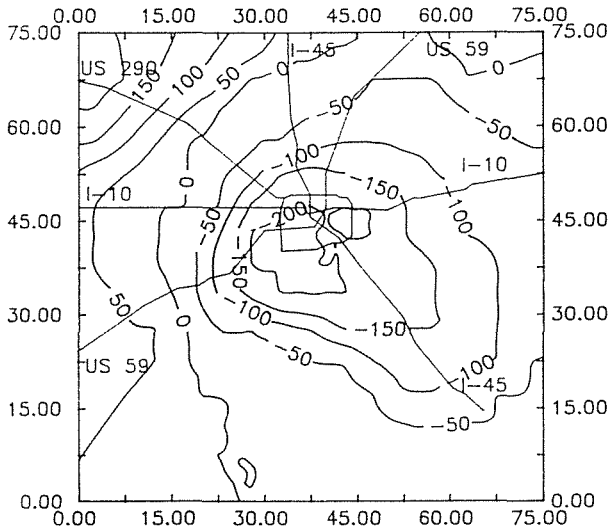

FIG. 4 Chicot aquifer 1984 heads (observed).

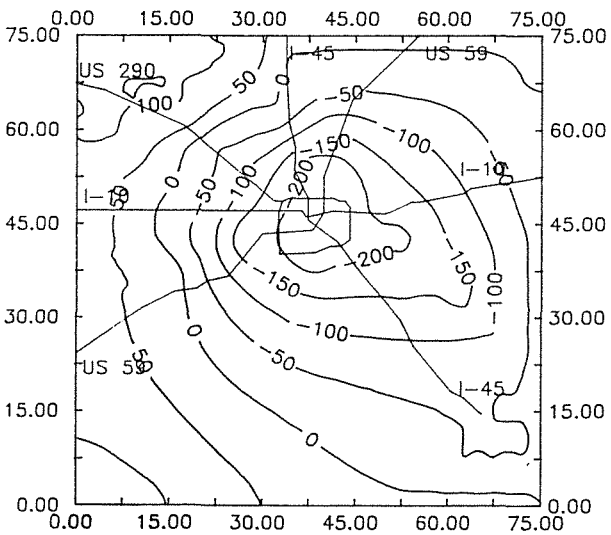

FIG. 5 Chicot aquifer 1984 heads (simulated).

$$RPE(x,y) = \frac{\phi^{predict}_{(x,y)} - \phi^{actual}_{(x,y)}}{\phi^{actual}_{(x,y)}} \tag{9}$$

where RPE(x,y) is the relative prediction error of the flow model.

Figure 8 shows a map of RPE for the Chicot Aquifer. The model performed well in predicting piezometric heads in the Chicot Aquifer at locations where actual data were available. Figure 9 shows a map of RPE for the Evangeline Aquifer. Again the model performs well for those locations where there were data. What is remarkable is that no

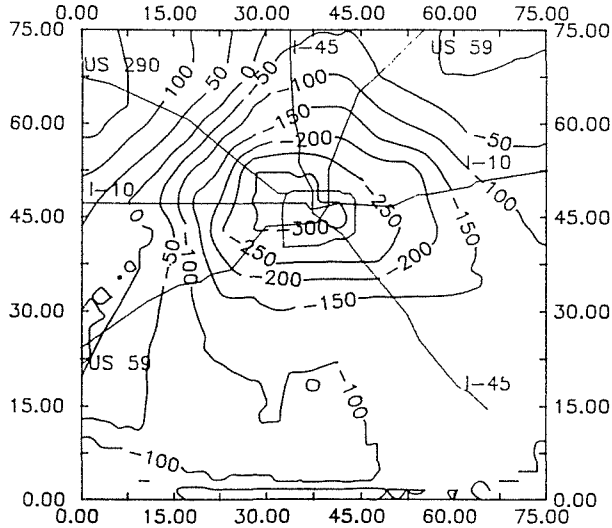

FIG. 6 Evangeline aquifer 1984 heads (observed).

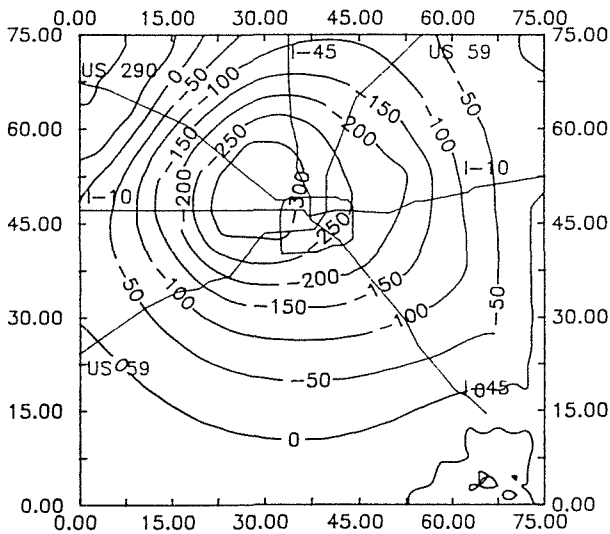

FIG. 7 Evangeline aquifer 1984 heads (simulated).

parameter identification (inverse estimation) procedures beyond determining the boundary conditions were used; yet the model performed adequately.

Subsidence was calculated but without an initial condition. Figure 10 presents a subsidence prediction for 1984 assuming there is zero subsidence in 1983. This can be interpreted as a map of change in subsidence, much like a ground water drawdown map.

CONCLUSIONS

The University of Houston Civil and Environmental Engineering group has developed a new ground water flow and land subsidence model of the Houston area. Based on the

1983 to 1984 simulation the flow and subsidence model appeared to perform well in areas where data were available; the change in subsidence was consistent with predicted head changes.

The model used regional variable theory for estimating initial conditions at locations where there were no data, and a radial flow analog to estimate flux boundary conditions in the Houston area. The techniques used may be applicable to similar regions; the flux boundary condition eliminates the need to model areas that are greater than the given area of interest.

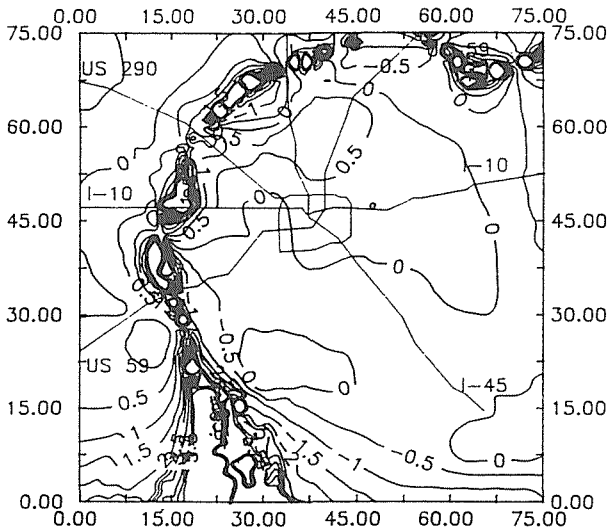

FIG. 8 Relative prediction error for the 1984 Chicot aquifer heads.

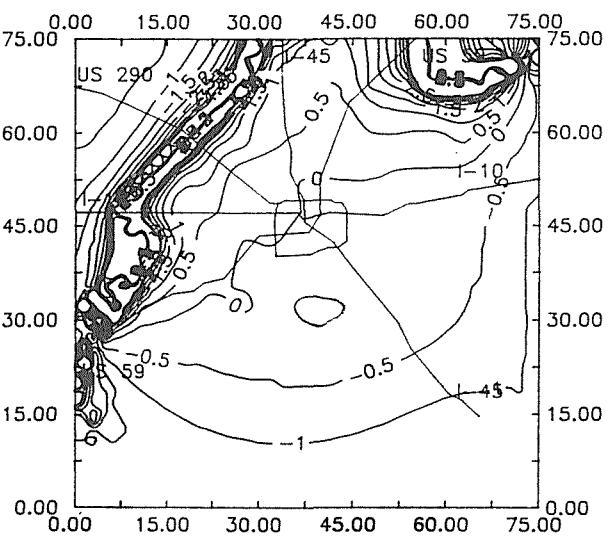

FIG. 9 Relative prediction error for the 1984 Evangeline aquifer heads.

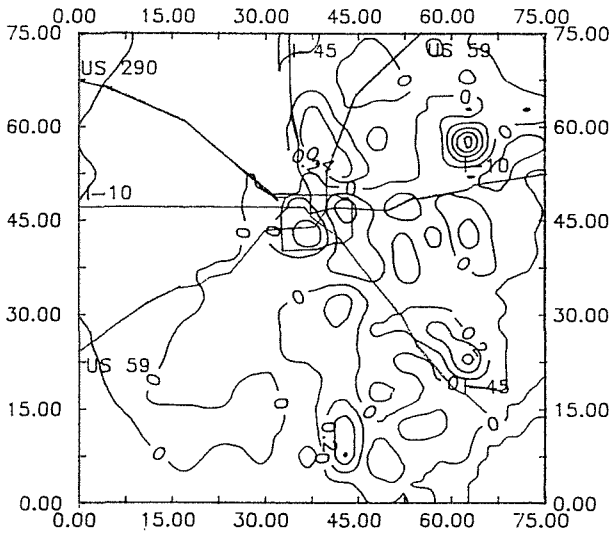

FIG. 10 Subsidence prediction for 1984.

Further research includes a study to determine the sensitivity of the model to changes in aquifer parameters, a study of the influence of storage in the clay layers when the vertical flow assumption is relaxed, and a study of the influence of the search pattern in the kriging algorithm when the assumption of statistical independence of the variation of head with direction is relaxed.

ACKNOWLEDGEMENTS The authors wish to thank Mr. Robert K. Gabrysch, Chief of the Houston Subdistrict of the United States Geological Survey and his staff for providing much of the background data and reports. Thank you to the Harris-Galveston Coastal Subsidence District for providing the information about pumping in the district.

REFERENCES

Bear, J. & Verruijt, A. (1987) Modeling Ground water Flow and Pollution. D. Reidel, Boston.

Bravo, R. (1990) A new Houston ground water flow and subsidence model utilizing three dimensional finite differences. Ph.D. Dissertation, University of Houston, Houston, Texas.

Bravo, R., Rogers, J. R. & Cleveland, T.G. (1990) Prediction of water heads in the Houston area, presented at American Water Resources Association, Texas Section, Austin, Texas, November, 1990.

Bravo, R., Rogers, J.R. & Cleveland, T.G. (1991) Analysis of ground water level fluctuations and borehole extensometer data from the Baytown area, Houston, Texas. Proceedings of the Fourth International Symposium on Land Subsidence, Houston, Texas.

Bravo, R., Rogers, J. R. & Cleveland, T. G. (1991) On the determination of the compressible soil properties required to model subsidence in the area of Houston, Texas. Proceedings of the Fourth International Symposium on Land Subsidence, Houston, Texas.

Davis, J.C. (1986) Statistics and Data Analysis in Geology. Wiley, New York.

Jorgensen, Donald G. (1975) Analog model studies of ground water hydrology in the

Houston district, Texas. U.S. Geological Survey, report 190.
Keys, W.S. & MacCary, L.M. (1971) Applications of borehole geophysics to water resources investigations. U.S. Geological Survey Techniques of Water Resources Investigations Book 2-E1.
Leake, S.A. & Prudic, D.E. (1988) Documentation of a computer program to simulate aquifer-system compaction using the Modular Finite-Difference Ground-Water Flow Model. U.S. Geol. Survey, Open File Report 88-482.
Marsily, Ghilsan de (1986) Quantitative Hydrogeology. Academic Press, New York.
McDonald, M.G. & Harbaugh, A.W. (1988) A modular three-dimensional finite-difference ground-water flow model. U.S. Geological Survey, Techniques of Water Resources Investigations, Book 6-A1.
Meyer, W.R., and Carr, J.E. (1979) A digital model for simulation of ground water hydrology in the Houston area, Texas. Texas Dept. Water Resources LP-103.
Ryder, Paul D. (1988) Hydrogeology and predevelopment flow in the Texas Gulf Coast aquifer system, U.S. Geological Survey water resources investigation report 624-B.
Trescott, P.C., Pinder, G.F. & Larson, S.P. (1975) Finite difference model for aquifer simulation in two dimensions with results of numerical experiments. U.S. Geological Survey, Techniques of Water Resources Investigations, Book 7-C1.
Wood, L.A. & Gabrysch, R.K. (1965) Analog model study of ground water in the Houston district, Texas. Texas Water Commission Bulletin 6508.
Williams III, James F., & Ranzau, Jr., C.E. (1987) Ground water withdrawals and changes in ground water levels, ground water quality, and land surface subsidence in the Houston District, Texas, 1980-1984. U.S. Geological Survey, Water-Resources Investigation Report 87-4153.

Land Subsidence (Proceedings of the Fourth International Symposium on Land Subsidence, May 1991). IAHS Publ. no. 200, 1991.

Detection of Aquifers Susceptibility to Land Subsidence

N. P. PROKOPOVICH
3333 Braeburn Street
Sacramento, CA 95821, U.S.A.

ABSTRACT Consolidometer testing of aquifer sediments can be used to determine: (1) the confined aquifer systems susceptible to subsidence due to a piezometric decline; and (2) the amount of such subsidence. "Undisturbed" core samples of aquifer sediments should be preconsolidated using a loading equal to the estimated weight of the overburden minus the supporting pressure of the existing piezometric head. The following second consolidation test under the total weight of overburden (without the subtraction) will indicate (1) the susceptibility of sediments to compaction after a complete or partial decline of piezometric head, and (2) the amount of subsidence. With some modifications, similar testing may be applied also for prediction of subsidence in unconfined aquifers.

INTRODUCTION

Confined and unconfined aquifer systems are an important source of water. In many areas, the development of such aquifers, particularly their overdraft, leads to a costly geological hazard--land subsidence (Bolt et al., 1975). Such subsidence is now known on all continents except Antarctica, and its future spread seems to be unavoidable with the growth of world population and the increasing need for water (Prokopovich, 1972). To be able to predict aquifers which have sediments that are susceptible to compaction that causes such land subsidence is, therefore, an important and challenging task in engineering geology (Prokopovich, 1978).

The following paper summarizes some ideas that were developed gradually by the author during some 30 years of studies of land subsidence for the Federal Bureau of Reclamation. Most of the studies were conducted on the west central portion of the San Joaquin Valley in California, United States of America, and were made in connection with the design and construction of the Federal San Luis Canal (Anonymous; 1974a, 1981), which is also incorporated as one of the reaches of the California Aqueduct (Anonymous, 1974b) (Figure 1). The valley (Figure 1) is one of the world's largest areas affected by man-induced land subsidence (Poland et al., 1975). In places, the amount of subsidence in the valley has approached 10 m (Figure 2), and has caused damage to several existing canals (by flooding of their lining), pipe crossings, bridges, etc. (Figure 3) costing multimillions of dollars.

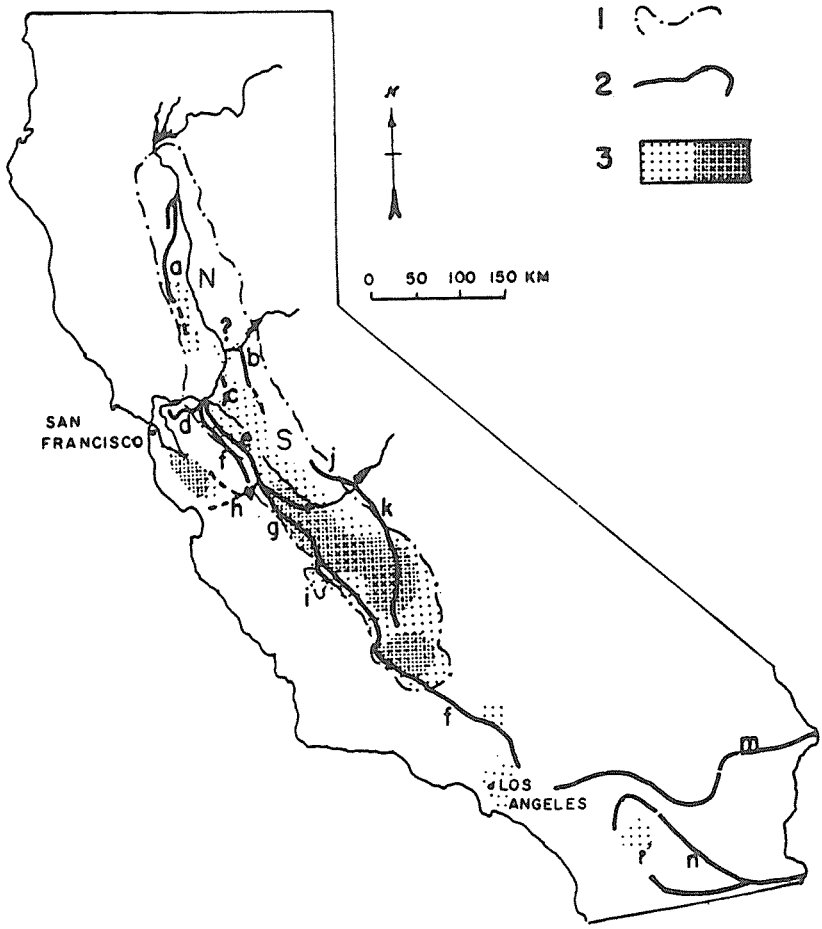

FIG. 1 Land subsidence due to an overdraft of ground water in California, U.S.A. (1) Outline of California's Central Valley, composed of Sacramento (N) and San Joaquin (S) Valleys; (2) major canals; (3) subsiding areas. Darkened pattern indicates major subsidence.

Major irrigation canals: (a) Tehama-Colusa; (b) Folsom South; (c) Peripheral (Proposed) Canal; (d) Contra Costa; (e) Delta-Mendota; (f) California Aqueduct; (g) San Luis; (h) San Felipe Division; (i) Coalinga; (j) Madera; (k) Friant-Kern Canal; (m) Colorado Aqueduct; (n) Coachella and All American Canals.

The ideas expressed in the paper are, however, those of the author and may not represent the official views of the Bureau of Reclamation. Unfortunately, the present concept was finalized after construction of the San Luis Canal and, therefore, was not properly field-laboratory tested.

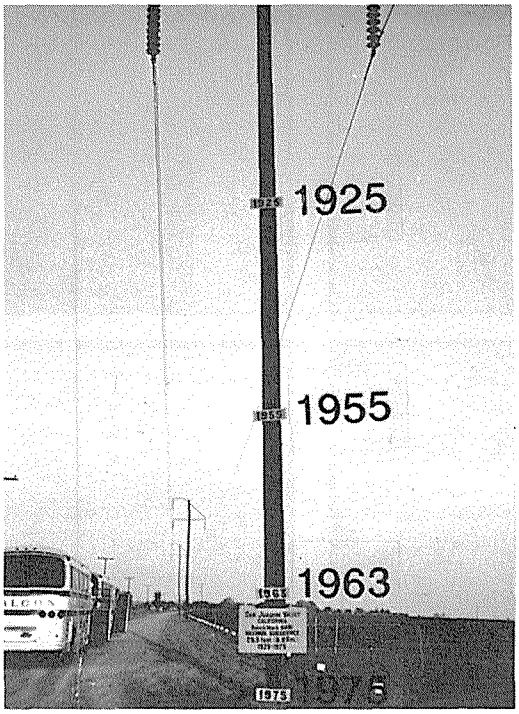

FIG. 2 Past changes of elevation of land surface in the San Joaquin Valley in an area of maximum subsidence (west of Mendota). Signs show the position of land surface in different years (photograph by B. Lofgren).

BASIC CONSIDERATIONS

Subsidence caused by a decline of ground-water levels is a surficial expression of the compaction of aquifer sediments at depth (Poland and Davis, 1969). Such compaction will take place only if these sediments are not already precompacted by the weight of their overburden.

In the case of a confined aquifer, the aquifer sediments will be practically compacted and not susceptible to subsidence if the piezometric head was developed after deposition of the overburden. Decline of piezometric head under such conditions with already preconsolidated sediments will increase the effective loading on the aquifer, but will not cause a major compaction--subsidence. On the contrary: if the piezometric head was developed prior (or during) the deposition of overburden, the head's decline by pumping and the resulting increase in the effective loading will cause subsurface-compaction of sediments and land subsidence (Prokopovich, 1983).

METHODOLOGY OF PREDICTIONS

The consideration discussed above allows to (a) determine theoretically the susceptibility of an aquifer sediment to

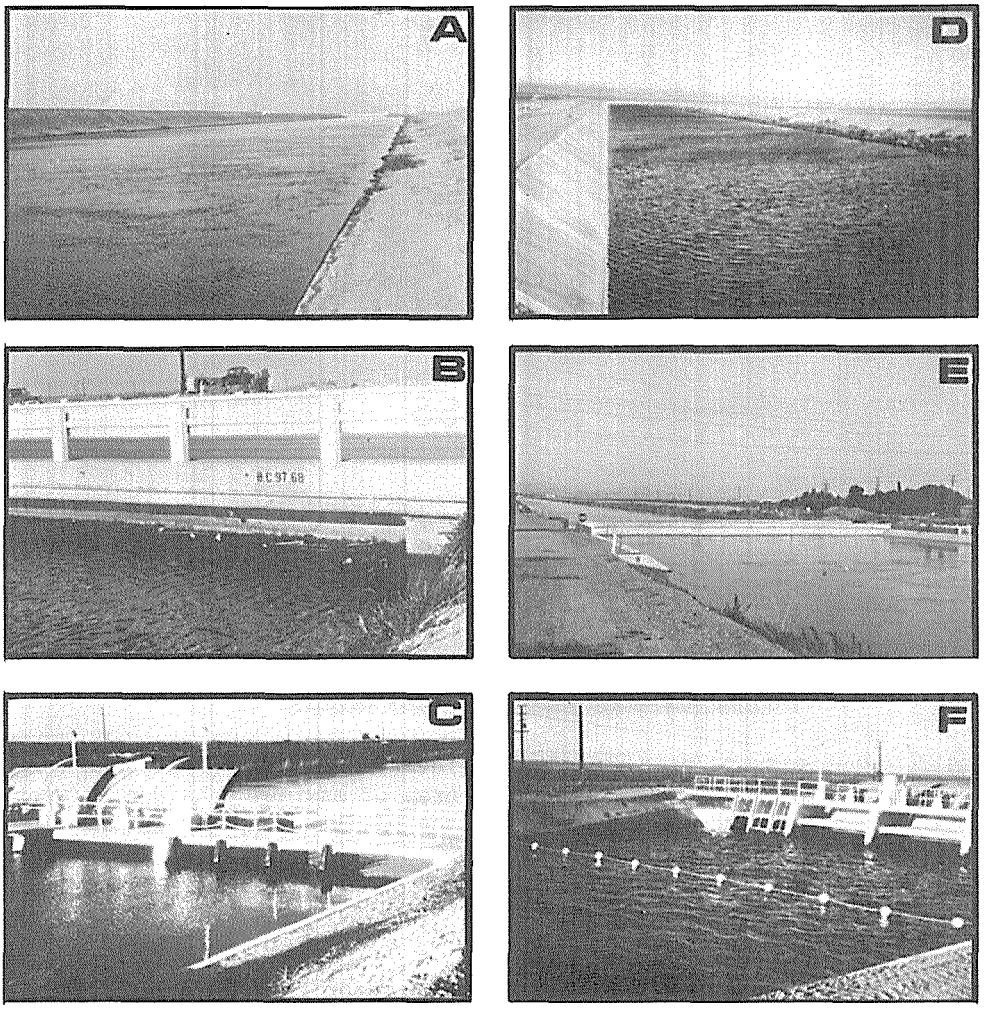

FIG. 3 Impacts of subsidence on the Delta-Mendota Canal, California (see Fig. 1). (a) Concrete canal lining is submerged below water; (b) highway bridge is partially submerged and canal side lining is completely flooded; (c) check structure is partially flooded; side lining is submerged; (d) partially rehabilitated concrete lining; lining on the opposite bank is flooded; (e) rehabilitated highway bridge and its approaches; (f) rehabilitated check structure.

subsidence, and (b) estimate ultimate amounts of such subsidence: using "undisturbed" (Anonymous, 1974c) samples of the overburden and of aquifer sediments obtained by drilling (Figure 4); and following laboratory consolidometer testing of samples. The following procedure is recommended:

(1) The total weight of overburden capping of an aquifer system should be established using "field" (="wet") densities (Anonymous,

1974c) of typical overburden sediments obtained at different depth intervals and the thinness of the overburden.

(2) Using these data, laboratory consolidation tests of typical samples of sediments of an aquifer system should be conducted using at least two consecutive loadings for each sample. The first loading should be equal to the total weight of overburden minus the relief of the loading created by the existing piezometric head. Such loading will eliminate possible rebound of sediments during sampling.

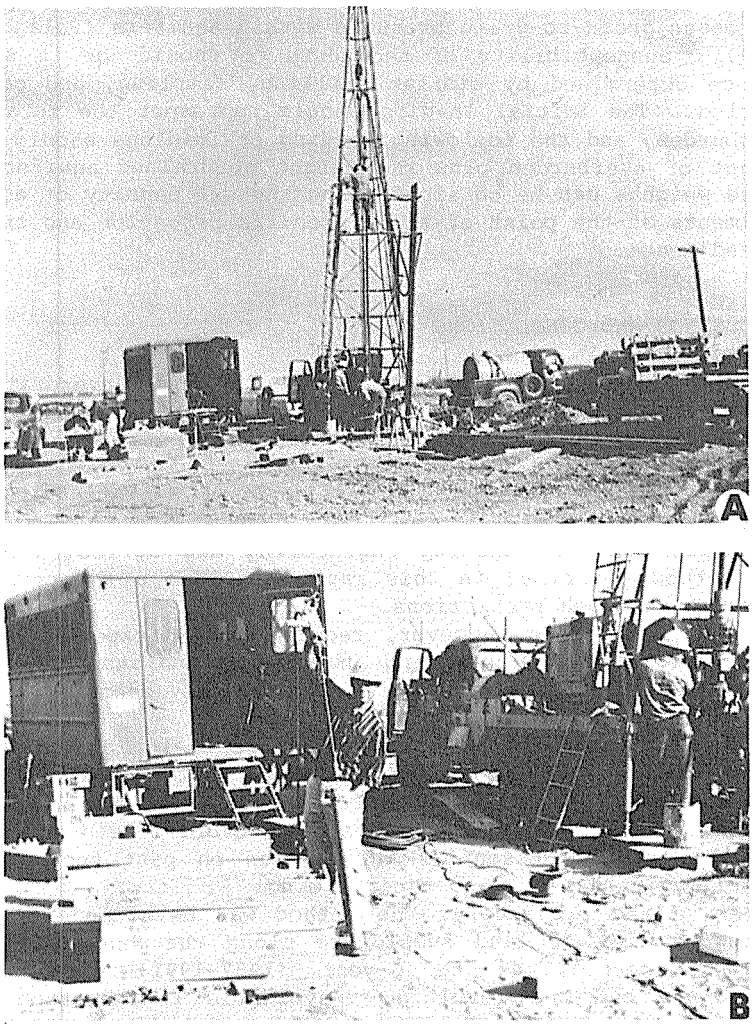

FIG. 4 Preconstruction drilling and sampling along the San Luis Canal alignment. (a) Drillrig of the test hole SE-501. The trailer is used by geologists for logging and field measurements of push samples; (b) geologist trims push sample in a 3-inch diameter Shelby Sampler for determination of field (wet) density and moisture content of sediments.

(3) The following, second test should be conducted on the already precompacted samples using the total weight of overburden without such subtraction. Additional compaction during this second test will indicate: (1) aquifers susceptible to subsidence due to a decline of piezometric head, and (2) the ultimate amount of possible subsidence.

In some cases (for example in California's San Joaquin Valley), a piezometric head probably was created both prior to and after the deposition of overburden (Prokopovich, 1983). A fractional increase of loading between the two basic tests may provide important data in this field.

In cases of unconfined aquifers, a decline of water levels increases grain-to-grain pressure within aquifers (Poland and Davis, 1969). Susceptibility of sediments to subsidence in such systems may be determined by similar drilling, sampling, and consolidation testing. The initial loading should represent the total weight of overburden, and the following loading or loadings should include the weight of overburden plus the weight of drained aquifer sediments. These weights can be obtained using the wet density of aquifer sediments at the point of their specific retention and the thickness of sediments.

DISCUSSION AND CONCLUSIONS

Land subsidence, including subsidence due to an overdraft of ground water is now a well-recognized geologic hazard causing a multimillion dollar expense. Determination of aquifer systems with sediments capable of creating subsidence, and prediction of its ultimate amounts under different rates of depletion of an aquifer system are essential for the development of new and the rehabilitation of existing engineering and agricultural projects. The method described in this paper provides a theoretically sound approach for such predictions.

The predictions, however, require rather expensive drilling of deep core holes, obtaining numerous "undisturbed" samples of sediments, and a slightly modified laboratory consolidometer testing of samples.

With an application of more than two basic loadings during such consolidometer testing, the method may help to establish a "safe piezometric decline" of an aquifer system (Prokopovich, 1976); i.e., piezometric decline which causes no notable subsidence. Such data may also provide essential information on past tectonic movements (or climatic changes) and their timing.

As stated previously, the method was developed but not tested during studies of land subsidence along the San Luis Canal. The present, record, 4- to 5-year (1987-1991) drought spell in California and the resulting unavoidable rejuvenation of intense ground-water pumping, and the following subsidence could, however, require such testing.

REFERENCES

Anonymous (1974a) San Luis Unit - Technical Report of Design and Construction, Design of Waterways and Detention Dams, Vol. VI.

United States Bureau of Reclamation: U.S. Government Printing Office, Denver, CO.

Anonymous (1974b) California State Water Project. California Department of Water Resources Bulletin 200, Sacramento, CA, Vol. 1, 173 p, Vol. 2, 349 p.

Anonymous (1974c) Earth Manual. United States Bureau of Reclamation, A Water Resources Technical Publication, Second Edition: U.S. Government Printing Office, Washington, DC, 810 p.

Anonymous (1981) Project Data. United States Water and Power Resources Service (Now Bureau of Reclamation) Technical Publication: U.S. Government Printing Office, Denver, CO, 1463 p.

Bolt, B. A., Horn, W. L., MacDonald, G. A, and Scott, R. F. (1975) Geological Hazards. Springer-Verlag, New York.

Poland, J. F. and Davis, G. H. (1969) Land Subsidence due to withdrawal of Fluids, Reviews in Engineering Geology II: Geological Society of America, pp. 187-269.

Poland, J. F., Lofgren, B. E., Ireland, R. L. and Pugh, R. G. (1975) Land Subsidence in the San Joaquin Valley, California, as of 1972. United States Geological Survey Professional Paper 437-H: U.S. Government Printing Office, Washington, DC.

Prokopovich, N. P. (1972) Land Subsidence and Population Growth. Engineering Geology: Proceedings 24th International Geological Congress, Section 13, Montreal, Canada, p. 44-54.

Prokopovich, N. P. (1976) Some Geologic Factors Determining Land Subsidence. Bulletin of the International Association of Engineering Geolog. No. 14, Krefield, West Germany, p. 75-81.

Prokopovich, N. P. (1978) Prediction of Land Subsidence for Irrigation Canals. Evaluation and Prediction of Subsidence, Engineering Foudnation Conference in Pensacola Beach, Florida, Proceedings: American Society of Civil Engineerings, New York, New York, pp. 234-251.

Prokopovich, N. P. (1983) Neotectonic Movements and Subsidence caused by Piezometric Decline. Bulletin of the Association of Engineering Geologists, Vol. XX, No. 4, pp. 393-404.

Land Subsidence (Proceedings of the Fourth International Symposium on Land Subsidence, May 1991). IAHS Publ. no. 200, 1991.

Subsidence of the Former Texcoco Lake

R. MORALES Y M.
Comisión Nacional del Agua, Proyecto Lago de Texcoco
R. MURILLO-FERNANDEZ
Comisión Nacional del Agua, Instituto Mexicano de Tecnología del Agua
A. HERNANDEZ-RUBIO
Comisión Nacional del Agua, Proyecto Lago de Texcoco, Mexico

ABSTRACT A report is made of the piezometric drawdowns and of the settlements recorded at the region since 1972 due to the extraction of water from underground aquifers, as well as the evolution of the subsidence at the zone where the largest lake at the Valley of Mexico basin existed.

INTRODUCTION

The Valley of Mexico is actually a closed basin which was provided with a man-made exit for its waters by means of works constructed in the past, which in turn induced the dessication of the former lakes. This basin is divided into 11 hydrologic sub-basins out of which the most important correspond to those of Mexico City, Churubusco, Xochimilco, Chalco and Texcoco on account of their economic and politic importance since the large Mexican metropolis has been developed above them. In addition, and with the purpose of supplying drinking water to the inhabitants, the aquifer of the Valley has been exploited since the end of the 19th century by means of deep wells and as a result there is an ever increasing drawdown rate of the piezometric levels, which in turn induces consolidation of the lacustrine deposits in the lower part of the Valley where the former lakes of Mexico, Texcoco and Chalco-Xochimilco are located.

The subsidence phenomenon affects buildings and municipal facilities by inducing cracking, rupturing of conduits, apparent emergence of piled foundations, differential settlements and loss of hydraulic gradients.

BACKGROUND

The former Texcoco Lake is located in the lowest part of the Valley of Mexico to the NE of Mexico City and it is used at present as a regulating reservoir of the surface runoff in the southern and southeastern regions of the basin. It forms a plateau at an average elevation of 2234 m above mean sea level and it is bounded to the East by the Sierra de Río Frío, to the West by the Sierra de Guadalupe, and to the North and South by the former Xaltocan and Chalco lakes, respectively. Some isolated volcanic cones can be seen as outcrops, such as those known as Peñón de los Baños, Peñón del Marqués and Cerro de Chimalhuacán (Fig. 1).

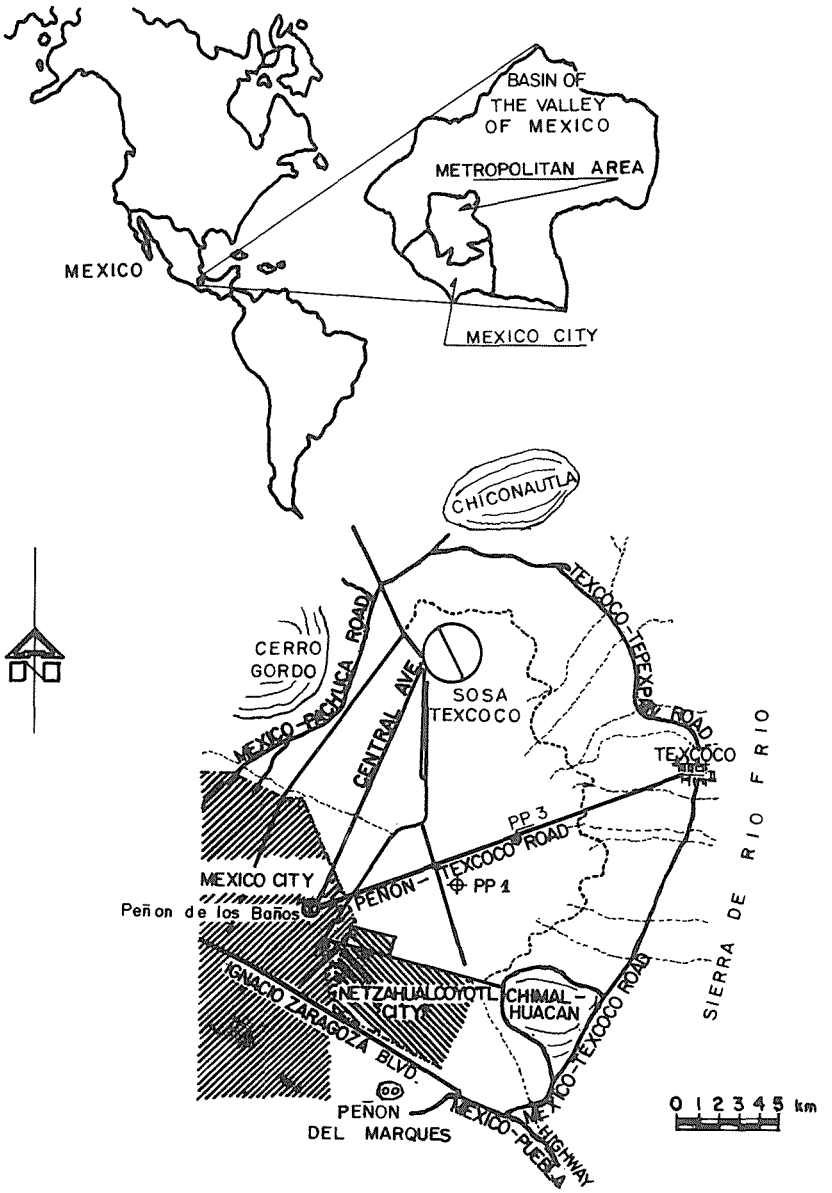

FIG.1 Geographical location of the former Texcoco Lake.

GEOLOGY

The basin of the Valley of Mexico is situated at the center of the volcanic belt that crosses the Mexican Republic from East to West and it has been subjected to major tectonic stresses and to volcanic eruptions from the beginning of the Tertiary to recent epochs.

In order to determine the deep geology of the Valley, several studies have been carried out among which mention should be made of

the gravimetric survey of the Texcoco Lake performed from 1952 to 1953 as well as the drilling of the deep wells known as PP1 (2065 m) and PP3 (589 m) in 1967-1968 (SHCP & NF, 1969).

The Texcoco sub-basin corresponds to a plateau underlaid by a highly compressible clay of lacustrine volcanic origin that covers alluvial and pyroclastic permeable materials from the Quaternary which in turn form the main aquifer of the region. Below these materials, igneous rocks of the Tertiary are encountered and they form the lower impervious barrier. The basal rock is constituted by marine limestone of the Cretaceous. The last cycle of vulcanism began during the Quaternary and there are still some manifestations. This period is representative of the volcanoes Cerro Gordo, Chimalhuacán and Chiconautla, among which the Texcoco sub-basin is located.

Deep well PP1

The lithologic profile of the PP1 well is characterized by 60 m of lacustrine clays interbedded with thin strata of silt and sand; by sands, silt and clay from 60 to 180 m; from 180 to 505 m by clays, lutites, sandy clays, sands, sandstone and lacustrine limestone; from 505 to 1437 m by tuffs and igneous rocks, breccias and conglomerates; from 1437 to 1980 m by lithic tuffs, igneous rocks and sands; from 1980 to 2045 m by clayey anhydrites and marls; and finally, from 2045 to 2065 m by clays, marls and calcareous conglomerates (SHCP & NF, 1969).

UNDERGROUND WATERS

Geophysical surveys point towards the presence of two seismic refractors inclined to the SE, at depths of 770 and 1850 m, respectively. Geoelectric studies have identified four units related to boring PP1 as follows: the first unit shows a seismic wave velocity of 600 m/s and it corresponds to the surface clay layer saturated with brackish water which has a saline concentration in excess of 10 000 mg/L, and a thickness of 30 m that decreases to the North; the second unit or stratum is mostly clayey and it behaves as an aquitard saturated with brackish water with a saline concentration ranging from 5000 to 10 000 mg/L, has a seismic wave velocity of 1700 m/s and a thickness varying from 30 to 50 m. The third unit, with a wave velocity of 2200 m/s, has water of medium quality with a concentration of dissolved solids equal to 2000 mg/L and a thickness from 300 to 500 m, and it corresponds to the main aquifer and is constituted by a clayey-sandy alluvial deposit. The thickness of this formation augments towards the West - Mexico City - and decreases to the East and South. Finally, the fourth geoelectric unit, which belongs to the lower refractor, is formed by tuffs and marls with very low permeability, and therefore it constitutes the lower boundary of the main aquifer; it has a wave velocity of 4500 m/s and has been interpreted as faulted blocks (SHCP & NF, 1969; Morales *et al*, 1989). Magnetic and gravimetric anomalies have been detected which indicate the presence of a buried volcano at the northern part of the zone under study, as well as magnetic minimums starting at the crater, that make evident former erosion courses. The high contents of solids dissolved in the water of the formations existing in the former

Texcoco Lake are attributed to the fact that this was the lowest zone since the valley was closed during the Quaternary and consequently the floods of the fresh water lakes of Mexico, Xaltocan and Chalco-Xochimilco were discharged into it and after evaporation the salts became concentrated during filling of the basin.

Pumping

During 1980 a total of 1685 wells were surveyed in the region which extract a volume equivalent to 12.59 m3/s, from which 5.3 are used to supply potable water to Mexico City and 0.5 correspond to the exploitation of brackish water for the alkali industry "Sosa Texcoco". The distribution of these flows as related to their use is shown in Table 1 (SARH, 1972).

TABLE 1 Uses of the underground water.

Use	Wells (No.)	Mean flow rate (m3/s)
Municipal services	121	6.817
Agriculture	431	3.110
Industry	647	1.540
Domestic	301	0.951
Electric power generation	2	0.057
Other uses	183	0.057
TOTAL	1685	12.590

PIEZOMETRIC EVOLUTION

Static level in wells

At the center of the lacustrine zone wells PP1 and PP3 are located; their casing is grooved from 213 to 1844 m in depth and from 222 to 527 m, respectively, and they provide an outstanding reference of the evolution of the piezometric levels at great depths. From 1968 to 1984 an average annual loss of hydraulic head of 0.93 m was recorded starting at a static level found at a depth of 6.8 m; at depths ranging from 56 to 95 m the static level showed a drawdown rate of 1.38 m/year. From 1984 to 1990 the static level recedes at a rate of 1.1 m/year at a depth beyond 200 m (Murillo, 1984; 1990).

Piezometric levels

Figure 2 depicts the evolution of the static level at wells PP1 and PP3 and in piezometers of the Casagrande type mounted at the center of the region. The water table elevation has varied from 0.0 to 1.2 m in

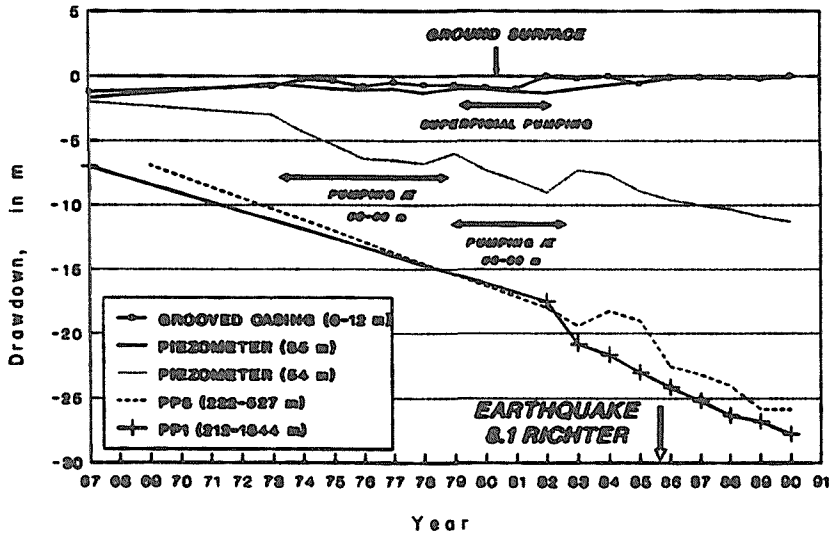

FIG.2 Evolution of the piezometric levels from 1967 to 1990.

depth and it shows the effects of the shallow pumping from 1979 to 1992. The hydraulic pressure at a depth of 35 m evidences the effect of pumping from 50 to 65 m in depth at an approximate distance of 3 km, from 1973 to 1982. The piezometer tip placed at a depth of 54 m, within a silty and sandy stratum, clearly registers the effect of pumping operations carried out from 1973 to 1982 and it shows a rate of drawdown equal to 0.4 m/year from 1973 to 1984 and to 0.63 m/year during the last five years (Murillo, 1984; 1990). It can be observed in figure 2 the effect of a smaller recharge in 1982 which has been the driest in the last 18 years.

Overexploitation of the aquifer

It has been assumed at present that the aquifer reaches down below the former lacustrine zone and that its formations emerge towards the sierras surrounding the basin where the largest part of the recharge takes place. In 1975 (DDF) a recharging equivalent to 38 m3/s was reported for the period 1920-1970 as well as an extraction of 30.3 m3/s in 1960 and consequently the geohydrological balance was positive. However, in the lower part of the basin the piezometric levels went down. It has been estimated that a flow rate of about 57 m3/s is extracted nowadays with a recharge of 25 m3/s and therefore the overexploitation amounts to 32 m3/s (Murillo, 1990) and it becomes evident in the fastest rate of piezometric drawdown and in the acceleration of the subsidence, in addition to the saline intrusion toward the periphery of the former lake which was reported since 1972 (SRH).

SUBSIDENCE

In 1972 a W-E leveling axis was established with a precision of 1 mm/km which starts in a fixed reference point. Figure 3 shows the

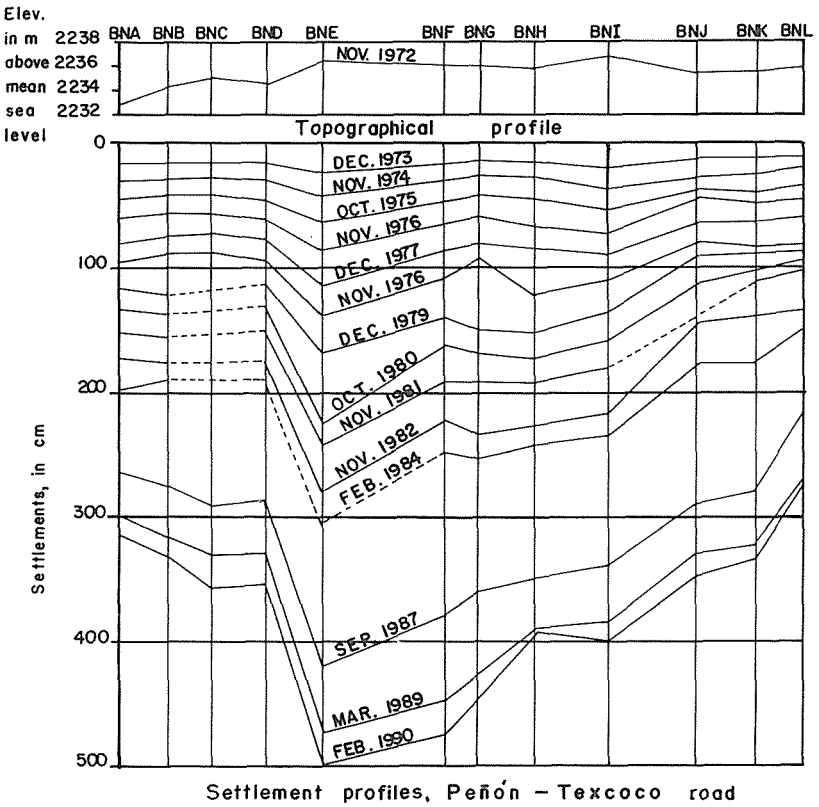

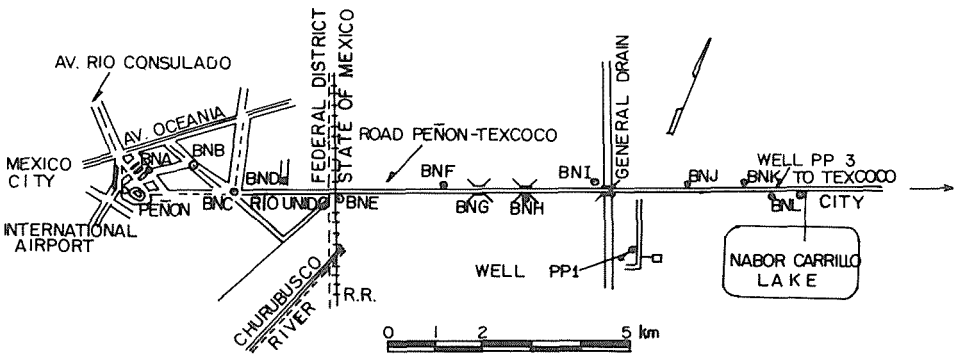

FIG.3 Settlement profiles, Texcoco Lake.

topographic profile in 1972, the settlement profiles as of 1990 and the location of the control points.

The maximum regional subsidence has reached 5 m in 18 years and the minimum is equal to 3.15 m toward the East, and consequently there exists a differential settlement of 1.85 m in that same period. It is worth mentioning that the thickness of the clay strata becomes smaller in that direction.

It is evident that several settlement rates exist among the benchmarks BNA and BND; the mean rate was equal to 16.9 cm/year up to 1984. This zone corresponds to urban areas developed before 1972; the benchmark BNE showed then a higher rate of 28 cm/year induced by artificial fills, and urban development occurred from 1968 to 1982. Among reference marks BNF and BNJ, with an average rate of 21.6 cm/year, no recharges were placed and no pumping took place. Between points BNJ and BNL pumping in the vicinity has been carried out from 1973 to 1978 and from 1978 to date and an average settlement rate of 14.2 cm/year has been recorded from 1972 to 1984. This irregular behavior in the zone has not been satisfactorily explained. In general terms, the rate of subsidence has shown an increase since 1978 at the benchmarks placed near Mexico City and from 1981 to date in other parts (Murillo, 1984; 1990). Table 2 shows the settlement rates.

TABLE 2 Settlement rate at Texcoco Lake.

	1972-1977 cm/year	1977-1982 cm/year	1982-1987 cm/year	1987-1990 cm/year
Maximum	22.8	33.4	27.8	33.1
Average	16.7	23.6	22.7	28.0
Minimum	12.0	14.4	16.6	26.0

Compression of the clay strata

In areas subjected to heavy pumping operations from the pervious layers found at depths from 30 to 31 m and from 50 to 60 m, with no superficial surcharge, the contribution of the settlement at the surface, expressed in percentage, was determined (Table 3).

TABLE 3 Distribution of the compression.

Layer	Depth (m)	Contribution (%)
Upper Clay Formation	0-30	15.0
Lower Clay Formation	31-50	70.5
Deep Deposits	> 50	14.5

Additional observations

At wells PP1 and PP3 it was observed that their casings emerged 1.7 and 2.3 m from 1968 to 1984, which represent emersion rates of 10.6 and 14.5 cm/year, respectively (Murillo, 1984), and they showed an

emersion of 1.1 m from 1984 to 1990 at the PP1 and of 0.9 m from 1984 to 1988 at PP3, i.e. rates of 18.3 and 22.5 cm/year, respectively, for the last few years. The casing of well PP1 emerges at a smaller rate than that of the regional subsidence and it is subjected to a strong negative friction, whereas the casing of well PP3 emerges at a rate equivalent to the subsidence.

ARTIFICIAL RECHARGE OF THE AQUIFER

The National Water Commission treats 50 L/s of residual waters to a tertiary level to be infiltrated in the ground by means of absorption wells, with the purpose of determining the technical and economical feasibility of achieving the artificial recharging of the aquifer at an accelerated rate and of reducing its overexploitation. Although highly permeable zones are found in the surrounding mountain ranges, the cost of rising with pumping the residual waters located in the lower part of the basin restrains the use of this alternative, and therefore it was decided to carry out the experiment in grooved infiltration wells from 70 to 200 m in depth. The permeability of those layers ranges from 10 E-2 to 10 E-4 cm/s. The static level in the recharge wells was found between 23 and 29 m in depth and in the pumping tests specific capacities from 1.1 to 4.7 L/s/m were determined for flow rates smaller than 100 L/s (Murillo & Piñón, 1986). The first results of the recharging point toward a rapid decrease of the infiltration capacity from 27 to 11 L/s in the first five months and from 11 to 4 L/s in the following five months, with a recovery of the static level equal to 11 m which in turn diminished subsequently although at a slower rate (Morales & Piñón, 1990). It has been estimated that the flow rate during recharging is quite slow because upon injection of fluorescein this substance was never detected in the test wells (Leor, 1986-1987).

CONCLUSIONS AND RECOMMENDATIONS

As a result of the overexploitation of the aquifer in the region, particularly in the perimetric zones, the regional subsidence will proceed with rates ranging from 26 to 33 cm/year. Out of this superficial settlement, 70% corresponds to the consolidation of the Lower Clay Formation found at depths varying from 31 to 50 m.

Since it is not possible to diminish appreciably the water extraction and therefore the overexploitation of the aquifer, it has been proposed to carry out an exchange of treated residual waters by the underground supplies for farming purposes and for industrial uses; to perform an artificial groundwater recharge with residual water treated to a tertiary level; and to expand the projects of reforestation, overturning of the surface layer, terrace construction and building of infiltration dams to increase the natural recharging of the sierras surrounding the Texcoco sub-basin.

REFERENCES

DDF (1975) Memoria de las Obras del Sistema de Drenaje Profundo del

Distrito Federal (Proceedings of the Works for the Deep Sewer System of Mexico City), Vol. I, Mexico.

Leor, S.A. (1986-1987) Estudios de transmisibilidad del acuífero y segunda aplicación de trazadores en los pozos de recarga (Studies of transmissibility of the aquifer and second application of tracers in the recharge wells), Mexico.

Morales R., Piñón N., Alvarez A. & Lesser J.M. (1989) Resistividades en el Ex-Lago de Texcoco (Resistivities in the Former Texcoco Lake). Tópicos Geológicos del Valle de México, Sociedad Mexicana de Mecánica de Suelos, Mexico.

Morales R. & Piñón N. (1990) Resultados de un módulo experimental de recarga de acuíferos (Results from an experimental module for recharging the aquifers). Proceedings of the 11th National Congress of Hydraulics, Asociación Mexicana de Hidráulica, Zacatecas, Mexico.

Murillo R. (1984) Comportamiento regional del Ex-Lago (Regional behavior of the former lake). Obras Recientes en el Lago de Texcoco, Sociedad Mexicana de Mecánica de Suelos, Mexico.

Murillo R. & Piñón N. (1986) Módulo experimental de recarga de acuíferos en el Valle de México (Experimental module for recharging the aquifers in the Valley of Mexico). Proceedings of the 9th National Congress of Hydraulics, Asociación Mexicana de Hidráulica, Querétaro, Mexico.

Murillo R. (1990) Sobreexplotación del acuífero de la Cuenca del Valle de México: efectos y alternativas (Overexploitation of the aquifer of the Valley of Mexico Basin: effects and alternatives). El Subsuelo de la Cuenca del Valle de México y su Relación con la Ingeniería de Cimentaciones a Cinco Años del Sismo, Sociedad Mexicana de Mecánica de Suelos, Mexico.

SHCP & NF (1969) Proyecto Texcoco (Texcoco Project).

SRH, Comisión Hidrológica de la Cuenca del Valle de México (1972) Aguas subterráneas de la zona de Texcoco (Underground waters of the Texcoco zone), Mexico.

Land Subsidence (Proceedings of the Fourth International Symposium on Land Subsidence, May 1991). IAHS Publ. no. 200, 1991.

Nonlinear Modeling of Groundwater Flow and Total Subsidence of the Mexico City Aquifer-Aquitard System

A. RIVERA & E. LEDOUX
Paris School of Mines- CIG. 35, Rue
Saint-Honoré 77305 Fontainebleau, France
G. de MARSILY
University P. et M. CURIE 4, Place Jussieu, 75230,
Paris Cedex 05, France

ABSTRACT The water budget in the Mexico city closed basin was in equilibrium until the begining of the thirties, natural recharge, of approximately8 $m^3\ sec^{-1}$ for a 1500 km^2 surface area, was the main source of some springs to the west and groundwater exploitation only represented less than 1 %. In 1980 the water pressure had diminished under the effect of a heavy groundwater pumping which exceeded natural recharge by more than 260 %. As a consequence the aquitards in the system have compacted to a total land subsidence of about 6.5 meters in downtown area for that period. In this study a numerical model is presented to simulate groundwater flow and total subsidence of multiaquifer systems. The model accounts for the non-linear compaction and total subsidence on multilayered systems by coupling a simultaneous numerical solution of the groundwater flow equation with the one-dimensional consolidation equation of aquitards through the Terzaghi's effective-stress concept. An important issue of this investigation is the model's capabilities to simulate the phenomenon at a regional scale. The application of this model to the Mexico city's basin has proved of great interest, its aim is to quantitatively analyse: (1) the water budget in the basin, (2) the land subsidence due to overexploitation, and (3) the response of the system to artificial recharge. The analysis of the water budget in the basin permits the calibration of the model in steady-state. Simulations in unsteady-state are performed for the period of 1930-1986 using the steady-state results as the initial conditions. The calibration process for this period is done through two variables: observed groundwater heads and land subsidence. The simulations are done with the linear and non-linear versions of the model. The observed subsidence is reproduced with a great detail with the non-linear version of the model. The linear version fails to reproduce the observed phenomenon.

INTRODUCTION

The compaction of clayey layers is a phenomenon generally studied through the optic of soil mechanics. In hydrogeology "the aquitard drainage models" are succesfully applied if previously known levels fluctuations are imposed as boundary conditions.

In this work, we propose a deterministic model combining the mechanics of the compaction of semi-pervious layers with the three-dimensional groundwater flow.

In Mexico, as is the case in general, reliable data are scarce when dealing with aquitard parameters. Due to the time dependent response of aquitards to pumping in aquifers and to the lack of adequate technics to analyse pumping tests in leaky aquifers,

many modelers are "forced" to infer aquitard parameters or to use the soil mechanics techniques to obtain them. In the best of the cases vertical permeability (K') of clay samples can be obtained from consolidation tests through the consolidation coefficient C_v (see for instance Scott, 1963), and compressibility (α) derived graphically from void ratio-applied effective stress ($e - log\bar{\sigma}$) curves (Jorgensen, 1980). The latter may in turn be used to estimate the storativity of the aquitard in which the sample was taken.

A problem associated with this is the non-linear response of the clay sample to the applied stress wich obviously also happens in the whole aquitard itself. In the last few years some modelers have circumvented this problem by using different constitutive relationships between soil engineering equations and groundwater flow equations so that both K' and α can be stress-dependent parameters (Helm, 1976; Narasimhan and Witherspoon, 1977; Neuman et al, 1982). Unfortunately most of this type of models have only been applied at a local scale.

Various efforts to simulate the aquifer-aquitard system of the Mexico basin have already been made (Cruickshank, 1982; Herrera et al, 1989; and Rudolph et al, 1989). Only the last of these deals with the non- linearities of K' and α but is restricted to a local analysis. Compaction and land subsidence from groundwater pumping have been documented in many areas (see Poland, 1984) but only few models of regional groundwater flow include the effects of permanent compaction.

The present model is based in the Paris School of Mines code *NEWSAM* (Marsily et al, 1978) originally developed to simulate multiaquifer systems and modified to account for aquitard storativity changes and compaction, distribution of stresses in aquitards through the discretization of these layers with nested square meshes, and the non-linearities of vertical permeability and compressibility (hence storativity) of the aquitards (Rivera, 1990).

The application of this methodology to the case of Mexico city has shown the representativity of the model allowing the reproduction of the observed land subsidence, to a regional scale, during more than 50 years. A complete study of the Mexico basin including the effects of pumping , in the last 50 years, on groundwater levels decline, on land subsidence, and on the response of the system to artificial recharge was proposed by Rivera (1990). In this paper we present a summary of the results.

THE MODEL

The classical approach for quasi-3D models is used here. Let us consider a multiaquifer system consisting of a number of aquifers separated by aquitards. All aquifers are heterogeneous and isotropic in the horizontal plane, aquitards have variable thickness in the horizontal direction, and their hydraulic parameters are functions of the vertical coordinates, time and effective stress. Flow is then assumed to be 2D (horizontal) in the aquifers, and 1D (vertical) in the aquitards.

For these conditions, the governing equations for any given aquifer is :

$$\frac{\partial}{\partial x}\left(T\frac{\partial h}{\partial x}\right) + \frac{\partial}{\partial y}\left(T\frac{\partial h}{\partial y}\right) = S\frac{\partial h}{\partial t} + Q(x,y,t) + q_L \qquad (1)$$

where h is the hydraulic head,
T is the isotropic transmissivity,
S is the storativity,
t is time,
Q is the strength of a source or sink function
(e.g. pumping from the aquifer and areal vertical
recharge of top aquifer),
q_L is a term representing the drainage.

If one wishes to account for storage changes in compressible aquitards, then q_L represents the aquitard areal leakage flux into the aquifer (variable in time). The complexity of the q_L term is dependent on whether or not head changes in aquifers can be assumed to occur throughout the aquitard layers within the time of integration.

Equation (1) is supplemented by appropriate initial and boundary conditions in the (x, y) plane.

In any given aquitard groundwater flow is supposed to take place in the vertical direction. This flow is governed by the one-dimensional vertical diffusion equation :

$$\frac{\partial}{\partial z}(K'(n)\frac{\partial h'}{\partial z}) \;=\; S'_s(n,\overline{\sigma})\frac{\partial h'}{\partial t} \tag{2}$$

where z is the coordinate taken vertically upward as positive,
h' is the hydraulic head in the aquitard,
K' is the vertical permeability,
S'_s is the specific elastic storage coefficient in the aquitard,
n is porosity,
$\overline{\sigma}$ is the effective stress.

The effective stress is related to the total vertical stress, σ, and to the pore pressure p by Terzaghi's relationship :

$$\overline{\sigma} \;=\; \sigma - p \tag{3}$$

Since the hydraulic parameters in (2) are function of n and $\overline{\sigma}$ which depend at the same time of the pressure, equation (2) is then non-linear. This equation which represents the vertical flow including the compaction of aquitards, is solved simultaneously with equation (1) by the finite-difference method with an implicite-explicite scheme.

The specific storage coefficient S'_s related with the compressibilities of the fluid and the porous matrix, is defined as :

$$S'_s \;=\; \rho g(\alpha + n\beta) \tag{4}$$

where ρ is the mass per unit volume of water, g is the acceleration due to gravity, and β is the water compressibility. In general the contribution of water elasticity to specific storage is relatively small and is ignored. We will nontheless keep it in equation (4) in order to be consistent with volume changes during compaction when porosity diminishes.

The values of the coefficient α vary as a function of effective-stress ($\overline{\sigma}$) and void ratio (e). This coefficient is estimated from consolidation tests from the slope of a semi-log curve void ratio-applied effective stress ($e - log\overline{\sigma}$), mathematically defined as :

$$\alpha(e,\overline{\sigma}) = 0,434\frac{C}{(1+e)\overline{\sigma}} \tag{5}$$

The coefficient C takes the value of C_c (compression index) when $\overline{\sigma}$ is greater than the "preconsolidation" stress; and the value of C_s (swelling index) when it is smaller.

Combining equations (4) and (5), using the relation $n \;=\; \frac{e}{1+e}$, we get :

$$S'_s(n,\overline{\sigma}) = \rho g\Big(0,434\frac{C}{\overline{\sigma}}(1-n) + n\beta\Big) \tag{6}$$

An empirical relationship was used to account for permeability changes as a function of porosity [$K' = f(n)$] (Rivera, 1990) :

$$K' = K'_o \left(\frac{n(1-n_o)}{n_o(1-n)} \right)^m \tag{7}$$

K'_o is the initial permeability, n_o is the initial porosity, m is an exponent, which for the case of Mexico city is equal to 3.

Finally, the total land subsidence $L(t)$ at a regional scale, is computed as the sum of the compaction of each layer, in the vertical direction, as :

$$L(t) = \sum_i \rho g \Delta Z_i \alpha_i \Delta h'_i(t) \tag{8}$$

ΔZ_i is the thickness of layer i.

This methodology was tested and verified through the comparison with various existing analytical solutions; the non-linear model was validated precisely reproducing a real case: the observed subsidence at Pixley, California (Rivera et al, 1990).

WATER SUPPLY AND OBSERVED LAND SUBSIDENCE IN MEXICO CITY

Potable water supply to the city of Mexico was assured by sources and springs located to the west and south of the city until the end of the last century. Between 1900 and approximately 1930, when the city's population was less than one million inhabitants, the water supply shifted progressively to the use of artesian wells. With time these wells, and other new wells were drilled deeper and deeper and were equipped with pumps, rapidly modifying the regional piezometry.

In order to catch up with the problem of a bigger water supply, needed for economic growth (figure 1), the city authorities created a very ambitous program of groundwater exploitation. From 1934, the construction of deep wells (-50 m) started in downtown area and to the north and west, and later continued to the south, towards the fifties.

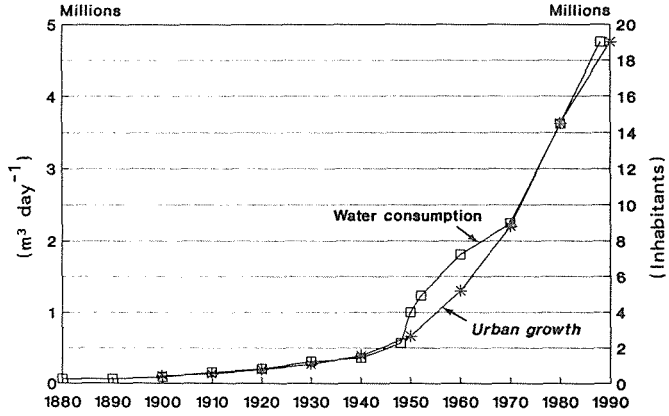

FIG. 1 Urban growth and water consumption in Mexico city.

In 1980, total pumping rate exceeded 21 $m^3\ s^{-1}$ with more than 600 wells. Figure 2 presents, as an histogram, the pumping data in Mexico city for the period of 1934-1986.

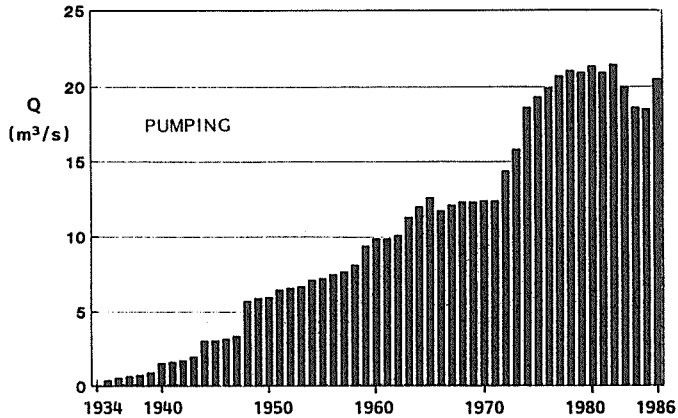

FIG. 2 Groundwater pumping for the period of 1934-1986.

In the same period of time, a maximum of more than 6 meters of land subsidence was observed at some locations (see figure 3), constituing one of the most remarquable cases in the word due to its magnitudeand its extension.

It has been shown since the forties, that the principal cause of this phenomenon, observed at a regional scale, is the groundwater exploitation.

The evolution of subsidence is marked by three periods (fig. 3). A first phase, between 1935 and 1948, is marked by a weak slope in a plot of the observed subsidence: the average speed is approximately 8 $cm\ year^{-1}$. Between 1947 and 1957-58 the observed subsidence averaged around 29 $cm\ year^{-1}$. The third phase, after 1959, is characterized by a decrease of the subsidence: in a long period of 27 years the observed subsidence averaged 5 to 6 $cm\ year^{-1}$.

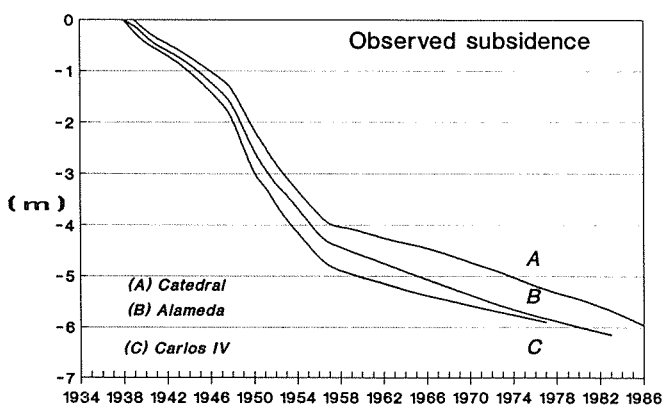

FIG. 3 Observed subsidence at three selected sites in downtown area.

A likely explanation is that the consolidation phenomenon alters the physical properties of the aquitards and causes significative variations of the hydraulic parameters K' ans S'_s; this would affect, in turn, the hydraulic response of the whole aquifer-aquitard system. The effect of the diminishing of these parameters during

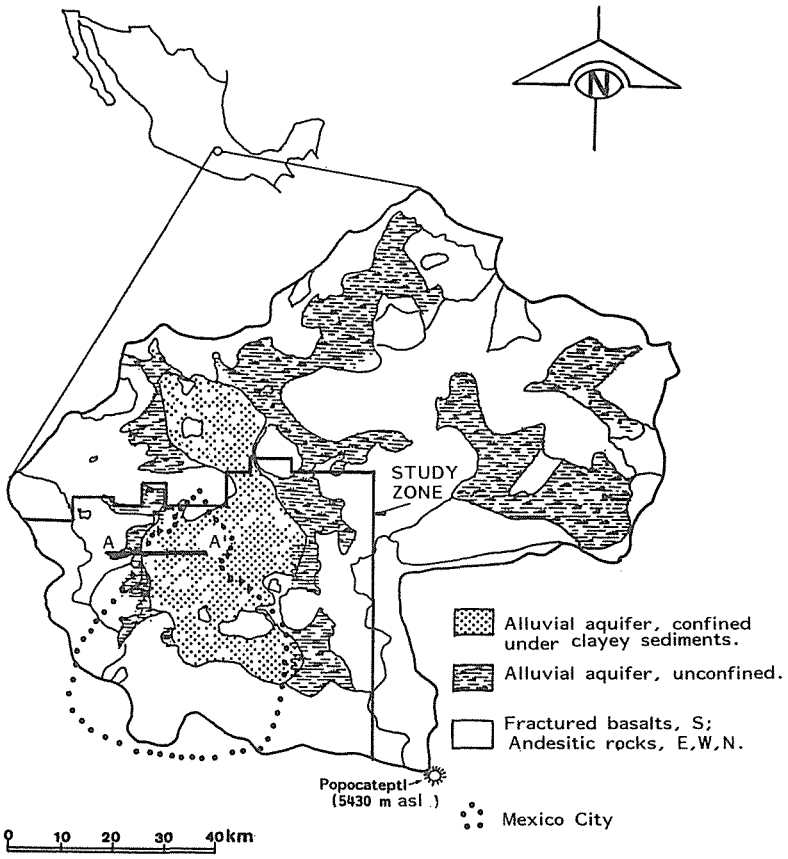

FIG. 4 The Mexico city basin and location of study area.

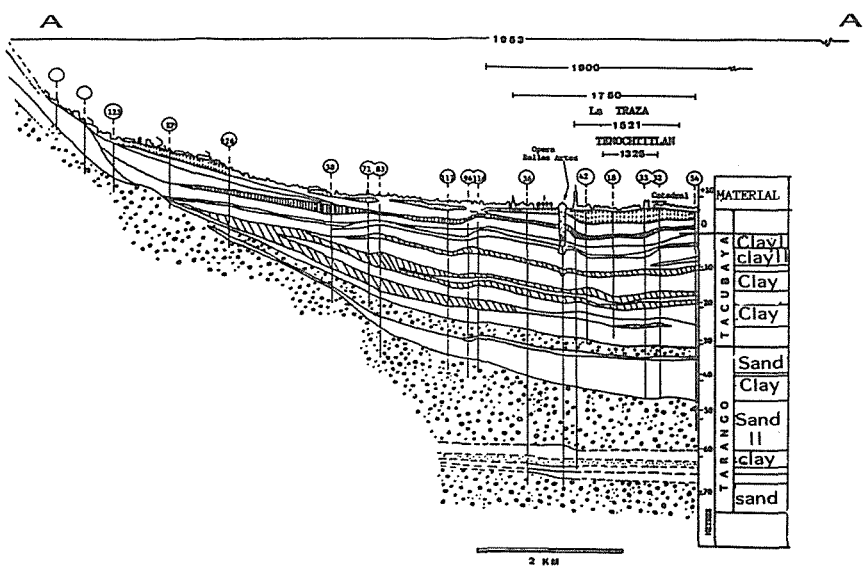

FIG. 5 Detailed cross section, A-A', of clayey sediments.

consolidation has, as a consequence, a decrease of the aquitard leakage, implying a longer time to reach steady-state, and a subsidence smaller than the one that would be predicted by a standard linear analysis.

We will try to reproduce, with our model, this phenomenon of non-linear subsidence observed in Mexico city.

CONCEPTION AND IMPLEMENTATION OF THE MEXICO CITY SIMULATION MODEL

Figure 4 shows a map of the hydrogeological formations in the basin of Mexico city.

This basin is formed by a series of closed sub-basins, more or less independent; it is considered that the main aquifer underlying the city of Mexico forms an entity relatively isolated from the aquifers in the north of the basin. This aquifer is separated by a line forming the volcanic cone of Sierra Guadalupe traversing the basin from west to east in its meridional part.

In the same figure is shown the study zone of approximately 2900 km^2 surface area. The main alluvial aquifer is confined in most of the valley by the lacustrine sediments of clays and silts, 50 m thick in downtown area. Figure 5 shows a detailed cross section, west-east, of these sediments.

The main assumptions adopted in the simulations are:

- the aquifer units, alluvial material (confined and unconfined, from the center of the basin to the piedmonts), fractured basalts (to the south), and andesitic rocks (to the east, west and north), function as a single continous aquifer;
- groundwater flow in the aquifer is considered horizontal, in the x,y directions, and is represented by a single layer in the model;
- the distinction between the three types of rocks is done as a function of their hydraulic characteristics (T, S, n);
- the lacustrine sediments constituing the aquitards are divided into three formations: the upper clay formation (UCF), the "Capa Dura" (or hard stratum, CD), and the lower clay formation (LCF). The flow in the aquitard is considered as essentially vertical and is represented by 22 horizontal layers in the model.

Figure 6 shows, in a west-east diagrammatic profil, the adopted conceptual model.

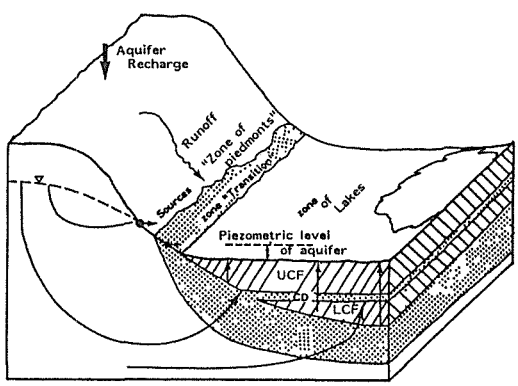

FIG. 6 Conceptual model of the aquifer-aquitard system.

Discretization of Study Area

Horizontal discretization

In order to better represent the boundaries and heterogeneities of the study area we adopted a grid of variable size using nested square meshes of three different sizes:

a big square mesh of 2000 m side, an intermediate mesh of 1000 m, and a small mesh of 500 m (figure 7).

The small meshes are used at the boundaries between the three zones ("zone of lakes", "zone of transition", and "zone of piedmonts", fig. 6), at the contact with the volcanic cones (impermeable), and at the zone of the "ancient city" where the maximum subsidence is observed.

The total number of elements used to discretized the aquifer layer is 1181 square meshes.

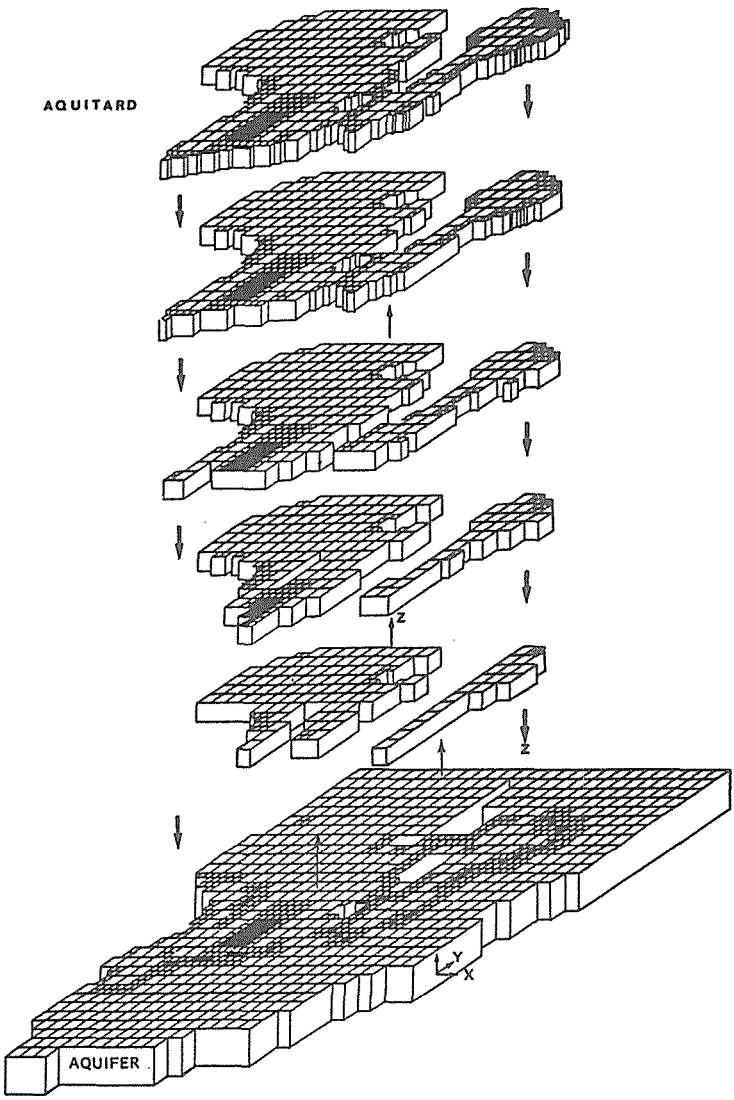

FIG. 7 Schematic perspective of the aquifer-aquitard system.

Vertical discretization

Since one of our principal objectives in this study is to analyze in detail, in the vertical direction, the distribution of pressures associated to the compaction of

aquitards, we used a very much finer grid with 22 layers to discretize the three aquitard formations UCF, CD, and LCF.

Figure 7 shows a schematic perspective of the aquifer-aquitard system as it is discretized in the model. The hydraulic connection between the aquifer and the aquitard is done exclusively in the lacustrine zone ("zone of lakes").

The total number of layers for each formation varies depending on the zone. For the ULF, the number of layers may be from 3 to 7; the CD is represented by a single layer (the 8^{th} one); the number of layers used to discretize the LCF may vary from 1 to 14.

The 22 layers representing the aquitards have 6523 meshes, making, for the whole model, a total of 7704 square meshes.

The adopted boundary conditions, with a possible combination between them are:

- constant flux (aquifer)
- prescribed drainage elevation combined with a limited vertical flux (aquitards),

The model also includes the eventual loss of water pressure in the confined aquifer (a change from a confined to an unconfined condition).

SIMULATIONS AND RESULTS

In order to identify and better understand the different components of the flow and their spatial distribution through the aquifer-aquitard system, we first analysed the water budget in the basin.

A simulation in steady-state permitted a first calibration of the model (before the aquifer exploitation) using the available data, and the review of some of the initial assumptions.

We considered in our simulations that a steady-state persisted until 1930.

Values of aquifer transmissivities, obtained from pumping tests (Lesser, 1985), were used in the model. Initial values of permeability for the aquitard were obtained from consolidation tests performed on clay samples (several references cited in Rivera, 1990).

In order to calibrate T and K' in steady-state, a twofold criteria was adopted. Firstly, a water budget in the basin (INS and OUTS) was calculated with the model to match a value of a classical hydrologic budget using data of mesured precipitation, evapotranspiration and runoff. Unfortunately there exist no reference piezometric levels that would allow the calibration in steady-state using the piezometry.

Secondly, it was search to reproduce the discharge zones of the aquifer, that is, the springs as well as the artesian zones which implied an upward vertical drainage through the semi-pervious layers.

The results of the simulations for this stage are totally coherent as a whole, they reproduce the orders of magnitudeof the different components of the water budget. The water budget calculated by the model is schematically summarized in figure 8.

The aquifer recharge rate by infiltration from precipitation calculated by the model was 8.1 $m^3\ s^{-1}$ and is equivalent to a mean annual infiltration rate of 15 $l\ s^{-1} - km^2$. Other authors (Ortega and Farvolden, 1989) propose an infiltration rate of 10 to 29 $l\ s^{-1} - km^2$.

The adopted initial permeabilities of the aquitards as calculated with the model are summarized in the following table:

FORMATION	LAYER	K' (m s^{-1})
FAS	1-6	2×10^{-8}
	7	1×10^{-8}
CD	8	910^{-5}
FAI	9-22	1×10^{-8}

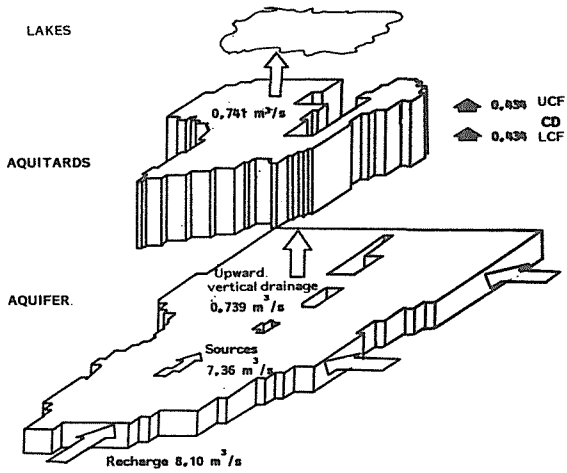

FIG. 8 Components of the water budget simulated in steady-state.

From the thirties, and after the begining of the heavy pumping in the aquifer, the behaviour of the aquifer-aquitard system has been marked by a progression of four processes:

- gradual drying up of the springs and sources,
- downward vertical drainage (leakage) of the aquitards,
- compaction of aquitard layers and land subsidence observed at the surface, and
- dewatering of the confined aquifer (a change from a confined to an unconfined condition).

The numerical model was adapted to account for these processes during the simulations in unsteady-state, for the period of 1934-1986. The observed values of the two unknowns: piezometry and subsidence, were used to calibrate the model at this stage.

The model parameters (besides T and K' already calibrated in steady-state) for this stage are the compression index C_c, the swelling index C_s, and porosity, n. From C_c and/or C_s, the model estimates the specific storage coefficient S'_s (eq. 6), the latter will vary as a function of piezometry and porosity.

The input values of C_c and C_s were obtained directly from consolidation tests performed in the laboratory on clay samples coming from approximately 65 borings in the valley of Mexico city.

Porosity was determined from values of void ratio (e) obtained from the same tests. The mean value of void ratio for the UCF is 6.7, with some maximum values of 9 mesured in the Texcoco zone. For the LCF, the mean value of e is 4.7, and for the Capa Dura, this value is 0.66. From those values, we input into the model the following values of porosity:

FORMATION	LAYER	n
UCF	1-7	0.87
CD	8	0.4
LCF	9-22	0.82

Permeability will vary as a function of porosity (eq. 7) which, itself varies with compaction.

Figure 9 shows a comparison between observed and calculated piezometric levels for two selected piezometers. The evolution of the observed piezometry for PC190 is

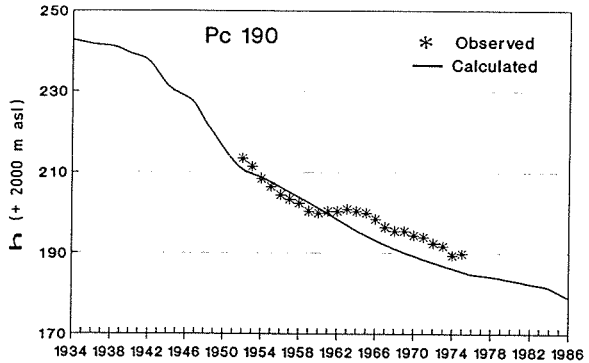

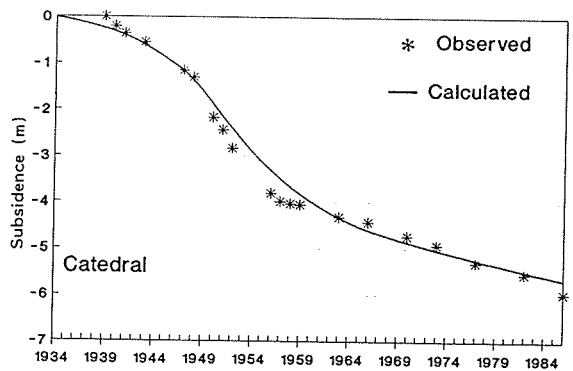

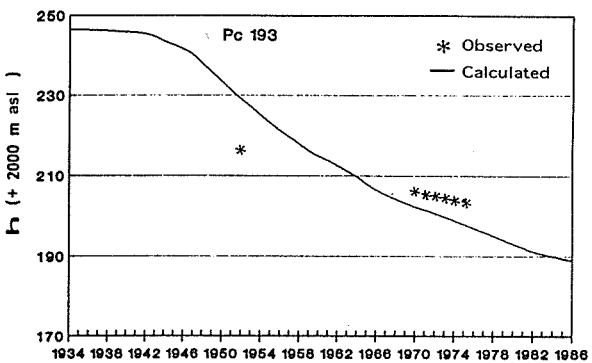

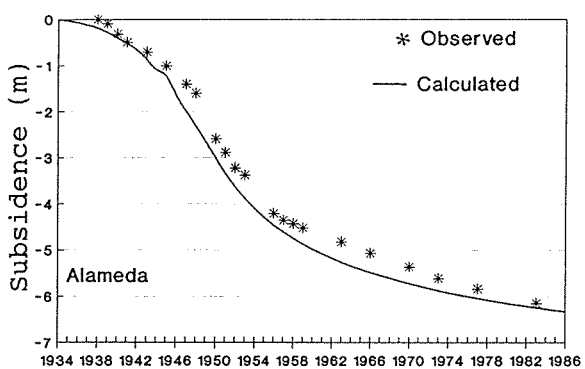

FIG. 9 Observed and calculated piezometric levels at selected sites. FIG. 10 Observed and calculated subsidence between 1934 and 1986.

adequately reproduced by the model; this piezometer has the largest series of observed data available. The comparison of the other piezometer is less good but it should be emphasized that the series of data is shorter. A comparison between the observed piezometry and the calculated piezometry at a regional scale and for different years is presented in Rivera (1990).

Figure 10 shows the results of the calculated subsidence compared with the observed subsidence at two selected sites. The agreement is very good. We believe that the fact that the model allows the correct reproduction of the three different periods of the subsidence, clearly shows the importance of considering the non-linear phenomenon.

The effects of the non-linearities on the aquitard layers, the variation of K', S'_s, n, and of the preconsolidation stress are presented in Rivera (1990).

The water budget estimated with the model is presented schematically on figure 11 for the year 1986, and is summarized in the following table:

	INS ($m^3\ s^{-1}$)	OUTS ($m^3\ s^{-1}$)
Recharge	8.1	
Aquifer storage	12.5	
Pumping		20.6
Leakage of aquitards	2.1	
Sources		2.1

In the light of these results, it is clear that the aquifer is overexploited.

The evolution in time of the water budget for the whole period of the study, 1934-1986, is shown in figure 12. It is noted that the dewatering of aquitards does not start until 1940, identified by a downward drainage, with 0.217 $m^3\ s^{-1}$ flow rate; the maximum flow rate coming from the aquitards appears in 1965 with a total of 2.35 $m^3\ s^{-1}$. The overexploitation of the aquifer starts in 1958 when total pumping exceeded natural recharge.

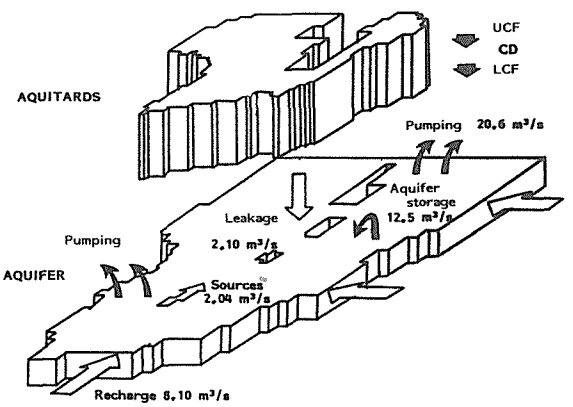

FIG. 11 Components of the water budget simulated in unsteady-state, year 1986.

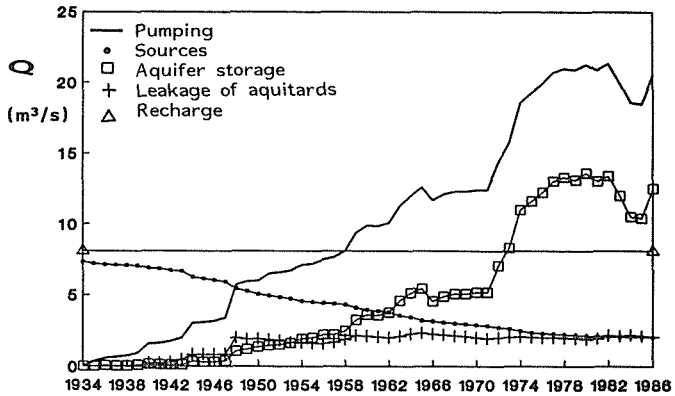

FIG. 12 Components of the water budget for the whole period of simulation.

CONCLUSIONS

The implemented model *NEWSAM-compaction* may simulate:

→ quasi-tridimensional groundwater flow,
→ the compaction of interbeds and total subsidence in a heterogeneous system,
→ the variation of hydromechanic properties as a function of applied stress.

• The results clearly show that the mechanical properties obtained from laboratory tests allow the explanation of the regional system. The conceptual model is then acceptable.

• The simulations for the Mexico city case permitted a better appreciationof both the groundwater flow and the water budget of the aquifer-aquitard system, both quantitatively and qualitatively.

• The subsidence phenomenon observed from 1934 to 1986 was nicely reproduced thanks to the non-linear hydraulic-mechanic coupled model.

• Predictions for a rational management of the Mexico city aquifer system will be possible with the implemented model.

REFERENCES

CRUICKSHANK, V.C., 1982. Modelos matematicos para acuiferos del valle de México. in : El sistema hidráulico del Distrito Federal, DDF-DGCOH, pp. 6.1-6.23.

HELM, D.C., 1976. One-dimensional simulation of aquifer system compaction near Pixley, California. 2. Stress-dependent parameters. Water Resour. Res. 12(3) ; 375-391.

HERRERA I., R. MARTINEZ, & G. HERNANDEZ, 1989. Contribución para la administracion cientifica del agua subterránea de la cuenca de México. Symposium "El Sistema Acuífero de la Cuenca de México", Mexico city; Geofísica Internacional vol. 28, n° 2, pp 297-334.

JORGENSEN, D.G., 1980. Relationships between Basic Soils-Engineering Equations and Basic Ground-Water Flow Equations. U.S. Geol. Survey Water-Supply Pap. 2064, p.40.

LESSER & Asoc, 1985. Actividades Geohidrologicas en el Valle de México, Plano 3-5 (29.V.85), México, D.F.

MARSILY, G. de, E. LEDOUX, A. LEVASSOR, D. POITRINAL, & A. SALEM, 1978. Modelling of large multilayered aquifer systems : theory and applications. J. of Hydrol. 36, 1-33.

NARASIMHAN, T.N., & P. WITHERSPOON, 1977. Numerical model for saturated-unsaturated flow in deformable porous media, 1. Theory, Water Resour. Res. 13(3) : 657-664.

NEUMAN, S.P., C. PRELLER, & T.N. NARASIMHAN, 1982. Adaptive explicit-implicit quasi three-dimensional Finite Element model of flow and subsidence in multiaquifer systems. Water Resour. Res. 18(5) ; 1551-1561.

ORTEGA, A. & R.N. FARVOLDEN, 1989. Computer analysis of regional groundwater flow and boundary conditions in the basin of Mexico. J. of Hydrol. 110 , pp 271-294.

POLAND, J.F., 1984. Guidebook to studies of land subsidence due to ground-water withdrawal. UNESCO, PHI Working Group 8.4, p.305.

RIVERA, B. A., 1990. Modèle hydrogéologique quasi-tridimensionnel non-linéaire pour simuler la subsidence dans les systèmes aquifères multicouches. Cas de Mexico. Ph.D. thesis. Ecole Nationale Supérieure des Mines de Paris, CIG. Paris, France.

RIVERA, B.A., E. LEDOUX, & G. de MARSILY, 1990. Modèle hydrogéologique quasi tridimensionnel non-linéaire pour simuler la subsidence. Cas de Pixley, Californie et de la ville de Mexico. Revue d'Hydrogéologie. BRGM, n° 1, pp. 27-39.

RUDOLPH, D., I. HERRERA, & R. YATES, 1989. Groundwater Flow and Solute Transport in the Industrial well fields of the Texcoco Saline Aquifer Symposium "El Sistema Acuífero de la Cuenca de Mexico", Mexico; Geofísica Internacional vol. 28 n° 2, pp. 363-408.

SCOTT, R.F., 1963. Principles of Soil Mechanics. Addison-Wesley Reading, Mass.

Land Subsidence (Proceedings of the Fourth International Symposium on Land Subsidence, May 1991). IAHS Publ. no. 200, 1991.

Subsidence Phenomena in the Industrial Area of Thessaloniki, Greece

B. ANDRONOPOULOS, D. ROZOS & I. HADZINAKOS
Institute of Geology and Mineral Exploration, 70 Mesogeion Av., 115 27 Athens, Greece

ABSTRACT The subsidence phenomena affecting the area of Gallikos - Sindos - Kalohori, lying to the west of the town of Thessaloniki are examined. The intense ground water extraction taking place in the area during the 50's, 60's and 70's, in combination with the presence of a black silty clay horizon, which is characterized by high plasticity and compressibility and low uniaxial and shear strength parameters, are considered to be the main factors which lead to the manifestation of the subsidence phenomena. A further examination of the black silty horizon revealed a low activity value and the presence of montmorillonite only in traces. Therefore, the subsidence phenomena were attributed to the changing of the structure of the formation and especially of the mica particles, from flocculent to "layered".

INTRODUCTION

Severe geotechnical problems occur in an area to the west of the town of Thessaloniki in the last three decades, the second largest town in Greece, which shows a continually increasing industrial development. It is an almost flat area with smooth morphology and low mean elevation (4-5m) mainly consisting by marine-lacustrine deposits. Three main rivers with an intense deposition rate, are or were converging in the area (Aliakmonas, Axios and Gallikos), causing significant changes to the morphology which has only recently been developed (before the 2nd World War). The recent action of the above rivers in combination with other factors (Valalas 1988) also caused significant and visible fluctuations in the seashore line during the last 40 years.

Because of the above unfavourable conditions the area has only recently been developed as an industrial zone for the necessities of the town of Thessaloniki. However, this development was followed by the manifestation of subsidence phenomena which are examined here.

GEOLOGICAL SETTING

The broader area lies in the geotectonic zone of Axios and more specifically in the Paionia sub-zone which is characterized by the presence of Mesozoic semi metamorphic to metamorphic rocks such as phyllites, gneisses, crystalline limestones and conglomerates as well as ophiolitic bodies of gabbric composition (IGME 1978).

The area under study constitutes a part of an old and extended

basin, in which the rocky basement is covered by Neogene deposits and Quaternary formations, which acquire considerable thickness towards the coastal area (Fig.1).

The Neogene deposits outcrop in the north and north-eastern parts of the examined area and consist of two main horizons. Quaternary formations cover the Neogene deposits throughout the rest of the area acquiring a significant thickness towards the coast which exceeds that of 200m. The upper layers of these, mainly lagoon or deltaic loose formations, can be distinguished into three horizons, which show changes in both the horizontal and vertical directions and different compositions which are attributed to the conditions, prevailing in such a changeable sedimentation environment. One of the above horizons consists mainly of sand, the other mainly of silt and the third of black silty clay with thin sandy intercalations. The latter is also characterized by the presence of shell fragments mainly occurring in the sandy intercalations.

HYDROGEOLOGICAL CONDITIONS

The alternating layers of coarse and fine grained phases, on both the horizontal and vertical directions, in the Quaternary deposits and their continuous supply with water from the nearby rivers resulted to the development of significant water aquifers. These horizons form today an underground water table at a depth of 3-6m from the surface. The intense and continuous enrichment of the different aquifers with water, allowed the intensive extraction of water during the 1955 - 1981 period and resulted to the lowering of the ground water table, which reached a depth of 37m from the surface (Fig.2).

Unfortunately, no records on the amount of water being extracted exist, although Demiris (1988) refers to a number of tenths of thousand of cubic meters of water per day.

GEOTECHNICAL CHARACTERISTICS OF THE FORMATIONS

In order to examine the geotechnical characteristics of the Quaternary deposits existing in the area, both the horizontal development of the formations and their vertical alternations up to a depth of 40-45m, were studied and lead to the construction of the engineering - geological map of the area (Fig.1). As it can be seen from this map, the sandy horizon shows the largest horizontal development while the black silty clay horizon is rather restricted and mainly appears in the southern part of the area.

In addition, the knowledge concerning the geotechnical characteristics of the formations, up to a depth of 40-45m from the surface, was thought to be necessary and to that purpose three boreholes were executed in the wider area by IGME, while the data from a large number of geotechnical boreholes, executed by other agencies and held in a data bank in IGME, were also used.

Based on the study of the boreholes and the mapping of the area, three Quaternary horizons are distinguished in the engineering geological map, namely sandy, silty and black silty clay horizons. Grain size distribution ranges for these are shown in Fig.3, while their physical characteristics and mechanical properties values are

FIG. 1 Engineering Geological Map of the wider area of Kalohori - Gallikos - Sindos.

given in Table 1.

Sandy horizon

The horizon acquires the largest surface development, consists mainly of fine to medium grained sand with a varying percentage of silt, clay not exceeding 20%, and an abundance of mica at places. Atterberg

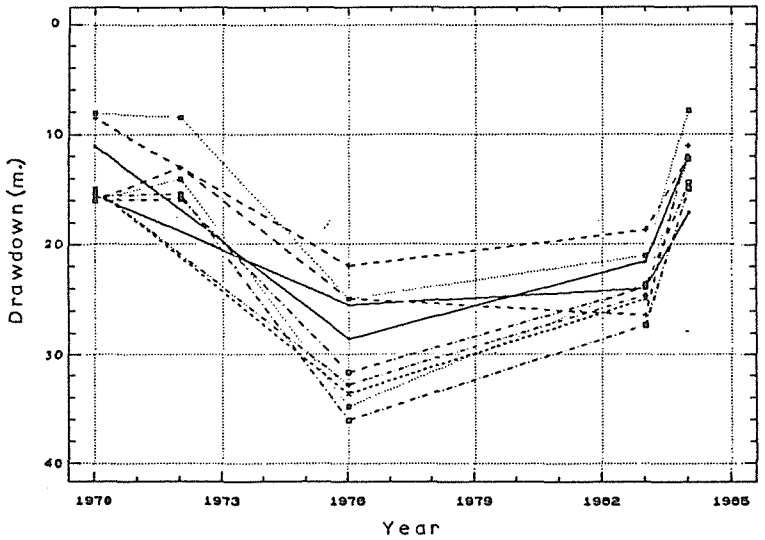

FIG. 2 Ground water level fluctuations based on data collected from Water Authority boreholes.

limits, and especially liquid limit, show a rather large variation, but in most cases the horizon shows no plasticity. Moisture content also varies significantly, between 3.1% and 39.1%.

Compressive strength values show a soft to stiff soil formation (B.S. 1975, Lambe and Whitman 1979, B.S. 1981) with cohesion ranging between 1 and 50 kPa and angle of friction values, with a very small variation, between 28° and 30°. Finally, the consolidation test produced values such as those expected from this kind of soil formation, with compression index varying between 0.116 and 0.293 and void ratio between 0.622 and 0.990 (Table 1).

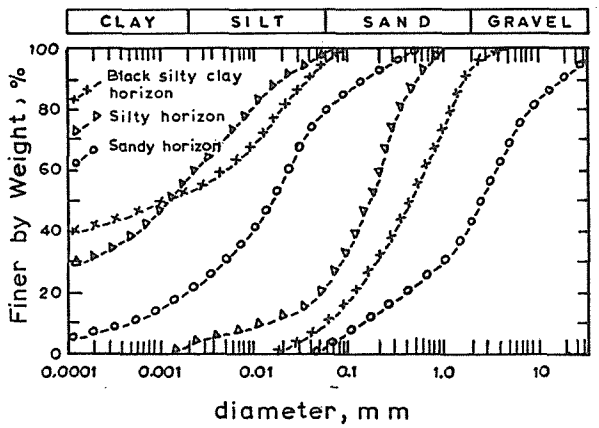

FIG.3 Particle-size limits for the three horizons of the Quaternary deposits.

TABLE 1 Minimum and maximum values for the physical characteristics and mechanical properties of the Quaternary formations.

Physical Characteristics

	Atterberg Limits w_L/w_P %		w_L/w_P %		Water Content w %		Dry and Wet Density kN/m³	kN/m³
	min	max	min	max	min	max	min	max
Silty Horizon	21.0/17.5		49.0/32.2		23.2	53.0	12.3/16.5	15.2/19.9
Sandy Horizon	8.7/11.8		39.0/21.4		3.1	39.1	11.8/14.8	18.4/21.7
Black Clay	17.8/10.0		94.8/38.0		4.0	69.4	8.7/14.8	18.2/23.0

Mechanical Properties

	Unconfined Compression kPa		Triaxial Test kPa/° c_u/ϕ_u	kPa/° c_u/ϕ_u	Consolidation Test C_c/e_o	C_c/e_o
	min	max	min	max	min	max
Silty Horizon	17.0	25.0	5.0/ 7	80.0/28	0.10/0.677	0.47/1.332
Sandy Horizon	14.0	117.0	1.0/28	50.0/30	0.12/0.622	0.29/0.990
Black Clay	4.0	120.0	3.0/ 1	170.0/37	0.08/0.413	1.01/2.047

Silty horizon

It is a brown to yellow coloured horizon, with silt as the major constituent and mica in abundance, while sand and clay also participate in the composition. Atterberg limits show a rather small variation, with ranges equal to 28 for the liquid limit and 14.7 for the plastic limit. Moisture content also shows a range of 29.8, which in comparison with the other horizons, can be considered small. The above should be attributed to the rather large proportion of mica particles participating in the silt and clay fractions of the horizon.

Unconfined compression values characterize a soft to very stiff soil formation with cohesion ranging between 5 and 80 KPa and angle of friction between 7° and 28° (Table 1). Consolidation test results show a soil formation with compression index lower than 0.470 and void's ratio ranging between 0.677 and 1.332.

Black silty clay horizon

It consists of a black to black-grey silty clay with an abundance of mica. Tests carried out also show the presence of organics at places. The horizon includes scattered sandy intercalations with a thickness not exceeding 1.00m. It is a loose horizon, mainly composed of silt and clay, with a restricted surface development in the examined area. However, it acquires an extended depth development since it is found at a small depth under the above mentioned horizons, with a thickness of up to 30.00m. Atterberg limits present a rather large range of values with a plasticity ranging from low to high. Moisture content

also varies from low (sandy intercalations) to high (for the silty clay).

Taking into consideration the results of the tests for the determination of the mechanical characteristics of the horizon, uniaxial compressive strength shows that the black silty clay horizon can be characterized as a very soft to stiff soil formation.

Cohesion and angle of friction values vary significantly, depending on whether the test was carried out on the sandy intercalations (c_u=2.5-90 kPa, φ_u=5-37°) or the silty clay part of the horizon (c_u=10-170 kPa, φ_u=1-20°). Finally, consolidation tests carried out in samples from this horizon, revealed high values for the compression index (C_c=0.305-1.014). Only when the test was executed on samples from the thin sandy intercalations of this horizon lower C_c values (0.075-0.300) were obtained. These high values of the thick silty clay part indicate that special problems, connected with this part, are to be expected.

SUBSIDENCE PHENOMENA IN THE AREA

From the above description of the lithological types participating in the engineering geological construction of the area under study, is made clear that no geotechnical problems are to be expected from the presence of the sandy and silty horizons of the Quaternary formations, which in general present satisfactory geomechanical behaviour.

However, the area is affected by the manifestation of extensive subsidence phenomena which cause serious obstacles to its industrial development. The phenomena were firstly observed in 1955, and since then were gradually increasing, resulting to sea intrusion up to the last line of Kalohori village houses. In order to face the problem, a sea embankment was constructed by the local technical authorities in the beginning of the 70's and since then it keeps increasing in height. Today the sea level is above that of the ground and a pumping system is used for the drainage of the area.

From the investigation program carried out in the area, certain characteristics were found to be associated with the subsidence phenomena:

(a) The affected area is mainly focused in the Gallikos river and Kalohori village wider area, and extends up to the village of Sindos (Fig. 1). A study of aerial photographs taken at different periods between 1945 and 1980, carried out by the Surveying Department of IGME, distinguished two areas as far as changes in the seashore line are concerned (Fig.4):
-In the first area, located between the village of Kalohori and the town of Thessaloniki the seashore remains practically unchanged.
-In the second area, to the south and east of Kalohori village, significant changes are distinguished: From 1945 up to 1960, the expected expansion of the Gallikos delta river is taking place, while from 1960 up to 1979 (a period which coincides with the heavy underground water extraction), a progressive seashore line withdrawal is marked, becoming more intense in the periods of 1960-1968 and 1975-1979. Especially, in 1979 the sea reached the southern outskirts of Kalohori. Reclamation works carried out during 1979-1980, brought the seashore line in the same position to that of 1970-1972 period (Fig.4).

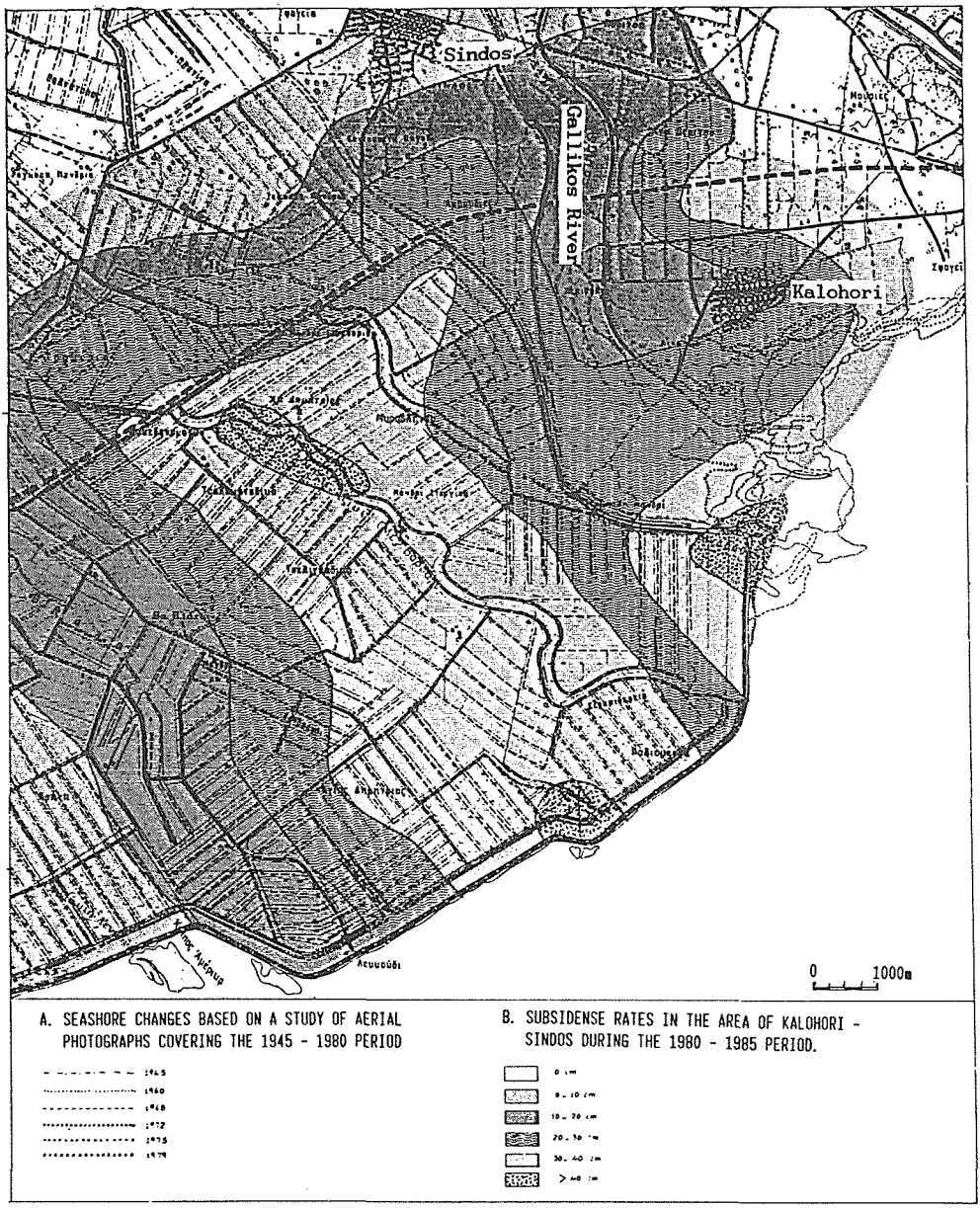

FIG. 4 Elevation changes and fluctuations of the seashore line in the wider area of Kalohori - Gallikos - Sindos.

(b) Geodetic measurements carried out by the Surveying Department of IGME covering the period between 1980-1985, distinguished 6 zones of different compaction rates (Fig.4). Three areas, to the south and west of Kalohori, show vertical movements in excess of 40cm. The relatively small amount of subsidence observed, is attributed to the fact that during this period the intense ground water extraction had been stopped and a restoration of its level was taking place.

(c) No differential settlements are observed in the area. Instead, the ground is uniformly subsiding and the greatest compaction varies between 2m and 3m, as it can be seen from both technical works in the area (protrusion of well casings, outside stairs of houses, etc.) and information collected locally.
(d) In all the affected area the black silty clay horizon is found in a small depth from the surface, covered by either the sandy or silty horizons, and for a considerable thickness.

From the above, a connection between the presence of the thick black silty clay horizon and the affected area is suspected. Therefore, the need for a more detailed look into the properties of the black silty clay horizon was thought to be necessary. To this direction, a number of boreholes drilled in the area by various authorities was closely examined up to the depth of 50m, and the following underground structure was deduced: A silty or sandy horizon with satisfactory mechanical behaviour extends up to a maximum depth of 5m, followed by the highly compressible silty clay with sand intercalations, up to the depth of 30-35m from the surface. A layer of sand with grits and good geomechanical characteristics, which acquires a maximum thickness of 14m is then observed, followed by a relatively thin layer of the black silty clay in the depth of 40-45m. Below that depth, the horizons consist of yellow to brown coloured sands to sandy and clayey silts with grits and gravels at places with a very satisfactory geomechanical behaviour.

With regard to the hydrogeological conditions the above formations develop a rich aquifer, with a today's underground water level at the depth of 3-4m. The reduction of the ground water table resulted to a draining of the formations above the depth of 40m (Fig.2), causing them to become unsaturated or partly saturated.

Therefore, it can be concluded that most of the 3m of compaction has occurred in the top 45-50m below land surface, chiefly in two very highly compressible silty clay beds of 25-30 and 5-7m thick respectively. The dominant fraction in this horizon is clay, and is characterized by a high to very high plasticity.

A mineralogical analysis which was carried out, indicated that clay minerals of the chlorite group (klinochlore), the mica group (muscovite) and the smektite group (montmorillonite) as well as quartz and albite are present. Results of a semi quantitative analysis carried out in twelve samples, shown in Table 2, clearly indicate that montmorillonite exists only in traces, while mica is in abundance. Finally, the activity value was calculated equal to 0.74 with the fitted line lying between that of illite and kaolinite (Fig.5).

DISCUSSION

The subsidence phenomena in the Gallikos - Sindos - Kalohori area originate from the extensive and intensive ground water extraction in combination with the presence of the black silty clay Quaternary formation. The latter acquires a rather large thickness to the south of the examined area (where the highest compaction rates are generally recorded) and shows low mechanical characteristics (high compressibility and low uniaxial and shear strength parameters). However, this material does not contain active clay minerals (montmorillonite) in large quantities which would explain the high rates of subsidence in the area. This is also substantiated by the calculation of the ac-

TABLE 2 Semi quantitative mineralogical analysis of the black silty clay horizon.

SAMPLE NUMBER	BOR/LE	DEPTH	MICA	CHLORITE	QUARTZ	ALBITE	MONTM/NITE
1	K1	5.00- 5.60	VM	M	F	F	VF
2	K1	14.00-15.00	M	F	F	F	VF
3	K1	18.00-19.40	M	VF	VF	VF	VF
4	K1	29.40-29.60	F	VF	VF	VF	VF
5	K1	47.00-47.50	M	M	F	M	VF
6	K1	47.50-48.50	VM	M	F	M	VF
7	K1	57.00-57.50	M	F	F	M	VF
8	K1	64.00-64.50	VM	M	F	F	VF
9	K2	9.20-10.05	F	F	VF	VF	VF
10	K2	21.60-22.80	M	M	F	F	VF
11	K3	4.80- 5.50	VM	VM	M	VM	TR
12	K3	25.30-27.50	M	M	F	M	TR

TR-TRACES, VF-VERY FEW, F-FEW, M-MUCH, VM-VERY MUCH

tivity value of the formation (0.74), which characterizes a non active material.

Attention is therefore drawn to the presence of mica particles in abundance, in both the clay fraction and the sandy intercalations. These particles, when present in high proportions, in unconsolidated formations which were deposited in a salty and kept remaining in an aqueous environment, show a scattered arrangement and result in a flocculent structure of the formation (e_o up to 2.047). The lowering of the ground water table brought the saturated sediments to a partly saturated or even dry condition, which resulted to a "layered" structure of the mica particles, a reduction in both the buoyant stresses and the void's ratio and a corresponding increase of the active stresses. A natural consequence of the above mentioned processes was the reduction of the volume of the loose sediments, which was expressed as a subsidence of the surface.

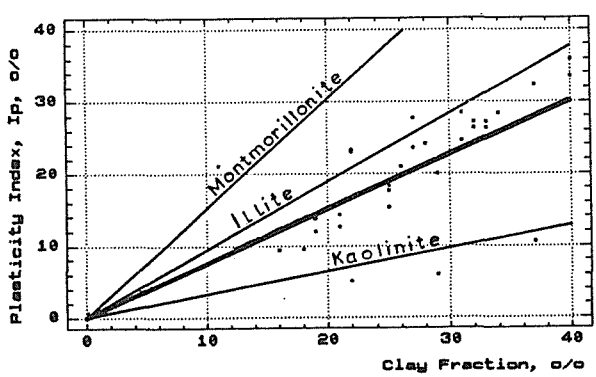

FIG. 5 Relation between plasticity index and clay fraction for the black silty clay horizon (activity 0.74).

Today, with the continuous decrease in the amount of ground water being extracted, which started in 1980, looks like the subsidence phenomena have either been reduced or even eliminated (in certain areas at least).

CONCLUSIONS

(a) The affected area is mainly focused in the Gallikos river, the village of Kalohori and reaches almost up to the village of Sindos. Throughout the above area the black silty clay horizon can be found at a small depth from the surface and for a considerable thickness. High compressibility and low uniaxial and shear strength parameters characterize this horizon.
(b) Extensive and intensive ground water extraction was taking place in the 50's, 60's and 70's and caused a considerable lowering of the ground water table, which reached to a maximum depth of almost 40m from the surface.
(c) The subsidence phenomena are mainly attributed to the ground water extraction which resulted to an altering of the structure of the black silty clay horizon, and especially of the mica particles, from flocculent to layered, with a corresponding reduction of both the pores and the volume of the formation, which was expressed as a uniform subsidence of the surface.
(d) A controlled operation of all water boreholes in the area seems to be the only solution of the problem, while certain large boreholes used exclusively for the irrigation of the town of Thessaloniki, should completely close down. In addition, a continuous checking of the operation of the sea embankment, and where necessary its local strengthening and protection, must be carried out.

REFFRENCES

Allen, A.S. (1984) Types of land subsidence. Guidebook to studies of land subsidence due to ground water withdrawal. p.133-142. Poland, J.F. (ed). UNESCO.

Andronopoulos, B. (1979) Geological and geotechnical study in the Kalohorion (Thessaloniki) area. Engineering Geology Investigations No 10, IGME, Athens.

Andronopoulos, B., Rozos, D., Hadzinakos I. (1990) Geotechnical study of the subsidence phenomena in Kalohori area. Unpublished Report, IGME.

B.S.1377 (1975) Methods of test for soils for civil engineering purposes. 143 p. British Standards Institution. England.

B.S.5930 (1981) Code of practice for Site investigation, 147 p. British standards Institution. England.

Demiris, K.A. (1988) Geological data and their influence in the development of the areas to the west of Thessaloniki. in Technical problems in the development of the area west of Thessaloniki.

Hadzinakos, I., Rozos D. & Apostolidis E. (1990) Engineering geological mapping and related geotechnical problems in the wider industrial area of Thessaloniki (Greece). 6th Int. IAEG Cong., Balkema, Rotterdam, pp 127-134.

Hunt, R.E. (1984) Geotechnical engineering investigation manual. 951pp. McGraw-Hill, USA.

IGME. (1978) Geological map of Greece. Thessaloniki sheet. Scale 1:50,000.

Lambe, T.W. and Whitman, U.R. (1979) Soil Mechanics, S.I. Version, J.Wiley and Sons, New York.

Technical Problems in the Development of the area west of Thessaloniki (1988) One day Symposium. Technical Chamber of Greece. Thessaloniki.

Valalas, D. (1988) An introduction to the symposium for the development of the area west of Thessaloniki. in Technical problems in the development of the area west of Thessaloniki.

Land Subsidence (Proceedings of the Fourth International Symposium on Land Subsidence, May 1991). IAHS Publ. no. 200, 1991.

Study of the Subsidence in the Bolognese Area

M. BALESTRI, B. VILLANI
Idroser S.p.A. - Bologna, Italy

ABSTRACT

For about 50 years, the lowland area surrounding the city of Bologna (see fig.1) has been subject to soil subsidence corresponding to the onset of systematic exploitation of the underground water resources. This subsidence is considerably more intense than the natural levels of regional subsidence, thus including it among the best-known cases in the world (Tokyo, Mexico City, Long Island, Po Delta, Ravenna, Venice).

Two categories of causes, geological and anthropic, are generally quoted to explain the origins of this subsidence.

The anthropic causes, including the extraction of fluids from the subsoil, make the greatest contribution to the acceleration and differentiation of the rate of subsidence, thus having serious effects on human activity.

In the case of Bologna, an initial quantification of the extent of the subsidence was made at the end of the Seventies; in the area to the north of the city and to a certain extent in the historic centre of Bologna, it was found that ground level had fallen by several tens of centimetres, with peaks of over a metre, in the last 25-30 years, and with gradual increase in speed (Pieri & Russo 1980).

Using a mathematical simulation model of the piezometric subsidence/topographical subsidence ratio, calibrated on the basis of the results of the experimental surveys, the Idroser study, comissioned by the Municipal Council of Bologna and the Regional Council of Emilia-Romagna, was able to determine the main connections between the physical quantities involved and to assess the trend of the subsidence on the basis of different possible cases for the reduction of underground water extraction.

1. INTRODUCTION

Geomorphologically the land in question consists of two distinct areas: the band at the foot of the Appennines and the lowlands in front. The land at the foot of the mountains is well-compacted and bonded and

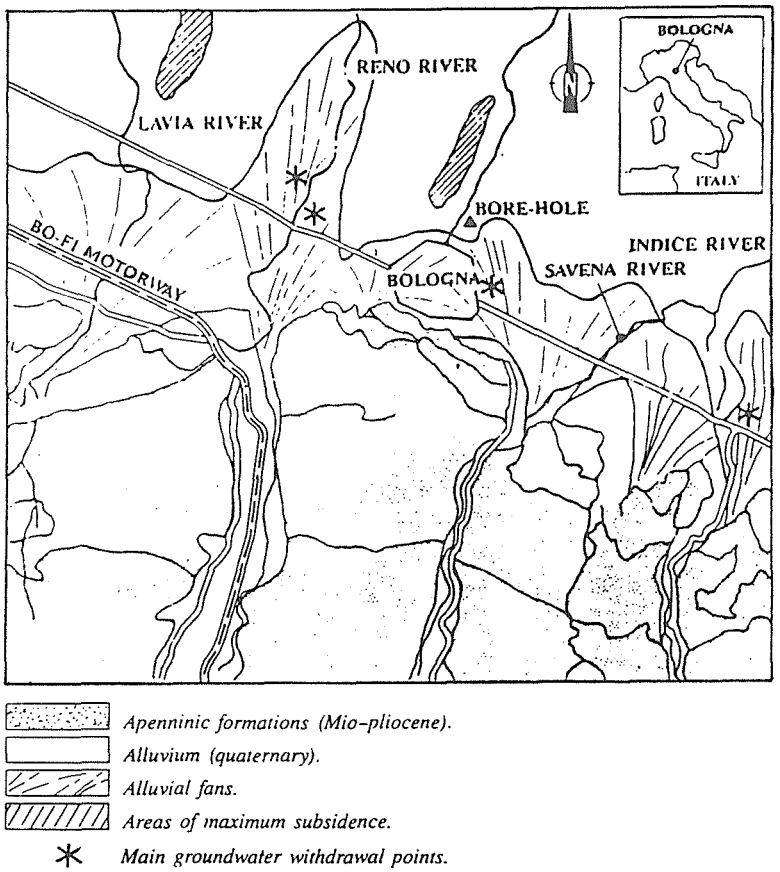

FIG. 1 Geological map.

therefore not subject to compaction; in fact, given its tectonic position, it is more likely to be subject to slight phenomena of folding. The quaternary covering of the lowlands, however, consists of normally loose soils, of relatively recent sedimentation, and containing water in the form of impregnating water and groundwater. These are the most favourable conditions for both natural and artificial compaction.

At their outlet in the lowlands, the watercourses have formed fan systems whose composition alternates between sandy or gravelly lentiform sediment, juxtaposed in a fan shape, extending far out into the lowlands. Finer, mainly clay deposits are found between one fan and another.

As regards the relation between the schematized lithostratigraphical situation and subsidence, it is possible to note how the presence of fine, highly compressible materials between two sectors with large gravelly and sandy accumulations leads to the anomalous development of the subsidence in progress. In fact the

maximum ground subsidence was found to correspond to the areas between the fans, remote from the centre with respect to those of maximum draining.

From a hydrogeological point of view, the group of fans create a single communicating system; it is fed by the direct infiltration of rain water into the ground and by the underbed dispersions.

In the medium and low lowland areas, featuring loam-clay sequences with thin sandy intercalations, the water-bearing layers in the sandy levels are fed by the water-bearing layers of the fans, of which they are the continuation.

For this reason they are fed by rather remote sources while the direct infiltration from the surface is negligible, since the surface consists mainly of loams and clays. The basis of this, which from a hydraulic point of view can be considered a single aquiferous system, is at a depth of between 250 and 500 metres and coincides with the presence of brackish and/or salt waters in the sediments of marine origin.

It is thus in the interval between the surface and a depth of 250-500 m in which there are a large number of perforated wells, that the phenomena of compaction can be found, subsequently causing soil subsidence.

2. DIVISION OF THE STUDY

The project was divided into the following parts:

a) Collection of existing data on piezometric levels, on the lithological and geotechnical characteristics of the grounds and on topographical surveys.

b) Experimental surveys carried out with integration and completion of the data considered particularly significant for the calibration of the model; they specifically refer to:

- Geoelectrical samples taken over an area of about 200km^2 around the city of Bologna, enabling the reconstruction of the stratigraphical series of the recent alluvial covering of the lowlands;
- a geognostic survey including a sample boring of 300m to define the geotechnical parameters of the ground;
- an assessment of the samples of underground waters;

c) quantitative forecast of the soil subsidence

This was defined in relation to various theories of groundwater exploitation, using the subsidence model. This model consists of two integrated parts:

- the hydrogeological models used to forecast mechanical ground stress (these models calculate the evolution of piezometry in aquifers and aquitards respectively, and thus the variation in pressure according to groundwater samples):
- the model of vertical compaction of the clays which, from the evolution of mechanical ground stress, calculates the state of compaction and consequently the subsidence of the surface.

3. RESULTS OF THE EXPERIMENTAL SURVEYS

The geophysical survey was made to supply a schematic reconstruction of the stratigraphical series. The results of the survey have been summarized in a series of papers which show the distribution of different types of sediments on the surface and at various depths (up to 300-400 m).

The geognostic survey enabled the stratigraphical pattern and the geomechanical properties of grounds to be characterized. Exploratory boring was carried out to 300 m using the wire-line system, with registration of the stratigraphical series and collection of undisturbed, semidisturbed and altered samples.

During the boring operations, wire-line static penetrometrical tests were made at prefixed depths using an electric tip and a piezocone and, at the end of the boring operation, tests were made of the dissipation of the excess of pore pressure, induced by penetration of the boring equipment itself.

The samples taken were subjected to tests of identification and classification, edometric compression and resistance to cutting. The results were summarized in a series of diagrams indicating the parameters identified according to the depth (see Fig. 2).

The analysis of these results has led to the division of the stratigraphical profile into two groups of layers according to the schematization used by the model.

More specifically, consideration was made of the layers composed mainly of loamy-clay materials, of compaction characteristics defined by the coefficient Cv and of medium compressibility, as well as the layers composed mainly of sandy-gravelly soils, which, for practical purposes, can be considered practically incompressible and providing sufficient drainage.

Geotechnical instrumentation was installed in both boring holes in order to define the extent and the distribution of ground subsidence in relation to the depth and to determine the piezometric levels according to different permeable horizons (see Fig. 3).

More specifically the monitoring system includes:

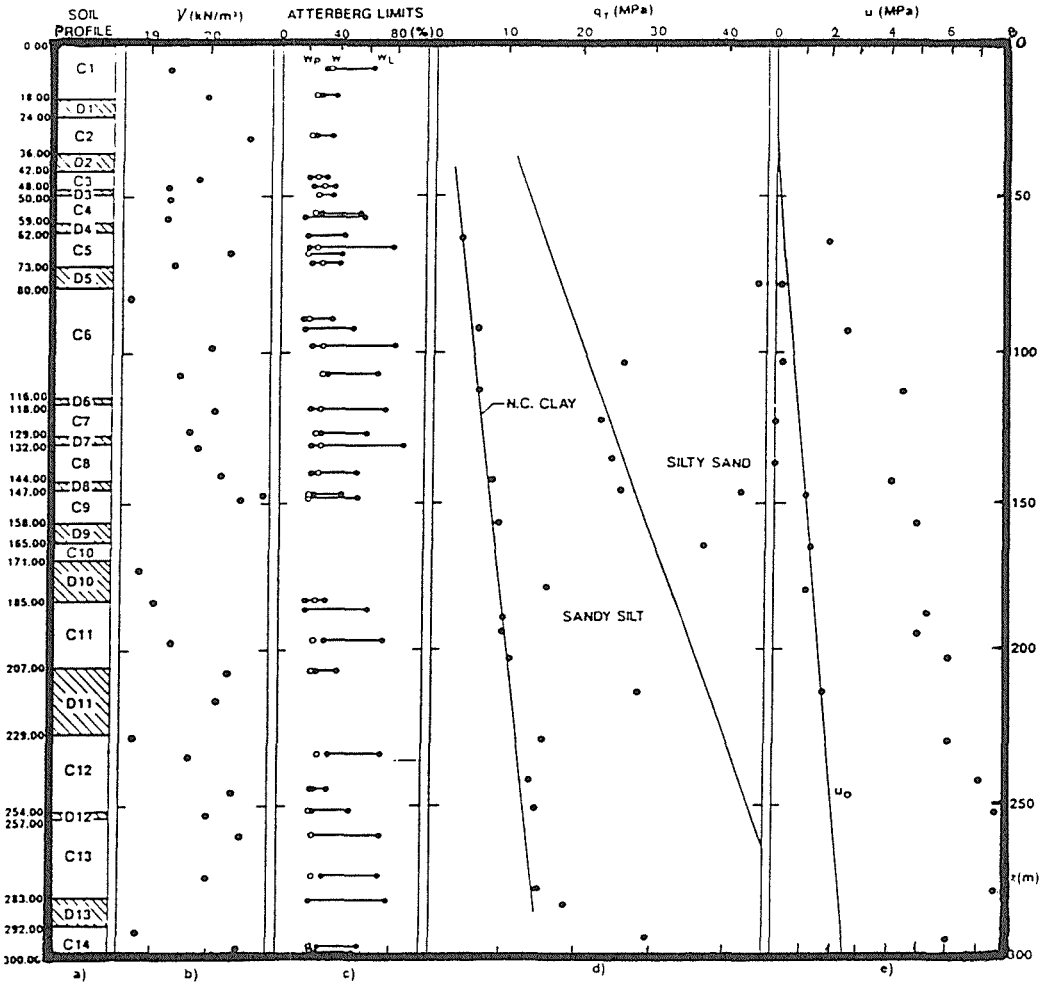

FIG. 2 Stratigraphic profile and geotechnical characteristics.

- 3 subsidence measuring stations positioned at 50.00 m, 146.90 m and 245.97 metres from the surface.
- 5 hydraulic piezometers, including 2 of the traditional Casagrande type and 3 of the purpose-built Casagrande type, at the following depths below the surface: 42 m, 72.57 m (BO3), 116.20 m, 167.20 m and 222.20 m (BO1).

The readings of the subsidence meters and the piezometers available at the moment refer to a period between September 1987 and April 1989. Measuring the subsidence registered by the subsidence stations is useful in separating the different contributions to the

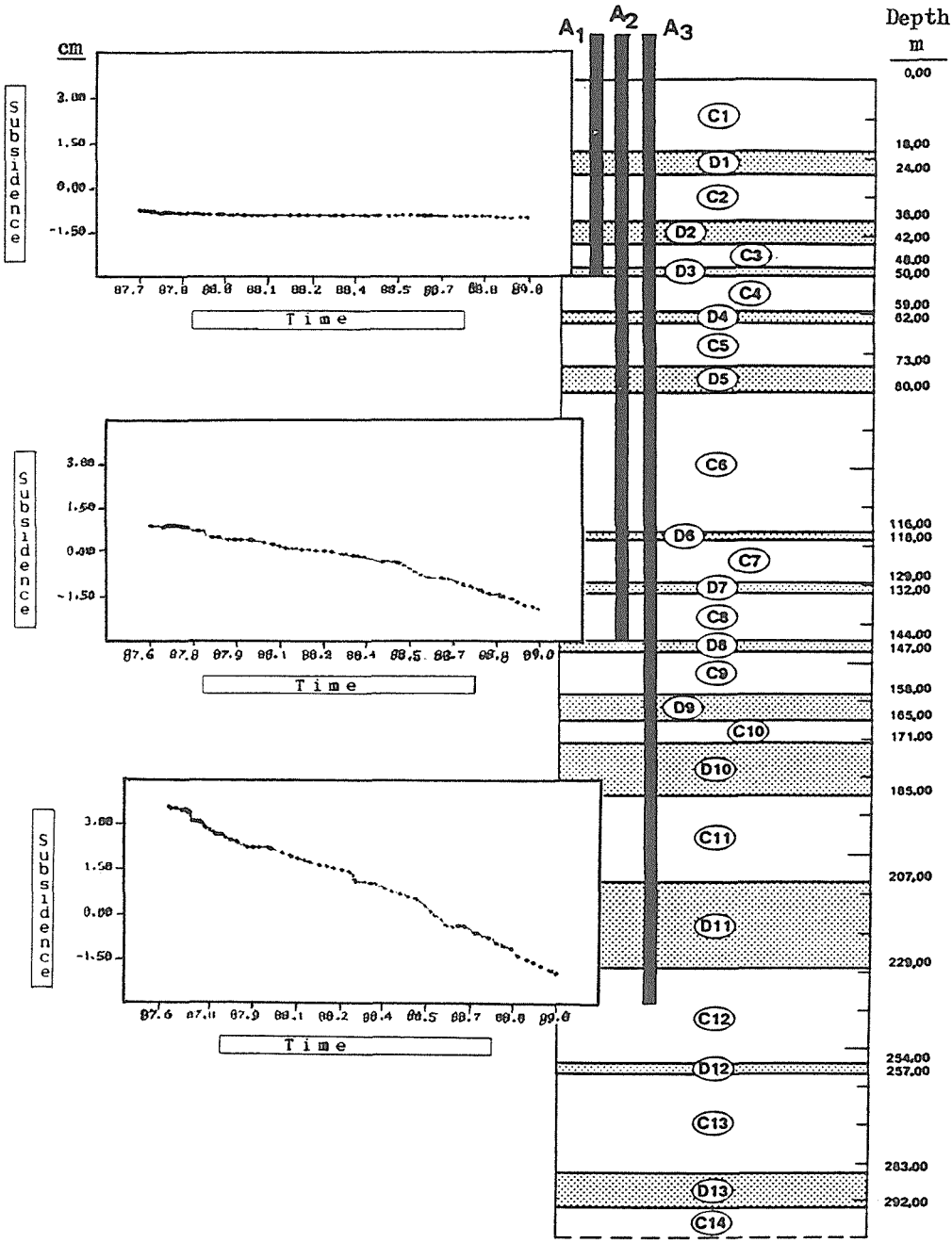

FIG. 3 Subsidence measured on the subsidence meter.

total subsidence of layer I (0 50 m), layer II (50 147 m), layer III (147 246 m) and layer IV (below 246 m). The annual subsidence rate values connected with the depth variations of a bench mark (71/2 and/or 71/3) situated near the boring site, showed that 84% of the

total subsidence takes place between the surface and a depth of 246 m. The first 50 m, with a rate of 0.21 cm/year, constitute only 4% of the total while layer II, with an average rate of 2.40 cm/year and layer III, with an average rate of 4.47 cm/year are those which appear most subject to compaction, constituting 41% and 39% of the total respectively.

3. MATHEMATICAL MODEL OF SUBSIDENCE

The study on the quantitative forecast of subsidence generally includes the use of two integrated models:

- a hydrogeological model which calculates the evolution of the piezometry according to the groundwater samples, for the determination of the mechanical ground stress following the hydraulic load variations identified;
- a model of subsidence that, taking the evolution of the mechanical stress, calculates the subsidence of the surface.

The hydrogeological model assumes the hydraulic behaviour of the aquiferous system to be comparable to that of an equivalent single layer: this assumption is legitimate and suitable for calculating the piezometric level in the sandy layers (aquifers), but does not enable the piezometric level within the cohesive layers (aquitards) to be calculated.

Given the importance of the pattern of the piezometric level within the cohesive layers on the phenomena of subsidence, the model has been integrated with a monodimensional hydrogeological model which calculates the time pattern of the piezometric level along the thickness of the aquitards from the piezometric level of the aquiferous layers.

The model of subsidence used is based on Terzaghi's theory according to which the increase of effective tensions, from an undisturbed reference condition, is equal to the variation of the piezometric level. The calculation of the subsidence derives from the integration along the vertical of the product of the compressibility of the ground multiplied by the variation of piezometric level at each point of the column.

The compressibility of the ground is shown from the curve of edometric compression where the effective pressures exceed the previous maximum value, or from the section of recompression/swelling where the effective tensions are below this value.

Calibration stage

The calibration stage of a complex system

constituting a succession of sandy and clay layers, as in the case of the Bolognese lowland, is complicated by the fact that the parameters used in the calculation of the subsidence are numerous and usually uncertain. For each point the thickness and the geotechnical characteristics of all the cohesive layers must be known. Even considering all the aquitards to be homogeneous, as was done in this case, the following factors have to be known for each of them:

- thickness
- compaction coefficient
- compressibility relative to the section of compression
- compressibility relative to the section of recompression/drainage
- the time series of the piezometric levels and of the subsidence measurements

8 sample areas were chosen for the definitive calibration of the model while the results of the on-site and laboratory tests were also used, made as part of the geotechnical boring BO1/BO3.

Given the importance of the contribution of data from the boring in the calibration stage, a detailed study was carried out on this.

Results of the simulations and indications appearing

The possible cases of gradual reduction of groundwater extractions were defined, differentiating them according to size and location. In simulation no. 1, maximum reduction, the extractions were reduced by 445 L/s (maximum recovery >35 m), in simulation no. 3, minimum reduction, 243 L/s were reduced (maximum recovery between 20 and 25 m), in simulation no. 2, (medium reduction), 358 L/s were reduced (maximum recovery >30m).

These draining theories formed the basis for the simulations of the pattern of soil subsidences in the lowlands from 1989 to 2000. After completing the calibration stage in the points specially chosen to determine the geotechnical parameters to be used, the simulation stage was begun.

At this stage, on the basis of the theories of exploitation of the underground aquifer, defined with the hydrogeological model, using the model of subsidence, the partial and total subsidence of the ground was determined, from 1989 to 2000, the year for which new situations of hydrodynamic groundwater equilibrium are forecast.

For the simulations, meshes were chosen in which it was possible to reconstruct the historic series of the piezometric patterns, using the undisturbed situation, the stratigraphy and using the geotechnical

parameters obtained during the calibration stage.

The calculation of the subsidence relative to each mesh has reproduced the ground subsidence until 1988; on the basis of water recovery an immediate reduction in rate is determined after 1988 in the three previously defined possible cases of exploitation of the aquifer.

Variations of the topographical measurements in the period 1989-2000

It should be remembered that the aquifer system responds immediately to the variation of pressure and recovers the water levels in a very short time (about 1 or 2 years). This produces a sort of barrier to the progress of the subsidence, generating a rapid reduction in subsidence (Fig. 4).

It should be noted that the residual subsidences are very similar whatever the reduction of the extractions, both in extent and in position: for this reason even the adoption of the minimum reduction alone

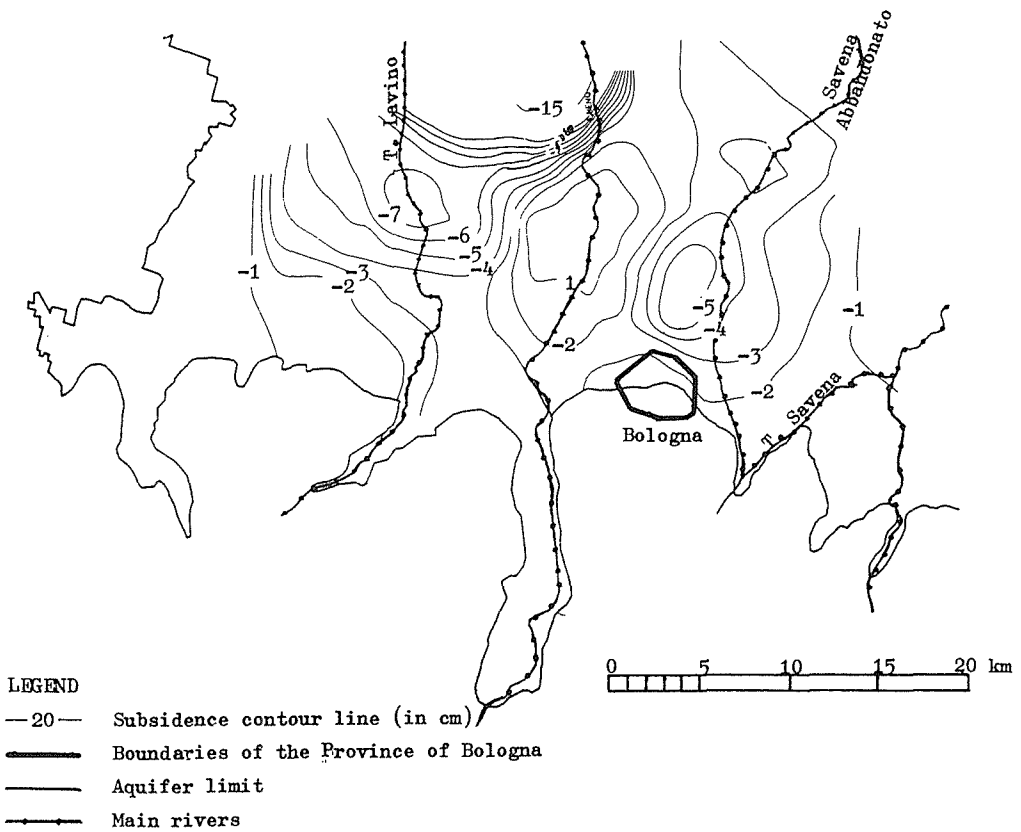

FIG. 4 Topographic variations in the 1989-2000 period as per simulation.

(-245 L/s) would be sufficient in order to stop the phenomenon in progress.

Besides the simulations relative to the 3 possible cases of reduction of the extractions, a fourth simulation has been carried out in which, up to the year 2000, the current extractions and the water levels are kept constant: the results obtained in this case have shown that a constant pattern of the groundwater levels produces only a slight reduction in the subsidence rate: therefore a threshold value exists in keeping extractions at a level below which further reductions are not to be considered convenient for a significant reduction in the subsidence rate, and above which there is no direct proportionality between reductions of extractions and the subsidence rate, as shown in the analysis of the simulations 1, 2 and 3. This value was identified as about 150 L/s of reduction, to be applied in an evenly distributed fashion.

Land Subsidence (Proceedings of the Fourth International Symposium on Land Subsidence, May 1991). IAHS Publ. no. 200, 1991.

The Monitoring and Investigation of Ground Subsidence in Southwest Taiwan

J. S. LIAO & K. L. PAN
Energy and Resources Laboratories, Industrial Technology Research Institute, Bldg 64, 195 Sec. 4, Chung Hsing Road, Chutung, 31015 Hsinchu, Taiwan, China
B. C. HAIMSON
Geological Engineering Program, University of Wisconsin-Madison, Madison, WI 53706, USA

ABSTRACT The overwhelming fluid withdrawal into fishery farms has caused a serious subsidence at Linpien, Chiatung, and Shuitiliao, the districts located at Southwest Taiwan. To figure out the relations between the current subsidence and decline of water level, several monitoring systems including multipoints wire-flex extensometer and multilevel water-head monitoring system have been installed in the area investigated. Meanwhile, the on-site borehole drilling and laboratory soil tests are also conducted to provide the soil properties data. The behavior of subsidence incurred by the decline of water head is predicted by the improved Biot's three-dimensional consolidation theory through computer simulation. The results show that the subsidence rate in the investigation area has been gradually alleviated. Ground subsidence incurred by the decline of water level can be fairly predicted from the mathematical modeling.

INTRODUCTION

The occurrence of major land subsidence due to the withdrawal of groundwater is relatively usual in highly developed areas, such as the cases at Shanghai in Mainland China, Taipei Basin in Taiwan, Cheshire district in Great Britian, Po Delta and Venice in Italy, Tokyo and Osaka in Japan, Mexico City in Mexico, Bangkok in Thailand, San Joaquin Valley and Santa Clara Valley in the United States, Wairakei in New Zealand, Far West Land in South Africa and Latrobe Valley in Australia, etc. (Poland, 1984). In general, the subsidence in these districts is mainly due to over-withdrawal of fluid, while the effects of natural factors, such as tectonic effects on subsidence is not significant. For instance, the subsidence in the east coast of America is approximately 2.5 mm/yr due to the raising of seawater (Davis, 1987); the crustal movements in Taiwan Geosyncline causes a 5 mm/yr raising in the Coast Mountain Chain, and a subsidence in the Coastal Plain in western Taiwan (Pingtung Coast Plain is included) (Chern, 1984). In Taiwan, ground subsidence in Taipei Basin, which began in mid-1950's has caused great concern during the past two decades. Besides Taipei Basin, the Choshui River Alluvial and Pingtung Coastal Areas are other hot-spot areas in which there has occurred tremendous ground subsidence due to withdrawal of groundwater to fishery farms. The action of withdrawing groundwater has led to piezometric head decline in confined aquifer, that, thus, increases the effective stress in earth materials. The Pingtung Coastal Area, geologically being the Lili River Alluvial Fan, circled by Linpien River,

Lili River, and Peishui River with a area of 73 km^2, has the withdrawal of groundwater, 165 x 10^6 m^3/yr, which is equal to average amount of withdrawal of 6.19 mm/day (Yang, 1987). Due to the large amount of water withdrawal and an uncompacted sediments (fine grains) distribution in the area, the subsidence is, generally, greater than those expected. The contour lines of land subsidence in the Pingtung Coastal Area is illustrated in Fig. 1. The maximum ground subsidence occurs at Wenfong where the accumulated subsidence has been over 2.43 m during February 1970 to June 1988 (TWCB,1988).

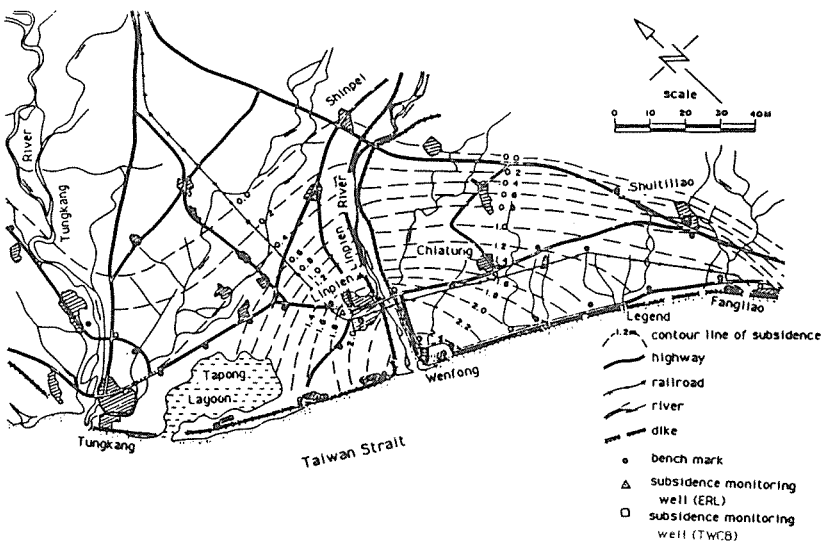

FIG. 1 The contour lines of land subsidence in the coast of Pingtung County (TWCB, June 1988).

The geological materials in the area are composed of various types of soil, they are SM (silty sand), SP-SM (sand to silty sand), SP-SC (sand to clayey sand) and SC (clayey sand). The grain size distribution ranging in 0.3 to 0.03 cm is ranked between fine sand and silt (ERL, 1988). The thickness of alluvium at Wenfong and Shuitiliao is in the range of 165-200 m. To understand the relations between the change of water level and ground subsidence, some monitoring systems, such as multipoints extensometer and multilevel water-head piezometer were installed at Linpien, Wenfong and Shuitiliao and mathematical modeling was also conducted to approach these relations.

The investigation area in this paper covers Linpien and Lili River allvial fan including Chiatung and Shuitiliao. Numbers of studies including the analyses of hydrogeological data, field measurements and mathematical modeling have been carried out in this area to investigate the ground subsidence.

SUBSURFACE GEOLOGY AND HYDROLOGY

The major structure in this region is Chaochou fault, located at eastern part of the

investigation area, which is a high-angled reverse fault with a dip of 75° - 80° eastward. Raising block of stratum is in the east of the fault plane. The downward faulted block with a striking of NNE-SSW formed Pingtung anticline and syncline. The topographic and geophysical data show that this region is currently in subsiding due to tectonic force (Chern, 1984). The subsurface geology of this region is identified from the borehole logs and rock/soil mechanical properties data. The reading of Gamma-ray log, generally, is less than 40 cps in this area (ERL, 1988). The contrast between high readings and low readings of Gamma-ray log is not significant. Core logs data show that the formation in the area is a type of the sand or sandy argillaceous formation formed by the erosion of river. It seems that the formation is uncompacted and has a high porosity.

HISTORY OF LAND SUBSIDENCE IN SOUTHWEST TAIWAN

The rate of subsidence in the coastal plain of Southwest Taiwan, is approximately 0-3 cm/yr during 1914-1979 (Chern, 1984); however, the raising rate is only 2-5 mm/yr based on the study of geomorphology (Hsu, 1954, 1962, 1980; Hsu & Chai, 1974; Li, 1976) and radiometric dating (Konishi, Omura & Kimura, 1968; Peng, Li & Wu, 1977; Taira, 1975). Obviously, the raising rate of ground is much less than the subsiding rate in the Southwest Taiwan. To be concluded, the withdrawal of groundwater might not be the only cause of ground subsidence in the Southwest Taiwan, but was being a major cause.

The historical data of elevations of various bench marks in the Pingtung Coastal Area is illustrated in Fig. 2. The accumulated land subsidence amounted to 2.43 m, from February 1970 to June 1985, was found at Wenfong.

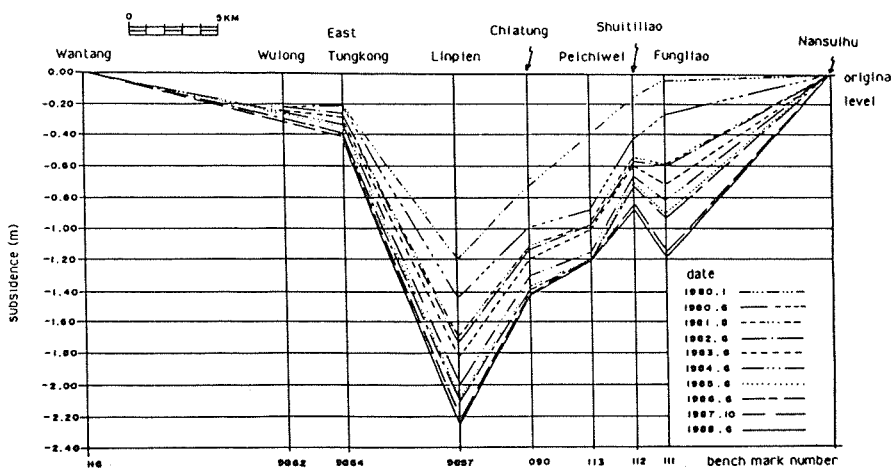

FIG. 2 The historical data of elevations of various bench marks in the Pingtung Coastal Area (TWCB, June 1988).

It is explainable since Wenfong has the highest soil compressiblity, C_c, among the three districts, while $C_c = 0.4$ at Wenfong, 0.3 at Shuitiliao, and 0.2 at Linpien(ERL, 1988). The subsidence has been recorded at there since January 1979. The subsidence rate was found accelerating during January to June in 1981, the beginning stages for

over-withdrawal groundwater in the Southern Taiwan, recording the amount of 5 cm/month for land subsidence (Lin, 1986). As noted previously, the over-withdrawal of groundwater for a long time has resulted in a lowering groundwater level and severe land subsidence. The viewpoint might be proved by the following facts: the area of fishery farm increased from 6 hectares in 1972 to 980 hectares in 1982. Wells have being increased rapidly responding the expansion of fishery farm. For example, the number of illegal wells in the groundwater restricted districts of Pingtung County is about 3871 (conservative estimation). The annual consumption of groundwater in this area is about 320 x 10^6 m^3 in 1983, of which, approximately 176 x 10^6 m^3 is for the purpose of the fishery farms (Lin, 1986).

The whole picture of the stratigraphic profiles in this region is illustrated in Fig.3.

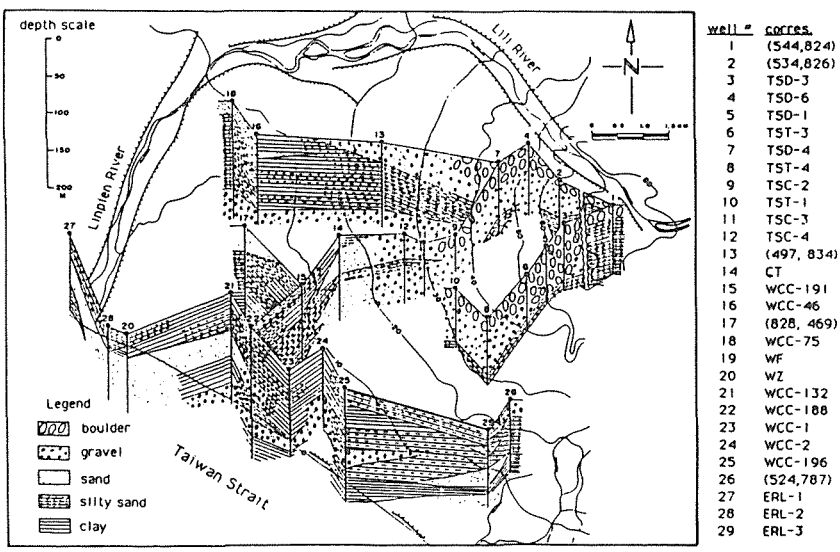

FIG. 3 Stratigraphic cross-section in the Pingtung Coastal Area.

The abbreviations in Fig. 3 are represented by the followings: TS= Taiwan Sugar Company, WCC= Taiwan Water Conservancy Council, WF= Wenfong, WZ= Wentz Elementary School, CT= Chiatung. The Chaochou fault is crossing between 1-2 and 1-3. The Lili alluvial fan aged in Quaternary, is composed of uncompacted gravel, boulder, sand, silt and clay, etc. Around this area, boulder and gravel distribute toward inland; gravel, coarse sand and clayey sand distribute in the central region of the fan. The minerals in the shallower formations (less than 100m) in the area are composed of chlorite, illite and other non-swelling clay minerals with litter amounts of swelling clay minerals (ERL, 1988). It is, thus, concluded that there is not a significant influence of swelling clay minerals on ground subsidence in the shallower formation. The clay layer is thicker near seashore. The clay layer with a maximum thickness of 80 m, is located near seashore and west of fault. The gravel is thin at east of fault; it becomes thicker at west of fault and disappears at middle part of the area. Generally, the apex (#1) and middle part (# 13, 14 and 25) of alluvium is a free water area; the end of alluvium (#18, 28 and 20) is a semi-confined water aquifer; coastal plain (#21-26) is a confined aquifer (Chang, 1985). The resistivity logs show the salinity of groundwater is decreasing with increasing depth (ERL, 1988), it means the shallower formation might

be intruded or polluted by seawater.

The change of groundwater level in rainy season (Sept. 1984) and dry season (April 1985) is in the range of 25-30 m at apex of alluvial fan, and 7-12 m near sea shore (Chang, 1985). To realize the variation of groundwater quality and seawater intrusion, the conductivity of groundwater was measured through the area in the shallow formation during sept. 1984-April 1989 (Fig. 4).

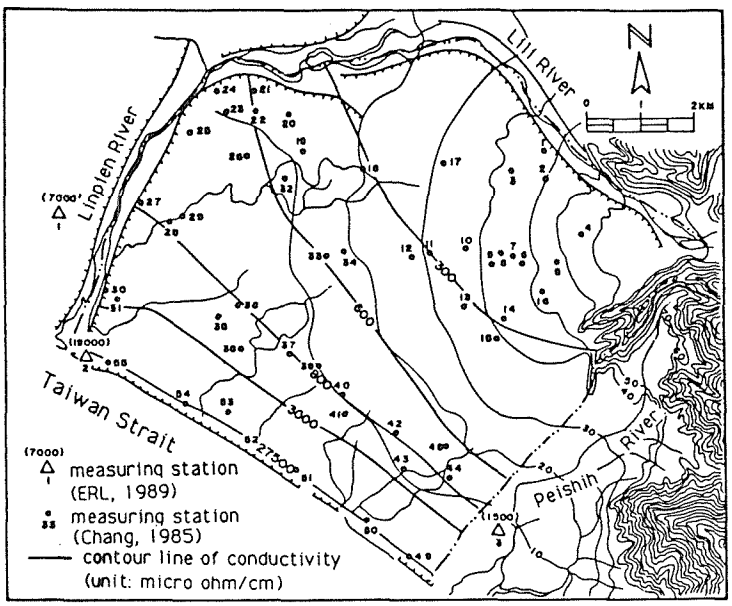

FIG. 4 The distribution of groundwater conductivity in the shallow formation (10m-50m).

Generally, the formation could be thought as intruded or contaminated by seawater if salinity is higher than 2000 micro ohm/cm. Since the well-water around Linpien River (ERL #1, #2) was recorded a high conductivity, which is 7000 and 19000 micro ohm/cm, respectively, the groundwater at shallower formation, around depth 30m, nearing coast was possibly intruded or contaminated by seawater and the confined water aquifer at deeper formation is still kept uneffected.

CONCEPT OF AQUIFER SYSTEM AND THE MATHEMATICAL MODELS

The water-head data (see Fig. 11) show two aquifers separated by a fine-grained interbed (sand with clay) at Wenfong. This conclusion can be proved by the geological core logs (ERL, 1988). Generally, due to the aspects of uncompacted formation and the thinning of clayey formation, it is reasonable to assume that the water flow in beds, is mainly, restricted in vertical direction. The aquifer systems in the investigation area, are thus, simplified to a single aquifer system with different lithologies.

The mathematical model based on the improved Biot's consolidation theory (Biot, 1941) is used to predict the relations between groundwater level and ground subsidence. The model is shown as follows (Liao & Haimson, 1989):

An incompressible solid and fluid field equation (see equations 3 and 4) can be modified to a compressible solid and fluid field equation. Equations 3 and 4 are based on the Biot's theory (Biot, 1941) which was formulated for solid-fluid interaction. According to Biot's theory, the soil skeleton is treated as a porous elastic solid and the laminar pore fluid is coupled to the solid under the conditions of compressibility and continuity. Biot's theory assumes some basic material properties including isotropy of the material, linearity of stress-strain relations, incompressible water in the pores, and water flow in the porous media according to Darcy's law.

The derivation of equations 3 and 4 is based on the following equilibrium and continuity equations in the absence of body forces (Smith, 1982):

$$\mathbf{K}_m\ \mathbf{R} + \mathbf{K}_c\ \mathbf{X} = \mathbf{f}$$

$$\mathbf{K}_c^T \frac{\partial \mathbf{R}}{\partial t} - \mathbf{K}_p\ \mathbf{X} = \mathbf{0} \qquad (1)$$

where $\mathbf{X}$ = fluid potential
$\mathbf{R}$ = displacement vector
$\mathbf{f}$ = applied external force
t = time
$\mathbf{K}_m$ = elastic stiffness
$\mathbf{K}_p$ = fluid stiffness
$\mathbf{K}_c$ = coupling matrix ; $\mathbf{K}_c$ is the connection matrix that has the same shape functions as the solid element governing the variation of pore water pressure within the element and the variation of displacements. The formula for $\mathbf{K}_c$ is as follows:

$$\mathbf{K}_c = \int \mathbf{VOL}\ .\ \mathbf{N}^T\ dx\ dy \qquad (2)$$

then, the following formula for composite continuum (solid + water) was presented (Smith, 1982):

$$\theta\ x\ \mathbf{K}_m\ x\ \mathbf{R}_1 + \theta\ x\ \mathbf{K}_c\ x\ \mathbf{p}_1 =$$
$$(\theta - 1)\ x\ \mathbf{K}_m\ x\ \mathbf{R}_0 + (\theta - 1)\ x\ \mathbf{K}_c\ x\ \mathbf{p}_0 + \mathbf{f} \qquad (3)$$

$$\theta\ x\ \mathbf{K}_c^T\ x\ \mathbf{R}_1 - \theta^2\ x\ \Delta t\ x\ \mathbf{K}_P\ x\ \mathbf{p}_1 =$$
$$\theta\ x\ \mathbf{K}_c^T\ x\ \mathbf{R}_0 - \theta(\theta - 1)\ x\ \Delta t\ x\ \mathbf{K}_P\ x\ \mathbf{p}_0 \qquad (4)$$

where θ = time stepping interpolation parameter
Δt = increment of real time
$\mathbf{p}$ = pore pressure
o = initial time (beginning of time step)
1 = after initial time (end of time step)
$\mathbf{N}$ = shape function (see equations 9)
$\mathbf{VOL}$ = volumetric strain (see equation 15)

In the axisymmetric case, the stiffness for solid, liquid, and coupling matrices can be written as

$$\mathbf{K}_m = 2\pi \iint \mathbf{U}^T \mathbf{D}\, \mathbf{U}\, r\, dr\, df \tag{5}$$

where **U** is strain-displacement matrix and **D** is elasticity matrix.

$$\mathbf{K}_P = 2\pi \iint \mathbf{DERIV}^T \times \mathbf{KAY} \times \mathbf{DERIV}\, r\, dr\, df \tag{6}$$

$$\mathbf{K}_c = 2\pi \iint \mathbf{VOL}^T \times \mathbf{N}\, r\, dr\, df \tag{7}$$

where N is a shape function for the quadrilateral element and r and f is polar coordinates.

$$\mathbf{N} = [\, N_1\ N_2\ N_3\ N_4 \,] \tag{8}$$

$$\begin{aligned} N_1 &= 0.25\,(1-\xi)(1-\eta) \\ N_2 &= 0.25\,(1-\xi)(1+\eta) \\ N_3 &= 0.25\,(1+\xi)(1+\eta) \\ N_4 &= 0.25\,(1+\xi)(1-\eta) \end{aligned} \tag{9}$$

where ξ and η are natural coordinates.
The explicit form of the elasticity matrix **D** can be written as:

$$\mathbf{D} = \frac{E(1-\nu)}{(1+\nu)(1-2\nu)} \begin{bmatrix} 1 & \frac{\nu}{1-\nu} & 0 & \frac{\nu}{1-\nu} \\ \frac{\nu}{1-\nu} & 1 & 0 & \frac{\nu}{1-\nu} \\ 0 & 0 & \frac{1-2\nu}{2(1-\nu)} & 0 \\ \frac{\nu}{1-\nu} & \frac{\nu}{1-\nu} & 0 & 1 \end{bmatrix} \tag{10}$$

for plane strain and axisymmetry. Only the first 3 x 3 portion indicated will be employed in the plane strain case. The
strain-displacement matrix, **U**, is a function of the natural coordinates in isoparametric elements.

$$\mathbf{U} = \mathbf{A}\,\mathbf{N} \tag{11}$$

where

$$\mathbf{A} = \begin{pmatrix} \frac{\partial}{\partial r} & 0 \\ 0 & \frac{\partial}{\partial z} \\ \frac{\partial}{\partial z} & \frac{\partial}{\partial r} \\ \frac{1}{r} & 0 \end{pmatrix} \tag{12}$$

and

$$\mathbf{KAY} = \begin{bmatrix} K_x & 0 \\ 0 & K_y \end{bmatrix} \tag{13}$$

$$\mathbf{DERIV} = [J]^{-1} \times \begin{bmatrix} \frac{aN^T}{a\xi} \\ \frac{aN^T}{a\eta} \end{bmatrix} \tag{14}$$

$$\mathbf{VOL} = [\ \frac{\partial N_1}{\partial x}\ \frac{\partial N_1}{\partial y}\ \frac{\partial N_2}{\partial x}\ \frac{\partial N_2}{\partial y}\ \frac{\partial N_3}{\partial x}\ \frac{\partial N_3}{\partial y}\ \frac{\partial N_4}{\partial x}\ \frac{\partial N_4}{\partial y}\ ] \tag{15}$$

Equations 3 and 4 are only valid for full saturation and incompressible fluid and solid (Smith, 1982). However, it is necessary to consider the incompressible fluid and solid as a compressible fluid and solid in the real situation. For the compressible solid case, equation 7 can be written as (Ghaboussi &Wilson, 1973; Rice & Cleary, 1976; Detournay & Roegiers, 1987):

$$\mathbf{K_c} = 2\pi \iint \alpha\ \mathbf{VOL}^T \times \mathbf{N}\ r\ dr\ df \tag{16}$$

where

$$\alpha = \frac{3(\nu_u - \nu)}{B(1+\nu_u)(1-2\nu)} \tag{17}$$

In equation17, ν_u is undrained Poisson's ratio and B is Skempton's coefficient. a is Biot's coupling coefficient. It measures the ratio of the water volume squeezed out to the volume change of the total medium if the latter is compressed while the water is allowed to escape. For incompressible solid grains, $\alpha \approx 1$; for compressible solid grains, $0 < \alpha < 1$. Equation 6 can be modified to a case of compressible fluid by considering Biot's storativity coefficient, M:

$$\begin{aligned} &\theta \times \mathbf{K_c^T} \times \mathbf{R_1} - \theta \times \mathbf{K_L} \times \mathbf{P_1} - \theta^2 \times \Delta t \times \mathbf{K_p} \times \mathbf{P_1} \\ &= \theta \times \mathbf{K_c^T} \times \mathbf{R_o} - \theta(\theta - 1) \times \Delta t \times \mathbf{K_p} \times \mathbf{P_o} - \\ &\quad \theta \times \mathbf{K_L} \times \mathbf{P_o} \end{aligned} \tag{18}$$

where $\mathbf{K_L}$ can be written as (Ghaboussi & Wilson, 1973; Rice & Cleary, 1976):

$$\mathbf{K_L} = 2\pi \iint \frac{1}{M} N^T N\ r\ dr\ df \tag{19}$$

with

$$M = \frac{2GB^2(1+\nu_u)^2(1-2\nu)}{9(\nu_u - \nu)(1-2\nu_u)} \tag{20}$$

where, G is shear modulus. For an incompressible fluid, $M \approx \infty$, leading to $\mathbf{K}_L = 0$. Based on equations 3 and 18, after discretization in space, a time-stepping scheme for Crank-Nicolson type of approximation ($\theta = 0.5$) has the form:

$$\begin{bmatrix} \mathbf{K}_m & \mathbf{K}_c \\ \mathbf{K}_c^T & -(\frac{\Delta t}{2}\mathbf{K}_P + \mathbf{K}_L) \end{bmatrix} \begin{Bmatrix} \mathbf{R}_1 \\ \mathbf{P}_1 \end{Bmatrix}$$

$$= \begin{bmatrix} -\mathbf{K}_m & -\mathbf{K}_c \\ \mathbf{K}_c^T & \frac{\Delta t}{2}\mathbf{K}_P - \mathbf{K}_L \end{bmatrix} \begin{Bmatrix} \mathbf{R}_0 \\ \mathbf{P}_0 \end{Bmatrix} + \begin{Bmatrix} 2\mathbf{f} \\ \mathbf{0} \end{Bmatrix} \tag{21}$$

Based on a hybrid method which set $\theta = 1$ (fully implicit) for the equation 3 and $\theta = 0.5$ for equation 18 can lead to the following equation:

$$\begin{bmatrix} \mathbf{K}_m & \mathbf{K}_c \\ \mathbf{K}_c^T & -(\frac{\Delta t}{2}\mathbf{K}_P + \mathbf{K}_L) \end{bmatrix} \begin{Bmatrix} \mathbf{R}_1 \\ \mathbf{P}_1 \end{Bmatrix}$$

$$= \begin{bmatrix} \mathbf{0} & 0 \\ \mathbf{K}_c^T & \frac{\Delta t}{2}\mathbf{K}_P - \mathbf{K}_L \end{bmatrix} \begin{Bmatrix} \mathbf{R}_0 \\ \mathbf{P}_0 \end{Bmatrix} + \begin{Bmatrix} \mathbf{f} \\ \mathbf{0} \end{Bmatrix} \tag{22}$$

Here, let

$$\mathbf{K}_E = \begin{bmatrix} \mathbf{K}_m & \mathbf{K}_c \\ \mathbf{K}_c^T & -(\frac{\Delta t}{2}\mathbf{K}_P + \mathbf{K}_L) \end{bmatrix} \tag{23a}$$

$$\delta_1 = \begin{Bmatrix} \mathbf{R}_1 \\ \mathbf{P}_1 \end{Bmatrix} \tag{23b}$$

$$\mathbf{K}_D = \begin{bmatrix} \mathbf{0} & \mathbf{0} \\ \mathbf{K}_c^T & \frac{\Delta t}{2}\mathbf{K}_P - \mathbf{K}_L \end{bmatrix} \tag{23c}$$

$$\delta_o = \begin{Bmatrix} \mathbf{R}_o \\ \mathbf{P}_o \end{Bmatrix} \tag{23d}$$

$$\mathbf{f} = \begin{Bmatrix} f \\ 0 \end{Bmatrix} \tag{23e}$$

then, equation 22 becomes

$$\mathbf{K}_E \, \delta_1 = K_D \, \delta_0 + \mathbf{f} \tag{24}$$

By solving equation 24 for unknown $\mathbf{d}_1$, displacements and pore pressure at each node can be determined.

The physical data input in the problem are shown in the Table 1. The elastic modulus, Poisson's ratio (drained), and permeability are determined from the laboratory tests, while the undrained Poisson's ratio and Skempton's coefficient are based on the estimation. The averaging water-level in the area was from 2m in Wantang to 26m in Linpien counted from ground surface during August 1985 to May 1987.

In order to formulate a boundary value problem for analyses, it is necessary to define the following items: (a) the geometry; (b) the materials; (c) the loads; and (d) the boundary conditions. The mesh is divided into three different lithologies ranging from silty sand to clayey sand with a concave water-level (Fig. 5). The bottom of the mesh is constrained.

TABLE 1 Physical properties used in the mathematical model.

properties\ layers	*A	*B	*C
elastic modulus (10^7 kg/m^2)	0.21	0.49	0.42
Poisson's ratio (drained)	0.25	0.35	0.25
Poisson's ratio (undrained)	0.30	0.40	0.30
Skempton's coef.	1.0	1.0	1.0
x-permeability (10^5 m/day)	0.01	0.01	0.01
y-permeability (10^5 m/day)	0.1	0.1	0.1

* A- loose silty sand; B- compacted silty sand; C- clayey sand

in the vertical direction and only vertical displacements are allowed on the sides of the mesh. The pore pressure on the whole boundaries is relaxed and only the gravity load is considered in the study. It shows, the more declining of the water level, the more subsiding of the ground due to that the rock (or soil) grain subjected to more overburden pressure. The magnitude from computer modeling (Fig. 6) is greater than (around 1.5 of) those from field measurements (Fig. 2). However, the trend for subsiding is approximately the same in both cases.

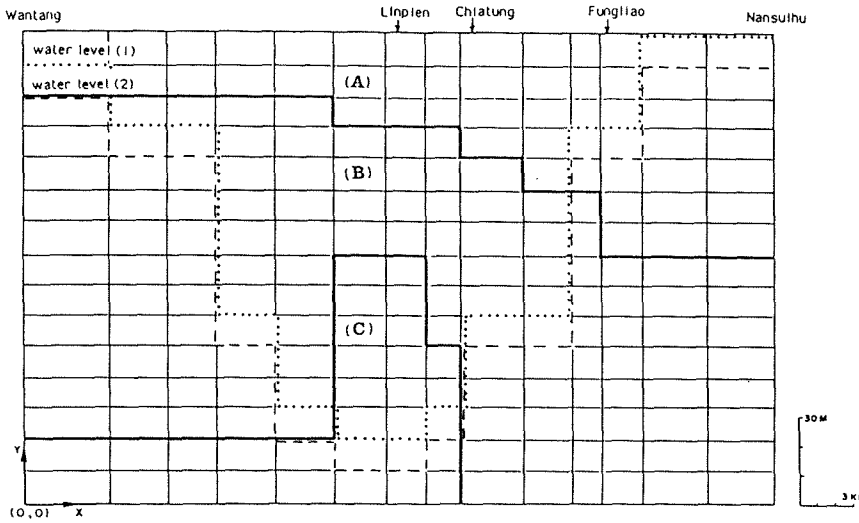

FIG. 5 Finite element mesh in the Pingtung Coastal Area.

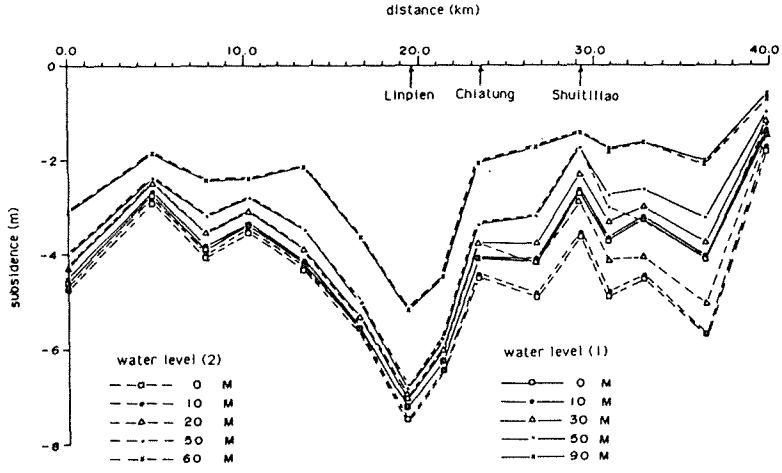

FIG. 6 Computational results from the mathematical modeling.

RESULTS OF FIELD MONITORING

Wire-flex extensometer (Fig. 7) with ten measured points is used to monitor the small deformations of the ground paralleling to the axis of borehole. The system designed by RocTest Inc. (Canada), is comprised of the three parts, which are

(a) mechanical head assembly (covering (1) to (4))
(b) rods and their protective tubing (covering (5) to (7))
(c) anchors ((8))

The anchors are fixed individually to the rods. The array of rods is protected by an external sheath which is in contact with the cement grout and allows for some displacement in shear. The deformations measured are the differences between the

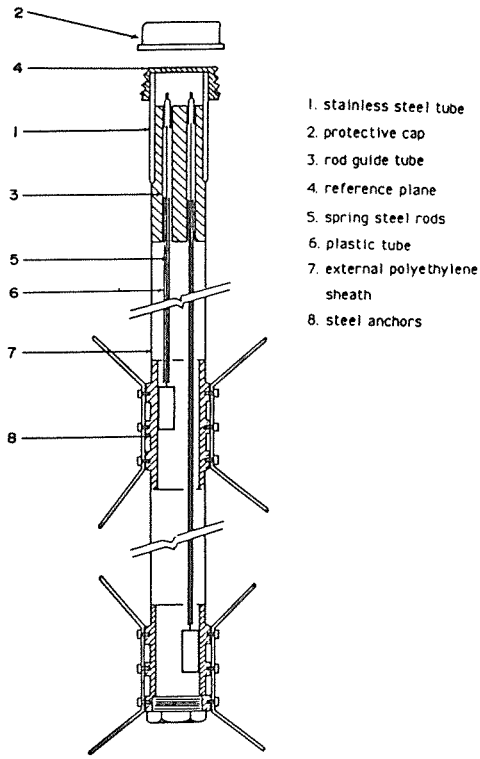

FIG. 7 Wire-flex Extensometer.

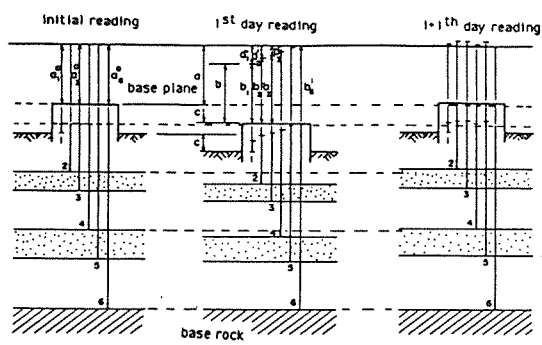

Assumptions:

1. spring steel rod = constant length
2. taking base plane as an initial reading
3. the deformation at the bottom of rods is responded from those in the tops of rods

" + " : rebound

" − " : compression

significance of reading:

. reading per day b^i_n ← i^{th} day, ↖ anchor No.

. subsidence based on initial reading

c^i

. deformation of rods

$d^i_n = b^i_n - a^i_n +/- c^i$

. deformation in each sublayer

$\Delta^i_n = d^i_{n-1} - d^i_{n(n=2-n)}$

$\Delta^i_1 = c^1 - d^i_1$

FIG. 8 Conceptual model for Wire-flex Extensometer.

movements of the deepest anchor and each anchor or head. The conceptual model is shown in Fig. 8. The Wire-flex system has been installed and started working since January 1988. The depth of key layer causing subsidence is expected in 50m counted from ground surface.

The subsidence of the individual layers can be observed clearly from multi-point wire line extensometer as shown in Fig. 9.

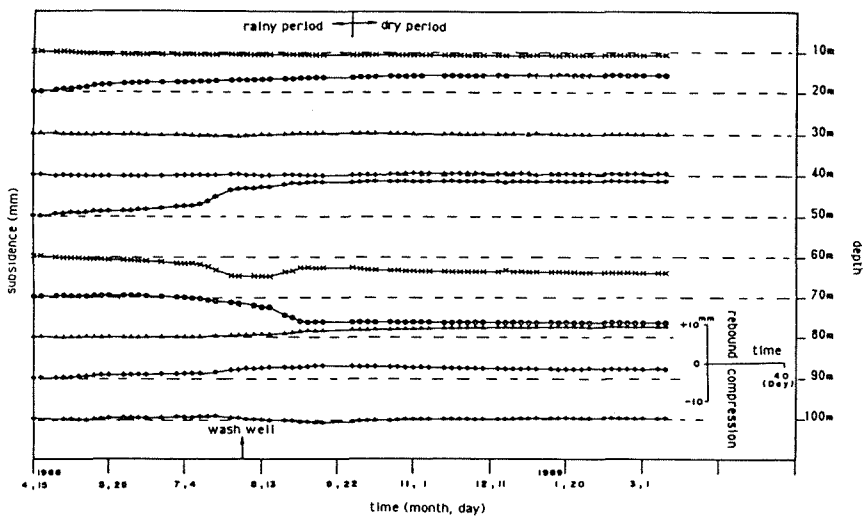

FIG. 9 Deformation in each sublayer from Wire-flex Extensometer at Wenfong monitoring well.

The compression and rebound of earth occurs in the interval of 40-70m at Wenfong. The rebound might be due to the stop to withdraw groundwater. Both the rebounded upper soil and compressed lower soil occurred at Shuitiliao and Linpien are also located in the depth of 40 to 70m. The deformation started to occur during the raising period of water level(i.e., rainy period) while there is no significant change in sublayer deformation during dry period. Besides the effects of water fluctuation in rainy and dry period, the sickness of shrimps which have activated since 1989 causes a less use of groundwater, it, thus, slows down the subsidence rate. The conceptual design of multilevel water-head observation system using piezometer is shown in Fig. 10. The piezometer was installed at depth of 10 to 68m. Each different interval, under which measurements of subsidence are conducted, is isolated and separated by bentonite. There are two water levels identified at Wenfong (Fig. 11). The first aquifer, between 10 to 20m, is composed of sandy clay or sandy silt. The water pressure is close to static condition. It, thus, shows the interval between 10 to 20m is not a key layer for withdrawing groundwater. The water fluctuation in this layer is around 1 to 4 m. The second aquifer is between 25 to 65m. The water pressure at this depth is lower than static pressure. Water fluctuation is more significant at this interval; it is, thus, projected that, the second aquifer is the key aquifer where the local resident is over pumping groundwater.

CONCLUSIONS

From the results of field monitoring, the subsidence rate in the investigation area has become alleviated since May 1988. The compression and rebound of earth are found at

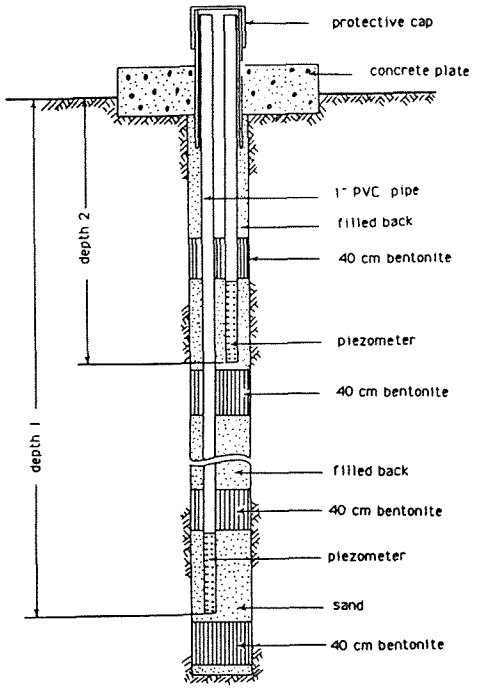

FIG. 10 Diagramatic cross-section for the monitoring well of multilevel water-head.

around the depth of 40 to 70m. The ground is predicted to be stable in the near future if not over pumping groundwater. The seawater intrusion is available in the near-shore area. The mathematical model fairly predicted the relations between the decline of water-level and ground subsidence.

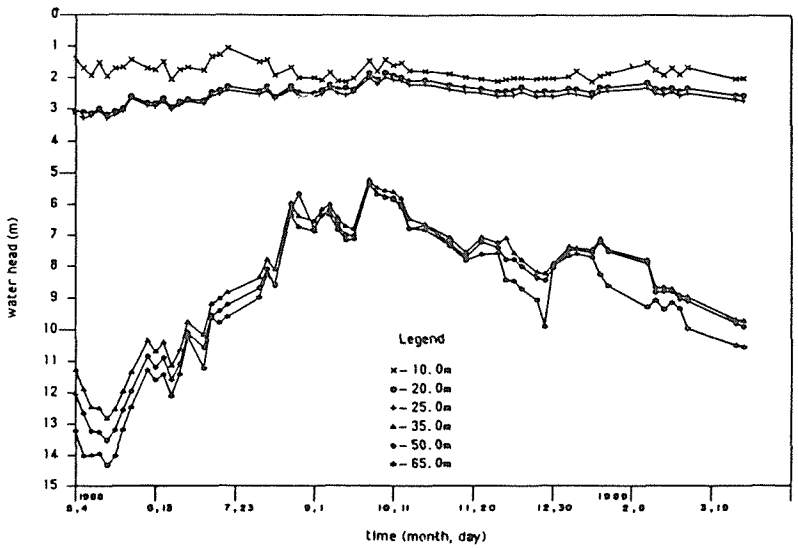

FIG. 11 Multilevel water head at Wenfong.

ACKNOWLEDGMENTS The authors would like to express their gratitude to the MOEA (Ministry of Economic Affairs) for its financial support through the research. Thanks are also due to TWCB (Taiwan Water Conservancy Bureau) for its valuable suggestions.

REFERENCES

Biot, M. A. (1941) General theory of three-dimensional consolidation. J. Appl. Phys., 12, 155-164.

Chang, C. C. (June 1985). The investigation of ground subsidence at Chiatung and Fungliao in Pingtung County. M. S. thesis, Dept. of Geography, National Taiwan Normal University .

Chern, H. F. (1984) The raise and subsidence of Taiwan Island based on the data of bench markes measurements. Central Geological Survey, No. 3, 127-140.

Davis, G. H. (1987) Land subsidence and sea level rise on the Atlantic Coastal Plain of the United States. Environ. Geol. Water Sci., 10, No. 2, 67-80.

Detournay, E. and J. C. Roegiers (April 1987) Poroelastic consolidations in in-situ stress determination. in "Forced Fluid Flow Through Strong Fractured Rock Mass", International Workshop held at the Centre de Formation de Garchy.

Energy & Resources Laboratories, ITRI (July 1988) Ground Subsidence Investigation, Final Report.

Ghaboussi J. and E. L. Wilson (1973) Flow of compressible fluid in porous elastic media. Int. J. Num. Meth. in Engng., 5, 419-442, 431.

Hsu, T. L. (1954) The topogrpahy of coastal mountain in East Taiwan and recent raising movement. Taiwan Provincial Geological Survey, No.7, 3-5.

Hsu, T. L. (1962) A study on the coastal geomorphology of Taiwan. Proc. Geol. Soc. China, No. 5, 29-45.

Hsu, T. L. (1980) The relations between the topography and the new structure of Taiwan. Geol. Soc. China, No. 23, 3-5.

Hsu, T.L. & M. S. Chai (1974) Coastal features of Northern Taiwan and their neotectoric significance. Proc. Geol. Soc. China, No. 17, 123-130.

Konishi, K., A. Omura, and T. Kimura (1968) ^{234}U - ^{230}Th dating of some late Quaternary coralline limestones from Southern Taiwan. Geology and Palaeontology of Southeast Asia, 5, 221-224.

Li, Y. H. (1976) Denudation of Taiwan Island since the Pliocene Epoch. Geology, 4, 105-107.

Liao, J. S. and B. C. Haimson (Nov. 27-29, 1989) Stability of near-surface excavations in weak rock. Symposium on Underground Excavations in Soils and Rocks, Including Earth Pressure Theories, Buried Structures and Tunnels , Bangkok, Thailand, Sponsored by Asian Institute of Technology (AIT) and Southeast Asian Geotechnical Society (SEAGS).

Lin, Y. T. (April 1986) Information on land subsidence in Coastal Areas of Taiwan. Council of Agriculature, Executive Yuan, R.O.C., p. 6.

Peng, T. H., Y. H. Li and F. T. Wu (1977) Tectonic uplift rates of the Taiwan Island since the early Holocene. Mem. Geol. Soc. China, No. 2, 57-69.

Poiand, J. F. (1984) Guidebook to studies of land subsidence due to groundwater withdrawal. United Nations Educational, Scientific and Cultural Organization, 8-10.

Rice, J. R. and M. P. Cleary (May 1976) Some basic stress diffusion solutions for fluid-saturated elastic porous media with compressible constituents. Review of Geophysics and Space Physics, 14, No. 2, 227-241.

Smith, I. M. (1982) Programming the finite element method with application to geomechanics. John Wiley & Sons, New York.

Taira, K. (1975) Holocence crustal movements in Taiwan as indicated by radiocarbon dating of morine fossils and driftwood. Tectonophysics, 28, T1-T5.

Taiwan Water Conservancy Bureau (June 1988) The monitoring of ground subsidence in Pingtung Coastal Area. Final Report.
Yang, W. C. (June 1987) The ground subsidence in Taiwan. The Symposium on Ground Subsidence in Taiwan (I), held in Taipei, Sponsored by Energy & Resources Laboratories, ITRI, p. 235.

Land Subsidence (Proceedings of the Fourth International Symposium on Land Subsidence, May 1991). IAHS Publ. no. 200, 1991.

Land Subsidence Due to Gas Extraction in the Northern Part of The Netherlands

JAN J.E. PÖTTGENS
State Supervision of the Mines
P.O. Box 90
NL-2280 AB Rijswijk, The Netherlands
FRITS J.J. BROUWER
Survey Department of Rijkswaterstaat
P.O. Box 5023
NL-2600 GA Delft, The Netherlands

ABSTRACT Via precision levelling the motion processes are monitored over the gasfields in the North of The Netherlands. Monitoring in relation to subsidence prognosis is important to take timely action to prevent or reduce damage as a result of subsidence. A description of the precise levelling is given with also an outlook how geodetic monitoring can be improved. In addition a method to statistically test various subsidence models as a result of reservoir compaction against actual subsidence is presented to be able to improve the prognosis.

INTRODUCTION

Due to the location of The Netherlands by the North Sea (N.B. 60% of the country lies below high tide level!), the dense infrastructure of towns, roads and waterways and the very intensive land use (375 inhabitants per km^2), the country is very vulnerable to land subsidence in general.
The most important kinds of damage that may occur due to land subsidence are:
- less production in farming and agriculture due to an increase of soil wetness;
- decrease of safety as a result of lower dikes and erosion of the dunes;
- ecological damage due to an other hydrological regime in the Waddenzee of currents and associated sand transport;
- decrease of quality of water management in the subsidence region.

After World War II, in The Netherlands large scale lowering of polder water levels has been applied to increase the carrying-capacity of the soil for agriculture. As a result of the fact that the upper soil of The Netherlands mainly consists of clay and peat, an unequal subsidence occured with structural damage to buildings at different places.

In 1964 the exploitation of natural gas started. The major part of the Dutch natural gas reserves are located in the two Northern Provinces, Groningen and Friesland, and under the Waddenzee (Fig. 1). The gas extraction causes in general a very slow and smooth subsidence. To prevent damage, measures are needed to adapt primarily the water management systems. To monitor the actual movements, over all gasfields in The Netherlands regularly precise levellings are made. The observed subsidence resulting from these levellings is composed of several factors:
- subsidence of the benchmark in a house or bridge due to the own mass of the construction, depending on the constitution of the soil;

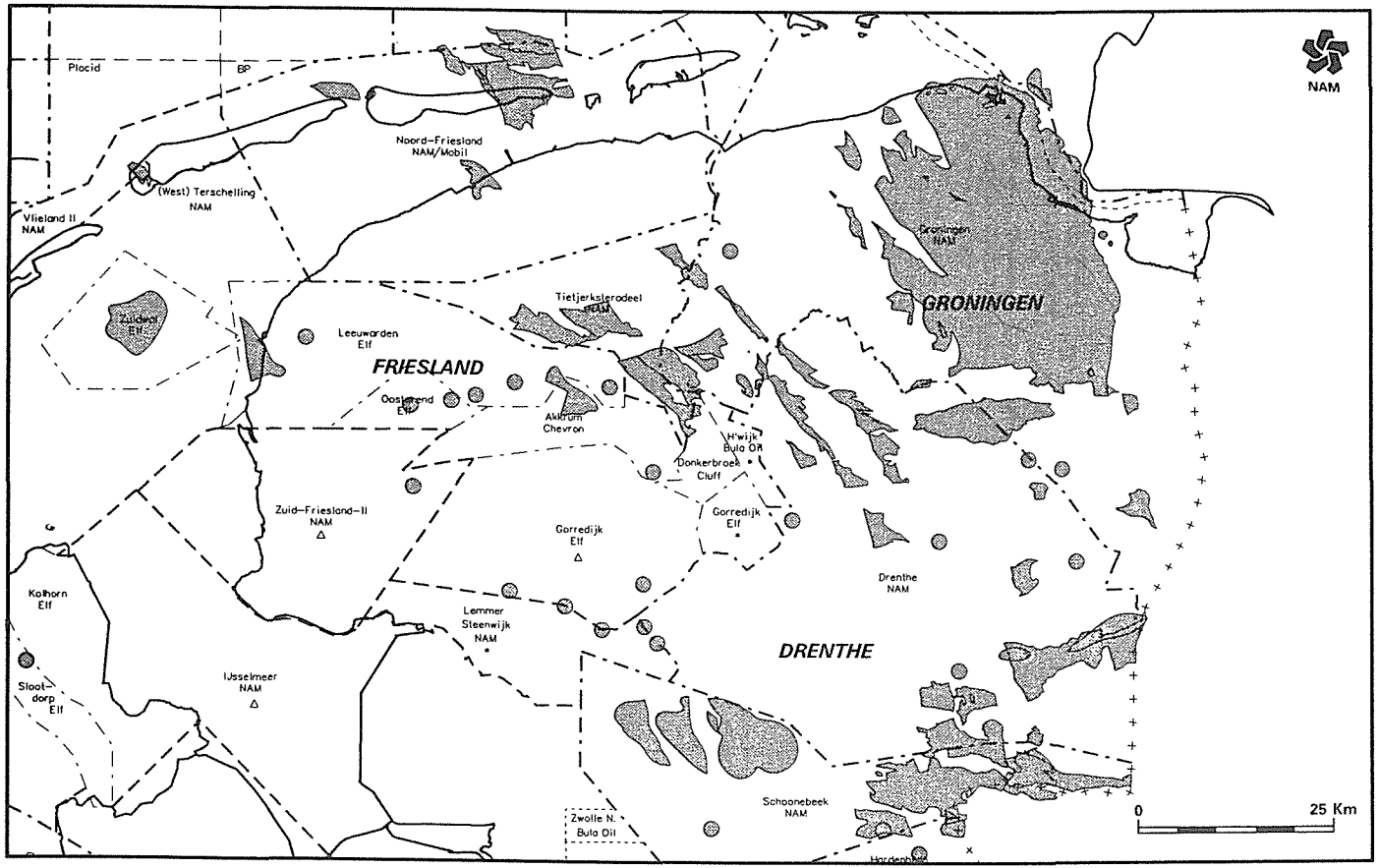

FIG. 1 Map of gasfields in the Northern part of The Netherlands.

- natural compaction of unconsolidated sediments of Holocene, Pleistocene or Tertiary;
- compaction in the Holocene layers due to changes in the hydrological regime as a result of adaptations of polder water levels;
- subsidence due to depressurization in the gasfield.

The major problem - both scientifically and practically in view of financial compensation for damage due to gas extraction - is the difficulty to separate the influences of the four factors. See e.g. Fig. 2 where the annual subsidence of benchmarks in Groningen is shown *before* the start of the gas extraction.

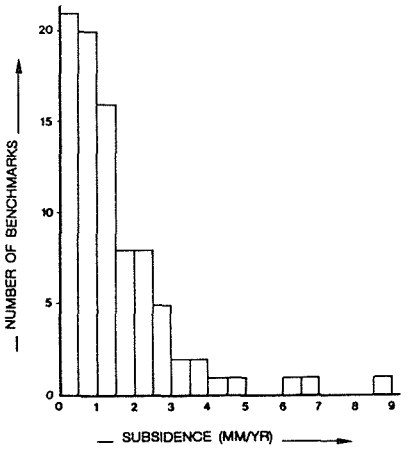

FIG. 2 Subsidence of the benchmarks in Groningen which were placed before 1965.

THE GRONINGEN GASFIELD LEVELLINGS

Background

Soon after the start of the production of natural gas from the Groningen gasfield, a first prediction was made of the land subsidence caused by the production. The originally predicted number was 100 cm for the centre of the field, the latest prediction of 1990, however, is 33-43 cm.
As a natural means to verify this prediction and to monitor actual subsidence, the State Supervision of the Mines (SodM), the responsible Government Agency, imposed the concessionaire (the Nederlandse Aardolie Maatschappij B.V., NAM) the organization of a regular series of levellings. These levellings should be executed conform the regulations of the Survey Department of Rijkswaterstaat (MD), who are in charge of the national NAP network (Amsterdam Height Datum). The actual procedure is now such that NAM instructs one (or more) private companies to measure the network in accordance with the MD measurement scheme. NAM itself measures the connections of the network to the underground benchmarks (OM) of the NAP, because of the extreme importance of maintaining a good connection to one's reference. Next, NAM computes the free network adjustment and the constrained adjustment to the OM, and MD verifies the results. Finally the findings are reported to SodM and the Province of Groningen.

Past Measurements

One can divide the levelling networks in two types: the so-called 'large' and 'small' networks. The smaller ones are somewhat less

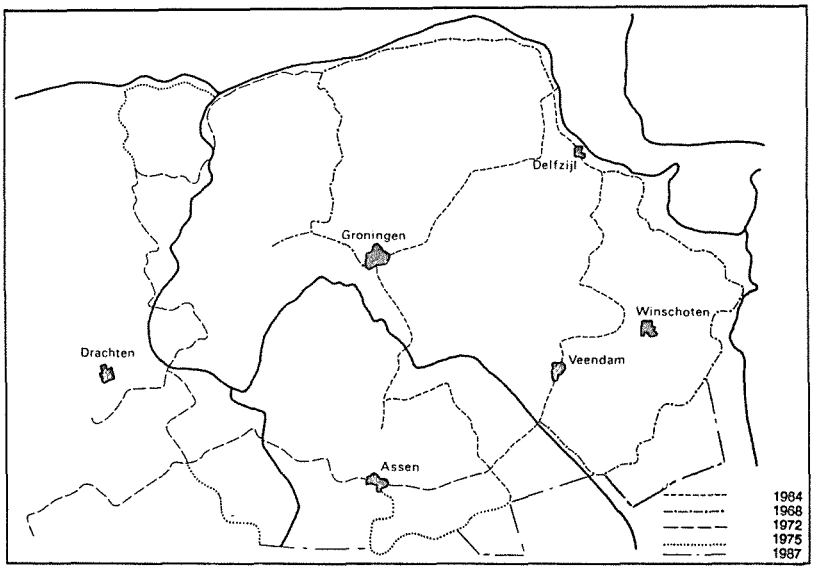

FIG. 3 Boundary of networks for subsequent levelling campaigns.

dense and of a smaller extent than the large ones. The latter have been observed in 1964 for the first time and subsequently in 1968, 1972, 1975, 1978, 1981 and 1987. Small ones have been observed in 1973, 1976, 1977, 1979, 1980, 1982, 1983, 1984, 1985, 1986, 1988, 1989 and 1990. A few numbers may illustrate the dimensions of the project: the last 'large' network had 1393 km of levelling sections and included some 2600 benchmarks; the 1989 'small' one consisted of 803 km.

The policy now is to measure a 'large' network every six years, which has not always been the case as one can see from the years mentioned above. Also the size of the network changed as the area of production and thus the area of land subsidence grew wider (Fig. 3). The measurements are made with invar rods and precise automatic levels.

This whole set-up makes a final adjustment of the network possible using an a priori standard deviation of 1 mm/$\sqrt{\text{Lkm}}$. [Verhoef & Brouwer, 1991].

Analysis Method

For the analysis by MD, section tolerances are checked; runs are formed from sections, with special emphasis on the selection of junction points and on levelling runs which are not part of closed loops. Next the closures per loop are computed, which is still a very powerful means to detect and restore (measuring) errors.
As a final result a free network adjustment (only one known height fixed) to detect any inconsistencies in the observed data and a constrained network adjustment are made. The latter serves to check on the stability of one's reference benchmarks and yields the final heights of all benchmarks of interest. These adjustment computations are made using the WSCAN-software suite, which performs a Least Squares adjustment, including quality control by statistical testing and reliability description on the basis of conventional alternative hypotheses, as developed by the Delft Geodetic Computing Centre [Teunissen, 1988]. NAM follows the same computational strategy, using

its own software. The whole procedure is fully automated, but still takes a lot of time when errors are suspected and have to be found and restored. And so far no network ever was without errors, as should be the case when collecting some 120.000 raw observations!

Results

All finally computed heights of relevant benchmarks are stored in the ORSNAP database of MD. At present the actual land subsidence is assessed by comparing the heights of benchmarks following from the 1964 (reference) network to the ones computed from the newest levellings, by simple subtraction, i.e. a so-called *static* approach. The subsidence is visualized - as a final product to SodM and the Province of Groningen - in three ways:

- a contour map with iso-subsidence lines (Fig. 4);
- selected profiles, following from levelling runs (Fig. 5);
- separate subsidence diagrams of some benchmarks.

The accuracy of the presented subsidence is of course a function of the standard deviation of the height determination. Using the 1 mm/$\sqrt{\text{Lkm}}$ assumption, for most benchmarks the standard deviation of the estimated heights is between 2-5 mm, relative to the chosen datum point (Gasselte). In view of this number, for the interpretation of the subsidence, it should be noted that the difference in height between two epochs should be at least 1 cm to be statistically significant.

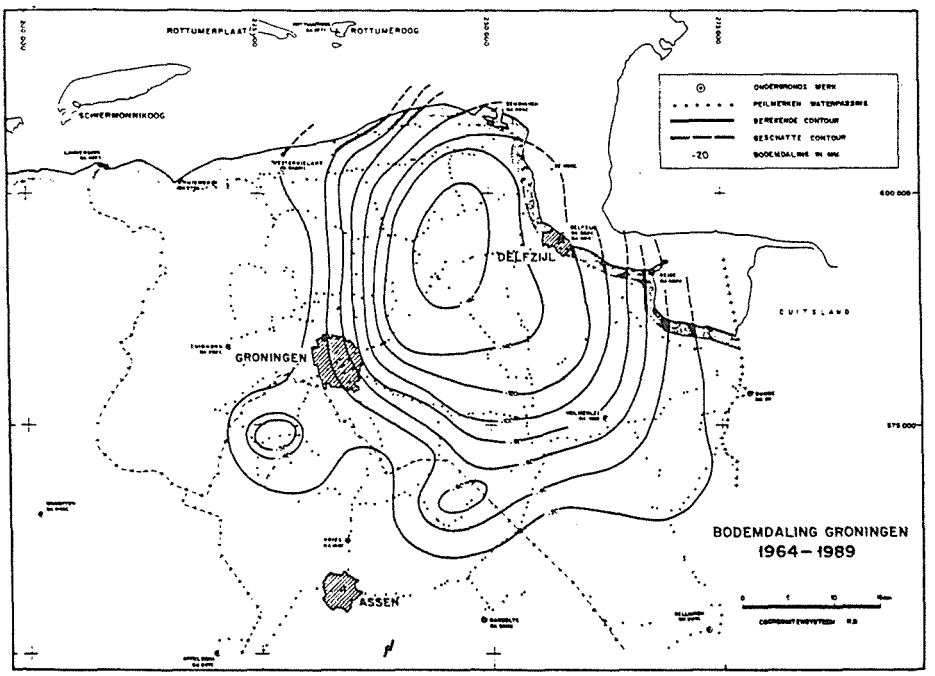

FIG. 4 Contour plot of subsidence.

OUTLOOK FOR GEODETIC TECHNIQUES

As concerned to levelling there are still a number of problems to be solved.

A. Stability of underground benchmarks (OM).
It is obvious that OM within the subsidence area are not usable

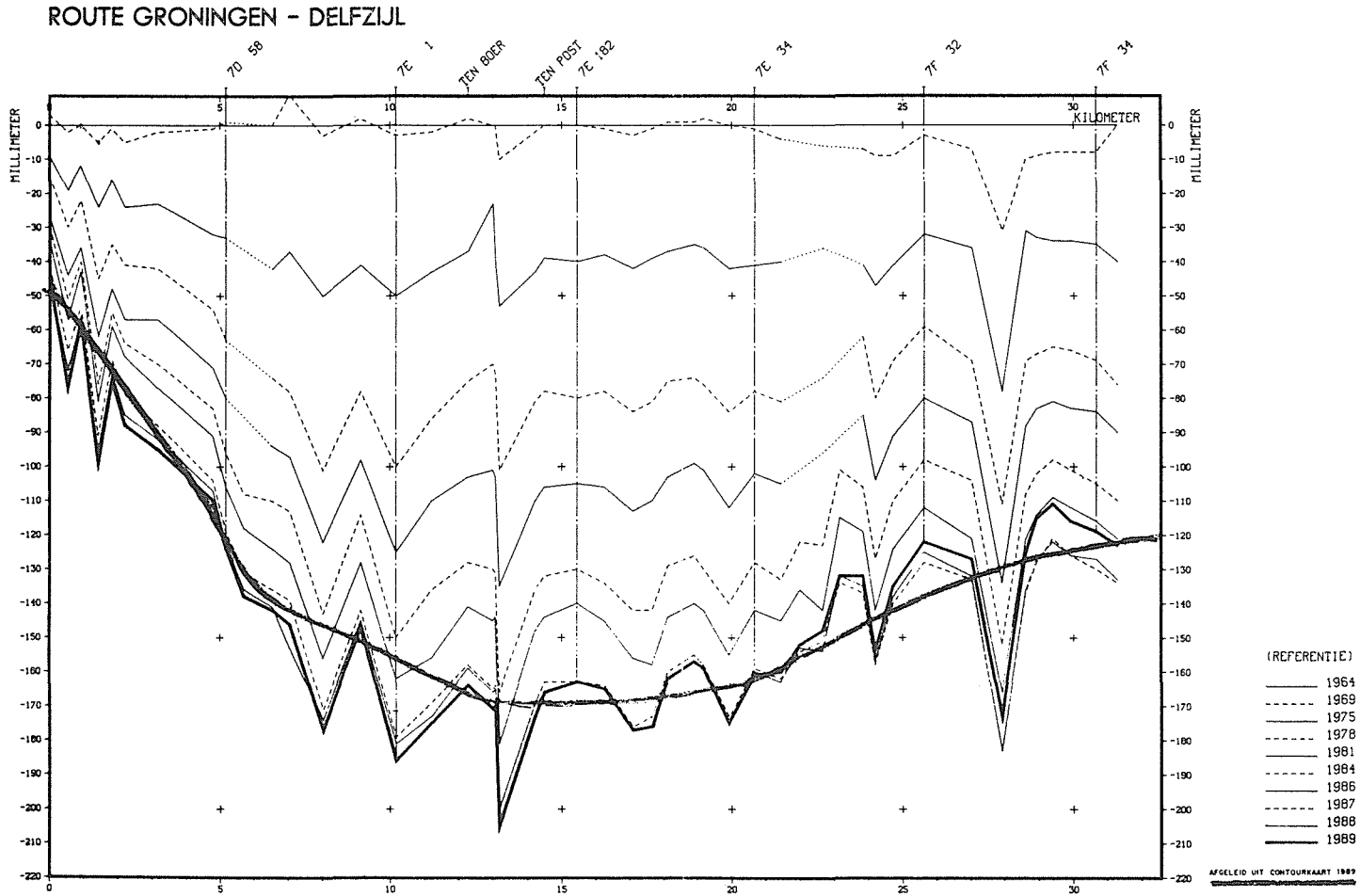

FIG. 5 Example of levelling profiles.

to serve as a reference. However, also the OM outside the area are not free of motions, due to e.g. geological processes or influence of groundwater extraction [Groenewoud et al., 1991]. What is therefore a safe way to assess stability of the OM?

B. Local instability of benchmarks.
Some benchmarks show a very deviating subsidence from its surroundings. Very probably this tells more about the foundations of the building where the benchmark is located than about subsidence due to gas extraction. However, it poses the very real problem to discern between different causes of motion: is it a trend or a local disturbance?

C. New benchmarks.
In The Netherlands some small percentage of the benchmarks disappear each year. Replacements are of course installed. However, the problem still remains to connect old and new benchmarks, and to avoid the introduction of 'fictive' heights at epoch 1964 for benchmarks installed only after 1964.

To tackle these kinds of problems, recently the MD, NAM and the Geodetic Computing Centre of the Delft University of Technology joined forces to perform a completely new analysis of all levelling data of the Groningen gasfield using another computing method, the so-called *kinematic* adjustment. In a kinematic adjustment next to heights of stations at a certain epoch, also velocities and where required accelerations are estimated, according to specified models: linear, polynomials, splines, etc. For this purpose also new software will be developed.

The objective is to improve our knowledge about the actual subsidence over the Groningen gasfield by solving the problems mentioned above on the one hand and to improve the quality description of the results in terms of precision and reliability on the other hand [Teunissen, 1988].

A quite other aspect concerning the outlook, is the application of GPS (Global Positioning System), the satellite navigation and positioning system of the U.S. Department of Defense. Measurements with geodetic - i.e.(sub)cm - precision to determine height differences are possible by working in a differential mode, even on long distances [Ashkenazi et al., 1990; Groenewoud & Brouwer, 1991].

The use of GPS for determining land subsidence in Groningen offers two attractive possibilities. Firstly, GPS is competitive to spirit levelling in a economical sense: measurements can be made faster - and thus cheaper - and one needs not to determine the heights of a lot of stations in between, which are not of relevance to the subsidence problem. This also means that stable reference benchmarks can be chosen further away from the subsidence area. In addition, the subsidence is essentially a pure deformation problem, so that uncertainty about the geoid - to which levelling refers - is irrelevant.

Secondly, the verification of models is of interest. The prognosis models for reservoir compaction predict a horizontal motion at the surface for the rim of the gas reservoir of 50% of the vertical motion. Three-dimensional GPS measurements can thus verify the prediction models integrally!

Investigations of how exactly to set up a GPS control network for the Groningen gasfield have just started.

PROGNOSIS OF SUBSIDENCE

The Mine Act demands at regular intervals (mostly 5 years) a prognosis of the subsidence for the Dutch gasfields, on the basis of the

most recent geological and mine engineering information. To compute the reservoir compaction and the resulting subsidence of the surface, the following input parameters are used:
- dimension of the reservoir (extension, depth and thickness);
- depressurization in the reservoir;
- uniaxial compaction coefficient C_m;
- permeability of the rock formation.

In the computing model, the gasfield is divided into blocks by an orthogonal coordinate grid. In addition, every block has a vertical division into layers. To compute the expected subsidence of the surface, all characteristic parameters of the reservoir per subblock are specified, and next both a "nucleus of strain" [Van Opstal, 1973] and a finite element [Thomas, 1984] approach are used. In 1990 NAM made its last prognosis in cooperation with KSEPL (Royal Dutch/Shell Exploration and Production Laboratory). This prognosis stated that the subsidence in the centre of the field would be between 33 and 43 cm in the year 2050, with 36 cm as the most probable value. The diameter of the subsidence bowl within the 2 cm subsidence contour would be approx. 60 km.

Here, the subsidence for the year 1989 according to the model is presented for the levelling line Groningen-Delfzijl as a solid line (Fig. 5). It is obvious that the measured subsidence deviates considerably at some benchmarks from the model. Further research is needed to assess whether deviations are the result of local effects in the undeep underground or that they follow from uneven compaction along fault surfaces in the gas reservoir.

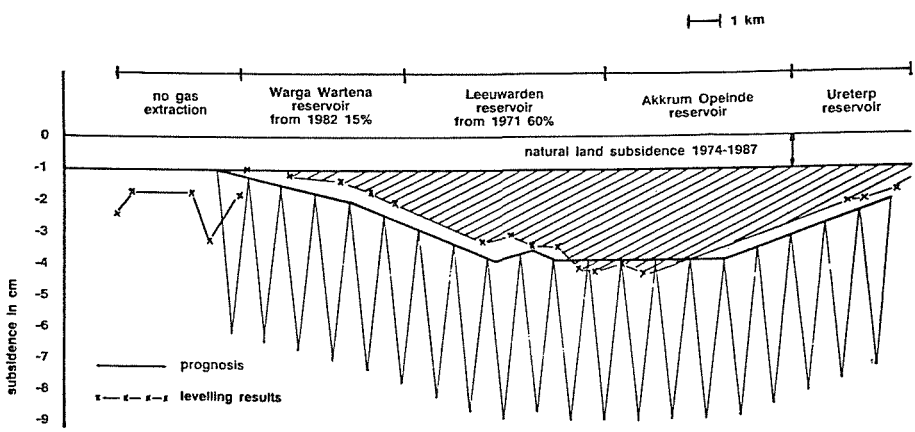

FIG. 6 Comparison of levelling results and model prediction.

TEST PROCEDURE FOR SUBSIDENCE MODELS

Using statistical techniques, an attempt is made to ascertain what motion hypothesis most resembles the actually observed subsidence, taking into account the stochasticity of the heights of benchmarks determined from levelling. As an example the levelling line Warga - Ureterp (Fig. 6) is used [Pöttgens, 1989]. On the basis of the above mentioned linear elastic model a prognosis for subsidence in the period 1974-1987 is shown by the solid line. The actually observed subsidence is shown by the dashed line. Fig. 6 shows generally a clear relation between the subsidence of benchmarks at the surface and the gas extraction at greater depths. To have a statistical measure for the conformity of the two datasets, standard deviation

(s) and mean (x) of the difference at all benchmarks are computed. Then the test quantity $t=|x|\sqrt{(n-1)}/s$ is formed. This t has a Student distribution with expectation zero. As an alternative for the linear elastic model, the subsidence model of the unequal zig-zag line at the bottom of Fig. 6 is hypothesized, which was at some point suggested in the press ("lightnings"). The results of statistical testing for both motion hypotheses are shown in Table 1.

TABLE 1 Student test of motion hypotheses.

	Linear elastic motion model	Unequal zig-zag motion model
Number of benchmarks	16	16
Mean difference observed minus model	-2.30	-25.01
Standard deviation observed minus model	3.59	16.29
Student test statistic	2.48	5.94

Comparing the resulting test statistics with Student's critical values shows that the second hypothesis is more than 99,9% improbable, whereas an almost smooth subsidence in large areas is very likely.
All levelling line results are now confronted with the most recent models of the prognosis to have a better insight in the actual processes.

CONCLUSIONS

On the basis of the combined knowledge of rock mechanics, reservoir science and geodesy, as presented in the previous sections and many more studies of other aspects connected to surface subsidence in the North of The Netherlands, e.g. [Theeuw, 1973] and [De Waal,1986], it can be stated that:

1. The geodetic measurements of the surface subsidence are reliable;
2. In general the levelling results and the prognosis on the basis of a linear elastic computing model are in correspondence;
3. Major deviations between model and observed height changes can mostly be explained by local factors, and are often related to changes in the water management system in combination with an inhomogeneous composition of the undeep subsoil.
4. Geodetic and geological knowledge as a result of the Groningen gasfield levellings and associated actions are also very valuable for the study of the natural, regional subsidence in The Netherlands [Groenewoud et al., 1991]. The latter is also closely related to the reliable prediction of relative sea level rise and its consequences for the low country by the North Sea, called The Netherlands.

REFERENCES

Ashkenazi, V. & G. Ffoulkes-Jones (1990) Millimeters over hundreds of kilometers by GPS. GPS World, November/December 1990.
Groenewoud, W. & F.J.J. Brouwer (1991) NEREF: a new 3-D reference frame for The Netherlands. In: (Eds.: H. Pelzer & A. Witte) Precise Vertical Positioning. DÜmmler Verlag, Bonn.

Groenewoud, W., G.K. Lorenz, F.J.J. Brouwer & R.E. Molendijk (1991) Geodetic Determination of Recent Land Subsidence in The Netherlands. Proceedings of the Fourth International Symposium on Land Subsidence, Houston, Texas, USA, 12-18 May 1991.

Opstal, G.H.C. van (1973) The effect of base rock rigidity on subsidence due to reservoir compaction. Proceedings of the Third Congress of the International Society of Rock Mechanics, Denver, National Academy of Sciences, Washington D.C., part B.

Pöttgens, J.J.E. (1989) Deformatie boven gasvelden + bijlagen. Report of the State Supervision of the Mines.

Teunissen, P.J.G. (1988) Mathematical Geodesy I+II, lecture notes, Delft Geodetic Computing Centre (LGR), Faculty of Geodesy, Delft University of Technology.

Thomas, J.N. (1984) An improved accelerated initial stress procedure for elasto-plastic finite element analysis. International Journal for numerical and analytical methods in geomechanics, Vol. 8, 359-379.

Verhoef, H.M.E. & F.J.J. Brouwer (1991) Some Reliability Aspects of the Kinematic Modelling of Land Subsidence. In: (Eds.: H. Pelzer & A. Witte) Precise Vertical Positioning. Dümmler Verlag, Bonn.

Waal, J.A. de (1986) On the rate type compaction behaviour of sandstone reservoir rock. PhD dissertation, Delft University of Technology, The Netherlands.

Land Subsidence (Proceedings of the Fourth International Symposium on Land Subsidence, May 1991). IAHS Publ. no. 200, 1991.

Surface Subsidence in Natural Gas Fields

T. ESAKI & K. SHIKATA
Kyushu University, Fukuoka, 812, Japan
K. AOKI
National Research Institute for Pollution and Resources, Tsukuba, 305, Japan
T. KIMURA
The National Research Institute for Environmental Studies, Tsukuba, 305, Japan

ABSTRACT A large volume of ground water, which contained water-soluble natural gas, has been pumped from a certain aquifer system. The volume of pumpage water was increased step by step. Surface subsidence has occurred due to the subsequent decline in groundwater level. A quasi-three dimensional simulating system has been developed and applied to evaluate the aquifer system. The simulating system consists of a quasi-three dimensional finite-element computer program for simulating groundwater flow and an influence function method to estimate the incidental land subsidence. Contour maps of water level and land subsidence can have also been obtained. This system gives useful simulation results based on past, present and future conditions and has contributes for development without environmental hindrance.

INTRODUCTION

In Japan, natural gas is coming into wide use as energy for power plants, public use, and so on. The development of domestic natural gas fields has been accelerated, yet most of natural gas demand in Japan is now served by other countries. The gas field examined in this paper is one of the largest ones in Japan, located in the northern area of the Miyazaki Plain in Kyushu island as shown in Fig.1. During the 16 years, about 50 wells have been developed at intervals of roughly 500m in an area of 40km^2. The geologic formation of the aquifer system is classified into seven layers, which involves two sandy gas beds, Pliocene age, and intermediate between muddy beds. The sandy ones contain water-soluble natural gas and concentrated iodine. These layers are 180-310m, 400-490m in thickness, respectively. The daily volume of pumpage water has increased from 6,600kl in 1975 to 7,700kl in 1989. The subsequent decline in water level results in a corresponding increase in effective stress on the sandy layer sequence in the aquifer system. The compaction of the permeable layers affects the above layers in succession. As a result, land subsidence has occurred at the surface.

Due to these circumstances, it is necessary to predict the ground movement and to consider how to minimize the movement from the viewpoint of environmental control. In this study, a new environmental

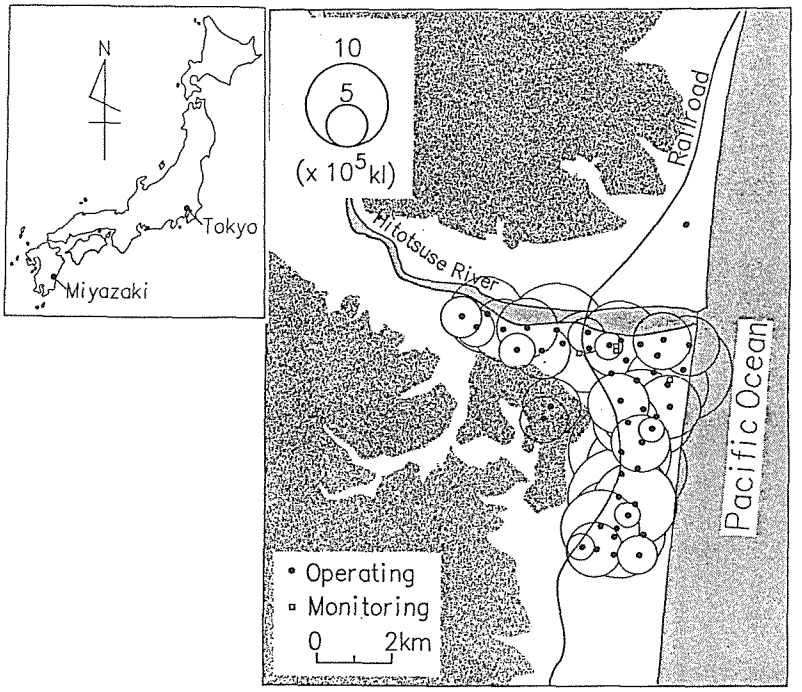

FIG. 1 Distribution of operating and monitoring gas wells and total volume of pumpage water from 1974 to 1988.

system which can predict and check surface subsidence is proposed. This analytical method consists of two stages:

(a) Water flow analysis by the finite element technique gives the distribution of water level in a gas seam;
(b) The gas seam deformation is given by the above calculated change of water level head. Nextly, by using Influence function method, the surface subsidence due to the gas seam deformation at arbitrary points can be obtained.

This new analytical system is applied to the Miyazaki gas field.

QUASI-THREE DIMENSIONAL GROUNDWATER FLOW - SUBSIDENCE COUPLING SIMULATION SYSTEM

For a long time, many studies for groundwater flow and land subsidence due to discharge of water have been done at different water withdrawal sites (e.g. Nishida et al., 1981). Evaluating aquifer compaction has been the object of most studies, and the amount of land subsidence was usually assumed to be equivalent to this aquifer deformation. However, land subsidence will occur as a result of three-dimensional propagation of the deformation of aquifer, characterized by an influence factor within a limit angle, as shown in Fig.2. In this paper, groundwater flow, aquifer compaction, and land subsidence are systematically simulated using a quasi-three dimensional simulation system, which is formed by combining the following three stages:

(a) Simulation of groundwater flow and the water-level decline due to

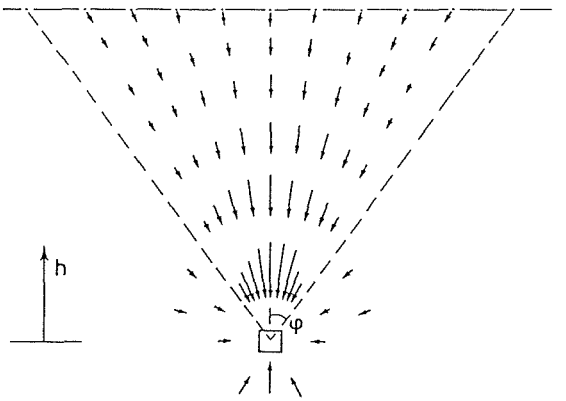

FIG. 2 Movement of points within a circular cone of the overlying rock mass caused by a deformation of an element (after Kratzsch, 1983).

water pumpage from the aquifer system are given using a quasi-three dimensional finite element computer program. The program can consider the depth of aquifer, which is based on the following equation:

$$K\frac{\partial^2 H}{\partial x^2}+K\frac{\partial^2 H}{\partial y^2}+Q=0 \tag{1}$$

where K is permeability in the x and y directions, H(x,y) is hydraulic head, and Q is discharge rate. The model uses a square grid with a certain horizontal spacing. This size of spacing is dependent on the nature of the problem.

(b) The decline in water level is directly related to the increase in effective stress, while the total stress on the solid phase of the ground remains constant. So the gas seam compaction is caused by this increase of effective pressure. While most analytical methods for predicting subsidence are based on the well-known Terzaghi's consolidation theory which is suitable for cases of relatively shallow and/or unconsolidated strata such as soft clay, the proposed method is based on the assumption that elastic behavior dominates for the relatively deep and/or compact strata. In other words, the calculation of the gas seam deformation is based on generalized Hooke's law:

$$d=\left(\frac{m}{E}\right)(1-2\nu)\gamma g\Delta H \tag{2}$$

where s is deformation of gas seam, m is thickness of gas seam, E is young's modulus of gas seam, ν is Poisson's ratio of gas seam, γg is unit weight of water containing natural gas, and ΔH is the amount of water level decline in the aquifer system. This is for a single seam. If there are multiple gas seams, we have to sum up the effects of each gas seam deformation.

(c) Surface subsidence is not proportional to the decline in water level in the aquifer system, while the gas seam deformation is. This is because the influence of gas seam deformation at a certain depth propagates and spreads three-dimensionally to surface. Surface subsidence attributed to gas seam compaction is obtained by the influence function method, which is a three dimensional method that can be used to obtain displacement at a large number of points and distribution of subsidence both accurately and efficiently (Esaki et al., 1987).

$$s = e \times a \times d \times z \tag{3}$$

where s is land subsidence at a point, e is an influence factor, a is coefficient of subsidence, d is amount of seam compaction, and z is a time factor. And when analyzing a gas field in which many wells have been developed one by one, time factors should also be considered. Surface subsidence increases over long periods of time, while the change in water level is small except for the initial steep loss of head. It is shown that surface subsidence is related to both the change in water level and the time since development. The time factor should be used appropriately.

PRACTICAL APPLICATION

In Japan since 1932, groundwater containing natural gas has been pumped in different places, such as Hokkaido, Chiba, Niigata, Miyazaki, and Okinawa. Following the advance of industry, the amount of pumpage water and extracted natural gas have increased rapidly. The overdevelopment of groundwater and natural gas has resulted in a type of mining damage, i.e. land subsidence. Especially in Niigata, subsidence has exceeded 50cm per year, and in Chiba the total subsidence since 1961 amounts to over 100cm. However, the subsidence phenomena have decreased steadily since 1970 when laws and ordinances restricting the groundwater usage were established (Yamamoto & Kobayashi, 1984).

The area studied here is located in the northern portion of the Miyazaki Plain in Kyushu, southern Japan. This area is alluvial lowland, approximately 20km long and 2km wide facing the Pacific Ocean in the east and divided by the river Hitotsuse into northern and southern regions. The typical geological sequence underlying this area is shown in Table 1.

TABLE 1 The typical geological sequence underlying the study area.

Depth	Bed		
surface-300m	Takanabe	muddy	impermeable
300-600m	Sadohara	sandy	permeable (gas seam)
600-1100m	Niinazume	muddy	impermeable
1100-1500m	Uryuno	sandy	permeable (gas seam)
1500-	Ikime	muddy	impermeable

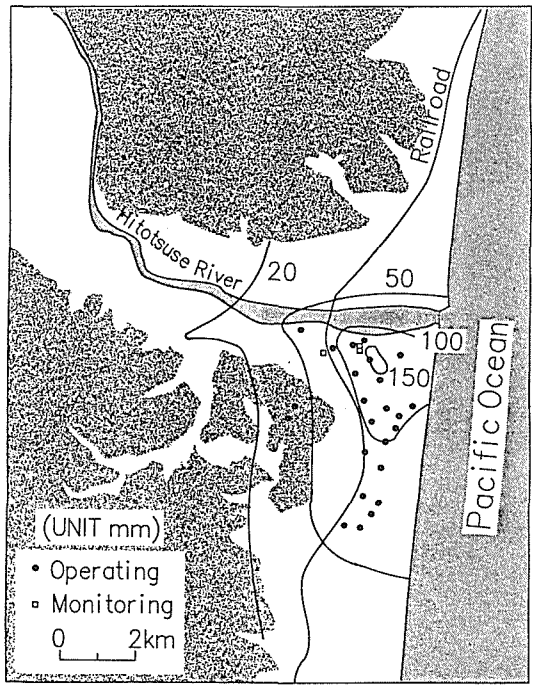

FIG. 3-a Measured contour map of subsidence from 1974 to 1978.

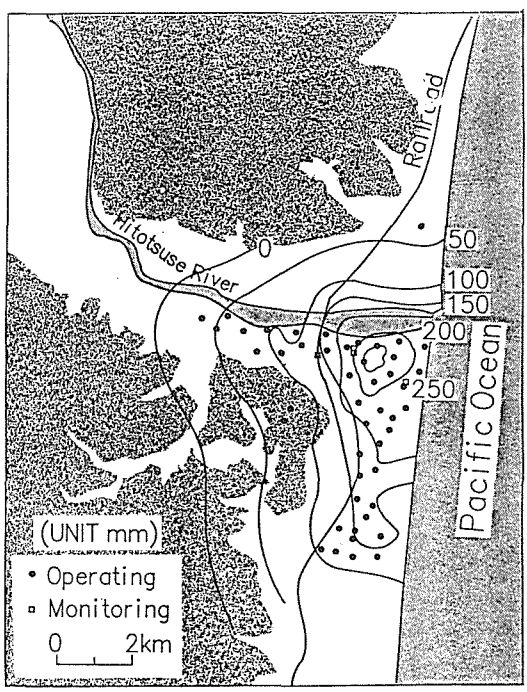

FIG. 3-b Measured contour map of subsidence from 1974 to 1988.

That is, this geological formation has packed groundwater containing water-soluble natural gas and allows no natural recharge to the aquifer system. The locations of 47 operating wells are shown in Fig.3-a and Fig.3-b. Each well is located at intervals of roughly 500m, at depths of 400-1,300m. In 1989, the daily volume of pumpage water and extracted natural gas amounted to 7,700kl and 11,300Nm3, respectively. The subsequent decline in water level results in a corresponding increase in effective stress on the sandy layer sequence in the aquifer system. The compaction of the permeable layers affects the above layers three dimensionally. As a result, shown in Fig.3-a and Fig.3-b, land subsidence has occurred in the vicinity of well field.

First, the distribution of water level decline was evaluated using a quasi-three dimensional computer program, under the following conditions:

(a) initial condition: water level at all nodes is the surface.
(b) boundary condition: water level at boundary nodes is the surface.

Input data for water head decline at each of the wells were modified according to Thiem's equation:

$$\Delta h_w = \frac{Q}{2\pi \times K \times m} ln\left(\frac{R}{r}\right) \tag{4}$$

where Δhw is local drawdown, Q is discharge rate, K is a permeability index, r is radius, and R is the influence limit. In the case that the upper seam of the aquifer system is of low permeability, the water level in the vicinity of well will decline locally and intensively(as shown in Fig.4). Some input data are modified according to the interval of grids.

Hydraulic properties used as input data were deduced from laboratory tests, which are shown in Table 2.

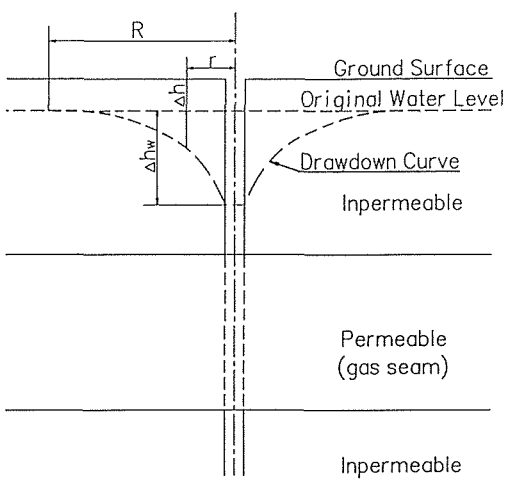

FIG. 4 Schematic diagram showing variation in drawdown curve due to the extraction of water containing natural gas.

TABLE 2 Hydraulic properties.

Seam	m(m)	E(kg/cm^2)	ν	K(cm/sec)
Sadohara	240	$2x10^4$	0.25	$4x10^{-5}$
Uryuno	480	$4x10^4$	0.25	$4x10^{-5}$

Interatively, a contour map of water level, which was obtained by the post-processing program, was proportional to the contribution of gas seam deformations. This was done because water level withdrawal will lead the increase of effective stress in the aquifer system, and gas seam compaction will be caused by the stress increase. The gas seam deformation was estimated by equation 2.

Next, land subsidence caused by the seam compaction was obtained using an influence function method. The program used is performed in three steps:

(a) a pre-processor for data input together with a digitizer, accurately reproduces the irregular layout of the water level contour map;
(b) a main-processor calculates the influence coefficient of each point on the surface, at 25m intervals;
(c) a post-processor graphically displays the computed results.

Fig.5-a shows the contour map for the predicted land subsidence four years after development in 1978. Fig.5-b is after 14 years, 1988. The shape of the contour lines is fairly similar with one of the field data in Fig.3-a and Fig.3-b.

As shown in Fig.5-a and Fig.5-b, subsidence is large where the volume of pumpage water is relatively large(Fig.1). Even if the pumpage volume is similar, the time lag since development may affect the subsidence phenomena. In order to cope with this condition, a time factor was applied, according to the period since development and the decline in water level. This procedure was also applied to the two profiles shown in Fig.6 and Fig.7, which compare field data and predicted subsidence in 1988, according to cross sections A-A' and B-B'. This system provides the simulation of land subsidence in the aquifer system appropriately. The differences in shape of two profiles, can be attributed to local variance in the local geological structure, e.g. small faults or the depth of alluvium.

SUBSIDENCE MONITORING AND ENVIRONMENTAL CONTROL

In order to protect surface affairs from subsidence and to develop valuable domestic resources in agreement with local inhabitants, the Technical Committee for natural gas development has been established at Kyushu Branch of MITI in 1974, just before development of the Miyazaki field. By recommendation from the committee, level surveying(126 measuring points over a total length of 53km), measuring of ground water level at the monitoring wells(four wells: one 1300m and three 60m), and prediction of subsidence have been carried out in collaboration with the authorities and the mining company every year.

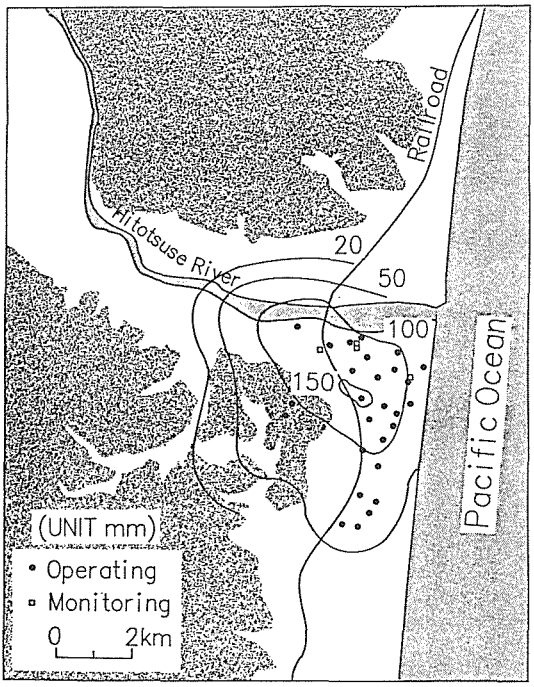

FIG. 5-a Calculated contour map of subsidence from 1974 to 1978.

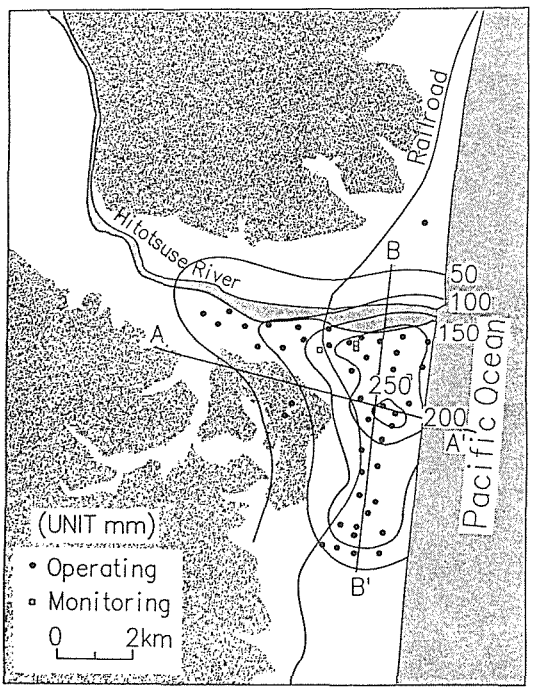

FIG. 5-b Calculated contour map of subsidence from 1974 to 1988.

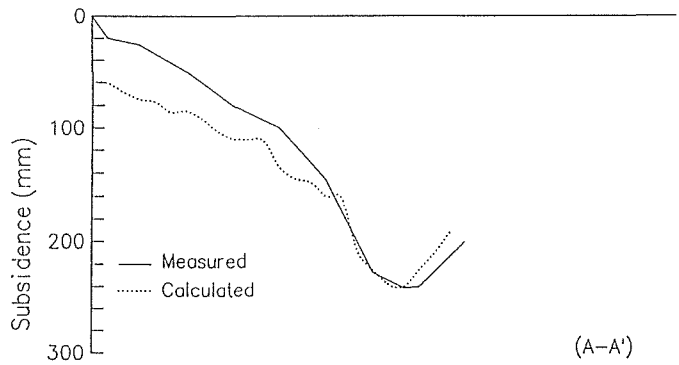

FIG. 6 Subsidence profile from 1974 to 1988(section A-A').

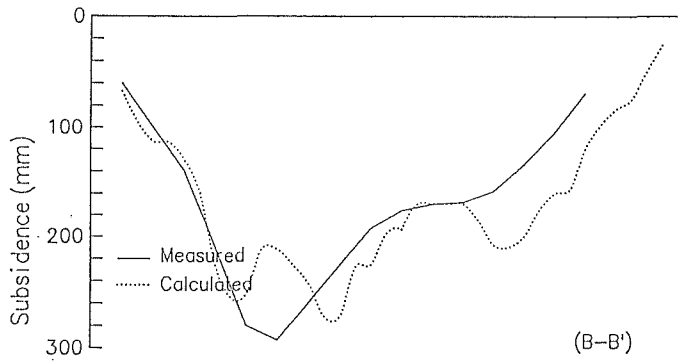

FIG. 7 Subsidence profile from 1974 to 1988(section B-B').

The progress of ground water withdraw and subsidence has been checked and the simulation system also has been modified several times following the field data. During the 14 years since the beginning of operation, subsidence has been restricted to within 30mm per year and withdraw of each well has also within 200m from sea level. In the next decade, 20 new wells are planning in the northern field. The committee will continue to make efforts at environmental control by the use of monitoring system.

CONCLUSION

The interrelation between the volume of pumpage water, groundwater flow, aquifer compaction, and land subsidence can be clarified and simulated according to an aquifer system with dominantly elastic character. This system will also be able to predict the future conditions, which is useful for developing new wells in the northern field.

ACKNOWLEDGMENT

The authors are much indebted to the staffs of the Ministry of

International Trade and Industry in Japan and Ise Chemical Industries Co. Ltd. for providing the valuable data and to Associate Professor M. Nishigaki, Okayama University, offering us PC-GWAPG computer program.

REFERENCES

Esaki, T., Kameda, N., Nishida, T., Kimura, T., & Shikata, K. (1987) Subsidence analysis for complex irregular tabular extraction by use of personal computer. Proc. 7th Japan Symp. on rock mechanics, 413-418.

Kratzsch, H. (1983) Mining Subsidence Engineering. Springer-Verlag, 74-91.

Nishida, T., Esaki, T., Aoki, K., & Kameda, N. (1981) On the surface subsidence in natural gas fields. Proc. Int. Symp. on weak rock, 701-705.

Yamamoto, S. & Kobayashi, A. (1984) Groundwater resources in Japan with special reference to its use and conservation. Proc. 7th Japan Symp. on rock mechanics, 381-389.

Land Subsidence (Proceedings of the Fourth International Symposium on Land Subsidence, May 1991). IAHS Publ. no. 200, 1991.

Numerical Analysis of Land Subsidence at Ravenna Due to Water Withdrawal and Gas Removal

G. GAMBOLATI & G. RICCERI
University of Padova, Padova, Italy
W. BERTONI
Municipality of Ravenna, Ravenna, Italy
G. BRIGHENTI
University of Bologna, Bologna, Italy
E. VUILLERMIN
University of Ferrara, Ferrara, Italy

ABSTRACT Land subsidence at Ravenna has been caused by both groundwater withdrawals from the Quaternary multiaquifer system and gas production from a number of deep prequaternary reservoirs discovered starting from the early fifties and scattered over the area. Water pumpage grew steadily until the middle 70's when consumption was drastically curtailed owing to the economical crisis and the activation of a new aqueduct. Gas removal is currently under way and the search for new fields is still in progress. Geodetic levelling indicates that the overall subsidence, including a natural geologic settlement of perhaps 2 mm/y, achieved a maximum value of 1.30 m from 1950 to 1986 in the industrial zone of Ravenna. In 1980 the Municipality promoted a reconnaissance study with the aim at providing the informative base needed to reconstruct the event, understand correctly the physical behavior and develop a mathematical model relating land sinking to grounwater withdrawal and gas production with an emphasis on the respective influence. The results fron the 3-D numerical analyses, performed with the aid of finite differences, finite elements and integral equations, show that the primary responsability for the regional land sinking is to be placed upon water overdraft. Gas withdrawal exerts a more restricted but netherveless measurable influence which may be expected to have a high environmental cost if gas production occurs from reservoirs underlying the Adriatic coastline.

INTRODUCTION

An excellent review of the worldwide most famous events of land subsidence caused by groundwater withdrawal can be found in the guidebook published by UNESCO (1984) some years ago. Land settlement due to gas/oil production is also extensively reported in the scientific literature. Ravenna, Italy, is a recent case of particular interest since land sinking that occured there has been

caused by both postwar groundwater overdraft from Quaternary confined aquifers and gas pumpage from a number of deep Pliocenic reservoirs scattered over the area and detected as early as 1952 by AGIP S.p.A., the Italian National Oil Company.

Ravenna is located 60 km south of the Po river Delta and 120 km far from Venice, a city which also experienced an alarming ground sinking in the late 60's, and lies close to the Adriatic coast (Figure 1a). The settlement process involved a large area and displayed its major effects in the late 70's (Carbognin at al., 1978) when the occurence started to threaten the industrial zone, the urban districts, the nearby reclaimed marshland and several beautiful historical monuments.

In 1980 the Municipality of Ravenna appointed a Committee with the specific aim at analysing quantitatively the event and providing the informative data base needed for its mathematical simulation with the aid of numerical models. The major objective of the study was the detection of the responsability for land subsidence to be placed upon water pumping and gas production, respectively. The Committee completed his activity in 1987 and presented his conclusive report to the Municipality in early 1988 (Committee for the Study of the Subsidence of Ravenna, 1988).

The present note summarizes the most significant findings obtained with the numerical simulations of the Ravenna land settlement as it is related to both water and gas withdrawal and gives a short account on the "ad hoc" reconnaissance study promoted by the Committee to properly integrate the existing information about the physical scenario and the history of the event.

GEOLOGICAL SETTING AND HISTORICAL RECORDS

The Ravenna area is part of the south-estern edge of the wide sedimentary Po river basin (Figure 1a). The underlying quaternary deposits consist mostly of sandy and silty-clayey layers laid down in different environments, from continental, lagoonal and deltaic in the upper zone to littoral and marine in the lawer one. The thickness of the Quaternary soils ranges between 1500 and 3000 m (Figure 2). The basement of the system is characterized by a structure of Pliocenic folds and faults which constitute the reservoirs containing gas (chiefly methane).

For what concerns the present study three different environments can be recognized in the Ravenna underground system. These are the upper multi-aquifer system down to the interface between fresh and brackish water, the transition zone where the latter turns progressively into salty water and finally the bedrock saturated with salty water and including several gas reservoirs, mainly made from Pliocenic and occasionally Quaternary deposits.

Fluid removal at Ravenna occurs from the 1st and the 3rd environments upon which therefore the present investigation is focused.

The information collected and analyzed by the Committee comes from a number of boreholes, soil drillings and pumping tests unevenly scattered over the Municipality area (Figure 1b). Particularly important are the core samples taken from the deep

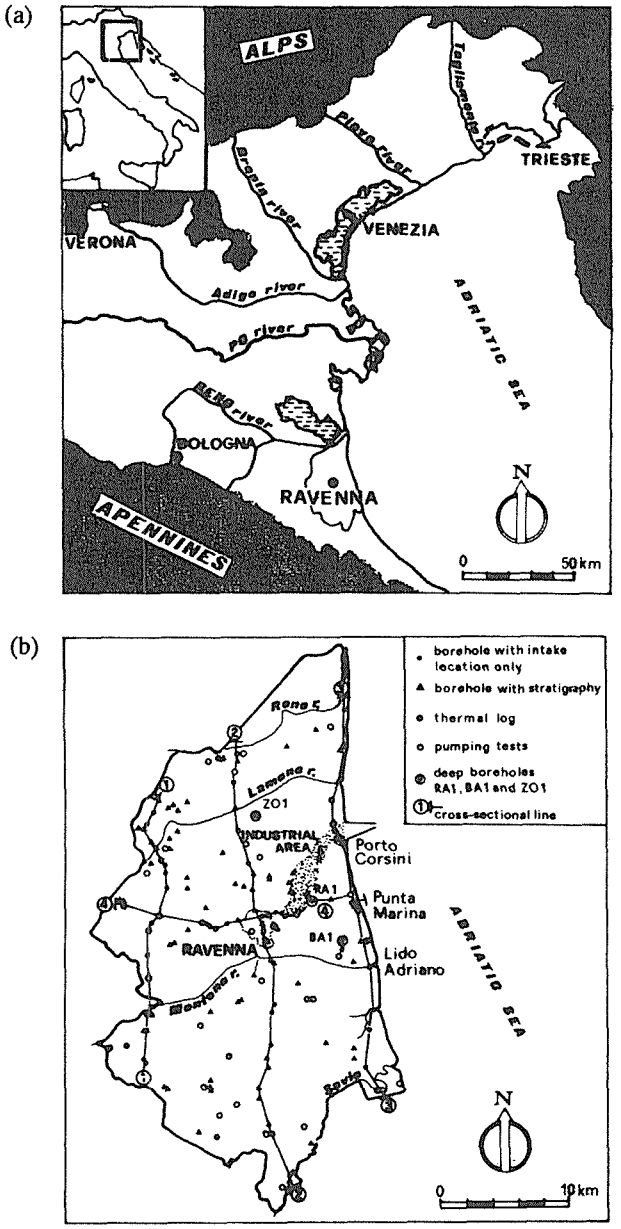

FIG. 1 Map of (a) the eastern end of the Po river basin, and (b) the Ravenna Municipality showing the location of several test holes and four hydro-geologic profiles.

wells BA1, RA1 and ZO1 (Figure 1b) which, together with the geologic profiles reconstructed along the four cross-sectional lines indicated in Figure 1b, have much helped define the multi-aquifer structure summarized in Figure 3 and used in the mathematical groundwater flow model. The in situ test pointed out a horizontal aquifer transmissivity between 2×10^{-6} and 7×10^{-3} m^2/s while the

FIG. 2 Schematic geological cross section of the subsurface system between Venice and Ravenna (after Carbognin et al., 1978).

laboratory analyses performed on the deep holes RA1 and ZO1 and other wells of the Po river basin have provided soil compressibility values α as shown in Figure 4 for both granular and cohesive soils. In the depth 100-4000m α varies between $7x10^{-3}$ and $6x10^{-5}$ cm^2/kg, sand being only slightly less compressible than clay (Figure 4).

The settlement after 1950 of the benchmark Porta Adriana in Ravenna is shown in Figure 5a while Figure 5b gives a map of the subsidence bowl over the Municipality area as of 1977, the most critical year in relation to groundwater pumping rate (Figure 6a) which greatly increased during the 50's and 60's and was progressively reduced after 1977 due to both a severe economical crisis and the activation of a new fresh water aqueduct. The behavior in time of the piezometric decline paralleled the consumption rate. Following a drowdown in the deepest aquifer of

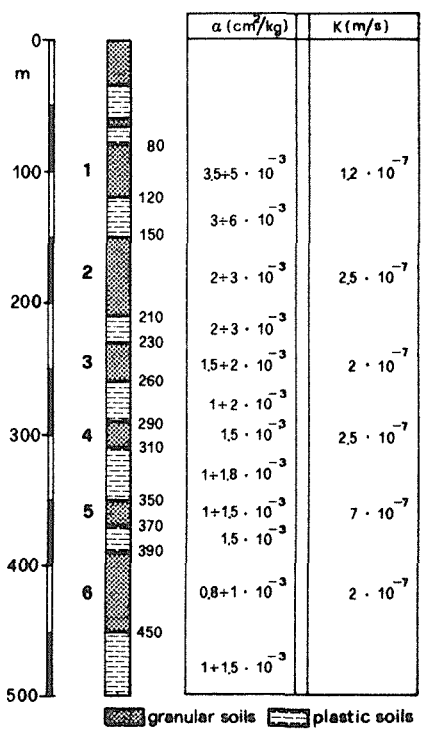

FIG. 3 Schematic littro-stratigraphic profile used to define the multi-aquifer structure of the quasi 3-D hydrological model.

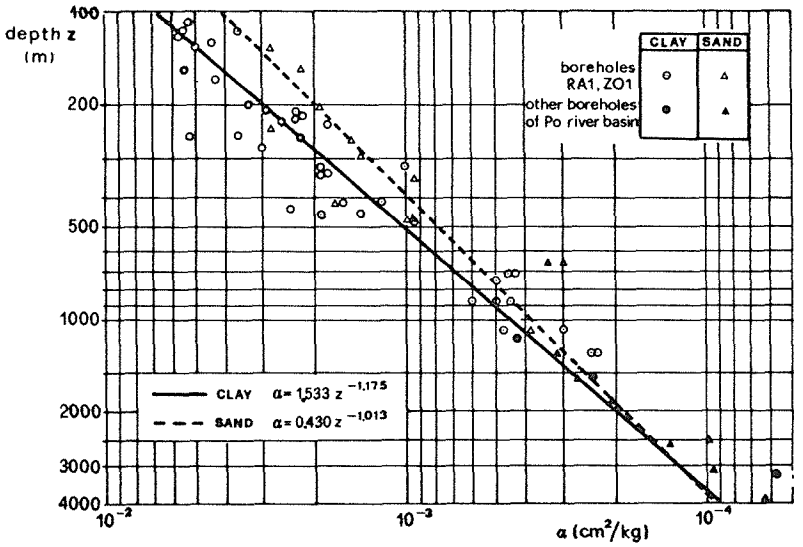

FIG. 4 Vertical soil compressibility vs. depth as measured on core samples taken from the Ravenna area. Two regression straight lines fitted against sand and clay measurements are shown.

more than 40 m recorded in the middle 70's, a recovery of the flow field has been observed (Figure 6b).

Concerning land subsidence due to gas production, the Committee decided to analyse the Ravenna Terra reservoir, which is the oldest field detected and exploited by AGIP, since its production was completed in 1982, 30 years after its discovery, the essential data were made available by AGIP and its location is totally inland where ground leveling was carried out. The Ravenna Terra field consists of two pools A and B situated beween 1720 and 1957 m depth. The gas production amounted to 21.77×10^9 Nm^3 and the maximal pressure decline in 1975 achieved the values of 90.5 and 95.5 kg/cm^2 in the upper and lower pool, respectively. The behavior in time of the pressure drawdown in both pools was provided by courtesy of AGIP S.P.A.

NUMERICAL ANALYSES

Land subsidence at Ravenna is simulated with the aid of two separate models. The first model consists of a quasi 3-D hydrologic model of subsurface flow on a regional scale (Gambolati et al., 1986) followed by a 1-D vertical consolidation model applied to the site where an accurate lithostratigraphic column of soil is available down to the depth of the pumped interval. Conceptually this approach is similar to the one applied to predict the subsidence of Venice (Gambolati and Freeze, 1973 and Gambolati et al., 1974) and properly accounts for the hysteretic behavior of silt and clay in rebound.

The second model is a 3-D calculation of the settlement occured over the Ravenna Terra field from the beginning up to the end of the production life. Due to the shortage of data concerning

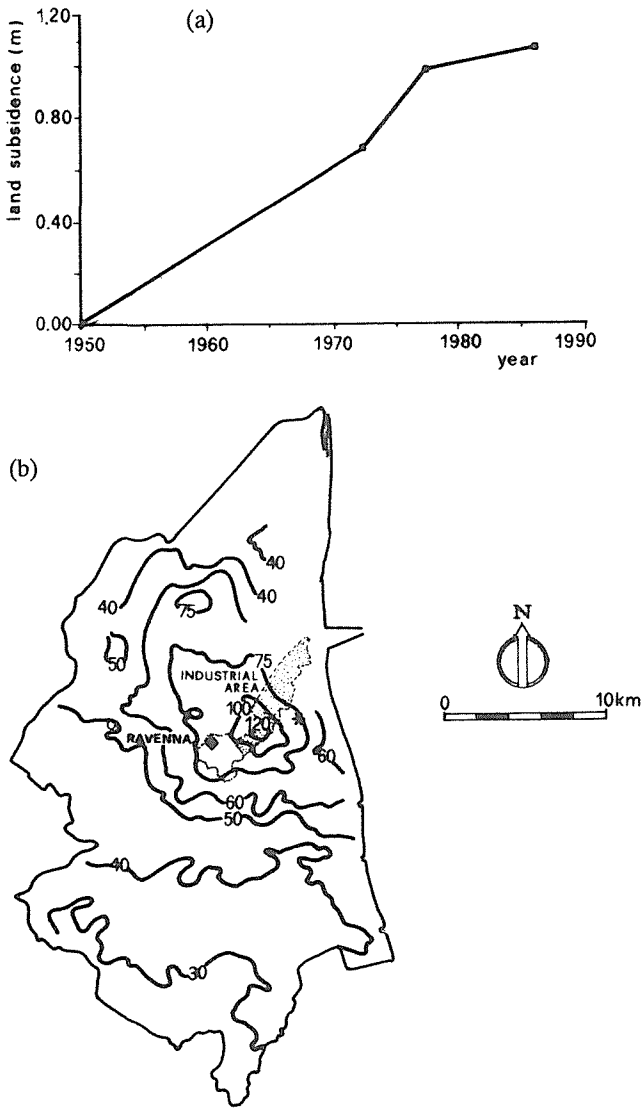

FIG. 5 (a) Settlement vs. time of the benchmark Porta Adriana at Ravenna, and (b) map of land subsidence (in centimetres) in the Ravenna area between 1949 and 1977.

the mechanical properties of the rock at the reservoir depth, the use of a more realistic non-linear model is precluded. Hence the simulation has been performed by a linear pro-elastic model (Geertsma, 1973) solved by a boundary element method (Gambolati et al., 1987) over a 3-D heterogeneous layered seminfinite medium. We are aware that the results from a linear model may not be very accurate. However we believe this analysis to be suitable for a useful comparison with the prediction made by the more realistic non linear groundwater model.

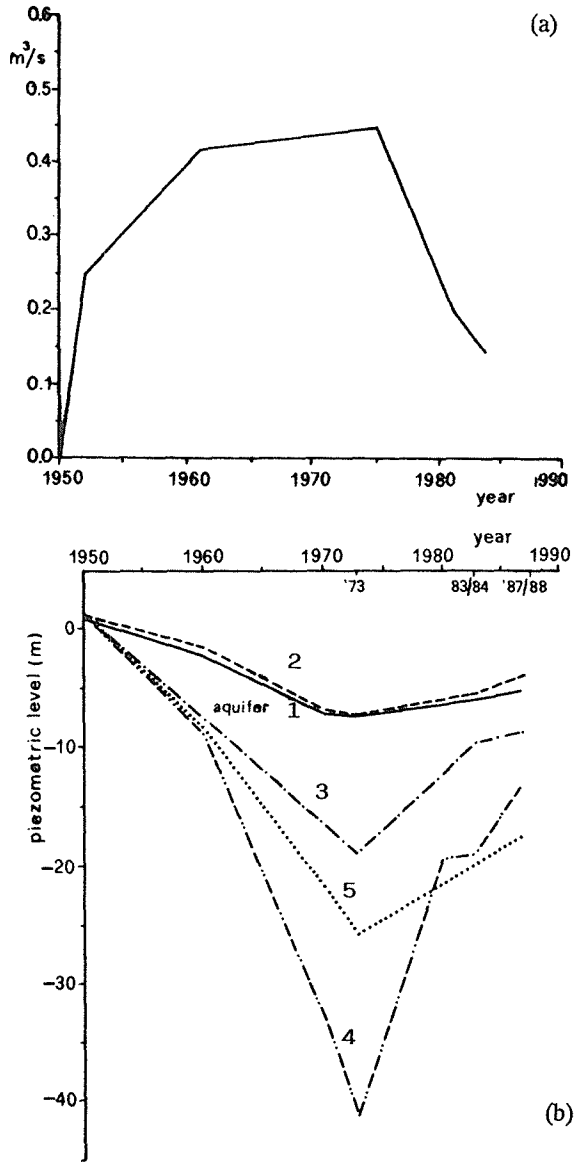

FIG. 6 (a) Cumulative groundwater pumping rate vs. time in the Ravenna area, and (b) piezometric level a.m.s.l. vs. time at Ravenna as reconstructed on the basis of available records.

Figure 7a and 7b show a perspective view of the triangular finite element and boundary element (Sartoretto et al., 1990) mesh adopted for the regional flow simulation of the Ravenna multi-aquifer system and the compaction simulation over the Ravenna Terra field, respectively.

Land subsidence at Ravenna due to water pumpage as simulated with the mathematical model is shown in Figure 8a. The largest settlement appears to have occured in the late 70's with a value of 1.10 m. This prediction is quite consistent with the

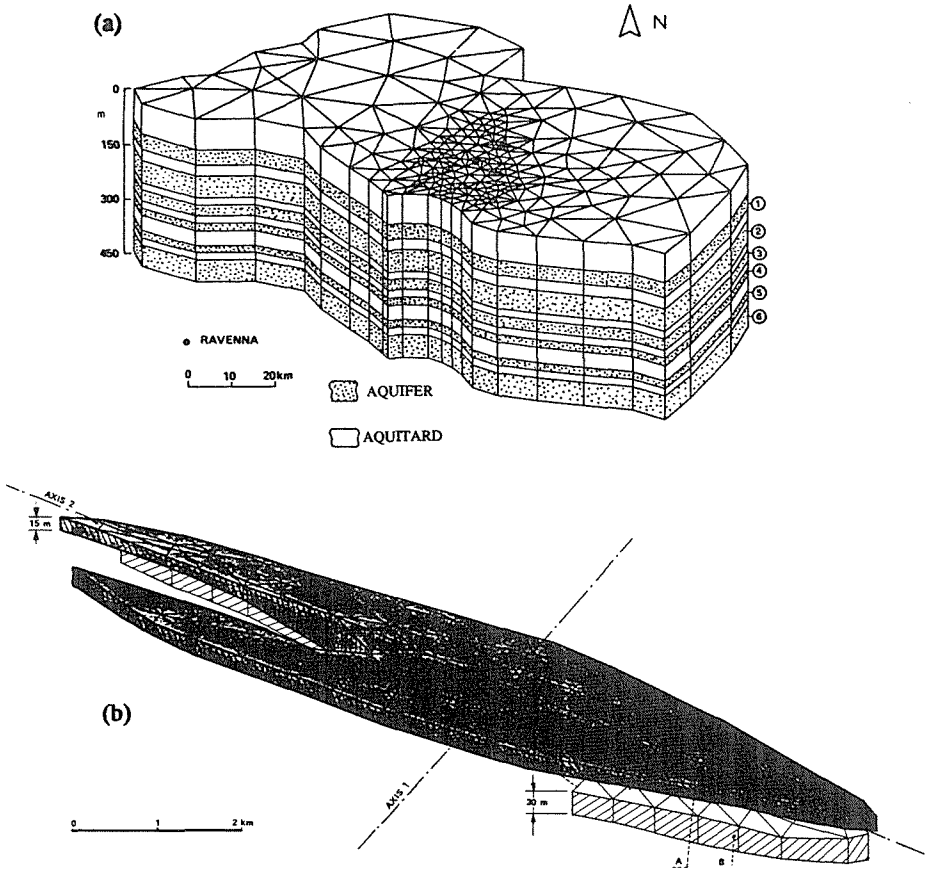

FIG. 7 (a) View of the regional quasi 3-D flow model of the aquifer system underlying the southeastern Po river basin, and (b) of the main pools A and B of the Ravenna Terra gas field.

benchmark record of Figure 5a and the equicontour map of Figure 5b and points out that water pumpage is likely to account almost entirely for the surface lowering observed at Ravenna.

Figure 8b gives the sinking over the major and minor axis of the Ravenna Terra field as simulated in 1975, i.e. when the largest pressure decline occurred. Figure 8b indicates a maximum settlement equal to 0.65 m and shows that the measurable subsidence is pratically restricted to the area overlying the gas reservoir and the occurrence in quickly dampened out beyond the boundary of this area.

CONCLUSION

The results from the 3-D numerical analyses show that the primary responsability for the regional land sinking that occurred in the Ravenna area is to be placed upon the subsurface water overdraft recorded until the middle 70's. Gas withdrawal plays a role restricted to the area overlying each reservoir with a

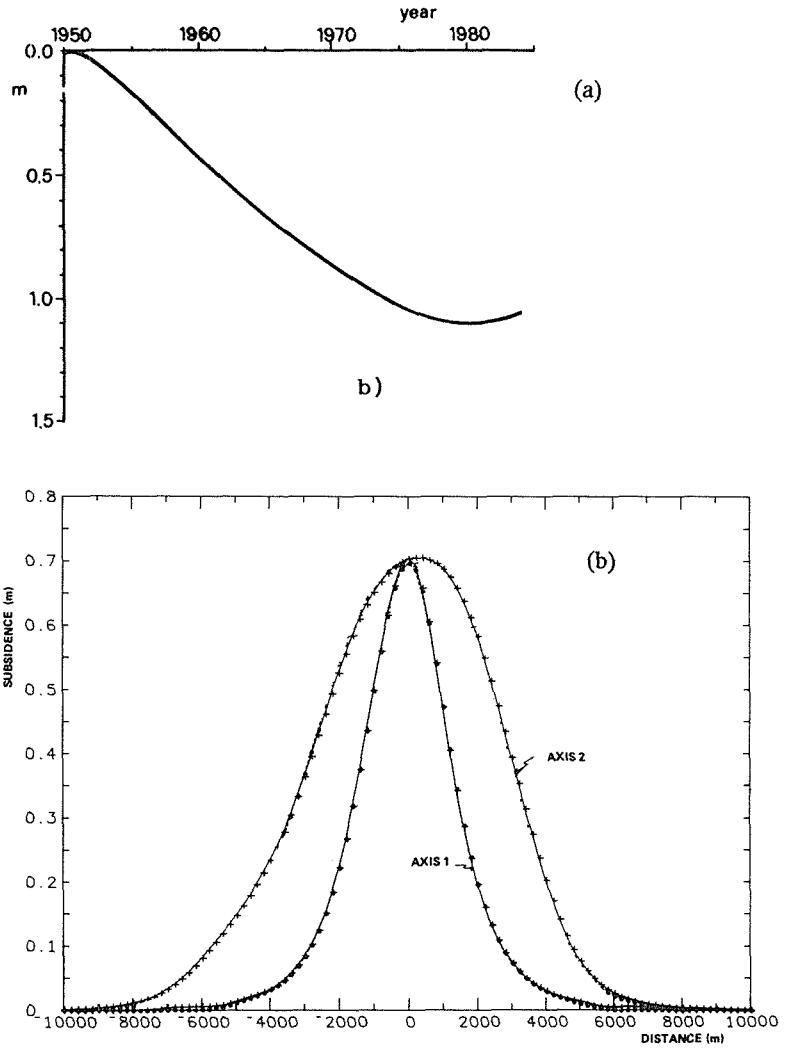

FIG. 8 (a) Land subsidence due to groundwater withdrawal at Ravenna as predicted by the mathematical model, and (b) land settlement due to gas production over the Ravenna Terra field in 1975 as predicted by the linear model along the major and minor axes of the reservoir.

magnitude depending on the depth of burial, thickness of mineralized rocks and gas pressure drawdown. A major environmental impact may be expected where the gas subsidence bowl is intersected by the Adriatic coastline.

ACKNOWLEDGMENTS

The authors are much indebted to AGIP S.p.A. for providing part of the data used in the mathematical model and to the Municipality of Ravenna for the financial and technical support and the continuous encouragement.

REFERENCES

Carbognin L., P. Gatto, G. Mozzi and G. Gambolati (1978) Land subsidence of Ravenna and its similarities with the Venice case. in "Evaluation and Prediction of Subsidence", S.K. Saxena Ed., ASCE, 254-266, N.Y.

Committee for the Study of the Subsidence of Ravenna (W. Bertoni, G. Brighenti, G. Gambolati, G. Ricceri and E. Vuillermin) (1988) Final Report to the Municipality of Ravenna, pp. 147.

Gambolati G. and R.A. Freeze (1973) Mathematical simulation of the subsidence of Venice. 1.Theory. Water Resour. Res., 9, 721- 733.

Gambolati G., P. Gatto and R.A. Freeze (1974) Mathematical simulation of the subsidence of Venice. 2.Results. Water Resour. Res. 10, 563-577.

Gambolati G., F. Sartoretto and F. Uliana (1986) A conjugate gradient finite element model of flow for large multi-aquifer systems. Water Resour. Res., 22, 1003-1015.

Gambolati G., F. Sartoretto, A. Rinaldo and G. Ricceri (1987) A boundary element solution to land subsidence above 3-D gas/oil reservoirs. Int. J. Num. Analyt. Methods Geomech, 11, 489-502.

Geertsma J. (1973) Land subsidence above compacting oil and gas reservoirs. J. Pet. Tech., 25, 734-744.

Sartoretto F., G. Gambolati and A. Rinaldo (1990) Land subsidence due to gas/oil production in inhomogeneous transversally anisotropic half-space by a boundary element method. Int. J. Num. Analyt. Methods Geomech., 4, 379-399.

UNESCO, (1984) Guidebook to Studies of Land Subsidence due to Groundwater Withdrawal. J. Poland Ed., Paris.

Land Subsidence (Proceedings of the Fourth International Symposium on Land Subsidence, May 1991). IAHS Publ. no. 200, 1991.

Subsidence Due to Oil Production in Western Venezuela: Engineering Problems and Solutions

JUAN MURRIA

Maraven S.A., Apartado 173, Codigo Postal 4016A, Lagunillas, Venezuela

ABSTRACT Ground subsidence associated with oil production in the east coast of Lake Maracaibo (Western Venezuela) was detected as early as 1929. Maximum cummulative subsidence as of April 1990 is 5.03 m. Typical subsidence rates range from 5 cm/year along the coast to 20 cm/yr in inland areas subjected to intensive oil production. The geomorphology of the area (low, swampy lands) prompted the need to protect inhabitants and oil industry installations from lake waters.

The construction of a coastal protection system was started in 1932 and is still in progress. The system consists of coastal and inner dikes as well as drainage networks, all conforming the "polders" of Tia Juana, Lagunillas and Bachaquero, which correspond to the oilfields of the same names, collectively know as the Costa Oriental oilfields.

This paper summarizes the origin, development, and monitoring of the subsidence describes the aforementioned coastal protection system, highlighting design and construction problems and the engineering solutions implemented and, finally, describes four subsidence prediction models (two operational and two being developed).

BRIEF HISTORICAL SUMMARY

Geomorphologically the eastern coasts of Lake Maracaibo are typical of lacustrine environments: flat and swampy (Lagunillas in Spanish means small lagoons or marshes), barely above lake level and composed mostly of sandy-silty soils. These swamps were separated from the lake by a comparatively narrow strip of land slightly higher than mean lake water level, so that these strips were flooded during high tides, storms, and strong on-shore winds.

Venezuelan Oil Concessions (VOC), Ltd., a subsidiary of the Royal Dutch Shell, was the concessionaire of the on-land area and started oil operations in the area in 1926. This company was renamed Compañia Shell de Venezuela in 1953, and, in 1976, became Maraven, S.A., as a result of the nationalization of oil industry (Abi-Saab & Murria, 1985).

VOC established their base of operations in Lagunillas; because of the region's topography, a small earthen dike, a few meters wide, less than one meter high and several hundred meters long was built by hand to protect the installations and dwellings from lake waves.

In 1929 the Lagunillas dike was breached and the resulting flooding led to suspicion of the ocurrence of ground subsidence, since the foreshore became permanently submerged.

Almost from the start of the subsidence it became necessary to construct inner dikes and a drainage system to dispose of the run-off by pumping it into the Lake.

As new oil was discovered, the oil companies extended their operations and established new oil fields, Tía Juana to the north and Bachaquero to the south (Figure 1), which had to be also protected by means of the construction of polders similar to the one in Lagunillas.

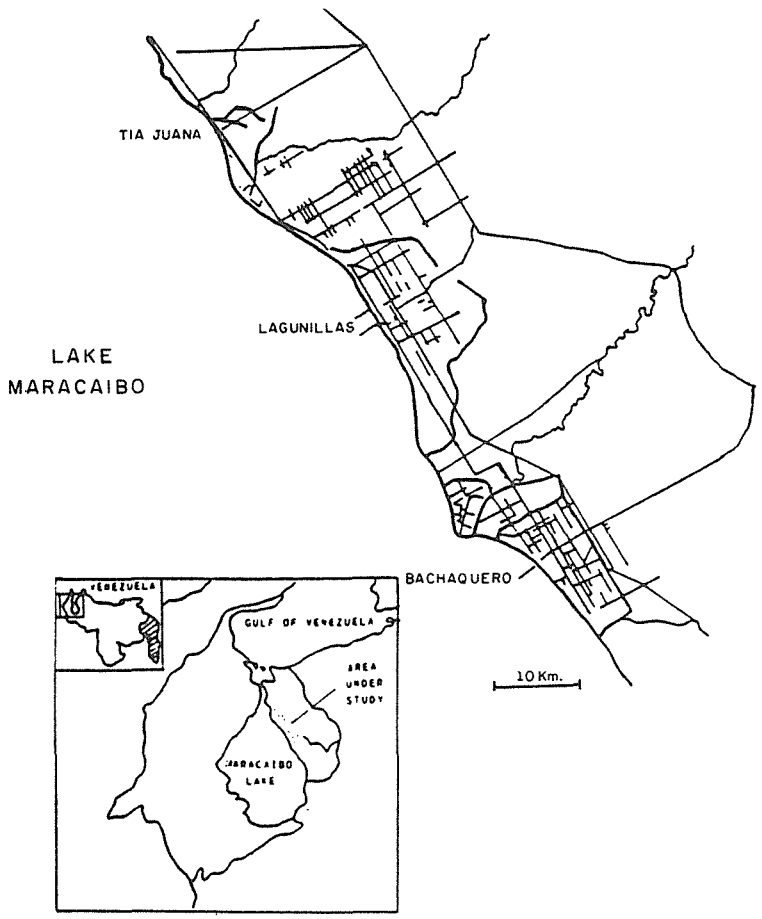

FIG. 1 Costa Oriental oil fields.

Initially, these dikes were built along the coast as "simple" elevated roads behind sheetpiles (Collins, 1935). The continued subsidence made it necessary to continually raise and widen the dikes. With time, the initial simple elevated roads became fully developed earth dams. Figure 2 shows the progressive rising of the coastal dikes.

On the basis of present subsidence predictions it is expected

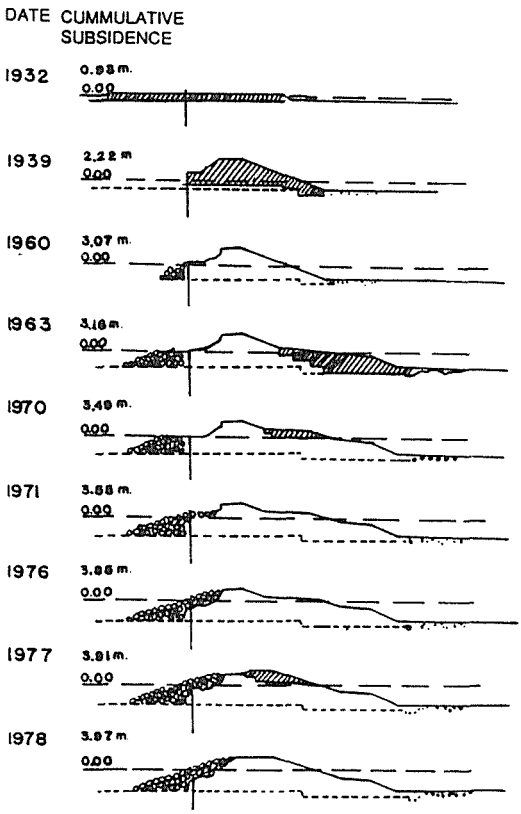

FIG. 2 Progressive raising of the dike.

that the Tía Juana and Bachaquero dikes will have to be raised only an additional 1.00-1.50 meters, while the Lagunillas dike may have to be raised as much as 4.00 meters as additional subsidence is expected due to the exploitation of two superposed reservoirs, Laguna and Lower Lagunillas.

As construction proceeded, the coastal protection system gradually took shape and conformed proper "polders" in Tia Juana, Lagunillas and Bachaquero (Murria & Abi-Saab, 1988) consisting of:

(a) The coastal dike to protect the subsided area from Lake flooding.
(b) The inner diversion dikes to prevent run-off from the area outside getting into the subsided polder area.
(c) Drainage channels to convey the water to the pumping stations constructed along the coast.
(d) Pumping stations to dispose of the water over the dike and into the Lake.

Figure 3 shows the main features of the Lagunillas polder. The Bachaquero and Tía Juana polders show similar features.

SUBSIDENCE MONITORING

A levelling network was established in Lagunillas in 1929 and later extended to cover the Cabimas, Tia Juana, Bachaquero, and Mene Grande

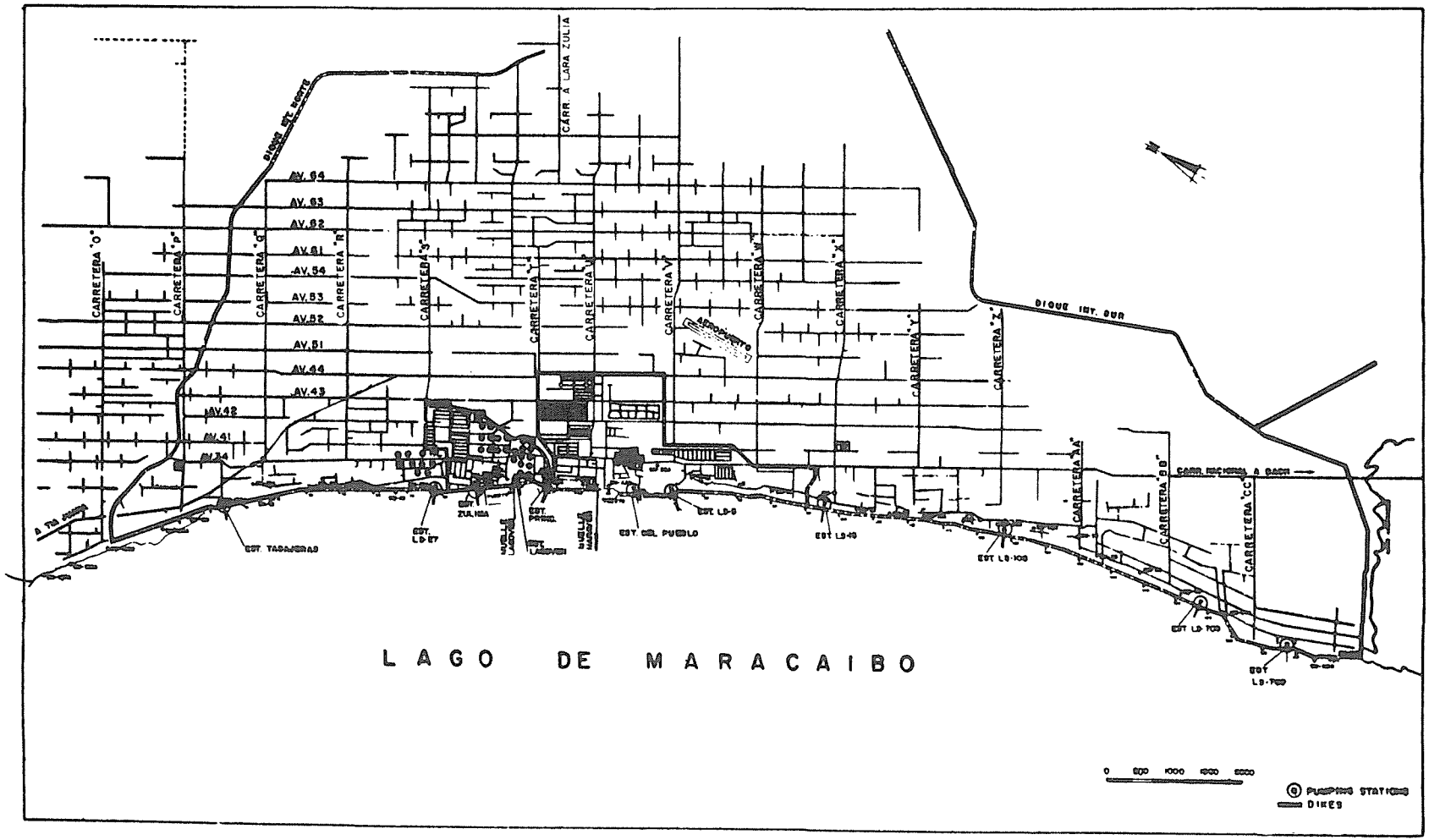

FIG. 3 Lagunillas polder.

as well as nearshore lake oilfields. To date the network covers an area of about 800 km^2 and comprises over 1.600 bench marks.

The subsidence monitoring surveys are still conducted at two year intervals. The historic records kept since the very beginning consist basically of the bench mark elevation, relative subsidence between the two most recent surveys, and the cumulative subsidence since the beginning of explotation of each field. This information has been represented graphically in the form of isoline maps showing the cumulative and the biannual subsidence Figure 4 shows cummulative subsidence as of March, 1990.

In 1988 GPS (Global Positioning System) techniques were incorporated in the levelling campaign (Figure 5) with encouraging results (Chrzanowski et al, 1988), but problems developed because of poor satellitar geometry. In 1990 GPS was again used together with traditional levelling and the results improved considerably.

The computational scheme includes a model that allows the combination of GPS with levelling in a geodynamic adjustment. For more details on the computational methodology the reader is referred to Leal (1989).

The maximum subsidence rate is about 20 cm per year inland in the area of El Polvorin, Lagunillas. The maximum subsidence rate along the coastal dikes is 7 cm/yr. The maximum cumulative subsidence up to March 1990 has reached a value of 5 m in Lagunillas.

There are 60 years of subsidence history, significant treasure from a scientific point of view and probably one of the few cases in the world.

DESCRIPTION OF THE COASTAL PROTECTION SYSTEM

Design and construction of coastal dikes

The gradual nature of subsidence, together with the possibility of predicting future subsidence, has allowed for staged construction of the coastal dikes as shown in Figure 2.

The characteristics of the coastal dikes have been influenced, not only by subsidence but also by geotechnical, hydrographic, and seismicity and seismic geology aspects (Abi-Saab et al, 1982).

Geotechnical aspects

The Delft Soil Mechanics Laboratory has studied the stability of the dikes based on soil investigations and the results showed that, for a dike with a height of 8-10 m on a subsoil of silty sand, an outer (Lake) slope is required not steeper than 1:2.5, and an inner (land) slope not steeper than 1:3.

Hydrographic aspects

The height of the dike is determined by the water level and wave run-up, all in accordance with the expected subsidence; as a criterion for the height of the dike it has been assumed that no more than 2% of the waves during a storm should reach the crest.

Based on theoretical calculations confirmed by model tests a minimum dike height of 1.8 m above MLWL was defined.

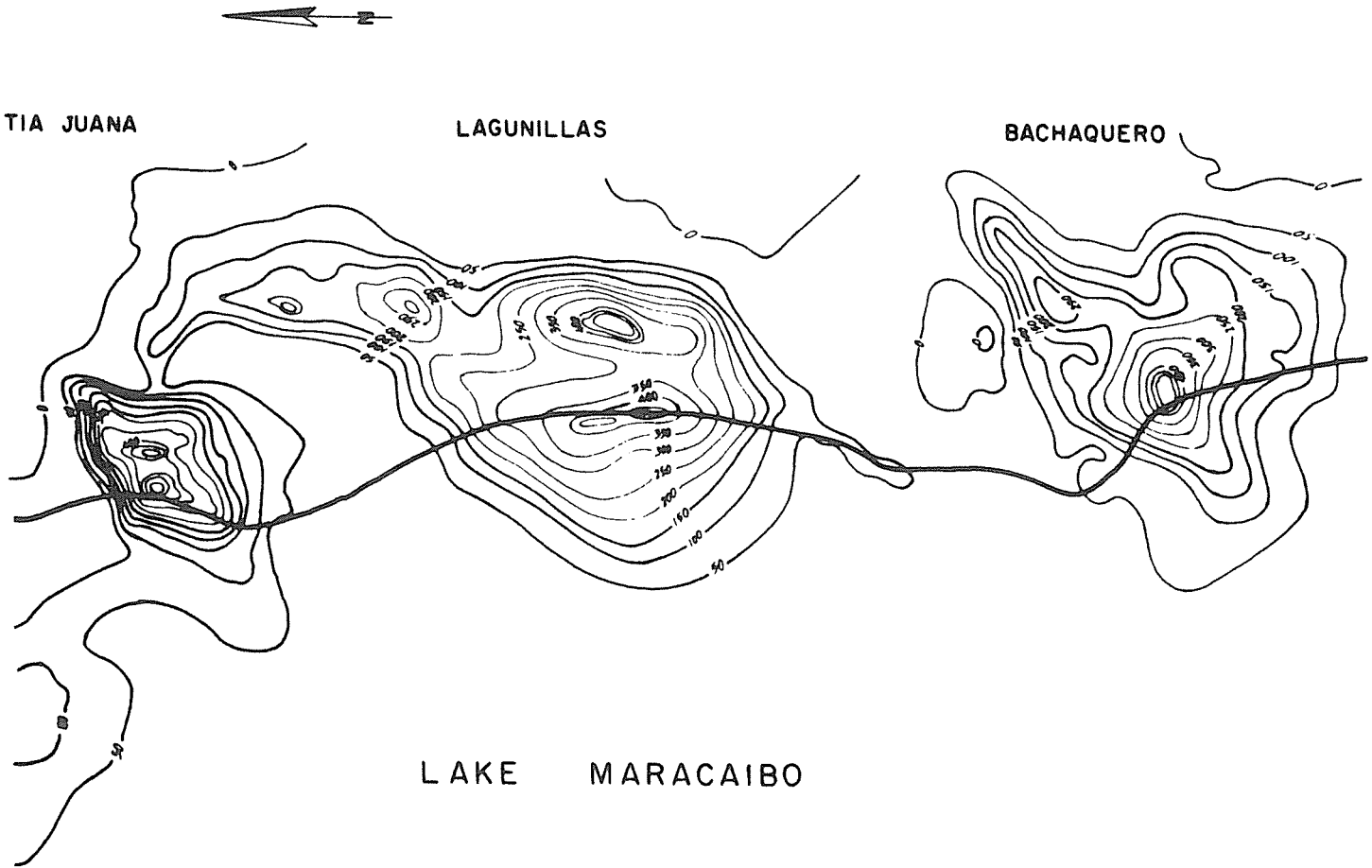

FIG. 4 Total cumulative subsidence (1990).

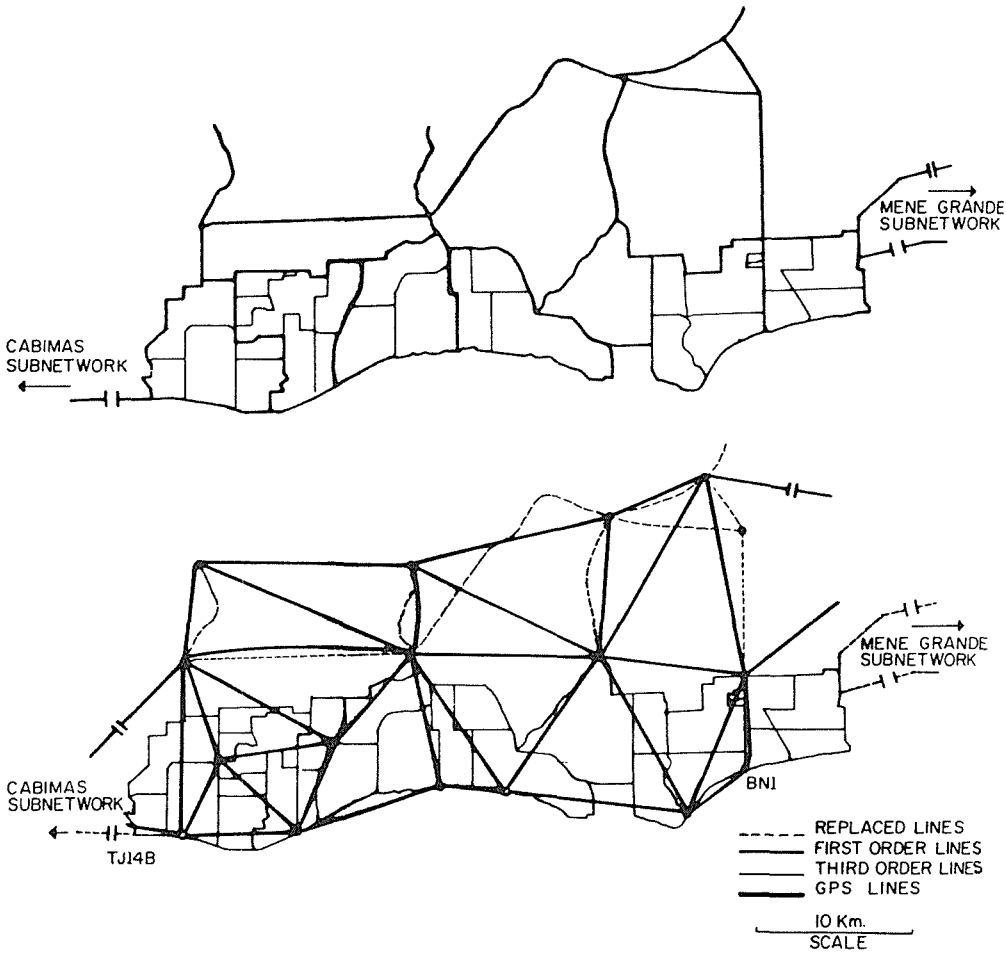

FIG. 5 Original and GPS aided subsidence monitoring main levelling network.

In 1982, it was decided to raise this minimum freeboard to 2.30 m to account for tidal variations (± 30 cm) and the possibility of lake body oscillations (± 20 cm) in an east/west direction.

Seismicity and seismic geology aspects

The coastal dikes are located in a seismic area of low to moderate intensity, corresponding to Zone 2 of the 5 zones in which Venezuela is divided for seismic design purposes.

Seismic geology and seismicity studies were carried out from 1985 to 1988. These studies showed a moderate seismic risk, mainly due to the possibility of liquefaction of a fairly loose, saturated, silty sand layer in the dike foundation soils.

Mitigative measures, consisting basically of downstream berms, with or without soil improvement, and, in some sections, an upstream artificial beach, are being implemented in about 25 of the 47 km of coastal dikes (see Figure 6).

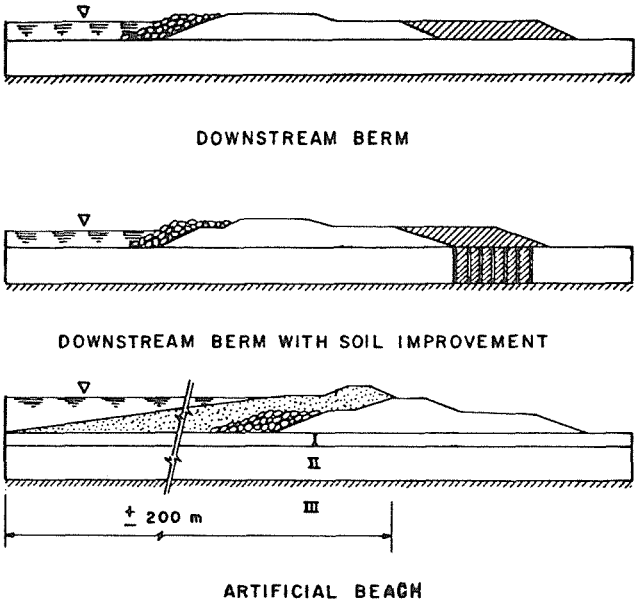

FIG. 6 Mitigative measures.

Work in the three polders was started in 1988 and it is estimated that it will be completed by 1995.

The implementation of the mitigative measures will increase the return period of the design earthquake from about 130 to 3000 years, the return period typically used worldwide for the design of earth dams in seismic areas.

Drainage masterplan

The nonuniformity of subsidence is obviously reflected in topography and, therefore, in surface drainage patterns. In recognition of this problem, Maraven undertook in 1984 the development of a Drainage Master Plan (Irazabal et al 1986) with a 50 year planning scenario with an intermediate 25 year scenario, both based on subsidence forecasts using the "ANALYTICAL" model (see below).

This masterplan was finalized in 1986 when detailed drainage projects were undertaken. Actual construction of the first project started in 1988.

SUBSIDENCE PREDICTION MODELS

In the case of the Costa Oriental oilfields, subsidence predictions allow appropriate planning and scheduling of the engineering activities needed to guarantee the protection function of the coastal and diversion dikes as well as the satisfactory performance of the drainage system.

Maraven and its predecessors have been studying subsidence, as it relates to reservoir compaction, practically since the beginning of oil production in the late 1920's. For a thorough and extensive

description of the studies performed, the reader is referred to Van der Knaap and Van der Vlis (1967) and Nuñez and Escojido (1976) and Mendoza and Murria (1989).

Since 1980, Maraven has been working in the development of two subsidence prediction models, HUNDCALC and the "ANALYTICAL" model. In 1983, and based on an approach suggested by Delft Geotechnics, The Netherlands, work was started in the development of the SINK model. Finally, INTEVEP, the research and development sister company, has been developing the SUB 3D model since 1984.

A general description of these models is given below.

The HUNDCALC Model

The HUNDLAC model was the first empirical method developed by Maraven to estimate future ground subsidence in the Costa Oriental oil fields. The technique for prediction of surface subsidence involves calculating reservoir compaction from actual or estimated production. Subsidence is then calculated from these compaction results. The model will also calculate the maximum comparative value of the sand and shale and therefore the maximum surface subsidence expected.

The area was covered with a grid system of 828, 1.4 x 1.2 km rectangles ("blocks"). The subsidence is calculated for each block. The individual grid block results are fused together and contoured to produce an areal landscape.

The "ANALYTICAL" model

The analytical model is the most widely used for the Costa Oriental. It is the results of combined historical data, laboratory measurements and the usual analytical and simple equations of surface deformation due to pore pressure reduction in the subsurface layers with variable compressibility.

This methodology has been applied successfully is easy to handle, with low cost and does not use excessive data.

The SINK model

The SINK model is an approach suggested in 1983 by Delft Geotechnics.

The objective is the simulation of surface subsidence due to fluid withdrawal from the subsurface. A simple solution is not available due to its complex nature, mechanical effects in a heterogeneous reservoir with environment or surface consequences. The behavior is typically non-linear and related to the pore fluid behavior.

The SINK model is an analytical formulation of the consolidation/deformation process explicity in terms of reservoir pressure, which in turn are determined numerically in order to account for heterogeneity in the geological system, whereas the true coupling between both is established iteratively. The integration in time is not required, reducing the cost of long term predictions.

The SUB-3D model

The Sub-3D is a fully-coupled model that uses finite element techniques to calculate the compaction of the reservoir and associated

surface subsidence. The model follows the principle that the soil above the reservoir will not be on equilibrium after fluid extraction and the corresponding decrease of the pore pressure. This will cause deformation until the whole system achieves steady state conditions. Consolidation is the physical law which governs the compaction phenomenon. An elastoplastic constitutive law based on critical soil mechanics is used.

The calculation of the plastic behavior of the soil is done by using a flow rule, a field surface and an evolution law. A solution algorithm taking into account the equilibrium equations, Darcy's Laws and an assumed rheological model for the soil has been chosen.

The model is in experimental stage but has been tested on the Costa Oriental oilfields in small sections of the coastal area. A preliminary evaluation indicates that the model may be useful for small areas where specific deformation problems arise. An observed disadvantage is the excesive computing time needed specially in 3D problems. It has the advantage, on the other hand, of representing many features of soil behavior using a small number of parameters which can be obtained from standard soil testing procedures.

FINAL REMARKS

This paper has attempted to summarize the development of the Costa Oriental Coastal Protection System, the studies performed, the problems encountered, and the engineering solutions implemented.

Perhaps the most salient characteristic of this system is its multidisciplinary diversity. Disciplines apparently as diverse as geodesy and earthquake engineering, hydraulics and seismic geology, oceanographly and subsidence modeling, have been successfully integrated and, as a result, the Venezuelan oil industry can proudly state that the main objective of the system, protection of life and installations, has been successfully achieved.

REFERENCES

Abi-Saab Soto J., Roest, P. W., Velsink, H. "Polders and dykes of the Bolívar Coast, Venezuela". Int. Symp. on Polders of the World, October 1982, Netherlands, Vol. I, 134-145.

Abi-Saab S. J. and J. Murria (1985) "Origen y desarrollo del sistema de protección costanera, Costa Oriental del Lago de Maracaibo". I Jornadas de Tecnología de Producción, INTEVEP, Los Teques, Venezuela.

Chrzanowski A., Y. P. Chen, R. Leeman, and J. Leal (1988) "Integration of the global positioning system with geodetic levelling surveys in ground subsidence studies". Proc. of the 5th Int. (FIG) Symp. on Deformation Measurements and 5th Canadian Symp. on Mining Survey and Rock Deformation Measurements, Fredericton N. B., Canada, 142-151.

Collins, J. J. "New type sea-wall built for subsiding lake shore in Venezuela". Engineering News Record, V. 114, No. 3, 1935, 405-408.

Irazabal A., Abi-Saab J., Murria J., Groot, J. "Drainage problems in areas subject to subsidence due to oil production". Proc. of the 2nd Int. Conf. on Hydraulic Design Water Resources Engineer-

ing: Land Drainage, Southampton University, U.K., April 1986, Springer Verlag, Berlin Heidelberg-New York-Tokyo, 545-554.

Leal J. "Integration of GPS and levelling in subsidence monitoring studies at the Costa Bolivar oil fields". M.S.C. Thesis in prep. Department of Surveying Engineering, Univ. of New Brunswick, Fredericton, N. B., Canada, 1989.

Mendoza, H. and Murria J. "Ground subsidence modelling in western Venezuela". Submitted for acceptance to the Organizing Committee of the Int. Symp. on Land Subsidence, Dhanbad, Bihar, India, 1989.

Murria, J. and Abi Saab J. "Engineering and construction in areas subjected to subsidence due to oil production". 5th Int. (FIG) Symp. on Deformation Measurements and 5th Canadian Symp. on Mining Surveying and Rock Deformation Measurements, Fredericton, N. B., Canada, 1988, pp. 367-373.

Nuñez, O. and Escojido, D. "Subsidence in the Bolivar Coast", Publication No. 121 of the IAHS, Proc. of the Annaheim Symp., December 1976, 257-266.

Van der Knapp, W. and Van der Vlis, A. C. "On the cause of subsidence in oil producing areas". Proc. of the 7th World Petroleum Congress, Mexico City, 1967, 85-95.

Land Subsidence (Proceedings of the Fourth International Symposium on Land Subsidence, May 1991). IAHS Publ. no. 200, 1991.

Subsidence Due to Abandoned Mining in the South Wales Coalfield, U.K.: Causes, Mechanisms and Environmental Risk Assessment

I. STATHAM & G. TREHARNE
Arup Geotechnics, Cambrian Buildings, Mount Stuart Square, Cardiff, CF1 6QP, U.K.

ABSTRACT Recent research on South Wales mining subsidence has assembled a database of over 400 subsidence incidents attributable to abandoned mining. Over 75% were collapses into workings at outcrop; or mine entrances. The remainder were almost always crownholes, whose upper limit of migration through rock was generally 8 to 12 times the void height.

Two thirds of the incidents occurred in open land and their environmental and economic impact was nominal. About 16% caused damage to roads and structures. Only one example of injury was traced, although about 20% occurred in areas where people pass frequently.

Taken as a whole, the database has shown a very low probability of a subsidence causing damage to property or injury to people. Expenditure on preventive measures vastly exceeds remedial expenditure, indicating that perception of the risk is out of proportion with the consequences. Engineering strategies for protecting existing and proposed developments should recognise that different levels of risk apply to different mining situations, so that resources are used to best advantage.

INTRODUCTION

South Wales has a tradition of mining on an industrial scale extending back more than 200 years. Mining has now virtually ceased, although periodically surface subsidence occurs as the abandoned workings continue to deteriorate.

Recent Department of Environment/Welsh Office research contracts (see Statham et al 1987) have assembled a database of over 400 subsidence incidents, for the South Wales Coalfield allowing a review of the risk to be carried out on a coalfield wide basis. Such opportunities are rare, although similar assessments have been made by Bruhn et al (1980) for the Pittsburgh Coal Bed and Cole et al (1984) for Limestone Mining in the West Midlands of the U.K.

In this paper, causes, mechanisms and environmental effects of subsidence due to abandoned mineworkings are discussed. The level of risk and economic consequences are then assessed, in the light of current expenditure on remedial and preventive measures. In

the past, subsidence processes and effects have been severe at, and shortly after, the time when the mining occurred. The purposes of this study, however, are to identify the current, residual subsidence effects since it is these, and the prospects for the future, which are relevant to present day development and planning.

THE SOUTH WALES COALFIELD

Geology

The South Wales Coalfield is an elongate synclinal structure, some 100km by 40km; see Figure 1. It is divided by a major fault system, the Neath Disturbance, which crosses from NE to SW with a downthrow of over 650m to the west. To the east, the northern limb of the syncline dips at about 1 in 10, whilst the southern limb is steeper, at up to 1 in 2. West of the Disturbance the structure is complex, with many reverse faults and thrusts.

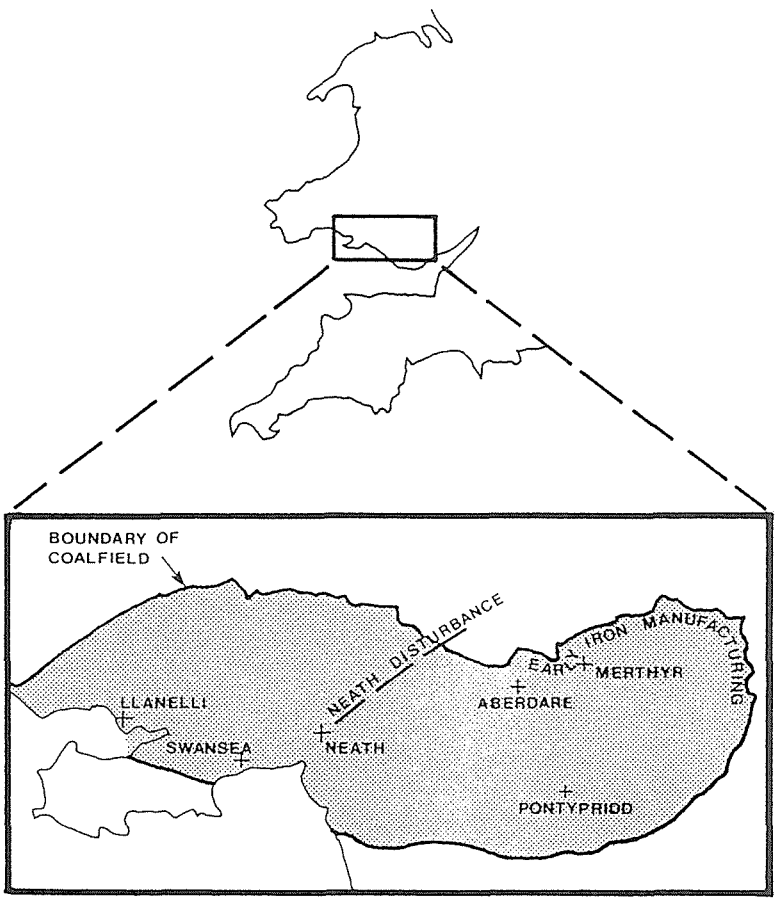

FIG. 1 The South Wales Coalfield.

A characteristic of the coalfield is the large number of coal and stratigraphic iron ore horizons which have been worked in a relatively small thickness of strata. This is particularly so in the Lower and Middle Coal Measures. The seams are normally thin, 0.5m to 2.0m being typical, although collectively they add up to a considerable thickness of extraction in many places.

Mining History

Coal and iron ore have been mined for centuries in some parts of the coalfield. However, pre-industrial mining has largely been obliterated by later operations.

Large scale mining started in the south-west of the coalfield in the 16th and 17th centuries, serving a sea-based export trade centred on Llanelli; see Figure 1.

Widespread industrial mining began in the north-east from about 1760 onwards, see Figure 1, associated with iron manufacture. Rapid expansion occurred as communications developed and the area was almost completely worked out by the end of the 19th century. Iron smelting spread slowly to other areas around the margins of the coalfield, but not to the same extent. In particular, progress was inhibited in the north-west, since the anthracite grade coals found in this area were unsuitable for smelting in early iron technology.

Mostly, the centre of the coalfield remained undeveloped until the mid 19th century. Here, the seams were deep and it took the enormous demand for steam coal in the mid 19th century to stimulate the necessary improvements in mining technology to exploit these deep reserves. Development peaked around the First World War at more than 50 million tons per year.

There has been a steady decline throughout the 20th century, accelerated recently by major rationalisation of the British Coal Industry. Now, only five collieries remain open and over most of the coalfield, mining is rapidly passing into history.

CAUSES AND MECHANISMS OF SUBSIDENCE

Data

Records of over 400 subsidence incidents have now been collected, forming a comprehensive database of recent subsidence processes associated with abandoned mining. Most records have been collected from the British Coal Corporation and local government departments, the majority dating from 1960 onwards.

Causes

Records usually consist of scanty details of location, consequences and sometimes remedial measures. Establishing the cause of subsidence involved a review of the geology and available mining records for each incident. Table 1 summarises the findings. The main points arising are:

(a) Some 75% of incidents were caused by collapses at mine

TABLE 1 Causes of subsidence incidences.

CAUSE	NUMBER OF INCIDENTS	PERCENTAGE OF TOTAL	
Recorded Adit Entrances	120	30.3	77.2% of incidents relate to collapses through superficial deposits or in fill
Unrecorded Adit Entrances	25	6.4	
Recorded Shafts	64	16.1	
Unrecorded Shafts	7	1.8	
Recorded Outcrop Workings	12	3.0	
Unrecorded Outcrop Workings	78	19.6	
Recorded Adits below Rockhead	21	5.3	22.8% of incidents relate to collapses of workings below rockhead
Unrecorded Adits below Rockhead	1	.3	
Recorded Workings below Rockhead	37	9.7	
Unrecorded Workings below Rockhead	31	7.9	
Cause Unknown	8	Excluded	

entrances or at the outcrop of the seam; i.e. there was no rock cover to the part of the mine which collapsed to cause the subsidence.
(b) Mine entrances pose by far the biggest risk, over 50% of the total, most of which are recorded.
(c) More than 80% of the mine entrance incidents occurred at recorded features.
These three points are encouraging. Clearly the vast majority of subsidence incidents occur within well defined, easily locatable zones which form a very small part of the total area of the coalfield.

Failures of Mine Entrances

Mechanisms of subsidence due to collapse of adits and shafts have been discussed elsewhere (e.g. Dean 1962, Edmonds 1989, Statham and Gordon 1990; NCB 1982). The main causes are:
(a) Structural failure due to decay, e.g. of adit supports within the superficial deposits (masonry, timbers or steel rings) or shaft liner.
(b) Failure of backfill to a shaft or adit by consolidation, or rapid slumping due to washing out.
(c) Failure of inadequate or decayed cappings placed over open entrances.

Subsidence Due to Collapse of Workings below Rockhead

As Table 1 shows, subsidence due to adits and workings below rockhead only account for 90 incidents, about 25% of the whole set. However, it is particularly important to understand their mechanisms because:
(a) Their locations are less predictable than mine entrances and outcrop workings.
(b) They define the 'upper bound' of the subsidence process and hence the limits of areas at risk.
The vast majority of subsidence incidents where a rock cover was formerly present over the workings are 'crownholes' in form. That is, they have developed by migration of the void upwards through the roof strata by progressive collapse, forming a chimney; see Figure 2.

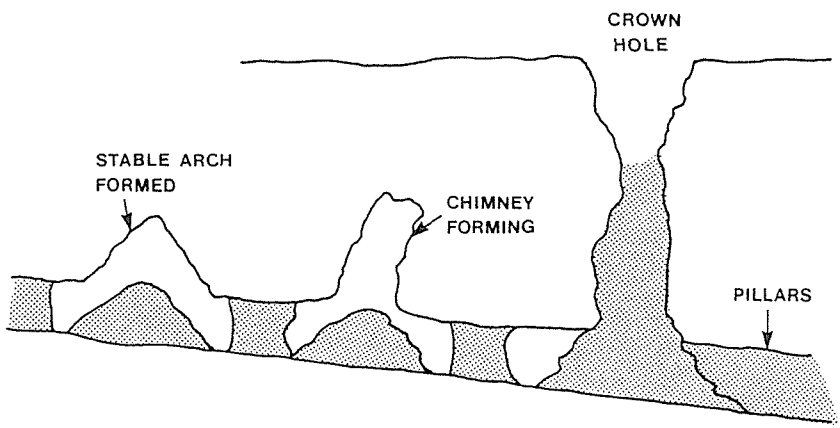

FIG. 2 Formation of chimneys, stable arches and crown holes.

The upper limit to this process has been the subject of many papers on abandoned mining subsidence for over 30 years. Most efforts have been directed at deriving empirical relationships between maximum height of void migration and the geometry of the collapse chimney, taking bulking of the collapse debris into account (for example, Tinscelin, 1958; Piggott and Eynon, 1978; Whittaker and Reddish, 1989). Most calculations arrive at an upper bound for chimney height (H) of around 8T, where T is the thickness of strata extracted, or original height of void.

Recently, Garrard and Taylor (1988) presented the results of a study of abandoned workings found at British opencast sites and concluded, by a combination of theoretical and empirical analysis, that the upper limit of migration was controlled by the formation of stable arches, not choking by bulked collapse debris. Height of migration was generally limited to less than 3W, where W is the width of the void.

There is a third possibility, where no stable arch can form, e.g. in shattered or faulted zones with groundwater ingress and where no bulking occurs. The latter may be due to washing away of collapse debris by water moving through the mine, or by slipping

to greater depth down steeply inclined workings. In these cases, the height of migration is indeterminate and could greatly exceed the limits given above.

In South Wales, the process of collapse of workings generally results in the formation of crownholes. Only two examples of general subsidence, i.e. subsidence of a wider area without formation of a collapse feature, have been found in the studies. These probably related to pillar failures.

The height of migration of crownholes has been analysed for the 90 incidents where a rock cover was formerly present above the workings. In some cases, the actual values of H and T were recorded at the time of collapse but in most cases assumptions had to be made. H was derived from topographic maps, mine plans and geological maps, whilst a standard roadway height of 2m was assumed for T. The results are, therefore, not necessarily absolute but if they are applied consistently they can be used as a predictive tool within the area from which they were derived, i.e South Wales. For other areas, a similar coalfield wide study of subsidence would be necessary, since the limit to migration would not necessarily be the same.

Figure 3 is a histogram of H/T vs percentage of incidents. It shows that the upper bound for South Wales is about 18, although in 90% of cases H/T was less than 6. A comparison is made with data in Bruhn et all (1981) which shows that different coalfields can have different forms of histogram and upper limit to

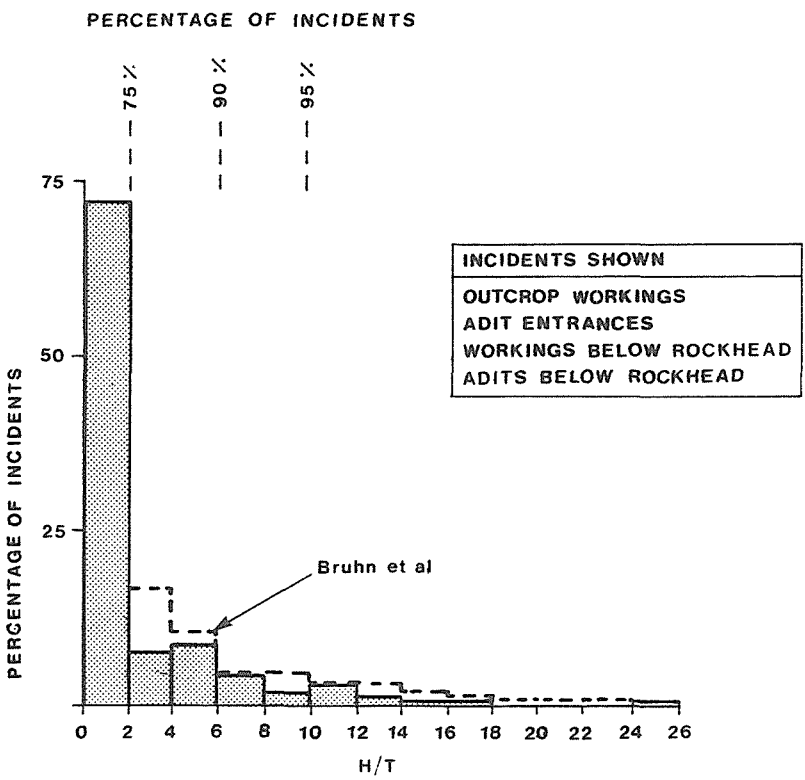

FIG. 3 H/T vs percentage of incidents.

subsidence. The differences reflect variations in mining methods and geological conditions.

The form and upper limit to the histogram give some clues about controlling mechanisms; stable arching or bulking. H/T on Figure 3 could be read as W/T, since roadways are also typically about 2m wide. Reading it this way, around 80% fall below W/T <3, suggesting that stable arching could well be a controlling mechanism in most cases. However, for incidents where 3<W/T<18, stable arches could not have formed and thus bulking is the limiting mechanism. Typically, stalls (rooms) in South Wales mines were approximately 5m width; hence even if the higher values of W/T related to stalls, the maximum ratio would still be 18 x (2/5) = 7.2, well above Garrard and Taylor's limit for stable arching. It follows that, whilst stable arching may be a common controlling collapse mechanism, it does not control the upper bound and cannot be used to predict areas at risk of crownholing. It is worth noting that more than a dozen incidents on well recorded mine adits have been collected where the H,T and W were accurately known and where calculated values of H/T (or W/T) were in the range 6 to 10.

ENVIRONMENTAL IMPACT AND PROBABILITY OF SUBSIDENCE

Nearly two-thirds of incidents (64%) occurred in open ground, well away from structures. A further 14% occurred close to buildings but caused no actual damage.

Damage occurred in 16% of the incidents; 9% to roads and 7% to buildings. Mostly, the damage to buildings has been minor. In a few cases, substantial works have ensued but these have largely been towards preventing the spread of damage or future occurrence of similar subsidence. There have been occasional examples where demolition has been considered necessary.

Incidents causing damage have averaged less than 3 per year over the last 30 years, a low rate of occurrence when the size of the coalfield is considered.

About 6% of incidents occurred on construction sites, and could be regarded as a threat to life. Actually, only one injury has been recorded and there have been no fatalities.

An estimate of the assumed probability of subsidence occurring at any site can be made as follows:

$$P = N_i . A_i \ / \ T \ A_c$$

Where P = probability, N_i = no of incidents recorded, T = time period, A_i = area affected by an incident (taken as 5m x 5m), A_c = area of coalfield. This results in an average probability for any point in the coalfield of about $1x10^{-7}$/annum. For mine entrances and areas within 100m of seam outcrops, values of $1x10^{-4}$/annum and $5x10^{-6}$/annum respectively apply. The level of risk for the remainder of the coalfield is in the region of $1x10^{-8}$/annum.

Cole (1987) has considered the notions of 'degree of risk', 'severity of consequences' and 'public tolerance' to derive a matrix of risk acceptance or tolerance by society. The levels of risk given above for subsidence in South Wales are compared in Table 2. The Table is a first approximation at a strategy for tackling the mining subsidence risk in South Wales. It highlights the importance of seam outcrops and mine entrances and shows that,

TABLE 2 Annual risk of subsidence due to abandoned mining in South Wales.

LOCATION IN COALFIELD	ANNUAL RISK LEVEL	RISK CLASSIFICATION* TO LIFE	TO PROPERTY	PUBLIC EXPECTATION
Whole Coalfield	1×10^{-7}	Very unlikely	Negligible	About what would be expected in a mining area for structures
At Mine Entrance	1×10^{-4}	Some Risk	Unlikely	Not acceptable in public buildings, work places or houses
Near Seam Outcrops	5×10^{-6}	Slight Chance	Unlikely	About what would be expected in open spaces in a mining area
Elsewhere (away from entrances and outcrops)	1×10^{-8}	Practically Impossible	Negligible	Better than would be expected in a mining area for structures

* see Cole (1987)

in any event, there are areas where preventive measures would be expected in construction projects. Elsewhere, there is a much lower risk, well within that which would be normally tolerated by the public. These generalisations are no substitute for detailed site assessment and a judgement of the level of risk at each site still has to be made. Nevertheless, they do serve to show that the concept of risk can be introduced into engineering decisions.

REMEDIAL VERSUS PREVENTIVE EXPENDITURE

It is interesting to compare the costs of remedial works to properties affected by abandoned mining subsidence with the costs of preventive measures, used to protect existing and new buildings 'at risk'. A pilot survey of a large property estate in the coalfield revealed an average expenditure over 6 years on remedial works was about £3000/annum; the range per incident was from nominal expenditure to over £35,000. These figures represent the cost of rectifying the actual damage and do not allow for consequential costs, or preventive measures deemed necessary to stabilise the remainder of the site. A study of over 30 sites where preventive measures were carried out revealed that the average annual expenditure was about £200,000, an average contract costing over £40,000.

It is clear that the preventive expenditure is out of proportion with the risk; the amount spent on preventive measures exceeding that spent on remedial work by a factor of 60. This, in conjunction with the assessment of risk to property and people

discussed above, shows that the response to the abandoned mining hazard tends to be irrational, leading to an unbalanced use of funds.

CONCLUSIONS

The following conclusions can be made:
(a) Subsidence incidents due to abandoned coal mining in South Wales are confined mainly to occasional crownholes and collapses at mine entrances; very few examples of general subsidence are now occurring.
(b) The majority of migrating voids are limited by the formation of stable arches. However, the upper limit of crownholing appears to be controlled by bulking of collapse debris, and therefore bulking should be taken as the 'design process' for engineering decisions.
(c) The risks of future subsidence incidents are by now low; at an average of some $1x10^{-7}$/annum for the coalfield as a whole. Locally, the risks of future subsidence incidents, are much higher at mine entrances and near to seam outcrops.
(d) Overall the risk of subsidence incidents causing damage to property or injury to people, are overestimated, resulting in unwarranted expenditure on preventive measures in relation to existing and new structures. Only around mine shafts and near to seam outcrops is the risk high enough to warrant extensive preventive expenditure in the ground. Elsewhere, measures incorporated into the structures, e.g. raft foundations, are a more appropriate solution.

ACKNOWLEDGEMENTS The research on which this paper is based was jointly sponsored and financed by the Welsh Office and Department of Environment. The support provided by various officers, particularly Aubrey Waters, David Brook and Hugh Payne has been much appreciated.

REFERENCES

Bruhn, R.W., Magnusson, M.O. & Gray, R.E. (1978) Subsidence over the Mined Out Pitsburgh Coal. ASCE Convention 'Coal Mine Subsidence', Pittsburgh, USA, 26-55.

Cole, K.W. (1987) Building over Abandoned Shallow Mines: A strategy for the engineering decisions on treatment. Ground Engineering, May 1987.

Cole, K.W., Turner, A.J. & O'Riordan, N.J. (1984) Limestone Workings in the West Midlands. In Forde, M.J. Mineworking 84; Proceedings of the First International Conference on Construction in Areas of Abandoned Mineworkings. Engineering Technics Press, 40-51.

Dean, J.W. (1967) Old Mine Shafts and Their Hazards. Mining Engineer, Paper No. 4161, 368-380.

Edmonds, C.N. (1989) Review of Underground Mines in the English Chalk; Form, Origins, Distribution and Engineering Significance. International Chalk Symposium. Telford Press 229-237.

Garrard, G.F.G. & Taylor, R.K. (1988) Collapse Mechanisms of Shallow Coal Workings. In Bell, Culshaw, Cripps & Lovell (Eds) Engineering Geology of Underground Movements. Geological Society Engineering, Geology Special Publications No. 5, 3-32.

National Coal Board (1982) The Treatment of Disused Mineshafts and Adits. NCB Mining Department.

Piggott, R.J. & Eynon, P. (1978) Ground Movements arising from the Presence of Shallow Abandoned Mineworkings. In Geddes, J.D. Large Ground Movements and Structures Pentech Press, 749-780.

Statham, I., Golightly, C. & Treharne, G. (1987) Thermatic Mapping of The Abandoned Mining Hazard: A Pilot Study for the South Wales Coalfield. In Culshaw, Bell, Cripps & O'Hara (Eds) Planning and Engineering Geology. Geological Society Special Publication No. 4, p255-268.

Statham, I. & Gordon, T. (1990) Problems of Land Reclamation on De-Commissioned Colliery Sites in South Wales. In Whyte I.L. (Ed) De-Commissioning and Demolition 90, Proceedings of 2nd International Conference, Manchester. Telford Press 106-112.

Tinscelin, R.K. (1958) Pressions et Deformations de Terrain dans les Mines de fer de Lorraine. Jouve Editeurs Paris.

Whittaker, B.N. & Reddish, D.J. (1989) Subsidence, Occurrence, Prediction & Control. Developments in Geotechnical Engineering No. 56. Elsevier, Amsterdam.

Land Subsidence (Proceedings of the Fourth International Symposium on Land Subsidence, May 1991). IAHS Publ. no. 200, 1991.

Inclusion of an Intensity Function for Subsidence Prediction with the Influence Function Approach

T. L. TRIPLETT & D. W. YURCHAK
U.S. Bureau of Mines, Twin Cities Research Center, Minneapolis, Minnesota, USA

ABSTRACT This paper presents research, conducted by the Bureau of Mines, on modifying the influence function method to predict subsidence. According to theory, this technique must incorporate an intensity function to represent the relative significance of the causes of subsidence. This paper shows that the inclusion of a reasonable intensity function increases the accuracy of the technique, then presents the required functions for a case study of mining subsidence in Illinois. Finally, the paper discusses the application of the technique to subsidence caused by ground water withdrawal.

INTRODUCTION

Subsidence persists as a damaging manifestation of several phenomenon, including mining and ground water withdrawal. To insure the coexistence of these ventures and desired surface activities, possible subsidence damages should be minimized or prevented. However, the first requirement for the development and implementation of reasonable damage reduction and mitigation techniques is the knowledge of the magnitude of the surface displacements caused by the subsidence event.

Because of the difficulties which exist in characterizing rock mass properties for use in analytical subsidence prediction techniques, the empirical profile function and influence function methods are widely used for the prediction of subsidence due to mining. Since the shape of the subsidence curve predicted by a profile function is limited by the form of that function, the influence function approach seems to offer the greatest potential for accurately predicting mine subsidence for various conditions. Therefore, the objective of this research, conducted by the Bureau of Mines, is to review and modify the influence function method to predict mine subsidence in Illinois. This paper shows that the inclusion of a function to describe the intensities of the causes of subsidence increases the accuracy of the technique. For example, in the case of subsidence above longwall mines, the intensity function must represent the caving of the roof and subsequent ground movement around the longwall panel. The procedure for using the technique to predict subsidence for a mining case study in Illinois, as well as from other causes such as ground water withdrawal, then are described.

LINEAR EQUATIONS IN CAUSE AND EFFECT

Linear equations frequently can be used to model physical problems in which the effects of several causes are to be superimposed (Hildebrand, 1965). In these problems, a distribution of causes, $c(\xi)$, is assumed to exist over the volume, V, in the region $\mathfrak{R}$, and the resultant distribution of effects, $e(x)$, is to be determined. The variables x and ξ are defined as representing position in space of any dimension within some interval in the region $\mathfrak{R}$.

If the effect at x due to a unit cause (value=1) at ξ is denoted by $G(x,\xi)$, the effect at x due to a uniform distribution of causes of actual intensity $c(\xi)$ within a small interval of the region is $c(\xi)G(x,\xi)d\xi$. Thus, assuming superposition is valid, the total effect at a point x due to a distribution of causes within the entire region is (Hildebrand, 1965):

$$e(x) = \int_{\mathfrak{R}} G(x,\xi)c(\xi)dV \qquad (1)$$

The function $G(x,\xi)$ is called the influence function of the problem and represents the effect at x due to a unit concentrated cause at ξ. However, to determine $e(x)$ from equation 1, this influence function must be multiplied by an intensity, $c(\xi)$, at every point and summed for the region $\mathfrak{R}$. This region is assumed homogeneous, with material effects being inherent in the shape of the chosen influence function. Figure 1 shows two exponential influence functions for points above the centerline and edge of a longwall coal mine panel. These functions give the influence of a cause at mine level on a particular surface point, and, obviously, decrease with distance between the cause and the surface point. However, to calculate the effects (subsidence) on the surface by equation 1, these causes must be assigned intensities.

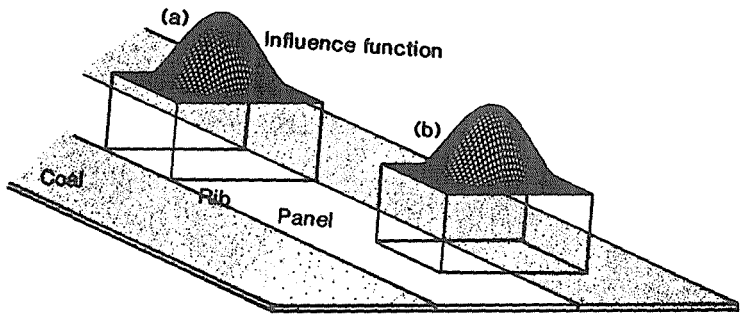

FIG. 1 Position of influence function for surface point located above (a) centerline of panel, (b) edge of panel.

From the explanation of procedure as given by Brauner (1973), the intensities initially used for subsidence prediction above longwall coal mines can be shown to be represented by a step function equal to one over the extracted area and equal to zero elsewhere (Triplett and Yurchak, 1990). Employing a step function for the intensities may be appropriate under the conditions for which the influence function approach was first applied, that is, for stowed panels (Kratzsch, 1983). However, the intensity function may have to be modified for caved panels. Several changes in the technique have essentially modified the intensity function, as shown in figure 2 (Berry and Sales, 1962; Kratzsch, 1983; Adamek and Jeran, 1985; Heasley and Saperstein, 1986). Since each of these changes has increased the accuracy of the technique, a rigorous definition of the intensity function seemed appropriate.

By inspection of an assumed caving configuration above a longwall panel, such as failure of the immediate roof up to some strata that spans the caved zone, the necessary changes can be hypothesized. The total caving region can be represented by an intensity function which changes across the width of the panel (figure 2), thereby including such factors as the break angle of the immediate roof and incomplete convergence near the edge of the extraction. This intensity function also can incorporate convergence of the entries adjacent to the mined panel. For this case, a reasonable intensity function would increase from zero at some distance away from the panel to one somewhere over the extracted area, remain constant across some central width, then decrease similarly over the opposite edge.

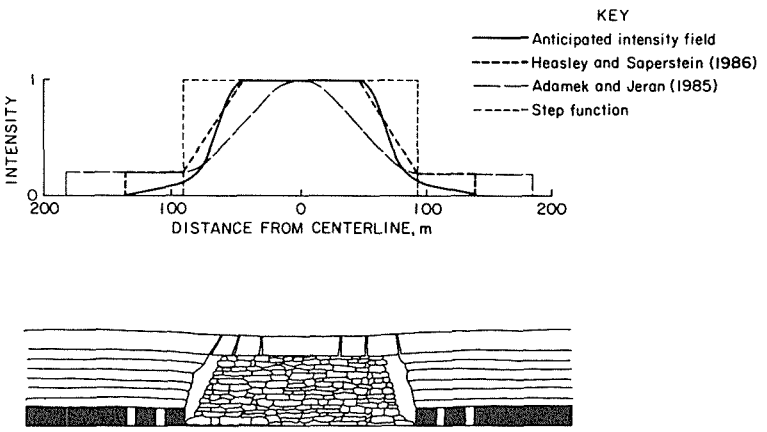

FIG. 2 Caving configuration with approximate intensity functions.

Even though the intensities are hypothesized to be related to the factors mentioned above, at this time the intensities cannot be written as a function of specific physical quantities. Therefore, the intensity of an extraction is necessarily represented as a relative, dimensionless quantity between zero and one. The assumed intensities

shown in figure 2 vary along only one dimension. The function actually varies across both the width and length of the panel. In this paper, the function was assumed to be constant along the length of the extraction, which is appropriate for a transverse subsidence profile unaffected by the ends of the extraction.

DETERMINING THE INFLUENCE AND INTENSITY FUNCTIONS FOR A LONGWALL PANEL

From working with various influence and intensity functions the location of the predicted inflection point, or the point where the curvature of the subsidence profile changes sign, was found to depend only on the intensity function. That is, given a particular intensity function to be used in equation 1, the predicted location of the inflection point remains constant when different symmetrical influence functions are substituted in the equation. The relationship between the intensity function and the location of the inflection point allows an iterative process to be developed which provides an influence and intensity function for a given case study.

First, a particular form of intensity function is varied and used with a constant symmetrical influence function in equation 1 until the actual and predicted inflection points correspond, thereby identifying a possible intensity function. In general, the shape of the actual and predicted profiles will not match after this first step. Thus, in the second step, the determined intensity function is used in equation 1 along with various influence functions until a best fit to the entire profile is found. If the measured and predicted profiles will not match, another form of intensity function is chosen and the process repeated until the entire profile is duplicated. The accuracy of this process is increased by matching the measured slope and curvature with the first and second partial derivatives of equation 1. For example, the derivatives with respect to the northing, or x_1, direction are:

$$\frac{\delta s(x_1,x_2)}{\delta x_1} = \int_{\mathfrak{R}} \frac{\delta G(x_1,x_2,\xi_1,\xi_2)}{\delta x_1} \, c(\xi_1,\xi_2)\,d(\xi_1,\xi_2) \qquad (2)$$

$$\frac{\delta^2 s(x_1,x_2)}{\delta x_1^2} = \int_{\mathfrak{R}} \frac{\delta^2 G(x_1,x_2,\xi_1,\xi_2)}{\delta x_1^2} \, c(\xi_1,\xi_2)\,d(\xi_1,\xi_2) \qquad (3)$$

where $s(x_1,x_2)$ is the subsidence at the surface.

In these equations, ξ_1 and ξ_2 represent the northing and easting coordinates of a mine level point, and the above integrals are taken over the area in which intensities occur. Since x_1 and x_2 represent the northing and easting coordinates of a surface point, equation 2 yields the slope and equation 3 yields the curvature along a surface subsidence profile in the x_1 direction. If both the influence and intensity functions chosen to match the measured subsidence are correct, then the slopes and curvatures given by equations 2 and 3 should match the slopes and curvatures calculated along the measured profile.

Actual field data from southern Illinois was used to demonstrate this approach. In this case study, a 260 m (850 ft) wide and 190 m (625 ft) deep panel was mined from west to east. Measurements in the mine show convergence at a distance of more than 23 m (75 ft) away from the edge of the panel (Janes, 1983), and a barrier pillar was located at 38 m (125 ft) outside the panel. Furthermore, studies have shown that the barrier pillar may deform in certain instances in Illinois (Chugh, 1989). Thus, the limit of convergence was varied between 23 and 53 m (75 and 175 ft), with this point defining the limit of the intensity field. The distance from the edge of the panel to the zero subsidence point was 91 m (300 ft); therefore, the distance from the outermost point of non-zero intensity to the subsidence limit varied between 38 and 68 m (125 and 225 ft). These values were equated to the radius of the base of the influence function, B.

In figure 3, actual subsidence data above the longwall panel were matched using the influence function:

$$G(x_1,x_2,\xi_1,\xi_2) = \frac{nS_{max}}{B^2} \exp\left[-n\pi \left(\frac{(x_1 - \xi_1)^2 + (x_2 - \xi_2)^2}{B^2} \right) \right] \qquad (4)$$

with n equal to 3 (Triplett and Yurchak, 1990). In this equation, x_1 and x_2 are northing and easting coordinates on the surface and ξ_1 and ξ_2 are northing and easting coordinates at mine level.

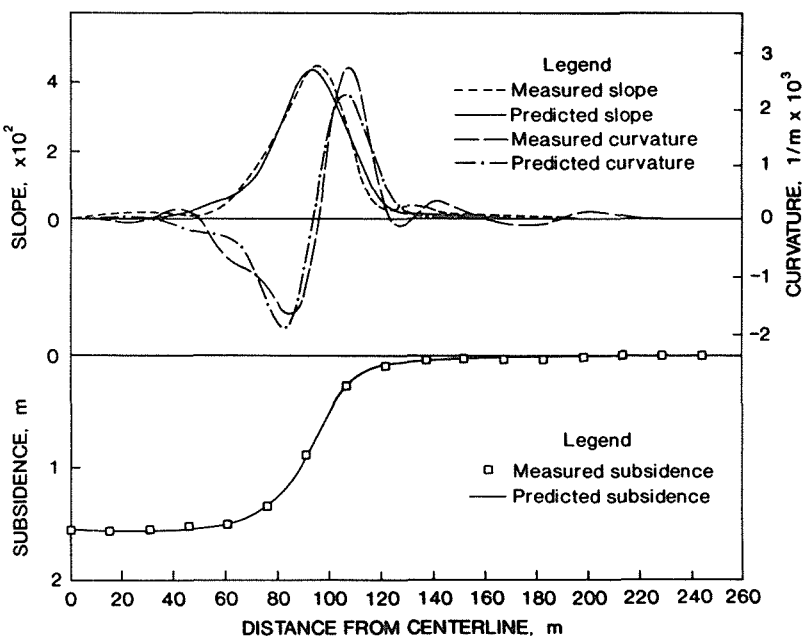

FIG. 3 Actual and predicted subsidence.

The corresponding intensity field was:

$$
\begin{aligned}
c(y) &= .00106y && y = 0 \text{ to } 47.2 \\
&= .91 - \{.043/(.05 + .81e^{-.282(90.5-y)})\} && y = 47.2 \text{ to } 90.5 \\
&= .86 + .00459(y-90.5) && y = 90.5 \text{ to } 121 \\
&= 1 && y = 121 \text{ to centerline}
\end{aligned} \qquad (5)
$$

where y in meters corresponds to the ξ_1 direction and is measured toward the panel centerline from the point of no convergence, found by matching the data to be 45 m into the entries beside the edge of the panel. This function is similar to that shown in figure 2. Assuming the validity of the intensity field, the caving characteristics within the extracted area close to the edge seem to be important, since the intensity function is small in this area. These characteristics may include the shape of the caving zone and incomplete convergence near the edge.

As a check, the first and second derivatives of the influence function were taken in the x_1 direction, and the predicted slopes and curvatures were compared with actual values produced by the derivatives of a fifth-order spline function fit to the subsidence data (figure 3). The ability of these functions to predict the slopes and curvatures suggests that the functions are appropriate for this case study.

The above functions were determined from one case study and must be verified using independent subsidence data. The influence function is expected to remain constant for similar overburden geological properties. The intensity function, however, should change with varying mine geometry; thus, the influence function first should be verified using data from mines with similar geometry. However, since this work has shown that the prediction technique is not overly sensitive to the choice of influence function, the function shown in equation 4 is expected to be suitable for areas of Illinois with geology similar to the test site. Given positive results, intensity functions then can be found for varying mine-level conditions and mine geometries. Finally, if the appropriate influence and intensity functions are known, equations 2 and 3 can be used to predict the slopes and curvatures along the profile.

PREDICTING SUBSIDENCE FROM GROUND WATER WITHDRAWAL

According to equation 1, two functions are required to predict an effect, e(x): an influence function, $G(x,\xi)$, and an intensity function, $c(\xi)$. Typically, measurements are used to determine these functions. For example, to find the influence function of a material, both the intensities of the causes as well as the effects are measured, and the influence function is calculated. This influence function then can be used to predict the effects of causes of various intensities. Consequently, from equation 1, either the influence function can be calculated from known intensities and measured effects, or the intensities can be calculated from a known influence function and measured effects.

Unfortunately, in the problem of longwall mining subsidence, only the effects are measured as subsidence, and neither the influence nor intensity functions are known. Both the influence and intensity

functions cannot be calculated mathematically from subsidence data. Of course, the form of either function can be assumed, as with the intensity functions shown in figure 2, and then the remaining function can be calculated by fitting the field data. However, a good fit to the field data could be provided if both the influence function and intensity function were correct or if both functions were incorrect but compensating. Therefore, a good fit to the field data does not insure that the correct functions have been found. Thus, at this time, a procedure is being sought which will mathematically prove the validity of the calculated functions.

However, these limitations may not exist in the case of subsidence due to ground water withdrawal. Under these conditions, the cause of subsidence at the surface is the compaction of aquifers or aquitards at depth. Given the development of numerous models for the prediction of compaction of aquifers and aquitards due to a lowering of the hydraulic head (Vega et al, 1984; Helm, 1984), the intensities of the causes can be equated to this compaction, analogous to Salamon (1963) using a convergence distribution at mine level when predicting subsidence from longwall mining. If the resultant subsidence is also measured, the influence function for a particular geologic setting can be calculated from equation 1. In this case, the effects, $e(x_1,x_2)$, are the subsidence and the intensity function, $c(\xi_1,\xi_2)$, is given by the compaction of the aquifer or aquitard. The influence function, $G(x_1,x_2,\xi_1,\xi_2)$, then can be calculated or determined by matching field data.

An example using simplified data from subsidence due to ground water withdrawal in the Los Banos-Kettleman City area of California can be used to demonstrate this approach. Figure 4 shows the estimated compaction as well as the subsidence from 1943 to 1959 in the lower perforated zone along a cross section from Anticline Ridge to Fresno Slough (cross section B-B′ in Bull and Poland, 1974; Bull 1975). To simplify the example, the total compaction, and therefore the intensities, were applied at the top of the lower zone. Since the compaction was an estimate based on several factors, including the subsidence, the values were used only as a guide to the intensity field. The subsidence values then were matched using the intensity field shown in figure 4 along with the influence function:

$$G(x_1,x_2,\xi_1,\xi_2) = \frac{0.877n}{B^2} \exp\left[-n\pi \left(\frac{(x_1 - \xi_1)^2 + (x_2 - \xi_2)^2}{B^2} \right) \right] \qquad (6)$$

with n equal to 3 and B equal to 115 m (375 ft). Figure 4 shows the variations in the intensity field necessary to produce the measured subsidence. These variations are required to match slopes and curvatures along the subsidence profile, but are omitted by the sparse compaction data. The intensity field was assumed constant perpendicular to cross section B-B′, and is valid only for this particular data.

Even though the data was simplified for this example, the illustration demonstrates several strengths of the technique. First, the technique can be used to predict subsidence from separate aquifers or aquitards, with the total subsidence being given by summation of the subsidence from all causes. Second, the elevation of the top of

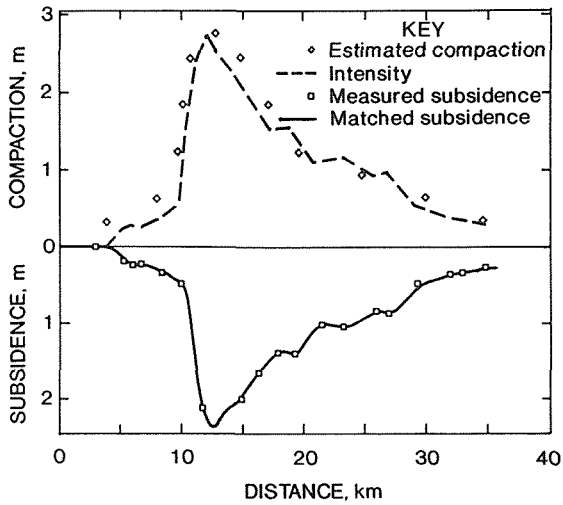

FIG. 4 Actual and predicted subsidence and compaction from ground water withdrawal.

the lower zone varied, but, since the influence is based on distance between the intensity and the surface point, the technique can incorporate varying elevation of intensities or surface points. Finally, the subsidences were measured for a specific time increment; therefore, the intensity function is valid for the years 1943-1959. Analogously, the technique can be made time dependent by changing the intensities over time.

Note that the versatility of the technique may allow the unique determination of an influence or intensity function when only subsidence is measured. That is, given data, it is a simple process to determine influence functions for different geologic settings and intensity functions for diverse sources of subsidence, such as various types of mining or ground water withdrawal. For example, to determine an influence function for predicting mining subsidence, compaction can be calculated in a nearby pumped aquifer, an intensity function can be inferred, and subsidence measurements can be used to calculate the appropriate influence function. Alternatively, to determine an intensity function for ground water withdrawal in a geologic setting similar to a mining case study, the same influence function can be assumed. Subsidence measurements then can be used along with this influence function to calculate the intensity function for ground water withdrawal. In this way, subsidence data from various areas can be used to develop a comprehensive prediction technique.

CONCLUSIONS

The inclusion of a reasonable intensity function in the influence function technique can produce a more accurate prediction of subsidence for mining conditions in southern Illinois. The use of an intensity function is based on the mathematical principles of the influence function technique, that is, linear equations involving cause and effect. A comparison of earlier influence function

techniques has shown that a step function was used by Brauner (1973) to represent extraction intensities, and subsequent modifications to these techniques have essentially changed the intensity function. Several intensity functions were hypothesized and used with various influence functions until measured subsidence from southern Illinois was predicted. Derivatives of the influence function then were used to predict the slopes and curvatures along the profile as a check on the accuracy of the functions. Finally, the versatility of the technique was demonstrated by matching subsidence from ground water withdrawal in California. This versatility may be used to develop appropriate influence or intensity functions for various areas and causes of subsidence.

REFERENCES

Adamek, J. & Jeran, P.W. (1985) Precalculation of Subsidence over Longwall Panels in the Northern Appalachian Coal Region. BuMines IC No. 9042,34-56.

Berry, D.S. & Sales, T.W. (1962) An elastic treatment of ground movement due to mining-III, three dimensional problem, transversely isotropic ground. J. Mech. Phys. Solids 10,73-83.

Brauner, G. (1973) Subsidence due to Underground Mining (in two parts) BuMines IC Nos. 8571 & 8572.

Bull, W.B. & Poland, J.F. (1974) Land Subsidence due to Ground-Water Withdrawal in the Los Banos-Kettleman City Area, Part 3. Interrelations of Water-Level Change, Change in Aquifer-System Thickness, and Subsidence. U.S. Geol. Survey Prof. Paper 437-G.

Bull, W.B. (1975) Land Subsidence due to Ground-Water Withdrawal in the Los Banos-Kettleman City Area, Part 2. Subsidence and Compaction of Deposits. U. S. Geol. Survey Prof. Paper 437-F.

Chugh, Y.P. (1989) Private communication.

Heasley, K.A. & Saperstein, L.W. (1986) Recent insight into longwall strata movements deduced from subsidence analysis. SME Preprint No. 86-331.

Helm, D.C. (1984) Field-based computational techniques for predicting subsidence due to fluid withdrawal. In: Man-Induced Land Subsidence. T.L. Holzer, ed. Boulder, CO: Geological Society of America, Inc.

Hildebrand, F.B. (1965) Methods of Applied Mathematics. New Jersey: Prentice-Hall, Inc.

Janes, J. (1983) A Demonstration of Longwall Mining. Final report, BuMines Contract J0333949, OFR Nos. 86(1)-85 and 86(2)-85.

Kratzsch, H. (1983) Mining Subsidence Engineering. New York: Springer-Verlag.

Salamon, M.G.D. (1963) Elastic analysis of displacements and stresses induced by the mining of seam or reef deposits. J. of S. African Inst. of Mining and Metallurgy, 128-149.

Triplett, T.L. & Yurchak, D.W. (1990) Inclusion of an intensity function for subsidence prediction in Illinois, In: 3rd Conference on Ground Control Problems in the Illinois Coal Basin (Proc. Mt. Vernon, IL, August 1990), 276-284.

Vega, G.F., Yamamoto, S. & Helm, D.C. (1984) Techniques for predicting subsidence. Chapter 5 in Guidebook to Studies of Land Subsidence due to Ground-Water Withdrawal. J.F. Poland, ed. Chelsea, MI: Unesco.

Land Subsidence (Proceedings of the Fourth International Symposium on Land Subsidence, May 1991). IAHS Publ. no. 200, 1991.

Environmental System for Subsidence Engineering

T. ESAKI & S. DOHZONO
Faculty of Engineering, Kyushu University, Fukuoka, 812, Japan
T. KIMURA
The National Institute for Environmental Studies, Tsukuba, 305, Japan
N. KAMEDA
Faculty of Engineering, Kyushu Kyoritsu University, Fukuoka, 806, Japan

ABSTRACT The extraction of mineral and energy resources from underground causes not only visible damage such as surface subsidence but also many invisible ones, which involve changes in ground water flow, cave-in of cavities remaining at shallow depths, and so on. In addition, the land disturbed by extracting is of less economic value and certain ground environments are influenced. The land tends to become flooded, construction of buildings on the land requires special considerations, and residents on the land always feel restless under such dangerous conditions. The problem of restoring disturbed lands is difficult because of various social factors and thus should be considered in an environmental system. This paper describes the actual state of damage caused by extracting resources and by developing underground openings in urban areas and the factors which influence the surrounding environment. The present paper also describes certain features of time delayed cave-ins in the field of coal mining and discusses the long term stability of underground structures from an environmental point of view.

INTRODUCTION

Underground mining of solids such as coal or mineral and extraction of gas or liquid such as natural gas or oil from underground have been developed throughout the world and are continuing at an increasing rate with the development of modern industrial societies. Though most resources are extracted from underground, they are indispensable for human activity at present and their increasing development cannot be avoided in the future. Considering the volume of tailings and subsidence rate, for example, production of three billion tons of coal induces about two billion cubic meters of subsidence basins every year. Subsidence due to mining is large, and has a severe effect on ground environment of the earth because similar degrees of subsidence have been experienced by other mining activity. The exhaustion of mineral resources is an important subject in the near future, and in addition, it is also important to preserve environmental control in presently operating mines. It is, needless to say, that the securing of resources is essential to human life, and nobody can live for a day without resources. Considering the current condition demanding a

better harmony of resource developments and environments, the problem of subsidence requires further examination on not only control of subsidence and preventing damages, but also ground environment harmonizing with human community and securing of resources.

This research aims at discussing subsidence from the point of view of environmental system. This paper describes and discusses the present condition of subsidences and the related problems.

SUBSIDENCES AND DAMAGE CAUSED BY MINING

Subsidence caused by mining has been studied for a long time (Nishida, 1962; Braeuner, 1973; Kratzsch, 1974; British Coal, 1975; Fukuoka Branch; MITI, 1975). Their theories have been almost accomplished solutions to the problems, and can be applied to most cases in the field. The schematic of a subsidence trough is shown in Fig.1. Extraction of a deposit lying at a depth causes subsidence in the surface area defined by a limit angle at the edge of the extraction area. This subsidence does not arise in a moment, but increases slowly with progress of extraction. For example, a face, whose width is a hundred meters or more in long wall mining, proceeds usually a few meters a day. In addition, ground movement also depends on time and continues for several months to years after extraction. Therefore, it is usual that damages are found a long time later after mining. The rate of subsidence, which is a ratio of maximum subsidence, S_{max}, to the thickness of an extracted seam, is about 75-90%. If the mining area has spread to a large area, the convergence between roof and floor in the extracted area should develop and the consequent surface subsidence becomes extensive. From the point of view of damage to surface features, it is convenient to resolve the deformation at a point into five components: subsidence (vertical movement), slope, curvature, horizontal movement and horizontal strain. Kinds of damage caused by these components are briefly described as follows:

(a) Subsidence
If subsidence arises uniformly, additional stresses will not be transmitted to surface structures. When a mining area is extended widely, however, life lines would be deformed with a big arc and their joints be damaged. In the lowland, surface structures are liable to sustain inundation and poor drainage, and paddy fields can become damp.

(b) Slope
Slope changes a gradient of structures. Stress changes may be induced within the structures, and severe slope would destroy the structures. Damage also occurs in waterways, paddy fields etc..

(c) Curvature
There are two cases; the foundation of a structure bends as the ground does; the structure separated from the ground behaves like a beam. In either case, bending stress and shear stress are induced within the structures, and their framework is deformed.

(d) Horizontal movement
If the magnitude and direction of the horizontal movement are different at each point in a structure, a structure is damaged. In particular, when the structure needs to be kept in a straight line, it may suffer severe damage.

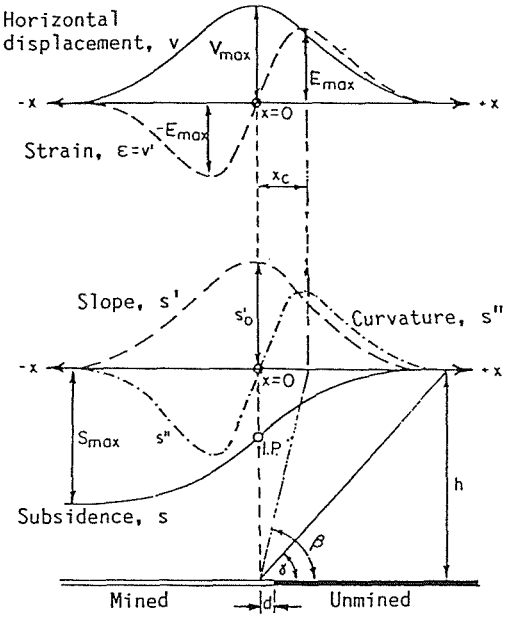

FIG.1 Extraction area and surface movements.

(e) Horizontal strain

Horizontal movement produces shear, tension and compression strains, and causes cracks in structures. This results in leakage of water from a reservoir etc. Regarding mining under the sea, the tensile strain accumulated beneath the sea may cause flooding in the pits.

Generally the greater the magnitude of subsidence, the heavier is the damage. However, high levels of subsidence do not always cause extensive damage. Namely, actual damage cannot be related to an acceptable limit of subsidence. In an actual fact, many damage phenomena are indirectly due to subsidence, and there is peculiar damage that can not be predicted at the beginning. Such phenomena are described in this chapter; sinkhole and trough will be described in the next chapter in more detail.

Except for visible damage, some of environmental impacts are latent.

(a) Resistance from disaster

Storm tides or inundations in a subsidence area could induce greater damage to the area than ones in which have not experienced subsidence. In a region where severe subsidence has been experienced for more than a few meters, the surface run-off water derived from precipitation can not flow down to the river, and pumping up is often necessary. Then the cost is huge. On the lowland, ever a trifling rainfall causes inundations. This phenomenon appears only in limited areas in Japan because the plain area is small. But it is spreading in some European countries and China. Some subsidence areas have remained, forming a large pond as shown in Fig.2.

FIG.2 Subsidence due to deep multiple seam extractions in North China.

(b) Influence on newly constructed structures
When big heavy structures such as railways, roads, waterways or dams are constructed on the mined area, suitable measurements are necessary because cavities remaining since mining operations may cause additional subsidence and sinkholes. A leakage of water may occur at a dam. An example is a working shield tunnel that was flooded all at once because the existence of old goafs was not taken into account at site. The cost for countermeasures usually is very expensive. Sometimes the cost of the foundation is much higher than the upper structure.

(c) Other impacts
The land disturbed by extraction is of less economical value. Surface structures might be injured in the future, and the possibility of the occurrence of damage might impact also the mental state of local residents.

COUNTERMEASURE AGAINST SUBSIDENCE

Many efforts have been made to prevent and/or minimize damage due to subsidence. The allowable strain and slope of a surface structure depend on not only its function but also its habitability. In a wooden house, the allowable value on habitability will be smaller than one on structural stability in many cases. If the slope reaches 2-2.5mm/m, an opening takes place between the door and the frame, and the door becomes poorly fitted. It is sensible that slope of the floor reaches 5mm/m. If plaster wall has 1 mm/m slope, opening may take place between the column and it.

Concrete is brittle and extremely weak for tensile stress. 0.2-0.5mm/m tensile strain makes slight cracks. An allowable deformation of a precision machine may vary with its type. The acceptable value is supposed to be smaller than one of the usual structures mentioned above. Because a machine can be amended and controlled when it is established, the acceptable deformation may be permitted as well as for building in many cases.

The values of allowable deformation are given according to experience in different countries, type of structure and the definition of damage. Table 1 shows representative examples of the allowable values (Peng, 1986). The ground movement, which causes little or insensible damage, can be permitted. Table 2 is an example

TABLE 1 Maximum allowable structural deformations in major coal-producing countries.

Country	Compressive Strain (mm/m)	Tensile Strain (mm/m)	Slope (mm/m)	Radius of Curvature (km)	Remark
China		2	3	5	
France	1-2	0.5			Pipeline
Germany	0.6	0.6	1-2		
	0.5	0.5			Reinforced concrete foundation
Japan	1	1			Frame
	5	5			Waste impoundment
Poland	1.5	1.5	2.5	20	
Donets Coal-field(USSR)	2	2	4	20	
Karaganda Coal-field(USSR)	4	4	6	3	
United Kingdom	1	(30-ft-long building)			

TABLE 2 Categories of protection, Donets district, USSR. α is the angle of dip of the seam. The coefficient of safety is the ratio of safe depth to seam thickness.

Category	Allowable Tilt, $\times 10^{-3}$	Allowable Radius of Curvature (m)	Allowable Strain $\times 10^{-3}$	Coefficient of Safety	
				$\alpha \leqq 45°$	$\alpha > 45°$
I	4.0	20,000	2.0	400	500
II	4.5	18,000	2.5	350	400
III	5.0	12,000	3.5	250	300
IV	8.0	5,500	6.0	150	200
V	10.0	3,000	7.5	100	150
VI	25.0	1,000	14.0	50	75

at Donets coal field (VNIMI, 1958). The category of protection is suggested according to importance or sensitivity of structures. The category I is applicable to a crane foundation or a power plant, the category II is to over five-story structures, and the category VI is to one-story ones.

Once the underground is developed, subsidence cannot be kept to zero. However, if countermeasures are taken in advance, actual damage

can be prevented or be minimized. There are two types of measures, which have been executed, as follows:

(a) Mining design
This type of measures includes partial extraction, filling after mining, harmonic extraction, safety pillar, rapid mining and avoiding undesirable mining shape.

(b) Surface structures
This type of measures includes stiff structures, flexible structures and reducing the stress (a small plane size, division of a structure, reducing the bond between the ground and structures, trenching ditch).

SINKHOLE PHENOMENA

Sinkhole phenomena and their characteristics

The ground with old coal workings often has many unfilled cavities at shallow depths. The cavities are naturally unstable, while weathering of the roof of the cavities, construction of new structures on the ground surface, change in the level of ground water or occurrence of earthquakes may accelerate the deterioration of roof strata above the cavities (Gray, 1982). These effects may become so severe in old abandoned areas that the deteriorated zones fall into the cavities and extend to the ground surface, and eventually cave-in occurs suddenly.

Sinkholes often happen associated with mining. In Japan, sinkholes caused by coal mining are experienced at northern Kyushu and Ube field, and ones by lignite mining at Miyagi, Gifu and Oh-ita Prefectures. It is well-known that sinkholes happen at Appalachia coal fields in the U.S. and diamond mines in the Republic of South Africa. In addition, it is well known that sinkholes happen at limestone areas; they happen at about 50 airports every year which are located on limestone areas in the U.S. The cave-ins at an abandoned tuff quarry in the suburbs of Tokyo caused a severe social problem in the residence area. When the overburden of a tunnel is thin, cave-ins are often experienced during constructing the tunnel.

Sinkhole phenomena are classified in two modes: a sinkhole and a trough. A sinkhole is a phenomenon caused by collapse of the roof of cavities. In this case, the boundary between the ground surface and cave-in is clear. The deeper a cave-in, the larger the diameter. As erosion progresses, the diameter near the surface increases. Most surface shapes of sinkholes are circles and ellipses. A trough is also one kind of sinkhole phenomenon. A cave-in that happens at an underground cavity and does not reach the surface, but the surface sinks like a tray. A cave-in in the underground cavity is caused not only by collapse of roof but also by destruction of pillars or punching. The strength of pillars is reduced due to the movement of ground water levels, weathering of rock beds and so on. If a pillar is crushed by concentration of stress, a redistribution of stress is weak. The surface shape of trough is generally ellipse and the diameter is about 15-150 m.

Collapse process of a cavity

The occurrence of sinkhole is promoted by rainfall, earthquake and so

FIG. 3 Cave-ins due to ground water drainage.

on. The influence of rainfall is proved because occurrences of sinkhole increase in the rainy or typhoon season in Japan. It is indicated that sinkhole development in many cases is related to precipitation in preceding three to eight months in U.S.A. (Bruhn, 1978). Drawing up of ground water also heavily influences occurrence of sinkhole. It is the example that some sinkholes have caused by drawing up for construction of new railroad, Shinkansen (Fig.3). The influence by drawing up of ground water is much greater than one by rainfall. These influences originated in ground water are explained by a rise of pore pressure inside underground and an increase of unit volume weight of the ground.

Because a sinkhole is the phenomenon that a collapse of a roof of cavity reaches to the surface, it is important to investigate the behavior of roof of cavity. When the ground is assumed to be homogeneous, the shape of collapse is an arch i.e. the middle of the arch is the highest, and the edge of the arch becomes an abutment. If a cavity is at shallow depth, this arch reaches the surface and a sinkhole happen. On the other hand, in the case that the ground is regarded as bedding ground such as seamy ground, the immediate roof of a cavity falls first, and it progresses to upper beds one by one. In this case, because each beam is fallen by bending, the collapse height tends to be larger than one at homogeneous ground. But if a cavity is deep, sinkhole is hard to occur.

Time dependence of collapse of a cavity

The time when a cavity can be kept without support after excavation is called "stand-up time". Stand-up time depends on characteristics of ground discontinuity (i.e., a joint), a strike direction, filling in a joint, and so on. Lauffer (1958) and Bieniawski (1984) studied the stability of cavities considering the lapse of time (Fig.5). Their "unsupported span" stands for the maximum width of a stable unsupported opening as defined in Fig.4. The stand-up time is the

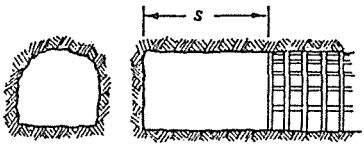

(a) In case of Tunnel width < Unsupported span

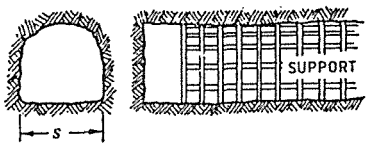

(b) In case of Tunnel width > Unsupported span

FIG.4 Definition of Unsupported span.

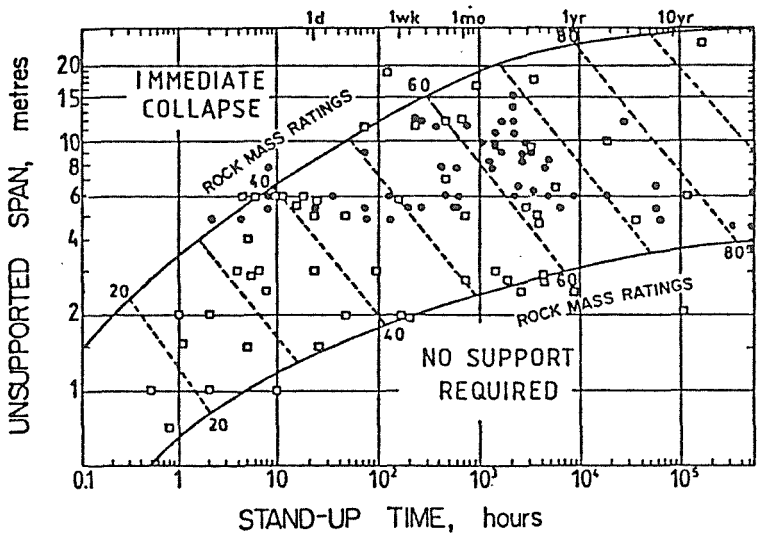

FIG.5 Geomechanics Classification of rock masses: output for mining and tunneling after Bieniawski (1984);
● = case histories of roof falls in mining;
□ = tunneling roof falls;
contour lines = limits of applicability.

period of time that a tunnel will stand unsupported after excavation, but long term stability is not considered. There is no key to calculate concretely the long term stability. Therefore, it is supposed to be important to analyze the actual instability phenomena that occurred in the past. The lapse of time from excavation of a cavity to cave-in occurrence has been investigated statistically, as an example, in northern Kyushu. We have experienced 1,211 cave-ins from 1974 to 1990 in the area of 500 km². The record of excavation is not clear in most cases. Therefore, the opening and closing year of mining is examined for each coal mine located in the fields where

sinkholes happened in the past. As a result, three cases is assumed as the time of excavation. (A): it is at the mine opening, (B): at the mine closing, (C): The middle of the mine opening and closing. Fig.6 shows the lapse time for 1,211 cave-ins on a normal probability graph. The abscissa axis is the lapse time taken from excavation of a cavity to cave-in occurrence, while the ordinate is accumulated probability. In the case of (A), the average lapse time, X, is 19.4 years, the standard deviation, σ, is 6.57 years. In the case of (B), X=71.5 years, σ =23.4 years and in the case of (C), X=45.5 years, σ =12.6 years. Then, 90% of the whole occurrence will take 62 years after mining in the case of (C).

The relation between the lapse time and the accumulated probability in the Pennsylvania coal field also is shown in Fig.6. 50% of the whole occurred by 52 years after mining. Comparing these with a couple of data in Northern Kyushu and Pennsylvania, their averages are slightly different, but the data of sinkhole occurrence in Pennsylvania fall between the cases (B) and (C). This reason is that mining at the shallow depth was executed at early times of mine development. In either case, it can be said that cave-ins continue for a long time after mining. As clear records, the lapse time such as 118 years in England, and 73 years in Colorado State are recorded.

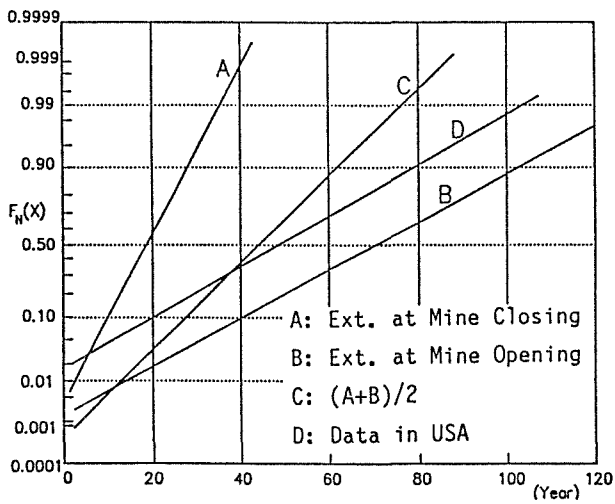

FIG.6 Time interval between extractions and cave-ins occurred in the northern Kyushu. Lines A, B and C are obtained under assumptions that coal was extracted at opening of mine, at closure of mine and at the middle of the mine opening and closing.

CONCLUDING REMARKS

Subsidence problems related to resource development are introduced and discussed based on many examples, and some problems are reviewed from the point of ground environment. As a result, it is clarified that a subsidence problem is not related to only physical values. Mining

activity might change ground characteristics, since present mining plans are not always considered from the environmental point of view. Once ground conditions change, visible damage may take place in the future. In other words, some kinds of damage are not visible at present, but they might be caused by changes of the other conditions. The compensations and restorations for visible damage have been investigated only by affected ones, but they should be also considered from the environmental viewpoint. It would therefore be necessary and pressing to consider and accomplish an environmental system for settling these problems.

REFERENCES

Bieniawski, Z.T. (1984) Rock Mechanics Design in Mining and Tunneling. A.A.Balkema, Rotterdam, 97-135.

Braeuner, G. (1973) Subsidence due to underground mining. Information Circular 8571, US Bureau of Mines.

British Coal (1975) Subsidence Engineers' Handbook, 2nd ed. London.

Bruhn, R.W., Mangnuson, M.O. & Gray, R.E. (1978) Survey of ground surface conditions affecting structural response to subsidence. ASCE Spring convention, Pittsburgh, ASCE Preprint 3293, 26-55.

Burns, K. (1981) Prediction of delayed subsidence, Proc. Workshops on Surface Subsidence due to Underground Mining, Morgantown, 220-224.

Gray, R.E. & Bruhn, R.W. (1982) State of the art of ground control in longwall mining and mining subsidence. SME, AIME, 253-271.

Kratzsch, H. (1974) Bergschadenkunde, Springer Verlag, Berlin.

Lauffer, H. (1958) Gebirgsklassifizierung fuer den Stollenbau. Geologie und Bauwesen, 24 (1), 46-51.

Fukuoka branch, the ministry of international trade and industry (1975) An Introduction to Mining Damage, Fukuoka, Japan (in Japanese).

Nishida, T. (1962) Mining subsidence. The Reports of Research Inst. of Industrial Science, Kyushu University, 32, 1-74.

Nishida, T., Esaki, T., Kimura, T. & Kameda, N. (1988) Environmental impacts of coal mining and preventive measures in Japan. Proc. Symp. on Modern Mining Technology, Taian, 85-92.

Peng, S.S. (1986) Coal Mine Ground Control, 2nd ed. John Wiley & Sons, N.Y.

VNIMI (1958) General institute of mining surveying, Soviet Union. The Movements of the Rock Masses and of the Surface in the Main Coalfields of the Soviet Union, 250, Moscow.

Land Subsidence (Proceedings of the Fourth International Symposium on Land Subsidence, May 1991). IAHS Publ. no. 200, 1991.

Modelling and Prediction of Ground Subsidence Using an Iterative Finite Element Method

A. SZOSTAK-CHRZANOWSKI & A. CHRZANOWSKI
Department of Surveying Engineering, University of New Brunswick, Fredericton, N.B., E3B 5A3, Canada

ABSTRACT Several years of intensive research on modelling and prediction of ground subsidence in mining areas have led the authors to the development of a method, known as the S-C method, which is based on iterative linear elastic analysis combined with an empirical knowledge of the general behaviour of rock masses and their in situ mechanical properties above mine workings. The non-linear behaviour of the rock masses is modelled by a linear elastic finite element analysis in which zero values of Young's modulus are iteratively introduced in the directions of the critical tensional stresses in individual (anisotropic) elements.The concept of a so-called "weak" zone of rocks is introduced in order to reduce propagation of tensional stresses. The "weak" zone represents the distressed and tensiond rocks above the mine opening. It is delineated by the elements with maximum shearing stresses. The S-C method is supported by software FEMMA for two- and three-dimensional finite element analyses.

INTRODUCTION

Ground subsidence, like any other type of ground or structural deformation, may be modelled by using either empirical (statistical) or deterministic prediction theories.The empirical (statistical) model, through a regression analysis of the post-survey data and observed causative effects (loads), gives the load-deformation relationship which in turn may be used for predicting deformations as a function of known loads.The deterministic model, obtained from the a priori known properties of material, from mechanical relations between the loads (surface and body forces) and internal stresses, and from the physical laws governing the stress-strain relation, describes the expected deformation.

Most of the empirical theories for predicting subsidence have been developed in central Europe and the United Kingdom, where systematic and accurate monitoring surveys have been conducted in mining areas for several decades. The empirical models have been obtained through a correlation of the observed deformations with the causative effects which are usually expressed only in terms of the geometry and depth of the mined deposit and, in some theories, with qualitative information on geology and the strength of rocks. Since other parameters, such as mechanical properties of the rock and tectonic stresses, are not taken into account, the prediction theories are applicable only to the areas where the mining, geologic, and tectonic conditions are the same or very similar to the area where the empirical data for the theory had been collected. Since the conditions in different areas are never the same, any attempt to adapt, for instance, the European empirical models for ground subsidence prediction to the North American continent requires the calibration of the model parameters through many years of comparisons with the observed deformations in the new area. Usually, this approach is unrealistic because very few, if any, mines in North America have a well organized and systematic program of monitoring surveys. It also should be stressed that the empirical theories are generally not reliable in cases of complicated geometry of mined deposits, in the presence of faulting, and in areas of previous extensive mining operations.

For the above reasons, the authors in their research on the development of a prediction theory concentrated on the use of deterministic modelling of ground subsidence, rather than on the adaptation of empirical models from other areas to North American conditions. The deterministic methods are definitely more universal than the empirical theories because they can be applied in any geological and mining conditions, and they provide information not only on surface subsidence but also on deformations within the rock masses and within the mine workings. The deterministic methods, however, require reliable information on the in-situ properties of rocks, initial stresses, and tectonics of the area. The in-situ properties of rocks are of particular importance. They are difficult to determine and they change in time according to the progress of the mining activity. In addition, due to discontinuities in the rocks (cracks, faults, etc.) they cannot be treated as linear elastic material. The uncertainty in the determination of the mechanical properties and the non-linear behaviour of the rocks are the main reasons why despite intensive research at various centres over the last two decades, no successful method for predicting ground subsidence has been developed when using deterministic modelling alone.

Several years of intensive research on modelling and prediction of ground subsidence in mining areas have led the authors to the development of a method, known as the Szostak-Chrzanowski or, briefly, the S-C method, in which the theory of deterministic modelling has been combined with an empirical knowledge of the global behaviour of rock masses and their in-situ mechanical properties. Preliminary results of the authors' research were presented at the Third International (IAHS) Symposium on Land Subsidence (Chrzanowski and Szostak-Chrzanowski, 1984) held in Venice in 1984. Over the past few years the method has undergone some final refinements and has been expanded from two- to three-dimensional applications. The method is supported by software FEMMA (Finite Element Method for Multi-purpose Applications) which has been developed by Szostak-Chrzanowski (1988). This paper gives a brief review of the S-C method and FEMMA followed by a practical example.

THE S-C METHOD OF GROUND SUBSIDENCE MODELLING

Basic Concepts and Calculation Procedures

Modelling of ground subsidence involves rock masses which, due to existing discontinuities (cracks, faults, etc.), can generally be treated as non-linear elastic material. Following Zienkiewicz et al. (1968), the S-C method accepts (with some limitations) the concept of the rock masses being "no-tension" material (having zero tensional strength).

Changes of stresses in the rock masses due to the mining activity and resulting changes in the in-situ mechanical properties of the rocks are time dependant. The problems of time dependancy and of the aforementioned non-linearity of the material are solved in the S-C method through the iterative superposition of static linear elastic solutions using the finite element method (FEM).

The S-C method has been developed for the determination of the final (static) state of deformation when the excavation process has been completed and a new state of equilibrium of forces has been achieved after a long enough period of time.

The basis of the S-C method is the introduction from empirical models of ground subsidence (Figure 1) of a so-called "weak" zone of the rock strata above the distressed mine opening. The weak zone is delineated by maximum shearing stresses which develop at the boundary between the zone of loosened rocks subjected to tensional stresses above the opening and the surrounding rocks subjected to compressive stresses. The boundary surface of the maximum shearing stresses had been identified by Kratzsch (1983) as a slippage surface of rocks which reduces the transfer of tensional stresses beyond the surface. In shallow mines, the slippage surfaces of the "weak" zone may extend to the surface. In the S-C method, the limitation of the transfer

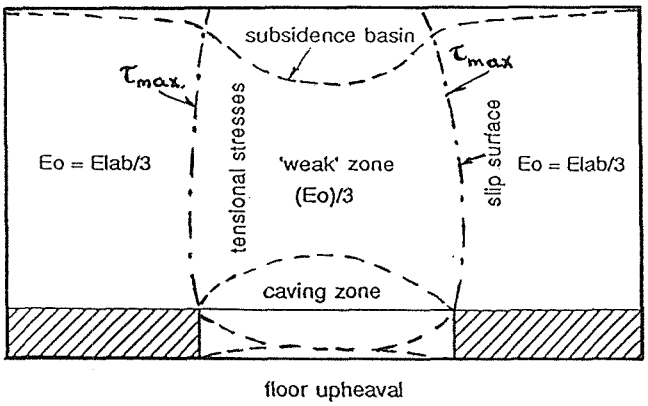

FIG. 1 Basic Model of Ground Subsidence.

of tensional stresses is achieved by decreasing the initial value of Young's modulus of elasticity of the rocks within the "weak" zone by an empirical factor of 3. If any geological faults or any other major discontinuities are identified within the expected influence of the mining activity, the "weak" zone is expanded to the discontinuity. The "weak" zone is delineated after obtaining the first linear elastic FEM solution with the introduced mine openings, initial displacement and force boundary conditions, and initial mechanical properties of the rocks.

Once the "weak" zone is introduced into the FEM model, the basic task of the S-C method is to change iteratively the values of Young's modulus E in the constitutive matrix according to the assumption that the rock mass is a "no-tension" material. All elements in which tensional stresses develop are determined through the subsequent iterative FEM solutions. In the case of elements within the "weak" zone in which both principal stresses are tensional, the value of E = 0 is placed in all directions (isotropic elements). In cases of only one principal stress being tensional, the material is assumed to be anisotropic with E = 0 in the direction of the principal stress. Typically, when the extracted area is sufficiently large, the elements in the immediate roof of the mining opening develop tensional stresses in all directions and thus their E value is decreased isotropically to zero (practically it is taken as equal to 0.01 of its initial value). These elements are then treated as being "caved-in" into the mine opening. In coal mines, the caved-in zone may reach 70 m or even more above the opening. The displacements of the caved-in elements are limited (by introducing additional boundary conditions) to be smaller than the expected maximum vertical convergence of the opening. If a backfill is used in the mined opening then the coefficient of compactivity of the backfill must be estimated. If any tensional stresses develop outside the "weak" zone, the value of E = 0 is introduced only in the direction of the tensional stress which exceeds the tensional strength of the rock in the given element. The iterative FEM calculations are repeated untill no more tensioned elements are developed in the "weak" zone.

Basic Parameters of the S-C Method

To carry on the quantitative analysis, following parameters must be specified:
- geometry of the problem, which includes geometry of mine openings, surface topography, geology, and geometry of tectonic disturbances,
- loads, which include body forces, tectonic stresses and external forces,
- mechanical parameters of rocks,
- strength criteria,

• boundary conditions, with information on degrees of freedom of each point and location of the points with zero degrees of freedom.

Geometry of the Problem
The location and shape of the mine opening and rock profile are factors which have to be considered in defining the geometry of the problem. The location of the opening is in most cases easy to define. In the two dimensional analysis it is important to place the cross section of the investigated mining field in such way that the perpendicular dimension of the field is equal or larger than the diameter of the so-called critical area of the opening which would cause the maximum subsidence. To determine the approximate radius of the critical area, one of the empirical subsidence prediction methods may be used. In a geometry of tectonics the most important factor is localisation of the tectonic discontinuities.

Definition of Loads
The existing state of equilibrium of stresses, often termed as the initial or in-situ stress is disturbed by the mining activity. The initial state of stress is a function of the weight of the material and, in some cases, the tectonic forces. The initial state of stress is usually defined by the vertical stress and the ratio 'k' of the horizontal to vertical stress. The direct determination of the in-situ stress is very difficult, and in some cases even impossible. Therefore, the initial state of stress is usually calculated only from the known unit weight of the material. In this case, the gravity loads are included in the analysis as body forces. If, from other measurements, the aforementioned coefficient 'k' is known, one can introduce also horizontal stresses calculated from $s_x = k\, s_y$, where s_y is the vertical stress obtained from gravity forces. The value of the coefficient k varies in practice from 0.2 to 2 or even more.

Material Properties
The basic parameters of the S-C method which describe the rock mass are: elasticity parameters such as Young's modulus and Poisson's ratio, the unit weight and compressive and tensional strengths. The elasticity parameters are included in the constitutive matrix which describes the relation between the strain and stress in the rock mass (general Hook's low).

Usually, the values of the basic parameters are determined through laboratory tests using rock samples from the given mining area. Since the in-situ rock masses are inhomogenuous and very often discontinuous, the laboratory determined parameters have large errors which depend on the quality of the sample and type of the test (uniaxial or triaxial). In most cases the parameters obtained from laboratory tests have higher values than in-situ values. Following the empirical data published by Bieniawski (1984), the S-C method accepts the in-situ values of E of the intact rock mass as being three or five times smaller than the laboratory values for intact or disturbed (by previous mining operation) rocks respectively. If the laboratory values from the investigated mining area are unknown (a frequent case) then the E value is taken as the average value published for similar type of rocks and similar geological conditions.

Laboratory values of Poisson's ratio are accepted in the S-C method as equal to the in-situ values.

The laboratory determined tensional strength R_r is usually, at least, four times smaller than the critical compressive strength R_c. The empirical data from coal mining areas (Kleczek, 1986) show, that the in-situ critical tensional strength is about 40 times smaller than the compressive strength in the immediate roof of the opening and about 10 times smaller in the higher strata. In the S-C method, the tensional strength within the "weak" zone is accepted as equal zero, while in the rocks outside the "weak" zone

the tensional strength is accepted either as given by laboratory tests or 10 times smaller, whatever is smaller. If the laboratory values for the investigated mining area are not known, then commonly known values for similar type of rocks and similar geological conditions are taken.

FINITE ELEMENT PROGRAM "FEMMA"

The computer program FEMMA has been developed by the co-author (Szostak-Chrzanowski) for two and three dimensional linear and visco-elastic analyses. The two dimensional version has been adapted for PC computers while the three dimensional version is still usable only on mainframe computers.

The programme is characterized by the following specifications:

- linear eleastic or visco-elastic analyses (Kelvin model)
- in the two-dimensional analyses, options for either plane stress or plane strain cases are available
- unlimited number of elements (the limit is given only by the capacity of the computer);
- unlimited number of nodes, (limit is as above);
- unlimited number of material types (limited only by the number of elements);
- analysis with isotropic and anisotropic materials (the direction of anisotropy does not have to coincide with the axes of the coordinate system);
- four nodal or eight nodal elements for two- or three-dimensional analyses respectively
- application of four or six integration points
- banded format of the total stiffness matrix (to decrease the dimensions of the total stiffness matrix)

The programme may utilize the following input data:

- initial stress,
- initial strain,
- initial thermal strain,
- body forces (as a unit weight),
- force boundary conditions,
- displacement boundary conditions,
- elasticity parameters (E and ν) for isotropic and anisotropic material,
- orientation of anisotropy,
- strength parameters,
- choice of a criteria,
- time iterval

The output of the programme gives:

- displacement vectors at the nodal points, (x and y components, total displacement, and its direction),
- elastic strain vector in each element,
- strain vector in each element with elastic and creep components,
- stress vector in each element,
- principal stresses and their orientation,
- list of elements in which the tensional stresses exceeded the given value,
- list of elements in which the compressive stresses exceed the critical values

EXAMPLE OF A PRACTICAL APPLICATION

The S-C method has been succesfully employed in modelling and predicting ground deformation in coal, copper, potash, and lead and zinc mines. Some applications have been described in Szostak-Chrzanowski (1988) and in Chrzanowski and Szostak-Chrzanowski (1987). One example is given below.

The investigated mining operation is located at the central east coast in the People's Republic of China. Two side-by-side panels (Figure 2) of an inclined (11°) and 4.2 m thick coal seam have been extracted at an average depth of 150 m using the long wall mining method with roof caving. The geological strata (Figure 3) consisted mainly of sandstone and shale.The exploitation of the two panels took place in 1966. Subsidence measurements had commenced prior to the exploitation and ended in 1968. The finite element analysis, using the S-C method, was performed along the A-A cross section which coincides with the line of survey benchmarks (Figure 2). The actual mechanical parameters of the rocks were not available to the authors. Therefore, average values (Table 1) have been accepted as published by Kidybinski (1982) for the similar types of rocks in coal mines in Poland.

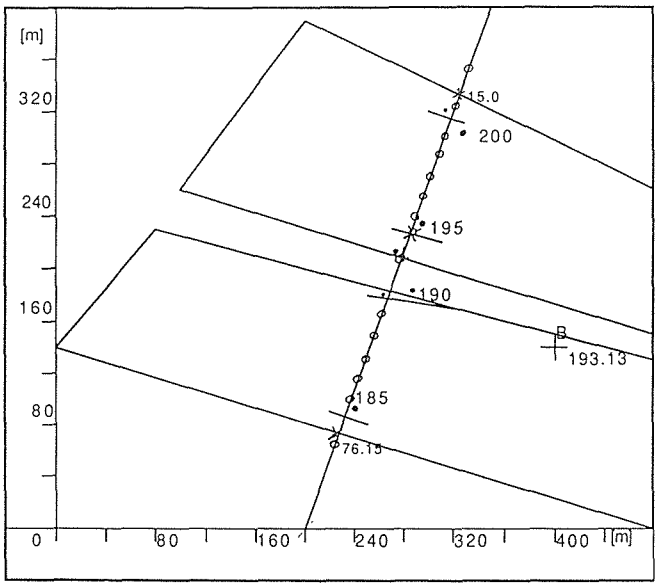

FIG. 2 Coal mine, East Coast of People's Republic of China.
o - surveying points ; x - elevations [m] in the mine; • - elevations on the surface

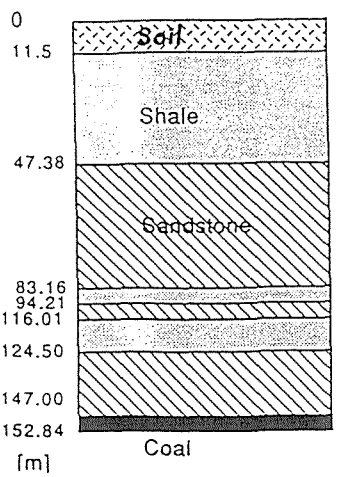

FIG. 3 Geological profile at point B.

TABLE 1 Average properties of rocks (laboratory); coal mine in East China.

Material	Rc [MPa]	Rr [MPa]	E [GPa]	ν	γ [kN/m^3]
Sandstone	60.0	4.2	11.0	0.20	26.0
Shale	40.0	4.8	12.2	0.20	26.0
Shale + soil	10.0	4.9	3.0	0.30	26.0
Coal	20.0	0.8	3.5	0.25	13.0

Figures 4 and 5 show the FEM mesh and the comparison of the subsidence results, respectively. The final results were obtained after five iterative solutions. Despite the poor knowledge of the mechanical properties of the rocks, a very good agreement has been obtained between the observed and modelled subsidence.

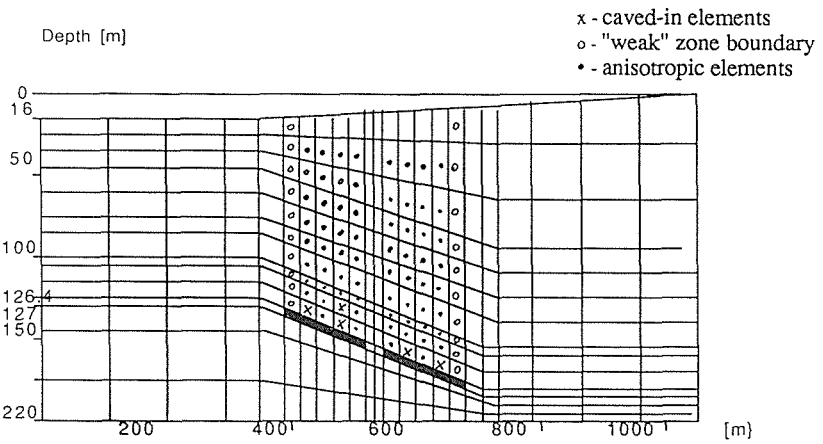

FIG. 4 FEM model.

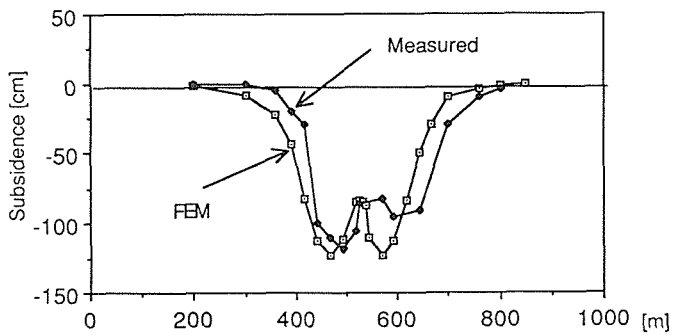

FIG. 5 Calculated and observed ground subsidence.

CONCLUSIONS

The S-C method gives good results in two-dimensional deterministic analyses of ground deformations produced by deep mining activity. The method has also been adapted for three-dimensional analyses but, at the time of writing this paper, no practical examples have yet been available.

The program FEMMA, thanks to its modular structure, is a very flexible software allowing for easy expansions into solving time dependant deformation problems. At present, visco-elastic modelling is possible using Kelvin model. Any other models of the material behaviour can easily be added to the program

REFERENCES

Bieniawski, Z. T. (1984) Rock Mechanics Design in Mining and Tunnelling. Balkema.

Chrzanowski, A. and A. Szostak-Chrzanowski (1987) Some new developments in monitoring, analysis and prediction of ground subsidence. CIMM Bulletin, vol.80, No.901, pp. 46-50.

Kidybinski, A. (1982) Podstawy geotechniki kopalnianej (in Polish). Wydawnictwo Slask, Katowice.

Kratzsch, H. (1983) Mining Subsidence Engineering. Springer-Verlag, Berlin.

Szostak-Chrzanowski, A. (1988) An iterative modelling of ground subsidence using non-linear elastic finite element analysis. Proceedings, 5th International (FIG) Symposium on Deformation Measurements (ed. Chrzanowski and Wells), University of New Brunswick, Canada, June 6-9, pp.524-535.

Zienkiewicz, O.C., S.Valliappan and I.P. King (1968) Stress analysis of rock as a 'no-tension' material. Geotechnique, vol.16, pp.56-66.

Land Subsidence (Proceedings of the Fourth International Symposium on Land Subsidence, May 1991). IAHS Publ. no. 200, 1991.

Subsidence Management in Jharia Coalfield, India — A Concept

N. C. SAXENA
Central Mining Research Station
Dhanbad 826001, India

ABSTRACT Jharia coalfield in India having been blessed with about 17-billion tonne coal in 40 coal seams is facing problems of subsidence management due to successive extraction of the seams. More than 50 Km^2 of land in the coalfield has so far been degraded. Many surface properties have been damaged. A maximum subsidence of about 25 m is anticipated in the coalfield. The subsidence shall be taking place repeatedly and therefore subsidence management measures shall have to be planned accordingly. A methodology for such a subsidence management has been suggested.

JHARIA COALFIELD

The importance of Jharia coalfield in India lies in the fact that this is the only source of prime coking coal in the country. From the point of view of coal mining India occupies an important position with about 205 million tonne production in 1989-90. The projected target for the year 2000 is 400 million tonne. As per available records coal mining in India was started in 1774.

The Indian coalfields, covering more than 15,000 Km^2 area, generally belong to Lower Gondwana group of Permian age and Tertiary group of Eocene to Miocene age. Lower Gondwana deposits account for 90% of the total coal production. The coal reserves of the country are estimated as 176,330 million tonne.

The Jharia coalfield is located in Dhanbad district of Bihar. It lies about 250 km west of Calcutta. Various details of the coalfield are listed below.

1.	Longitude & Latitude	-	86°11' to 86°27' and 23°39' to 23°48'
2.	Ground elevation above mean sea level	-	140 to 240 m
3.	Surface topography	-	Slight undulations
4.	Shape of coalfield	-	Sickle shaped coalfield
5.	Average length	-	40 km
6.	Average width	-	12 km
7.	Area	-	450 sq.km.(approximate)
8.	Formation	-	Gondwana Group of Permian age

9.	Measures	-	Talcher,Barakar,Barren & Ranigunj
10.	Coal bearing measures	-	Barakar and Ranigunj
11.	Number of coal seams	-	Barakar measures = 40 Ranigunj measures = 10
12.	Reserves	-	17,077 million tonne
13.	Rock mass composition (average)	-	Coal = 12%, Sandstone = 45%, Shales=20%, Intermixed sandstones and shales =16%, Jhama= 3%, and Sub-soil = 4%
14.	Dip of seams	-	Generally flat. But up to 55° in extreme western part
15.	Mining history	-	Mining was started about 100 years ago in 1890.
16.	Present production	-	28 million tonne (1990)
17.	Target for 2000	-	43 million tonne
18.	Production from underground	-	15 million tonne (1990)
19.	Production target from underground for 2000	-	30% (17.2 million tonne)
20.	Coal blocked below surface properties	-	6,143 million tonne
21.	Coal blocked below fires	-	1,864 million tonne
22.	Important surface properties	-	Rivers and Jores,e.g.,Damodar, Jamunia,Khudia,Ekra,Katri,Chatkori,Kari,Sulunga,etc.

Roads,e.g.,National Highways (No.2 and 32),PWD,District Board and Private roads. The total length of roadway network in the coalfield may be around 500 km by the end of 1995.
Railway lines,e.g.,Grand Chord of Eastern Railway,Adra-Gomoh link line of South Eastern Railway,and a network of local railways,railway yards and assisted siding. The total length of rail network in the coalfield was about 110 km in 1990.
Townships and Colonies(14 Urban and 113 Rural settlements), e.g.Jharia, a part of Dhanbad town,Karkend,Katras,Digwadih, Chasnala,Patherdih,etc. All constructions in these settlements are either Kutcha (mud construction), Pucca single and double storey without basement in general. There are only a few multistorey buildings.
Plants and Structures, like,thermal power plants,washeries, coal handling plants,ropeways,high and low tension transmission lines,small factories,pipe lines,bridges,etc.

23.	Population	-	About 1.5 million (1989)
24.	Land use pattern(1989)	-	Mining and other industries=24%, Agriculture=11%, Forest=1.2%, Settlements=12%, TISCO,IISCO, Roads,Railways,water bodies, barren fallow land,etc. =51.8%
25.	Degraded land in BCCL leasehold (1989)	-	Area under subsidence=35 sq.km, Area under fire(70 fires)= 17 sq.km, Area under dumps=6 sq. km,and Area under abondoned opencast mines=4 sq.km.

UNDERGROUND MINING SITUATION

As stated earlier,Jharia coalfield has about 100 years history of coal mining and has 40 seams in Barakar and 10 seams in Ranigunj measures. The present day (1990) mining situation in the coalfield is briefly described below.

1. Old workings - The yester-year mining practices in the field have left a legacy of unapproachable abondoned underground mine workings standing on small pillars in a large number of places. With the passage of time these workings have became waterlogged and their accurate plans are generally not available. Many of these workings are below and by the side of important surface properties.

About a dozen of the unapproachable old workings have subsided in recent past causing severe damages on the surface in the form of wide-cracks,large depressions,sink holes (pot-holes), blockage of roads and rails, damage to buildings and other surface properties,etc. The main characteristics of these subsidence were that -
indications on the surface are seen only a few hours in advance, they do not follow any pattern, they cause marked depressions with wide cracks and steppings, and they are associated with rumbling sound.

2. Extraction thickness - Generally seams less than 1.2m in thickness are considered unworkable. The maximum extraction thickness may be upto 4.8m in one lift. In case of multi-lift and multi-section mining the extraction has been up to about 12m.

3. Depth - The underground workings in the coalfield are generally at depths less than 250m. Only about 20% of the workings are at greater depths. The maximum depths of the workings may be around 500m while the minimum may be about 15m.

4. Multi-seam extraction - As stated earlier there are 40 coal seams in Barakar measures and 10 in Ranigunj measures in the coalfield and the total thickness of seams is on average 12% of coal measures. In these conditions almost everywhere multi-seam mining has been done. In some situations two or three seams are standing on developed pillars.

5. Multi-section extraction - The maximum thickness of coal seams in the coalfield is around 20m. In the seams, more than 6-7m in thickness, multi-section development has been extensively done on bord and pillar pattern. Suitable methods of exploitation of the thick seams developed in two to three sections are being looked for.

6. Method of underground extraction - About 80% of production from underground mining is obtained by bord and pillar system and the remaining 20% from longwall mining.

7. Percentage of extraction - The percentage of extraction from the panels in workings without longwall system varied greatly from about 60 to 80 in both caving and stowing cases.

SUBSIDENCE IN JHARIA COALFIELD

Jharia coalfield is facing subsidence problems from the point of view of the presence of old workings which are generally waterloged and about a dozen of them have subsided in recent past causing severe damages to surface topography and properties, extraction of coal seams below the old workings as also below workings standing on developed pillars, exploitation of coal seams below the old workings as also below workings and in the vicinity of surface properties, fires due to subsidence and then further subsidence due to fires and general degradation of surface land and environment.

Salient points of subsidence parameters in the coalfield after subsidence studies under the leadership of the author are described below.

1. Visual subsidence impacts of subsidence in Jharia coalfield over different categories of surface properties are as given below.

(a) Subsidence upto about 500 mm were generally not visually felt in barren areas.

(b) Subsidence upto a magnitude of about 650 mm over hydraulically sand stowed workings did not cause any visual distortion in the surface topography or impact on surface vegetation.

(c) Over caved workings at depths upto about 100m discontinuous subsidence took place with stepping.

(d) Over caved workings at depths less than 50m sink-holes/pot-holes were also developed.

(e) Subsidence over unapproachable workings also caused pot holes, discontinuities and steps.

(f) Discontinuities were more prominent over the workings (both current and old) in thick seams and at a few place stepping was of the order of 2m and more.

(g) The width of cracks on the surface varied and the maximum observed was over 1000 mm due to extraction of 8m thick seam at a depth of about 70m.

(h) In general the impact of subsidence on surface topography was very prominent over caved workings at shallow to very shallow depths.

(i) Subsidence of the order of 600 mm and more caused severe disturbances in sub-surface and underground water regime resulting in loss of water from aquifers and water tables.

(j) Subsidences with cracks retarded growth of vegetation on the surface due to loss of water from top-soil.

(k) Subsidence over unapproachable old workings and also over current workings at depths upto about 100m were generally sudden (taking place within a few hours to a few days of initial indications).

(l) Damage to buildings took place even with subsidences as low as 300-500 mm over workings at a depth of about 300m.

(m) Waterlogging of central portion of subsided areas was very commonly seen.

(n) All major cracks over underground workings were generally within extraction perimeter,i.e.,the angle of break was inside the goaf.

2. Maximum subsidence over hydraulically sand stowed underground workings in the coalfield was not more than 6.5% of extraction thickness even with multi-lift and multi-seam extractions at depths ranging from about 35 to 400m. Over caved workings the subsidence varied but was less than 60% of extraction thickness at depths upto about 480m. Non-settlement of overlying old workings at a few places caused an increased subsidence due to settlement of both the seams. In general the magnitude of subsidence was more over the areas having rock mass disturbed due to previous underground mining activities. The maximum possible subsidence and maximum subsidence for any given width-depth ratio of extraction (Fig.1) can be computed with the aid of CMRS com-

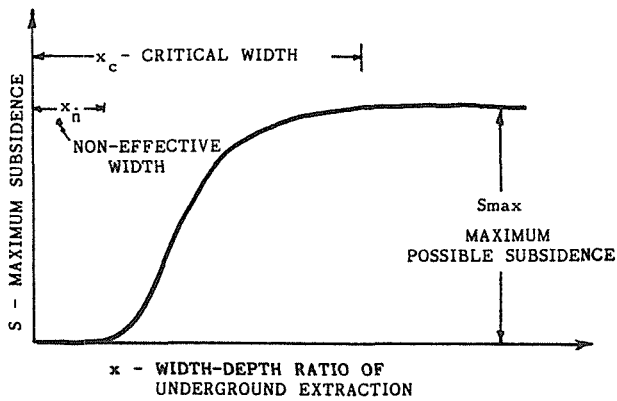

FIG. 1 Maximum possible and maximum subsidence in underground coal mining.

puter model which uses the following simple expressions.

$$Smax = 0.5(1+M)(e'.a'.h'.m') \quad (1)$$

$$S = \frac{Smax}{9}[4+5 \tan h(4- \frac{x-x_n}{x_c - x_n} -1.1)] \quad (2)$$

where Smax = maximum possible subsidence, m, M = rock mass factor,0.4 for predominently hard sandstones to 1 for totally disturbed rock mass, e' = extraction percentage factor,0.95 for longwall and 0.5-0.8 for bord and pillar, a' = goaf treatment factor, 0.95 for caving and 0.07-0.1 for hydraulic sand stowing, m' = extraction thickness, m, h' = depth factor, 1 for depths up to 250m, 1.1 for depths from 251 to 400m and 1.15 for still greater depths, S = maximum subsidence for a given width-depth ratio x, m, x_n = non-effective width-depth ratio, and x_c = critical width-depth ratio.

The maximum subsidence, anticipated for the various coal measure thickness in the coalfield, on the basis of 12% coal availability and 50-80% effective extraction is as given below:

Depth	Seam thick-ness*	Effective extraction	Maximum possible subsidence With stowing**		With caving	
m	m	m(5)	%	m	%	m
100	12	9.6(80)	5-7	0.48-0.67	50-60	4.8-5.76
200	24	16.8(70)	5-7	0.84-1.18	50-60	8.4-10.08
300	36	21.6(60)	5-7	1.08-1.51	50-65	10.8-14.04
400	48	24.0(50)	5-7	1.2-1.68	50-70	12.0-16.80
500	60	30.0(50)	5-7	1.5-2.10	50-70	15.0-21.00
600	72	36.0(50)	5-7	1.8-2.52	50-70	18.0-25.20

*12% of depth **hydraulic sand stowing

It is noted that a maximum subsidence of about 25m can be expected to take place in the coalfield. There are more than 40 coal seams in the coalfield and in most places these seams are being/shall be extracted one after the other. Therefore the surface area in the coalfield can be anticipated to have subsidence in steps as depicted in Fig.2. The incremental magnitude of the steps and their interval would depend upon the underground mining parameters and time lag between successive extraction of the seams. The programme for the management and utilisation of surface land under these circumstances should have possibilities of intermediate steps for end use corresponding to each step of subsidence.

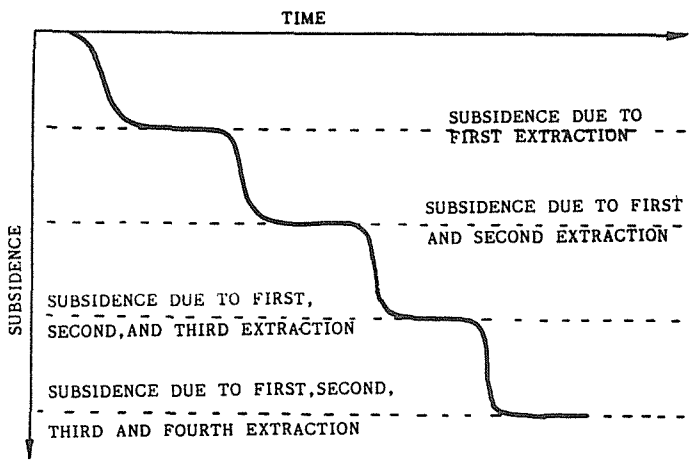

FIG. 2 Subsidence in steps due to multi-seam extraction.

3. Volume of subsidence troughs - Underground mining of coal seams never lands clean sweep of coal from large areas as panel barriers, protection pillars for roadways, shafts, surface properties,etc.,stooks,small pillars,etc.in bord and pillar workings,etc. are left underground. This is all the more true in a situation obtaining in the Jharia coalfield which has multiple number of seams in close proximity. In such situations subsidence can be expected to take place in patches and the volume of subsidence

troughs for successive extraction of seams and thereby the volume of subsidence at each step can be computed by using the following empirical relationship:

$$v = 0.53 \frac{SV}{m'} \quad (3)$$

where v=volume of subsidence trough,m^3, S=maximum subsidence,m, V=volume of underground,m^3,and m'=extraction thickness,m.

4. Subsidence-time relationship - Subsidence over underground coal mining areas continues for some time after extraction is completed. The time lapse for final subsidence depends upon the state of overlying rock mass. About 70-90% of subsidence, over workings with undisturbed rock mass above, takes place immediately after extraction (extraction period) is completed and the remaining 10-30% subsidence takes about 300-500 days. Over disturbed rock mass about 90-95% subsidence takes place during extraction period and remaining 5-10% takes about 50-100 days. The above subsidence-time relationships are illustrated in Fig.3.

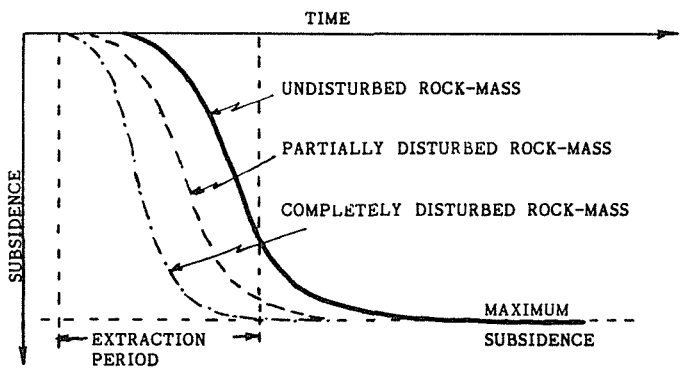

FIG. 3 Subsidence-time relationship.

Thus, in a situation as obtained in Jharia coalfield subsidence due to extraction of lower seams (in descending order extraction with caving) can be expected to take a maximum of about 100 days to complete after finish of underground extraction.

5. Subsidence impacts - Subsidence movements,i.e., subsidence, slope and strains, in different magnitude have different impacts on surface, sub-surface and underground properties, water regime and surface topography and environment. On the basis of the experience and subsidence observations the author has made a categorisation of subsidence impacts which are incorporated in CMRS subsidence model. For assessing the feasibility of management and utilisation of subsided land in Jharia coalfield it would be necessary to anticipate impacts of subsidence at every step due to extraction of successive seams.

SUBSIDENCE MANAGEMENT - A CONCEPT

Surface land, especially in a thickly populated country like India, is the most precious assest and therefore it should be put to optimum use. Depending upon climate, availability of infrastructure, etc. the subsided land can be used for storage of water, paddy fields, orchards, pastures and housing and other constructions. The author suggests that the following steps be taken for this purpose.

A. Planning stage

1. Prepare upto-date surface plans of the area (mine leasehold and about 500 m around it) showing surface contours at 1m interval, water courses on the surface, ponds, houses,colonies, villages, townships,etc., railway lines and roads, aerial ropeways, high tension lines,etc. The plans should also depict the land use pattern on the surface. These plans will also be useful in deciding the mining methods to be adapted.
2. Obtain all possible information and plans of previous mine workings in the area under review.
3. Obtain all borehole records for the area under review.
4. From the above information construct plans, for individual seam, showing seam thickness, seam contours, surface confugeration etc.so as to ascertain the areas which can be caved and which need be stowed during extraction.
5. Anticipate subsidence movements separately for individual seams and then collectively for successive extraction of the seams.
6. Using the anticipated subsidence and original surface contours probably surface contours and thereby the change in surface topography, as every mining stage and also at the final stage, can be computed.
7. Anticipate impacts of subsidence at every mining stage on underground, sub-surface and surface properties, features and structures. These impacts should be critically assessed for collapse of any overlying workings thereby adding to subsidence and its impacts, disturbances in overlying virgin seams, possibilities of fires in overlying and the working coal seams, possibilities of damage to water bodies and inundation of underground workings, disturbances in top-soil characteristics, nature and magnitude of damage to buildings,structures,railway lines,roads,etc., disturbances in water regime on the surface including water table,etc.

B. End use

On the basis of the above preparations and anticipations at planning stage itself it should be decided that to what purpose the subsided land can be used at different stages during extraction of seams in sucession and then after final subsidence. The use of subsided land at various stages would depend upon the extent and magnitude of degradation caused by subsidence, socio-economic requirements of the area, availability of resources,e.g., money, manpower, water, fertilizer, etc.

C. Minimise land damage

The author feels that the most critical subsidence factor causing damage to surface land is development of steep slopes, wide cracks and stepping. If by orienting the underground mining pattern this can be reduced/minimised then the damage can be

reduced to a considerable extent. The following means can be adapted to reduce subsidence.

- By stowing the underground goaves with sand and/or other suitable solids hydraulically.
- By resorting to partial extraction methods.
- By planning underground workings in such a manner that wider subsidence troughs are obtained.

Hydraulic stowing may not be feasible in most situations because it adds to the cost of coal production, it retards the production rate, sufficient quantity of sand and suitable solids are not readily available in and in the vicinity of the coalfields, and stowing is required for extraction of coal seams below surface properties,etc.where caving can not be done. Hence the adaptation of stowing-methods is not being suggested for reducing subsidence and its impacts.

In partial extraction methods, with stowing and caving, a large quantity of coal is left insitu which amounts to loss of coal and the probabilities of fires in such conditions become more. Hence, as a rule partial extraction methods should be avoided as far as possible.

Subsidence trough shape control by planning underground extraction can be done in the manner show in Fig.4. Two methods

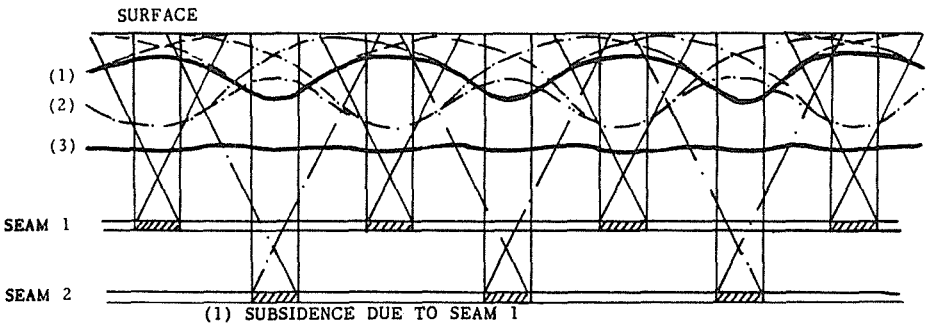

(1) SUBSIDENCE DUE TO SEAM 1
(2) SUBSIDENCE DUE TO SEAM 2
(3) SUBSIDENCE DUE TO BOTH THE SEAMS.

(a) SUBSIDENCE TROUGH SHAPE CONTROL IN TWO SEAM MINING SITUATION

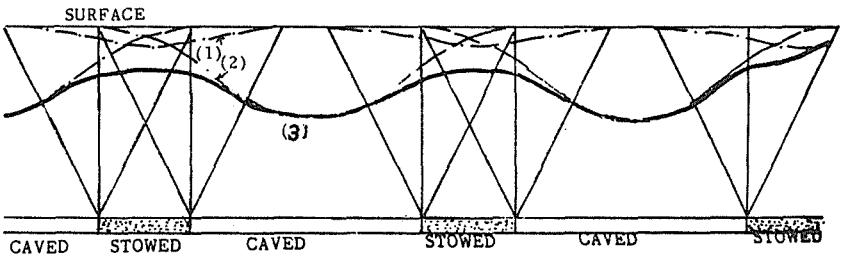

(1) SUBSIDENCE DUE TO STOWED WORKINGS
(2) SUBSIDENCE DUE TO CAVED WORKINGS
(3) SUBSIDENCE DUE TO TOTAL EXTRACTION

(b) SUBSIDENCE TROUGH SHAPE CONTROL IN SINGLE SEAM MINING SITUATION

FIG. 4 Underground extraction planning for subsidence trough shape control.

shown in the figure can be planned, specially in multi-seam mining situations, to reduce development of steep slopes, wide cracks and steppings on the surface and thereby degradation of surface land.

D. Management of subsided land for various end uses - a few suggestions

As stated earlier the subsided land in Jharia coalfield can be used for storage of water, paddy fields, orchards, pastures, housing and other construction, forestry,etc. The most important operation for any end use of land is plugging of cracks. The cracks in general in undisturbed rock mass have been found to appear with strains reaching 4.5-5.0 mm/m level.

Any use of subsided land in coal mining areas is full of danger of underground fires if steps are not taken at proper time. Plugging of cracks is not only important from the point of view of prevention of mine fires but also important from the stand-point of improving water retention capacity of sub-soil and for reducing loss of surface water which finds way to underground workings through cracks (Fig.5).

In the areas having only one seam cracks due to subsidence are likely to develop only once. But in case of multi-seam mining situations, as in Jharia coalfield, the cracks can be expected

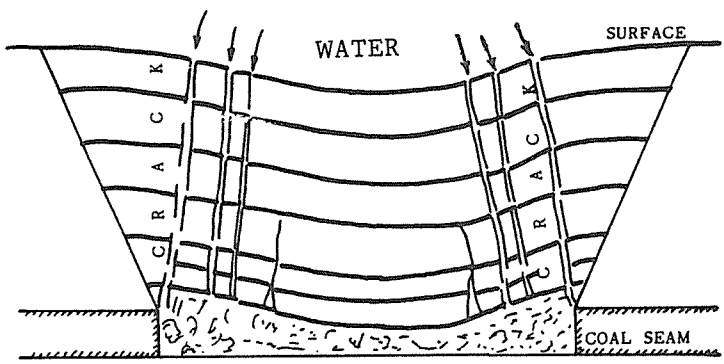

FIG. 5 Seepage of water to underground workings through cracks.

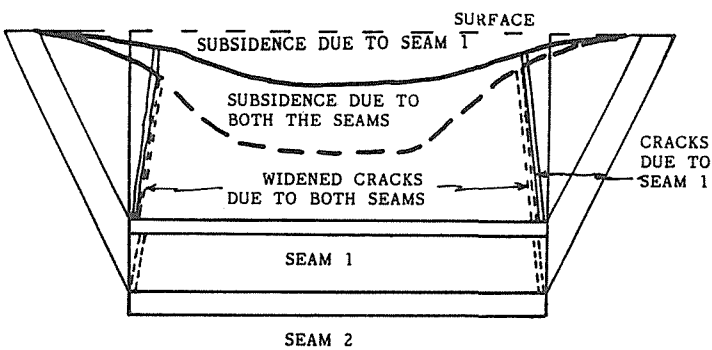

FIG. 6 Widening of cracks due to multi-seam extraction.

to form repeatedly. In case of superimposed workings the cracks formed due to extraction of top seam tend to widen further with addition of new cracks as illustrated in Fig.6. Whether single or multiple seam underground mining, in Jharia coalfield, the cracks formed due to subsidence should be plugged/filed as soon as they are formed and the operation of plugging should continue to the time till then the cracks do not appear and widen further. Since, most areas in the coalfield have multiple number of coal seams, such a situation is not likely to be obtained in near future, i.e., in next 10-15 years. In these situations it would be advisible to use subsided land in the following manner.

Pasture land - Subsided land with or without prospects of further subsidence can be affectively developed as pasture land. Grass and other suitable vegetations can be planted after taking care of cracks developed due to subsidence in the first instance. Later it may be necessary to do re-planting of grass,etc.in the zones affected by the development of cracks due to subsequent subsidences. For such an intermediate use of subsided land it is not necessary to bring the subsided land to original topography. The author feels that it is not at all necessary to do any reclamation work. However, it would be necessary to make arrangements for drainage of water from the subsided areas to be used as pastures.

Forestry and plantation - Forestry and plantation has assumed national importance in India due to its various advantages. A large area (about 10 sq.km) of subsided land in Jharia coalfield has been covered in such schemes and all these areas have to undergo further subsidences in future due to extraction of lower seams. It has been observed at a few places that plantations done up to about 2-3 years before subsidences over caved workings were severely affected as almost all the plants over subsided areas dried out. This indicates that for multi-seam mining situatios due care is required to be taken for the plants so that they are not affected by subsequent subsidences. Underground extractions can be planned for larger intervals between successive subsidences so as to allow the plants to overcome the effects of each subsidence. And during each active subsidence period care be taken that the cracks are plugged and the plants get water.

For plantation in subsided land also it is not at all necessary to reclaim the subsided land. But due care is necessary in plugging surface cracks due to subsidence. Planting can be done within a few months of first subsidence. The choice of plants and timing of plantation should depend upon local climate and nature of top-soil.

In the TISCO leasehold area in the coalfield about 47,000 plants were planted over 47 acres of subsided land and 29,000 plants over 29 acres of fire area. In these plantation the most surviving species has been popular with a survival rate of 70% and an average daily growth of about 12 mm/day. Under normal circumstances the growth rate of this plant should be about 60 mm/day.

In the situation obtaining in Jharia coalfield it would be advisible to use a suitable mix of grassland and plantation to maintain/restore eco-system. The plants to be chosen for plantation

should also have mixed root system, because the plants with wider spreading root system have top-soil binding capacity and thus may have a tendancy to reduce damage to top-soil due to subsidence. This aspect needs a detailed study.

It may take more than 20-25 years for extraction of all the seams from the areas where seams up to No.10 have already been exploited. The plantations can be expected to yield plenty of wood, which could be helpful in rehabilitation of area in and around the coalfield.

Construction of buildings and structures - There are 14 urban and 113 rural settlements in the Jharia coalfield and about 6,143 million tonne of coal is blocked below them. Every year hundreds of small and medium size buildings are being constructed in the coalfield by private citizens as well as nationalised coal mining industry. Most of these constructions are over barriers between goaves, on the goaves, and in the areas where there is practically no extraction and seams are standing on developed pillars. The more the construction in the coalfield the more the quantity of coal blocked below them.

Under the built-up areas it may not be possible to extract all the seams even with partial extraction and stowing methods. The most appropriate step would be to stop all further construction in the coalfield and then progressively shift as many settlements as possible so as to release maximum possible surface area to effectively plan underground extraction for better management of surface area after subsidences.

The author suggests for better management of subsided land and other lands all construction should be planned for the following situations.

- Temporary structures for 5-10 years life with provision to take care of minor subsidences may be built over the areas planned for extraction after the life of the structures.
- Permanent or semi-permanent buildings and structures should be planned over the areas where practically no further subsidence is anticipated in future and where all the seams have been extracted. A time lapse of about 300-500 days be given to allow for consolidation of rock mass after subsidence. While constructing buildings and structures in such areas several precautions may be necessary in making the foundation, superstructure and service facilities.

For construction of the buildings,etc.it may again not be necessary to bring the surface to original level. Depending upon the magnitude of subsidence and resulting surface topography necessary levelling need be done. Once again plugging of cracks due to subsidence is a must.

CONCLUDING REMARKS

The underground coal mining propositions in Jharia coalfield call for a long-term planning of underground mining to affect subsidence without many steeper slopes, wide cracks and stepping. Due to extraction of a large number of seams in succession subsidence and resulting impacts on surface are to take place again and therefore it would be advisible to use the surface area for grass-

land and plantation till all the seams are exhausted and then construction of permanent and semi-permanent buildings and structures should be planned. For the intermediate period wherever necessary temporary constructions for a life of 5-10 years be made such as not to interfere with the underground extraction programme.

There are about 127 settlements in the coalfield blocking more than 6,000 million tonne of coal and every year hundreds of small and medium size constructions are coming up. In order to effect proper exploitation of coal seams and then manage subsided land it would be advisible to stop all further construction in the coalfield and then progressively shift as many settlements as possible.

A maximum subsidnce of about 25m is anticipated to take place in the coalfield and this shall be taking place in steps as the successive seams are extracted. The development of many steep slopes, wide cracks and stepping can be reduced by adapting the mining methodologies suggested.

For any end use of subsided land the most important operation is plugging of cracks developed due to subsidence, specially in situations such as in Jharia coalfield.

It is felt that a long-term planning is necessary for the coalfield and this planning should include anticipation of subsidences and impacts at every stage of mining to decide upon intermediate and ultimate management of subsided land.

ACKNOWLEDGEMENT The author is thankful to the Director,Central Mining Research Station,Dhanbad, for according necessary permission to present this paper. The views expressed in this paper are those of the author and not necessarily of the CMRS.

Land Subsidence (Proceedings of the Fourth International Symposium on Land Subsidence, May 1991). IAHS Publ. no. 200, 1991.

Overburden Deformation and Hydrologic Changes Due to Longwall Coal Mine Subsidence on the Illinois Basin

J.T. KELLEHER , D.J. VAN ROOSENDAAL , B.B. MEHNERT
Illinois State Geological Survey, Champaign, Illinois, USA
D.F. BRUTCHER
Collier County Government, Naples, Florida, USA
R.A. BAUER
Illinois State Geological Survey, Champaign, Illinois, USA

ABSTRACT Subsidence-induced deformation and hydrologic changes were studied at two active longwall coal mines in Illinois using surveying and geotechnical monitoring. Surface subsidence characteristics fall into a range common to other Illinois longwall operations. Subsidence-induced water level fluctuations correlated with mining activity and the passing of the dynamic subsidence wave. Aquifer thickness and lateral extent affect these fluctuations. Bedrock water levels completely recovered at site 1 and partially recovered at site 2. Comparison of pre- and post-subsidence logs showed increased fracture frequency and decreased seismic velocities in the overburden at site 1. Deformation monitoring at site 2 showed only small vertical differential displacements within the overburden, suggesting a nearly uniform drop of the subsided rock mass and a caved zone extending less than 6 m above the mine. Mechanisms of overburden deformation observed at both sites include bedding separations and shear within incompetent formations.

INTRODUCTION

The purpose of this investigation is to characterize the surface expression, hydrologic impacts and overburden-deformation mechanisms of subsidence above active longwall coal mines in Illinois. Results from two mines are presented.

Site 1 is a 221-m deep operation in south-central Illinois. Site 1 was characterized before, during and after subsidence using core drilling, geophysical logging, surveying, in situ aquifer testing and geotechnical instrumentation monitoring.

Site 2 is a 122-m deep mine in southeastern Illinois. Investigations are still in progress, therefore only results from surveying and monitoring during subsidence are presented. Post-subsidence drilling and aquifer characterization at site 2 are planned.

SITE 1: 221-m DEEP LONGWALL OPERATION

Site 1 description

Site 1 is located in the flat to gently rolling farmland of south-central Illinois. The Herrin (No. 6) Coal seam, which is approximately three meters thick in this area, is

mined by the longwall method at a depth of 221 m. The overburden consists primarily of Pennsylvanian-age shales and siltstone overlain by six to eight meters of glacial drift. The aquifer monitored is a 26-m thick, laterally continuous argillaceous sandstone (Mt. Carmel Sandstone), located 21 m below the ground surface. Panel dimensions are 1524 m long by 183 m wide with 61 m between panels (double-chain pillars). Two adjacent east-west longwall panels were instrumented.

Site 1 monitoring program

Frost-protected survey monuments were installed 10.7 m apart (5% of depth of mining) in transverse and longitudinal lines over one panel to document dynamic and static surface subsidence and strain. Level surveys were performed using a WILD NA-2 with a micrometer; strain was measured with a tape extensometer.

Core holes were drilled before and after subsidence at the panel centerline. Both boreholes were inclined 10 degrees from vertical to intersect vertical joints and fractures. The pre-subsidence borehole was drilled to a depth of 214 m. Problems associated with loss of circulation prevented post-subsidence drilling below 158 m. Field description of drill cores included lithology, percent recovery, rock quality designation (RQD), and the fracture frequency of each 3.3-m core run. Geophysical logs including gamma ray, density and sonic velocity were run in the open boreholes.

Open-standpipe piezometers were installed in the glacial drift and the Mt. Carmel Sandstone aquifer to monitor the hydrogeologic effects of subsidence in these units. Drift and sandstone piezometers were positioned over the chain pillars, on the centerline and on the edge of the panel. Piezometric levels were monitored hourly using pressure transducers and data recorders.

The hydraulic conductivity of the sandstone aquifer was determined by in situ tests before and after subsidence. A pump test was conducted before and after undermining in a large-diameter well located at the panel centerline. Slug tests were performed in the piezometers before undermining and during active subsidence. Hydraulic injection tests were conducted in the pre- and post-subsidence inclined holes.

Time Domain Reflectometry (TDR) cables were used to document strain and fracture development in the overburden. Two 1.27-cm diameter unjacketed Cablewave System FXA 12-50 coaxial cables were grouted into deep boreholes at the center and edge of a panel. The cables were crimped at 6.1 m intervals to produce evenly-spaced signals that increase the resolution of distance measurements. Time domain reflectometry signals were monitored at regular intervals during and after subsidence. The mode of TDR cable deformation (shear or tension) was determined using the method of Dowding et al. (1988, 1989) and correlated with subsidence characteristics and lithology.

Site 1 results

Surface subsidence The transverse subsidence profile developed as mining progressed (Fig 1). Subsidence recorded at the center of the trough after one and one-half months was 1.89 m. Residual subsidence recorded after two years of monitoring is an additional 0.1 m for a total of 1.99 m. The ratio of maximum subsidence to extracted thickness at the transverse line of this panel is 0.69 or 69%. Subsidence of 0.40 m was observed over the chain pillars between the instrumented panel and the

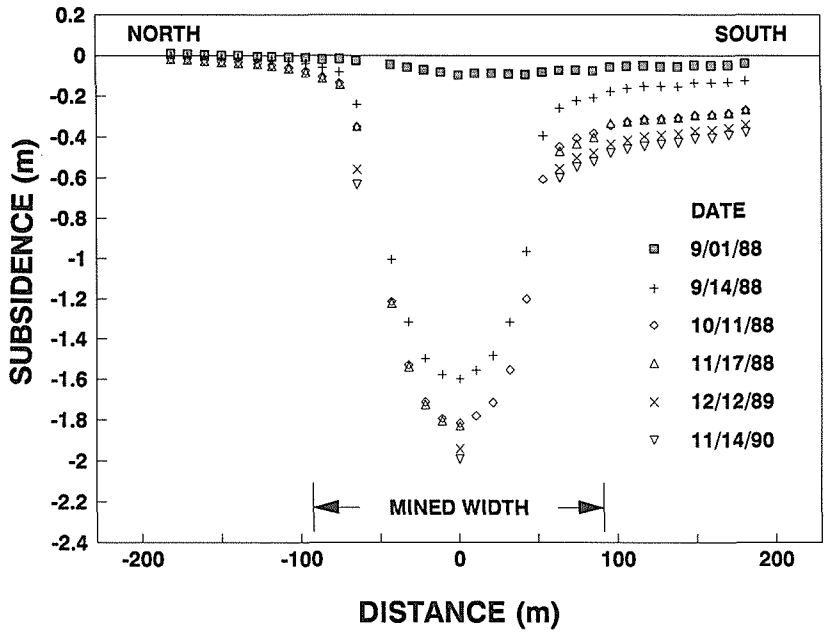

FIG. 1 Transverse subsidence profile at site 1.

previously-mined panel to the south. A 23-degree angle of draw was measured on the north side of the profile, where no previous mining had occurred.

Using static subsidence characteristics, maximum slope of 0.041 was calculated 38.16 m inside the edge of the panel (distance/depth ratio of 0.174). A maximum tensile strain of 0.0134 was measured 22.07 m inside the edge of the panel (distance/depth ratio of 0.101). The maximum surface compression is located 59.59 m inside the edge of the panel, which gives a distance/depth ratio of 0.272. These static subsidence characteristics at site 1 agree with values for the Illinois Basin published by Bauer & Hunt (1982).

Geotechnical and geophysical logging Figure 2 shows comparison of pre- and post-subsidence core logs. Core recovery was excellent before and after subsidence. Changes in the RQD of the respective cores was not unique to any particular lithology, but more a function of the position of mining-induced fracture zones within the overburden. Fracture frequency increased dramatically due to undermining (Fig 2).

A plot of changes in shear-wave velocity (Fig 2) shows four spikes that represent velocity decreases of 12 to 18%. These spikes directly correlate with coals and thin calcareous zones within the overburden. The general decrease of 1 to 10% in the shear-wave velocity throughout the rest of the overburden is the result of wave attenuation through a fractured medium filled with fluid.

Water level response Hydrographs from Mt. Carmel Sandstone-piezometers located on the centerline and chain pillars of the first panel are shown in Fig 3. Water levels declined as the mine face approached the instruments, reached maximum lows when tensile events passed, showed a temporary recovery spike as the maximum compressive strain passed, and then steadily recovered until passage of the mine face of

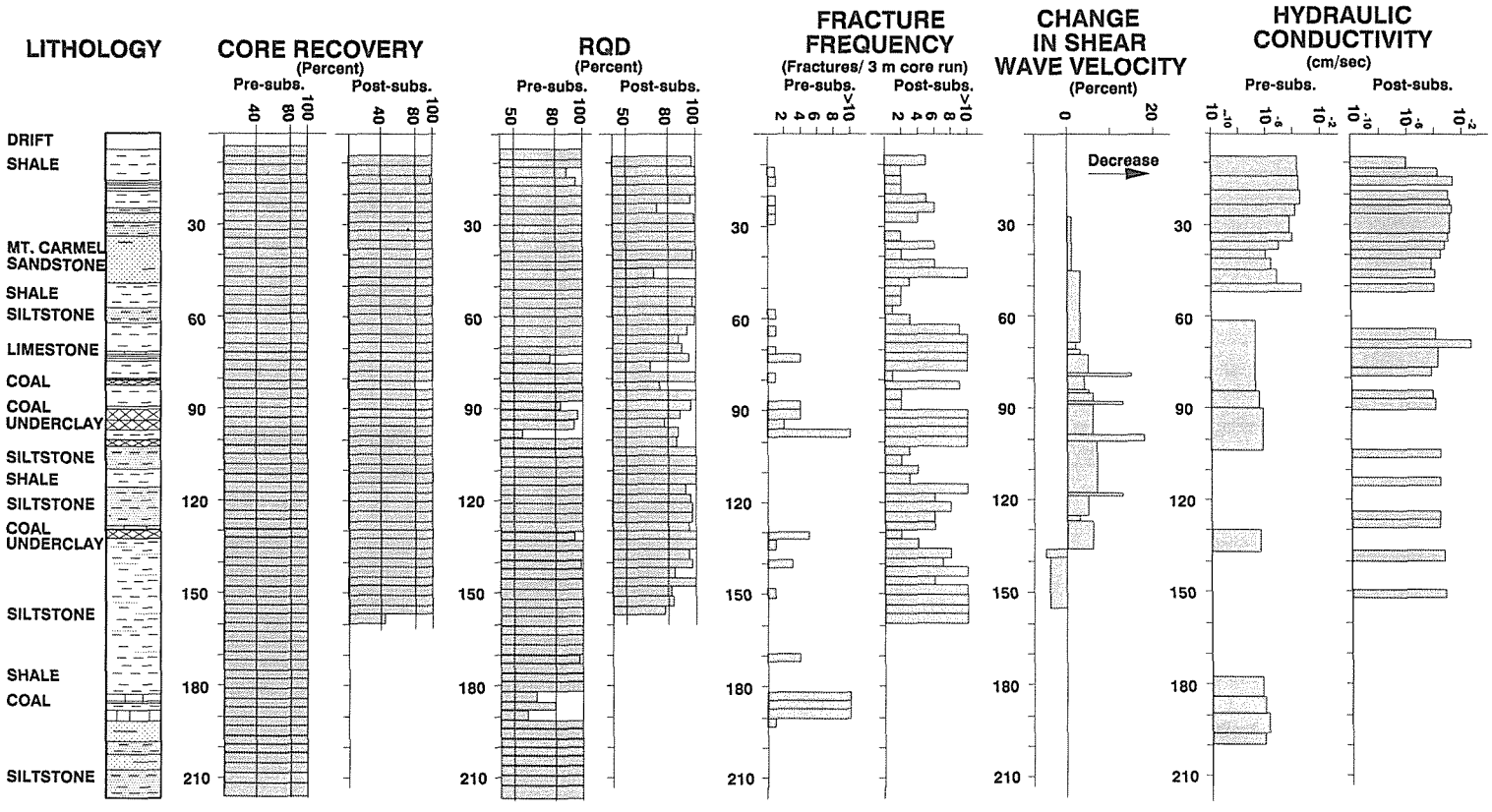

FIG. 2 Comparison of pre- and post-subsidence logs from site 1 (Mehnert et al. 1990).

the adjacent panel. In each piezometer, maximum tensile events occurred when the mine face was 15 to 30 m past the instruments. Water levels from piezometers on the adjacent panel began to decrease when the approaching mine face was about 610 m away. Bedrock water levels recovered two or three months after undermining.

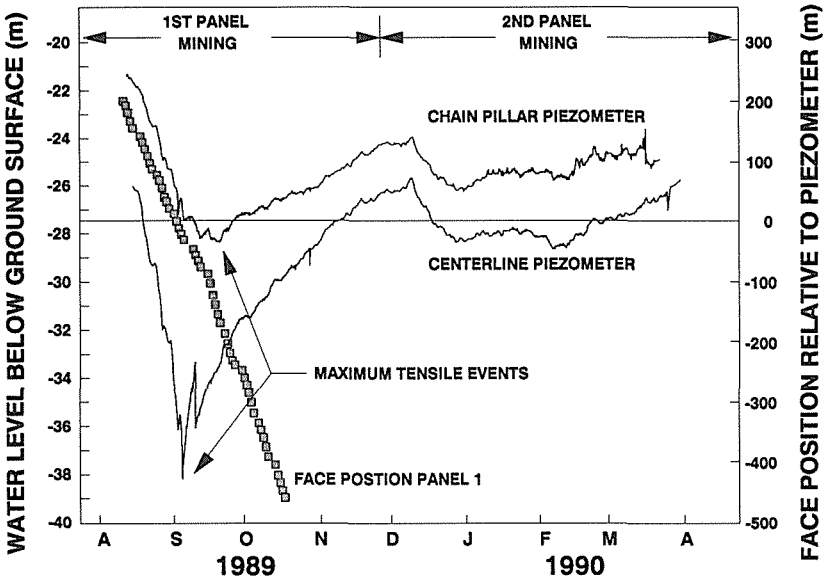

FIG. 3 Water level response at site 1 (after Van Roosendaal et al. 1990).

Piezometric drops are caused by increased secondary porosity resulting from developing and opening fractures in the tensile part of the wave. Recovery occurs when the compressive part of the subsidence wave passes the piezometer, the fractures partially close and the cone of depression associated with the advancing longwall face (tensile event) moves away. The association between water-level fluctuations and dynamic-subsidence strains was also documented by Walker (1988).

Pre-subsidence hydraulic conductivities of 10^{-7} to 10^{-6} cm/s (shales), and 10^{-6} to 10^{-4} cm/s (sandstone) were measured by pump, slug and hydraulic injection tests. Post-subsidence values increased approximately two to three orders of magnitude for the shale and one order of magnitude for the Mt. Carmel Sandstone (Fig 2). The increase in hydraulic conductivity is attributed to mining-induced fracturing in the overburden (Booth et al. 1989). Drift water levels and local water-supply wells showed no appreciable change during mining.

Overburden deformation Figure 4 shows digitized TDR signals for the cable located at the panel edge. Each signal shows the crimps (every 6.1 m) and subsidence-induced changes in this cable for a particular mine-face position. Cable crimps and shear deformations produce sharp negative signals that increase in amplitude as deformation increases (see insert Fig 4). As shown in Fig 4, the cable located at the edge of the panel deformed in shear. Shear deformation occurred at interfaces between strong and weak lithologic layers or within weak layers such as claystones, to accommodate the bending deformation found near the edge of the panel. Shear signals increased in amplitude prior to cable failure, indicating the rate of deformation.

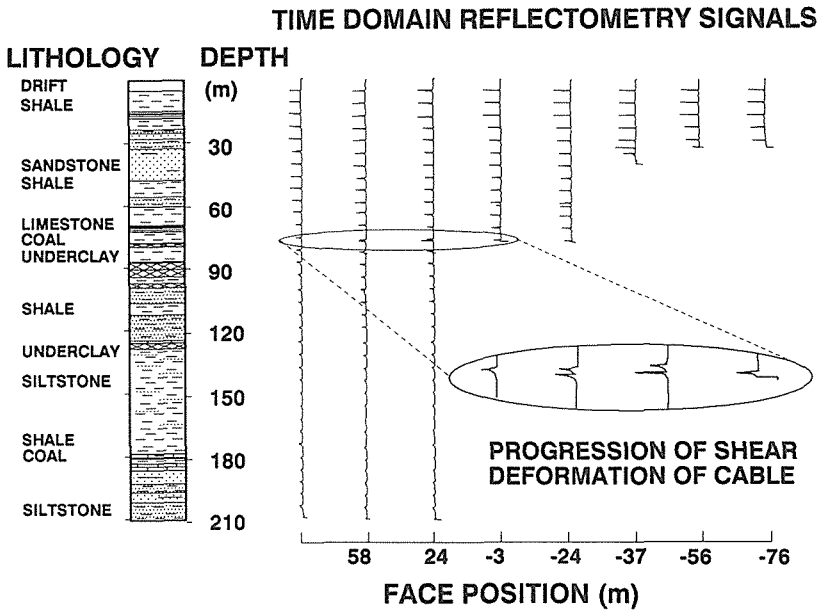

FIG. 4 TDR signals from cable at panel edge at site 1. Horizontal axis indicates mine-face position relative to cable when readings were taken (Brutcher et al. 1990).

Terminal breaks in the cable progressed upward through the overburden as the mine face advanced. The cable at the centerline also showed shear deformation due to bending as the dynamic subsidence wave passed.

SITE 2: 122-m DEEP LONGWALL OPERATION

Site 2 description

Site 2 is located in the gently rolling farmland of southeastern Illinois, where topographic relief is 12 m. The overburden was monitored over a longwall mine working in the 1.7-m thick Herrin (No. 6) Coal seam at a depth of 122 m. Pennsylvanian-age shales and siltstones comprise the bulk of the bedrock overburden. The three to five meter thick Trivoli Sandstone aquifer, which is a medium-grained, slightly argillaceous and micaceous sandstone, is at a depth of 56.3 m. The Trivoli Sandstone has limited lateral extent at this site. Glacial deposits 24- to 27-m thick overlie the Pennsylvanian-age rocks. These glacial deposits consist of loess overlying glacial drift. Gravel is common at the base of the till.

One isolated east-west longwall panel was studied. The panel is 203.6-m wide by 2.4-km long. Double-chain pillars extend 61 m and 46 m from the north and south sides of the panel, respectively.

Site 2 monitoring program

Frost-protected survey monuments were installed 6.1 m apart (5% of mining depth) in transverse and longitudinal lines over the panel to document surface subsidence and

strain. Subsidence was monitored as described for site 1.

Piezometers were installed in a gravel unit at the base of the drift and in the Trivoli Sandstone. Drift and bedrock piezometers were positioned at the panel centerline, just inside the panel edge at the anticipated zone of maximum static tension, and over the chain pillars. Control piezometers were installed 206 m north of the panel edge. Water levels were monitored hourly using pressure transducers and data recorders.

A single 1.27-cm diameter TDR cable was installed in a 129.5-m deep borehole at the panel centerline. TDR monitoring was identical to the procedure followed at site 1.

Two six-anchor multi-position borehole rod extensometers (MPBX) were installed at the panel centerline to monitor vertical overburden deformation. The deep MPBX had grouted anchors every 6.1 m from 85.3 to 115.8 m, and at depths of 36.6 to 67.1 m for the shallow MPBX. Extensometers were measured and the elevation of the MPBX reference heads were surveyed three to four times daily during active subsidence.

Site 2 results

Surface subsidence Maximum subsidence measured at the center of the panel is 1.37 m. The ratio of maximum subsidence to extracted thickness is 69 percent.

An examination of the static subsidence profile gives a maximum tensile strain of 0.021 located 13.4 m inside the north edge of the panel (distance/depth ratio of 0.110). A maximum surface compressive strain of 0.0146 was measured 43.9 m inside the panel edge (distance/depth ratio of 0.360). The maximum slope of 0.0396 is located 31.7 m inside the south panel edge (distance/depth ratio of 0.26).

Water level response The water level response of two Trivoli Sandstone piezometers and one glacial drift piezometer is plotted in Figs 5 and 6. Trivoli Piezometer 2 (TP2) (Fig 5) is located 271 m from the transverse survey line at the panel centerline. Drift Piezometer 2 (DP2), and Trivoli Piezometer 3 (TP3) are on the transverse line and within the maximum static tensile zone at the panel side (Fig 6). In each figure, face positions are plotted relative to the location of the piezometers.

Water levels in the Trivoli wells began to decline when the mine face was about 457 m away and then partially recovered after subsidence occurred. Trivoli Piezometer 2 (Fig 5) experienced a rapid response because the face advance was continuous when it was undermined. Trivoli Piezometer 3 (Fig 6), however, showed a prolonged and irregular depression. The mine advance was slow and sporadic when these wells were undermined. Water levels partially recovered during periods of mine inactivity.

The water-level fluctuations of DP2 (Fig 6) are typical of all drift piezometers installed in the basal gravel regardless of position relative to the mine panel.

Overburden deformation Absolute anchor displacements for the shallow and deep MPBXs and surface subsidence are plotted against time in Fig 7. The largest relative displacement between any anchor and the reference head was 15 cm. The relative strains between anchors were less than one percent for all extensometers. The extensometers clearly show no evidence of large vertical differential displacements in the overburden to within 6.1 m of the mine roof. Therefore, the caved zone extends less than 6.1 m above the mine, or less than 3.3 times the mined height. The caved zone is within the values of two to eight times the mined height predicted by Peng & Chiang (1983). At the panel centerline the overburden rocks subsided as a fairly contiguous mass without caving or large bedding separations.

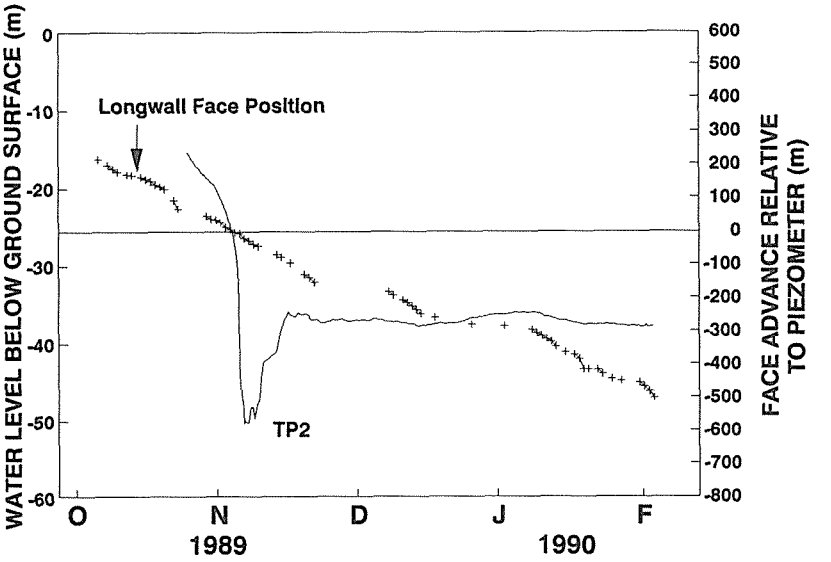

FIG. 5 Water level response for Trivoli Piezometer 2 (TP2) at site 2 (Van Roosendaal et al. 1990).

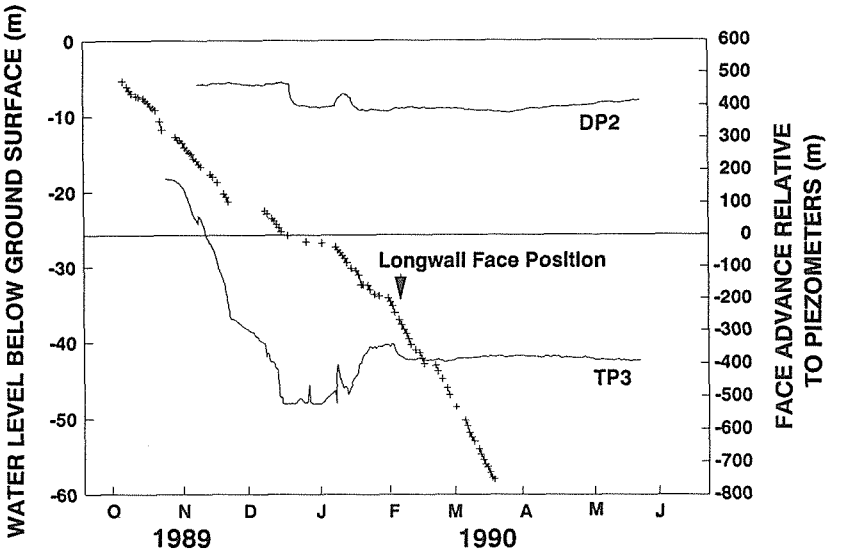

FIG. 6 Water level response for Trivoli Piezometer 3 (TP3) and Drift Piezometer 2 (DP2) at site 2 (Van Roosendaal et al. 1990).

The TDR cable at the centerline deformed predominantly in shear. The cable showed subsurface movements about 61 m in advance of the moving face, agreeing with results presented by Dowding et al. (1989) from another Illinois longwall mine. Shear breaks correlate with weak lithologies and pre-existing joints. No clear correlation exists between the location of TDR cable deformation and the amount of differential strain between MPBX anchor positions. Cable deformation took place in the glacial drift as well as in the bedrock overburden.

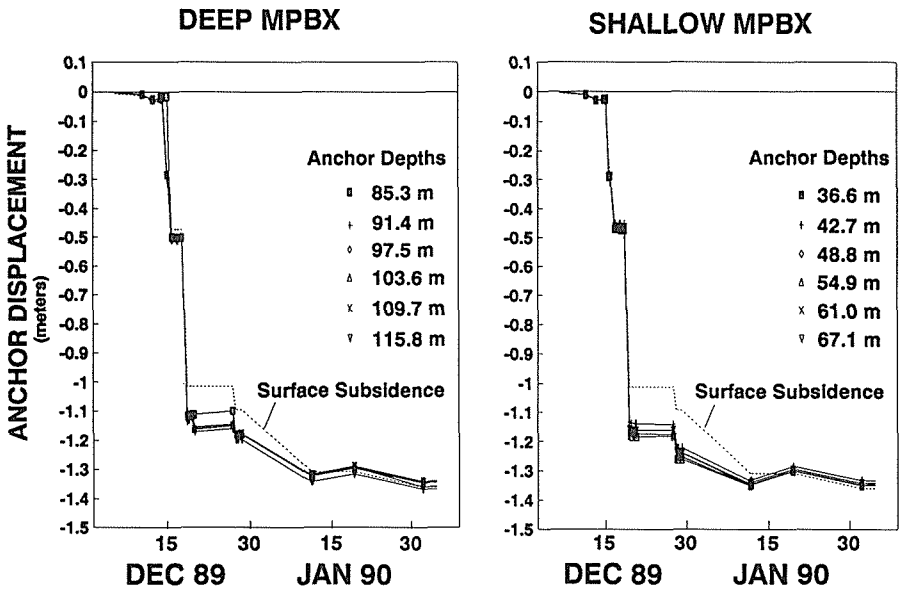

FIG. 7 Absolute displacements of MPBX anchors at site 2 (Van Roosendaal et al. 1990).

CONCLUSIONS

(a) The surface expressions of longwall mining observed at these sites are typical of those experienced in the Illinois Basin.

(b) Piezometric levels in the overburden decreased as fractures developed due to the tensile portion of the dynamic (traveling) subsidence wave. Recovery began when the fractures closed due to the compression portion of the wave; the mine face advance carried away the cone of depression associated with the dynamic tensile event.

(c) At site 1 water levels in the shallow Mt. Carmel Sandstone aquifer recovered within two to three months. The thickness and lateral extent of this aquifer facilitated the rapid recharge to the newly created fractures. At site 2 water levels in the deep Trivoli Sandstone aquifer, however, have only partially recovered. This thin, discontinuous sandstone does not have sufficient storage capacity to recharge the fractures.

(d) Mining increased the bedrock hydraulic conductivities at site 1 by two to three orders of magnitude in the shale, and one order of magnitude for the Mt. Carmel Sandstone, producing improved aquifer characteristics.

(e) Fracture development in the overburden at site 1 was documented by a decrease in RQD and shear-wave velocity, and an increase in fracture frequency and hydraulic conductivity. Time domain reflectometry (TDR) signals indicated shear deformation between strong and weak lithologic layers near the panel edge.

(f) Bedrock deformation monitoring on the panel centerline at the shallower site 2 shows shear deformation 61 m in advance of the mine face and only minor differential vertical deformation. The overburden subsided as a contiguous rock mass with a caved zone within the size range predicted by Peng & Chiang (1983).

ACKNOWLEDGMENTS This research was supported by the Illinois Mine Subsidence Research Program funded by the U.S. Bureau of Mines, and the Illinois Coal Development Board of the Illinois Department of Energy and Natural Resources, and administered by the Illinois State Geological Survey. B. Trent and C. Bough assisted with manuscript preparation.

REFERENCES

Bauer, R.A. & Hunt, S.R. (1982) Profile, strain and time characteristics of subsidence from coal mining in Illinois. Proc. Workshop on Surface Subsidence Due to Underground Mining, Morgantown, WV, 207-218.

Booth, C.J., Spande, E.D., Brutcher, D.F. & Mehnert, B.B. (1989) Hydrological response to longwall coal mining in Illinois. GSA Abstracts with Programs, vol. 21, A230.

Brutcher, D.F., Mehnert, B.B., Van Roosendaal, D.J. & Bauer, R.A. (1990) Rock strength and overburden changes due to subsidence over a longwall coal mining operation in Illinois. In: Rock Mechanics Contributions and Challenges (Proc. 31st U.S. Symp., June 1990) 563-570. Balkema, Rotterdam.

Deere, D.U. & Miller, R.P. (1966) Engineering Classification and Index Properties for Intact Rock. Technical Report No. AFWL-TR-65-116, Kirtland AFB, NM.

Dowding, C.H., Su, M.S. & O'Connor, K. (1988) Principles of time domain reflectometry applied to measurement of rock mass deformation. International Journal of Rock Mechanics and Mining Science, vol. 25, 287-297.

Dowding, C.H., Su, M.S. & O'Connor, K. (1989) Measurement of rock mass deformation with grouted coaxial antenna cables. Rock Mechanics and Rock Engineering, vol. 22, 1-23.

Mehnert, B.B., Van Roosendaal, D.J., Bauer, R.A. & Brutcher, D.F. (1990) Effects of longwall coal mine subsidence on overburden fracturing and hydrology in Illinois. In: Mine Subsidence - Prediction and Control (Proc. Assoc. Engineering Geol. 33rd Annual Meeting, October 1990) 105-112.

Peng, S.S. & Chiang, H.S. (1983) Longwall Mining. John Wiley & Sons Inc., New York.

Van Roosendaal, D.J., Brutcher, D.F., Mehnert, B.B., Kelleher, J.T. & Bauer, R.A. (1990) Overburden deformation and hydrologic changes due to longwall mine subsidence in Illinois. In: Ground Control Problems in the Illinois Basin (Proc. 3rd Conf., August 1990) 73-82. Southern Illinois Univ. at Carbondale.

Walker, J.S. (1988) Case study of the effects of longwall mining induced subsidence on shallow ground water sources in the Northern Appalachian Coalfield. U.S. Bureau of Mines Report of Investigations 9198.

Land Subsidence (Proceedings of the Fourth International Symposium on Land Subsidence, May 1991). IAHS Publ. no. 200, 1991.

Analysis of Mining Subsidence Using the Large Deformation Theory

HE MANCHAO & CHEN ZHIDA
Beijing Graduate School, China University of Mining and Technology

ABSTRACT Mining subsidence relates to the problem of large deformation. Strictly speaking, however, the theory of classic deformation mechanics as used at present is a mini-deformation theory from the viewpoint of geometric field equations, although the non-linear behavior of material has been considered. An absurd result is obtained when we analyze a typical slide in the Fushun open pit mine by using the classic theory of deformation mechanics, and a correct solution can be obtained by using the modern theory of large deformation mechanics. At last, the finite element method of large deformation theory is used for analyzing the land subsidence due to open pit mining. The analysis shows that the step deformation occurs in the ground surface. It correlates well with engineering practice in the field.

INTRODUCTION

Until now, the classic theory of mining subsidence engineering has been unable to give a good result under the condition of complicated structure, for example, mining in faulted rock masses, sharply inclined layers and closed folds. In recent years, with the development of the computer, the finite element method (FEM) of rock mechanics has been used to estimate mining subsidence. Generally speaking, the result of the FEM application is far from the best use for mining subsidence. The reason is that there are three complex theoretical problems in the classic FEM of rock mass mechanics: (a) continuum problem, i.e. a rock mass is usually believed to be a kind of medium of high discontinuity, and on the other hand, the continuum theory is almost always used in all analyses of deformation of rock masses; (b) constitutive equation problem, i.e. the constitutive equation of rock masses is scarcely determined, but it must be used in every analysis of rock masses stability; (c) large deformation problem, i.e. the deformation of rock masses is usually quite large, but the analysis theory used at present belongs to the mini-deformation theory. So these three absurd problems are the three main contradictions of the deformation theory used in the practice of mining subsidence engineering. In this paper, however, only the problem of large deformation is discussed. The other two problems, the continuity of rock masses or the constitutive equation of rock masses, have been discussed by the authors in previous papers. At last, we use the modern FEM technique which depends upon the theories of rock masses continuity, constitutive equation, and large deformation

mechanics to analyze the real example of mining subsidence under the condition of the very complicated structure in the Fushun open pit coal mine.

NON-RATIONALITIES OF CLASSIC DEFORMATION THEORY

Strictly speaking, the classic deformation theory is the mini-deformation theory from the viewpoint of geometric field, although the non-linear behavior of material has been considered. In order to prove the non-rationalities of the classic deformation theory, the error that results when the classic theory is used to calculate the deformation of a typical slide in the Fushun open pit mine is discussed first.

As shown in Figs 1 and 2, for a typical circular slide, the curvature of sliding plane is constant. When the sliding block A is sliding, it can be considered as a rigid body moving from A to A', with the rigid rotation angle of $(\phi' - \phi)$.

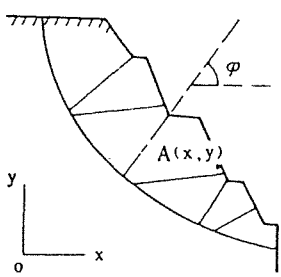

FIG. 1 A circular slide before sliding.

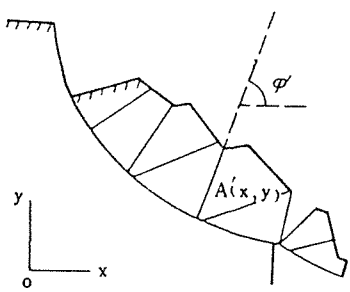

FIG. 2 A circular slide after sliding.

So the displacement equation of each point within the block A is

$$\left.\begin{aligned} u &= (\cos\theta - 1) \cdot x - \sin\theta \cdot y + a \\ v &= \sin\theta \cdot x + (\cos\theta - 1) \cdot y + b \end{aligned}\right\} \tag{1}$$

where:

u,v -----Components of displacement vector along χ,y axis direction

a,b -----Components of translation of particle center

$\theta = (\phi' - \phi)$

According to the classic theory, the strain components ε_{ij}

$$\left.\begin{aligned} \varepsilon_{xx} &= \frac{\partial u}{\partial x} \\ \varepsilon_{yy} &= \frac{\partial v}{\partial y} \\ \varepsilon_{xy} &= \frac{1}{2}\left(\frac{\partial v}{\partial x} + \frac{\partial u}{\partial y}\right) \end{aligned}\right\} \tag{2}$$

Mini-rotation angle ω_z

$$\omega_z = \frac{1}{2}\left(\frac{\partial v}{\partial x} - \frac{\partial u}{\partial y}\right) \tag{3}$$

From the equation (1) above, one can obtain:

$$\varepsilon_{xx} = \cos\theta - 1 \qquad \varepsilon_{yy} = \cos\theta - 1$$
$$\varepsilon_{xy} = 0 \qquad \omega_z = \sin\theta$$

For $\theta = \phi' - \phi = 10^{\circ}$, one obtains

$$\varepsilon_{xx} = -0.015 \qquad \varepsilon_{yy} = -0.015$$
$$\varepsilon_{xy} = 0 \qquad \omega_z = 0.1737$$

It is clear that the results are quite ridiculous, since there is no strain in block A. So strictly speaking, it is unrealistic to describe the body movement by using the classic theory of deformation mechanics.

In a real slide movement (as shown in Fig. 3), every element in the sliding masses can have a large displacement or large deformation. For solving this problem, the FEM theory that depends upon the classic deformation mechanics is irrational not only from the geometrical point of view but also is against the law of energy conservation. As shown in Fig. 3, the classic FEM analysis is carried out using a fixed coordinate system. When slope masses are deformed, the shaded element in Fig. 3 is changed into a distorted one. If, as usual, the FEM mesh elements are created by fixed coordinates, the element boundaries must be straight. Obviously, the element is very different from the real deformed one. So the particles in the element also differ from the actual deformed ones. These facts are against the law of energy conservation according to the mass-energy relation.

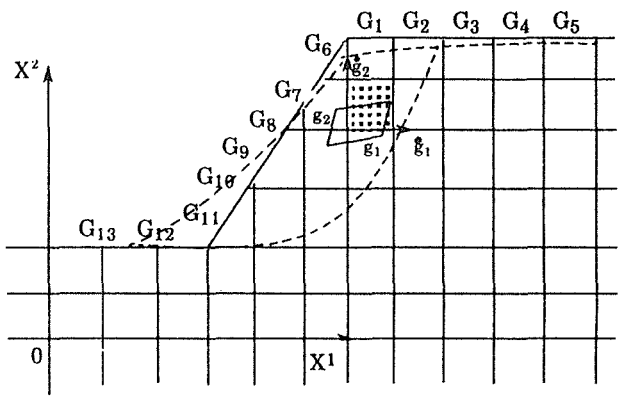

FIG. 3 Theoretic model of subsidence due to open mining.

NONLINEAR LARGE DEFORMATION THEORY

Co-moving coordinate system

As shown in Fig. 4, we chose two reference systems, a co-moving system X^i and a fixed system X^i.

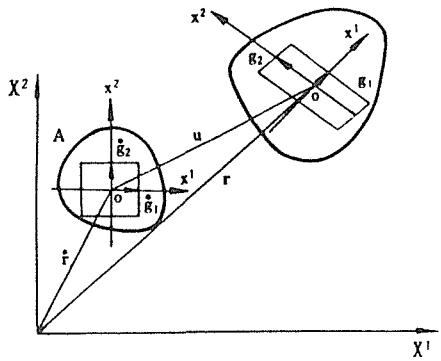

FIG. 4 The co-moving coordinate system.

For a large deformation theory, the method of a co-moving system developed by Chen (1988) is suitable for describing the motion of a deformed body. Fig. 4 shows a transformation of continuum body A_0 in large rotation and large deformation. In a time process sequence, A_0 is continuously transformed, i.e. $A_0(t_0) \rightarrow A(t)$.

At the moment t_0, the embedding coordinate system $\{\chi^i\}$ is initially isomorphic with a fixed coordinate system $\{\mathring{X}^i\}$, i.e.

$$X^i = X^i(\chi^i, t_{0)} = \chi^i$$

At the moment t,

$$X^i = X^i(\chi^i, t)$$

the local basic vectors:

$$\mathring{\vec{g}}_i = \frac{\partial \mathring{\vec{r}}}{\partial x^i} \qquad \vec{g}_i = \frac{\partial \vec{r}}{\partial x^i} \tag{4}$$

where, $\mathring{\vec{r}}$, $\vec{r}$ is the location vectors of any point of the deformable body A_0 at the moment of t_0 or t.

S-R decomposition theorem

The basic vectors $\mathring{\vec{g}}_i$ of the undeformed state is changed to $\vec{g}_i$ in the deformed state, the transformation tensor F_i^j gives

$$\vec{g}_i = F_i^j \mathring{\vec{g}}_j \tag{5}$$

By the S-R decomposition theorem, where

$$F_j^i = S_j^i + R_j^i = \textit{Strain tensor} + \textit{rotation tensor} \tag{6}$$

Finite strain tensor:

$$S_i^j = \frac{1}{2}(u^i|_j + u^j|_i^r) - (1 - \cos\theta) L_k^i L_j^k \tag{7}$$

Finite mean local rotation

$$R_i^j = \delta_j^i + L_j^i \sin\theta + (1 - \cos\theta) L_k^i L_j^k \tag{8}$$

Mean angle of local rotation θ:

$$\theta = \arcsin\left\{\frac{1}{2}[(u^1|_2 - u^2|_1)^2 + (u^2|_3 - u^3|_2)^2 + (u^3|_1 - u^1|_3)^2]^{1/2}\right\} \tag{9}$$

Axis of local rotation:

$$\begin{aligned} L &= L^i g_j \\ L_i^j &= \left(\frac{1}{2\sin\theta}\right)(u_i|^j - u_i|^r) \end{aligned} \tag{10}$$

Verification of the rationality

For a large deformation of the slide in Figs 1 ~ 2, we shall use the large deformation theorem (equations 6 ~ 10) to calculate the strain at every point of the sliding masses, to obtain:

$$\begin{aligned} \|S_j^i\| &= \begin{bmatrix} S_1^1 & S_1^2 \\ S_2^1 & S_2^2 \end{bmatrix} \\ &= \begin{bmatrix} \dfrac{\partial u}{\partial S_1} + (1 - \cos\theta) & \dfrac{1}{2}\left(\dfrac{\partial u}{\partial S_1} + \dfrac{\partial v}{\partial J_2}\right) \\ \dfrac{1}{2}\left(\dfrac{\partial u}{\partial S_2} + \dfrac{\partial v}{\partial S_1}\right) & \dfrac{\partial v}{\partial S_1} + (1 - \cos\theta) \end{bmatrix} \\ &= \begin{bmatrix} \dfrac{\partial u}{\partial x} + (1 - \cos\theta) & \dfrac{1}{2}\left(\dfrac{\partial u}{\partial x} + \dfrac{\partial x}{\partial y}\right) \\ \dfrac{1}{2}\left(\dfrac{\partial v}{\partial x} + \dfrac{\partial u}{\partial y}\right) & \dfrac{\partial v}{\partial y} + (1 - \cos\theta) \end{bmatrix} \\ &= \begin{bmatrix} 0 & 0 \\ 0 & 0 \end{bmatrix} \\ \omega_z &= \frac{1}{2}\left(\frac{\partial v}{\partial S_1} - \frac{\partial u}{\partial S_2}\right) = \frac{1}{2}\left(\frac{\partial v}{\partial x} - \frac{\partial u}{\partial y}\right) = \sin\theta \end{aligned}$$

For the movement of the circle slide in Figs 1–2, the strain components within the sliding masses are zero, but the rotation is taking place along the circular sliding plane. These results are clearly rational.

Considering the general case of large deformation of the slope shown in Fig. 3, two coordinate systems--a fixed system and a co-moving system--are used in accordance with the FEM equations for a nonlinear large deformation geometrical

field. The deformed element is described by the co-moving coordinate system. So the boundary of the element is the same as the actually deformed one, the energy after or before the deformation is kept constant. Obviously, this FEM technique of nonlinear large deformation is quite rational for describing the large deformations.

MINING ENGINEERING BACKGROUND

The Fushun open coalmine pit is the largest one in China. It is 6000m long, 2500m wide and 300m deep at present. It will be 500m deep at the end of this century. There is an important refinery on the ground surface at the north wall of the open pit. The location is shown in Fig. 5. Since 1984, ground displacement in the refinery area has been taking place with the mining. There was some damage to the refinery equipment due to a discontinuous ground deformation.

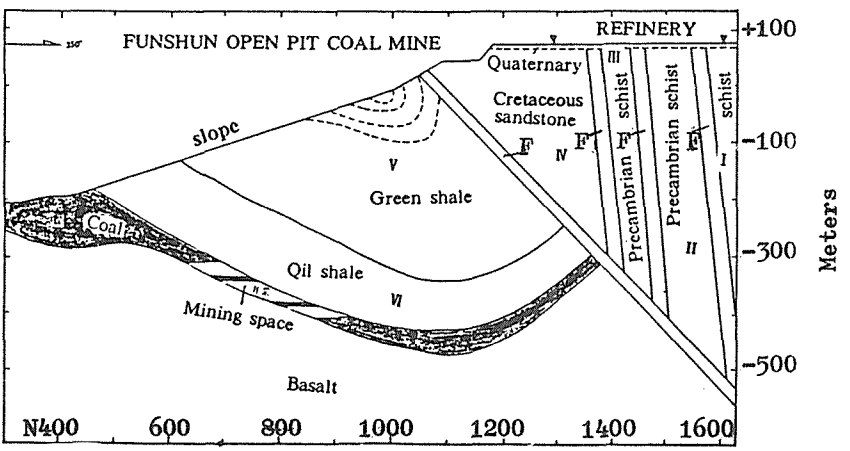

FIG. 5 The location of Fushun open pit and Refinery factory.
I--The damage area of rock masses
F--The damage area of fractured zone
-------- Mudded shear zone in V damage area

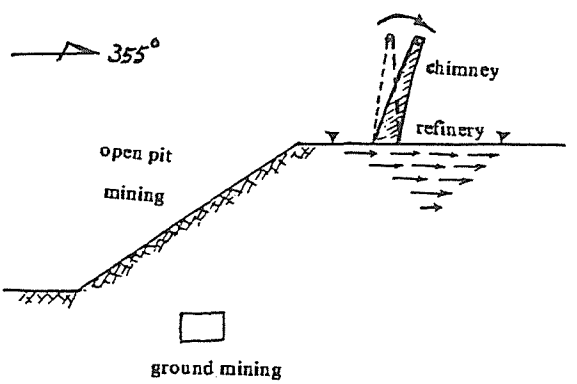

FIG. 6 The curious phenomena of displacement in the refinery area.

Some curious phenomena have occurred. For instance, the chimneys were inclining in the direction away from the open pit, and the displacement vector of the refinery area was oriented almost north. The above phenomena is shown in Fig. 6.

DISPLACEMENT ANALYSIS WITH MINING

The displacement of the refinery area due to mining has been carried out by using the large deformation FEM technique. The analysis results are shown in Fig. 7 to 12.

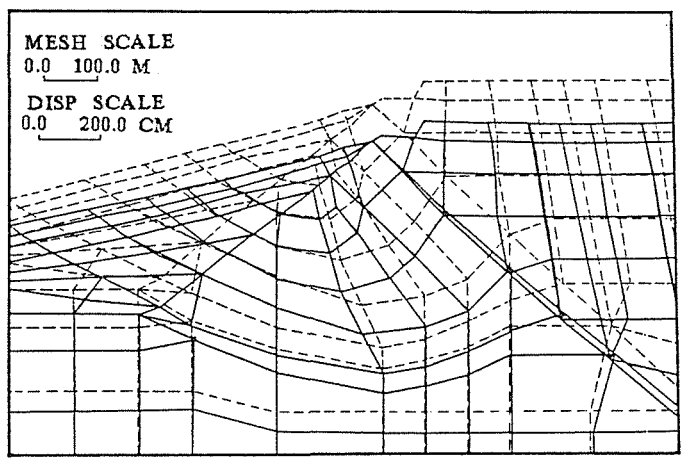

FIG. 7 The location of ground subsidence in 1979.

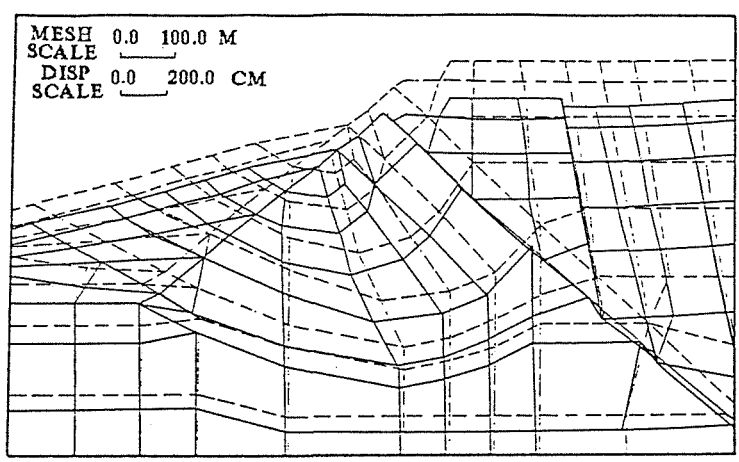

FIG. 8 The step deformation of ground in 1987.

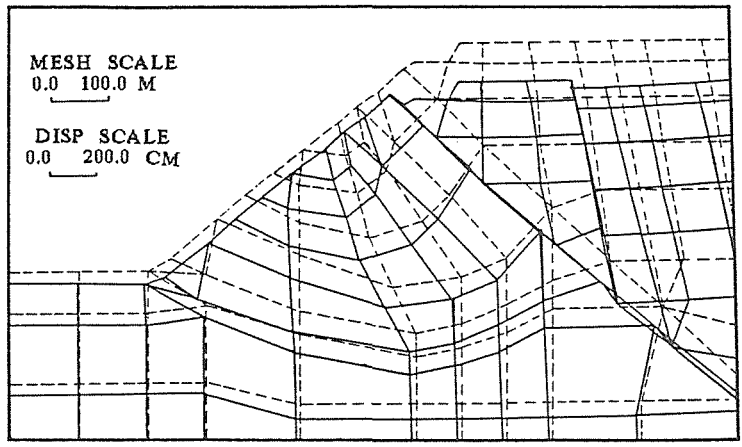

FIG. 9 The step deformation of ground in 2002.

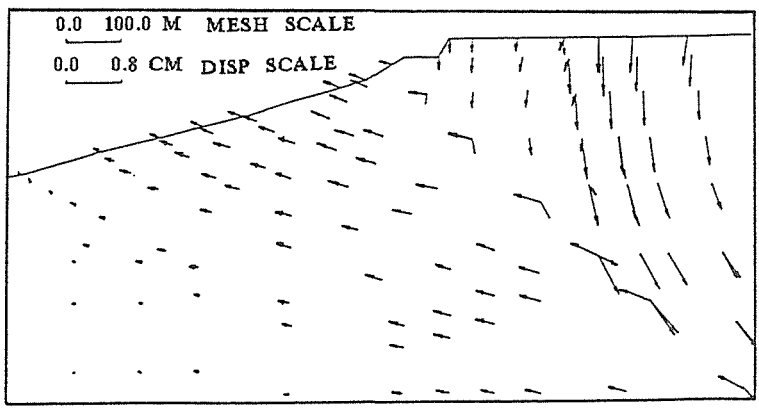

FIG. 10 Increment displacement vector of ground during 1979-1982.

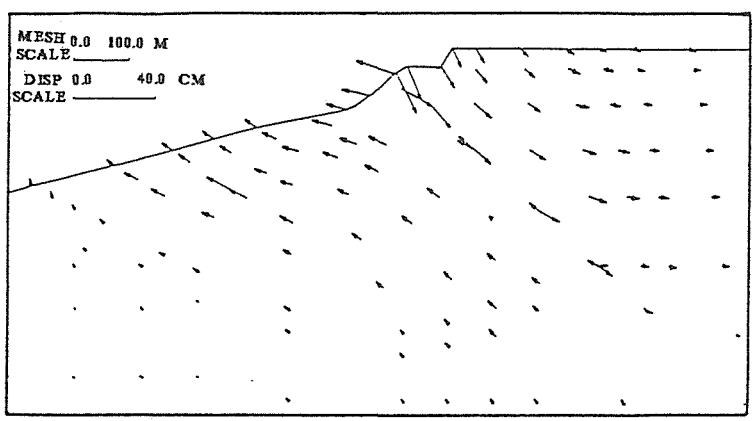

FIG. 11 Increment displacement vector of ground during 1984-1987.

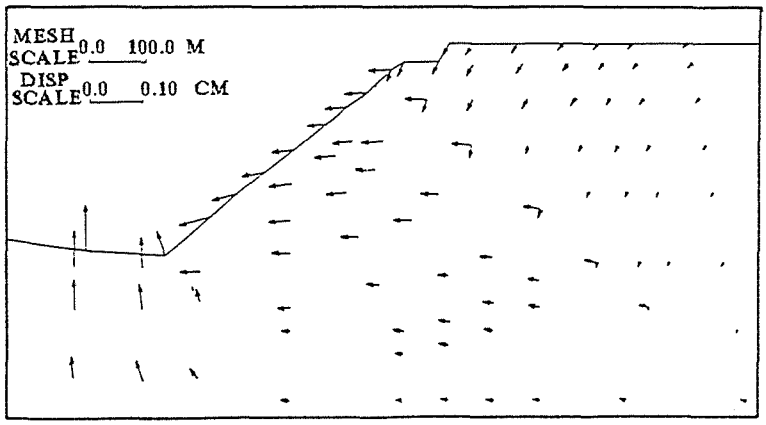

FIG. 12 Incremental displacement vector of ground during 1999-2002.

In the figures, the dashed line shows the outline before mining, while the solid line is the deformed outline. Fig. 7 shows clearly that the plastic dilatance occurred in the deep fracture zones, but there is no shear deformation along the fault planes, when mining is carried out of shallow depth. As slope deepens, the plastic dilatancy is further developing in the deep part of the fracture zone, while the shear deformation occurred in the shallow fracture zone. The step deformation has formed on the ground surface of the refinery area (as shown in Fig. 8 and 9). It is the step deformation that produced the inclination of the chimney toward the North, because the chimney is located on the fracture zone. Fig. 10 to 12 show displacement vectors for various mining time intervals. Fig. 10 shows that the ground subsidence is greatest when mining is at shallow depth. With open pit mining to a certain depth, the displacement vectors of the ground change their direction to the North (See Fig. 11); when mining depth is very great (as shown in Fig. 12), the displacement vector direction will turn to the South.

ACKNOWLEDGEMENTS The author would like to thank Prof. Ma Weimin for his valuable discussion. The author greatly appreciates the financial support by the National Expert Bureau in the fiscal years 1988 and 1989.

REFERENCES

Chen Zhida (1988) Rational Mechanics. China Mining University Press (in Chinese, with English abstract).

He Manchao (1991) High Slope Geomechanics, Coal Science Press (in Chinese).

He Manchao (1990) Constitutive Relation of Plastic Dilatancy due to weak Intercalation in Rock Masses. Proceedings of 26th Annual Conference of the Engineering Geology of Weak Rock, Sept. 1990.

Eringen, A. Cemal (1980) Mechanics of Continua. Krieger Publishing Company, New York.

Land Subsidence (Proceedings of the Fourth International Symposium on Land Subsidence, May 1991). IAHS Publ. no. 200, 1991.

Abandoned Limestone Mines in the West Midlands of England — A Strategy for Action

D. BROOK
Land Stability Branch, Minerals and Land Reclamation Division, Department of the Environment, 2, Marsham Street, London, SW1P 3EB, U.K.

ABSTRACT Abandoned limestone mines in the West Midlands of England present a risk of subsidence to urban areas. Over £25M has been spent in the last 7 years on investigation, monitoring and mine infilling. The role of the independent Black Country Limestone Advisory Panel in advising the Secretary of State for the Environment has been crucial in developing the necessary strategy for action.

INTRODUCTION

The geological situation in the West Midlands of England (Fig. 1) favoured easy exploitation during the Industrial Revolution of the raw materials for iron making. Rocks of Silurian age are overlain unconformably by Middle Coal Measures and thus thick seams of high quality Silurian limestones occur close to or directly underlie abundant seams of coal, iron ore and fireclays.

The presence of abandoned mines in the Silurian limestones of the West Midlands has been known for many years. Ground movements due to the collapse of the mines have occurred from time to time over the last 150 years, largely in open land. However, in 1978, collapse of part of the Cow Pasture Mine at a depth of 150m caused significant damage to industrial buildings in Sandwell. This changed the previous appreciation of the limestone problem and it became clear that the potential problems were on a scale which was beyond the means of private landowners or local authorities to remedy.

Assistance was sought from Central Government and legislation was enacted in 1980 to enable the grant-aiding of remedial works to prevent dereliction being caused by subsidence of abandoned mines. Whilst this legislation was triggered by the problems due to limestone mines in West Midlands County, it was recognized that there were wider applications, eg to similar limestone mines in the Wrekin District of Shropshire. It was also clear that there was insufficient information about the mines to allow priorities and the form of remedial action to be determined.

In consequence, a research study to assess the degree of risk of surface collapse and to consider what action was required was jointly funded by the Department of the Environment and the local authorities concerned.

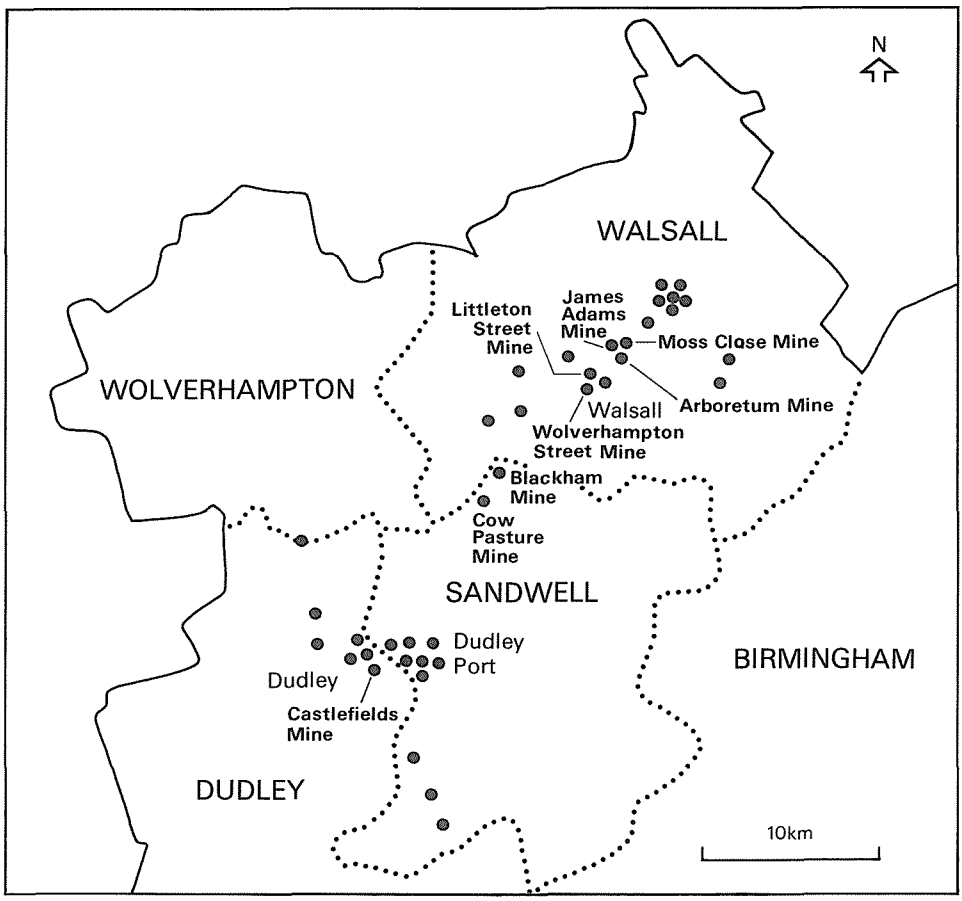

FIG. 1 Location of abandoned limestone mines in the West Midlands.

THE OVE ARUP STUDY

This study (Ove Arup and Partners, 1983) comprised two separate but complementary activities :

(a) the search for data about the limestone mines; and
(b) an engineering study to develop a risk strategy.

The objective of the data search was to discover the extent of information concerning limestone mines that remains. The objectives of the engineering study were to investigate the extent and characteristics of the mines and the rocks surrounding them, to establish the degree of risk of ground movements occasioned by their collapse and to consider and recommend what remedial and other works should be undertaken.

38 mines were identified at depths of <10m to >200m. For some mines reasonably accurate plans were available but for others only the general location could be determined from the information available. Only if two or more independent pieces of information referred to the existence of a mine was it shown on the mine plans prepared at 1:2,500 scale.

Visual inspections were made of accessible workings in Dudley and Walsall and site investigations of flooded workings in Sandwell and Walsall were carried out using rotary core drilling, geophysical logging, ultrasonic surveying and closed circuit television.

Working had been by galleries and by room and pillar mining with room heights of 4-6m in the Upper Wenlock Limestone and 7-10m in the Lower Wenlock Limestone. 100 surface disturbances recorded in the past 150 years took the form of :-

(a) crown holes - sudden collapses of the ground surface due to void migration from shallow workings at depths of <70m; and
(b) general subsidence - gentler but more widespread subsidence due to collapse of pillars or "pseudo-pillars" in the strata above the limestone from depths of >70m.

A statistical approach was adopted taking account of the stratigraphy and the age, depth and layout of the mines to define the potential for collapse. This was combined with an importance factor to derive the relative risk for the defined Consideration Zone (CZ ie the area above the mine within which structures and services are likely to suffer more than minor damage due to subsidence and thus consideration should be given to the need to investigate the ground in relation to surface movements that could be caused by abandoned limestone mines). CZs, bounded by the predicted 0.2% strain line, were produced as overlays to the detailed mine plans.

Options for future action indicated in the risk strategy were :

(a) minimum work;
(b) monitoring ;
(c) investigation;
(d) treatment of the mine; and
(e) treatment of structures and services.

POLICY CONSIDERATIONS

A parallel study by the commissioning bodies of the policy considerations examined the roles of planning, building regulations, other legal issues and the land use and financial implications (DOE. 1983).

It was estimated that about 486Ha could potentially be affected by subsidence due to limestone workings including town centre areas with important surface uses which could not readily be replaced elsewhere. Within the total area thus affected, there were estimated to be about 12,000 jobs, a resident population of 9,000 and property valued (conservatively) at £152 million.

Codes of Practice covering planning and building regulations matters prepared during this study have since been adopted by the local authorities concerned. These codes have been modified for adoption by local authorities in Shropshire, where there are similar mining problems (Wrekin Council, no date) and have formed the basis for general policy guidance on the development of contaminated (DOE, 1987) and unstable land (DOE, 1990).

THE LIMESTONE PROGRAMME 1983-90

On publication of the reports of these studies, a commitment was given by the Secretary of State for the Environment to make funds

available through derelict land grant for investigation, monitoring and treatment of the limestone mines where appropriate (Brook & Cole, 1986; Cole et al, 1986). Further research has examined methods of monitoring the condition of the mines using acoustic emission techniques (eg Miller et al, 1988) and monitoring of ground movements (Longworth, 1988). In addition, full-scale pumping trials for a novel method of infill were carried out by the Building Research Establishment (Ward & Hills, 1987; Ward, 1988).

Subsequent investigations of the mines have been reported by eg Braithwaite & Cole (1986), Jackson & Braithwaite (1988), Brook (1988). Almost all have now been investigated to some degree and many of the previous uncertainties have been resolved. Whilst there have been minor extensions to CZs, substantial areas have been removed because investigation has shown the mines to be fully collapsed or the limits of mining have been defined more accurately than was previously possible.

Techniques for infilling the mines to preclude the possibility of surface damage have also been progressed (eg Stevens & Seago, 1987; Braithwaite & Cole, 1988; Cole & Stevens, 1989). The use of rock paste made from colliery spoil or pulverised fuel ash as infill material has proved to be much cheaper than conventional grouting techniques. Following a trial infill of part of the Castlefields Mine, Dudley, in 1985, rock paste has been used successfully to infill the Littleton Street mine in Walsall. 600,000 tonnes of colliery spoil from three derelict spoil heaps were injected into the mine as a thick paste at an average rate of 6,500m^3 per week at a total cost of £6 million, enabling 15.5Ha of CZ to be removed.

THE BLACK COUNTRY LIMESTONE ADVISORY PANEL

To assist him in his decision-making, in November 1983, the Secretary of State for the Environment established a panel of outside experts. This Black Country Limestone Advisory Panel, chaired by Sir Edward Parkes, was established to :

- "advise the Secretary of State for the Environment on proposals for monitoring, site investigations and remedial works in relation to old limestone mines in the Black Country; and to consider other related issues as necessary".

After an initial period of familiarization with the limestone problem, the Panel's main role has been in the provision of :

(a) advice and recommendations on the annual round of programme submissions for derelict land grant by the local authorities;
(b) detailed comments, advice and recommendations on individual schemes subsequently submitted for pre-tender approval;
(c) independent views on engineering and risk assessment; and
(d) advice on a long-term strategy to achieve acceptable cost-effective solutions to the limestone problem.

Research recommended by the Black Country Limestone Advisory Panel

Land use affected by limestone workings Land use and planning aspects of the limestone problem were briefly examined during the 1983 policy study by individual local authorities in the preparation

of their strategies for action. However, the Panel advised the Department of the need for an independent assessment of the value of potentially affected land in relation to the overall strategy for land use and economic development within the region.

Therefore, the Department commissioned Roger Tym & Partners (1985) to carry out research to :

- "provide an evaluated information base to assist the Limestone Advisory Panel and the Department in assessing the programmes and bids submitted by the local authorities".

Having assessed the regional social, economic and planning context, this study examined land use and activities within 13 CZs comprising a total of 364Ha. The value of properties on the basis of the market as it then existed was about £100 million (excluding the value of roads, properties owned and operated by Statutory undertakings and churches, schools, hospitals and museums) and the estimated increase on completion of satisfactory remedial works was just over 11%. The CZs were then ranked on the basis of priority to confirm existing use and to create development opportunities.

Risk analysis and cost-benefit study Recognizing the limitations of the relative risk assessment carried out during the Ove Arup study and the need to combine it with the land use information described above, the Panel recommended the development of a computerised system to provide an expert analysis of data about the limestone mines in relation to risk assessment and cost-effectiveness of treatment. This was developed by Blockley and Henderson (1988) using FRISP (Fuzzy Relational Inference Language with Support Logic) to provide a measure of uncertainty.

Technical audit of limestone investigations The Ove Arup study had developed techniques of investigation designed to gain the maximum amount of information from a limited number of boreholes. These techniques were applied by the local authorities in their strategies for staged investigations of the mines to determine their extent and condition and to provide information for the design of remedial measures. Once a sufficient number of investigations had been completed, the Panel advised of the need for an independent technical audit of investigation techniques to ensure that cost-effectiveness was being achieved.

The findings of this independent assessment (Geoffrey Walton Practice, 1988) endorsed the general approach adopted but recommended a reconsideration of certain aspects and identified a number of actual and potential savings. These areas of savings were recognized by the local authorities and their consultants and some had already been identified and implemented.

Reports by the Black Country Limestone Advisory Panel

The Advisory Panel has reported to the Secretary of State for the Environment on a number of specific issues and, since September 1989 has also reported progress on an annual basis (BCLAP, 1989; 1990).

Cow Pasture Mine, Sandwell Subsidence at the Cow Pasture mine in Sandwell had been responsible for the change in the appreciation of the limestone problems in the West Midlands. Following the Ove

Arup study, further investigation of this mine revealed that it was largely open and remained vulnerable to further subsidence. It was also clear that treatment of the mine would involve considerable expenditure.

Following further work by the local authority and its consultants and by the Department, the Panel reported to the Secretary of State (BCLAP, 1986) on the most cost-effective means of dealing with the problems caused by the Cow Pasture mine. Options considered included :

(a) infilling at a cost of up to £14 M;
(b) inducing subsidence at up to £6-7 M;
(c) structural protection at £2.3-3.5 M (up to £2.5 M now and £1 M over the next 15-20 years);
(d) relocation of surface development at £11-13 M; and
(e) monitoring and compensation at up to £2-3 M (spread over the next 15-20 years).

The Panel's recommendation of a programme of monitoring and damage-repair as the most sensible and cost-effective approach enabled the Department to devise and implement a package of central and local government and private sector measures to help alleviate the element of blight on property transactions in the area caused by the existence of the limestone mines. In particular, assurances were received from insurers and building societies that they will not discriminate in their offers of subsidence cover and mortgages solely on the grounds that property is in a limestone area.

This package was successfully tested in 1988-89 when further collapse of a different part of the Cow Pasture mine caused subsidence of up to 1.3m leading to severe damage to residential and industrial properties. 12 houses were written off for insurance purposes, with payments to individual owners dependent on the extent of their cover. The difference between the insurance payments and the value of the properties is being made up by local authority purchase of the properties which will then be demolished.

A strategy for limestone mines In 1988, the Panel reviewed the achievements of the limestone programme and considered what still needed to be done (BCLAP, 1988a). It recommended a strategy which involves defining the extent and stability of the mine workings by staged investigations; initiating treatment methods; programming the works by priorities based on the risk to public safety and property and on the potential use of the overlying land; and completing the programme as quickly as resources and knowledge will allow. The mid-1990s target for completion of treatment of all mines to be treated (at a cost at 1987 prices of up to £40 M) was amended to the middle to late 1990s by the Secretary of State in endorsing the Panel's strategy.

Technical audit of limestone mine investigations Following the technical audit which it had recommended and the response to it by the local authorities' consultants, the Panel reported on the benefits which would ensue (BCLAP, 1988b). This report included guidelines for the preparation of bids for derelict land grant to assist in future decisions and ensure that the potential cost-savings which had been identified by the technical audit could be achieved.

Other reports by the BCLAP Progress with the limestone

programme is now reported on an annual basis and further consideration is being given to specific issues. In particular, a report on monitoring of the limestone mines is currently being finalised and consideration is being given to the development of an overall treatment strategy in the near future, as the investigation phase is nearing its completion.

THE LIMESTONE PROGRAMME - THE CURRENT POSITION

As a result of works carried out to date, a number of mines can now be removed from further consideration. Of the 486Ha identified in the Ove Arup study, 90-100Ha have been removed from CZs, including :

(a) 3 mines in Sandwell have been deleted following reappraisal of the historical evidence;
(b) 6 mines in the Dudley Port area of Sandwell have had their CZs deleted following investigation by drilling as they were found to be fully collapsed;
(c) Blackham mine in Sandwell has had its CZ reduced as drilling found the upper mine to be collapsed;
(d) Moss Close mine has had its CZ reduced since drilling showed that the mined area was substantially less than the leased area on which the CZ had been based;
(e) infilling of the Littleton Street mine is complete and the CZ can now be removed;
(f) parts of several other mines have been infilled, including emergency infilling of limited areas where chimneys had been identified approaching the surface;
(g) infilling of the Moss Close and Arboretum mines and of parts of the James Adams mine is under way; and
(h) design for the infilling of the Wolverhampton Street mine (16Ha at a cost of £10 M) is under way.

Since the scale of the limestone problem was recognized in the late 1970s, over £25 M has been spent on investigation, monitoring and treatment of the limestone mines with a further £1.5-2.0 M on research. Current expenditure is at the rate of £6 M per annum and the programme is now moving from the investigation to the treatment phase of the overall strategy.

ACKNOWLEDGEMENTS The ready assistance and cooperation of colleagues within the Department of the Environment, the Metropolitan Borough Councils of Dudley, Sandwell, Walsall and Wolverhampton and their consultants, Ove Arup and Partners is hereby acknowledged. I would particularly thank Sir Edward Parkes and the members of the Black Country Limestone Advisory Panel for their forbearance over the last 7 years.

Any views expressed are, however, those of the author alone and do not necessarily represent the views of the Department of the Environment or any other organisation.

REFERENCES

Black Country Limestone Advisory Panel (1986) Cow Pasture Mine, Sandwell, West Midlands. Rpt to Sec. of State for Environ.

Black Country Limestone Advisory Panel (1988a) A strategy for limestone mines. 2nd Rpt to Sec. of State for Environ.

Black Country Limestone Advisory Panel (1988b) Technical audit of limestone mine investigations and Guidance notes on applications for derelict land grant - limestone. 3rd Rpt to Sec. of State for Environ.

Black Country Limestone Advisory Panel (1989) Report for 1988-89. Rpt to Sec. of State for Environ.

Black Country Limestone Advisory Panel (1990) Second Annual Report - 1989-90. Rpt to Sec. of State for Environ.

Blockley, D.I. & Henderson, J.R. (1988) Knowledge base for risk and cost benefit analysis of limestone mines in the West Midlands. Proc. Instn. Civil Engrs, 84.

Braithwaite, P.A. & Cole, K.W. (1986) Subsurface investigations of abandoned limestone workings in the West Midlands of England by use of remote sensors. Trans. Instn Mining Metall., 95, A165-214.

Braithwaite, P.A. & Cole, K.W. (1988) The use of colliery spoil in the infilling of limestone caverns. In: "Mine Scape 88" Int. Sympos., Instn Mining Engrs, Harrogate.

Brook, D. (1988) Abandoned limestone mines in the West Midlands of England - underground dereliction in an urban area. In: Cities and subsurface use. Rotterdam, A.A. Balkema, 121-28.

Brook, D. & Cole, K.W. (1986) Subsidence of abandoned limestone mines in the West Midlands of England. In: Land subsidence. Proc. 3rd Int. Sympos. on Land Subsidence, Venice, Italy, 19-25 March 1984), IAHS Publication No. 151, 675-85.

Cole, K.W., Braithwaite, P.A., Dauncey, P.C. & Seago, K.L. (1986) Removal of actual and apprehended dereliction caused by abandoned limestone mines in the West Midlands of England. In: Building on marginal and derelict land. Lond., Thos. Telford.

Cole, K.W. & Stevens, D.W. (1989) Infilling abandoned limestone mines in the Black Country. Land & Mineral Surveyors. 7.

Department of the Environment (1983) Policy considerations arising from the study of limestone workings in the West Midlands. Rpt of Steering Group for Limestone Study., Birmingham, Dept Environ.

Department of the Environment (1987) Development of contaminated land. Dept Environ. Circular 21/87, Lond., HMSO.

Department of the Environment (1990) Development on unstable land. Planning Policy Guidance Note 14, Lond., HMSO.

Geoffrey Walton Practice (1988) Investigation of limestone workings in the West Midlands- a technical audit. London, Dept Environ.

Jackson, C.V. & Braithwaite, P.A. (1988) The identification of abandoned limestone mines by site investigation methods. In: Mine workings 88 (Proc. 2nd Int. Conf. on Construction in areas of abandoned mine workings), Edinburgh, Engineering Technics Press.

Longworth, T.I. (1988) Monitoring of ground movements above an abandoned underground limestone mine. In: Engineering geology of underground movements. Geol. Soc. Engng Geol. Spec. Publication No. 5.

Miller, A., Richards, J.A. & McCann, D.M. (1988) Micro-seismic monitoring experiments in abandoned flooded limestone mine. In: Engineering geology of underground movements. Geol. Soc. Engng Geol. Spec. Publication No. 5.

Ove Arup & Partners (1983) Limestone mines in the West Midlands: the

legacy of mines long abandoned. London, Dept Environ.
Roger Tym & Partners (1985) Land use affected by limestone workings in the Black Country. Rpt to Dept Environ., December 1985.
Stevens, D.W. & Seago, K.L. (1987) Sources study - the identification and selection of sources of colliery spoil for use in the infilling of abandoned limestone mines in the Black Country. In: 2nd Int. Sympos. on Reclamation, treatment and utilization of coal mining wastes, Nottingham.
Ward, W.H. (1988) Full-scale mixing, pumping and surface spreading trials of rock paste for filling mines. In: Engineering geology of underground movements. Geol. Soc. Engng Geol. Spec. Publication No. 5.
Ward, W.H. & Hills, D.L. Rock paste for filling abandoned mines. Ground Engineering, 20.
Wrekin Council, no date. Mineral workings - Town Planning and Building Regulation Codes of Practice., Telford, Wrekin Council.

Land Subsidence (Proceedings of the Fourth International Symposium on Land Subsidence, May 1991). IAHS Publ. no. 200, 1991.

Prediction of Subsidence Resulting from Creep Closure of Solutioned-Mined Caverns in Salt Domes

JAMES T. NEAL
Underground Storage Technology Division 6257, Sandia National Laboratories, Albuquerque, NM, USA

ABSTRACT The prediction of subsidence over solution-mined caverns in salt domes is based on some fifty years' solution mining history. Several approaches contribute to predictions: site-specific observations obtained from subsidence monitoring; numerica modeling, now becoming more practicable and credible; salt-creep data from testing; and rule-of-thumb methods, based on experience. All contribute to understanding subsidence but none are totally reliable alone. The example of subsidence at the Strategic Petroleum Reserve sites demonstrates several principles of cavern creep closure, the main cause of the subsidence, and shows that reliable projections of future subsidence are possible.

INTRODUCTION

Solution mining in salt is now a mature technology, having been practiced for more than 50 years, first in Europe and now extensively along the U. S. Gulf Coast. More than 500 permits for solution mining have been issued by the State of Texas alone, with the Barbers Hill dome at Mont Belvieu, Texas, having more than 100 caverns. Caverns are created as a result of dissolution during extraction of brine, and intentionally for storage of liquid or gaseous hydrocarbons, or other material such as industrial waste.

Frasch mining of sulphur from the caprock overlying salt domes is a type of solution mining, strictly speaking, and the accompanying subsidence and collapse effects are reasonably well known (Deere, 1961). The phenomenology associated with subsidence induced from sulphur extraction differs from that associated with the creep closure of caverns or mine openings in salt. However, subsidence associated Frasch sulphur mining is not discussed here, but nonetheless is often concurrent with subsidence resulting from solution mining in salt.

Although common in occurrence, subsidence has not been widely reported on, possibly because of the perception of

adverse publicity which most companies and institutions wish to avoid, and because of difficulty in obtaining accurate measurements. Subsidence is an acknowledged fact of life wherever large underground voids have been created, and openings in salt follow specific rules related to the rheologic behavior of salt. Some ten years of history of Strategic Petroleum Reserve (SPR) operations demonstrate subsidence phenomenology and point to means of prediction. Observations of subsidence from leveling surveys, numerical modeling, lab creep testing, and rules-of-thumb have all been used to predict subsidence.

The 65 SPR caverns now contain some 500 million barrels (MMB) of crude oil in five salt domes [Fig. 1] and when full will contain about 675 MMB. An additional 73 MMB is contained in a former room and pillar mine at Weeks Island dome, LA, but the subsidence phenomenology there differs because of more shallow depth and much different geometry compared to solution-mined caverns.

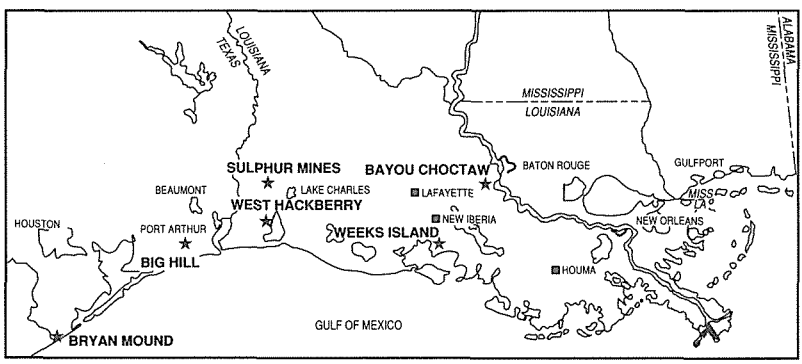

FIG. 1 The six Strategic Petroleum Reserve sites (star) are located in Louisiana and Texas.

ORIGIN OF CAVERN SUBSIDENCE IN SALT CREEP

The process of creep closure in underground caverns is understood qualitatively to occur radially into the cavern, with the largest amounts at the cavern bottom [Fig. 2]. The closure requires the concomitant flowage of salt from all directions and therefore a gradual lowering of the surface, i.e. subsidence. Factors that influence the observed variations in creep closure in caverns are the constitutive properties of the salt, the depth, which controls temperature and lithostatic pressure, the differential pressure between that in the cavern and lithostatic pressure, cavern shape, and the configuration of multiple caverns.

Laboratory tests conducted at 32° C revealed large variations in salt creep response between sites and within a single site and may be due to experimental and/or

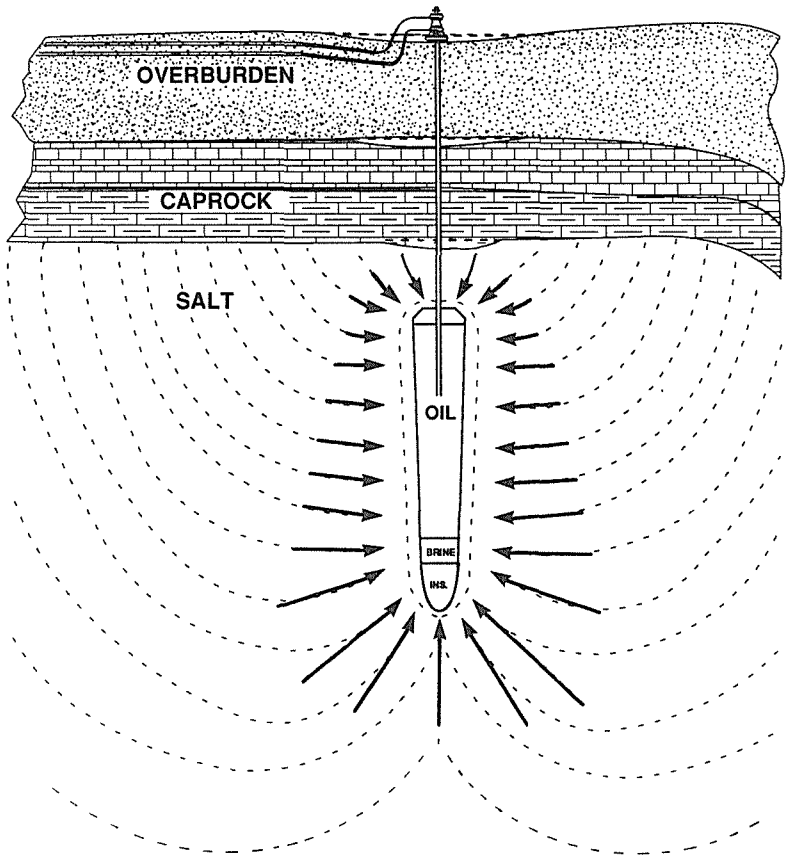

FIG. 2 Creep closure and subsidence associated with caverns in salt. Arrows show vector quantities of relative closure; dashed lines are flow patterns in salt. Some 10% of cavern volume is lost by this process in 30 years.

constitutive differences (Nelson & Kelsall, 1984). Many authors believe that the data scatter between samples results from characteristics at the molecular level, as attempts to correlate impurities, fabric, or crystal size have been unsuccessful. Some samples show greater sensitivity than others to temperature change. Cavern shape influences creep by virtue of surface area and depth; an equal-volume sphere possesses about 61% of the area of a 10:1 cylinder and consequently has less creep closure and more uniform pressure and temperature. Multiple cavern arrays display synergistic effects that result in additional subsidence over what would be expected for single caverns (Chow, 1974; Sutherland & Preece, 1986).

Observations in mines, boreholes, caverns, laboratory creep tests, and in calculations all show that salt under

constant loading displays a rapid but transient initial strain response (primary creep), followed by a longer-term steady-state deformation (secondary creep), and sometimes an increasing rate of deformation leading to rupture (tertiary creep) [Fig. 3].

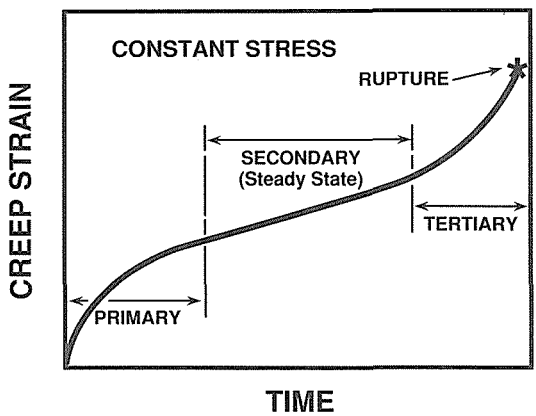

FIG. 3 Phases of creep deformation in salt.

OBSERVED SUBSIDENCE AT SPR SITES

Subsidence observed at SPR includes multiple caverns and sites and illustrates various principles of salt creep and associated subsidence, demonstrating varying salt properties, differing cavern shapes, depths and configurations, and variable site geology. Regional subsidence from other sources is also occurring in addition to that induced by the SPR caverns but this contributes only a small amount to the overall subsidence. Repetitive surveys at approximately annual intervals have been conducted at each of the SPR sites (Table 1), showing values of average annual subsidence that ranged from 9 to 63 mm. A total of some 350 survey points include cavern wellheads, concrete foundations, and constructed monuments, all located over a total area of about 7 km^2 . A wide range in values is observed both within and between sites; thus understanding the phenomenology is essential to establishing a predictive capability.

The data of Table 1 show a sevenfold variation between the smallest (Bryan Mound) and largest (West Hackberry) subsidence rates. Upon initial inspection basic parameters appear similar, but detailed examination reveals possible reasons for the variation. Laboratory creep rates of Bryan Mound salt are among the lowest of any salt studied (Wawersik & Zeuch, 1984), and the West Hackberry caverns are some 180 m deeper on average. While this may not seem significant, the exponential increase in

TABLE 1 Summary of measured subsidence, SPR sites, 1982-88 (Goin and Neal, 1988).

SITE (Capacity, in MMB)	WEST HACKBERRY (219)	WEEKS ISLAND* (73)	SULPHUR MINES (26)	BAYOU CHOCTAW (72)	BRYAN MOUND (226)
Ave. Subsidence (mm year^{-1})	62.5	34.8	29.1	18.7	9.0
Min./Max., (mm year^{-1})	27/82	12/58	21/38	12/34	3/20
Standard Error (mm year^{-1})	3.14	4.02	3.84	1.83	2.93
Cavern Depth,m top/bottom	823/ 1372	140/ 226	823/ 1106	762/ 1220	640/ 1250
Salt Roof Thickness,m	186	99	375	670	320
Caprock Thickness,m	152	0	305	61	99
Volume Area^{-1} (MMBBL ha^{-1})	1.92	0.64	1.46	1.24	1.98
Other Activity	oil	salt; oil	sulphur; oil	oil	sulphur
Extraction Ratio, %	~7	~25	---	---	~7

*Data from Weeks Island is included here, but storage is in a former room-and-pillar salt mine; Big Hill dome is not included, being now developed, and subsidence monitoring is just beginning.

creep with depth can account for the majority of creep occurring in the bottom 20% of the cavern [Figs. 2 & 4] (Todd, 1989; Heffelfinger, 1990).

Some of the data is not entirely consistent, and this difficulty has been attributed to inaccurate or shifting reference monuments, to instabilities in individual monuments, and possibly to leveling inaccuracy. Changes in survey practices, monuments, and reference points are expected to improve future measurements. The West Hackberry data are the most consistent, and this site has high interest within SPR because of the low surface elevation and location within coastal marshlands.

TREND FORECAST OF WEST HACKBERRY SUBSIDENCE

Projections of subsidence trends of the lower elevation areas of the West Hackberry site are shown in Table 2, based on rates established over some eight years of measurements. No indications of rate change were noted in any of the data, thus it is assumed to represent steady-state (secondary) creep primarily, with most of the primary creep closure [Fig. 3] having occurred early during the three-year leaching process to create the caverns. Thus the projections are linear, based entirely on observed rates. The projections allow for no change in regional subsidence or uplift rates, but this is only an insignificant small portion of the total subsidence measured. The results show that the already low areas of

TABLE 2 Projected Surface Elevations for Selected West Hackberry Stations in Meters, Relative to Mean Sea Level, based on 68 months data, 1982-88.

STATION	DELTA	ELEV (9/88)	SUBSIDENCE RATE (mm mo.$^{-1}$)	Projected Elevations 1995	2000	2005	2010	2015
SMS 3	0.162	0.909	2.38	0.72	**0.57**	**0.43**	**0.29**	**0.15**
SMS 4	0.320	2.13	4.71	1.75	1.47	1.18	0.90	0.62
SMS 5	0.329	1.70	4.84	1.31	1.02	0.73	**0.44**	**0.15**
WH 6C*	0.332	1.58	4.89	1.18	0.89	**0.60**	**0.30**	**0.01**
WH 8A*	0.271	4.01	3.99	3.69	3.45	3.21	2.97	2.73
WH 108*	0.165	2.28	2.42	2.08	1.94	1.79	1.65	1.50
WH 110*	0.399	2.03	5.87	1.55	1.20	0.85	**0.50**	**0.14**
WH 111*	0.387	2.08	5.69	1.62	1.28	0.94	**0.59**	**0.25**
WH 113*	0.408	1.86	6.01	1.37	1.01	0.65	**0.29**	**-0.07**
WH 114*	0.412	1.84	6.05	1.35	0.99	0.62	**0.26**	**-0.10**
WH 115*	0.466	2.32	6.86	1.76	1.35	0.94	**0.53**	**0.12**
WH 116*	0.378	2.10	5.30	1.67	1.35	1.03	0.71	**0.40**

* Wellhead elevations are measured at unknown height above the ground surface. **Bold** values are below mean tide level of Black Lake, 0.60 m.

the site within a few years will be at or below the level of Black Lake on the northern perimeter, which has a mean tidal elevation of 0.6 m. These projections allow time to consider engineering solutions, e.g., diking.
Another mitigating measure would be to operate the caverns at the highest possible differential pressure (~90% of lithostatic at casing seat) to slow creep to the extent practicable. The effects of operating pressure on closure vs depth are shown dramatically in the calculations by Heffelfinger, 1990 [Fig. 4]; operating at lower pressures could exacerbate existing subsidence.

NUMERICAL PREDICTION METHODS

Finite element modeling can be used to predict the creep of materials under loading and is commonly applied to engineering problems such as this. Segalman (1989) calculated creep closure and subsidence of a generic (average material properties and depth) West Hackberry cavern, using the JAC code (Biffle, 1984). Cavern volume loss rates are plotted along with subsidence volume and show close parallelism [Fig. 5]. The ratio of subsidence volume to cavern volume loss is also plotted and shows that after 10 years some 70% of the closure will have manifested in subsidence, increasing only to 80% after 30 years, and showing the same steady-state trend. These calculations reveal volumes close to measured subsidence rates, and they appear useful primarily in explaining phenomenology at this point.

A more direct method of predicting cavern performance has been proposed by Thoms and Gehle (1983) in which the borehole that is constructed for the eventual cavern is observed over a period of several years and its measured closure rate is ratioed with the projected cavern

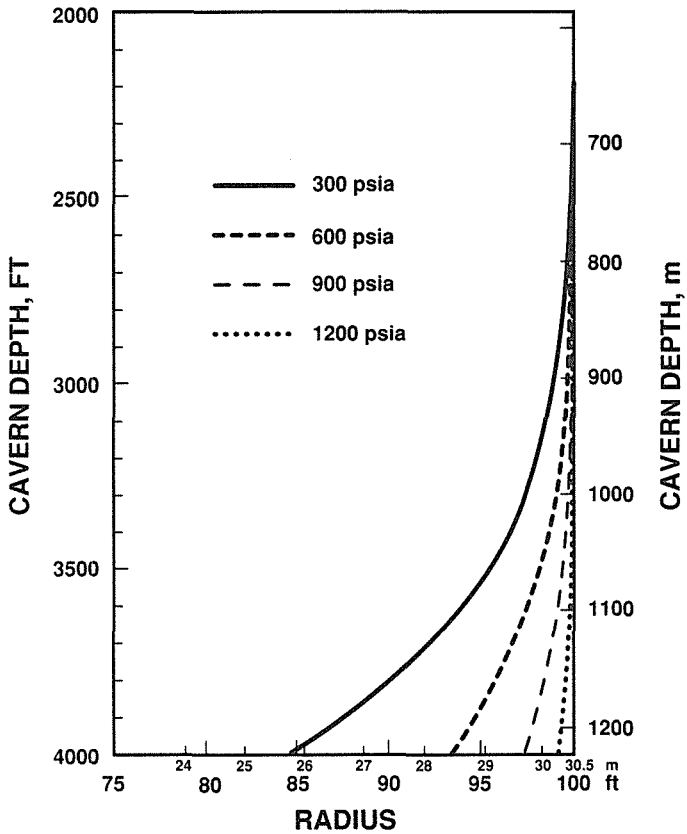

FIG. 4 Calculated effects of differential pressure at 600, 900, & 1200 psi (4.1, 6.1, 8.2 MPa), plotting cavern diameter vs depth at 30 years. From Heffelfinger, 1990.

dimensions. A limiting factor is that all measurements of closure are time dependent; thus long-term behavior can be estimated best when steady-state closure is indicated. Field tests are normally limited in duration, making it difficult to obtain such information. However, long term projects that emplace multiple caverns offer excellent opportunities to use this method. Once the creep closure behavior is known, then subsidence estimates can follow, using other geologic information on caprock and overburden in conjunction. In this regard, similar experience and conditions are needed for extrapolation, unless modeling as described above is used.

SUBSIDENCE ESTIMATION

Frequently it is desirable to estimate subsidence effects in advance of actual cavern development, given the

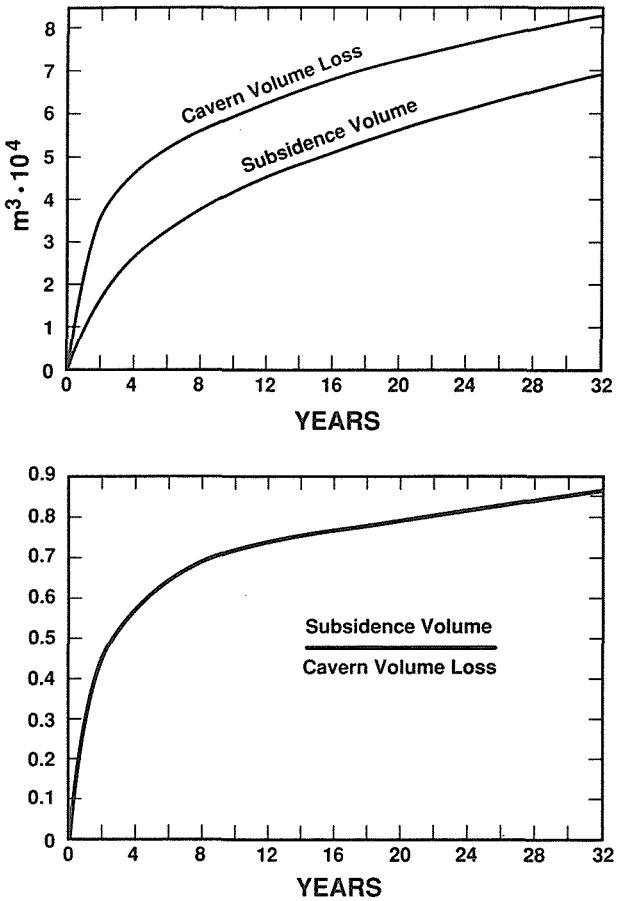

FIG. 5 Top: Calculated creep closure and associated subsidence for a generic West Hackberry cavern. Initial rapid closure (primary creep) gives way to longer-term (secondary) creep. Bottom: Ratio of subsidence to cavern closure, showing some 80% of closure is manifested in subsidence in 30 years. From Segalman, 1989.

large investment in such operations. Approximations of the potential subsidence pattern was estimated for a 200 MMB generic cavern field [Fig. 6]. The estimate of about 1.5 m maximum subsidence over 30 yrs is based on a rule-of-thumb for volume loss used in SPR (10% in 30 yrs), comparisons with domes having caverns at similar depths (Bayou Choctaw), similar group patterns observed in the cavern field at West Hackberry dome, and knowledge of creep principles obtained from numerical calculations (Segalman, 1989; Heffelfinger, 1990) [Figs. 4 & 5]. The estimate appears reasonable based on experience observed elsewhere, but there is no material property data or salt core to substantiate it.

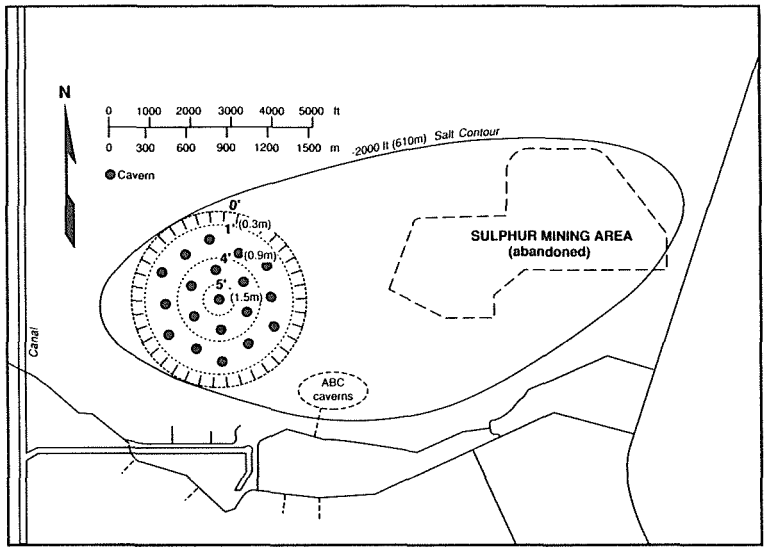

FIG. 6 Probable 30 yr subsidence pattern resulting from 200 MMB cavern field.

ACKNOWLEDGMENTS Prepared by Sandia National Laboratories for the U. S. Department of Energy under Contract DE-AC04-76DP00789. I thank B. L. Ehgartner and G. S. Heffelfinger for their critical review and helpful suggestions in improving the manuscript.

REFERENCES

Biffle, J. H. (1984) JAC - A two-dimensional finite element computer program for the non-linear quasistatic response of solids with the conjugate gradient method. SAND81-0998. Sandia Nat'l. Labs., Albuquerque, NM. Note: the users manual for JAC-3D is not formally documented.

Chow, R. (1974) Long term creep closure of solution cavity system. Proc. 4th Int. Symp. on Salt, 119-127, Northern Ohio Geol. Soc. Cleveland, OH.

Deere, D. U. (1961) Subsidence due to mining - a case history from the Gulf Coast region of Texas. Proc. 4th Symp. on Rock Mech. 59-64.

Goin, K. L. & Neal, J. T. (1988) Analysis of surface subsidence of the Strategic Petroleum Reserve crude oil storage sites from December 1982 to January 1988. SAND88-1309, 39 pp. Sandia Nat'l. Labs., Albuq., NM.

Heffelfinger, G. S. (1990) Creep closure modelling of the U. S. DOE Strategic Petroleum Reserve caverns (abs). EOS, Trans. Am. Geophys. Un., 71, No. 17, p. 627.

Kelsall, P. C. & Nelson, J. W. (1983) Geologic and engineering characteristics of Gulf region salt domes applied to underground storage and mining. Proc. 6th

Int. Symp. on Salt, vol. I, 519-544. Salt Institute, Alexandria, VA.
Nelson, J. W. & Kelsall, P. C. (1984) Prediction of long-term creep closure in salt. 25th Symp. on Rock Mech., preprint. Northwestern Univ., Evanston, IL.
Preece, D. S. & Sutherland, H. J. (1986) Physical and numerical simulations of fluid-filled cavities in a creeping material. SAND86-0694, 40 pp. Sandia Nat'l. Labs., Albuquerque, NM.
Russell, J. E. (1980) A creep model for salt. Proc. 5th Int. Symp. on Salt, 349-353. Cleveland, OH.
Segalman, D. R. (1989) Informal communication of calculational results. Sandia Nat'l. Labs., Albuq., NM.
Thoms, R. L. & Gehle, R. M. (1983) Borehole tests to predict cavern performance. Proc. 6th Int. Symp. on Salt, vol. II, 27-33. Salt Inst., Alexandria, VA.
Todd, J. L. (1989) Informal communication of calculational results. Sandia Nat'l. Labs., Albuquerque, NM.
Wawersik, W. R. & Zeuch, D. H. (1984) Creep and creep modeling of three domal salts - a comprehensive update. SAND84-0586, Sandia Nat'l. Labs., Albuquerque, NM.

Land Subsidence (Proceedings of the Fourth International Symposium on Land Subsidence, May 1991). IAHS Publ. no. 200, 1991.

A Case of Induced Subsidence for Extraction of Salt by Hydrosolution

G. GISOTTI
Servizio Geologico Nazionale
Largo S. Susanna, 13, Roma 00186, Italia

ABSTRACT In the commune of Belvedere (Calabria, Italy), at a depth varying from 200 to 600 m, lies a mine of rock salt. The layers are intercalated by an evaporitic formation of Messinian Age, trasgressively covered by Plio-Pleistocene sandy clayey deposits. Since 1970, the salt has been extracted by hydrosolution, which caused subterranean cavities inducing a wide subsidence. From the beginning the extraction was worked out by the "multiple wells" method, which didn't allow a safe control of the forming of dissolution cavities. The subsidence caused collapses (sinkholes, landsliding, etc.). Presently, extraction methods that have a more concern for the environment ("single wells") are used. The National Geological Survey is checking the mining area from a geological point of view and is looking after the subsidence.

GEOLOGICAL AND MINING SITUATION OF BELVEDERE SPINELLO ROCK SALT MINE

The evaporitic formation of Messinian Age in the "Crotonese Basin" (Calabria - Southern Italy) has intercalations of salt bed. It's trasgressively covered with sandy-clayey deposits of the Plio-Pleistocene period. In the commune of Belvedere Spinello, on the left side of Neto River, locality Timpa del Salto, lies a rock salt mine, useful from an industrial point of view, exploited since 1970 (Figs. 1 and 2).

The mine consists of two main salt layers, one of which, the first, is exploited; it is made up of breccia (clayey marl, gypsum, etc.), cemented by salts; it has a mineral percentage of about 60 and an average thickness of about 150 m. The depth from the ground level of the surface of this layer varies from 200 to 600 m.

The salt layers are overhung by an alternance of clays and gypses; they are folded and create an anticline with the axe oriented from NNE to SSW.

Three faults run parallel to the axe: Timpa del Salto, oriented from North to South and the two faults of Serra Filetto and TS 3-TS 4,

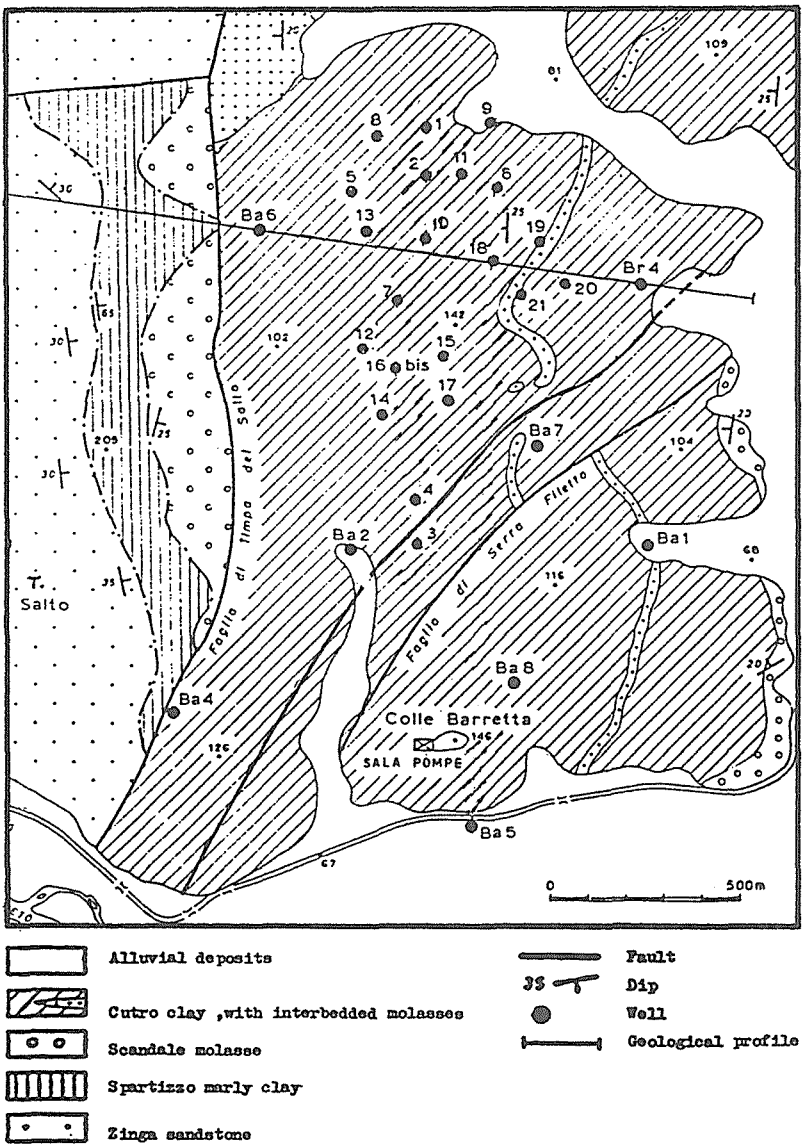

FIG. 1 Field brine geological map.

oriented from NNE to SSW.

The anticline is asymmetrical; its western side is vertical, or locally overturned, and the eastern side degrades eastward with an inclination of 15-20°.

The salt in the mine is schistose, and this indicates a plastic deformation with a vertical component, so that the mine looks like an incipient diapir.

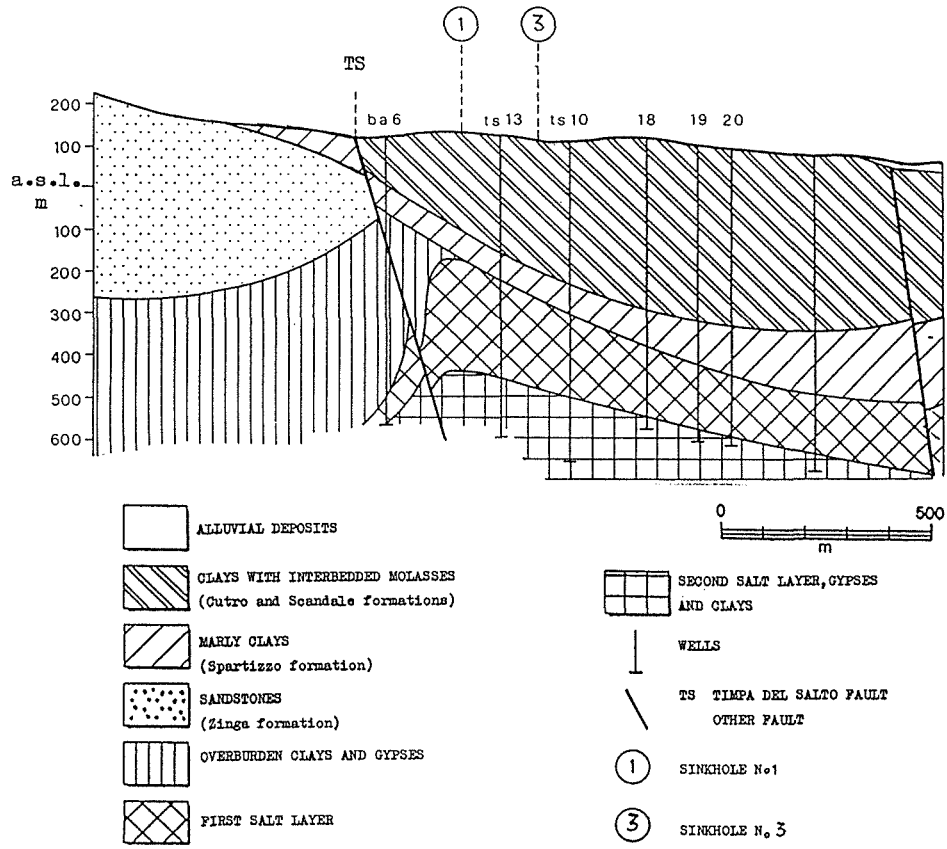

FIG. 2 Geological profile.

THE EXTRACTION METHODS IN BELVEDERE SPINELLO MINE

A quantity of mineral was estimated in about 250 millions of tons of sodium chloride.

The mine is connected to the refinement plant of Cirò Marina by the pipe-line. Here, the brine is purified, the salt recrystallized and shipped to the chemical plants of Porto Marghera (Venice).

From the beginning of the activity of Belvedere Spinello the concessionary company adopted the method of multiple wells. It consists with the introduction in a borehole of fresh water under a pressure of 200 atmospheres, to gain the solution of the salt layers (hydrofracturing) and the connection with another well. The production is allowed using a pressure of 25-30 atmospheres and the salty solution, called brine, goes up to the surface, beginning a continuous productive cycle.

The company used this method until 1984, when a lot of environmental problems arose.

In 1987, when the mining activity restarted, the company adopted a program of gradual passage from multiple to single wells, in which

the descending column of fresh water and the reascending one of the brine can be in coaxial tubes inside the well itself.

The activity of the mine is concentrated on two allined zones called "North basin" and "South basin".

From the beginning of mining, more than forty wells were opened, fifteen of which are active, with a production of about 300 m^3/hour of brine and 300 g/l of NaCl.

THE SUBTERRANEAN CAVITIES CREATED AFTER THE EXPLOITATION

On account of the described method of exploitation, subterranean cavities formed and replaced the salt and the insolubles mixed with it: moreover, such wastes remained underground, deposited on the bottom of the cavity.

The original condition of the subsoil and the conditions after 15 years of exploitation, as results from a geoelectrical prospecting carried out in 1984 by electrical vertical drillings, are shown in Fig. 3.

The creation of cavities caused quick subsidence and "sinkholes". Moreover, the subsidence was foreseen as a phenomenon connected with this mining method.

The geoelectrical prospecting carried out in 1984 allowed the rebuilding of the first salt layer's roof and of dissolution and saturation zones. The results permitted the location of the hazard zones in the brine field, summarized in a map. The zones with higher hazard are those with higher subsidence and microsysmic intensity.

A general valuation can be done of the existing subterranean cavities, considering the content of extracted salt, the grade, the total outer subsidence volume and the sinkholes.

The water injected in the wells during the exploitation by multiple wells reached a volume of about 34 Mm^3, to which corresponded a quantity of extracted salt of 12 millions of tons, with a specific weight of the undisturbed material of 2.16 t/m^3, that is 5.5 Mm^3.

Since the weight of the average grade of the salt is about 60% in NaCl, nearly 8 millions of tons of insolubles deposited on the bottom of the subterranean cavities have been removed during the dissolution process. We can consider as specific weight of the removed wastes 2.455 t/m^3; we have therefore a volume of the undisturbed material of 3.3 Mm^3, that is 5.2 Mm^3 of refilling, taking into account a rising of volume of 1.6.

The outer subsidence caused a sinking of 640,000 m^3, with a consequent refilling of about 0.8 Mm^3, considering with prudence a coefficient of rising volume of 1.3 (in fact it's not certain that the roof of the cavities in its whole will break).

The three sinkholes caused a subterranean refilling of about 2 Mm^3.

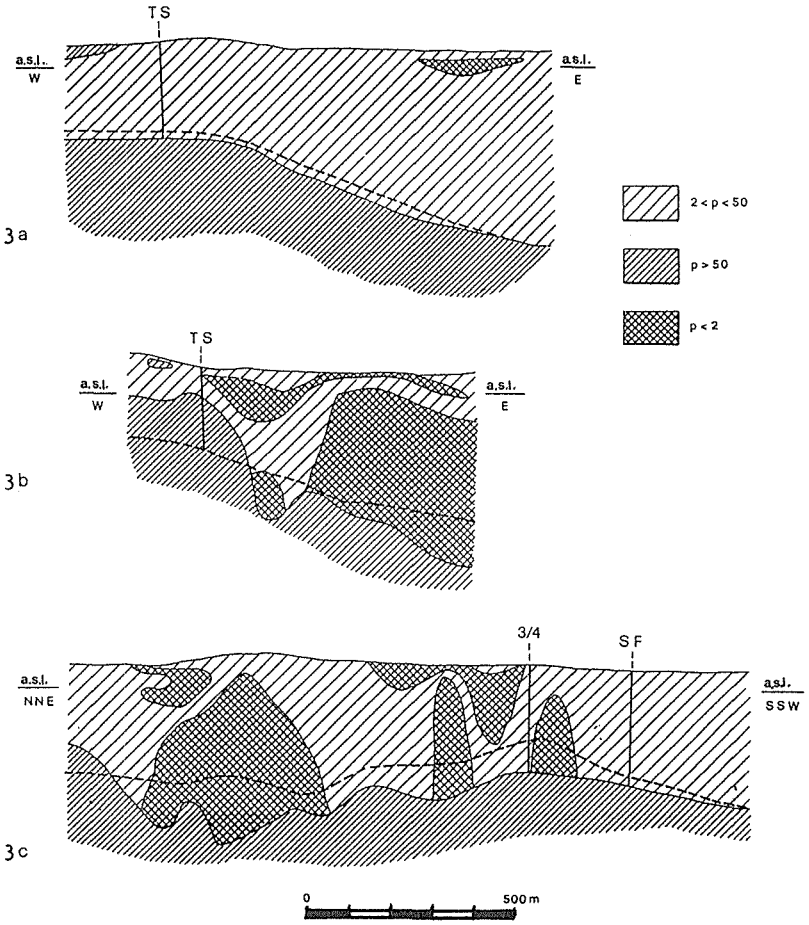

- - - - Overburden of 1st salt layer

TS /Timpa del Salto fault

SF /Serra del Filetto fault

3/4 /TS3 - TS4 fault

Fig.3a represents terrain original condition,before mining. Terrains are divided into 3 resistivity classes(p by ohm·m):

p > 50 salt ore body

50 > p > 2 cover terrains

p < 2 very conductive terrains(clays)

Fig. 3b and 3c represents brine field condition at 1984,after 15 years mining.Terrains are divided into 3 resistivity classes:

p > 50 materials remained of original salt ore body

50 > p > 2 cover terrains

p < 2 very conductive terrains,defined as "impregnated masses" and consisting of:terrains in wich circulate brine,terrains liquefied and re-deposited on the bottom of solution cavities(insolubles),brine (p=0,08 ohm·m)

FIG. 3 Brine field profiles as regards the electrical resistivity (source: Mining Italia, 1985).

Summarizing, we have a volume of residual subterranean cavities of about 0.8 millions of m^3.

Some of these spaces are marginal, with limited dimensions, disconnected to the main structure of the cavities, out of the area of subsidence, so probably they will not be filled, but remain fix because of the pillars.

SUBSIDENCE CAUSED BY EXTRACTION AND CONSEQUENT EFFECTS

The most remarkable lowerings have been surveyed in the North basin, where the exploitation was mainly concentrated. The other productive zones are less concerned by the subsidence.

The concessionary company ordered topographic levellings to follow the evolution of the subsidence, starting from october 1980; at present, the National Geological Survey carries out two levellings a year.

The first measurements, though made on a topographic surface already influenced by previous exploitations, are the reference for the following ones.

The subsidence in its hole shows a main depression in the North basin (Fig. 4). In detail, the main depression corresponds to the sinkholes n. 1 and 3.

The levelling measurements show a general increase of the subsidence values respect to the previous data, reaching values of more than 90 cm in the North basin, in a round area with the barycentre in the well TS 13; notice that the two sinkholes of the North basin are less than 100 m away from the well TS 13. The average speed of the subsidence in this limited area is 12 cm per year. At present, a decreasing course of these values (3-4 mm/month) is noticed.

Also in the South basin on the right of Fosso Barretta, another subsidence cone occurred.

In the course of the mining, the exploited cavities came in touch with faults at least three times. As a consequence, emissions of water, close to the zone of "Barretta" and East of the Timpa del Salto fault, have been noticed, during the hard works of hydraulic connection between the multiple wells TS 3 and TS 4.

All this shows the remarkable difficulties to control the extending of cavities and the development of destabilizing stresses caused by the multiple wells, with the widening or forming of fractures through which the brine may flow, even a long way from the wells to connect.

The main effects caused by the subsidence were the sinkholes, wide and deep subcircular depressions with subvertical walls opening in the ground.

These collapse cylinders are characterized by the lack of

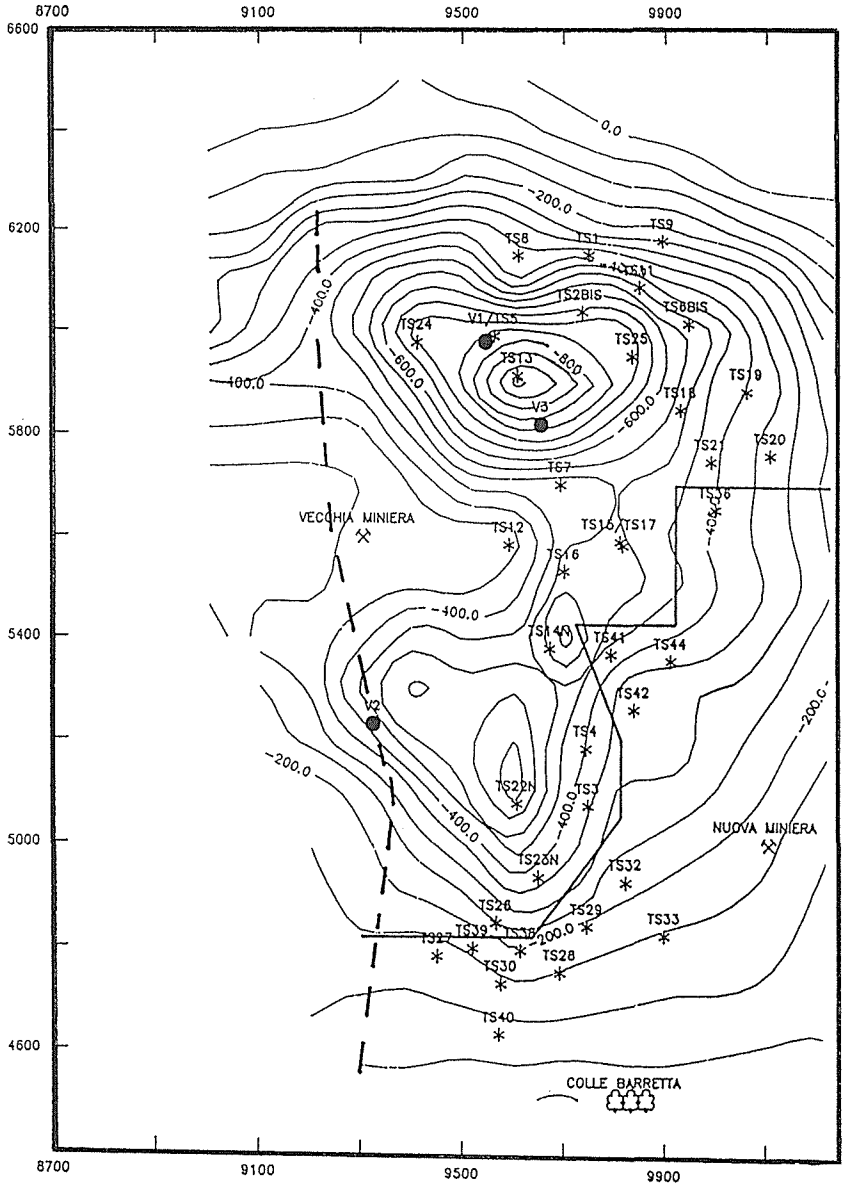

FIG. 4 Cumulative subsidence (source: Servizio Geologico).

macroscopic concentric superficial fractures, often observed in sliding phenomena.

The first sinkhole occurred around the well TS 5 in January 1983. After the collapse, a round abyss opened in the ground, with a diameter of 50 m and an area of about 2000 m^2, filled with brine.

Presently, the depth of the lake is about 6 m, the continuous erosion of the walls causing the progressive refilling of the abyss itself.

The estimated volume of such mass of water is about 20,000 m^3. The salinity is 30 g/l of NaCl.

The second sinkhole revealed itself in april 1984, on the right of Fosso Barretta, south-western edge of the brine field. It occurred on the foot of a hilly slope, causing the sliding of a terrain in the lake of the sinkhole itself, with consequent violent expulsion and projections of a huge mass of brine.

A volume of about 100,000 m^3 of brine produced a flood, first in the river bed of Fosso Barretta, then in the plain of Neto River, extending through an area about 120 hectares wide. The brine moved straight to the fluvial stream of Neto River, polluting it, and also polluting the local ground waters by percolation.

The sinkhole was formed along the fault of Timpa del Salto, joining the "Marly clay of Cutro" (that suffered the sliding), downstream, to the "Molasse of Scandale", upstream.

The landsliding material has a volumetric consistence lower than the landsliding body; this means that the missing rock filled the sinkhole because of the collapse of the roof of a subterranean cavity.

The barycentre of the collapsed block isn't placed on the vertical of any productive wells; migrations of brine, causing hollows, may therefore occurr, even in zones far from the injection well, or far from the reflow well.

After the landslide and the consequent flood, the works were interrupted and began again in the first months of 1987.

A direct effect of the described phenomenon was the saline pollution of waters. The salinity of fluvial waters, after the flood of brine, reached values of 19.7 g/l. Step by step, the salinity has then returned to normal values; in that interval, the salt made the waters completely unusable for any purpose.

The ground waters of alluvial fill of Neto River, the most important of the zone, are placed at an absolute elevation of about 20-30 m. The brine in the dissolution cavities should be instead placed at a maximum elevation of -200 m and thus it shouldn't pollute the ground waters of the alluvial fill, being deeper.

In fact, the complexity of the circulating brine in the mining basin allows one to believe that in some strict areas it may be placed at an elevation higher than the replaced salt, as shown by the sinkholes with expulsion or emerging of brine.

The third sinkhole formed in september 1986, in the area of Barretta Asciutta, North basin, inside the triangle whose vertexes are the wells 13, 10 and 7, at an elevation of 120/130, on a quite steep hilly slope.

This new abyss is about 200 m away from the first sinkhole, the one close to the well TS5.

The concerned terrains are the "Marly Clays of Cutro". In the

beginning, the diameter of the hole was about 30 m: the bottom of the abyss was made of a small brine lake and the depth of the surface of this water body was about 20 m below the hole mouth. The width of the sinkhole has increased because of the subsequent collapses, the brine dispersed underground and, at present, the diameter of the hole is about 50 m, with an area of about 8,000 m^2. The depth is about 25 m.

As observed in field, and as results from scientific literature, these sinkholes are the consequence of a quick subsidence area caused by the extraction of salt.

CURRENT METHODS OF EXTRACTION

On account of the disastrous events caused by the multiple wells, in the last years this method was given up and now the extraction is

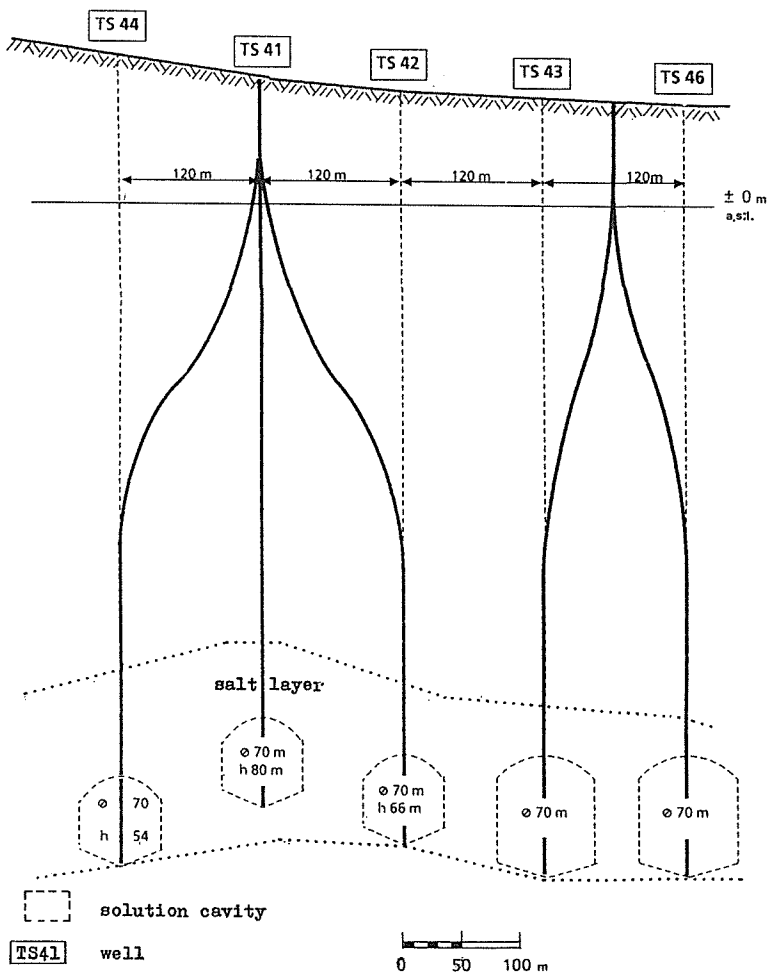

FIG. 5 Single wells mining, by "chambers and pillars" method.

worked only by single wells.

Presently, the plan of mining activity is to control strictly the development of subterranean cavities caused by the dissolution, so that the induced subsidence can be avoided. That's why the cavities are created with programmed dimensions, with a diameter of 70 m and a height of 50-150 m depending on the characteristics of salt, separated by pillars so strong to support the "slab" of brine substaining the covering clays. The dimensions of cavities are yearly checked by the Sonar Survey and daily by a geometric model "cavita" set on computer. In other words, we adopt the method by "chambers and pillars", fit to the particular mining (Figs 5 and 6).

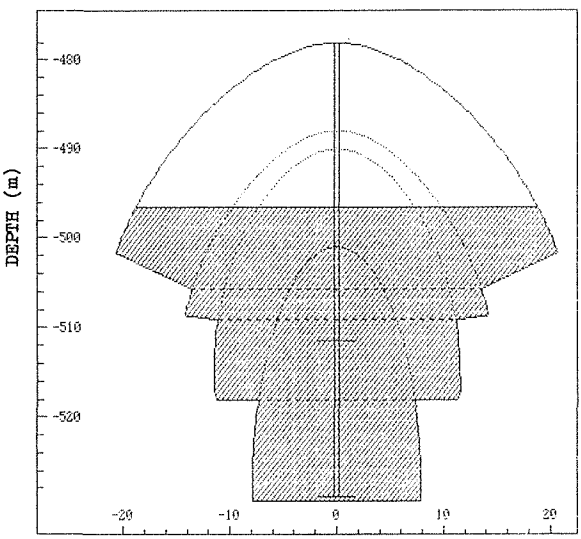

Shaded = insolubles White = brine

FIG. 6 "CAVITA" model.

CONCLUSIONS

In the described geological situation, the most induced subsidence occurs where the following two geological conditions happen: a) maximum height of the salt roof; b) minimun thickness of the Plio-Pleistocenic cover of the brine field.

To these geological factors is added the anthropic ones: the maximum exploitation of the mine.

The sinkholes n. 1 and 3, identified on figures, are placed in correspondence of the bend of the anticline and of the zone of highest subsidence.

The faults are also very important, creating preferential ways for the circulation of subterranean waters and the brine, particularly where the latter is subject to the high pressures of injection of the

fresh water, required for the hydrofracturing in the multiple wells.

The subsidence continues in the mining zone slower than in the past. At the moment, it's difficult to make hypotheses about the time necessary to stop the phenomenon.

REFERENCES

Carbognin L. (1986) La subsidenza indotta dall'uomo nel mondo. I casi più significativi. Boll. Assoc. Min. Subalpina. XXIII, 4, dec.

Gisotti G. Problemi geo-ambientali inerenti la miniera di salgemma di Belvedere Spinello (Catanzaro) . Un nuovo caso di subsidenza in Italia. Boll. Serv. Geol. It., Roma (in press).

Guarascio M., Martina E., Musso L., Solution mining development with single wells in a salt deposit with a high content of insolubles. Solution Mining Research Institute. Fall Meeting, Paris, Oct. 1990.

Dusseaud M., Fiore L., Musso L., Tijani Modeling and control of cavities development in a brine field. Solution Mining Research Institute. Fall Meeting, Paris, Oct. 1990.

Land Subsidence (Proceedings of the Fourth International Symposium on Land Subsidence, May 1991). IAHS Publ. no. 200, 1991.

Land Subsidence and Earth Fissuring on the Central Arizona Project, Arizona

J. P. SANDOVAL & S. R. BARTLETT
US Bureau of Reclamation, Arizona Projects Office, Phoenix, Arizona, USA

ABSTRACT Land subsidence and earth fissures have significantly impacted the design, construction and operation of the CAP. Reclamation and the USGS began geologic investigations in 1977 to determine subsidence design parameters and to identify fissure hazard zones. The investigations consisted of field mapping, test drilling, borehole instrumentation, and geophysical surveys. The subsequent designs accommodated 0.1 to 4.6 meters of subsidence over the 50-year operating period and included resteel within the canal lining to bridge fissures. To monitor the rate of subsidence, several methods have been employed including GIS and GPS. Fissure mitigation is extremely difficult because fissures propagate upward from the water table to the ground surface. Following construction, remedial treatment including buried barrier walls, filling, and capping have been required adjacent to CAP structures. To coordinate current and future mitigation techniques, a fissure committee was formed. Key elements of a successful fissure mitigation program include education, early detection, and prompt remedial treatment.

GENERAL

The Central Arizona Project (CAP) is being constructed by the Bureau of Reclamation (Reclamation) to deliver Colorado River water to central and southern Arizona. This water will replace existing groundwater uses and supplement surface water supplies. The CAP will deliver an average of 1.8×10^9 m^3/s of water yearly to cities and industries, Indian communities, and farmers. The 536 km long CAP system of concrete-lined canals, inverted siphons, tunnels, pumping plants, pipelines, turnouts, and check structures will convey Colorado River water across Arizona. The system consists of three aqueducts (Hayden-Rhodes, Salt-Gila, and Tucson) which are similar in design but vary in the size of canal prisms and the number of pumping plants (Fig. 1). The system capacity varies from 85 m^3/s at the Colorado River (Havasu Pumping Plant) to 5.7 m^3/s at the end of the Tucson Aqueduct. The total lift of 880 meters from the Colorado River to Tucson is accomplished by 14 pumping plants. In addition to its major components, the CAP system has many associated features such as dams, roadway bridges, wildlife crossings, drainage overchutes and culverts, protective dikes with related outlet structures, and environmental mitigation features. All of the remote pumping plants, turnouts, and check structures are operated from the project operations and maintenance center in Phoenix by a computerized control and

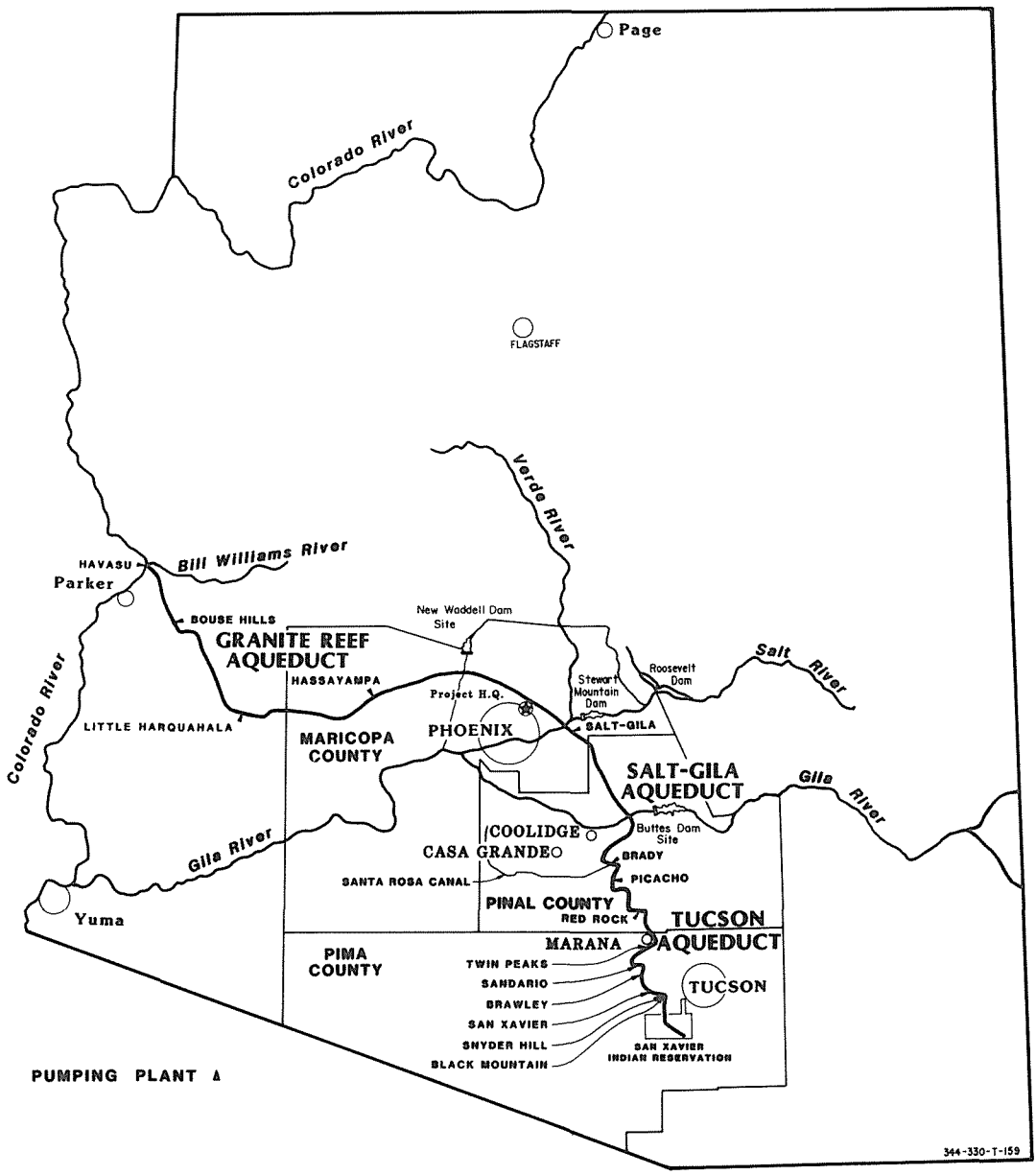

FIG. 1 General location map of the Central Arizona Project, Arizona.

communications system through line-of-sight microwave relay stations and buried fiber-optic communications cables. Actual construction began in 1977 and will be completed by 1992.

REGIONAL GEOLOGY

The CAP is located in central and southern Arizona within the Basin and

Range Physiographic Province. The geology of this province is characterized by large-scale block faulting and associated volcanism. The basins formed by the downfaulted blocks have been partially filled with material eroded from the higher surrounding mountain ranges. Also included in the basins are lacustrine deposits and interbedded middle to late Tertiary and Quaternary volcanics. Alluvial deposits commonly occur adjacent to the mountain fronts and cover both the bedrock and the range bounding faults. The cores of the mountain ranges are composed of Precambrian granitic and metamorphic rocks that are often overlain by early to middle Tertiary sedimentary and volcanic rocks. Younger Tertiary volcanic flows and pyroclastics in turn commonly cap the mountains. Alluvial materials deposited in the basins consist of heterogeneous unconsolidated mixtures of clay, silt, sand, and gravel which locally contain cobbles and boulders. This material grades from coarser to finer grained with increasing distances from their sources in the surrounding mountains and is variably cemented by calcium carbonate. Rock hills and knobs protrude through the alluvial materials (USBR 1982 & 1986). During the Pleistocene Epoch when climatic conditions were much wetter than current conditions, the alluvial basins were charged through the percolation of excess surface flows. This initial charging created large groundwater basins with abundant groundwater resource which in turn has influenced greatly recent development in south-central Arizona.

REGIONAL HYDROLOGY

As a consequence of the geological history, the groundwater table lies within the alluvial fan and basin fill deposits resulting in a groundwater surface that slopes gently away from the mountain fronts and occurs at greatest depths in the center of the basins. Streams and washes which drain the area flow only during and immediately after periods of heavy rainfall providing little recharge to the groundwater table. During the past century, groundwater use has increased in central and southern Arizona primarily due to expanded agriculture. Since 1950, groundwater levels have dropped dramatically due to rapidly increased pumping rates. This excessive pumping of the groundwater for agriculture has caused the water table to decline approximately 46 to 152 meters (USBR 1976). Overdraft of groundwater from the basin has resulted in dewatering and compaction of sediments at depth and downwarping of the land surface. The downwarping of the land surface, commonly referred to as land subsidence, has affected the region to varying degrees. Land subsidence is a slow regional process resulting in a downward change in the elevation of the basin relative to the adjacent mountains. Post-construction subsidence along the aqueduct could change the invert gradient of the canal causing local sags in the canal and allowing water to overtop the lining. Therefore, design of the aqueduct required accommodation of anticipated future subsidence estimated to occur by the year 2035.

GEOLOGIC INVESTIGATIONS AND SUBSIDENCE PREDICTIONS

Reclamation and the US Geological Survey (USGS), began investigations of land subsidence and earth fissuring along the Salt-Gila and Tucson Aqueducts in 1977. The purpose of these investigations was to define

the hydrogeologic conditions that produce land subsidence and earth fissuring, to estimate the amount of subsidence for use in designing the aqueduct, to identify earth fissure hazard zones, and to develop methods for monitoring future land subsidence along the aqueducts (Schumann 1986).

Geologic investigations consisted of field reconnaissance and mapping, test drilling, borehole instrumentation, borehole geophysical surveys, and surface geophysical surveys. A total of 83 test holes were completed along the aqueduct that ranged in depth from 38 to 670 meters. Forty-eight of the test holes were equipped with multiple piezometers to determine the depths to groundwater and to serve as observation wells. Ten of the test holes were equipped with both piezometers and compaction recorders. Water level and aquifer compaction measurements were recorded to provide a direct measurement of the relative movement for each aquifer penetrated (USGS 1985 & 1986). The relationships between water level changes, aquifer compaction, and land subsidence were identified. Recognizing that groundwater overdraft and land subsidence would continue, land subsidence predictions were completed along the aqueduct for a 50-year period extending to the year 2035. In areas where borehole information was available, aquifer compaction amounts were determined from one-dimensional consolidation tests along with borehole geophysics and applied soil mechanics. Projections of future water declines were obtained using a groundwater flow model developed by the USGS. In areas where borehole information was not available, aquifer compaction was prepared using historic ratios of long-term land subsidence to water level decline from adjacent or nearby geologically similar areas.

Estimates of future subsidence were determined by computing the ratio of the amount of aquifer compaction or land subsidence to the groundwater level decline. This subsidence to water level decline ratio was then multiplied by the projected future water level decline to produce a projected subsidence quantity. These estimates were then adjusted for horizontal and vertical variations in lithology and distributions of future pumping patterns (Schumann & Anderson 1988). Estimated amounts of predicted future subsidence over a 50 year period along the CAP ranged from 0.1 to 4.6 meters on the Salt-Gila Aqueduct (USBR 1985) and ranged from 0.6 to 2.4 meters on the Tucson Aqueduct (USBR 1985).

SPECIAL AQUEDUCT REQUIREMENTS AND DESIGN CONSIDERATIONS

The large amount of predicted subsidence required special engineering design techniques to mitigate potential impacts. These techniques included additional canal freeboard, reinforced concrete lining, overbuilt overchutes, trapezoidal road crossings, and modified check structures (USBR 1985).

In general, canal freeboard is determined by the hydraulic properties for different design capacities. Canal lining and embankments are extended above the normal water surface to protect the conveyance system from overtopping. Freeboard provides for a canal water surface higher than normal caused by sedimentation in the canal, misuse of the system, excess flows entering the canal, and waves produced by winds or surges which accompany sudden changes in flow. Special requirements for canal bank freeboard were mandatory for the canal where the system traversed areas in which land subsidence is

occurring. In areas of predicted subsidence, the canal prism freeboard was increased by raising the lining to a height sufficient to contain the water surface after the 50-year predicted subsidence, unless the 50-year predicted subsidence exceeded 10 feet, then the canal prism freeboard was raised to contain the water surface after the 35-year predicted subsidence or 10 feet above the initial water depth, whichever is greater. The interval and magnitude of the lining increments were set to balance the cost of additional materials against the efficient use of the contractor's equipment and forces.

Reinforced concrete lining was used along the canal for two reasons. Reinforced lining was used upstream and downstream of the trapezoidal road crossings to lengthen the potential percolation paths by decreasing the amount of construction joints required and thus increasing the length of the concrete slabs. This longer path was necessary so that the road subgrade across the trapezoidal crossings does not become saturated after subsidence occurs, because after subsidence occurs, the water elevation in the canal is higher than the road subgrade. The lengths of the reinforced lining adjacent to the trapezoidal road crossings depends upon the predicted 50-year subsidence for that location. Reinforced lining was also used in the potential fissure hazard areas that occur along the canal as discussed later.

Additional subsidence mitigation designs involved the overchute structures. Overchute structures along the aqueduct carry storm runoff or drainage water over the canal. The structures are located in narrow washes and sized for a maximum assumed full pipe velocity for the design flow. The cross drainage area was designed on estimated 100-year frequency flood values and 50-year sediment accumulations. Two types of overchutes were considered for the aqueduct; pipe overchutes and post-tensioned concrete open-flume overchutes. Whenever possible, the pipe overchute option was selected instead of the open-flume type so that the Operation and Maintenance roads along side the canal would not be interrupted. The pipe overchutes used on the aqueduct go above the initial water surface but through the canal lining rather than over it. As subsidence occurs, the pipes on the overchutes become submerged, subjecting the pipes to lateral loads and uplifting. Therefore, the pipes are bolted down to withstand the upward and lateral loadings. The abutments for these overchutes have spread footings where the earth on these footings resist the uplift on the pipe. The total downward force from the deadload of the overchute and the earth resist the maximum upward force on the pipe with a minimum factor of safety.

In order to mitigate the effects of subsidence, a trapezoidal road crossing configuration was chosen over a standard bridge to avoid the bridge's required high approach ramps and possible costly future jacking incurred as a result of the expected deep subsidence. The trapezoidal crossing provides a structure which is capable of handling subsidence of an equal magnitude to that designed into the canal lining. The trapezoidal road crossings were constructed to provide for the entire 50-year subsidence value plus 50 percent of this value. In areas where the designers, geologists, and field personnel felt that the design criteria was too conservative, only the 50-year subsidence value was used. Initially, the trapezoidal section in line with the canal allows free flow in the canal. After subsidence occurs, the trapezoidal section becomes a siphon. An earthen cover on the trapezoidal section provides ballast against possible flotation after

the 50-year predicted subsidence. There is a possibility that the road on the trapezoidal section could become saturated if leakage from the canal percolates to the road at some future date. Should leakage occur, road drains can be added to collect and drain the percolated water. In addition, as subsidence raised, the height of the sidewalls of the structure can be increased as the lining heights of the canal are raised.

Check structures located along the canal to regulate the canal water surface upstream of the structure and control the downstream flow have also been affected by subsidence design requirements. In addition, in the event of a break in the canal bank, checks can be used to limit the volume of escaping water to the pool confined between them and thus, prevent the entire canal from being drained. Check structure spacing was also influenced by the predicted subsidence estimates. The checks in areas of predicted subsidence were located where the 50-year subsidence prediction was 1.5 meters or less. This caused the maximum interval between checks to be 14.5 km. Checks not located in subsidence areas were located at intervals ranging from 9.7 to 11.3 km. Checks in areas of predicted subsidence were constructed with the floor of the check raised enough to allow for the predicted 50-year subsidence. This allows the checks to operate for the present conditions as well as for the future subsidence conditions.

SUBSIDENCE MONITORING

In order to monitor the effectiveness of the aqueduct design to check and the accuracy of the subsidence predictions, a subsidence monitoring program has been incorporated into the operation of the CAP. Three methods are currently in use to accomplish this monitoring. Conventional surveying methods were used during preconstruction to establish an accurate reference baseline. Control points were established along centerline and three-wire levels were used to collect the data. After construction, the control points were reestablished on structures, reference monuments were established within the aqueduct right-of-way, and K & M Bolts were installed on top of the canal lining. In areas of active subsidence the K&M bolts were located on 30 meter centers, and in semiactive subsidence areas the K&M bolts were located on 150 meter centers. Regional subsidence runs are completed at 1 to 5 year intervals depending upon the amount of subsidence and criticalness of the structure. The data is displayed on spread sheets using Lotus and D-Base III software.

Alternative methods have been used to monitor subsidence and local settlement. The Geographic Information System (GIS) has been used in conjunction with a Close Range Photogrammetric System to produce data with a horizontal and vertical tolerance of 2 centimeters. Horizontal wing points are located on the ground and field tied by first-order triangulation. Low level flights are completed and aerial photographs obtained. The aerial photographs are used to prepare a stereographic model that performs real-time measurements on the APPS-IV Analytical Stereoplotter. The plotter then locates the position of a point, measures the coordinates and establishes an elevation. The results are transfered to a data file having a format consistent with existing Reclamation profile compilation software. Periodic aerial flights prepare on-going subsidence data. Isopach maps are produced displaying horizontal movement and vertical settlement. This method has been used

successfully in areas where active settlement is occurring at a rapid rate.

Future monitoring will incorporate the use of the Global Positioning System (GPS) system. Once fully operational, the system will be used as a management tool to schedule periodic maintenance, to identify accelerated subsidence areas, and to evaluate areas of potential problems. Currently, static GPS surveying is used on Reclamation dams in Arizona to produce topographic information. It is anticipated that a kinematic GPS system will soon be used as engineering support to monitor future subsidence. The GPS system is proving to be the most economical method for gathering data. Preliminary cost comparisons between conventional and GPS system indicate that the GPS system is one-quarter the cost of conventional surveying. Additional cost savings are expected upon implementing the kinematic GPS system. It is anticipated that future subsidence monitoring on the CAP will be completed strictly by using the GPS system.

EARTH FISSURE ORIGIN AND DEVELOPMENT

Earth fissures as they affect the CAP in South Central Arizona are consequential to and directly related to groundwater withdrawal and land subsidence. The majority of these fissures have occurred within the last 50 years as the rate of groundwater withdrawal has accelerated. Earth fissures for the purpose of this presentation are defined as surface cracking in unconsolidated sediments associated with land subsidence resulting from excessive groundwater withdrawal.

Earth fissures occur in unconsolidated sediments, typically near the outer margins of alluvial basins or near outlying bedrock outcrops where groundwater levels have declined in excess of 60 meters. Surfical appearances are noted progressively by: (1) thin linear ribbons of vegetation, (2) lineations of a series of small holes or depressions (25 to 150 cm in diameter) often as the result of animal burrowing along the soft traces of the fissure, (3) small linear or in echelon hairline cracks (less than 5mm wide), (4) irregularly spaced depressions resulting from surface sloughing along the hairline cracks, (5) followed by larger open holes resulting from the collapse of subsurface piping channels, and (6) the classic "mature" expression of large gullies (up to 4.5 meters in depth) where surface drainage has been captured and has extensively eroded the previously developed cracks. Earth fissures "heal" through filling of the open trace with alluvium; however, rejuvenation and reactivation can occur at any time during their life cycle. Earth fissures older than 40 years are known to exist; however, 40 years is the probable life span of a fissure, provided that geologic conditions remain constant. Most earth fissures result from horizontal tensile stresses developed as a consequence of differential compaction of a depleted aquifer influenced by local bedrock configurations. Earth fissures differ from other types of surface cracking in that they propagate upward from the groundwater surface and the surface expressions of an earth fissure represents the last phase of development. Due to the relationship between earth fissures and the subsurface bedrock configuration, earth fissures generally develop perpendicular to the normal drainage. Consequently they intercept surface flows causing extensive erosion and gullying. Because earth fissures act as sinks, dense vegetation

characteristically outline a fissure's trace.

Surface, geophysical, and subsurface investigations indicate that earth fissures most often develop over buried salt domes, ridges, fault scarps or other irregularities in the bedrock surface, generally where these structures are buried by less than 300 meters of alluvial basin fills. In addition, the thickness of alluvium generally varies significantly across these structures, causing tensile stresses through differential compaction of the alluvium.

Five different combinations of mechanisms and hydrogeologic conditions are believed to produce earth fissures at different locations within groundwater basins. These five conditions included: (1) deep subsurface structural conditions, (2) alluvial facies changes, (3) local differential subsidence and near-surface conditions, (4) soil-moisture stress conditions as a result of vegetation, and (5) hydrocompaction or near-surface subsidence conditions. The conditions of primary importance to CAP are the deep bedrock configurations and the alluvial facies changes. The configuration of the bedrock surface is believed to be the most important controlling factor on earth fissure development along the CAP alignment. Basically, the area of thinner alluvium near the mountain fronts experiences lesser amounts of subsidence than the thicker alluvium in the central portion of the basins, where the largest amounts of subsidence have been measured. The differential subsidence between these two diverse areas cause the maximum flexure over buried fault scarps, steep slopes, or ridges. Thus, the maximum tensile stress is concentrated at these points resulting in tensional breaks or earth fissures. This scenario is similar to the origin of "hinge faults" or "pivotal faults" in sedimentary rocks along the edges of large sedimentary basins. Where the controlling mechanisms are facies changes in alluvial sediments, compaction rates vary between the larger sediments (coarse sands and gravels) from the heads of the buried alluvial fans and the finer sediments (fine sands and clays) from the toes of the buried fans. Greater amounts of subsidence occur near the centers of the basin, causing differential horizontal displacement which in turn builds stress and ultimately results in earth fissure development at these abrupt facies changes.

INVESTIGATION AND DESIGN FEATURES

Generally, the same investigations performed for subsidence determinations were also utilized to predict fissure occurrence. These investigations included mapping from aerial photographs, deep boreholes to determine soil types and depths to bedrock, seismic refraction surveys to determine top of bedrock profiles, and surface mapping to delineate existing fissures within approximately two miles of the canal alignment. Upon completion of these studies, potential fissure hazard zones were delineated along the canal alignment. An earth fissure hazard zone was defined as an area within a groundwater basin experiencing excessive groundwater withdrawal, having a depth to bedrock of less than 300 meters, and having a bedrock surface which displays a characteristic buried peak and ridge profile. These three conditions make the zone conducive to earth fissure development.

The primary design feature for fissure hazard zones involved moving the canal away from these zones wherever possible. However where rerouting was not possible the canal design treatment for fissure

hazard zones consisted of embedding No. 4 resteel mats on 0.3 meter centers (horizontally and vertically); where-as, the canal lining outside these zones remained unreinforced. The resteel was included for the purposes of supporting the entire filled canal prism in the event of fissure development so that remedial measures could be completed without disrupting water deliveries downstream. A total of 5 fissure hazard zones ranging from 480 to 3,000 meters in length were delineated along the Salt-Gila and Tucson Aqueduct alignments.

POST CONSTRUCTION FISSURE MITIGATION

The basic problem of post construction earth fissure mitigation stems from the upward propagation resulting in an earth fissure appearing on the surface after it has fully developed. In addition, any mitigation is made more difficult due to the inability to treat the fissure down deep where it is most extensive. Water within the fissure flows primarily in a downward direction and flows laterally only when the downward movement is blocked, typically by collapse of the sidewalls. Piping then occurs on top of the blockage and ultimately results in surface expression results through these alternate piping and collapsing cycles.

Due to the large dependance of municipal, industrial, and agricultural users on the CAP system, outages during any part of the year cannot be tolerated. Therefore, monitoring and rapid mitigation of earth fissures has become critical. To date, a total of nine fissures have required remedial measures. These remedial measures have included: (1) sheet piling cutoff walls, (2) geotextile cutoff barriers, (3) filling with gravel, (4) total rebuilding of fissure damaged areas, and (5) sealing the earth fissure in combination with diversion of adjacent drainage. The intent of the sheet piling cutoff walls and geotextile cutoff barriers is to force any water flowing through an earth fissure deep enough below the ground surface that it will exit downslope of the structure far enough to preclude stability problems (much like increasing the seepage path for water retention structures). The intent of the gravel is to fill and bridge the earth fissure; however, little success has been noted with this method. By

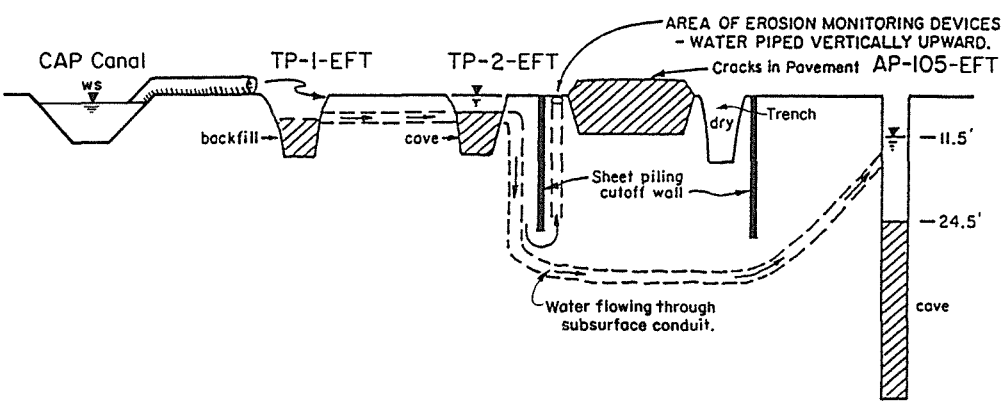

FIG. 2 View along an earth fissure trace showing the method of failure induced at a sheet piling cutoff wall intended to mitigate earth fissure development.

far the most successful remedial method tried to date has been the sealing of earth fissures in combination with rerouting of drainages away from the afflicted area. The intent of sealing earth fissures and diverting the drainages is to prevent surface flows from eroding the earth fissures, and creating the large gullies that are characteristic of mature earth fissures. To seal the enlarged earth fissures, combinations of clay, bentonite mixed with soil, and soil cements have been used to fill and mound up to 2 meters of material over the fissure. Rerouting of the drainage often requires several readjustments to achieve adequate results. Upon completion of any earth fissure mitigation, continued close surveillance and immediate corrections are necessary to prevent rejuvenation of the afflicted earth fissure.

To test methods of mitigation, one of the sheet piling cutoff walls, which was constructed along both sides of a paved access road, was tested to failure (Figure 2). The results of this test indicate that these cutoff wall methods can prevent immediate failure of a structure long enough to make corrective fixes. However, hairline cracks developed between of the sheet piling walls during testing which will ultimately result in failure of the road.

FUTURE EARTH FISSURE MITIGATION ON THE CAP

To coordinate earth fissure activities, a fissure hazard committee has been formed between USBR project personnel and water district personnel. The charge of this committee, is to share information on earth fissure development and monitoring, to report on remedial earth fissure treatments that can be related to CAP earth fissures, to initiate work requests for earth fissure mitigation, develop a Standard Operating Procedures (SOP) manual for earth fissure mitigation and control, and to develop future earth fissure mitigation techniques through research.

Among the earth fissure prediction techniques that look promising for future research and development are acoustic emission surveys, and extensometer monitoring techniques. To date, extensometers have been used by the USGS to monitor and predict earth fissure development with good results. No work has been accomplished to date with acoustic emissions; however, the conditions are suitable for this type of monitoring. Tensile stress buildups give off acoustic signatures and listening posts in the form of fence posts are embedded approximately every three meters along the canal perimeter to provide data points for the monitoring of these emissions.

Geophysical methods have also been tried to locate near surface earth fissure openings with some success. However, the openings must be wide enough to attenuate the refracted waves. In conjunction with the Arizona Geological Survey an attempt has been made to predict fissure development rates by using dated aerial photographs. This method has some potential; however, complete photographic records in areas of fissure development are rare.

The cornerstone of the continuing earth fissure mitigation program is the early detection and treatment of these fissure before they can enlarge and cause extensive damage to engineering structures such as the CAP. Due to the method of development of fissures (emanating from the groundwater level and migrating to the ground surface), early detection will continue to involve mapping of known traces and

subsurface irregularities, and periodic monitoring to determine growth rates, direction, and proximity to engineering structures. The most successful methods of mitigation for the foreseeable future will involve sealing the surface trace and diverting adjacent drainage.

Efforts have been most successful in preventing damage on the mainstem of the CAP canal where the proper expertise is available and the responsible employees have been educated in the origin and destructive potential of these earth fissures. Conversely, the most troubles with earth fissure damage has been experienced on the offstream canals and distant laterals where the expertise and funding has not been available to adequately mitigate earth fissures. To be successful in the future, the education, expertise and funding must be made available to the smaller water districts to insure adequate fissure mitigation offstream from the CAP. In summary the key elements of a successful earth fissure mitigation program are education, early detection, and prompt remedial treatment.

REFERENCES

Holzer, T.L., Davis, S.N. and Lofgren, B.E. (1979) Faulting Caused by Groundwater Extraction in South Central Arizona, J. Geophys. Res. 84 (B2) 603-612.

Larson, M.K. and Pewe , T.L. (1986) Origin of Land Subsidence and Earth Fissuring, Northeast Phoenix, Arizona. Bull. Assoc. Eng. Geol. 23 (2) 139-162.

Schumann, (1986) Groundwater Depletion and Land Subsidence in Western Pinal County, Arizona. Focus Conference on Southwest Groundwater Issues October 20-22, 1986, Tempe Arizona Proceedings.

Schumann, H.H. and Anderson S.R. (1988) Land Subsidence Measurements and Aquifer Compaction and Monitoring in the Tucson Basin and Avra Valley, Arizona. USGS Water Resources Investigations Report 88-4167.

Slaff, S., Jackson, G.W. and Pearthree, P.A. (1989) Development of Earth Fissures in Picacho Basin, Pinal County, Arizona from 1959 to 1989. Arizona Geological Survey Open - File Report No. 89-10.

U.S. Department of the Interior, Geological Survey (1986) Geohydrologic Data along the Salt-Gila Aqueduct of the Central Arizona Project in Maricopa and Pinal Counties, Arizona. Open-File Report 86-236, Tucson, Arizona.

U.S. Department of the Interior, Geological Survey (1985) Geohydrologic Data along the Tucson Aqueduct of the Central Arizona Project in Pinal and Pima Counties, Arizona. Open-File Report 85-565, Tucson, Arizona.

U.S. Department of the Interior, Bureau of Reclamation (1985) Design Summary - Salt-Gila Aqueduct; Central Arizona Project, Arizona.

U.S. Department of the Interior, Bureau of Reclamation (1976) Geology and Groundwater Resources Report, Maricopa and Pinal Counties, Arizona. Arizona Projects Office, Phoenix, Arizona.

U.S. Department of the Interior, Bureau of Reclamation (1982) Salt-Gila Aqueduct Reach 4 - Solicitation No. 3-SB-30-00010/Specification No. DC-7527; Central Arizona Project, Arizona.

U.S. Department of the Interior, Bureau of Reclamation (1985) Subsidence and Earth Fissure Predictions for Reaches 4, 5, and 6, Tucson Aqueduct and Twin Peaks, Sandario, Brawley, San Xavier,

Snyder Hill, and Black Mountain Pumping Plants. Central Arizona Project, Arizona.

U.S. Department of the Interior, Bureau of Reclamation (1986) Tucson Aqueduct Reach 3 Completion and Reach 4 - Solicitation No. 6-SI-30-04380/Specification No. DC-7668; Central Arizona Project, Arizona.

Land Subsidence (Proceedings of the Fourth International Symposium on Land Subsidence, May 1991). IAHS Publ. no. 200, 1991.

Use of Low-Sun Angle Photography for Identification of Subsidence-Induced Earth Fissures

G. H. BECKWITH
Sergent, Hauskins & Beckwith Geotechnical Engineers, Inc., Phoenix, AZ 85009, USA
D. B. SLEMMONS
Consulting Geologist, Las Vegas, NV 89117, USA
R. E. WEEKS
Dames & Moore, San Diego, CA 92123, USA

ABSTRACT Geotechnical studies for repair of a flood control dam near Phoenix, Arizona required investigation of the presence of subsidence-induced earth fissures. The dam was damaged by extensive cracking of uncertain origin. Low-sun angle (LSA) photographic methods were used successfully to detect recent earth fissures near the dam. It was demonstrated that LSA aerial photographs enabled the identification of earth fissures having only minor surface expression and unlikely to be discovered by conventional surface methods. This allowed trenching of recent fissures to obtain information critical to remedial design.

INTRODUCTION

McMicken Dam is a 10 mi. (16 km) long homogeneous flood control structure of 31.5 ft. (10 m) maximum height which was constructed in the 1950s to protect Luke Air Force Base near Phoenix, Arizona (Figure 1). Inspections in the 1960s revealed surface irregularities and distortians and led to a detailed geotechnical investigations beginning in 1972. These studies detected extensive transverse cracks in the embankment. The dam was declared unsafe by regulatory authorities and breached.

Geotechnical investigations for remedial design revealed that many of the foundation soils were subject to hydrocompaction. The site is in a typical area of groundwater withdrawal, subsidence and earth fissuring of the type described by Holzer (1984) for basins of the southwestern United States. A program of LSA photography was undertaken to determine if fissures created by groundwater withdrawal had caused any of the cracking of the dam or were likely to do so in the future.

DESIGN ISSUES & ENGINEERING SOLUTIONS

At the outset of design studies for repairs, it was apparent that the existing cracks in the dam could lead to rapid internal erosion and failure. Although it was clear that many cracks were caused by hydrocompaction, it was uncertain whether some subsidence-induced cracks might be present. Cracks that were clearly attributed to hydrocompaction extended up to 14.5 ft. (4.4 m) deep and were no more than 0.4 in. (1 cm) wide, while experience indicated subsidence-induced fissures were up to

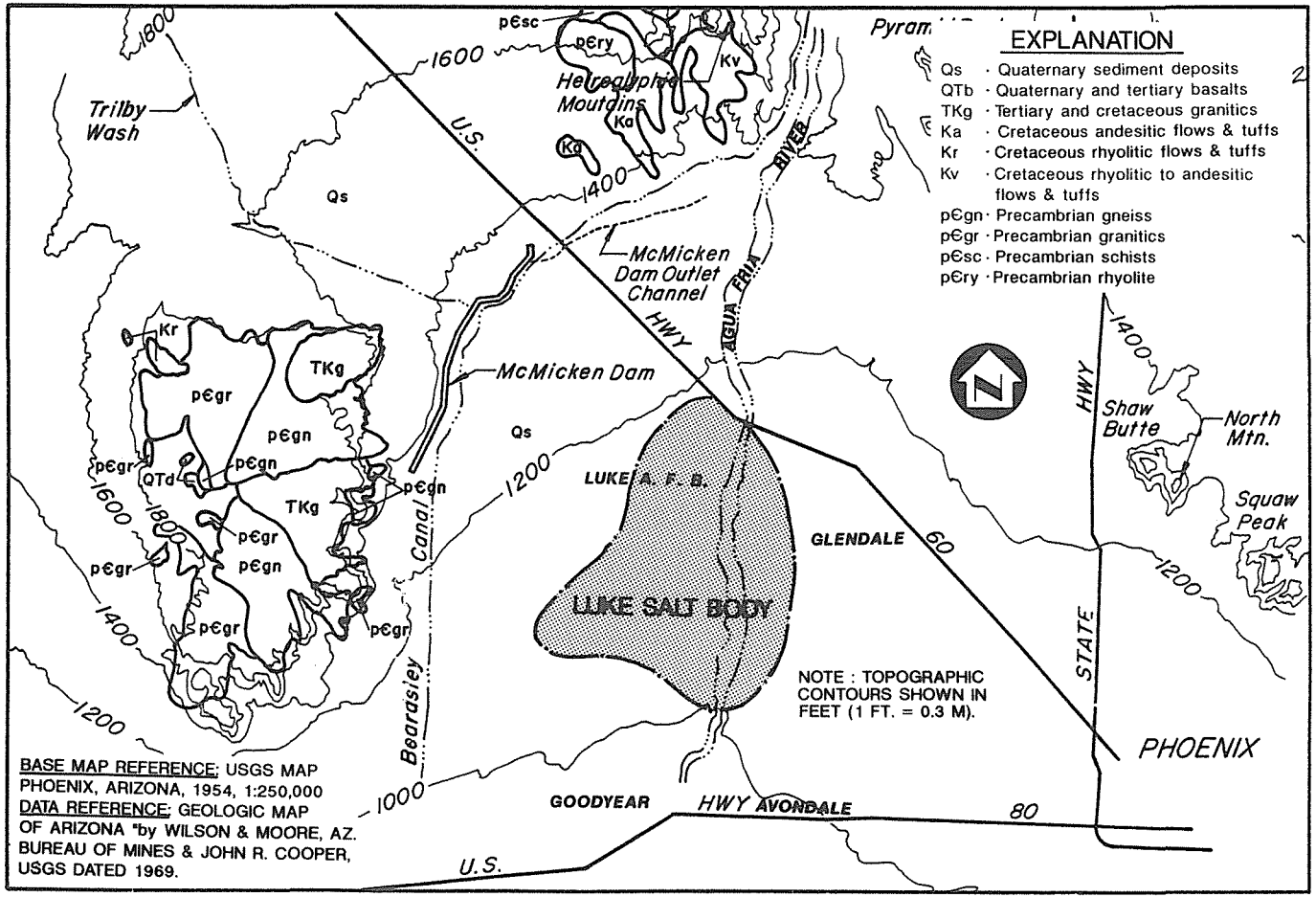

FIG. 1 Geological map.

3/4 in. (2 cm) wide and extended to great depths. It was thought that considering the age of the dam there was little possibility of future cracks due to hydrocompaction. A crucial question was the potential of earth fissuring created by subsidence affecting the dam in the future and what might be the width and hydraulic properties of such fissures. The LSA photographs helped establish that none of the existing fissures were related to subsidence, but fortified the conclusion there is a strong probability of such fissures developing in the future. It allowed the identification and trenching of fresh fissures to determine their geometry. Knowing the fissure geometry that controlled design with a high degree of confidence, a system of center, finger and toe drains consisting of gravel encasulated with geomembranes and geotextiles were designed as a repair method (Deatherage et al.,1986). Special tests to simulate cracks were performed to ensure that the geotextiles and geomembranes could withstand the opening of 3/4 in. (2 cm) wide fissures.

GEOLOGY

The McMicken Dam study area lies within the southern Basin and Range Physiographic Province (Hunt, 1974) which is characterized by linear mountain ranges separated by broad alluvial basins containing thick unconsolidated deposits. The dam is situated near the western fringe of such an alluvial basin, commonly referred to as the Phoenix Basin. As depicted in Figure 1, bedrock is composed of Precambrian granitic rocks, gneiss and schist, and Tertiary- Cretaceous granitic rocks (Wilson et al., 1969). The contact between the bedrock and the Phoenix Basin alluvium is quite irregular, with several bedrock highs protruding through the alluvial cover. One of these protrusions, Fenne Knoll, is within 1/2 mile (0.8 km) of the southern end of McMicken Dam.

Geophysical data interpreted by Oppenheimer and Sumner (1980) indicate that the depth of bedrock is in excess of 1,600 feet (490 m) below the northern two thirds of McMicken Dam, decreasing in thickness abruptly to 500 feet (150 m) near its southern end. Southeast of the dam the depth to bedrock increases to a maximum of about 10,000 feet (3,000 m) near Luke Air Force Base. Eaton and others (1972) provide geophysical and hydrological evidence for the existence of a large salt body located in the vicinity of the air force base.

Valley fill deposits of the western Phoenix Basin have been described (Stulik & Twenter, 1964) as unconsolidated to semiconsolidated clay, silt, evaporites, and sand and gravel with subordinate caliche. The deposits appear to be highly lenticular and laterally discontinuous. The alluvium in the general vicinity of McMicken Dam is estimated (Stulik & Twenter, 1964) to consist of 40 percent to in excess of 60 percent fine grained material throughout the profile penetrated by water wells. Water well logs identify highly discontinuous clay and gravel deposits to a depth of 1,000 feet (300 m) below McMicken Dam.

The McMicken Dam study area is a typical intermontain basin in the southwestern United States where the deeper sediments were formed in closed basins (Reeve, 1977). Alluvial fans tend to predominate around the perimeter of the basin and lacustrine clays in the interior creating the potential for differential subsidence in response to groundwater declines. Buried faults and irregularities in the bedrock are often factors that contribute to differential subsidence. At least 14 basins with similar geologic settings have been identified in California, Nevada,

Utah, Arizona and New Mexico where similar phenomina have occurred (Contaldo & Mueller, 1988; Holzer, 1984; Poland, 1981).

HYDROGEOLOGY

Water level elevations within 1 mile (1.7 km) of McMicken Dam, varied from 800 to 950 feet (250 to 290 m) above mean sea level in 1977 (Ross, 1978). Water levels decrease significantly southeast of the dam to a minimum of 650 feet (200 m). These elevations correspond to a depth of water of 450 to 500 feet (140 to 150 m) near the dam, and 550 feet (170 m) at its lowest elevation.

As is typical of several Arizona basins, groundwater pumpage has far exceeded natural recharge rates in the Phoenix Basin. Within the study area, in excess of 100 wells are pumped for irrigation, public water supply and domestic use. Groundwater level declines from 1923 to 1977 (Ross, 1978), vary from 200 feet (60 m) to in excess of 300 feet (90 m). Contours of groundwater decline are plotted in Fig. 2. About 25 wells are present within 2 miles (3.2 km) downstream of McMicken Dam. Figure 3 presents water table variations for 11 of these wells for the period 1938 to 1982. The depth to water in these wells has generally increased during this period from 200 to 500 feet (60 to 150 m).

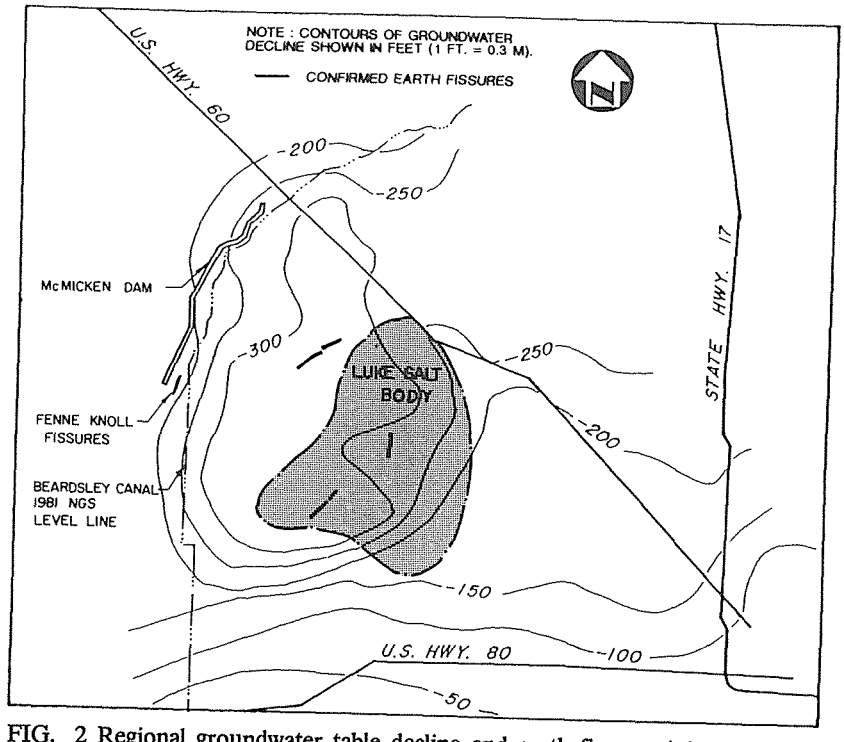

FIG. 2 Regional groundwater table decline and earth fissures (after USGS Water Investigation Report, 1977).

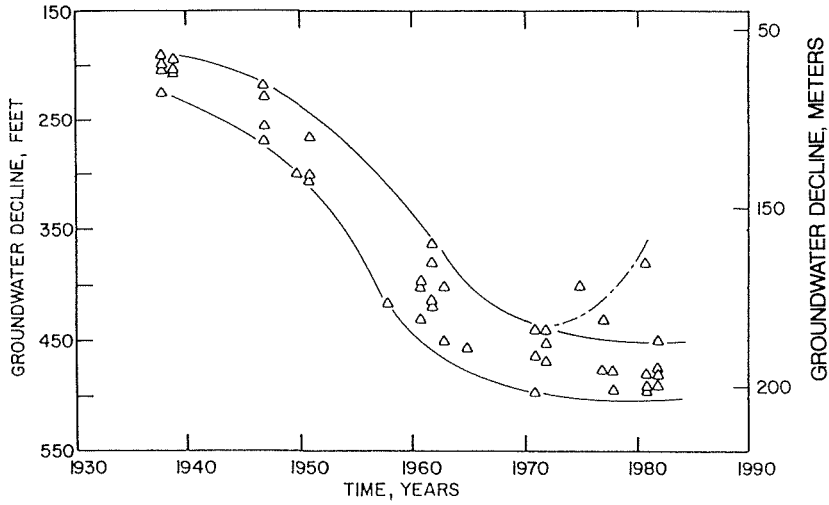

FIG. 3 Groundwater table decline.

SUBSIDENCE & EARTH FISSURING

Elevation change of 11 National Geodetic Survey level line points downstream McMicken Dam near the wells for which water level declines have been plotted on Figure 4 have been monitored between 1948 and 1981. The elevations of these points decreased between 2 and 4 feet (0.6 and 1.2 m) from 1948 to 1982. The rate of subsidence is generally increasing, though the groundwater decline to which it is related is decreasing. There is a time lag between the change in total stress due to the groundwater decline and the resulting subsidence due to consolidation of the fine grained alluvial soils. Subsidence values for the period 1948 to 1981, which approximates the history of McMicken Dam, are shown on Fig. 4 for

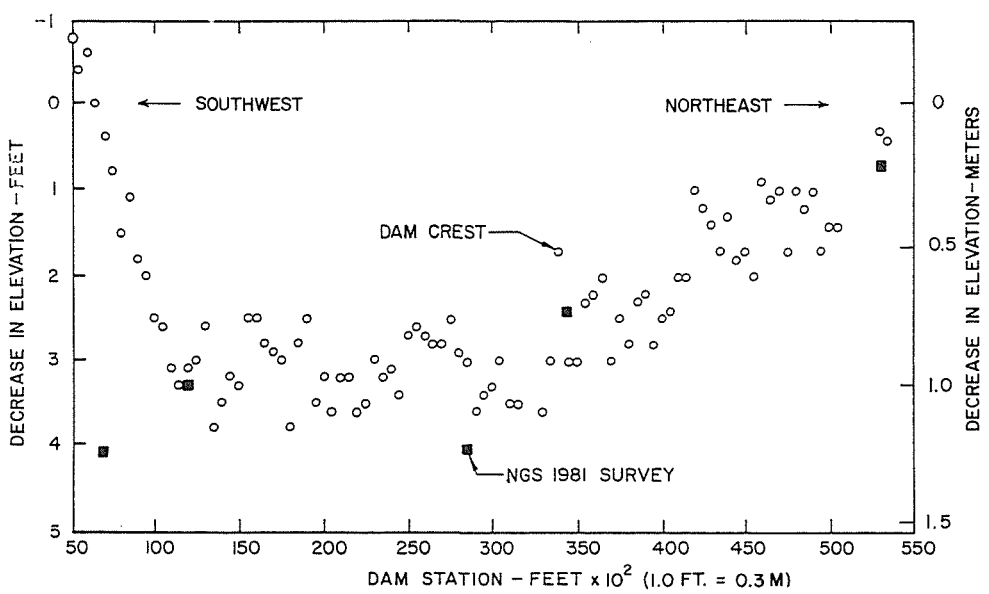

FIG. 4 Dam crest elevation and regional subsidence profile.

comparison with changes in elevation of the McMicken Dam crest. The magnitude and trend of both survey point subsidence and crest elevation change are similar. The close comparison indicates that the overall trend in settlement of McMicken Dam is related to subsidence due to groundwater withdrawal.

Fissures have developed around the perimeter of the western part of the Phoenix basin since the 1950s (Eaton et al., 1972). Most fissures have occurred near the perimeter of the area of water level declines shown on Fig. 2. Several have occurred in the westerly part of the Luke Salt Body. Fig. 5 illustrates older fissures near the dam found in 1973 investigations and confirmed and possible fissures identified in the LSA photography studies.

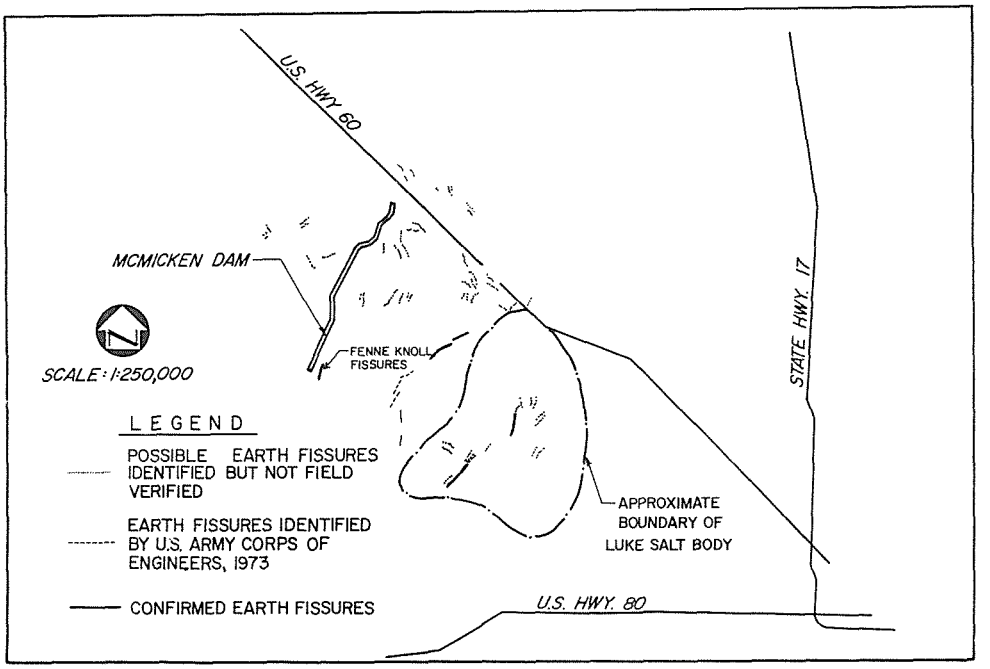

FIG. 5 Suspected and field verified earth fissures near McMicken Dam.

LOW-SUN ANGLE PHOTOGRAPHY

The detection and delineation of active faults and lineaments is commonly shown by youthful geomorphic features. The single most important method for searching for young fault scarps is by use of special LSA aerial reconnaissance and photography. The method was first described by Slemmons (1969), and Cluff and Slemmons (1972), and independently by Clark (1971). Detailed descriptions of the methods of application are in Walker and Trexler (1977), and Glass and Slemmons (1978). The conventional method for aerial photography is to use the uniform sun illumination of topography with the light directly from above. In contrast the low-angle method is based on the highlighting or shading effect of oblique lighting in the early morning or late afternoon. The ideal azimuth and altitude of the sun can be selected for illumination by using the daily and seasonal

variations. Since these effects greatly enhance the minor cracks and fissures associated with surface faulting, it appeared to be ideal for the search for earth fissures in the McMicken Dam area. This method generally reveals many minor branch faults than are unlikely to be recognized on the ground.

APPROACH & METHOD OF APPLICATION

Application to this site used an initial aerial reconnaissance of the study area to familiarize the participants with the area and to plan and schedule the mission for the optimal time.

Two sets of photographs were obtained--a 1:3,000 detailed scale along the axis of McMicken Dam and outlet channel, and a 1:9,000 scale flown for a 200 square mile area on east-west lines from White Tank Mountains on the west across Aqua Fria River on the east. The detailed scale photographs permitted high resolution of small-scale features, and the larger scale photographs of a large region permitted detection of any major trends that could affect the site. Independent analyses of all photographs were made by different observers in two offices. A search was made for topographic expression of fault scarps, straight drainage lines, fissures, alignment of depressions and piping cones, and vegetational lineaments.

The lineament analysis led to detection of 200 suspect earth fissures or lineaments. All features within 1,000 feet of the dam were field checked, and after elimination of those caused by cultural activity or erosion, a final list of eight sites remained. These were trenched with a back hoe to depths of from 12 to 21 feet and logged for evidence of subsurface fissures or paleo-fissures. These studies led to identification of two fissures in a zone with minor surface expression (Figure 6) about 600 to 1,000 feet east of the dam's toe. The two fissures of this zone were explored and evaluated in five trenches. The trenches were extended to as deep as 25 ft (7.7 m) and showed maximum uneroded width of fissures of 3/4 in. (2 cm). It is believed that open fissures extend to depths of hundreds of feet. A profile perpendicular to the axis of the dam at this location is of a zone that has undergone a differential subsidence of approximately 3 feet (0.9 m) since 1956. The depth to bedrock appears to be less than 800 feet (243 m) and the close proximity of bedrock knolls suggest that a bedrock ridge or other irregularity could underlie these fissures. To correlate the activity of known, larger scale fissures, three trenches were made at the south end of the study area. Although these features were longer and more conspicuous, they were similar to those in trenches near the dam.

CONCLUSIONS

This was the first known application of the low sun angle method for detection of ground fissures. The use of low-sun angle aerial photographs with detailed scales from 1:3,000 to 1:9,000 were successful in discovering earth fissures having minor surface expression that would probably not have been discovered by conventional ground methods. Features of importance in fissure recognition in this area included cracks, cone-shaped depressions, vegetational alignments, and straight stream segments.

The physical setting of McMicken Dam proved to be excellent for the application of the technique. The cemented surficial soils were

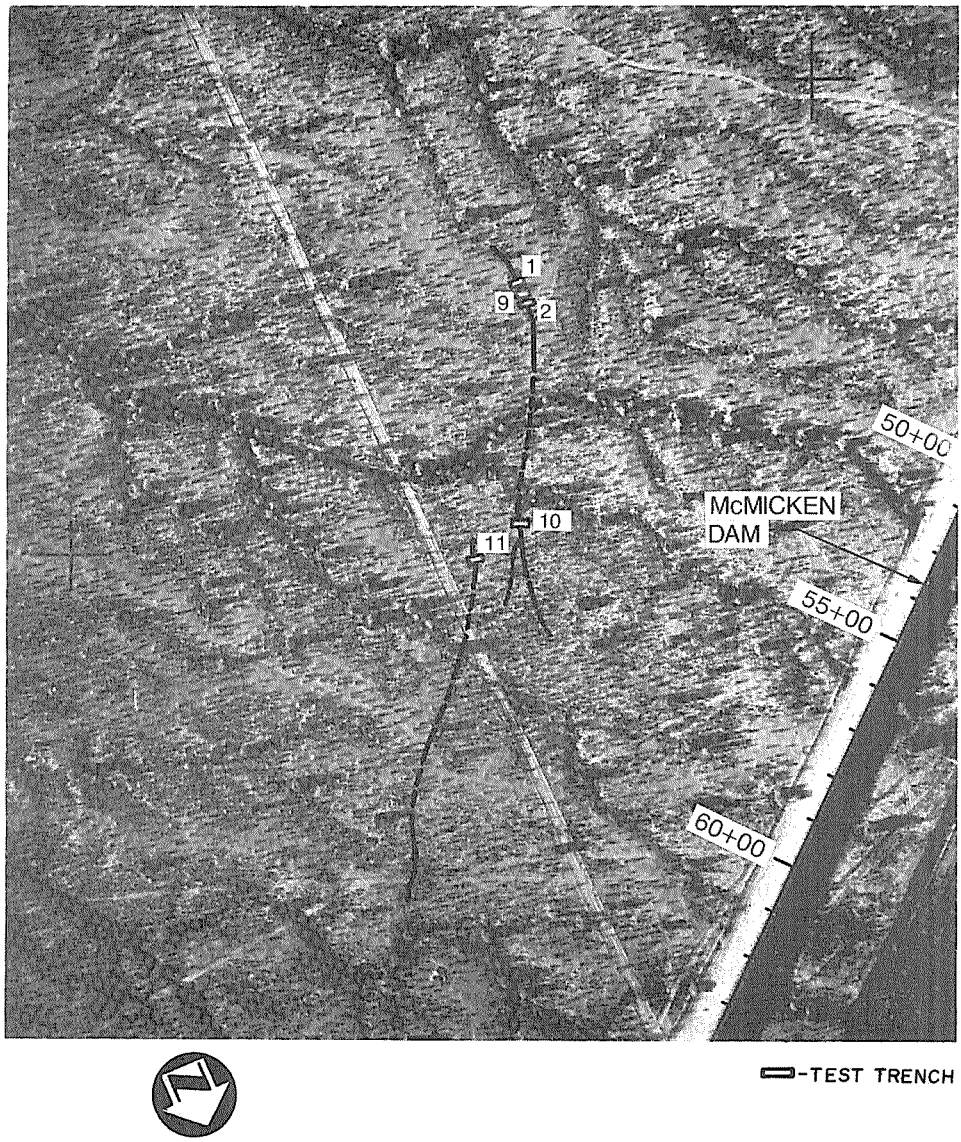

FIG. 6 Fenne Knoll fissures.

responsible for distinct, recognizable fissures, even in the early stages of their formation. The sparse vegetative cover in the semi-arid climate made a high percentage of the ground surface visible.

The physical character of the fissures were typical of those which have been found in other basins. The formation of this type of fissure through a homogeneous water impounding dam or dike of cohesive material would probably lead to rapid failure by internal erosion. This type of fissure may also create high permeability conduits to the groundwater table that would be of concern in the design of land disposal facilities for hazardous or toxic wastes.

REFERENCES

Clark, M.M. (1971) Solar position diagrams - solar altitude, azimuth, and time at different latitudes: in Geological Survey Research 1971, U.S.G.S. Prof. Paper 750-D, 145-148.

Cluff, L.S. & Slemmons, D.B. (1972) Wasatch fault zone--features defined by low-sun-angle photography: in Hilpert, L.S. (ed.), Environmental Geology of the Wasatch Front, Utah Geol. Assoc. Pub. 1, G1-G9.

Contaldo, G.J. & Mueller, J.E. (1988) Earth fissures in the Deming area, Cretaceous and Laramide Tectonic Evolution of Southwestern New Mexico, G.H. Mack, T.F. Lawson & S.G. Lucas, Eds. N.M. Geol. Soc., Socorro, N.M., USA, 3-6.

Deatherage, D.T., Beckwith, G.H. & Hansen, L.A. (1986) Restoration of McMicken Dam, 3rd Intl. Conf. on Geotextiles, Vol. 1, Vienna, Austria 261-266.

Eaton, G.P., Peterson, D.L. & Schumann, H.H. (1972) Geophysical, geohydrological and geochemical reconnaissance of the Luke Salt Body, Central Arizona. U.S.G.S. Prof. Pap., 753.

Glass, C.E. & Slemmons, D.B. (1978) Imagery in earthquake analysis: a State-of-the-art for Assessing Earthquake Hazards. U.S. Army Engineer Waterway Experiment Station, Vicksburg, Mississippi, Misc. Paper S-73-1, Report 10.

Holzer, T. (1984) Ground failure induced by groundwater withdrawal from unconsolidated sediment. Man-Induced Land Subsidence, T. Holzer, Ed., Reviews in Engr. Geol., Vol. VI, Geol., Soc. of Am. Boulder, Colo, USA, 67-106.

Hunt, C.B. (1974) Natural regions of the United States. W.H. Freeman & Co., San Francisco.

Oppenheimer, J.M. & Sumner, J.S. (1980) Depth-to-bedrock map of southern Arizona. Dept. of Geosciences, Univ. of Arizona, Tucson, Arizona, USA.

Poland, T.F. (1981) Subsidence in United States due to groundwater withdrawal. J. Jrr. & Dr. Div., ASCE, Vol. 107, No. IR2, 115-135.

Reeves, C.C. (1977) Intermontane basins of the arid western United States. Geomorphology in arid regions, D.O. Doehring, Ed. George Allen & Unwin, London, 7-26.

Ross, P.P. (1978) Maps showing groundwater conditions in the western part of the Salt River valley area, Maricopa County, Arizona, 1977. U.S.G.S. Water Res. Invest., Open-File Report, 78-40.

Slemmons, D.B. (1969) New methods for studying regional seismicity and surface faulting. Trans. AGU, EOS, Vol. 50, 397-398.

Stulik, R.S. & Twenter, (1964) Geology and groundwater of the Luke area, Maricopa County, Arizona. U.S.G.S. Wat. Supply Pap. 1779.

Walker, P.M. & Trexler, D.T. (1977) Low sun-angle photography. Photogrammetric Engineering and Remote Sensing, Vol. 43, 493-505.

Wilson, E.D., Moore, R.T. & Cooper, J.R. (1969) Geologic map of Arizona, Prepared by U.S.G.S. and Ariz. Bur. of Mines.

Land Subsidence (Proceedings of the Fourth International Symposium on Land Subsidence, May 1991). IAHS Publ. no. 200, 1991.

Geophysical Characterization of Soil Deformation Associated with Earth Fissures near San Marcial and Deming, New Mexico

WILLIAM C. HANEBERG
New Mexico Bureau of Mines and Mineral Resources, New Mexico Institute of Mining and Technology, Socorro, New Mexico, U.S.A. 87801
CHARLES B. REYNOLDS
Charles B. Reynolds & Associates, 4409 San Andres Avenue NE, Albuquerque, New Mexico, U.S.A. 87110
IRENE B. REYNOLDS
Geological Associates, 4409 San Andres Avenue NE, Albuquerque, New Mexico, U.S.A. 87110

ABSTRACT Seismic reflection profiles across two earth fissures show that surficial strata are draped over a buried normal fault scarp beneath one fissure and over a buried channel deposit beneath the other. P-wave velocity contour plots also show anomalies near both fissures. Gravity profiles suggest the presence of buried structures, but provide comparatively little information about the geologic setting of the fissures. Mechanical analysis of a compressible elastic soil layer draped over steps shows that the most tensile stresses will develop along the upper free surface if the steps are wide and along the base of the layer if the steps are narrow. We conclude that geometric details of buried irregularities control whether a fissure propagates upward from depth or downward from the ground surface. Moreover, details of stress trajectory fields can control the position of a fissure at the earth's surface relative to bedrock irregularities at depth.

INTRODUCTION

Earth fissures are a geologic hazard in many parts of the southwestern United States, and can be associated with land subsidence due to fluid withdrawal, neotectonic activity, or mining. Beyond the obvious danger of unexpected cavernous openings to humans and livestock, the appearance of fissures can affect the siting and construction of highways, aqueducts, or hazardous waste storage facilities. In this paper we present the results of shallow seismic and gravity surveys across two earth fissures in New Mexico, one apparently related to aseismic fault movement and the other to groundwater overdraft, and then use a simple mechanical model for flexure of a compressible elastic layer to interpret our observations.

We define earth fissures as narrow openings of considerable length and depth formed in unsolidated sediments, engineering soils, or regolith. Although the two earth fissures we describe here apparently began in zones of tension, we have not incorporated any genetic terms into our definition. There are two reasons for this. First, we believe that earth fissures, particularly if any amount of time has passed since the fissures appeared, are as much the products of surface and subsurface erosion (e.g., Slaff et al., 1989) as they are products of fracturing. Second, we believe that there is much more to be gained by using purely descriptive observations as boundary conditions for mechanical models, from which genesis can be elucidated by comparing theory and observation, than by incorporating genetic terms into our descriptions.

Holzer (1984, also see references therein) reviews occurrences and postulated origins of earth fissures associated with groundwater overdraft in Arizona, California, and Nevada. In general these fissures are associated both in space and in time with the dewatering of phreatic

aquifers, and the preferred mechanism of fissuring is localized differential compaction of unconsolidated aquifer material over bedrock irregularities. Earth fissures have also been attributed to vadose zone dessication, horizontal seepage forces, and regional compaction. Some fissures, however, occur in areas where groundwater withdrawal is insignificant. For example, Bell et al.(1989) and Bell & Hoffard (1990) describe fissures in unconsolidated materials above known bedrock faults in western Nevada. Haneberg et al. (1990) describe in detail their geophysical and mechanical investigations of the San Marcial earth fissure, the results of which are summarized in this paper. Zellmer et al. (1985) attribute two intersecting systems of earth fissures - one composed of long, curvilinear fissures and the other of shorter, en echelon fissures– to strain accumulation along the Garlock fault zone in southeastern California. Pampeyan et al. (1988), however, conclude that groundwater withdrawal may be partially respsonsible for Garlock fault zone fissures. Keaton & Shlemon (1990) describe a fissure system at a proposed low-level radioactive waste repository in western Texas, but do not identify a probable mechanism of formation. Whittaker & Reddish (1989) summarize both field and laboratory studies of fissures associated with underground mining in sedimentary sequences. We belabor the diversity of geologic settings in which earth fissures occur, because we are impressed by the similarities among fissures from different areas described by different workers. As such, we suggest that any mechanical model of the processes responsible for fissuring must incorporate driving forces of an arbitrary nature; that is, the model must not be specific to fissures associated with only fluid withdrawal or tectonic activity or mining.

Both local and regional gravity survey results have been used by other researchers in attempts to correlate the locations of earth fissures with bedrock irregularities (e.g., Jachens & Holzer, 1979, 1982; Schumann & Poland, 1969; Sanford et al., 1982; Schuman, 1989). In each of these cases, the purpose of gravity surveys was not to detect subsurface voids representing fissures, but rather to elucidate irregularities in buried bedrock topography that might have given rise to differential compaction of overlying sediments. Although gravity surveys can provide a generalized profile of basin geometry, they cannot be used to infer displacement fields produced by differential compaction or draping of unconsolidated sediments. During the past few years, however, multi-channel seismic reflection surveys have been successfully used to investigate shallow structure and stratigraphy near the Borah Peak fault in Idaho (Miller & Steeples, 1986; Treadway et al., 1988), the Meers fault in Oklahoma (Miller et al., 1990), and the San Andreas fault in California (Shedlock et al., 1990). Shallow reflection surveys have also been used to determine water table position during pump tests (Birkelo et al., 1987) and investigate shallow structure and stratigraphy as part of a groundwater contamination study (Miller & Steeples, 1990). Encouraged by these recent developments and our own experience with shallow reflection surveys, we decided to investigate the applicability of this method to earth fissure studies.

GEOLOGIC BACKGROUND

Southwestern New Mexico consists of predominantly Tertiary volcanic fault-block mountain ranges, with minor amounts of Paleozoic and Precambrian rocks, separated by basins filled with Quaternary and Upper Tertiary sediments (Fig. 1). The Rio Grande rift, a major topographic and structural feature, bisects the state from south to north along a corridor between longitude 106° and 107° W. The first fissure described below runs along a tributary arroyo of the Rio Grande, near the settlement of San Marcial, in unconsolidated sands and gravels of the Quaternary Sierra Ladrones Formation (Osburn, 1984). The second fissure was formed in unconsolidated Quaternary sands and gravels of the Mimbres basin some 12 km south of Deming.

The San Marcial fissure was discovered after a heavy rainstorm during August, 1981, when it formed a graben about 1 m wide across an unpaved embankment for the southbound lane of Interstate Highway 25. Sanford et al. (1982, 1983) conducted preliminary geophysical investigations over a period of two years after the fissure appeared. They described a 1345 m long linear feature, which grew about 15 m at each end during the first week after its appearance, and striking NW-SE, roughly parallel to an un-named tributary arroyo along the Rio Grande.

No other fissures were found, either in the field or on 1:1000 aerial photographs taken approximately one month after the original discovery. Width of the fissure ranged from greater than 1 m immediately upstream from the highway embankment, where the ground surface collapsed into small grabens, to 10 cm or less farther away from the embankment. Repeated surveys of monuments on either side of the fissure show a maximum opening of 0.008 m between August, 1981, and February, 1982, with no recorded movement afterwards. Population in the vicinity of the fissure is sparse, and groundwater withdrawal is insignificant. San Marcial is in a seismically quiet area, with no siginificant earthquakes from 1849 to 1980 (Sanford, 1981; Sanford et al., 1982). Moreover, there were no earthquakes of magnitude 0.2 or greater at or near the crack between January and August, 1981, the period immediately preceding appearance of the fissure. Analysis of five seismic refraction lines along the unpaved embankment for the southbound lane of Interstate 25 (Sanford et al., 1982) suggests a 900 m/s average velocity layer from 0 to 50 m in depth, an 1800 m/s average velocity layer from 50 to 80 m in depth, and a 3600 m/s average velocity layer of unknown thickness beneath 80 m. Regional gravity and magnetic surveys showed no definite relationship between the San Marcial fissure and regional structures; as a result, Sanford et al. (1982) concluded that the fissure may have formed due to either differential compaction of alluvium over a northwest trending bedrock ridge or movement along a northwest-southeast striking bedrock fault.

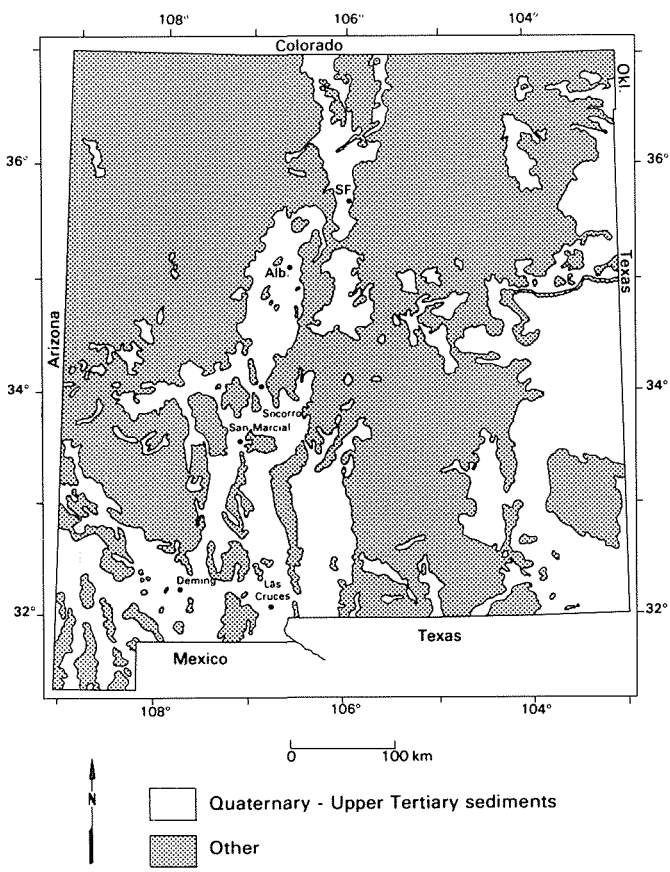

FIG. 1 Index map showing surface exposures of Quaternary-Upper Tertiary sediments, which are susceptible to fissuring, in New Mexico. Fissures described in this paper are near San Marcial and Deming.

The Deming fissure described in this paper is located in NE/4, NE/4, Sec. 32, T25S, R9W of the USGS Midway Butte 7.5' quadrangle. It is one of 12 fissure locations described in the Deming area, where groundwater mining for irrigation has lowered the water table by as much as 35 m since 1908 (Contaldo, 1989). This fissure, which appeared during a heavy October, 1984, rainstorm, is a north-south trending linear feature some 360 m long, and is probably the continuation of a shorter fissure immediately to the south, which appeared two years earlier. The northern fissure was originally up to 2.5 m wide and 7 m deep where it crossed an unchanneled topographic depression. On higher ground, the fissure originally ranged in width from a hairline crack to several centimetres. Both of the fissures have been significantly altered by erosion, piping, and human activity since they appeared. For example, erosion and sedimentation has changed the 2.5 m wide portion of the northern fissure from a steep-walled arroyo photographed in 1985 (Contaldo, 1989, p. 36) to a smoothed, sediment-filled depression in early 1990; therefore, it is difficult to say much about the details of original fissure morphology. Static water level upon completion of a domestic well (state permit number M-5379) on the property during April, 1981, was approximately 36.6 m below ground level. Water level was 42.0 m below the ground level during our geophysical investigations in late January, 1990. The driller's log describes sand from 0 to 1.8 m, clay with minor sand from 1.8 to 26.2 m, and interstratified sand, gravel, and clay from 26.2 to 61.0 m.

GEOPHYSICAL SURVEYS

Methods

We recorded gravity readings every 50 m, to correspond with every tenth seismic drop point, using a LaCoste & Romberg Model G gravimeter. The gravity data were reduced using standard methods (Dobrin, 1976) with a combined free-air and Bouguer correction of 0.1969 mgal/m. Preliminary calculations showed terrain effects to be negligible, so no corrections were applied. In order to eliminate the effects of regional gravity gradients, we subtracted a straight-line trend, fitted using the standard least-squares method, from each data set to find first-order residual Bouguer anomalies.

Energy source for our seismic surveys was a leather bag filled with 250 kg of lead shot and dropped from a height of 2 m. Data were collected for 1 s at 1 ms intervals, using an EG&G ES1210F 12 channel digital seismograph and 10 Hz Mark Products G-21 gimbal-mounted, self-orienting drag geophones. Drop point spacing was 5 m, with one to three drops required per point, and geophone spacing was 10 m. The data processing sequence consisted of 1) transcription of data from field tapes to an office microcomputer; 2) data editing; 3) refraction break analysis (Reynolds et al., 1990); 4) application of an F-K filter to remove refractions, ground roll, and air waves; 5) three-operator, time-variant deconvolution with 40 ms operators; 6) 1200% common depth point stacking; 7) 2:1 horizontal stacking; 8) dip filter enhancement of events dipping 20° or less; 9) frequency filtering with a 0-30 Hz passband; 10) trace normalization; and 11) plotting of variable area wiggle traces. Total lengths of the San Marcial and Deming reflection lines were 800 m and 1500 m, respectively; however, we will show only 600 m portions from each of the lines.

Results

Results of the San Marcial profiles show no sign of a residual gravity anomaly across the fissure (Fig. 2A), although there is -1 mgal anomaly, approximately 200 m wide, centered around drop point 40. Half-width analysis gives a maximum depth of about 150 m, providing some evidence of a relatively shallow structure. Several strong reflectors above 0.3 s two-way time, defining a structural sag between drop points 40 and 95, are apparent on the reflection profile (Fig. 2B). Reflector R_1 coincides with a refraction break approximately 16 m deep, with P-wave velocities of 481 m/s over 741 m/s. Reflector R_2 coincides with a refraction break approximately 78

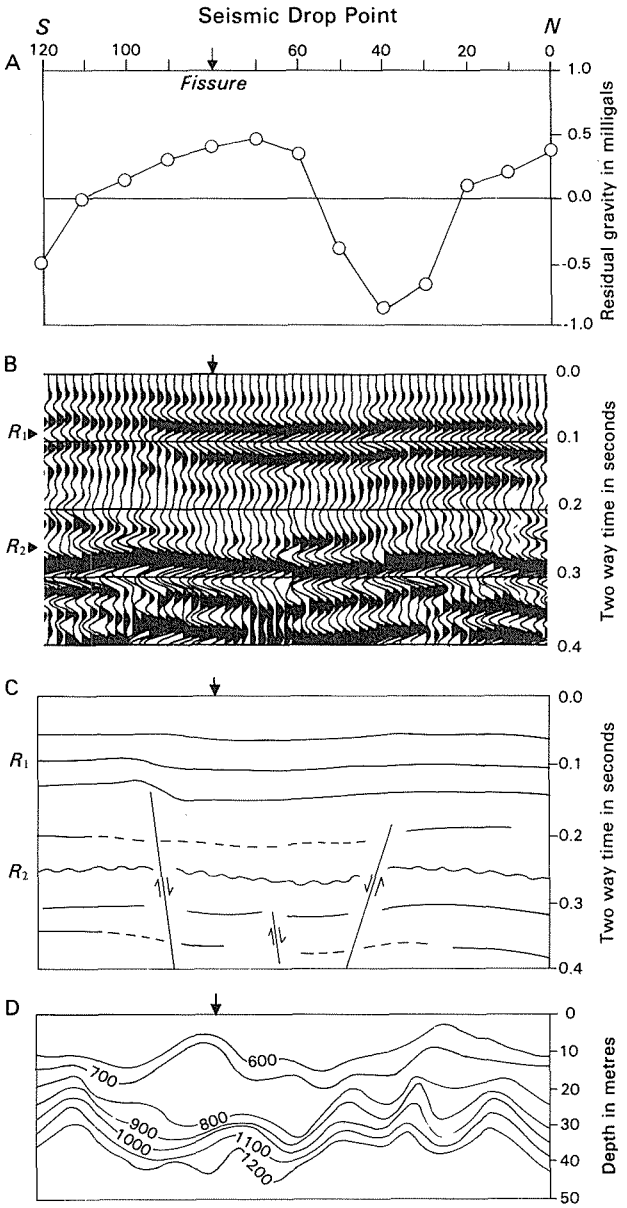

FIG. 2 Results of geophysical surveys across the San Marcial earth fissure. A) 1st order residual gravity anomaly. B) Seismic reflection profile. C) Tracing of prominent refelctors from reflection profile, with interpreted faults (arrows indicate offset) and unconformity (wavy line). Reflectors dashed were uncertain. D) P-wave velocity distribution for uppermost 50 m of the reflection profile, with contours in m/s.

m deep, with P-wave velocities of 1795 m/s over 3658 m/s; this appears to be the same refraction break identified by Sanford et al. (1982), which they interpreted as the contact between unconsolidated Quaternary deposits and Tertiary volcanic rocks. Using these velocities, maximum vertical offset along R_1 is approximately 2 m and maximum vertical offset along R_2 is

approximately 9 m. The reflection section contains no direct evidence of the fissure, which intersects the line at drop point 80; however, reflectors above 0.2 s two-way time do show a small step between drop points 80 and 90, just south of the fissure. An abrupt break in R_2 beneath drop point 40 corresponds with the negative gravity anomaly. Fig. 2C is a tracing of strong reflectors from 2b, with faults interpreted on the basis of reflector discontinuties. The negative gravity anomaly thus appears to be caused by faulting not directly associated with the earth fissure. High and low P-wave velocity contours bifurcate across the sag, producing a noticable bulge (Fig. 2D). Note that the vertical scales of Figs. 2a,b are in seconds, whereas the vertical scale of Fig. 2D is in metres. As such, the velocity contours in Fig. 2D represent two-way times of approximately 0.15 s and less; that is, only the upper 1/3 or so of Figs. 2a,b.

Our Deming gravity profile shows only an approximately 200 m wide, -0.20 mgal anomaly across the fissure (Fig. 3A). Half-width analysis gives a maximum depth of 110 m. Reflectors on the Deming reflection section (Fig. 3B,C) are fairly continuous before 0.2 s two-way time, but later reflectors are discontinuous. We infer several buried down-to-the-west normal faults beneath an angular unconformity on the basis of the discontinuous reflectors. Refraction analysis yields four distinct breaks, with average depths and velocity contrasts of 5 m and 333 m/s over 481 m/s for R_1, 30 m and 481 m/s over 1325 m/s for R_2, 75 m and 1325 m/s over 1600 m/s for R_3, and a depth of 235 m for R_4. Arrival times for R_1 decrease about 0.014 s to form a small structural high between drop points 40 and 85; using an estimated velocity of 333 m/s, this corresponds to 2.3 m of structural relief along R_1. Moreover, wavelets along R_1, which are simple on either side of the high, take on complicated forms directly over the high; this disturbance may be related to void space created by the fissure. Figure 3d shows a marked zone of P-wave velocities lower than 200 m/s directly beneath the surface expression of the fissure. Velocities well below the speed of sound in air (approximately 335 m/s), although theoretically impossible, are commonly calculated for highly weathered surficial deposits (Steeples et al., 1990). The combination of a gravity low and a structural high leads us to believe that the Deming fissure may have developed due to differential compaction of sediments over a comparatively incompressible, coarse-grained channel-fill deposit. Beneath 10 m depth, low-velocity zones split to follow the buried normal faults inferred from the reflection sections. Note that Fig. 3D covers only the upper 0.16 s of the reflection sections (Fig. 3B,C). As such, velocity contour section (Fig. 3D) shows signs of faults at much shallower depths than on the reflection sections (Fig. 3B,C).

MECHANICAL ANALYSIS

Haneberg et al. (1990) give exact analytical expressions for stresses and displacements in a compressible elastic layer draped over a symmetric pair of steps. Dimensionless variables controlling stress and displacement fields are layer thickness T/L, step width h/L, step height 2B/L, and Young's modulus $E/(\rho gT)$. Horizontal displacement along the lower boundary is required to vanish, and vertical displacement along the lower boundary is specified by a Fourier cosine series given in Haneberg et al. (1990). Our objective in this section is to compare the effects of draping a thin soil layer over narrow versus wide steps, so we have chosen two hypothetical elastic layers with $T/L = 0.1$, $2B/L = 0.04$, $E/(\rho gT) = 100$, and Poisson's ratio $\nu = 0.25$. Tensile stresses are defined as positive, and compressive stresses as negative. However, we specify a dimensionless step width of $h/L = 0.02$ for the first layer and $h/L = 0.2$ for the second layer. Comparison of Fig. 4A and B shows that the steps act as stress concentrators for both compression and tension. Lithostatic compression due to the weight of the layer counteracts tensile stresses developed at depth due to draping over a wide step. However, the tensile stresses developed due to draping over a narrow scarp can be large enough to overshadow lithostatic compression.

Stress fields also affect the direction in which a fracture propagates. A propagating mode I, or tensile, fracture will remain perpendicular to the least compressive (or most tensile) principal stress and parallel to the most compressive principal stress in order to maximize propagation energy per increment of fracture growth (Pollard & Aydin, 1988). Inspection of the stress trajectory field in Fig. 4A shows that a mode I fracture that nucleates near the toe of a buried

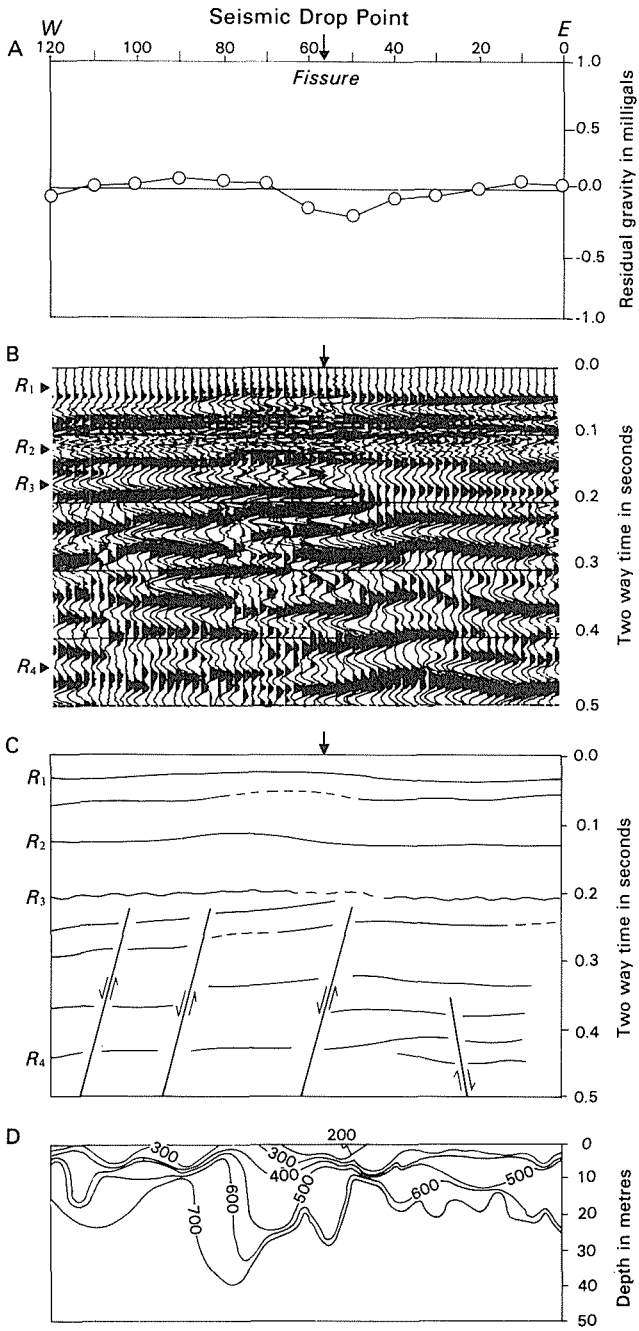

FIG. 3 Results of geophysical surveys across the Deming earth fissure. A) 1st order residual gravity anomaly. B) Seismic reflection profile. C) Tracing of prominent refelctors from reflection profile, with interpreted faults (arrows indicate offset) and unconformity (wavy line). Reflectors dashed were uncertain. D) P-wave velocity distribution for uppermost 50 m of the reflection profile, with contours in m/s.

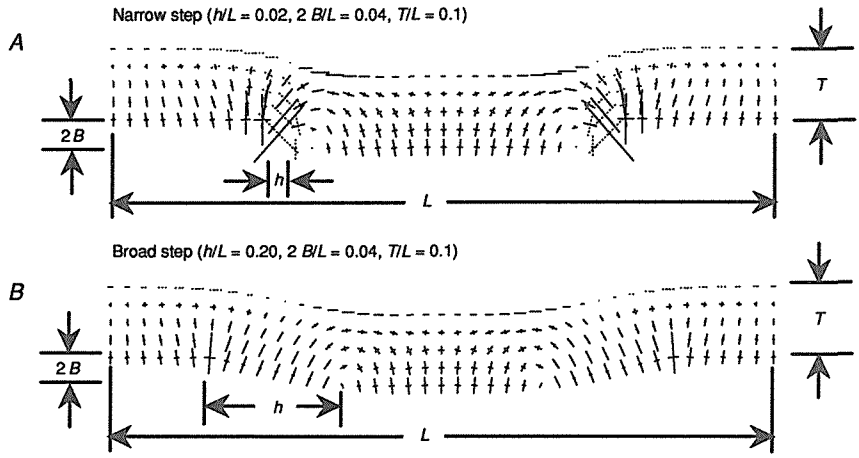

FIG. 4 Principal stress trajectories and displacement fields for compressible elastic layers draped over narrow (A) and wide (B) steps. Dotted lines represent tensile stresses, and solid lines represent compressive stresses. Horizontal and vertical displacements magnified 10×.

step will propagate upward and away from the step. A mode I fracture that nucleates along the ground surface, where principal stress axes are nearly horizontal and vertical (Fig. 4B) will propagate almost straight downward. Therefore, it can be misleading to infer the origin of an earth fissure by comparison with structures directly beneath the fissure.

SIGNIFICANCE OF VELOCITY ANOMALIES

The significance of the P-wave velocity anomalies associated with the flexure and faulting of surficial strata is largely speculative. However, it is interesting to compare the velocity contour sections (Figs. 2D and 3D) with stresses in a flexed elastic plate or beam. We note that velocity lows tend to occur in areas where we would expect tension or reduced compression, whereas velocity highs occur in zones where we would expect increased compression. For example, shallow velocities are abnormally high and deep velocities are abnormally low beneath drop point 80 in Fig. 2D, which corresponds roughly to principal stress magnitudes in Fig. 4A. Likewise, near-surface velocities are low along both flanks of the structural high in Figs. 3B,C, but increase somewhat towards the center of the high. This distribution corresponds roughly to the principal stress magnitudes along the upper surface of the hypothetical layer in Fig. 4D. We further imagine that shear-induced dilation may be responsible for the correspondence between low-velocity zones and buried faults in Fig. 4D. The well-know relationship between P-wave velocity and elastic constants (e.g., Jaeger & Cook, 1971, p. 172)

$$V_P = \sqrt{\frac{E(1-\nu)}{\rho(1+\nu)(1-2\nu)}}$$

suggests that the effect of tension or shear is to reduce E in a flexed or faulted surficial layer, whereas the effect of compression is to increase E. Although these findings are preliminary, the possibility that shallow seismic surveys might yield information on both geometry and in situ strains in deformed near-surface strata is encouraging. To this end, our ongoing research is directed towards the integration of both P- and S-wave data to elucidate variations in elastic constants and residual stresses associated with near surface structures. Future work may include trenching, drilling, and installation of instruments to monitor seasonal water level changes, temperature changes, and displacement patterns on either side of the Deming fissure.

ACKNOWLEDGEMENTS Portions of this research were supported by the New Mexico Bureau of Mines and Mineral Resources and the New Mexico Institute of Mining and Technology Research Council. William Bedford, Eric Beornsen, Phil Goetz, John Hawley, Ellen Limburg, and David Love all assisted with field work. Jon Cheney and Monte Brown produced most of the illustrations, and Mark Geddings of the U.S. Geological Survey loaned the gravity meter used for the San Marcial and Deming projects. We also appreciate the permission of June Cox to work on her property near Deming.

REFERENCES

Bell, J.W., Ramelli, A.R., DePolo, C.M., Maurer, D.K. and Prudic, D.E. (1989) Extensional cracking along an active normal fault: A case for creep on a Basin and Range fault? (abs.). Seismol. Res. Lett. 60, 30.

Bell, J.W. and Hoffard, J.L. (1990) Late Quaternary tectonic setting for a possible fault creep event in the Pine Nut Mountains area, western Nevada (abs.). Geol. Soc. America, Abstr. Prog. 22, 7.

Birkelo, B.A., Steeples, D.W., Miller, R.D. and Sophocleous, M. (1987) Seismic reflection study of a shallow aquifer during a pumping test. Ground Water 25, 703-709.

Contaldo, G.J. (1989) Earth fissures and land subsidence near Deming, New Mexico. M.S. thesis, Las Cruces, New Mexico State University.

Dobrin, M.B. (1976) Introduction to Geophysical Prospecting (3rd edn.). McGraw-Hill, New York.

Haneberg, W.C. (1990) Use of seismic reflection profiles to characterize soil deformation associated with earth fissures and groundwater withdrawal near Deming, New Mexico. New Mexico Bureau of Mines and Mineral Resources Open-File Rpt. 367.

Haneberg, W.C., Reynolds, C.B. and Reynolds, I.B. (1990) Monoclinal flexure of surficial strata and the origin of an earth fissure near San Marcial, New Mexico. J. Geophys. Res., in review.

Holzer, T.L. (1984) Ground failure induced by ground-water withdrawal from unconsolidated sediment. In: Man-Induced Land Subsidence, ed. T.L. Holzer. Rev. Engrg. Geol. VI, Geol. Soc. America, Boulder, Colorado, 67-105.

Jachens, R.C. and Holzer, T.L. (1979) Geophysical investigations of ground failure related to ground-water withdrawal– Picacho Basin, Arizona. Ground Water 17, 574-585.

Jachens, R.C. and Holzer, T.L. (1982) Differential compaction mechanism for earth fissures near Casa Grande, Arizona. Geol. Soc. America Bull. 93, 998-1012.

Jaeger, J.C. and Cook, N.G.W. (1971) Fundamentals of Rock Mechanics. London, Chapman and Hall, Ltd.

Keaton, J.R. and Shlemon, R.J., (1990) The Fort Hancock, Texas, earth fissure system: Possible causes and site selection issues for critical facilities. Pocatello, Idaho State University,Proc. 26th Symp. Engrg. Geol. Geotech. Engrg., in press.

Miller, R.D. and Steeples, D.W. (1986) Shallow structure from a seismic-reflection profile across the Borah Peak, Idaho, fault scarp. Geophys. Res. Lett. 13, 953-956.

Miller, R.D. and Steeples, D.W. (1990) A shallow seismic reflection survey in basalts of the Snake River Plain. Geophysics 55, 761-768.

Miller, R.D., Steeples, D.W. and Myers, P.B. (1990) Shallow seismic survey across the Meers fault, Oklahoma. Geol. Soc. America Bull. 102, 18-25.

Osburn, G.R. (1984) Socorro County geologic map (1:200,000). New Mexico Bureau of Mines and Mineral Resources Open-File Rpt. 238.

Pampeyan, E.H., Holzer, T.L. and Clark, M.M. (1988) Modern ground failure in the Garlock fault zone, Fremont Valley, California. Geol. Soc. America Bull. 100, 677-691.

Pollard, D.D. and Aydin, A. (1988) Progress in understanding jointing over the past century.

Geol. Soc. America Bull. 100, 1181-1204.

Reynolds, C.B., Reynolds, I.B. and Haneberg, W.C. (1990) Refraction velocity sections– an aid in shallow reflection interpretation (abs.). 1990 Society of Exploration Geophysicists Annual Meeting Technical Program Abs., in press.

Sanford, A.R. (1981) Earthquakes in New Mexico, 1978-1980. New Mexico Institute of Mining and Technology, Geoscience Department and Geophysical Research Center, Geophysics Open-File Rpt. 36.

Sanford, A.R., Schlue, J.W., Budding, A.J. and Payne, M.A. (1982) Report on San Marcial crack, August, 1981 - August, 1982. New Mexico Institute of Mining and Technology, Geoscience Department and Geophysical Research Center, Geophysics Open-File Rpt. 41.

Sanford, A.R., Budding, A.J., Schlue, J. and Oravecz, K. (1983) Investigations of the San Marcial crack, August, 1982 through August, 1983. New Mexico Institute of Mining and Technology, Geoscience Department and Geophysical Research Center, Geophysics Open-File Rpt. 46.

Schumann, H. and Poland, J.F. (1969) Land subsidence, earth fissures, and groundwater withdrawal in south-central Arizona. Land Subsidence, Vol. 1, IAHS-UNESCO Publication No. 88, 295-302.

Schumann, H.H. (1989) Geophysical investigations of earth fissures caused by land subsidence near Apache Junction, Arizona (abs.). Proc., 28th Inter. Geol. Congr., Washington, D.C, July 9-19, 1989, Vol. 3, 58.

Shedlock, K.M., Brocher, T.M. and Harding, S.T. (1990) Shallow structure and deformation along the San Andreas fault in Cholame Valley, California, based on high-resolution reflection profiling. J. Geophys. Res. 95, 5003-5020.

Slaff, S., Jackson, G.W. and Pearthree, P.A. (1989) Development of earth fissures in Picacho Basin, Pinal County, Arizona from 1959 to 1989. Arizona Geological Survey Open-File Rpt. 89-10.

Steeples, D.W., Miller, R.D. and Black, R.A. (1990) Static corrections from shallow reflection surveys. Geophysics 55, 769-775.

Treadway, J.A., Steeples, D.W. and Miller, R.W. (1988) Shallow seismic study of a fault scarp near Borah Peak, Idaho. J. Geophys. Res. 93, 6325-6337.

Whittaker, B.N. and Reddish, D.J. (1989) Subsidence: Occurrence, Prediction, and Control. Amsterdam, Elsevier.

Zellmer, J.T., Roquemore, G.R. and Blackerby, B.A. (1985) Modern tectonic cracking near the Garlock fault, California. Geol. Soc. America Bull. 96, 1037-1042.

Land Subsidence (Proceedings of the Fourth International Symposium on Land Subsidence, May 1991). IAHS Publ. no. 200, 1991.

The Fort Hancock Earth Fissure System, Hudspeth County, Texas: Uncertainties and Implications

JEFFREY R. KEATON
Sergent, Hauskins & Beckwith Engineers, 4030 South 500 West, Suite 90, Salt Lake City, Utah 84123
ROY J. SHLEMON
Roy J. Shlemon and Associates, P.O. Box 3066, Newport Beach, California 92663

ABSTRACT A previously unknown northwest-trending curvilinear system of discontinuous earth fissures about 150 m long was discovered in 1988 on a gently sloping alluvial apron in the Hueco Bolson about 80 km southeast of El Paso during an independent, third-party engineering geologic reconnaissance of a site being considered for disposal of low-level radioactive waste. Individual depressions comprising the fissure system are as much as 10 m long, 0.4 m wide, and 1.1 m deep. The depressions display steep sidewalls and sharp edges at the ground surface in Holocene fine sandy silt floodplain deposits. Approximately 53.6 Mg of sediment have moved vertically downward creating these depressions. Excavations across the fissure system reveal voids and filled cracks which extend downward into late Pleistocene calcic soil horizons formed on older alluvial floodplain deposits. Clayey bolson-fill deposits of mid-Pleistocene to Pliocene age are present at depth, but the characteristics of the fissure system in these deposits are unknown.

The cause of the fissuring is not known; it could be tectonic (aseismic fault slip, neotectonic folding, or induced by earthquake shaking) or nontectonic (subsidence, subsurface dissolution, differential compaction, desiccation, pedogenisis, or strain release from a nearby buried stream channel incision). Two additional earth fissure systems and two buried paleo-fissures were discovered in 1989 within about 1 to 2 km of the Fort Hancock fissure system. These were not within the boundaries of the proposed site in 1988, but the boundaries, expanded in 1989 in an attempt to avoid the 100-year floodplain, encompassed the additional fissures. So much uncertainty exists about the cause and location of the fissures, and the possibility of future fissuring, that serious questions could not be answered with the level of assurance necessary to satisfy conventional site selection requirements for critical facilities, such as the proposed low-level radioactive waste disposal facility.

INTRODUCTION

The State of Texas established an agency in the early 1980s to provide for disposal of low-level radioactive waste at the most suitable site in Texas. The agency started by assessing the volume of waste generated within the state and screening the state to identify those areas relatively more suitable for waste disposal. Several areas of the state were identified as potentially suitable and ranked. Two preferred sites, both on private land, were identified in 1985 but were excluded from further consideration because of political pressures. The agency reacted to the exclusion by focusing on land owned by the State of Texas, most of which is located in west Texas.

By 1988 it was becoming clear to local governments in west Texas that the State's preferred site was going to be the Fort Hancock Site in southwest Hudspeth County, about 80 km southeast of downtown El Paso (Fig. 1). Several local governmental agencies (Hudspeth County, Hudspeth County Conservation and Reclamation District No.1, Hudspeth County Underground Water Conservation District No. 1, and El Paso County) retained a team of engineers and geologists to conduct an independent evaluation of the Fort Hancock Site. The team issued a three-volume report in April 1989 documenting several serious deficiencies with the site (Sergent, Hauskins & Beckwith, 1989); the Fort Hancock fissure system is one of these deficiencies.

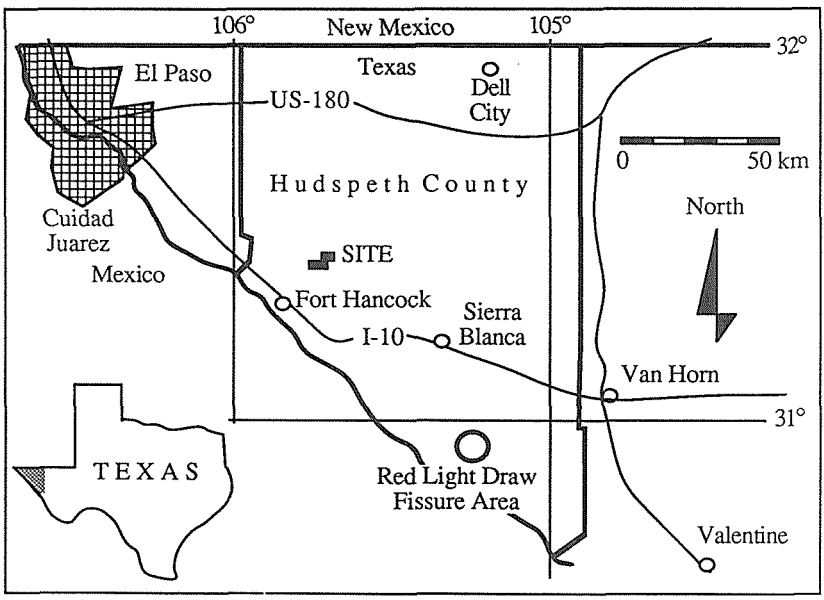

FIG. 1 Map showing locations of key features in the Fort Hancock, Texas, area.

THE FISSURE SYSTEM

The Fort Hancock fissure system is a 152-m long curvilinear series of elongated to circular topographic depressions ranging up to 1.2 m across, 9.1 m long, and 1.2 m deep (Fig. 2 and 3). The edges of the depressions are vertical to overhanging, showing very little modification by running water. Piping tunnels connecting adjacent topographic depressions are common. However, it appears that these piping tunnels represent the present positions of upward-migrating subsurface voids rather than hydraulic pipes because of the lack of fluvial erosion features and deposits in the pipes. The surface expression of the fissure system probably is no more than a few years to a few tens of years old because living creosote bushes are located on the edges of depressions and on earth bridges over piping tunnels. The edges of the depressions are sharper near the northwest end of the fissure system than near the southeast end, suggesting that the system may be propagating toward the northwest. The fissure system does not appear to be visible on aerial photographs taken by the U.S. Department of Agriculture in 1951; it may be present on photos taken in 1981, but the evidence is equivocal.

The fissure system was mapped by establishing a baseline with the aid of a compass and a 30-m tape. Reference points were placed by driving 5-cm square wooden stakes

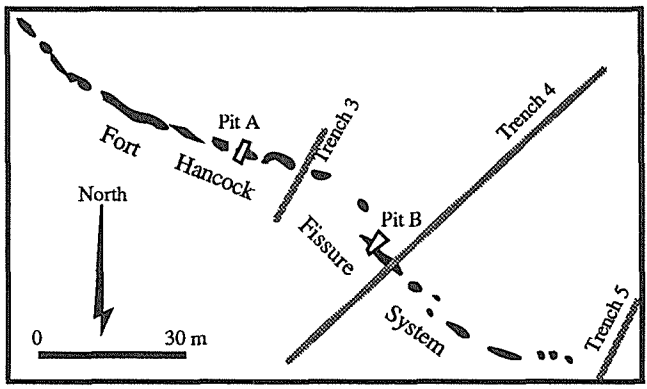

FIG. 2 Map of the Fort Hancock fissure system showing trench and test pit locations.

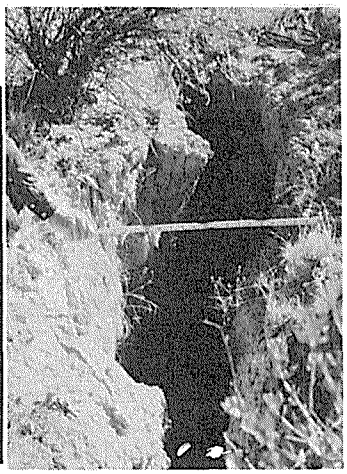

FIG. 3 Photograph showing fissure expression at Pit A.

into the ground at 15-m intervals. While the 30-m tape was stretched on the ground, a second tape was used to measure the distance from the baseline to the surface features of the fissure system. The locations of the edges of the elements of the fissure system and the depths from the ground surface to the bottom of the ground crack were recorded. The mass of earth missing from the site along the fissure system was computed by determining the volume of the ground crack and multiplying by a total unit weight of 17.27 kN/m^3 (110 lb/ft^3). The volume, estimated by average-end-area and frustrum-of-a-cone methods, was found to be 26.0 to 29.8 m^3, respectively. Thus, approximately 53.6 Mg (58 tons) of sediment are missing from the site surface at the fissure system. The fissure system was investigated by excavating two hand-dug pits and five trenches at locations shown on Fig. 2. The shallow stratigraphy of the site is shown in Fig. 4. The upper 2 m is Holocene fluvial fine sandy silt with rare gravel channel deposits; this unit has a weak calcareous A-C pedologic profile, several buried weak calcic horizons, and represents the modern floodplain alluvium. The upper fine sandy silt unit is underlain by high-energy fluvial gravel including individual boulders up to 30 cm long weighing nearly 15 kg. Well-developed (Stage V) calcrete horizons have formed in the gravelly parent material, as shown on Fig. 4.

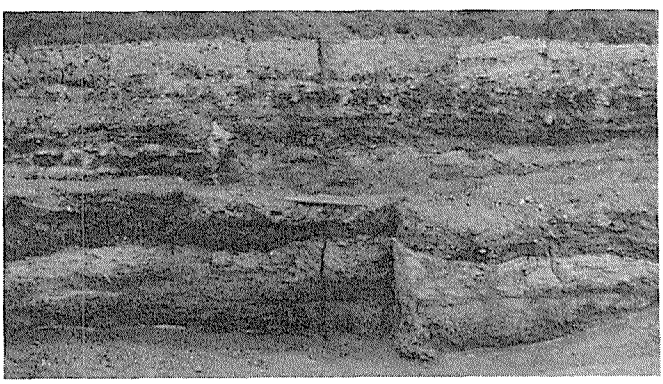

FIG. 4 Stratigraphy exposed in the east wall of Trench 3. Wall is 6 m high. Fissure crosses photograph center from top to bottom.

The ground crack was found to be associated with a subsurface fracture which in some places was an open void and in other places was filled with sediment (Fig. 4 and 5). In a few places, open voids were found within infilled sediment in cracks in the calcrete, suggesting several episodes of crack opening and infilling. However, no consistent evidence was found to indicate a recurring sequence of opening and infilling. Three trenches were excavated across projections of the fissure system beyond its surface expression. Cracks were found in shallow subsurface sediments in all trenches; in most cases, these cracks extended downward into the upper calcrete horizon which was exposed in the bottom of the trenches. The character of sediments filling the cracks indicate multiple occurrences of crack opening and filling.

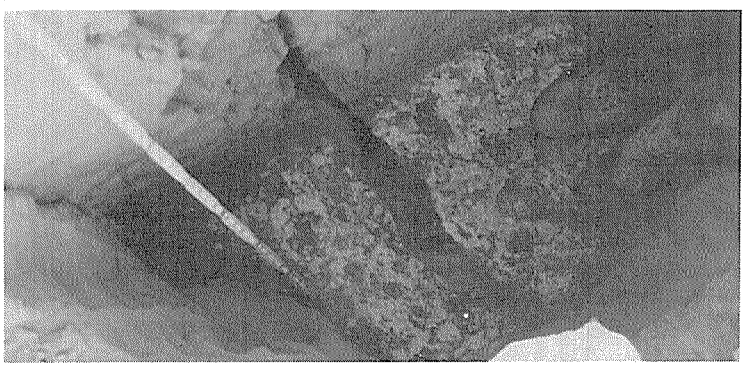

FIG. 5 Void and filled crack in calcrete exposed in Pit A.

The subsurface expression of the fissure system clearly is directly related to crack in the shallow subsurface sediments and calcrete. The presence of subsurface cracks beyond the surface expression of the fissure system, and the very youthful appearance of the ground cracks strongly suggest that propagation or expansion of the Fort Hancock fissure system should be expected in the near future. Critical questions regarding the fissure system at the site are: (a) What caused it?; (b) Why is it located where it is?; (c) Could similar fissure systems develop elsewhere on the site during the 500-year "design" life of a low-level radioactive waste disposal facility?; and (d) Can they be predicted with confidence?

POSSIBLE CAUSES

The cause of the fissure system is unclear, but it could well be related to tectonic processes or to surface geologic processes. Tectonic processes include slip along faults unrelated to earthquakes (aseismic slip), continued development of a fold along the nearby Diablo Plateau Rim, or cracking of the ground owing to earthquake shaking. Surface geologic processes include subsidence possibly induced by water well pumping, dissolution of gypsum in a geologic formation at depth, differential compaction or collapse of the sediments under the site, shrinkage owing to desiccation of sediments under the site, volume changes caused by pedogenic processes, or strain release caused by a nearby deeply cut arroyo which is now buried.

Earth fissures have been observed at various locations including arid regions of the western United States, regions of limestone with active karst processes, and in areas of underground mining. The causes of earth fissures which have been investigated most extensively consist of subsidence associated with fluid (water, oil, and gas) withdrawal from porous media, oxidation of peat, solution and collapse in limestone terrain, and collapse of shallow mine workings (Griggs and Gilchrist, 1983). Many aspects of fissure formation are unclear and problematical. Some fissures have been noticed following earthquakes and have been attributed directly or indirectly to earthquake

shaking (Albritton and Smith, 1965); others have been observed in tectonically active areas, but at times when association with shaking is improbable (Shlemon and Davis, 1988; Swadley and Scott, 1988; Bell et al., 1989). Many uncertainties exist regarding fissure formation and propagation and extensive research would be required to advance scientific understanding to the point that reliable predictions could be made.

Tectonic

Aseismic Fault Slip A probable west-northwest-trending fault was identified under the southwest corner of the Fort Hancock Site in 1986 during a geophysical survey conducted by Phillips et al. (1986). The geophysicists interpreted their data to indicate that the fault came to within at least 15 to 18 m of the ground surface.

Faults in the Fort Hancock region display chiefly normal separation. Some evidence exists for lateral separation on the nearby Amargosa fault in Chihuahua, Mexico (Keaton et al., 1989); however, this evidence is not consistent along the fault. The seismic reflection profiles interpreted by Phillips et al. (1986) indicate different senses of vertical separation from profile to profile and from older to younger reflecting horizons. Thus, if the interpretation by Phillips et al. (1986) is accurate, the postulated fault under the southwest part of the Fort Hancock Site must be a lateral fault. The west-northwest-trending Texas Lineament (Albritton and Smith, 1957; 1965; Henry and Price, 1985) passes virtually under the site (Fig. 6) and has been a persistent structural boundary with left-lateral transcurrent separation since Precambrian time. Consequently, if the Fort Hancock fissure system were caused by aseismic creep on the subsurface fault, it would be reasonable to expect features consistent with left-lateral shearing. The map of the fissure system (Fig. 2) shows it to be curvilinear and discontinuous. At two locations near Pit B (Fig. 2), the fissure system steps to the right; right-stepping en echelon strands are found on shear zones with left-lateral separation. Thus, the surface expression of the fissure system does not contradict aseismic creep on the geophysically located fault under the Fort Hancock Site. The relationship between the geophysically located fault and the Texas Lineament remains unknown.

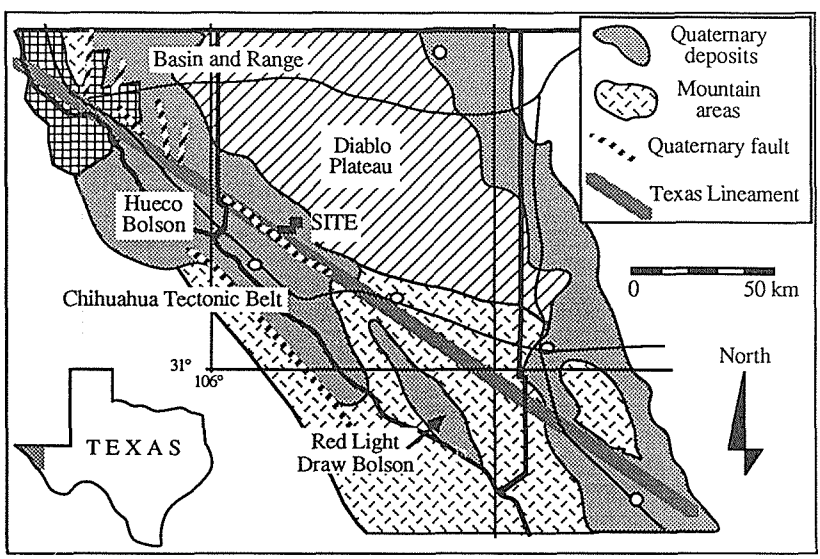

FIG. 6 Tectonic map of the Fort Hancock Site region. Modified from Sergent Sergent et al. (1989). Place names are shown on Fig. 1.

Neotectonic Folding The site is located in the Hueco Bolson within 5 km of the Diablo Plateau Rim (Fig. 1). The transition from the Diablo Plateau to the Hueco Bolson is marked by the Diablo Rim fault zone and a monoclinal fold with relative deformation consistent with the Plateau being higher than the Bolson. The highway from El Paso, Texas, to Carlsbad, New Mexico, was surveyed in 1934, 1943, and 1958 (Reilinger et al., 1979; 1980). These surveys indicate that the Diablo Plateau is moving upward while the Hueco Bolson is moving downward. The geodetic movement of the Diablo Plateau with respect to the Hueco Bolson could cause continued development of the Diablo Rim fold which would induce horizontal extensional stresses oriented roughly perpendicular to the edge of the Diablo Plateau Rim. Such stresses would be expected to generate earth fissures roughly parallel to the Rim.

The Fort Hancock fissure system is roughly parallel to the south edge of flat-lying limestone of the Diablo Plateau Rim, as well as to the Campo Grande fault, the Amargosa fault, the Texas Lineament, and the north edge of the complexly folded rocks of the Chihuahua Tectonic Belt (Fig. 6). Thus, any neotectonic stresses in the site region should be expected to cause or contribute to surface features with a northwest trend, such as the fissure system. Since the Diablo Plateau is moving upward with respect to the Hueco Bolson, neotectonic folding may be a likely candidate for the cause of the stresses leading to formation of the Fort Hancock fissure system.

Earthquake-Induced Ground Failure The closest reported earth fissures to those at the Fort Hancock Site are located in alluvium of Red Light Draw (Quitman Canyon), approximately 24 km south of Sierra Blanca (Albritton and Smith, 1965). Three sets of fissures exist in the valley; two older sets and one young set. One of the older sets was attributed to the Valentine, Texas, earthquake of 1931, the epicenter of which was about 80 km east of Red Light Draw. This set consists of three main fissures aligned roughly parallel to the draw but west of it; smaller connecting fissures were oriented roughly perpendicular to the main ones. Albritton and Smith (1965) observed these fissures in 1949, 17 years after the Valentine earthquake, and found cracks still partly open to depths as great as 2.1 m and widths as great as 0.9 m. These fissures were observed in 1989, and found to be up to about 0.9 m deep and as wide as 2 m (Fig. 7).

An additional set of fissures in Red Light Draw not mentioned by Albritton and Smith (1965) was also observed in 1989. This set of fissures had similar character to those

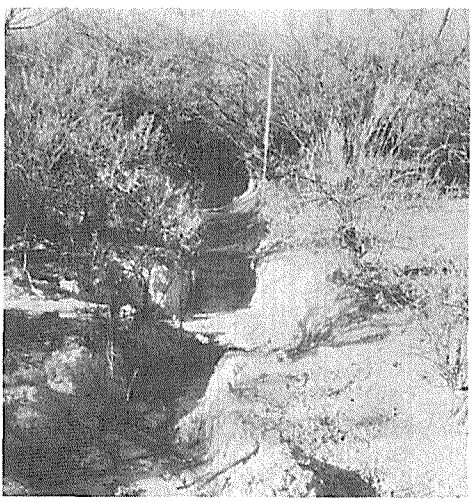

FIG. 7 Photograph of older fissures in Red Light Draw.

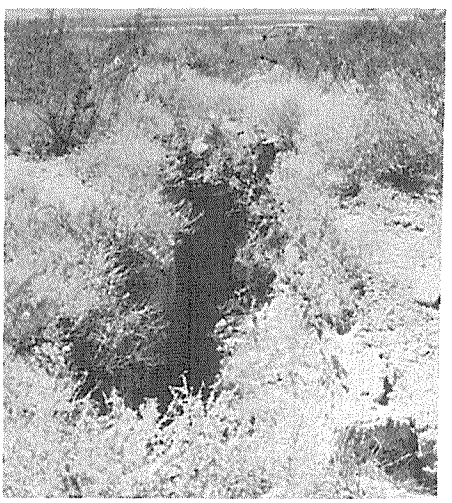

FIG. 8 Photograph of younger fissures in Red Light Draw.

described by Albritton and Smith (1965), but were located east of the draw, about 2.5 km east of the set described above. The younger set of fissures was discovered by local residents of Hudspeth County in September, 1985, the day following the Mexico earthquake (Sheriff Richard Love and Deputy Sheriff Rusty Wilbanks, 1989, personal communication). These fissures crossed the unsurfaced county road in Red Light Draw, making it impassable to vehicles. These fissures were observed in April, 1989, and found to form a rectilinear pattern approximately 300 m long. The surface expression of these fissures (Fig. 8) is similar to that at the Fort Hancock Site but appear to be even younger. The largest topographic depression along the young set of fissures in Red Light Draw is approximately 1.8 m wide and 1.5 m deep.

The timing of the discovery of the younger fissures with respect to the occurrence of the Mexico earthquake suggests that the fissures may have been caused by earthquake shaking. This is problematical because the epicenter of the earthquake was on the west coast of Mexico, about 1600 km from Red Light Draw. Ground motions at the site should have been negligible. The authors visited these fissures again in December, 1989, and found fresh cracks in the shoulder of the county road and on the valley floor in close proximity to the fissure. These cracks clearly indicate an ongoing process that does not require earthquake shaking. Baumgardner (1990) cites a reference to a person who observed fissures in Quitman Canyon in 1924; therefore, he believes they are not caused by earthquake shaking.

Nontectonic

Subsidence Ground cracking has been caused by subsidence induced by water well pumping. This process is well known from Phoenix, Arizona, Las Vegas, Nevada, and Houston, Texas. Holzer (1984) notes that ground failure occurs on earth fissures and surface faults; the fissures are tensile failures while the faults are shear failures. Fissure locations can be controlled by the positions of subsurface faults even though the stresses responsible for opening the fissures are induced by groundwater withdrawal. The nearest water well to the Fort Hancock Site is approximately 5 km to the east and is a single low-volume domestic well. Two paleo-fissures were exposed in a large trench excavated at the direction of the State. One paleo-fissure is present below the well-developed calcrete (Fig. 9); the other paleo-fissure cuts the calcrete, but has no surface expression (Fig. 10). These paleo-fissures clearly are prehistoric and indicate that groundwater pumping is not necessary to produce fissures.

Water has been pumped from exploration wells drilled on the site by the Authority's geological consultant. The volumes pumped from these wells has been small and it is unlikely that subsidence has been induced. If these wells did cause subsidence, it would indicate that the site is very sensitive to minor water level declines.

FIG. 9 Photograph of older paleo-fissure. Note multiple calcrete horizons.

FIG. 10 Photograph of younger paleo-fissure. Note lack of surface expression.

Dissolution Ground cracking could be caused by dissolution of gypsum in a geologic formation under the Site. Large selenite crystals are littered on the ground surface in Alamo Arroyo, approximately 6 km southwest of the Site, in a formation known to underlie the site. If a concentrated zone of gypsum were to become dissolved, a subsurface void would be created. Such a void gradually would work its way to the ground surface, resulting in a series of cracks. If this process is responsible for the Fort Hancock fissure system, the predicting locations of future fissures would be virtually impossible.

Differential Compaction or Hydrocompaction Ground cracking could be caused by compaction of the sediments under the Site. Sediments gradually become more compact with age; ultimately becoming sedimentary rock. The process of natural compaction affects different sediments in different ways. For example, clay-rich sediment will compact a larger amount than sediment made of gravel. Some sediments are susceptible to hydrocompaction when wetted. Usually, such sediments have substantial eolian material or were deposited rapidly as debris flows or mudflows on alluvial fans, and have not been wetted since deposition. If a major change in the type of sediment occurs under the Site, cracking of the ground could occur due to differential compaction. Such an abrupt change of sediment type could be associated with a subsurface fault.

Desiccation Under limited circumstances, ground cracking could be caused by shrinkage owing to desiccation of sediments under the Site. Ground cracks caused in this way usually are roughly polygonal, commonly hexagonal, and rarely have sides as long as 30 m. The fissure system at the Site is curvilinear for 150 m. Shrinkage is most pronounced in clay-rich sediments, particularly smectite clay. The sediments at the Site above the calcrete are eolian and alluvial deposits derived from erosion of limestone in the cliffs on the Diablo Plateau Rim. Multiple, slightly developed buried paleosols are present in these sediments, indicating a few periods of landscape stability. These sediments are not rich is smectite and probably exhibit only small shrinkage potential even though some of the horizons contain substantial clay.

The older bolson deposits at depth under the calcrete do contain significant amounts of clay, including smectite. Shrinkage cracks can be observed in those areas where the older bolson deposits crop out. However, the shrinkage normally would be distributed in such a way that systems of earth fissures, such as the Fort Hancock System, are very unlikely to form, especially since the stresses would have to be transmitted through the calcrete horizon. Nonetheless, despite the small probability of the fissure system being caused by desiccation, this process cannot be ruled out.

Pedogenesis It is well known that the process of soil formation results in sediment acquiring soil structure. The primary element of soil structure is the ped. Ped surfaces are commonly vertical, particularly in clayey parent material. The Fort Hancock fissure system is vertical but much larger than would be associated with normal pedogenic processes. Furthermore, only three active earth fissures have been found on the site; pedogenesis should be expected to produce hundreds or thousands of fissures on a smaller scale. The State's consultant has identified extensive, deeply-buried paleo-vertisols (Gustavson, 1990) but has not related these to fissure genesis.

Strain Release An arroyo cutting a deep channel through the calcrete could induce horizontal tension which could, in turn, crack the calcrete parallel to the arroyo bank. Such an arroyo, if it exists, would have been completely buried by younger sediments and would be much larger than any of the channels exposed in the trenches excavated to investigate the fissure system. Additional exploration would be required to evaluate this possible cause for the fissure system.

DISCUSSION

Critical questions regarding the Fort Hancock fissure system are: (a) What caused it?; (b) Why is it located where it is?; (c) Could similar fissure systems develop elsewhere on the site during the 500-year "design" life of a low-level radioactive waste disposal facility?; and (d) Can they be predicted with confidence? Based on the discussion presented in this report, we offer the following answers to these critical questions: (a) The cause of the fissure system is unknown, and likely to remain unknown. (b) The reason for the fissure system's location is unknown, but a geophysically located subsurface fault is suggestive. (c) It is not possible to rule out similar fissure systems developing elsewhere on the site during the 500-year "design" life of the proposed facility; in fact, other fissure systems may presently exist in the subsurface but not yet be expressed at the ground surface. (d) Predicting with confidence the locations, timing and size of future fissures, and their vertical and horizontal extent is not possible. So much uncertainty exists about the cause and location of the Fort Hancock fissure system, and the other active earth fissures on the site, that serious questions can not be answered with the level of assurance necessary to satisfy conventional site selection requirements for critical facilities, such as the proposed low-level radioactive waste disposal facility.

Baumgardner (1990), on behalf of the Texas Low-Level Radioactive Waste Disposal Authority, concluded that: (a) "Three surface fissures in the study area formed as a result of surface collapse and piping along preexisting tension fractures." (b) "All three surface fissures are in local topographic lows, which indicates that concentrated overland flow is an essential component in their development." (c) "The source of tensional stress that formed the tension fractures is unknown." and (d) "Fissure development appears to be a natural geomorphic phenomenon in arid desert basins." However, Baumgardner (1990) has not offerd any opinion regarding the significance of the fissure systems to the proposed low-level radioactive waste disposal facility. The State selected the Fort Hancock Site, stating publicly that it was selected for its technical merit, despite the active fissures and other geotechnical studies indicating that it is within the 100-year floodplain and subjected to earthquake ground motions exceeding 0.6 g. The local governmental agencies in Hudspeth and El Paso counties sued the State for violating their own site selection criteria established in 1982 (e.g., the Fort Hancock Site is within a Wildlife Management Area, yet the State's criteria require such areas to be excluded from site selection consideration). The case was tried in the 34th Judicial District Court in El Paso from September 6 to 22, 1990. The judge had not ruled by the time this manuscript was prepared; it is likely that the decision will be appealed and the final ruling made in the Texas State Supreme Court.

ACKNOWLEDGEMENTS The authors benefitted from discussions with George Beckwith, Jamie Barnes, Mary Gillam, Douglas Clark, Barbara Matz (Sergent, Hauskins & Beckwith), David B. Slemmons (consultant), and John Hawley (New Mexico Bureau of Mines & Mineral Resources). Mark Turnbough provided logistical support. Darcy Frownfelter, Special Assistant Attorney for El Paso County, authorized preparation of this report.

REFERENCES

Albritton, C. C. & Smith, J. F., Jr. (1965) *Geology of the Sierra Blanca area, Hudspeth County, Texas*. U. S. Geological Survey Professional Paper 479, 131 p.

Albritton, C. C. & Smith, J. R., Jr. (1957) The Texas Lineament. Mexico City, *20th International Geological Congress* [1956], Section 5, Relaciones entre de tectonica y la sedimentecia.

Baumgardner, R. W., Jr. (1990) *Geomorphology of the Hueco Bolson in the vicinity of the proposed low-level radioactive waste disposal site, Hudspeth County, Texas.*

Austin, Texas, The University of Texas Bureau of Economic Geology Final Contract Report for Texas Low-Level Radioactive Waste Disposal Authority, 98 p.

Griggs, G. B. & Gilchrist, J. A. (1983) *Geologic hazards, resources and environmental planning*. Belmont, CA, Wadsworth Publishing Co. 502 p.

Gustavson, T. C. (1990) *Sedimentary facies, depositional environments, and paleosols of the Upper Tertiary Fort Hancock Formation and the Tertiary-Quaternary Camp Rice Formation, Hueco Bolson, West Texas*. Austin, Texas, The University of Texas Bureau of Economic Geology Final Contract Report for Texas Low-Level Radioactive Waste Disposal Authority, 94 p.

Henry, C. D. & Price, J. G. (1985) *Summary of the tectonic development of Trans-Pecos Texas*. Austin, Texas, The University of Texas Bureau of Economic Geology Miscellaneous Map no. 36.

Holzer, T. L. (1984) Ground failure induced by groundwater withdrawal from unconsolidated sediment, in Holzer, T. L., ed., *Man-induced ground failure*. Boulder, CO, Geological Society of America Reviews in Engineering Geology, v. VI, p. 67 - 105.

Keaton, J. R., Shlemon, R. J., Slemmons, D. B., Barnes, J. R. & Clark, D. G. (1989) The Amargosa fault - a major late Quaternary intraplate structure in northern Chihuahua, Mexico: *Geological Society of America Abstracts with Programs*, v. 21, no. 6, p. A148.

McClure, C. R., Jr. & Hatheway, A. W. (1979) An overview of nuclear power plant siting and licensing, in Hatheway, A. W., and McClure, C. R., Jr., eds., *Geology in the siting of nuclear power plants*. Boulder, CO, Geological Society of America Reviews in Engineering Geology, v. IV, p. 3 - 12.

Phillips, J. D., Dean, D. R. & Riherd, P. S. (1986) *Preliminary seismic reflection study of the Fort Hancock area in Hudspeth County, Texas*. Austin, Texas, The University of Texas Institute for Geophysics Technical Report TR-45, Final Report for the Texas Low-Level Radioactive Waste Disposal Authority, Contract No. IAC (86-87)-0994, 35 p.

Reilinger, R. E., Brown, L. D. & Powers, D. (1980) New evidence for tectonic uplift in the Diablo Plateau region, west Texas: *Geophysical Research Letters*, v. 7, no. 3, p. 181 - 184.

Reilinger, R. E., Brown, L. D., Oliver, J. E. & York, J. E. (1979) Recent vertical crustal movements from leveling observations in the vicinity of the Rio Grande Rift. in Riecker, R. E., ed., *Rio Grande Rift, tectonics and magmatism*. Washington, D.C., American Geophysical Union, p. 223 - 236.

Sergent, Hauskins & Beckwith (1989) *Preliminary geologic and hydrologic evaluation of the Fort Hancock Site (NTP-S34), Hudspeth County Texas, for the disposal of Low-Level Radioactive Waste*. Unpublished consultant's report prepared for Hudspeth County, Texas, Hudspeth County Conservation adn Reclamation District No. 1, Hudspeth County Underground Water Conservation District No. 1 and El Paso County, Texas, El Paso SHB Job No. E88-4008B, 3 volumes.

Shlemon, R. J. & Davis, P. (1988) Ground fissures in the Rancho California area, Riverside County, CA. *Geological Society of America Abstracts with Program*, v. 20, no. 7. p. A145.

Swadley, W. C. & Scott, R. B. (1988) Modern fissures in the Pahranagat shear system northeastern Nevada. *EOS*, v. 69, no. 44, p. 1459.

Land Subsidence (Proceedings of the Fourth International Symposium on Land Subsidence, May 1991). IAHS Publ. no. 200, 1991.

Earth Fissures, Urbanization and Litigation: A Case Study from the Temecula Area, Southwestern Riverside County, California

E. J. CORWIN, S. C. ALHADEFF, S. P. OGGEL
Lorenz Alhadeff Lundin & Oggel, 101 West Broadway, Suite 1500, San Diego, CA 92101, USA
R. J. SHLEMON
P.O. Box 3066, Newport Beach, CA 92659, USA

ABSTRACT Ground fissures occurring in 1987 extended discontinuously along a 12-km long zone in the rapidly-urbanizing Temecula-Wolf Valley area of southwestern Riverside County, California. Impacted were new residential and industrial buildings. Litigation has ensued, and damage is now alleged to exceed about 50 million dollars. Defendants include County government, a local Water District, developers, and consulting engineers and geologists.

INTRODUCTION

In the mid-1980s, urbanization dramatically increased in the Temecula area of southwestern Riverside County, California. From a population of 8,324 in 1980, the previously serene town, about 41 km north of San Diego and 53 km southeast of Los Angeles, jumped to a population of over 29,000 in 1988 (Fig. 1). Developers seized on the increasing popularity of southern California as a desirable place to live, and vast new residential and light industrial complexes ("Business Parks") were built. The rapid urbanization produced the usual plethora of environmental constraints for both the developers and residents of Temecula. The most unexpected problem was the mid-1987 occurrence of earth fissures, the resulting allegations of property damage and general loss of value, and the perhaps inevitable litigation that has since followed.

GEOLOGICAL FRAMEWORK

The Temecula area lies in the Murrieta-Temecula-Wolf Valley, an approximately 20-km long and 1.5 to 2.0-km wide structural graben bounded by major splays of the Elsinore fault system: namely, the Wildomar fault on the east and the Willard fault on the west (Mann, 1955; Kennedy, 1975; Fig. 1). The Wildomar fault is active,

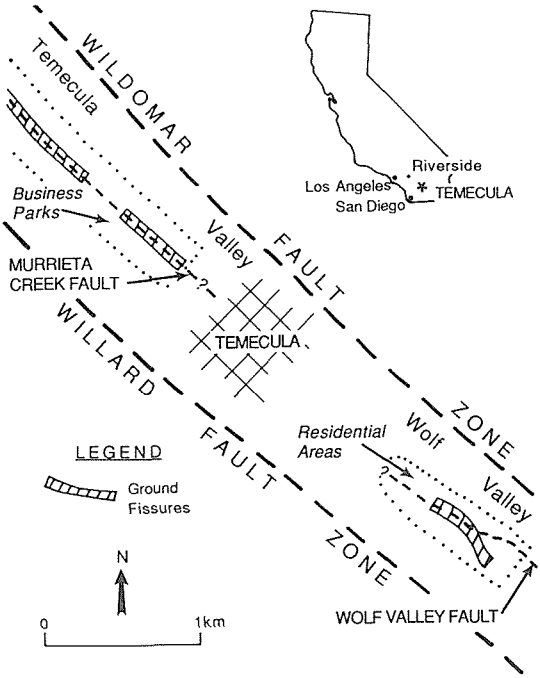

FIG. 1 Location of 1987 ground fissures and adjacent fault zones in the Temecula-Wolf Valley area, southwestern Riverside County, California.

according to State of California criteria, for it has geomorphic expression and has offset Holocene sediments and soil profiles (Hart, 1985). Accordingly, habitable structure "setback zones" have been established for the fault (Calif. Div. Mines and Geology, 1990). In contrast, recent investigations show that last movement of the Willard fault occurred in pre-Holocene time, and the fault is therefore presently deemed "not active" for purposes of engineering design (Schaefer Dixon Associates, 1988a). Prior to mid-1987, no other active faults had been identified in the Temecula-Wolf Valley area despite the fact that literally tens of engineering-geological investigations had been conducted in support of residential and industrial development. Neither identified were buried stream terraces or older faults underlying valley alluvium, geologic discontinuities that often control the surface location of ground fissures (Holzer, 1984).

Quaternary sediments underlying the Temecula-Wolf Valley area are more than 800 m thick, and have yielded abundant water for both domestic and agricultural use (Scheliga & McGoldrick, 1984). Two principal aquifers are the upper "Pauba beds," generally producing from

depths within about 100 m from the surface, and the lower, more prolific "Temecula sands" generally encountered between about 200 and 400 m. The Temecula aquifer is a source of relatively high quality and inexpensive water, and two Temecula-Wolf Valley wells, pumping since at least 1982, have the capacity to produce 8,000 to 9,000 1/min. In 1984 it was pointed out to the Rancho California Water District (RCWD) that: "Because of the depth of saturated sediments and the potential for construction of additional high capacity wells, the Murrieta-Wolf [hydrologic] Unit offers a location for development of a substantial increase of ground water resources to RCWD supplies" (Scheliga & McGoldrick, 1984, p. 3-21). By late 1986 an additional six, deep wells tapped the Temecula aquifer. After initial tests, most started production in 1987 (Leighton & Associates, 1987).

THE TEMECULA FISSURE

In August 1987, a northwest-trending curvilinear system of earth fissures about three km long was discovered in recently-developed residential tracts in the southern part of the Temecula area. In October 1987, similar northwest-trending fissures were observed in a new Business Park approximately four km to the northwest. Despite diligent search, no fissures were identified in the intermediate area (Fig. 1).

The fissures were expressed at the surface by 10 to 20 m long cracks in street pavement and in adjacent gutters and curbs. Most fissures were en-echelon, the overlapping width generally less than about three or four m. Vertical relief was typically less than a few cm with the east side down. In the residential area, fissure damage was mainly displaced curbs and floor slab cracks in four or five buildings. However, some homeowners several blocks away alleged that small cracks in their residences were caused by the fissures, rather than the "normal" settlement typical of new construction in the area. In the northern business parks, the fissures promulgated through up to five m of compacted fill, and eventually widened along widely dispersed "sinkholes" up to a meter wide.

The cause and specific location of the fissures has been argued in the press and by technical experts. Two general hypotheses have been advanced: the 1987 fissures were caused by increased groundwater withdrawal, and localized along either previously-unrecognized, graben-bounding discontinuities such as faults or buried channel escarpments; or by aseismic creep occurring on heretofore unrecognized active faults (Shlemon & Davis, 1988).

Arguments to support both hypotheses abound: on the one hand, several new wells began production just

prior to fissure occurrence, and no obvious fissure rejuvenation has taken place since certain "suspect" wells were shut down; on the other hand, post-1987 investigations now show that the fissures are localized along a previously-unrecognized active (Holocene) fault, although no microseismic events have been recorded (Leighton & Associates, 1987; Geowest Soils Consultants, 1987; Schaefer Dixon Associates, 1988b). The southern residential area fissure coincides in part with the previously-recognized Wolf Valley fault (Kennedy, 1987); and the northern fissure is now informally designated as the "Murrieta Creek fault" (Bergmann & Rockwell, 1989; Fig. 1).

LITIGATION

Shortly after ground fissure stories and photographs appeared in the local and regional newspapers, Plaintiffs' attorneys signed up clients in the residential areas affected by fissures. By early 1988, over 200 lawsuits alleging over $25 million in damages had been filed against the developers, the County of Riverside, the local water district, and several geologic and soils engineering consulting firms. The individual suits were later consolidated into a few large actions which ultimately proved too large for the Riverside County Superior Court system to handle. As a result, the parties to the lawsuits stipulated to have the cases litigated before a retired judge, who was given all of the powers of a Superior Court judge.

Plaintiffs as a group and Defendants individually hired their own technical experts, including specialized geologists, geohydrologists, soils engineers, and construction experts. In the first year of the litigation, the judge also hired additional "joint experts" in order to investigate the fissure-related problems. However, the Business Park developers, the private landowners affected by the business park fissures, the County of Riverside, and the local water district each hired their own technical consultants to investigate the Business Park fissures. In 1990, three years after fissure occurrence, owners of a large Business Park commercial building damaged by the fissures, filed a lawsuit against the developer, the County of Riverside, and the local water district.

The cost to date for technical investigations is in the range of $2- to $3 million; and the studies continue. Legal fees for the residential area litigation alone are conservatively estimated at more than $2 million for all parties. Total costs will ultimately exceed at least ten-fold the value of the structures allegedly damaged by the fissures.

The News Media

Predictably, the local and regional news media, including television, radio and print, provided alarmist coverage of the ground-cracking for the first year after fissures occurrence and periodically thereafter. Television stations and newspapers in Temecula, Riverside, San Diego, and Los Angeles all carried stories about the assumed catastrophic impact of a major earthquake on the families and businesses situated near the Temecula ground fissures. Headlines such as "Crack-Watchers Turn Homeowners Into Tour Guides" and "On Uncertain Ground: Homeowner Says Yard Is Sinking" were common.

The County of Riverside

The County, as a defendant in the litigation, initially instituted a total ban on new building permits, then later adopted a local "Subsidence Report Zone" ordinance. The subsidence zone, approximately 1.6 km wide and 15 km long, encompassed the known fissure area in length and extended in width from the Wildomar fault on the east to the Willard fault on the west (Fig. 1). The intent of the County ordinance was to ensure that no new buildings were constructed across known or potential fissures and it required, among other things, that structural and geotechnical engineers formally document possible seismically-induced liquefaction and subsidence problems. The area of the zone was much greater than even the typical 240-m wide active fault "Special Study Zone" required by the State of California (Hart, 1985). The impact on development was therefore almost immediate, with many escrow closings frequently delayed or even failing as real estate agents sought to ensure the public that the Temecula Valley was as geologically "safe" as almost any other place in California.

The Water District

Almost immediately after the fissures appeared, the Water District shut down several wells near the fissures. The Water District has since been extremely cautious and defensive in its water management policy for the Temecula-Wolf Valley area. Owing to court injunction, several of the deep wells have remained inoperative since the onset of the 1987 fissures; while others, apparently based on Water District decision, have subsequently pumped less than about one-half their pre-fissure production. The Water District has thus been obliged to increase import of water from sources outside the local groundwater basin, resulting in a

more costly and generally lower quality supply. Consultants for the Water District, as those for some of the developers, continue to monitor fissures for evidence of any further movement, usually by periodic observation of lines painted across the cracks and by quadrilateral-survey readings.

The Developers

Several developers of both residential and business parks were named in the original litigation. The developers and their insurance carriers retained various geotechnical consultants to determine the cause of the 1987 fissures and to recommend appropriate setback zones commensurate with public safety and the requirements of the State of California and the County of Riverside. The numerous studies following the 1987 fissure events demonstrated that the fissures were, for the most part, controlled by faults. And these faults were judged to be Holocene in age, and therefore active according to State of California criteria (Leighton & Associates, 1987; Geowest Soil Consultants, 1987; Schaefer Dixon Associates, 1988b). Developers of the residential tracts in the southern fissure area bought back several recently-constructed houses, and eventually moved houses astride the fissure to other yet unbuilt lots in the area. One developer in a northern Business Park provided technical data to the owner of a large industrial building through which the fissure passed, as well as assisted in obtaining a County occupancy permit. In all cases, new, extensive geotechnical investigations were required, including the backhoe trenching of previously-compacted fill in order to determine the exact location of the fault-controlled fissures, and to establish an active fault setback zone. A beneficial side effect of the 1987 ground fissures is that almost all builders in Riverside County generally, and in the Temecula area specifically, have since become aware of potential "ground cracking" and subsidence problems, and thus have taken a much more conservative view with regard to buying and developing various parcels.

State of California

The California Division of Mines and Geology (CDMG) is the state agency given the authority to identify and designate active fault zones. According to California law, no habitable structures may be placed across known active (Holocene) faults. Based mainly on consultants' reports and on the CDMG's own observations, "Special Study Zones" are established for active faults (Hart, 1985). The developers' consultants then typically

perform appropriate geotechnical investigations to locate active fault traces within the Zone, recommend a setback zone for habitable structures, and document all findings in reports that are reviewed by local agencies. The typical Special Study Zone is about 240 m wide and is intended to encompass, within geological uncertainty, all faults that may be active, based on geomorphic expression and on subsurface (usually trenching) information. An actual building setback zone is usually much less wide, dependent on the amount and quality of geological data obtained.

In July 1989, following critique of consultants' reports and field verification, the CDMG issued a preliminary Special Study Zone for the Temecula area. After a six-month period during which developers and other interested parties had the opportunity to provide additional information as to the location and dimensions of the new fault, the CDMG issued final Special Studies Zone maps in January 1990 (California Div. Mines and Geology, 1990). As a result, ground fissures and active faults are now often combined in the minds of the layman, regardless of any cause-and-effect relationship.

The Temecula Residents

The response of Temecula area residents to the ground fissures has been mixed. Some have moved out of the area, fearing a large earthquake; but others have simply accepted the fact that earthquakes are a way of life in California, and that nobody has yet been killed by a ground fissure. However, as revealed during the litigation, some homeowners sought the help of health care providers for alleged emotional problems resulting from the fear of living on or next to what they perceive as an active fault. Ironically, several ground fissures elsewhere in Riverside County have been shown to be not located along near-surface active faults (Lofgren, 1976; Morton, 1978).

In 1988, some of the residents living near the ground fissures allegedly had difficulty in selling their homes, and there were reports that many real estate brokers were refusing to become involved in sale of homes located near the ground fissures. Also alleged was that near-fissure homes decreased in value because of the fissures, the lawsuits, and the resulting press coverage. It is probably more accurate to say, however, that most homes may have experienced a slower rate of appreciation, rather than an absolute decline in sale price.

LITIGATION STATUS

At the time of this writing (October 1990), the litigation involving the residential homes has in most respects been settled. Except for one defendant developer who conducted preliminary engineering and sold a tract of land to others who eventually constructed houses, all defendants have settled with the plaintiff homeowners, for about $2.8 million. Ironically, the Water District, which still refuses (at least publicly) to accept the theory that its deep groundwater pumping caused the 1987 Temecula ground fissures, paid the largest pro rata share of the overall settlements.

In contrast to the residential litigation, the lawsuit involving ground fissuring in a Temecula Business Park has just started, and promises to be nearly as costly.

The Temecula area fissure litigation points out that urbanization, especially in geologically sensitive locations, will continue to cause increasing friction between developers, federal, state and local regulatory authorities, utility concerns, and private business and residential interests. Cooperation at the earliest stages of development planning is therefore crucial to prevent disruption or injury to the environment, to property, and to the health and safety of individuals, and to minimize related litigation.

ACKNOWLEDGMENTS

We thank the Riverside County Geologist, S. Kupferman, and Consultant Hydrogeologist, W. Hardt, for discussions over the past few years regarding ground fissures in the Temecula area. We also thank D. Klimmek, Chief Counsel, Bedford Properties (Lafayette, California), for general support in the course of the litigation; and S. Davidor for drafting.

REFERENCES

Bergmann, M. & Rockwell, T. (1989) The Murrieta Creek fault, a new branch of the Elsinore fault, Rancho California area, Riverside County, California. Geol. Soc. America Abs. with programs, 21 (5).

California Division of Mines and Geology (1990) Special Studies Zones Maps, Pechanga, Murrieta and Temecula Quadrangles, Sacramento, California, scale 1:24,000.

Geowest Soil Consultants (1987) Geotechnical investigation, Tract 19939 fissure, Pala Road between Via Gilberto and Via Eduardo, Wolf Valley area, County of Riverside, California:

Consultants' report prepared for Jostri, Inc. (Temecula, California), Proj. File 742-002, 10 Dec. 1987.

Hart, E. W. (1985) Fault rupture hazard zones in California, Alquist-Priolo Special Studies Zone act of 1972 with index to Special Studies Zones Maps. Calif. Div. Mines and Geol. Special Studies Rept. 131, Sacramento, California.

Holzer, T. L. (1984) Ground failure induced by ground-water withdrawal from unconsolidated sediment. In: Man-Induced Land Subsidence. Geol. Soc. America Reviews in Engineering Geology vol. VI, 67-105.

Kennedy, M. P. (1975) Recency and character of faulting along the Elsinore fault zone in southern Riverside County, California. Calif. Div. Mines and Geol. Special Studies Rept. 131, Sacramento, California.

Leighton & Associates, Inc. (1987) Geotechnical investigation of "ground crack," Tract 19872, Wolf Valley, Rancho California area, County of Riverside, California: Consultants' report prepared for Richmond American (Irvine, California), Project No. 6851602-03, 7 Dec. 1987.

Lofgren, B. E. (1976) Land subsidence and aquifer-system compaction in the San Jacinto Valley, Riverside County, California--a progress report. J. Res. USGS 44 (1).

Mann, J. F. (1955) Geology of a portion of the Elsinore Fault Zone, California. Calif. Div. Mines Special Rept. 43, Sacramento, California.

Morton, D. M. (1978) Ground fissuring in part of the San Jacinto Valley, southern California. Geol. Soc. America Abs. with Programs, 10 (3).

Schaefer Dixon Associates (1988a) Report on geotechnical investigation of the Willard Fault, Parcel C-16. Consultants' report prepared for Bedford Properties (Temecula, California), Project No. 70-299, 4 April 1988.

Schaefer Dixon Associates (1988b) Geologic investigation of the Wildomar Fault, Parcel Map 19582. Consultants' report prepared for Bedford Properties (Temecula, California), Job No. 8R1208A, 18 April 1988.

Scheliga, J. T. & McGoldrick, J. P. (1984) Rancho California Water District, Water Resources Master Plan 1984. Consultants' report prepared for Rancho California Water District (Temecula, California), 10 Chapts.

Shlemon, R. J. & Davis, P. (1988) Ground fissures in the Rancho California area, Riverside County, CA. Geol. Soc. America Abs. with Programs, 20 (7).

Land Subsidence (Proceedings of the Fourth International Symposium on Land Subsidence, May 1991). IAHS Publ. no. 200, 1991.

Earth Fissures and Land Subsidence of the Mimbres Basin, Southwestern New Mexico, U.S.A.

G. J. CONTALDO
Geoscience Consultants, Ltd., NASA-WSTF, P.O. Drawer MM, Las Cruces, New Mexico, U.S.A. 88004
J. E. MUELLER
New Mexico State University, Department of Earth Sciences, P.O. Box 3AB, Las Cruces, New Mexico, U.S.A. 88003

ABSTRACT Earth fissures have formed in response to tensile failure of unconsolidated alluvium in the Mimbres Basin of southwestern New Mexico. A comparison of the location of earth fissures to areas of water-level decline reveals that the two are spatially associated. Total maximum and average water-level declines from 1910 to 1990 are approximately 35 m and 0.44 m year^{-1}, respectively. Dating the fissures also reveals their temporal association with water-level decline. Data from leveling surveys and protruding water wells indicate that the area of maximum land subsidence coincides with the area of greatest water-level decline. Maximum measured subsidence, 36.2 cm, occurs in an area where the groundwater level has declined at least 30 m. The fissures are suspected to be a result of land subsidence caused by the compaction of unconsolidated alluvium due to dewatering of an unconfined aquifer.

INTRODUCTION

The Mimbres Basin earth fissures of southwestern New Mexico are long, narrow, eroded tension cracks. Similar earth fissures have been described from other alluvium-filled basins of the southwestern United States (Holzer, 1984; Lister & Secrest, 1985; Ireland, 1986; Love et al., 1987; Péwé et al., 1987; Pampeyan et al., 1988). The process that produces the stress necessary for the formation of earth fissures has been attributed to both man-induced and natural causes (Holzer, 1984).

The study area encompasses 12 townships (approximately 1120 km^2) of the Mimbres Basin, a closed drainage basin in southwestern New Mexico (Fig. 1). Highway access to the study area is provided by Interstate 10, U.S. 180, and New Mexico 11, 26, 331, 332, 377, 418, and 594.

Associations related to formation of the Mimbres Basin earth fissures are based on integrating earth fissure data with water-level and land subsidence data. Particular attention is given to documenting earth fissures, total water-level decline, and land subsidence. This study is the first to address earth fissures and land subsidence of the Mimbres Basin.

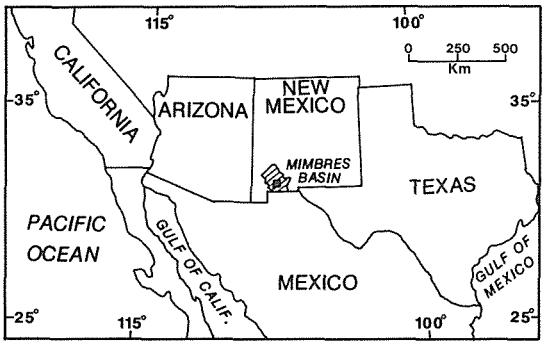

FIG. 1 Mimbres Basin study area.

GEOLOGY

The geology of the study area is highly varied in petrology and structure. Lithologies range from Cambrian plutonic rocks to basin-fill alluvium of Recent age. North- to northwest-trending Basin and Range normal faults are superimposed on northwest-trending Laramide reverse faults.

According to Clemons (1986) and Clemons & Mack (1988), most of the study area was covered by Eocene to early Miocene volcanic rocks before the onset of Basin and Range deformation. As areas subsided along normal faults, volcanic rocks exposed in uplifts provided most of the source material for the basin-fill alluvium. Clemons (1986) analyzed cuttings from four wildcat oil and gas exploration wells and suggested that the boundary between bedrock and overlying basin-fill alluvium may be at the top of the consolidated Miocene-Oligocene volcanic sequence. Overlying this sequence is late Tertiary to Holocene age basin-fill alluvium. Basin-fill alluvium can be distinguished from the volcanic sequence because drill cuttings of the former generally contain a greater percentage of well-rounded grains (Clemons, 1986).

The basin-fill alluvium consists of irregular lenses of gravel, sand, silt, and clay. Individual beds or lenses vary greatly in thickness and lateral extent. Sorting and rounding are irregular in these sediments, which have been derived from the nearby fault-block mountains. The basin-fill alluvium can be separated further into upper and lower units.

In general, the lower unit is composed of sediments which extend from 1220 m above sea level down to bedrock. This unit is finer-grained than the upper unit and consists primarily of reddish clays. Hawley (personal communication) indicated that sediments of the lower unit represent alluvial fan and playa deposits which are middle Pleistocene or older.

The upper unit extends from 1220 m above sea level to the present land surface. According to Hawley (personal communication) much of the upper unit is composed of admixtures of gravel, sand, silt, and clay, and represents fan-delta or splay sedimentation by the Mimbres River within late Quaternary time. Braided channels of ancient Mimbres distributaries in uppermost basin-fill have been mapped in detail by Seager (in press).

GROUNDWATER HYDROLOGY

The major aquifer in the study area is the upper basin-fill unit. Thickness of sand and gravel deposits within this unit generally varies between 12 and 15 m, though in many places the thickness is much less, commonly in the range 1.5 to 5.5 m (Darton, 1916). Determination of the lateral extent of water-bearing strata is very difficult due to the wide spacing of water wells and the lenticular nature of the water-bearing sand and gravel.

The aquifer in the unconsolidated basin-fill alluvium is generally unconfined (water-table aquifer). Local confinement and artesian conditions have been described previously (Darton 1915, 1916; White, 1929; Theis, 1938). The transmissivity of the alluvial aquifer varies from 173.8 to 2358.2 $m^2 day^{-1}$, and specific capacity of wells developed in this unit ranges from 9.6×10^{-3} to 2.0 l s^{-1} per meter of drawdown (McLean, 1977). The range of these aquifer characteristics may be correlated with the lenticular character of the alternating clayey and sandy beds of the basin-fill alluvial deposits.

Most groundwater in the study area is used for domestic consumption and irrigation. Development of groundwater began in 1908, when a large number of homesteaders settled in Luna County (Fiedler, 1928). As the population grew, the amount of irrigated acreage increased, and the demand for groundwater also increased (Doty, 1959). Darton (1916) estimated that the total groundwater withdrawal in about 1915 was no more than 12.3×10^6 m^3 $year^{-1}$. Wilson (1985) estimated the groundwater withdrawal and depletion from storage in 1985 at 131.7×10^6 and 62.4×10^6 m^3, respectively.

The effect of pumping groundwater upset the balance between recharge and discharge (discharge being much greater than recharge). As a result, the water levels in the area began to decline in 1913 and continue to decline. Numerous workers, such as Darton (1915; 1916; 1917), Fiedler (1928), White (1929; 1932), Theis (1938), Conover & Akin (1942), Doty (1959), and McLean (1977) have documented the amount and extent of water-level declines during specific time intervals.

The most recent and comprehensive maps showing the long-term decline of water levels were produced by McLean (1977). His maps show the decline of water levels for various periods from 1910 to 1970 in the Mimbres Basin. Most apparent is a circular to elliptical cone of depression that expanded in areal extent from 1910 to 1970. Also evident is the fact that the rate of groundwater decline has increased through time, and the cone of depression has migrated somewhat southward. The increased rate and southward migration are probably due to increased development of irrigated land and increased pumpage associated with groundwater development in the area.

EARTH FISSURES

Earth fissures occur in 13 discrete locations in the Mimbres Basin (Fig. 2). Table 1 provides the earth fissure location number, the date fissures appeared, and the type of fissure pattern at each location.

Earth fissures in the area have two types of patterns: (a) orthogonal to polygonal and (b) curvilinear. An orthogonal to polygonal pattern consists of a series of fissures interconnected to form triple

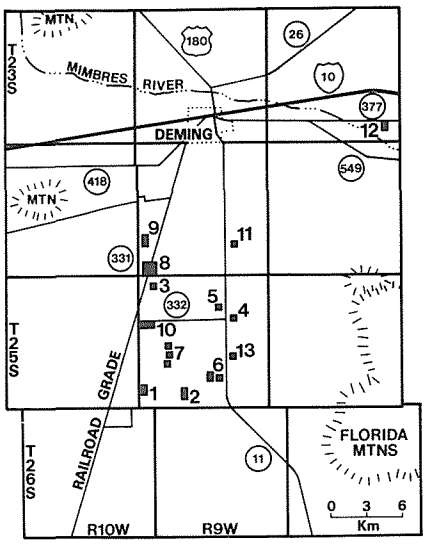

FIG. 2 Earth fissure locations in the Mimbres Basin.

TABLE 1 Fissure location numbers, date fissures appeared, and type of earth fissure pattern.

Location number	Date fissures appeared	Fissure type	Location number	Date fissures appeared	Fissure type
1	June 1982	intersecting curvilinear	7	post 1954 pre 1984	curvilinear & intersecting curvilinear
2	June 1982 and October 1984	curvilinear	8	mid 1950s	orthogonal-polygonal
3	mid 1950s	orthogonal-polygonal	9	post 1954 pre 1984	orthogonal-polygonal
4	post 1977 pre 1984	curvilinear	10,11	post 1954 pre 1977	intersecting curvilinear
5	post 1954 pre 1984	curvilinear	12	post 1954 pre 1984	curvilinear
6	post 1954 pre 1984	curvilinear	13	post 1954 pre 1977	curvilinear

junctions (Fig. 3). Individual polygons range from 30 to 366 m across. Curvilinear fissures are arcuate and exist isolated from each other within seven of their ten areas of occurrence; their lengths range from 16 to 615 m.

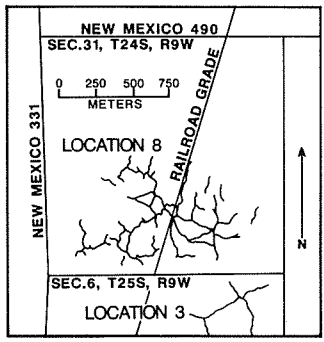

FIG. 3 Fissures at locations three and eight mapped from a 1984 aerial photograph.

Measurable fissure depths range from less than 0.3 to 12.8 m. Fissure depth measurements are conservative and represent the limit to which a weighted tape can be lowered into the fissures. Depth measurements are actually measurements of surface features (e.g., potholes, hair-line cracks, and surface depressions) rather than measurements of total fissure depth. Field evidence indicates that the near-surface void space of surface features is generated by transport of shallow soils to greater fissure depths. Holzer (1984) suggested that the near-surface void space is a measure of the total void space created during the formation of a tension crack. Based on the observed size of surface features and the amount of material transported to greater fissure depths, the actual depths of fissures are probably at least an order of magnitude greater than measured fissure depths.

The width of fissures ranges from incipient hairline cracks to 9.7 m. Their width and morphology, as exposed at the surface, appear to be the result of secondary erosion rather than horizontal separation. The appearance of aligned potholes at the surface at many fissure locations, and the fact that no vertical offset was observed along fissures, indicates that fissures initially form as tension cracks in the subsurface. The formation of tension cracks creates preferred pathways for infiltrating water. Infiltrating water promotes enlargement of the cracks through subsurface piping erosion. Once large voids are created in the subsurface, soil above the voids can no longer support itself and eventually collapses, typically forming aligned potholes at the surface. Erosion through tributary gullying, slumping, and subsurface piping continues to enlarge many potholes. Potholes generally enlarge along the trend of fissures and may eventually become interconnected, completely opening fissures to the surface (Fig. 4). As erosion at the surface and concomitant deposition within the fissures proceeds, the width of fissures generally increases, whereas the apparent depth decreases. Many of

the fissures appear to be almost completely filled with slump and runoff material. These fissures are marked on the surface by curvilinear surface depressions.

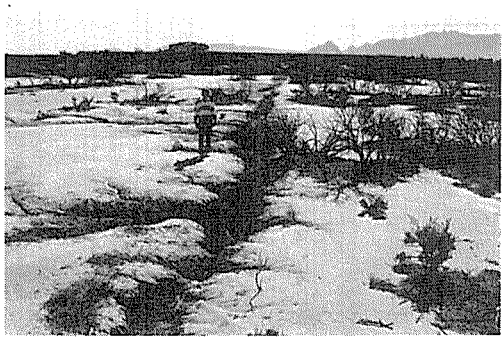

FIG. 4 One of numerous fissures at location eight. This fissure is well defined at the surface and displays tributary gullying on left (north). Photograph was taken in April 1988.

Additional conspicuous characteristics of the earth fissures are that a) almost without exception, fissures occur in areas where the land surface is currently undisturbed by cultivation; the fissures typically form either between or immediately adjacent to cultivated fields; b) most curvilinear fissures trend north-south; and c) fissures are generally narrower and shallower across roads as compared to adjacent undisturbed land. The reader can refer to Contaldo & Mueller (1988) for a citing of problems related to the Mimbres Basin fissures and Contaldo (1989) for a more detailed description and map of each fissure location.

FISSURES, WATER-LEVEL DECLINES, AND LAND SUBSIDENCE

Fig. 5 shows the total water-level decline from 1910 to 1990. Conspicuous is a circular to elliptical cone of depression that is elongated north-south. An area of about 880 km^2 has been affected by water-level declines. The maximum water-level decline from 1910 to 1990 in the Mimbres Basin is slightly greater than 35 m. The average rate of water-level decline in the area of greatest depletion is 0.44 m $year^{-1}$.

A comparison of the location of earth fissures (Fig. 2) to areas of water-level decline (Fig. 5) reveals that the two are spatially associated. The majority of fissures, including those at locations two through 11, occur near the apex of the cone of depression in an area where the water level has declined at least 25 m. Earth fissures at location one and location 12 are also in the cone of depression where the water level has declined about 20 and 12 m, respectively.

Earth fissures are also temporally associated with water-level declines. The date the fissures first appeared is based on analysis of aerial photographs and interviews with local residents. Earth

fissures first appeared as early as the mid 1950s, and others as recently as October 1984 (Table 1). Analysis of water-level decline maps provided by McLean (1977) reveals that groundwater level had declined as much as 13.7 m by the mid 1950s. Relatively precise dates

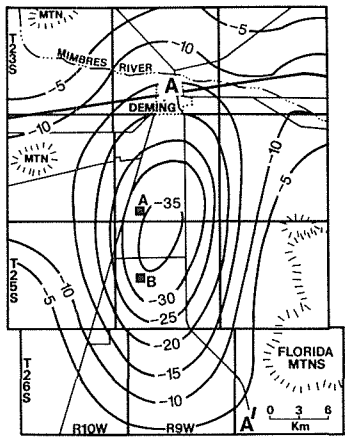

FIG. 5 Total water-level decline from 1910 to 1990. Contours are in meters.

on the appearance of fissures indicate that fissures nearest the apex of the cone of depression are older than those found farther from the apex. Because the more recent fissures are located farther from the cone of depression apex, the fissures appear to be spatially and temporally associated with the expanding cone of depression.

Fig. 6 shows the amount of land subsidence in the study area along line A-A′ in Fig. 5, based on leveling data obtained by the National Geodetic Survey. The original leveling line, line L4486, which is along New Mexico 11 (line A-A′) was first surveyed in 1935. This leveling line is used as the datum. Benchmarks along this leveling line are spaced less than 1600 m apart. Unfortunately, leveling line L4486 has never been releveled. Only certain benchmarks along this leveling line have been resurveyed during surveys conducted along other leveling lines. Benchmarks A134, Z133, Y133, and X133 along leveling line L14850 were resurveyed in 1953. Fig. 6 reveals that a minor amount of land subsidence occurred in the area between 1935 and 1953. Benchmark A134 along leveling line L24557 was resurveyed in 1980. Elevation data from this benchmark indicate that the amount of land subsidence increased greatly from 1953 to 1980.

Additional indirect evidence for determining the amount of land subsidence during certain time periods was obtained from two protruding water wells. At both wells, the top of the surface casings, the pumps, and the concrete slabs supporting the pumps stand farther from the ground surface than when the wells were first completed. The location of these wells is provided in Fig. 5.

Water well "A" was completed in April 1958 to a total depth of 122 m. According to Paul Smith (personal communication), a local well driller who installed the well, the base of the concrete slab which supports the pump for this well was originally flush with the ground

surface. The discharge pipe connected to the pump continued to bend over a period of years, resulting in damage to the flow valve which is connected to the discharge pipe. Measurements taken from the ground surface to the base of the concrete slab in July 1990 indicated that the land surface had subsided 36.2 cm since 1958 (Fig. 7). This measurement is plotted in Fig. 6.

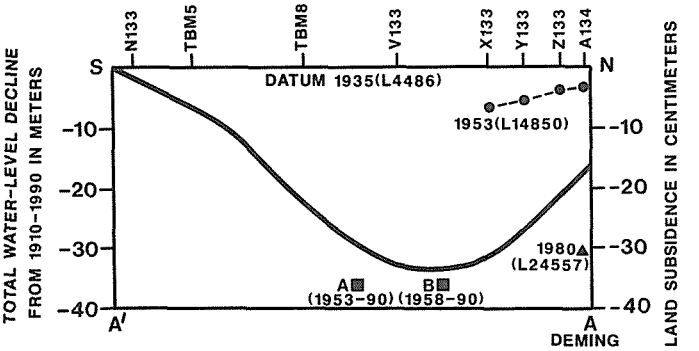

FIG. 6 Total water-level decline from 1910 to 1990 (solid line) and land subsidence along line A-A' (Fig. 5). Benchmark designations are provided at top. Leveling line designations are shown in brackets. Protruding water wells "A" and "B" are shown by squares.

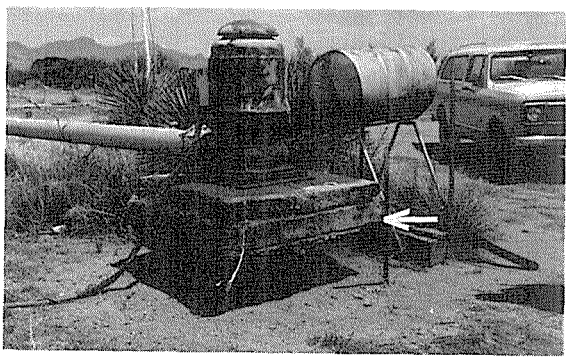

FIG. 7 Protruding water well "B". Original land surface is marked by arrow. Photograph was taken in July 1990.

Water well "B" was completed in April 1953. The total depth of this well is unknown. Similar in construction to protruding well "A", the base of the concrete slab which supports the pump of well "B" was flush with the ground surface when it was installed. Measurements taken from the ground surface to the base of the concrete slab in July 1990 indicated that the land surface had subsided 36.2 cm since 1953. This measurement is also plotted in Fig. 6.

Total water-level decline from 1910 to 1990 is plotted in Fig. 6 and suggests a cause and effect relationship between water-level decline and land subsidence. The amount of subsidence, as determined

from benchmarks along leveling line L14850, increases as the amount of water-level decline increases. Maximum subsidence, as determined by measurements of protruding water-wells "A" and "B", has occurred near the apex of the cone of depression, where the groundwater level has declined at least 30 m (Fig. 5).

The spatial and temporal association of water-level decline with earth fissure formation in the Mimbres Basin suggests a cause and effect relationship. The land subsidence data presented suggest that land subsidence is a manifestation of groundwater depletion. The fissures are therefore suspected to be a result of land subsidence caused by compaction of unconsolidated sediments. Compaction may be due to increased effective stresses as a result of dewatering of an unconfined aquifer.

The United States Geological Survey is presently involved in studying land subsidence in this area utilizing the Global Positioning System (GPS). The New Mexico Bureau of Mines and Mineral Resources recently conducted gravity and seismic reflection surveys across a fissure at location two in order to characterize the distribution of alluvial units and their physical properties. Information obtained by these studies may provide greater insights to the mechanisms responsible for land subsidence and the initiation, development, and propagation of earth fissures in the Mimbres Basin.

ACKNOWLEDGEMENTS Critical reviews by Russell Clemons, William King, Richard Marston, and Robert Myers are greatly appreciated. Financial support was provided by the New Mexico Geological Society and New Mexico Bureau of Mines and Mineral Resources. The preparation of the maps by the Laboratory for Cartography and Spatial Analysis at New Mexico State University is also appreciated.

REFERENCES

Clemons, R.E. (1986) Petrography and stratigraphy of Seville-Trident exploration wells near Deming, New Mexico. New Mexico Geol. 8, 5-11.

Clemons, R.E. & Mack, G.H. (1988) Geology of southwestern New Mexico. In: Cretaceous and Laramide Tectonic Evolution of Southwestern New Mexico, ed. Mack, G.H., Lawton, T.F., & Lucas, S.G., New Mexico Geol. Soc. Guidebook to 39th Field Conf., Socorro, New Mexico, 45-57.

Conover, C.S. & Akin, P.D. (1942) Progress report on the ground-water supply of Mimbres Valley, New Mexico, 1938-1941. In: New Mexico State Engr. 14th and 15th Biennial Reports, 235-282.

Contaldo, G.J. & Mueller, J.E. (1988) Earth fissures in the Deming area. In: Cretaceous and Laramide Tectonic Evolution of Southwestern New Mexico, ed. Mack, G.H., Lawton, T.F., & Lucas, S.G., New Mexico Geol. Soc. Guidebook to 39th Field Conf., Socorro, New Mexico, 3-5.

Contaldo, G.J. (1989) Earth fissures and land subsidence near Deming, New Mexico. M.S. thesis, New Mexico State University, Las Cruces, New Mexico.

Darton, N.H. (1915) Underground water of Luna County, New Mexico. USGS Wat. Supply Pap. 345-C, 25-40.
Darton, N.H. (1916) Underground water of Luna County, New Mexico. USGS Bull. 618.
Darton, N.H. (1917) Geologic atlas of the United States, Deming folio. USGS Folio 207.
Doty, G.C. (1959) Mimbres Valley, Luna County. Annual water level measurements in observation wells, 1951-1955, and atlas of maps showing changes of water levels for various periods from beginning of record through 1954, New Mexico. In: New Mexico State Engr. Tech. Report 13, 299-339.
Fiedler, A.G. (1928) Report on the reconnaissance of the ground-water area of the Mimbres Valley, Luna County, New Mexico. In: New Mexico State Engr. 8th Biennial Report, 159-171.
Holzer, T.L. (1984) Groundfailure induced by groundwater withdrawal from unconsolidated sediments. In: Man-Induced Land Subsidence, ed. T.L. Holzer, Rev. Engrg. Geol. VI, Geol. Soc. America, Boulder, Colorado, 67-105.
Ireland, R.L. (1986) Land subsidence in the San Joaquin Valley, California, as of 1983. USGS Wat. Resour. Invest. Report 85-4196.
Lister, L.A. & Secrest, C.D. (1985) Giant desiccation cracks and differential surface subsidence, Red Lake Playa, Mojave County, Arizona. American Assoc. Engrg. Geol. Bull. 22, 299-314.
Love, D.W., Reimers, R.F., Hawley, J.W., Johnpeer, G.D. & Bobrow, D.J. (1987) Summary of geotechnical investigations near Espanola, New Mexico. In: Quaternary Tectonics, Landform Evolution, Soil Chronologies and Glacial Deposits - Northern Rio Grande Rift of New Mexico, ed. C. Menges, New Mexico Depart. Geol., Albuquerque, New Mexico, 133-157.
McLean, J.S. (1977) Hydrologic maps and data in the Mimbres Basin, New Mexico. USGS Open-file Report 77-314.
Pampeyan, E.H., Holzer, T.L. & Clarke, M.M. (1988) Modern ground failure in the Garlock fault zone, Fremont Valley, California. Geol. Soc. Amer. Bull. 100, 677-691.
Péwé, T.L., Raymond, R.H. & Schumann, H.H. (1987) Land subsidence and earth-fissure formation in eastern Phoenix metropolitan area, Arizona. In: Geologic Diversity of Arizona and its Margins - Excursions to Choice Areas, ed. Davis, G.H., & VandenDolder, E.M., Arizona Bur. Geol. Min. Tech., Geol. Survey Branch Special Paper 5, 199-211.
Seager, W.R., in press, Geologic map of the southwest quarter of the Las Cruces and northwest part of the El Paso 1° by 2° sheets. New Mexico Bur. Mines Min. Res. Geol. Map 57.
Theis, C.V. (1938) Progress report on the ground-water supply of the Mimbres Valley, New Mexico. In: New Mexico State Engr. 12th and 13th Biennial Reports, 135-153.
White, W.N. (1929) Preliminary report on the ground water supply of the Mimbres Valley, New Mexico. In: New Mexico State Engr. 9th Biennial Report, 131-152.
White, W.N. (1932) Progress report on the ground-water supply of the Mimbres Valley, New Mexico. In: New Mexico State Engr. 9th Biennial Report, 131-152.
Wilson, B. (1985) Water use in New Mexico in 1985. New Mexico State Engr. Tech. Report 46.

Land Subsidence (Proceedings of the Fourth International Symposium on Land Subsidence, May 1991). IAHS Publ. no. 200, 1991.

Sinkhole Collapse Resulting from Pumping of Karst Groundwater: A Problem and its Solutions

J. CHEN & S. XIANG
Institute of Karst Geology, Ministry of Geology and Mineral Resources, Guilin, Guangxi 510004, China

ABSTRACT In recent years, sinkhole collapse caused by pumping of groundwater in karst terrains has been recognized as a hazard resulting in heavy property losses. Therefore, it is necessary to decrease the hazard by reducing the number of sinkholes triggered by human influence. Solving such problems is complicated and involves several considerations:
-predicting development of sinkhole collapse in areas of karst groundwater resources;
-developing effective water exploitation plans which will prevent sinkholes;
-determining the ground surface area of potential sinkhole collapse;
-predicting the intensity and extent of sinkholes;
-evaluating the developing trends in the sinkhole area;
-estimating the influence of sinkholes on construction and suggesting feasible and appropriate remediation and countermeasures.
This paper deals with four aspects of resolving sinkhole collapse problems, based on the authors' experiences with such problems in China.

INTRODUCTION

In recent years, karst collapse caused by pumping groundwater in karst areas has been recognized as a hazard which will result in heavy loss of lives and property. Therefore it is necessary to decrease or even prevent collapse caused by human efforts. Preventing human-caused sinkhole collapses requires:
(a)predicting the development of sinkhole collapse;
(b)deciding the best groundwater exploiting design to prevent sinkhole collapse;
(c)delineating the area of possible collapse and predicting its intensity and extent;
(d)estimating its influence on constructions and suggesting suitable preventive measures;
(e)monitoring and evaluating developing trends in the collapse area, and suggesting feasible countermeasures and remediations. Thus, the solution of collapse problems

involves four aspects: prediction, prevention, monitoring/forecast, and remediation. Collapse prediction is the basic prerequisite, and the other aspects are concrete countermeasures for preventing collapse hazard.

PREDICTION OF SINKHOLE COLLAPSE

Since the potential threat of sinkhole collapse due to pumping is extensive in covered karst areas, it is critical to predict its possibility during planning and design stages. The primary purpose is to make full use of the karst groundwater resources, and to prevent the hazard of pumping collapse--or at least to minimize it, for the sake of economy, society and environment. Prediction involves place, time, intensity, and range of sinkhole collapse. In fact, there is still a great gap in our ability to predict the first two, which can be narrowed by accumulating a great amount of information on geology, hydrogeology, engineering characteristics of earth mass, and the regime of groundwater pumping. To predict sinkhole collapse, geological setting is fundamental, and knowledge of factors leading to collapse is key. There is a general procedure of prediction which includes qualitative and quantitative/semi-quantitative, as seen below.

TABLE 1 Collapse prediction procedures.

1.QUALITATIVE PREDICTION:
Geological setting analysis
Sinkhole collapse site investigations
Qualitative prediction
2.QUANTITATIVE/SEMI-QUANTITATIVE PREDICTION:
Geological setting analysis
Sinkhole collapse site investigation
Synthetical statistical analysis or Empiric formula calculations
Quantitative/semi-quantitative prediction

Prediction based on geological setting information and sinkhole site investigation

Knowledge of features of the geological environment in the prediction area This includes topography and geomorphology of the area; amount of rainfall; surface water distribution; original types of overburden (lithological texture and assemblage characters, physical mechanical properties, distribution areas and thickness); development of soil cavities; lithology and assemblage characteristics

of underlying karst conduits and their distribution in horizontal and vertical directions; undulation of the karst bedrock surface; occurrence of groundwater in karst aquifer and soil, and their hydrodynamic features.
Diagrams and maps (synthetical or single-factor) for the hydrogeology or engineering geology of the prediction area should be plotted after summarizing the above factors. For instance, one could plot contours of the overburden thickness or groundwater level, sections of intense karst development, distribution of soil cavities, or areas of confined or unconfined karst groundwater.

Investigation and analysis of the sinkhole sites This includes the detailed records and statistics of the features of individual sinkhole collapse, as well as the dissemination, extent, history and process of collapse. Based on this, patterns of collapse in space and time and their relationship with the conditions of collapse development may be further discussed. Patterns of collapse distribution have been characterized as (1) distributed in the area where shallow karst is intensely developed and the loose overburden is generally less than 10 m thick; (2) distributed in areas where shallow karst is intensely developed and cavities are unfilled or incompletely filled; (3) distributed in topographic depressions such as a riverbed and its sides; (4) occurring along the geostructural zones; (5) distributed within the cone of depression caused by pumping in the intensely developed zone of shallow karst; (6) distributed in areas of original natural recharge and discharge of groundwater but later influenced by pumping; (7) surrounding the pumping points; (8) occurring in the initial stages of pumping or in the period when groundwater level changes from artesian to nonartesian; (9) occurring during pumping following periods of long-term aridity and abrupt rainfall.

Prediction map Formation and distribution of patterns of sinkhole collapse can be compared to the conditions of the existing geological environment; then surface stability of the prediction area should be characterized as regions of collapse, possible collapse, reasonably stable, and stable. Plotting these regions produces prediction maps.

Prediction from geostatistic and empiric formula calculations

Generally correlative statistics In accordance with the analysis of geological conditions and sinkhole collapse, a series of curves and tables of factors related to the sinkhole collapse may be worked out. For instance, comparison of collapse frequency with diameter, depth or volume; collapse sections compared to degree of karst development; relationship between collapse and time, drawdown, hydraulic gradient, pumping rate from karst

aquifer, lithology thickness, and parameters of the soil overburden. From these, one can determine the correlation between frequency and intensity of collapse and the variety of factors listed above. Where collapse has not yet occurred, prediction may be applied by using experimental geostatistical data derived from areas of similar geological and hydrogeological conditions which contain sinkhole collapses. Where collapse has already developed, regionalized maps of collapse prediction or collapse trend statistics may be extrapolated by extending the curves discussed above.

Stepwise discriminant analysis Many factors affect collapse, such as porosity, indexes of plasticity and liquidity, cohesion, angle of internal friction and thickness of overburden, and the amplitude of fluctuation of groundwater level. One can apply stepwise discriminant analysis to analyze the degree of correlation between the above factors and the collapse. Once the critical values of the major factors (among the multiple factors influencing collapse) have been identified, they can be used to help regionalize surface stability. Using this method, over one hundred collapse spots near Guilin city, Guangxi Zhuang autonomous region, were analyzed in 1984. Discriminant functions were set up by variations of cohesion, angle of internal friction, thickness of overburden, differences between the thickness of overburden and high or low level of groundwater, etc. Results were fairly coincident with the actual situation.

Empiric formula calculation Based on many years' experience in preventing railway subgrade calamities, a formula (G. Chen, 1983) has been derived from the equilibrium conditions of collapse earth mass to calculate the height of cracking arch in soil cavities, as follows:

$$h = B/2*\epsilon*tg\alpha$$

where h=height of cracking arch of soil cavity; B=width of underlying cavity; ϵ=lateral pressure coefficient, $\epsilon=tg^2(45-\phi/2)$; α=angle of friction of slip plane, $\alpha=(0.5\sim0.7)\phi$. Comparing h with the thickness of overburden allows estimation and prediction of whether soil cavities will result in surface collapse.

One can predict the radius of the sinkhole collapsed area by taking into account the development of shallow karst. A study of the collapse along the Yanshi railway showed that the main collapse area was a part of the cone of depression caused by pumping where the water level fell below the overburden; where water level was lowered to the base of the shallow karst zone, the collapse area was largest. A formula was suggested by use of the average hydraulic gradient in shallow karst aquifer to calculate the influenced area of collapse, as follows:

$$L = (S - Sf)/Ic$$

where L=radius of predicted area of collapse; S=drawdown by pumping; Sf=value of drawdown in overburden; and Ic=average hydraulic gradient in shallow karst aquifer.

The empiric values of Ic for very developed and developed karst in the fracture and fissure zones are respectively 1-2.5% and 2-3%; for developed and rather developed karst in network of fissure zones, respectively 3-4% and 4-6%.

PREVENTION OF SINKHOLE COLLAPSE

Sinkhole collapse may be prevented on the basis of collapse prediction. According to prediction data and actual demand of the district, reasonable preventative measures could be taken to reduce the losses by collapse to a minimum.

In the possible collapse area, significant engineering construction should be avoided; the density of common buildings should be reduced; and structural design against collapse, or setting the foundation on firm bedrock, should be considered.

Reasonable arrangement of wells and selection of pumping mode should be adopted; and pumping wells should be located as far away from buildings as possible. Important construction areas should be situated outside the radius of pumping influence, and wells should be arranged in a dispersed form to reduce the interferential influence of multiple wells in the same section by superimposed effects of drawdown. In the water source area where pumping wells is concentrated, the pumping discharge and drawdown should be controlled to keep groundwater level above the surface of bedrock. A great discharge or drawdown of pumping should be avoided, and the rate of water level decline should be slowed down, to reduce failure of soil caused by rapid increase of hydraulic gradient. Pumping wells should be equipped with a reasonable filter to prevent or reduce soil particles brought into wells by water flow. In sections with shallow karst well developed, it is necessary to exploit water in the deeper part and to seal up that in the shallow part.

The efficiency of controlling pumping to prevent sinkhole collapse has been proven in practice. For instance, numerous collapses caused by pumping occurred in the water source area of Jiangchun county, Guangdong province. In order to prevent collapse from developing continuously, the local water company reduced pumping discharge of a well from 4000m^3/day to 2500 m^3/day, and the drawdown from 5.6 m to about 4 m in 1981. In consequence, no new collapse has been discovered surrounding the well in recent years. As another example, the water source of the Hongqi cement plant of Guangxi is situated in limestone terrain with an overburden of less than 5 m; the groundwater level is about 3-5 m below the surface, and fluctuations

range from 2 m to 3 m per year. Sinkholes have commonly been found to occur in such geological and hydrogeological settings. At the Hongqi cement plant, pumping drawdown has been controlled to less than 2 m, resulting in a single collapse in over ten years of pumping.

Furthermore, in order to prevent infiltration of surface water accelerating the development of collapse, the ground surface should be leveled and the perfect drainage system for surface water set up.

MONITORING/FORECAST OF SINKHOLE COLLAPSE

This includes long-term observation of ground surface, buildings and wells, as well as the monitoring of phenomena premonitory of sinkhole collapse. The long-term observation generally proceeds during the early stage of pumping, in the first three to five years. The cycle of observation depends on the stage of pumping; in early stages, observations should be every 5-10 days, and in later stages, once a month. Elements to be observed are mainly cracks, displacement settlement and collapse of ground surface and buildings by pumping; variations of water level and sand content of wells, etc. Premonitory phenomena of collapse are primarily seen as drying up of ponds or springs; gushing air or water in ground surface; browning of some plants; cracks or tilting of buildings; circular cracks on ground surface, subsurface crashing of soil; rapid change of discharge, water level and sand content in pumping wells; animals appearing terrified anomalously; and so on. For areas of important construction, it may be useful to telescope benchmarks to get warning of collapse for protection of people (Fig. 1).

REMEDIATION OF SINKHOLE COLLAPSE

Once the collapse occurs, it is necessary to promptly take appropriate remedial measures, based on detection of collapse origin and the possibility of its further development. Remedial measures should primarily affect three factors (water, soil and karst openings) related to collapse: blocking up or reducing groundwater flow, consolidating loose overburden or fill in soil cavities, and filling in karst openings. Specific methods include the following.

Backfilling

This is a most common method. When a sinkhole pit exposes bedrock, it may first be filled with blocks, rubble and sand to form an inverted filter on the bottom of the pit, or backfilled by explosion of the bedrock, then overlain by clayey material and rammed. To improve the strength of the

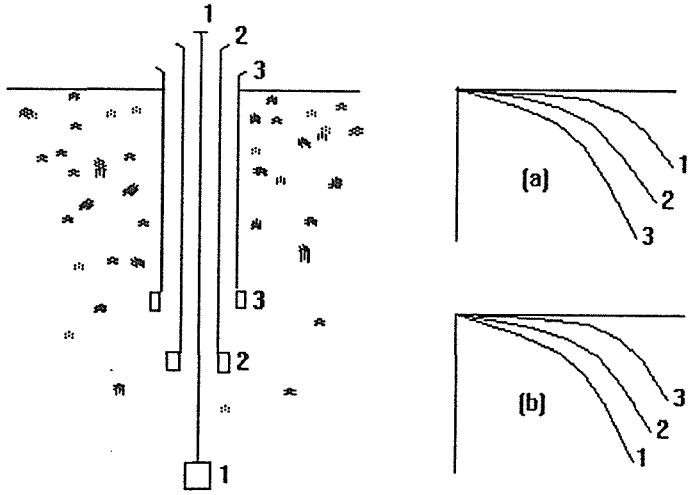

FIG. 1 Telescopic benchmarks give early warning of the development of a doline or a sinkhole. (a) movement rates for compaction conditions as in doline development; (b) movement rates for arching condition as in sinkhole development (Jennings, 1966).

backfill, cement paste may be added to consolidate the filling material while the pit is being filled (Fig. 2). If the pit does not expose bedrock, it may be simply rammed with clay.

Spanning

This method is useful for bigger and deeper collapse pits or cavities which cannot be easily backfilled. The loads above

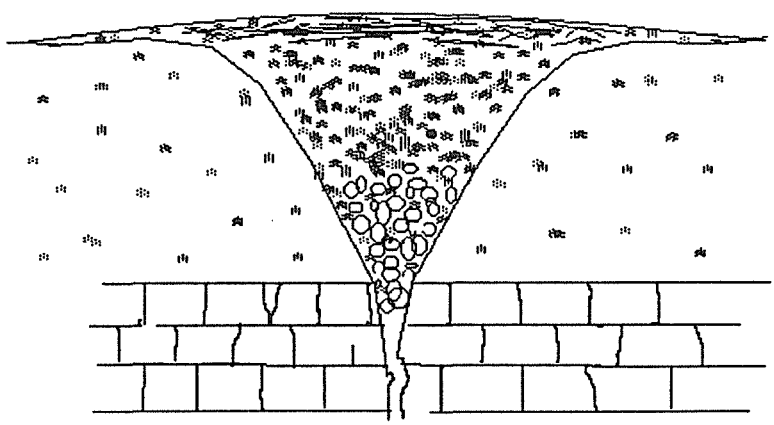

FIG. 2 Filling sink with graded filter fill (George, 1984).

the collapse or cavity can be transmitted to dependable soil or rocks by the firm, stable spanning structure. Spans of concrete beam, slab, arch or bridge are commonly used (Fig. 3).

Forced ram

This method involves use of a 10- to 40-ton ram lifted 10-40 m high and then dropped to generate a strong impact (6-80 tons per meter) on the soil. It can compact the soil layer and reinforce the foundation; on the other hand, it may also lead to discovery of soil cavities and weak zones (Fig. 4).

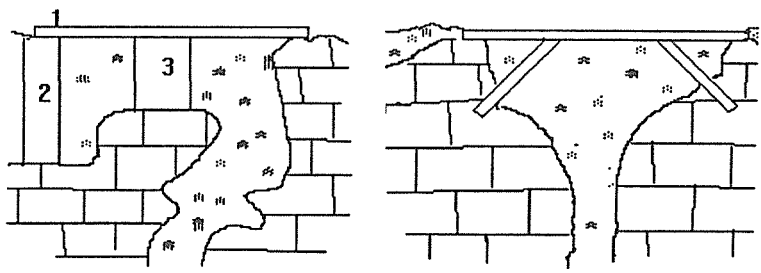

FIG. 3 Spanning methods. 1.simple beam; 2.deep converted caisson; 3.pier-type foundation.

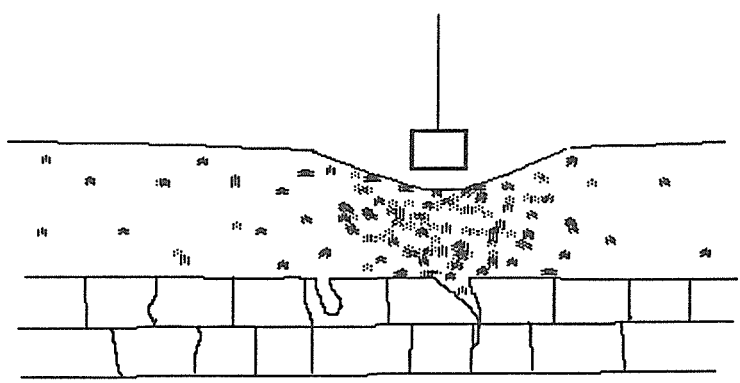

FIG. 4 Impact collapsing soil domes (George, 1984)

Grouting

This method can be used to consolidate soil layers or the fillings of cavities, fill caves or openings, intercept groundwater flow, and reinforce building foundations. Grouting material is commonly cement paste with added sodium silicate or fine aggregates.

Reinforcement of deep foundations

Building foundations may be set on deep bedrock by steel piles, reinforced concrete-perfused piles, driven piles, shafts, caissons, spiral spray piles, and pier-type foundations (Fig. 5).

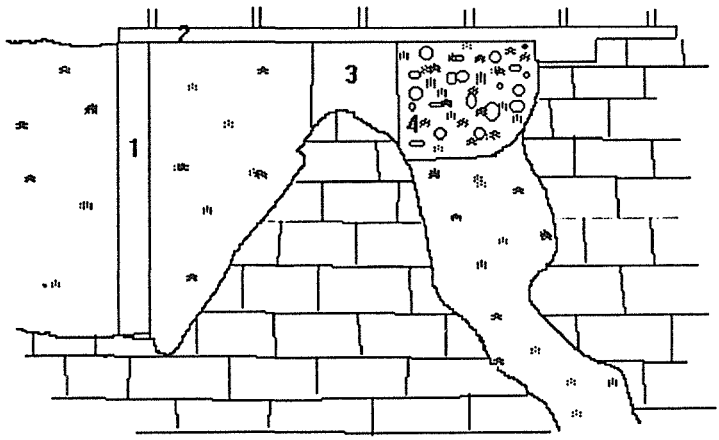

FIG. 5 Procedure of karst foundation of Liu Panshui cinema, Guizhou province. 1.converted caisson; 2.concrete beam; 3.pier-type foundation; 4.backfill concrete.

Remedial measures for surface water

Collapse pits often become inlets for surface water; thus, it is necessary to dredge and drain surface water away from the collapse area. In flooding areas, collapse pits should be surrounded with a dike or backfilled and rammed as soon as possible. When collapse occurs near or in the riverbed, pits may be backfilled if minor; otherwise, changing the course of the river should be considered, based on local geological conditions. In addition, thinner overburden in the bottom of the riverbed can be cleaned and paved with impermeable material to prevent leakage collapse sinkholes.

Adjustment of underground atmospheric and hydraulic pressure

Ventilation and decompression may be used to eliminate the influence of atmospheric and hydraulic pressure. A ventilating drill hole penetrating into karst caves or openings in bedrock can be used to prevent collapse caused by high pressure or subatmospheric pressure resulting from rapid fluctuations of groundwater level.

ACKNOWLEDGEMENTS Authors would like to thank Professor Yuan Daoxiang for his helpful advice, and thank Toni Trees for correcting the English and typing the manuscript.

REFERENCES

Aley, T. J. (1972) Ground water contamination and sinkhole collapse induced by leaky impoundments in soluble rock terrain. Missouri Geological Survey and Water Resources, Engineering Geological Series, No.5.

Chen, J. (1988) Karst collapse in cities and mining areas, China. Environmental Geology and Water Sciences, Spring-Verlag,Inc., New York, Vol. 12, No. 1, 29-35.

Foose, R. M., and others (1979) Engineering geological approaches to foundations in the karst terrain of the Hershey Valley. Bull. of the Association of Engineering Geologists, Vol.16 No.3, 355-381.

Jennings, J. E. (1966) Building on dolomites in the Transval. Transactions of the South African Institution of Civil Engineers, Vol.8, No.2, 41-62.

Sinclair, W. C.(1982) Sinkhole development resulting from ground water withdrawal in the Tampa area, Florida. U.S. Geological Survey, Water Resources Investigation Report 81-50, 1-24.

Sowers, G. F. (1975) Failures of limestones in humid subtopics. Civil Engineering, ASCE, Vol.101, 771-787.

Sowers, G. F. (1984) Correction and protection in limestone terrain. Sinkholes--Their geology, engineering and environmental impact, A. A. Balkema Publishers, 373-378.

Sweeting, M. M. (1973) Karst landforms. New York, Columbia Press.

Tan, J. & Chen, J. (1987) Preliminary study of karst collapse on forecast method. Endins, Spain, No. 13, 99-104.

Xiang, S., Chen, J. & Qing, Y. (1988) Evaluation and prediction of karst collapse--as exemplified by the Daguangshan iron mine. Proceedings of the IAH 21st Congress, China Geological Publishing House, Vol. 2, 1169-1177.

Xiang, S. & Chen, J. (1987) Karst collapse induced by pumping and draining ground-water, its forming conditions and factors affecting. Proceedings of the International Symposium on Human Influence in Karst, 65-75.

Xiang, S., Kan, Y., Lui, Z., Xie, D. & Chen, J., et al. (1986) Karst collapse in Yangtze River basin. Carsologica Sinica,Vol. 5, No. 4, 255-277.

Land Subsidence (Proceedings of the Fourth International Symposium on Land Subsidence, May 1991). IAHS Publ. no. 200, 1991.

Sinkhole Evolution in Alluvial Deposits within the Central Ebro Basin, Northeast Spain

G. BENITO
Department of Geosciences, University of Arizona, Tucson, Arizona 85721, USA
P. PEREZ DEL CAMPO
Dirección de Coordinación e Inversiones (RENFE), Avda. Ciudad de Barcelona 4, 28007 Madrid, Spain

ABSTRACT We have used aerial photo analysis and geophysical data to study the evolution of sinkholes developed on alluvial deposits covering Tertiary gypsum. This data can be interpreted as indicating different mechanisms by which sinkholes form. Negative gravity anomalies reflect the movement of alluvial particles into deeper subsurface caves. Ground penetrating radar (GPR) anomalies may indicate formation of caves in the alluvial material which can later create sinkholes by collapse and compaction.

INTRODUCTION

In recent years, the environmental and engineering impact of sinkhole collapses has been subject to increased attention in the geomorphological, hydrological and engineering literature (Beck, 1984, Beck & Wilson, 1987 and Waltham, 1989). Most of these studies have dealt with collapses produced in carbonate rocks. However, little analysis has been performed for on karst processes in evaporitic rocks such as gypsum, which is dissolved in flowing water at rates about 100 times faster than limestone. Previous studies of sinkhole development in gypsum areas have primarily emphasized Permo-Triasic rocks (Nicod, 1976 and Cooper, 1986), where the subsidence is strongly controlled by folds, faults and joints. Few studies deal with sinkhole development in areas with subhorizontal gypsum formations.

The processes facilitating sinkhole development in gypsum areas are cavity formation and collapse (similar to processes in limestone karst areas) as well as gradual downward movement and piping of overlying materials. Solution rates of gypsum rocks can range from 0.01 m per annun (Sweeting, 1966) to 1.7 m per annum in extreme conditions (James & Lupton, 1981). The resulting subsidence from all of these processes can cause significant environmental impact on high density

population areas. Studies of mechanisms inducing sinkhole development are needed to predict unstable areas and to develop remedial strategies. This study deals with the genetic processes and evolutionary stages of sinkhole formation and their detection. In order to do that, surface analyses using a time series of aerial photographs as well as geophysical surveys have been carried out.

THE STUDY AREA

The study area is in the central sector of the Ebro Basin (NE-Spain), few kilometers north of the city of Zaragoza (700,000 inhabitants). The research was performed along 20 kilometers of the railroad right-of-way between Zaragoza and Barcelona (Fig. 1). The railroad runs north from Zaragoza along the Gállego River valley, which is a tributary of the Ebro River. The climate is continental mediterranean with semiarid characteristics. The average annual rainfall is 322 mm and the average monthly temperature range between 24.2°C in July and 5.8°C in January.

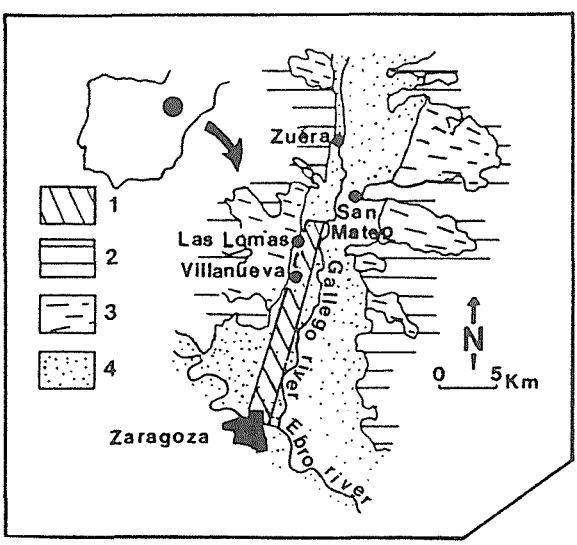

FIG. 1 Location of the railroad right-of-way Zaragoza-Barcelona. 1: Study area. 2: Tertiary rocks. 3: Quaternary pediments. 4: Quaternary terraces.

The Ebro Basin is filled with horizontally-bedded continental Miocene sediments. Within this stratigraphy, there is a thick formation of evaporites (primarily gypsum and halite) with interbedded marl layers. Quaternary terraces and pedimentation levels have formed

in response to episodic downcutting of the Ebro River and its tributaries into the Tertiary evaporite formation. These fluvial systems have deposited layers of alluvial materials on top of the evaporites. The alluvial deposits are comprised of gravel and sand with interstratified clays and silts. In the study area, the dissolution of the Tertiary evaporites by the Gallego River during the Pleistocene has resulted in a thickness increase from 4m to 110m in the overlying alluvial deposits over 15 kilometers (Benito & Pérez González, 1990).

The railroad right-of-way between Zaragoza-Barcelona is set on a Late Pleistocene terrace 12 m above the Gállego River. The alluvial materials of this terrace are about 4 m thick and overlie 35-80 m of Early Pleistocene alluvium deposited by the Gállego River. The Early Pleistocene deposits are fractured and folded in response to old sinkhole collapses and diapiric movements (Benito & Casas, 1987).

Presently, solution processes are producing extensive areas of dolines on the alluvial cover (Gutiérrez et al. 1985; and Benito 1987) which are an important environmental impact both on the agriculture and on civil engineering works on the Zaragoza outskirts (Benito & Gutiérrez, 1988; Pérez del Campo & Lanzarote, 1988; Soriano, 1988; and Pérez del Campo 1989). The occurrence of sinkholes has increased during the last 30 years due to human activities such as irrigation areas and excessive groundwater withdrawal. The resulting problems include cracks in buildings, road subsidence and damage of irrigation channels. Despite the local importance of subsidence, processes and evolutionary stages associated ground subsidence are poorly understood.

METHODS

For this study, both surface and subsurface analyses were performed to detect and evaluate the genetic processes and the evolutionary stages of sinkhole formation. The spatial and temporal sequence of surface sinkhole development was analyzed with a series of aerial photographs taken in 1928, 1957 and 1985. Geophysical studies were carried out in 1987 within a project of building a new railroad right-of-way for a high speed train between Madrid and Barcelona. The aim of these analyses were to detect subsurface caves along the railroad right-of-way in the Zaragoza area that were in danger of collapsing. The geophysical data were obtained from gravimetric studies and ground penetrating radar (GPR). These methods were chosen because data from seismic refraction and electrical logs surveys obtained in 1986 could not be confidently used in the location of subsurface caves.

The gravimetric survey was performed in order to detect negative anomalies caused by subsurface density

contrasts, especially those resulting from caves and pipes. In this study, a Lacoste-Romber gravimeter with 0.01 mGal precision was used. Measurements were taken at 150-200 meter intervals and the results were drawn on large-scale topographic maps.

The ground penetrating radar emits high electromagnetic frequecy waves that are reflected from subsurface interfaces and discontinuities in response to contrasting dielectric properties. For this study, the data were obtained from a GPR using the OYO Corporation system. The instrument was composed of 250 Mz transmitting-receiving antennas, a control unit and a graphic recorder. The antennas are pulled along the ground surface and record profiles 55 m in length. The reflected waves are processed by the control unit and printer by the graphic recorder. Resolution of the subsurface discontinuities was achieved to depths of 2 to 5 m. Shallower effective penetration was recorded in wetter areas and in zones with ambient electrical noise. The instrument was first tested at locations of known natural pipes, water-supply pipes, and in areas of karst cavities in order to determine the signals associated with those features.

RESULTS

The gravimetric data obtained along 20 kilometers of the railroad right-of-way between Zaragoza and Barcelona (Fig.2) show five areas with negative anomalies that appear to be the result of heterogeneities within the alluvial cover. The gravity anomalies are located between kilometers 2.75-4, 6.15-7.4, 8.3-11, 14.45-15.5 and 18.8-19.8 with 2 mGal, 1.25 mGal, 0.5 mGal, 0.3 mGal and 0.8 mGal, respectively. GPR anomalies were found along 3,037 m (15% of the studied area)(Fig.2).

In Figure 2 the locations of dolines and depressions observed in the series of aerial photographs are indicated. The dominant forms are bowl-shaped with diffuse or sharp edges. The diffuse-edge dolines are the largest with diameters up to 20 m. Generally, dolines observed in the series photographs remain in the same position. However, some of the dolines apparently disappear and later reappear between photographs because local farmers fill them in.

From the results of the surface and subsurface studies the following cases can be established:

(1) Areas of observed sinkholes coincide with:
    (a) Gravity anomalies
    (b) GPR anomalies
    (c) Both gravity and GPR anomalies

(2) There are areas of dolines where neither gravity nor GPR anomalies have been detected.

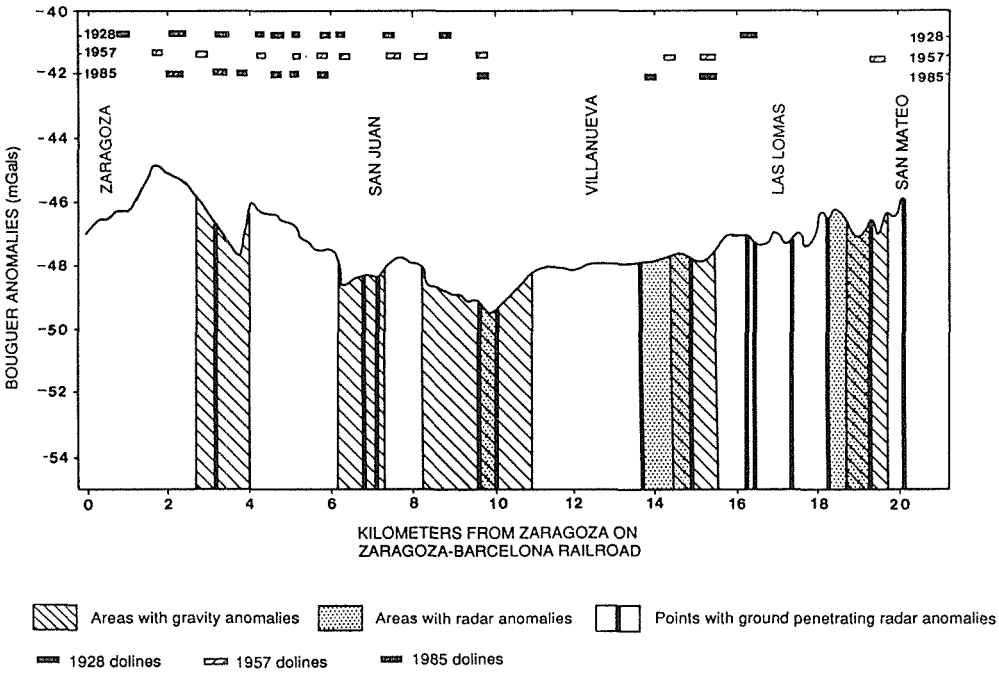

FIG. 2 Location of geophysical anomalies and sinkholes observed in 1928, 1957 and 1985 aerial photographs of the Zaragoza-Barcelona railroad.

The greatest concentration of dolines observed on the aerial photographs are in the first six kilometers of the right-of-way. However, their locations do not always correspond to areas of geophysical anomalies (Fig. 3). Gravity and GPR anomalies do coincide between kilometers 3.15-3.2 and 6.7-6.76. However, the lack of coincidence of observed dolines and geophysical anomalies along kilometers 2.200-5.900 may be explained by occurrence of noise and wet areas.

From kilometer 8, both gravity and GPR anomalies do always not match; nevertheless, there is a good correlation between geophysical anomalies and the development of dolines in the surface (Fig.2). The relationships between specific geophysical anomalies and subsidence areas can be interpreted as indicating different evolutionary stages and processes in the sinkhole formation. Geophysical data also provide information about subsidence as well as predict the growth and development of sinkholes areas.

INTERPRETATION

Ground subsidence on overlying alluvial materials can result from downwarping or collapse of an underground cavity. The main processes fostering sinkhole development

are: 1) cavity formation and collapse, 2) gradual downward by solution in the gypsum-alluvium interface and 3) piping of the overlying alluvial materials. The initial amount of space necessary to create a void is produced in the Tertiary bedrock by gypsum solution. Where alluvium overlies karst, the groundwater can erode and transport the loose alluvial material by mechanical subsurface erosion or piping. Two different processes for subsurface transport are envisioned; (1) through large pipes that originate in gypsum rock caves that may migrate into the alluvial cover by debris fall from walls, (2) debris particles can be washed down and transported through smaller voids and fractures producing subsidence by compaction.

In the study area, the solution processes cannot solely explain the collapse phenomena in the alluvium because of the large thickness of the Quaternary deposits (40-80 m). For producing surficial subsidence, the span of the caves is one of the most important factors (Stefanko, 1973; Ege 1984). The opening required to produce the roof collapse in a cavity depends on the thickness of the overlying material and the degree of consolidation and cementation. For sinkhole formation on the Gállego alluvial deposits, both evaporite solution and mechanical erosion in the debris need to be considered. The void created by solution in the gypsum formation migrates to the surface through the alluvium by piping processes. A condition is achieved where the stress exceeds the strength in the overlying alluvial deposits and the roof ruptures to produce a sinkhole on the surface. The creation of cavities by subsurface mechanical transportation of sediment have been indicated in few studies but this process may occur more frequently than has been recognized (Allen 1969; Ege 1984). In the study area, piping processes are confirmed by detecting caves and pipes by the ground penetrating radar surveys in the alluvial deposits.

The results of the surface and subsurface analyses can be interpreted as indicating different mechanisms of sinkhole formation (Fig.3). Subsurface density contrasts produced by small voids in the alluvial material are reflected as negative gravity anomalies. In some cases, these voids cannot be recorded by the ground penetrating radar because of their small size or their location in the Early Quaternary deposits at depths greater than 5 m from the surface. In this process, alluvial particles are moved down through small voids and cracks into deeper subsurface caves (Fig.3) resulting in a decreased alluvial density. Subsequent compaction of these alluvial deposits produces bowl-shaped dolines in the surface.

The cavities and voids created in the evaporites can migrate into the surface through the alluvial deposits as large pipes. In this case, gravity anomalies and ground penetrating radar anomalies should be detected where the voids are not further than 4-5 m from the surface. When

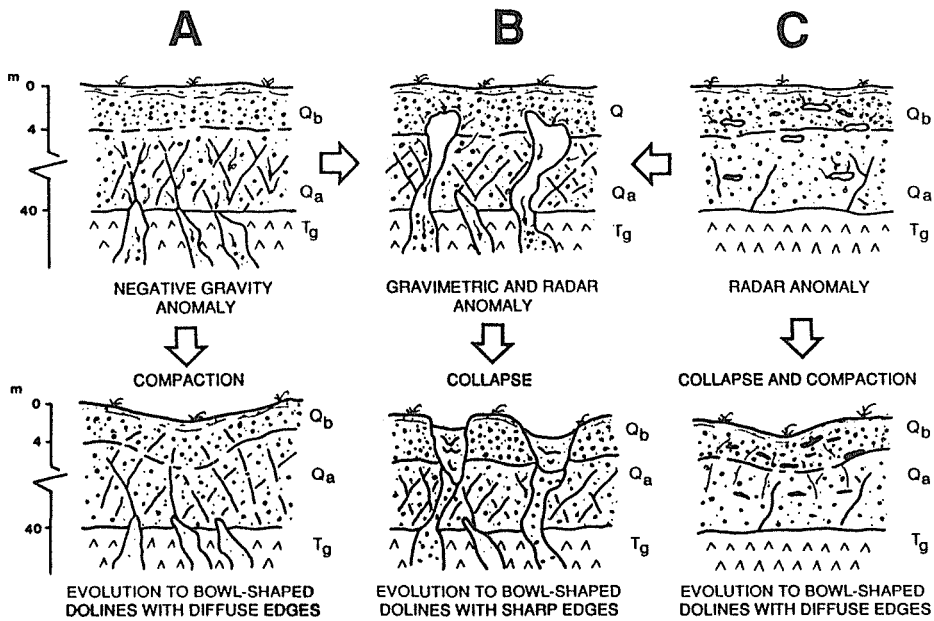

FIG. 3 Interpretation of sinkhole evolution from the aerial photography and geophysical data. T: Tertiary gypsum. Qa: Early Pleistocene deposits. Qb: Late Pleistocene deposits (Terrace + 20m).

recorded whereas gravity anomalies would not. Sinkhole development has been observed in these areas with ground penetrating radar. The sequence of processes in the sinkhole development is: gypsum solution, piping through the overlying alluvium, and then failure of the roof or alluvial compaction (Fig.3).

The areas that have sinkholes but are without geophysical anomalies cannot be easily explained. It is possible that subsequent to sinkhole formation the compaction closes voids.

Summarizing, the geophysical data may indicate three stages of sinkhole formation: 1) karst solution processes forming caves in the Tertiary gypsum formation, 2) subsurface mechanical erosion of the detritical cover (piping) and 3) the compaction or collapse of the caves and pipes in the alluvial deposits (Fig.3). Subsurface mechanical erosion can produce either the migration of caves originating in the gypsum bedrock into the alluvial surface or density reduction by transporting detritus particles through small voids, cracks and pipes.

These preliminary ideas as to the different mechanisms of sinkhole formation can be inferred from the the stress on the overlying alluvium becomes large enough, the roof may fail catastrophically. If the size of the subsurface cavity is large enough, the rupture may

occur along concentric planes resulting in bowl-shaped dolines with sharp edges (Fig.3). For the case of less catastrophic failures, slow downwarping may result. This type of failure probably occurs along a series of stages in which surface concentric cracks appear and bowl-shaped dolines with diffuse edges are formed.

In certain instances, near surface voids may be too small to yield detectable gravity anomalies. Also, because gravimetry is a vertical measurement, pipes connected horizontally with cavities may not be detected by the gravimeter. In these cases, GPR anomalies may be results of surface and subsurface studies. Nevertheless, new geomorphological and geophysical tools should continue to be applied in order to further develop and test sinkhole evolution models.

ACKNOWLEDGEMENTS The authors are very grateful to Dr. J.E. O'Connor (University of Arizona) for reviews of the manuscript and useful suggestions.

REFERENCES

Allen, A.S. (1969) Geologic settings of subsidence. In: D.J. Varnes and G. Kiersch (Eds.). Reviews in engineering geology 2, Geological Society of America, 305-342.

Beck, B. F. (Ed.) (1984) Sinkholes: Their Geology, Engineering & environmental impact. Proceedings of the first multidisciplinary conference on sinkholes, Orlando, Florida. A.A. Balkema, Rotterdam.

Beck, B. F. & Wilson, W.L. (Eds.) (1987) Karst Hydrogeology: Engineering & Environmental applications. Proceedings of the second multidisciplinary conference on sinkholes and the environmental impacts of karst, Orlando, Florida. A.A. Balkema, Rotterdam.

Benito, G. (1987) Karstificación y colapsos kársticos en los yesos del sector central de la Depresión del Ebro (Aragón, España). Cuaternario y Geomorfología 1, (1-4), 61-76.

Benito, G. and Casas, A.M. (1987) Small-scale deformations in Quaternary deposits in the northeastern Iberian Peninsula. Géologie Méditerranéenne 15, (4), 233-243.

Benito, G. and Gutiérrez, M. (1988) Karst in gysum and its environmental impact on the Middle Ebro Basin, Spain. Environ. Geol. Water Sci. 12, (2), 107-111.

Benito, G. and Pérez González, A. (1990) Modelo de respuesta compleja de las terrazas del río Gállego en el tramo Zuera-Zaragoza. I Reunión Nacional en Geomorfología. Teruel (in press).

Cooper, A.H.(1986) Subsidence and foundering of strata

caused by the dissolution of Permian gypsum in the Ripon and Bedale areas, North Yorkshire. In: G.M. Harwood & D.B. Smith (Eds.), The English Zechstein and related topics. Geological Society Special Publication 22, 127-139.

Ege, J.R. (1984) Mechanisms of surface subsidence resulting from solution extraction of salt. In: T.L. Holzer (Ed.) Man-induced land subsidence, Geological Society of America. Reviews in Engineering Geology 6, 203-221.

Gutiérrez, M., Ibáñez, M.J., Peña, J.L., Rodríguez, J. and Soriano, M.A. (1985) Quelques exemples de karst sur gypse dans la dépression de l'Ebre. Karstologia 6, (2), 29-36.

James, A.N. and Lupton, A.R.R. (1978) Gypsum and anhydrite in foundations of hydraulic structures. Geotechnique 28, 249-272, London.

Nicod, J. (1976) karst des gypses et des evaporites associées. Ann. de Géog. 471, 513-554.

Pérez del Campo, P. and Lanzarote, A. (1988) La problemática de los colapsos kársticos en las infraestructura de la Depresión del Ebro. Congreso Geológico de España 1988. Comunicaciones 2, 333-336.

Pérez del Campo, P. (1989) Nuevos datos sobre los colapsos kársticos en la Depresión del Ebro. Detección e incidencia en la nueva línea de alta velocidad Madrid-Barcelona. Segunda Reunión sobre el Cuaternario Ibérico. ITGE, 10p. (in press).

Soriano, M.A. (1988) Dolinas aluviales y su impacto ambiental en las proximidades de Zaragoza. Congreso Geológico de España 1988. Comunicaciones 2, 495-498.

Stefanko, R. (1973) Roof and ground control-subsidence and ground movement. In: A.B. Cummins and I.A. Given (Eds.). SAME mining engineering handbook. Society of Mining Engineers of American Institute of Mining, Metallurgical, and Petroleum Engineers 2, sec.13, 2-9.

Sweeting, M.M. (1966) The weathering of limestones, with particular reference to the Carboniferous Limestone of northern England. In: G.H. Dury (Ed.) Essays in Geomorphology, Heinemann, London.

Waltham, A.C. (1989) Ground subsidence. Blackie & Son, London.

Land Subsidence (Proceedings of the Fourth International Symposium on Land Subsidence, May 1991). IAHS Publ. no. 200, 1991.

Sand Drain Induced Subsidence of a Peat

E. GREGORY McNULTY
Fuller, Mossbarger, Scott and May, Civil Engineers, Inc., Lexington, Kentucky, U.S.A.

ABSTRACT Several investigators have suggested that sand drains cannot accelerate the consolidation of peat because of the predominance of creep effects. In addition, some have claimed that radial decreases in hydraulic conductivity due to increases in effective stress will greatly retard consolidation with sand drains. The author compares predictions from a nonlinear, large-strain finite element analysis with field measurements. This paper shows that accounting for field disturbance caused by construction activities correctly predicts field settlements. In addition, these analyses show that ignoring a radial variation in properties results in a small error in predicted rates of settlement.

INTRODUCTION

Several investigators such as Lake (1961 and 1963) and Casagrande & Poulos (1969) have concluded that sand drains fail to accelerate the settlements of a peat deposit. In particular, Lake (1961) concluded that drainage distance had no effect on the rate of settlement. This conclusion implies that creep, not dissipation of excess pore pressures, controls the subsidence of peats. In addition, Barron (1978) postulated that radial changes in hydraulic conductivity due to changes in effective stress would greatly affect sand drain performance. This paper shows that dissipation of excess pore pressures controls the subsidence of a peat when one accounts for field disturbance caused by construction activities. Furthermore, this paper shows that radial decreases in the hydraulic conductivity near the sand drains only slow the rate of settlement slightly. The following sections discuss a case history involving detailed field measurements, comprehensive laboratory testing, and analysis by a finite element code.

FIELD MEASUREMENTS

In 1974, the widening of the Eastern New Hampshire Turnpike of I-95 provided an excellent opportunity to investigate the efficacy of drains in peat. Construction included about 244 m (800 ft.) of roadway built through a tidal marsh of peats, organic silts, and clays near Hampton-Hampton Falls in the area of Taylor River. The site consisted mostly of tidal marsh whose ground elevation ranged from about -1m (msl) in the tidal backwater to 1.5m (msl) to the toe of the existing embankment. Before placement of pavement, construction of high embankments of about 5m served as surcharge with sand drains to accelerate settlements. To avoid slope stability failures of the embankment during construction, the New Hampshire Department of Public Works and Highways installed settlement platforms, piezometers, slope indicators and alignment stakes.

The most critical section involved soils between Stations 5913 m (194+00 ft) and 5944 m (195+00 ft). Figure 1 gives an approximate profile view of the soil stratigraphy and the final embankment at Station 5928 m (194+50 ft). Table 1 summarizes the subsurface stratigraphy before start of construction.

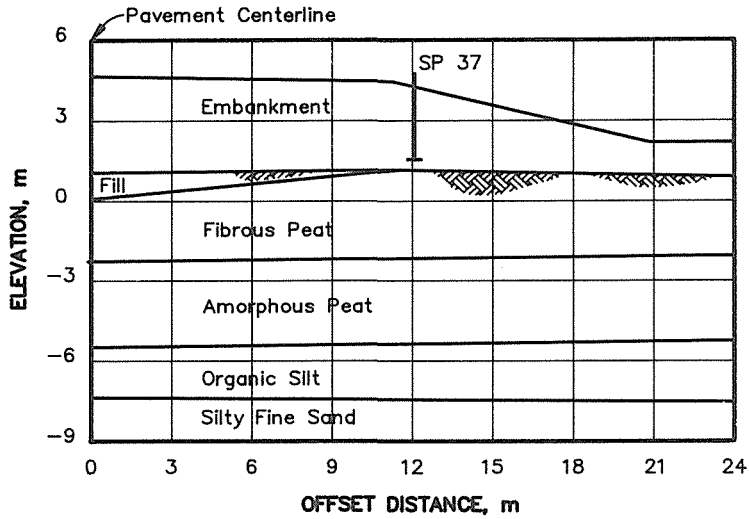

FIG. 1 Profile view of embankment and underlying stratigraphy near Station 5928 m (194 + 50 ft) at Taylor River.

TABLE 1 Subsurface stratigraphy before start of construction.

Layer	Soil	Thickness m	Total Unit Weight kN m^{-3}
1	Fibrous Peat	2.9	102.1
2	Amorphous Peat	3.4	103.7
3	Organic Silt	1.7	142.9
4	Sand	----	------

Because of the gradual transition from one peat to another, uncertainty exists in the layer thicknesses shown in Figure 1. Unpublished analyses subsequent to those given by McNulty (1982) suggest that the numerical solution has only a small sensitivity to the individual peat layer thicknesses.

Figure 1 shows the cross-section at the location of Settlement Platform (SP) 37 where readings started on June 22, 1974. Subsequent discussion will refer to June 22, 1974 as Construction Day 22. A slope inclinometer at R29.1m (R95.5 ft) and alignment stakes at R48.8m (R160 ft) allowed measurement of horizontal movements during construction of the embankment. Construction of a layer of clean sand started at Day 20 to serve as a drainage layer for the sand drains. Recker (1982) observed mud waves as bulldozers pushed the sand into place. By Day 46, lateral movements about 2.1m (7 ft) and ultimately reaches 2.4m (8 ft) shortly after installation of sand drains around Day 50. A jetting tool installed the sand drains into 7.9m (26 ft) of compressible soil. Each drain had a radius of 0.15m (0.5 ft) in a triangular pattern with a 1.2m (4 ft) spacing. The water table lay at the original ground surface. Throughout construction of the 5m high embankment, the alignment stakes showed no further lateral movements.

Installation of slope inclinometers at Day 90 resulted in no slope inclinometer data during movement of the alignment stakes. Nevertheless, the settlements observed at SP 37 probably relate directly to the mass movements induced by the placement of the sand blanket by the bulldozers. Analyses to be discussed later in this paper suggest that observed settlements occurred at stresses too low to be associated with subsidence due to dewatering or dissipation of pore pressures during consolidation.

Construction of the main embankment started on Day 87 and continued until Day 157 when the elevation reached about 5 m. At Day 340, bulldozers cut the embankment back to an elevation of about 3.8 m for construction of the pavement.

LABORATORY DATA

Laboratory data included index tests, incremental and radial inflow consolidation tests. Table 2 (adapted from McNulty, 1982) summarizes ranges in index properties for the compressible soils.

TABLE 2 Soil properties.

Soil Type	Total Unit Weight kN m-3	Natural Water Content %	Liquid Limit %	Plastic Limit %
Fibrous Peat	92.7 - 113	200 - 875	325 - 650	100 - 375
Amorphous Peat	102 - 121	125 - 375	150 - 300	50 - 150
Organic Silt	132 - 157	45 - 175	45 - 135	30 - 60

While Table 2 gives high natural water contents and Atterberg limits, Casagrande & Poulos (1969) and Murray (1971) have found similarly high values.

Haley & Aldrich (1974) performed 21 conventional, incremental tests on 6.35 cm (2.5 in) diameter by 1.9 cm to 2.54 cm (0.75 to 1.00 in) thick undisturbed specimens taken from 7.62 cm (3 in) Shelby tubes. Trautwein (1980) performed 3 inflow radial and 2 vertical flow tests on undisturbed specimens of fibrous peat taken from 7.62 cm (3 in) Shelby tubes. Trautwein (1980) used free strain theory to reduce data for the radial inflow tests. No completely remolded specimens underwent laboratory tests.

Figure 2 gives the consolidation coefficients for the fibrous peat. Figure 2 shows that the radial coefficients typically exceeded the vertical by about factor of 10. Space limitations prevent the showing of the vertical consolidation coefficients for the amorphous peat and organic silt. McNulty (1982, Figure 7.4b and c) gives these data and recommends using the upper range of the scatter bands. Because the fibrous peat had C_r/C_v ratio equal to 10, it was assumed that C_r/C_v also equaled 10 for the amorphous peat and organic silt.

Figure 3 gives the ranges in stress-strain behavior for the peats and organic silt. As the next section will discuss, calibration of predicted against observed settlements yielded the disturbed curves.

In a finite element analysis involving layered systems one must convert the consolidation coefficients to the fundamental parameters of hydraulic conductivity, k, and specific storage, S_s. The vertical coefficient of consolidation C_v equals $k/(\gamma'_w m_v) = k/S_s$, where m_v equals the soil compressibility and γ'_w equals the unit weight of water. The use of consolidation coefficients to satisfy continuity of flow between soils of different compressibilities results in an incorrect ratio in the hydraulic gradients at the layer interfaces (McNulty, 1982, Pg. 40). Instead, one can calculate the compressibility, m_v, from the stress-strain curves in Figure 3. Then one calculates the hydraulic conductivity as a function of vertical strain from the corresponding consolidation

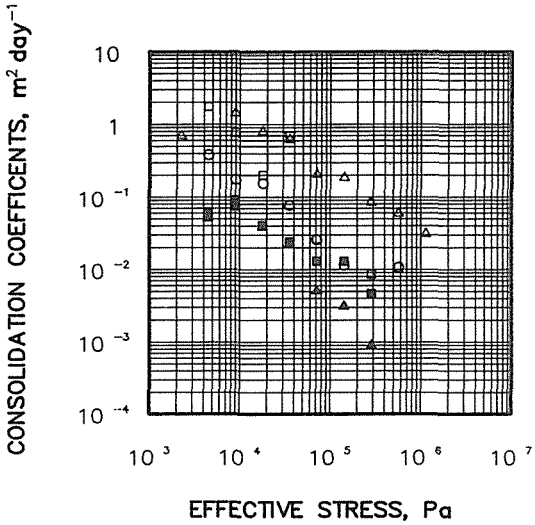

FIG. 2 Consolidation coefficients for fibrous peat: radial (open symbols) and vertical (solid symbols).

coefficients. A regression fit of the resultant k versus strain data with a low degree polynomial allows transformation of k to a function of effective stress. Mapping of strains to the stress-strain curves transforms k to a function of effective stress. Given the new smoothed relationship of k with effective stress, one can then calculate specific storage from k and C_V: $S_S = k/C_V$. Figure 4 shows the variation of hydraulic conductivity and specific storage with effective stress for the fibrous peat. Note that the hydraulic conductivity decreases smoothly as the effective stress increases. In contrast, the specific storage shows radical changes with effective stress. Typically, S_S will increase an order of magnitude or more as the effective stress exceeds the preconsolidation stress.

TIME-SETTLEMENT ANALYSES

The code SUBFE, an extension of the one developed originally by McNulty (1982), predicted settlements versus times at SP 37 using laboratory and calibrated (backed-in) soil properties. The code allows nonlinear variations in the specific storage and hydraulic conductivity through input of the coefficients of consolidation and hydraulic conductivity with effective stress. Finite element shape functions interpolate the state variable excess pore pressure at each gauss point from the element nodes. SUBFE assigns different soil properties to each gauss point to allow a pointwise radial and vertical variation of hydraulic properties with effective stress. An Updated Langrangian formulation (Belytschko, 1983) continuously adjusts the finite element mesh to account for large one-dimensional vertical strains calculated with small strain incremental theory. In addition, the code represents any external loadings as equivalent fill elevation with time. Furthermore, SUBFE accounts for settlement dependent submergence effects on applied load due to changes in the elevation of the water table. The code allows for changes in boundary conditions at any time, including the installation of sand drains or recovery wells at any time. McNulty (1982, Chapter 5) has verified this code with closed-form solutions, a nonlinear finite difference algorithm, and published results for a nonlinear, large-strain theory. McNulty (1982, Chapter 5) has also partially validated the code with independent experimental data from a large-strain consolidation test.

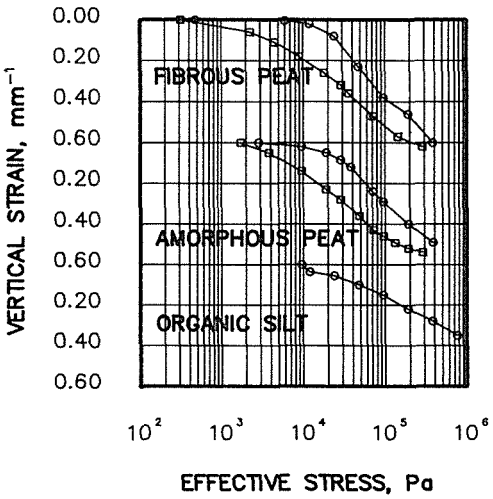

FIG. 3 Ranges in stress-strain curves for laboratory tests where upper curves (open circles) represent undisturbed and lower curves (open squares) represent disturbed soils.

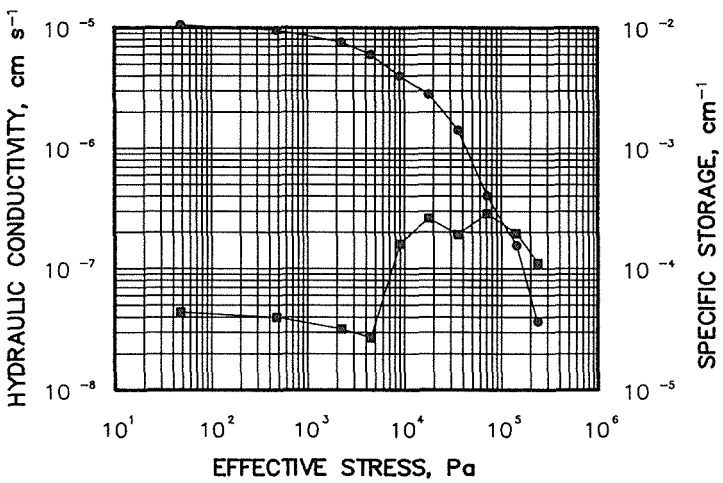

FIG. 4 Variation of hydraulic conductivity (solid circles) and specific storage (solid squares) of fibrous peat with effective stress.

Analyses with Laboratory Soil Properties

Figure 5 compares the measured settlement with those from finite element analyses based on "undisturbed" laboratory properties for cases of no drains and drains installed. Sand drains appear to have substantially reduced the consolidation times. However, predicted settlements with drains underpredicted the rate of settlement before drain installation and overpredicted the rate of settlement after drain installation. Before installation of the sand drains, measured settlements occurred at stresses too low to be associated with subsidence due to dewatering. In addition, the alignment stake data strongly suggest that mass flow caused these movements. Consequently, predicted initial settlements should include settlements caused by mass flow to

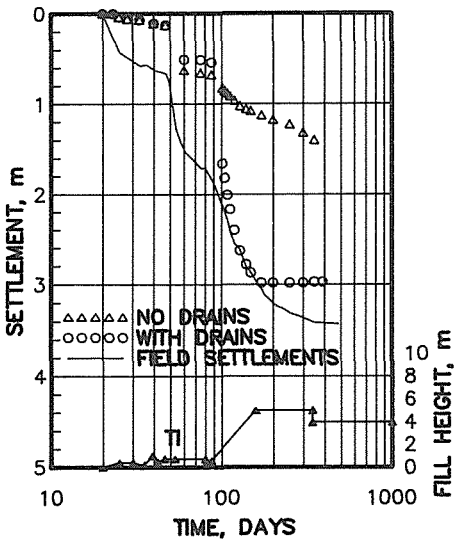

FIG. 5 Finite element prediction based on "undisturbed"laboratory properties assuming no drains installed (open triangles), drains installed at day 50 (open circles), and measured field settlements (curve without symbols).

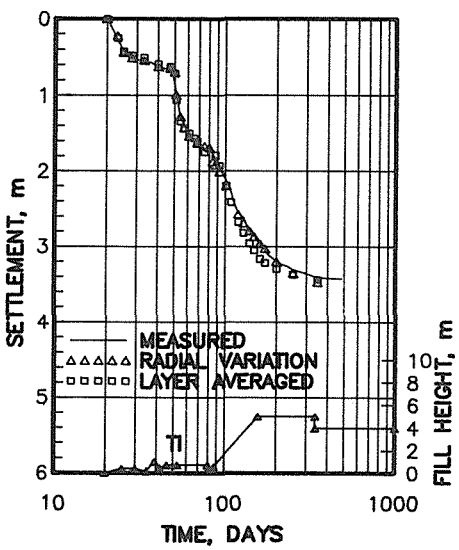

FIG. 6 Finite element predictions based on "calibrated" (or backed-in) properties with radial variations of soil properties (open triangles) and averaged layer properties (open squares) as compared to measured field settlements.

allow proper consideration of settlements caused by subsidence due to dewatering or consolidation due to dissipation of excess pore water pressures.

However, even without adjusting the predicted settlements for mass movements, Figure 5 shows that the predicted settlement rates exceed the measured rates after drain installation. Disturbance caused by mass movements and jetting of the sand drains may explain the slower than predicted time rate of settlement in the field. Because of such disturbance, the soils in the

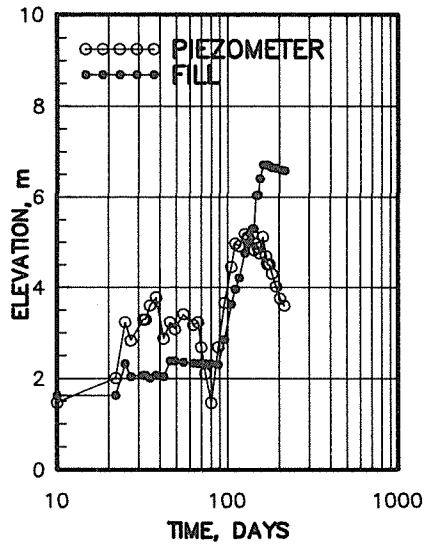

FIG. 7 Comparison of measured piezometric response to applied fill load with time.

field probably incurred corresponding reductions in the hydraulic conductivity. Therefore, the hydraulic properties measured in the laboratory probably exceed those controlling settlement in the field.

Analyses with Calibrated Soil Properties

Trial and error adjustment of soil properties can produce calibrated soil properties that can predict measured settlements. Because the number of unknowns exceeds the knowns in our problem, this inverse formulation will not yield a unique solution. However, such calibrated data can confirm the physical effects of soil disturbance in the field. Figure 2 gives the disturbed stress-strain curves derived for the peat materials used in the final calibration analyses. McNulty (1982, Figures 7.8 and 7.9) gives the related data on hydraulic conductivity and specific storage. Figure 6 shows the finite element predictions based on "calibrated" or "backed-in" soil properties for two cases: one with radial variation of properties and another with soil properties averaged over the entire layer. Note that the settlements predicted before drain installation now include those associated with mass flow. Figure 6 shows that the prediction using a radial variation of properties closely matches measured settlements after sand drain installation. This close agreement among predicted and measured settlements in a peat deposit strongly suggests that dewatering caused by consolidation of peat controls the observed settlement. This result strongly contradicts the earlier conclusions drawn by Lake (1961), Lake (1963), and Casagrande & Poulos (1969). Furthermore, Figure 7 confirms that fill construction generated piezometric heads directly correspond to the applied fill loads. Finally, Figure 6 shows only a slight increase in rate of predicted settlements with time for the case using soil properties averaged over an entire layer. These data suggest that ignoring the radial variation of properties in a sand drain analyses introduces only a small error.

ACKNOWLEDGEMENTS The National Science Foundation supported this research through Grant CME-7918195. Also, the New Hampshire Department of Public Works and the firm of Haley & Aldrich, Inc., provided some of the necessary data. Eric Schieve at the University of Texas performed the radial flow laboratory tests. J.T. Collins and S.J. Trautwein of the University of Texas performed the field sampling.

REFERENCES

Barron, R. A. (1978) Discussion of "Analytical Solutions of Sand Drain Problems." J. Geotech. Engng. Div. ASCE 104, 1330.

Belytschko, T. (1983) An overview of semidiscretization and time integration procedures. Computational Methods for Transient Analysis, 37. Edited by T. Belytschko and T.J.R. Hughes, Elsevier Science Publishers B.V.

Casagrande, L.F. & Poulos, S.J. (1969) On effectiveness of sand drains. Can. Geotech. J. 6 (3), 287-326.

Haley & Aldrich (1974) Report on laboratory results on undisturbed soil samples Eastern New Hampshire Turnpike, I-95 Taylor River crossing Hampton-Hampton Falls, New Hampshire. New Hampshire Department of Public Works.

Lake, J.R. (1961) Pore-pressure and settlement measurements during small scale laboratory experiments to determine the effectiveness of sand drains in peat. In: Conf. on Pore Pressure and Suction in Soils (Proc. London Symp., 1961), 103-107.

Lake, J.R. (1963) A full-scale experiment to determine the effectiveness of vertical sand drains in peat under a road embankment in Dunbartonshire, Scotland. (Proc. European Conf. on SMFE), vol. 1, 351-356.

McNulty, E.G. (1982) Consolidation with axisymmetric flow in soils having radial and vertical variation of properties. Dissertation - The University of Texas at Austin.

Murray, R.T. (1971) Embankments constructed on Soft Foundations: Settlement study at Avonmouth. Rd. Res. Lab., Rp LR 419.

Recker, K.L (1982) Personal Communication, Haley & Aldrich Inc.

Rendulic, L. (1935) Der hydrodyamische spannungsausgleich in zentral entwasserten tanzylindern Wasserwritschaft and Technik, Wein, vol. 2, 250-253.

Terzaghi, K. (1923), Die berechnung der durchlassigkeitsziffer des tones aus dem verlauf der hydrodynamischen spannungserscheinungen, Sitz, Akademie de Wissenschaffen in Wein, part iiA, vol. 132, Vienna, Austria, 125-138.

Trautwein, S.J. (1980) Practical measurement of radial flow consolidation properties of clays. M.S. thesis, The University of Texas at Austin.

Land Subsidence (Proceedings of the Fourth International Symposium on Land Subsidence, May 1991). IAHS Publ. no. 200, 1991.

Active Subsidence Controlled by Basement Structures in the Marañon Basin of Northeastern Peru

J. F. DUMONT
ORSTOM, C. P. 9214, La Paz, Bolivia
F. GARCIA
ORSTOM, A. P.18-1209 Lima Perú & Instituto Geofísico del Perú, A. P. 3747, Lima, Perú

ABSTRACT The Marañon Basin is located between the Brazilian shield and the Andean foothills. The southern part of the basin, called Ucamara depression, comprises large swamp and lakes, with more or less straight edges and nearly geometrical shapes. The Punga swamp is an historical example of tectonic related subsidence. Large swamps overlay structural blocks limited by faults, and uplifted or pulled down basement structures. The main trend of the swamps is related to the reactivation of basement faults. The implications for the regional geodynamic context are briefly discussed.

INTRODUCTION

The Marañon Basin in northeastern Peru is located between the Brazilian shield to the east, represented by the Iquitos uplands, and the Andean foothills to the west (Fig.1). The drainage area of the Marañon Basin is the largest of the Andean piedmont, extending from just below the Equator to near Lake Titicaca, over about 14º of latitude. This provides large water supplies from the Andes, concentrated in two large rivers, the Ucayali and the Marañon. The wet tropical climate generates heavy precipitation over the lowland areas of the basin, drained by a dense network of local rivers and extended wetlands. In the context of active subsidence, this region appears to be a good case-study of fluvial and wetland patterns in relation to neotectonics.

While neotectonic studies in uplifted areas are well documented and based on various basic methods (landform analysis, fault scarps and fault plane measurement), subsiding areas are poorly documented because current neotectonic methods do not apply. Neotectonic studies in the Amazonian Basin began probably with Sternberg's (1950, 1955) considerations on tectonic grain and river systems. In the western Amazonian regions, Rüegg (1952) mentions fold deformations in the late Tertiary lacustrine deposits, attributed to a Plio-Quaternary tectonic phase, which effect was supposed to be presently active. Later, Iriondo & Suguio (1981) pointed out the relative effect of tilting and subsidence over the Amazon River valley. In the Beni Basin of Bolivia, whose position is similar to that of the Marañon Basin, Allenby (1988) suggested the aligned, rectangular shaped lakes as controlled by an orthogonal fracture pattern propagated upward from the underlying granitic basement. Because of the lack of precise structural data for the basement, the Allenby's hypothesis remains speculative. The case provided here is based on closer relations between surface patterns observed on Landsat and SLAR images and basement structures interpreted from seismic data (Laurent & Pardo 1975; Laurent, 1985). We present here new data on the subsidence of the region, gathered through field studies.

GEOLOGICAL BACKGROUND

The Marañon Basin (Fig.1) has been mainly developed during Cenozoic. According to Laurent & Pardo (1975) and Laurent (1985), upper Triassic to Jurassic deposits exist only in the western part of the basin, and the Cretaceous deposits (Aptian-Maastrichtian) overlap eastward on the Paleozoic and crystalline basement. Thickness of post Jurassic sediments rises to 5000m in the central part of the basin (Sanz, 1974). But the more striking tectonic features of the basement are inherited from the Hercynian tectonics reinforced in part by the late Kimmeridgian phase. These features are represented by isolated horsts of crystalline basement or thin sedimentary cover overlain by Cretaceous deposits (from north to south, the Concordia, Samiria, Santa Elena and Santa Lucia uplifts). Transcurrent faulting is reported for the late Hercynian tectonics.

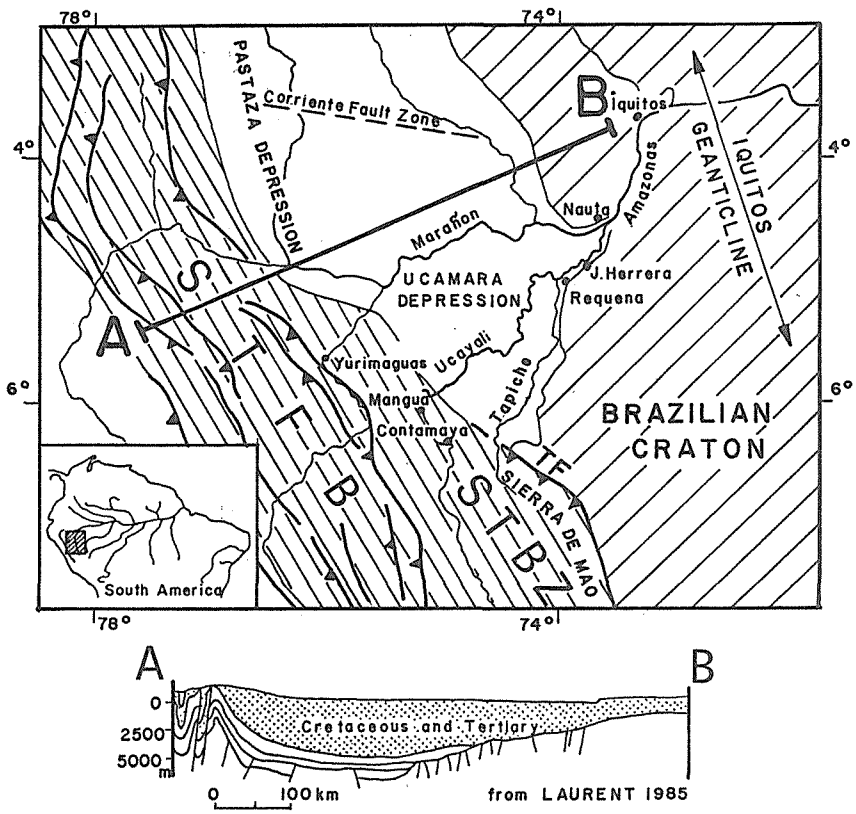

FIG. 1 Structural scheme of the Marañon Basin and surrounding areas. STFB: Subandean Thrust and Fold Belt and STBZ: Subandean Tilted Block Zone, TF: Tapiche fault. A-B, cross-section through the Marañon Basin, located on the structural scheme.

The subsidence of the basin was accompanied by positive tendencies in the Iquitos geanticline. During the late Tertiary the subsidence accelerated over the whole area and Mio-Pliocene deposits extended over the geanticline. During Mesozoic and Cenozoic the Andean foredeep basin was much more extended than now, longitudinally along the

Andean range of Peru and also laterally over the present foothills. The basin was reduced to its present extension as a result of the late Tertiary and early Quaternary tectonics in the Subandean Thrust and Fold Belt (Ham & Herrera, 1963; Pardo, 1982; Mégard, 1984), as well as in the subandean foreland of central Peru, which was completely uplifted as a result of tilted block tectonics (Dumont, 1989) related to the initiation of flat slab subduction beneath the Andes (Jordan et al., 1983). During these tectonic phases most of the Hercynian faults were reactivated, mostly in reverse motion (Laurent & Pardo, 1975; Laurent, 1985).

The present subsiding areas of the Marañon Basin are characterized by the occurrence of large swamps located from north to south along the Pastaza River, at the confluence of the Marañon and Huallaga Rivers (Laurent & Pardo, 1975), and over the southern part of the Marañon-Ucayali watershed area, known as the Ucamara depression (Villarejo, 1988). These areas of active subsidence fit approximately with the axis of the structural basin, which appears to be arcuate, trending N-S in the northern part and NW-SE in the southern (Sanz, 1974; Laurent & Pardo, 1975; Laurent, 1985).

THE UCAMARA DEPRESSION

The Ucamara depression (Fig.2) is extremely flat, drained by an intricate network of meandering rivers and permanent or semi-permanent swamps and lakes (Cabrera la Rosa,1943; Villerejo, 1988). The depression is subtily delimited on the north by the Marañon River (except in the lower Chambira and Tigre Rivers area) and on the west by the north-south branch of the Samiria River. While, the southern and eastern borders are sharp morphostructural boundaries formed by the Tapiche fault along the Sierra de Moa uplift and the bluffline at the margin of the Iquitos geanticline.

Three white water rivers cross the depression, from north to south respectively: the Marañon, the Ucayali and the Tapiche. Large swamps are located either along the course of the main rivers which cross them, or are located adjacent to the river courses.

THE MODERN RIVER REGIME

The annual rainfall average in western Amazonia is over 2000mm. Precipitation falls in all month of the year, but is heavier between January and May. As commonly occurs in Amazonian regions, the lowland drainages are separated into large white water rivers (silty water from the Andes and foothills areas) and smaller black water rivers (rain water high in organic acids, flowing out of the swampy areas).

The difference between high water level (January to May) and low water level (June to December) is up to 11m at Iquitos (García & SHNA, 1987) but decreases significantly westward: 9.5m in Jenaro Herrera on the border of the depression and of less than 2m in the Ucamara depression (personal observation). These differences are probably due to the weir effect of the Iquitos upland.

Very few and relatively imprecise topographic data are available for the area. According to the elevations of Iquitos (105m), Nauta (111m) and Requena (114m) (Ministerio de Guerra, 1984), the gradient for the Marañon and Ucayali rivers crossing the Iquitos geanticline is of about 0.06m km^{-1} (location on fig.3). Toward the Marañon Basin a similar mean gradient is found between Requena and Contamana (134m) along the Ucayali River. Data from Stiglish (1904) show a gradient of 0.04m km^{-1} between Mangua (present name Carolina) and Requena along the Ucayali River, through the Ucamara depression. Downstream from Iquitos to the sea, the Amazon River has a mean slope of 0.03m km^{-1}, the same value being mentioned by Baker (1978) between Manaus and the sea.

THE EXTENDED SWAMPS

The permanent swamps (Fig.2) are large flooded areas which are not directly related to fluvial landforms. Nevertheless, some flooded fluvial landforms like oxbow, swale, or part of channel may have been incorporated into the more extensive swamps. Three permanent swampy areas have been identified. The Chambira-Tigre (Concordia) swamp on the northern side of the Marañon River, the Puinahua swamp over the central part of the Puinahua channel, and the Punga swamp along the Tapiche River. All these swamps drain black water. When they are crossed by white water rivers, as the Punga swamp by the Tapiche River, white and black waters are separated by more or less wide fluvial levees.

The Chambira-Tigre (Concordia) swamp is located between the Chambira River westward and the Tigre River eastward, and extends about 25km to the north of the Marañon River. This area is characterized more by wetland forest than the deep swamps, represented by flooded fluvial landforms, such as ria type lakes.

The Puinahua swamp covers an area of about 25km by 60km, following the axis of the Puinahua Channel. Northeastward, the permanent swamps are discontinuous, with the flooded areas located around large oxbows. Southwestward, the swampy

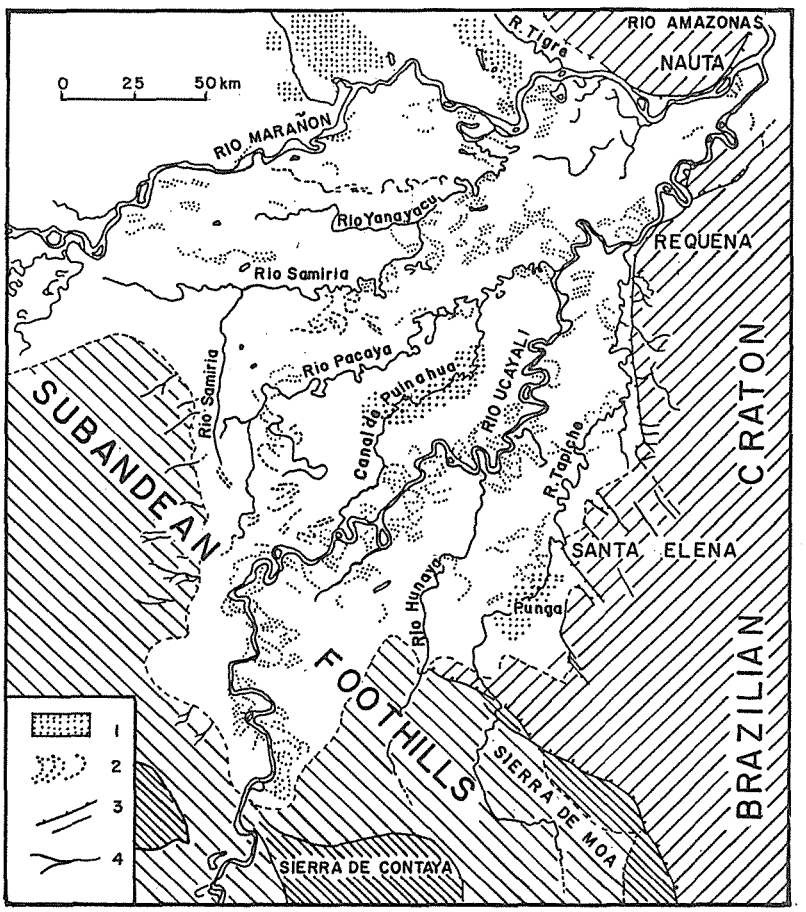

FIG. 2 Morphostructural scheme of the Ucamara depression: 1: Major swamp areas; 2: fluvial landforms (ridge and swale arrays); 3: morphological scarps; 4: Drainage in uplands.

areas are more continuous, and the relationships with fluvial landforms are obvious. While the northeastern limit of the Puinahua swamp is not clearly delimited, the southwestern limit is very distinct, and fits with a NNW-SSE trending line. The superimposition of the swamp over fluvial landforms suggest the first postdate the second.

The Punga swamp is rectangular shaped, 675km2, located between Santa Elena and Wicungo, on both sides of the Tapiche River (5 by 15km on the western side and 15 by 40km on the eastern). Stiglish (1904) described the area as an upland (bosque de altura), and convincing testimony supported by morphological observations suggest that the flooding of the area occurred about only 60 years ago. According to the testimony of two inhabitants (Arturo Pereira in Iquitos and Santiago Panduro in Santa Elena) the Punga area began to sink between 1927 and 1929, after some earthquakes occurred (Santiago Panduro, personal communication). The area was progressively flooded; settlers and Capanahuas Indians had to leave as each year the remaining dry land was reduced by flooding. According to travel accounts (Faura, 1964; Villarejo, 1988), the lower part of the tributaries of the Tapiche River (especialy the Loboyacu) were not completely flooded in the years 1930-1940. After an initial (relatively short ?), high rate of flooding, the present extension of the area was reached very progressively. All that remains of the forest are the tree trunks, preserved by the black water, and just rising above the low water level. The bases of the dead trees are presently under 2m of water during low flows. Estimates based on the present river bank (1.5m high) and the water level during high flows which overpass the levees of about 50cm, suggest a total subsidence of more than 4m.

We suggest that the flooding of the Punga is related to tectonic subsidence. We dismiss the hypothesis of flooding due to the rising of the base-level downstream, because this should have had flooded not only the Punga area, but also the watershed between the Tapiche and the Ucayali River which is barely higher than the high water level. Some change in the hydrographic network of the region resulted from the subsidence of the Punga. The valleys of the Loboyacu and Camungo Rivers, eastern tributaries of the Tapiche River, were completely flooded, and the Tapiche river migrated southward toward the center of the subsiding area. The Tapiche River is presently reconstructing its sedimentary channel through the Punga Swamp. The white, silty water of the Tapiche river is separated from the black water of the swamp by a levee 1m to 1.5m high and less than 5m wide, colonized in some places by a single row of Cecropia (trees of the pioneer stage of forest succession, Salo et al., 1986).

EVIDENCE FOR BASEMENT STRUCTURE CONTROL

According to Laurent & Pardo (1975), few deformations are reported from the Mesozoic and Cenozoic deposits in the Marañon Basin, but on the contrary, the pre-Mezosoic basement is divided in several faulted and uplifted blocks. A comparison between the scheme of the basement structures on one hand and the scheme of fluvial landforms and large swamps on the other suggest an active structural control over the surface landforms by the basement. The most striking cases will be reported here (Fig.3).

The Chambira-Tigre swamp is located over a generally depressed zone in the basement. The lower and upper Paleozoic zones are bounded by normal faults, of which a part was reversely reactivated during the late Tertiary (Quechua) tectonic phases. The western part of the swamp (Chambira River) overlays an area of horsts (e.g., the Concordia uplift) and deep grabens, with a general westward tilt which ends against the Patayacu horst zone. The western branch of the Concordia uplift has been reversely reactivated during late tertiary tectonic phase. The eastern part of the swamp (Tigre River) overlays a NNW-SSE deep, lower Paleozoic zone bounded by normal faults. To the north, the eastern faults were reversely reactivated recently. According to Laurent & Pardo (1975) the effect of the Quechua tectonic phase on the Marañon Basin

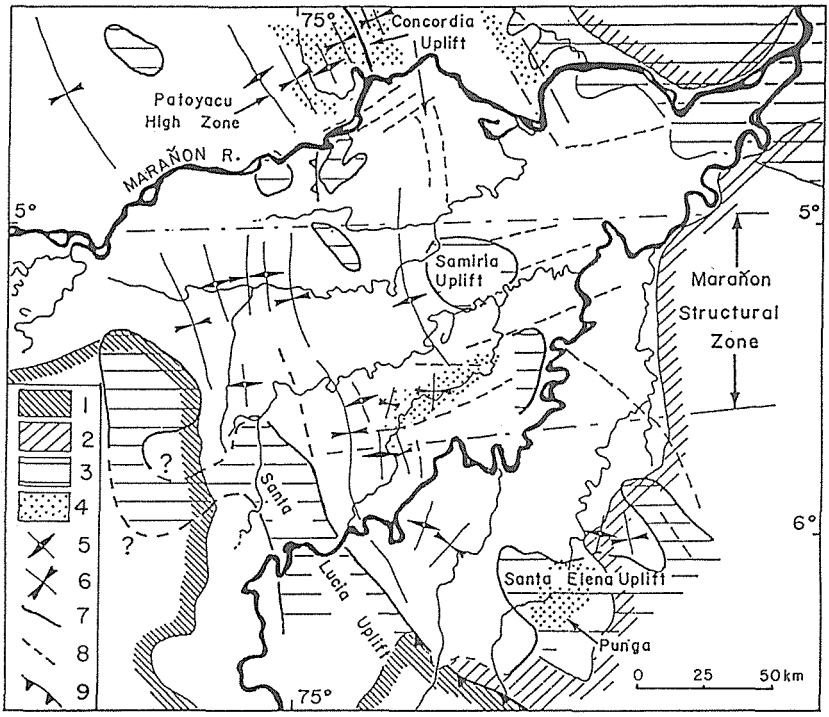

FIG. 3Sketch of the basement structures of the Ucamara depression, from Laurent (1985) and Laurent & Pardo (1975), completed with surface morphostructures: 1: Limit of the Subandean foothills. 2: Limit of the uplands of the Iquitos Geanticline. 3: Late Hercynian uplifts of crystalline rocks overlay by cretaceous deposits. 4: Major swamps. 5: Pre-cretaceous anticlines. 6: Pre-cretaceous synclines. 7: Basement fault reactivated during late Tertiary tectonic. 8: Pre-cretaceous basement faults. 9: Tapiche fault zone with post-Pleistocene uplift.

was characterized by differential vertical block motion.

The limit of the Punga subsidence fits relatively well with the northwestern part of the Santa Elena uplift defined in Laurent (1985). The structure of the Santa Elena uplift (Alto de Santa Elena) is interpreted as a crystalline horst surrounded by Paleozoic layers. The NNE-SSW direction of the Punga swamp is parallel to a few of the structural features reported by Laurent (1985), just northward and northwestward from the Santa Elena high zone. The position of the Punga swamp suggests that underlying block faults are still active in the basement. The NNE-SSW orientation of the Punga is sub-parallel to the "en echelon" system of the Marañon Fault Zone reported for the late Paleozoic (Laurent, 1985). The location of the present active subsidence just over an historically uplifted zone suggests an inverse recurrent motion of the probably normal or normal-transcurrent Paleozoic faults.

The Puinahua swamp is located within Paleozoic depressions limited toward the north, east and south by transcurrent faults in the basement. The western limit of the swamp, which is also the most evident, is defined by a fold belt parallel to the eastern border of the Santa Lucia Paleozoic uplift (Laurent, 1985). The case of the Puinahua swamp shows that the occurrence of Paleozoic faults in the basement determines the boundaries of the subsiding blocks.

The migration of the Ucayali River extends over an area characterized by NNE-SSW to W-E transcurrent late Paleozoic faults, related to the Marañon Fault Zone. On

the contrary, the Marañon River which enters the basin through the northern part, flows through an structural depression located between the Marañon Fault Zone southward and the Corrientes Fault Zone northward. The common course of the Ucayali and Marañon Rivers during the Samiria stage, which corresponds to the limit of the area of extreme migration for each river, follows precisely on the belt of higher fault density, identified as the Marañon Fault Zone by Laurent (1985).

RELATIONS WITH REGIONAL TECTONICS

The geometrical relations between swamp and basement structures are not the same throughout the depression. On the north of the Marañon fault zone, swamp and basement structures are parallel to the main Andean structures (NNW-SSE). In the southern part of the depression, the direction of elongation of the swamps appears to be controlled by transverse structures, NE-SW to NNE-SSW, related to the Marañon fault zone.

The most active subsidence of the Marañon Basin occurs presently in front of the Subandean Thrust and Fold Belt (STFB) in the northern part of the basin, and extends southward in front of the northern part of the Tapiche reverse fault. This can be interpreted as a tendency of the present basin to extend toward southeast, along the preexisting Cretaceous axis of the basin that extended over the Pastaza-Ucamara-Acre areas.

The state of stress in the Ucamara depression is not known, but the case of the Punga swamp suggests that the basement is submitted to compressional stress. In our opinion this compression is weaker than that in Central Peru, where the whole Subandean foreland and Craton margin are submitted to uplift. The combination of a good compressional linkage in Central Peru and a weak one in Northern Peru may produce some adjustments in the Craton margin, like the normal faulting observed in the Iquitos Upland (Dumont et al., 1988). These faults of relatively small throw have a major control over the flood plain limits; they may be interpreted as superficial and small scale neotectonic joint generation (Hancock & Engelder, 1989). The faulting tectonic is contemporaneous with the rising of the Iquitos Upland during Quaternary. Increasing tectonics lead to a more active subsidence of the foredeep, as well as positives tendencies of the craton margin (rebound effect). A dam effect resulted, and caused the merging of all the drainages comprising the Marañon Basin toward only one exit, giving rise to the Amazon River.

CONCLUSION

In the actively subsiding Ucamara depression, relations between large swamps and basement structure is obvious. Some cases are clearly related to Hercynian structures and faults inversely reactivated during late Tertiary and Quaternary tectonic phases. Other cases are less evident, but most probably related to inverse or transcurrent reactivation of basement structures, although the transmission of the deformations through the sedimentary column is not observable on the present structural documents.

ACKNOWLEDGEMENTS This work is a UR 105 ORSTOM project supported by two agreements, ORSTOM-IGP and ORSTOM-IIAP. This is a contribution to IGCP project 279 "Terrane in Latinoamerica", and 281 "Climas Quaternarios de America del Sur". Structural data from the basement shown on Fig. 3 have been reviewed and corrected by H. Laurent, who provided several comments on the faults and the major basement structures. We thanks also A. Pardo, V. Benavides, J. Paredes and M. Sébrier for helpful discussions. D. Smith revised the English text, for which we are grateful.

REFERENCES

Allenby, R. J. (1988) Origin of rectangular and aligned lakes in the Beni Basin of Bolivia. Tectonophysics 145, 1-20.

Baker, V. E. (1978) Adjustment of fluvial system to climate and source terrain in tropical and subtropical environments. In: Fluvial Sedimentology, A D.Miall, (Editor), Can. Soc. Pet. Geol., Mem. no. 5, 211-230.

Cabrera La Rosa, A. (1943) Caracteristicas geomorfológicas de los ríos en la región Amazonica. Bol. Soc. Geol. Perú 14 & 15, 38-58.

Dumont, J. F. (1989) Neotectónica y dinámica fluvial de la baja Amazonía peruana. Bol. Soc. Geol. Perú 80, 51-64.

Dumont, J. F., Lamotte, S. & Fournier, M. (1988) Neotectónica del Arco de Iquitos (Jenaro Herrera, Perú). Bol. Soc. Geol. Perú 77, 7-17.

Faura, G. S. (1964) Los ríos de la Amazonía peruana. Ed.Colegio Militar Leoncio Prado (Callao, Peru).

García , J. S. & Servicio de Hydrografía y Navigación de la Amazonía (1987) El Río que se aleja: Cambio del curso del Amazonas, historia y estudio técnico. Centro de Estudios Teológicos de la Amazonía, Iquitos.

Ham, C. K. & Herrera, L. J. (1963) Role of Subandean fault system in tectonics of Eastern Peru, and Ecuador. In: O.E. Childs and B.W. Beebe (Editors), Backbone of the Americas. Am. Assoc. Pet. Geol., Mem. no.2, 47-61.

Hancock, P. L. & Engelder, T. (1989) Neotectonic joints. Bull. Geol. Soc. Am. 101, 1197-1208.

Iriondo, M. & Suguio, K. (1981) Neotectonics of the Amazon plain. INQUA Neotec. Bull. 4, 72-78.

Jordan, T. E., Isacks, B. L., Allmendinger, R. W., Brewer, J. A., Ramos, V. A. & Ando, C. J. (1983) Andean tectonics related to geometry of subducted Nazca plate. Bull. Geol. Soc. Am 94, 341-361.

Laurent, H. (1985) El pre-Cretáceo en el oriente peruano: su distribución y sus rasgos estructurales. Bol. Soc. Geol. Perú 74, 33-59.

Laurent, H. & Pardo, A. (1975) Ensayo de interpretación del basamento del Nororiente Peruano. Bol. Soc. Geol. Perú 45, 25-48.

Mégard, F. (1984) The Andean orogenic period and its major structures in central and northern Peru. J. Geol. Soc. London 141, 893-900.

Ministerio de Guerra (1984) Mapa físico-político del Perú.

Pardo, A. (1982) Caracteristicas estructurales de la faja subandina del norte del Perú. In: Symposium "Exploración Petrolera en las Cuencas Subandinas de Venezuela, Colombia, Ecuador y Perú", Asoc. Colomb. Géol. Geofis. Petr., Bogotá.

Rüegg, W. (1952) La depresión del Ucayali y Amazonas superior. Rev. Assoc. Geol. Argentina 7, 106-124.

Salo,J., Kalliola, R., Häkkinen, I., Mäkkinen,I., Niemelä, P., Puhakka, M. & Coley, D. (1986) River dynamics and the diversity of Amazon lowlands forest. Nature, 322, 254-258.

Sanz, V. P. (1974) Geología preliminar del Río Tigre-Corrientes en el Nororiente peruano. Bol. Soc. Geol. Perú 44, 106-127.

Sternberg, H. O'. R. (1950) Vales tectônicas na planicie amazonicas? Rev. Bras. Geogr. 4 (12), 511-534.

Sternberg, H. O'. R. (1955) Sismicité et morphologie en Amazonie brésilienne. Annales de Géographie 342, 97-105.

Stiglish, G. (1904) Ultimas exploraciones ordenadas por la Junta de vías fluviales a los ríos Ucayali, Madre de Díos, Paucartambo y Urubamba. Oficina tipográfica de "La Opinión Nacional".

Villarejo, A. (1988) (first publication 1943) Así es la Selva. Centro de Estudios Teológicos de la Amazonía, Iquitos.

Land Subsidence (Proceedings of the Fourth International Symposium on Land Subsidence, May 1991). IAHS Publ. no. 200, 1991.

Subsidence and Quaternary Glaciation

N. P. PROKOPOVICH
3333 Braeburn Street
Sacramento, CA 95821, U.S.A.

ABSTRACT Following are five subsidence and "subsidence-like" processes associated with Pleistocene-Holocene glaciations: (1) Local subduction of continental crusts; (2) subsidence related to the drainage of alluviated valleys by a postglacial isostatic uplift of the previously subsided portions of the earth's crust; (3) flooding of near-shore lowlands with ocean levels rising by melting of continental ice cappings and warming of the ocean water; (4) thermokarst; and (5) freeze-drying of some unconsolidated, originally water-saturated sediments created deposits susceptible to hydrocompaction.

INTRODUCTION

Many natural processes are closely genetically related, no matter how different they may appear to us. A good example of such a relationship is the Quaternary continental glaciations resulting in several forms of past and present land subsidence. Such subsidence is now a well-recognized geologic hazard causing multimillion dollars in damages (Holzer, 1984; Prokopovich, 1984. The following brief communication is an attempt to discuss briefly some forms of subsidence and subsidence-like processes genetically relative to the Pleistocene-Holocene glaciations.

FACTUAL DATA

A critical evaluation of the readily available factual data indicates that at least the following five types of subsidence and "subsidence-like" processes are related to the Quaternary glaciations:

I. The enormous weight of giant continental icecaps (Snead, 1972) caused an isostatic subsidence of several parts of continental plates. The process was studied particularly well in the Fennoscandia. Maximum subsidence here probably locally exceeded 100 m (Flint, 1971; Bowen, 1978).

II. Melting of these icecaps resulted in an unloading, and in a major Holocene isostatic dome-shaped uplift of the Fennoscandia and on Canadian shields. The present-day rates of the uplifts in the Fennoscandia are locally up to 9 mm/yr, and the total Holocene uplift is locally over 80 m (Flint, 1971; Bowen, 1978). Similar uplifts were reported also on the Canadian shield in North America. The surface of hard, Fennoscandia crystalline bedrock is cut by

numerous alluviated valleys. Natural drainage of this alluvium caused by the Holocene uplift and, in recent time, by man-induced drainage of the unconsolidated fill resulted in a widespread and frequently devastating land subsidence and associated structural damage (Broms et al., 1977 and Karlsrud and Sander, 1979).

III. Melting of large masses of Pleistocene continental ice returned enormous amounts of water into the oceans and raised the global ocean level. An additional increase in the volume of ocean water was caused by an increase of its temperature by the postglacial global warming. Both processes resulted in a "subsidence-like" flooding of coastal plains and islands (Shlemon and Begg, 1975; Atwater et al., 1977; Fairchild and Wiebe, 1977); and Louderback, 1952 (Figure 1).

FIG. 1 Sacramento-San Joaquin "Delta" in California, U.S.A. Prior to reclamation, the area was located at the sea level. Late Pleistocene sea level here was locally about 12 m below the present sea level.

IV. Modern and past melting of buried ice blocks and so-called pingo in formerly glaciated and periglacial areas resulted in soil collapses, usually known as "thermokarst" (Gary et al., 1972) (Figure 2). Numerous water-filled and dry depressions of such origin are scattered in the formerly glaciated areas of Europe (Bijlsma, 1983) and North America (Shwartz and Thiel, 1955). Present-day formations of such features are common in Alaska, northern Canada, and Siberia (Bailey, 1983; Harry and French, 1983; Pewe, 1983; Thomas and Ferrell, 1983).

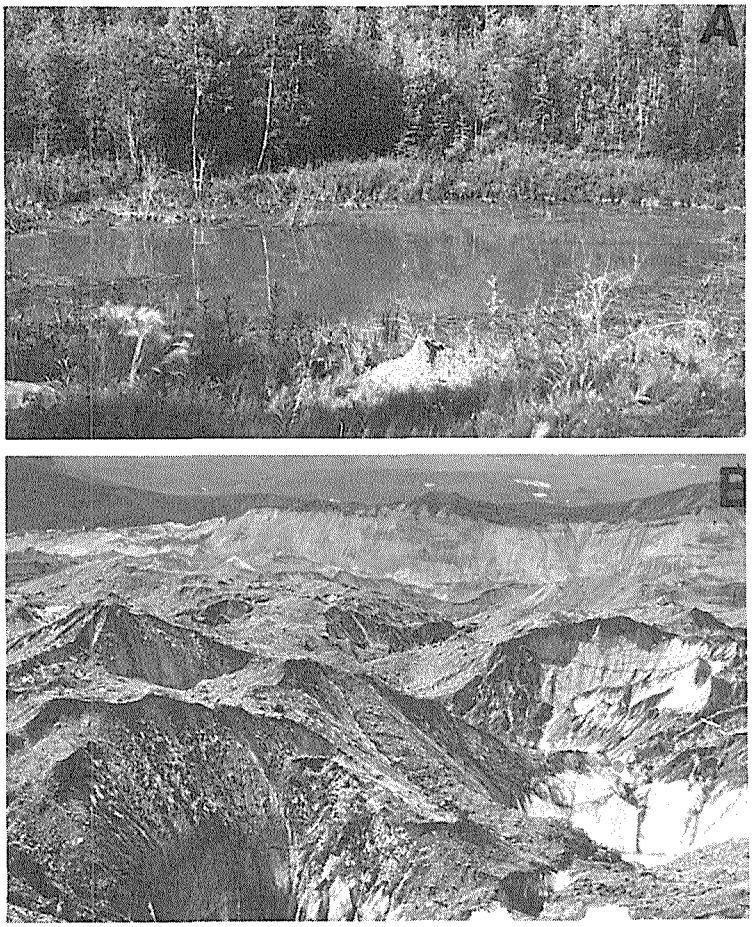

FIG. 2 Examples of thermokarst in (A) Alaska and (B) Yukon (courtesy of Dr. H. Wright).

V. Cold air is more dense than warm air. Cooling of the air over continental icecaps and, to a lesser degree, air cooling over major mountain glaciers may cause local barometric maxima. Such pressure differences could easily create dry, foehn-like winds blowing from glaciated areas into periglacial terrains. Freeze-drying of some originally wet periglacial sediments expanded by freezing of pore-water could create some additional porosity. In clayey-silty sediments with a high-dry strength. In a dry, postglacial climate, such excessive porosity may create sediments susceptible to hydrocompaction (Prokopovich, 1984). This frequently catastrophic form of subsidence (Figure 3) is common in loess deposits in Northern America (Figure 4), Europe, and Asia (Lofgren, 1960, 1969 and Krayev, 1969). In California, hydrocompaction is known in the western San Joaquin Valley, along the San Luis Canal-California Aqueduct (Bull, 1961, 1964 and Lofgren, 1960, 1969). Here the hydrocompaction was treated by costly preconstruction flooding of the canal alignment (Prokopovich, 1984) (Figure 5).

FIG. 3 Hydrocompaction damages to a test section of the State of California prototype canoe in the San Joaquin Valley.

FIG. 4 Distribution of loess in the U.S.A. (modified from several USBR publications.

VI. Another more indirect impact of glaciation on postglacial subsidence or, better, on porosity of aquifers is overcompaction of sediments by the weight of capping ice. Such overcompaction, however, may be reduced by past "cementation" of sediments by frozen ground moisture.

FIG. 5 Preconstruction flooding of one of the sections of San Luis Canal, California.

DISCUSSION

Several forms of past and contemporary land subsidence and subsidence-like processes are related to Pleistocene-Holocene glaciations. All such prehistoric subsidence processes were strictly natural. The contemporary processes, however, are frequently man-induced. Examples of such man-induced processes are soil collapses in permafrost areas, hydrocompaction in irrigated semiarid terrains, etc. Future global warming due to a "greenhouse" effect may cause costly "subsidence-like" flooding of nearshore areas, several islands, etc.

REFERENCES

Atwater, B. F., Hedel, C. W. and Helley, E. J. (1977) Late Quaternary Depositional History, Holocene. Sea-Level Changes, and Vertical Crustal Removement, Southern San Francisco Bay, California. U.S. Geological Survey Professional Paper 1014, 15 p.

Bailey, P. K. (1983) Periglacial Geomorphology in the Kokrine-Hodzana Highlands of Alaska, in Permafrost Forth International Conference. Proceedings, National Academy Press, Washington, DC .

Bijlsma, S. (1983) Weichselian Pingo Remnants in the Eastern Part of the Netherlands, in Permafrost Forth International Conference. Proceedings, pp. 62-67.

Bowen, D. Q. (1978) Quarternary Geology. A Strategraphic Frame work for Multidisciplinary Work, Pergamon Press, Oxford, Toronto, Paris, Frankford.

Broms, B. B., Fredriksson, A. and Carlsson, L. (1977) Land subsidence in Sweden due water leakage into deep-lying tunnels and its effects on pile-supported structures, in Land Subsidence-Symposium. Proceedings of the Second International Symposium on Land Subsidence held at Anaheim, California, December 1976. IAHS-AISH Publication, No. 121, pp. 375-387.

Bull, W. B. (1961) Causes and Mechanisms of Near-Surface Subsidence in Western Fresno County, California. In United States Geological Survey Professional Paper 424-B. U.S. Government Printing Office, Washington, DC, pp. B-187 to B-189.

Bull, W. B. (1964) Alluvial Fans and Near-Surface Subsidence in Western Fresno County, California, United States Geological Survey Professional Paper 437-A. U.S. Government Printing Office, Washington, DC.

Fairchild, J. B. and Wiebe, K. H. (1977) Subsidence of Organic in Soils and Salinity Barrier Design in Coastal Orange County, in Land Subsidence, Symposium, Proceedings of the Second International Symposium on Land Subsidence, in IAHS-AISH Publication N121, pp. 334-346.

Flint, R. F. (1971) Glacial and Quaternary Geology. John Wiley and Sons , New York .

Gary, M., McAfee, R., Jr. and Wolf, C. L. (Editors) (1972) Glossary of Geology. American Geological Institute, Washington, DC.

Harry, D. C. and French, H. N. (1983) The Orientation and Evolution of Thaw Lakes, Southwest Babns Island, Canadian Arctic, in Permafrost Forth International Conference. Proceedings, pp. 456-461.

Holzer, T. L. (editor) (1984) Man-Induced Land Subsidence: The Geological Society of America, Boulder, Colorado.

Lofgren, B. E. (1960) Near-Surface Land Subsidence in Western San Joaquin Valley, California. Journal of Geophysical Research, Vol. 65, No. 3, pp. 1053-1062.

Lofgren, B. E. (1969) Land Subsidence Due to the Application of Water, in Reviews in Engineering Geology II. The Geological Society of America, Boulder, Colorado.

Louderback, G. D. (1952) Development of San Francisco Bay, of the Geological Society America, Bull, V52.

Karlsrud, K. and Sander, L. (1979) Subsidence Problems Caused by Rock Tunneling in Oslo, in K. Saxena (Editor), Evaluation and Prediction of Subsidence - Engineering Foundation Conferences, American Society of Civil Engineers, New York, pp. 197-213.

Krayev, V. F. (1969) On Subsidence of Loess Soils of the Ukraine, in Land Subsidence, IAHS Publication No. 88, Vol. 1, IAHS-UNESCO IAHS-UNESCO, pp. 321-324.

Péwé, T. (1982) Geologic Hazards of the Fairbanks Area, Alaska. Division of Geological and Geological Surveys, Colege, Alaska, 109 p.

Prokopovich, N. P. (1984) Hydrocompaction along the San Luis Canal and its service area in the San Joaquin Valley, California, U.S.A., in State-of-the-art--Irrigation Drainage and Flood Control, No. 3, International Commission on Irrigation and Drainage, The Central Electric Press, New Delhi, (India), pp. 424-443.

Schwartz, G. M. and Thiel, G. A. (1955) Minnesota's Rocks and

Waters--Geological story. University of Minnesota--Minnesota Geological Survey, Bulletin 37, The University of Minnesota Press, Minneapolis.

Shlemon, R. J. and Begg, E. L. (1975) Late Quaternary evolution of the Sacramento-San Joaquin Delta, California, in Suggate, R. P. and Cresswell (Editors), Quaternary Studies, The Royal Society of New Zealand, Wellington, New Zealand, pp. 259-266.

Snead, R. E. (1972) Atlas of World Physical Features, John Wiley and Sons, New York.

Thomas, H. P. and Ferrell, J. E. (1983) Thermokarst Features Associated with Buried Sections of the Trans-Alaska Pipeline, in Permafrost Fourth International Conference. Proceedings, pp. 1245-1250.

Land Subsidence (Proceedings of the Fourth International Symposium on Land Subsidence, May 1991). IAHS Publ. no. 200, 1991.

Controlled Subsidence during Pile Driving

K. R. PEAKER
Geotechnical Division, Trow Consulting Engineers Ltd,
1595 Clark Boulevard, Brampton, Ontario L6T 4V1, Canada
I. GORE
Trow Ontario Ltd, 1074 Webbwood Drive, Sudbury,
Ontario P3C 3B7, Canada
S. A. AHMAD
Geotechnical Division, Trow Consulting Engineers Ltd,
1595 Clark Boulevard, Brampton, Ontario L6T 4V1, Canada

ABSTRACT The Provincial Building located in the downtown core of Sudbury, Ontario is an 11-storey concrete frame building supported on long driven concrete piles. At an immediately adjacent site, the general ground surface settled 0.9 m over a brief time period during pile driving for the foundations.

The subsoil stratigraphy beneath the Sudbury Provincial Building comprises 6 m of loose recent alluvial material with a groundwater table 1 to 2 m beneath the ground surface, followed by 12 m of soft to firm silty clay. Beneath this clay layer and continuing to a depth of 46 m is a stratum of 27 m of loose to dense fine becoming coarse silt. Bedrock is at a depth of 65 m with 15 m of dense till over bedrock.

Soon after pile driving began at the adjacent Civic Regional Building, water was noted rising adjacent to the piles. During the operation when a damaged pile was removed, water gushed freely from the hole. Up to 0.9 m of subsidence was recorded with the center of the settlement occurring near the pile driving operation. The zone of influence for this subsidence extended well beyond the property lines into adjacent roadways; fortunately no buildings were immediately adjacent to this site. The lateral movement of piles close to the center of the zone was measured up to 150 mm toward the center of the zone of influence.

Because of the problem on the adjacent building, it was known that a similar subsidence could occur at this site. To avoid complications of the subsidence effect of this construction on the Civic Regional Building the foundations for the Provincial Building were constructed immediately after the pile driving was completed for the Civic Regional Building. By modifying the construction sequence the overall subsidence was reduced to 15 percent of that experienced at the Civic Regional Building.

INTRODUCTION

The Ontario concept of Regional Government in the mid 1970's

gave rise to the Sudbury Civic Square project. This project included a Civic Regional Building and a Provincial Building. The project in the downtown core consisted of a 5-storey single parking basement level structure with adjacent West Tower Building and a proposed future 11-storey Provincial Building. These proposed structures were to wrap around the existing Bell Canada Tower a 5-storey single basement office complex.

The site had been used as a parking lot for several years after demolition of smaller commercial type stores and residential housing. This area had, during earlier times, been the site of Junction Creek that meandered through the development. The flood plain occupied most of the area prior to infilling and redirecting the creek through a concrete culvert. The Bell Building immediately north of the proposed buildings and forming part of the complex was founded on a raft below a single basement level (see Figure 1).

This paper briefly discusses the geological conditions at the site and describes the discovery of the subsidence settlement conditions during the driving of piles for the Civic Regional building (Figure 1). The treatment of the foundations for the Provincial Building in this problem area is presented and the successful results are discussed.

SUBSOIL DATA

The geology of the Sudbury area is noted for its extreme variations in bedrock elevation soft clays and loose silts. The geology is further complicated by silts and clayey silt whose capacity is difficult to predict when subjected to dynamic loading, i.e., pile driving.

The original design concept for the Provincial Building and Civic Regional Building was to incorporate a raft foundation for the major buildings and spread footings for the connecting links. The initial investigation indicated that it would probably be more economic to support the building on piles. Further investigations to select pile founding levels were subsequently undertaken.

The subsoil was found to be reasonably uniform over the entire site, with the exception of the depth of fill and alluvium overlying the firm silty clay. This alluvium was found to vary from 2 to 6 meters in depth with the deeper depths reflecting old creek channels or flood plains that had traversed the site in a random fashion. Figure 2 shows a typical subsoil profile consisting of 6 meters of fill and recent alluvial material over a firm silty clay to a depth of 18 meters; below 18 meters the clay grades to a stratified silt gradually becoming more sandy and at 30 meters changes to a silty sand. To the 40 meters depth the silt and sandy silt exist in a compact to dense state. Below 40 meters and to 46 meters, a layer of loose silty sand was encountered overlying dense sand, gravel and cobble till. Below 46 meters, bedrock was not proven, but is anticipated at 65 meters depth.

The geotechnical properties of each layer are included in abbreviated form on Figure 2. Figure 3 indicates typical

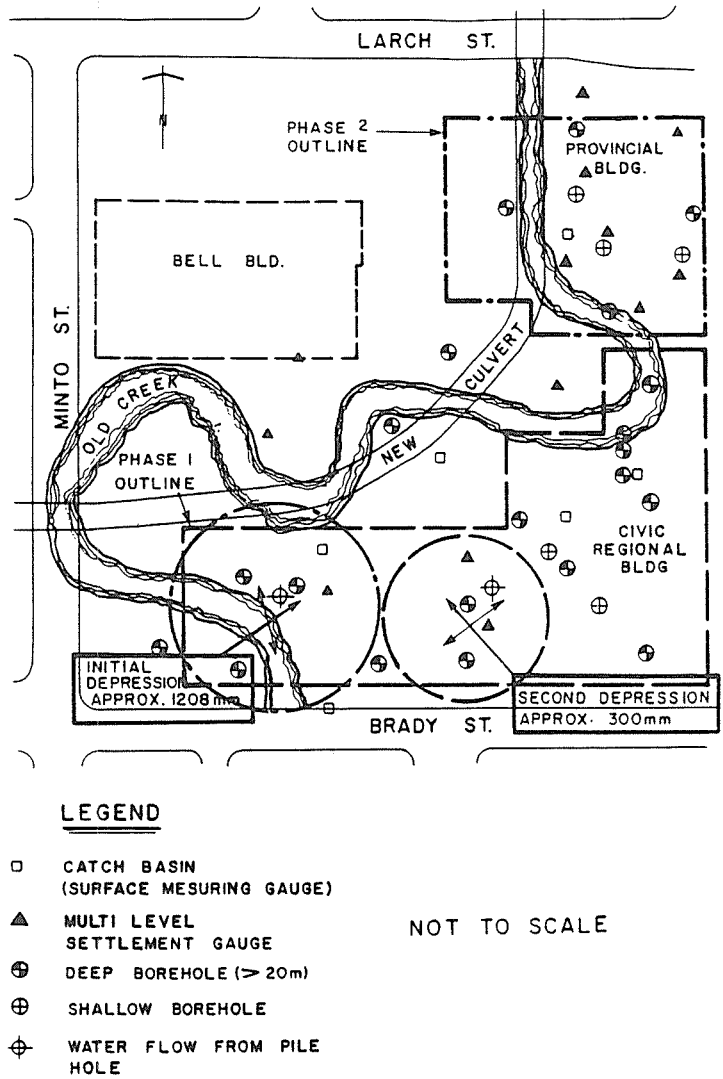

FIG. 1 Borehole and settlement gauge locations.

gradings for representative depths. The groundwater level in the upper fill and alluvium was near old creek level some 2 meters below existing surrounding ground surface. The sand, gravel and cobble till at a depth of 46 meters showed a piezometric head at least 1 meter above the existing ground surface, i.e., Elevation 257 meters.

FOUNDATION CONSIDERATIONS

Prior to construction the designers decided to eliminate the raft and utilized driven piles. Experience in this area showed low displacement H piles would penetrate 3 to 4.5 meters beyond

Elevation (m)	Depth (m)	Description	Comments
256	0		
		FILL - sand, organics, loose	N < 4
252.4	3.0		
		SILTY CLAY ALLUVIUM (organic) loose	N < 3
250	6.0		
		SILTY CLAY, FIRM	C = 40 kPa γ = 18.4 kN/m³ W = 35% 40 LL = 33% PL = 19%
237.8	18.2		
		SILT - STRATIFIED with clay seams compact to dense MORE SAND	N > 20<40 γ = 20.1 kN/M³ W = 20%
225.6	30.4		
		SILT SANDY compact to dense	N>20 <70 γ = 20.1 kN/m³ W = 18-20%
216.4	39.6		
		SANDY SILTY loose, compact	N < 12 W = 22%
209.7	45.7		
		SAND GRAVEL & COBBLES (TILL) very dense	N >100
	57.8		

FIG. 2 Subsoil stratigraphy.

the depth of displacement piles. Because of the potential cost saving displacement piles were considered most practical. Based on this requirement it was estimated that piles carrying nominal loads, i.e., 445 kN on a 250 mm and 710 kN on a 300 mm displacement pile would meet refusal at an average depth of 35 meters or Elevation 221 meters. This depth was determined by the standard penetration test results in the boreholes and to a

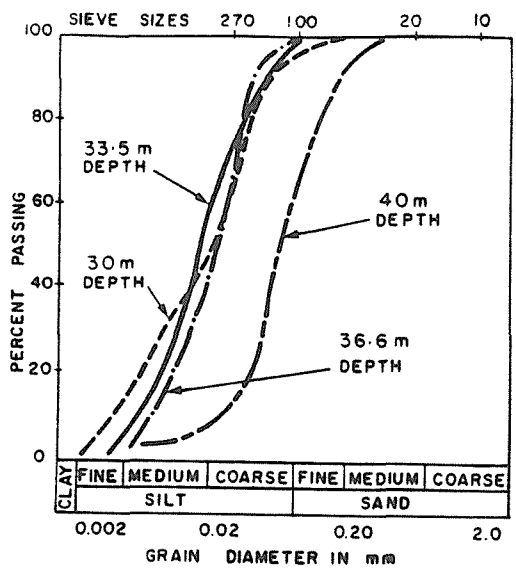

FIG. 3 Typical grain size distribution over entire depth.

larger extent by the dynamic cones driven at the base of the boreholes. Local experience had shown that typical pile 'refusal', i.e., 15 blows/25 mm would be achieved for displacement piles 4.5 to 6 meters below the refusal to driving of the dynamic cone i.e., more than 100 blows/300 mm.

The actual load carrying capacity of the piles was to be determined by load tests, however, the most economic pile for the deep depths was one that was driven to a capacity equal to the structural capacity of the pile. The piles selected were precast concrete piles with quick attach patented full moment splices. The nominal 200 mm pile was to carry 620 kN while the 300 mm size should be driven to carry maximum loads of 1020 kN. These capacities were to require sets of 20 blows/25 mm with the maximum safe capacity to be confirmed by the load test.

Test Results Three piles were selected for testing. The result of these tests is presented as Figure 4. It can be seen that the 300 mm piles were capable of carrying a 1020 kN design load and the 200 mm pile obtained the necessary safe capacity of 620 kN.

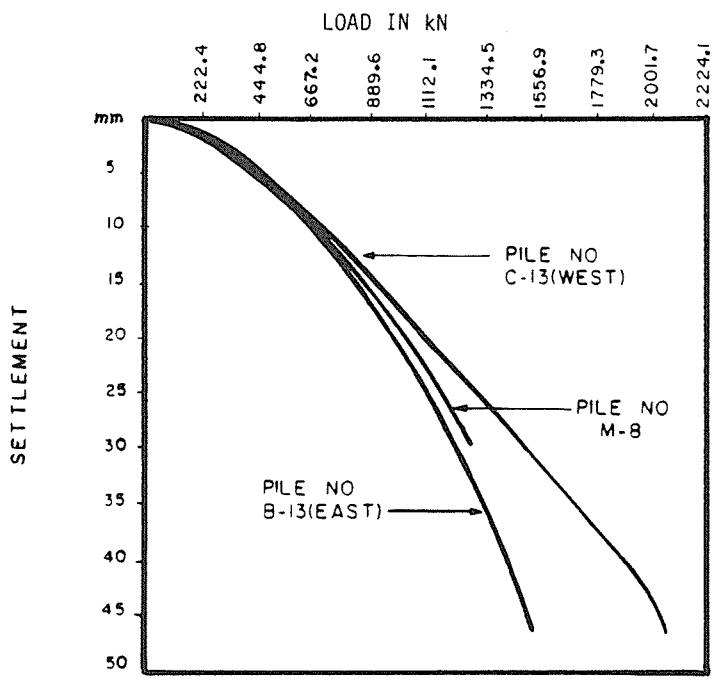

FIG. 4 Pile load test results.

PILE DRIVING - CIVIC REGION BUILDING

Pile driving began with the driving of the test piles January 13 and 31, 1975. Production driving commenced late January of 1975. During the early days on site, significant problems associated with pile breakage occurred and the driving schedule was very much behind by mid February when it was decided to bring

a second pile driver on site. From January to mid February only 20 of the 437 piles for the civic region complex had been driven. The initial hammer, a Linkbelt 520 rated at 35 kJ was supplemented with a Linkbelt 440 (24 kJ). Both hammers when checked with the Pile Driving Analyser were delivering up to the designated 24 kJ of energy to the pile.

By March 5, both units working side by side were driving up to 6 piles per day. On one pile a maximum of 2000 blows was required to penetrate the upper 0.3 to 0.6 meters of frozen ground, however, this was exceptional as most piles penetrated the frost zone with less than 150 blows.

During the first week of March, a local depression around the pile drivers, approximately 36 meters in diameter and 1.2 meters in depth with a volume of 1200 cubic meters was recorded. This depression occurred rapidly, i.e., within 2 days. Elevations taken on catch basins in the depression indicated a settlement of 1 meter below original level. The extent of this subsidence is shown on Figure 1. As this depression was forming driving continued. Silt laden water was noted to be flowing up around some of the piles. An analysis of the silt showed that it corresponded to the grain sizes of the material from the deeper silt strata below 21.5 meters.

Piles within the depression moved more than 200 mm laterally towards the center of the zone of influence and there was concern for their integrity. A retapping program carried out on the piles that were obviously affected showed that their original resistance to driving remained unchanged.

Figure 5 and 6 indicate some of the magnitude of the settlement; Figure 7 shows the intensity of the piles, although no cap contained more than 8 piles.

Speculation as to what was the source of the settlement and the consequences for continuing work were of immediate concern. To determine if the settlement was deep-seated or occurred as a result of consolidation of the upper loose fill and alluvial material, settlement points were installed at ground surface, within the fill/alluvium and into the silty clay. During installation of the settlement gauges a pile suspect of being damaged was withdrawn from the position shown on Figure 1 and water gushed from the 18 meter deep hole for a 38 to 48 hour period and settlement of 1 foot over large (30 meter cone) area resulted.

It was obvious that the pile driving was causing the problem regardless of where the problem originated from. To reduce this effect, the pile drivers were separated to opposite ends of the site and pile driving was restricted to 1 or 2 piles a day per pile group. Piling continued until the 437 piles were in place and little, i.e., less than 25 mm of movement was detected over the remainder of this site. No pattern of movement at depth could be obtained from the settlement points.

Based on all the data that could be assembled, it was possible to show that serious damage could result to structures within 30 meters of any similar occurrence. Since the adjacent Provincial Building would be constructed within this zone there was concern that damage to the Civic Regional Building could occur during construction of the Provincial Building.

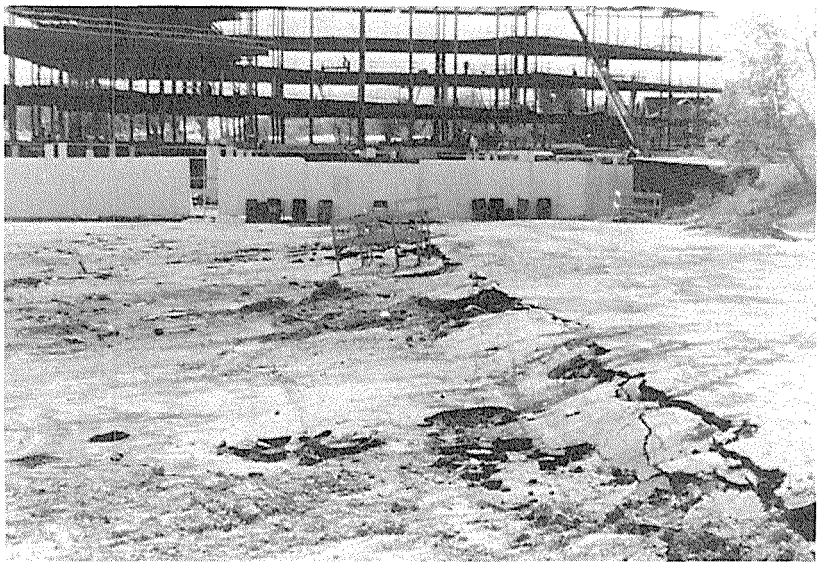

FIG. 5 Magnitude of settlement.

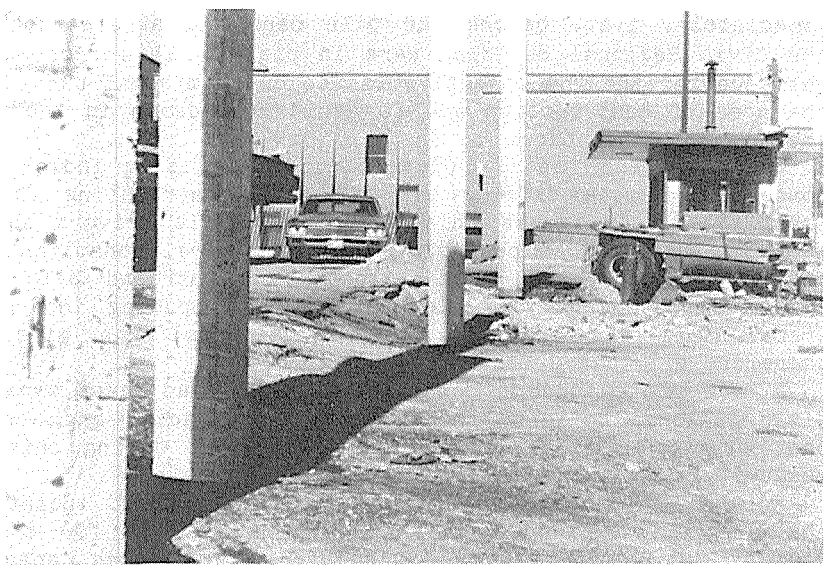

FIG. 6 Subsidence adjacent to piles.

PILE DRIVING - PROVINCIAL BUILDING

The foundations for the Provincial Building were scheduled to begin construction 18 months after the completion of the Civic Regional Building. Measurements of the potential zone of influence in which subsidence could occur showed that construction of the Provincial Building would adversely affect

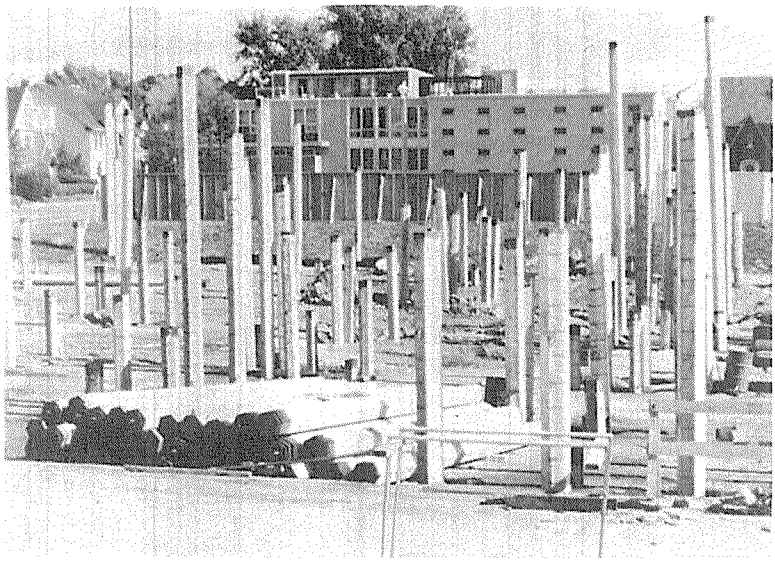

FIG. 7 Intensity of piles.

the Civic Regional Building. The owner was advised that it was imperative to drive the piles for the Provincial Building immediately, i.e., before the pile caps and superstructure for the Civic Regional Building were in place. This recommendation was accepted and the objective was to cause minimal subsidence in the area of construction and to avoid subsidence in the area of the adjacent structure.

The experience at the Civic Regional Building indicated that concentrated pile driving was the main contributing factor to subsidence. To reduce this subsidence, pile drivers should be kept as far apart as possible. The structural consultant agreed that instead of the heavily loaded concentrated pile support system proposed, that a wide spread pile spacing incorporating grade beams was possible. A redesign of the pile layout therefore eliminated large pile groups.

A hold was placed on construction in the adjacent area of the Civic Regional Building and by carefully spacing and separating the driving of piles the overall settlement during driving was measured to be less than 150 mm.

Prior to beginning driving six settlement points were installed in the Provincial Building area. As for the Civic Regional Building at each location the gauges enabled an assessment of subsidence at the ground surface, in the alluvium and fill and below the silty clay. A review of this data showed that only minor movements could be attributed to the fill and alluvium and that the major settlement took place below the silty clay layer.

Vibration Monitoring Throughout the entire driving program a vibration consultant was retained to assess the vibrations and potential damage resulting from pile driving. The results of this monitoring showed that at no time did maximum vibration

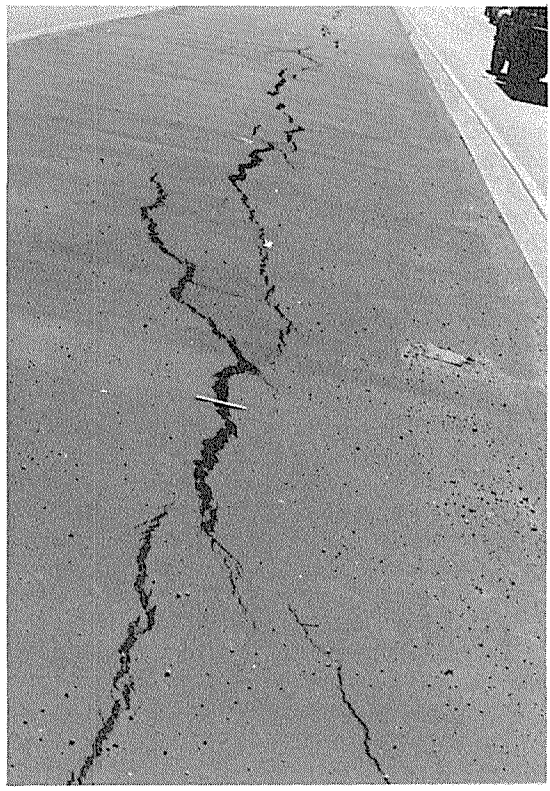

FIG. 8 Damage adjacent to roads.

FIG. 9 Damage adjacent to roads.

amplitudes reach 50 mm per second at a distance of 5 meters from the pile. Apart from significant cracking to adjacent roads no off site damage was recorded for this project (Figure 8 and 9).

Long Term Performance Monitoring of the site over the past 10 years shows no adverse effect from the subsidence to either of the projects described or to the neighbouring Bell Building. It is interesting to note that no other buildings in this area have been or are likely to be founded on piles, since the construction of the Civic Center Buildings.

Related Comments It was not possible to accurately assess the source of the large measured subsidence at the adjacent Civic Regional Building since instrumentation was not in place in this area until the movement was virtually complete. At the Civic Regional Building it could have been argued that the upper fill and the alluvial material were loose initially and could have been a potential source of subsidence. Tests carried out in these materials after the subsidence showed an increased density and decreased water content. This could have resulted from vibration induced consolidation and densification or it could also have resulted by driving a large number of displacement piles. The silt encountered at a depth of 40 meters is described as loose and possibly the driving could have resulted in vibrations that densified this material -water was noted emerging from extracted pile holes and this could have originated at this level. At the Provincial Building it was clearly established that the subsidence was caused by deep seated densification of the silt.

CONCLUSIONS

1. The choice of pile type should be carefully related to all site conditions and economics should not be the prime consideration.
2. The potential for densification of loose layers of cohesionless material can be of greater significance than is often considered for most sites.
3. Ground control measurements must be well thought out and be in place prior to construction if they are to provide the control and information to warrant their cost.
4. The long-term effect of the subsidence in this case was negligible for both the constructed buildings and for adjacent property.

REFERENCES

1. J. E. Thomson, "Geology of the Sudbury Basin", Ontario Department of Mines, Annual Report, 65(3), 1957, 1-56.
2. Trow, "Foundation Investigation Proposed Civic Regional Building Sudbury, Ontario", Report prepared for the Regional Municipality of Sudbury, 52047, 1973, 6-10.
3. K.R. Peaker, S.A. Ahmad, "Pile Driving Triggers Subsidence" Proceedings XII International Conference on Soil Mechanics and Foundation Engineering, Rio de Janeiro, 1989, 1-3.

Land Subsidence (Proceedings of the Fourth International Symposium on Land Subsidence, May 1991). IAHS Publ. no. 200, 1991.

Engineering and Environmental Impacts Caused by Land Subsidence Due to Subsurface Extraction of Solid Raw Materials from Poland

J. LISZKOWSKI
Institute of Geology, Department of Geographical and Geological Sciences, Adam Mickiewicz's University, Poznań, Poland

ABSTRACT Poland is a country of intensive and extensive mining activities for coal, zink, lead and copper ores, native sulphur and salts. However, the principal mineral mined is and has been for more than 200 years, coal. Collapse of underground working results in ground-surface subsidence, both continous and discontinous. The paper present the most new data concerning the mechanisms, areal distribution, amplitudes, rates and hazards of mining subsidence from Poland.

INTRODUCTION

Land subsidence is a common exogeodynamic phenomenon in Poland. Both natural and man-made (anthropogenic) categories of land subsidence are known. The last category is of special interest from the standpoint of engineering geology since it is much more hazardous for life and property. Table 1 list the main types of anthropogenic subsidence in terms of geologic processes and man's activities as known from Poland. The individual types of anthropogenic land subsidence listed differ in their sources of ground surface level disequilibrium, physical nature and kinematics and these characteristics are qualitatively summarized in Table 1 too.

Anthropogenic subsidence is in general - with few exceptions only - of one to three orders faster than natural one. Thus it is well justified to speak from accelerated subsidence in the case of man-made one.

Only one type of accelerated land subsidence from Poland will be discussed below, namely: subsidence due to subterranean extraction of solid raw materials. Other types of anthropogenic subsidence where described elsewhere (Liszkowski, 1989).

THE DISTRIBUTION OF ANTHROPOGENIC LAND SUBSIDENCE IN POLAND

Although the main objectives of the paper will be subsidence due to subsurface mining of solids, it seems to

TABLE 1 Types of anthropogenic /accelerated/ land subsidence as known from Poland.

No.	Type of ground-surface subsidence	Sources of subsidence	Physical nature of ground surface subsidence	Kinematics
1	Accelerated subterranean erosion	mass loss	continuous & discontinuous	slow & rapid
2	Accelerated hydrocompaction	yield strength reduction	continuous & discontinuous	rapid
3	Excessive withdrawal of groundwater	relative increase of vertical		
3a	- for water supply	stresses /consolida-	continuous	slow
3b	- in pre-mining drainage	tion/	continuous & discontinuous	slow
4	Drainage of organic deposits	compaction /consolidation/ & biochemical degradation	continuous & discontinuous	rapid
5	Subsurface extraction of solids by:	mass loss; relative increase of		
5a	- mining	vertical stresses yield strength	continuous & discontinuous	rapid
5b	- brining /solution/	reduction	discontinuous	rapid
5cc	- melting-out		discontinuous	rapid

be of interest to discuss shortly the collocation of various types of accelerated subsidence in Poland. Fig. 1 is a simplified graphic representation of accelerated land subsidence occurences in Poland.

It can be seen from Fig. 1 that as a rule land subsidence is strongly localized and coincide either with large urban-industrial complexes (Warsaw, Lodz, Gdańsk, Szczecin, Poznań) and the location of major open-pit mines of brown coal, sulphur and some earth material resources, e.g. aggregates (assigned H on Fig. 1), either with the location of intensively exploited major subterranean mineral resources (assigned G on Fig. 1) or with areas of intensive drainage of organic deposits (assigned T on Fig. 1).

Subsidence due to heavy extraction of ground-water for different uses is usually extensive but rather slow (rates of subsidence < 0.01 m/y) and may pass unnoticed without the use of precise geodetic techniques. However, intensive extraction of solids by mining techniques and drainage of organic deposits is more localized and rapid (rates of subsidence > 0.01 m/y). There is one area in Poland where subsidence is both extensive and fast; this is the case of the Upper Silesian Coal Basin (USCB), heavily mined for coal and zinc and lead ores for more than two hundred years. Here individual subsidence lows overlap together to form complex subregional subsidence troughs of more than $10^0 - 10^1$ km^2 area.

SOME REMARKS ON THE MECHANISMS OF MINING SUBSIDENCE

The geometric and kinematic characteristics of mining subsidence are in part dependent on the extraction technologies and techniques used. Actually the following extraction

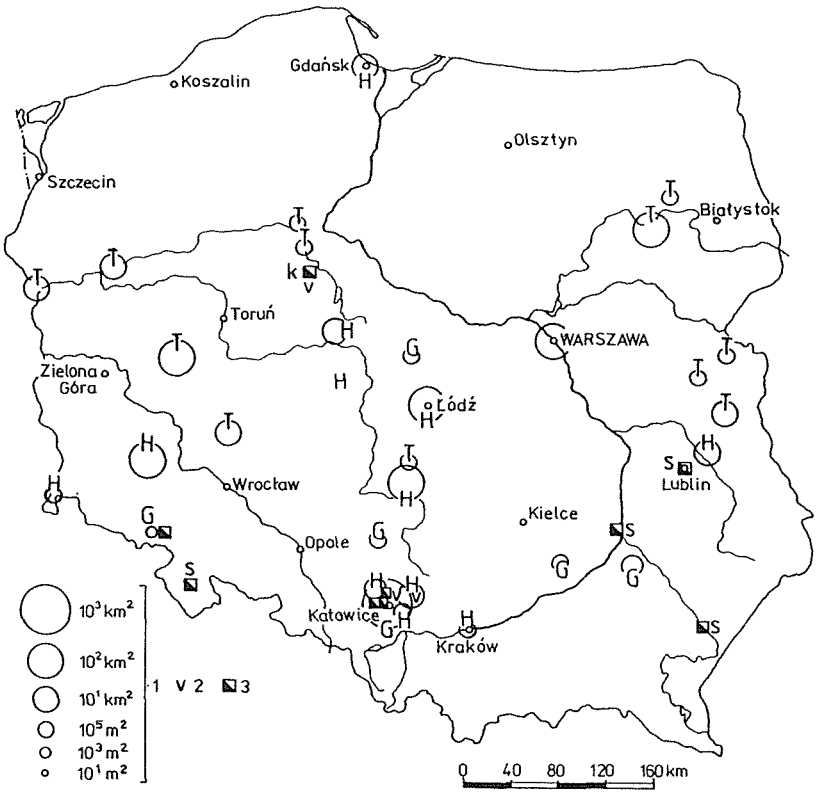

FIG. 1 Distribution of anthropogenic land--subsidence in Poland.
1 - area affected by land subsidence due to: G - mining, H - excessive extraction of ground water, T - drainage of organic deposits; 2 - discontinnous subsidence and collapses; 3 - some more known sites of residentional building failures; s - due to accelerated piping and hydrocompaction.

technologies are used in Poland: mining; controlled and bastard brining and subsurface melting-out. The most common extraction technology used is mining.

Three mining techniques are put into operation: pillar and stall working, a partial extraction mining method used for extraction of copper, zinc and lead, ironstones (now ceased) and salt; vein stoping in the case of steeply dipping ore or other mineral veins or lodes (e.g. baryte in the Sudetes) and longwall mining, a full extraction mining method used for pit-coal mining. In the 19th and the early 20th centuries bell pits were a common used mining method for coal, ironstones, clays and building stones. Controlled brining was used only in the salt-mine at Inowrocław but after a heavy catastrophic subsidence disaster in the Wapno salt mine, this practice has ceased. Bastard

mining is practised in the Wielician and Bochnia salt mines. And at all subsurface melting-out technique is used for the extraction of native sulphur in the Grzybow and Jeziorko areas, Carpathian Foredeep, Southern Poland.

Full extraction mining method usually result in complete (flat-bottomed), continuous subsidence depressions; all other extraction technologies result either in incom - plete (concave-bottomed), regular or irregular, continuous subsidence depressions or linear and or isometric discontinuous subsidences, often of catastrophic rate of ground-surface displacement (collapses).

The mining cavities represent strain nuclei. The strains migrate from the roof of the mining cavities towards the ground-surface with strain rates depending on the stresses created, which depend itself on the dimensions of the cavities - and the rheological behaviour of the rock masses immediately above the void roof ("direct roof" material). The final result of this strain migration process is the ground-surface subsidence. It is clear that the radius of subsidence will be a function of depth of the strain nucleus since "limit angles" and "angles of break" have finite values. As rock and rock mass properties vary from one mining area to another, no general and closed physical formulations of the subsidence mechanisms are at present known. However, for a given mining area the variability of material properties may be assumed as constant. Then empirical and exact solutions, based on different approaches to the problem, may be obtained and are widespread used for predictive purposes (H.M.S.O., 1949; National Coal Board, 1966; Kratzsch, 1974; Surface ..., 1980).

If the amount of subsidence (s max) and the radius of influence (r) are known, either from measurements or calculations, all other geometric, physical and kinematic parameters of subsidence may be predicted. The forecasting equations used in Poland (Fig. 2) are based on Budryk - Knothe's and Kochmanski's theories which are successful used in the USCB for more than 35 years. However, both s max and r may be calculated using following empirical equations:

$$s\ max = a \cdot d_c \tag{1}$$

$$r = z \cdot \cot\bar{\beta} \tag{2}$$

or $$r = \Sigma d_i \cdot \cot\beta_i \tag{2'}$$

where: s max and r as defined above, a - coefficient of subsidence which depend on the roof management techniques used (fall or stowing methods), d_c - thickness of coal seams exploited, z - mining depth, $\bar{\beta}$ - mean limit angle (for USCB conditions $tg\bar{\beta} = 1{,}5 - 2{,}5$), d_i - thickness of individual complexes or formations, β_i - limit angles of the individual complexes or formations (for explanations - see Fig. 2). Moreover, the rate of subsidence is pre-

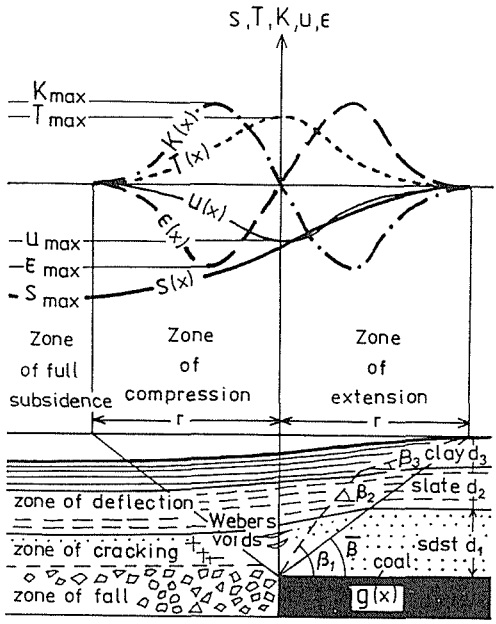

radius of influence	$r = z \cdot ctg\,\overline{\beta}$ $= \sum_{1}^{n} d_i \cdot ctg\,\beta_i$
max. vertical displac.	$s_{max} = a(x) \cdot g(x)$
max. slope	$T_{max} = -\frac{s_{max}}{r}$
max. curvature	$K_{max} = \pm 1{,}52\,\frac{s_{max}}{r^2}$
min. radius of curvature	$R_{min} = K_{max}^{-1}$
max. horizontal displac.	$u_{max} = 0{,}4\,s_{max}$
max. horizontal strain	$\epsilon_{max} = \pm 0{,}6\,\frac{s_{max}}{r}$

FIG. 2 Components of mining subsidence and prediction equations used in Poland to calculate geometric characteristics of subsidence troughs.
Explanation of symbols in the text.

dictable, too (cf. **Surface ....**, 1980, p. 75, Fig. 2.31).

Thus, the topographic effects of mining may be controlled using up - to - date technologies and or various coordination and organization practices. However, there are no possibilities to eliminate mining subsidence completely.

Despite all the preventive possibilities, subsidence due to subterranean extraction of pit-coal results in many, often disastrous effects for both life and property.

CONSEQUENCE OF MINING SUBSIDENCE FOR PROPERTY AND LIFE IN THE USCB

As mentioned, mining subsidence cannot be completely eliminated, despite various possibilities to minimalize the amount of subsidence, the horizontal displacements and strains created a.s.o. Thus subsidence is an overall existing constraint for land-use development in areas of intensive mining activities. Within Poland this is especially true for the USCB where extensive mining activity coincide with large urban and industrial development and a dense population. As a result, quite frequent loss of property, and casualties too, occur.

There is a broad literature on various kinds of threats or hazards due to mining subsidence for specified activities and to people living in the vicinity. All these are known from the USCB and they are here concentrated to an extremely high degree. 21% of the whole area of the Katowice province, i.e. about 1300 km^2 are totally materially altered; any further land-use development and any natural recovery of the primary environment are impossible. The area affected directly by mining subsidence exceed 650 km^2 and indirectly - 1100 km^2. The amount of subsidence actually exceed locally 20 m and will exceed locally more than 40 m in year 2025. The mean rate of subsidence equals to 100 mm/month and may exceed 500 mm monthly. The costs that arise due to constructional damages and failures in residential, commercial and industrial buildings, liners, road and train communications, changes in soil productivity, loss of cropland and pastureland, degradation of quality of groundwater and surface water, land reclamation, loss of coal and aggregate resources a.s.o., exceeds 1.0 to 2.5 billion dollars yearly (Piatek, 1989). As an instance Table 2 lists the losses of property in the Katowice province for the year 1985. The list is not complete and do not include losses which resulted from soil degradation, accelerated gullying, landsliding, a.s.o. which are difficult to fix. Fortunately, loss of life due to the direct consequences of mining subsidence and the failure of residential buildings and or other constructional works were seldom noticed, even in the cases of rapid ground-surface subsidence, i.e. collapses. The last mentioned type of subsidence in the form of crown holes collapses is mainly related to areas of old abondoned, bell - and - pit and pillar - and - stall working mines. The area occupied by this kind of mining subsidence in the USCB exceed 350 km^2. Fig. 3 presents a more detailed picture of the areal extent of ground-surface subsidence due to mining activities in the USCB. Areas of strong mining-induced rock bursting and seismicity are also delineated. Rock bursting and induced seismisity are an important secondary hazard related to extensive coal extraction. Within the time interval between 1980-1985 more than 17500 seismic events of energies $E > 10^5 J$ where registered; 25 events had energies $E > 10^8 J$ and 10 above

TABLE 2 Loss of property as the result of mining subsidence in the Katowice province for 1985 (after Piatek, 1989, 90-91, Table 19).

No.	Property	Units	Quantity	Approximate costs Thousands US$
1	Loss of land	ha	1521.0	101 760
	: cropland	ha	1175.0	82 250
	: woodland	ha	189.0	13 230
	: investment 1.	ha	157.0	6 280
2	Import and redistribution of drinkable water	10^6m^3	488.0	102 701
3	Loss of constructional works			
	- residential	m^2	5198.7	3 120
	- commercial	m^2	492.8	1 132
	- industrial	m^2	787.4	2 680
	- one-family houses	No.	27	2 106
	- others	m^2	273.3	10 040
4	Loss of infrastructural systems			
	- water-supply serv.	km	59.1	5 932
	- severage	km	16.9	932
	- gas pipes	km	47.8	823
5	Communications damages			
	- road communications	km	326.8	66 644
	- rail communications	km	238.3	3 000
	- bridges, viaductes	No.	18	4 892
	- trackage systems	No.	73	2 922
	- others	No.	46	2 670
6	Loss of resources			
	- coal	10^6t	80.8	2 329 390
	- aggregates	10^3m^3	228.3	34 700

10^9J. The energy of the last events equals to local Richter magnitudes $M_L \geq 5$ (Zuber, Mutke, Żogala, 1986). It is this secondary mining-induced hazard which may, and in fact, results in heavy loss of life.

In all other mining areas of Poland similar consequence of land-subsidence were noticed, although on a much more local scale.

CONCLUSION

In Poland ground-surface subsidence due to subsurface exploitation of solid raw materials by mining, brining and melting-out technologies are a common, although mostly localized, man-made (anthropogenic) phenomenon. There

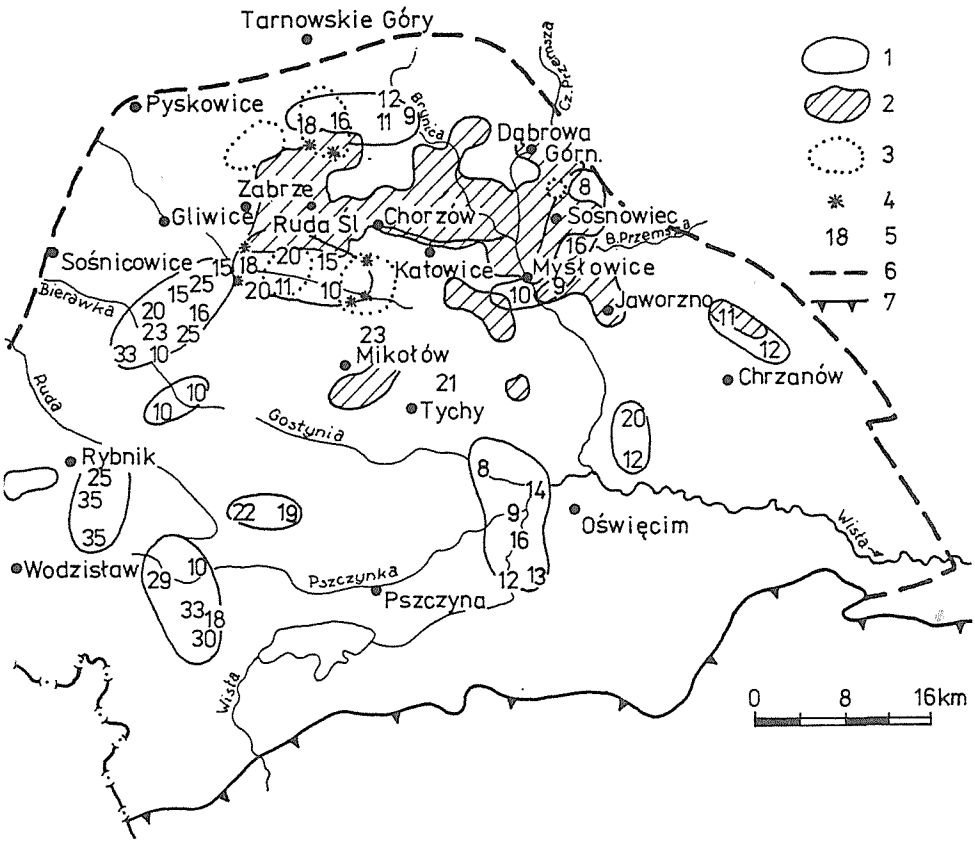

FIG. 3 Hazards related to coal mining in the USCB, southern Poland.
1 - continuous mining subsidence; amount of subsidence above 5 m; 2 - areas of collapses and other kinds of discontinuous subsidence; 3 - areas of increased seismicity for 1980-1985; 4 - localities of catastrophic rock bursts ($E > 10^9$ J of events) for 1980-1985; 5 - predicted values of subsidence in meters; 6 - the boundaries of the USCB; 7 - northern boundary of the Carpathian orogen.

is one area - the Upper Silesian Coal Basin - where mining subsidence is both extensive and fast. And it is here, that all the negative consequences of mining activities are concentrated to an extent, that they are not only a potential but real hazard for property and life. The loss of property equals yearly from 1 to 2.5 billion dollars. The threat of life, mainly as the result of catastrophic rock bursting and or mining-induced seismicity is a heavy stress to all the people living within this area. And these are more than 3 million residents.

The socio-economic situation in Poland is such that it is not possible to resettle people away from even the

most hazardous areas. Thus, we can only hope that there will be better times for preservation, more exactly: for restoration and reclamatioan of the environment in the USCB.

ACKNOWLEDGMENTS I wish to thank Arnold I. Johnson for thoughtful and constructive review of the manuscript and G. Rozmiarek for manuscript preparation. Financial support from the U.S. National Science Foundation which allows me to attend the Fourth International Symposium on Land Subsidence in Houston, Texas, USA is especially gratefully acknowledged.

REFERENCES

H.M.S.O. (1949) Inter-Departmental Committee Report on Mining Subsidence. Report of Committee of Mining Subsidence, Cmd 7637.

Kratzsch, H. (1974) Bergschadenkunde. Springer-Verlag, Berlin.

Liszkowski, J. (1989) Anthropogenic ground-surface deformations in Poland: their formation, distribution, geometric and kinematic characteristics and engineering-geological risks (in Polish). In: Inżyniersko-geologiczne problemy środowiska człowieka (Engineering-geological problems of the Environment), 258-301, Warszawa.

National Coal Board (1966) Subsidence Engineers Handbook, London.

Piatek, F. (ed.) (1989) Costs of ground-surface degradation in the Katowice province (in Polish). Polish Academy of Sciences, Wrocław.

Surface ... (1980) Surface protection against mining damages (in Polish). Wyd. Śląsk, Katowice.

Zuberek, W., Mutke, G. Żogala, B. (1986) Mining induced seismicity of the Upper Silesian Coal Basin (in Polish). In: Konstantynowicz, E. (ed.), Problemy ochrony środowiska i zasobów naturalnych w województwie katowickim. PTPNoZ, Oddz. Górnośląski, Sosnowiec.

Land Subsidence (Proceedings of the Fourth International Symposium on Land Subsidence, May 1991). IAHS Publ. no. 200, 1991.

Filled "Subsidence" Cracks in San Luis Canal Excavations, California, U.S.A.

N.P. PROKOPOVICH
3333 Braeburn Street, Sacramento, CA 95821, USA
J. ISOM
PO Box 18, Los Banos, CA 93635, USA

ABSTRACT About 9,000 nearly vertical, usually 3±1-cm-wide, tension cracks with mostly vertically laminated clay filling, were encountered in the Holocene-Pleistocene Coast Range piedmont alluvium in canal excavations in the west-central San Joaquin Valley in California, U.S.A. The number of cracks ranged from less than 10 to about 856 cracks per one km of the alignment. The alluvium is underlain by folded, Late Pleistocene, lacustrian Corcoran Clay. Two reaches of the canal were affected by hydrocompaction (=shallow subsidence) caused mostly by irrigation. The hydrocompaction caused up to 5 m of settling and up to 1- to 2-m-wide cracks. The filled cracks were assumed to be caused by a prehistoric hydrocompaction although they hardly resembled typical hydrocompaction cracks. The most numerous, filled cracks occur in areas of Holocene anticline uplifts and are probably tension features caused by folding. Their laminated fillings were injected from compressed, deeply seated, water-saturated alluvium. Scattered cracks on fold limbs could be created by a lateral extension by tilting. The clay-filled cracks interrupt lateral migration of ground water in the piedmont alluvium and interfere with its drainage. Neotectonic movements probably are present in the area at the present time.

INTRODUCTION

This paper is based on: original observations; literature and file data; and an evaluation of field notes made by several geologists of the Federal Bureau of Reclamation. The paper discusses the origin of peculiar filled cracks noted in construction excavations of a major Federal San Luis Canal in California (Anonymous, 1974a and b and 1981) (Figure 1). The discovery of cracks was made by Mr. M. K. Bradley. An excellent detailed description of cracks was published by Bull (1972). He and several other geologists assumed prehistoric hydrocompaction (=shallow subsidence) as the origin of cracking. The present paper suggests a new theory of a neotectonic origin of these features.

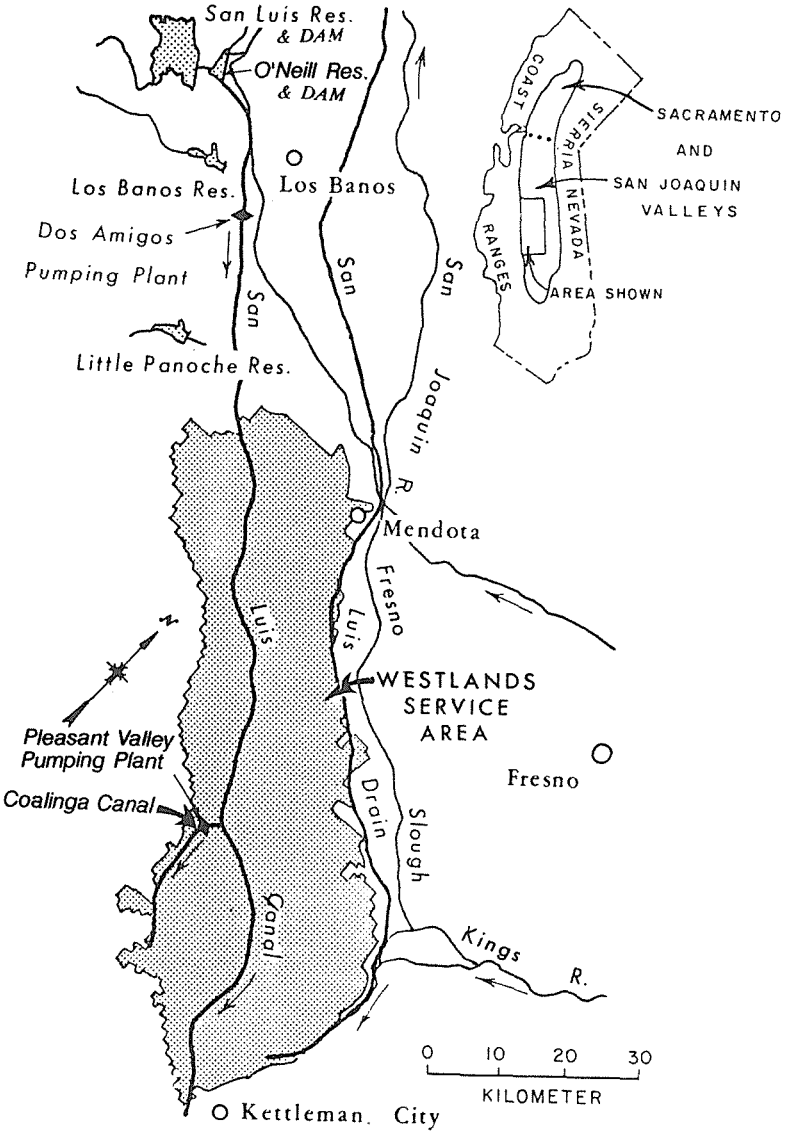

FIG. 1 San Luis Unit of the Federal Central Valley Project, California, U.S.A.

LOCATION AND REGIONAL GEOLOGY

The San Luis Canal is located some 160-300 km southeast of the city of San Francisco, California, in the west-central portion of the semi-arid, deeply alluviated San Joaquin Valley in California (Bailey, 1966 and Hinds, 1952) (Figure 1). The Federal San Luis Canal is also acting as one of the reaches of the California State Aqueduct (Anonymous, 1974c and d). The canal alignment is underlain by buff, mostly clayey-sandy, westside piedmont alluvium derived from Coast Ranges and deposited either as alluvial fans of several

major intermittent streams, or as "interfan" alluvium composed of minor fans of ephemeral streams and slopewash. The alluvial apron is underlain by Late Pleistocene lakebed-Corcoran Clay deformed by a neotectonic folding (Frink and Kues, 1954; Miller et al., 1971).

The area is affected by deep subsidence caused mostly by the overdraft of a sub-Corcoran aquifer system for irrigation (Poland et al., 1969) and, locally, by hydrocompaction (=shallow subsidence) (Bull, 1961 and 1964; Lofgren, 1960 and 1969). Wetting in areas susceptible to hydrocompaction results in soil cracking and up to 5 m of subsidence. Some cracks are up to 1 to 2 m wide (Figure 2). In order to prevent structural failures, two reaches of the canal totaling some 32.5 km were flooded by ponding prior to their construction (Anonymous, 1974a; Hall and Carlson, 1965). In the past, most of the hydrocompaction was caused by irrigation. A few cracks, however, were also induced by natural flooding (Figure 3).

FIG. 2 A hydrocompaction crack about 2 m wide that was caused by irrigation. San Luis Canal Service Area.

FIG. 3 Four filled cracks in the trimmed bank of the San Luis Canal. Clay layer (marked by hammer) is not offset by cracks.

FACTUAL DATA

Unexpectably, numerous unusual, clay-filled cracks (Figure 3) were encountered in the canal prism; they were mapped by several geologists of the Bureau of Reclamation.

All observations on thickness, dip and strike of cracks, their offsets, etc. were complicated by observations made on 2:1 canal side slopes, not on a vertical plane perpendicular to the cracks' stakes.

Filled cracks were absent in San Luis Canal excavations from the MP 70 (O'Neill Dam) to MP 98 (MP=Mile Post; the California Aqueduct Mile Posts were adopted also for the San Luis Canal). About 9,000 cracks were encountered from this point to the MP 168 near the downstream end of the San Luis Canal at Kettleman City. Lateral distribution of cracks along the Canal in this reach is shown in Figure 4. Downstream from Kettleman City, similar filled cracks were reported on the west side of the San Joaquin Valley in excavations for the California Aqueduct near Kings-Kern County Line, at Lost Hills, and west of Bakersfield (Anonymous, 1974a). Cracks were also encountered west of the San Luis Canal in the 2.4-km-long intake channel for the Pleasant Valley Pumping Plant, and at a few places along the Coalinga Canal (Figure 1). Some filled cracks were recorded also at a depth of over 90 m in a few preconstruction test holes in the San Luis Service Area. All cracks in the canal prism were nearly vertical and mostly straight. Some cracks showed tearing, zig-zag patterns. Several individual cracks crossed each other with or without offsets. Many cracks showed branching, splitting, and rejoining. No definite offsets of bedding by cracks were observed (Figures 3 and 5). In most cases, crack strikes were subperpendicular to the Canal axis. Similar trends also exist, however, in cracks in the intake channel of the Pleasant Valley Pumping Plant which is almost perpendicular to the San Luis Canal.

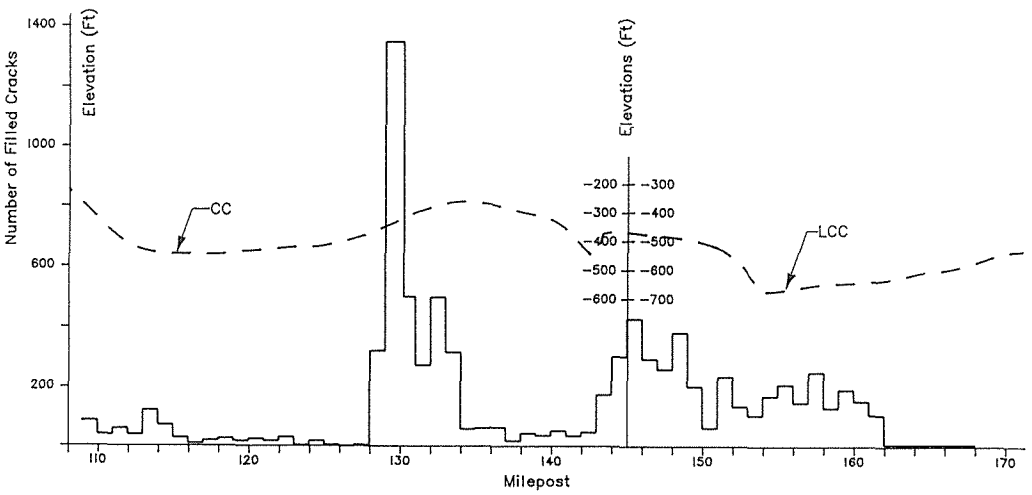

FIG. 4 Bar graphs showing lateral distribution of filled cracks in the San Luis Canal excavations and the profiles of the top of Corcoran Clay (based on a contour map prepared by USGS).

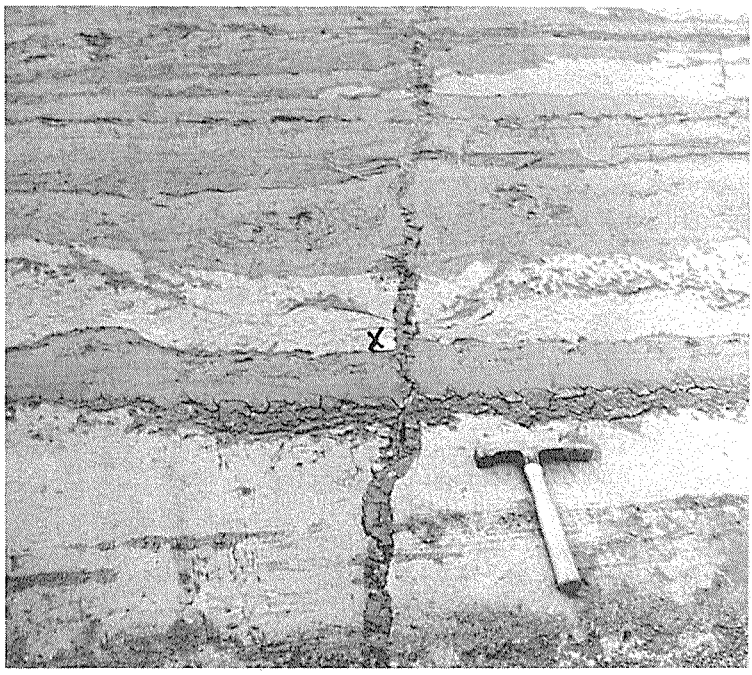

FIG. 5 Closeup view of clay-filled crack exposed in a bank of the San Luis Canal. A minor offset of bedding marked by "X" may be caused by an irregularity of the bedding plane. No other offsets of bedding are visible.

Many cracks in excavations extend to the top of the excavated canal prism, i.e., to a depth of 0.5 m ± below the original plowed ground surface. Some cracks and swarms of cracks, however, have their upper ends within the canal prism 2 to 5 m below the original ground. All cracks extend below the canal invert and no lower ends of cracks were ever observed in 8 to 10 m deep canal prism and in (up to over 40 m deep) the prism of the Pleasant Valley intake channel. Some cracks were noted at a depth in samples from test holes in the San Luis Service Area.

Most of the cracks have fillings composed of laminated fat clay (CH) (Figure 6). Only a few fillings were composed of lean clay (CL) and, rarely, of clayey sand (SC). Very typical is vertical lamination occurring parallel to the cracks' walls. Laminas of the same composition occur symmetrically on both sides of the central lamina, which sometimes is microfolded and contorted (Bull, 1972). Crack filling is never similar to the surrounding alluvium and always differs from it by color, lithology, and content of soluble salts (Bull, 1972).

ORIGIN OF FILLED CRACKS

The hydrocompaction origin of cracks seems to be highly questionable, if not impossible. The only common features of hydrocompaction and filled cracks are: (1) They are tension

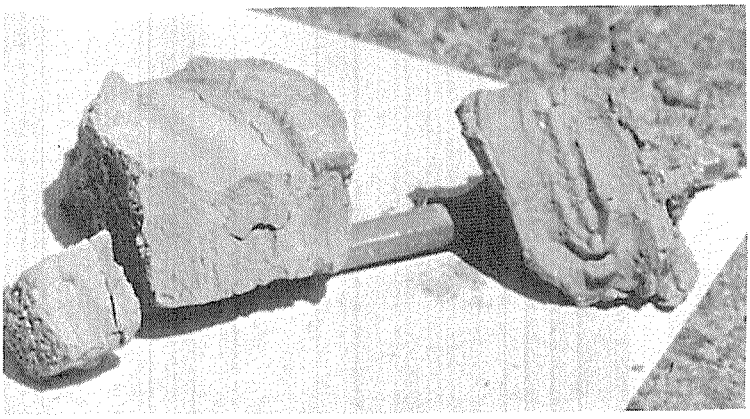

FIG. 6 Closeup view of two fragments of crack filling showing laminated fat clay.

features; (2) cracks of both types are nearly vertical; (3) they occur frequently as swarms; and (4) cracks frequently have subparallel orientation.

On the other hand: (1) Many hydrocompaction cracks are up to 1 to 2 m wide. Such wide hydrocompaction cracks are associated with smaller, 5 to 10 cm wide cracks. All filled cracks are narrow; (2) hydrocompaction cracks are wedge-shaped, and are narrowing with depth. Filled cracks are uniformly thin fissures which extend below the invert. Only a few filled cracks are wider in their upper ends, while many thin cracks feather . out in the alluvium; (3) hydrocompaction cracks are filled with local sediments and are frequently poorly or not visible in excavation. The filling of all filled cracks differs in its color and composition from the local alluvium; (4) typical vertical lamination of filled cracks cannot be explained by a gravity deposition of washed-in material; (5) the largest number of filled cracks were observed in areas known to be not susceptible to hydrocompaction; (6) Bull (1972) noted some microfolding in central laminas in some filled cracks. Development of such contortion by gravelly filling is improbable; and

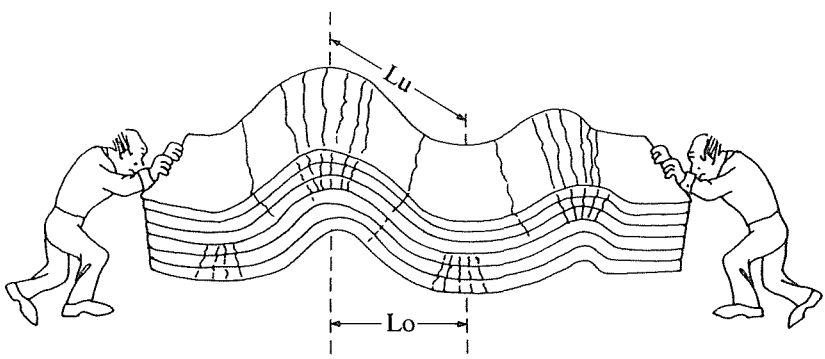

FIG. 7 Distribution of cracks in folded sedimentary beds. The distance Lu is larger than the distance Lo.

(7) hydrocompaction is not "an endless" process. After wetting and collapsing, deposits susceptible to hydrocompaction became stable. In some areas, there are several generations of filled cracks of different ages; hence, earlier cracking failed to stabilize the alluvium.

Most probably, both tension cracks in alluvium in canal excavations and their filling were caused by stresses generated by Holocene and very Late Pleistocene folding as shown in Figure 7. The folding created tension cracking in upper beds near the crest of an anticline, and increased compression stresses in underlying beds, thereby injecting water-saturated sediments into developing cracks. Such a process explains the development of symmetrical lamination in filled cracks and the orientation of minute mica flakes in crack fillings (reported by Bull, 1972).

On the contrary, the topmost beds near a sinkline axis experience a compaction and develop no tension cracks. Minor extensions of the surface due to tilting on fold limbs results here in some less extensive cracking. Such cracks may be filled either with injection or with cave-in materials.

Such origin of filled cracks in the San Luis Canal excavations is well supported in the Figure 4, which shows the largest number of cracks coinciding with anticline uplifts of the Corcoran Clay.

DISCUSSION AND CONCLUSIONS

Structural features discussed in this paper are caused not by hydrocompaction (=shallow subsidence), but by neotectonic Holocene and Late Pleistocene folding. Due to such origin and the small thickness of filled cracks, the most proper name for this feature is "clastic dikelets."

The presence of Holocene folding in the area and its continuation at the present time is important for a better understanding of local land subsidence, and the design of new, and, due to earlier phases of folding, the rehabilitation of existing water conveyance systems and other engineering projects. The number of clastic dikelets at depth probably is much larger than at the surface. Such dikelets with fat-clay filling should interfere with lateral movements of ground water in the westside piedmont alluvium.

REFERENCES

Anonymous (1974a) San Luis Unit - Technical Record of Design and Construction, Vol. 1 - History, General Description and Geology. U.S. Department of the Interior, Bureau of Reclamation, Denver, Colorado, p. 164.

Anonymous (1974b) San Luis Unit - Technical Report of Design and Construction, Design of Waterways and Detention Dams, Vol. VI, United States Bureau of Reclamation. U.S. Government Printing Office, Denver, Colorado.

Anonymous (1974c) California State Water Project. California Department of Water Resources Bulletin 200, Sacramento, California, Vol. 1.

Anonymous (1974d) California State Water Project, California

Department of Water Resources Bulletin 200, Sacramento, California, Vol. 2.

Anonymous (1981) Project Data, a United States Water and Power Resources Service (now Bureau of Reclamation) Technical Publication. U.S. Government Printing Office, Denver, Colorado.

Bailey, E. H. (editor) (1966) Geology of Northern California. California Division of Mines and Geology Bulletin 190, Sacramento, California.

Bull, W. B. (1961) Causes and Mechanisms of near-surface subsidence in western Fresno County, California. In United States Geological Survey Professional Paper 424-B. U.S. Government Printing Office, Washington, DC, pp. B-187 to B-189.

Bull, W. B. (1964) Alluvial Fans and Near-Surface Subsidence in Western Fresno County, California, United States Geological Survey Professional Paper 437-A. U.S. Government Printing Office, Washington, DC, p. 71.

Bull, W. B. (1972) Prehistoric Near-Surface Subsidence Cracks in Western Fresno County, California, U.S. Geological Survey Professional Paper 437-C: U.S. Government Printing Office, Washington, DC, p. 85.

Frink, J. W. and Kues, H. A. (1954) Corcoran Clay - Pleistocene Lacustrine Deposit in San Joaquin Valley, California, in Bulletin of the American Association of Petroleum Geologists, Vol. 38, No. 11, pp. 2357-2371.

Hall, C. E. and Carlson, J. W. (1965) Stabilization of soils subject to hydrocompaction: Engineering Geology, Bulletin of the Association of Engineering Geologists, Vol. 2, No. 2, pp. 47-58.

Hinds, N. E. (1952) Evolution of the California Landscape, California Division of Mines, Sacramento, California, 240 pp.

Lofgren, B. E. (1960) Near-surface land subsidence in western San Joaquin Valley, California. Journal of Geophysical Research, Vol. 65, No. 3, pp. 1053-1062.

Lofgren, B. E. (1969) Land subsidence due to the application of water. in Reviews in Engineering Geology II. The geological Society of America, Boulder, Colorado, pp. 271-303.

Miller, R. E., Green, J. H. and Davis, G. H. (1971) Geology of the Compacting Deposits in the Los Banos-Kettleman City Subsidence Area, California. United States Geological Survey Professional Paper 497-E. U.S. Government Printing Office, Washington, DC, p. 46.

Poland et al. (1969) Land Subsidence in the San Joaquin Valley, California, as of 1972, United States Geological Survey Professional Paper 437-H. U.S. Government Printing Office, Washington, DC, 78 p.

Land Subsidence (Proceedings of the Fourth International Symposium on Land Subsidence, May 1991). IAHS Publ. no. 200, 1991.

A Study of the Relationship between Subsidence and Flooding

ALAN J. POTOK
Turner Collie & Braden, Inc., Houston, Texas 77057, USA

ABSTRACT At the same time the conversion to surface water was occurring in eastern Harris County, continual increases in ground water pumpage were occurring in the western and northern metropolitan areas not affected by tidal flooding. The result has been the gradual shifting of the regional concentration of subsidence westward. The relationship between subsidence and riverine flooding in inland areas, however, is not as clear as in coastal areas where one foot of subsidence corresponds to a one-foot increase in the depth of flooding. This report presents the results of a study to specifically evaluate the impact of subsidence on riverine flooding. The study focused on the impacts of subsidence on three major areas of the inland drainage system: riverine flooding on major watersheds, localized drainage in small watersheds, and the Addicks and Barker flood control reservoir system. This paper summarizes the results of the riverine and reservoir analyses.

HISTORICAL SUBSIDENCE

As early as 1918, land-surface subsidence due to the withdrawal of oil and gas was noted in the Baytown, Texas area. Also during this time, substantial ground water withdrawals were occurring in the Baytown area from large-capacity industrial water wells with resulting reduced aquifer pressures and associated land-surface subsidence. By 1925, these withdrawals had caused as much as 3.25 feet of subsidence near the Goose Creek Field. While surface water was being introduced as an alternative source through the construction of the City of Houston's East Water Purification Plant in 1954, pumpage continued to increase throughout the greater Houston area such that by 1973, the levels of subsidence exceeded nine feet in the Pasadena area, eight feet on the western side of the Baytown area, and a localized center of at least nine feet on the southeastern side of Baytown in the Goose Creek area. This subsidence resulted in permanent flooding of some land adjacent to the coast and substantially increased flooding in areas subject to tidal surges associated with tropical storms.

In 1976 and 1977, conversion to surface water began in the heavily industrial area east of downtown Houston along the ship channel where the maximum amount of subsidence had occurred. As a result, the rate of subsidence in this area has declined. The areas west of downtown Houston, however, have experienced continued growth and increased ground water withdrawal. While the western area experienced about four feet of subsidence between 1906 and 1978, it is currently experiencing subsidence at a rate of about one foot every seven years.

SCOPE OF STUDY

The scope of this study includes three major components of the drainage and flood control systems in the greater Houston area: riverine drainage systems, localized drainage systems, and the Addicks and Barker flood control reservoir system. The

Riverine Flooding Analysis portion of the study is an evaluation of flooding that may result from potential subsidence along main drainage channels with the objective of determining if a relationship exists between gradient change caused by subsidence and storm flows or floodplain area. The Localized Drainage Analysis is an evaluation of the impacts of regional subsidence and well field placements on localized drainage systems and the resultant effects on minor drainage channels, storm sewer systems, and street ponding. The Reservoir Capacity Analysis addresses the effects that subsidence-caused gradient changes have on the maximum flood storage capacities and 100-year pool levels of the Addicks and Barker flood control reservoirs. Only discussion of the Riverine Flooding analysis and the Reservoir Capacity analysis are presented herein.

RIVERINE FLOODING ANALYSIS

Subsidence in coastal areas can be directly correlated to an increase in tidal flooding. While the land surface is lowered, the sea level and storm surge levels remain constant. Thus, each foot of subsidence results in an increased depth of flooding of one foot. However, in the areas that are not subject to tidal influence, the relationship between subsidence and flooding is not so evident. In riverine flooding, the channel capacity and rate of flow, rather than the tidal elevation, are the controlling factors. Channel capacity is primarily a function of the geometry of the channel cross-section and the slope of the energy gradient for a given flow. Of these two parameters, only the slope of the energy grade line is significantly impacted by land subsidence. Unless extremely severe differential subsidence occurs, the change in any channel cross-section is so insignificant that no discernible impact on a cross-section can be reflected in an analysis. The energy grade line, however, extends for the entire length of the channel and is directly related to the ground elevation. Therefore, relatively minor changes in ground slope, when extended for the length of a stream channel, can have significant impacts on the slope of the energy gradient and, thus, the channel capacity.

Flow rate in a channel is a function of several factors including the time of concentration (how quickly water gets to a stream and travels down the stream) and the quantity of storm water that is within the channel and its adjacent floodplain (generally referred to as storage). Since the time of concentration can be affected by ground and channel slope and since the storage is dependent upon the configuration or geometry of a channel cross-section and the depth of flooding, it becomes evident that flow rate and channel capacity are not independent.

Because of the interrelationship among these factors, the net impact of subsidence on flooding is unknown, although it has been generally assumed that increased slopes would result in decreased flood elevations and decreased slopes would result in increased flood elevations. However, the typical subsidence pattern results in an increased slope on one portion of a channel and a decreased slope on another portion. The net result of changing slopes on channel capacity, time of concentration, and storage for this situation is even less clear. It is important, however, that these impacts also be understood since the current subsidence patterns are increasing the possibility of this situation occurring.

TECHNICAL APPROACH

Overview

This riverine flooding analysis was performed on nine channels in five major watersheds integral to drainage in the Houston area. The five watersheds studied, shown on Fig. 1, are Brays Bayou, Sims Bayou, Buffalo Bayou, Addicks Reservoir tributaries, and Barker Reservoir tributaries.

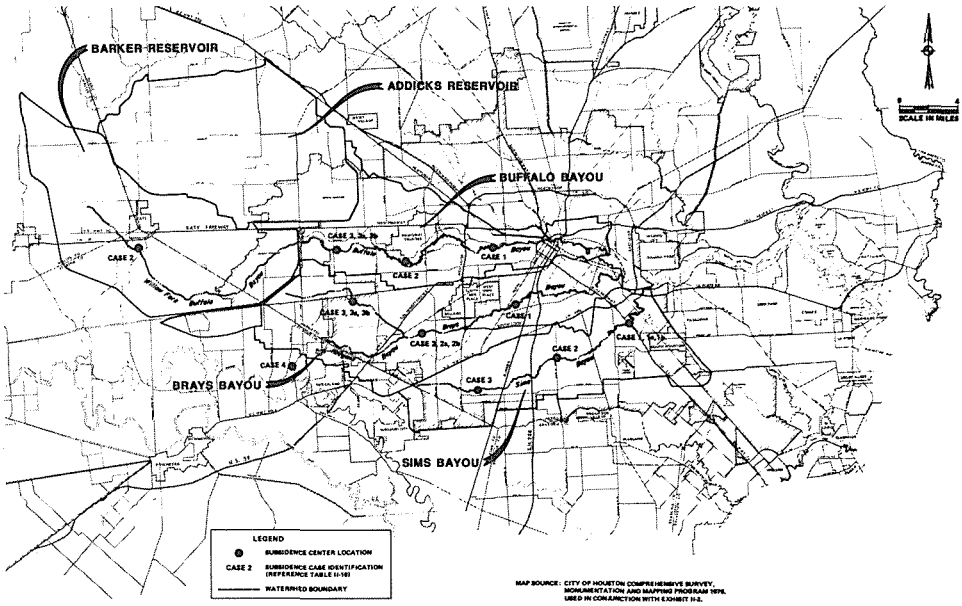

FIG. 1 Riverine Areal Subsidence Contour Base Map.

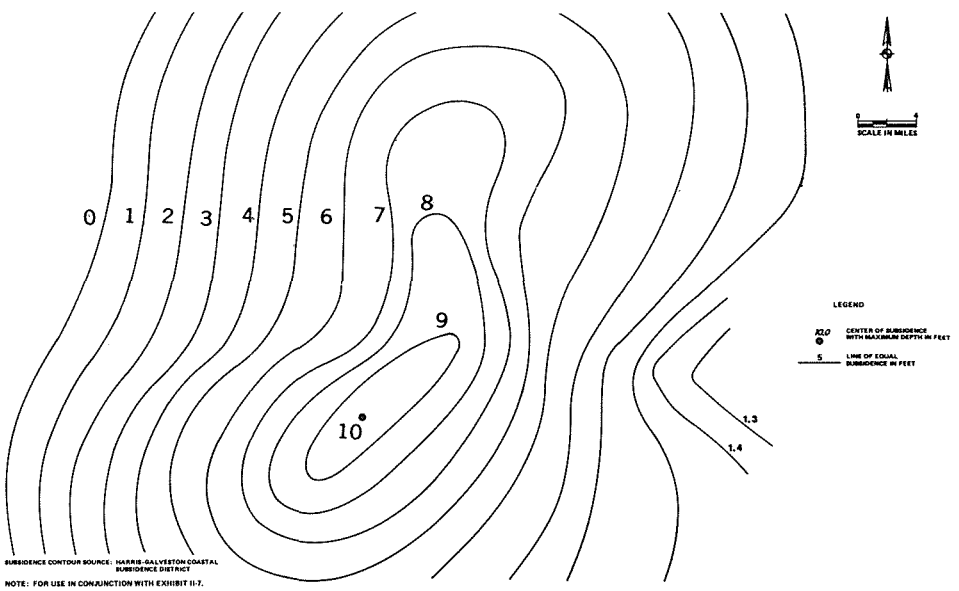

FIG. 2 Areal Subsidence Overlay.

The subsidence pattern shown in Fig. 2 was the primary condition of areal subsidence to be used in this analysis. It represents the projected subsidence pattern over 35 to 40 years assuming limited future surface-water conversions including the City of Houston's East Water Purification Plant and its current expansion.

The technical approach used in this analysis was composed of two parts. The

first part was an evaluation of idealized situations targeted at identifying and quantifying what parameters are affected by gradient change. To perform this portion of the analysis, the watersheds upstream of the Addicks and Barker reservoir system were selected for investigation because they exhibit a relatively wide range in characteristics of slope, urbanization, and channel rectification.

A total of 30 cases of gradient change were evaluated on the six study channels upstream of the reservoirs. These cases included increasing the existing channel slopes by steepening as much as 25% or decreasing the slope as much as 50%. This range of change was selected to represent the maximum slope of the subsidence cone realized by the condition represented by Fig. 2 and comparing this slope of subsidence to channel gradients in the Houston area.

Of the 30 cases studied, 20 were used to simulate a uniform change in gradient in a single direction to characterize a subsidence condition centered outside of the watershed boundaries. The remaining 10 cases considered a combination of steepening and flattening on the same channel.

The second portion of the analysis involved investigations of the more complex watersheds downstream of the reservoirs and their response to more complex conditions of gradient changes.

The location and magnitude of the subsidence pattern shown in Fig. 2 was varied so that 17 additional investigations were performed. For 10 of the investigations, the subsidence pattern was shifted to varying points within each watershed to identify the channel response if the largest magnitude of subsidence was to occur in the upper, middle, or lower portion of the watershed. An additional seven cases were investigated by varying the magnitude of subsidence at common locations in an effort to identify any relationship between magnitude of subsidence and increase in flood levels.

Figure 1 indicates the location of the center of the subsidence cones used in Cases 1, 2, 3, and 4. Each case simulation can be visualized by shifting the areal subsidence (Fig. 2) to the center location on Fig. 1.

ANALYSIS OF RIVERINE SUBSIDENCE

Overview

The impacts of subsidence on the various watersheds have been quantified by changes from the base condition for storm flows, floodplain area, and depth of flooding. The results are shown graphically as a series of trends summarizing the analysis performed on all watersheds.

Subsidence and its Effect on Storm Flows

The 10- and 100-year frequency peak storm flows were computed for each case of subsidence that was analyzed. Data were evaluated in terms of absolute values and the percentage change in values.

From Mannings Equation, channel discharge capacity (Q) is related to the channel slope by the equation

$$Q = 1.49AR^{2/3}S^{1/2}/n \tag{1}$$

or Q is a function of slope when the geometry of the section and flow depth remain unchanged

$$Q = F(S^{1/2}) \tag{2}$$

Accordingly, changes in channel slope should correspond to changes in channel discharge capacity by the relationship

$$Q_2 = F\,[Q_1(S_2/S_1)^{1/2}] \tag{3}$$

Figure 3(a) shows a consistency with equation (3) in that increases in channel slope

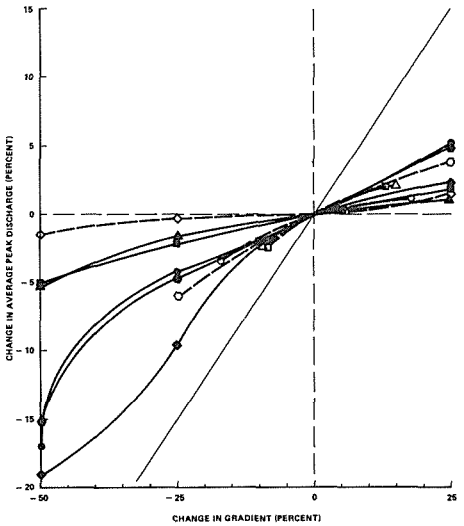

FIG. 3(a) Percent Change in Average Peak Discharge vs. Percent Change in Gradient.

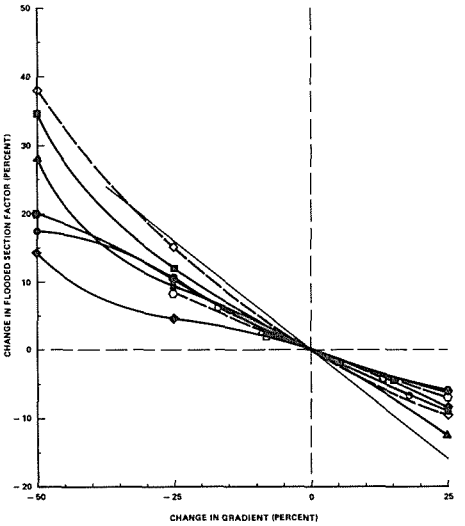

FIG. 3(b) Percent Change in Hydraulic Carrying Capacity vs. Percent Change in Gradient.

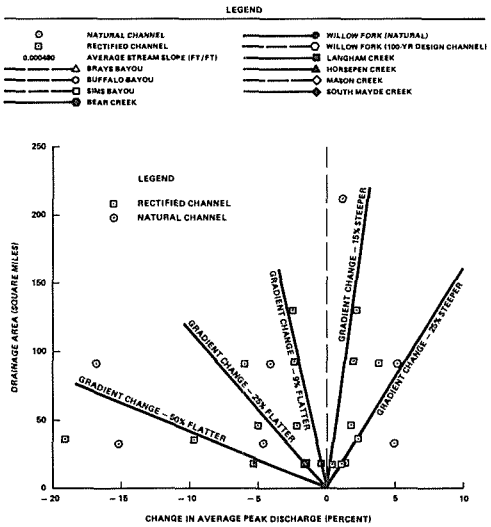

FIG. 3(c) Drainage Area vs. Percent Change in Average Peak Discharge for Changes in Gradient.

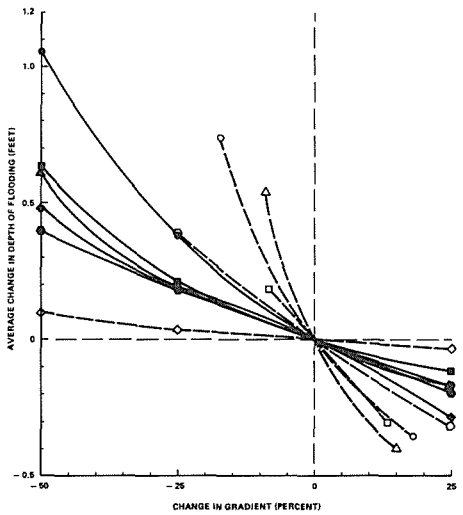

FIG. 3(d) Average Change in Depth of Flooding vs. Percent Change in Gradient.

resulted in increases in discharge capacity. Correspondingly, decreases in slope were accompanied by decreases in discharge capacity. In all cases, however, the magnitude of change in discharge capacity was significantly less than theorized by equation (3). The difference between the observed data and theoretical equation can be attributed to the change in channel storage and conveyance associated with a change in channel slope.

Figure 3(a) indicates that channels with steeper slopes conform more closely to the theoretical relationship than do those with flatter slopes. This can be attributed to the fact that steeper slopes are often associated with narrower floodplains (less storage) and require less section conveyance to pass a given channel flow than do channels with flatter slopes.

Figure 3(b) confirms the conclusion that channel storage and section conveyance accounts for the differential between observed and theoretical changes in discharge capacity. A rearrangement of Mannings equation, equation (1), will give

$$Q/S^{1/2} = 1.49\frac{AR^{2/3}}{n} \tag{4}$$

For purposes of this study, the left-hand side of equation (4) is referred to as the flooded section factor required to pass a given storm flow. The flooded section factor conforms to the same relationship noted in equation (3). Figure 3(b) describes the increase (or decrease) in the flooded section factor associated with a change in slope. Similar to that witnessed in the change in discharge, the change in flooded section factor is less than would be predicted by the theoretical equation. This indicates the shared participation in discharge and channel storage, or flooded section factor, in responding to channel slope changes created by subsidence.

The size of the contributing drainage area also had an impact on the degree of change in discharges caused by changes in stream gradients for both 10- and 100-year storms. Generally, the larger the contributing drainage area, the greater the extent of the change in discharges for each gradient change condition as shown on Fig. 3(c). For flattened gradients, discharges generally decrease and the magnitude of decrease is greater for larger drainage areas. The relationship between magnitude of increase or decrease and drainage area is a result of the cumulative effects of changes in channel storage along the stream. Generally, the larger the drainage area, the longer the length of channel involved and the greater the cumulative effects of gradient changes on channel storage.

Subsidence and its Effect on Depth of Flooding

Figure 3(d) shows the average change in depth of flooding compared to the change in channel gradient. In general, increases in gradient resulted in decreases in the depth of flooding and, conversely, decreases in gradient caused increases in the depth of flooding. No general trends could be identified between the existing channel gradients, or channel type, and the resultant change in depth of flooding because of the anomalies produced by localized conditions of the streams. However, the maximum increase in depth of flooding was observed to occur downstream from the center of subsidence cone in all cases.

Figure 4 indicates that for the 48 case studies, the maximum increase in flooding depth was found to be less than one-third of the related ground subsidence. An average of the conditions tested indicates that in areas where increased flooding occurred, the increase in flooding depth was one-tenth of the related subsidence. A similar magnitude of impact was found to occur in conditions when flood levels decreased. Of these 48 cases, 26 were of the simplified condition of either steepening or flattening the channel slopes and 22 were of the more complex cone simulations. The subsidence simulated for the 26 simplified cases ranged from 1.4 to 39.2 feet with a maximum increase in depth of flooding ranging from -1.7 to 4.0 feet for the 100-year event. The

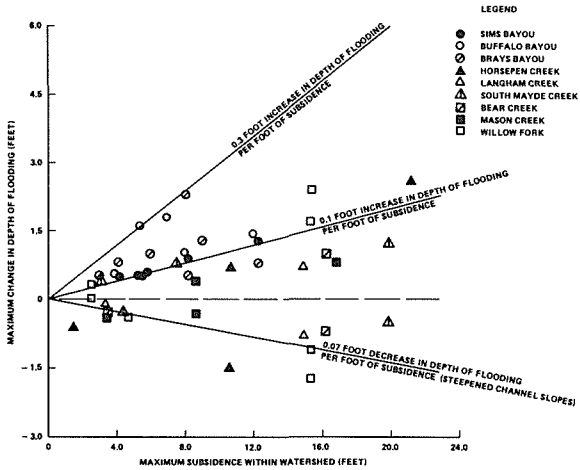

FIG.4 Maximum Change in Depth of Flooding vs. Subsidence (100-Year Event).

subsidence simulated for the 22 cone cases ranged from 2.6 to 12.4 feet with a maximum increase in depth of flooding ranging from 0.0 to 2.3 feet for the 100-year event.

ACKNOWLEDGEMENTS This manuscript was extracted from a report jointly prepared by Turner Collie & Braden Inc., Houston, Texas; Winslow & Associates Inc., Houston, Texas; and Pate Engineers Inc., Houston, Texas.

Land Subsidence (Proceedings of the Fourth International Symposium on Land Subsidence, May 1991). IAHS Publ. no. 200, 1991.

Re-evaluation of the Causes of Subsidence Along the Texas Gulf of Mexico Coast and Some Extrapolations of Future Trends

J. M. SHARP, JR. & R. H. RAYMOND
Department of Geological Sciences, The University of Texas at Austin, Austin TX 78713-7909, USA
S. J. GERMIAT
Hart Crowser, Inc., 1910 Fairview Avenue E., Seattle, WA 98102-3699, USA
J. G. PAINE
Texas Bureau of Economic Geology, The University of Texas at Austin, Box X, Austin TX 78713, USA

ABSTRACT Analyses of National Ocean Service tidal gauge data from the Texas Gulf Coast and first-order releveling surveys conducted by the National Geodetic Survey indicate very high rates of regional relative sea-level (RSL) rise (eustatic level-level [ESL] rise plus subsidence) up to 20 mm/year. The highest overall recent rates (> 10 mm/year) are found in the northeastern area gauge data, from Sabine Pass on the Texas–Louisiana border southwest to Freeport. Lower, but still high rates (4-6 mm/year) are common near the alluvial valleys of the Brazos and Colorado rivers and south to the Rio Grande Valley. Such rates for natural subsidence are not realistic over geologic time. RSL rise on the "stable" Florida platform is about 2 mm/year, which is a conservatively high estimate of regional ESL rise in the Gulf of Mexico. Estimates of natural subsidence for the Texas Coast range between 0.1 and 2.4 mm/year. While extraction of ground water is a well-known cause of subsidence along the Gulf Coast, these areas are localized and some of the highest subsidence (or RSL rise) is in areas with little ground-water production. Extraction of hydrocarbons on a regional basis remains a possible cause for the enhanced rates of observed subsidence. Extrapolation of the trend of the past 20 to 30 years predicts a regional subsidence of nearly one meter by the end of the next century. Furthermore, tidal gauge data from Pier 21 in Galveston demonstrate an increasing rate of RSL rise. Finally, a delphic analysis of the risk of future ESL rise yields a reasonable change that the rise in sea level over the same time frame will be of about the same order of magnitude as that of the extrapolated subsidence. A 2-meter rise in RSL will result in considerable economic dislocations along the Texas Coast because of shoreline retreat and local inundation. These problems will be exacerbated by diminished sediment input to the Gulf by major coastal streams and intensive coastal development. Final determination of the relative amounts of natural and fluid-extraction–induced subsidence will require, among other data, a better areal delineation of subsidence trends over the whole coast.

INTRODUCTION

The Texas coast borders the northwestern quadrant of the Gulf of Mexico (Fig. 1), where up to 15 kilometers of sediments have been accumulating steadily since the Jurassic. These sediments hold America's greatest concentration of mineral wealth, including lignite, uranium, petroleum, base metals, industrial minerals, and ground water. The Texas Gulf Coast has experienced several decades of growth--industrial, municipal, and recreational. Thus, historical and projected subsidence is of great interest.

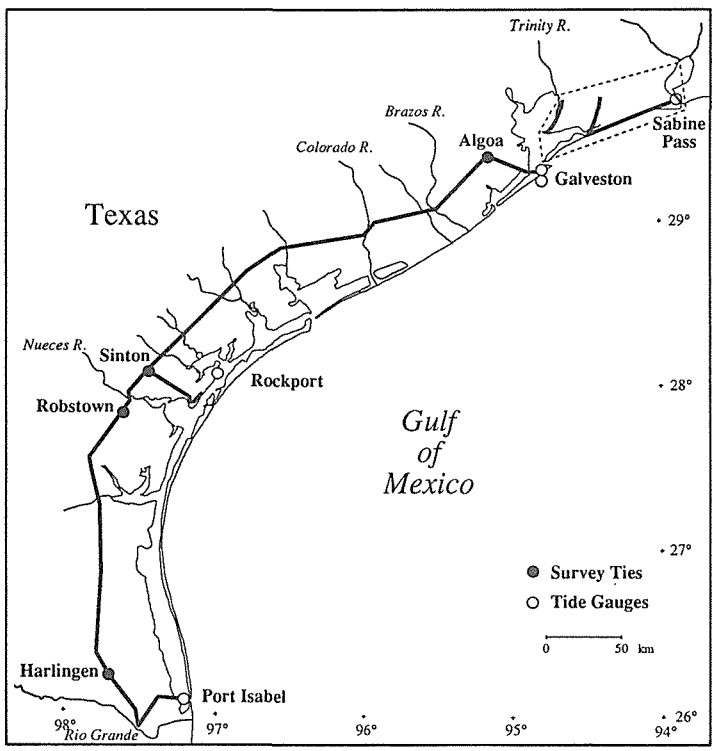

FIG. 1 The Texas coast, showing tidal gauges and releveling lines used. The northwestern coast is evaluated as a special study area.

This important coastal region has experienced significance shoreline retreat during the last century (Morton, 1979) and subsidence caused by ground-water withdrawals has been very well documented (Pratt and Johnson, 1926; Kreitler, 1977; Ratzlaff, 1982; Gabrysch, 1982 and 1984; Holzer and Bluntzer, 1984). Spectacular rates of subsidence (over 2 m in 40 years) have caused inundation and a variety of geotechnical problems. The gradual transition of water supply sources from ground water to surface water has alleviated many of these effects, but recent studies (Germiat and Sharp, 1990; Paine, 1990; and Sharp and Germiat, 1990) have indicated regional relative sea-level (RSL) rises of up to 20 mm/year. These rates encompass wide areas of the region, even where there is little ground-water pumpage. RSL change is the sum of subsidence plus eustatic sea-level (ESL) change; regional tectonic uplift or downwarping could also be included in estimates. Subsidence has numerous causes. The most important of these are: natural

consolidation of sediments, collapse over mined cavities (a very local effect), and subsidence created by withdrawal of subsurface fluids (water or petroleum). Changes in ESL reflect long-term climatic changes as well as anthropogenic factors such as the "Greenhouse effect" on ESL rise. In this paper, we discuss regional geology and subsidence trends, evaluate the Trinity Bay–Port Arthur region as a case study, and present general implications of the observed trends and their extrapolation.

REGIONAL TRENDS

The northwestern Gulf of Mexico contains a thick sequence of clastic sediments deposited on passive (since the Middle Jurassic) continental margin. Clastic sediments covered extensive evaporites that deform, flow, and create salt diapirs. The depocenters (Sharp and others, 1988, their Fig. 1-1) were in the general Houston area (Paleocene-Eocene), then the Rio Grande embayment (Oligocene), and then the Mississippi River embayment (Miocene to present). These sediments are characterized by excess pore-fluid pressures at depth, and the sediments have been undergoing relatively continuous consolidation with fluids expelled upwards and laterally out of them. The basin is classified as a young, compacting basin by Kreitler (1989). Along the Texas coast, the uppermost sediments contain clay layers of high compressibility, which are intercalated with and confine the coastal aquifers. The most important of these aquifers are the Chicot, Evangeline, and Jasper (youngest to oldest); their hydrostratigraphy is discussed by Sharp and others (in press, their Table 1). Natural rates of subsidence are difficult to ascertain, but a range between 0.1 and 2.4 mm/yr is suggested. These figures are based upon tilting of exposed shorelines and estimated sediment cycle thicknesses, 0.1 to 0.15 mm/yr by Winker (1979); the slope of Pleistocene formations, 0.3 mm/yr by Bernard and LeBlanc (1970); and submergence of a Holocene strand line, 2.4 mm/yr by Morton (1979).

Numerous oil-and-gas reservoirs are also present in these sediments. Many are found in young sediments, offshore and near onshore equivalents to the aquifer units, and in other units at depths of up to 20,000 feet (6,000 m). Thick clays and shales are present in Paleocene and Oligocene (including the abundant reservoirs of the Frio Formation) sediments. More significantly, similar low-permeability units also cap and are intercalated with petroleum reservoirs of Wilcox and Claiborne Group sediments. These clays and shales, as well as the reservoirs themselves, are subject to additional consolidation upon petroleum production. Kreitler (1989) demonstrated that many petroleum fields in the Frio Formation have undergone considerable depressurization (Figure 2).

Recent rates of RSL rise for the middle and lower Texas coast (Fig. 1) were estimated from first-order leveling surveys conducted by the National Geodetic Survey (GS) between 1951 and 1982 and monthly sea-level averages from several Texas tide gauges operated by the National Ocean Service (NOS) (Paine, 1990). Relative rates of vertical movement were calculated from elevation differences between an early survey and a later survey relative to an arbitrary datum (benchmark F46 at Sinton) and dividing by the time between the surveys. Survey lines were then tied to tide gauges at Galveston (upper coast), Rockport (central coast), and Port Isabel (lower coast), which allowed RSL rise calculated for these gauges to be correlated across the leveling network. An estimate of sea-level rise relative to the arbitrary vertical datum was made from this correlation, which in turn allowed estimation of rates of RSL rise all along the levelling network (Fig. 3).

Rates of vertical movement along the 500-km-long strike line between Algoa and Harlingen were calculated from elevation changes between leveling surveys completed in 1951 and either 1978 (northern part) or 1982 (southern part). The line between Algoa and Harlingen was connected to tide gauges at Galveston (Pier 21), Rockport, and Port Isabel along three short (40- to 85-km) lines completed in 1978

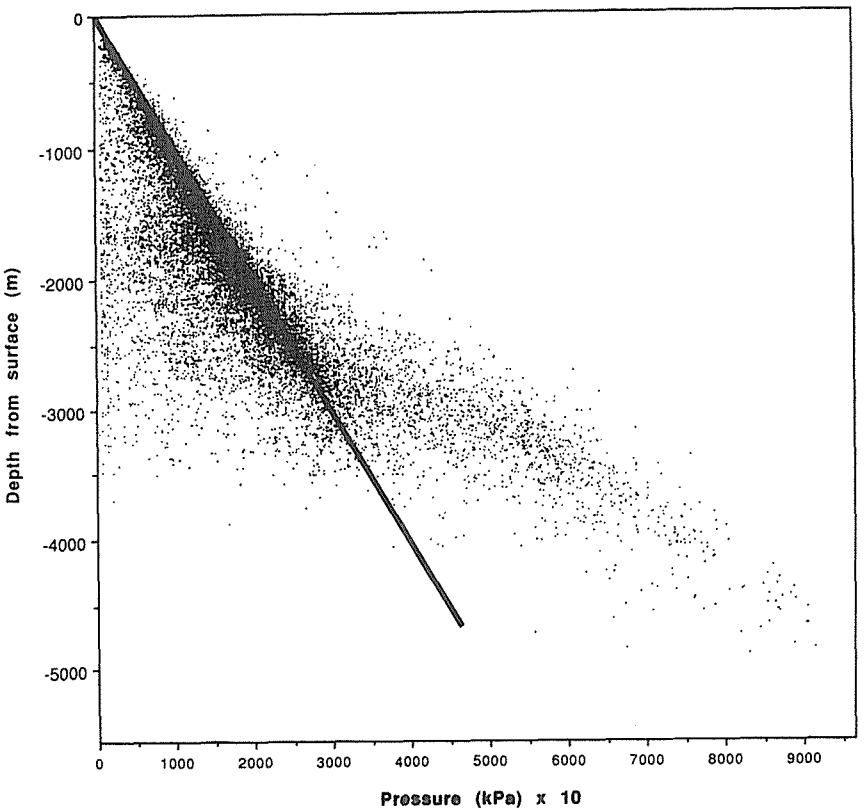

FIG. 2 Fluid pressures versus depth in the Frio Formation, Texas Gulf Coast (Kreitler, 1989; Sharp and others, in press). The solid line represents hydrostatic pressure. Hydrostatic and geopressured sections are evident as is the significant degree of shallow (<3,000 m) reservoir depressurization, plotting left of the hydrostatic line.

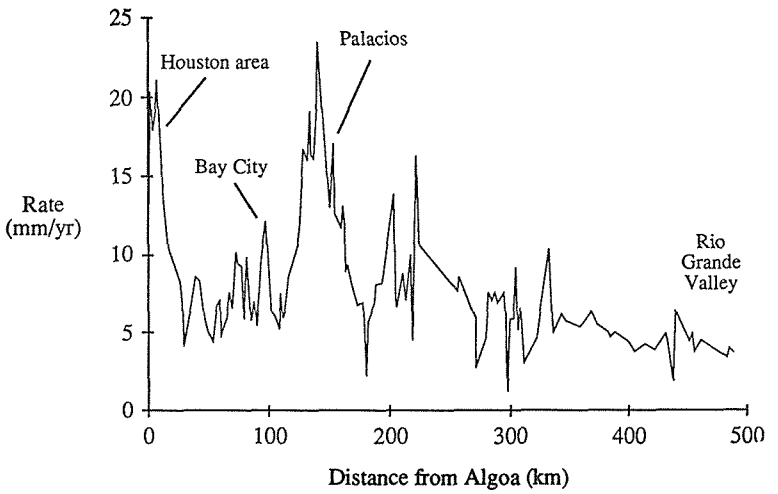

FIG. 3 Rate of RSL rise along the Texas coast between Algoa and Harlingen, from 1951 to 1978-1982.

and 1987 (Algoa to Galveston line), 1950 and 1978 (Sinton to Port Aransas), and 1951 and 1982 (Harlingen to Port Isabel). Connecting the tide gauges across the levelling network demonstrates relative vertical movement. Galveston Pier 21 subsided at the highest rate, about 2.5 mm/yr, relative to benchmark F46; Rockport moved up relative to F46 at about 2 mm/yr; Port Isabel moved up at a slightly higher rate of about 3 mm/yr. Because the rate of ESL rise should be similar for each of these gauges, the rate of relative rise at the gauges should differ by amounts corresponding to their differential vertical movement.

The rate that sea level rose relative to benchmark F46, and thus all other points along the leveling network, was calculated by examining monthly average sea levels for the tide gauges at Pier 21, Rockport, and Port Isabel. For consistency, only the period between the leveling surveys was used; furthermore, only the months during which all three gauges were operating were used. Linear regression of monthly tidal data indicates that sea level rose at an annual rate of 8.2 mm/yr at Galveston, 5.4 mm/yr at Rockport, and 4.6 mm/yr at Port Isabel between 1951 and 1982. These rates of RSL rise are consistent with the differences in rates of vertical movement of these gauges calculated from the leveling data.

By combining rates of sea-level rise at Pier 21, Rockport, and Port Isabel with relative vertical movement along the leveling network, rates of RSL rise can be calculated for the line between Algoa and Harlingen (Fig. 4). These rates were generally between 4 and 8 mm/yr between 1951 and 1982, but reached 15 to 25 mm/yr locally.

There are several areas along the Texas coat that underwent anomalous elevation changes between 1951 and 1984 (Fig. 3). Most of thee areas are moving down relative to the nearby benchmarks, including the Algoa area (-22 mm/yr relative to sea level), Bay City (-13 mm/yr relative to sea level), and Palacios (-23 mm/yr relative to sea level). These correspond to areas of ground-water withdrawals. The Rio Grande valley moved down at 3 to 5 mm/yr relative to sea level, the lowest rate of any large area.

EVALUATION OF SUBSIDENCE IN TRINITY BAY/SABINE PASS AREA

The northeast Texas coast between the Texas–Louisiana border and the Houston–Galveston metropolitan area, bordering Galveston and Trinity Bay, is highly susceptible to rising RSL. Almost 50% of the area is below 1.5 m of elevation and 75 to 80% of the area is below 3.0 m (Fisher and others, 1972; 1973). The shoreline has a narrow beach zone which grades inland to coastal marshes. Data from tidal gauges that border the area are shown in Fig. 4. These indicate rates of RSL rise from 1958 to 1986 of 11.4, 11.1, and 7.3 mm/yr for Sabine Pass and the Galveston gauges (Pier 21, and Pleasure Pier), respectively. These rates are significantly higher than the presumed ESL rise rate of 2 to 2.4 mm/yr, inferred from tidal gauge data from the Florida stations (Sharp and Germiat, 1990). This range is significantly higher than world-wide estimates of 1 to 1.5 mm/yr (e.g., Gornitz and Lebedeff, 1987). Pirazzoli (1986) suggests that even their rates are too high. We speculate that downwarping of the Earth's crust by sediment loading in the northern Gulf of Mexico may be the cause. We cannot differentiate tectonic downwarping and rising ESL effects.

Ground-water withdrawals and related subsidence near Galveston are documented by Gabrysch (1982) at rates of about 4 mm/yr between 1906 and 1978. There has been, however, a general switch to surface-water resources to control subsidence; in the Sabine Pass area, poor water quality has limited ground-water pumpage. Water levels have not declined in the past 20 years (Germiat, 1988), although local subsidence in Orange County, north of Sabine Pass, can be attributed to ground-water withdrawals (Ratzlaff, 1980; Bonnet and Gabrysch, 1982). The

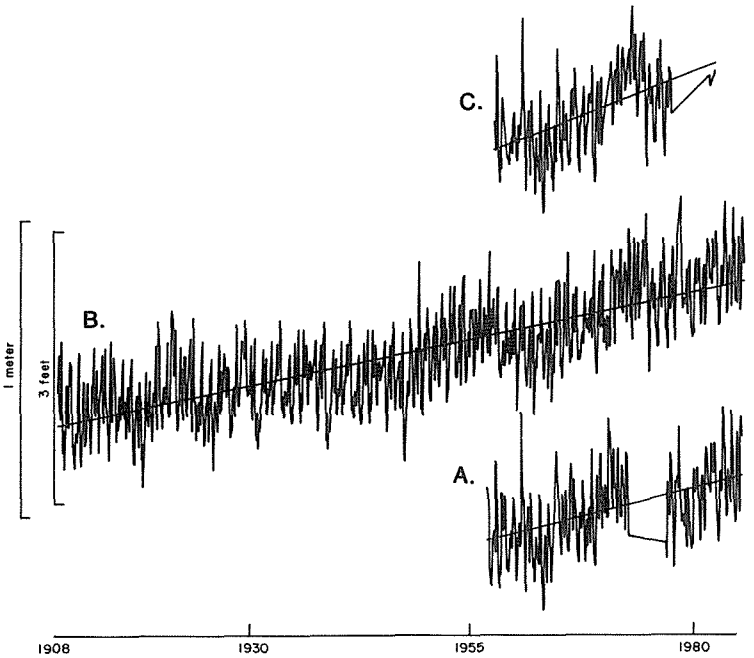

FIG. 4 Tidal gauge data bordering the Trinity Bay/Port Arthur area: A, Pleasure Pier; B, Pier 21; C, Sabine Pass.

regional subsidence trend between Sabine Pass and Trinity Bay was analyzed with synthetic leveling lines, based upon unadjusted elevations using data from Balazs (1980). These do not provide absolute elevation changes, but do indicate spatial variability. As reported by Germiat and Sharp (1990), these analyses indicate that tidal gauge rates are not localized, but they are generally representative of the entire study area. Rates of subsidence are greater near the coast, where there is little ground-water pumpage.

Subsidence caused by petroleum production is well documented within the study area on a local basis at Goose Creek by Pratt and Johnson (1926) and at High Island–Caplen by Ewing (1985). Using Geerstma's (1973) model, Sharp and Germiat (1990) and Germiat and Sharp (1990) analyzed potential reservoir consolidation in eight fields within the study area. Depressurization of the reservoirs could account for 1 to 16 cm of subsidence above the fields. These analyses did not analyze the compressible clay layers above, below, and within the reservoirs. We believe that depressurization of petroleum reservoirs and adjacent reservoirs is widespread. This is borne out by the recent studies of whose data show significant underpressuring of shallow oil and gas reservoirs (Fig. 2). Because the observed rates of undifferentiated RSL rise/subsidence are 1 to 2 orders of magnitude greater than estimated of "natural" subsidence rates, we suggest that broad-scale regional depressurization of oil and gas reservoirs and adjacent clays and shales is a major factor in subsidence in Gulf Coast sediments. The total RSL change in the area is about 11.4 mm/yr with components as follows: 2-2.4 mm/yr in undifferentiated eustatic sea-level rise; 0.1-2.4 mm/yr of natural subsidence; 0-4.1 mm/yr of subsidence caused by ground-water withdrawal; and 2.5 to 9.2 mm/yr of subsidence induced by petroleum reservoir depressurization. The relative magnitudes of the last three components are still

uncertain. This remains a critical issue for future investigations because both absolute and relative magnitudes of subsidence vary along the coast and with time.

IMPLICATIONS

Given the historical rates of Texas shoreline retreat, the high and apparently accelerating rate of RSL rise has important implications for coastal management and geotechnical engineering. An important additional factor of uncertainty involves possible increases in ESL because of predicted global climatic changes. Sharp and Germiat (1990, their appendix 1) used a probability questionnaire to estimate the uncertainties of ESL rise. The responses are shown on Fig. 6) for 2050 and 2100. At 2050 a low-rise scenario (50% probability) and a high-rise scenario (10% probability) yield ESL rises of 0.28 and 1.52 m, respectively. These scenarios at 2100 yield ESL rises of about 0.9 and 3.5 m, respectively. These possible ESL rises

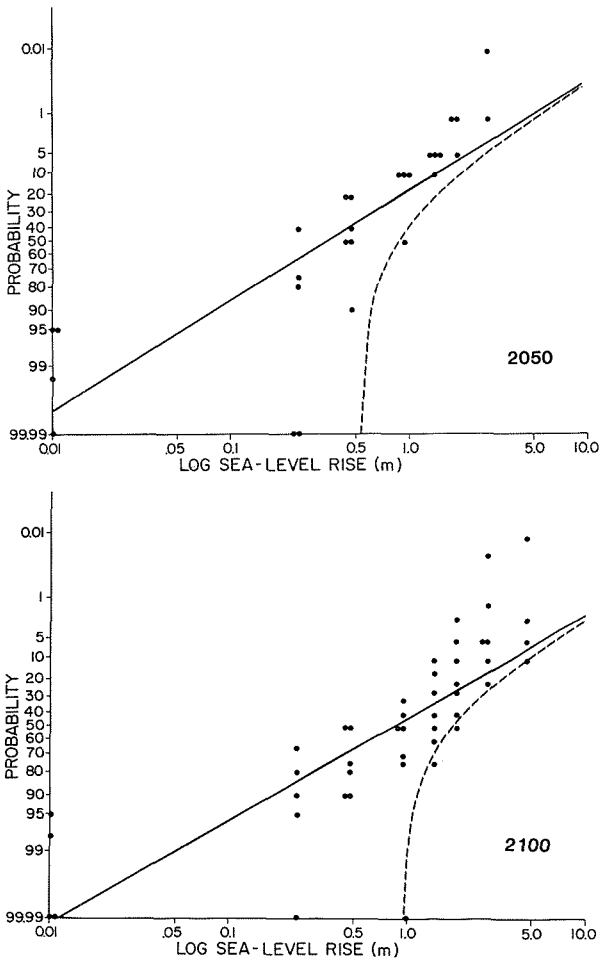

FIG. 5 Probability estimates for ESL rise. Dashed line adds 9 mm/yr subsidence. Note the near log-normal appearance of the data.

coupled with the documented high rates of subsidence provide a threat of inundation and coastal retreat.

Germiat and Sharp (1990) linearly extrapolated historical coastal rates using historical and projected RSL rises. This analysis predicted shoreline retreat rates to 2050, ranging up to 9.2 m/yr and 28.5 m/yr for low-rise and high-rise scenarios. Coastal retreats of over a kilometer are possible; tens of square kilometers of valuable coastlands are predicted to be lost by coastal retreat. Furthermore, their analysis did not consider direct inundation.

There is considerable uncertainty in these projections, but the general trends are clear: high and apparently accelerating rates of RSL rise; areally extensive subsidence; depressurization of petroleum reservoirs; high rates of actual and projected coastal retreat. Additional research is vitally needed on the following: spatial and temporal quantification of subsidence; analysis of regional subsidence caused by petroleum reservoir depressurization; better predictions of future ESL rise; analysis of the effects of diminished sediment input to the Gulf of Mexico coast; and a clearer understanding of probable coastal geomorphic response to both observed and anticipated geologic changes.

CONCLUSIONS

Re-evaluation of regional subsidence along the Texas Gulf Coast led to interesting implications. We conclude that:

a) Regional RSL rise (mostly subsidence) is occurring at rates varying between 4 and 15 mm/yr;

b) High rates of subsidence occur in many areas where ground-water pumpage is minimal and rates significantly greater than previous estimates of natural subsidence;

c) Regional depressurization of petroleum reservoirs is likely a major cause of this regional subsidence; and

d) Significant coastal retreat and inundation will occur in the next century.

ACKNOWLEDGEMENTS Partial support from the Petroleum Research Fund of the American Chemical Society, Sigma Xi, and Gulf Coast Association of Geological Societies is gratefully acknowledged. Thanks also to Emery Balazs, Samuel Moore, and the National Geodetic Survey for providing leveling data and to the Texas Department of Water Resources for providing historical water-level record for coastal index wells. Manuscript preparation was funded by the Owen-Coates Fund of the Geology Foundation of The University of Texas at Austin.

REFERENCES

Balazs, E. L. (1980) The 1978 Houston–Galveston and Texas Gulf Coast Vertical Control Surveys. National Ocean and Atmospheric Administration Technical Memorandum NOS NGS 27. U.S. Government Printing Office, Washington DC.

Bernard, H. A. & LeBlanc, R. J. (1970) Résumé of the Quaternary geology of the north-west Gulf of Mexico province. In: Recent Sediments in Southeast Texas. Guidebook 11. Bureau of Economic Geology, University of Texas, Austin, Tex.

Bonnet, C. W. & Gabrysch, R. K. (1982) Development of ground-water resources in Orange County, Texas, and adjacent areas in Texas and Louisiana, 1971-1980. U.S. Geological Survey Open-File Report 82-330.

Ewing, T. E. (1985) Subsidence and surface faulting in the Houston–Galveston area, Texas--related to deep fluid withdrawal? In: (Dorfman, M. H., and Morton, R. A., eds.), Geopressured-Geothermal Energy. Proceedings of the 6th U.S. Gulf Coast Geopressured-Geothermal Energy Conference, University of Texas, Austin, Tex., 289-298.

Fisher, W. L., McGowen, J. H., Brown, L. F. & Groat, C. G. (1972) Environmental geologic atlas of the Texas coastal zone--Galveston–Houston area. Bureau of Economic Geology, University of Texas, Austin, Tex.

Fisher, W. L., Brown, L. F., McGowen, J. H. & Groat, C. G. (1973) Environmental geologic atlas of the Texas coastal zone--Beaumont–Port Arthur area. Bureau of Economic Geology, University of Texas, Austin, Tex.

Gabrysch, R. K. (1982) Groundwater Withdrawals and Land Surface Subsidence in the Houston–Galveston Region, Texas, 1906-1980. U.S. Geological Survey Open File Report 82-571. U.S. Government Printing Office, Washington DC, 68 p.

Geerstma, J. (1973) Land subsidence above compacting oil-and-gas reservoirs. J. Petroleum Technology 25, p. 734-744.

Germiat, S. J. (1988) An Assessment of Future Coastal Land Loss in Galveston, Chambers, and Jefferson Counties, Texas. Unpublished M.A. thesis, University of Texas, Austin, Tex.

Germiat, S. J. and Sharp, J. M., Jr. (1990) Assessment of future coastal land loss along the upper Texas Gulf Coast. Bull., Assoc. Engineering Geologists 27, in press.

Gornitz, V. & Lebedeff, S. (1987) Global sea-level changes during the past century. In: (Nummedal, D. et al., eds.) Sea-Level Fluctuations and Coastal Evolution. Special Publication No. 41, Society of Economic Paleontologists and Mineralogists, Tulsa, Okla., 3-16.

Kreitler, C. W. (1989) Hydrogeology of sedimentary basins. J. Hydrology 106, 29-53.

Morton, R. A. (1977) Historical shoreline changes and their causes. Gulf Coast Assoc. Geol. Societies Trans. 27, 352-364.

Morton, R. A. (1979) Temporal and spatial variations in shoreline changes and their implications, examples from the Texas Gulf Coast. J. Sedimentary Petrology 49, 1101-1112.

Paine, J. G. (1990) Recent vertical movement and sea-level changes, Texas coastal zone [abs.]. EOS 71, 479.

Pirazzoli, P. A. (1986) Secular trends of relative sea-level (RSL) changes indicated by tide-gauge records. J. Coastal Research 1, 1-26.

Pratt , W. E. & Johnson, D. W. (1926) Local subsidence of the Goose Creek oil field. Jour. Geology 34, 577-590.

Ratzlaff, K. W. (1980) Land-surface subsidence in the Texas coastal region. U.S. Geological Survey Open-File Report 80-969, 19 p.

Sharp, J. M., Jr. & Germiat, S. J. (1990) Risk assessment and causes of subsidence along the Texas Gulf Coast. In: (Fairbridge, R. W., and Paepe, R., eds.) Proceedings of NATO Conference on the Greenhouse Effect, Sea Level, and Drought. Kluwer Academic Publishers, Dordrecht, in press.

Sharp, J. M., Jr., Kreitler, C. E. and Lesser, J., in press, Ground Water. In: (Salvador, A., ed.) The Gulf of Mexico, The Geology of North America. Geological Society of America, Boulder, Colo.

Winker, C. D. (1979) Late Pleistocene Fluvial-Deltaic Deposition of the Texas Coastal Plain and Shelf. Unpublished M.A. thesis, University of Texas, Austin, Tex.

Land Subsidence (Proceedings of the Fourth International Symposium on Land Subsidence, May 1991). IAHS Publ. no. 200, 1991.

Land Subsidence and Flooding in Bangkok

R.N. YONG
Geotechnical Research Centre, McGill University, 817 Sherbrooke St. West, Montreal, Canada H3A 2K6
P. NUTALAYA
Asian Institute of Technology, Dept. of Geotech. and Transportation Engineering Bangkok, Thailand
A.M.O. MOHAMED and D.M XU
Geotechnical Research Centre, McGill university, 817 Sherbrooke Str. West, Montreal, Canada H3A 2K6

ABSTRACT

In the last thirty years, the area affected by land subsidence in the Bangkok Metropolitan Region (i.e. City of Bangkok and surrounding region) has grown to more than 4,550 km^2 in size, with maximum subsidence in many localized regions exceeding 1600 mm. the extremely flat and low-lying nature of the terrain, together with differential ground subsidence, renders the region very susceptible to excessive flooding. Unless corrective action is undertaken, the situation will continue to deteriorate, and the socioeconomic penalties will also continue to mount.

INTRODUCTION

The Bangkok (Thailand) metropolitan area is located on the delta and flood plain of the Chao Phraya river. The river has developed a meander belt of about 10 km wide in the Lower Central Plain (known also as the Lower Chao Phraya Basin) as it courses to the Gulf of Thailand. The Basin extends 200 km to the north (from the gulf of Thailand) and about 175 km from east to west. The underlying geology of this Basin consists of a thick sequence of sediments formed in the later Tertiary to Quartenary period, with sediment thickness in excess of 500 m. The region is principally low lying and flat,and is about 1.5 m above mean sea level.

As reported by Yong and Nutalaya, (1988),the Lower Central Plain was formed by fault tectonics during the Tertiary time and filled with clastic sediment during the Quarternary period. The basement bedrock consists of quartzite, gneiss, granitic gneiss, and gently inclines southwards to the Gulf of Thailand. The strata overlying the basement complex are unconsolidated to semi-consolidated sediments of Tertiary to Quarternary geologic age-as noted above-with depositional features considered as river plain and deltas with occasional shallow marine incursions.

The drainage system in the Basin consists of the Pasek, Chao Phraya, and Suphan rivers and their tributaries, and the total drainage area is about 55,000 km^2. There are at least 8 aquifers identified in the substrate system, with a corresponding number of aquitards. It is the nature of these aquitards, and their subsequent reduction in thicknesses, that has contributed significantly to the problem of land subsidence and prolonged flooding of the region.

As a result of rapid industrial and population growth, Bangkok is confronted with many of the problems faced by other metropolitan centers where rapid and controlled urban growth occur- i.e. inadequate infrastructure and related facilities, traffic congestion, low-cost housing problems, mass transportation problems,

environmental pollution and waste management problems, inadequate (delivered) water supply, etc. In coastal metropolitan centres founded on soft deposits, the problems can become more complicated if the underlying hydrogeology is utilized for water supply and is inadvertently mismanaged in the process of utilization. In the particular situation being reported herein, i.e. land subsidence and aggravated flooding of Bangkok, the root cause of the problems appears to be a direct function of excessive (and long-term) groundwater withdrawal. Because of the present inadequate water supply, well pumping (withdrawal) rates have exceeded 1 million cubic meter per day, causing thereby significant lowering of the piezometric levels of the aquifers.

LAND SUBSIDENCE AND FLOODING

The low-lying flat nature of the terrain which characterizes the landform on which Bangkok is founded, renders the region very susceptible to flooding if depressions in the terrain surface become dominant. With present ground elevations ranging from 0 to 1.5 meters above mean sea level, flooding is a regular event during the rainy season and seasonal high tides. According to Nutalaya et al. (1989), with the present drainage system, a 30 mm rain can cause flooding of a few centimeters on some streets which would last for up to 6 hours. If rainfall is grater than 60 mm, extensive flooding occurs, - lasting for periods of 6 to 24 hours.

The problem becomes more severe during the high tide season in October to December, when tides can rise up to 1.35 m above mean sea level. When this occurs,the chao Phraya river is raised (as are the other rivers), and water will flow back into the series and canals. Hence land subsidence can pose a particularly undesirable situation. The effect of flooding on the population, the buildings and infrastructure, conduct of business, etc. is not easily calculated. For example, it is estimated that in the most severe flood of the 1980's (1983), which lasted 4 months, the losses and damage amounted to about 6,600 million Baht 1 billion Baht is approximately 40 million U.S. (*Sodsathit*, 1989).

The dilemma that faces the decision makers centres around several difficult issues: (1) continued exploitation of groundwater to augment surface water supply - i.e. conjunctives use of both surface and subsurface water; (2) the need to reach a steady-state or positive condition between recharge of aquifers supplying the groundwater and well pumping (withdrawal), and (3) economic trade-offs if groundwater water utilization is curtailed or totally discontinued, - substituted by increasing surface water supply (*at what cost?*)

The link between land subsidence and groundwater extraction via well pumping - for the Bangkok Metropolitan Region - has been well established, e.g. Nutalaya et al (1989), Yong and Nutalaya, (1988), A.I.T., (1978 ,1980,1981). From the network of monitoring stations installed in previous studies by A.I.T. and the Royal Thai Survey department, the extent of land subsidence between the year 1978 and1986 can be seen in Figure 1. Since the many wells located in the region are not necessarily terminated at the same depth,the data shown in Figure 1 indicate measurements for monitoring points located at various depths, to measure subsidence due to consolidation of the subsurface layers within those depths. Thus for example the top "curve" shows surface subsidence caused by the consolidation of the subsurface sediment in the 1 to 10 m depth (below ground surface). Correspondingly, the other two "curves" show surface settlement in the 1 to 27 m and 1 to 196 m depth. The bottom "curve" which shows the effect of water extraction from the layer of sediment up until the 194 m depth, suggests that subsidence is still continuing, albeit at a slower rate. The slower rate is reflective of the characteristics of subsidence and its secondary effects, and also

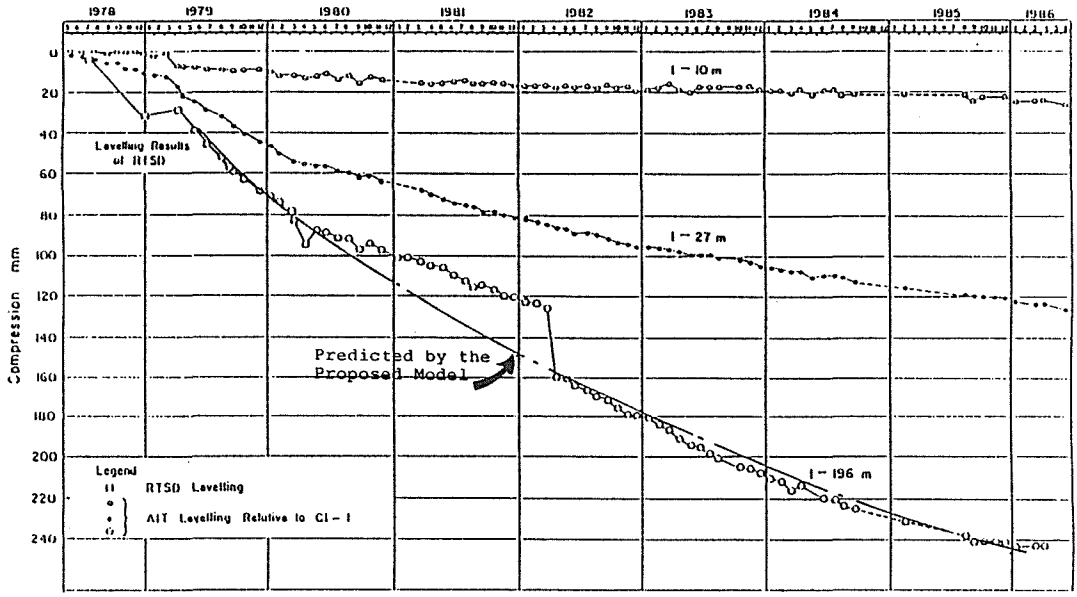

FIG. 1 Subsidence at Station 8 observed from deep instruments.

of the fact that the rate of well pumping (extraction) has been decreased. We should note that the 245 mm "compression" of the 196 m of sediment has occurred over a ten-year period, and that this should be added on to the previous amounts of "compression" (not recorded) occurring prior to 1978.

RESEARCH AND REMEDIATION

In the study undertaken on a cooperative basis between A.I.T. and the Geotechnical Research Centre (GRC)of McGill University, under the sponsorship of IDRC, it was agreed that if alleviation of ground subsidence was to be obtained, the balance between aquifer input and output must be realized. Whilst this mass flux balance requirement appears obvious and should apparently be simple to implement, the reality of the situation is far from simple. The tasks and research needed to obtain mass flux balance required the following items to be addressed:

1. determination of the continuity (or lack thereof) of the aquifers and communication between aquifers - *hydrogeology of the Basin;*
2. physical, mechanical and hydraulic properties and characteristics of aquifers and quitards;
3. physical/analytical modeling of the Basin aquifer system accounting for input /output fluxes and resultant land subsidence, and
4. natural recharge augmentation requirements (*artificial recharge?*, technology, economic feasibility, and viability.

Two prominent indicators (of the problem) can be readily measured: (a)the surface subsidence, (*identified as the problem itself to be studied)* , and(b)the piezometric levels in the aquifers, (*pressure head drops or phreatic levels*). The cooperative study undertaken between A.I.T. and GRC (begun in 1986) has been reported in detail by Yong and Nutalaya (1988). Some of the reported results are given in the following:

Underlying Geology

The geologic classification of the sediments overlying the basement bedrock was made on the basis of soil type, depositional environment and geologic age. The stratigraphic profiles from north to south and from east to west show that the subsurface strata below 50 m depth can be grouped into two major types:

(1) sand layer: - coarse-grained sediments with high permeability and low compressibility, and
(2) - fine-grained sediments with low permeability and relatively high compressibility.

The depths and thicknesses of the first five aquifers and aquitard were obtained during the course of the subsurface exploration program.

Compositional Features

Compositional analyses of borehole samples from the Ban Tamur area, for the fine-grained sediments, showed that the clay minerals consist of mainly kaolinite, illite, smectite and a small amount of possible chlorite with mixed-layer clay minerals. Non-clay minerals identified include quartz, K- feldspar, plagioclase, calcite, dolomite, and siderite. It would appear (from the results obtained) that smectite generally increases with depth, while kaolinite decreases with depth (of deposit). The dominant water soluble ions in the soil pore fluids of the borehole samples were sodium and chloride, in the range of 10 to 30 meq/100g of soil, while alkaline cations (Ca and Mg) range from 0.5 to 5 meq/100 g of soil. The soluble ion concentrations with depths do not show any distinct variation except the highest Na and Cl contents in the uppermost (layer) samples reflect the marine compositional environment of the top soft clay. The major adsorbed cations on the solids are Ca and Na. The higher concentration of Ca in the samples appear to be consistent with the relative abundance of smectite in the samples.

Hydrogeochemistry

The groundwater in the Lower Central Basin was characterized on the basis of hydrochemical facies and can be grouped into five major types: Type I, fresh Ca-HCO_3, Type II, Ca-HCO_3-Na-Cl, type III, Na-HCO_3, Type IV, moderately saline Ca-Na-Cl,and Type V, saline Na-Cl. Type I water occurs at shallow depths, in the areas covered by recent alluvial deposits. Type III water appears to be the most common hydrocehmical facies in the study area, occurring at depths of 100 to 500 m in the central region of the Basin. Type IV water occurs in the south-eastern region, at depths between 50 and 100 m, while Type V water appears confined to the first aquifer.

Chemical analyses of samples collected in the summer of 1986, from the Bangkok area, showed unexpected wide ranges of hydrochemical composition. A sample from the third aquifer (Phra Pradaeng aquifer) showed type III water with dissolved solids of 60 mg/l, whereas a sample from the fourth aquifer (Nakhon Luang aquifer) showed a greater enrichment of Ca, Na, and Cl with total dissolved solids of 14,000 mg/l. Whilst the hydrochemical distribution in the Bangkok area appear to be similar to that of the Basin, the Type IV water which is predominant in the 50 to 100 m depths shows a highly variable bottom boundary-indicative of the deterioration of groundwater quality.

The isotopic ages of the groundwater, determined by ^{14}C analyses indicates that the bulk of the groundwater in the Basin is considerably younger than the corresponding sediments of the Basin, but older than the last regression in the

area. The data suggest that the formation water of the sediments had been flushed out by recharge water during deep groundwater circulation , and has evolved to the present water type

The ^{18}O and ^{2}H isotopic analyses of the groundwater indicate that the Type I water is a recharge water of "modern" origin, obtained most likely through infiltration processes through the alluvia, deposits. The groundwater flow, established on the basis of the ^{18}O enrichment suggests that the recharge water in the Mae Klong river basin moves towards the Chao Phraya river basin,and that the recharge water in the northern region moves to the south along a flow path similar to the Chao Phraya river.

Geotechnical Properties

The geotechnical tests conducted served to provide information concerning the consolidation and hydraulic properties of the underlying soil sediments. Of particular importance was the determination of the coefficients of consolidations of the aquitards, and the permeabilities of the aquitards and aquifers.

Physical and Analytical Modeling/Prediction

Fundamental to the capability for prediction of the performance of the aquifers and resultant subsidence, is the requirement for a realistic model representing the well pumping (withdrawal)/subsidence phenomenon. The sketch shown in Figure 2 which idealizes the problem at hand, shows horizontal groundwater flow in the aquifer in response to the extraction well demands. At the same time, because of the pressure drop in the aquifer, water from the aquitard will flow downward

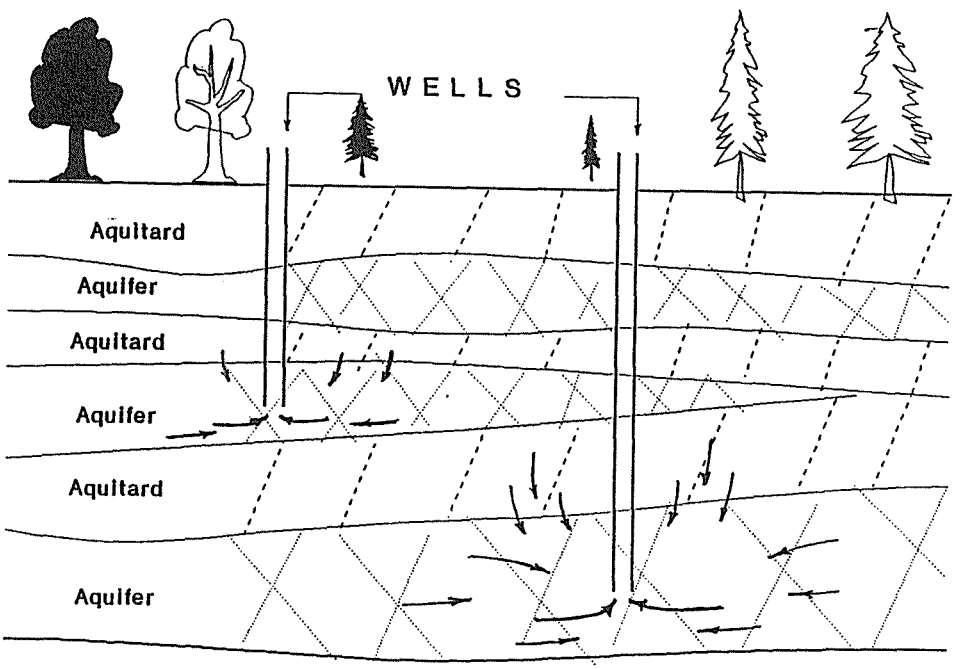

FIG. 2 Pictorial representation of well pumping (withdrawal) and flow response in a multi-aquifer system.

into the aquifer (Figure 3). It is this particular response action (pore water depletion in the aquitard) that causes the subsidence observed at the ground surface - since water flow from the aquitard cause a compression of the aquitard. The "pear-shaped" pressure drop "surface" shown in Figure 3 is indicative of the piezometric head, and represents the effect of well pumping (withdrawal). Since this is a boundary "effect", the physical phenomenon can be analyzed by studying the pressure drop-time (piezometric head- time) relationships in both the aquifer and aquitard. The sketch in Figure 4 shows the "modeling" scheme adopted by Yong et al., 1989 and 1991, using a radial coordinate system. The system is considered to be axially symmetric-for simplicity in computations.

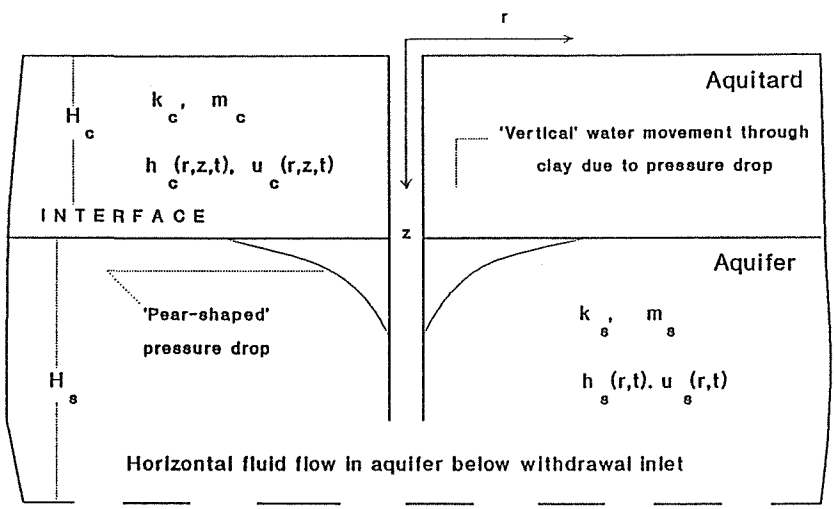

FIG. 3 Double aquitard-aquifer model showing pressure head drop as "pear-shaped" boundary in the aquifer.

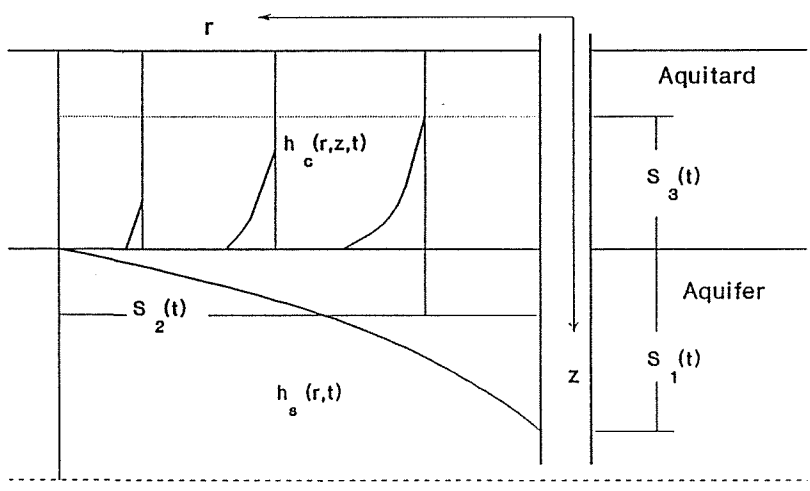

FIG. 4 Pressure drop profiles in aquitard and aquifer.

The analytical model essentially seeks to determine the pressure head drops in the aquifer, $h_s(r,t)$, an aquitard, $h_c(r,t)$, as a function of the transmission and compression properties of the aquifer and aquitard layers respectively. It is reasoned that if one can express the shape of the pressure head drops in terms of radial distance r (away from the centerline of the well), time t, and depth z, in both types of soil layers - as a function of the controlling soil properties - a reasonable analysis or prediction of the groundwater regime could be obtained. The fundamental consideration herein is the requirement for a measurable set of parameters. The pressure head drop (piezometric heads) is easily measured in the field via monitoring wells, and the compression (consolidation) and hydraulic transmissivity properties of the soils can be obtained through laboratory testing. One obviously presumes that proper care and procedures are used for monitoring and laboratory testing.

The analytical/computer model develops at the Geotechnial Research Centre McGill university and identified as IDRC BASIC COUPLED MODEL provides the capability for assesment and prediction for the deterioration of the drawdown of the phreatic surface and its progress over time based on groundwater withdrawal from a single well. This model is described by Yong et al. 1989 and 1991. A trial-function technique is implemented whereby a polynomial function describes the shape of the phreatic surface based on the governing equation for hydraulic pressure head. This method assumes a two-dimensional, semi-infinite medium, wherefrom, water is pumped. Flow is assumed to be one- dimensional in the horizontal direction. Initial conditions are assumed to be hydrostatic. For a multi-well system all wells are considered active simultaneously and are averaged in a single, equivalent well. The model is capable of predicting the variation of the phreatic-surface drawdown with time around a single or cluster of wells.

Input Requirement

The input requirements for the IDRC BASIC COUPLED MODEL are summarized as follows: 1) discharge rate for a single well or for a cluster of wells represented by a single equivalent well; 2) well readius; 3) depth/length of well; 4) horizontal/radial permeability, and 5) horizontal/radial coefficient of consolidation.

Field Validation

Using data from AIT Comprehensive Report 1978-1981, the station 8 measurements are used for comparison with the theory. The physical parameters as well as geometric parameters can be calculated as follows:

(1) aquifer thickness (H_s): since the model simulates the subsidence of one aquifer and one aquitard, H_s must be calculated in a global sense. An approximate estimation of total aquifer thickness can be taken as H_s=100m;
(2) well's diameter: From the comprehensive report titled "Groundwater resources in Bangkok area: development and management study", 19878-1981, AIT, the well's diameter is 76.2 and 63.5mm for different stations. Choose d=63.5 mm;
(3) η: which indicates the leakage percentage from one aquifer layer to the neighboring aquifer layers. Since the aquifer layers thickness has been combined in a global sense, therefore should be taken as zero;
(4) well's pumping rate: which refers to the rate of pumping of one individual well. The total pumping rate in Bangkok area is $Q = 1.35 \times 10^6 m^3/day$ which comes from approximately 11000 wells. The pumping rate of each individual well can be calculated by averaging as follows:

$$Q = 1.35 \times 10^6/11000 = 122.73m^3/day \tag{1}$$

(5) K_s, which equals to aquifer conductivity, can be assumed to have a value of 100 m/day;
(6) K_c, which equals to aquitard conductivity, can be taken as $K_c = 10^{-4}m/day$;
(7) compressibility of aquifer: $\rho_w g m_s = 10^{-6}m^{-1}$, and
(8) compressibility of aquitard: $\rho_w g m_c = 5 \times 10^{-3}m^{-1}$.

The generalized coordinates $S_1(t), S_2(t)$ and $S_3(t)$, (Yong et. al. 1991) which refer to pressure head front moving in aquitard in vertical direction, pressure head front moving in aquifer horizontally and water pressure head drop, can be calculated as follows:

$$S_3(t) = \left\{6\frac{K_c}{\rho_w g m_c}\right\}^{\frac{1}{2}} t^{\frac{1}{2}} \tag{2}$$

$$= 6.618m \left\{\frac{t(year)}{year}\right\}^{\frac{1}{2}}$$

$$S_2(t) = \left\{\frac{72(1-\eta)r_o H_s K_s}{[6K_c m_c \rho_w g]^{\frac{1}{2}}}\right\}^{\frac{1}{3}} t^{\frac{1}{6}} \tag{3}$$

$$= 632m \left\{\frac{t(year)}{year}\right\}^{\frac{1}{6}}$$

$$S_1(t) = \frac{Q_i}{4\pi r_o H_s K_s} S_2(t) \tag{4}$$

$$= 19.44m \left\{\frac{t(year)}{year}\right\}^{\frac{1}{6}}$$

And the total subsidence can be calculated as follows:

$$\bar{u}(t) = \frac{1}{18(1-\eta)} \rho_w g S_1(t) \{3H_s m_s + S_3(t) m_c\} \tag{5}$$

$$= 0.000324 \quad m \left\{\frac{t(year)}{year}\right\}^{\frac{1}{6}} + 0.0715m \quad \left\{\frac{t(year}{year}\right\}^{\frac{2}{3}}$$

It can be seen that the first term is much smaller than the second term, therefore,

$$\bar{u}(t) \approx 0.0715 \quad m \left\{\frac{t(year)}{year}\right\}^{\frac{2}{3}} \tag{6}$$

If one takes the beginning of 1980 as a reference time and assumed that the pumping continuously functioned for 1 year, therefore the initial subsidence value form Fig. 1 is 42 mm. With such initial value , the subsequent calculated subsidence for each year will be added to the initial value to get the total subsidence. The dotted line in Fig.1 is the predicted subsidence for station 8. The comparison between the predicted and measured values shows the ability of the developed model to predict the subsidence.

CONCLUSION

The urban hydrogeological problem in Bangkok is detailed in regard to the underlying site charactersics, properties, and subsidence development. In addition field validation of the developed analytical/computer coupled model for assessment and prediction of the effects of well pumping is addressed. It can be noted that the coupling effect between the horizontal hydraulic field in the aquifer, generated in response to well withdrawal, and the vertical subsidence stress field in the aquitard, generated as a result of fluid flow from the aquitard to the aquifer below, in response to the pressure head drop in the aquifer is central to the expression describing the pressure head-time relationships sued in the modeling protocol. From the results obtained some salient features are noted:

(1) subsidence is caused mainly by consolidation of the aquitard;
(2) the pressure head front (in vertical direction), $S_3(t)$, progresses in the aquitard in a typically slow fashion in comparisons with the front in a horizontal direction, $S_2(t)$, in the aquifer, and
(3) the basic average subsidence in a single well system is proportional to $t^{\frac{2}{3}}$.

The effectiveness of the geometric, physical, and mechanical properties of the soil substrate is reflected in $S_1(t), S_2(t)$ and $S_3(t)$ explicit formulae, i.e. the $S(t)$ functions.

ACKNOWLEDGMENTS

In addition to the research team members for both A.I.T and GRC McGill who contributed greatly to the study, acknowledgments need to be made to the project officers of IDRC who at one time or another, were responsible for the project - on behalf of IDRC, and who provide valuable input to the Project. These included: Dr. M. Tremblay,Dr. R. Vincencio, Dr. S. Mukerji, Dr. D. Anton,Dr. A. Gyi, and Mr.C. Pilon. Special thanks should be extended to Dr. Paket Kiravanich of the Ministry of Science, Technology and Energy (Thailand), for his continued encouragement and support.

REFERENCES

Asian Institute of Technology (1978) Investigation of Land Subsidence Caused by Deep Well Pumping in the Bangkok Area, Phase I Final Report, AIT Research Report No. 87.

Asian Institute of Technology (1980) Investigation of Land Subsidence Caused by Deep Well Pumping in the Bangkok Area, Phase II Final Report, AIT Research Report No. 89.

Asian Institute of Technology (1981) Investigation of Land Subsidence Caused by Deep Well Pumping in the Bangkok Area, Comprehensive Report 1978-1981, AIT Research Report No. 91.

Nutalaya, P., Yong, R.N., Chumnankit, T. and Buapeng, S. (1989) Land Subsidence in Bangkok During 1978-1988. Proc. Workshop on Land Subsidence - Whats Next, Bangkok.

Sodsathit, A. (1989) Bangkok Flood and Control. Proc. Workshop on Land Subsidence - What Next, Bangkok.

Yong, R.N. and Nutalaya, P. (1988) Impact of Quarternary Sediments on Urban development and Land Use of the Central Plain of Thailand. Final Report, Report to International Development Research Centre (IDRC), Canada

Yong, R.N., Xu, D.M. and Mohamed, A.M.O. (1989) Ground Water Resource

Management Model Final Report, Report to International Development Research Centre (IDRC), Canada

Yong, R.N., Mohamed, A.M.O. and Xu, D.M. (1991) Analytical Solution for a Coupled Hydraulic and Subsidence Model Using a Characteristic Surface Method. ASCE, Geotech. Eng. Congress, Boulder, Colorado, June 10-12.

Land Subsidence (Proceedings of the Fourth International Symposium on Land Subsidence, May 1991). IAHS Publ. no. 200, 1991.

Use of the Global Positioning System (GPS) for Ground Subsidence Measurements in Western Venezuela Oil Fields

A. CHRZANOWSKI & Y.Q. CHEN
Department of Surveying Engineering, University of New Brunswick, Fredericton, N.B., Canada, E3B 5A3
J. LEAL & J. MURRIA
Maraven S.A., Apartado 173, Lagunillas 4016-a, Venezuela
T. POPLAWSKI
The BSC Group, Inc. 425 Summer Street, Boston, MA 02210, USA

ABSTRACT Oil production along the east coast of Lake Maracaibo in Western Venezuela produces ground subsidence which affects an area of about 1000 km^2 in the form of three subsidence basins. Since 1929 the accumulative subsidence has reached 5 m with the present rate of subsidence reaching 0.2 m per year in some locations. A levelling network consisting of over 1600 benchmarks has been remeasured every two years to monitor the subsidence. The levelling surveys are slow and expensive. In 1986, Maraven together with the Department of Surveying Engineering at the University of New Brunswick in Canada, initiated a project to test and implement the satellite Global Positioning System in the monitoring surveys. The new monitoring scheme which combines GPS with terrestrial levelling surveys is expected to bring a savings of over 30% in time and money. After initial test surveys in Canada and in Venezuela between 1986 and 1988, the full implementation of GPS has been performed in 1990 obtaining the average standard deviation of 11 mm of the adjusted GPS height differences over average distances of 10 km. A further increase in the accuracy is expected when more GPS satellites become available. A mathematical model and software for the integrated analysis of subsidence have been developed.

INTRODUCTION

Oil production along the east coast of Lake Maracaibo in Western Venezuela began in the late 1920s in Lagunillas. The extraction from the comparatively shallow (300-1000 m deep), unconsolidated, and highly porous reservoir resulted in ground subsidence which affects an area of about 1000 km^2 in the form of three separate subsidence basins (Murria, 1991) corresponding to the Tia Juana, Lagunillas, and Bachaquero oil fields as shown in Fig. 1. The accumulated subsidence has reached 5 m with the maximum rate of subsidence being about 0.2 m per year at some points. The subsidence in the whole area has been monitored since 1929 using conventional geodetic levelling with over 1600 benchmarks connected to some points considered to be outside of the subsidence area. The levelling network consists of 800 km of primary (main network) and 600 km of second-order densification surveys. A recent accuracy evaluation of the levelling surveys (Leal, 1989) indicates that the main levelling network has been measured with a standard deviation of 2 mm$\sqrt{K}$, where K is in kilometres, and the second-order levelling with a standard deviation of 4 mm$\sqrt{K}$ giving an overall average accuracy (standard deviation) of 10 mm in the subsidence determination. The complete survey has been repeated every two years with a portion of the network (about a third of the whole area)

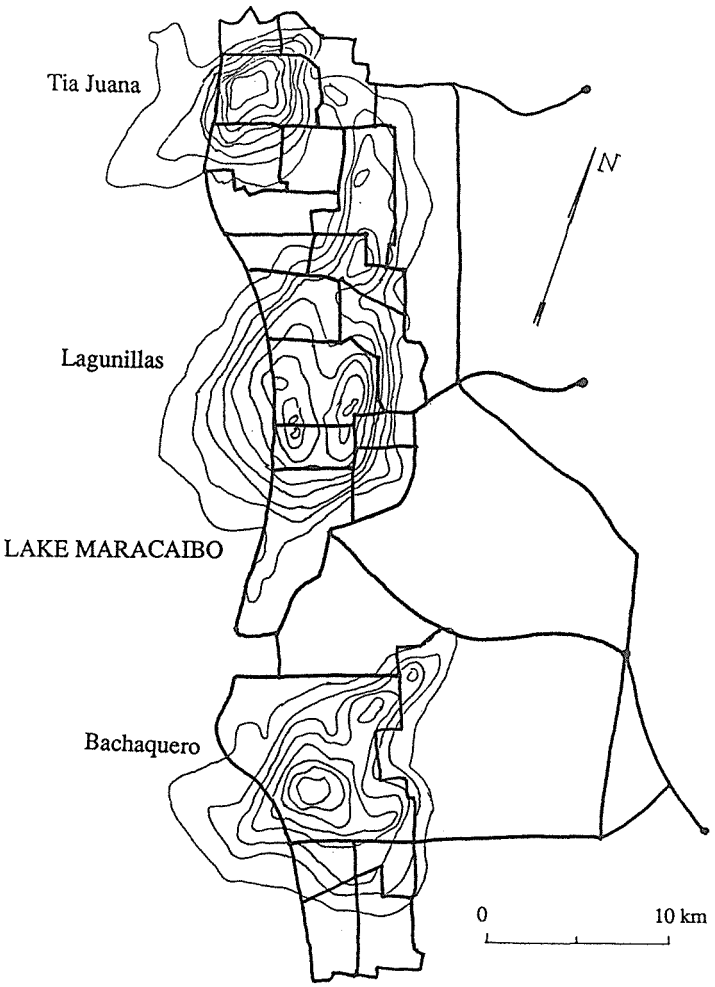

FIG.1 Subsidence basins with 0.5 m contour interval and the main levelling network.

remeasured every six months for the purposes of upgrading protective coastal dykes, updating the irrigation system, and controlling the stability of offshore platforms and plants.

The levelling survey is a slow, expensive, and labour intensive operation. Five survey crews need about three months to measure the whole subsidence area at a total cost of over US$200,000 per campaign (Leal, 1989). In 1986, in a search for a more economical monitoring method, the co-authors from the University of New Brunswick (UNB) suggested that the satellite Global Positioning System (GPS) be introduced into the monitoring scheme to replace the main levelling network and the long lines connecting to the stable points with a GPS network combined with the second-order levelling surveys (Fig. 2). The new monitoring scheme has been expected to bring a savings of over 30% in time and money.

An accuracy pre-analysis of the combined monitoring scheme has indicated that in order to achieve the accuracy of ground subsidence compatible with the accuracy obtainable with levelling surveys alone, the GPS surveys should give the standard

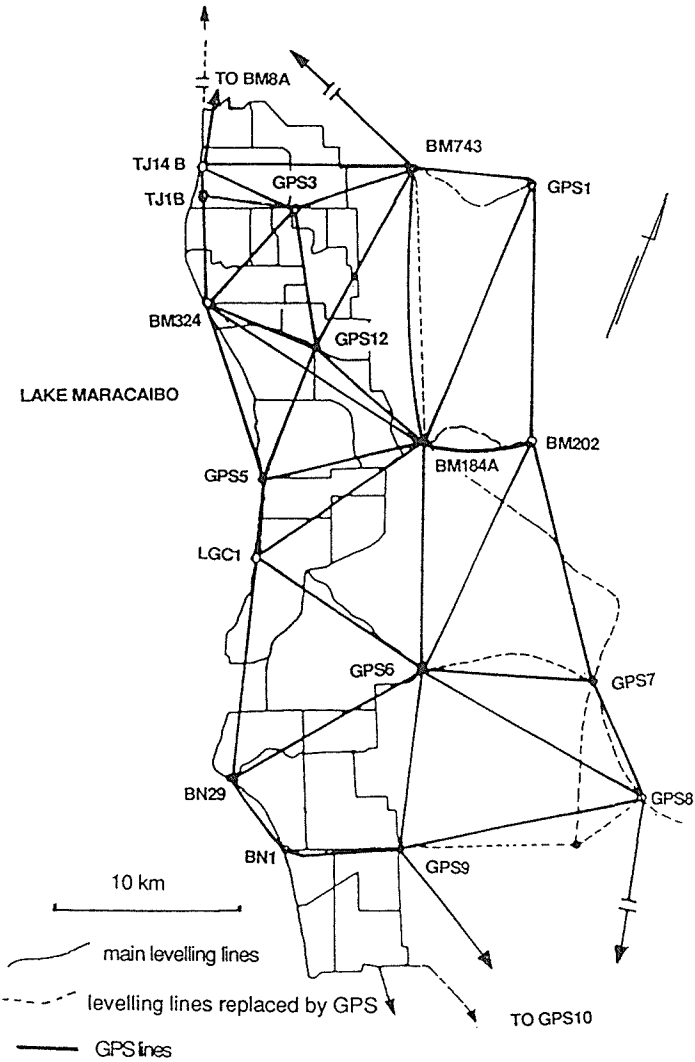

FIG.2 GPS aided monitoring scheme.

deviation of the observed height differences smaller than 15 mm over the average lines of 10 km long. Therefore, before implementing the GPS in the subsidence surveys, extensive tests had to be done on the achievable accuracy of GPS in the hot and humid climate of the subsidence area. In addition, a mathematical model and software for the integration of GPS with geodetic levelling had to be developed. In 1986 and 1987, a total of five test measurements were performed with three survey campaigns on a test network established by UNB near Fredericton, N.B., Canada, and two test surveys on a portion of the monitoring network in Venezuela. The full implementation of GPS in the monitoring surveys in Venezuela was attempted in 1988 and repeated in 1990.

This paper, after reviewing the basic principles of GPS, outlines the methodology developed for the integrated analysis of ground subsidence and gives a summary of the test and implementation results.

USE OF GPS IN DEFORMATION SURVEYS

Basic principles of GPS surveys

GPS is a satellite-based positioning system developed by the U.S. Department of Defence. When fully operational (1993) it will consist of 24 satellites arranged in six orbital planes, each with a 55° inclination with respect to the equator. Currently (1990), about fourteen satellites are operational which allow for a partial use of the system during selected periods of a few hours per day. The satellites have a 12-hour period, and orbit at an altitude of 20 200 km above the Earth. The satellite signals consist of two carrier frequencies: L1 at 1575.42 MHz and L2 at 1227.60 MHz, which correspond to wavelengths of approximately 0.19 m and 0.24 m. The L1 frequency is modulated by the so-called C/A code at 1.023 MHz, and P code at 10.23 MHz. The L2 frequency carries only the P code. Superimposed on each code, at 50 bits per second, is the satellite message consisting of satellite ephemeris, the almanac for all the other satellites, clock error parameters, and satellite status information.

To determine the absolute position of a ground point in a selected coordinate system, at least four satellites must be simultaneously observed with a GPS receiver. The GPS system, when fully operational, will fulfil the requirement that at least four satellites be visible from any point on the earth's surface at any time. There are two main GPS observables: namely, pseudoranges and carrier phase measurements. In the latter case, the integer number (so-called ambiguity) of the carrier wavelengths between the receiver and each satellite is unknown at the initial epoch of tracking, but it can be solved for during the data reduction. The accuracy of absolute positioning, which is typically several tens of metres, is not sufficient for engineering surveys. If two or more ground receivers are used simultaneously, however, and the same satellites are observed in a so-called differential mode using the carrier phase differences as the observables, then relative positioning between the two stations (determination of differences of coordinates in a three-dimensional coordinate system) of high precision is obtained.

Compared with terrestrial surveys, GPS surveys have several merits. Intervisibility between stations is not needed, which simplifies the design of monitoring schemes and allows for the optimal location of points. It also makes it easier to select the reference points outside the deformation area. In addition, GPS surveys provide simultaneously three-dimensional information on the deformation status. Over the past few years, GPS has been extensively tested and applied in deformation measurements in various projects. The examples include the herein discussed ground subsidence study in the oil fields in Venezuela, deformation surveys of dams (Goad, 1989; Chrzanowski et al., 1990a), the application of GPS to monitoring ground subsidence due to water withdrawal (Strange, 1989), and the determination of tectonic movements (Bock & Murray, 1988; Kleusberg et al., 1988), just to mention a few. A number of aspects concerning the use of GPS in integrated deformation surveys has been discussed in Chrzanowski et al. (1990b).

Sources of errors

The accuracy of GPS relative positioning depends on the geometrical distribution of the observed satellites and the quality of the observations. The observation errors are categorized into three sources: satellite-related errors (mainly orbital errors), receiver-related errors (multipath due to the reflection of the satellite signals, variation in the antenna's phase centre, receiver noise, biases in the coordinates of the reference station, etc.), and signal propagation errors (ionospheric and tropospheric refraction effects). The effect of the orbital error on the baseline components is approximately proportional to the baseline length. Most of the receiver-related errors are independent of the baseline length and, therefore, their effect on the overall accuracy is more significant over short distances. The bias in the height (in an ellipsoidal coordinate

system) of the fixed reference station, however, produces a scale error, while the biases in the horizontal coordinates will cause the baseline to rotate in a vertical plane affecting the height difference in proportion to the baseline length. The ionospheric and tropospheric effects, though partially cancelled out in the differential mode of observations, are still the most dangerous sources of error. The receivers, which have a capability of measurements using both L1 and L2 signals, reduce 99% of the ionospheric refraction delay but increase the noise level by a factor of 3. Thus, use of dual frequency combinations is generally not advisable for short baselines, say up to 10 km or even longer. The tropospheric refraction can be partially eliminated by applying refraction corrections. A number of factors, however, influence the accuracy of the corrections. For instance, instrumental errors of standard meteorological equipment introduce biases in the measured temperature, pressure, and humidity. A more severe problem is that the meteorological conditions measured near the ground surface at the receiver sites are not representative of the atmospheric model above the site due to local micro-climate effects. Therefore, in practice, in small diameter networks (less than a few tens of kilometres) it is recommended that some kind of average local atmospheric conditions be used, the same for the entire network, rather than the observed meteorological values (Chen & Chrzanowski, 1989). Also, in order to minimize the atmospheric refraction effects, the GPS observations of each baseline should be repeated with the different geometrical distribution of the satellites. The effect of the geometrical distribution of the satellites on the overall positioning accuracy is usually expressed by a so-called Geometrical Dilution of Precision (GDOP) which is given as a ratio of the actual positioning (and time) accuracy to the measurement accuracy. The smaller the numerical value of GDOP the better the geometry.

From the above discussion, the accuracy (error model) of GPS relative positioning can be generally expressed as:

$$\sigma^2 = a^2 + b^2S \qquad (1)$$

where S is the baseline length. The values of a and b depend on the type of receiver, observation environment, satellite geometry, observation time, processing data technique, and so on.

With the current (1990) configuration of satellites and technology of receivers, and with the observation time of one to two hours, typical values for a and b for horizontal components are 5 mm and 1 ppm, respectively. The accuracy of the vertical component is usually about 1.5 to 2 times worse. With the improvement of the geometry of the satellite distribution and improvements in modelling of some systematic errors, the overall accuracy of GPS is expected to increase in the near future.

Observation methods

As aforementioned, some of the systematic errors, particularly the effects of the atmospheric refraction, are minimized or, at least, randomized, if the observations are repeated in various conditions of the geometrical distribution of the satellites. Therefore, in precision surveys, each baseline is usually observed over a prolonged period of time (say two hours) in a static mode to allow for a sufficiently large change in the satellite geometry. The prolonged observation time helps also in solving for the aforementioned ambiguities. Recent tests show, however, that the same accuracy may practically be achieved, if the receivers remain at the stations for only a short period of time (few minutes) and the survey is repeated after a sufficiently long period of time (say one to three hours) when the geometrical distribution of the satellites has significantly changed. This approach is particularly attractive when a large number of points with comparatively easy access to them are to be positioned within a small area. Within the approach, one may distinguish semi-kinematic (known also as a "stop-and-go") and rapid-static

methods which can significantly shorten the total observation time and increase productivity.

The semi-kinematic survey refers to the case when one receiver is kept stationary at one known point while the second (roving) receiver moves from one station to another with only short stops on each. In order to be able to solve for the ambiguities, the roving and the stationary receivers must be continuously locked to the signals coming from, at least, four satellites. After the short observation time, say one to two minutes, the roving receiver can be moved to another point where again one or two minutes of observations are made. To randomize the effects of atmospheric refraction, the survey should be repeated with different geometry of the satellites. The requirement on the continuous tracking of the satellites by the roving receivers limits the practical use of the semi-kinematic surveys to open areas only without any obstacles which could block the intervisibility between the satellites and the moving receiver.

In the rapid-static survey method, which is still under development, the continuous tracking of the satellites during the transfer of the receivers from one station to another is not necessary (Ashkenazi & Summerfield, 1989). The receivers occupy the stations for a few minutes and collect the data in the same way as in the long duration static surveys. The survey is repeated after one to two hours when the geometry of the satellites has sufficiently changed. In this method, the main problem is to obtain the solution for the ambiguities. Here, a combination of two or more short duration observations may be used in an iterative solution for the ambiguities or the P code signals may be utilized. More investigation on the rapid-static method and on the development of an appropriate software is still needed. In the future, this method will, perhaps, dominate in engineering applications of GPS.

INTEGRATED MODELLING OF GROUND SUBSIDENCE USING COMBINED GPS AND LEVELLING SURVEYS

The subsidence w of a point P(x,y) at any time t with respect to reference time t_0 can be modelled by

$$w(x,y;\, t) = \mathbf{b}(x,y;t\text{-}t_0)\mathbf{c} \qquad (2)$$

where $\mathbf{b}$ is a raw vector of some selected base functions, and $\mathbf{c}$ is a vector of unknown coefficients to be estimated.

In order to combine results of GPS measurements with levelling surveys one has to remember that the GPS-derived heights are referred to a reference ellipsoid (presently, an international ellipsoid of the World Geodetic System WGS84 is used), while the levelling heights (orthometric heights) are referred to the geoid (mean sea level). Due to the irregular shape of the geoid, the separation (geoidal height N) between the geoid and the reference ellipsoid varies from one point to another and, usually, its value is not precisely known. Therefore, the geoidal heights must be included in the combined deformation model as unknown parameters. Thus the GPS-derived height difference $\Delta h_{ij}(t)$ at time t and levelled height difference $\Delta H_{kl}(t)$, for all k, l, i, j, and t, are related to the deformation model (2) by

$$\Delta h_{ij}(t) + v_{hij}(t) = H_j(t_0) - H_i(t_0) + (N_j - N_i) + [\mathbf{b}(x_j,y_j;\, t - t_0) - \mathbf{b}(x_i,y_i;\, t - t_0)]\, \mathbf{c} \qquad (3a)$$

$$\Delta H_{kl}(t) + v_{Hkl}(t) = H_l(t_0) - H_k(t_0) + [\mathbf{b}(x_l,y_l;\, t - t_0) - \mathbf{b}(x_k,y_k;\, t - t_0)]\, \mathbf{c} \qquad (3b)$$

where v corresponds to the observation error, $H_i(t_0)$ is the expected orthometric height of point P_i at the reference epoch, and N_i is the geoidal height at point i. The geoidal heights either can be solved for individual GPS stations from the above equations or can

be modelled. Let us assume that the geoidal heights N in equation (3a) do not significantly change with time and can be modelled using a polynomial of a general form:

$$N(x,y) = \mathbf{g}(x,y)\,\mathbf{e} \tag{4}$$

where **g** is a raw vector of selected base functions, and **e** is the vector of unknown coefficients. Substituting equation (4) into equation (3a), one obtains:

$$\Delta h_{ij}(t) + v h_{ij}(t) = Hj(t_0) - H_i(t_0) + [\mathbf{g}(x_j,y_j) - \mathbf{g}(x_i,y_i)]\,\mathbf{e} +$$

$$+[\mathbf{b}(x_j,y_j;\, t - t_0) - \mathbf{b}(x_i,y_i;\, t - t_0)\mathbf{c} \tag{3a'}$$

If one is interested in single point displacements rather than in the determination of the surface of subsidence, and if the vertical movements of the point may be considered as linear in time, then the deformation model for point P_i becomes

$$w(x_i,y_i;\, t - t_0) = (t - t_0)\,\dot{H}_i \tag{5}$$

where $\dot{H}_i$ is the subsidence rate of point P_i. Then the deformation model in equations (3) is expressed in terms of the rates of subsidence of individual points:

$$[\mathbf{b}(x_j,y_j;\, t - t_0) - \mathbf{b}(x_i,y_i;\, t - t_0)]\mathbf{c} = (t - t_0)\,(\dot{H}_j - \dot{H}_i) \tag{6}$$

As discussed earlier, some systematic errors cause the GPS network to rotate in a vertical plane. The magnitude of the effect depends on the visible satellite distribution and the nature of the error. Changes in the visible satellite distribution and the systematic errors between two GPS campaigns yield additional errors to the subsidences measured with GPS. To accommodate this type of error, one can introduce into equation (3a) the additional term:

$$(x_j - x_i)\delta a(t) + (y_j - y_i)\delta b(t) \tag{7}$$

where the unknown coefficients $\delta a(t)$ and $\delta b(t)$ are related to the GPS campaign at epoch t with respect to the initial one.

Summarizing the above discussion and combining all the measurements, one can write the observation equations in the matrix form as

$$\boldsymbol{\ell} + \mathbf{v} = \mathbf{A}\mathbf{x} + \mathbf{B}\mathbf{c} + \mathbf{G}\mathbf{e} + \mathbf{D}\delta\mathbf{a} \tag{8}$$

where **x** is the vector of orthometric heights at reference epoch t_0, $\delta\mathbf{a}$ is the vector of unknown coefficients which model the systematic errors (see equation (7)), **c** and **e** have been defined before, and **A**, **B**, **G**, and **D** are the corresponding design matrices. Using the least-squares criterion, one can solve for the unknown parameters and perform statistical analysis of the deformation model. For a detailed discussion on deformation analysis and statistical testing of the deformation parameters the readers are referred to Chen (1983), Chrzanowski et al. (1983), and Chrzanowski et al. (1986).

TEST MEASUREMENTS WITH GPS

Test surveys at UNB in Canada

The aforementioned UNB test network (Fig. 3) consists of seven points with interstation

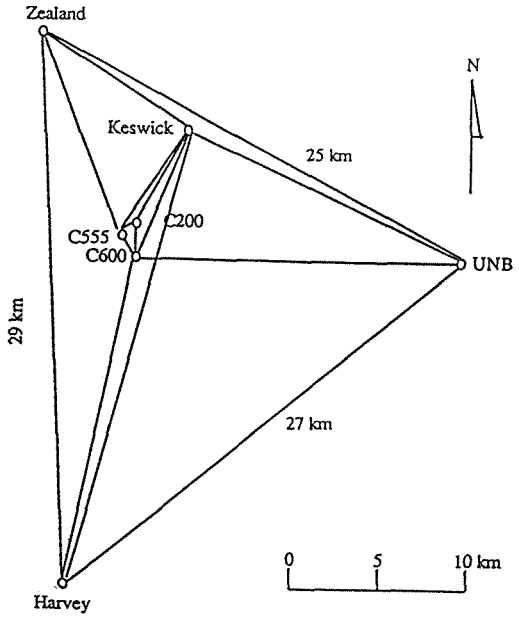

FIG.3 UNB test network.

distances ranging from 0.7 to 29 km. The following three survey campaigns have been analysed:

- WM86 campaign (October 1986 with WM101 receivers)
- Trimble87 campaign (April 1987 with Trimble 4000SX receivers)
- WM87 campaign (October 1987 with WM101 receivers).

Fifteen baselines were observed in the WM86 and WM87 campaigns with average observation time for each baseline being 1.2 and 2.0 hours, respectively. Seventeen baselines were observed in the Trimble87 campaign with average observation time being 1.5 hours. Table 1 gives loop closures of height differences in each of the three campaigns, and Table 2 gives a comparison of the height differences for each baseline.

TABLE 1 Loop misclosures of GPS height differences (UNB Test Network).

Loop	Perimeter (km)	WM86 (mm)	(ppm)	WM87 (mm)	(ppm)	Trimble87 (mm)	(ppm)
HY-UN-C6	71	22	0.3	25	0.3	46	0.7
KE-UN-C6	41	40	1.0	1	0.0	30	0.7
KE-UN-ZE	51	8	0.2	34	0.7	130	2.5
HY-ZE-C5-C6	69	77	1.1	27	0.4	14	0.2
KE-C6-C5	15	31	2.1	5	0.3	34	2.3
C6-C2-C5	3	4	1.3	6	2.0	12	4.0
UN-HY-ZE	82	98	1.2	6	0.1	74	0.9
Mean:			1.4		0.5		1.6

TABLE 2 Comparison of observed height differences (UNB Test Network).

Baseline	Length (km)	WM87-WM86 (mm)	WM87-WM86 (ppm)	Trimble87-WM87 (mm)	Trimble87-WM87 (ppm)
C5-C6	1.0	12	12.0	9	9.0
C6-C2	1.4	7	5.0	-19	13.6
C6-KE	7.1	-8	1.1	28	3.9
C6-UN	17.5	-35	2.0	-18	1.0
C6-HY	17.9	-68	3.8	20	1.1
KE-C2	5.8	12	2.1		
C5-C2	0.6	17	28.3	24	40.0
KE-C5	6.4	-36	5.6	- 2	0.3
KE-ZE	9.3	-37	4.0	23	2.5
KE-UN	16.1	-41	2.5	-102	6.3
KE-HY	25.0	-27	1.1	- 5	0.2
UN-ZE	25.4	-38	1.5	29	1.1
UN-HY	27.5	14	0.5	-33	1.2
ZE-C5	11.6	-52	4.5		
ZE-HY	29.0	-120	4.3	6	0.2

Fig. 4 shows the typical geometrical distribution of the satellites during the optimal observation "windows" of the test surveys. The optimum GDOP value was 3.0.

The accuracy of the GPS-derived height differences was estimated using Minimum Norm Quadratic Estimation (MINQE) theory as described in Chen & Chrzanowski (1985) and Chen et al., (1990). The results are:

$\sigma^2_{\Delta h} = (10\ \text{mm})^2 + (2.2 \times 10^{-6}\ S)^2$ for Trimble87 campaign and

$\sigma^2_{\Delta h} = (7\ \text{mm})^2 + (1.4 \times 10\text{-}6\ S)^2$ for the average of WM86 and WM87 campaigns.

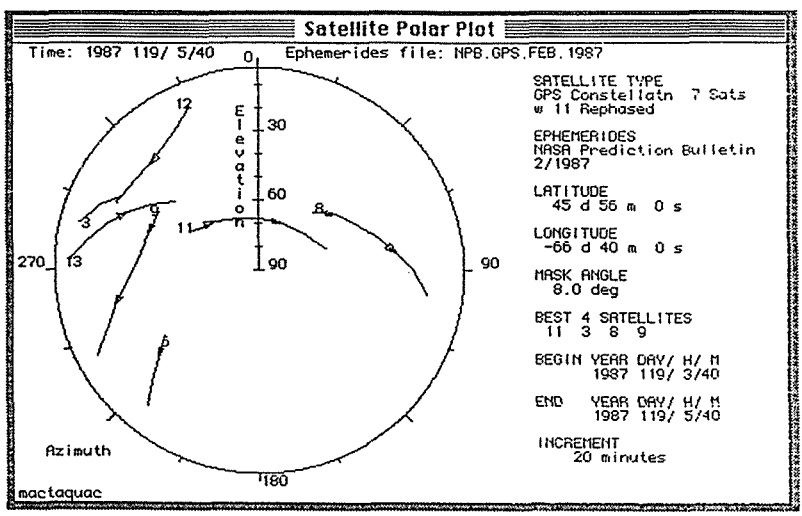

FIG.4 Satellite polar plot (1987 GPS test survey in Canada).

The above results indicated that in the case of average GPS lines of 10 km length, the WM101 receivers could give standard deviations of height differences in the order of 16 mm which would be only slightly below the required accuracy of 15 mm.

Test and implementation surveys in Venezuela

In April 1987 and October 1987, two test surveys were performed on a portion of the monitoring network within the area encompassed by points GPS1, BM202, TJ14B, and GPS5 (Fig. 2). Both surveys were conducted in cooperation with Usher Canada Ltd. using their WM101 receivers. The GPS surveys had been planned to be performed at the same time as the conventional levelling surveys were conducted in the same area.

In both campaigns, the observation data on some baselines were noisy and difficulties were encountered in their processing (solving for the ambiguities). Some observation data had to be rejected. This was caused, perhaps, by a rather poor geometrical distribution of the satellites (GDOP larger than 5) and unstable atmospheric conditions in the hot and humid climate. Table 3 shows a comparison of changes in height differences obtained from two campaigns of GPS and levelling surveys.

TABLE 3 Changes in the GPS and levelling height differences (mm).

Baseline	Length (km)	October 1987-April 1987			April 1988-October 1987		
		GPS	level	GPS-level	GPS	level	GPS-level
GPS1-BM202	15.8	-4	12	-16	43	-8	51
GPS1-BM743	7.3	-14	1	-15	46	-11	57
BM202-BM184A	4.6	11	6	5	-42	0	-42
BM743-GPS3	7.0	-8	-7	-1	-50	-14	-26
BM743-BM184A	17.0				22	3	19
GPS3-TJ1B	6.4	-17	-3	-14	-63	22	-8
GPS3-BM324	8.0				22	11	11
TJ1B-BM324	7.6	30	10	20	12	15	-3
BM324-BM184A	16.6	5	-1	6	-42	18	-60
BM324-GPS5	12.1	-118	-23	-85	83	-15	98
GPS5-BM184A	10.6	39	26	13	-56	20	-76

Despite the aforementioned difficulties, the 1987 test results were rather encouraging because, except for one baseline (BM324-GPS5), the differences between GPS and levelling surveys were within the expected confidence intervals at 95% probability. Therefore, Maraven and UNB decided to go ahead with the full implementation of GPS during the levelling campaign of 1988.

The 1988 campaign was performed also in cooperation with Usher Canada Ltd. using the same receivers (four WM101 units) as during the test surveys. Balloon measurements of atmospheric conditions were made at two stations, up to 1000 m elevation, using a telemetric data acquisition system constructed at UNB. Some results of the meteorological investigations have been discussed in Chrzanowski et al. (1989). The geometrical distribution of the satellites was poor (Fig. 5), particularly for the height determination. All observed satellites were low above the horizon giving GDOP = 5 or more. Table 3 shows a comparison between the GPS-derived and levelling changes of height differences on the baselines observed in October 1987 and April 1988. Table 4 lists loop misclosures of height differences obtained from the 1988 GPS surveys. The

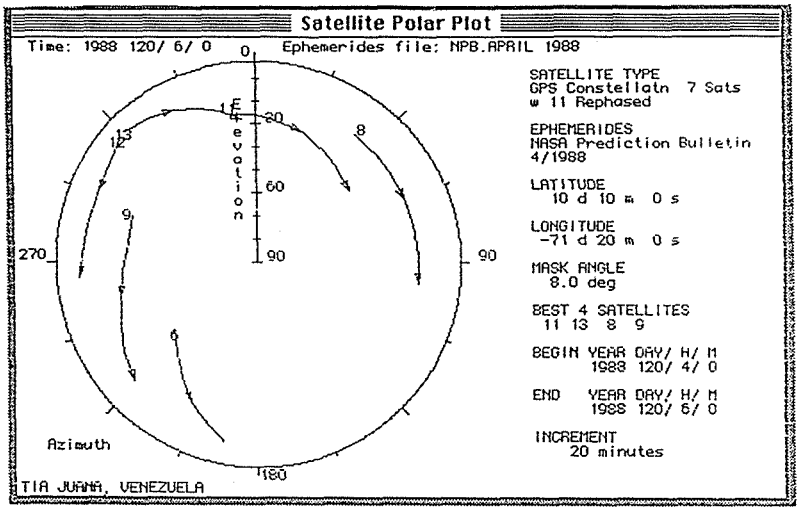

FIG.5 Satellite polar plot (1988 GPS survey in Venezuela).

results have been disappointing. Evaluation of the variance components using MINQE gave the standard deviation of 29 mm (independent of the baseline length) for the observed height differences of individual baselines, and 20 mm for their adjusted values (Chrzanowski et al., 1989). The poor geometry of the satellites distribution has been

TABLE 4 Loop misclosures in GPS campaigns 1988 and 1990 in Venezuela.

Loop	Perimeter (km)	1988 campaign (mm)	(ppm)	1990 campaign (mm)	(ppm)
TJ1B-BM8A-BM743	58.2	-18	0.3	18	0.3
TJ14B-BM743-GPS3-TJ1B	29.0	-101	3.5	30	1.0
TJ1B-GPS3-BM324	22.0	36	1.6	5	0.2
BM324-GPS3-GPS12	24.5	41	1.7		
GPS3-BM743-GPS12	28.1	-5	0.2	4	0.1
GPS12-BM743-BM184	38.3	117	3.1	27	0.8
BM184-BM743-GPS1	40.9	-87	2.1	-4	0.1
BM202-BM184-GPS1	28.5	-94	3.3	2	0.1
GPS12-GPS5-BM324	28.9	11	0.4	28	1.0
BM324-BM184-GPS5	39.3	4	0.1		
LGC1-GPS5-BM184A	26.0	-32	1.2	10	0.4
LGC1-BM184-GPS6	39.0	-32	0.8	35	1.0
BM184-BM202-GPS6	33.5	61	1.8	28	0.9
GPS7-GPS6-BM202	40.3	-40	1.0	0	0.0
BN1-BN29-GPS6-GPS9	36.8	30	0.8	-42	1.1
GPS6-GPS7-GPS8	34.0	25	0.7	34	1.0
GPS9-GPS6-GPS8	41.2	-13	0.3	-38	0.9
GPS9-GPS8-GPS10	71.5	-36	0.5	33	0.5
Mean:			1.3		0.6

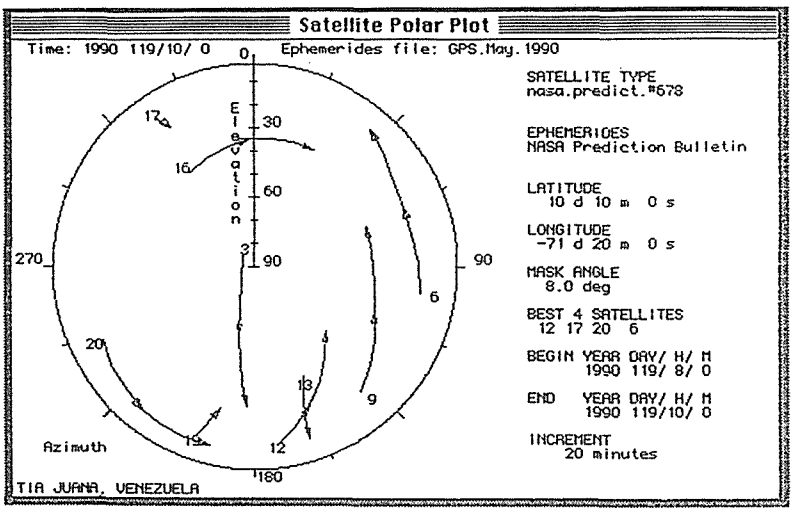

FIG.6 Satellite polar plot (1990 GPS survey in Venezuela).

recognized as the prime reason for the worse than expected results. The distance-independent nature of the error could be explained by the dominant relative tropospheric effects due to the hot and humid climate in the area. Since some of the survey stations are located along the coast of Lake Maracaibo and some are located in dry areas about 20 km inland, large local changes in humidity of air could have been expected.

Between 1988 and 1990, significant improvement to the geometry of the GPS constellation has taken place due to recent launching of several new GPS satellites. Also, a new generation of GPS receivers has become available. Therefore, Maraven and UNB decided to repeat the GPS survey during the 1990 levelling campaign. Four Trimble 4000ST receivers were used in the campaign in cooperation with Coler & Colantonio (USA) survey company using the static mode of differential positioning with about two hours of observation time at each baseline. Fig. 6 shows the geometrical distribution of the satellites during an optimal window of observations with GDOP = 2.5 (twice better than in 1988). Table 4 shows the loop misclosures obtained in 1990. They are, on average, twice better than in 1988. The MINQE evaluation of the 1990 results gave the standard deviation of 17 mm for the GPS observed height differences and 11 mm for their adjusted (network adjustment) values. Thus the required accuracy of 15 mm has almost been reached. Further increase in the accuracy is expected when additional GPS satellites are launched. Based on the 1990 results, Maraven plans to purchase three GPS receivers in 1991 and use them on a regular basis in all the future subsidence surveys as designed.

CONCLUSIONS

The present constellation of GPS satellites and present technology of GPS receivers allow for the determination of height differences with an average standard deviation slightly larger than 15 mm over average distances of 10 km in unfavourable atmospheric conditions (hot and humid climate) when using the static observation mode of about two hours duration. Further increase in the accuracy is expected in the near future when more GPS satellites become available.

Use of GPS in combination with levelling densification surveys provides significant

economical advantages over conventional monitoring surveys with levelling measurements alone.

REFERENCES

Ashkenazi, V. & Summerfield, P.J. (1989) Rapid static and kinematic GPS surveying: with or without cycle slips. Land and Minerals Surveying, 7, 489-494.

Bock, Y.& Murray, M.H. (1988) Assessing the long-term repeatability and accuracy of GPS: Analysis of three campaigns in California. Proceedings, 5th Int. (FIG) Symp. Deformation Measurements, Univ. of New Brunswick, Fredericton, Canada, 6-9 June, 91-102.

Chen, Y.Q. (1983) Analysis of deformation surveys—A Generalized Approach. Technical Report No. 94, Dept. Surveying Eng., Univ. of New Brunswick, Canada.

Chen, Y.Q. & Chrzanowski, A. (1985) Assessment of levelling measurements using the theory of MINQE. Proceedings, Third Int. Symp. on the North American Vertical Datum (NAVD'85), Rockville, Md., 21-26 April, NOAA, 389-400.

Chen, Y.Q. & Chrzanowski, A. (1989) Experimental study on the methods for processing GPS observation data (in Chinese). J. Wuhan Technical University of Surveying and Mapping, 14 (1) (P.R.China) 1-10.

Chen, Y.Q., Chrzanowski, A. & Kavouras, M. (1990) Assessment of observations using minimum norm quadratic unbiased estimation (MINQUE). CISM J. ACSGC, 4, (1), Spring, 39-46.

Chen, Y.Q., & Chrzanowski, A. (1990) Integration of GPS with levelling in ground subsidence studies: Mathematical modelling. Proceedings, 8th Int.(IAG) Symp. on Geodetic Computations,Wuhan, China, May 1990 (in prep.)

Chrzanowski, A, Chen, Y.Q. & Secord, J.(1983) On the strain analysis of tectonic movements using fault crossing geodetic surveys. Tectonophysics, 97, 297-315.

Chrzanowski, A., Chen, Y.Q. & Secord, J.M. (1986) Geometrical analysis of deformation surveys. Proceedings, Workshop on Deformation Measurements, Massachusetts Institute of Technology, Cambridge, Mass.,October, 170-206.

Chrzanowski, A., Chen, Y.Q., Leeman, R. & Leal, J. (1989) Integration of the Global Positioning System with geodetic levelling surveys in ground subsidence studies. CISM J. ACSGC, 43, (4), Winter, 377-386.

Chrzanowski, A., Chen, Y.Q., Leal, J. & Poplawski, T. (1990a) Combination of space and terrestrial surveys in deformation monitoring of dykes. Presented at 7th Annual Conference of Assoc. of State Dam Safety Officials, New Orleans, USA, 14-18 Oct.

Chrzanowski, A., Chen, Y.Q., Poplawski, T. & Leal, J. (1990b) Use of GPS in integrated deformation surveys: monitoring and implementation. Proceedings, GPS '90 Conference, Canadian Inst. Surveying & Mapping (in press), Ottawa, 6-9 Sept.

Goad, C.C. (1989) Kinematic survey of Clinton Lake Dam. J. Surv. Eng., 115, (1), 67-77.

Kleusberg, A., Georgiadou,Y. & Dragert, H.(1988) Establishment of crustal deformation networks using GPS: A case study. CISM J. ACSGC, 42,(4), 341-351.

Leal, J. (1989). Integration of satellite Global Positioning System and levelling for the subsidence monitoring studies at the Costa Bolivar oil fields in Venezuela. Tech. Rep. No. 114, Dept. Surveying Engineering, Univ. New Brunswick, Canada.

Murria, J. (1991) Subsidence due to oil production in Western Venezuela: engineering problems and solutions. Presented at the Fourth Int. Symposium on Land Subsidence, Houston, Texas, 12-18 May.

Strange, W. (1989) GPS determination of groundwater withdrawal subsidence. J. Surveying Engineering, 115, (2),198-206.

Land Subsidence (Proceedings of the Fourth International Symposium on Land Subsidence, May 1991). IAHS Publ. no. 200, 1991.

The Positioning System GPS for Subsidence Control of the Terminal Reach of the Po River

F. GAMBARDELLA & S. BORTOLOTTO
Magistrato per il Po, Rovigo, I 45100, Italy
M. ZAMBON
Istituto di Scienza e Tecnica delle Costruzioni
University of Padua, I 35100, Italy

ABSTRACT The present Delta of Po river is of new formation. Its origin is of 1604 due to the intervention of venetian engineers, that cut the right bank of the Po river near its mouth to remove the cloudy water from the Venice lagoon. In the 1960s' the Delta river suffered a great soil subsidence, which reached 3 meters in some areas, due to withdrawal of groundwater and solution gas. In the region there still exists a bench-mark network which is periodically controlled by traditional methods, but requires a long time and high costs. This project consists in the execution of some geodetic positioning by GPS of the existing bench-marks. The purpose of these operations is to determine possible variations in the height of the region round the terminal reach of the Po river by GPS satellite technique, which guarantees precision, rapidity of execution and comparative economy. In fact, contrary to traditional methods, GPS allows large areas to be kept under control in a precise, speedy and cheap manner. Besides, if the traditional operations are in concurrence with soil subsidence phenomenon, it's possible to accumulate intolerable systematic errors. This does not happen using GPS technique. The measured ellipsoidal heights may be, thanks to consistent algorithm, transformed into geoidal heights. In this manner it's always possible, and in a short time, to postpone the geoidal heights of existing bench-marks of the region measured by traditional techniques. Moreover the method from ellipsoidal heights permits to determine geoidal heights of every point of the region.

THE PO RIVER

The Po is the biggest and most important river in Italy. It is 652 km long, with a basin of 70 000 km^2 and an average capacity of 2000 m^3 that can in certain periods reach more than 9000 m^3.
In the upper reaches the water flows rapidly due to the steep slopes taking down large quantities of debris into the valley. In the lower reaches where the slopes are less steep, the debris

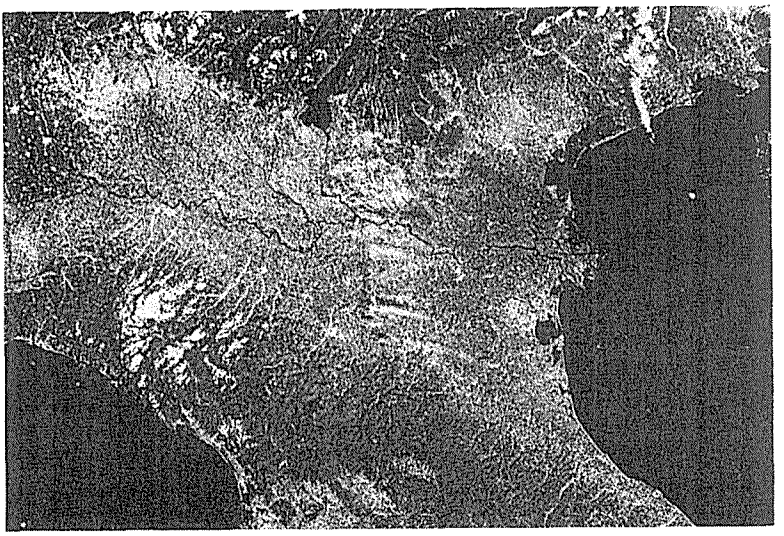

FIG. 1 The Po river basin from satellite.

brings about a continual filling up of the river bed and so the water level is higher than the surrounding countryside. The river flows into the Adriatic sea with a seven branch delta (fig. 1).

THE PO DELTA

The present delta is of recent formation. This present-day situation must be considered as a result of a series of events both natural and artificial, substantially beginning during the 12th century. The first important fundamental event goes back to 1150 when a flood modified the river course. However the event that brought about the greatest modification was in 1604, when the Venetian engineers, wanting to block the torbid waters from the lagoon, cut the right bank of the river directing it towards the south-east (Porto Viro Opening). After this the Delta markedly stretched out towards the sea, reaching increases of approx. 130 ha/year up to 1840 (figs 2, 3, 4).
The morphological evolution of the Delta came about due to both natural events (natural subsidence, strong tides, etc.) and man's intervention (territorial reclamation, bank construction, intervention in the fluvial basin, etc.).

SUBSIDENCE OF PO DELTA DURING THE '60S

The natural subsidence, characteristic of all the coastal tract of the northern Adriatic including the Delta, consists of a slow lowering of the land estimated at about 15-30 cm each century.
This subsidence is essentially due to glacial eustatism and is presently evaluated at around 15 cm/century in relation to the average sea level and the compaction of the alluvial deposits that

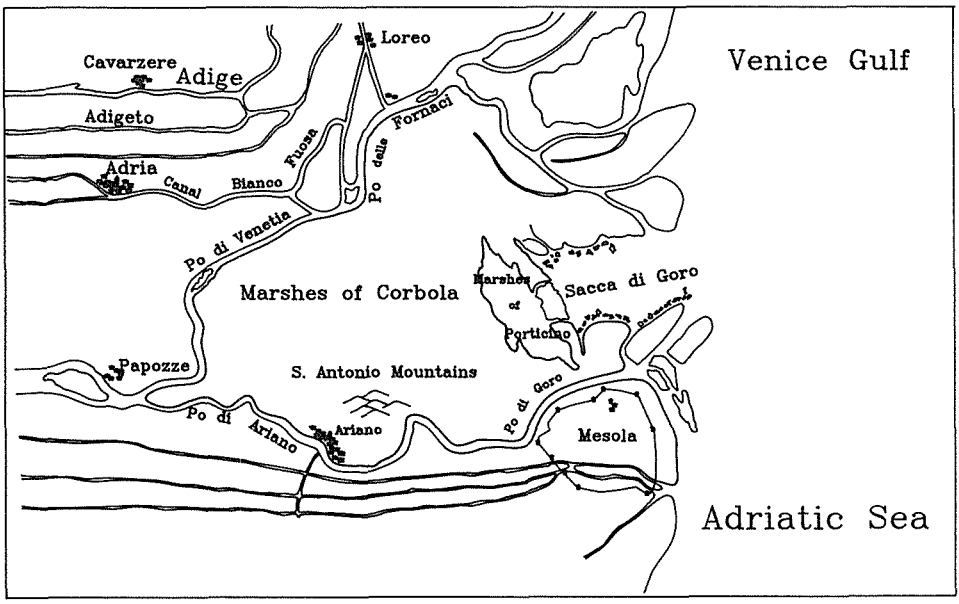

FIG. 2 The Po Delta before the opening of Porto Viro (Biblioteca Vaticana, 1604).

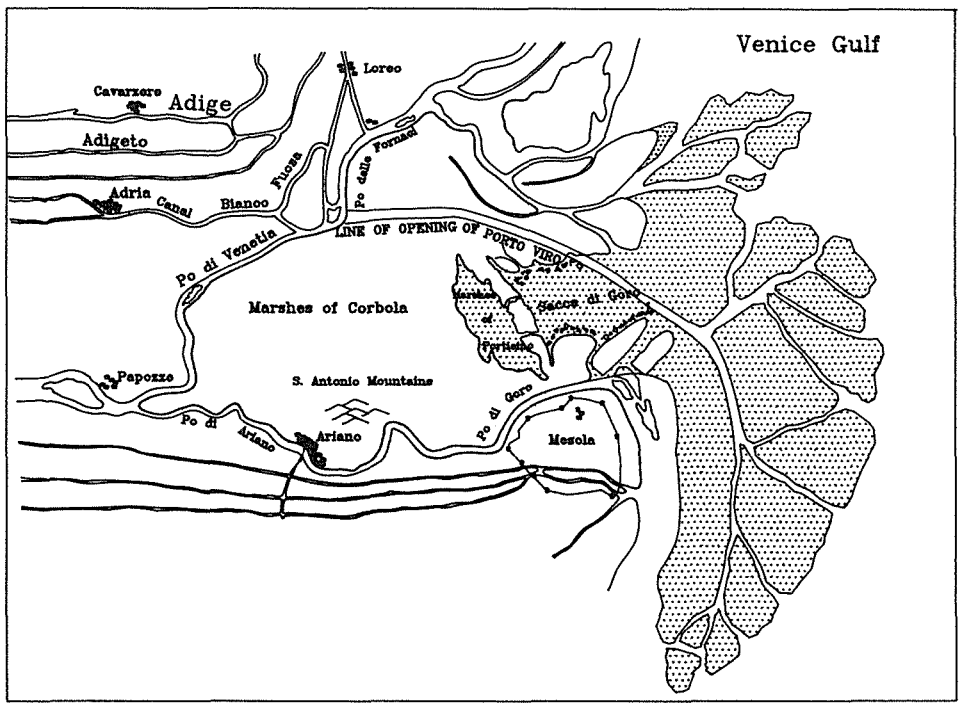

FIG. 3 Superposition of the Delta shape before and after some years from the opening of Porto Viro.

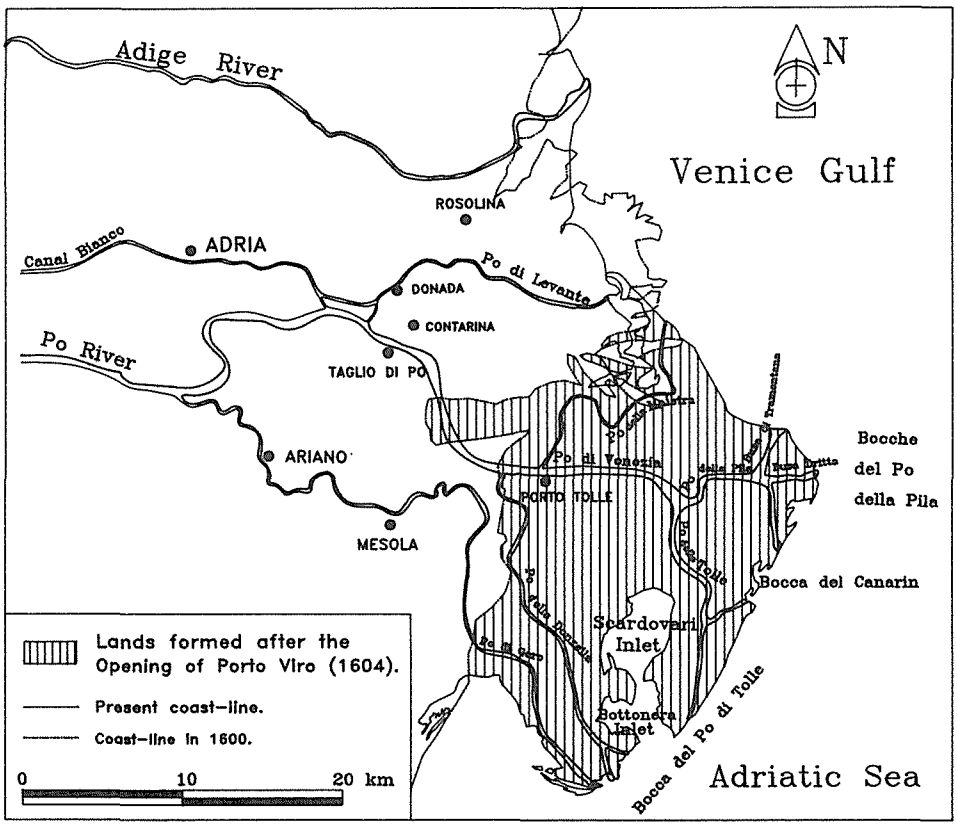

FIG. 4 The present Delta of Po river.

can, in the delta area, reach approx. 15-25 cm/century.
However the real and true lowering of the Delta was provoked by the extraction, during the years 1950-1960, of water and methane gas from layers found up to 600 meters of depth. After this activity an abnormal rapid and obvious lowering of the land was verified and in some places was 3.5 meters (fig. 5).
The phenomenon covered an area of 7-800 km² and disrupted all the water courses of the zone and in particular the Delta, creating a necessity for bank construction. The surrounding countryside was also affected.
The strict connection between withdrawal activity and the abnormal lowering is demonstrated in fig. 6 in which a comparison is made between the annual methane production and the average lowering of the whole delta area.
A further confermation of this can be seen from the lowering of the two bench-marks shown in figs 7 and 8.

THE GPS FOR SUBSIDENCE CONTROL

The GPS (Global Positioning System) is based on the use of satellites created for the static positioning and terrestrial

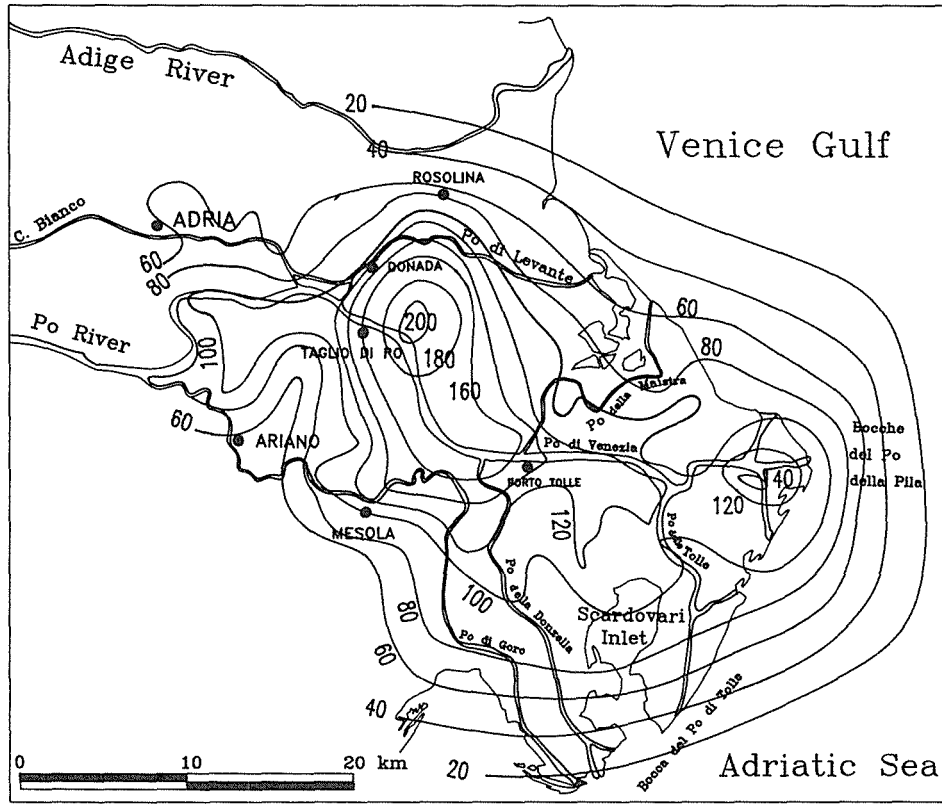

FIG. 5 Subsidence of the Po Delta from 1951 to 1960.

navigation. The complete constellation of the satellites foreseen for 1992 will be made up of 18 operating satellites, placed on six separated orbits inclined 55° with respect to the equatorial plane and also of three spare satellites.

At the moment there are 13 operating satellites in orbit placed in such a way as to permit simultaneous vision of 4 of them from any point on Earth during 7.5 hours of the day. The average height of the satellites is approx. 22 000 km above sea level with an orbiting time of about 12 hours.

The satellites continously transmit on two carrier frequencies denominated L1 (1 575.42 MHz) and L2 (1 227.60 MHz) which allow determination of the ionospheric effects on the signal propagation speed. The carrier frequencies are modulated with the navigation signal that consists of a pseudo-casual binary code generated by a mathematical algorythm in relation to time.

Other than the code, a message containing all the necessary parameters for the determnation of the satellite orbit is transmitted.

Every GPS measurement consists of the simultaneous observation from 2 stations, positioned in relation to two bench-marks of the continously transmitted signals from the NAVSTAR satellite (NAvigation Satellite Time And Ranging).

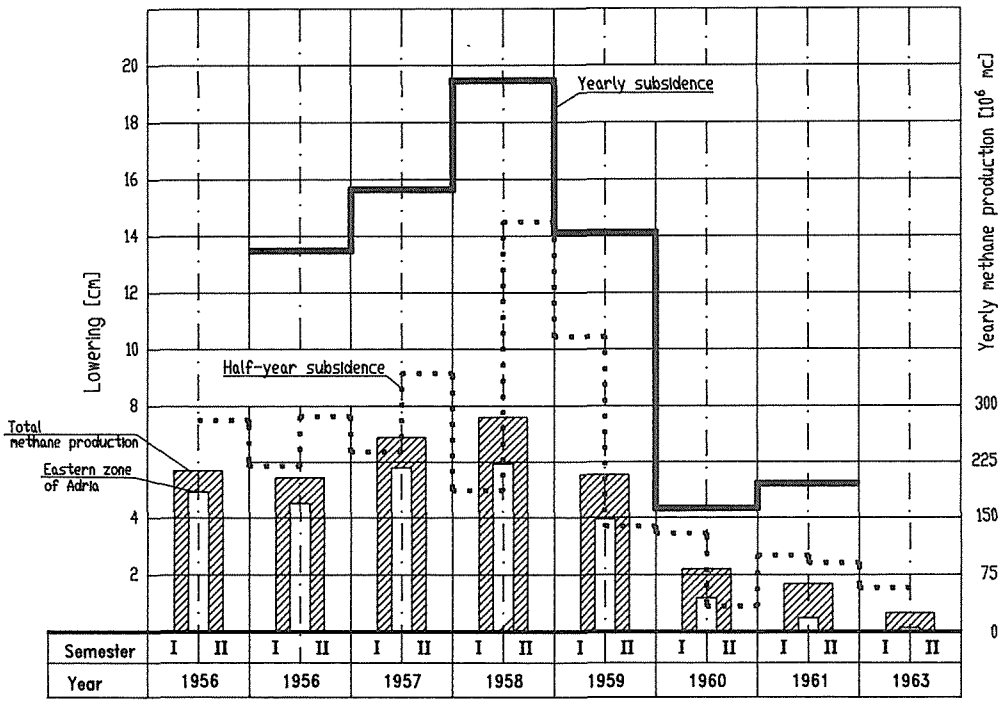

FIG. 6 Correlation between methane extraction and subsidence.

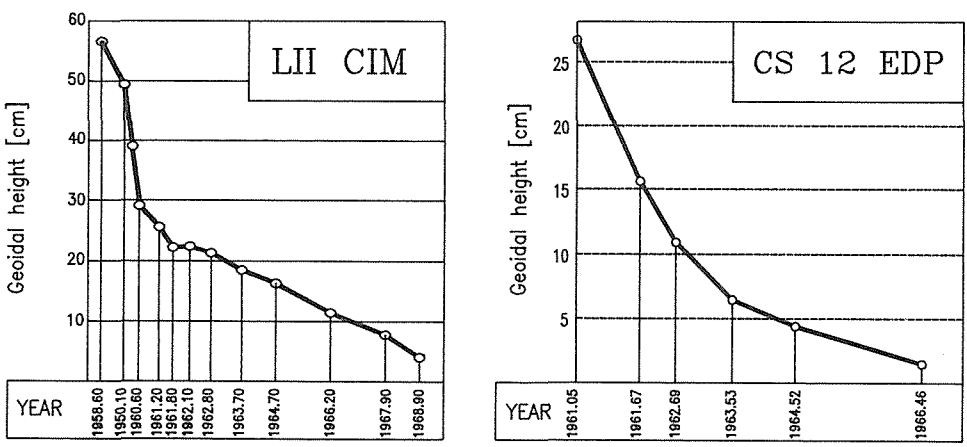

FIGS. 7 and 8 geoidal height of 2 bench-marks in the Po Delta region.

The signals, appropriately elaborated, are recorded onto a magnetic tape and then re-elaborated at the computer by a relevant programme with an appropriately developed calculation. In such a way the geocentric co-ordinates of the observation sites are obtained in reference to the WGS84 (World Geodetic System 1984). Working with the GPS technique the probable error is nominally 5 mm

± 1 ppm which can be decreased carrying out copious measurements, with respect to that strickly necessary.
For a tract of 1 km this error result in 6 mm, which corresponds to that allowed for the traditional leveling methods (precision levelings).
Only this evidence places the GPS technique, with reference to the variation measurement of the height to the amount of a few centimeters, on the same plane as the traditional one (by precision levelling methods), but it is important to note that the error with the GPS technique presented exclusively accidental characteristics given that the measurement is pratically carried out in real time and therefore excludes the accumulation of systematic errors that can influence the traditional levellings if one operates in subsident areas.
In the graphs of fig. 9 a comparison was made between the expected deviation in the levellings adopting the GPS technique and the traditional one in different hypothesis of subsidence, evidenced by different coefficent K values that express the average daily lowering relative to 2 points 1 km apart. Therefore for example K=1/50 mm/km days is equivalent to a lowering relative to 1 mm/day between 2 points 50 km apart.
It must be noted how the errors due to subsidence phenomenon exceeds, even after a short distance, the deviation for the precision levelling, with a land lowering value analogous to that found in the Po Delta.
This is due to the time needed for completion levellings with the traditional system which is much longer with respect to evolution of the subsidence phenomenon.
In fact one can demonstrate that with some simplified hypothesis, the precision and high precision levellings are able to estimate

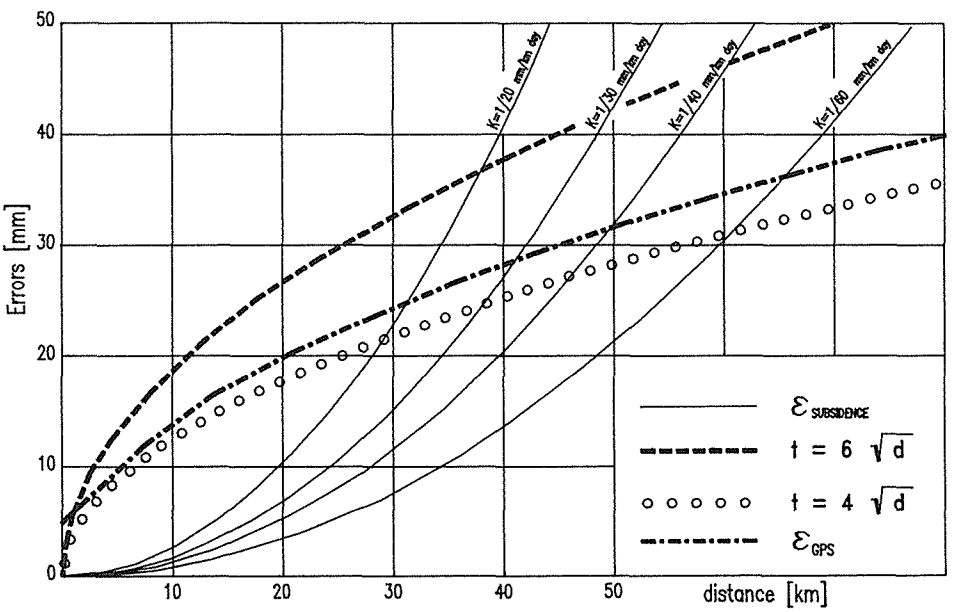

FIG. 9 comparison between different deviation.

half of the subsidence from the beginning to the end of the operations.
In conclusion, the GPS technique offers such as to be preferred to that of normal precision levellings. However where the zone requires measurements of small height variations the utilization of the GPS technique cannot be replaced, with reference both to the precision and high precision levellings.
A control example, using the GPS technique, of the eventual movements of a vast territory is being done on the Po Delta and its lower reaches on behalf of the Po Magistrato. The plan shown in fig. 10 represents the vertices subject to periodic controls.

TRANSFORMATION ELLIPSOIDAL-GEOID

GPS refers the co-ordinates of the prominent points to the WGS84 ellipsoid so furnishing for the height, the distance between the same points and the ellipsoid; a mathematical surface the separation of which from the geoidal surface varies from point to point and can even reach 60-70 m.
The problem of tranformation from the ellipsoidal height to the geoidal one is quite complicated, so that the geoidal variation is influenced by numerous parameters that are difficult to evaluate.
It has been established that it is possible to resolve the problem for small areas, adopting for the geoidal surface a model obtained hypothesizing a linear variation, in a certain direction, of the orthometric heights (intended as the height differences between ellipsoid and geoids).
The hypothesis of variation can therefore be expressed by the following linear equation:

$$N = a_o + a_1 X + a_2 Y \qquad (1)$$

If the zone is not sufficiently small enough the above mentioned variation could be expressed by the following squared equation:

$$N = a_o + a_1 X + a_2 Y + a_3 XY + a_4 x^2 + a_5 Y^2 \qquad (2)$$

where X and Y are the co-ordinates of the observed points and the coefficients a_i are determined by resolving the system of equations obtained imposing (1) or (2) for the points where one knows both the geoidal and ellipsoidal heights are known, utilizing the squared minimun method.
Such model was successfully applied for the Po Delta where the GPS surveys were carried out at points of notable geoidal height.
In particular we were able to establish that for territories of the Po delta, model (1) can easily be adopted for areas of 30 km diameter remaining within the precision margins of the adopted recording system (± 1 cm) whilst model (2) is valid for all the the zones; it was not possible with the available data to determine the validity limits of the same model.

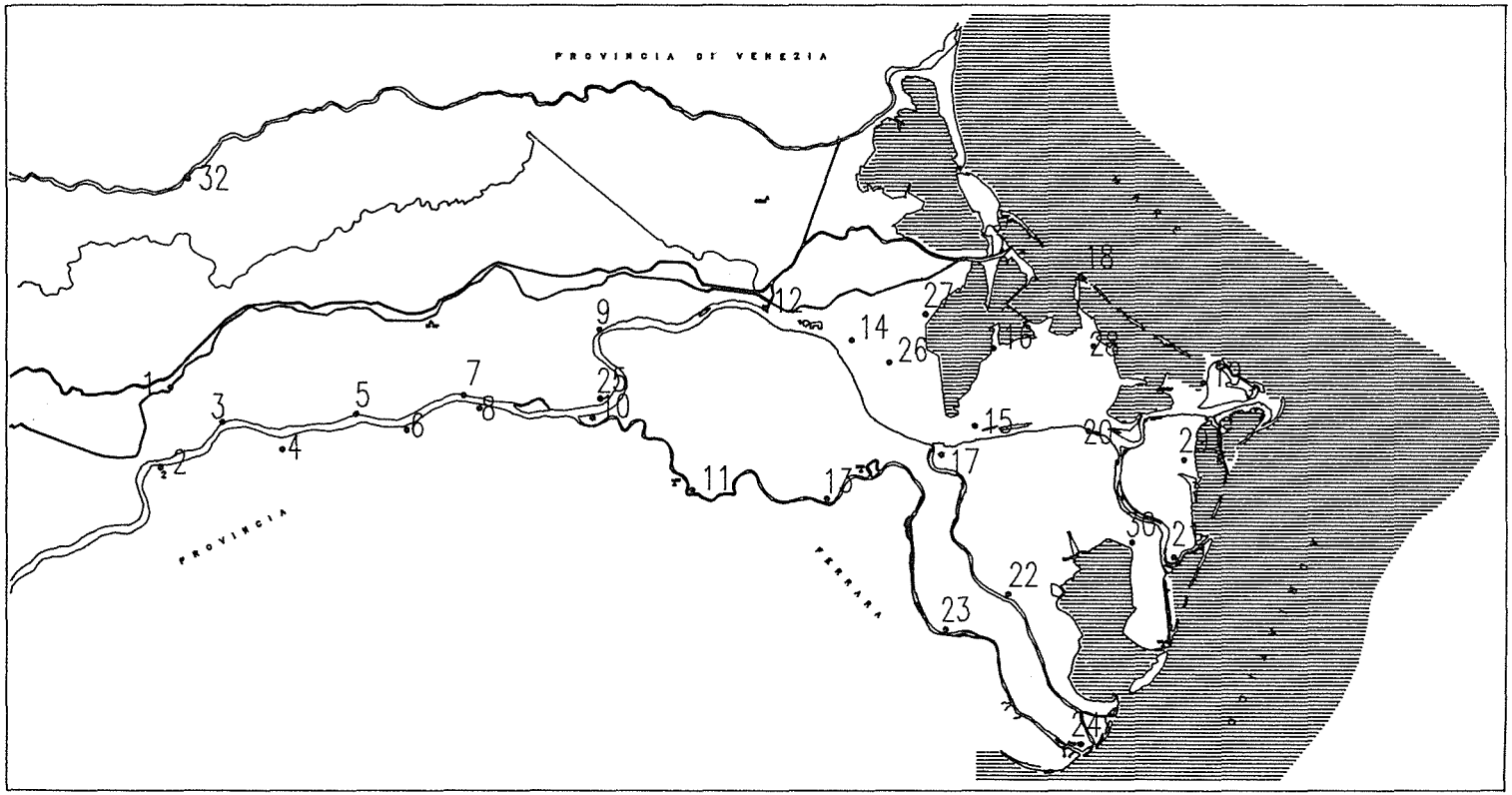

FIG. 10 Plan of the vertices subject to periodic controls.

Land Subsidence (Proceedings of the Fourth International Symposium on Land Subsidence, May 1991). IAHS Publ. no. 200, 1991.

Subsidence Controls in the Town of Bologna

A.CAPRA & G.FOLLONI
Istituto di Topografia,Geodesia e Geofisica Mineraria, University of Bologna,Italy
P.RUSSO
Dipartimento di Ingegneria dei Trasporti, University of Napoli,Italy

ABSTRACT Land subsidence in the town of Bologna is actually the most remarkable case in Italy, with regard to the extent of the subsiding area and to the velocity of ground vertical movements. Recent levellings of a vertical control network established in 1983 and repeated in 1987 point out subsidence values ranging from less than 1 cm/year to about 8 cm/year. From a geometrical point of view, the most interesting aspect of the phenomenon is the sharp gradient which movements present in some places (1 cm/ 100 m per year), one of which is the historical centre of the town. Here damages produced by differential foundations sinkings have been detected in several buildings for about ten years.

In order to study the correlation between such differential sinkings and subsidence, a densification of the main network has been performed in the North East area of the town centre, where the gradient of ground movements, as well as the presence of damaged buildings, is considerable. The results of five levellings, performed in the period August '87 - March '89, are here presented and discussed.

INTRODUCTION

The phenomenon of land subsidence in the Po river valley has been known for at least thirty years. The first studies (Salvioni, 1953,1957) were based on the comparison of the heights coming from the surveys of the old (1897-1903) and the new (1943-1950) Italian fundamental levelling network . In particular a slight ground sinking, ranging from 2 mm/year to 4 mm/year,resulted to be acting in the plain of the town of Bologna. The relevelling of some I.G.M.I. (Italian Geographical Military Institute) lines in the period 1970-1973, pointed out that many bench marks situated in a wide area comprising Bologna, had remarkably lowered later then 1943-50 (Pieri et

al.,1977). The most considerable movements occurred in the north-east and northern parts of the territory, the former comprising also a portion of the historical centre of the town. The average value of subsidence in these areas in the period 1943-50 / 1970-73 was of several tens of cm with a maximum value of about 140 cm. An interesting geometric feature of this new phenomenon was a sharp gradient of movements in the town center, along the direction south-west/north-east.

In the period 1974-1981 some people have carried out other levellings which brought up to date our knowledge on ground movements. Most significant results of these measurement campaigns, which confirmed the phenomenon pointed out by previous surveys, concern the maximum value of subsidence and of its velocity which are respectively about 2 m (1943-50/1981) and 11 cm/year(Pieri et al.,1984).

A research program for the study of the subsidence started in 1981 and was planned entailing historical, hydrogeological, geophysical, geomechanical and other types of research. The foundation of the project was the periodical determination of ground movements, within a period of four years, by means of a survey of the vertical control network.

This network was established in 1983, over a territory of about 460 km^2 and comprises 475 new bench marks. Heights and, by consequence, movements are computed with reference at two bench marks placed in areas at the base of the Appennines which are not affected by subsidence. Four different levels of bench mark density were used in order to determine with adeguate detail ground movements occurring in the territory under control . In order to have accurate detection of local changes in the gradient of movements, the average distance between consecutive points in the center of Bologna is 250 m .

Two levellings of the whole network have been performed up to now: in 1983 and in 1987 instruments and method of high precision levelling were used in both measurement campaigns. The results of such levellings point out that subsidence is occuring in the whole area under control with values ranging from 1 to 32 cm. Ground movements, moreover, are characterized in the North-West and South-East part of the historical center by a sharp gradient with a maximum of about 1 cm - 100 cm per year (Barbarella et al., 1990).

THE UNIVERSITY CONTROL NETWORK

The subsidence gradient is more evident in the area located between the Asinelli Tower and Porta San Donato, along Zamboni Street (Fig.1), where many historical buildings, typical of Bologna architecture, are found.

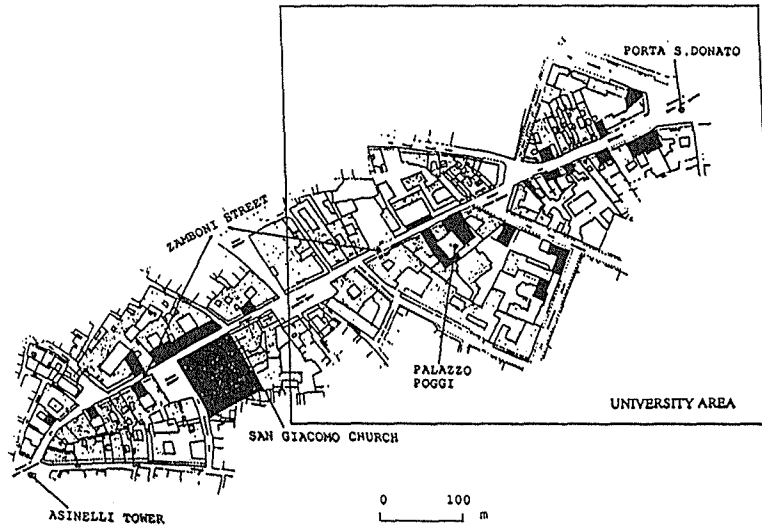

FIG. 1 Map of damaged buildings.

The Asinelli Tower, the San Giacomo Church and the near-by Conservatory, located in this area,are controlled, respectively, since 1972 (Borgia et al.,1977, 1978, Gubellini,1984,Cavani,1912) and since 1979 (Gubellini et al.,1984); the high precision levellings, periodically maked, showed that the movements of the foundations of these monuments are surely due to subsidence.In particular differential ground vertical movements which occured along the Church of San Giacomo have probably caused the observed structural damages and the consequent rod breaks.

Recent rebuilding works of the damaged university buildings, located in this area, were done. On the basis of the subsidence phenomenon and of the builings seriously damaged, we decided to collect, for the first time, subsidence data in order to the best recommendations for restructuring work. Before planning and realizing the appropriate survey for the detection of vertical ground displacements corresponding to damaged buildings, it was obviously necessary to perform a systematic investigation of the probable causes of damages.

The results of this investigation (Alessi, 1985) have been summarized in a planimetric map (Fig.1) ; the buildings with significant damages have been categorized and divided into four classes :

(a) Class I - greatly damaged structure mostly through subsidence;
(b) Class II - greatly damaged structure, owing to uncertain causes;
(c) Class III - slightly damaged structure;
(d) Class IV - not damaged structure.

One observes that many universitary buildings belong to Class II : particularly the Jurisprudence Building , the Rectorate and the Administratives Offices , the

University Library , the seats of Chemistry, Geography and Geology Departments.

The control network has been designed in order to detect movements of the ground, as well as of the structures of the buildings; it has to be surveyed periodically by high precision levelling. The bench marks are particularly numerous in the buildings corresponding to the first and second classes; in case of some significant vertical cracks, a pair of bench marks have been applied astride the same cracks.
The network, that we could define as the "University network " , is a densification of the general Bologna network and has many bench marks in common with it.
The total length of lines is about 6 km., most of which form independent loops (Fig.2): the open branches have always been surveyed with forward and backward measurements. A total number of 99 new bench marks have been established.

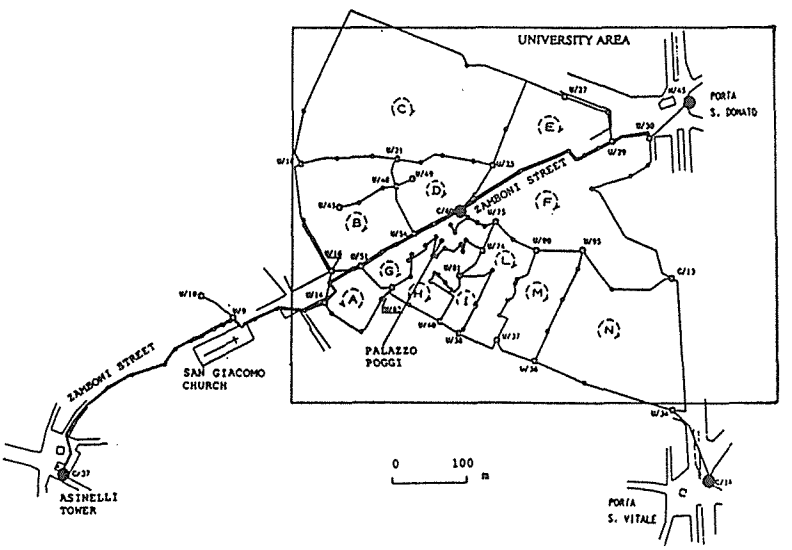

FIG. 2 University control network.

GROUND VERTICAL MOVEMENTS

The first four levellings had quadrimestral periodicity; the last one was made later for bad metereological conditions. The first survey was made in August 1987 and the last in March 1989.Instruments and observing methods of high precision levelling have always been adopted for every campaign; moreover measurements were performed as quickly as possible in order to reduce the influence of ground movement on the results of levelling.

From the least square adjustment of the network the

following mean square errors were obtained in the five levellings campaigns: 2.0,1.1,1.1,2.0 and 1.1 mm/Km.

The differences among values are probably due to atmospheric conditions: the first and fourth surveys (m.s.e.of 2.0 mm/Km) were performed in the summer when the disturbance on the levelling measurements is greater. Table 1 shows the adjusted heights of nodal bench marks of the network : the heights have been computed with respect to bench mark C/37 (Asinelli tower) assumed to be steady in time.

TABLE 1 Adjusted heights of nodal bench marks (August 1987) and their variations.

Nodal Bench Marks	Height (m)	Δ H 8/87-12/87 (mm)	Δ H 8/87-4/88 (mm)	Δ H 8/87-8/88 (mm)	Δ H 8/87-3/89 (mm)
C/37	59.7039				
U/9	53.9819	- 3.2	- 6.7	- 15.2	- 23.0
U/14	53.2136	- 5.6	- 11.5	- 23.0	- 36.7
U/16	52.0567	- 6.8	- 13.3	- 25.7	- 41.3
U/18	51.4328	- 8.5	- 15.9	- 29.6	- 48.9
U/21	50.5692	- 9.3	- 17.2	- 28.4	- 49.3
U/25	50.6672	- 8.3	- 16.9	- 28.1	- 48.4
U/27	49.3866	- 7.6	- 14.9	- 27.9	- 47.3
U/29	49.6064	- 6.6	- 13.7	- 22.5	- 40.3
U/30	49.9277	- 5.7	- 12.6	- 20.7	- 36.9
U/34	52.9495	- 4.5	- 10.4	- 17.6	- 34.7
U/36	51.1969	- 7.4	- 14.3	- 20.3	- 41.5
U/38	51.3343	- 7.2	- 14.5	- 22.9	- 42.7
U/40	51.1272	- 7.3	- 14.8	- 23.3	- 43.1
U/45	51.8223	- 7.3	- 15.7	- 26.2	- 45.3
U/48	50.6853	- 9.1	- 17.4	- 28.7	- 49.5
U/49	50.5869	- 11.6	- 20.2	- 31.1	- 52.7
U/51	51.9032	- 6.0	- 13.0	- 24.2	- 41.7
U/54	50.9115	- 9.0	- 17.6	- 28.0	- 49.1
U/62	50.9231	- 7.7	- 14.8	- 23.3	- 43.2
U/74	51.0182	- 7.0	- 14.8	- 24.1	- 43.7
U/75	50.5872	- 8.4	- 16.8	- 25.6	- 45.5
U/81	51.3471	- 8.2	- 16.0	- 25.4	- 46.1
U/90	50.6889	- 7.2	- 14.4	- 23.0	- 40.9
U/95	51.6480	- 7.7	- 14.9	- 22.2	- 40.8
C/13	52.1043	- 6.6	- 13.3	- 20.1	- 38.1
C/14	53.6584	- 4.3	- 11.0	- 25.5	- 33.8
C/60	50.1700	- 8.8	- 17.7	- 29.2	- 49.9
N/45	50.6481	- 8.4	- 15.3	- 23.6	- 40.7

The data obtained from five surveys permit us to map out contour lines of ground vertical displacement in the period August '87 - March '89. The contouring map was elaborated with SURFER 4.0 software. Contour lines were made by gridding, with grid cell size of 25 by 25 meters; the method of interpolation in the grid nodes is the inverse of the square distance with the research method of octants for the nearest points. Because the distribution of all bench marks of the University control network is not uniform, the representation area was reduced; in fact

a uniform distribution of measurement points was necessary to obtain a correct contour line representation of the investigated phenomenon.

The applying of a c^2 test verified that the distribution of bench marks can be considered uniform in the reduced area. Figs. 3,4,5,6 show contour lines of vertical movements of the successive surveys related to the first.

We have also made the vertical displacement profile of the control points located near the axis of Zamboni Street, as reported in Fig.7.

The examination of vertical movement contour lines and of the displacement profile allow us to make some observations:

(a) the subsidence phenomenon show a local trend much more irregular than could be hypothized;
(b) the gradient of movements increases progressively and shows variations in absolute value and in direction in some precise areas;
(c) some gradient variations correspond to strongly damaged buildings (the Church of San Giacomo, the Rectorate and the Universiy Library and the Geology Department).

Therefore it seems that detected damages in some buildings of Class II assigned to uncertain causes, instead are to be, totally or partially,assigned to subsidence movements. Moreover one can observe that

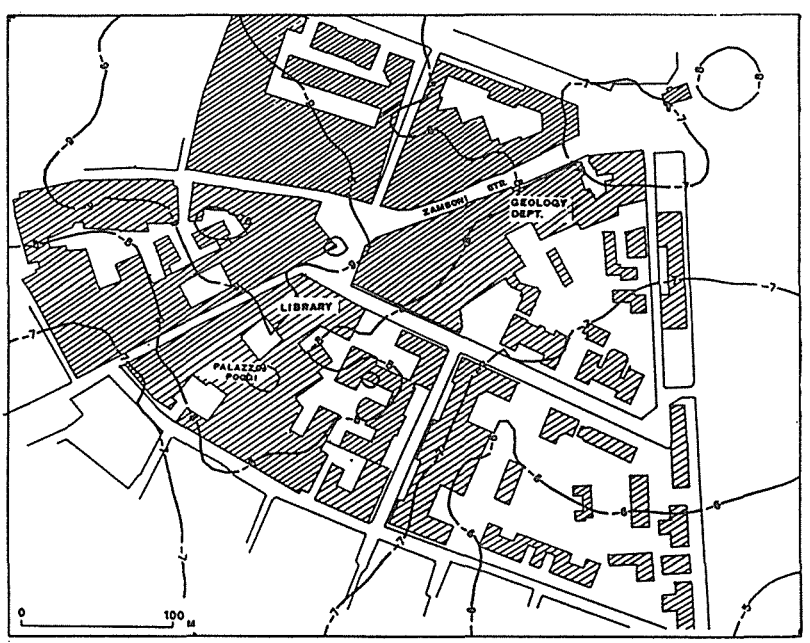

FIG. 3 Contour lines of subsidence (mm) for the period August '87- December '87.

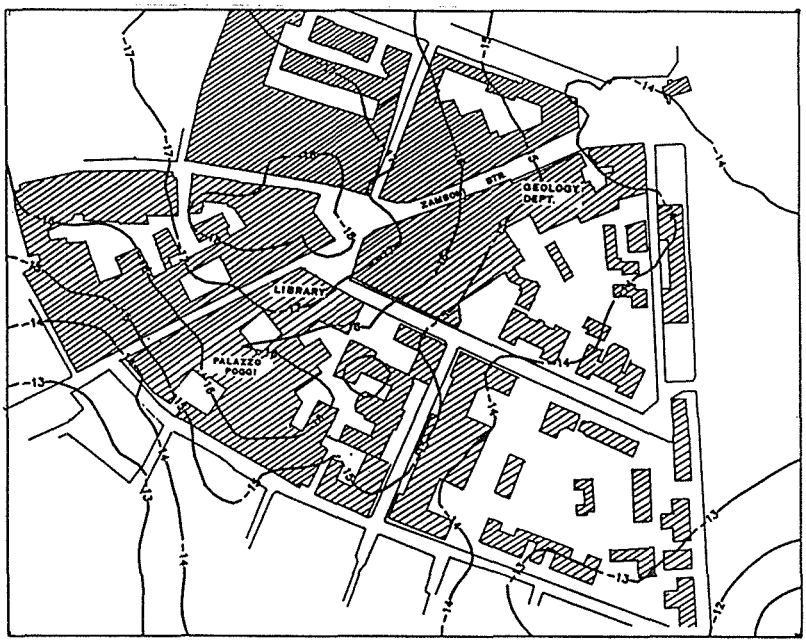

FIG. 4 Contour lines of subsidence (mm) for the period August '87- April '88.

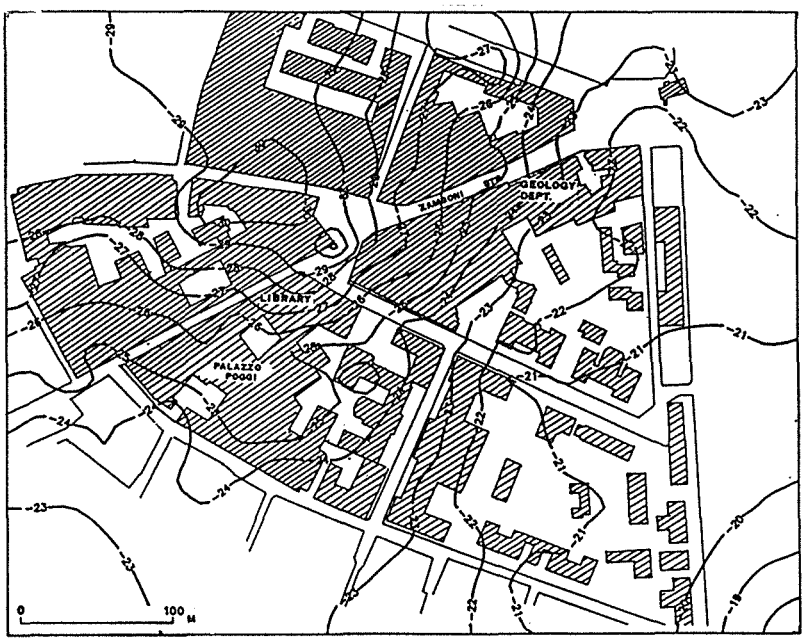

FIG. 5 Contour lines of subsidence (mm) for the period August '87- August '88.

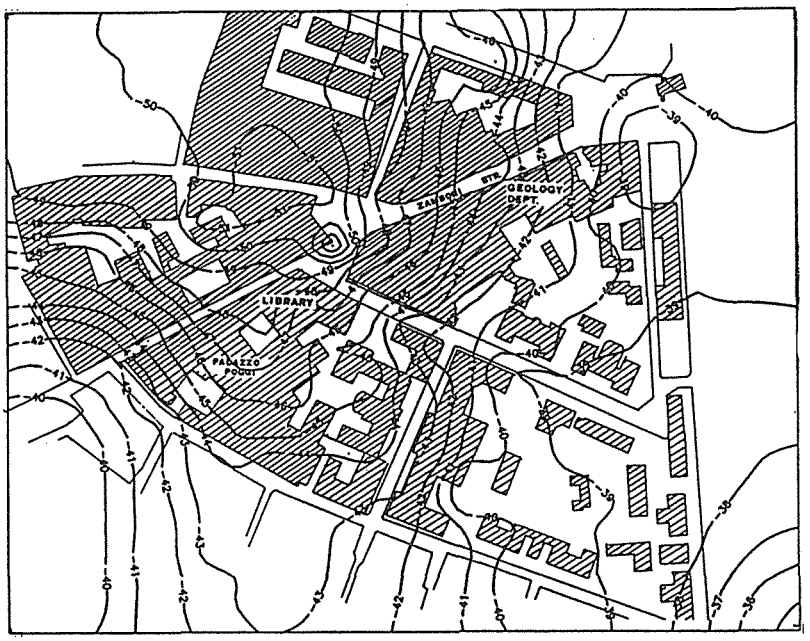

FIG. 6 Contour lines of subsidence (mm) for the period August '87- March '89.

buildings located in the same strongly subsident area showed different damages, since some buildings are ancient and were built using traditional masonry techniques (the University Library) while other ones are more recent and were built with a concrete structure (Economic Science Faculty).

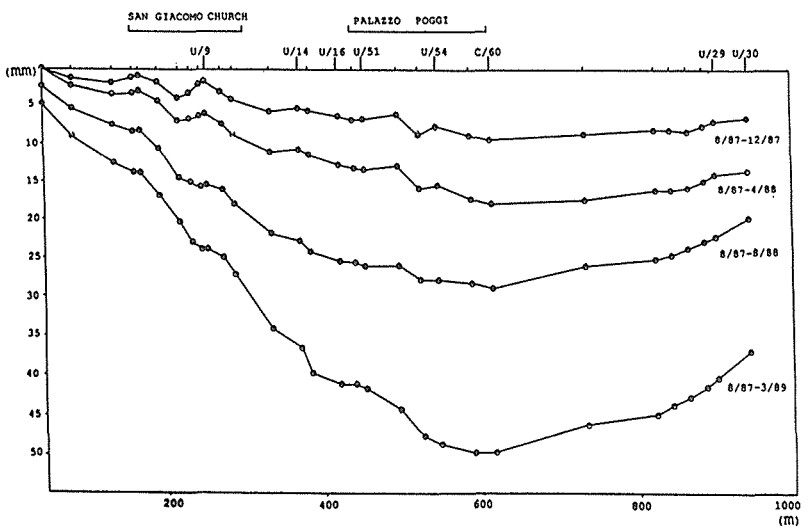

FIG. 7 Vertical displacement profile along Zamboni Street.

CONCLUSIONS

The period of observation is not long enough to draw reliable conclusions on a clear correlation between ground subsidence and building damages in the area under control. However it is sure that vertical ground displacements are still active : relative vertical displacement speeds in the period of observation (eighteen months) are of the same size as those measured in the high precision levelling network in the last years (1983 - 87). The results obtained indicate that the geometry of the phenomenon is much more irregular than could be expected on the basis of the main network and show that a high density of control points is indispensable for a correct analysis of the effect of subsidence on structures.

It is however necessary to complete the control measurements of vertical ground displacements with geotechnical and hydrogeological surveys and to monitor movements of more significant damages . The realization of such a program and of its repetition for a sufficient period will reliably quantify the correlation level between ground subsidence and structural building damages.

REFERENCES

Alessi, R.(1985) La subsidenza nel centro storico della città di Bologna:il grado di dissesto dei fabbricati nella zona di via Zamboni.Inarcos 456 (2) 62-71.

Barbarella, M., Pieri, L., Russo, P. (1990) Studio dell'abbassamento del suolo nel territorio bolognese mediante livellazioni ripetute.Inarcos 506 (1) 1-19.

Borgia, G.C., Folloni,.G, Gubellini,A.(1977) Movimenti attuali delle fondazioni della torre degli Asinelli. Inarcos 374 (2).

Borgia, G.C., Folloni, G., Gubellini, A.(1978) Nuovi rilievi sull'assetto della Torre degli Asinelli. Inarcos 388 (5).

Capra, A., Folloni,G., Russo, P.(1990) A levelling network for the control of ground subsidence and its effects on buildings in the town of Bologna.In:Engineering geology of ancient works,monuments and historical sites (Proc.Athena Symp.,Sptember 1988), vol. Balkema Publ.,Rotterdam,1990.

Cavani, F.(1912) Sulla pendenza e la stabilità della torre Asinelli di Bologna. Accademia delle scienze , Bologna.

Davis, J.C. (1986) Statistics and data analysis in geology.John Wiley & Sons, New York.

Gubellini, A.(1984) L'inclinazione della torre degli Asinelli: recenti rilievi e tendenza attuale. Tecnoprint, Bologna .

Gubellini, A., Lombardini,G., Russo, P.(1986) Application

of high precision levelling and photogrammetry to the detection of the movements of an architectonic complex produced by subsidence in the town of Bologna. In: Third International Symposium on Land Subsidence (Proc. Venice Symp., March 1984),257-271 IAHS Publ.no.151.

Pieri, L., Russo, P. (1977) Studio del fenomeno di abbassamento del suolo in atto nella zona di Bologna. Bollettino di Geodesia e Scienze Affini , Anno XXXVI , n.3.

Pieri, L. , Russo, P.(1984) The survey of soil vertical movements in the region of Bologna.In: Third International Symposium on Land Subsidence (Proc. Venice Symp., March 1984),235-247.IAHS Publ.no. 151.

Salvioni, G.(1953) Primo contributo sulla comparazione fra la nuova rete altimetrica fondamentale alla vecchia livellazione di precisione. Bollettino di Geodesia e Scienze Affini , vol. XII ,87-99.

Salvioni, G.(1957) I movimenti del suolo nell'Italia centrosettentrionale. Dati preliminari dedotti dalla comparazione di livellazioni. Bollettino di Geodesia e Scienze Affini , vol.XVI ,325-366.

Land Subsidence (Proceedings of the Fourth International Symposium on Land Subsidence, May 1991). IAHS Publ. no. 200, 1991.

Levelling Data Management for the Monitoring of Land Subsidence

G. BITELLI
Istituto di Topografia, Geodesia e Geofisica Mineraria, University of Bologna, Bologna, Italy
P. RUSSO
Dipartimento di Ingegneria dei Trasporti, University of Naples, Naples, Italy

ABSTRACT The main source of geodetic measurements for the detection of ground vertical movements is usually levelling. A considerable amount of data from different sources must be often elaborated in order to have informations on subsidence. Such data may be disomogeneous with regard to quality, epoch and space. The purpose of this paper is to present the use of a relational data base for the storage, retrieval and elaboration of levelling data. The integration of the system in a GIS can play an important part in a multidisciplinary approach to a subsidence problem.

INTRODUCTION

Geodetic data which allow ground vertical movements and in particular subsidence to be determined, derive for the most part from repeated spirit levelling. The development of new altimetric survey techniques linked to the use of motorized trigonometric levelling and of Global Positioning System (GPS) will shortly make available a considerable quantity of other types of data. At the present moment however, the results of spirit levelling provide the richest store of information.

As is well-known, there are two main stages in the study of a case of subsidence:

(a) collecting and processing existing levelling data concerning the area being studied;
(b) the creation, and repeated surveys, of a new control network.

A stage in which exclusively "historical data" from various origins are processed is followed by one in which these data are compared with data obtained directly from field operations.

In a region in which bench marks exist, and in which surveys are continually being carried out the altimetric data situation is continuously changing: bench marks are lost, new bench marks created, survey campaigns are undertaken concerning different parts of the region and at dif-

ferent times. There are therefore many data, arriving not only from the control networks, which can be used to form a picture of ground subsidence in any given period.

Storing the original survey data in a traditional archive, based on paper documents, is a simple operation. What is however time-consuming and problematic is the procedure of searching for data relating to one particular area and moment in time, the selection of these data in function of their suitability for use in the study of ground movements and the preliminary operations for homogeneizing data.

It would therefore be helpful to have an information instrument that could store already existing levelling data, after a suitable selection process, and further data as they progressively become available; such an instrument would automatically answer queries concerning available data and would allow them to be processed, using internal and easy-to-perform procedures so as to make data usable in mathematical models for determining and representing subsidence.

LEVELLING DATA AND PROBLEMS CONNECTED WITH THEIR MANAGEMENT

As already mentioned, through the years spirit levelling campaigns are carried out in a geographical region for different reasons. A levelling campaign is characterized by considerable amount of data, concerning:

(a) the agency which carried out or ordered the survey;
(b) the period in which field operations were carried out;
(c) the territory involved;
(d) the design of the network;
(e) the adopted observing procedures and instrumentation;
(f) the height reference system;
(g) the bench marks surveyed;
(h) the results of measurements;
(i) the heights determined and their errors.

The aim of any survey can cause variations in the criteria governing the network design, techniques of building elevation points, observing procedures and data processing: therefore wide variations in the types of data are found.

For a levelling campaign to be of use in the study of ground movements, the following basic needs must be met:

(a) the elevation points must be based on reliable bench marks;
(b) survey operations must be carried out using known instruments and procedures;
(c) bench mark positions, and the plan of the network surveyed, must be documented in an exhaustive manner.

Absence of these minimum requirements leads to a survey being excluded from the group of those which can be used.

Once the survey campaigns have been selected, there is the problem of how to process the data so that they can be used together as input of a model to describe the land sub-

sidence in the same height reference system. Ground vertical movements are calculated and represented using mathematical models (Carrera & Vanicek, 1986) which utilize either redetermined bench mark elevations, or remeasured elevation differences relative to the segments.

This paper deals with the work phase that leads to supply data to the mentioned models; this phase, as delineated above, concerns storage, retrieval and pre-elaboration of the levelling data.

The aim of the authors is to describe the main characteristics of an information system which answers the above needs. The system has been conceived as an open system, both to other altimetric data, and to other types of data concerning the geographical region and particularly useful for studying the causes and effects of subsidence.

DATA MANAGEMENT IN A DEDICATED INFORMATION SYSTEM

The database type of information approach to the problem has been chosen. It is common knowledge that this approach allows the different types of data to be considered as a single organized set, and this set maintains the correlations among the data, is exhaustive from the information point of view and eliminates or minimizes information duplication (Bitelli & Russo, 1988). So the key instrument adopted is a Data Base Management System (DBMS); the advantages which accrue from adopting this technology can be briefly summarized as follows:

(a) all the information stored is available to more than one user and application, each of whom is interested in, and/or has access to, specific data subsets ("views");
(b) data integration minimizes data redundancy and duplication, and eliminates the risk of inconsistency, which happens when there is simultaneous access to two or more copies of the same data, which however are not identical copies;
(c) a series of services is provided for database use and maintenance (security, integrity, data reset, etc...);
(d) physical independence of data, which ensures that the physical set-up and data access strategies can be modified without changing the application programs that refer to the data;
(e) logical independence of data, which ensures that the database logical design can be modified (for example when new requirements come into being, or some elements are changed) without changing application programs not involved in modifications;
(f) availability of a language, in general non-procedural, for designing the logical data model, for access to data and for modifying them, for formulating queries and reports.

An information system must be created in following five accepted main successive stages:
(a) analysis of the functional requirements;
(b) creation of a a conceptual model of the data;
(c) logical design of the database;
(d) physical design of the database;
(e) implementation of the system in accordance with the model and the resulting specifications.

Analysis of the functional requirements

The system has to deal with the integrated management of data, i.e. data retrieval and utilisation in specialized procedures oriented towards the study of ground vertical movements; it must be underlined that such procedures may at some stage become a part of the system, but they are not a key element in it. The only topographical procedures that are internal and essential to the system are those which allow data in output to be prepared so that they can be used effectively by other programs, and which guarantee their quality in terms of congruence, reliability and standardisation.

Key requisites of the system are therefore a maximum of flexibility in use and the guarantee of being open to the outside world.

The system must allow the following main operations:
(a) Data entry, with procedures which show up possible risks of duplications and coincidences, which can be frequent when historical data such as those being considered are dealt with (in particular in the identification of bench marks: for example, it often happens that two or more agencies use the same code to designate different bench marks); this calls for the use of data validation techniques. The constraints which the system manages are of the implicit, or static type, and the explicit or dynamic type; the former are conditions linked to the actual definition of data (for example the type, the field of values permitted, etc...), while the latter concern the significance of data (for example verification of prerequisites). In many situations look-up tables are active, narrowing down to a predetermined list an item's permitted values. The system thus helps the user to avoid errors and omissions which could compromise the congruence of the information apparatus;
(b) modification and cancellation of existing data;
(c) management of procedures for free queries to the database, with the possibility of memorising queries for re-use; it is unacceptable that data queries be restricted to a predetermined and limited number of standard requests;
(d) management of reports both on screen and printed;
(e) procedures to homogeneize data produced by a query.

Considering that the data dealt with by the system are continually being added to, but are rarely modified, it can be stated that the most frequently occurring operations when using the system are entry of new data and production of output in consequence of a query. The latter operating sequence is shown in Fig. 1: following a free query to the database, a subset of information is generated responding to the filter criteria, and if the user deems this result satisfactory, depending on the characteristics of the data a homogeneization procedure is carried out upon it; finally the set of data obtained can be used for generating reports, or to constitute input for specialized procedure and other programs.

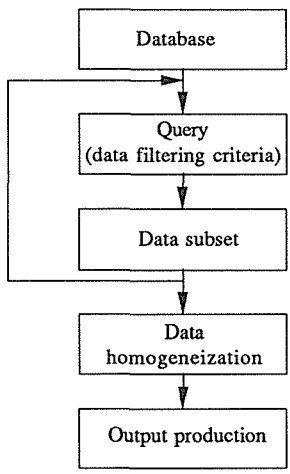

FIG. 1 Operating sequence for output data production.

Definition of the conceptual data model

The concept modelling stage aims to achieve an effective representation of the reality which is the subject of the information system, by attributing a semantic structure and classification, i.e. linked to intrinsic information content, to the data which describe the reality; it must be observed that this reality is independent of which type of DBMS will be used.

It is therefore necessary to define the entities and attributes which make up the information system, as follows.

Agency: a public or private organisation which carries out or order a levelling campaign. Its attributes concern: denomination, address, period of activity.

Survey: a levelling campaign. Its attributes concern: period of field operations, agency, measured network, height reference system, area involved, observing procedures, instrumentation.

Bench mark: a point materialized in order to allow its height to be determined with spirit levelling. Its attributes concern: denomination, localization, description, constructing technique, agency which commissioned it, set-up date, possible disappearance date.

Reference bench mark: a bench mark whose height is assumed as known for a survey. Its attributes concern: denomination, height, reference date.

Segment: a levelling line between two consecutive bench marks. Its attributes concern: bench mark names, length.

Height: height resulting from the adjustment of a network. Its attributes concern: bench mark to which it refers, the levelling campaigns in which it was determined and the mean square error associated.

Height difference: measured height difference between the extremes of a segment. Its attributes concern: segment, survey, date of measure.

References: any publication concerning levelling campaigns. Their attributes concern: title, authors, publishing informations, levelling campaigns described, areas involved.

Widely used is the so-called "Entity-Relationship" (E-R) conceptual design method, according to which the information universe is described in terms of entities, relations and attributes. The simplified E-R design shown in Fig. 2 illustrates the relations among the entities involved in the system.

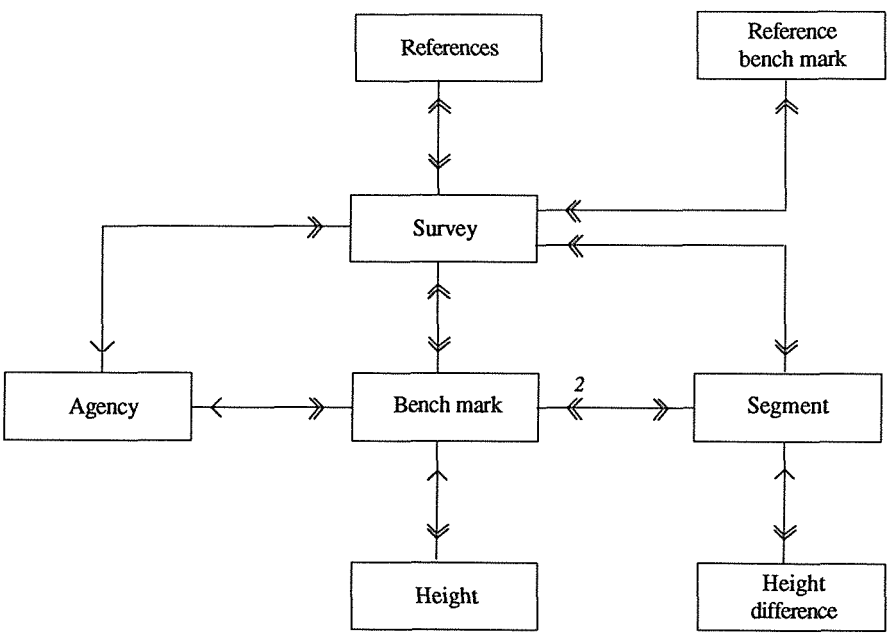

FIG. 2 Entity-Relationship diagram.

In the figure the double arrow sign indicates a "one-to-many" relation between two entities in the direction of the arrow, while the single arrow sign indicates a "one-to-one" relation; considering for example the relation between the "bench mark" entity and the "height" entity, it will be seen that each bench mark may correspond to two or more heights determined in different surveys, while vice versa each height refers to one bench mark alone.

The logical database design

The conceptual model must be translated into a logical model which expresses the internal structure of the database and consequently defines the operators which it will be possible to activate.

The logical model which has been chosen, and which today is most widely used, is the relational model, introduced by E Codd in 1970 (Codd, 1970). It represents the store of information by basing itself on the mathematical concept of "relation": given the sets D1,D2,..., Dn (called the domains of the relation), a relation R is made up of "n-ples", and in each of these the first element belongs to the domain D1, the second D2 and so on; R is therefore a subset of the Cartesian product D1 x D2 x ... x Dn. The simplest way to represent a relation is to use a two-dimensional table, in which the lines are the n-ples and in which each column (attribute) is identified by a name and contains values belonging to the corresponding domain. The conditions must also be met that all the lines (n-ples) differ from one other and that the names of the attributes are unique within the relation; finally neither the order of the lines nor that of the columns is important, and two or more attributes can belong to the same domain.

The attribute or the set of attributes, which allow each single line of the table to be identified uniquely, is defined as the "primary key".

The process of normalizing relations must be carried out during the logical design stage: it is a progressive and reversible process of substituting a collection of relations with successive collections of relations where the structure of the relations becomes progressively simpler and more regular. The final goal is a representation of relations in which the totality of the information is contained in the values of the n-ples of the relations, each relation has a primary key and the attributes of each relation depend in a simple and immediate manner on the primary key. Normalization is achieved by well-defined "normal forms" (first, second, third normal form, etc...). Briefly, a relation is in first normal form (1NF) when the attributes are of the elementary type, in other words when it is a real table. The 2NF is present when the relation is in 1NF and all its attributes which are not part of the key depend in a direct and nontransitive manner on the key

itself. The relation is in 3NF if it is in 2NF and every attribute which is not a part of the key depends in a direct and nontransitive manner on the key itself. Higher standard forms exist, but in practice it is generally sufficient to stop here so as not to excessively fragment the data store.

Relational algebra makes operators which act on the relations available, these being a "projection operator" (which creates a relation from another wider one, selecting only certain attributes), "restriction" operator (which selects only those lines in a relation which satisfy certain predetermined conditions), and a "join" operator (which joins two relations in terms of where the values of one or more common attributes coincide). These operators are powerful instruments, enabling the user to manipulate entire data blocks present in the database, whilst at the same time being simple to use.

Some interesting features of the relational model can be underlined: simplicity and flexibility, data independence, considerable symmetry of approach to the data base (there are no requests that are more efficient or simpler than others as opposed, for example, to a hierarchical model of data in which an item of information is identified following a hereditary mechanism), possibility of using high level programming languages which enable blocks of several items of stored data to be manipulated with a single instruction, in contrast to traditional types of languages.

The physical design and the implementation of the system

The tables forming the database result from the analysis of the E-R model; for each table a key and some columns (corresponding to the above listed attributes) has been defined,

To implement the system software and hardware had to be chosen.

For the choice of the software product a 4th generation language relational DBMS was chosen, providing the following characteristics:

(a) simple and user-friendly interface, suitable for use by non-experts (environmental planners, etc...);
(b) a maximum of flexibility and simplicity in the creation, activation and saving of different data "views", following non-procedural query methods;
(c) communication capabilities: possibility of linking up to networks, of access to remote databases resident on mainframes, of accepting input from field data recorders;
(d) possibility of entering special processing procedures already availables, written in traditional computer languages;

(e) flexible data import procedures from other systems, and flexible data export in formats usable by external application programs.

Regarding hardware, the decision was taken to use personal computers to create the system, the reasons for this decision being as follows:

(a) widespread availability and low cost of instrumentation, while processing and data storage capacity is sufficient for the aims of the system;
(b) availability on personal computer of most of the processing programs which are commonly used in studying ground vertical movements;
(c) simple manner in which data are collected from and transferred to different operating contexts, using procedures which have become common.

The realization of the system is going to be completed; first results point out that the base requirements are satisfied.

FUTURE EXTENSIONS

The system presented constitutes the first element in the framework of a general information system for altimetric data management.

As for data processing, the system envisages a further module, for management of GPS satellite data. However this constitutes a structurally different and separate system from the one presented here on account of the different type of information, the different characteristics of the surveys and the particular problems they involve; the capacity for linkage, integration and comparison between these two environments are first and foremost linked to the possibility of comparison of elevations (referred to the geoid in the case of spirit levelling, ellipsoidal in the case of GPS), and secondly to the possible availability of linkages between elevations obtained from levelling bench marks and GPS bench marks.

A second prospect is the integration of the database within a Geographic Information System (GIS) dedicated to the study of land subsidence; such a system would have to organize, on a geographical referenced basis, data connected directly or indirectly with the phenomenon of land subsidence, from whatever source and of whatever type, thus making it possible to provide powerful instruments for analysing subsidence; it would allow different thematic views of an area to be superimposed and to deduce hypotheses on the correlations existing between ground level displacement and its effects or causes. To achieve these goals it is therefore extremely important to have available a topographical database such as that presented in this paper, well-structured and directly transferable into a numeric cartography environment, a stock of information which

otherwise would be lost or scattered or in any case difficult to utilize.

In order to proceed with this operation it is however necessary to make a preliminary analysis of the precision with which data are geographically located, with reference to the use envisaged in the GIS, in particular to the dimensions of the region under study, to the wealth of detail required in relation to the other types of data contained in the system, and to what procedures are planned to be used.

The characteristics of the database itself, and in particular the possibility of selecting a particular "temporal window" on the data, permit, if other databases referring to the time variable are available, the creation of a time-related geographic information system, capable of managing constantly changing information; such a system would certainly be most suited for the study of a highly dynamic phenomenon such as subsidence.

CONCLUSION

From the above considerations it is clear furthermore that availability of instruments of this type could also not be limited to storing information differently, but could exert great influence on the methods and practices followed in the use of altimetric data.

On one hand in fact, the knowledge that the data will be entered and managed in an integrated information system could lead to requesting right from the start that the agency carrying out the survey provide data and descriptive records documented in a better and different manner, thus setting definitive data standards.

Finally, being able to use instruments of this type when processing the data collected, will allow, naturally with due caution, a series of new studies to be undertaken on the complementary use of altimetric data of different origins, type and nature.

REFERENCES

Bitelli, G. & Russo, P. (1988) A data base for levelling data. In: Geodetic Meeting Italy-Poland (Proc. Bologna Symp., June 1988), 235-248. CUSL Publ.

Carrera, G. H. & Vanicek, P. (1986) Review of techniques for determining vertical ground movements from levelling data. In: Third International Symposium on Land Subsidence (Proc. Venice Symp., March 1984), 195-201. IAHS Publ. no. 151.

Codd, E. F. (1970) A Relational Model of Data for Large Shared Data Banks. Comm. ACM 13 (6).

Land Subsidence (Proceedings of the Fourth International Symposium on Land Subsidence, May 1991). IAHS Publ. no. 200, 1991.

Elevation Changes Associated with Subsidence in Las Vegas Valley, Nevada

JOHN W. BELL
Nevada Bureau of Mines and Geology, University of Nevada, Reno, NV 89557, USA

ABSTRACT Subsidence in Las Vegas Valley, Nevada, is characterized by a primary regional subsidence bowl punctuated by several localized bowls. Previous studies indicate that from 1963 to 1980 the valley-wide bowl had subsided more than 49 cm with the secondary bowls subsiding as much as 79 cm. Vertical-control data obtained from releveling benchmarks in 1986-1990 indicate that the same patterns and trends of movement have continued to occur since 1980. Nearly constant rates of subsidence on several benchmarks outside of major pumping areas suggest that subsidence does not simply reflect the location of major pumping or the location of major water-level decline. Releveling of nine short vertical-control lines from 1978 to 1989 indicates that preexisting geologic faults are the sites of preferred differential subsidence, and that these faults should be regarded as zones of high subsidence risk.

INTRODUCTION

Location

Land subsidence in the Las Vegas area, Nevada, is primarily related to groundwater withdrawal. Although the rate of subsidence has remained relatively constant for the last decade, recent rapid urban development has highlighted the longer term effects, in particular, the appearance of fissures and an increase in structural damage.

The metropolitan Las Vegas area is located in southern Nevada, within a 1295 km^2 (500 mi^2) alluvial valley which receives between 12 to 20 cm (5 to 8 in) of average annual precipitation. Nevada is the fastest growing state in the USA and Las Vegas is the most rapidly growing city in Nevada. The present permanent population (1990 statistics) of the Las Vegas metropolitan area is about 800,000.

Hydrogeologic setting

Las Vegas Valley is a fault-bounded basin containing hundreds of metres of Tertiary and Quaternary sediments derived from lacustrine, paludal, and

alluvial deposition. These sediments consist predominantly of coarse-grained alluvial fan deposits around the periphery of the valley and predominantly of fine-grained (silt and clay) sediments in the central portion of the valley. Areas presently exhibiting significant amounts of subsidence are underlain by compressible deposits having fine-grained contents ranging from 25% to more than 75% by volume (Plume, 1984). Poorly permeable clay and calcium carbonate (caliche) beds occur throughout the alluvial sequence. A series of linear and curvilinear north- to northeast-trending tectonic Quaternary faults cut the valley floor creating a succession of prominent scarps as much as 50 m (160 ft) high, with displacements all down to the east.

Nearly all of the groundwater supply in Las Vegas Valley comes from a zone of confined and semi-confined principal aquifers at depths of 200-300 m (Maxey & Jameson, 1948; Harrill, 1976). Recharge to the principal aquifers is primarily through an artesian flow system. Between 31 and 43 hm^3/year (25,000 and 35,000 acre-feet/year) of water are estimated to enter the Las Vegas Valley hydrologic system in the recharge area (Maxey & Jameson, 1948).

Water has been withdrawn from the valley-fill reservoir through artesian discharge and pumped wells since 1905. In 1946, annual groundwater withdrawals began to exceed annual recharge (Maxey & Jameson, 1948). In 1955, withdrawals and discharge from the principal aquifers were estimated to be about 49.3 hm^3/year (40,000 acre-feet/year) (Malmberg, 1965); by 1968 this had increased to an all-time maximum of 108.6 hm^3/year (88,000 acre-feet/year) (Harrill, 1976). Since 1968, annual groundwater withdrawals have gradually been reduced (Katzer, 1977), and since 1980, withdrawals have remained at about 82.7 hm^3/year (67,000 acre-feet/year) (T. Katzer, 1990, personal communication). Increased demand in the last decade has been satisfied by the importation of Colorado River water.

PREVIOUS SUBSIDENCE STUDIES-- 1935-1980

Using vertical control data from the 1935 National Geodetic Survey (NGS) first-order network through Las Vegas Valley, Maxey & Jameson (1948) first noted as much as 7.5 cm (3 in) of movement in the central portion of the valley. By 1963, a distinct subsidence bowl with a maximum depth of more than 1 m (3.3 ft) had affected an area of 518 km^2 (200 mi^2) (Mindling, 1971). Releveling of the first-order NGS network in 1980 showed that the affected area had enlarged to more than about 1030 km^2 (400 mi^2), and that three distinct secondary subsidence bowls had developed, superimposed on the larger valley-wide bowl (Bell, 1981). From 1963 to 1980, the valley-wide bowl subsided more than 49 cm (1.6 ft) with the secondary bowls subsiding as much as 79 cm (2.6 ft).

SUBSIDENCE DATA-- POST-1980

Elevation data acquired since the last tabulation in 1980 (Bell, 1981) consist of two sets: a) vertical-control data obtained from releveling of selected NGS

benchmarks by the Clark County Surveyors Office in 1986-1990, and b) vertical-control data derived from a 12-year leveling program by the Nevada Department of Transportation designed to monitor localized differential movement across geologic faults.

Clark County data

During 1986-1990, the Clark County Surveyors Office releveled most of the existing city, county, and NGS benchmarks in Las Vegas Valley in order to update a major portion of the valley-wide vertical-control network. Leveling procedures were comparable to second-order, class II accuracy standards. Since the last NGS survey in 1980, many of the NGS benchmarks have been destroyed by urbanization.

A total of 28 NGS benchmarks are used here to determine the elevation change throughout Las Vegas Valley for the period 1963-1986 (Fig. 1). Many of these points were releveled by the NGS in 1963 but not in 1980; too few 1980 points remain to allow a 1980-1986 comparison. The Clark County survey assumed that benchmark W51 was fixed and determined all other elevations relative to this point. Since benchmark W51 is situated within alluvial fill and therefore susceptible to subsidence, all Clark County elevations were normalized to benchmark A109 located in bedrock about 10 km (6 mi)

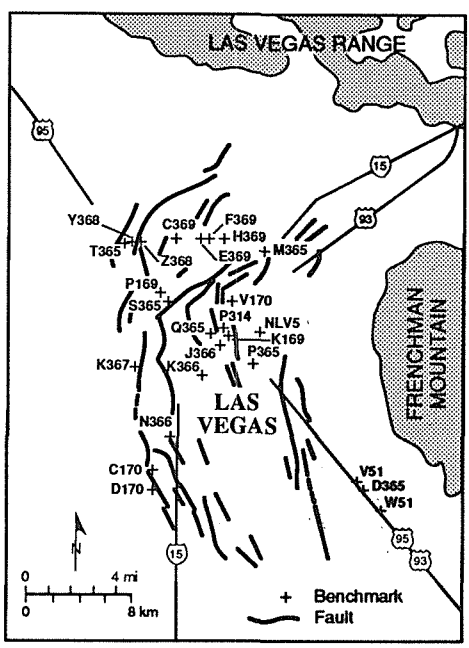

FIG. 1 Location of NGS benchmarks used in study.

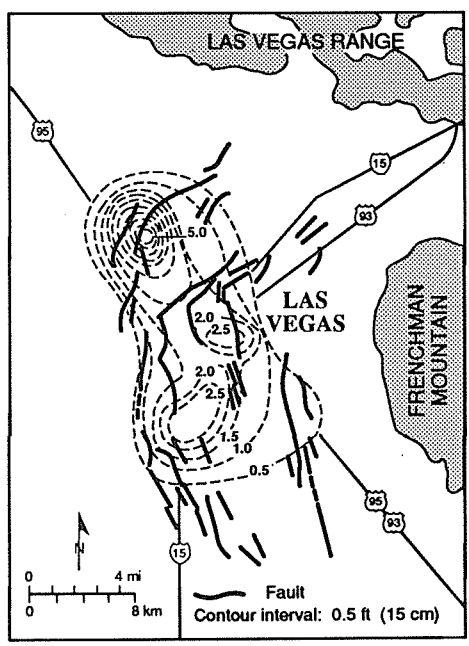

FIG. 2 Contour map showing subsidence for the period 1963-1986, with Quaternary fault base.

southeast of benchmark W51. The elevation adjustment applied to all Clark County points based on this assumed fixed datum is about 2.1 cm (0.07 ft).

Subsidence in Las Vegas Valley for the period 1963-1986 is shown in Figure 2. Contouring is based on proportional interpolation, and since the data set consists of only 28 points, the subsidence contours are only approximately located. In particular, the centers of the secondary subsidence bowls are contoured on the basis of maximum measured change on a benchmark within the existing network. Because of the relatively sparse coverage, other areas of large elevation change may be present but undetected. The outer 15 cm (0.5 ft) contour is relatively well defined in the eastern, western, and southern parts of the valley. The location of the 1986 zero-change contour is not precisely known, but it is outward at least as far as in 1980, which in general was near the perimeter of the valley fill.

In order to analyze long-term subsidence rates and trends on individual benchmarks, the 1986 data were compared to a combined set of elevation data derived from several different surveys. The second-order county data were combined with first-order data from the 1935, 1963, and 1980 NGS surveys, and with second-order data from a survey by the Nevada Department of Transportation in 1972. Five benchmarks (K169, P169, Z368, N366, and H369) are shown here (Figs. 3 & 4) to illustrate the trend of subsidence with time. Benchmark K169 has the most complete vertical-control record dating back to the original 1935 survey. Benchmark Z368 shows the greatest amount of vertical movement for the 1963-1986 period.

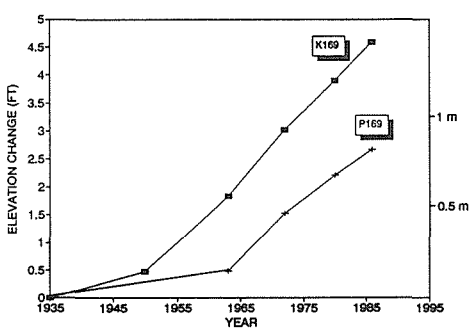

FIG. 3 Subsidence trend for benchmarks K169 and P169 for the period 1935-1986.

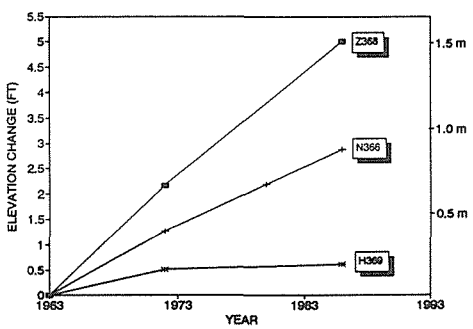

FIG. 4 Subsidence trend for benchmarks Z368, N366 and H369 for the period 1963-1986.

Nevada Department of Transportation Level Lines

Much of the subsidence in Las Vegas Valley is preferentially focussed on the numerous Quaternary faults which cut the alluvial sediments (Fig. 2) and serve as preexisting planes of weakness. In 1978-1980, a series of short (1.5-4 km [0.9-2.5 mi]) vertical-control lines were established by the Nevada Department of

Transportation (Fig. 5) to verify the hypothesis that the faults may be at the sites of incipient vertical rupture due to large amounts of differential subsidence in the immediate vicinity of the faults (Holzer, 1978). Benchmarks were set at 60-90 m (200-300 ft) intervals across nine faults and monitored at second-order accuracy annually or semiannually through 1989. All elevation measurements were based on assumed fixed benchmarks along each line, so that only relative differential changes were determined.

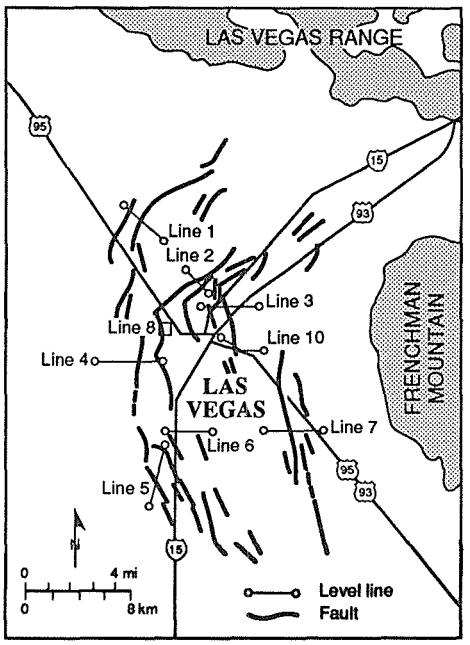

FIG. 5 Location of level lines established by the Nevada Department of Transportation in 1978-1980 across geologic faults.

All lines show differential movement during the monitoring period with total displacements across the fault zones ranging from a few centimeters to more than 40 cm (1.3 ft) (Varnum, 1987). The results from four of these lines are presented here. Level line 1 extended across a prominent Quaternary fault -- the Eglington fault-- in the northern part of the valley (Fig. 6). The line was destroyed in 1985. Line 2 (Fig. 7) crosses a compound scarp and lies 1 km (0.6 mi) northeast of a subdivision which recently experienced more than $12 million in subsidence-related damage. Lines 3 and 10 (Figs. 8 & 9) cross a large scarp in downtown Las Vegas.

DISCUSSION

Subsidence in Las Vegas Valley is characterized by two distinct modes: a) regional vertical movement primarily centered in the valley and secondarily centered in three localized areas, and b) differential vertical movement associated with preexisting geologic faults. Regional and localized horizontal strains induced by the vertical subsidence may be present, based on the distribution of earth fissures (D. Helm, 1990, personal communication), but have not been systematically measured.

The pattern of valley-wide subsidence for the 1963-1986 period follows the same trend delineated for the 1963-1980 period (Bell, 1981), with the exception that the localized subsidence bowl in the northwest part of the valley is much more pronounced. This deep secondary bowl was present in 1980 but undetected because the 1980 survey did not relevel benchmarks in this area.

The 1986 Clark County survey did include these benchmarks, which are here compared to 1963 NGS and 1972 Nevada Department of Transportation data.

Individual benchmark trends indicate that in many cases subsidence has continued at an approximately constant rate at least since 1963. Trends of subsidence in each of the localized bowls are reflected by benchmarks K169 and P169 (Fig. 3) and Z368 and N366 (Fig. 4). Benchmark K169 has the most detailed record of any point in the actively subsiding part of the valley, and it indicates that the downtown Las Vegas area has been subsiding uniformly since 1950. The average rate of movement on this benchmark has been 3.6 cm/year (1.4 in/year). The 1935-1950 rate was substantially lower because significant overdrafting of the groundwater system did not commence until the mid-1940's (Maxey & Jameson, 1948). Several benchmarks (P169, N366, & H369) show reduced rates of movement since 1972, probably in response to reduced pumping.

Benchmark Z368, which is located in the deep localized subsidence bowl in the northwest part of the valley, shows the most movement (1.5 m [5 ft]) for the period (Fig. 4) with an average subsidence rate of 6.6 cm/year (2.6 in/year). It lies within a few kilometers of two other benchmarks (T365 &

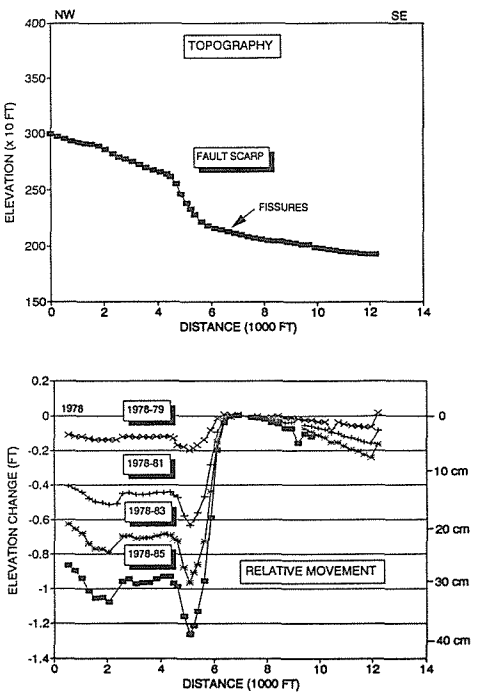

FIG. 6 Topography and corresponding relative movement for level line 1 for the period 1978-1985.

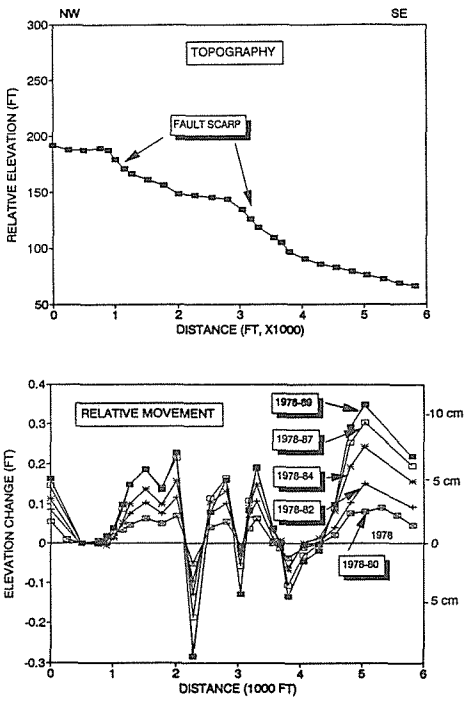

FIG. 7 Topography and corresponding relative movement for level line 2 for the period 1978-1989.

Y368) which subsided comparable amounts: 1.2 m (3.9 ft) and 1.4 m (4.7 ft), respectively.

The subsidence trend data suggest that the amounts and rates of subsidence may be semi-independent of the location of major pumping and the location of major water-level decline. The relatively constant rate of subsidence on benchmark K169 is significant because of the lack of intense groundwater pumping in this part of the valley (Harrill, 1976; Wood, 1988). The location of the deep subsidence bowl around benchmark Z368 does not clearly coincide with either the location of major pumping or the location of major water-level decline. The closest heavily pumped area lies 3-5 km (1.8-3.6 mi) to the southwest (Wood, 1988) where it is associated with a zone of large (>55 m [180 ft]) water-level decline. Such observations suggest that the relations between pumping, water-level decline, and long-term subsidence are complex, and may be related to other variables such as thickness and compressibility of sediments, residual compaction, and hydraulic partitioning.

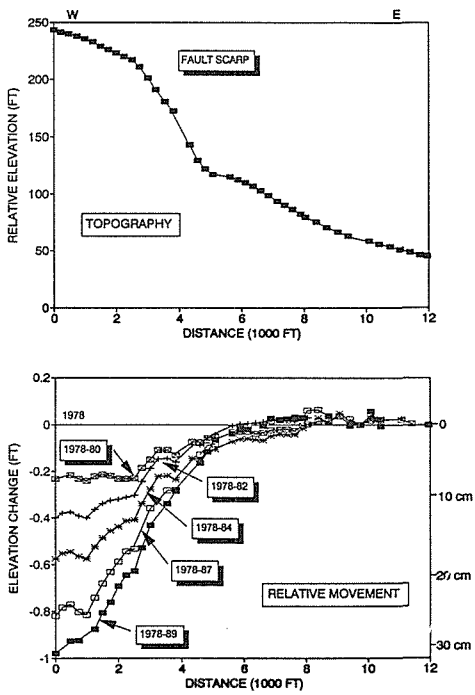

FIG. 8 Topography and corresponding relative movement for level line 3 for the period 1978-1989.

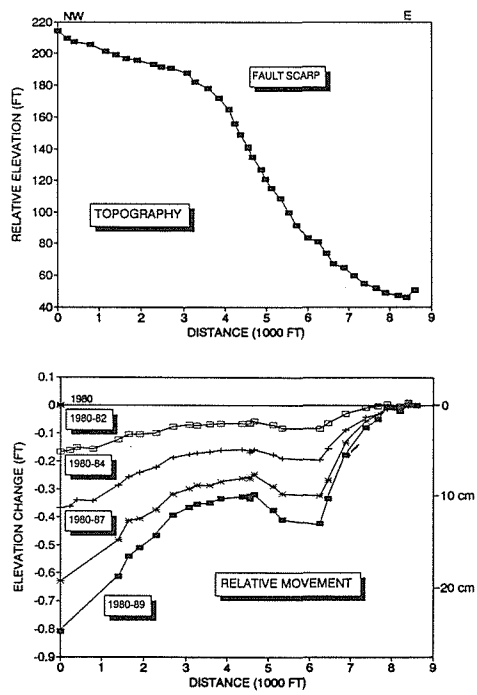

FIG. 9 Topography and corresponding relative movement for level line 10 for the period 1980-1989.

Localized differential vertical movements are occurring along the preexisting geologic faults. The direction of movement across the faults is controlled by the location of adjacent subsidence bowls, resulting, in several instances, in the movement being antithetic to the original sense of displacement along the fault. For example, level line 1 shows a large (52 cm [15.6 in]) displacement across

the Eglington fault scarp for the 1978-1985 period (Fig. 6), with the northwest end of the line moving down relative to the southeast end. The sharpest relative elevation deflection coincides with the location of both the topographic fault scarp and the location of numerous fissures lying along the toe of the scarp. Similar, but less striking, antithetic movements are also seen along faults on lines 2, 3, and 10 (Figs. 7, 8, and 9).

The displacement along level line 1, although coinciding in part with the deep localized subsidence bowl, indicates that the area to the northwest of the fault trace is subsiding more rapidly than the area to the southeast. Since benchmark Z368 is situated on the southeast (downthrown) side of the fault, deeper portions of the subsidence bowl may exist to the northwest but be undetected because of sparse benchmark density.

Line 2 is situated between the subsidence bowl surrounding benchmark Z368 and the bowl surrounding benchmark K169 in downtown Las Vegas. The elevation change profile along this line is an irregular pattern of individual benchmark displacements across a compound set of fault scarps, probably reflecting an influence from both subsidence bowls. The largest displacement between adjacent benchmarks across any fault occurs on this line, where more than 15 cm (6 in) of differential movement has occurred between two points for the 1978-1989 period.

Lines 3 and 10 both cross a large (45 m [150 ft]) fault scarp that cuts through downtown Las Vegas. The patterns and magnitude of the elevation change for both of these lines are similar; displacement is down to the west, antithetic to the original geologic offset, with about 30 cm (1 ft) of cumulative movement measured on line 3 for the period 1978-1989, and about 24 cm (0.8 ft) of cumulative movement measured on line 10 for the period 1980-1989. Differential offset on these lines is distributed across zones about 1.6 km (1 mi) in width, and the largest differential offset between adjacent benchmarks is about 4.5 cm (1.8 in) for the monitoring period.

Although differential elevation changes related to subsidence are observed across several principal faults in the valley, the patterns of displacement are not suggestive of imminent surface faulting. The elevation changes are, as noted, either antithetic to the dip of the existing fault plane, or are distributed across relatively broad zones. The location of deep secondary subsidence bowls is the primary factor influencing the sense and style of renewed movement on the faults. The fault traces, however, are clearly preferred sites of enhanced movement (and fissuring) in comparison to the regional subsidence and thus are regarded as zones of high subsidence risk.

REFERENCES

Bell, J.W. (1981) Subsidence in Las Vegas Valley. Nevada Bureau of Mines and Geology Bulletin 95.

Harrill, J.R. (1976) Pumping and ground-water storage depletion in Las Vegas, Nevada, 1955-74. Nevada Department of Conservation and Natural Resources, Water Resources Bulletin 44.

Holzer, T.L. (1978) Documentation of potential for surface-faulting related to ground-water development in Las Vegas Valley, Nevada. U.S. Geological Survey Open-file Report 78-79.

Katzer, T. (1977) Water-level changes associated with ground-water development in Las Vegas Valley, Nevada, March 1976 to March 1977. Nevada Department of Conservation and Natural Resources, Water Resources Information Series Report 27.

Malmberg. G.T. (1965) Available water supply of the Las Vegas ground-water basin, Nevada. U.S. Geological Survey Water-Supply Paper 1780.

Maxey, G.B. & Jameson, C.H. (1948) Geology and water resources of the Las Vegas, Pahrump, and Indian Springs Valley, Clark and Nye Counties, Nevada. Nevada Department of Conservation and Natural Resources, Water Resources Bulletin 5.

Mindling, A.L. (1971) A summary of data relating to land subsidence in Las Vegas Valley. University of Nevada Desert Research Institute Publication.

Plume, R.W. (1984) Ground-water conditions in Las Vegas Valley, Clark County, Nevada: Part I. Hydrogeologic framework. U.S. Geological Survey Open-file report 84-130.

Varnum, N.C. (1987) Results of leveling across fault scarps in the Las Vegas Valley, Nevada, April 1978- April 1987. Nevada Bureau of Mines and Geology Open-File Report 87-7.

Wood, D.B. (1988) Water-level changes associated with ground-water development in Las Vegas Valley, Nevada, 1979-81. U.S. Geological Survey Water-Resources Information Report 31.

Land Subsidence (Proceedings of the Fourth International Symposium on Land Subsidence, May 1991). IAHS Publ. no. 200, 1991.

Elevation Changes Associated with Groundwater Withdrawal and Reinjection in the Wilmington Area, Los Angeles Coastal Plain, California

STEPHEN M. TESTA
Applied Environmental Services
22313 Plaza Pointe Drive, Suite 100
Laguna Hills, California 92653, USA

ABSTRACT Subsidence in the Wilmington area due to deep fluid withdrawal is well documented in published literature. A recorded decrease in elevation of nearly 30 feet between 1928 and 1974 has been attributed to oil production operations at the Wilmington field. Reinjection of water beginning in 1953 essentially stabilized most of the affected area within the Wilmington field by 1966. Available first order leveling data indicates that areas adjoining the northern boundary of this field experienced subsidence as early as 1933, prior to significant oil production, and at least two feet of localized subsidence preceding approximately one-half foot of uplift since 1975. Plots of elevation change with time for selected benchmarks demonstrated a pattern of elevation change that is not adequately explained by withdrawal and injection of fluids at the Wilmington field. Piezometric surface maps and hydrographs of wells producing from freshwater aquifers show strong correlation between changes in piezometric head and localized elevation changes. Observed elevation changes at individual benchmarks are probably the result of the interaction of several contributing factors including pumpage and injection. The primary factor reflects lowering and raising of piezometric surface levels in the three principal aquifers. Pumpage from the Silverado aquifer accounts for an estimated one foot of subsidence. The influence of local tectonism may account for slightly greater than 0.001 feet per year of subsidence. The amount of elevation change attributable to each factor has been estimated from models and analogy with documented subsidence and rebound in other areas.

INTRODUCTION

Ground surface elevation changes as a result of subsidence is well documented in many places within the United States and throughout the world, especially where associated with fluid withdrawal (Strehle, 1989; Holzer, 1984). Areas of appreciable subsidence due to fluid extraction can be divided into those caused by oil and gas

exploitation and those caused by groundwater withdrawal. Tectonic subsidence is widespread, but typically occurs at much slower rates than events induced by man.

One of the best documented cases of oil- and gas-related subsidence occurred at the Wilmington oil field situated within the Los Angeles coastal plain (Allen, 1974; Gilluly & Grant, 1949; Kosloff *et al.*, 1980; Strehle, 1987). Although geodetic leveling surveys established that the coastal area from San Pedro to Seal Beach had been subsiding since the early 1900s, it was not until after this field was developed in the late 1930s that appreciable subsidence was observed.

Early studies noted the relationship between the subsiding area and the Wilmington oil field outline, suggesting oil production as the cause of subsidence. From 1946 to 1951, development of the Wilmington oil field increased to a peak production of over 50 million barrels per year. The rate of subsidence also peaked in 1951 at 2.4 feet per year; at this time, the center of the subsidence bowl had subsided 15 feet. The subsidence rate gradually diminished after 1952.

Repressuring of oil zones by reinjection of water was suggested as a method of curbing additional subsidence. In 1956, the first reinjection project was initiated near the southern boundary of the field to prevent coastal inundation. By 1961, almost all oil producers had formed cooperative water injection units covering most of the field. By 1966, the land surface had been stabilized over almost the entire field, and some areas were beginning to rebound.

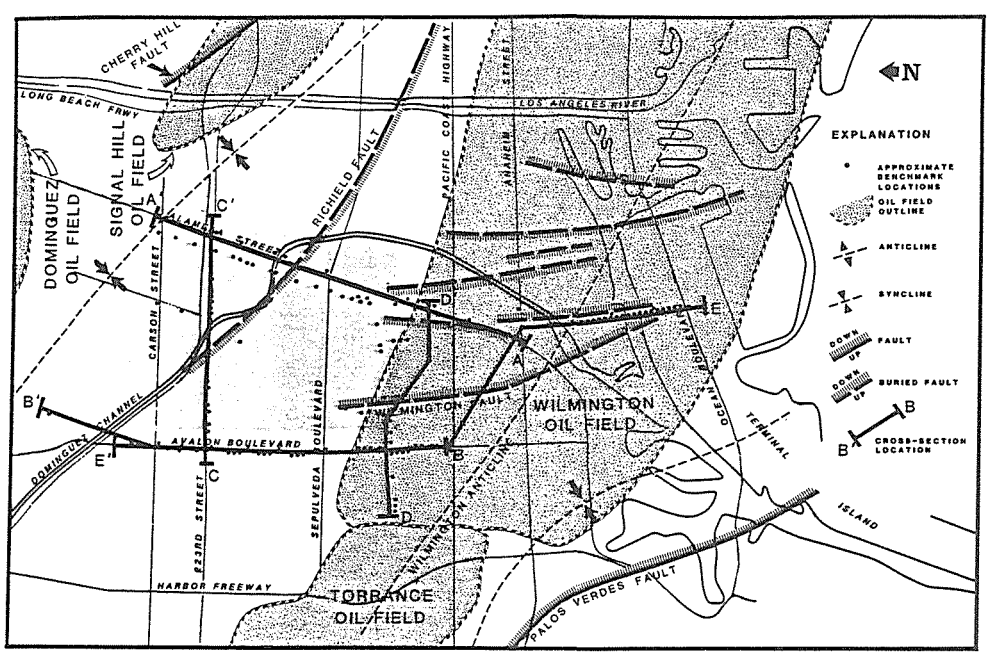

FIG. 1 Location of study area.

Total subsidence had reached over 28 feet with a 20-square mile area subsiding two feet or more. Currently, the area of partial rebound included most of the field, with some areas regaining over a foot of lost elevation (Strehle, 1987).

However, further inland the Los Angeles coastal plain is characterized by other factors which all play a role in evaluating changes in ground surface elevations. These factors include freshwater injection as part of the seawater intrusion barrier project; pumpage of groundwater for industrial, drinking water usage, aquifer restoration- related activities, and tectonic influences (Testa, 1989; Testa & Winegardner, 1990).

This study was conducted to evaluate the potential for ground surface elevation changes along the northern perimeter of the Wilmington oil field (Figure 1). Causes for past elevation changes in the vicinity of the study area were evaluated with respect to 1) fluid withdrawal from oil-bearing zones resulting in known elevation changes associated with Wilmington oil field activities ; 2) groundwater withdrawal from the Gage, Lynwood, and Silverado aquifers resulting in lowering of piezometric surfaces; 3) water injection into the Gage and Lynwood aquifers as part of the Dominguez Gap Barrier Project; and 4) tectonism, including regional subsidence of the Los Angeles Basin and possible vertical movement associated with local structures.

Following evaluation of past elevation changes, assessment of potential subsidence in the area was conducted. Based on interpreted causes of past evaluation changes and published models, potential for future elevation change was estimated.

REGIONAL HYDROGEOLOGIC SETTING

The study area is situated on the Los Angeles Coastal Plain, about fifteen miles south of the city of Los Angeles Civic Center (Figure 1). Regional geology is discussed by Yerkes & others (1965), Poland et al. (1956), and the California Department of Water Resources (1961). The study area is directly underlain in part by deposits which comprise the unconformable upper Pleistocene Lakewood Formation, and in part by Recent alluvium. The Lakewood Formation, called the "unnamed upper Pleistocene deposits" by Poland & Piper (1956) and Yerkes & others (1965), includes both marine and continental sands, gravels, silts and clays. In this formation, shallow marine deposits of sand with some gravel alternate with silt and clay deposits beneath the Torrance Plain. The thickness of the Lakewood Formation varies up to a maximum of 250 feet.

Hydrogeologic conditions beneath the study area were investigated by evaluating all available information on water wells within a one-half mile radius of the site boundaries. A large amount of information was available because the Los Angeles County Department of Public Works (LACDPW; formerly Flood Control District) has constructed and is operating numerous monitoring wells and four recharge wells within the study area. These wells were installed as part of the Dominguez Gap Barrier Project to repel sea water intrusion into beneficial aquifers. In addition, numerous deep wells have been drilled in the area, many of which are presently producing from the Silverado aquifer.

Named aquifers, in descending order from the surface, are the Semiperched aquifer within the Bellflower aquiclude, the Gaspur aquifer, the Gage aquifer ("200-foot sand"), the Lynwood aquifer ("400-foot sand"), and the Silverado aquifer. Beds of fine-grained materials which act as aquicludes or confining layers separate the aquifers in some but not all places. Detailed discussion is provided by Testa et al. (1989).

Inadequate surface water supplies encouraged early development of groundwater sources in the West Coast Basin (Mendenhall, 1905). Springs east of the Newport-Inglewood structural zone were utilized as early as 1870. Shallow wells were soon required; by 1904, these wells produced approximately 10,000 acre-feet per year. After introduction of the deep-well turbine pump, groundwater use spread throughout the basin. Eventually, demand exceeded recharge, and water levels dropped below sea level throughout the basin in the 1920s. As a result, seawater encroached beneath coastal areas of the basin by 1932. Groundwater quality continued to deteriorate until several regional water suppliers filed suit in 1945 to control groundwater extractions from the basin. Demand for groundwater increased rapidly after 1943 due to population and industrial growth before leveling off in 1970 (Figure 2). Today the West Coast Basin

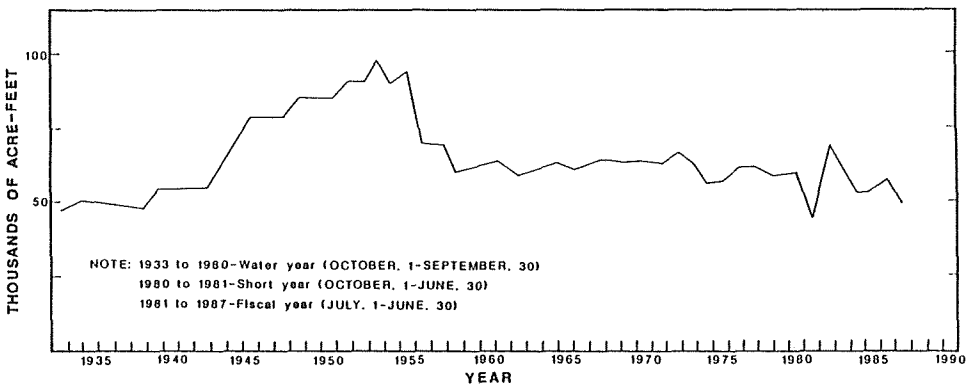

FIG. 2 Historic groundwater use.

is an adjudicated basin and all groundwater pumped must be reported to the Watermaster. All wells produce from the Silverado aquifer. All pumped water is used by refineries for industrial purposes except for two acre-feet pumped by Southern California Edison. The total pumpage in this area for a typical 12-month period of July, 1985 through June, 1986 was about 9,762 acre-feet.

Sea water intrusion barrier projects have been established to protect West Coast basin groundwater supplies. The Dominguez Gap Barrier Project was set up along San Pedro Bay and began operating in February, 1971. The nearest artificial recharge of groundwater by injection through Dominguez Gap Barrier Project wells via 29 operational recharge wells are located in the southern and eastern portion of the study area (Figure 1). The Gaspur, Gage and Lynwood aquifers are replenished in this program. The total amount of water

purchased for Dominguez Barrier Gap recharge for a typical 12-month period ending September, 1987 was 6,230 acre-feet.

RELATIONSHIP BETWEEN HISTORIC GROUND SURFACE ELEVATIONS AND GROUNDWATER LEVELS

Surveying data acquired and used in this report were obtained from the City of Long Beach, City of Los Angeles, Los Angeles County Department of Public Works (LACDPW), and National Geodetic Survey. Useful data were restricted to resurveyed benchmarks (e.g., a piece of metal embedded in concrete) whose location is documented in detail (Figure 1). Only first order leveling data were utilized in this study. In evaluating the relationship(s) between historic ground surface elevations and groundwater levels, detection of absolute elevation changes is dependent upon a common, stable reference point. To compare elevations obtained from different sources. All data collected during this study are relative to Tidal Bench Mark Number Eight (Tidal Bmk-8), which has been adopted by the National Geodetic Survey as the "stable reference point" within southern California. Benchmarks have been tied directly to Tidal Bmk-8 by surveying from this point, or indirectly by tying into another survey which originated at this point. For data shot at different times to be comparable, the reference point, Tidal Bmk-8, must be stable. It is assumed that this condition is satisfied, although the effects of potential instability of Tidal Bmk-8 on interpretations is discussed later.

Subsidence in relation to ground surface elevation changes is presented relative to a period of subsidence which continued from the 1920s to the late '60s-early '70s, recent uplift of the area (1965-75 to 1985), a summary of the areal distribution of elevation changes, and finally a summary of the timing of elevation changes.

Subsidence: 1920's to 1965-75

All available data show subsidence throughout the area dating back to the earliest available resurveys. Lowering of the ground surface continued, with exception of minor reversals, until stabilization and/or rebound was initiated. The time of ground surface stabilization varies geographically but in general commenced between 1965 and 1975. Subsidence and uplift can be demonstrated by documenting changes in benchmark elevation as illustrated by subsidence profiles (Figure 3). Surveying events used on subsidence profiles are normalized to the labeled year even though surveying may not have taken place entirely during that year. The locations of the subsidence profiles are shown in Figure 1.

Elevation changes are plotted for specific years relative to a base year. Each benchmark must be surveyed during the selected base year for effective comparison to other years. For this reason the base year is not always the earliest year that a survey was made, although an attempt was made to designate the base year as early as possible. Profiles indicate subsidence if earlier surveying events plot above the base year and more recent surveying events plot progressively below the base year. The vertical lines on the profiles represent benchmarks and show the years in which the

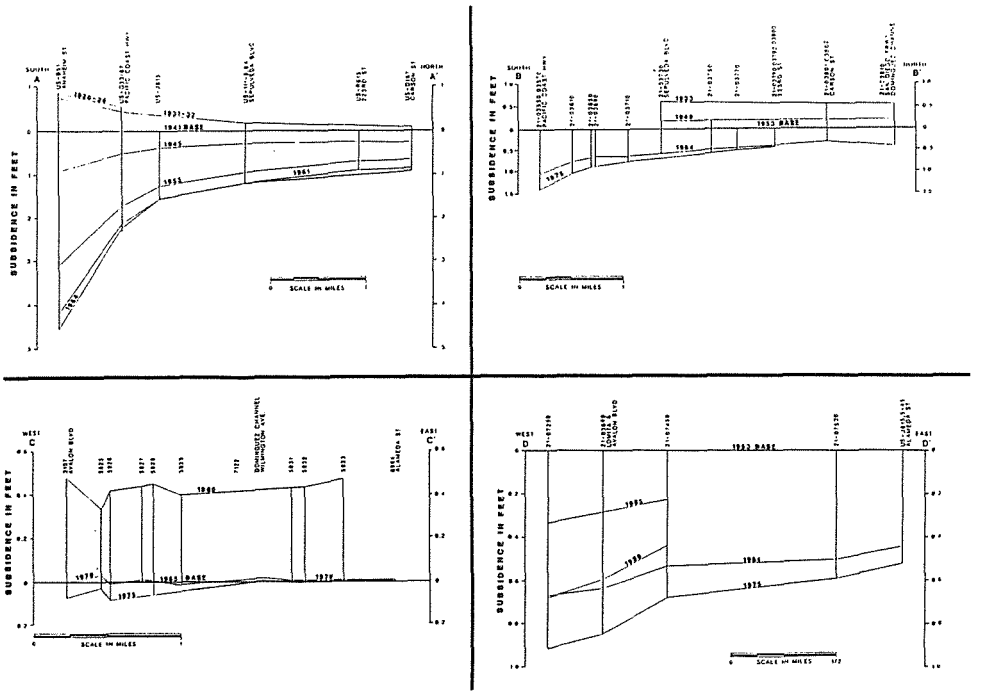

FIG. 3 Subsidence profiles documenting changes in benchmark elevations.

individual benchmark was surveyed; therefore, showing the duration of the record at each benchmark. Subsidence rates have been determined from profiles by dividing elevation change by the number of years between surveys.

Profile of subsidence A-A′ Subsidence profile A-A′ is a N-S transect situated along Alameda St. from Anaheim St. to Carson St. Limited data show a low initial rate of subsidence between the 1920-26 and 1931-32 surveys. Subsidence accelerated after 1931-32 to rates ranging from 0.08 ft/yr at Anaheim St. to 0.02 ft/yr at Sepulveda Blvd. North of Sepulveda Blvd. the rate of subsidence remained low during this time period and was equal to approximately 0.01 ft/yr. By 1945, subsidence rates more than doubled in comparison to rates of the previous period, reaching peak rates of 0.23 ft/yr at Anaheim St. and 0.07 ft/yr from Sepulveda Blvd. to Carson St. Subsidence rates remained high, but below peak levels in the period from 1945 to 1955, showing a regular decrease from south to north. Rates continue to decrease along the entire transect after 1955. Between 1955 and 1961 rates decreased rapidly north from Anaheim St. to Lomita Blvd., and then gradually from Lomita Blvd. to Carson St. By 1964, subsidence had decreased to less than half its peak levels. It appears that the ground surface had essentially stabilized along a one mile path extending south from Sepulveda Blvd. Total subsidence values are 5.3 feet at Anaheim

St., 1.4 feet at Sepulveda Blvd. and 1.0 feet at Carson St. for the period between 1931/32 and 1974.

Profile of subsidence B-B' Subsidence profile B-B' is a N-S transect situated along Avalon Blvd. from Pacific Coast Highway (PCH) to the Dominguez Channel. Initial subsidence rates between 1933 and 1949 vary from 0.027 ft/yr at Sepulveda Blvd. to 0.021 ft/yr at the Dominguez Channel. Subsidence rates during the 1949 to 1953 period are approximately double the earlier rates. Rates increase slightly northward from Sepulveda Blvd. Peak subsidence rates along this transect occurred in the southern portion of this transect during the period from 1953 to 1964. To the north, rates declined from peak levels reached during 1949 to 1953 period. From south to north, rates dropped sharply from 0.094 ft/yr at PCH to 0.057 ft/yr at Lomita Blvd., then gradually from Lomita Blvd. to 0.029 ft/yr at Carson St. and then increased to 0.039 ft/yr at the Dominguez Channel. Rates drop off markedly after 1964 to 0.034 ft/yr at PCH decreasing regularly to 0.003 ft/yr at 223rd St. for this period extending to 1975. Due to the limited duration of benchmarks, total subsidence values span different periods of time. Net subsidence totaled 1.4 feet at PCH from 1953 to 1975, 1.2 feet at Sepulveda Blvd. between 1933 and 1964, 0.3 feet at 223rd St. from 1953 to 1975, and 0.85 feet at Carson St. between 1933 and 1964.

Profile of subsidence C-C' Subsidence profile C-C' is an E-W transect situated along 223rd St. from Avalon Blvd. to Alameda St. The earliest subsidence rates cover the period from 1960 to 1965. During this period rates vary from 0.096 ft/yr to 0.68 ft/yr along the transect, but do not show a regular pattern of change. The 1965 to 1970 period demonstrates relative stability of the ground surface. During the 1970 to 1975 period, there is a regular pattern of decreasing subsidence rates eastward. Rates vary from 0.015 ft/yr immediately east of Avalon Blvd. to slightly greater than zero at Alameda St. Total subsidence is relatively constant across this profile between 1960 and 1975. The high and low values are in close proximity near Avalon Blvd., varying from a low of 0.37 feet to a high of 0.54 feet.

Profile of subsidence D-D' Subsidence profile D-D' is an approximately E-W transect parallel to surrounding oil field trends. During the period from 1953 to 1964, rates decrease from 0.061 ft/yr 0.5 miles west of Avalon Blvd. to 0.040 ft/yr at Alameda St. Rates are lower between 1964 and 1975, decreasing sharply eastward from 0.048 ft/yr west of Avalon Blvd. to 0.008 ft/yr at Alameda St. Total subsidence from 1953 to 1975 decreases from 0.92 feet west of Avalon Blvd. to 0.52 feet at Alameda St.

Uplift: 1965-75 to 1985

The most recent available surveying data suggest that following subsidence the ground surface within the study area and surrounding areas has been rising in recent years. Rebound is demonstrated

using two elevation change profiles, benchmark elevation profiles, and published data from Wilmington oil field studies. The timing of uplift initiation varies geographically and will be discussed later.

A consistent rate of uplift equal to 0.048 ft /yr occurred between 1975 and 1980 along Lomita Blvd. from 1500′ west of Avalon Blvd. to Wilmington Ave. as illustrated in subsidence profile D-D′. Rates between 1980 and 1985 decreased eastward from 0.070 ft/yr 1500′ west of Avalon Blvd. to 0.043 ft/yr at Wilmington Ave. Transect E-E′ is a north-south profile demonstrating total uplift (Figure 4). This profile extends north from Ocean Blvd. across the Wilmington oil field to Anaheim St., then is offset one mile west before continuing north along Avalon Blvd. from PCH to north of Carson St. The south end of this profile passes just west of the area of maximum uplift in the Wilmington oil field, where uplift exceeds 1.4 feet (Port of Long Beach, January, 1988). Along the transact, total uplift is almost 1.2 feet near the center of the Wilmington oil field, and then decreases to 1.0 feet at Anaheim St. A second peak is evident at PCH and Avalon Blvd. where total uplift again approaches 1.2 feet. Uplift values drop rapidly northward,

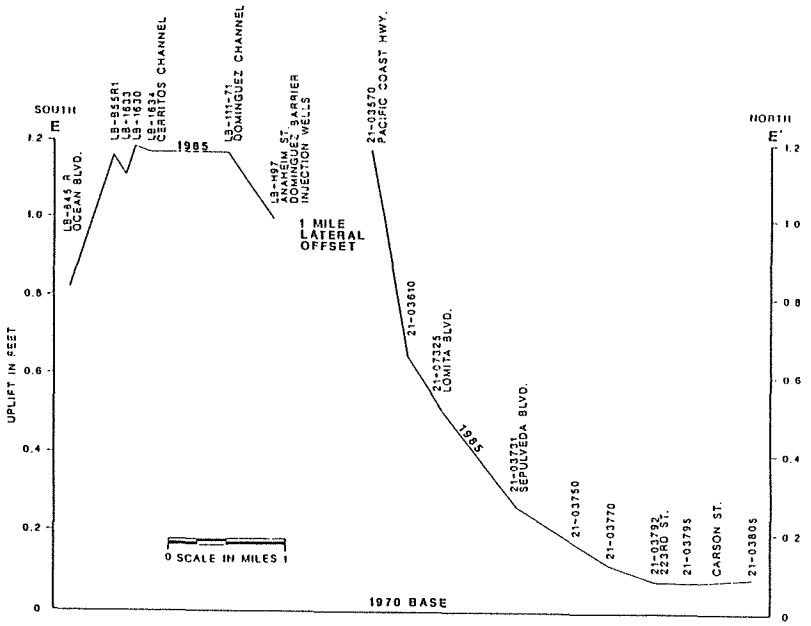

FIG. 4 Uplift profile E-E′ documenting changes in benchmark elevations.

measuring 0.5 feet at Lomita Blvd. and 0.1 feet at 223rd St. On the east side of the study area uplift values through 1975 decrease from about 0.10 feet on Alameda St. a half mile south of Sepulveda to about 0.3 feet at the intersection of Alameda St. and 223rd St. The most rapid uplift is recorded between 1975 and 1985 at Avalon Blvd. and PCH as shown by the elevation change of benchmark 21-03570 which averages 0.118 ft/hr. Available data show that the uplift rate decreases northward from this point. Uplift rates vary down to zero, as some benchmarks show little or no uplift. From limited data, uplift appears to decrease eastward.

Uplift in the Wilmington oil field has occurred over a longer period of time; in some cases over 25 years, since it was initiated in the early '60s. In general, benchmarks there have reversed directions three to five times, and the average uplift rate is lower than values along Avalon Blvd. High rates, in excess of 0.2 ft/yr occur over short time periods (Strehle, 1987). The amount of ground surface subsidence regained varies from approximately 3 percent near the center of the subsidence bowl up to 15 percent near the northwestern edge of the field. Some benchmarks (e.g. 21-03570 and 21-07450) in the western portion of the study area have risen by an amount exceeding half of their post-1953 subsidence loss.

Areal Distribution of Elevation Changes

Precise leveling data gathered from government agencies have been used to determine the total amount of subsidence and rebound in the vicinity of the study area. The regional distribution of subsidence rates from 1928 to 1975 is shown in Figure 5. Contoured values reflect subsidence rates calculated during the period in which each

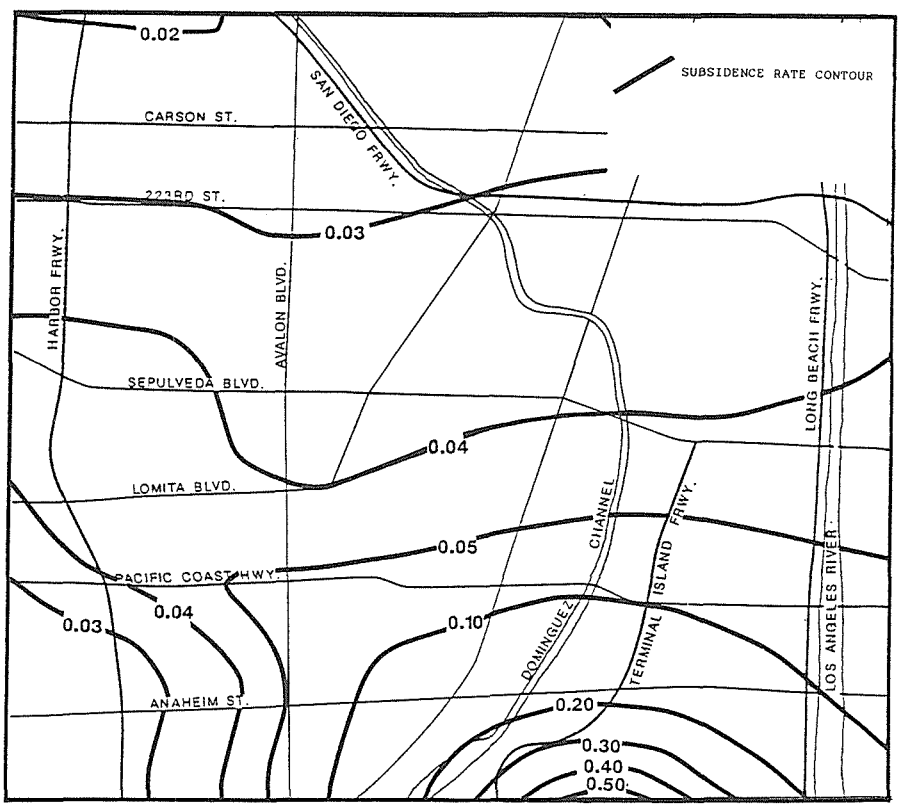

FIG. 5 Average annual rate of subsidence from 1928 to 1975.

benchmark was active. Benchmarks of less than ten-year duration were not used. Highest subsidence rates, up to 0.63 ft/yr, occur south of the study area in the Wilmington oil field. Subsidence rates within the study area range up to 0.04. Estimated total subsidence between 1933 and 1975 is shown in Figure 6. In general,

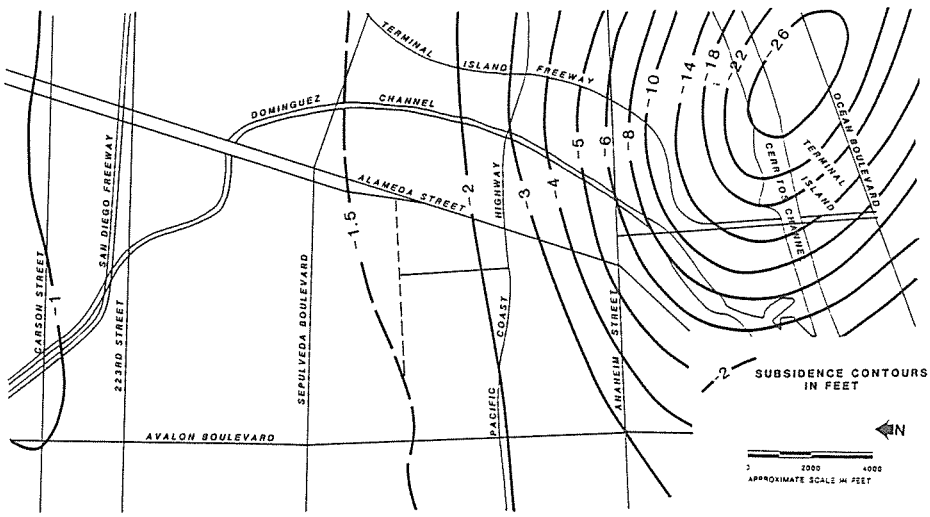

FIG. 6 Estimated total subsidence.

decreased from south to north away from the Wilmington oil field. Within the study area, values range from approximately 1.5 to 1.2 feet.

A total uplift map was not constructed due to the variable durations of the records of resurveyed benchmarks and the lack of post-1980 data in the eastern portion of the study area. However, distribution of uplift can be gleaned from profiles D-D′ and E-E′.

Timing of Elevation Changes

The study area had been subsiding since the earliest available records. Subsidence accelerated through the 1930s and 1940s. Subsidence continued west of the study area until the late 1960s, albeit at diminishing rates after 1945. These relationships are shown by benchmarks along Avalon Blvd. To the east along Alameda St., the ground surface stabilized between 1960 and 1970, with stabilization occurring earlier to the north. The ground surface began to rise as early as 1965 and entirely by 1970 along Alameda St. With the exception of a short term pulse, uplift did not begin along Avalon St. until about 1975. An east to west delay in the initiation of uplift identified in the Long Beach harbor area (Port of Long Beach, 1988) appears to extend across the study area. Within the study area, subsidence ceased and uplift began between 1965 (east) and 1975 (west).

Piezometric Surface Levels

Mendenhall (1905) shows groundwater levels at the study area in 1904 to have averaged about 18 feet above sea level. Water levels were somewhat lower along Dominguez Channel, and slightly above 20 feet farther west. The water levels in shallow wells within the study area had dropped to about 10 to 20 feet below sea level by 1929-1930. Although early maps did not differentiate between shallow and deep coastal plain aquifers, a deeper zone was also contoured with elevations ranging from 25 to 35 feet below sea level. Initiating in 1951, two sets of contour maps were prepared; however, the deep contour map did not contain data for the West Coast Basin. By 1951, shallow aquifer groundwater elevations had fallen to 30 to 40 feet below sea level. At this time, measurements in wells adjacent to the study area showed elevations of about 90 feet below sea level in deeper gravels corresponding to the Silverado aquifer.

In 1963, the LACFCD prepared separate maps for the deep (Silverado) and shallow (Gage) aquifers. Piezometric surface levels continued to fall in the Gage aquifer, reaching elevations of 35 to 45 feet below sea level in 1963 within the study area. Piezometer elevations remained over 80 feet below sea level in the Silverado aquifer at the time of this gauging. By 1970, levels in the Gage aquifer had fallen to 45 to 50 below sea level and ranged from 90 to over 95 feet below sea level in the Silverado aquifer.

The most recent shallow aquifer contour map constructed by the LACFCD corresponds to a 1977-78 gauging (Figure 7). On this map, a depression 60 feet below sea level is present south of Sepulveda Blvd. and west of Wilmington Ave. Levels in the Gage aquifer beneath the study area remained at about 45 to 50 feet below sea level. Deep aquifer contour maps constructed from 1986 data show that water levels in the Silverado aquifer had rebounded and are approximately 70 feet below sea level within the study area (Figure 8).

Prior to 1940, LACDPW water level measurements appear to support a general head decline in the Gage, Lynwood and Silverado aquifers. From the early '40s to the mid '50s, levels declined sharply in the principal aquifers. Rapid head loss diminished due to reduced pumping after 1955 (CDWR, 1987). The lowest levels occurred between the mid-50s and mid-70s within the study area. The time of minimum piezometric surface levels varies with the aquifer and the proximity of observation wells to pumping centers.

Maximum head loss and rise can be ascertained from water level data. Maximum head loss in the Gage aquifer appears to be between 60 and 80 feet and increasing to the southwest, considering an initial level about 20 feet above sea level. Piezometric surface decline between 1930 and 1970 was about 35 to 45 feet. Data for the Lynwood aquifer is spotty; a head loss of about 45 feet since 1934 has been estimated. Head loss in the Silverado aquifer was somewhat greater. Piezometric surface levels declined between 45 and 65 feet since 1947 alone. A previous head loss of 20 feet between 1934 and 1945 is suggested by sparse data.

Overall piezometric surface rise ranges between 20 and 30 feet in the Gage aquifer, and 25 to 30 feet in the Lynwood aquifer. Silverado water level rebound appears to increase from the east and west toward the study area with levels rising about 40 feet.

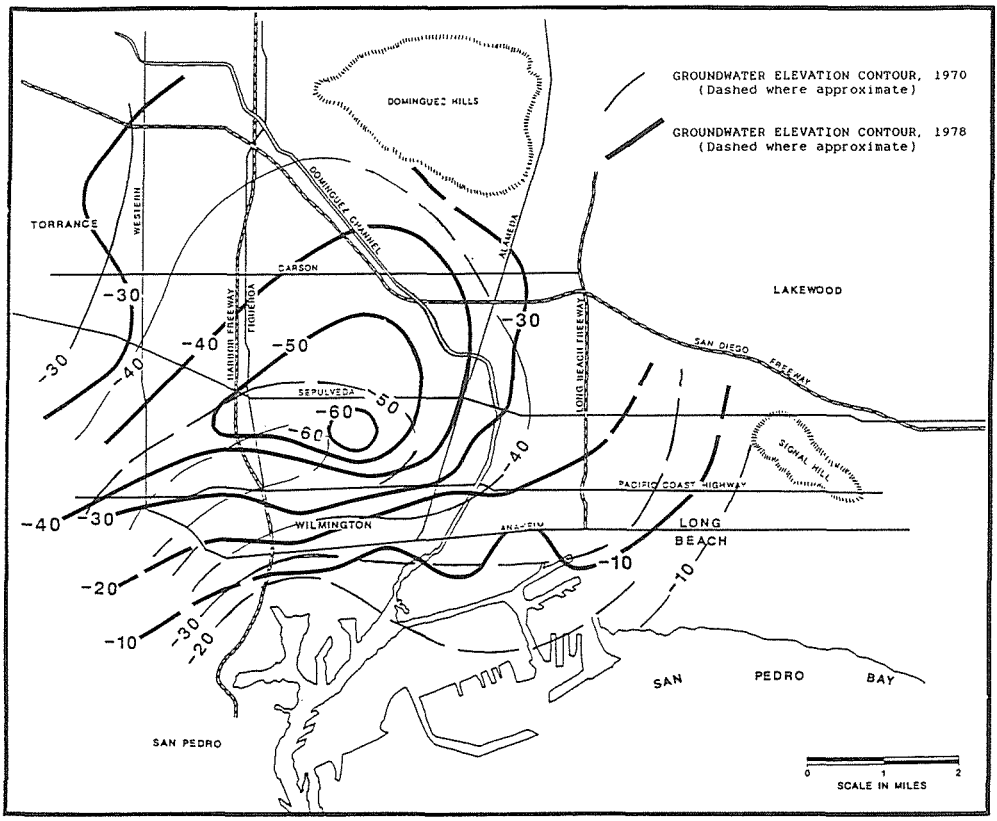

FIG. 7 Piezometric surface contour map for the Gage/Lynwood aquifer for 1970 and 1978.

DISCUSSION

Although most of the study area lies north of the Wilmington field production area, oil operations appear to have had some influence on surface elevations within the study area. Fluid production depletes reservoir pressure in oil-bearing zones. Where these zones continue past field boundaries, pressure reduction occurs, possibly resulting in consolidation and subsidence of the ground surface. The amount of subsidence depends in part on the stratigraphic continuity of these zones.

Numerical modeling of reservoir pressure reduction is beyond the scope of this report; however, the amount of subsidence can be quantified using the shape of an idealized subsidence curve extending out from the field. The postulated shape of the subsidence profile extending out from the subsidence bowl is hyperbolic. Kosloff & others (1980) show this curve to flatten and approach zero approximately 3.1 miles from the center of their modeled depression. This model predicts zero subsidence from the Wilmington oil field within the study area, except in the southeast portion. This zero subsidence arc crosses profile A-A' at Sepulveda Blvd.

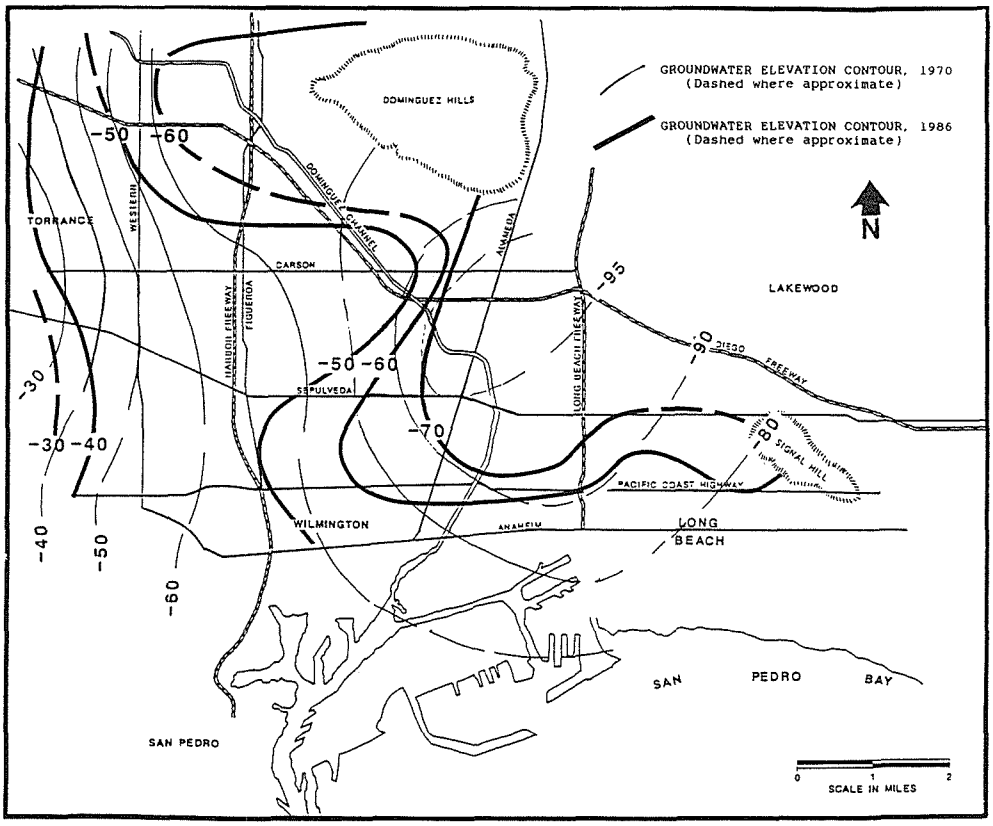

FIG. 8 Piezometric surface contour map for the Silverado aquifer for 1970 and 1986.

A qualitative approach suggests that the flat portions of the subsidence profiles A-A′ and B-B′ represent non-oil contributions. If production from the Dominguez and Signal Hill fields together contributes to subsidence in the study area, then total oil-related subsidence may exhibit a flat response on the central portion of N-S subsidence profiles. Therefore, oil field operations may still contribute to subsidence throughout the area. Regardless, published theoretical models and shapes of subsidence profiles suggest that other causes may be responsible for the majority of subsidence within the study area north of Sepulveda Blvd.

Water flood projects are apparently responsible for rebound over almost the entire area of the Wilmington oil field. Because uplift appears to be related to the previous subsidence event, it is considered to represent a rebound of the ground surface. Recent rebound falls off sharply to the north away from the Wilmington field as shown in profile E-E′, supporting oil zone repressuring as the cause.

In California alone, there are many examples of subsidence caused by head decline in aquifer-aquitard systems (Poland & Davis, 1969). Locally, almost a foot of differential elevation loss was induced by lowering water levels in the Gaspur aquifer 75 feet

during construction of the U.S. Naval Graving Dock No. 1 in Long Beach (Gilluly & Grant, 1949).

The study area is underlain by an interbedded aquifer-aquitard is documented by Zielbauer et al. (1962) and Testa, et al. (1989). Ratios of subsidence to head loss are higher in interbedded aquifer-aquitard systems than in aquifers alone. These ratios also increase with increasing amounts of dispersed clays and clay lenses within aquifers. Confined aquifers experience both elastic or reversible aquifer compression and inelastic compression or permanent compaction of interbedded clay layers and surrounding aquitards. Unconfined or groundwater table aquifers produced subsidence only where dewatered clays compact. Aquifer compression and consolidation of confining clay layers during aquitard drainage evidently occurred in response to lowered head in the Silverado aquifer, and also the Lynwood aquifer where separated from the Gage aquifer.

Subsidence mechanisms vary in the three principal aquifers. Consolidation of clays probably has occurred as a result of dewatering the upper portions of the Gage aquifer, including dewatering of the perched zone by oil recovery operations. A small amount of subsidence would be due to the regional lowering of water levels in the Gage aquifer. Compaction of clays and elastic aquifer compression has also occurred as a result of lowered head in the Silverado aquifer and confined portions of the Gage and Lynwood aquifers. These contributions from confined water-bearing zones are thought to represent the most important cause of subsidence within the study area.

With consideration of different subsidence mechanisms, and using examples presented by Poland & Davis (1969), a conservative estimate of the ratio of head loss to subsidence is 50:1 for the Silverado aquifer, and 100:1 for each of the Lynwood and Gage aquifers. Relating piezometric surface declines and head loss to subsidence ratios, overall subsidence due to groundwater withdrawal has been estimated for the period between 1930 and 1970. Calculated values range from 2.1 to 2.5 feet for southern portions of the study area, and from 2.2 to 2.3 feet for the northern portions. These calculated subsidence estimates exceed measured and extrapolated subsidence (Figure 6).

Indirect evidence supporting groundwater withdrawal as the cause of subsidence is evident on the subsidence profiles, where shapes are different than those anticipated if subsidence was due entirely to oil field operations. Profile shapes should be hyperbolic with subsidence decreasing northward if entirely controlled by Wilmington oil field fluid withdrawal. Profile A-A′ demonstrates about 0.1 feet of subsidence between the 1920-26 and 1931-32 leveling events prior to discovery of the Wilmington oil field. The subsidence curve on this profile appears to flatten at the one-foot subsidence value suggesting a total of at least a foot of subsidence unrelated to oil production. Profile B-B′ is essentially flat between 1933 and 1953; the northward decrease away from the Wilmington oil field is as expected if subsidence was controlled by oil field operations. In addition, there is an increase in subsidence north of Carson Street during the 1953 to 1964 period. Profile C-C′ shows a westward increasing subsidence wedge between 1970 and 1975. This is difficult to explain in the terms of Wilmington oil field operations. Finally, Profile D-D′ was constructed parallel to structural trends in the oil fields and therefore should show a reasonably flat

response. Instead, subsidence increases to the west into the area of greater head loss in shallow aquifers. Figure 9 demonstrates a positive correlation between benchmark elevations and water levels in the shallow and Silverado aquifers, respectively. In combination with estimations of subsidence due to piezometric surface decline, consumptive groundwater withdrawal appears to be the predominant cause of subsidence in the study area.

Surveying data suggest ground surface uplift in recent years. Existence of high uplift values outside of the Wilmington oil field suggests that causes other than oil field repressuring have helped cause rebound of the ground surface. Uplift is interpreted to represent rebound of the ground surface largely due to increased water levels. Elastic expansion of the Silverado aquifer due to increased head should theoretically match previous elastic compression. Unfortunately, the proportion of elastic to inelastic compaction in the Silverado aquifer is unknown. Pressures in the Gage and Lynwood aquifers have been enhanced by injection in conjunction with the Dominguez Gap Barrier Project. Some elastic expansion may occur, but the majority of the initial subsidence is thought to be attributable to inelastic consolidation of clays.

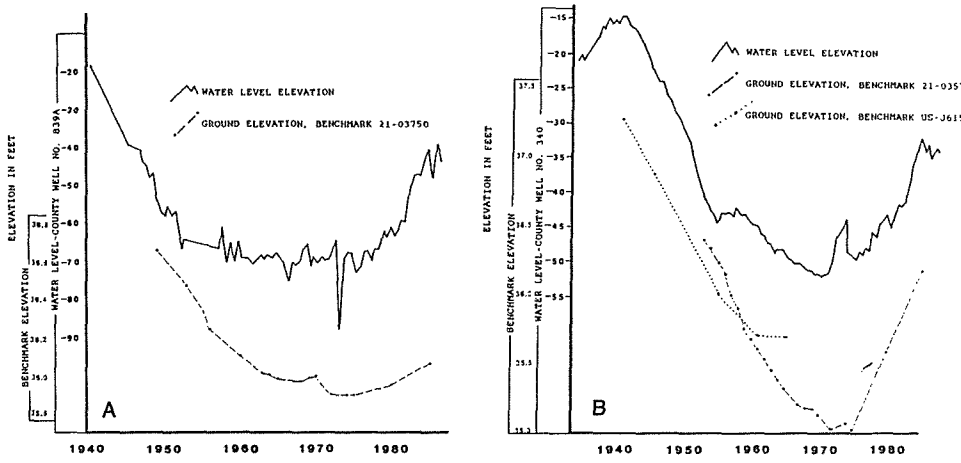

FIG. 9 Comparison of changes between shallow aquifer (a) and Silverado aquifer (b) water levels, and ground surface elevations.

Expected aquitard expansion or expansion of clays is only about one-tenth the value lost to compression (Freeze & Cherry, 1979). Because of the probably dominance of inelastic over elastic compression, it is anticipated that uplift should eventually amount to not much more than a tenth of the observed subsidence values. Measured values may exceed this fraction because ratios are based only on subsidence since 1930. Uplift to subsidence ratios are as expected in the northern portion of the study area. However, uplift proportions are greater than would have been expected as the result of only piezometric surface increase in the southern portion of the study area. It is possible that the close proximity of Dominguez Gap Barrier

Project injection wells contributes to high rebound values to the south, as head gain in the Gage and Lynwood aquifer significantly increases southward. In addition, uplift values fall off exponentially away from Dominguez Gap injection wells. Higher than expected elastic expansion of the Silverado aquifer as the piezometric surface has risen may also contribute to high uplift values.

Aquifer restoration related-activities probably have negligible effects on ground surface elevations due to the small amount of water level lowering. Net fluid recovered is relatively small and produced water is reinjected into the Gage aquifer. Overall, the effect of locally depressing the groundwater table by fluid recovery has been overshadowed by a regional rise in piezometric surface levels in the Gage aquifer. In contrast, usage of water from the Silverado aquifer may have a substantial effect on groundwater elevations.

Reduced pumpage has helped restore piezometric levels in the Silverado and appears to have helped cause rebound of the ground surface. A continued rise in water levels may extend the present phase of elevation gain. Substantial amounts of past subsidence was due to irreversible dewatering of clays. Therefore, future groundwater withdrawal from the Silverado should not cause significant amounts of subsidence unless water levels are depressed below the historically lowest level.

The influence of local tectonism has not yet been documented, but may account for appreciable local elevation change. Potential tectonic movements could change interpretation of causes of elevation changes, or could affect interpretation of absolute elevation changes if our assumed stable reference point, Tidal Benchmark-8, has moved.

Tectonism may contribute in part to local elevation changes. Regionally, the Los Angeles Basin is an actively subsiding alluvial basin and has undergone a period of accelerated subsidence from 4 to 1 million years ago before reaching its present high rate of 0.005 ft/yr near the center of the basin (Yeats, 1978). A lower rate of basinal subsidence, equal to 0.0013 ft/hr, has been assigned to the Long Beach area by Clarke (1987). Movements on local structures such as the Newport-Inglewood structural zone, or on presently unidentified structures could have a significant effect on ground surface levels. However, downward movement associated with the syncline lying between the Richfield and Cherry Hill faults would be anticipated. Geologically, vertical movements in the active Los Angeles Basin could be relatively rapid. Uplift rates of 0.05 ft/yr are not uncommon in parts of tectonically active areas such as Southern California. Rockwell & others (1988) have documented uplift rates as high as 0.66 ft/yr on the Ventura Avenue anticline. Tectonic uplift may help explain at least a portion of the recent rapid uplift within the study area.

Another important consideration is movement of the assumed stable reference point. Tidal Bmk-8 is located on an offshore extension of the upthrown Palos Verdes Peninsula fault block. Studies by Strehle & Clarke (1986), using Los Angeles County elevation data, indicated 0.03 and 0.04 ft/yr of relative movement along the Palos Verdes fault. Of this amount, Clarke (1987) assigns 0.005 ft/yr of tectonic movement across the fault. Uplift of Tidal Bmk-8 would result in measurement of more subsidence than has actually occurred. On the other hand, Tidal Bmk-8 is located

adjacent to documented subsiding areas in the Los Angeles and Long Beach harbor areas. Subsidence of Tidal Bmk-8 would infer less subsidence or exaggerated uplift to be measured.

CONCLUSIONS

The ground surface beneath the study area has subsided since the earliest resurveys, prior to 1940, until approximately 1970, about 1.2 to 1.5 feet. Recent rebound extending through 1985 has occurred and accounts for 0.1 to 0.5 feet of uplift. Wilmington oil field operations substantially affected ground surface elevations south of the study area, but apparently has had minimal effect beneath the study area.

Fluctuations in piezometric surface levels correlate positively with ground surface elevation changes. Lowering and raising of piezometric surface levels in the three principal aquifers accounts for the majority of elevation changes in the study area reflecting pumpage from the Silverado aquifer and injection into the upper Gage and Lynwood aquifers.

REFERENCES

Allen, D. R. (1974) Subsidence, rebound and surface strain associated with oil producing operations, Long Beach, California. Geol., Seismicity, and Environ. Impact. Assoc. of Eng. Geol. Spec. Publ., 101-111.

California Department of Water Resources (1961) Planned utilization of the groundwater basins of the Coastal Plain of Los Angeles County. Bull. 104, Appx. A, Groundwater Geology

Central and West Basin Water Replenishment District (1988) Annual Survey Report on Groundwater Replenishment. Prep. by Bookman-Edmonston Engineering, Inc., Glendale, California.

Clarke, D. P. (1987) The structure of the Wilmington Oil Field. In: Geological Field Guide to the Long Beach Area. D. Clarke and C. Henderson eds. The Pac. Sect. Am. Assoc. of Petr. Geol., Los Angeles, California, 43-55.

Freeze, R. A. & Cherry, J. A. (1979), Groundwater. Prentice-Hall, Inc., Inglewood Cliffs, N.J.

Gilluly, J. & Grant, U. S. (1949) Subsidence in the Long Beach Area, California. Geol. Soc. of Am. Bull. 601, 461-530.

Holzer, T. L. (1984) Ground failure induced by groundwater withdrawal from unconsolidated sediment. In: Reviews in Engineering Geology VI Man-Induced Land Subsidence. T. L. Holzer ed. Geol. Soc. of Am., Boulder, Colorado, 67-105.

Kosloff D., Scott, R. F. & Scranton, J. (1980) Finite element simulation of Wilmington Oil Field subsidence I. linear modeling. Tectonophysics, 65, 339-368.

Mendenhall, W. C. (1905) Development of underground waters in the Western Coastal Plain Region of Southern California. U.S.G.S. Water Supply Paper 139.

Poland, J. F. & Davis, G. H. (1969) Land subsidence due to withdrawal of fluids. In: Reviews in Eng. Geol. II, Geol. Soc. of Am. Spec. Publ. 187-270.

Poland, J. F., Piper, A. M., & others, (1956) Groundwater geology of the coastal zone Long Beach-Santa Ana area, California. U.S.G.S. Water Supply Paper 1109.

Rockwell, T. K., Keller, E. A. & Dembroff, G. R. (1988) Quaternary rate of folding of the Ventura Avenue Anticline, Western Transverse Ranges, Southern California. Geol. Society of America Bulletin, 100 (6), 850-858.

Strehle, R. W. & Clarke, D. P. (1986) Study of non-oil field induced elevation changes in the Long Beach area. Unpublished report.

Strehle, R. W. (1987) Subsidence in Long Beach. In: Geologic Field Guide to the Long Beach Area. D. Clarke and C. Henderson eds. The Pac. Sect. Am. Assoc. of Petr. Geol., Los Angeles, California, 69-79.

Strehle, R. W. (1989) Subsidence hazards - a history. S. M. Testa, ed. Am. Assoc. of Petr. Geol. Symp., May 1989, 107-116.

Testa, S. M. (1989) Regional hydrogeologic setting and its role in developing aquifer remediation strategies. Geol. Soc. of Am. Abs. 21 (7).

Testa, S. M., Baker, D. & Avery P. (1989) Field studies on occurrence, recoverability, and mitigation strategy for free phase liquid hydrocarbon. S. M. Testa, ed. Am. Assoc. of Petr. Geol. Symp., May 1989, 57-81.

Testa, S. M. & Winegardner, D. (1990) Restoration of petroleum-contaminated aquifers. Lewis Publ., Chelsea, Michigan.

Yeats, R. S. (1978) Neogene acceleration of subsidence rates in Southern California. Geology, 6, 456-460.

Yerkes, R. F., McCulloh, T. H., Schoelhamer, J. E. & Vedder, J. G. (1965) Geology of the Los Angeles Basin, California - an introduction. U.S.G.S. Prof. Paper 420-A.

Zielbauer, E. J., Kues, H. A., Burnham, W. L. & Keene, A. G. (1962) Dominguez Gap Barrier Project, Geologic Investigation. Los Angeles County Flood Control Dist.

Land Subsidence (Proceedings of the Fourth International Symposium on Land Subsidence, May 1991). IAHS Publ. no. 200, 1991.

Grouting in Deep Flooded Mines

WILLIAM C. MORRISON
United States Department of Interior
Office of Surface Mining,
Eastern Service Center,
Pittsburgh, Pennsylvania, USA 15122

ABSTRACT A methodology developed to place a cement based grout in the Mary Lee coalbed in Graysville, Alabama. The coal seam is situate in excess of 700 feet below the ground surface. Several difficulties to be overcome were the disintegration of the grout mix from downhole flow of water and the separation of grout ingredients in long overland and downhole delivery systems.

BACKGROUND

In January, 1980, a subsidence event that affected approximately 14 homes, a shopping center, and a service station was reported in the City of Graysville, Alabama. In March, 1980, the Alabama Department of Industrial Relations reported the severity of the event to the Office of Surface Mining field office in Knoxville, Tennessee.

The area involved lies adjacent to U.S. Highway 78 in the city of Graysville, Jefferson County, Alabama and is located 8 miles north-west of Birmingham. It is located on the U.S. Geological Survey 7.5 minute Adamsville Quadrangle (Fig. 1). Beneath the affected subsidence area, there are two abandoned coal mines. The Bessie Mine is in the Pratt coalbed approximately 180 feet below the surface. The Flat Top Mine is in the Mary Lee coalbed, approximately 540 feet below the Pratt coalbed, or 720 feet below the surface.

The Office of Surface Mining (OSM) was requested to investigate the severity and extent of this event. OSM was also requested to make appropriate recommendations for mine subsidence stabilization.

In July, 1980, personnel from the OSM conducted an in depth investigation of the site and concluded that the affected area was larger than originally reported. The revised area embraced a total of 42 homes, two shopping centers, two service stations, and two churches (Morrison, et al, 1987).

EXPLORATORY DRILLING PROGRAM - Phase 1

The OSM team evaluated the need for mine stabilization in the project area and the various methods that could be employed. To make this evaluation, the condition of the mine in the project area had to be determined. Aside from the drilling conducted in 1981 around the strip shopping center, there was no information available concerning conditions at mine level. OSM initiated an exploratory drilling program to obtain the additional required information.

The exploratory drilling program consisted of drilling six borings (ATB-3, 4, 5, 6, 8 and 9) at the locations shown on Fig. 2. Staff engineers located the exploratory holes on the mine and topographic maps. They were located to provide information concerning the openness of the mine voids and the height of the coal pillars.

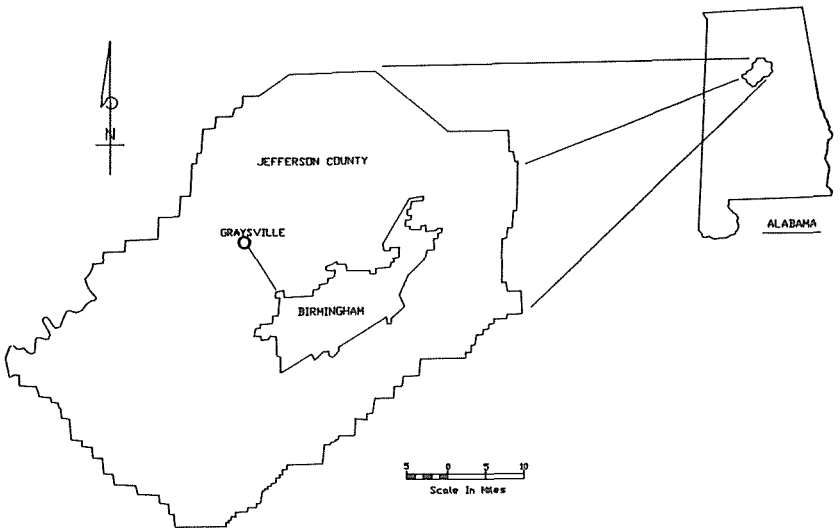

FIG. 1 Location map.

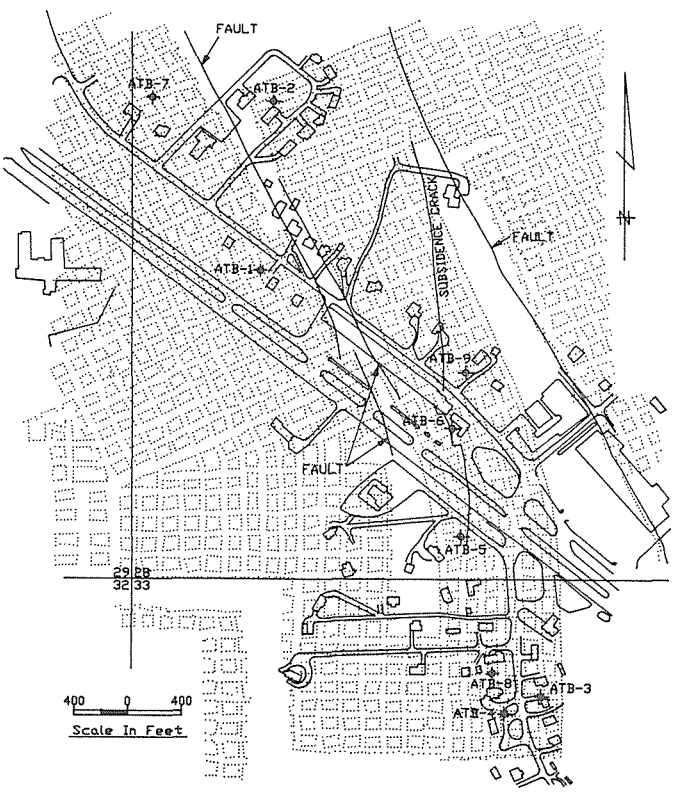

FIG. 2 Location plan: test core holes for 1983 grouting project.

ANALYSIS OF DATA

The OSM team analyzed the data from the coring to determine the condition of the mine and the amount of subsidence, if any, that occurred. The void height and amount of infilled material were compared to the coal sections and mine heights given on the mine maps. This comparison showed that between 2 and 6 feet of reduction in mine height had occurred and there was roof fall material in the remaining void. Water level readings taken in the boreholes show that the mine was flooded and the phreatic surface in the mine is 70 to 80 feet above the mine roof.

CONCLUSIONS FROM INTERIM TEST CORING

It was apparent from the data collected that the mine in the Mary Lee coalbed was subsiding. The surface expression, as reflected in the damage to structures, indicated that not all the subsidence had migrated to the surface. The only exception to this was in the strip shopping center area. Also, the potential for more collapse at the mine level existed as open voids up to 5 feet in height were recorded. The presence of loose unconsolidated roof fall material in the mine made the building of point support columns difficult.

STABILIZATION METHOD AT MINE LEVEL

Effective stabilization of the project area required that future subsidence at the mine level be prevented from migrating to the ground surface. Subsidence that had already migrated up into the rock overburden, but had not yet expressed itself as surface movement must be kept from doing so.

OSM engineers believed that a stable mine could be obtained if saturation grouting could produce large zones or areas of support, similar to the unmined panel pillars. They also believed that no structure in the project area should be more than 150 horizontal feet from support at the mine level. Also, the support at the mine level should extend laterally so that the assumed 15° angle of draw is taken into consideration. The material injected into the mine should be designed to permeate the roof fall material and travel a substantial distance from the hole (150 +/- feet) prior to setting up. The flow of down hole water had to be contained to prevent washing of the material. Engineers decided to place water stops at the project perimeter to reduce the flow of water at the mine level through the project area. The conceptual stabilization program at mine level is shown as it was envisioned on Fig. 3.

STABILIZATION OF OVERBURDEN

The stabilization of the top 350 feet of overburden to prevent latent movement from expressing itself at the surface required pressure grouting. The presence of unmined zones at the mine level results in high shear stress levels at the base of the Pratt coalbed and for a distance of 150 feet below this coal. It is possible to eliminate latent movement by strengthening this zone (Craft, et al, 1987). Also, the overburden above the Pratt coalbed can be strengthened in the same manner. It was therefore important on this site to grout the upper 350 feet of overburden. The presence of open vertical fractures in this section, as recorded from the core drilling, reduced the ability of the rock mass to resist movement.

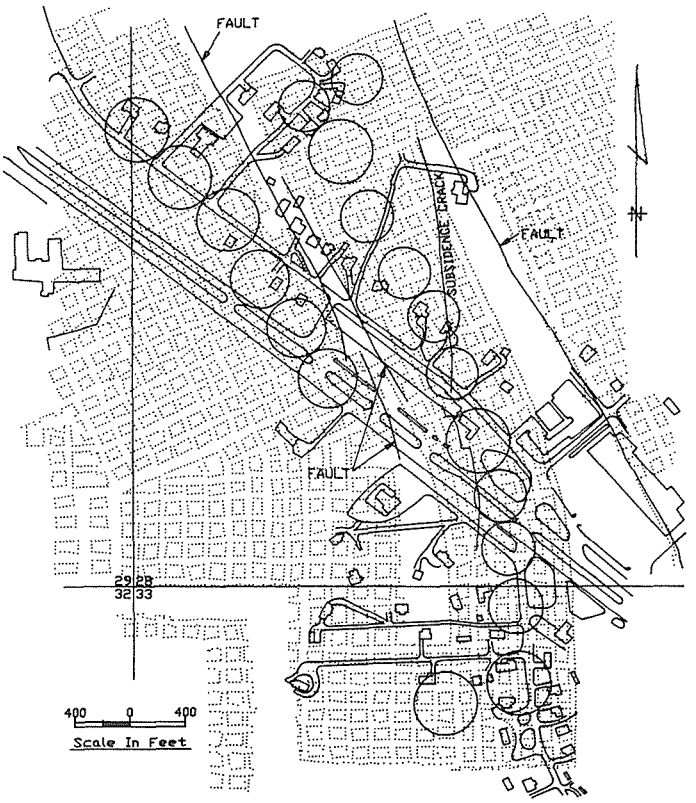

FIG. 3 Conceptual stabilization program, 1983 project.

DRILLING AND GROUTING-PHASE II

In August 1983, OSM sent out specifications for bidding on a drilling and grouting program in the Graysville Area. Since there were specific requirements to be met in the preparation of the bids, there was a limited time frame for bid preparation.

The contractor had to design a rapid set grout for water containment barriers. The grout had to attain an initial set in thirty (30) minutes with a compressive strength of 1000 psi in twenty-four (24) hours. The specifications also defined the compressive strength for the saturation grout to be used in the mine as pillar and overburden support. This grout had to attain a compressive strength of 1500 psi in twenty-eight (28) days.

The contractor started drilling operations in December 1983. The first set of holes drilled were the water barrier holes in the south end of the project area. The engineers selected these holes to be drilled first because of the dip in the mine. The contractor drilled fourteen (14) holes for water barriers in the Mary Lee coalbed. Seven (7) holes were drilled in the south end of the project and seven (7) in the north end of the project (Fig. 4 and Table 1)

The rapid-set grout for the containment barriers was composed of cement, sand, lime kiln dust and calcium chloride. The proportions of the various ingredients were:

Cement	769 pounds
Sand	576 pounds
Lime Kiln Dust	618 pounds
Calcium Chloride Flake	16 pounds
Water	427 pounds

This mix worked very well in all holes except S-10 which took a total of 2662 tons of grout. The contractor was directed to increase the amount of calcium chloride to further accelerate the set time.

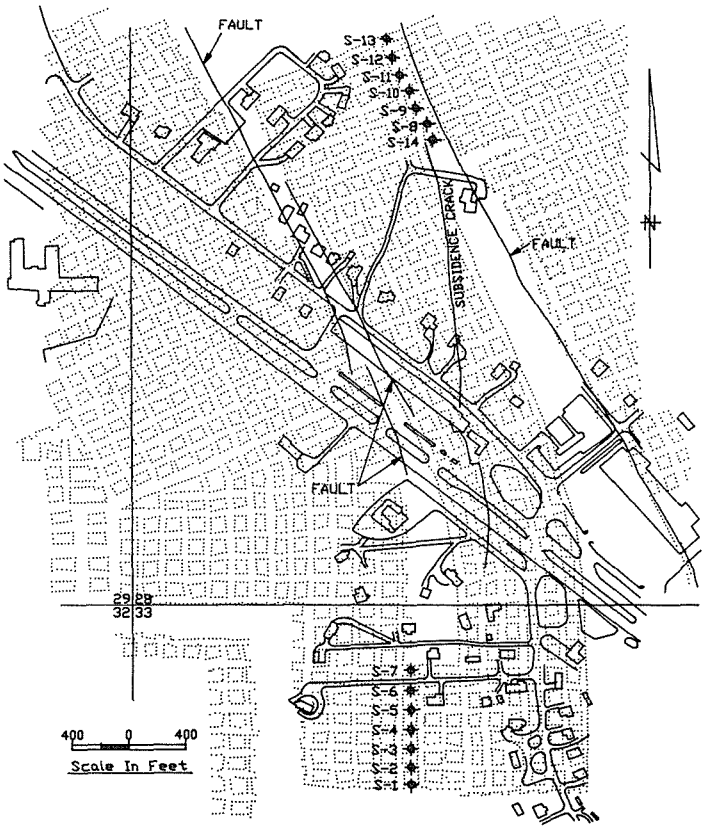

FIG. 4 Water barrier grout holes.

TABLE 1 Water barrier grout holes and grout quantities.

Hole No.	Depth Ft.	Void Ft.	Grout Tons	Hole No.	Depth Ft.	Void Ft.	Grout Tons	Hole No.	Depth Ft.	Void Ft.	Grout Tons
S1	699	4	132	S6	700	9	242	S11	762	B*	77
S2	699	5	286	S7	705	2	77	S12	663	2.5	588
S3	695	8	484	S8	706	B*	264	S13	655	2	44
S4	689	8	66	S9	684	B*	1221	S14	700	B*	121
S5	687	9	1067	S10	682	B*	2662				

B* = Broken zone, no recorded open void

These water barrier plugs controlled water flow in the mine to permit the saturation grouting. By creating a quiescent pool in the mine, or reducing the water flow, the grout would stay in place. Also, the grout would not separate as it had in previous efforts.

In February 1984, the contractor started drilling the saturation grout holes. Drilling started at the north end of the project area and proceeded in a south-easterly direction toward the intersection of Route 78 and Main Street. Originally, sixteen (16) holes were to be drilled for saturation grouting. (See Fig. 5).

The original saturation grout was composed of cement, flyash, sand and water. The grout mix was composed of:

Cement	257 pounds
Fly Ash	184 pounds
Sand	1559 pounds
Water	43 gallons

The grout was pumped about 300 feet overland then 700 feet down into the mine. While testing the grout mix by pumping it through the delivery system, it was determined that the sand in the grout was separating and settling to the bottom of the horizontal grout line. This settlement caused a bridging or clogging of the grout line. The contractor, in consultation with the engineer altered the mix to the following:

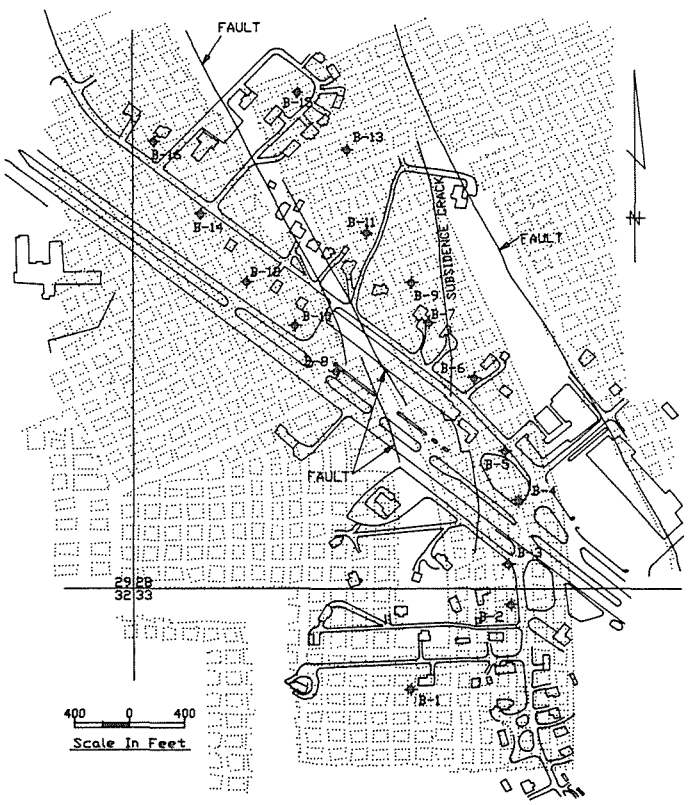

FIG. 5 Control saturation grout holes.

Cement	300 pounds
Fly Ash	200 pounds
Sand	1500 pounds
Bentonite	6 pounds
Water	54.7 gallons
Water reducing agent	75 ounces

This produced a cohesive, pumpable grout mix that would not separate as it was being pumped through the system and into the mine. The contractor grouted the original design holes, B-1 through B-16, with the modified grout mix (Fig. 5 and Table 2)..

TABLE 2 Saturation grout holes.

Hole No.	Depth Ft.	Void Ft.	Grout Cu.Yds.	Hole No.	Depth Ft.	Void Ft.	Grout Cu.Yds.	Hole No.	Depth Ft.	Void Ft.	Grout Cu.Yds.
B 1	703	7	1160	B 6	711	B*	372	B11	711	B*	734
B 2	705	B*	1411	B 7	728	3	797	B12	689	3	473
B 3	700	2	51	B 8	694	3	19	B13	710	B*	20
B 4	700	B*	7	B 9	722	6	718	B14	689	5	1011
B 5	703	4	456	B10	695	3	385	B15	722	4	4968
								B16	689	2	509

B*= Broken Zone, no recorded open void

When the initial sixteen saturation grout holes had been grouted to refusal, the contractor then grouted the test holes drilled in 1983 (Table 3 and Fig.2).

OSM analyzed the amount of grout placed into the mine in the original sixteen holes. By doing a plot on a project map, it was determined there were areas that received very little if any additional support in the mine due to very small grout takes. Therefore, to provide the desired results, additional holes were required. The engineers located six additional holes to intercept the areas that needed more grout (Table 4 and Fig. 6).

While the contractor drilled and pumped grout into the mine through the six "AB" holes, another crew drilled the pressure grout holes. These holes were 350 feet deep, or approximately 150 feet below the Bessie Mine in the Pratt coalbed. A total of 124 holes were drilled for this purpose.

There was always the possibility of drilling into, or through a mine void in the Bessie Mine (Pratt coalbed). This possibility was in the area north of Main

TABLE 3 Exploratory holes, 1983.

Hole No.	Depth Ft.	Void Ft.	Grout Cu.Yds.	Hole No.	Depth Ft.	Void Ft.	Grout Cu.Yds.
ATB 1	689	2	972	ATB 6	700	1	85
ATB 2	722	-0-	D.P.	ATB 7	680	-0-	D.P.
ATB 3	709	5	1040	ATB 8	716	B*	745
ATB 4	715	B*	19	ATB 9	714	B*	7
ATB 5	721	5	25				

D.P.= Drilled into Pillar
B*= Broken Zone, no recorded open void

TABLE 4 Additional grout holes, 1984.

Hole No.	Depth Ft.	Void Ft.	Grout Cu.Yds.	Hole No.	Depth Ft.	Void Ft.	Grout Cu.Yds.
AB 17	689	2	653	AB 20	714	6	1779
AB 18	710	2	1037	AB 21	700	2	720
AB 19	728	B*	22	AB 22	703	7	2070
AB 19A	728	7	6247				

B*= Broken Zone, no recorded open void

Street and at the extreme eastern end of the project site. To overcome this eventuality, grouted gravel columns were planned where the drill hole penetrated mine voids. The drilling was advanced through this column to the lower bed, the Mary Lee. This concept is more fully described in "Recent Developments In Grouting For Deep Mines" (Ackenheil and Dougherty, 1970).

As the drill hole advanced, the return drilling fluid was closely monitored as it carried the drill cuttings to the surface. When, and if, the drill broke through the mine roof in the Pratt coalbed, the hole was then advanced into rock in the mine floor. The hole was then reamed and cased through the overburden with 10-inch I.D. pipe and a 2-inch I.D. steel slurry grout injection pipe was installed into the hole into the floor of the mine. Gravel up to 3/4 inch in size

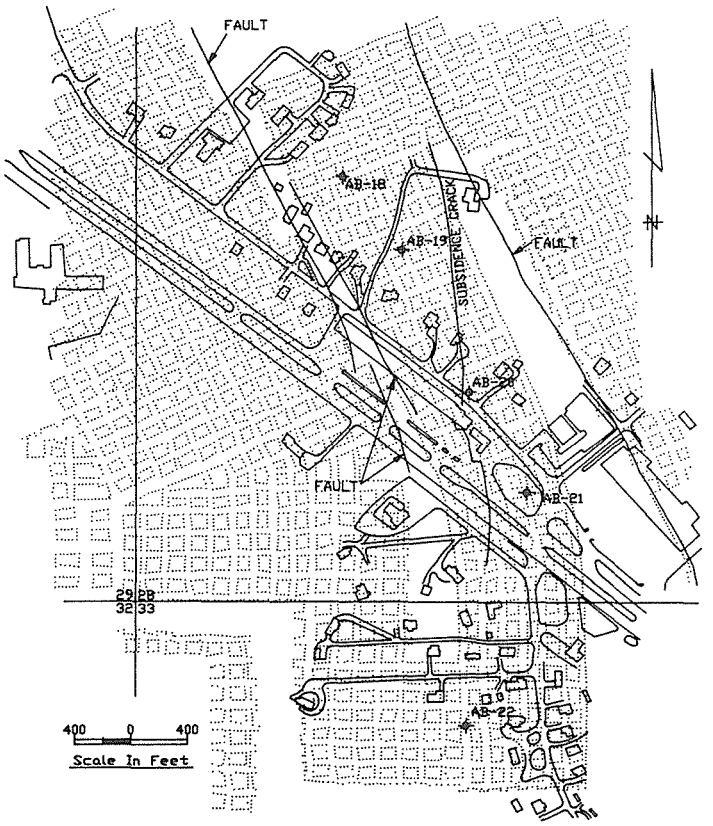

FIG. 6 Additional controlled saturation grout holes.

was then loaded down the hole around the injection pipe. The amount of gravel per hole was based on a chart that was developed in the Ackenheil-Dougherty paper defining volume of gravel versus void height (See Figure 7). With the gravel in place, grout slurry was pumped through the injection pipe into the gravel. The slurry was composed of one (1) part cement, four (4) parts flyash and four (4) parts water. The slurried gravel column was then allowed to set for a period of forty-eight (48) hours, then redrilled with the original size bit to completion at the 350 feet depth.

After the hole was drilled to the required depth, the grout slurry was pressure injected into the overburden. A balloon packer was set at a depth of two-hundred-twenty-five (225) feet, or into the first competent rock below the Pratt coalbed. Pressure was applied to the grout in the amount of one (1) psi for every vertical foot of overburden thickness including the gravity head of the slurry. This overburden thickness was measured between the Pratt coalbed and the ground surface. After the initial grout had set, the contractor retrieved the grout injection system to an elevation approximately twenty-five (25) feet above the Pratt coalbed to allow this section to be gravity grouted. This grout set for a minimum of sixteen (16) hours. The contractor then grouted the remainder of the hole by gravity in one (1) lift to the top of rock below the soil line.

During the pressure grouting, the contractor drilled five (5) holes for testing purposes. The holes were drilled and cored in two stages. The contractor first drilled the hole to within 10 to 15 feet of the roof of the mine in the Mary Lee coalbed with the pneumatic hammer. He retrieved the drill, cased the hole with NQ coring casing, then advanced the hole using a NQ wire-line core drill into the bottom rock of the mine. OSM sent the retrieved core to a laboratory for compressive strength tests and petrographic analyses.

Table 5 compares the break strengths of the grout before the grout was injected into the mine with the grout cores taken from the mine.

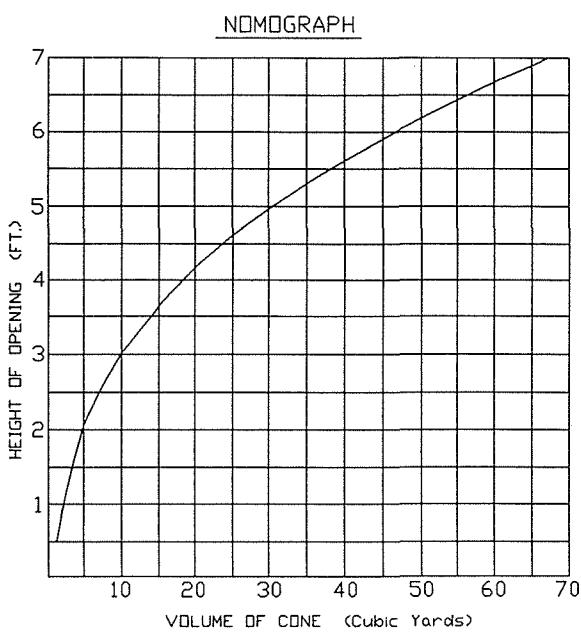

FIG. 7 Volume of gravel as function of void height (after Ackenheil and Dougherty, 1970).

TABLE 5 Compressive break strengths of grout.

HOLE NO.	GROUT ON SURFACE	GROUT FROM CORE SAMPLE	HOLE NO.	GROUT ON SURFACE	GROUT FROM CORE SAMPLE
B 3	1055 psi	3963 psi	B 5	1699 psi	1705 psi
B 14	457 psi	1760 psi	B 15	3752 psi	4785 psi
B 10	2433 psi	5022 psi			

TABLE 6 Comparison of grout mixes by petrographic analysis.

HOLE NO.		MIXER PROPORTION	LABORATORY PROPORTION
S 3	Cement	25.00%	50.00%
	Sand	75.00%	48.70
	Muscovite		1.30%
B 14	Cement	12.80%	43.20%
	Fly Ash	9.20%	9.0 %
	Sand	77.90%	47.70%
	Muscovite		0.10%
B 10	Cement	12.85%	54.30%
	Fly Ash	9.20%	14.80%
	Sand	77.95%	30.80%
	Muscovite		0.10
B 5	Cement	15.00%	51.80%
	Fly ash	10.00%	9.00%
	Sand	75.00%	38.70%
	Muscovite		0.50%
B 15	Cement	15.00%	60.30%
	Fly Ash	10.00%	12.70%
	Sand	75.00%	26.20%
	Muscovite		0.80%

Table 6 compares the composition of the grout mixes: first as they were prepared in the mixer for injection into the mine and second, the same mixes after they were retrieved from the mine as core samples.

The major conclusion determined from Table 5 is that the grout had a better chance to harden and set in a very controlled condition in the mine. This table, along with Table 6 show there was a definite reconstitution of the grout mix. This was accomplished during the pumping operation. Even with the bentonite and super-plastizer added, some of the larger sand grains separated from the grout mix.

From the beginning of this project through the pump testing on the ground, there was a need for a bonding agent such as bentonite to assure a cohesive grout mix. Without a bonding agent a grout pumped such a distance overland and to such a depth to a mine will separate. In effect, the larger grains of sand would not stay in suspension in the grout mix. According to the laboratory tests, specifically the petrographic analysis, a decided redistribution of grout mix constit-

uents occurred. With this redistribution of ingredients, the grout strengthened and densified to become a much higher compressive strength grout.

REFERENCES

Ackenheil,A.C., Dougherty, M.T. (1970) Recent Developments in Grouting in Deep Mines, Jour. of Soil Mech. and Foundations, A.S.C.E.

Craft, J.L., Crandall, T.M. (1987) Mine Configuration And Its Relationship To Surface Subsidence, OSMRE File Report, Eastern Field Operations, Pittsburgh, PA, 22 pps., Presented at the 1987 Annual Meeting, Association of Engineering Geologists.

Morrison, W.C., Elder, C.H., Craft, J.L. (1987) Subsidence Abatement Project Report, Graysville, Jefferson County, Alabama; OSMRE File Report, Eastern Field Operations, Pittsburgh, PA.

Land Subsidence (Proceedings of the Fourth International Symposium on Land Subsidence, May 1991). IAHS Publ. no. 200, 1991.

Land Subsidence Due to Thermal Water Withdrawal: The Case of Abano Terme, Northern Italy

G. BRIGHENTI
Mining Science Institute, University of Bologna, Viale Risorgimento,2 - Bologna, Italy

ABSTRACT The major geological features of Euganean thermal basin are recalled. It is then noted that excessive withdrawal of thermal waters, especially concentrated at Abano Terme, has caused serious lowering of the piezometric levels (2.5 m/years were measured during the period 1970-1973).
The intervention performed by the unitary Management imposed by Italian Government, led to the stabilization of these levels starting from 1975-1976. However, subsidence still takes place, with soil lowering of up to 2 cm/year in 1989 even if the phenomenon is following a decreasing trend.
Due to subsidence, the walls of various buildings show significant inclinations; studies performed, however, have shown that this does not create any danger for the stability of the buildings.

INTRODUCTION

Abano Terme is the main center of the Euganean thermal basin, which also includes Montegrotto and Battaglia (see fig. 1).

The thermal waters of Euganean basin, one of the largest thermal basin in Italy, have been known and studied since many centuries (see Piccoli et al., 1976) and are used for water and mud bath treatments.

These warm waters, which can reach over 86° C, circulate deeply in fractured carbonate rocks and originate from precipitations occurring at levels superior to 1500 m above sea-level. After a trip of 70-80 Km, during which depths of 2000-3000 m are reached, waters are mineralized and heated according to the local geothermal gradient. The waters, after an underground transit time estimated to be around 25-30 years, climb rapidly to the plains lying East to the Euganean Hills along fractures or faults, maintaining high salinity and high temperatures on the surface.

The main aquifer is formed by red scaglia-Jurassic limestone complex, whereas the other aquifers, which are localized in the alluvial Quaternary sequence, are formed by sands with interbedded

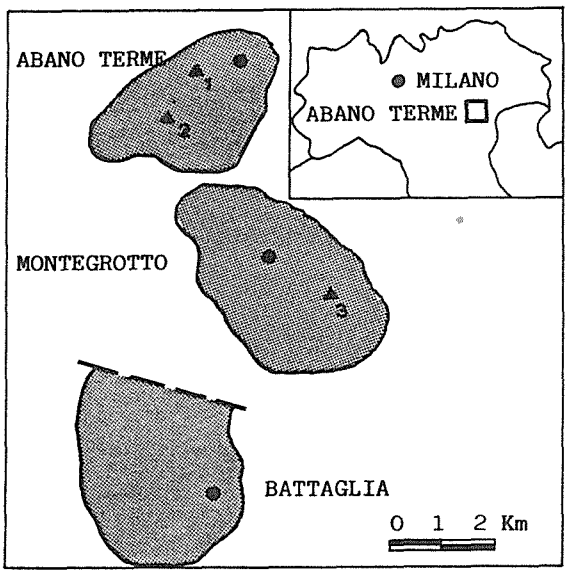

FIG. 1 Euganean thermal basin: water production areas of Abano Terme, Montegrotto and Battaglia.

layers of clays and silts . In this sequence the deep waters mix with the surface waters, thus reaching minor salinities and temperatures.

Till the end of the last century, the waters used for thermal baths in Abano originated from springs or lakes. Later they were produced by wells draining the Quaternary aquifers, still later sand production problems, along with formation of sinkholes, led to deepening the wells in order to produce directly from the fractured rock (Dainese, 1988).

In the Sixties, production surpassed 500 l/s and caused a progressive piezometric level lowering. The Italian Department of Industry, in order to protect the basin, decided to impose a united management of the local geothermal resources and in 1966 created the "Gestione Unica di Abano Terme e Teolo" (hereafter denominated with the abbreviation GU). However, due to local political reasons, the authority of the GU was limited only to the territory of Abano and Teolo.

The GU, in order to achieve a rational use of the thermal waters, proceeded both to measure the piezometric levels over the entire territory of its jurisdiction, and to evaluate the total production of hot waters. From the measurements taken, it was noted that the well SOJ 6 (indicated with the letter A in fig. 1) could be considered representative of the relative variations in piezometric levels in the entire Abano area and, beginning in the early 1970's, the GU proceeded with systematic measurements of the levels in this well. In this way a progressive lowering of the mean annual level, of approximately

2.5 m/years, was detected. To evaluate the effect of reduced production, in the winter of 1977-1978 the GU drastically reduced the withdrawal of water for over two months: the result was a rapid increase of the level, by over 15 m (Schiesaro, 1982 and 1985).

Given this result, it was decided to permanently reduce winter withdrawals which, since thermal activity is reduced during this period, were mostly used to heat the hotels. In 1977, the Venetia Region also imposed the installation of flow meters on all wells in production, thus allowing an exact evaluation of hot water withdrawal. A close look at figs. 2 and 3, showing, respectively, the withdrawal of thermal waters in Abano Terme and the average monthly levels in the SOJ 6 well, during the period 1977-1989, reveals that during this

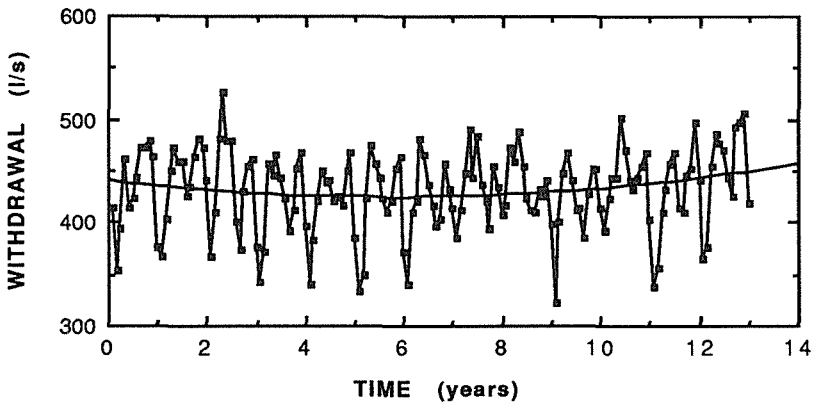

FIG. 2 Withdrawal of thermal water in Abano Terme from 1977 to 1989.

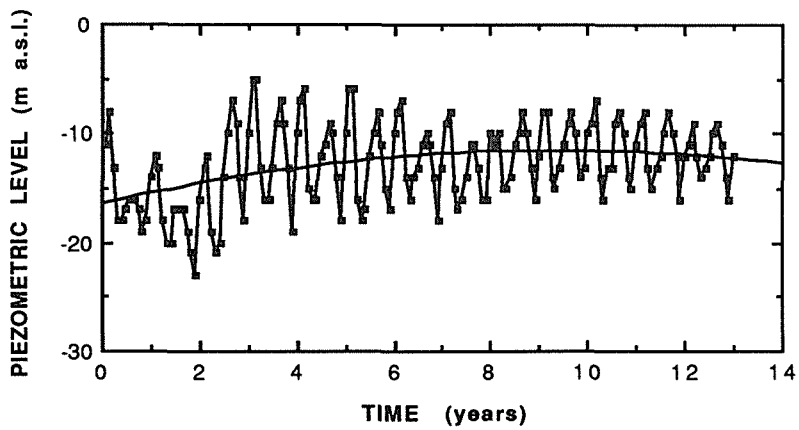

FIG. 3 Piezometric levels in Soj 6 Well from 1977 to 1989.

period production and average annual piezometric level were stabilized. An examination of these figures, however, also shows that the system is extremely sensitive, and that even slight increases in production cause significant reductions in the levels.

In the meantime, observations of the inclinations and lesions of some buildings and damage to some sewage systems induced local Authorities to feel that, as a consequence of the withdrawal of thermal waters, the soil has been lowered, with maximum estimated values of over one meter. It was thus decided to take periodic precision levellings in the area of GU jurisdiction and in the near Montegrotto area (during the period 1983-1989 five high precision levelings were taken) and to entrust the Mining Science Institute of the University of Bologna to study the phenomenon with particular regard to the possible correlation between land subsidence and decline of the water level in wells, and also to verify the effect of subsidence on the differential settlements and on the structural damages of the buildings. A preliminary examination was also requested concerning the reinjection of waste water into the subsoil (Brighenti et al., 1990).

CAUSES OF LAND SUBSIDENCE

The Euganean basin is formed by Quaternary alluvial deposits (mainly fine and very compressible sediments), accumulated on a pratically non-compressible pre-Quaternary substratum formed by the following formations (from the most recent to the more ancient):

(a) limestone-marly-tufaceous formation from the Middle-upper Eocene;
(b) limestone and marly limestone formations from the Upper Cretaceous (scaglia rossa);
(c) layered and compact limestone from the Lower Cretaceous (biancone).

The subsurface stratigraphy has been explored on the basis of a geophysical investigation (see Piccoli et al., 1976) and the examination of the stratigraphic columns obtained from several hundreds of hot water wells. These investigations have made it possible to identify - though with some discrepancies between the results of the geophysics and the stratigraphies - the depth of the pre-Quaternary substratum (see the cross sections shown in fig. 4). On the contrary, it was not possible to identify the lithotypes present in the Quaternary due the imprecisions of the stratigraphic columns. This fact thus made it impossible to characterize the alluviums from a geotechnical point of view, and, particularly, to differentiate the compressibilities of the different strata.

The historical piezometric data are also incomplete; however, the comparison of the mean water levels detected in 1986 (Dainese, 1986) and the subsidence rate between 1985 and 1987 shows a clear

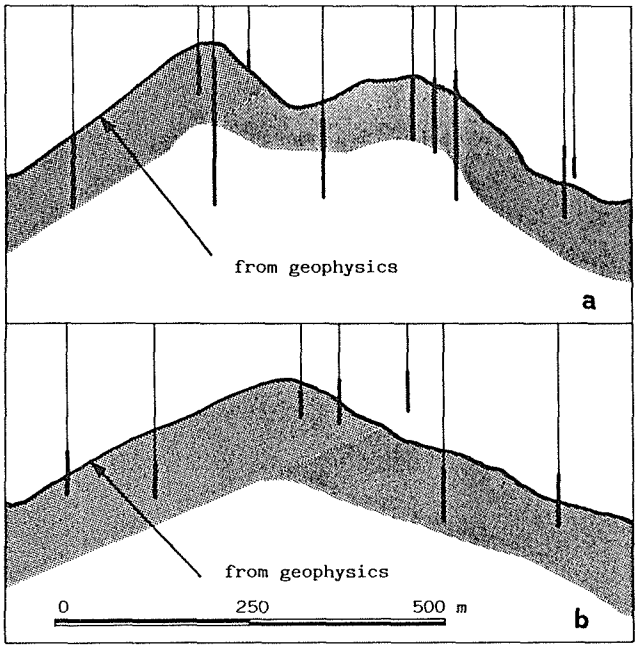

FIG. 4 Schematic cross-sections showing depth of pre-Quaternary substratum: a - North-South section; b - Northwest-Southeast section.

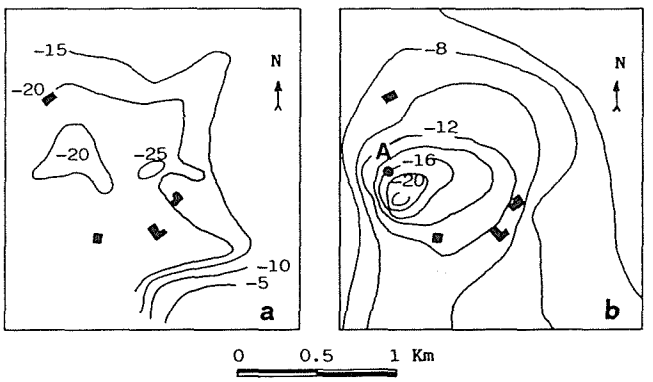

FIG. 5 a - average piezometric surface in m a.s.l. in 1986. b - countor lines of equal speed of soil sinking (cm/year) in the period 1985-1987.

correspondence between piezometric lowering and land subsidence (see fig. 5). The observed trend led us to conclude that the subsoil compaction was prevalent in the more compressible superficial layers; thus the thickness of the Quaternary alluviums does not influence the land subsidence: at times the areas with the greatest subsidence are those where the substratum is less deeper.

In conclusion, the study has shown that the major cause of subsidence is the strong lowering of the piezometric levels which took place before the withdrawal reduction imposed by the GU. Given the fact that this lovering ended in the years 1975-1976, the current land subsidence should be considered the final effect of a ceased cause, and it may be predicted that it will gradually slow down to a decrease trend. This prediction is confirmed by the examination of the subsidence trend which took place during the period 1983-1989: see for example fig. 6, showing the land settlement vs. time in one of the areas of greatest subsidence (A in fig. 5-b).

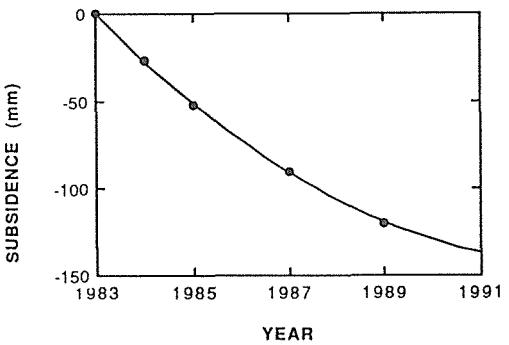

FIG. 6 Land settlement in one of the areas of greatest subsidence (A in fig. 5-b).

DAMAGES TO THE BUILDINGS

In early 1986, 13 representative buildings (all except for one were large hotel complexes) were chosen and bench-marks were attached to their structures in order to measure differential settlements. Five measurement series were taken over the period 1987-1989.

An examination of the results, for example those for the Hotel

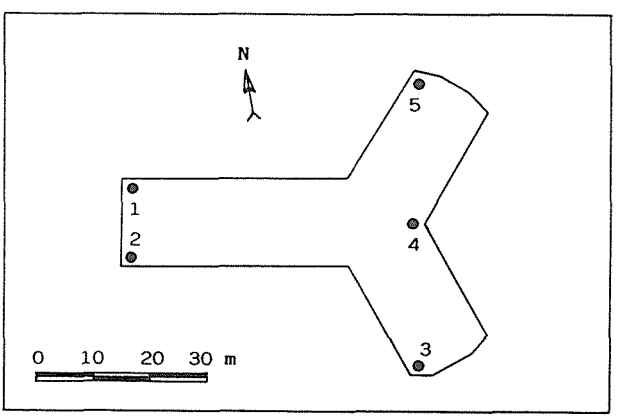

FIG. 7 Hotel Molino with the locations of the bench-marks.

Molino shown in figs. 7 and 8, shows that in most cases the structure settlements follow the global trend of soil lowering due to subsidence. However, these settlements have caused only slight inclinations of the buildings, without causing lesions to the structures.

On the other hand, serious damages were pointed out in those buildings which had been subsequently raised following their construction. In any case these damages are not to be attributed to subsidence, as the local Authorities feared.

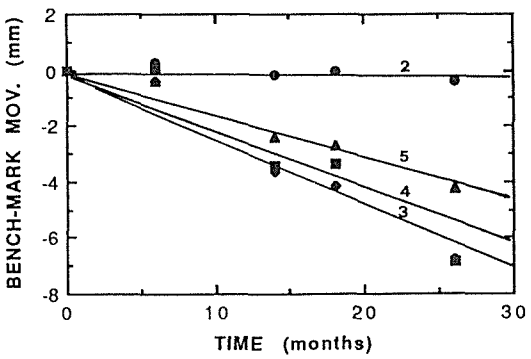

FIG. 8 Hotel Molino: vertical differential settlement with reference to bench-mark n. 1.

FUTURE WORK AND CONCLUSIONS

Reinjection of water into the subsoil was initially considered both as a way of disposing of waste water after thermal use (bath, mud bath treatments, etc.) and to contribute to repressurizing the aquifers and thus to slowing down the subsidence (see Dainese, 1989).

Given, however, the complex physical, chemical and biological problems caused by reinjecting into the aquifers waters which have undergone significant variations to their original composition and temperature, it is felt that the advantages of reinjection should be evaluated with extreme care, also keeping in mind the severe limits placed by current Italian legislation (see Caia, 1986).

In addition, if one considers the fact that:

(a) in recent years the soil has not been lowered by more than 2 cm/year in the most critical points;
(b) the lowering rate is slowly but constantly decreasing;
(c) no serious damage has been caused to the buildings due to subsidence;

it is felt to be more appropriate to turn public attention to other actions, first of all optimization of withdrawal.

The measurement of the piezometric level lowerings, made in recent years in some wells located in Abano Terme and Montegrotto (see the

average monthly levels vs. time of the three most representative wells in fig. 9, the location of which is shown in fig. 1) shows that strong piezometric lowerings were localized in the areas in which intensive withdrawals occur, but that the Euganean basin allows larger production of thermal waters than those currently produced. It is therefore a matter of rationally positioning the new wells.

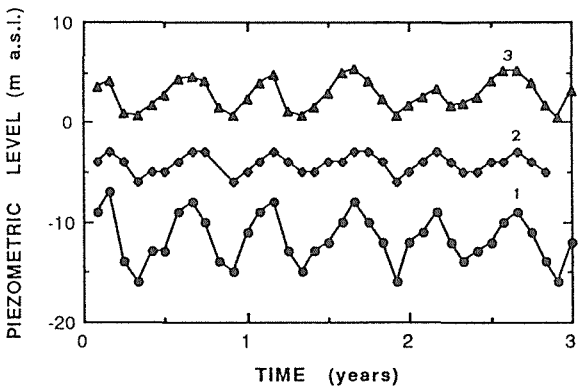

FIG. 9 Piezometric levels (m a.s.l.) of three wells in Abano Terme and Montegrotto. Location of the wells is reported in fig. 1.

It is thus felt that the essential first step towards a more rational utilization of the Euganean thermal water resources is a passage to a unitary Authority for the management of the entire basin. This Authority would have to further study the aquifer, through field and laboratory tests to obtain enough information on its hydraulic and geotechnical characteristics. All this should allow the construction of a mathematical model of the entire system to make it possible to determine the future piezometric fluctuations and soil lowerings on a long term basis as a function of the management policies of thermal water withdrawal.

AKNOWLEDGMENTS

The author acknowledges the Gestione Unica di Abano Terme e Teolo that released part of the field data. This research was partly supported by Grant N. 88.01664.05 from the Italian Consiglio Nazionale Ricerche.

REFERENCES

Brighenti, G., Ciancabilla, F. & Ballestrazzi, P. (1990) Ricerca sull' abbassamento del suolo nell' area termale di Abano Terme. Report of Mining Science Inst. University of Bologna, Italy.

Caia, G. (1986) Considerazioni sull' utilizzo delle acque termali e la disciplina giuridica degli scarichi idrici. Report of Mining Science Inst., University of Bologna, Italy.

Dainese, A. (1986) Il bacino idrotermale di Abano Terme. Alcuni studi sulla produzione e gestione della risorsa termale. PhD. thesis.

Dainese, A. (1988) Evoluzione delle opere di captazione nel Bacino Termale Euganeo. Proc. GEOFLUID Symp., Piacenza, Italy, 55-58.

Dainese, A. (1989) Campo idrotermale euganeo - considerazioni sulla possibilità di reimmissione in falda di reflui termali. Acque Sotterranee 6, 29-33.

Piccoli, G.,Bellati, R., Binotti, C., Di Lallo, E., Sedea, R., Dal Pra', A., Cataldi, R., Gatto, G., Ghezzi, G., Marchetti, M., Bulgarelli, G., Schiesaro, G., Panichi, C., Tongiorgi, E., Baldi, P., Ferrara, G.C., Massari, F., Medizza, F., Iliceto, V., Norinelli, A., De Vecchi, G., Gregnanin, A., Piccirillo, E.M. & Sbettega, G.(1976) Il sistema idrotermale Euganeo-Berico e la geologia dei colli Euganei. Mem. Ist. Geol. Univ. di Padova, 30, 1-266.

Schiesaro, G. (1982) La dinamica del Bacino Termale Euganeo: modello indiziario della produzione. L'Industria Mineraria 3, 47-52.

Schiesaro, G. (1985) Il tema della subsidenza quale capitolo significativo e qualificante di una ricerca geo-mineraria totale. Quarry and Construction 12, 49-54.

Land Subsidence (Proceedings of the Fourth International Symposium on Land Subsidence, May 1991). IAHS Publ. no. 200, 1991.

Countermeasures for and Monitoring of Land Subsidence in the Northwestern Part of the Kanto Plain, Japan

T. NAKAO
River Bureau, Ministry of Construction
Tokyo, Japan
A. KAMATA
Association of Groundwater Technology
Tokyo, Japan

ABSTRACT This paper briefly describes the groundwater condition and land subsidence in the northwestern part of the Kanto Plain, particularly the area of the Saitama Prefecture. The water level, land subsidence and countermeasures for it are presented and discussed.

OUTLINE OF THE AREA

The Kanto Plain is located in the central part of Japan and counts among the largest in the island. In its southern part are sited the capital of Japan and the other large cities along the coast of Tokyo Bay. All types of institutions and facilities are concentrated in this area.

The abstraction of groundwater, heavily made in the area during the period after World War II and primarily for industrial use, caused a severe land subsidence which continued through time, with this subsidence that were almost ceasing in the early Seventies due to the regulations enacted and the industrial waterway that was constructed.

Today, and for the purpose of municipal and agricultural water supply, groundwater is heavily abstracted in the northern part of the Kanto Plain. This has resulted to severe land subsidence, particularly in the area along the middle stream of the Tone River which flows through the plain.

HYDROGEOLOGY

The area occupies a northwestern portion of the Kanto Plain and is composed of alluvial and diluvial layers. Its sub-surface geology is subdivided into three groups, namely, alluvium, low terrace deposit and diluvium (A - D members).

The alluvium is distributed along the major rivers flowing through the plain and has a maximum thickness of 50 meters in the south. This thickness decreases towards the north however.

The "A" layer of diluvium forms a basin structure and has a maximum depth of 100 meters below sea level at the center of the basin. Also forming basin structures are the "B" and "C" layers with respective maximum depths at their centers of 260 meters and 350 meters below sea level.

Sand and gravel of upper alluvium and gravel of terrace deposits

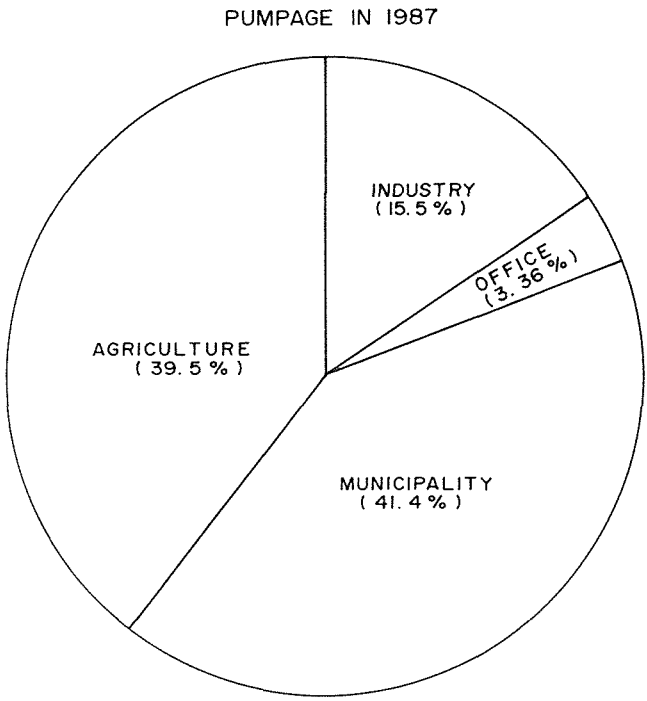

FIG. 1 Groundwater pumpage.

constitute phreatic aquifers. The sand and gravel of the layers of the diluvium form the artesian aquifers in the area.

The first confining bed between the phreatic and artesian aquifers is an alluvium clay which is distributed along the lowland and has a thickness of about 30 meters. Second and third main confining beds are thick clayey layers of the "A" and "B" members of diluvium. The respective maximum thicknesses of "A" and "B" clayey layers in the northern part of the area are 40 meters and 80 meters; volume compressibility range from 10^{-1} to 10^{-4} cm^2/kg and decreases in proportion to the depth.

GROUND WATER USE

The total groundwater pumpage in the area (within the northern part of the Saitama Prefecture) was about 500 MCM/year in 1987 (Fig. 1). Usage shares for groundwater-sourced water supply are: 41% for municipal supply; 39% for agricultural; 16% for industrial; and 4% for the water supply of offices.

Groundwater is mainly abstracted from the alluvium and the "A" layer for agricultural use, but is pumped from the "B" and "C" layers for municipal and industrial use.

Total pumpage varies yearly as shown in Fig. 2. It can be seen that the industrial use of supply decreased, but with municipal use gradually increasing since the start of the Eighties. The seasonal fluctuation of pumpage is mainly caused by the agricultural use of supply and the slight increase in the municipal water supply. Fig. 3 shows the seasonal fluctuation.

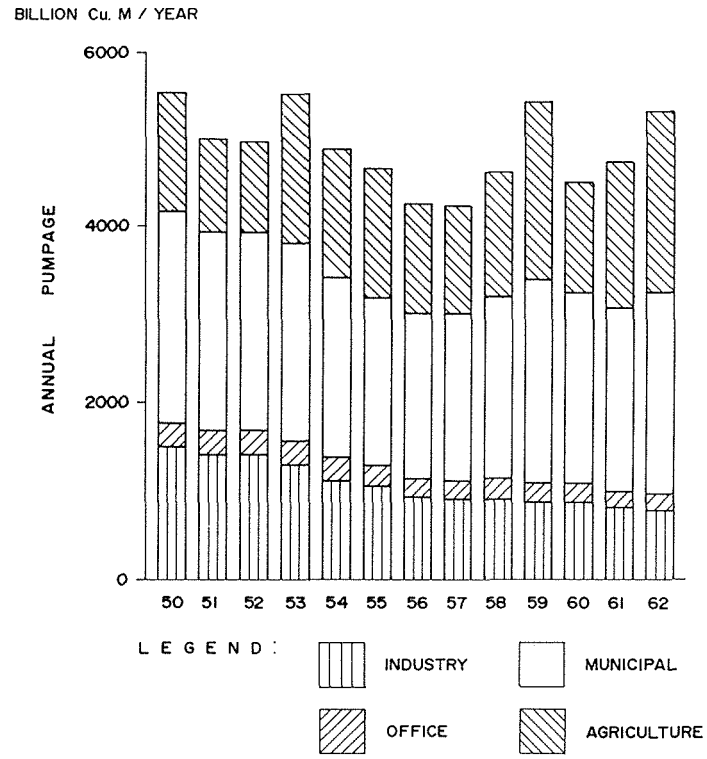

FIG. 2 Yearly change of pumpage.

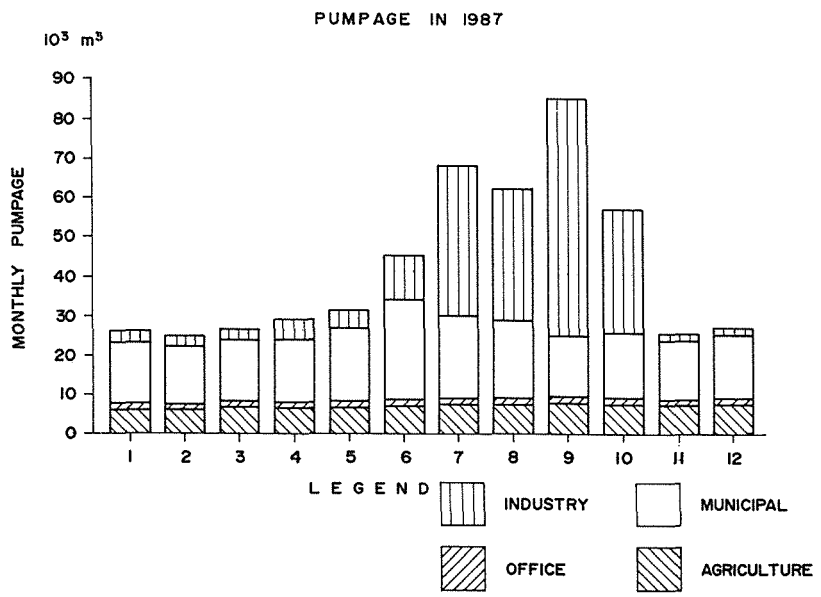

FIG. 3 Monthly change of pumpage.

MUNICIPAL WATER SUPPLY

The Saitama Prefecture sources its water supply from both surface water and groundwater. But the serious drought which happened in 1987, and which affected the upper stream of the Tone River, gave birth to the restriction that only a maximum of 30% of the surface water in the downstream of said river may be taken during three months of the summer season. (Fig. 4 shows the typical variation of storage

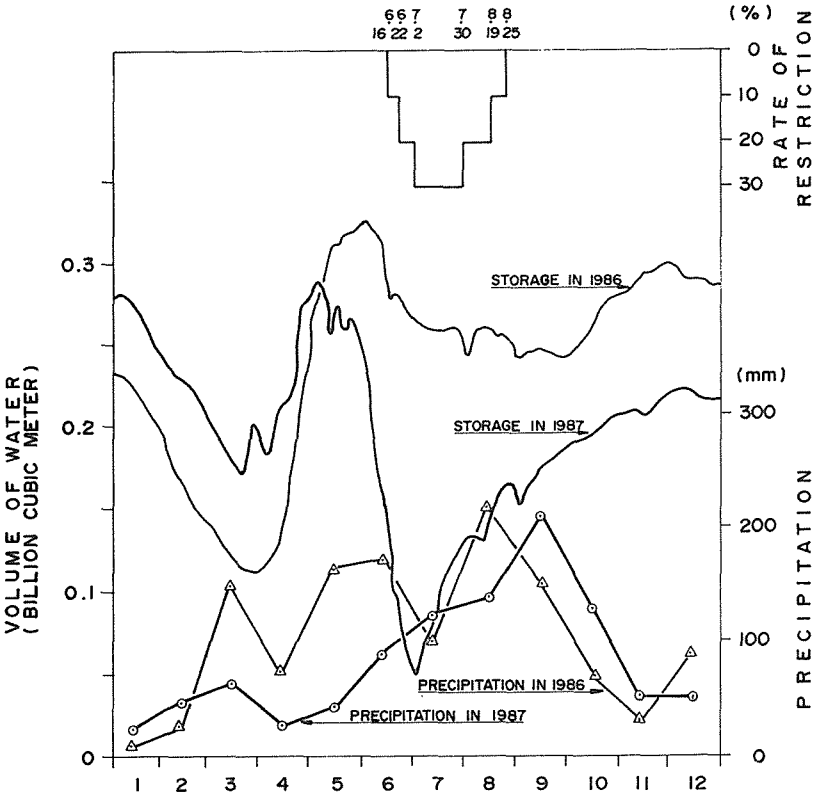

FIG. 4 Change of storage in reservoirs.

in six reservoirs on the upper stream of the Tone River during this drought.) As the southern part of the prefecture is largely dependent on surface water, the impact of the restriction was such as to have groundwater pumping heavily increased to compensate for the shortage.

GROUNDWATER LEVEL AND LAND SUBSIDENCE

The location of monitoring wells for groundwater level and land subsidence in the northwestern part of the Kanto Plain is shown in Fig. 5. Forty-six (46) of the wells (in 30 sites) are for subsidence monitoring; eighty-four (84) (in 62 sites) for groundwater level monitoring; and thirty-six (36) (in 34 sites) for shallow groundwater level monitoring. A piezometric surface of aquifers in the area for the year 1987 is shown in Fig. 6.

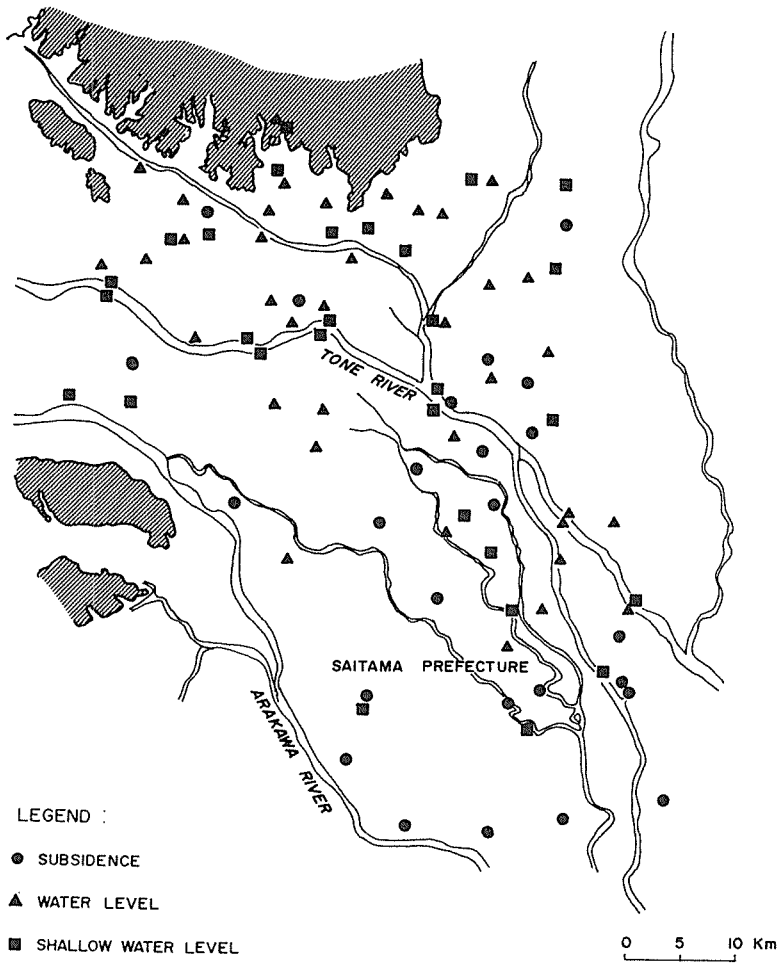

FIG. 5 Location of monitoring wells.

In the lowland along the Nakagawa River, the groundwater level has declined to more than 20 meters below sea level, with the zone of depression spreading from south to north. From a surface levelling of benchmarks, it was observed that an annual subsidence rate of more than 20 mm occurred in the cities of Kurihashi, Satte, Kazo and Washinomiya in 1987 (Figs. 7 and 8). Land subsidence at a rate of 20 mm/year was also observed for the southern part of the prefecture as a result of the increase in pumpage in response to the 1987 drought.

Based on the records of subsidence monitoring wells at Washinomiya, continuous subsidence occurred at a rate of 42 mm/year at the deepest well for the abovesaid year (Fig. 9). Further, the rate of subsidence was low for the period February to July and increases afterward. This may be caused by the pumping increase in summer as reflected by the water level fluctuation.

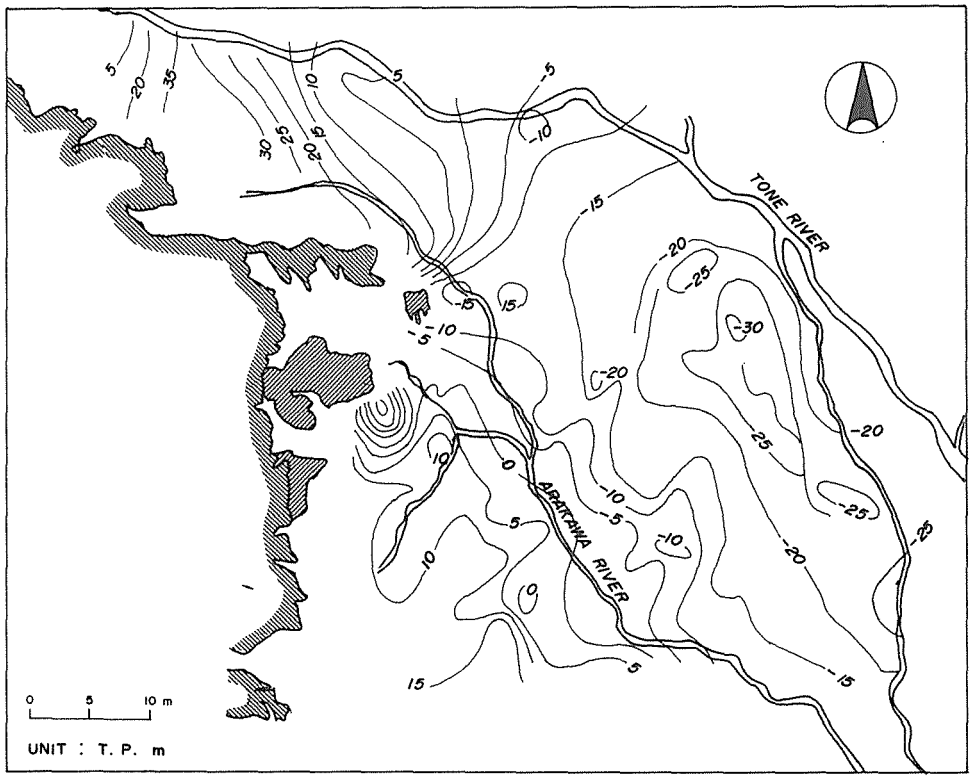

FIG. 6 Piezometric surface of aquifers in September 1987.

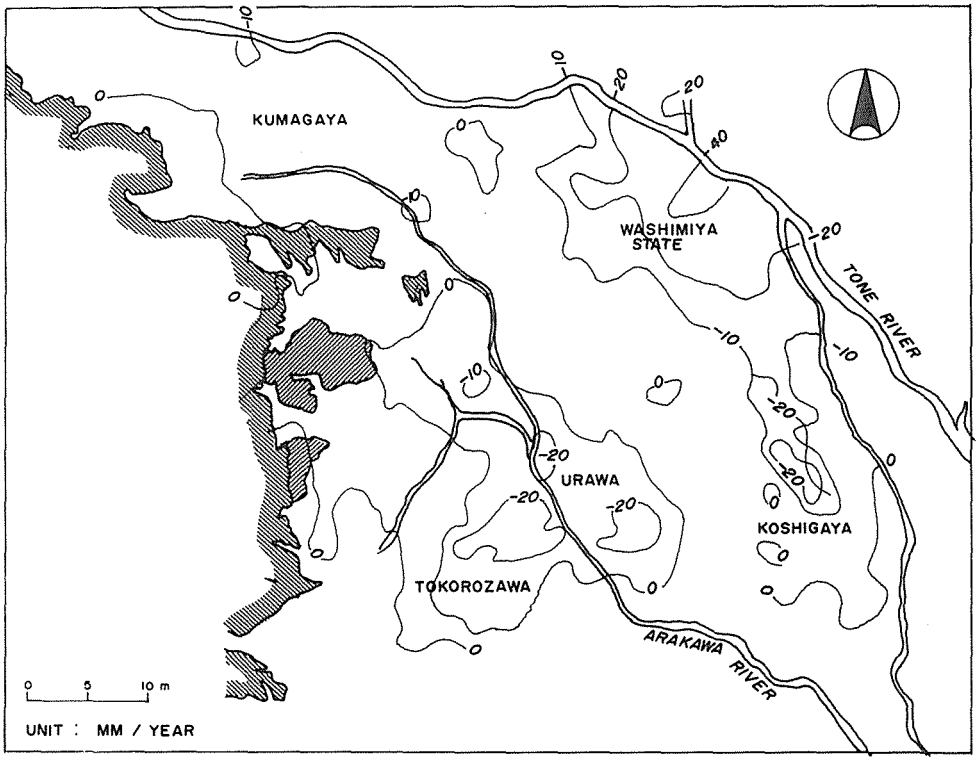

FIG. 7 Annual land subsidence in 1987.

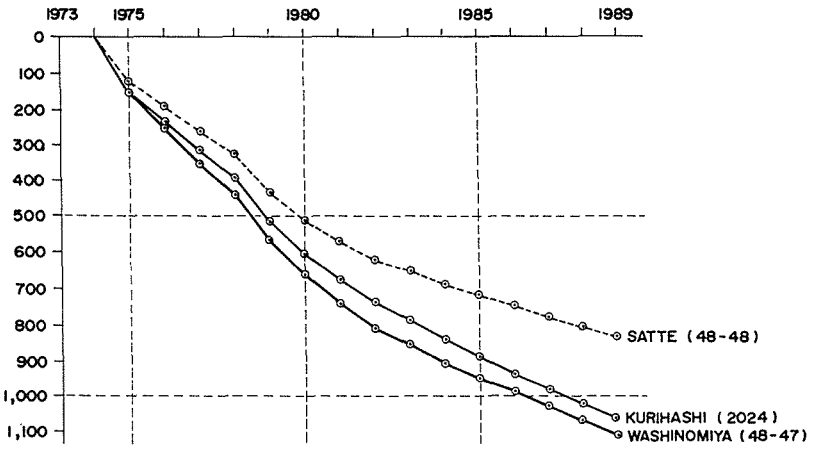

FIG. 8 Subsidence records at benchmarks.

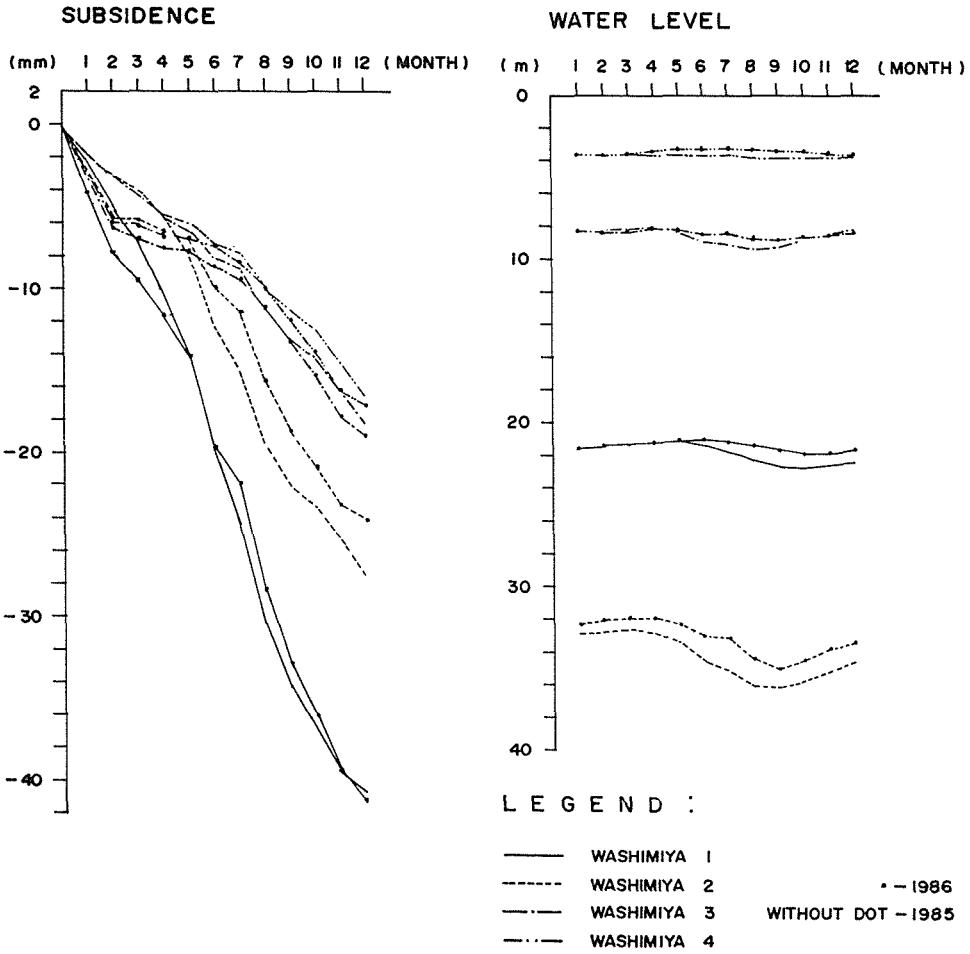

FIG. 9 Subsidence and water level records at monitoring wells.

COUNTERMEASURES FOR LAND SUBSIDENCE

To avert disasters which could arise out of the land subsidence problem, governmental agencies are undertaking regional countermeasures. These include the (1) regulation of groundwater pumping, (2) construction of alternative waterways, (3) rationalization of water use, and (4) improvement of drainage and restoration of facilities.

Land Subsidence (Proceedings of the Fourth International Symposium on Land Subsidence, May 1991). IAHS Publ. no. 200, 1991.

Control of Groundwater Withdrawal for Preventing Land Subsidence in the Owari Plain, Japan

K. DAITO
Department of Geotechnical Engineering, Nagoya University
Chikusa-ku, Nagoya, 464-01, Japan
M. MIZUNO
Department of Environment, Aichi Prefecture,
Naka-ku, Nagoya, 460-01, Japan
K. UESHITA
Department of Geotechnical Engineering, Nagoya University
Chikusa-ku, Nagoya, 464-01, Japan

ABSTRACT In Owari Plain, groundwater heads were extremely drawn down before 1973, but groundwater heads were recovered by the regulation of withdrawals after then. In this paper, safety groundwater heads and allowed withdrawal of groundwater in Owari Plain are shown which are based on the calculation for compression of aquitards according to the change of groundwater heads of aquifers using the one-dimensional F.E.M. analysis and the quasi-three-dimensional F.E.M. analysis. From these calculations, the proposed groundwater management plan in Owari Plain is introduced.

INTRODUCTION

Owari Plain is a part of Nobi Plain which is the central part of Japan as shown in Fig.1, and belongs to Aichi Prefecture. The history of land subsidence in this area by use of three bench marks is shown in Fig.2. Land subsidence of Owari Plain was mainly caused by lowering of piezometric heads of groundwater due to the withdrawal from the aquifers. Since 1974, the regulation on groundwater use has been put into effect by Aichi Prefecture. As a result of this regulation, lowered groundwater heads were recovered and subsidence has been recently retarded. The subsidence of Nobi Plain including Owari Plain for 29 years from 1961 to 1989 is shown in Fig.3. Land subsidence of Nobi Plain has been studied by many people (Iida, et al., 1976, Kuwahara, et al., 1976, Ohshima, et al., 1989, Sato, et al., 1978, 1986, Ueshita, et al., 1977, Ueshita & Sato, 1981, and Ueshita & Daito, 1984, 1990).

SAFETY GROUNDWATER HEADS OF OWARI PLAIN

These days, safety groundwater heads preventing land subsidence and optimal withdrawals with effective use of groundwater are required to be known for the groundwater management. When the groundwater basin is managed, withdrawals of groundwater must be controlled based on the allowable perennial yield. The allowable perennial yield of

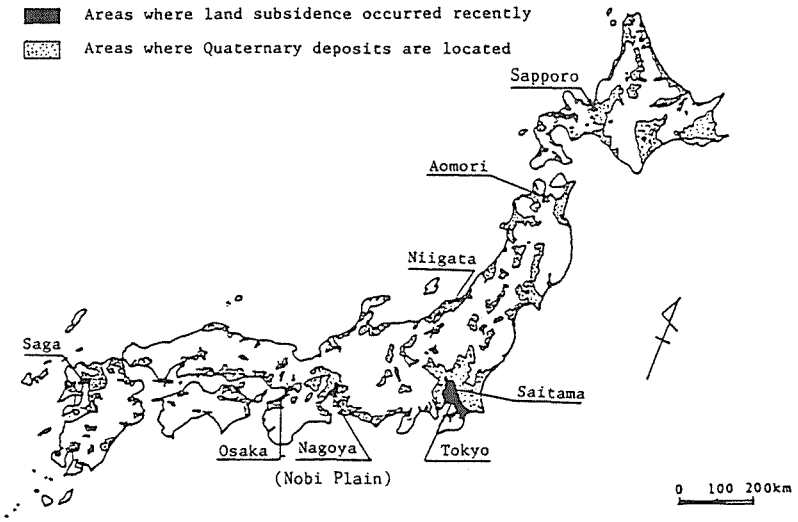

FIG.1 The location of Nobi Plain and Nagoya City.

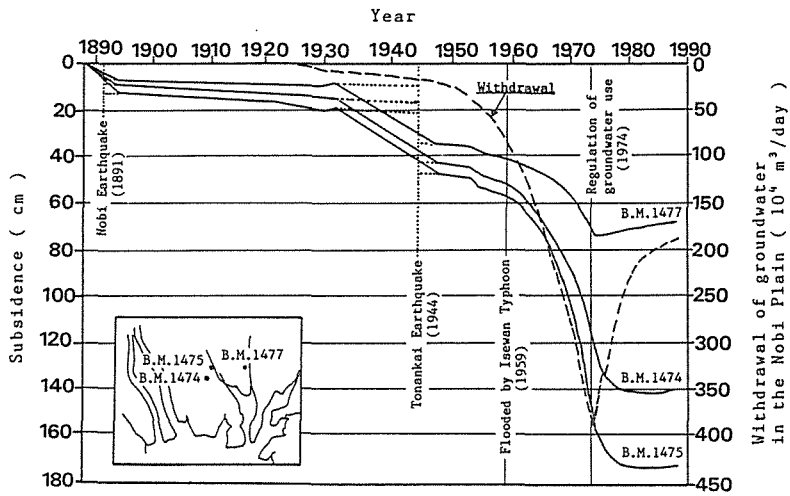

FIG.2 Subsidence of bench marks and withdrawal of groundwater (Recent data were added to the figure of Iida, et al. (1976)).

groundwater basin is considered as the rate at which water can be withdrawn perennially under specified operating conditions without producing undesired results (Todd, 1980). This allowable perennial yield is not to be found easily.

On the other hand, groundwater heads are easy to be measured in time. Therefore, safety groundwater heads at the allowable yield are obtained for the basin, management of groundwater basin is thought to be very easy and effective. Fortunately, groundwater heads and compression of layers have been measured at 97 observation wells in Nobi Plain (24 observation wells in Owari Plain) as shown in Fig.4.

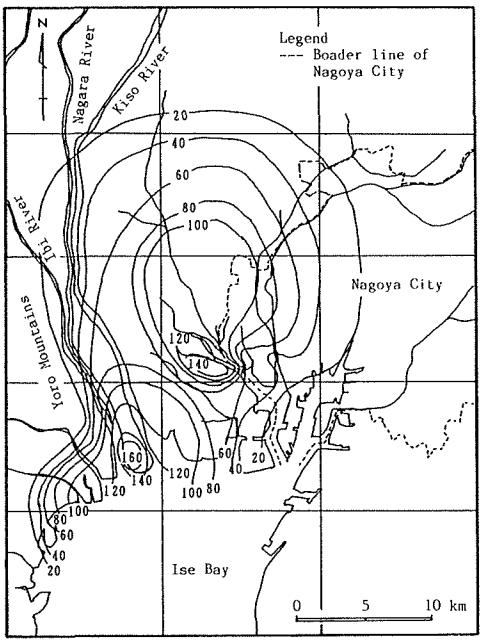

FIG.3 Subsidence for 29 years from 1961 to 1989 in Nobi Plain.

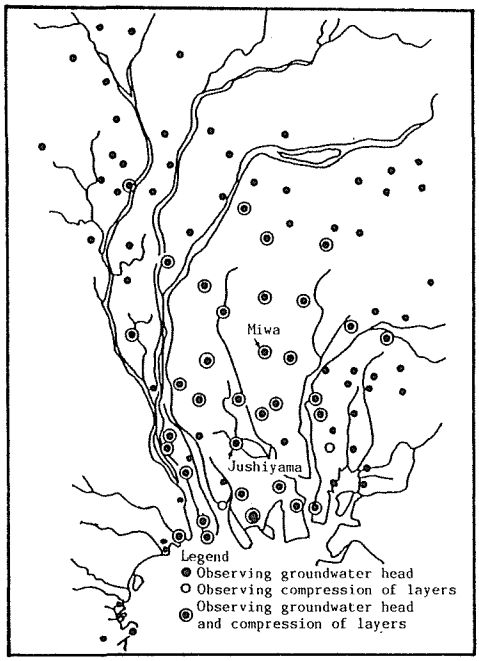

FIG.4 Observation wells in Nobi Plain.

The authors prepared the one-dimensional consolidation model in order to find out safety groundwater heads for preventing land subsidence. This model is able to compute the time dependent consolidation phenomena of aquitards due to lowering of piezometric heads which were drawn down by withdrawal of groundwater. As the displacement of soil as also one-dimensionally vertical one at each computational point, the continuous equation of groundwater flow in a saturated aquitards can be expressed as follows:

$$\frac{\partial}{\partial x} k_{zi} \frac{\partial h_i}{\partial z} = S_{si} \frac{\partial h_i}{\partial t} \tag{1}$$

where h_i denotes the piezometric head of groundwater, S_{si} denotes the specific storage of aquitard, k_{zi} denotes the vertical permeability, z denotes the vertical coordinate, and i denotes the i-th aquitard.

Finite element discretization of above equation was performed using Galerkin's procedure. Applying boundary conditions which the heads of top and bottom nodes of the aquitard were known, the inflow and outflow of groundwater through the aquitard were calculated as follows:

$$U_i = \frac{k_z}{L_1} h_2 - h_1 + S_{si} L_1 \frac{1}{6} \frac{\partial h_2}{\partial t} + \frac{1}{3} \frac{\partial h_1}{\partial t} \tag{2}$$

$$V_i = \frac{k_z}{L_n} h_n - h_{n+1} + S_{si} L_n \left(\frac{1}{6} \frac{\partial h_{n+1}}{\partial t} + \frac{1}{3} \frac{\partial h_n}{\partial t} \right) \quad (3)$$

where U_i denotes inflow from the upper aquifer to the aquitard, V_i denotes outflow from the aquitard to lower aquifer, L denotes the length of element of which the aquitard was made, and h_1 and h_{n+1} denote the known heads of top and bottom of the aquitard, respectively.

The amount of consolidation of the aquitard was thought to be equal to the amount of outflow from the aquitard by compression of the aquitard. This amount was calculated as follows:

$$S = \Sigma S_{si} \cdot \Delta h \cdot L = V_i - U_i \quad (4)$$

In this calculation, S_s at consolidation process was not equal to S_s at rebound process.

Results of calculation for Jushiyama observation well are shown as follows. At first, ground was modeled as shown in Fig.5 based on the results of borehole investigation and soil tests. Test results and soil parameters used in computation work are shown in Fig.6. Calibration of this calculation was performed with data measured by observation well and bench mark. The result of calibration is shown in Fig.7. This figure shows that calculated subsidence is similar to observed one, and until two or three years after 1975 when groundwater heads of aquifers became to rise, subsidence was stopped, or ground was rebounded. From this calculation, aparent safety groundwater heads which are based on the traditional definition, are obtained as M.S.L. -6.8 m for the 1st aquifer, M.S.L. -12.2 m for the 2nd aquifer, and M.S.L. -23.5 m for the 3rd aquifer.

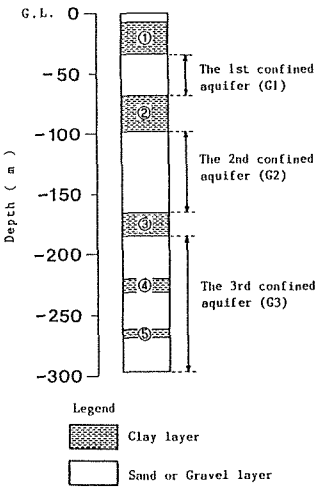

FIG.5 Ground model at the point of Jushiyama observation well.

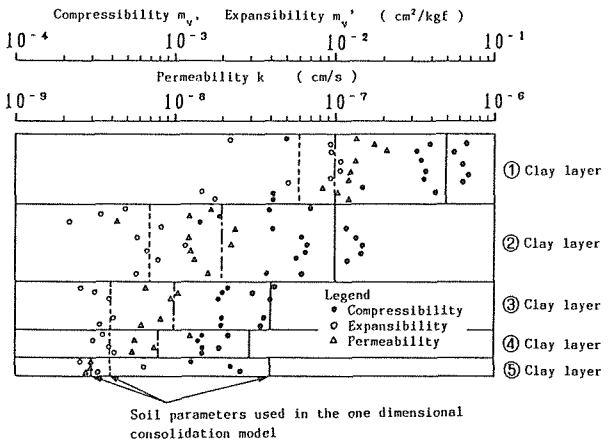

FIG.6 Results of oedometer tests.

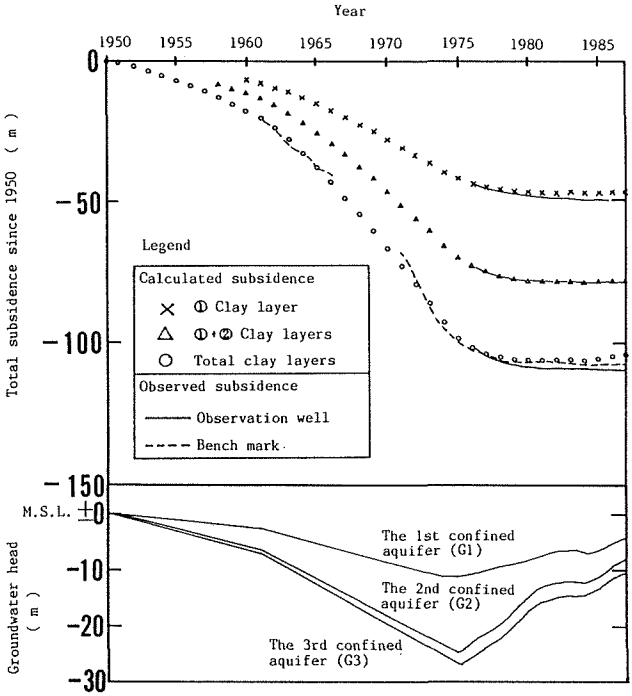

FIG.7 Calculated and observed subsidence at the place of Jushiyama observation well.

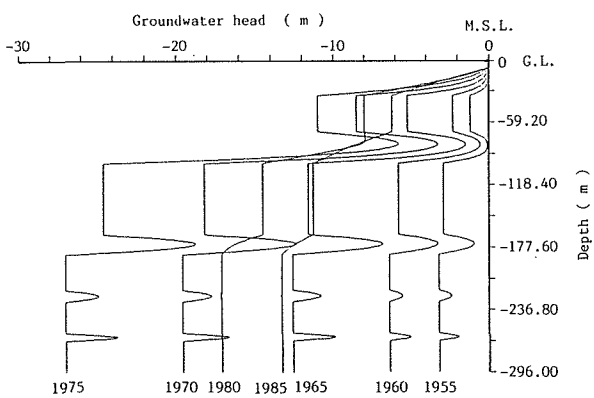

FIG.8 Time dependent change of calculated groundwater heads in the ground at the place of Jushiyama observation well.

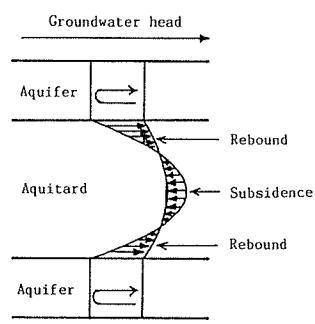

FIG.9 Change of groundwater head in aquitard by recovering groundwater heads in aquifers after drawing down of the heads.

Time dependent change of calculated groundwater heads in the ground at the point of Jushiyama observation well is shown in Fig.8. Excess pore water pressure in clay layers induced by lowering groundwater heads at the top and bottom of the clay layer becomes to disapear with time lag.

Generally when the subsiding speed is zero, various conditions are considered in the ground as follows:

(1) Excess pore water pressure in the all aquitard completely disapeared;
(2) According to change of groundwater heads in aquifers, rebounding clay layers by rising groundwater head in clay layers and subsiding clay layers by constant or lowering groundwater head in clay layers exist in the ground at the same time. And total subsiding speeed becomes to be zero; and
(3) According to rising groundwater head in aquifers, in the top and/or bottom part of aquitard excess pore water pressure disapered completely and in the center part of aquitard excess pore water pressure is disapering as shown in Fig.9. The former part is rebounding and the latter part is subsiding. But total subsiding speed becomes to be zero.

In the case of (3), when the groundwater heads are maintained to aparent safety groundwater heads which make aparent subsiding speed to be zero, the ground will go on subsiding for a few years.

So the authers defined the new safety groundwater heads based on the remained maximum excess pore water pressure in the aquitard. If groundwater heads are not drawn down below the new safety groundwater heads, plastic subsidences in the normal consolidation region do not occur in the aquitards. Deformation of the aquitards by change of groundwater heads in the aquifers above the new safety groundwater heads seem to be elastic. This deformation is not serious. The new safety groundwater heads at the place of Jushiyama observation well are obtained from Fig.8 as M.S.L. -6.2 m for the 1st aquifer, M.S.L. -11.0 m for the 2nd aquifer, and M.S.L. -19.0 m for the 3rd aquifer. These values are slightly higher than the aparent safety groundwater heads. The new safety groundwater head should be defined that the plastic subsidence in the range of normal consolidation dose not occur in the aquitard. The management of Owari groundwater basin should be performed based on the new safety groundwater heads.

SIMULATION MODEL FOR GROUNDWATER MANAGEMENT IN OWARI PLAIN

For estimating the allowable perennial yield, the groundwater movement in Owari Plain was computed by using the quasi-three-dimensional F.E.M. analysis of this groundwater basin. Fig.10 shows the area of the Nobi groundwater basin model which is 1164 km^2 and coveres about 90 percent of the Nobi alluvial plain. Boundary conditions in this calculation are shown in Fig.11.

Allowed withdrawals in 1994 has been decided by Aichi Prefecture according to "General Plan of Countermeasures for Land Subsidence of the Nobi Plain" of the Ministrial Conference in 1985. Groundwater condition in 1994 was predicted by using the data of this allowed withdrawals as shown in Fig.12. Fig.13 shows the calculated and observed groundwater heads distribution of each aquifer in 1986. Calculated groundwater heads of aquifers at the point of Miwa observation well are shown in Fig.15. From thses figures, it is known that groundwater heads of all aquifers will rise until 1994, and especially the groundwater head of G1 aquifer will rise to near ground surface. This groundwater condition is not desirable for earthquake because of liquefaction disaster. The groundwater head of the

aquifer G1 should be slightly lowered below the predicted head. So the reasonable plan of withdrawal of groundwater must be established for the effective use of groundwater in Owari Plain.

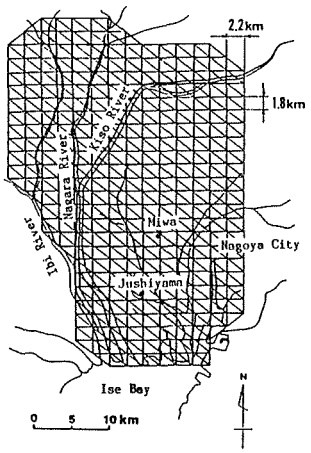

FIG.10 Finite element mesh for the quasi three-dimensional F.E.M. simulation of Owari Plain.

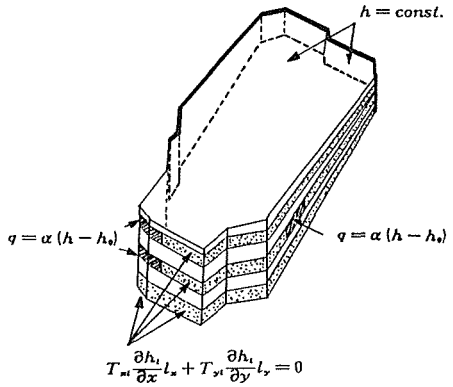

FIG.11 Schematic explanation of the boundary conditions of the quasi three-dimensional simulation model of Owari Plain.

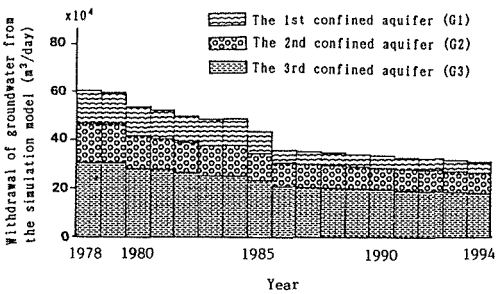

FIG.12 Yearly withdrawal of groundwater in the simulation model.

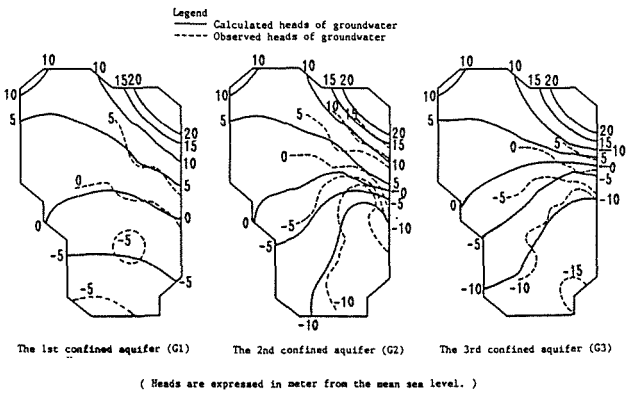

FIG.13 Comparison of calculated heads of groundwater with observed heads in 1986.

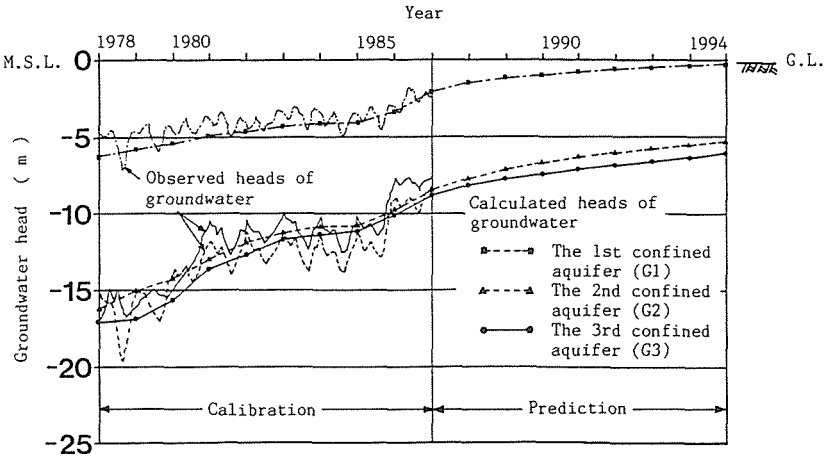

FIG.14 Calculated and observed groundwater heads of aquifers at the place of Miwa obervation well.

GROUNDWATER MANAGEMENT FOR EFFECTIVE USE IN OWARI PLAIN

Safety groundwater heads preventing land subsidence and optimal withdrawals with effective use of groundwater are required to be known for groundwater management in Owari Plain. Groundwater heads are easy to measured in time. Therefore, safety groundwater heads at allowable yield are useful for the reasonable groundwater management. This safety groundwater heads were discribed in the previous section. On the other hand, the relations of withdrawals, groundwater head of aquifer, and land subsidence have not been made clear perfectly in Owari Plain. And also the work of grasping the actual withdrawals takes much time. Therefore, based on some calculations of groundwater condition using the data of some patterns of withdrawals, the groundwater management plan of Owari Plain was introduced. The basic concepts of this management plan are as follows:

(1) Groundwater management in Owari Plain must be performed based on the long term withdrawal plan for going near the reasonable groundwater condition in this basin. In this case, amount and distribution of withdrawal for achieving the reasonable groundwater condition should be obtained by groundwater flow simulation conbined with optimization method;

(2) The short term and local change of groundwater condition can not be grasped by the above method. For achieving the long term plan of withdrawal, groundwater management will be performed by the regulation of the change of groundwater heads in some observation wells. In this case, safety groundwater head should be set as the lowest limit of groundwater head, and some warning limits should be also decided. And the regulation of groundwater use will be performed according to the condition of groundwater heads; and

(3) The short term and local condition of groundwater heads and withdrawal will be feedbacked to the long term plan of the distribution of groundwater head and withdrawal, and this long term plan should be modified according to the new condition.

The flow chart of this management process is shown in Fig.15. This management plan of groundwater basin combined with the long term management by the regulation of withdrawal which takes a much time to sum up, and the short term and local management by the regulation of the change of groundwater heads will make possible to manage the groundwater basin minutely.

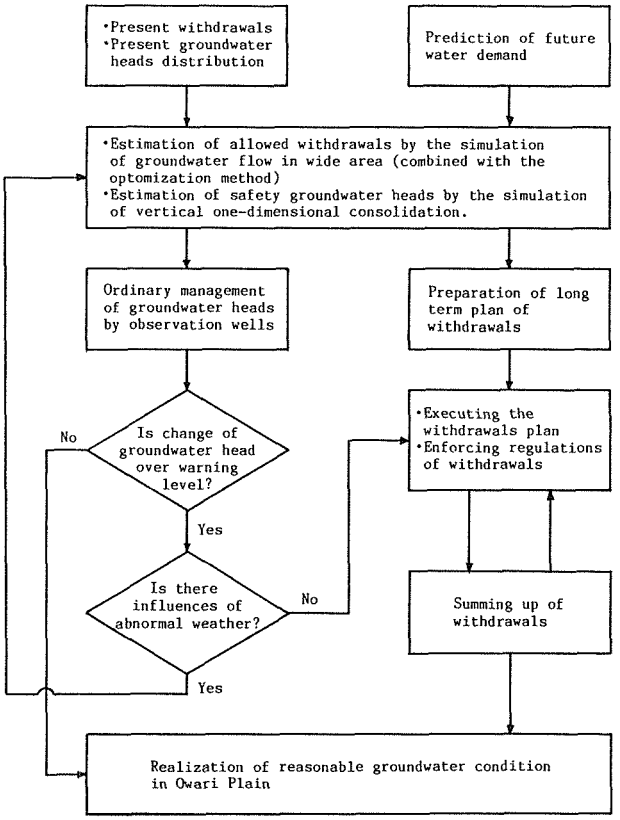

FIG.15 Flow chart of the proposed groundwater management plan for Owari Plain.

CONCLUSION

Safety groundwater heads in Owari Plain are shown in this paper which are based on the calculation for compression of aquitards according to the change of groundwater heads of aquifers. In this calculation, the one-dimensional F.E.M. analysis was used. In Owari Plain, groundwater heads were extremely drawn down before 1973, but groundwater heads were recovered by the regulation of withdrawals after then. From these calculations, it is found that safety groundwater head is not the head which made stop the subsidence aparently, and is not the lowest head of aquifers, but the lowest pore water head experienced in aquitards in the past.

Allowed withdrawal in 1994 has been decided by Aichi Prefecture according to "General Plan of Countermeasures for Land Subsidence of the Nobi Plain" of the Ministrial Conference in 1985. Calculated groundwater condition in 1994 assuming the condition of withdrawals is shown in this paper. In this calculation, the quasi three-dimensional F.E.M. analysis was used. From this calculation, it was thought that groundwater heads in some aquifers were over recovering in 1994.

The groundwater management plan in Owari Plain is proposed in this paper. This management plan of groundwater basin combined with the long term management by the regulation of withdrawal, and the short term and local management by the regulation of the change of groundwater heads will make possible to manage the groundwater basin minutely.

ACKNOWLEDGEMENTS The authors would like to express their hearty gratitude to the members of Department of Environment, Aichi Prefecture and the organs and persons concerned.

REFERENCES

Iida, K., Sazanami, K., Kuwahara, T. & Ueshita, K. (1976) Subsidence of the Nobi Plain. Proc. 2nd Int. Symp. on Land Subsidence, IAHS-AISH Publication 121, 47-54.

Kuwahara, T., Ueshita, K. & Iida, K. (1976) Analysis of land subsidence in the Nobi Plain. Proc. 2nd Int. Symp. on Land Subsidence, IAHS-AISH Publication 121, 55-64.

Ohshima, T., Ueshita, K. & Daito, K. (1989) Land subsidence and groundwater condition in Nagoya. Proc. Int. Symp. on Land Subsidence, 193-204.

Sato, T., Itabashi, K. & Ueshita, K. (1978) Improved model of the Nobi ground water basin to solve the subsidence problem. Proc. Specialty Session on Geotechnical Engineering and Environmental Control, 9th ICSMFE, vol.2, 79-81.

Sato, T., Daito, K. & Ueshita, K. (1986) Analysis of land subsidence due to withdrawal of groundwater in the Nobi Plain. Proc. 3rd Int. Symp. on Land Subsidence, IAHS Publication 151, 89-99.

Tood, D.K. (1980) Groundwater Hydrology 2ed, 363-364.

Ueshita, K., Itabashi, K., Tanahashi, H. & Sato, T. (1977) Modelling of the Nobi ground water basin to solve the subsidence problem. Proc. Specialty Session on Geotechnical Engineering and Environmental Control, 9th ICSMFE, vol.1, 465-480.

Ueshita, K. & Sato, T. (1981) Study on subsidence of the Nobi Plain. Proc. 10th ICSMFE, vol.2, 387-390.

Ueshita, K. & Daito, K. (1984) Land subsidence in Japan, and a case study on the Nobi Plain. Proc. Int. Symp. on Geotechnical Aspects of Mass and Material Transportation, 439-460.

Ueshita, K. & Daito, K. (1990) Environmental geotechnics in Nagoya, Japan. Proc. 10th Southeast Asian Geotechnical Conference, Vol.1, 253-258.

Land Subsidence (Proceedings of the Fourth International Symposium on Land Subsidence, May 1991). IAHS Publ. no. 200, 1991.

The Prediction of Heave Associated with the Storage of Surface Water in the Midst of a Region of Ongoing Subsidence

DONALD C. HELM
Nevada Bureau of Mines and Geology, c/o University of Nevada, Las Vegas, NV U.S.A. 89154 (On leave from the CSIRO Division of Geomechanics, Melbourne, Australia)

ABSTRACT Heave of up to 200 mm occurred during one year in the mid 1980's near the Loy Yang Settling Pond, Latrobe Valley, Australia, and in early 1987 was in the process of continuing. For nearly three decades, the surrounding valley has been subsiding due to ground-water withdrawal. Using the computer code COMPAC, model parameter values were found by back calculating the observed history of subsidence and heave. The histories of water-level fluctuations within four identifiable aquifer systems at the site were constructed from sparse field data and served as input to the model. For overconsolidated material, stress-dependent parameter values that control subsidence appear to control heave also. In 1987 predictions of heave were made based on four scenarios of future water-level patterns. Time lag of residual heave is significant. Recent field measurements tend to confirm predictions into 1990.

INTRODUCTION

Earth movement survey measurements around the Loy Yang Settling Pond in the Latrobe Valley near Melbourne, Australia, indicate that a net heave of up to 200 mm occurred locally between August 1985 and August 1986. This heave is anomalous because the surrounding region is subsiding in response to ground water withdrawals. It is believed that the local rise in land elevation is associated with a rise in potentiometric heads beneath the settling pond. The observed local tilting of the land surface is probably related to the local stratigraphy and geologic structure (such as a truncated anticline) and the resulting hydraulic connections between the settling pond and the underlying aquifers. The truncated clay and coal confining beds (separators) and the lenticular interbeds (aquitards) are overconsolidated due to greater loading in the geologic past. The State Electricity Commission of Victoria (SEC) enlisted the Commonwealth Scientific and Industrial Research Organization (CSIRO) to investigate the mechanisms that cause this anomolous heave and to predict future behavior. A one-dimensional computer code, COMPAC, was applied to the problem.

Subsidence due to fluid withdrawal is known to occur in the Latrobe Valley due to the withdrawal of ground water from aquifers at Morwell Open Cut and more recently at Loy Yang Open Cut. The computer code COMPAC has successfully simulated observed subsidence in the Latrobe Valley at a number of sites (Helm, 1984a). Based on one-dimensional nonlinear

consolidation theory, COMPAC models the vertical compression and expansion of heterogeneous beds whose compression can be either completely recoverable, completely nonrecoverable, or partly recoverable (Helm, 1976). Compression/expansion of both unconfined and confined aquifer systems can be modelled.

The available hydrogeological data (both surface and subsurface, near the settling pond and regional) were examined. Water-level measurements as a function of time within various aquifers were translated into input to the computer program. Back analysis of observed subsidence data served as the procedure for deriving model parameter values. These, in turn, were used for predictions of future heave and subsidence.

BACK ANALYSIS

The model is able to treat in situ measurements of stress changes and the resulting compression and/or expansion as constituting a type of field laboratory. Back analysis is used to estimate field-scale values of vertical hydraulic conductivity (K) and compressibility (either specific storage S_S or compression ratio CR2) at a site of interest. The compression ratio CR is defined by the slope of the strain (namely a change in thickness divided by the initial thickness) versus the base 10 logarithm of effective stress evaluated over one log cycle of stress. It is essentially a stress-dependent specific storage value. CR2 represents recompression or swelling for stresses less than past maximum (overconsolidated material). Before beginning the calibration phase, one must estimate the thickness and depth distribution of compressible beds and their degree of hydraulic connection. This is done by stratigraphic interpretation.

A major problem during the calibration phase is the nonuniqueness of parameter values. In other words, more than one combination of hydraulic conductivity and compressibility values might yield similar calculated results for subsidence versus time. This problem of nonuniqueness is discussed by Helm (1984b) and can be solved (Helm, 1977) under many field conditions by using zero-error curves. An example is given later in this report.

A primary requirement for back analysis is that the observed aggregate compression and expansion in the field must in fact be in a direct cause-and-effect relation to the observed water level fluctuations. The more precise the causal connection is between the stress and strain parts of the field data, the easier the analysis becomes and the more confident one is in making predictions.

STRATIGRAPHIC INTERPRETATION

Thickness of beds

Back analysis can determine only two parameters. It presupposes that thicknesses of beds are already determined by an independent method. If thicknesses are approximate or in error, then the values of K and CR2 which are found from simulation of observed subsidence are merely model

values and can not be expected to correspond closely to laboratory values. Fortunately, the model values of K and CR2 can partly compensate for possible mistakes in the approximation of the thickness values. These model parameter values may still be used effectively for predictive purposes at a site of interest if the stratigraphic interpretation remains unchanged.

For example, if 100 m of compressible slow-draining material is interpreted to lie within a heterogeneous aquifer system whose total thickness is 150 m then a corresponding value of CR2 or vertical S_s will emerge from back analysis of field data. If these 100 m comprise ten slow-draining interbeds (aquitards) with an average thickness of about 10 m, then a corresponding value of vertical K will emerge. By way of contrast, if the average thickness is interpreted to be only 2 m thick, then a smaller model value of K (for 50 equivalent beds) will emerge from the back analysis than would have emerged for the 10-m case. If case 1 is the true thickness distribution and the case 2 thickness distribution is erroneously assumed (or vice versa), a compensating error in K should be found from back analysis.

The interests of a subsidence modeller in interpreting stratigraphy is distinct from the interests of a ground-water modeller. The latter is interested in horizontal flow and sometimes for the sake of computational convenience lumps lenticular interbeds (aquitards) within an aquifer with semi-confining beds (separators) above and beneath the aquifer. For the modelling of subsidence (or vertical flow), it is important to distinguish between the behavior and thicknesses of aquitards and separators. Hence a subsidence modeller cannot uncritically borrow the stratigraphic simplifications implicit within a previously developed ground-water model.

Loy Yang Settling Pond site

Figure 1 shows a simplified interpretation of stratigraphy at a site near the Loy Yang Settling Pond. Land surface elevation is 58.8 m. A semi-confined upper aquifer lies between land surface and an elevation of 48 m. Only the lowest two m is sand. The upper eight m is clay. A separator lies between this aquifer system (called the unconformity aquifer) and the underlying Morwell 2B aquifer system. There is one 3-m-thick aquitard (isolated lens) within the Morwell 2B aquifer system. A second separator lies between the Morwell 2B and the Morwell 2C squifers. At this site the Morwell 2C aquifer system contains no aquitard. The thickest separator (No. 3) lies between the Morwell 2C aquifer system and the Traralgon aquifer system. The lowest member of the Traralgon aquifer system is a 40-m-thick clay sequence that lies directly on bedrock. The bedrock is interpreted to be impermeable. A single 12-m-thick aquitard lies within the upper 22 m portion of the Traralgon aquifer system.

WATER LEVEL INTERPRETATION

The history of water level fluctuations within the four main aquifers was constructed by the SEC from sparse data. The heads within the Morwell 2B, Morwell 2C and Traralgon aquifers are believed to have declined from approximately land surface elevation beginning some time during the late 1960's. Figure 2 shows the most reasonable pattern through the years based

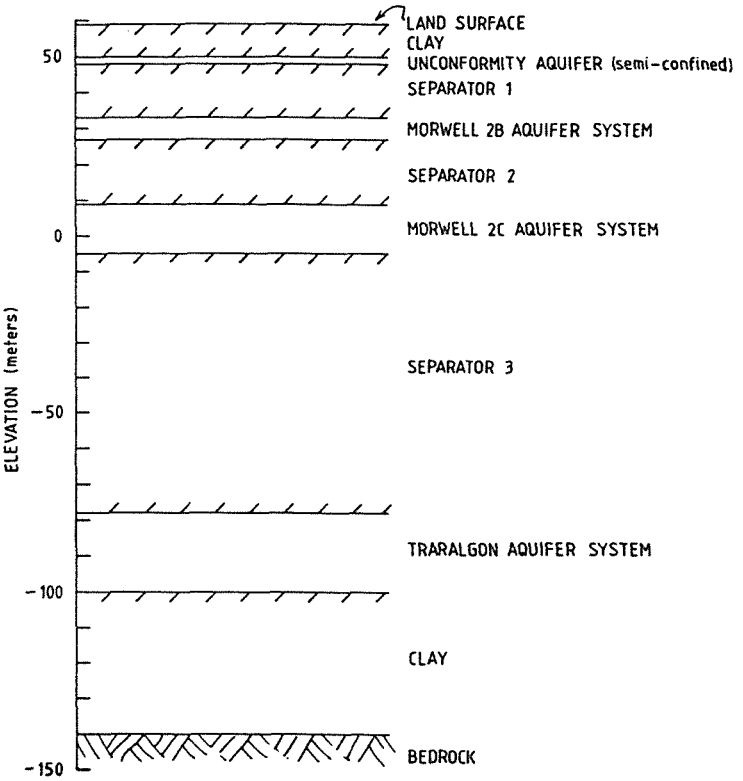

FIG. 1 Stratigraphic interpretation at Loy Yang Settling Pond.

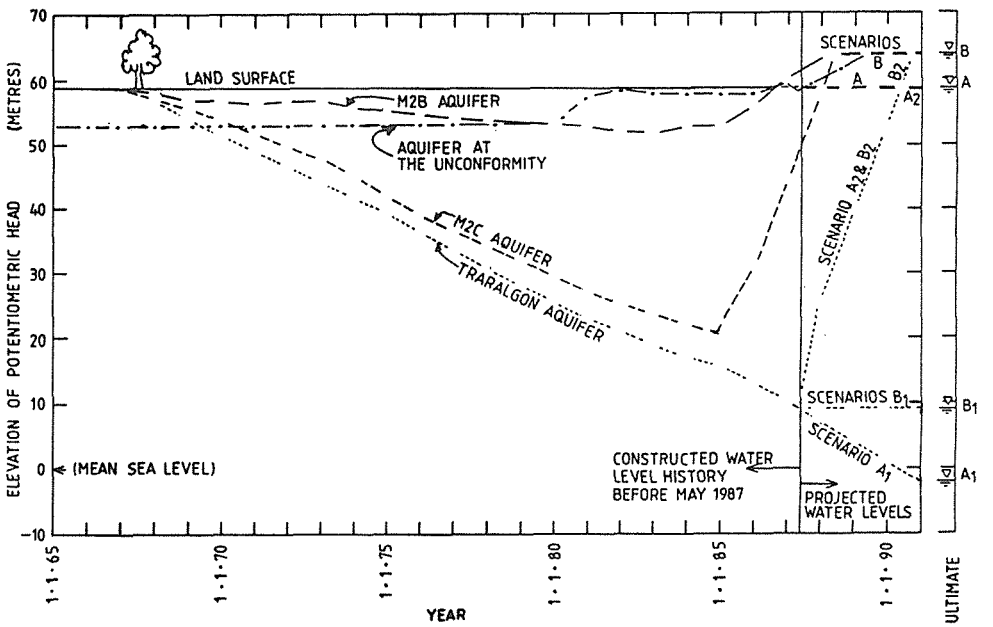

FIG. 2 Fluctuations of head within four aquifers.

on the best available evidence. Potentiometric head within the unconformity aquifer is believed to have started at a lower elevation and then to have risen during the early 1980's, probably in response to the impounding of surface water. The hydraulic head values prior to early 1987 were used as input to the computer code COMPAC. Time-dependent compression and expansion for eight hydraulic systems (Fig. 1) were calculated and summed.

ZERO-ERROR CURVES

Figure 3 shows a set of zero-error curves found by the calibration method described by Helm (1984b). Each individual curve in Fig. 3 signifies that by using any (K, CR2) value that falls along the curve, the calculated subsidence (between two specified dates) matches the observed subsidence between the same two dates. Hence any of an infinite number of parameter values (K, CR2) satisfies the required match for the specified two dates. Using several zero-error curves, rather than one, represents a method for overcoming the nonuniqueness problem. Zero-error curves A (representing the net observed land surface movement between 1965 and September 1979) and B (representing movement between September 1979 and May 1983) and D (between September 1985 and January 1987) converge near K = 2 x 10^{-3} m $year^{-1}$ and CR2 = 0.01.

Initially, zero error curve C (representing the net observed subsidence between May 1983 and September 1985) did not approach anywhere near

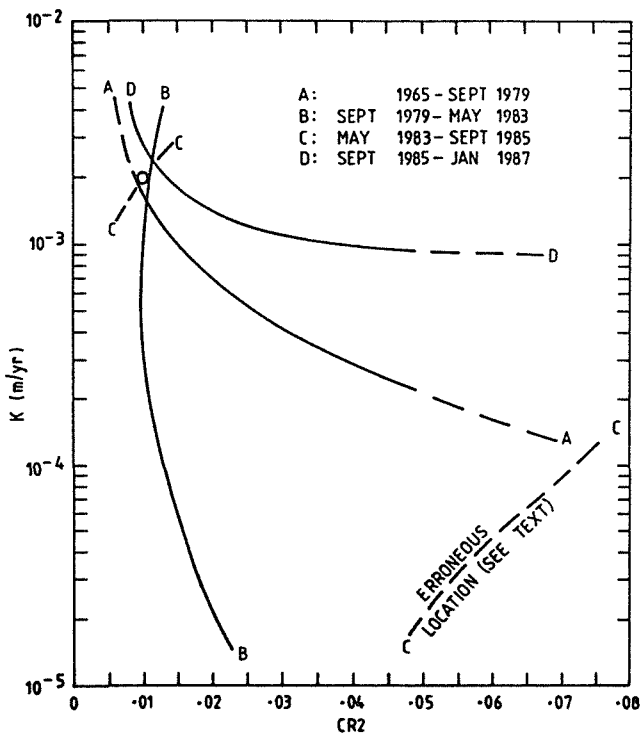

FIG. 3 Zero-error curves for Settling Pond analysis.

the part of (K,CR2) space where the other curves converged (Fig. 3). This prompted a careful look at the water-level measurements within all four aquifer systems between 1983 and 1985. It was found that a fortuitous cumulative rise in head of three m in the Morwell 2B aquifer had been accidentally estimated to have occurred between 1983 and 1985 (ref. to water-level measurements in observation wells 2003 and 2004). When correction to the input data was made, zero-error curve C passed also through the part of (K,CR2) space where curve B in Figure 3 intersects curves A and D. The diagnostic model values for CR2, therefore, lie between .008 and .012. The diagnostic model values for K lie between 1.5 x 10^{-3} and 2.3 x 10^{-3} m $year^{-1}$.

It should be pointed out that the zero error curves shown in Figure 3 are for the parameters of the slowly draining strata only. Ground-water flow within the more permeable (sand) members of each aquifer system is assumed to be horizontal. Hence within a vertical column, sand members are assumed to compress or expand instantaneously in response to the observed water level fluctuation. The model compressibility of sand members was found to equal 5 x 10^{-4} MPa^{-1} or about the compressibility of water.

SETTLEMENT AND HEAVE

Figure 4 shows the calculated subsidence (solid line) using the water-level data of Fig. 2 as input and the model K and CR2 values of 2 x 10^{-3} m $year^{-1}$ and 0.01 for all aquitards and semiconfining beds. The triangles between 1979 and January 1987 represent measured values. Those prior to 1979 are extrapolated from more distant measurements. The match between 1979 and 1987 is considered excellent.

The triangle at 1965 represents what the initial unperturbed elevation is estimated to have been. In other words, the actual cumulative total subsidence in 1979 is estimated to have been about 13% smaller than the calculated value. It is evident from curve A in Figure 3 that choosing a CR2 value between 0.008 and 0.009 instead of 0.01 would have matched the 1965 to 1979 period more accurately. However, for the selected K value, the match after 1979 would not have been as precise as the one plotted in Fig. 4. Alternatively, retaining a CR2 value of 0.01, one could decrease K from 2 x10^{-3} m $year^{-1}$ to 1.5 x 10^{-3} m $year^{-1}$ to match the 1965 to 1979 segment (curve A),

The same values of K and CR2 that yield a realistic settlement pattern as a function of time also yield a realistic pattern of heave during and after 1985.

TIME CONSTANTS

Based on the theory of consolidation, one can calculate a time constant for slow compression of saturated porous material. The time constant is the length of time required for a slowly draining bed to become 93% consolidated in response to an instantaneously induced stress at its boundary which is held constant thereafter.

The time constants for the various depth intervals control the time lags and residual subsidence (or heave). Using K and CR2 values of 2 x 10^{-3}

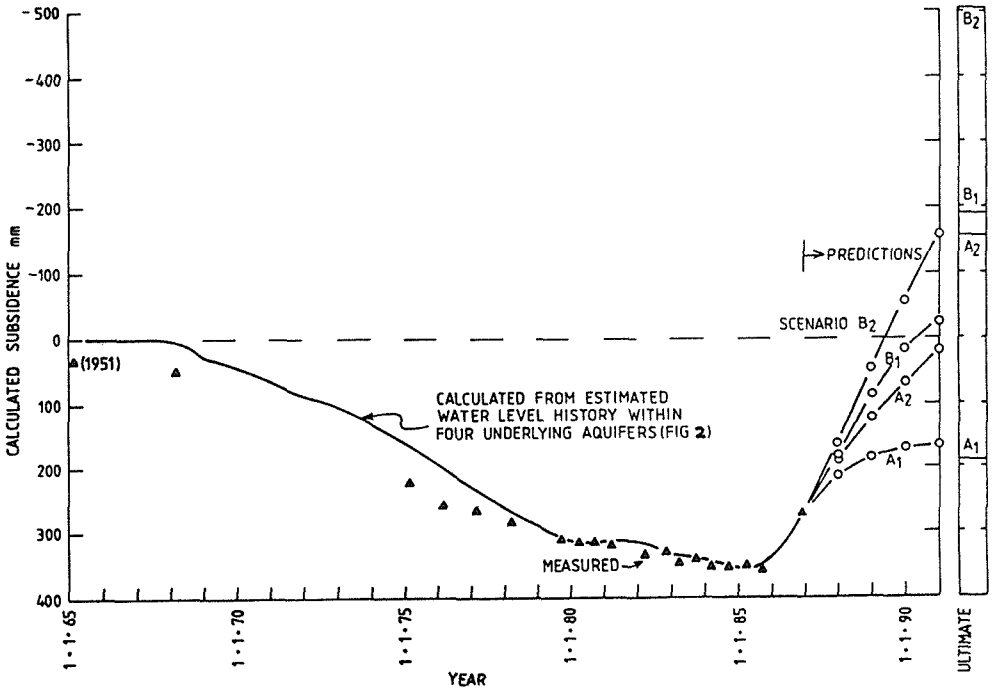

FIG. 4 1987 simulation and prediction of subsidence and heave based on four scenarios of future head fluctuations.

m year^{-1} and .001, the calculated time constant for the unconformity aquifer system is 37 years; for separator 1, it is 27 years; for the Morwell 2B aquifer system, it is 0.17 year; for separator 2, it is 17 years; for the Morwell 2C aquifer system, it is instantaneous; for separator 3, it is 116 years; for the top part of the Traralgon aquifer system, it is 0.53 year; for the lower clay member of the Traralgon system, it is 17 years.

1987 PREDICTION OF HEAVE

Once the model parameter values are determined from back calculation of observed field phenomena, prediction runs are straightforward. Four hypothetical scenarios for future ground-water development were devised by the SEC in 1987 (see Fig. 2) and prediction runs were made (Helm, 1987). Figure 4 shows the results. Scenarios A1 and A2 (Fig. 2) both require that after May 1987 the potentiometric heads within the upper three aquifer systems reach land surface elevation and remain constant thereafter. In scenario A1 the water level within the lowest aquifer system (namely, the Traralgon aquifer system) declines at a steady rate until about January 1991 and then it is held constant. In scenario A2 the potentiometric head within the Traralgon aquifer system rises to land surface joining those in the other three aquifer systems in 1990 and then remains constant. Figure 4 shows the predicted heave between 1987 and 1991 for scenarios A1 and A2. In scenario A1 the rate of heave decreases rapidly and may reach a maximum heave of about 200 mm above the 1985 maximum subsidence of 360 mm before settling ultimately back to a net heave of 163 mm above the 1985

value. In scenaro A2 the heave continues at a reasonably steady rate until the land surface ultimately reaches an elevation slightly greater than 500 mm above the 1985 level.

Scenarios B1 and B2 are "worst case" type of heave situations. The potentiometric heads within the upper three aquifer systems are required to rise swiftly to an elevation five m above land surface and thereafter to remain steady. For scenario B1 no change of the potentiometric head is allowed to occur within the lowest aquifer system (namely, the Traralgon aquifer system) after May 1987 (Fig. 2). For this latter scenario, the land surface is predicted to heave to its original (1965) elevation during 1990. It will continue to heave an additional 190 mm (about 545 mm above the early 1985 elevation) before reaching its ultimate value. For scenario B2 it is assumed that the head in the lowest aquifer system will rise to 5 m above land surface by late 1990 and remain constant thereafter. For this last case, an additional ultimate heave of 323 mm is calculated.

It is worth remarking that what causes a calculated net subsidence after 1991 in scenario A1 is caused by the slow draining beds within the Traralgon aquifer system and the lower portion of separator 3 (see Fig. 1). The upper several strata are calculated to register considerable expansion even for scenario A1.

Note that no change in stress is assumed to occur after January 1991. Hence the difference between the calculated 1991 value and the calculated ultimate value in Fig. 4 is the value of residual expansion due entirely to time lag (see the earlier section entitled Time Constant). It takes time for water to be absorbed into a system just as it takes time for water to be squeezed out of it. For practical design purposes one can reasonably assume that by the year 2020 the ultimate values listed in Fig. 4 will be reached.

1990 UPDATE ON EARLIER PREDICTIONS

Because the foregoing subsidence calculations include time as a function, predictions can be checked by commonly collected field data and when necessary can be updated. Water level and subsidencce measurements into 1990 are now available at the Loy Yang Settling Pond site and the 1987 predictions can thereby be checked. In three of the four idealized aquifers, the actual head fluctuations closely followed the previously assumed A1 scenario (see Fig. 2). The fluctuations in only the M2C aquifer deviated significantly from the A1 scenario by leveling off in 1987 and remaining constant at an elevation of about 48 m above mean sea level.

The solid-line curve in Fig. 5 shows the calculated (predicted) heave when the measured water-level fluctuations between 1987 and 1990 are used as input along with the K and CR2 parameter values of 2×10^{-3} m year^{-1} and 0.01 as shown in Fig. 3. The entire calculated heave is due to time lag of residual heave because no significant rise in water levels occurred during the period of interest. In fact the potentiometric head in the Traralgon aquifer system continued its long term gradual decline (about five m between May 1987 and May 1990).

The actual land surface movement is shown in Fig. 5 by triangles. Its pattern deviates from the predicted pattern in two distinct ways. A third curve (shown by circles) is plotted in Fig. 5 in order to help make the distinction between these two types of deviation. The third curve differs from measured data by a constant of 20 mm beginning with the first measurement in 1988. It illustrates that a sudden loss in land surface elevation occurred during late 1987. This loss of about 20 mm in elevation

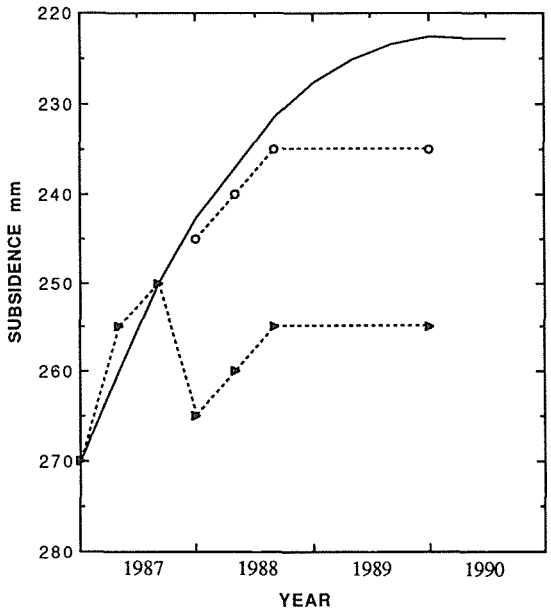

FIG. 5 Calculated heave (solid line), observed heave (triangles) and reconstructed heave (circles) after 1987.

cannot be accounted for by any manipulation of hydraulic parameter values. It would appear that the measured changes in potentiometric head are not what caused this one-time event.

The second deviation is that actual heave leveled off during late 1988, or slightly more than a year before it was predicted to occur. This means the model's time constants (which control the calculated time lag of residual heave) are too large. For a specified thickness of beds, the time constant can be decreased either by decreasing CR2 or by increasing K (or a combination of both). Decreasing the CR2 value from 0.01 to between 0.008 and 0.009 would have the double advantage of matching the 1965 unperturbed data point (discussed earlier) as well as having the calculated heave level off in early 1989. The circles in Fig. 5 can thereby be more closely matched by calculated heave.

It is encouraging that the behavior of highly heterogeneous material can be so closely simulated by a lumped parameter method. For over-consolidated beds it has been shown in this paper that the values which control subsidence can be used successfully to simulate heave. These values can in turn be fine-tuned as more data become available. For example, it has been found that the 1987 simulation using a CR2 value of 0.01 for predictive runs can be effectively improved by choosing instead a value between 0.008 and 0.009.

The SEC is able to quantify the gradual development of an "island" of heave as well as the surrounding "ocean" of ongoing subsidence for various future scenarios of water management. If preventative or ameliorative steps are eventually required to control ground movement, the SEC has a much improved idea of when, where, and how quickly these steps will need to be taken.

ACKNOWLEDGEMENTS The author gratefully acknowledges the subsidence research support of the State Electricity Commission of Victoria, both financial and technical. Information and suggestions given by Don Raisbeck and Ian Pedler were particularly helpful. The author would also like to thank the CSIRO for the opportunity to investigate subsidence related problems.

REFERENCES

Helm, D.C. (1976) One-dimensional simulation of aquifer system compaction near Pixley, California, 2, Stress-dependent parameters. Wat. Resour. Res. 12 (3), 375-391.

Helm, D.C. (1977) Estimating parameters of compacting fine-grained interbeds within a confined aquifer system by one-dimensional simulation of field observations. In: Land Subsidence (Procedings of the Anaheim Symposium, December 1976) 145-156. International Association of Hydrological Sciences Publ. no. 121.

Helm, D.C. (1984a) La Trobe Valley Subsidence Predictions: The Modeling of Time-Dependent Ground Movement due to Groundwater Withdrawal. Joint Publication of Fuel Dept. (DD195) and Design Engineering and Environment Dept. (GD9), 2 vols. State Electricity Commission of Victoria, Melbourne.

Helm, D.C. (1984b) Field-based computational techniques for predicting subsidence due to fluid withdrawal. In: Reviews in Engineering Geology, vol. VI, 1-22. Geological Society of America.

Helm, D.C. (1987) Mathematical simulation of heave associated with the storage of surface water. Internal Report 130. CSIRO Division of Geomechanics, Syndal, Victoria, Australia.

Land Subsidence (Proceedings of the Fourth International Symposium on Land Subsidence, May 1991). IAHS Publ. no. 200, 1991.

Solution of the One-Dimensional Consolidation Theory Equation with a Pseudospectral Method

N. SEPULVEDA
U. S. Geological Survey, Box 364424, San Juan, Puerto Rico 00936-4424

ABSTRACT The one-dimensional consolidation theory equation is solved for an aquifer system using a pseudospectral method. The spatial derivatives are computed using Fast Fourier Transforms and the time derivative is solved using a fourth-order Runge-Kutta scheme. The computer model calculates compaction based on the void ratio changes accumulated during the simulated periods of time. Compactions and expansions resulting from groundwater withdrawals and recharges are simulated for two observation wells in Santa Clara Valley and two in San Joaquin Valley, California. Field data previously published are used to obtain mean values for the soil grain density and the compression index and to generate depth-dependent profiles for hydraulic conductivity and initial void ratio. The water-level plots for the wells studied were digitized and used to obtain the time dependent profiles of effective stress.

Notation

a_v	aquifer matrix compressibility [$M^{-1}LT^2$]
C_c	compression index
c_w	water compressibility [$M^{-1}LT^2$]
$e(z,t)$	depth-dependent void ratio profile $(n(z,t)/(1-n(z,t)))$ at time t
f	dual variable of z in Fourier transforms
F, F^{-1}	Fourier and inverse Fourier transforms
g	acceleration due to gravity [LT^{-2}]
H_b	overburden thickness including the confining bed thickness [L]
H_0	pre-pumping or static water level in the observation well [L]
$K_z(e)$	hydraulic conductivity in the z direction, a function of e [LT^{-1}]
L	functional operator on $e(z,t)$
$n(z,t)$	depth-dependent porosity profile $(e(z,t)/(1+e(z,t)))$ at time t
$\overline{n}_b$	average porosity of the overburden, including the confining bed
$p(z,t), p_f(z,t)$	total pressure and fluid pressure [$ML^{-1}T^{-2}$]
$p_i(z,t)$	effective stress [$ML^{-1}T^{-2}$]
$s(t)$	drawdown [L]
S_s	specific storage [L^{-1}]
t	time [T]
z	coordinate in vertical direction (positive downwards) [L]
Γ	proportionality constant between K_z and e terms [LT^{-1}]
Δt	time step interval [T]
$\overline{\theta}_b$	average volumetric water content of the overburden
$\rho_f, \rho_s, \overline{\rho}_s$	fluid density, soil grain density, and average grain density [ML^{-3}]
$\overline{\rho}_{sb}$	average soil grain density of the overburden [ML^{-3}]

INTRODUCTION

The decline in artesian pressure in a confined aquifer system results in the increase of effective stress (intergranular pressure). An increase in effective stress causes the individual soil grain particles in fine-grained deposits to move relative to each other to produce a lower void ratio (Terzaghi & Peck, 1967), which in turn results in the compression and ultimate compaction of the granular medium. The resulting porosity decreases are related to the pore volume compressibility of the material, which depends on the effective stress and the void ratio. The compaction of sediment layers generally results in land subsidence. As the porosity is reduced, the aquifer system is reduced in volume by compaction, reducing the ability of the aquifer to store water (Green, 1964). Decreases in specific storage depend on the magnitude of the porosity decreases.

Helm (1975) simulated the one-dimensional (1-D) compaction of a series of confining units in an aquifer system by representing the vertical stress distribution within each unit with constant hydraulic conductivity and specific storage. This method was later extended to represent the vertical stress by time dependent hydraulic conductivity and specific storage values (Helm, 1976). In both studies, Helm (1975, 1976) linearized the consolidation equation as a simplification of the problem. The U.S. Geological Survey has developed a computer program to simulate compaction in an aquifer system using the finite-difference ground-water flow model (Leake & Prudic, 1988). This computer code provides a systematic way of accounting for all interbeds in an aquifer system that can contribute to the compaction process using water level data from the ground-water flow model.

The purpose of this paper is to present a pseudospectral method of solving the nonlinear 1-D consolidation theory equation. During the last two decades, spectral methods have been the subject of more research and development than either finite difference or finite element methods (Voigt et al., 1984). The pseudospectral method presented in this paper has been previously tested and used to solve an integro-differential system of partial differential equations (Sepúlveda, 1987). This method is more suited to handle the nonlinearities of the 1-D consolidation theory equation than the methods of finite differences or finite elements because it avoids the need to iteratively solve a large system of nonlinear equations. In the next section, the 1-D consolidation theory equation is presented and an expression for the effective stress as a function of depth z and time t is established. A numerical solution based on a pseudospectral method is explained after the formulation.

FORMULATION

Gibson et al. (1967) derived the 1-D partial differential equation that governs the spatial and temporal variations of void ratio for aquifer materials. This 1-D consolidation theory equation can be written as:

$$\frac{\partial e}{\partial t} = \left(\frac{\rho_s}{\rho_f} - 1\right)\frac{\partial}{\partial z}\left(\frac{K_z(e)}{(1+e)}\right) - \frac{1}{g\rho_f}\frac{\partial}{\partial z}\left(\frac{K_z(e)}{(1+e)}\frac{dp_i}{de}\frac{\partial e}{\partial z}\right) \tag{1}$$

In the derivation of equation (1), Darcy's law was assumed to be valid but was recast in a form in which the relative velocities of the aquifer skeleton and the pore fluid were related to the excess pore-fluid pressure gradient. The pore fluid and the soil grains were assumed to be incompressible, and the hydraulic conductivity was considered a function of void ratio. The dependence of K_z on the void ratio can be stated in the form:

$$K_z(e) = \Gamma\frac{e^3}{(1+e)} \tag{2}$$

which is a simplified version of the Kozeny-Carman equation (Lambe & Whitman, 1969). Changes in hydraulic conductivity brought about by changes in void ratio governed by equation (1) can be monitored using equation (2). For a deforming coordinate system fixed in the solid matrix, specific storage is defined as: $S_s = g\rho_f(nc_w + a_v)$ (Cooper, 1966), which could be expressed as: $S_s = g\rho_f(nc_w - de/dp_i)$ (Jorgensen, 1980). Thus, changes in specific storage also can be monitored from the void ratio solution of equation (1), because changes occurring in effective stress and void ratio will change the pore-volume compressibility of the fine-grained beds.

Terzaghi's laboratory results (Terzaghi & Peck, 1967) show that the relation between changes in void ratio and changes in the logarithm of effective stress (for sands, silts, and clays) is nearly linear. The assumption of linearity between these variables has been made in several subsequent studies (e.g. Lambe and Whitman, 1969; Helm, 1976; and Jorgensen, 1980). The slope of the linear section of the empirical e vs. $\log p_i$ curve defines the compression index C_c. The compression index C_c of an aquifer material can be expressed as:

$$C_c = -\ln 10\ p_i \frac{de}{dp_i} = -\frac{de}{d(\log p_i)} \approx \frac{e - e_0}{\log p_{i0} - \log p_i} \tag{3}$$

where e_0 and p_{i0} are fixed initial values. The substitution of equation (3) in equation (1) gives:

$$\frac{\partial e}{\partial t} = \left(\frac{\rho_s}{\rho_f} - 1\right)\frac{\partial}{\partial z}\left(\frac{K_z(e)}{(1+e)}\right) + \frac{\ln 10}{gC_c\rho_f}\frac{\partial}{\partial z}\left(\frac{K_z(e)p_i}{(1+e)}\frac{\partial e}{\partial z}\right) \tag{4}$$

where $K_z(e)$ is given by equation (2).

As can be seen from equation (4), an expression for p_i as a function of depth z is needed. As derived in Sepúlveda & Zack (1990), the total pressure p exerted at a point at distance z from the top of the artesian system is:

$$p(z,t) = gH_b\left\{(1-\overline{n}_b)\overline{\rho}_{sb} + \overline{\theta}_b\rho_f\right\} + g\int_0^z \left\{(1-n(z))\rho_s + n(z)\rho_f\right\} dz \tag{5}$$

The line $z = 0$ is the bottom of the uppermost confining bed of the artesian system. The coordinate z is assumed to increase downward. The uppermost confining bed properties should be taken into account when the $\overline{\rho}_{sb}$, $\overline{\theta}_b$, and $\overline{n}_b$ values are averaged throughout the overburden.

If $z = -H_0$ is the height of the water column in the observation well referenced to the top of the artesian aquifer, then the fluid pressure at point z can be expressed as:

$$p_f(z,t) = g\rho_f\left(H_0 + z - s(t)\right) \tag{6}$$

where $s(t)$ is the drawdown and H_0 is assumed to be constant. Positive drawdown denotes a decline in fluid pressure. The fluid pressure is a function of time because the drawdown is time dependent. Based on the principle of effective stress, p_i at point z and time t can be computed subtracting equation (6) from equation (5):

$$p_i(z,t) = p_{i0} + g\rho_f s(t) + g(\overline{\rho}_s - \rho_f)\int_0^z (1-n(z))\,dz \tag{7}$$

where $p_{i0} = gH_b\{(1-\overline{n}_b)\overline{\rho}_{sb} + \overline{\theta}_b\rho_f\} - g\rho_f H_0$ represents the effective stress at the line $z = 0$ when the water level is located H_0 meters above $z = 0$. The values of p_{i0} and C_c were chosen to be constant in time and independent of depth. The values of $\overline{\rho}_s$ and C_c were obtained by averaging the soil grain density and the compression index data over the thickness of the layer being studied.

NUMERICAL SOLUTION

If the Fourier transform of $n(z)$ is denoted by:

$$\hat{n}(f) = F(n) = \frac{1}{\sqrt{2\pi}} \int_{-\infty}^{+\infty} e^{2\pi i f z}\ n(z)\ dz \tag{8}$$

and its inverse by:

$$F^{-1}(\hat{n}) = \frac{1}{\sqrt{2\pi}} \int_{-\infty}^{+\infty} e^{-2\pi i f z}\ \hat{n}(f)\ df \tag{9}$$

then equation (4) can be Fourier transformed to obtain:

$$\frac{\partial e}{\partial t} = \left(\frac{\rho_s}{\rho_f} - 1\right) F^{-1}\left\{2\pi i f F\left\{\frac{K_z(e)}{(1+e)}\right\}\right\} - \frac{4\pi^2 \ln 10}{g C_c \rho_f} F^{-1}\left\{f F\left\{\frac{K_z(e) p_i}{(1+e)} F^{-1}\left(f F(e)\right)\right\}\right\} \tag{10}$$
$$\equiv L(e)$$

The time derivative in equation (10) was solved using a fourth-order Runge-Kutta scheme (Canuto et al., 1988). If $e(z, t_n)$ denotes the void ratio profile at time $t = t_n$ then the evolution of this $e(z, t_n)$ profile at time $t = t_{n+1}$, denoted by $e(z, t_{n+1})$, can be obtained by executing the following steps in the given order:

$$e_1(z) = e(z, t_n) + \frac{\Delta t}{2} L(e(z, t_n)) \tag{11}$$

$$e_2(z) = e(z, t_n) + \frac{\Delta t}{2} L(e_1(z)) \tag{12}$$

$$e_3(z) = e(z, t_n) + \Delta t\, L(e_2(z)) \tag{13}$$

$$e(z, t_{n+1}) = e(z, t_n) + \frac{\Delta t}{6}\left(L(e(z, t_n)) + 2\,L(e_1(z)) + 2\,L(e_2(z)) + L(e_3(z))\right) \tag{14}$$

where $\Delta t = t_{n+1} - t_n$ and $e_1(z)$, $e_2(z)$ and $e_3(z)$ are intermediate steps between the $e(z, t_n)$ and the $e(z, t_{n+1})$ profiles.

The function L in the scheme shown above, defined by equation (10), was computed using two Fast Fourier Transforms (FFT) (Cooley et al., 1969) for the first term on the right-hand side and four FFT's for the second term. The combination of this Runge-Kutta scheme to solve the evolution problem and the FFT technique to solve the spatial derivatives is an example of a pseudospectral method (Canuto et al., 1988). Throughout the numerical calculations, the z-coordinate was discretized uniformly, i.e., $\Delta z = z_{i+1} - z_i = 0.5$ meter, and was constant for each well studied. The value of $\Delta t = 0.005$ year, was chosen to be constant for all runs. The number of points used in the FFTs, a power of two, was 1024. The remaining points were filled with exponential decay to zero for void ratio to satisfy the periodic solution assumption (Voigt et al., 1984) inherent to a pseudospectral method.

APPLICATION OF METHOD

Specific clay and silt layers from two observation wells in Santa Clara Valley (7S/1E-16C6 and 6S/2W-24C7) and two in San Joaquin Valley, California (16/15-34N1 and 23/25-16N1) were chosen to test the numerical scheme presented here. The mean values used for $\overline{n}_b$, $\overline{\rho}_{sb}$, and $\overline{\theta}_b$ were taken from Johnson et al. (1968). Laboratory values of K_z (while simulating appropriate overburden stresses) and e were used to generate their profiles needed to solve (4). A cubic spline interpolant

(Akima, 1970) was used to generate the continuous void ratio and hydraulic conductivity profiles from the data listed in Johnson et al. (1968). This assured the profiles had a continuous derivative, which was required by equation (4). The effective stress profile was generated from equation (7).

The water level data needed in equation (7) were obtained by digitizing the hydrographs for the respective wells (Figs. 1-2). Hydrographs for wells 7S/1E-16C6 and 6S/2W-24C7 in Santa Clara Valley (Fig. 1) were obtained by digitizing Figures 40A and 38A from Poland & Ireland (1988), respectively.

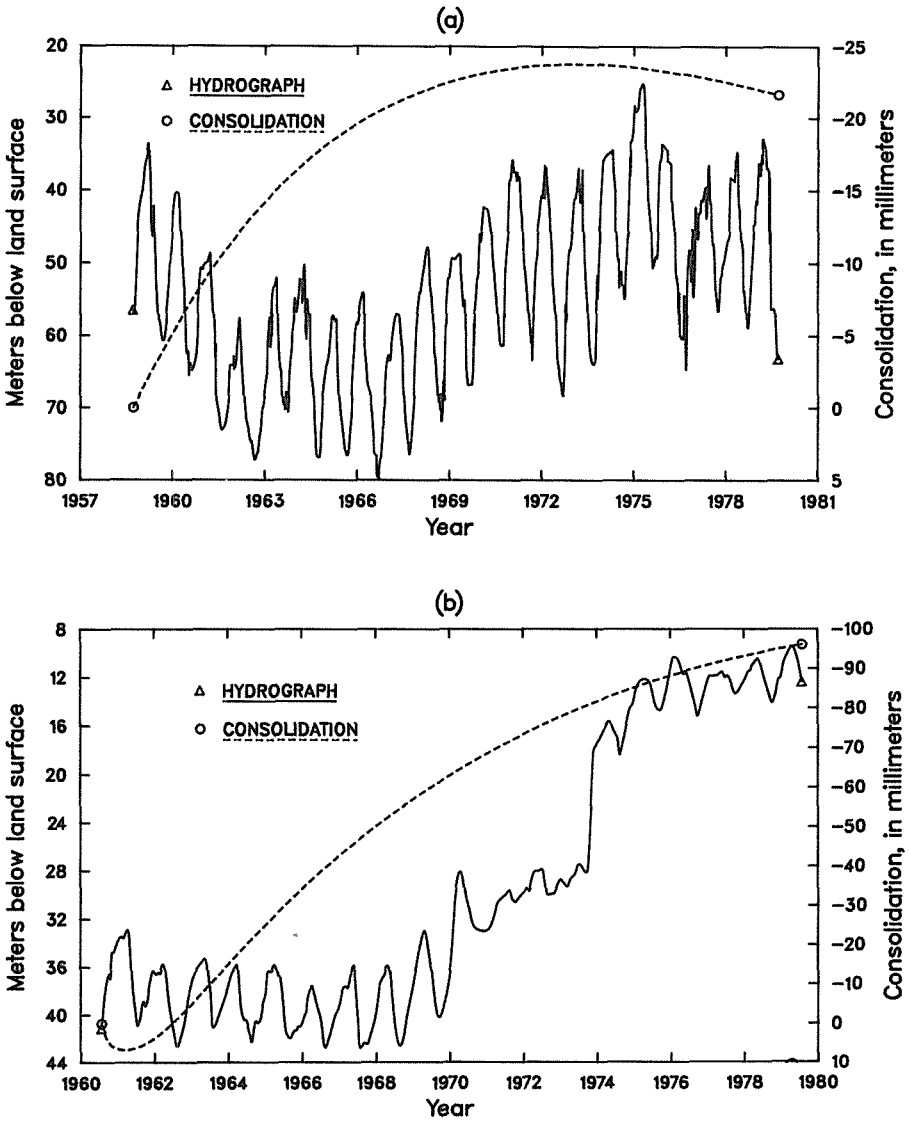

FIG. 1 Water levels and consolidation of a confining layer for wells (a) 7S/1E–16C6 and (b) 6S/2W–24C7 in Santa Clara Valley, California.

The hydrographs for wells 16/15-34N1 and 23/25-16N3 in San Joaquin Valley (Fig. 2) were obtained by digitizing Figures 49A and 58A from Ireland et al. (1984), respectively. Water levels are indicated in figures 1 and 2 by a continuous line. The assumption of constant compression index C_c made here has the effect of uniformly smoothing the depth-dependent initial void ratio profile. This effect occurs during the early periods of the simulation and is noticed in figures 1 and 2, where the water levels do not drive the consolidation curve. As time increases, the effects of a constant compression index C_c are less evident and the water levels drive the consolidation curve.

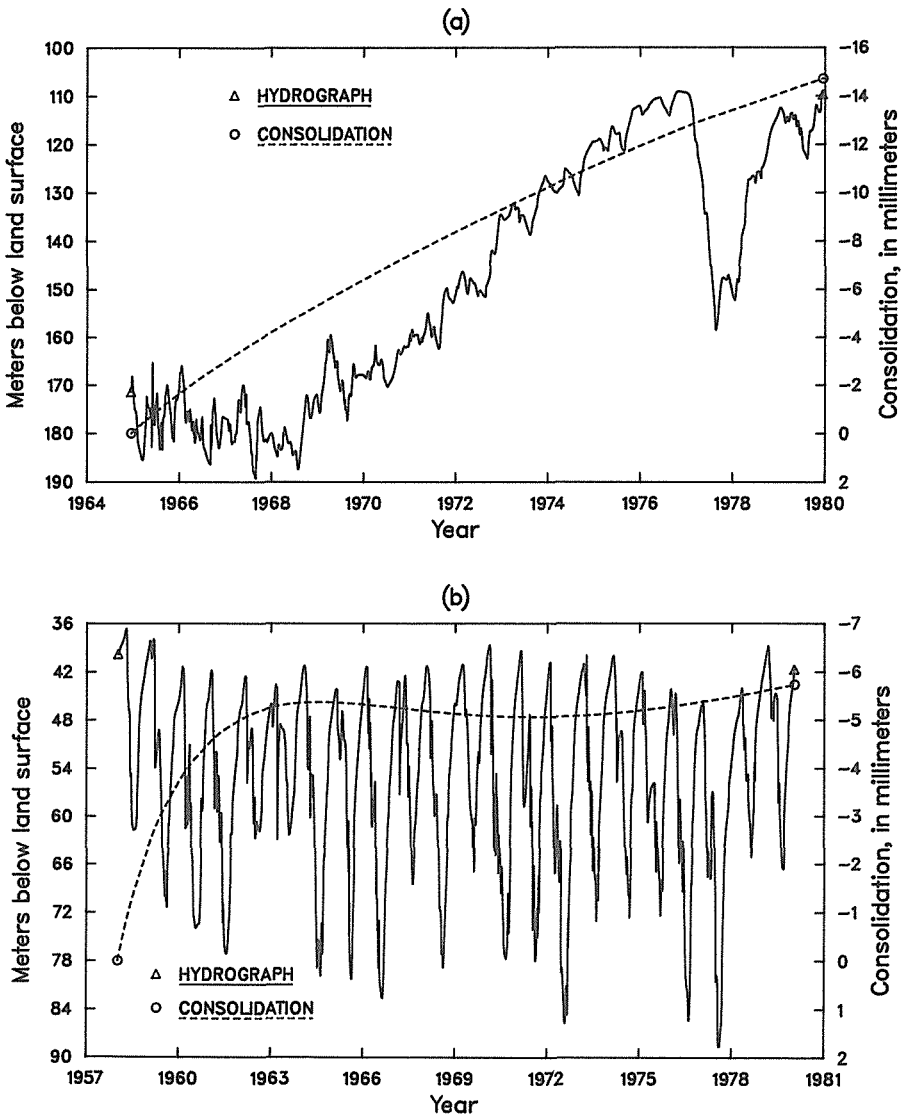

FIG. 2 Water levels and consolidation of a confining layer for wells (a) 16/15–34N1 and (b) 23/25–16N1 in San Joaquin Valley, California.

The water level data were used to compute the drawdown $s(t)$, which in turn was used to compute $p_i(z,t)$ from equation (7) for the time period simulated. The same water levels were assumed for all depth values at a given time because of the lack of information on water level variations with depth. The depth range (in meters) of the fine-grained layers, the initial effective stress (in mega Pascals) calculated from equation (7) at the top of the layer, the average value of the aquifer matrix grain density (in kilograms per cubic meter), the average compression index, and the simulated time period for the four wells studied are shown in Table 1. These data were derived from Johnson et al. (1968).

TABLE 1 Data Used in the Computer Simulation.

Well Number	Depth	p_i	$\bar{\rho}_s$	C_c	Time Period
7S/1E-16C6	144.2 - 177.2	2.112	2747.8	0.2417	09/58 - 09/79
6S/2W-24C7	100.0 - 127.0	1.474	2724.0	0.2616	07/60 - 07/79
16/15-34N1	272.8 - 297.8	2.572	2672.3	0.3485	12/64 - 12/79
23/25-16N1	171.7 - 200.7	1.958	2688.2	0.2814	01/58 - 01/80

The pseudospectral method presented here was tested and the numerical error was estimated by comparing the simulated compaction results of a special case problem with its analytical solution. If $K_z(e) = a(1+e)^2$ for a positive constant a is assumed, if $\partial s/\partial z = +1$, and if, in addition, $e(z,0) = e_o(z)$ is the initial void ratio profile for a given clay layer, then equation (1) has the analytical solution $e(z,t) = e_o(z + at(\rho_s/\rho_f - 2))$. This is a direct consequence of the solution of a one-dimensional linear hyperbolic partial differential equation. The initial void ratio profile $e_o(z)$ was assumed to be given by:

$$e_o(z) = e_f \exp\left\{\ln\left(\frac{e_i}{e_f}\right)\left(\frac{H-z}{H}\right)\right\} \tag{15}$$

where $z = 0$ and $z = H$ are the upper and lower boundaries of this hypothetical clay layer, respectively. The corresponding initial void ratio values at $z = 0$ and $z = H$ are e_i and e_f. A comparison of analytical with simulated compaction results for this case showed that the largest numerical void ratio error, for a time period of 22 years, was found to be 0.001.

The predicted consolidation of fine-grained layers within the artesian aquifer system is shown along with the hydrographs for wells 7S/1E-16C6, 6S/2W-24C7, 16/15-34N1, and 23/25-16N1 in figures 1 and 2. As effective stress decreases, shown by increases in water levels, expansion occurs within the sediment layers. Expansion is shown as negative consolidation whereas compaction is positive. The amount of compaction or expansion, determined according to Green (1964), applies to specific depth ranges within the wells where clay and silt were abundant.

The void ratio profiles for well 7S/1E-16C6 at the beginning and at the end of the simulation period are shown in Figure 3a. The area between the curves is proportional to the expansion during that period of time. Inflection points from the initial void ratio profile are eliminated through the simulated period. This is due to the assumption of constant compression index C_c. Other interpolation techniques could be used to generate the initial void ratio profile; however, with the data available, the cubic spline interpolant seemed the most natural approach. The definition of the initial void ratio profile increases as the amount of field data available increases. Figure 3b shows the variations in the hydraulic conductivity profiles for well 7S/1E-16C6. Changes in K_z (due to

changes in void ratio during the simulation) were computed from equation (2) where Γ was assumed to be constant in time. The hydraulic conductivity changes during the computer simulation will depend on the relation assumed between K_z and the void ratio. However, the magnitude of these changes does not vary considerably when variations of equation (2) are used.

The magnitude of the hydraulic conductivity values in a given layer of the aquifer will determine the time step required to satisfy the stability requirement of the pseudospectral method. The stability condition for the pseudospectral method presented here becomes more restrictive as the hydraulic conductivity

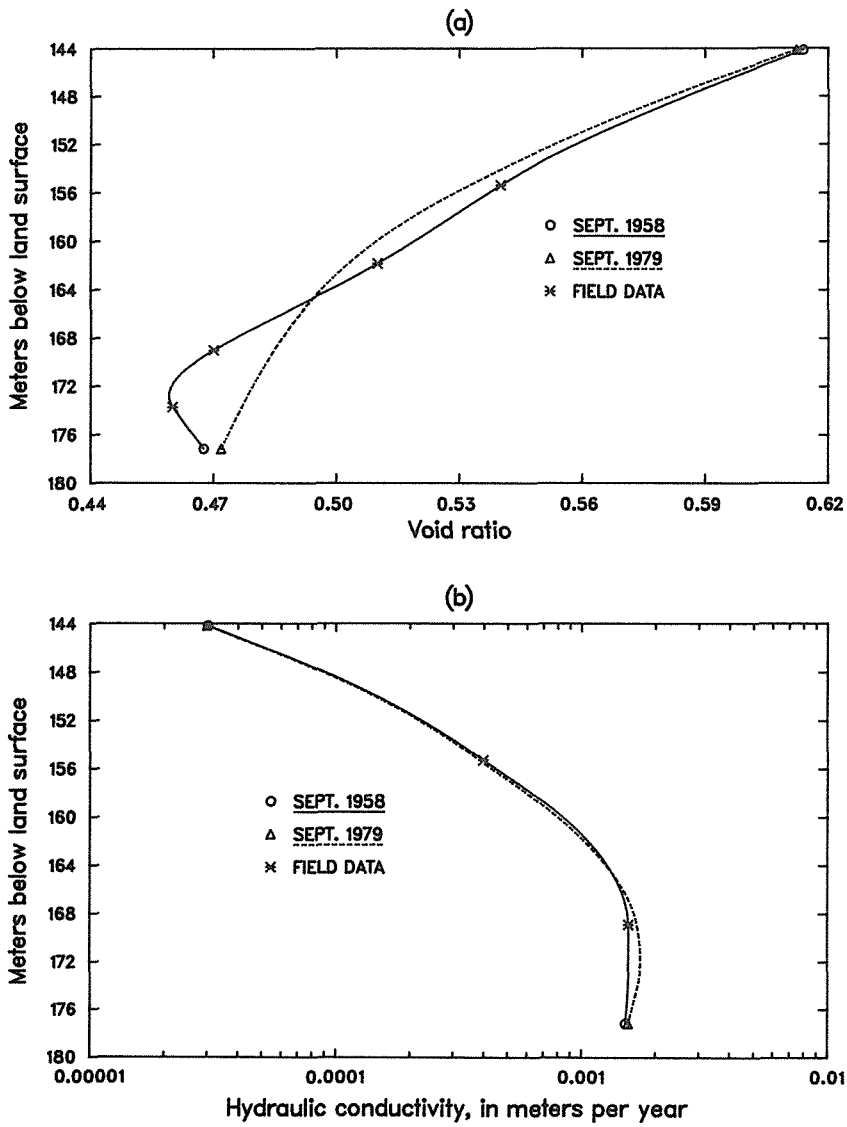

FIG. 3 (a) Void ratio and (b) hydraulic conductivity profiles for well 7S/1E–16C6 in Santa Clara Valley, California.

of the layer increases. This limits the depth ranges to which the method can be applied within the artesian aquifer system because K_z could differ by several orders of magnitude in a given section of the aquifer. However, the method presented here, based on the numerical solution of equation (1), can be used to simulate compaction or expansion at all depths in an aquifer system by treating each appropriate layer separately.

FUTURE WORK

The periodic solution assumption inherent in the pseudospectral method presented in this paper is based on the periodicity assumed by the FFT technique. This resulted in a need to use a domain of integration in depth sixteen times larger than the one occupied by the layers under study. This, in turn, increased the computing time. This could be avoided if a spectral method like Chebyshev's method is implemented (Gottlieb & Orszag, 1977).

At the present time, the computer code developed to implement this method can only simulate compaction and expansion of individual layers of sediment. The code needs to be expanded to cover the entire thickness of the artesian aquifer system. The value of C_c in equation (3) is assumed to be constant and unaffected by changes in effective stress. In reality, however, C_c decreases as water levels rise and the effective stress decreases. The method presented here can be used to solve equation (4) with variable C_c.

ACKNOWLEDGMENT

This research was partially funded by the Puerto Rico Aqueduct and Sewer Authority.

REFERENCES

Akima, H. (1970) A new method of interpolation and smooth curve fitting based on local procedures. J. of the ACM 17, 589-602.

Canuto, C., Hussaini, M. Y., Quarteroni, A. & Zang, T. A. (1988) Spectral Methods in Fluid Dynamics. Springer-Verlag, New York.

Cooley, J. W., Lewis, P. A. W. & Welch, P. D. (1969) The Fast Fourier Transform and its applications. IEEE Trans. on Education 12-1, 27-34.

Cooper, H. H. Jr., (1966) The equation of groundwater flow in fixed and deforming coordinates. J. Geophysical Res. 71 (20), 4785-4790.

Gibson, R. E., England, G. L. & Hussey, M. J. L. (1967) The theory of one-dimensional consolidation of saturated clays, 1. Finite non-linear consolidation of thin homogeneous layers. Geotechnique 17 (2), 261-273.

Gottlieb, D. & Orszag, S. A. (1977) Numerical analysis of spectral methods: Theory and applications. Society for Industrial and Applied Mathematics, Philadelphia.

Green, J. H. (1964) The effect of artesian-pressure decline on confined aquifer systems and its relation to land subsidence. USGS Wat. Supply Pap. 1779-T.

Helm, D. C. (1975) One-dimensional simulation of aquifer system compaction near Pixley, California 1. Constant parameters. Wat. Resour. Res. 11 (3), 465-478.

Helm, D. C. (1976) One-dimensional simulation of aquifer system compaction near Pixley, California 2. Stress-dependent parameters. Wat. Resour. Res. 12 (3), 375-391.

Ireland, R. L., Poland, J. F. & Riley, F. S. (1984) Land subsidence in the San Joaquin Valley, California, as of 1980. USGS Prof. Pap. 437-I.

Johnson, A. I., Moston, R. P. & Morris, D. A. (1968) Physical and hydrologic properties of water-bearing deposits in subsiding areas in Central California. USGS Prof. Pap. 497-A.

Jorgensen, D.G. (1980) Relationships between basic soils-engineering equations and basic ground-water flow equations. USGS Wat. Supply Pap. 2064.

Lambe, T. W. & Whitman, R. V. (1969) Soil Mechanics. Wiley, New York.

Leake, S. A. & Prudic, D. E. (1988) Documentation of a computer program to simulate aquifer-system compaction using the modular finite-difference ground-water flow model. USGS Open-File Rep. 88-482.

Poland, J. F. & Ireland, R. L. (1988) Land subsidence in the Santa Clara Valley, California, as of 1982. USGS Prof. Pap. 497-F.

Sepúlveda, N. (1987) Solitary waves in the resonant phenomenon between a surface gravity wave packet and an internal gravity wave. Phys. Fluids 30 (7), 1984-1992.

Sepúlveda, N. & Zack A. (1990) Laboratory simulation of the effects of overburden stress on the specific storage of shallow artesian aquifers. Tropical Hydrology and Caribbean Water Resources, American Water Resources Association TPS-90-2, San Juan, Puerto Rico, 349-356.

Terzaghi, K. & Peck, R.B. (1967) Soil Mechanics in Engineering Practice. 2nd ed., Wiley, New York.

Voigt, R. G., Gottlieb, D. & Hussaini, M.Y., eds. (1984) Spectral Methods for Partial Differential Equations. Society for Industrial and Applied Mathematics, Philadelphia.

Land Subsidence (Proceedings of the Fourth International Symposium on Land Subsidence, May 1991). IAHS Publ. no. 200, 1991.

Simulation of Vertical Compaction in Models of Regional Ground-Water Flow

S. A. LEAKE
U.S. Geological Survey, Tucson, Arizona, U.S.A.

ABSTRACT A new computer program was developed to simulate vertical compaction in models of regional ground-water flow. The program accounts for ground-water storage changes and compaction in discontinuous interbeds or in extensive confining beds. The new program is a package for the U.S. Geological Survey modular finite-difference ground-water flow model. Several features of the program make it useful for application in shallow unconfined flow systems. Geostatic load can be treated as a function of water-table elevation, and compaction is a function of computed changes in effective stress at the center of a model layer. Thickness of compressible sediments in an unconfined model layer can vary in proportion to saturated thickness. The new package was tested by comparison with an existing model of one-dimensional compaction.

INTRODUCTION

Digital models of ground-water flow are widely used tools to study the response of regional aquifer systems to pumping stress. For aquifer systems that include compressible fine-grained interbeds (Fig. 1), existing model programs have been modified to account for release of water from compacting interbeds and to compute resulting compaction[1] and land subsidence (Meyer & Carr, 1979; Williamson et al., 1989; Leake & Prudic, 1988). These computer programs keep track of head at which preconsolidation stress will be exceeded (preconsolidation head). Values of elastic or inelastic storage coefficients are selected on the basis of a relation between head in a model cell and the preconsolidation head. The programs are based on the assumption that elastic and inelastic skeletal specific-storage values are constant and that a unit decline in head results in a unit increase in effective stress.

Such assumptions may be appropriate for analyses of compaction in deep confined aquifer systems but are inappropriate for shallow unconfined systems. This paper extends previous models by presenting a method for simulating aquifer-system compaction in models that include unconfined ground-water flow. A computer program developed to test this approach expands on the earlier work by Leake & Prudic (1988). The program works as a part of the modular finite-difference ground-water flow model (also called MODFLOW) by McDonald & Harbaugh (1988).

Several previous programs have incorporated stress-dependent storage properties. One of the programs is COMPAC1 by Helm (1976). This program simulates compaction in

[1]In this paper, the term "compaction" refers to a decrease in thickness of sediments as a result of increase in vertical compressive stress. The identical physical process is referred to as "consolidation" by soils engineers.

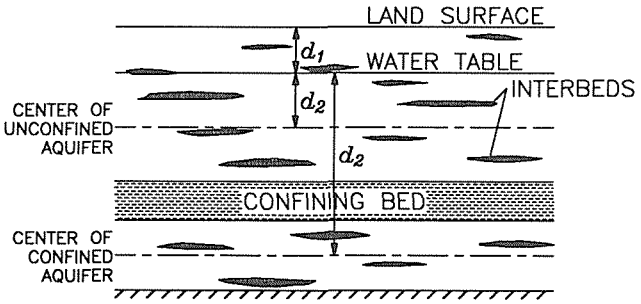

FIG. 1 Distances used for computing geostatic load for upper unconfined aquifer and lower confined aquifer.

compressible beds with specified stress changes at the boundaries. Another program, FLUMPS, by Neuman et al. (1982) is a finite-element ground-water flow model that calculates compaction of confining beds between model layers.

RELATION OF COMPACTION TO CHANGES IN EFFECTIVE STRESS

To incorporate calculations of compaction into ground-water flow models, a relation between compaction and change in effective stress must be established. The development of a relation presented here is based on the Terzaghi theory of vertical consolidation. Compaction (consolidation) occurs when effective stress or grain-to-grain load increases. According to the Terzaghi relation, effective stress, σ', is the difference between geostatic load, σ, and pore pressure, u. These quantities are commonly expressed in terms of force per unit area but may be expressed in terms of height of a column of water by dividing the quantities by the unit weight of water, γ_w. For many sediments, void ratio, e, decreases linearly with increase in logarithm of effective stress. The relation is:

$$\Delta e = -C_c \, \Delta \log_{10} \sigma' \qquad \sigma' > \sigma'_c \tag{1a}$$

$$\Delta e = -C_r \, \Delta \log_{10} \sigma' \qquad \sigma' \leq \sigma'_c \tag{1b}$$

where C_c and C_r are the dimensionless compression and recompression indices and σ'_c is preconsolidation stress. From empirical studies, C_c is much larger than C_r. Equation 1a is valid for increases in σ' beyond σ'_c and resulting reductions in e are permanent or inelastic compaction. Changes in e described by equation 1b result in elastic compaction or expansion.

Compaction, Δb, is related to changes in void ratio by the expression:

$$\Delta b = -\frac{b_0}{1+e_0} \Delta e \tag{2}$$

where b_0 is initial thickness and e_0 is initial void ratio. The sign convention for Δb as used in this paper is positive for compaction and negative for expansion. Inelastic compaction, Δb_i, and elastic compaction, Δb_e, can be computed by combining equations 1 and 2 and using the relation $\Delta \log_{10} \sigma' = 0.434 \, \Delta \sigma' / \sigma'$. Those expressions are:

$$\Delta b_i = \frac{0.434\ b_0\ C_c\ \Delta\sigma'}{(1+e_0)\ \sigma'} \tag{3a}$$

$$\Delta b_e = \frac{0.434\ b_0\ C_r\ \Delta\sigma'}{(1+e_0)\ \sigma'} \tag{3b}$$

According to Leake & Prudic (1988), Δb_i and Δb_e are related to $\Delta\sigma'$ by:

$$\Delta b_i = \frac{S_{skv}\ b_0}{\gamma_w}\Delta\sigma' \tag{4a}$$

$$\Delta b_e = \frac{S_{ske}\ b_0}{\gamma_w}\Delta\sigma' \tag{4b}$$

where S_{skv} and S_{ske} are inelastic and elastic skeletal specific-storage values, respectively. Equations 3 and 4 imply that S_{skv} and S_{ske} can be expressed as:

$$S_{skv} = \frac{0.434\ C_c\ \gamma_w}{\sigma'\ (1+e_0)} \tag{5a}$$

$$S_{ske} = \frac{0.434\ C_r\ \gamma_w}{\sigma'\ (1+e_0)} \tag{5b}$$

Equation 5a is consistent with expressions given by Helm (1976), Jorgensen (1980), and Neuman et al. (1982). Note that specific storage is inversely related to effective stress. For deep sediments, σ will be large and changes in u resulting from ground-water pumping are not likely to make large percentage changes in σ'. For that case, S_{skv} and S_{ske} can be treated as constants with little resulting error. On the other hand, for shallow sediments where σ' is relatively small, changes in u could result in relatively large percentage changes in σ'.

For this study, equations 3a and 3b are the basic relations between compaction and $\Delta\sigma'$. These equations can be combined into a general expression for compaction or expansion of sediments, Δb, between times t_{n-1} and t_n as follows:

$$\Delta b = \frac{0.434\ b_0}{(1+e_0)\ \sigma'}\left[C_n\left(\sigma'_n-\sigma'_{c,n-1}\right) + C_r\left(\sigma'_{c,n-1}-\sigma'_{n-1}\right)\right] \qquad C_n = \begin{cases} C_c\ , & \sigma'_n > \sigma_{c,n-1} \\ C_r\ , & \sigma'_n \le \sigma_{c,n-1} \end{cases} \tag{6}$$

where σ'_{n-1} and σ'_n are effective-stress values at times t_{n-1} and t_n, and $\sigma'_{c,n-1}$ is the preconsolidation-stress value at time t_{n-1}. Note that the relation of σ'_n to $\sigma'_{c,n-1}$ is used to select the value of C_n as C_c or C_r. The expression gives correct results for overconsolidated sediments, for normally consolidated sediments, and for sediments in transition from overconsolidation to normal consolidation.

INCORPORATING COMPACTION AND STORAGE CHANGES IN THE MODEL

The ground-water flow model (MODFLOW) by McDonald & Harbaugh (1988) is a modular computer program designed to allow addition of features without extensive modification of the

existing program. Each new feature is called a model package. For this study, a new Interbed-Storage package (IBS3) was developed. Previous interbed-storage packages are described by Leake & Prudic (1988) and Leake (1990).

The MODFLOW program solves a form of the three-dimensional ground-water flow equation:

$$\frac{\partial}{\partial x}\left(K_{xx}\frac{\partial h}{\partial x}\right) + \frac{\partial}{\partial y}\left(K_{yy}\frac{\partial h}{\partial y}\right) + \frac{\partial}{\partial z}\left(K_{zz}\frac{\partial h}{\partial z}\right) - W = S_s\frac{\partial h}{\partial t} \tag{7}$$

where x, y, and z are cartesian coordinates, aligned along the major axes of the hydraulic-conductivity tensor; K_{xx}, K_{yy}, and K_{zz} are principal components of the hydraulic-conductivity tensor; h is hydraulic head; W is volumetric flux per unit volume of sources and (or) sinks of water; S_s is specific storage of the aquifer; and t is time. To treat S_s as a scaler implicitly requires skeletal compressibility to be isotropic (Helm, 1987). Equation 7 is approximated with finite differences. The finite-difference equations are written in terms of volumetric flow rather than flow per unit volume. For model layers with a water table, values of horizontal hydraulic conductivity are multiplied by head so that the product, transmissivity, is a function of saturated thickness. Also for water-table layers, the specific yield of the aquifer is used in the storage term on the right side. As such, the storage term in the finite-difference equation approximates the rate of flow to or from storage at the water table.

To simulate compaction and storage changes in MODFLOW, an expression is added to the finite-difference equations to account for resulting rate of flow into or out of the compressible interbeds. The expression to be added to MODFLOW is derived from equation 6; however, because MODFLOW uses hydraulic head as a dependent variable, equation 6 must be rewritten. This is accomplished by using the Terzaghi relation $\sigma'_n = \sigma_n - u_n$. Pore pressure, u_n, can be expressed as $u_n = (h_n - z)\gamma_w$, where h_n is total head and z is elevation head. Substituting these two relations into equation 6 yields:

$$\Delta b = \frac{0.434\ b_0\gamma_w}{(1+e_0)\ \sigma'}\left[C_n\left(\frac{\sigma_n}{\gamma_w} - h_n + z - \frac{\sigma'_{c,n-1}}{\gamma_w}\right) + C_r\left(\frac{\sigma'_{c,n-1}}{\gamma_w} - \frac{\sigma'_{n-1}}{\gamma_w}\right)\right] \tag{8}$$

Note that geostatic load, σ_n, is a variable in this equation. In an unconfined aquifer, σ_n varies as a function of the position of the water table, which commonly is assumed to equal the head. Equation 8 is further modified to express the rate of flow into or out of interbeds. This modification is accomplished by multiplying by the area of the finite-difference cell, A; dividing by the length of the model time step, Δt_n; and rearranging the resulting expression as follows:

$$Q_i = \frac{A b_n}{\Delta t_n}\left[S_s\left(\frac{\sigma_n}{\gamma_w} - h_n + z_n - \frac{\sigma'_{c,n-1}}{\gamma_w}\right) + S_{ske}\left(\frac{\sigma'_{c,n-1}}{\gamma_w} - \frac{\sigma'_{n-1}}{\gamma_w}\right)\right] \quad S_s = \begin{cases} S_{skv}, & \sigma'_n > \sigma_{c,n-1} \\ S_{ske}, & \sigma'_n \le \sigma_{c,n-1} \end{cases} \tag{9a}$$

$$S_{skv} = \frac{0.434 C_c \gamma_w}{\sigma'_{n-1}(1+e_0)} \tag{9b}$$

$$S_{ske} = \frac{0.434 C_r \gamma_w}{\sigma'_{n-1}(1+e_0)} \tag{9c}$$

where Q_i is the volumetric rate of flow to or from compressible interbeds, Δt_n is t_n-t_{n-1}, and z_n

is average elevation of interbeds in the layer at time t_n. Note that all stress quantities in equations 8 and 9 are divided by γ_w. This division has the effect of converting stress to the height of a column of water. For simplicity, the IBS3 package makes all calculations using stress values expressed as a height of a column of water. Simulation of storage changes using equation 9 assumes that head changes in the coarse-grained aquifer material propagate through the fine-grained interbeds within each model time step. This assumption means that the method will work best for relatively thin, compressible interbeds. For relatively thick, extensive confining beds, the method can be applied by simulating each confining bed as one or more separate model layers. For further discussion of the effects of delay in release of water from compressible interbeds, see Leake (1990).

Thickness of interbeds

In equation 9, the thickness term, b_n, represents the total thickness of interbeds in a finite-difference cell at time t_n. In an unconfined aquifer, thickness of compressible interbeds can change because of (1) compaction or expansion of individual interbeds and (2) changes in the position of water table. Thickness changes from the first mechanism need not be considered because the ratio $b/(1+e)$ remains constant even though b and e vary as sediments compact or expand. The values of b and e for interbeds in the saturated flow system can be held constant.

The IBS3 package includes an option to vary the thickness of interbeds in proportion to changes in saturated thickness of an unconfined model layer. This treatment of thickness is analogous to varying transmissivity in response to changes in saturated thickness. Because the thickness at time t_n is used, the term in the finite-difference equations that includes thickness must be updated every iteration. An assumption of this option is that interbeds are distributed uniformly throughout the vertical, so that a given percentage change in saturated thickness results in an equivalent percentage change in thickness of interbeds in the saturated interval. Another assumption is that interbeds above the water table do not supply any water to the saturated flow system. Helm (1984) presented an approach to simulating continued compaction of fine-grained interbeds left behind by a declining water table.

Average elevation of interbeds

The average elevation of interbeds in a model layer is used in the calculation of geostatic load. For this value, the IBS3 package uses the center of the saturated thickness in a layer. This use of the center of the saturated thickness assumes that the interbeds are uniformly distributed throughout the vertical. For layers that do not contain a water table, the layer center is a fixed reference point. For layers that contain a water table, the layer center changes by half the amount of any change in the water table. For these latter layers, the center elevation is updated with every iteration as the MODFLOW program computes a new solution for head. The datum for elevation must be the same as that used in the model. The average elevation of interbeds is not adjusted for changes in elevation from compaction of sediments.

For layers that contain a water table or are capable of being converted between confined and unconfined conditions, the IBS3 package computes layer-center elevation using arrays defined for other packages. For other layers, center elevation must be read in at the start of a simulation.

Geostatic load

The IBS3 package includes the following options for treatment of geostatic load, σ : (1) σ is

calculated and treated as a constant, (2) σ is read in and treated as a constant, and (3) σ is calculated and treated as a variable. In calculating geostatic load, the IBS3 package uses the relation:

$$\frac{\sigma}{\gamma_w} = G_m d_1 + G_s d_2 \tag{10}$$

where G_m is average specific gravity of moist sediments over the distance, d_1, between the land surface and the water table (Fig. 1), G_s is average specific gravity of saturated sediments over the distance, d_2, between the water table and the center of the layer. Equation 10 was modified from Poland & Davis (1969, equation 4). Application of this equation for an entire model layer assumes that the geostatic load at the layer center may be applied as an average value for interbeds throughout the saturated thickness.

As the model iterates to compute head, the IBS3 package recomputes d_1 and d_2 so that the final values are consistent with the water-table elevation at the end of the time step. At a fixed point in the saturated flow system, a unit decline in the water table results in a change in geostatic load of G_m - G_s. Because G_m is smaller than G_s, the change is a decrease in geostatic load. In the IBS3 package, this relation applies for layers underlying an upper unconfined layer. For an unconfined layer, the change in geostatic load from a unit drop in the water table is G_m - $G_s/2$. This relation reflects the lowering of the layer center as the water table declines. For typical values of G_m and G_s, the decline results in an increase in geostatic load for the layer.

If σ is treated as a variable, arrays of moist and saturated specific gravity and elevation of land surface must be read in. A single two-dimensional array is read for each of these three data sets. This approach assumes that average values of specific gravity of overlying saturated and moist sediments are about the same for all layers with interbed storage.

Effective stress

The value of effective stress in the denominator of equation 9 is taken at time t_{n-1}. This approach has the effect of explicitly selecting storage properties on the basis of conditions at the end of the previous time step. At the end of a time step, the IBS3 package uses the Terzaghi relation to update effective stress with currently calculated geostatic load, head, and layer-center elevations.

The relations of head changes and effective-stress changes in the IBS3 package are dependent on the types of layers and treatment of geostatic load. If geostatic load is treated as a variable, a head change in the upper unconfined layer results in effective-stress changes in all model layers. For example, suppose that the head change in the upper unconfined layer is Δh_u and the head change in a lower confined layer is Δh_l. The corresponding changes in effective stress are $\Delta\sigma'_u$ and $\Delta\sigma'_l$. For the case with geostatic load treated as a constant, the relations are:

$$\Delta\sigma'_u = -\frac{\Delta h_u}{2} \tag{11a}$$

$$\Delta\sigma'_l = -\Delta h_l \tag{11b}$$

The computed effective-stress change in the upper aquifer is half that of the lower aquifer

because effective stress is computed at the center of the saturated thickness, which is a moving reference point. The reference point is lowered by half of Δh_u. A better approach than the foregoing is to treat geostatic load as a variable. For this case, the relations between change in head and change in effective stress are:

$$\Delta\sigma'_u = -\left(G_m - \frac{G_s - 1}{2}\right)\Delta h_u \tag{12a}$$

$$\Delta\sigma'_l = (G_s - G_m)\Delta h_u - \Delta h_l \tag{12b}$$

For typical values of G_m and G_s, equation 12a predicts an effective-stress change larger than the head change, reflecting the changing position of the layer center. For the lower aquifer, the change in effective stress is dependent on head change in the upper and lower layers. For typical values of G_m and G_s with the same head changes in both layers, equation 12b predicts an effective-stress change less than the head change.

Preconsolidation stress

Previous computer programs by Meyer & Carr (1979), Williamson et al. (1989), Leake & Prudic (1988), assume preconsolidation stress to be related to a preconsolidation head. The preconsolidation head was used to switch between elastic and inelastic storage properties—specific storage changed to inelastic values whenever the hydraulic head dropped below the preconsolidation head. In contrast, the IBS3 package uses preconsolidation stress as an effective stress. This approach is taken because for some model layers a single head-change value is not sufficient to specify an effective-stress value (see equation 12b).

Preconsolidation stress is read into the IBS3 package at the start of a simulation. Starting values are changed if the starting effective stress is computed to be greater than starting preconsolidation stress. The preconsolidation stress is changed to the effective stress at the end of each time step for model cells where the preconsolidation stress has been exceeded.

Specific storage

Values for inelastic and elastic specific storage for each model cell are read into IBS3 at the start of a simulation. These values are not saved but rather are used to compute the quantities $0.434\ A\ C_c/(1+e_0)$ and $0.434\ A\ C_r/(1+e_0)$, which are saved. These constants are multiplied by $b_n\ \gamma_w/\sigma'_{n-1}$ at each iteration to obtain coefficients needed for equation 9.

Void ratio

As was previously stated, the ratio $b/(1+e)$ is constant; therefore, b and e for interbeds in the saturated flow system can be held constant. Void-ratio values are read in for each cell with interbed storage at the start of a simulation. As outlined in the previous section, the values are used in computing constant parts of coefficients in equation 9.

TEST PROBLEMS

Several test problems were used to test the performance of the IBS3 package. The simplest

test problems involved simulation of a uniform ultimate head decline of 10 m over a flow field. Different options were used for treatment of geostatic load. From the test simulations, model-calculated values of effective stress, geostatic load, compaction, and storage change were compared with hand-calculated values. For these tests, model-calculated and hand-calculated values were consistent. The consistency indicates that relations outlined in this paper were implemented in the IBS3 package as intended.

A more complicated test problem was adapted from Helm (1975). For this test, referred to as the ramp-load test problem, the results of the IBS3 package were compared with results of the COMPAC1 compaction model by Helm (1975, 1976, 1984). The test problem simulated compaction in a 10-m thick fine-grained bed with water levels at the top and bottom of the bed varying cyclically over a 10-m range as shown in Fig. 2A. Hydraulic conductivity of the bed was 1×10^{-3} m year^{-1}, initial inelastic specific storage was 1×10^{-4} m^{-1}, and initial elastic specific storage was 1×10^{-6} m^{-1}. With these values, the initial inelastic and elastic time constants were 2.5 and 0.025 year, respectively.

The test problem was simulated with the IBS3 package with a string of 100 finite-difference cells of 0.1 m length and 1 m by 1 m cross section. An additional finite-difference cell was used on each end of the string to simulate the specified heads at the boundaries. Application of the IBS3 package in this manner is analogous to simulation of flow in a confining bed using 100 model layers. Hydraulic conductivity of the bed was held constant. Two simulations of the ramp-load test problem were carried out. The first simulation assumed a constant geostatic load of 1000 m, whereas the second simulation assumed a constant geostatic load of 40 m. The starting head was set to 15 m above the center of the layer so that starting average effective stress across the bed was 980 and 20 for the two runs, respectively.

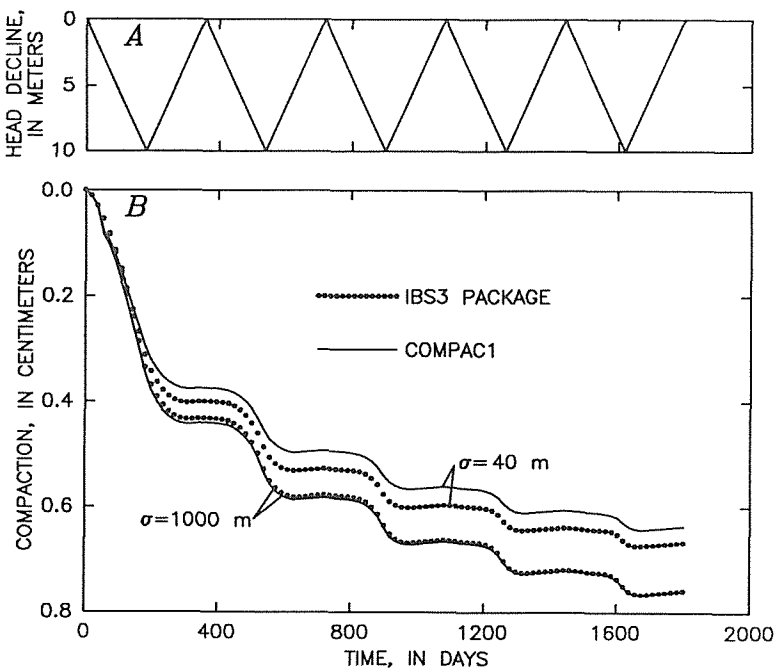

FIG. 2 Results of ramp-load test problem. *A*, Cyclical ramp load on upper and lower boundaries of bed. *B*, Compaction with geostatic load of 40 and 1000 meters of water.

Starting preconsolidation stress that was the same as starting effective stress meant that initial compaction was inelastic. For the COMPAC1 simulation, the finite-difference grid included 200 cells of 0.05-m length. A fine grid was used with COMPAC1 because the results for this problem were relatively sensitive to grid spacing. The nonlinear option of COMPAC1 varies hydraulic conductivity and specific storage as functions of effective stress.

Results of the simulations are shown in Fig. 2B. For the simulations with geostatic load set to 1000 m, results from IBS3 and COMPAC1 are virtually the same. These results also agree with previous test simulations by Leake & Prudic (1988, Fig. 3) in which specific storage was constant. For the simulations with geostatic load set at 40 m, compaction computed by the IBS3 package is more than that computed by COMPAC1. The results are different because the COMPAC1 simulation varies hydraulic conductivity whereas the IBS3 simulation holds hydraulic conductivity constant.

FUTURE APPLICATIONS AND LIMITATIONS

The IBS3 package was developed for analysis of aquifer-system compaction in ground-water reservoirs in alluvial basins of the southwestern United States. In this area, compaction can occur in relatively shallow unconfined aquifers and in underlying confined aquifers. Future application of the package to these or similar aquifers will provide a basis for assessing the importance of such features as stress-dependent specific storage, variable geostatic load, and variable thickness of interbeds in the saturated interval.

A major assumption in the simulation of compacting interbeds using the IBS3 package is that head changes in coarse-grained aquifer material occur throughout the fine-grained interbeds within a model time step. The package therefore is most applicable where time constants of the interbeds do not greatly exceed the length of model time steps. Another assumption is that interbeds are distributed uniformly throughout the vertical in each finite-difference cell. This is not a severe limitation, because the package could be modified to account for other distributions. Finally, if the package is applied to simulate compaction of a confining bed, one or more separate model layers must be used. For that case, the package would account for delay in compaction and release of water but changes in hydraulic conductivity from changing void ratio would not be considered.

A positive aspect of the IBS3 package is that it works as a part of the MODFLOW computer program. This model is widely used to simulate saturated ground-water flow. Simulations of aquifer-system compaction can make use of a variety of other features available in MODFLOW. Furthermore, the IBS3 package can be modified without extensive changes to the rest of the MODFLOW program.

REFERENCES

Helm, D. C. (1975) One-dimensional simulation of aquifer-system compaction near Pixley, California, 1. Constant parameters. Wat. Resour. Res. 11, 465-478.

Helm, D. C. (1976) One-dimensional simulation of aquifer-system compaction near Pixley, California, 2. Stress-dependent parameters. Wat. Resour. Res. 12, 375-391.

Helm, D. C. (1984) Latrobe Valley subsidence predictions: The modeling of time-dependent ground movement due to groundwater withdrawal. State Electricity Commission of Victoria, Australia, 2 vols.

Helm, D. C. (1987) Three-dimensional consolidation theory in terms of the velocity of solids.

Géotechnique 37, 369-392.
Jorgensen, D. G. (1980) Relationships between basic soils-engineering equations and basic ground-water flow equations. USGS Wat. Supply Pap. 2064.
Leake, S. A. (1990) Interbed storage changes and compaction in models of regional ground-water flow. Wat. Resour. Res. 26, 1939-1950.
Leake, S. A. & Prudic, D. E. (1988) Documentation of a computer program to simulate aquifer-system compaction using the modular finite-difference ground-water flow model. USGS Open-File Report 88-482.
McDonald, M. G. & Harbaugh, A. W. (1988) A modular three-dimensional finite-difference ground-water flow model. USGS Tech. of Wat. Resour. Investigations, Book 6, Chap. A1.
Meyer, W. R. & Carr, J. E. (1979) A digital model for simulation of ground-water hydrology in the Houston area, Texas. Texas Dept. of Wat. Resour. Report LP-103, Austin, Texas.
Neuman, S. P., Preller, C. & Narasimhan, T. N. (1982) Adaptive explicit-implicit quasi three-dimensional model of flow and subsidence in multiaquifer systems. Wat. Resour. Res. 18, 1551-1561.
Poland, J. F. & Davis, G. H. (1969) Land subsidence due to withdrawals of fluids. Rev. Eng. Geol. 2, 187-269.
Williamson, A. K., Prudic, D. E. & Swain, L. A. (1989) Ground-water flow in the Central Valley, California. USGS Prof. Pap. 1401-D.

Land Subsidence (Proceedings of the Fourth International Symposium on Land Subsidence, May 1991). IAHS Publ. no. 200, 1991.

Pore Water Pressures and Subsidence in Long Term Observations

M.A.VIERGEVER
Ministry of Transport and Public Works, Directie Flevoland, Lelystad, Netherlands

ABSTRACT In the central part of the Netherlands, polders were reclaimed by pumping out the water to a level of four to five meters below sea level. Over the first five to six meters the soil consists of compressible clay and peat layers. The change in pore water pressure due to reclamation and the load of a hydraulic fill both cause subsidence. The pore water pressure and subsidence is measured at several places during a long period. The observations are analysed using a simple model. It is shown when a simple model can be used and what should be taken into account in predictions.

INTRODUCTION

In the central part of the Netherlands, a former inland sea has been partly reclaimed by pumping out the water. The water table has been lowered about five meters. The soil consists of five to six meters of compressible clay and peat layers on a sandy subsoil. After reclamation a proces of ripening of the topsoil and subsidence of the lower layers starts.

New town development is started in these polders. As a start a hydraulic fill of one meter has been brought in place to get good accessibility and to be able to drain the building site. Change in pore water pressure and load by the hydraulic fill caused subsidence up to more then one meter. In order to check predictions several measuring sites were installed. The observations are analysed by a simple computermodel which will be described in this article. As a result the influence of the load history and the boundary can be seen.

SOIL DESCRIPTION

The compressible layers are holocene layers and in general deposited in water. From top to bottem the following layers are encountered:
(a) a light organic clay;
(b) a heavy organic clay;
(c) peat, sometimes with disturbed fabric;
(d) a heavy clay, organic;
(e) peat.
Average values of the most important parameters are listed in Table 1. The parameters are taken from auger borings and lab testing five to 10 years after reclamation and before bringing the hydraulic fill in place. Differences are caused by differences in soil composition such as water content, content of clay particles and content of

organic matter.

TABLE 1 Average soil parameters.

type of soil	unit weight [kN/m^3]	watercontent [% dry weight]	particles < 2 μm [%]
clay, light organic	17.5	50	26
clay, heavy organic	13.0	145-195	28.5-30
peat	10.5-11	425-600	10-36
heavy clay, organic	13 -15	80-150	35-40
peat	10.5-11	400-500	14-17

type of soil	angle of internal friction φ[°]	φ'[°]	cohesion c [kN/m^2]	c' [kN/m^2]
clay, light organic	17	35	10	5
clay, heavy organic	12-18	33-42	7.5-9	5-7
peat	17.5	40	8	7
heavy clay, organic	12-13	34-37	7.5-11	3.5-6.5
peat	18	46	9	8

type of soil	consolid. coëff. c$_v$ m/s	compressibill. coëff. m$_v$ m/kN	permeabill. coëff. k m/s
clay, light organic	5-18 $*10^{-10}$	4.5 $*10^{-4}$	3.8 $*10^{-10}$
clay, heavy organic	10-40 $*10^{-10}$	25-32$*10^{-4}$	6.7-11.8$*10^{-10}$
peat	12-30 $*10^{-10}$	23 $*10^{-4}$	8.7 $*10^{-10}$
heavy clay, organic	2-30 $*10^{-10}$	10-14$*10^{-4}$	3.9-6.8 $*10^{-10}$
peat	4-12 $*10^{-10}$	11 $*10^{-4}$	7.4 $*10^{-10}$

MEASURING SITES

Out of ten installed measuring sites at different places eight have been in use during several years. The first site is installed in 1972, only four years after the lowering of the water table in the former lake. It is still in use.

The sites are installed just before the hydraulic fill was placed in situ. Subsidence is measured with plates on the former surface and at the border of the different layers. The lower plates are placed as a screw plate and screwed to the wanted depth (see Fig. 1). Subsidence is measured by measuring the subsidence of iron rods fixed to the plates and surrounded by flexibele tubes to reduce friction alongside the rods.

At the same depth as the plates observation wells are placed to measure the pore water pressure. The wells are made of open pipes (3/4") with a filter of 0.20 m. The observation wells do not record

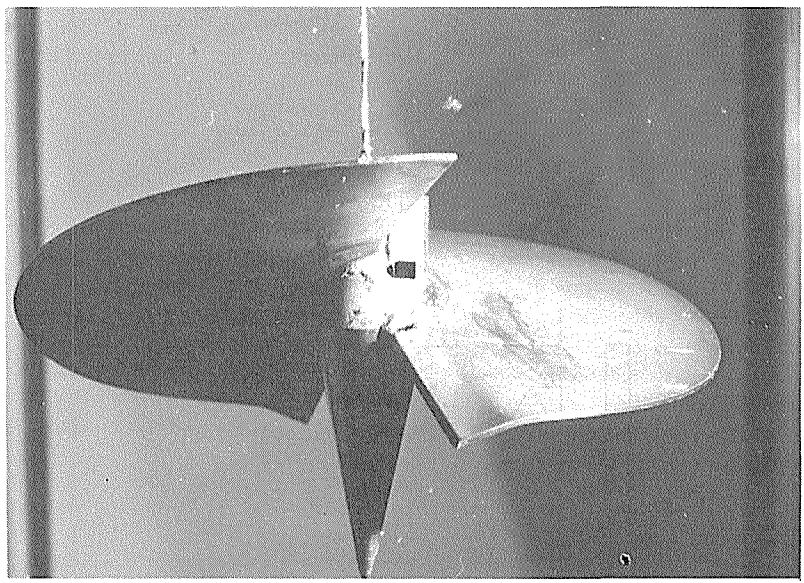

FIG. 1 Screw plate for measuring subsidence below the soil surface.

short range differences in pore water pressure, but are accurate to record changes that influence subsidence. Measurements were taken every two weeks during the first period. Now this period is longer.

CALCULATION OF CONSOLIDATION AND SUBSIDENCE

Evaluation of the testresults has been carried out with a simple computermodel based on the one dimensional consolidation theory of Terzaghi and the combined rule for subsidence from Terzaghi-Buisman-Koppejan.

Porewaterover-pressure and under-pressure are generated by a load or a change in conditions at the border of the compressible clay and peatlayers. A load at the top of the layer causes an increase of pore water pressure in the whole layer. The amount of pore water pressure increase equals the load at the surface. Changes in either waterlevel at the top or change in pore water pressure at the bottom cause a triangular pore water over pressure or under pressure in a layer of homogenous clay or peat. (see Fig.2)

The consolidation of pore water over and under pressure follows the formula given below (Terzaghi, 1951):

$$u = \sum_{m=0}^{m=\infty} \frac{4p}{(2m+1) * \pi} * \sin\left[\frac{(2m+1) * \pi}{h} * z\right] * e^{\left\{\frac{-k}{m_v * \gamma_w} * \left[\frac{(2m+1) * \pi}{h}\right]^2 * t\right\}}$$

with:

u = pore water over or under pressure at time t [kN/m_2]
p = pore water over or under pressure at time t=0 [kn/m^2]
h = thickness of the compressible layer [m]
z = depth at which u is calculated [m]
k = permeabillity [m/s]
m_v = compressibillitycoefficient [m^2/kN]
γ_w = volume weight of water [kN/m^3]
t = time of calculation u [s]

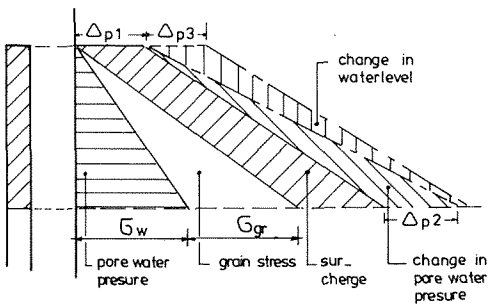

FIG. 2 Pore water pressure generation due to load or change in water level or pore water pressure at the bottom.

This calculation method gives the porewater over pressure at the wanted time t and wanted depth z for a uniform soil. In general the soil is layered. To get a uniform soil the actual soil with different layers is transformed to a soil with adapted thickness and uniform properties. This is done according to the finite difference method (Hansbo, 1987)

$$h_{uniform} = h_{original} \sqrt{\frac{k_{uniform} * m_{v\,original}}{m_{v\,uniform} * k_{original}}}$$

Each load or change in pore water pressure at the top or bottom of the compressible layers will cause consolidation. At any time the remaining pore water pressure is superposed to the original pore water pressure in the soil. Also the pore water pressures of former loads and changes in pore water are of influence because consolidation may not be finished yet.

Of course the starting level of the pore water is important. Before reclamation the waterdepth was about 4 m, after reclamation the waterlevel was equal to the soil surface. The pore water level at the bottom of the compressible layers was before reclamation one meter below sea level and shortly after reclamation about four meters below sea level. The drop in pore water pressure in the pleistocene sand below the holocene toplayers was caused by contact of the pore water in the sand with the surface water in the canals (see Fig. 3). The high pore water pressure inside the clay and peat layers cannot exist and the clay and peat are too impermeable to let the water dissipate. The soil will explode or fluidate. This situation was immitated in the lab. After a sudden drop of the waterlevel at top

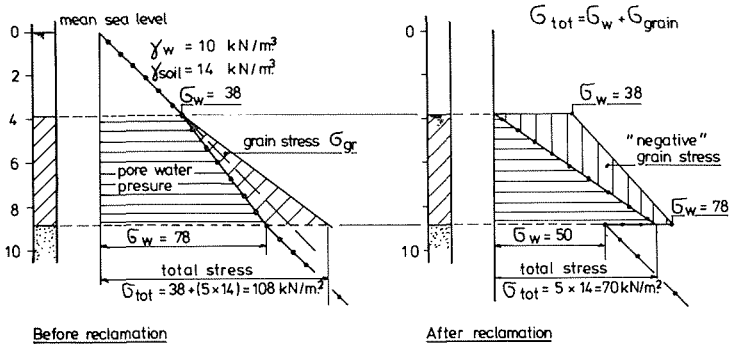

FIG. 3 Fluidation of soil due to reclamation.

and bottom, the soil raised and the pore water pressure became equal to the hydrostatic pressure of a fluid with a volume weight of about 1200 kN/m³. After fluidation the soil will be sedimented again and due to this effect starts to compact under its own weight. In situ this drop of water level and pore water pressure in the pleistocene sand took about nine month. This is believed to be so fast that it was not possible for the soil to consolidate completely and the soil will have been in a state of zero grain stress. Afterwards consolidation of the soil under its own weight starts. At the moment of the loading and the start of the measurement consolidation may not yet have been finished. In calculation a theoretical pore water pressure is taken, depending on permeabillity of the different layers, water level at the top and pore water pressure at the bottom of the layers instead of the measured value.

The total stress is equal to the sum of grain stress and pore water stress:

$\sigma_t = \sigma_{grain} + \sigma_{water}$

Subsidence is caused by an increase in grain stress. The decrease of pore water over pressure or decrease of pore water pressure caused by a change in conditions at the border means an equal increase in grain stress. The start of subsidence follows the rate of consolidation. Subsidence is calculated according to Terzaghi-Buisman-Koppejan:

$$s = h \left\{ \frac{1}{C_p} + \frac{1}{C_s} * \log(t) \right\} * \ln \frac{p_o + \Delta p_1}{p_o}$$

$$+ h \left\{ \frac{1}{C_p'} + \frac{1}{C_s'} * \log(t) \right\} * \ln \frac{p_o + \Delta p}{p_g}$$

with:

s = subsidence [m]
h = thickness of the layer [m]
C_p, C_s, C_p', C_s' = primary and secundary compressibillity coefficients
t = time [days]
p_o = original grainstress [kN/m$_2$]
$\Delta p, \Delta p_1$ = increase in grainstr. with $p_o + \Delta p_1 \leq p_g$ and $\Delta p \geq \Delta p_1$ [kN/m²]
p_g = ultimate stress level occured to the soil [kN/m²]

Different loads are calculated separately and afterwards added to the total subsidence. Increase of grain stress causes subsidence, decrease of grain stress swelling. For swelling the same coeficients are used, while the result from this calculation is multiplied with 0.10. The load on the surface is corrected for sinking under water of the soil, because in the calculation the original thickness remains the same.

TEST RESULTS

In this chapter a comparison will be made between test results and in situ measurements. For one of the measurement sites the schematisation of the water level and pore water pressure at the bottom is given in Fig. 4.

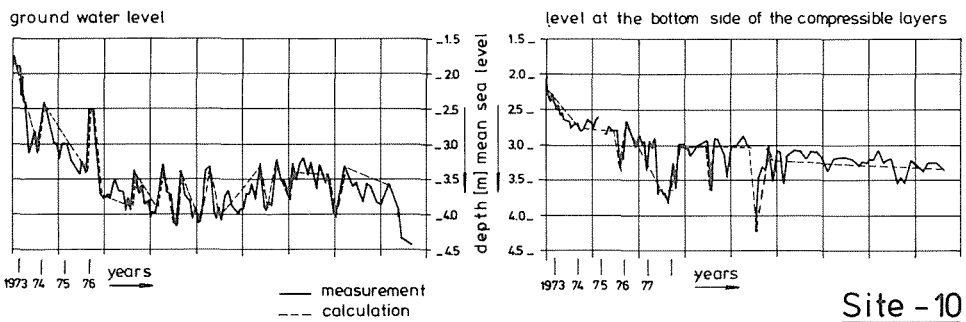

FIG. 4 Water level and pressure head in the underlaying sand.

(a) test results pore water pressure development

The pore water pressure is calculated at several times and compared with the measured value. The result of the calculations of some measuring sites are given in Fig. 5 and 6. From this results plots are made with differences between calculated and measured pore waterpressure at several depth as a function of time. The plots are given in Fig. 7. A summary of the testresults is given in Table 2.

The general conclusions that can be drawn from the comparison between the calculated pore water pressures and the measured values are:

(aa) The load of a sand layer with a volume weight of 18 kN/m³ has never caused a pore water pressure increase of the same amount. The differences are about the magnitude of the pore water pressure at the bottom of the hydraulic fill when the fill is still saturated. This could be explained when the pore water in the hydraulic fill contacts the pore water in the compressible layers. The water in the hydraulic fill generates in this case no pore water overpressure and from the sand only the weight under water is causing pore water over pressure.

(bb) The calculated pore water pressure consolidates faster than the measured pore water pressures, it starts too high and ends too low.

(cc) Measuring site E 9 reacts in a different way. The pore water

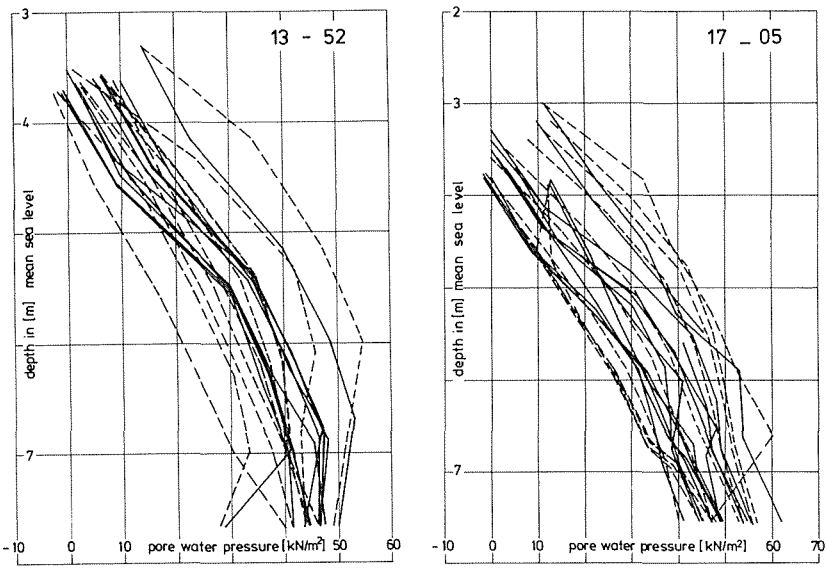

FIG. 5 Calculated and measured pore water pressure.

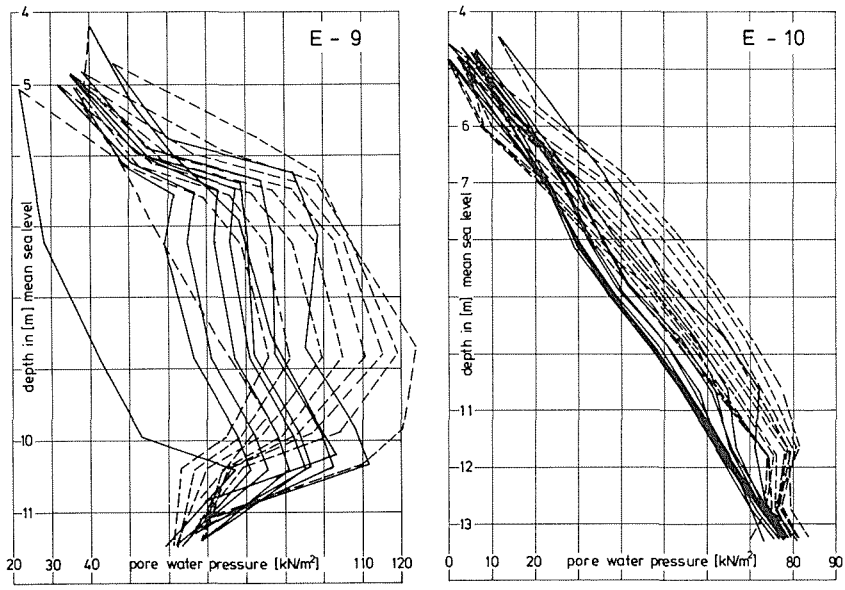

FIG. 6 Measured and calculated pore water pressures.

pressure increases strongly over the first 1.50 m, and then keeps constant over a depth of 2.50 m and increases slowly over a depth of 1.50 m followed by a sharp decrease over the last meter. After the removal of the load only pore water over pressure remains in the deepest layer. This behaviour does not fit the calculated consolidation proces (see Fig 6 and 7).

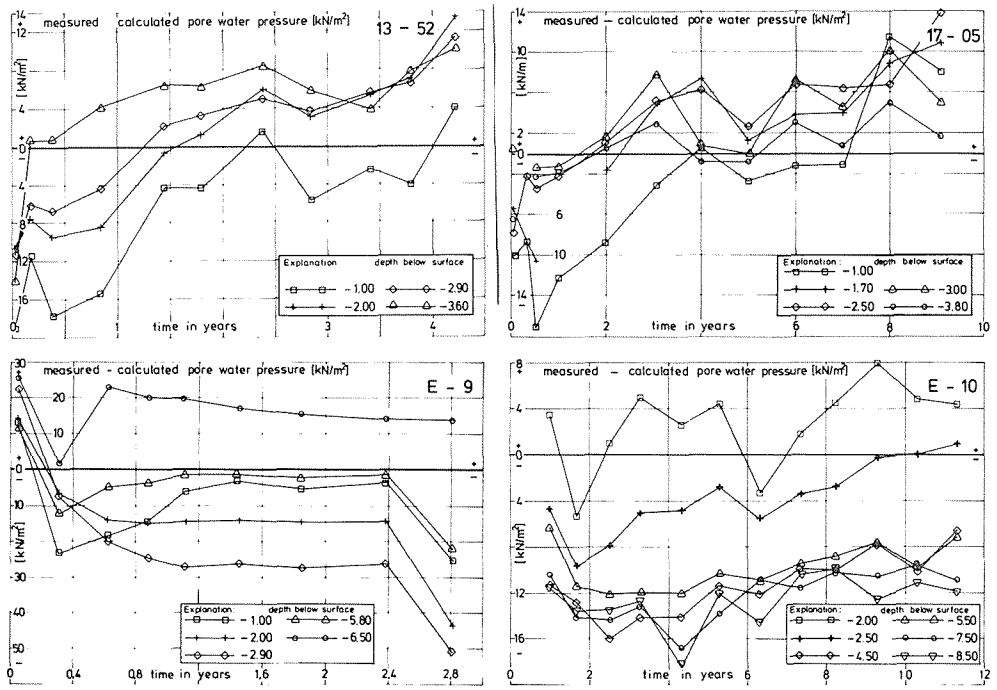

FIG. 7 Difference between measured and calculated pore water pressure.

(b) test results subsidence

Table 2 also gives the results of calculated and measured subsidence. Results of some meausuring sites are given in Fig. 8. The differences between calculated and measured values at different depth are given in Fig. 9. The following remarks can be made or conclusions may be drawn:

(aa) Differences between calculated and measured subsidence are not in the same order at the different sites.

(bb) Five out of ten are at the end within a range of +/- 0.15 m (20%).

(cc) In the first period differences are somewhat bigger. In spite of the slower in situ consolidation, the in situ subsidence takes place faster then calculated. The conclusion may be drawn that it is not correct to start primary and secundary subsidence as a result of increase or decrease of grain stress after consolidation. Primary and secundary subsidence should start directly after the load increase or decrease and be multiplied with a factor depending on the rate of consolidation.

(dd) The maximum difference is found at site E 13-10. The large predicted subsidence is caused by the condition of extreme high pore water pressure in the underlaying sandlayers at the start of the measurement at the bottom side of the compressible layers. When the pore water pressure is assumed lineair between surface and bottom than there remains a grain stress of only 3.3 kN/m² at a depth of 5.2 m. An applied load causes in this case a large increase in grain

TABLE 2 Summary of test results.

nr	measuring site	start measuring	end measuring	remarks
1	E 13-10	july 1972	still in use	many changes
2	E 13-52	july 1972	novemb. 1976	big changes
3	E 17-05	july 1972	febr. 1982	big changes
4	E 17-43	july 1972	still in use	changes in first period
5	E 5	april 1974	still in use	few changes
6	E 6	may 1976	still in use	few big changes
7	E 7	oct. 1975	still in use	
8	E 8	sept. 1976	still in use	
9	E 9	march 1976	sept. 1979	deposit of 4.70 m
10	E 10	march 1978	still in use	few changes

nr	pore water pressure calculated		subsidence calculated		remarks
	first period * [kN/m²]	last period [kN/m²]	first period [m]	last period [m]	
1	+ 10	- 5	+ 0.35 (50%)	+ 1.01 (96%)	
2	+ 10	- 14	- 0.12 (29%)	- 0.10 (18%)	
3	+ 10	- 12	- 0.09 (14%)	- 0.15 (15%)	
4	+ 5 / - 12	- 5	- 0.20 (40%)	- 0.11 (11%)	
5	+ 12	- 2	- 0.08 (18%)	- 0.10 (9%)	
6	+ 10	- 10	- 0.02 (6%)	+ 0.50 (82%)	
7	+ 12	- 12	- 0.08 (25%)	+ 0.12 (18%)	elastic behaviour
8	+ 12	- 3	+ 0.15 (43%)	+ 0.39 (61%)	
			+ 0.15 (43%)	+ 0.14 (22%)	elastic behaviour
9	+ 25	+ 50	- 0.55 (69%)	- 0.39 (37%)	
10	+ 14	+ 12	- 0.08 (15%)	+ 0.58 (77%)	
			- 0.12 (55%)	+ 0.26 (35%)	elastic behaviour

* first one to two years

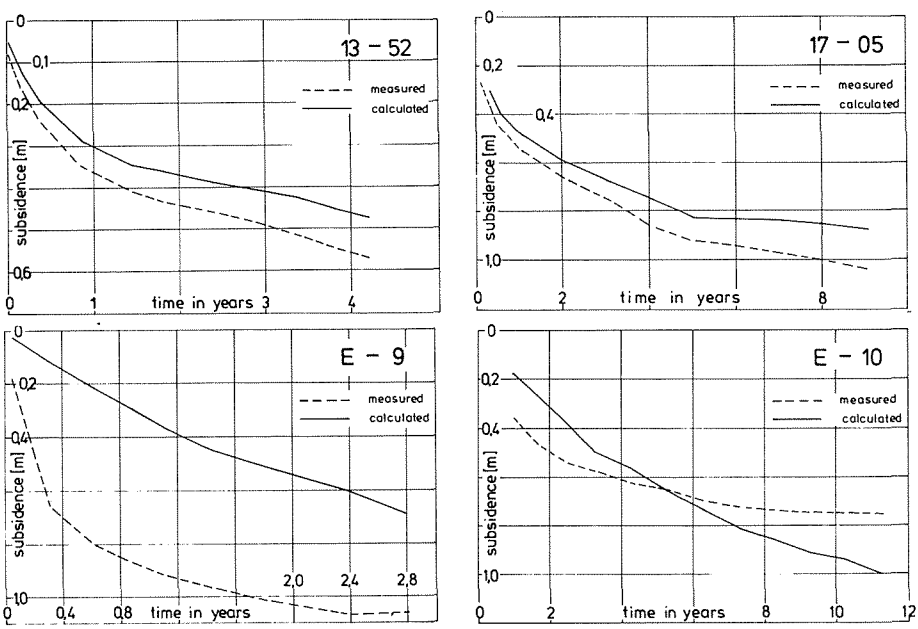

FIG. 8 Measured and calculated subsidence.

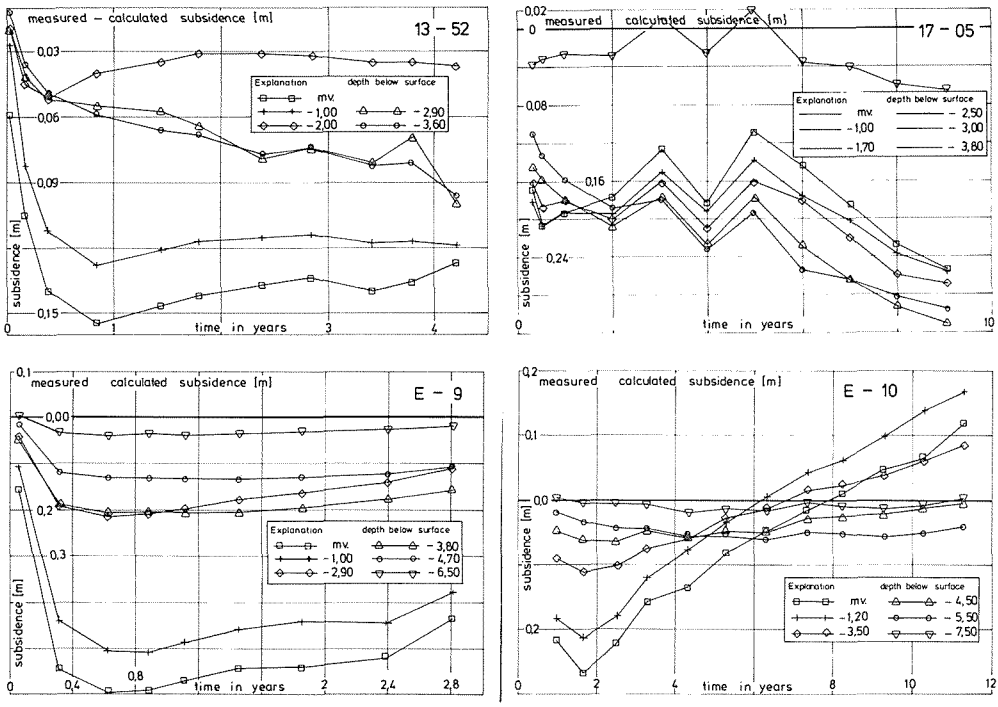

FIG. 9 Difference between measured and calculated subsidence at different depth.

stress. Unfortunately the pore water distribution in the compressible layer was not measured. Probably the assumption of lineair pore water distribution between top and bottom is wrong in this case.
(ee) At site E 6 pumping in wells were carried out in the neighbourhood during a period. This caused a large drop in pore water pressure in the underlaying pleistocene sand. This drop had a great effect on the subsidence calculations. To reach the range of +/- 0.15 m a multiplying factor of one has to be used for the swelling. This means that the soil reacts elastic.

REFERENCES

Terzaghi, K. Theoretical soil mechanics. New York, 1951
Schmidt, E. Über die Anwendung der Differenzrechnung auf technische Anheiz- und Abkühlungsprobleme.Beitrage zur technische Mechanik und technischen Physik, Berlin, 1924
Hansbo, S. State of the art report on groundwater problems in Sweden. IX ECSMFE, Dublin 1987

Land Subsidence (Proceedings of the Fourth International Symposium on Land Subsidence, May 1991). IAHS Publ. no. 200, 1991.

Probability Analysis of Shanghai Shallow Layer Subsidence

SU HE-YUAN
Shanghai Station of Environmental Geology, 930 Lingshi Road, Shanghai 200072, China
LIN GUO-MING
Southeast University, Nanjing, China
QIAN JIA-HUAN
Hohai University, Nanjing, China

ABSTRACT This paper endeavours to provide a suitable approach for the solution of the calculation about Shanghai shallow layer subsidence. An analytical study of deformation model concerning clay creep has been made by the optimization method, along with the observed data of the pore water pressure and deformation of Shanghai shallow layer under the pumping and recharging conditions. A viscoelastic Solution of Shanghai land subsidence derives from the selected model and the elastic solution of Shanghai land Subsidence. The statistical rule of the rheological parameters can be likewise obtained by the extended Lee's analogy method. The probability distribution of the deformation of shallow layer at a typical location in shanghai is calculated with Monte-carlo similation method. This new approach is intended for the prediction of land subsidence in Shanghai in the future ten years, which suggests a method for the reduction of the subsidence on Shallow layer.

INTRODUCTION

Shanghai land subsidence is chiefly attributed to groundwater pumping. This grave occurrence, since the beginning of 1960's has been kept under control by means of the limitation of the use of the groundwater in parallel with the application of the artificial recharage of the groundwater. However starting from 1972, there reoccurred minor subsidence, which, as shown by field observation, was concentrated in the upper part of Ovrburden (from the surface to the depth of 40m, hereinafter called shallow layer). And the laboratory tests further indicated that the creep of clay in shallow layer was an obvious cause of the minor subsidence (Su, 1979). So the adoption of proper measures both for the prediction of deformation and for the stabilization of the subsidence of shallow layer has become a key factor to further control of land subsidence in Shanghai.

GEOLOGICAL CONDITION AND DEFORMATION REGULARITY OF SHALLOW LAYER

In the area of Shanghai, there is a deposit of two compressible layers (Known as the 1st and 2nd compressible layers) in the upper part of

Bottom depth (m)	Thickness (m)	Columnar section	layer
3.50	3.50		Surface soil
6.00	2.50		Silt sand
19.00	13.00		Muddy loam clay
23.00	4.00	19.49	Fine silt sand
35.10	12.10		loam clay interlaminated With thin layers of silt
42.28	7.18		loam clay
49.99	7.71		Silt sand 1st aquifer

1st Compre. layer

2nd Compre. layer

FIG.1. Typical geological columnar section of shallow layer.

the Overburden, from the depth of 40m upward. The typical columnar section of the soil layers is shown in Fig. 1.

The 1st and 2nd Compressible layers are Composed of muddy clay with low permeability and high moisture content, which possess a higher compression and a long time lag during the process of groundwater pumping. This is considered to be an internal factor, which will lead to the high compression in the shallow layer. The cumulative deformation and water table fluctuation of the shallow layer in a typical site are both shown in Fig. 2, which states that the cumulative deformation of this layer has a tendency of continuous compression as well as cyclic swelling and compression with periodic fluctuation of groundwater level.Furthermore the peak valley value of deformation has a short lag of groundwater level. This phenomenon indicates the creep behaviour of the soft clay layer.

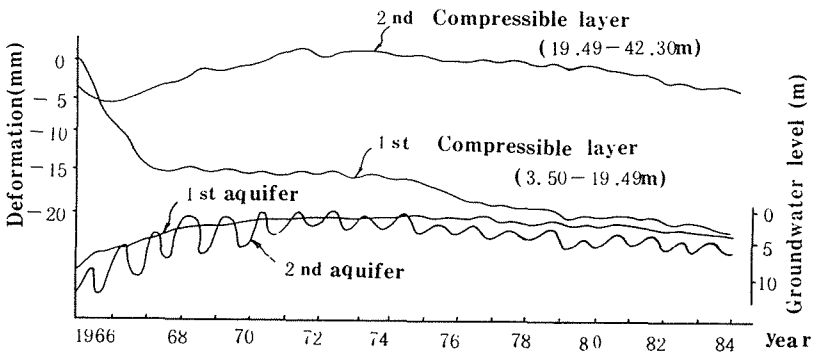

FIG.2. Curves showing the cumulative deformation of shallow layer and water level fluctuation in the typical site.

And the laboratory rheological test further reveals that the shallow soil has a creep behaviour. As shown in Fig. 3, the

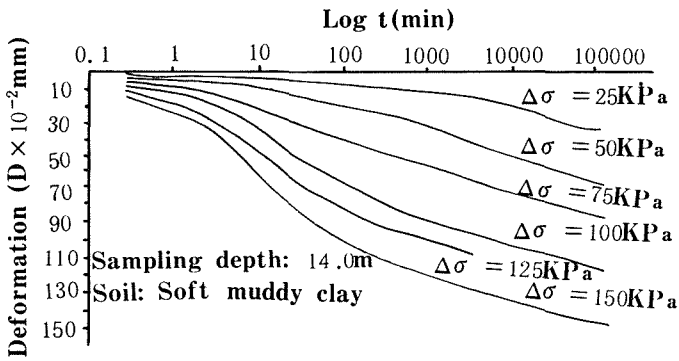

FIG.3. Curves showing the consolidated deformation (D) by odometer test versus time (t).

deformation of soil shows no tendency to approach stabilization during the 90 days testing and the ratio between the secondary consolidation and the principal consolidation is 3:1 (Su, 1979).

In view of the above mentioned cyclical variation of the groundwater level and of the deformation, in our computation, we divide one year's groundwater and deformation variation into a rising period and a lowering period. It is supposed that the variations of groundwater level both in the rising period and the falling period are with linear pattern. By the annual field observation data of the groundwater level and of the deformation, we can reverse the rheological model parameters individually for the compression period and the rising period. Only in this way, can the compression and the swelling deformation of the shallow layer be computed.

OPTIMUM ANALYSIS FOR RHEOLOGICAL MODEL AND THEIR PARAMETERS

Kelvin's model which connects with elastic elements and viscous elements is usually used to explain strain-stress. Thus, three-elements model shown in Fig. 4 can be selected.

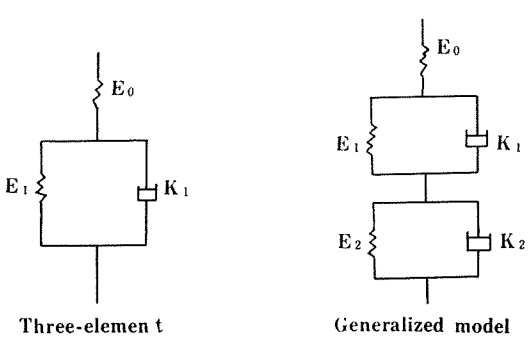

FIG.4. Schematic drawing of model structure.

Based on the principle of the creep mechanics, strain about generalized non-relax model, inclusive of three-elements, can be expressed as follows:

$$\varepsilon(t) = \sigma(t)\cdot J(o) + \int_o^t \sigma(\tau)\,\frac{dJ(t-\tau)}{d(t-\tau)}\cdot d\tau \qquad (1)$$

where $\varepsilon(t)$ = strain;
$\sigma(t)$ = stress;
t = time.

$$J(t) = \frac{1}{E_o} + \frac{t}{K_o} + \sum_{i=1}^{N}\frac{1}{E_i}\left[1-e^{-(E_i/K_i)\,t}\right]$$

is the strain acted by unit stress.

By substituting the pore water pressure observed in the field into Eq. 1, the layer strain at any time can be calculated. Optimum method is used to select rheological model and determine their parameters and target function is formed:

$$F(E_o, E_1, K_1, \cdots) = \sum_{i=1}^{N}\left[\varepsilon(t_i) - \varepsilon_i^*\right]^2 \qquad (2)$$

where ε^* = observed strain in certain period;
$\varepsilon(t_i)$ = calculated strain in the same period;
N = period numbers;
$E_o, E_1, K_1, \cdots$ = parameters of model.

So, value of target function $F(E_o, E_1, K_1, \cdots)$ becomes a measurement of coinciding precision. Three-elements model is accepted as a calculating model for shallow layer because it is relatively simple.

By putting the data of observed pore water pressure and deformation in rising and lowering preiod of water level individually into the target function, one set of parameters both in rising period and lwering period can be calculated.

DEFORMATIOM FORMULA OF SHALLOW LAYER

By assuming that soil is elastic and basing on the Terzaghi's one-dimensional consolidation theory, Qian, S.Y & Gu,X.Y have derived the solution of the deformation of layer (Fig. 5) under the

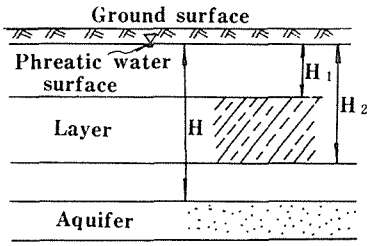

FIG.5. Schematic diagram of layer structure.

condition linear variation of central water level line. i. e.:

$$S(t) = \alpha M_v \left\{ \frac{1}{2H}(H_2^2-H_1^2)\, t - \frac{1}{24\, C_v\, H}(2H^2H_2^2-2H^2H_1^2-H_2^4+H_1^4) \right.$$

$$\left. +2\sum_{n=1}^{\infty}(-1)^n \frac{H^3\,[\cos n\pi\,(H_2/H)-\cos n\pi\,(H_1/H)]}{(n\pi)^4\, C_v}\, e^{-(n\pi)^n\, C_v\, t/H^2} \right\} \qquad (3)$$

where α = slope of variation of water level;
C_v = coefficient of consolidation;
M_v = coefficient of volume compressibility;
K = coefficient of permeability.

By extended Lee's analogy method, viscoelastic solution can be derived through following procedures:

(a) Selecting a three-elements viscoelastic model and write out it's physical equation

$$E_o K_1 \dot{\varepsilon} + E_o E_1 \varepsilon = \sigma(E_o + E_1) + K_1 \dot{\sigma} \qquad (4)$$

applying Laplace transformation to Eq.4

$$E_o K_1 S \bar{\varepsilon} + E_o E_1 \bar{\varepsilon} = \bar{\sigma}(E_o + E_1) + K_1 S \bar{\sigma} \qquad (5)$$

equivalent elastic modulus

$$E = \frac{\bar{\sigma}}{\bar{\varepsilon}} = \frac{(E_o K_1 S + E_o E_1)}{(K_1 S + E_o + E_1)} \qquad (6)$$

(b) Replacing Cv and Mv with elastic modulus
If one-dimensional compression, $M_v = 1 / E$, $C_v = K E / r_w$, assuming $D = (n\pi)^2 K / (H^2 r_w)$, $N = D E$, hence Eq. 3 becomes:

$$S(t) = \alpha \left\{ \frac{1}{2H}(H_2^2-H_1^2) \frac{t}{E} - \frac{r_w}{24\, K\, E^2\, H}(2H^2H_2^2-2H^2H_1^2-H_2^4+H_1^4) \right.$$

$$\left. +2\sum_{n=1}^{\infty}(-1)^n \frac{H^3\, r_w[\cos n\pi\,(H_2/H) - \cos n\pi\,(H_1/H)]\, e^{-Nt}}{(n\pi)^4\, K\, E^2} \right\} \qquad (7)$$

where E = elastic modulus;
r_w = unit weight of water.

(c) Apply Laplace transformation to Eq. 7

$$\bar{S}(S) = \alpha \left\{ \frac{1}{2H}(H_2^2 - H_1^2) \frac{1}{E S^2} - \frac{r_w}{24 K H}(2H^2H_2^2 - 2H^2H_1^2 - H_2^4 + H_1^4) \frac{1}{E^2 S} \right.$$

$$\left. + 2\sum_{n=1}^{\infty} (-1)^n \frac{H^3 r_w [\cos n\pi (H_2/H) - \cos n\pi (H_1/H)]}{(n\pi)^4 K} \left(\frac{1}{E^2 (S + N)} \right) \right\} \quad (8)$$

(d) Substitute E in Eq. 8 with expression of E in Eq. 6 and apply Laplace inverse transformation to Eq. 8, then viscoelastic solution can be obtained as follows:

$$S(t) = \alpha \left\{ \frac{1}{2H}(H_2^2 - H_1^2) L^{-1}\left(\frac{1}{E S^2} \right) \right.$$

$$- \frac{r_w}{24 K H}(2H^2H_2^2 - 2H^2H_1^2 - H_2^4 + H_1^4) L^{-1}\left(\frac{1}{E^2 S} \right)$$

$$\left. + 2\sum_{n=1}^{\infty} (-1)^n \frac{H^3 r_w [\cos n\pi (H_2/H) - \cos n\pi (H_1/H)]}{(n\pi)^4 K} L^{-1}\left(\frac{1}{E^2 (S + N)} \right) \right\} \quad (9)$$

where $L^{-1}\left(\frac{1}{E S^2}\right)$, $L^{-1}\left(\frac{1}{E^2 S}\right)$, $L^{-1}\left(\frac{1}{E^2 (S+N)}\right)$ are expression of Laplace inverse transformation.

PROBABILITY ANALYSIS OF SHALLOW LAYER DEFORMATION

By optimization method, model parameters from 1966 to 1986 can be calculated and their mean value and standard deviation are shown in table 1.

Using Kolmogorov-Smirnov method to examine the assumed distribution of paramaters, the results indicate that distribution of the model parameters can be assumed as normal distribution.

Putting the values of model parameters, depth of layer and coefficient of permeability into deformation Eq. 8, every year's value of compression in lowering period and value of swelling in rising period can be calculated, and the net cumulative values of deformation can also be evaluated. Fig. 6 shows the cumulative observed deformation values and cumulative calculated deformation values to be well coincided.

The deformation of shallow layer is affected by the variation of water level in underyling aquifer and also affected by meteorological phenomena, man's activity,measurement errors and other random factors. The parameters reversed from observed data also reflect the influence

TABLE 1. Statistic Value of rheological parameters.

Layer	Parameters	Rising period		Compression period	
		mean value	standard deviation	mean value	standard deviation
1st Layer	E_o(MPa)	34480	16100	11890	1342
	E_1(MPa)	267	28.0	164	21.7
	K_1(MPa)	11410	1342	7729	1488
2nd Layer	E_o(MPa)	38020	16590	36440	14980
	E_1(MPa)	416	137	538.6	128.4
	K_1(MPa d)	12330	2830	10410	10410

of all these random factors. So, a group of model parameters should be considered as random variables. Monte-Carlo simulation method is used to correlative sampling and calculating the deformation distribution regularity.

Monte-Carlo method is known as statistical examination method. It is a method of using random variables, which can be used to calculate deformation distribution regularity.

After 1000 times sampling and calculating based on the above mentioned method, the ten year's deformation distribution regularity for the typical site is calculated and shown in table 2.

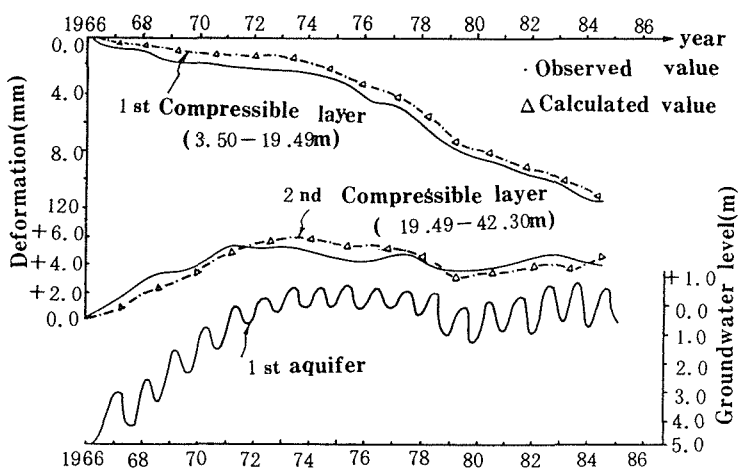

FIG.6 Curves showing the variation of deformation and water level in typical site.

TABLE 2. Deformation distribution from 1987-1996.

Depth of layer (m)	Deformation distribution	Deformation ranges when confidence interval is 0.8
3.5 -19.50	N [-8.00, 5.38]	[-10.97, -5.03]
19.50-42.30	N [4.5, 2.50]	[2.58, 6.50]

CONCLUSION

The three-elements model can be used to simulate the deformation regularity concerning about clay creep of shallow layer in Shanghai and optimization method can be employed to select model and inversely calculate parameters by the data observed in the field for pore water pressure and deformation.

Under the present pumping and recharging conditions, the shallow layer will continuously subside with a rate of 0.5-1.1mm per year.

Under the constant amount of pumping and recharging conditions, to prolong the period of recharging and shorten the period of pumping will be greatly useful to reduce the subsidence of shallow layer.

REFERENCES

Su, H. Y. (1979) Investigation of the Deformation Characteristics of various soil strata Under the influence of pumping out & back of groundwater in Shanghai. Chinese Journal of Ceotechnical Engineering, Vol. 1, No.1, PP. 24-30.

Qian, S. Y & Gu, X. Y. (1981) Computation of Shanghai Land Subsidence. Chinese Journal of Geotechnical Engineering, Vol. 3, No.1, PP. 1-10.

Qian J. H. (1985) Consolidation of Soils Under static and Dynamic loading. Proceedings of fifty international conference on numerical methods in geomechanics, NAGOYA, Japan, Vol. 1, PP. 105-110.

Alfredo H-S. & Wilso H. Tang. Probability Concepts in Engineering Planning and Design Vol. 2, PP. 274-320.

Land Subsidence (Proceedings of the Fourth International Symposium on Land Subsidence, May 1991). IAHS Publ. no. 200, 1991.

Mathematical Modelling of Land Subsidence Due to Pumping of a Multi-Aquifer System with Viscoelastic Properties

J. F. MIAO & L. G. WU
Department of Geotechnical Engineering, Tongji University, Siping Road 1239, Shanghai 200092, China

ABSTRACT A mathematical model of flow of a two-aquifer system (VEF model) is proposed in this paper, which represents viscoelastic hydraulic properties of the aquifer system and the characteristic of three-dimensional flow in the pumped aquifer. The model of the land subsidence (VES model) is suggested by coupling the VEF model to Merchant's one, which represents viscoelastic mechanical properties of the aquifer system matrix. The exact solution of the VEF model and that of the VES model are derived. All the results given by Hantush (1961), Neuman and Witherspoon (1969) can be obtained from the model of this paper.

NOTATION

S, S_1, S_2: drawdown in the pumped aquifer, aquitard, unpumped aquifer
K_r, K_z: radial and vertical permeability of the pumped aquifer
K_1, K_2: permeability of the aquitard and unpumped aquifer
M, M_1, M_2: thickness of the pumped aquifer, aquitard, unpumped aquifer
T_r: radial transmissibility of the pumped aquifer
T_1, T_2: transmissibility of the aquitard, unpumped aquifer
a, a_1, a_2: primary compressibility of soil skeleton of the pumped aquifer, aquitard, unpumped aquifer
b_1, b_2: secondary compressibility of soil skeleton of the aquitard, unpumped aquifer
q_1, q_2: viscosity of soil skeleton of the aquitard, unpumped aquifer
$\bar{n}$, $\bar{n}_1$, $\bar{n}_2$: porosity of soil skeleton of the pumped aquifer, aquitard, unpumped aquifer
α : reciporocal of Bulton's delay index
S_y: specific yield of the unpumped aquifer
Q : pumping rate
r : radial distance from pumping well center
t : pumping time
Z : vertical coordinate, positive downword, the zero is on the top of the pumped aquifer
$J_0(x)$: zero order Bessel function of the first kind
$K_0(x)$: zero order modified Bessel function of the second kind
β : elastic compressibility of water
ΔM, ΔM_1, ΔM_2: compression volume of soil skeleton of the pumped aquifer, aquitard, unpumped aquifer
D : total volume of the land subsidence
r_w : specific weight of water

INTRODUCTION

Land subsidence is the sinking or the settling of the land surface caused by natural conditions and people's actions. The withdrawal of groundwater causes compaction and leads to the land subsidence due to the addition of the effective stress resulting from

drawdown and the dissipation of the pore-water pressures of a saturated soil. Owing to the consolidation representing the response of a compressible porous medium to changes in the fluid flow field operating within it, it has long been understood that the land subsidence is best analyzed with reference to the theory of consolidation. A complete analysis of the land subsidence requires determination of the three-dimensional deformation field that accompanies the three-dimensional flow field, and this must be accomplished in a complex multi-aquifer system.

The phenomenon of the land subsidence is a type of consolidation known as in soil mechanics, the gradual dissipation of the pore-water pressures of a saturated soil and its settlement under an imposed load. Consolidation is generally considered to consist of a primary and a secondary phases. The primary consolidation is commonly assumed to be the deformation resulting from the elastic properties of the soil skeleton, which is coupled with the viscous flow of the pore-water. Thus, the primary consolidation is not immediate but graudal to allow the excess pore pressure to dissipate. The secondary consolidation or creep refers to the continued deformation that many soils such as clays or peats exhibit under a constant load. It results from a readjustment of the skeleton structure and, even though in a sense that it represents a viscous response, it has a stable limit with time. Most previous theoretical analyses of the land subsidence are based on one or other forms of Terzaghi-Jacob theory in which aquifer compaction has generally been assumed to be proportional to the pore-water pressure decrease; thus, only the primary consolidation has been considered; the secondary consolidation due to viscous properties of the aquifers and aquitards has not been included. Nevertheless, the secondary consolidation is recognized as an important factor causing soil compaction. In some recent literatures, the shortage of a theoretical analysis of the land subsidence based on linearly elastic consolidation theory has been considered and a rheological theory has been used to analyze the properties of soil compaction instead of the elastic theory and, by comparing the calculating results of the rheological and elastic theory with practice, the general conclusion is reached as follows:

Theoretical analyses and calculations based on the reological theory can explain the mechanical properties of the land subsidence more comprehensively and exactly and predict the total volume of the land subsidence more accurately than that based on the elastic theory. But when using rheological theory to analyze and predict the land subsidence, we have to face the new problem: the number of formation parameters is increased.

For most present theoretical analyses and calculations of the land subsidence there are such problems: usually only the compaction of pumped aquifers has been considered, but the response of the whole aquifer system has not been involved, and the respondence to the aquifer system of the storage release in the semipervious layer has usually been ignored. The theory of the land subsidence proposed in this paper would try to overcome the shortages mentioned above.

VISCOELASTIC THEORY OF FLOW IN A TWO-AQUIFER SYSTEM

The problem of flow in leaky aquifers has been studied by many scholars. The review of the literature (Hantush, 1955, 1960) (Neuman & Witherspoon, 1969) (Javandel & Witherspoon, 1983) (Chen et al, 1986) shows that the development of the present theories of flow in leaky aquifers is generally based on the coupling of elastic deformation theory to the classic diffusion equation, and the three-dimentional flow resulting from pumping with a partially penetrating well has not been included.

A viscoelastic deformation theory —— Merchant's model

The secondary consolidation is a specially important phase in the compaction of fine

soils. Owing to its deficiencies, the classic elastic theory can't explain the phenomenon of the secondary consolidation in the process of soil compaction. Viscoelastic theory provides a possible extension of the classic elastic theory that allows the inclusion of the secondary consolidation.

Merchant presented one of the most popular viscoelastic model —— Merchant's model (Taylor & Merchant, 1940). It forms the basis for several others. Its main advantage is that it represents some essential features of a consolidating soil, while requiring a minimal number of parameters.

Merchant's model corresponds a body consisting of a Hooking spring placed in series with a Kelvin body; a Kelvin body consists of a linear spring placed in parallell with a linearly viscous dashpot. And the stress-strain relationship shown by Merchant's model is as follows:

$$Eq_0'' \varepsilon + Eq_1'' \partial \varepsilon / \partial t = (E + q_0'')p + q_1'' \partial p / \partial t \tag{1}$$

where p = the incremental fluid pressure over and above the initial hydrostatic pressure under equilibrium conditions. E and q_0'' are the elastic moduli of the two components; q_1'' is the viscosity of the Kelvin body; and the total solid strain of the body $\varepsilon = \varepsilon_K + \varepsilon_H$, in which ε_K is the strain of the Kelvin body and ε_H is the strain of the Hooking spring.

In equation 1, the two terms of $Eq_0'' \varepsilon$ and $(E + q_0'')p$ represent the elastic deformation of soil under an incremental fluid pressure, stress p, whereas $q_1'' \partial p / \partial t$ and a part of $Eq_1'' \partial \varepsilon / \partial t$ describe the nonelastic deformation of soil under the secondary consolidation.

A viscoelastic flow equation in aquifers

By coupling the classic diffusion equation to equation 1 obtained from Merchant's viscoelastic model, Brustsaert and Corapcioglu (1976) proposed a viscoelastic flow equation of homogeneous, isotropic porous media with viscoelastic properties as follows:

$$(K/r_w)\Delta S = (\alpha_1 + \bar{n}\beta)\partial S / \partial t + \\ + (q_1'')^{-1} \partial / \partial t \int_0^t S(\tau) \exp [- (t - \tau)/\alpha_2 q_1''] \, d\tau \tag{2}$$

where α_1 and α_2 denote the primary and the secondary compressibilities respectively; K is the permeability of porous media.

The third kind of viscoelastic model of cross-flow in porous media

Consider an aquifer system comprising a non-confined and a confined aquifer separated by an aquitard as is shown schematically in Fig. 1. A partially penetrating well discharges only the lower confined aquifer at a constant rate. Each layer is homogeneous, anisotropic, horizontal, and of infinite radial extent. The flow in the aquifer system follows Darcy's law. Assume that flow is horizontal in the unpumped aquifer and vertical in the aquitard. The assumption is satisfactory so long as the permeability contrasts are greater than two orders of magnitude.

According to the data measured from field and model experiments, we may suggest that there is only elastic compaction in the lower confined aquifer comprising mainly sands, and the compaction caused by pumping has viscoelastic properties in the non-cofined aquifer and aquitard which consist of sandy loam or simply loam. With the help of the viscoelastic flow equation 2, in a manner similar to Neuman and Witherspoon's (Neuman & Witherspoon,1969), the third kind of viscoelastic model of cross-flow in the two-aquifer

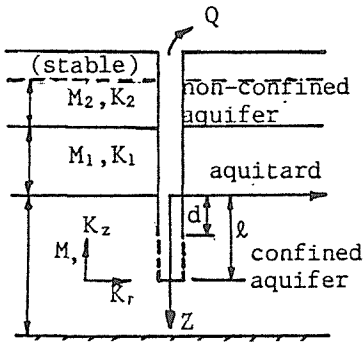

FIG. 1 Schematic diagram of two-aquifer system.

system with an aquitard (VEF model) is developed as follows:

In the aquitard:

$$\text{I}\begin{cases} (K_1/r_w)\,\partial^2 S_1/\partial Z^2 = (a_1 + \bar{n}_1\beta)\,\partial S_1/\partial t + \\ \quad + q_1^{-1}S_1 - (1/b_1q_1^2)\int_0^t S_1(Z, r, \tau)\exp[-(t-\tau)/b_1q_1]\,d\tau & (3) \\ S_1(Z, r, t)\,|_{t=0} = 0 & (4) \\ S_1(0, r, t) = S(0, r, t) & (5) \\ S_1(-M, r, t) = S_2(r, t) & (6) \end{cases}$$

In the non-confined aquifer:

$$\text{II}\begin{cases} (K_2/r_w)[\partial^2 S_2/\partial r^2 + (1/r)\,\partial S_2/\partial r] + (K_1/M_2r_w)(\partial S_1/\partial Z)\,|_{Z=-M1} = \\ \quad = (a_2 + \bar{n}_2\beta)\,\partial S_2/\partial t + q_2^{-1}S_2 - \\ \quad - (1/b_2q_2^2)\int_0^t S_2(r, \tau)\exp[-(t-\tau)/b_2q_2]d\tau + \\ \quad + (\alpha S_y/M_2 r_w)\int_0^t [\partial S_2(r, \tau)/\partial \tau]\exp[-\alpha(t-\tau)]\,d\tau & (7) \\ S_2(r, t)\,|_{t=0} = 0 & (8) \\ S_2(r, t)\,|_{r\to\infty} = 0 & (9) \\ \lim_{r\to 0} r(\partial S_2/\partial r) = 0 & (10) \end{cases}$$

In the lower pumped aquifer:

$$\text{III}\begin{cases} (K_r/r_w)[\partial^2 S/\partial r^2 + (1/r)\,\partial S/\partial r] + (K_z/r_w)\,\partial^2 S/\partial Z^2 - \\ \quad - (K_1/M' r_w)\,\partial S_1/\partial Z\,|_{Z=0} = (a+\bar{n}\beta)\,\partial S/\partial t & (11) \\ S(Z, r, t)\,|_{t=0} = 0 & (12) \end{cases}$$

$$|S(Z, r, t)| = 0 \tag{13}$$
$$r \to \infty$$

$$\text{III} \quad \lim_{r \to 0} r(\partial S/\partial r) = \begin{cases} 0, & \text{for } 0 \leqslant Z \leqslant d \\ -Q/2\pi K_r(\ell - d), & \text{for } d \leqslant Z \leqslant \ell \\ 0, & \text{for } \ell < Z \leqslant M \end{cases} \tag{14}$$

$$|\partial S/\partial Z|_{Z=0} = 0 \tag{15}$$

$$|\partial S/\partial Z|_{Z=M} = 0 \tag{16}$$

The main advantages of the VEF model are:

(a) both the variation of water head in the unpumped aquifer and the viscoelastic storage release from the aquitard are included;
(b) the three-dimensional flow resulting from pumping with a partially penetrating well is considered;
(c) the influence of free water delay is modified by applying Bulton's way;
(d) the viscoelastic properties of compaction caused by pumping is included. When $\alpha = 0$ the model consisting of equation groups I, II and III becomes one of a two-confined system with an aquitard.

VISCOELASTIC MODEL OF THE LAND SUBSIDENCE

Corresponding to the assumptions of the development of the VEF model, the stress ~ strain relationship of soil compaction in the aquifer system resulting from pumping are as follows:

In the pumped (lower) confined aquifer:

$$\varepsilon(Z, r, t) = a\, S(Z, r, t) \tag{17}$$

In the non-confined (unpumped) aquifer:

$$\varepsilon_2(r, t) = a_2 S_2(r, t) + q_2^{-1} \int_0^t S_2(r, \tau) \exp[-(t-\tau)/b_2 q_2] d\tau \tag{18}$$

In the aquitard:

$$\varepsilon_1(Z,r,t) = a_1 S_1(Z,r,t) + q_1^{-1} \int_0^t S_1(Z,r,\tau) \exp[-(t-\tau)/b_1 q_1] d\tau \tag{19}$$

where ε, ε_1, ε_2 are the strains of soil skeleton of the aquifer system.

The development of the VEF model produces a theoretical basis and a calculating tool for the theoretical analysis and prediction of the land subsidence. Coupling to the viscoelastic deformation models, equations 17, 18, and 19, with the model composed of the sets of integral-differential equations I, II, III, is the theoretical model of the land subsidence which represents the viscoelastic properties of soil compaction caused by pumping of the two-aquifer system. From the result of this coupling one can obtain the following formulas:

$$\Delta M(r, t) = a \int_0^M S(Z, r, t) dZ \tag{20}$$

$$\Delta M_1(r, t) = a_1 \int_{-M1}^{0} S_1(Z, r, t) dZ + q_1^{-1} \int_{-M1}^{0} \int_0^t S_1(Z,r, \tau) \exp[-(t-\tau)/b_1 q_1]\, d\tau\, dZ \tag{21}$$

$$\Delta M_2(r, t) = a_2 M_2 S_2(r, t) +$$

$$+ M_2 q_2^{-1} \int_0^t S_2(r, \tau) \exp[-(t-\tau)/b_2 q_2] \, d\tau \tag{22}$$

$$D(r, t) = \Delta M(r, t) + \Delta M_1(r, t) + \Delta M_2(r, t) \tag{23}$$

when $\alpha = 0$, the viscoelastic model of the land subsidence (VES model) becomes one of a two-confined aquifer system (with an aquitard).

THE EXACT SOLUTIONS OF THE VISCOELASTIC MODELS

After applying Laplace and Hankel and Fourior transforms to the sets of equation groups I, II and III and inverting the results, one can obtain the complete solutions to the viscoelastic models as follows:
In the lower confined aquifer (pumped):

$$S(Z, r, t) = [Q/4\pi K_r(\ell - d)] \int_0^\infty [1 - \exp(-y^2 t)]\{G_1(y) J_0(\sqrt{\omega_1(y)}) - G_2(y) J_0(\sqrt{\omega_2(y)}) + \sum_{n=1}^{\infty} \eta_n(y, Z) J_0(\sqrt{\delta_n(y)})\} dy/y \tag{24}$$

$$\Delta M(r, t) = [M a Q/4\pi K_r(\ell - d)] \int_0^\infty [1 - \exp(-y^2 t)]\{G_1(y) J_0(\sqrt{\omega_1(y)}) - G_2(y) J_0(\sqrt{\omega_2(y)}) + \sum_{n=1}^{\infty} \eta_n(y) J_0(\sqrt{\delta_n(y)})\} dy/y \tag{25}$$

In the non-confined aquifer (unpumped):

$$S_2(r, t) = [Q/4\pi K_r(\ell - d)] \int_0^\infty [1 - \exp(-y^2 t)]\{G_3(y) J_0(\sqrt{\omega_1(y)}) - G_4(y) J_0(\sqrt{\omega_2(y)}) - \sum_{n=1}^{\infty} \sim \eta_n(y) J_0(\sqrt{\delta_n(y)})\} dy/y \tag{26}$$

$$\Delta M_2(r, t) = [M_2 Q/4\pi K_r(\ell - d)] \int_0^\infty \{a_2 + b_2 + [b_2^2 q_2 y^2/(1 - b_2 q_2 y^2)] \exp(-t/b_2 q_2) - [(a_2 + b_2 - a_2 b_2 q_2 y^2)/(1 - b_2 q_2 y^2)] \exp(-y^2 t)\}\{G_3(y) J_0(\sqrt{\omega_1(y)}) - G_4(y) J_0(\sqrt{\omega_2(y)}) - \sum_{n=1}^{\infty} \sim \eta_n(y) J_0(\sqrt{\delta_n(y)})\} dy/y \tag{27}$$

In the aquitard:

$$S_1(Z, r, t) = [Q/4\pi K_r(\ell - d)] \int_0^\infty [1 - \exp(-y^2 t)]\{G_1(y) J_0(\sqrt{\omega_1(y)}) - G_2(y) J_0(\sqrt{\omega_2(y)}) + \sum_{n=1}^{\infty} \eta_n(y, 0) J_0(\sqrt{\delta_n(y)})\}\{\sinh[\sqrt{H_1(y)}(M_1 + Z)] / \sinh[\sqrt{H_1(y)} M_1]\} dy/y - [Q/4\pi K_r(\ell - d)] \int_0^\infty [1 - \exp(-y^2 t)] \times \{G_3(y) J_0(\sqrt{\omega_1(y)}) - G_4(y) J_0(\sqrt{\omega_2(y)}) - \sum_{n=1}^{\infty} \sim \eta_n(y) J_0(\sqrt{\delta_n(y)})\} \times \{\sinh[\sqrt{H_1(y)} Z] / \sinh[\sqrt{H_1(y)} M]\} dy/y, \quad -M < Z < 0 \tag{28}$$

$$\Delta M_1(r, t) = [Q/4\pi K_r(\ell - d)] \int_0^\infty \{a_1 + b_1 + [b_1^2 q_1 y^2/(1 - b_1 q_1 y^2)] \exp(-t/b_1 q_1) - [(a_1 + b_1 - a_1 b_1 q_1 y^2)/(1 - b_1 q_1 y^2)] \exp(-y^2 t)\} \times$$

$$\times (1/\sqrt{H_1(y)})[\coth(\sqrt{H_1(y)}\,M_1) - 1/\sinh(\sqrt{H_1(y)}\,M_1)]\,\{[G_1(y) +$$

$$+ G_3(y)]J_0(\sqrt{\omega_1(y)}) - [G_2(y) + G_4(y)]J_0(\sqrt{\omega_2(y)}) +$$

$$+ \sum_{n=1}^{\infty}[\eta_n(y,0) - \tilde{\eta}_n(y)]J_0(\sqrt{\delta_n(y)})\}dy/y \qquad (29)$$

where

$$G_i(y) = \{2[A(y) - \lambda_1(y)]/[\lambda_2(y) - \lambda_1(y)]\}\{[(\ell - d)/M] +$$

$$+ (2/\pi)\sum_{n=1}^{\infty}(1/n)[\sin(n\pi\ell/M) - \sin(n\pi d/M)][U(y) - \lambda_1(y)]/[U(y) -$$

$$- \lambda_1(y)]\}\,,\ i = 1,\ 2 \qquad (30)$$

$$G_{2+1}(y) = K_1\sqrt{H_1(y)}\,G_1(y)/\{T_2\sinh[\sqrt{H_1(y)}\,M_1]\times[A_2(y) - \lambda_1(y)]\}\,,\ i = 1,\ 2 \qquad (31)$$

$$\eta_n(y,Z) = (4/\pi)(1/n)[\sin(n\pi\ell/M) - \sin(n\pi d/M)]\{(K_z/K_r)(n\pi/M)^2$$

$$\times [U_n(y) - A_2(y)]/[(U_n(y) - \lambda_1(y))(U_n(y) - \lambda_2(y))] - 1 +$$

$$+ \cos(n\pi Z/M)\},\ n = 1,\ 2,\ \ldots \qquad (32)$$

$$\tilde{\eta}_n(y) = (4/\pi)\{K_1\sqrt{H_1(y)}/[T_2\sinh(\sqrt{H_1(y)}\,M_1)]\}(1/n)\times$$

$$\times[\sin(n\pi\ell/M) - \sin(n\pi d/M)]\{(K_z/K_r)(n\pi/M)^2/[(U_n(y) - \lambda_1(y))\times$$

$$\times (U_n(y) - \lambda_2(y))]\}\,,n = 1,\ 2,\ \ldots \qquad (33)$$

$$\overline{\eta}_n(y) = (4/\pi)(1/n)[\sin(n\pi\ell/M) - \sin(n\pi d/M)]\{(K_z/K_r)(n\pi/M)^2$$

$$\times [U_n(y) - A_2(y)]/[(U_n(y) - \lambda_1(y))(U_n(y) - \lambda_2(y))] - 1\}\,,n=1,2,\ \ldots \qquad (34)$$

$$\omega_i(y) = -\lambda_i(y)\,r^2\,, \qquad i = 1,\ 2, \qquad (35)$$

$$\delta_n(y) = -U_n(y)\,r^2\,, \qquad n = 1,\ 2, \qquad (36)$$

$$H_1(y) = -(r_w/K_1)[a_1 + \bar{n}_1\beta)y^2 + V_1/[q_1(V_1 - y^2)] - 1/q_1]\,,\ i=1,2 \qquad (37)$$

$$A_1(y) = [K_1\sqrt{H_1(y)}\,\coth(\sqrt{H_1(y)}\,M_1) - (a + \bar{n}\beta)r_w M y^2]/T_r \qquad (38)$$

$$A_2(y) = [K_1\sqrt{H_1(y)}\coth(\sqrt{H_1(y)}\,M_1) + T_2H_2(y) - \alpha S_y y^2/(\alpha - y^2)]/T_2 \qquad (39)$$

$$B_1(y) = K_1\sqrt{H_1(y)}/[T_r\sinh(\sqrt{H_1(y)}\,M_1)] \qquad (40)$$

$$B_2(y) = K_1\sqrt{H_1(y)}/[T_2\sinh(\sqrt{H_1(y)}\,M_1)] \qquad (41)$$

$$U_n(y) = (K_z/K_r)(n\pi/M)^2 - (a + \bar{n}\beta)r_w y^2/K_r\,, \qquad n = 1,\ 2,\ \ldots \qquad (42)$$

$$U(y) = -(a + \bar{n}\beta)r_w y^2/K_r \qquad (43)$$

$$\lambda_i(y) = 0.5\times[A_1(y) + A_2(y) +$$

$$+ (-1)^i\sqrt{(A_1(y) - A_2(y))^2 + 4\,B_1(y)\,B_2(y)}\,]\,,\ i = 1,\ 2 \qquad (44)$$

here, when $\omega_i(y) < 0$, $J_0[\sqrt{\omega_i(y)}\,]$ must be set to zero, i=1,2; and the same is true

of $J_0[\sqrt{\delta_n(y)}]$, when $\delta_n(y) < 0$, n=1, 2, ...

It can be proved that each function series is uniform convergent in equations 24~29, hence every integration in the above equations is convergent. The exact solutions of the VEF model and those of the VES model are expressed by equations 24 ~29, among which, equations 24, 26, and 28 can be applied to calculate the drawdown in the aquifer system, and equations 25, 27, and 29 can be used to compute the compaction volume of each layer in it caused by pumping.

The viscoelastic models and their exact solutions developed in the paper can be applied to explain the general rules of flow in a two-aquifer system (with an aquitard) in which only the lower confined aquifer is pumped, and of compaction of each layer in it, resulting from pumping. Also, it can be proved that all the results given by Hantush (1961), Neuman and Witherspoon (1969) can be obtained from the models in this paper (owing to the limit of this paper pages, we don't give the detailed deriving process).

APPLICATION

The viscoelastic models presented in the paper were applied to compute the land subsidence resulting from heavy pumping in digging the forth shaft in the engineering of diverting water from the upper reach of Huang Pu River in Shanghai City.

In the field, there was a sedimentary aquifer system deposited in Quaternary period, comprising one non-confined and five confined aquifers which were separated by semipervious and non-pervious layers. The field pumping conditions were similar to the two-aquifer system's: the non-confined aquifer is the unpumped one; the first, the second and the third confined aquifers were formed into a single one which was the pumped confined aquifer of this drainage due to the absence of aquitards and non-pervious layers between them; the layer of the grey and deep green loam underlying the non-confined aquifer was an aquitard. Owing to there being a non-pervious clay layer with large thickness overlying them and pumping mainly from the first confined aquifer, it was suggested that the underlied forth and fifth confined aqufiers be not influenced by the withdrawal. So the conditions of the withdrawal in the field were the same as in the viscoelastic models.

The wells were scattered in a ring of which the radius was 26 meters and with an equivalent interval. The big-well-method was used in calculation. The essence was: imagining a big well placed in the center of the ring with the same structure as of the wells instead of them equivalently, i.e. the pumping rate of the imagining well was the accumulation of the practical pumping rates of the wells. For a varying pumping schedule, drawdown and the land subsidence were computed by successive superposition of each pumping effect. The results of the calculations are shown in Fig. 2 and in Fig. 3.

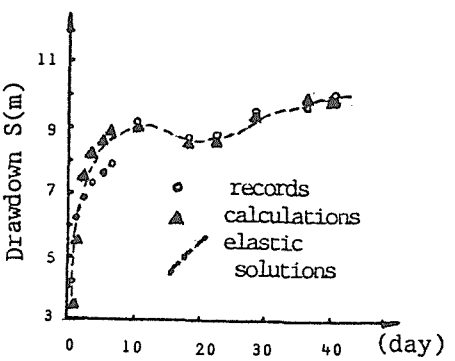

FIG. 2 Curve of drawdown versus time in No. 11 observed well.

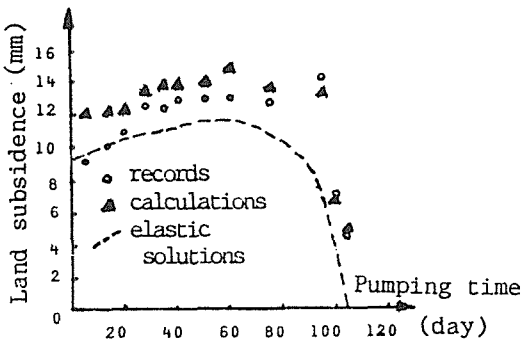

FIG. 3 Curve of the land subsidence versus time at No. 17 measuring point.

CONCLUSION

The VEF model is an extension of the elastic one. It represents viscoelastic properties of flow and deformation in aquifer system. The VES model can explain mechanism of the land subsidence more comprehensively and predict the land subsidence more accurately.

Owing to cross-flow, the deformation of soil skeleton of each layer in vertical direction and the effect of each layer must be considered in calculations of the land subsidence resulting from pumping only in the lower confined aquifer of a two-aquifer system.

The compaction of an aquitard caused by the release of non-elastic storage can't be neglected. Especially for the semipervious layers with large thickness and high compressibility it is important. And the compaction of an aquitard has been included in the viscoelastic model.

The viscoelastic theory presented in this paper has effectively explained the phenomenon of delay compaction resulting from the viscosity of fine soil and the influence of the delay phenomenon of drainage of free water on drawdown in aquifer system and on the land subsidence have been considered.

The elastic theory of cross-flow may be adequate to compute the drawdown in aquifers. However, it appears to be unsatisfactory to calculate the surface subsidence.

REFERENCES

Brutsaert, W. & Corapcioglu, M. Y. Pumping of aquifer with viscoelastic properties, Proc. ASCE HY. 11 Vol. 102, 1976, pp.1663-1675.

Hanthsh, M. S. & C. E. Jacob Steady three-dimensional flow to a well in a two-layered aquifer, Eos Trans. AGU 36, 1955, pp. 286-292.

Hantush, M. S. Modification of the theory of leaky auifers, J. Geophys. Res. Vol. 65, 1960, pp. 3713-3722.

Hantush, M. S. Drawdown around a partially penetrating well, J. Hydraul. Div. Am. Soc. Civ. Eng. 87(Hy4), 1961, pp. 83-98.

I. Javandel & P. A. Witherspoon, Analytical solution of a partially penetrating well in a two-layer aquifer, Water Resour. Res. Vol. 19, No. 2, April 1983, pp. 567-578.

Neuman, S. P. & P. A. Witherspoon Theroy of flow in a confined two-aquifer system, Water Resour. Res. 5(41), 1969, pp. 803-816.

Talor, D. W. & W. Merchant A theory of clay consolidation accounting for secondary compression, Journal of mathematics and physics Vol. 19, No. 3, 1940, pp. 167-185.

Z. X. Chen, Z. Y. Pang, L. S. Jiang & M. X. Liu exact solution for the problem of cross-flow in a bounded two-aquifer system with an aquitard, Water Resour. Res. Vol. 22, No. 8, August 1986, pp.1225-1236.

Land Subsidence (Proceedings of the Fourth International Symposium on Land Subsidence, May 1991). IAHS Publ. no. 200, 1991.

Analysis of Shanghai Land Subsidence

X. Y. GU & S. I. TSIEN
Institute of Mechanics, Chinese Academy of Sciences, Beijing 100080, China
H. C. HUANG & Y. LIU
Environmental Geology Station, Shanghai Bureau of Geology

ABSTRACT A synthetic analysis is carried out by means of incorporating computations and laboratory testing with field measurements. The field observations can be regarded as a large-scale in-situ test. Laboratory testing is used to study the mechanism of subsidence and the soil model as well as to obtain the soil parameters. In the computational analysis the actual boundary water level is resolved into several components and then the one-dimensional consolidation equation is solved in each case to obtain appropriate expressions for excess pore-water pressure and deformation. The computational results are comparable with the in-situ data. The results of analysis provide a scientific basis for determining the effective control measures and indicate the directions of future work.

NOTATION

A,B	-Fourier coefficients
C_v	-average coefficient of consolidation during cyclic loading
C_{vc}	-coefficient of consolidation
C_{vs}	-coefficient of rebound
e_o	-initial void ratio
G	-specific gravity
H	-thickness of soil layer
H_1,H_2	-depths of upper & lower boundaries of the compressible layer
h_2	-boundary water-level drawdown
K	-hydraulic conductivity
m_v	-coefficient of volume change
m_{vc}	-coefficient of volume compression
m_{vs}	-coefficient of volume rebound
$(m_{vc})_f$	-coefficient of compression from field data
$(m_{vs})_f$	-coefficient of volume rebound from field data
N	-number of cycles
n	-integral number
OCR	-overconsolidation ratio
P	-amplitude of cyclic water pressure
S	-deformation of soil layer
T	-time factor
t	-time
t_o	-equivalent time

U	-degree of consolidation
u	-excess pore-water pressure
W	-natural water content
W_L	-liquid limit
W_p	-plastic limit
z	-depth
α	-slope of linear variation of central water-level change
β	-attenuation factor
γ	-unit weight of soil
γ_w	-unit weight of water
$\sigma*$	-stress caused by loading or boundary water-level change
ω	-circular frequency of cyclic loading

INTRODUCTION

Land subsidence in Shanghai started in 1921. A dish-like depression has been forming continuously with increase of pumpage of underground water. The maximum accumulated subsidence had reached 2.63 m during 1921-1965, and the maximum subsiding rate - 200 mm per year. Since 1963, when pumping water had been reduced, the subsiding rate has decreased, and the average subsidence in 1965 was 23 mm. In 1966 the control measures like artificial water recharging into the aquifers was adopted, since then some rebound of the ground surface took place during 1966-1971. However, since 1972, in spite of the fact that the water recharging exceeds out-pumping, minor subsidence has been observed again. The minor subsidence can especially be demonstrated by the cumulative deformation curves of the compressible layers, which are shown in Fig. 1.

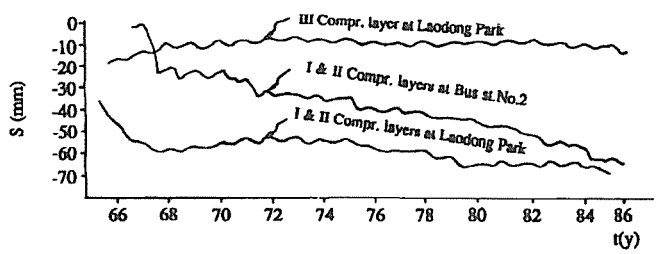

FIG. 1 Accumulated deformation curves of the compressible layers.

In order to study the land subsidence, a large amount of stratification benchmarks, observation wells and piezometers were set up, and many geotechnical boreholes were drilled by the Shanghai Geological Department (Su, 1979). Data from field observations serve as the basis for this analysis. Furthermore, analysis of the laboratory tests under the stress state simulating the field conditions provides the soil model and parameters for computations. Finally, through the computational analysis the theoretical and observed data of pore pressure and deformation are compared, and the validity of the computation method is warranted. Thus, the analysis provides a scientific basis for predicting subsidence and determining effective control measures.

ANALYSIS OF FIELD OBSERVATION DATA

Aquifers and aquitards

In Shanghai overlying the bedrock are sediments of Quaternary system with thickness of 300 m, within which one phreatic and five artesian aquifers are involved. The phreatic water surface is at +2m. Before the control measures were taken, underground water was pumped mainly from the II and III aquifers. The hydraulic gradient of the water level depression is very small, generally about 1/1000, and never exceeds 1/160. A typical curve of water-level changes in aquifer II is shown in Fig. 2.

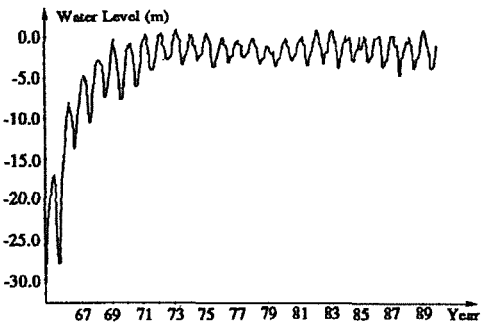

FIG. 2 Water level fluctuation in aquifer II.

The stratification benchmarks show that subsidence takes place mainly in three compressible layers above aquifer II, with a thickness of 70 m. The vertical profile of the soil layers is shown in Fig. 3. The geotechnical indexes of the three compressible layers are given in Table 1. Thicknesses of each compressible layer are less than 20 or 30 m, which is less than 2/1000 of the width of the overall pumping area. Therefore, seepage flow and deformation may be assumed to occur mainly in a vertical direction.

The distribution of soil layers in the whole urban area is not uniform. According to the different combination of soil layers, four engineering geological zones may be designated (see Fig. 4). Within each zone soil distribution and water-level changes in the aquifers are relatively uniform. But subsidences within zones III and IV are somewhat larger than that in zones I and II, and minor subsidence has been continuing in III and IV even after adopting the control measures. Thus, analysis of the zones III and IV is emphasized herein.

TABLE 1 Geotechnical indexes of three compressible layers.

Layer No.	W %	e_o	γ N/m^3	G	W_L %	W_p %	K cm/s	OCR
I	45-58	1.2-1.7	17.2-17.5	2.74	34-42	21-26	nx10^{-8}	1
II	32-42	0.9-1.2	18.0-18.4	2.72	33-35	19-21	nx10^{-7}	1
III	28-35	0.8-1.0	18.2-19.0	2.73	26-40	18-25	nx10^{-7}	1

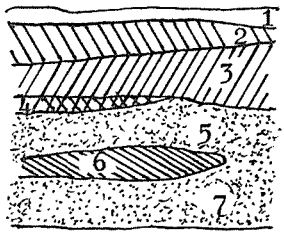

LEGEND
1-Surficial layer 2-I compressible layer
3-II compressible layer
4-Dark green clay 5-I aquifer
6-III compressible layer 7-II aquifer

FIG. 3 Scheme of soil profile.

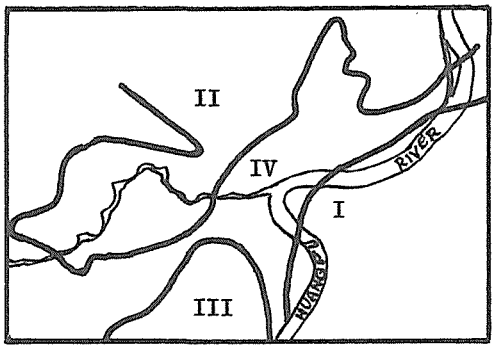

FIG. 4 Map of engineering geological zones.

Piezometric data

The mono-tubing piezometers of open type are used to adopt the long-term measurement and the prevailing negative pore-water pressures. Pore-pressure fluctuation curves at various depths are recorded. The fact that pore-pressure gradients in the compressible layers caused by the water-level fluctuations in the aquifers continue to exist implies that primary consolidation is continuing to the present.

Soil parameters from field data

Since the total overburden pressure of the soil-water system remains constant, if negative excess pore-pressure increases, the effective stress in the soil skeleton increases, in a like manner that tends to result in compression of the soil layer and vice versa.

The relationship between the pore pressure change and soil deformation is:

$$S = m_V \int_{H_1}^{H_2} \Delta u dz \qquad (1)$$

By differentiating the changing direction of the pore pressure m_{VC} and m_{VS} can be obtained. The average values of $(m_{VC})_f$ and $(m_{VS})_f$ are listed in Table 2.

ANALYSIS OF THE LABORATORY TESTS

Consolidation tests under pumping

To study the consolidation process under different loading conditions, consolidation tests with pumping at the lower boundary and the conventional consolidation tests with double drainage are compared (Gu, 1965). It is shown

TABLE 2 Coefficients of volume change obtained from field data (KPa^{-1}).

Site	Compressible layer	$(m_{vc})_f$	$(m_{vs})_f$
Bus station No. 2	I	$2x10^{-5}$	$1.9x10^{-5}$
	II	$0.46x10^{-5}$	$0.35x10^{-5}$
Laodong Park	I	$2.4x10^{-5}$	$1.4x10^{-5}$
	III	$0.55x10^{-5}$	$0.4x10^{-5}$

that the theoretical expressions for degree of consolidation are the same for both cases:

$$U = 1 - \sum_{n=0}^{\infty} \frac{8\exp[-(n+1/2)^2\pi^2 T]}{(2n+1)^2\pi^2} \qquad (2)$$

Similar results of the primary consolidation are also obtained from the experiments. It is concluded therefore that in the land subsidence studies soil.parameters may be obtained by following the routine consolidation test procedures.

To determine method of analyzing complicated water-level fluctuating conditions, tests with different water heads at top and bottom of a sample are conducted so as to set up a trapezoidal distribution of effective stress increments within the sample (Tsien, 1968). The deformation-time curves obtained are comparable to the ones obtained by superposing a rectangular and a triangular effective stress increment pattern, indicating the validity of the superposition theorem in this analysis.

Cyclic consolidation tests

The yearly water-level fluctuation data as demonstrated in Fig. 2 stress the importance of cyclic consolidation tests with low frequencies (Fu & Lou, 1968, Gu et al, 1988). Since load increment ratio has long been known to have an obvious effect on the consolidation behavior, the loading and unloading values are selected in conformity with the actual conditions.

Lowering of boundary water-level implies loading, so coefficient of consolidation C_{vc} is substituted in place of C_v in the one-dimensional consolidation equation:

$$\frac{\partial u}{\partial t} = C_v \frac{\partial^2 u}{\partial z^2} + \frac{\partial \sigma^*}{\partial t} \qquad (3)$$

Likewise, rising of boundary water-level means unloading, and C_{vs} is substituted instead. Fig. 5 shows the cyclic loading test results. On the absicissa N, odd and even numbers represent loading and unloading respectively. C_{vs} is larger that C_{vc} when N is not too large, but then they become close to each other. In both cases of unloading or during repeated loading after a certain number of cycles the consolidation process completes rapidly and no secondary consolidation is observed. Fig. 5 also shows that m_{vc} is always larger than m_{vs} in one cycle. With increase of N m_{vc} decreases, but m_{vs} changes moderately. Thus $(m_{vc}-m_{vs})$ declines exponentially. Therefore,

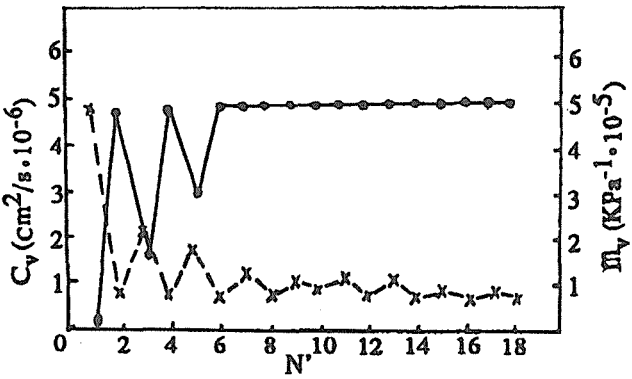

FIG. 5 Variation of C_v, m_v under cyclic loading.

for the condition of no appreciable secondary consolidation, the soil may be regarded as a nonlinear elasto-plastic medium which tends to behave elastically as the number of cycles increases.

COMPUTATION ANALYSIS

Computation method

As above mentioned, land subsidence caused by withdrawal of ground water may be considered as a one-dimensional consolidation problem as described by equation (3). Prior to pumping, excess pore pressure equals zero, $u(z,0) = 0$. The boundary conditions are: i) $u(0,t) = 0$, i.e. the water level at the upper boundary remains unchanged; ii) $u(H,t) = g(t)$ where $g(t)$ represents the water-level change of aquifer II. By using the superposition theorem it is possible to resolve the actual boundary water-level fluctuation into several simple components, namely: fixed drawdown, linear rising, and cyclic change (Tsien & Gu, 1981), in each of which only linear behavior is considered. By solving equation (3) separately, excess pore pressure for different boundary components are obtained:

Fixed drawdown:

$$u_1(z,t) = -\gamma_w h_2 \{\frac{z}{H}+2\sum_{n=1}^{\infty}\frac{(-1)^n \sin(nz\pi/H)\exp[-(n\pi)^2 C_{vc}t/H^2]}{n\pi}\} \qquad (4)$$

Linear rising:

$$u_2(z,t) = \alpha \{\frac{z}{H}t - \frac{z/H[1-(z/H)^2]}{6C_{vs}/H^2} + 2\sum_{n=1}^{\infty}(-1)^{n+1}\sin(n\pi z/H) \times \frac{\exp[-(n\pi)^2 C_{vs}t/H^2]}{(n\pi)^3 C_{vs}/H^2}\} \qquad (5)$$

Cyclic change:

$$u_3(z,t) = P \exp[-\sqrt{\frac{\omega}{2C_v}}(H-z)] \sin[\omega t - \sqrt{\frac{\omega}{2C_v}}(H-z)] \qquad (6)$$

Since many cycles have elapsed, only steady part of the analytical solution is considered here. An average value C_v is used. For the actual water-level fluctuation Fourier transformation must be carried out, then equation (6) becomes:

$$u_3(z,t) = \sum_{n=0}^{\infty} A(n)\exp\left[-\sqrt{\frac{n\omega}{2C_v}}(H-z)\right] \sin\left[n\omega t-\sqrt{\frac{n\omega}{2C_v}}(H-z)\right] +$$

$$+ \sum_{n=0}^{\infty} B(n)\exp\left[-\sqrt{\frac{n\omega}{2C_v}}(H-z)\right] \cos\left[n\omega t-\sqrt{\frac{n\omega}{2C_v}}(H-z)\right] \qquad (7)$$

Finally, total excess pore-water pressure $u = u_1 + u_2 + u_3$.

It should be noted that the water-level records started in 1964, which is far after the year consolidation process began in the soil strata. It may be considered that soil consolidation had been underway in an equivalent time t_0 (Tsien, 1988). Therefore, t_0 should be calculated beforehand according to the field data, then $t + t_0$ is used instead of t in equation (4).

By substituting equations (4) and (5) into (1), expressions (8) and (9) for deformation under different boundary conditions are obtained as follows:

Fixed drawdown component:

$$S_1 = -\frac{1}{2} m_{vc}\gamma_w h_2 H_2\{1-(\frac{H_1}{H_2})^2 - 4\sum_{n=1}^{\infty}(-1)\frac{n[\cos n\pi-\cos(H_1/H_2)n\pi]}{(n\pi)^2} \times$$

$$\times \exp[-(n\pi)^2 C_{vc}t/H_2^2]\} \qquad (8)$$

Linear rising component:

$$S_2 = m_{vs}\alpha H_2\{\frac{1-(H_2/H_2)^2}{2}t - \frac{[1-(H_1/H_2)^2]^2}{24C_{vs}/H_2^2} + 2\sum_{n=1}^{\infty}(-1)^n \times$$

$$\times \frac{[\cos n\pi-\cos(H_1/H_2)n\pi}{C_{vs}(n\pi)^4/H_2^2} \exp[-(n\pi)^2 C_{vs}t/H_2^2]\} \qquad (9)$$

Cyclic change component:

The stress-deformation relationship of the soil during one cycle is shown in Fig. 6. For an entire soil layer, the net deformation after one cycle S_3' is (Tsien & Gu, 1981):

$$S_3' = -2P(2C_v/\omega)^{1/2}(m_{vc} - m_{vs}) \qquad (10)$$

in which $(m_{vc}-m_{vs})$ declines exponentially by a factor β. After taking the Fourier transformation, deformation due to cyclic changes can be written as:

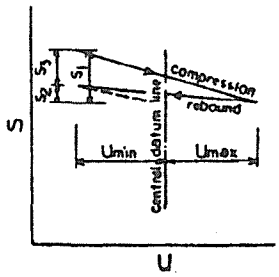

FIG. 6 Stress deformation diagram during one cycle.

$$S_3 = -2\sum_{n=0}^{\infty}[A(n) + B(n)]\,(C_v/n\pi)^{1/2}(m_{vc}-m_{vs})\beta \qquad (11)$$

For the case of using $(m_{vc})_f$ and $(m_{vs})_f$, which are the average parameters calculated from the field data in a specific time interval, β needs not be introduced. The expression for S_3 becomes:

$$S_3 = -2\sum_{n=0}^{\infty}[A(n) + B(n)]\,(C_v/n\pi)^{1/2}[(m_{vc})_f-(m_{vs})_f] \qquad (12)$$

Selection of soil parameters

After determining the computation method, the selection of soil parameters is the next important step to ensure correct results.

As described above, m_v and C_v values for different components are different. C_{vc} in equation (4) and m_{vc} in equation (8) and (11) are obtained from the conventional consolidation tests with load increment ratio = 1. The parameters in equations (5), (6), (9) and (11) are from the cyclic consolidation tests. $(m_{vc})_f$ and $(m_{vs})_f$ in equation (12) are from the field data.

Field observations can be regarded as large-scale in-situ tests, and laboratory testing can be used to study the mechanism of subsidence, the soil model as well as the relationships between various soil parameters. Therefore, the equivalent soil parameters obtained through the combination of laboratory testing and field observations can reflect the full range of soil layer behavior and the actual stress conditions (Tsien, 1981). The soil parameters obtained from the in-situ and laboratory testing together with the ones used in the computations are listed in Tables 2 to 4.

Computation results

Figs. 7 and 8 show the excess pore-water pressure and cumulative deformation curves at Bus Station No. 2 from zone III and at Laodong Park from zone IV respectively. It shows that the computation and the observed data are consistent. It indicated that the computation method based on primary consolidation is acceptable. Fig. 8 also shows the predictions of deformation to the year 2000 under the current water level condition.

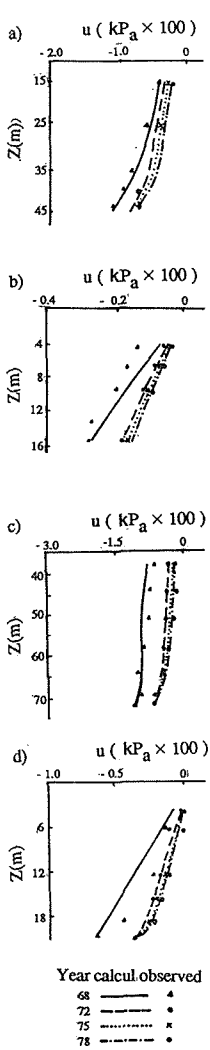

FIG. 7 Computed and observed pore pressure curves.

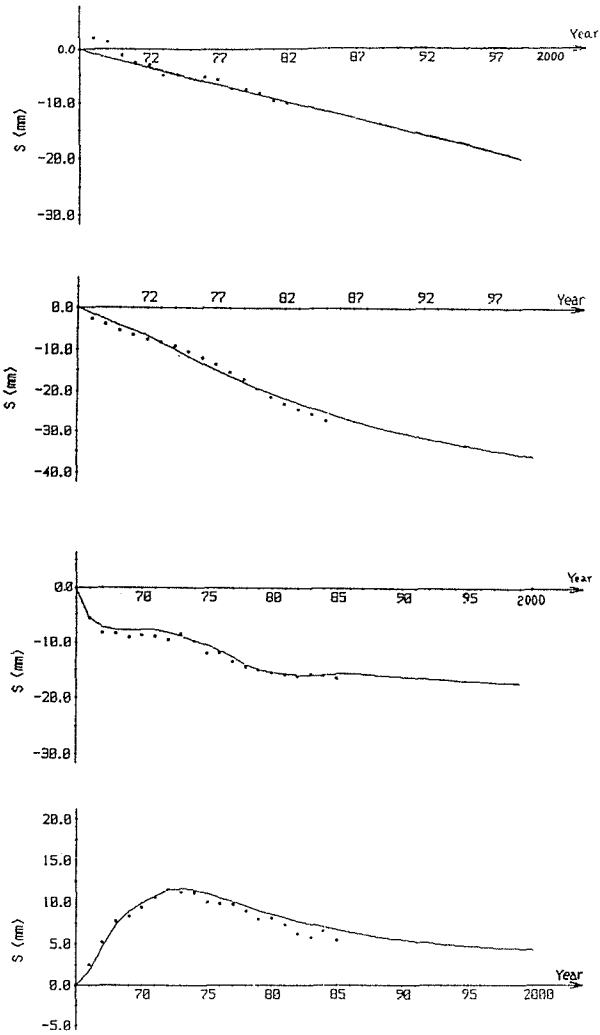

FIG. 8 Computed and observed curves of accumulated deformation.

TABLE 3 Coefficients of consolidation (m^2/year).

Site	Compr.layer	C_{vc}		C_{vs}		C_v	
		Lab	Comp.	Lab	Comp.	Lab	Comp.
Bus st. No. 2	I	3-8	4.7	30	22	30	22
	II	16-100	60	148	150	148	150
Laodong Park	I	5-7	7	20	20	20	20
	III	6-32	30	32-158	40	158	200

TABLE 4 Coefficients of volume change ($KPa^{-1}x10^{-5}$).

Site	Compr.layer	Lab		Comput. Components		
		m_{vc}	m_{vs}	S_1	S_2	S_3
Bus st. No. 2	I	42	2	42	1	$\beta(m_{vc}-m_{vs})$
	II	14	0.7	14	0.7	$(m_{vc})_f-(m_{vs})_f$
Laodong Park	I	35	3	18	2.8	$\beta(m_{vc}-m_{vs})$
	III	7	0.8	4	0.8	$\beta(m_{vc}-m_{vs})$

FUTURE WORK

Secondary consolidation due to soil viscosity and readjustment of its skeleton structure under constant effective stress and the development of excess pore-water pressure and deformation characteristics under cyclic loading are an ongoing part of the authors' future investigations.

Trends of continuing small rates of subsidence reveal that recharging the aquifers is not a cure-all remedy. Determination of the most effective recharging program, including implementation time, depth, frequency and intensity, deserves careful consideration.

REFERENCES

Fu, Y. S. & Lou, Y.Q. (1968) The behavior of Shanghai clay under repeated loading. Inst. of Mechanics (in Chinese).

Gu, X.Y. (1965) A preliminary experimental research on soil compression under pumping. Inst. of Mechanics (in Chinese).

Gu, X.Y., Huang H.C. & Xia, Q. (1988) Report on consolidation testing of Shanghai clay. Internal report (in Chinese).

Gu, X.Y., Gong, S.L., Huang, H.C. & Liu, Y. (1990) Quantitative study of land subsidence in Shanghai. Proc. VI Int. Congress of IAEG vol. 4.

Su, H.Y. (1979) Investigation of the deformation characteristics of various soil strata under the influence of pumping out & back of ground water in Shanghai. Chinese J. of Geotech. Engng. 1 (1), 24-35. (in Chinese)

Tsien, S.I. (1968a) Computation by an analytical method on land subsidence in Laodong Park due to pumping. Inst. of Mechanics (in Chinese).

Tsien, S.I. (1968b) Final report on research of land subsidence in Shanghai. Inst. of Mechanics (in Chinese).

Tsien, S.I. (1981) Some remarks on investigating land subsidence problems (oral discussion). Proc. X Int. Conf. Soil Mechanics & Found. Engng. vol. 4, 743.

Tsien, S.I. Gu, X.Y. (1981a) Computation of Land subsidence in Shanghai, China. X ICSMFE vol. 1, 251-254.

Tsien, S.I. & Gu, X.Y. (1981b) Supplementary remarks on "Computation of land subsidence in Shanghai, China" (written discussion). Proc. X ICSMFE vol. 4, 604-605.

Land Subsidence (Proceedings of the Fourth International Symposium on Land Subsidence, May 1991). IAHS Publ. no. 200, 1991.

Computing the Land Subsidence of Shanghai by a Finite Element Method

A. DASSARGUES
Laboratory of Engineering Geology, Hydrogeology and Geophysical Prospecting, University of Liège, B.19, 4000 Liège, Belgium

X.L. LI
Shanghai Geological Center 17 Guangdong road,Shanghai P.R. China, temporarily detached to the Laboratory of Engineering Geology, Hydrogeology and Geophysical Prospecting, University of Liège

ABSTRACT An accurate simulation by a FEM code has been performed on the case of the subsiding area of Shanghai. In this big city, the subsidence phenomena, caused by groundwater withdrawals, reached an approximate total value of 2.5 meters since 1920. Since 1962, the recharge of water during winters contributed to decelerate the phenomena but a residual consolidation about 3 mm a year is still recorded.
The study area is limited to the central zone of Shanghai and to the upper 70 meters of loose sediments. Quaternary geology, engineering geology and hydrogeology aspects have been examined in details previously to the mathematical simulation,in order to prepare all the needed data. A Finite Element Method (FEM) code has been chosen, allowing a very accurate spatial discretization taking into account heterogeneities and facies variations of the layers. The simulation has comprised a 3D flow model giving as results the values and spatial distributions of the water pressures at each time step. Then, a coupled non-linear flow-compaction model has computed the subsidence in function of time, taking the pressure variations in the aquifers as stress data. After the calibration procedure, simulations have been computed with "neutral" conditions (recharge ≥ pumping) and with "intensive pumping" conditions (pumping = 1.3*recharge). Additional compactions of 1.4 to 7.9 cm are computed for the 1989-2000 period with these last conditions.

INTRODUCTION

The city of Shanghai is situated in the vast low-lying coastal plain (usually called the Yangtze delta) characterized by the lower reach of the Yangtze river (Baeteman & Schroeder, 1990). Due to ground-water withdrawal, mainly from an aquifer situated between 60 and 80 m of depth, land subsidence occurred drastically. It was noticed as from 1921 but it reached 2.5 m to 3 m with a maximum annual rate of 98 mm between 1956 and 1959. Although the total thickness of the loose sediments is about 300 m, the observation data have indicated that 65 % to 85 % of the total subsidence occurred in the upper 70 m portion.

In order to manage the ground-water production and hence control the land subsidence, a mathematical model based on finite element method has been designed. Therefore intensive investigations of the quaternary geology, the hydrogeology and the engineering geology were carried out simultaneously, collecting new data and numerous old data from Shanghai geologists and engineers. This work has been completed together by the Shanghai Geological Center (P.R. China), the Belgian Geological Survey and the Laboratory of Engineering Geology, Hydrogeology and Geophysical Prospecting of the University of Liège (Belgium) (Monjoie et al. 1990). Very detailed data were thus available concerning the coastal lowland geology, the engineering geology and the hydrogeology, to provide the basic elements for the design of the mathematical model (Dassargues et al. 1990).
The geological setting of the Shanghai area (until a depth of about 70 m) has been subdivided into significant lithological units (Fig. 1) on basis of environmental analysis (Baeteman & Schroeder, 1990). The main hydro-engineering geology characteristics are summarized in the papers of Dassargues et al. (1990) and Baeteman & Schroeder (1990).
The total cumulative subsidence given by Fig.2 (Su, 1984 and Shi & Bao, 1979) shows a stabilization from 1963-1965 until 1985, due to the intensive recharge in the second aquifer (2A) in winter. Before the recharge has began the pore pressure maps showed two plate-shaped depression in the urban district, in accordance with the location of the main pumping. Fig.3 illustrates the lowest pore pressures reached in the subsoil of Shanghai before any recharge, in 1960. After 1965, a relative stabilization of the subsidence is obtained after the small elastic rebound, since this date a residual subsidence about 3 mm/year is still recorded and a lot of measurement data have been collected by the Shanghai Geological Center confirming this fact.

sedimentary environment		lithological unit	
fluvial	estuarine & coastal		HOLOCENE
	intertidal and subtidal	1C unit	
	salt marsh (supra tidal)	2C unit	
flood basin and backswamp		DGSC unit	UPPER PLEISTOCENE
natural levee and channel		1A upper unit	
	channel and sand bars	1A lower unit	
	intertidal and subtidal	3C unit	
	channel and sand bars	2A unit	

FIG. 1 Stratigraphic sequence of the Pleistocene and Holocene deposits (from Baeteman & Schroeder, 1990).

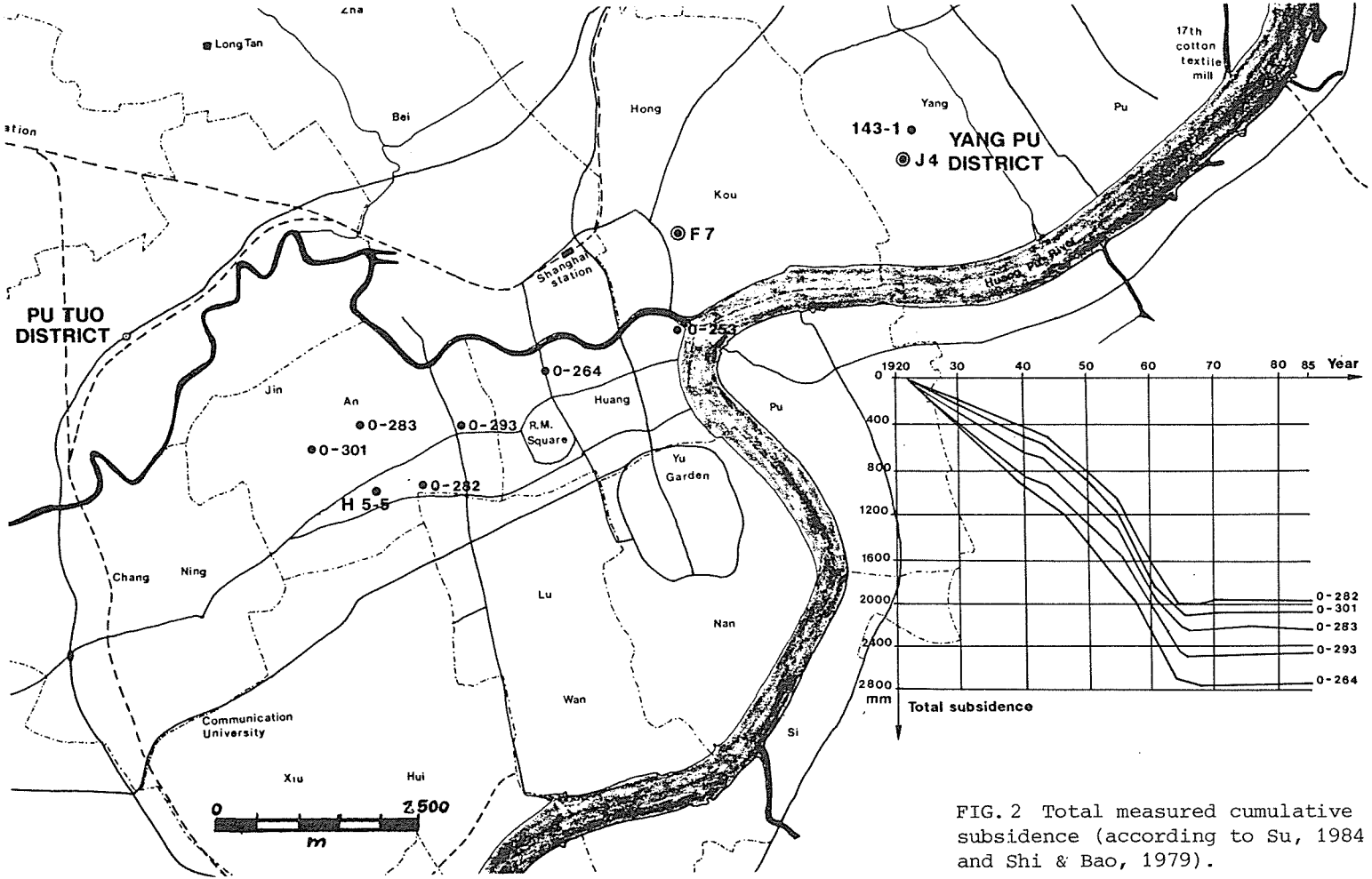

FIG. 2 Total measured cumulative subsidence (according to Su, 1984 and Shi & Bao, 1979).

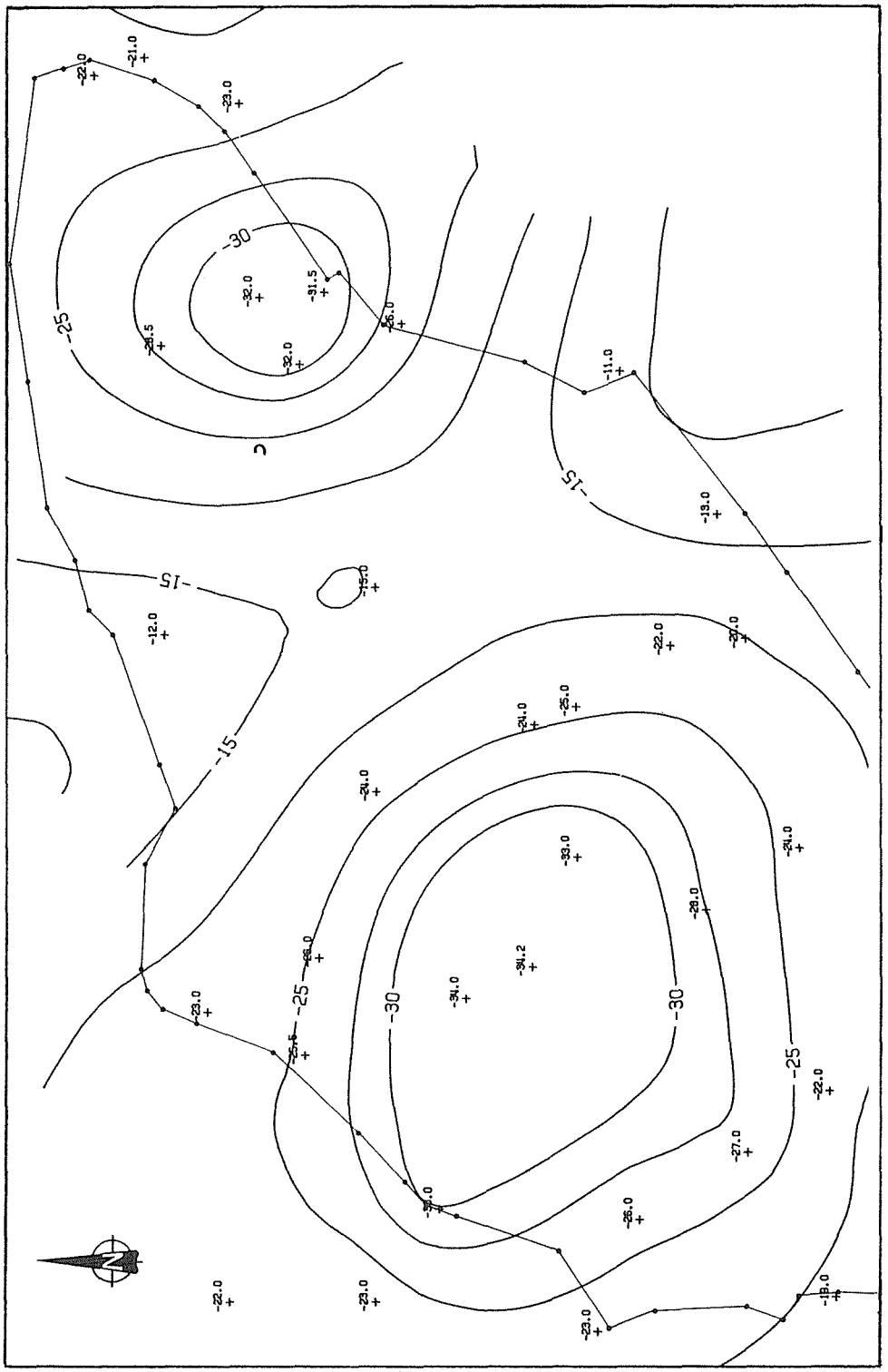

FIG. 3 Measured piezometric map in Shanghai, September 1960.

MAIN FEATURES OF THE NUMERICAL FORMULATION

The land subsidence model of Shanghai includes a transient 3D flow model and a coupled non-linear 1D flow-compaction model. The results of the flow model are the time dependent boundary conditions of the consolidation model. The models are implemented in the finite element code called LAGAMINE developed by the MSM department, University of Liège, since 1982. Large strains, both geometrical and material non-linear problems, mechanical problems, thermal conduction, seepage, ...can be modeled using this code (Charlier et al. 1988). It has been successfully applied in 1985-1987 to calculate the subsidence of the Ekofisk oil-field (Schroeder et al. 1988).

The Flow Model

The finite element method, based on the virtual power principle is applied. The internal virtual power (δW_i) and the external virtual power are expressed for a seepage problem (Charlier, 1987). The Gaussian numerical integration scheme is used on isoparametric 8-nodes brick-like elements.
Two constitutive laws are used : Darcy's law gives (Charlier et al. 1988) :

$$\underline{f} = - \frac{\underline{\underline{K}}}{\gamma_w} \underline{\text{grad}}\ p + \underline{\text{grad}}\ z \qquad (1)$$

where K is the permeability tensor, γ_w the specific weight of water, p the pore pressure and z the vertical coordinate.
For the 3D flow model, the law is considered to be linear : K is isotropic and assumed to be constant. We suppose also that the the volumetric strain variation f^v is equal to the volume of water expelled during the compaction ('storage flow'): $f^v = \dot{V}/V = 3\dot{\varepsilon}_m$ (2)
Using the Terzaghi principle expressed with mean stresses, $\sigma_m = \sigma'_m - p$ is written with tensions as positive stresses. If σ_m is supposed to be constant, we obtain $\dot{\sigma}'_m - \dot{p} = 0$ and $\dot{\sigma}_m = \dot{p}$. Equation (2) can be written :

$$f^v = 3\,\dot{\sigma}'_m / \chi = 3\,\dot{p} / \chi = C_p.\dot{p} \qquad (3)$$

C_p is the storage coefficient expressed in terms of pressure (Dassargues et al. 1988), $C_p = 3/\chi$ with $\chi = E / (1-2\nu)$
Time integration must be realized in the transient flow problem; a Galerkin time scheme has been used for the present model.

Coupled flow-compaction finite element model (Charlier et al. 1990).

The settlement of a "plate-like" aquifer system can be considered as essentially a unidimensional vertical problem. Hereafter, we use the Cauchy stress tensor $\underline{\sigma}$ and the Cauchy conjugated strain tensor $\underline{\varepsilon}$. For the 'oedometric' behaviour of the clayey soils, the effective stress tensor σ' and strain tensor are reduced to :

$$\begin{aligned} &\sigma'_{11} \neq 0\ ,\ \sigma'_{22} = \sigma'_{33} \neq 0 \text{ and } \sigma'_{12} = \sigma'_{23} = \sigma'_{31} = 0 \\ &\varepsilon_{11} \neq 0\ ,\ \varepsilon_{22} = \varepsilon_{33} = 0 \text{ and } \varepsilon_{12} = \varepsilon_{23} = \varepsilon_{31} = 0 \end{aligned} \qquad (4)$$

The virtual internal mechanical power is easily obtained by :

$$\delta W_{im} = \int_V \sigma_{ij}\ \delta\varepsilon_{ij}\ dv = \int_V \sigma_{11}\ \delta\varepsilon_{11}\ dv \qquad (5)$$

The axial strain rate of an element is : $\dot{\varepsilon} = \dot{L} / L_o$,
L represents the length variation rate, L_o is the initial length of the "element". Only flow in the vertical direction is allowed in oedometer tests, so that the expression of the internal

virtual flow power (δW_{if}) is reduced in consequence. We suppose that the elements are only subjected to gravity and the external virtual power (δW_E) is written consequently.
Based on the virtual power principle, equilibrium is obtained when $\delta W_{im} + \delta W_{if} = \delta W_E$ and nodal equivalent forces and flows are then easily got using the Gaussian numerical integration scheme (Charlier et al. 1990). A fully implicit time integration scheme has been adopted.
The following constitutive laws are concerned :

. The Terzaghi principle (Terzaghi, 1943) : $\sigma' = \sigma + p$ (6)

. The oedometer mechanical law (illustrated Fig. 4) can be transformed to an elastoplastic incremental form as follows :

$$\left.\begin{aligned} \dot{\sigma}'_{11} &= -\sigma'_{11}.A.\dot{\varepsilon}_{11} \\ \dot{\sigma}'_{11} &= -\sigma'_{11}.C.\dot{\varepsilon}_{11} \\ \dot{\sigma}_c &= \dot{\sigma}'_{11} \end{aligned}\right\} \quad \begin{aligned} &\text{if } |\sigma'_{11}| < |\sigma'_c| \\ &\text{if } |\sigma'_{11}| = |\sigma'_c| \\ &|\sigma'_{11}| > |\sigma'_c| \quad \text{impossible} \end{aligned} \qquad (7)$$

where σ' is the extreme stress encountered by the soil through its whole history, σ'_{11} represents the yield threshold, it is an internal variable.

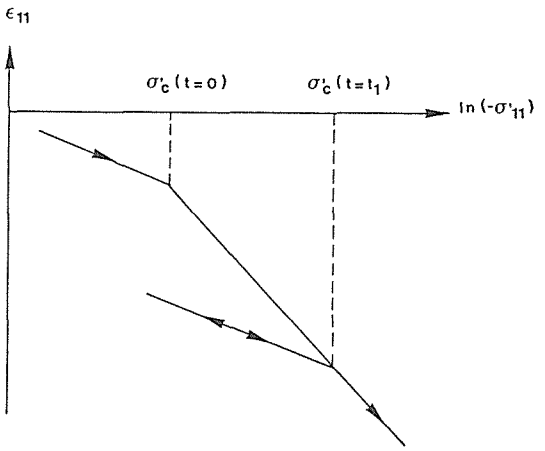

FIG. 4 Oedometer mechanical response.

.The storage is equal to the volumic strain rate because water and soil grains are assumed to be incompressible (equation 3).
.The Darcy's law with a non-linear relation concerning K is inducted. The chosen variation law was developed originally by Nishida & Nakagawa, 1969. Its transformed form is written (Dassargues, 1990) : $K = \exp(\alpha_p e + \beta_p)$ (K in m/s) (8)
where e is the void ratio, α_p and β_p are new material parameters related to plasticity index I_p and are obtained from laboratory tests providing I_p, e and K of the same samples.
We assume that volume variation is only due to void variation :

$$\dot{V}_{total} = \dot{V}_v = \dot{\varepsilon}_{11}(V_v + V_s)$$
$$\dot{e} = \dot{V}_v/V_s = \dot{V}_{total}/V_s = \dot{\varepsilon}_{11}.(V_v + V_s)/V_s = \dot{\varepsilon}_{11}(1+e) \qquad (9)$$

In summary, the relations mentioned above form, non-linear constitutive coupled laws. Where A, C, α_p, β_p, γ_p, γ_s are the parameters which can be determined from laboratory test and σ, σ', σ' and e are internal variables.
The Newton-Raphson technique is used to find the solution.

APPLICATION TO SHANGHAI SUBSIDENCE

The 3D flow model mentioned above with a complete discretization of the soil layers is implemented in the Lagamine code to compute the spatial distribution of the pore pressure in function of time. The study area is divided into 10 layers of 205 8-nodes brick elements each. Fig. 5 and Fig. 6 show the discretization pattern.

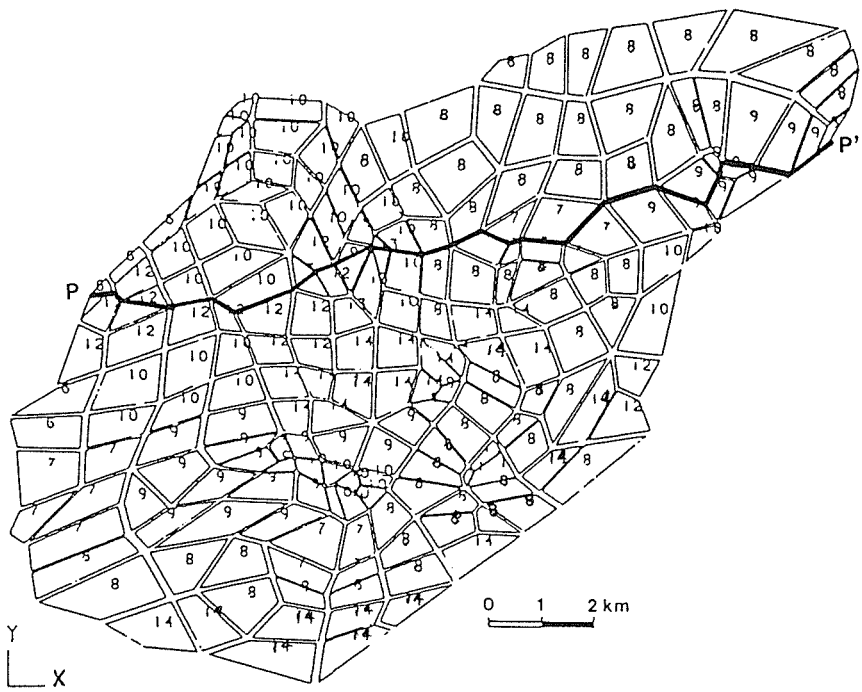

FIG. 5 Discretization of the fifth layer of the structure - Material classes distribution.

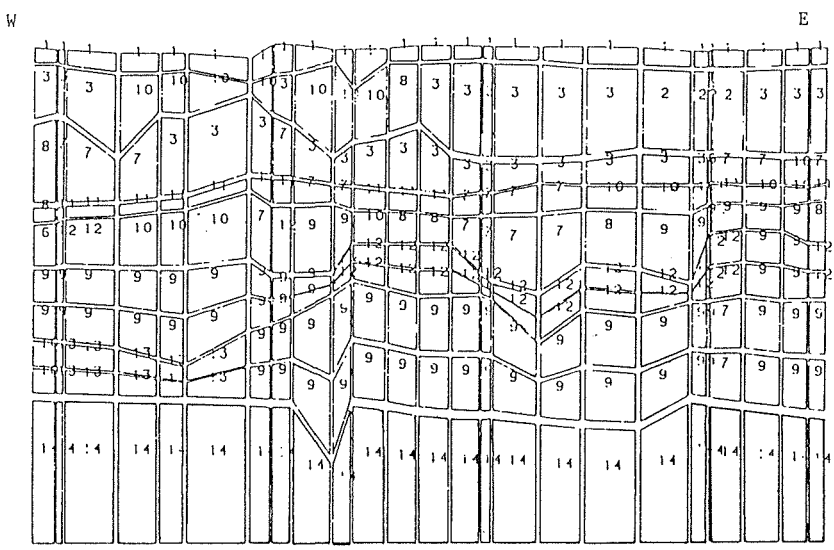

FIG. 6 One of the vertical cross-section in the mesh: section P-P'.

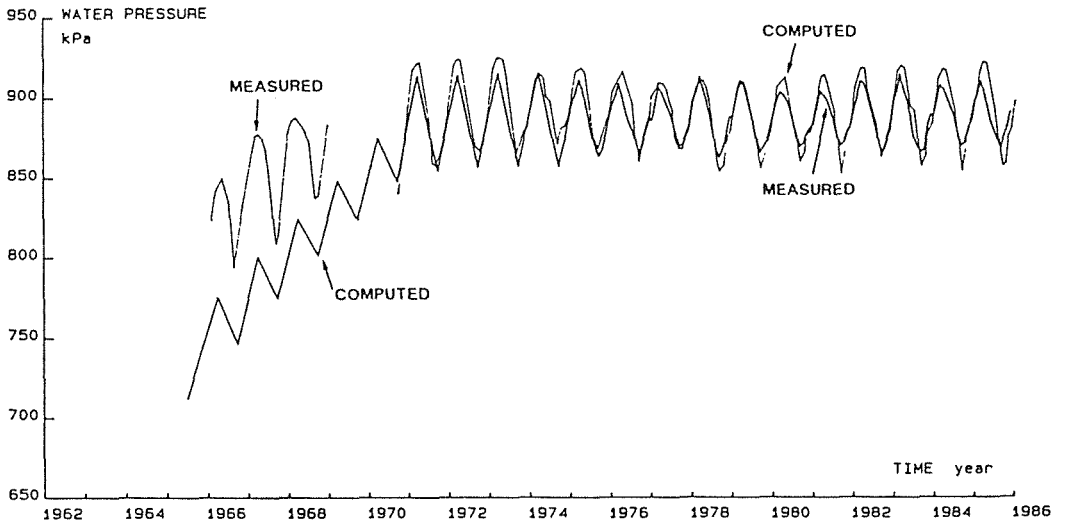

FIG. 7a Computed water pressure vs time at the column below the node 97.

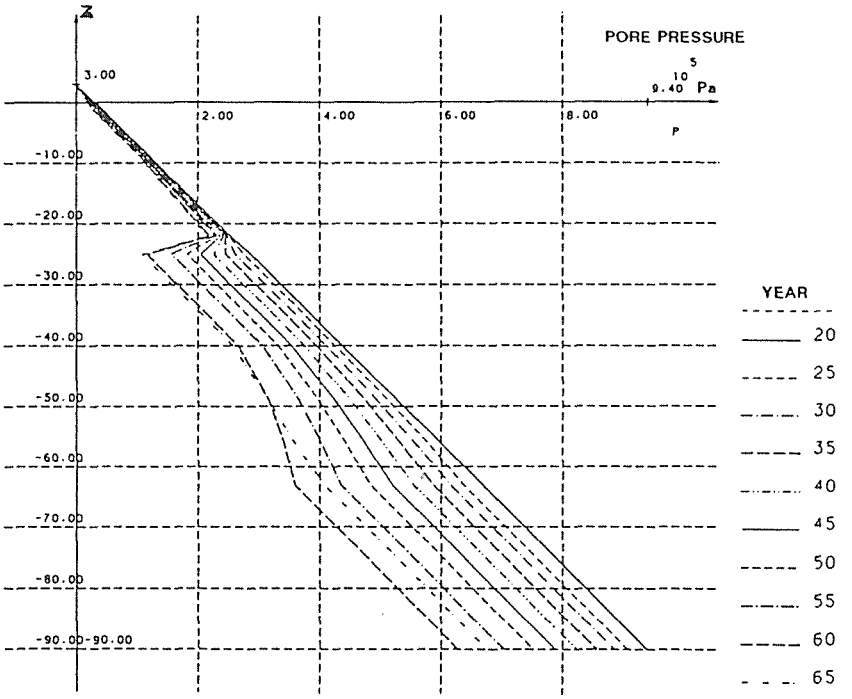

FIG. 7b Computed water pressure vs depth below the node 137 for different years.

The spatial distribution of the two parameters (K and S) is practically realized by using material classes for which the parameters are defined. Fourteen classes of materials are used in the model. As an example, Fig. 5 shows the material classes distribution in the 5th layer.

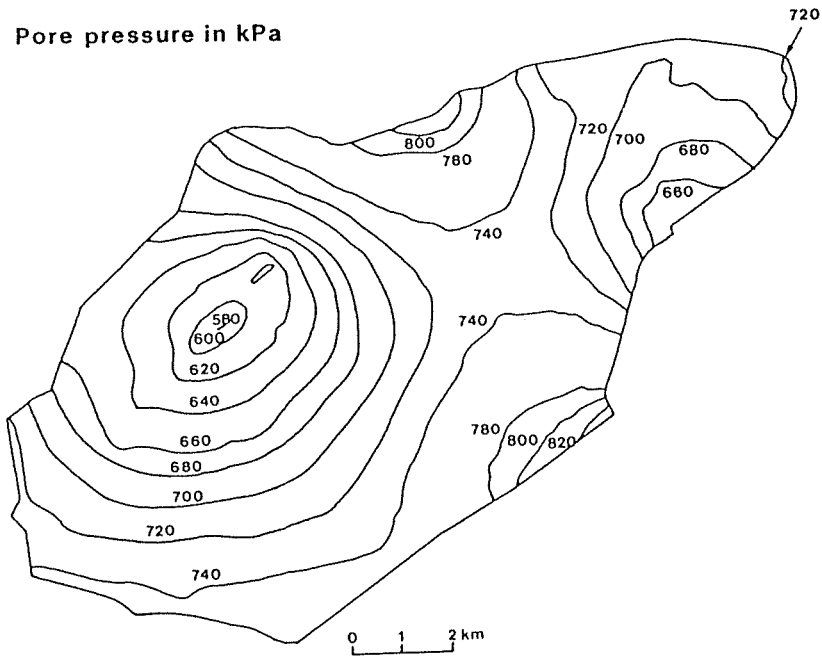

FIG. 8a Computed pore pressure map for the situation in 1960.

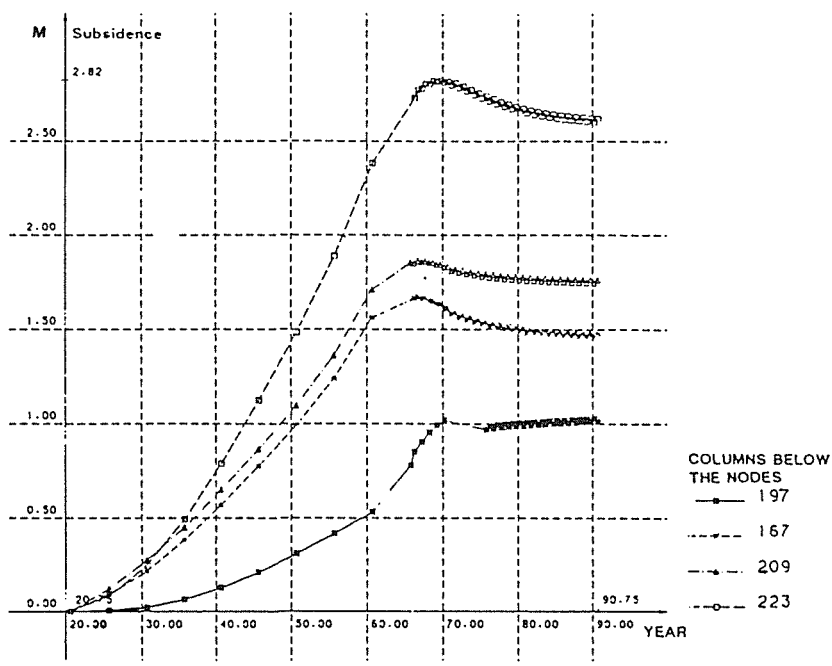

FIG. 8b Computed subsidence vs time in 4 of the 32 columns.

TABLE 1 Computed subsidence values for different running of the model.

Coupled and non-linear model (different running)					P=1.3xR -->2000	Additional subsidence
1st -> 1990	2nd	3rd	4th	1990		
0.55	0.960	1.019	-	1.019	1.033	0.014
1.02	1.470	-	-	1.470	1.507	0.037
1.62	1.754	-	-	1.754	1.779	0.025
2.80	2.683	2.611	-	2.611	2.643	0.032
1.25	1.623	-	-	1.623	1.687	0.064
2.17	2.198	-	-	2.198	2.238	0.040
1.67	2.048	-	-	2.048	2.096	0.048
2.33	2.325	-	-	2.325	2.380	0.055
0.52	0.827	0.998	-	0.998	1.033	0.035
1.63	2.278	-	-	2.278	2.311	0.033
1.58	2.259	-	-	2.259	2.303	0.044
2.17	2.280	-	-	2.280	2.319	0.039
1.23	1.542	1.708	1.881	1.881	1.946	0.065
1.97	2.525	-	-	2.525	2.577	0.052
1.40	1.688	1.832	-	1.832	1.877	0.045
1.51	1.982	-	-	1.982	2.031	0.049
0.95	1.492	-	-	1.492	1.519	0.027
1.72	1.718	-	-	1.718	1.761	0.043
1.42	1.563	-	-	1.563	1.602	0.039
0.96	1.207	-	-	1.207	1.235	0.028
2.06	2.032	-	-	2.092	2.125	0.033
2.05	2.085	-	-	2.085	2.124	0.039
1.34	1.807	-	-	1.807	1.855	0.048
1.58	2.281	1.532	1.867	1.867	1.912	0.045
1.29	1.630	-	-	1.630	1.677	0.047
1.05	1.250	-	-	1.250	1.276	0.026
1.23	1.697	-	-	1.697	1.740	0.043
0.82	1.288	1.319	-	1.319	1.345	0.026
3.12	2.948	-	-	2.948	3.027	0.079
1.79	2.187	-	-	2.187	2.250	0.063
1.72	1.602	1.742	-	1.742	1.778	0.036
1.63	1.556	1.549	1.815	1.815	1.849	0.034

In our analysis, initial state of pore-pressure is chosen in geostatic equilibrium corresponding to the situation before 1920. The boundary are assumed impervious at the bottom and at the top of the model, and imposed varying pressure with time laterally.

K and S determined by various soil test data and several pumping test data, have been slightly modified during "trial and error" calibration. Fig. 7 shows examples of pore-pressure computed results. The choice of the time step is mainly based on the measurements frequency in the pumping/recharge data.
As mentioned above, the subsidence computations are completed with a 1D coupled flow-compaction model. In our study area, 32 columns are chosen to calculate the subsidence. Each column contains 60 elements. The simulation is carried out prescribing the water pressure (obtained by the flow-model), at the aquifer/aquitard boundaries of the modeled columns. These prescribed water pressure are variable in time. Moreover, the non-linear variations of the permeability coefficient K and the specific storage coefficient S are taken into account in the model. Both K and S are actualized at each time step. The variation of K is performed by adapted Nishida relation and the S varies in the following way (Poland,1984 and Dassargues,1990):

$$S_s = \rho.g.\alpha \qquad (\alpha : \text{compressibility of the porous media}) \quad (10)$$

$$\text{and} \begin{cases} S_s = \gamma_w / A \;.\; \sigma'_{11} & \text{(in the elastic part)} \\ S_s = \gamma_w / C \;.\; \sigma'_{11} & \text{(in the plastic part)} \end{cases} \quad (11)$$

The parameters such as A,C,the preconsolidation stress σ' α , β , the initial void ratio of 1920 e are calculated element by element using laboratory test results and some empirical relations. Unfortunately, we have only a small amount of target points available for the calibration, where total subsidence is recorded before 1965 (located on Fig. 2), moreover the recorded subsidence is relative to the compaction of the 300 meters of loose sediments. The part due to the upper 70 m is not known with accuracy. During the calibration, the computed subsidence are checked to be comprised in the measurement ranges.
For the columns situated for away from these measurement points, the lack of available data has forced to make a kind of "blind calibration" to stay in a range of assumed logical values. Of course, the reliability of detailed results is affected by this fact. Some of the results are drawn on Fig. 8 , detailed computed results are shown in table 1.

PREDICTION OF THE LAND SUBSIDENCE

A simulation of the future water pressure distribution is completed with pumping = 1.3 x Recharge, and computed future subsidences between 1988 - 2000 are found out. The computed additional compactions would be comprised between 1.4 and 7.9 cm (table 1).

ACKNOWLEDGEMENTS This work has been carried out under an International Cooperation Agreement between the Ministry of Geology and Mineral Resources of the People's Republic of China and the Services of Scientific Policy and Planning of the Prime Minister of Belgium. The authors are grateful to the Chinese engineers of the Shanghai Geological Bureau for their participation in the works and discussions during the whole study. Thanks must also be expressed to Dr. Baeteman of the Belgian Geological Survey for the detailed Quaternary analysis.

REFERENCES

Baeteman, C. & Schroeder, Ch. (1990) Land subsidence in Shanghai. An application of the interaction between coastal-

lowland geology and engineering geology, Proc. 6th International IAEG Congress, Amsterdam August 1990, Balkema, pp. 191 - 199.

Charlier, R., Radu, J.P. & Dassargues, A. (1988) Numerical simulation of transient unconfined seepage problems, Proc. 1st Int. Conf. Computer Methods and Water Resources, Rabat, March 1988, Springer-Verlag, pp. 143 - 156.

Charlier, R. (1987) Approche unifiée de quelques problèmes non-linéaires de mécanique des milieux continus par la méthode des éléments finis, Doctorat or Ph. Thesis, University of Liège, Belgium, March 1987.

Dassargues, A., Radu, J.P. & Charlier, R. (1988) Finite element modelling of a large water table aquifer in transient conditions, Adv. in Water Resources, Volume 11, June, pp. 58 - 66.

Dassargues, A., Biver, P. & Monjoie, A. (1990) Geotechnical properties of the Quaternary sediments in Shanghai, accepted in Engineering Geology (to be published).

Dassargues, A., Schroeder, Ch. & Monjoie, A. (1990) Engineering geology in the central area of Shanghai : Preparation of the data for subsidence modelling, Proc. 6th International IAEG Congress, Amsterdam, August 1990, Balkema, pp. 1579 - 1588.

Nishida, Y. & Nakagawa, S. (1969) Water permeability and plastic index of soils, in land subsidence IAHS - Unesco, Publ.n° 89, pp. 573 - 578.

Poland, J.F. (1984) Guidebook to studies of land subsidence due to ground-water withdrawal, Unesco, Studies and reports in hydrology n° 40.

Schroeder, Ch., Monjoie, A., Radu, J.P., Charlier, R. & Fonder, G., Ekofisk subsidence compaction, mathematical modelisation synthesis report, internal report L.G.I.H. - M.S.M. for Fina Exploration Norway, 1988, Fina 881, (unpublished).

Shi, L.X. & Bao, M.F. (1979) Case history on subsidence in Shanghai, China, Guidebook to studies of land subsidence due to ground-water withdrawal, Edited by Poland, J.F., Unesco, Studies and reports in hydrology n° 40, pp. 155 - 160.

Su, H.Y. (1984). Mechanism of land subsidence and deformation of soil layer in Shanghai, Proc. of the 3rd International Symposium on land subsidence, Venice, IAHS, 1984, pp. 425 - 433.

Terzaghi, K. (1983) Theoretical soil mechanics, John Wiley and sons.

Land Subsidence (Proceedings of the Fourth International Symposium on Land Subsidence, May 1991). IAHS Publ. no. 200, 1991.

Prediction of Future Subsidence with Quantified Uncertainty by an Inverse Analysis Procedure

YUSUKE HONJO & PRABUDI DARMAWAN
Division of Geotechnical
& Transportation Engineering, Asian Institute of Technology,
P.O. Box 2754, Bangkok 10501, Thailand

ABSTRACT An inverse analysis procedure based on the Terzaghi's one-dimensional consolidation model is developed to predict the future compression of aquitards from available observation. The capability of the methodology is examined by artificial data as well as actual observation data in Nobi plain in Japan and in Bangkok.

INTRODUCTION

Many places of the world suffering from land subsidence have very complex multiple layers of aquifer and aquitard where subsidence takes place due to the drop of heads in the aquifers which result in increase of effective stress in the compressive aquitards. In order to analyze this complex aquifer-aquitard system, a two-step procedure is sometimes employed. (Gambolati & Freeze, 1974). In the first step, regional hydraulic head changes are predicted by using a (quasi-) three dimensional model which is capable of simulating the realistic behavior of this complex aquifer-aquitard system. The predicted head values in the aquifers are then used as time dependent boundary conditions in a set of one-dimensional consolidation models to calculate the compression of the aquitards. This procedure was also adopted in analyzing Nobi plain subsidence problem by Ueshita & Sato (1979, 1980) and Sato, Daito & Ueshita (1984). In this study, an attempt is made to improve the prediction capability of the second procedure, i.e. settlement prediction by a one-dimensional consolidation model.

In prediction, the future subsidence based on an one dimensional consolidation model, one at least needs to know the following information: (1) soil parameters such as compression indices, and coefficients of consolidation of compressive aquitards, (2) present distribution of excess pore water pressure in these layers, and (3) the future change of head distributions of the aquifers.

Purpose of this study is to provide a better solution to problems (1) and (2) mentioned above. An inverse analysis procedure based on the Terzaghi's one dimensional consolidation model, which is to estimate soil parameters as well as the initial excess pore water pressure distributions from the past aquifer head observations and the compression record of the aquitards, is developed and applied. The methodology developed is first examined by a set of artificial data to study the capability, then applied to a long term observation data from Nobi plain, Japan, as well as to a short term record from Bangkok.

METHOD OF ANALYSIS

The methodology employed in this analysis is illustrated in Fig. 1. A set of past observation data on head of aquifers as well as compression of aquitards are used to estimate the parameters in a one dimensional consolidation model. The model employed in this study is the Terzaghi's one-dimensional consolidation theory. The non-linear regression plays the main role in the parameter estimation; the estimation uncertainty involved is also quantified.

The estimated parameters are used to predict the future compression of the aquitards under given time-dependent boundary conditions which are expected to be given from the first step procedure discussed in the previous section. In order to quantify uncertainty involved in the prediction due to the uncertainty of the estimated parameters, the first order second moment (FOSM) method is used to calculate the propagation of uncertainty through the one-dimensional consolidation model.

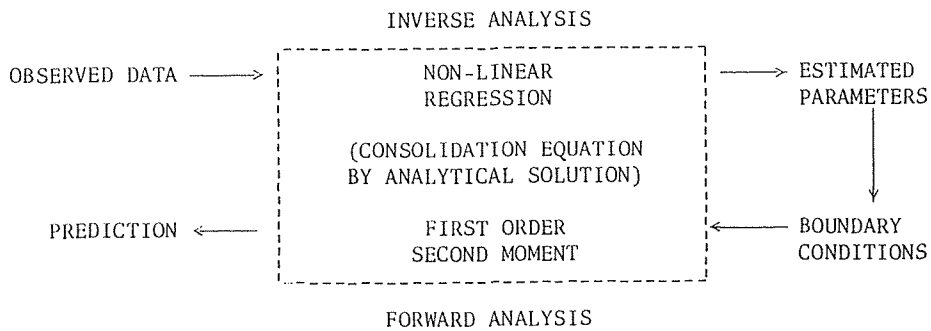

FIG. 1 General concept of the proposed prediction procedure.

The same type of methodology has been developed by Honjo & Morishima (1988) to predict the behavior of large regional aquifers.

One-dimensional consolidation model

A simple one-dimensional consolidation model employed in the calculation of aquitard compression is illustrated in Fig. 2. A homogeneous aquitard with thickness b is surrounded by top and bottom aquifers. For the convenience of the calculation, the time domain is discretized to n portions, and it is assumed that the heads of the aquifers only change at each discretized time, namely t_1, t_2, ..., t_n. It is also assumed that the excess pore pressure distribution at t = 0 is known, i.e. h_{eo} (Z). The total compression of this aquitard at arbitrary time t can be obtained by superposing the analytical solutions obtained for each boundary condition change.

The dissipation of the excess pore pressure can be calculated based on the Terzaghi's consolidation equation:

$$\frac{\partial^2 \Delta h_i}{\partial z^2} = c_v \frac{\partial \Delta h_i}{\partial t} \qquad (i = 0,1, \ldots ,n) \quad (1)$$

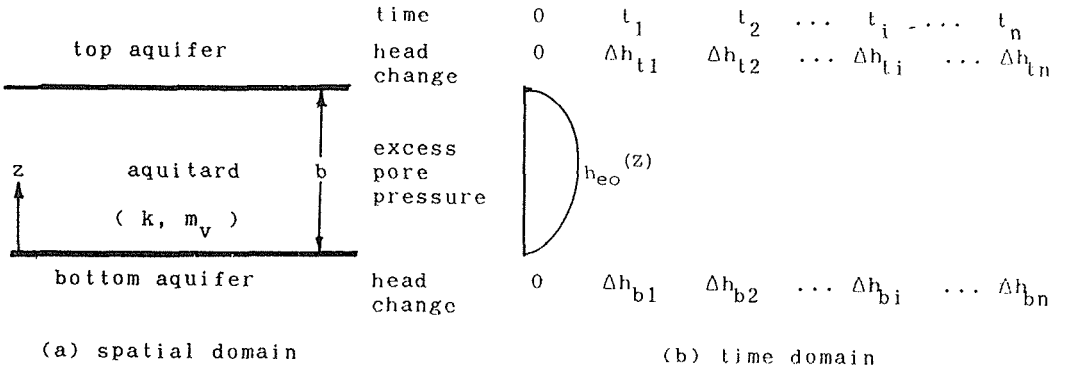

FIG. 2 One-dimensional consolidation model.

where Δh_i : excess pore pressure induced at time t_i
c_v : coefficient of consolidation (= $k/(m_v.\gamma_w)$).

The initial and the boundary conditons for $\Delta h_o(Z,t)$ are given as

$$\begin{aligned} &\text{I.C.} \quad \Delta h_o(Z,0) = h_{eo}(Z) \\ &\text{B.C.} \quad \Delta h_o(0,t) = 0 \qquad \text{for } t \geq 0 \\ &\qquad\quad \Delta h_o(b,t) = 0 \qquad \text{for } t \geq 0 \end{aligned} \tag{2}$$

those for general $\Delta h_i(Z,t)$ are given as

$$\begin{aligned} &\text{I.C.} \quad \Delta h_i(Z,t) = 0 \qquad \text{for } t \leq t_i \\ &\text{B.C.} \quad \Delta h_i(0,t) = 0 \qquad \text{for } t < t_i \\ &\qquad\quad \Delta h_{bi} \qquad \text{for } t \geq t_i \\ &\qquad\quad \Delta h_i(b,t) = 0 \qquad \text{for } t < t_i \\ &\qquad\quad \Delta h_{ti} \qquad \text{for } t \geq t_i \end{aligned} \tag{3}$$

The analytical solutions $\Delta h_o(Z,t)$ for Eqs. (1) and (2), as well as $\Delta h_i(Z,t-t_i)$ for Eqs. (1) and (3) can be obtained in the form of Fourier series (e.g. Taylor, 1948). Based on these solutions, the average degrees of consolidation are calculated as follows. For Eqs. (1) and (2):

$$\Delta U_0(t) = 1.0 - \left[\int_0^b \Delta h_0(z,t)\, dz \Big/ \int_0^b \Delta h_{e0}(z)\, dz\right] \tag{4}$$

and for Eqs. (1) and (3),

$$\Delta U_0(t) = \begin{cases} 0 & \text{for } t < t_1 \\ 1.0 - \left[\int_0^b \Delta h_i(z,t-t_i)\, dz\right] \Big/ \left[b(\Delta h_{bi} + \Delta h_{ti})/2\right] & \text{for } t > t_i \end{cases} \tag{5}$$

On the other hand, the final compression of the aquitard induced by each change of the initial and the boundary conditions can be also calculated. That induced by Eq. (2) is

$$\Delta S_0 = m_v \int_0^b h_{e0}(z)\, dz \tag{6}$$

and by Eq. (3) is

$$\Delta S_i = m_v b \left[\Delta h_{bi} + \Delta h_{ti}\right] / 2 \tag{7}$$

Finally, the total compression of the aquitard from t = 0 to t is obtained by combining Eqs. (4) through (7):

$$S(t) = \sum_{i=0}^{n} \Delta S_i \quad \Delta U_i (t - t_i) \tag{8}$$

Eq. (8) is the basic equation to calculate the compression of the aquitard. Throughout the calculation in this study, the excess initial pore pressure at t = 0, i.e. $h_{eo}(Z)$ in Eq. (2), is assumed to follow the function:

$$h_{e0}(z) = h_m \sin(\pi z/b) \tag{9}$$

Thus, the required parameters to calculate Eq. (8) are k, m_v and h_m ; therefore, Eq. (8) can be rewritten as,

$$S(t \mid k, m_v, h_m) = \sum_{i=0}^{n} \Delta S_i (m_v, h_m)\ \Delta U_i (t - t_i \mid k, m_v, h_m) \tag{10}$$

It should be emphasized that Eq. (10) is developed for the case an initial excess pore pressure exist at the start of calculation. It is developed in this way because most of the observation data on aquifers' heads and aquitards' compressions start from sometime after the occurances of subsidence where the excess pore pressure already exist at the start of the observation.

Inverse analysis procedure

From the past observation on heads of aquifers and compressions of aquitards, the model parameters for Eq. (10) is estimated. The estimation is based on the non-linear regression which is given as follow:

$$\text{min.} \qquad J(k, m_v, h_m) = \sum_{j=1}^{n} \left[S(t_j \mid k, m_v, h_m) - S^*(t_j)\right]^2 \tag{11}$$

where t_j : time at which the observations are given
$S^*(t_j)$: the compression observation at t_j
$S(t_j \mid .)$: the compression calculated by Eq. (10) at t_j
n : number of observations

k, m_v and h_m are estimated by minizing the function J. The set of parameters which minimizes J is indicated by $\hat{u} = (\hat{k}, \hat{m}_v, \hat{h}_m)^T$.

The estimation uncertainty of the parameters can be obtained by applying the method used in the linear regression. For this purpose, the function $S(t|k, m_v, h_m) = S(t|\underline{u})$ is linearized at $\underline{\hat{u}} = (\hat{k}, \hat{m}_v, \hat{h}_m)^T$ by Taylor expansion:

$$S(t|\underline{u}) \sim S(t|\underline{\hat{u}}) + \left\{\frac{\partial S(t|\underline{u})}{\partial \underline{u}^T}\right\}_{\underline{u}=\underline{\hat{u}}} (\underline{u} - \underline{\hat{u}}) \tag{12}$$

The estimation error covariance matrix can be obtained as follows:

$$V_s = \sigma_{ME}^2 \left[\sum_{j=1}^{n} \left\{\frac{\partial S(t_j|\underline{u})}{\partial \underline{u}^T}\right\}^T_{\underline{u}=\underline{\hat{u}}} \left\{\frac{\partial S(t_j|\underline{u})}{\partial \underline{u}^T}\right\}_{\underline{u}=\underline{\hat{u}}}\right]^{-1} \tag{13}$$

where

$$\sigma_{ME}^2 = \frac{1}{n-3} \sum_{j=1}^{n} \left[S(t_j|\underline{\hat{u}}) - S^*(t_j)\right]^2 \tag{14}$$

Thus, the mean and the covariance matrix by the estimated parameters are given as ($\underline{\hat{u}}$, Vs).

Forward analysis procedure

Based on the estimated model parameters and the given future time-dependent boundary conditions, the compression of the aquitard is predicted. Since there is uncertainty in the estimated parameters, the predicted future compression of the aquitard also contains uncertainty. This uncertainty is quantified by employing the First Order Second Moment (FOSM) method. As a result, the mean of the predicted compression at t is given as:

$$S(t) = S(t|\underline{\hat{u}}) \tag{15}$$

and the variance is given as:

$$\sigma_S^2 = \left\{\frac{\partial S(t|\underline{u})}{\partial \underline{u}^T}\right\}_{\underline{u}=\underline{\hat{u}}} V_S \left\{\frac{\partial S(t|\underline{u})}{\partial \underline{u}^T}\right\}^T_{\underline{u}=\underline{\hat{u}}} \tag{16}$$

More details of the methodology introduced in this section can be found in Darmawan (1990).

RESULTS AND DISCUSSION

The proposed method is first applied to a set of artificial observation data where all the true parameters as well as the future compression of aquitard are known to examine the capability of the methodology. Then applied to the data from Nobi, plane, Japan. The results for the Bangkok data are also briefly introduced. For more details, see Darmawan, (1990).

Artificial data to examine the capability of the method

In order to investigate the capability of this proposed methodology, a set of artificial data was prepared: Observation data generated by Eq. (10) using given parameters are used to estimate the parameters so that one can evaluate the estimation accuracy. Also, future prediction of the aquitard compression is made, and compared to the true value.

An isotropic and homogeneous aquitard of the thickness 5 m is assusmed. The permeability and the coefficient of volume decrease are set as $k = 4.2 \times 10^{-7}$ cm/sec and $m_v = 0.03$ cm^2/kg respectively. The initial excess pore pressure is given in the function form of Eq. (9) assuming that $h_m = -3.0$ m.

Instead of using actual time, a normarized time scale is introduced. It is termed "response time", t_{resp}, which is defined as follows:

$$t_{resp.} = T_{50} H^2 / c_v \qquad (17)$$

where T_{50} : time facter for 50% dissipation (= 0.197)
C_u : coefficient of the consolidation
H : thickness of the aquitard

t_{resp} for the present fictitious aquitard is about 41 days.

Based on these information, the artificial data is prepared for the 20 response time as shown in Fig. 3. In order to examine the effect of the duration of the observation, the aquitard compression prediction after 10 response time from the present based on different observation duration is used as a bench mark to measure the accuracy of the prediction.

The estimation errors for the model parameters and the prediction error are evaluated by comparing the estimated values with the true values.

The result of calculation is given in Fig. 4. The prediction errors decrease considerably as the duration of observation exceeds 5 response time, whereas that of k does not improve drastically. As a result the

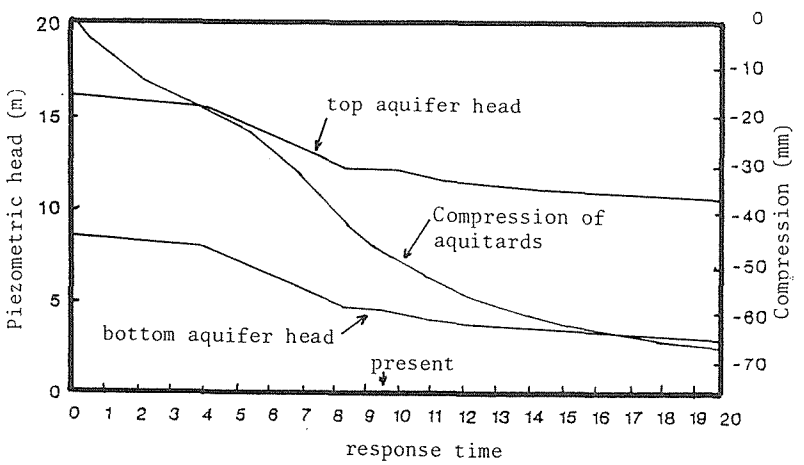

FIG. 3 Artificial data of piezometric head and compression.

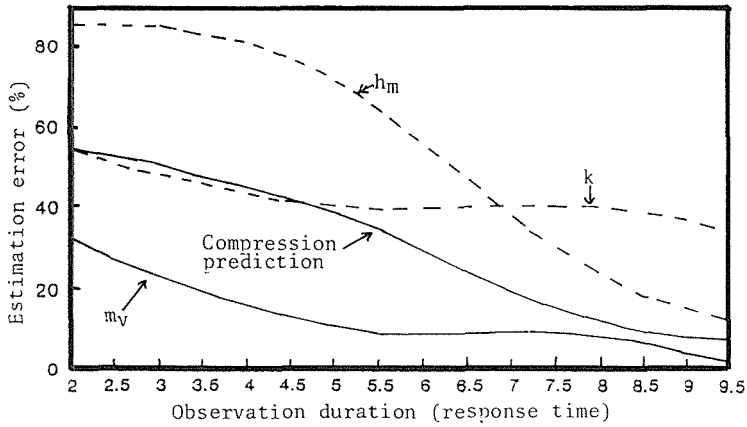

FIG. 4 Estimation and prediction accuracy vs observation duration.

prediction improves rapidly after 5 response time. Although it is difficult to draw any general conclusion from this result, the duration of observation is clearly reflected in the estimation and the prediction accuracy.

The influences of other facters such as the length of prediction time, the effect of the future head change trend etc. are also studied in Darmawan (1990).

Application to Nobi plain land subsidence

General description on Nobi plain land subsidence can be seen in, for example, Sato, Daito & Ueshita (1984) and Ohshima & Ueshita (1990). The observation record at Matsunaka Station during 1971-1987 is used in this calculation. The record of the head fluctuation in the second aquifer (Depth 40.6 m-66.5 m) and the third aquifer (Depth 105.3 m-156.0 m), and the compression of the second aquitard (Depth 66.5 m-105.3 m) are available. These observation data are shown in Fig. 5. Since 1973, the heads of aquifers are in the process of recovery, and some swelling has taken place in the second aquitard since 1980.

The calculation is carried out by assuming the second aquitard as a homogeneous layer although the actual aquitard consists of several layers. Furthermore, the value of the coefficient of volume expansivity, m_v , is taken as 1/7.5 of that of volume decrease, m_v . This ratio is determined based on the laboratory experiments.

Following three schemes are employed for the prediction:

Scheme A : Use first 6 years observation (1971-1976)
Scheme B : Use first 9 years observation (1971-1979)
Scheme C : Use first 13 years observation (1971-1983)

The response time (defined in the previous section) for this aquitard is about 10 months. Therefore, the total length of the observation at Matsunaka station is about 20 response time. The duration of observation used in the prediction for the schemes are about 7, 10 and

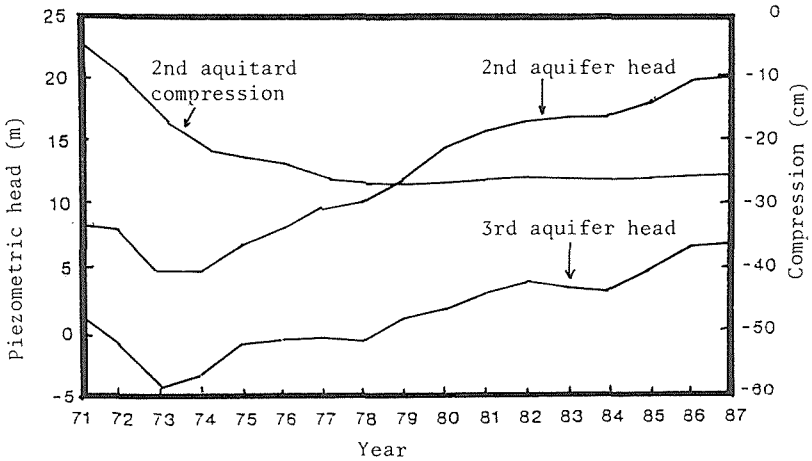

FIG. 5 Observed piezometric head and compression in Nobi plain.

15 response time respectively.

The comparison between the estimated parameters for each scheme and the laboratory test result are made in Table 1. Estimations in scheme A have larger errors compared to the other two schemes especially for h_m. The estimations for m_v and h_m are better than that for k. It seems that more than 10 resposne time of observation duration is required to get reasonable estimate of the parameters. The compression prediction by scheme C is shown in Fig. 6.

Application to Bangkok land subsidence

For the general description of Bangkok land subsidence, one can see Nutalaya, Yong, Chumnankit and Buapeng (1989). The observation record at the station 21 at Bang Na between 1978-1982 is employed for the

TABLE 1 Parameter estimation of Nobi plain land subsidence with various duration of observation.

Parameter	A	B	C	lab.
k^{*}(1) St. dev	-3.91 1.10	-3.48 0.71	-3.26 0.56	-4.66 ----
m_v^{*}(1) St. dev	-7.31 0.44	-7.62 0.26	-7.53 0.19	-7.42 ----
h_m(m)(2) St. dev (m)	-5.75 0.31	-11.60 0.23	-10.74 0.19	-11.5(3) ----

(1) k^{*} and m_v^{*} are in logarithmic scale for k in (m/year) and m_v in cm^2/kg

(2) h_m is maximum initial excess piezometric head in aquitard

(3) From Ueshita & Sato (1980)

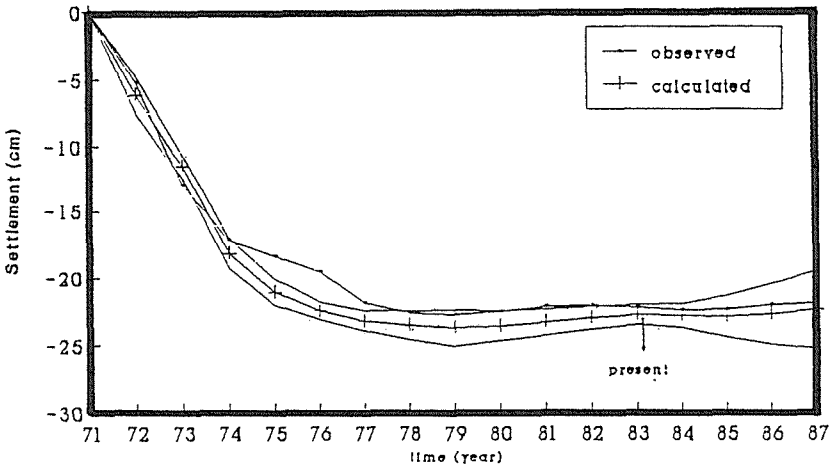

FIG. 6 Prediction of compression based on 13 years observation.

calculation. At this site, the first aquitard with thickness 39 m is sandwiched by the first aquifer (i.e. unconfined surface aquifer) and the second aquifer. It is believed that the head of the first aquifer remained unchange during this observation period, whereas the second aquifer exhibitied about 3 m head drop.

The calculation is carried out following three different schemes:

Scheme I : use monthly fluctuation data
Scheme II : use 6 months average data
Scheme III : use 12 months averaged data.

The response time for this aquifer is estimated to be about 12 months, which implies the length of the available observation record is only 4 response time.

Table 2 Parameter estimation of Bangkok land subsidence with various scheme of observation.

Parameter	I	II	III
k^*(1) St. dev	-4.52 0.43	-3.28 0.33	-3.39 0.46
m_v^*(1) St. dev	-8.78 0.07	-7.56 0.07	-7.57 0.11
h_m(m)(2) St. dev (m)	-12.73 0.33	-10.2 0.21	-10.2 0.23

(1) k^* and m_v^* are in logarithmic scale for k in (m/year) and m_v in cm^2/kg

(2) h_m is maximum initial excess piezometric head in aquitard.

The result of calculation for each scheme is presented in Table 2. The result of Scheme I is considerably different from the other two. It is speculated that the large monthly fluctuation of the head observation has disturbed the stable estimation of the parameters. The future prediction of the compression of the aquifer is also attempted. The result showed considerable amount of uncertainty as expected.

CONCLUSION

The methodology proposed in this study is considered to be useful in predicting the future subsidence. The major advantage of this method is its capability to estimate the initial excess pore pressure distribution as well as model parameters at the time observation started.

From the calculation, it is found the duration of observation measured by a normarized time length, "response time" (i.e. time requried for the aquitard to dissipate 50 % of the excess pore pressure), is a very important factor for the accurate prediction. As far as the calculation done in this study is concerned, ten resposne time may be requried for the reasonably accurate prediction.

REFERENCES

Darmawan, P. (1990) Prediction of subsidence with quantified uncertainty by an inverse analysis procedure. Masteral Thesis at AIT, GT-89-8.

Ganbolati, G. and Freeze, R.A. (1973) Mathematical simulation of the subsidence of Venice 1. Theory. Wat. Resour. Res. Vol. 9, No. 3, PP. 721-733.

Honjo, Y. and Morishima, A. (1988) Parameter estimation of numerical models of groundwater flow: estimation uncertainty and its influence on prediction. Proc. JSCE No. 400/III-10, PP. 215-224 (in Japanese).

Nutalaya, P., Yong, R.N., Chumnankit, T. and Buapeng, S. (1989) Investigation of land subsidence in Bangkok during 1978-1988. Proc. Workshop on Bangkok Land Subsidence - What's next?

Sato, T., Daito, K. and Ueshita, K. (1984) Analysis of land subsidence due to withdrawal of groundwater in the Nobi plain. Proc. 3rd Int. Symp. on Land Subsidence, PP. 89-99, Vanezia.

Ohshima, T. and Ueshita, K. (1989) Land subsidence and groundwater condition in Nagoya. Proc. Int. Symp. on Land Subsidence, Dhanbad.

Taylor, D.W. (1948) Fundamentals of Soil Mechanics, 700 pp. John Wiley, New York.

Ueshita, K. and Sato, T. (1979) Study on the reasonable recovery of groundwater in the Nobi plain. Proc. JSCE No. 287, PP. 137-146 (in Japanese).

Ueshita, K. and Sato, T. (1980) Study on the desiable groundwater level preventing land subsidence of the Nobi plain. Proc. JSCE No. 299, PP. 65-72 (in Japanese).

Land Subsidence (Proceedings of the Fourth International Symposium on Land Subsidence, May 1991). IAHS Publ. no. 200, 1991.

Time Delay Effect of Subsidence

D. M. XU, R. N. YONG & A. M. O. MOHAMED
Geotechnical Research Centre, McGill University
817 Sherbrooke St. West, Montreal, Quebec Canada H3A 2K6

ABSTRACT A model for the time delay effect of subsidence is derived. Numerical analysis of the developed model has shown that the two controlling factors, which govern the time delay effect in subsidence are: (1) water table recovery rate (speed),and (2) the ratios between $\frac{m_{ce}}{m_{cp}}$. The faster the water table recovery head, the shorter is the time lag. The greater the ratio $\frac{m_{ce}}{m_{cp}}$ of the aquitard, the shorter is the time required for subsidence to stop.

INTRODUCTION

Vertical and lateral movement of the ground surface have occurred in many parts of the world, resulting from a variety of causes, of which some are natural and some are manmade. The rate of occurrence varies from extremely rapid to long-term with time span varying from seconds to thousands of years. With the population increase, urbanization spreading over grater areas, and increasing industrialization, the consequences of subsidence have become very important.

Since surface movements caused by man's activities tend to have the shorter time scales and therefore important to construction, it has become desirable to establish the mechanisms by which these movements occur and to develop analysis techniques by which the amounts and distribution in time can be predicted. A number of previous reviews of subsidence, some from a particular point of view, or a special mechanism, have been reported (Allen, 1969; Sowers, 1976).

Subsidence due to underground pumping (extraction) is related to the phenomenon of consolidation. Generally speaking, when water is withdrawn from a well located in the aquifer layer, the hydraulic pressure reduces in the vicinity of the well, appearing as a pear-shaped hydraulic head drop profile. The effective stress which increases to compensate the hydraulic pressure drop is a direct result of the deformation-consolidation process which produces land subsidence. The greater the pumping (extraction) head, the larger the hydraulic head drop and correspondingly,the larger is the subsidence.

Because of the complexities of subsurface geology and hydrology, no single mathematical model can embrace all the specificities. In the mathematical sense, one is looking for two basic quantities: (1) deformation field; and (2) hydraulic head field. The solution is uniquely determined under precisely defined initial and boundary conditions.

This paper addresses the time delay effect of subsidence. The need to fully account for the time factor in subsidence becomes self evident when one wants to evaluate the effectiveness of natural or artificial recharge of the aquifers. Since the intent of recharge is to both replenish the groundwater and at the same time arrest subsidence (through recharge of the consolidating aquitards), the phenomenon of secondary compression or time delay effect will confuse calculations or when the recharge becomes successful.

It has been shown by Yong et al. (1989 and 1991) that subsidence is proportional to the characteristic line of water table $S_1(t)$ drop a the well. Remedial measures taken to raise the level of the water table through control of the pumping rate and groundwater recharging will not cause land subsidence to stop immediately. This is because of the consolidation process, which is responsible of the observed land subsidence, is controlled by diffusion mechanisms and thus are time dependent. As a demonstration of field example Yoshida and Aoki (1986) studied the Nigata plain in Japan and showed that subsidence continued to occur even after the water table had recovered slowly since 1965, and very rapidly since 1973.

MECHANICAL BEHAVIOR OF AQUITARD LAYER

The compression-rebound characteristics of the aquitard need to be considered in the analysis. When the aquitard layer is "compressed" the volume change-load relationship generally shows the volume compressibility m_{cp} is relatively large. If the aquitard layer is allowed to rebound, the volume change in rebound is seen to be small, due to the fact that the coefficient of volume expansion m_{ce} is relatively small in comparison to m_{cp}. This mechanical behavior of shown in Fig. 1. Physically, this indicates that some deformation is nonrecoverable once the same amount of effective stress is reversed, due to the non elastic behavior of the "electrolytic double layer".

MECHANISM OF TIME DELAY OF FIELD SUBSIDENCE

The time delay effect of subsidence for the aquitard aquifer model is shown in Fig. 2. We consider an infinitesimal element $A'A - BB'$ in the aquitard under

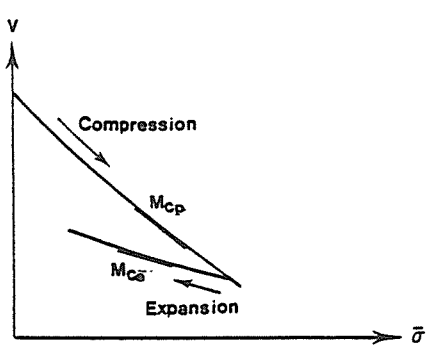

FIG. 1 Volume compressibility coefficient M_{ce} and expansion coefficient M_{cp} of aquitard soil.

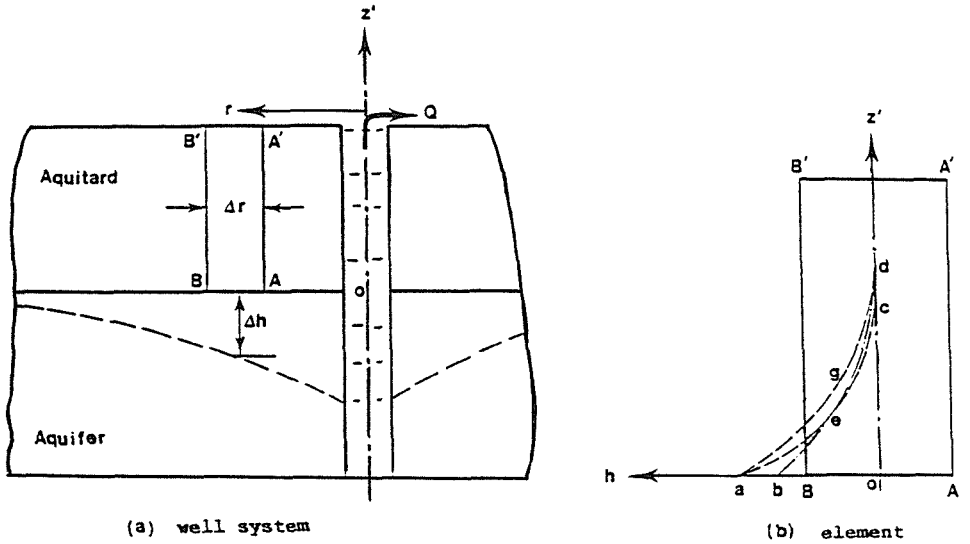

FIG. 2 Pressure head profiles.

investigation. Since $AB = \Delta r$, is very small, the pressure head in the element is only a function of z' and t. At $t = t_o$, because of previous pumping (extraction) of the water from the well, AB has a Δh pressure drop, which is indicated by the oa, is as shown in Fig. 2 (b). The vertical line $oc = S_3(r, t_o)$ indicates the pressure head progress in the z' direction from the time $t = 0$ to time t_o. As reported by Yong et al. (1991), $S_3(r, t)$ progresses very slowly because of the very small consolidation coefficient. The curves aec and agd in Fig. 2.(b) represent pressure profiles along the $z\prime$ direction at $t = t_o$and $t = t_o + \Delta t$ respectively. It is noted that within the $z\prime = 0d$ layer, the aquitard layer is being consolidated, i.e. subsidence continues.

SIMPLE MODEL FOR SUBSIDENCE FOR THE CASE OF WATER TABLE RECOVERY

Fig. 3 shows the pressure head profile in the element $AA\prime BB\prime$(Fig. 2a) in more detail. Consider the time period from $t = 0$ to $t = t_o$, when the water table drops from "o"to "a". For the period following let t^* denote the time commencing from $t = t_o$, i.e. $t^* = t - t_o$ for convenience. For $t* > 0$, the water table is assumed to recover. Let v_w denote the speed at which the water table recovers in t^*. Within the dt^* time period, "a" moves to "b". The water pressure profiles at $t* = 0, t*$ and $(t^* + dt)$ are represented by curves $ac\prime, a\prime fc$ and bfd respectively. We note that $aa\prime = t^* v_w$and $a\prime b = dt^* v_w$, and that at the water pressure head has progressed in the $z\prime$ direction to $c\prime, c$ and d at $t^* = 0, t^*$ and$(t^* + dt^*)$ respectively.

From Fig.3, it is seen that the aquitard (soil) at $0 < z < z^*$, (between "o"and "e", increases in volume (expands) during the dt^* time in view of the recovery of the water pressure i.e. reducing effective stress, while the soil at

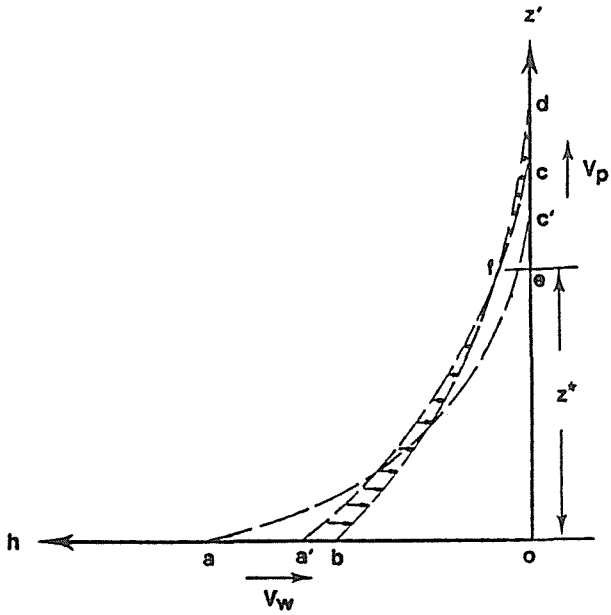

FIG. 3 Typical element analysis for time delay effect of subsidence.

$od > z > z^*$, (between "e" and "d"), consolidates as the pressure head front progresses. The arrows shown in Fig. 3 indicate the incremental effective stresses with the opposite directions within time dt^* in two different aquitard regions. From the geometric property of quadratic curves, the following relations can be obtained:

$$\text{Area} \quad a'fb = \frac{1}{3}z^*ab \tag{1}$$

$$\text{Area} \quad cfd = \frac{1}{3}efcd \tag{2}$$

The compression increment in the compression zone cfd is given by:

$$du_1(t^*) = m_{cp}\text{Area} \quad cfd \tag{3}$$

And the expansion (rebound) increment in the expansion zone $a'fd$ is given by:

$$du_2(t^*) = m_{ce}\text{Area} \quad a'fb \tag{4}$$

Therefore the net subsidence increments may take the following form:

$$du(t^*) = du_1(t^*) - du_2(t^*)$$

$$= m_{cp}\text{Area} \quad cfd - m_{ce}\text{Area} \quad a'fb$$

$$= \frac{1}{3}[m_{cp} \quad efcd - m_{ce}z^*a/b] \tag{5}$$

And the waterfront movement oc is given by:

$$oc = \left[\frac{k_c}{gm_{cp}}\right]^{\frac{1}{2}} [t + t_o]^{\frac{1}{2}} \tag{6}$$

Hence

$$cd = v_p dt^* \tag{7}$$

where v_p denotes the speed of the front movement and is given by:

$$v_p = \frac{1}{2}\left[\frac{k_c}{gm_{cp}}\right]^{\frac{1}{2}} [t^* + t_o]^{-\frac{1}{2}} \tag{8}$$

and

$$a/b = v_w dt^* \tag{9}$$

where v_w=recovering velocity of water table. Subsititing Eq. (7) and Eq. (9) into Eq. (5), one obtains:

$$du(t^*) = \frac{1}{3}[m_{cp}v_p ef - m_{ce}z^*v_w]dt^* \tag{10a}$$

or,

$$\frac{du(t^*)}{dt^*} = \frac{1}{3}[m_{cp}v_p ef - m_{ce}v_w z^*] \tag{10b}$$

The above procedure distinguishes between two different aquitard regions due to the fact that the pressure at $z = z^*$ does not changes after time dt^*. The first region is under compression whilst the second region is under expansion. The criterion which defines the boundary between the two regions can be stated mathematically as follows:

$$\frac{d}{dt^*}\left\{(\triangle h - v_w t^*)\left[1 - \frac{z^*}{S_3(t^*)}\right]^2\right\} = 0 \tag{11}$$

It leads to the following equation:

$$v_w\left[1 - \frac{z^*}{S_3(t^*)}\right]^2 - (\triangle h - v_w t^*)\left(\frac{\frac{dS_3}{dt^*}}{S_3(t^*)}\right)\left[\frac{2z^*}{S_3(t^*)} - 2\left(\frac{z^*}{S_3(t^*)}\right)^2\right] = 0 \tag{12}$$

where $S_3(t^*) = oc$ which is given by Eq. (6).Thus,

$$\frac{\frac{ds_3}{dt^*}}{S_3(t^*)} = \frac{1}{2(t_o + t^*)} \tag{13}$$

Let,

$$\xi = \frac{z^*}{S_3(t^*)} \tag{14}$$

then Eq. (12) becomes:

$$v_w[1-\xi]^2 = (\triangle h - v_w t^*)[\xi - \xi^2](t_o + t^*)^{-1}$$

or

$$(t_o + t^*)v_w(1-\xi) = (\triangle h - v_w t^*)\xi$$

Thus,

$$\xi = (t_o + t^*)\frac{v_w}{\triangle h + t_o v_w} \tag{15}$$

Using Eq. (14), z^* is obtained as:

$$z^* = \left[(t_o + t^*)\frac{v_w}{\triangle h_+ t_o v_w}\right]\left[\frac{k_c}{\rho_w g m_{cp}}\right]^{\frac{1}{2}}(t_o + t^*)^{\frac{1}{2}} \tag{16}$$

and

$$ef = (\triangle h - v_w.t^*)[1-\xi]^2$$

$$= (\triangle h - v_w t^*)\left[1 - (t_o + t^*)\frac{v_w}{\triangle h + v_w t_o}\right]^2 \tag{17}$$

Substituting Eq. (16) and Eq. (17) into Eq. (10), one gets:

$$\frac{du(t^*)}{dt} = \left(\frac{1}{3}\right)\left\{\frac{(\frac{k_c}{\rho g m_{cp}})^{\frac{1}{2}}}{(t_o + t^*)^{-\frac{1}{2}}}\right\} \times$$

$$\rho g m_{cp}\left\{(\triangle h - v_w t^*)\left[\frac{1 - v_w(t_o + t^*)}{(\triangle h + v_w t_o)}\right]^2 - \rho g m_{ce}.v_w(t_o + t^*)^2.\frac{v_w}{(\triangle h + v_w t_o)}\right\} \tag{18}$$

The stationary condition that defines when subsidence stops is given by:

$$\frac{du(t^*)}{dt^*} = 0 \tag{19}$$

This stationary condition leads to the following:

$$\frac{(\triangle h + v_w t_o)(\triangle h - v_w t^*_{stop})[1 - \delta v_w(t_{stop} + t_o)]^2}{[v_w(t_o + t_{stop})]^2} = \frac{m_{ce}}{m_{cp}} \tag{20}$$

where $t^*_{\text{stop}}$is the time lag between water table recovery and the moment that subsidence stops. Finally Eq. (18) represents the change in net subsidence with time as a function of : (1) compression volume change; (2) expansion volume change; (3) recovery rate of water table; 4) pressure head; (5) permeability. Eq.

(20) represents the stationary conditions at which subsidence stops. Eqs. (18) and (20) will be solved numerically for given values for h, t_o, m_{ce}, m_{cp} and v_w.

NUMERICAL RESULTS

A computer program has been written to numerically calculate the time lag, the subsidence and the water head profiles in the aquitard layer at a given value of aquitard parameters. The Range-Kutta method is used to intergrate Eq. (18) and the secant method is used to solve Eq. (20). The numerical results are shown in Figs. 4, 5 and 6 respectively. Fig. 4 presents the subsidence time lag under conditions of water table recovery. It can be seen that the time lag is controlled by two factors: (1) water table recovery rate (speed) v_w, and (2) the ratio between m_{cp} and m_{ce}. If v_w increases, the water table recovers quickly, and the time required for subsidence to stop is shortened. In addition, the value of $\frac{m_{ce}}{m_{cp}}$ is higher, which means grater rebounds. The subsidence stops promptly. From Fig. 4, we can easily obtain the time lag if these two factors are known.

For $\frac{m_{ce}}{m_{cp}} = 5\%$ and different water table recovery velocities the relationship between subsidence and time can be obtained as shown in Fig. 4. In the first five years, the water table neither recovers nor drops. However, after 5 years,

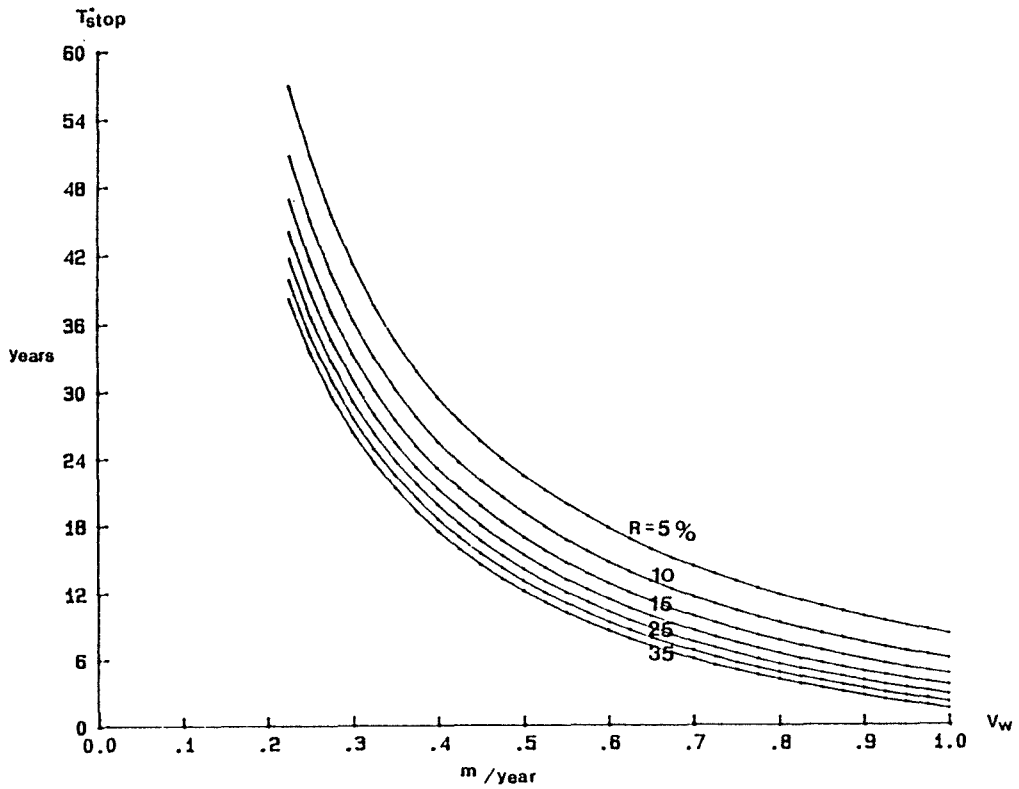

FIG. 4 Time lag of subsidence under conditions of water table recovery.

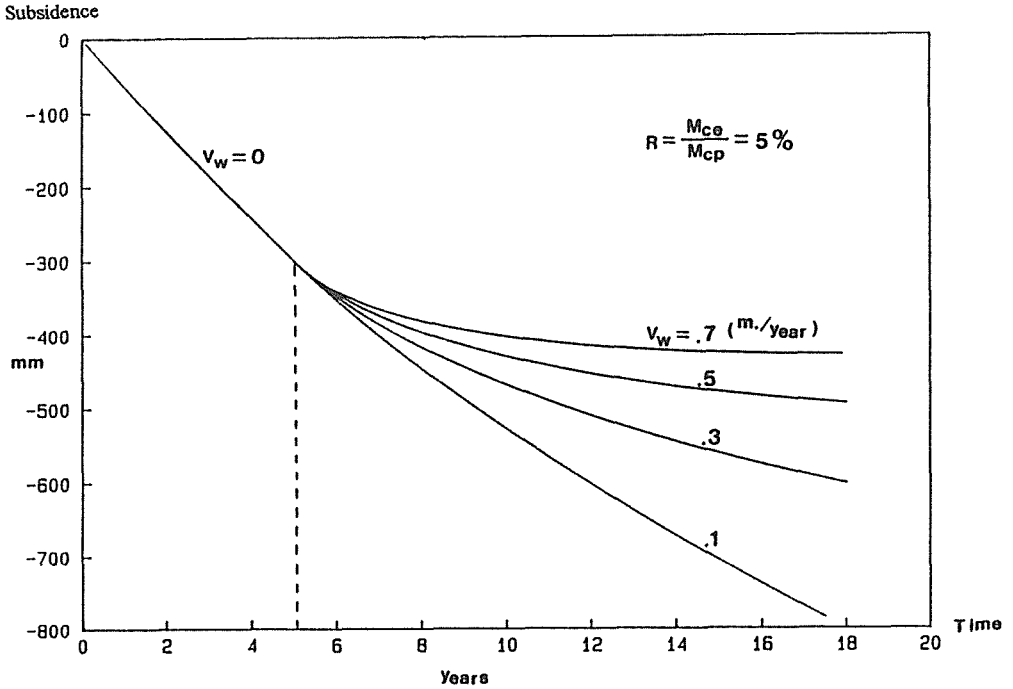

FIG. 5 Subsidence vs. time t at different water velocities (V_w).

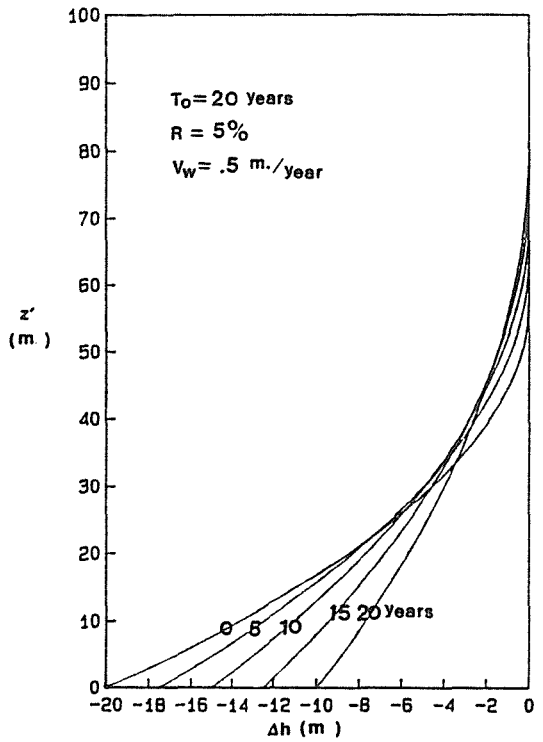

FIG. 6 Pressure head profiles at different times in the aquitard layer.

the water table starts to recover. It can be seen from Fig. 5 that the subsidence slows down depending on how fast the water table recovers. It is self evident that the faster the water table recovers, the shorter is the subsidence period, and the time required to terminate the subsidence is shortened.

Fig. 6 shows the water pressure head profiles along z' direction (vertically) at different time for $v_w = 0.5 \quad m/\text{years}$. It is shown that there are two regions: *aquitard compression regions and aquitard expansion region.* Since compression yields more deformation than expansion, due to $m_{cp} >> m_{ce}$, subsidence will continue to occur until a balance is reached.

CONCLUSIONS

This study has focused attention on the time delay effect in subsidence. The two controlling factors are: (1) water table recovery rate (speed),and(2) the ratio between $\frac{m_{ce}}{m_{cp}}$. The faster the water table recovery rate, the shorter is the time lag. The greater the ratio $\frac{m_{ce}}{m_{cp}}$ of the aquitard, the shorter is the time required for subsidence to stop.

ACKNOWLEDGMENT

This study was supported under a grant from the International Development Research Centre (IDRC) of Canada, Grant No. 3-P-1044- 02.

REFERENCES

Allen, A.S. (1969) Geologic Settings of Subsidence. G.S.A. Reviews in Engineering Geology, D.J. Varnes and G.Keirsch, eds., Vol. II, pp. 305-342.

Sowers, G.F. (1976) Mechanism of Subsidence Due to Underground Openings. Transportation Research Record, 612, pp. 2-8.

Yong, R.N., Xu, D.M. and Mohamed, A.M.O. (1989) Ground Water Resource Management Model. Final Report, Report to International Development Research Centre (IDRC), Canada p.

Yong, R.N., Mohamed, A.M.O. Mohamed and Xu, D.M. (1991) Analytical Solution for a Coupled Hydraulic and Subsidence Model Using a Characteristic Surface Method. ASCE, Geotech. Eng. Congress, Boulder, Colorado, June 10-12.

Yoshida, S. and Aoki, S. (1986) Mechanics of One-Dimensional Simulation of Land Subsidence During the Period of Head Recovery in Aquifers. In Land Subsidence edited by Johnson, A.I. et al., pp. 174-156.

Land Subsidence (Proceedings of the Fourth International Symposium on Land Subsidence, May 1991). IAHS Publ. no. 200, 1991.

Finite Element Analysis of Land Subsidence Due to the Variation of Groundwater Level

M. SHIMIZU
Faculty of Engineering, Tottori University,
Koyama-cho, Tottori, 680 Japan

ABSTRACT A one dimensional consolidation finite element analysis is made so as to simulate the behavior of a land subsidence experienced in a local city in Japan. The consolidation of an alluvial clay layer more than 10 m thick has been caused by the variation of the groundwater level in the sand layer beneath the clay layer. Field observation shows that the level of groundwater is likely to have been lowered and that it has so far been recovered with the seasonal and annual variations. Results of in-situ geotechnical surveying and laboratory tests, which were made in not sophisticated but practical ways, are applied for the analysis. The results of the analysis shows the ability and limitation of data obtained from practical surveys and tests for the land subsidence problem.

INTRODUCTION

In a local city, Tottori, in Japan, a subsidence has been observed since the 1960s and is attributed to the lowering of the groundwater level. It seems that the lowering of the level was caused by pumping for industrial uses. Recently, however, the level is gradually recovering and the subsidence has become less but not ceased.

The purpose of this study is to investigate the mechanism of the land subsidence occurring in the district and to simulate the settlement. To do so, it is examined if the variation of the groundwater level in the sand layer beneath the thick clay layer have caused the consolidation of the clay layer.

In-situ surveying and laboratory tests on undisturbed samples were performed in not sophisticated but practical ways. The data obtained were used for the analysis. Finite element analysis was adopted, in which the facts that the groundwater level varies in a complicated manner and that the clay layer is not uniform can be taken into account easily.

In this paper, first, the actual situation of the subsidence and the geological feature of the district will be described; second, the way for modeling the variation of the groundwater level will be described as well as that for modeling the constitutive behavior of soils; and finally, the calculated results will be shown and the ability and limitation of the approach adopted will be discussed.

GEOLOGICAL FEATURE

In the area in which remarkable subsidence has been observed, thick alluvial deposits lie as shown in FIG.1. The deposits consist of four or five layers: the surface layer (denoted by Um) of sand, silt and clay; the upper sand and gravel layer(Us); the upper clay layer (Uc); the lower sand and gravel layer (Ls); and the lowest clay and silt layer(Lc). The Lc layer is considered diluvial and it can not be found in some places.

Among these layers the consolidation mainly of the Uc layer causes the land subsidence, which will be confirmed later. The thickness of the Uc layer can be up to 20 m and the SPT N value is at most 5.

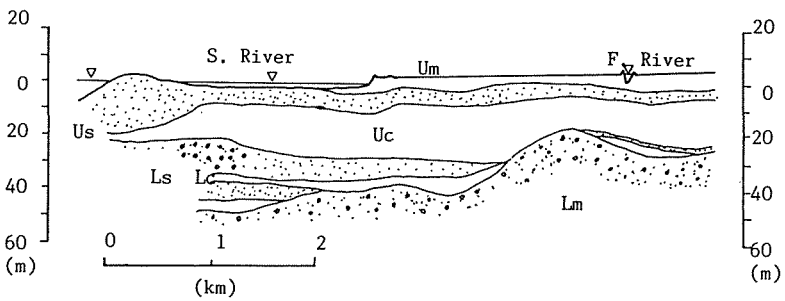

FIG.1 Subsoil profile on the cross section along AA' shown in FIG.2. (After Chugoku Branch of Japanese Society of Architecture (1981)).

SUBSIDENCE

The plan of the area of which the subsidence will be treated in this paper is presented in FIG.2. The subsidence in the area occurred earliest in the district. The level of groundwater in Us and Ls layers has been measured since 1978 in observation wells located at the point K. The leveling of bench marks BM1 to BM4 has been done; these bench marks are a part of the leveling system developed in this district.

FIG.3 shows those variations of levels of bench marks with time, which indicate the time history of the land subsidence in the area. From this figure we find that:

(a) the magnitude of the subsidence can be in the order of 30 cm at points BM2 and BM4;
(b) the rate of subsidence is gradually decreasing but not zero; and
(c) the subsidence is likely to have begun since 1960s as is seen in the record at the point BM2.

These findings will be used for assumptions adopted in the analysis.

The soil profile at the site K is shown in FIG.4, in which the domain and finite element mesh used in the analysis are also shown. It can be considered to be a representative soil profile in this area.

The dominant layer in the subsidence was identified by the Tottori Office of the Ministry of Construction. At the point K, two holes down to the surfaces of Us and Ls layers were bored; a rod was inserted in each hole. At the same time a plate was set on the ground surface.

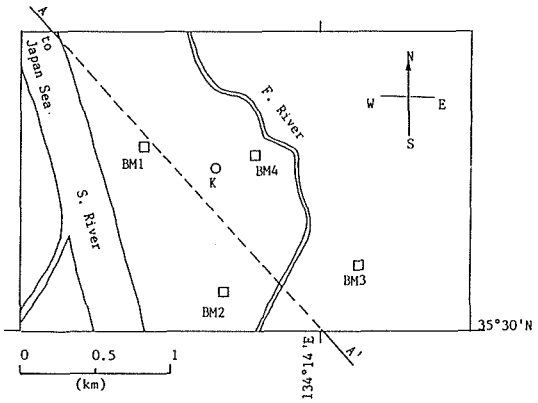

FIG.2 Locations of bench marks (BM1 to BM4) and the obsevation well (K).

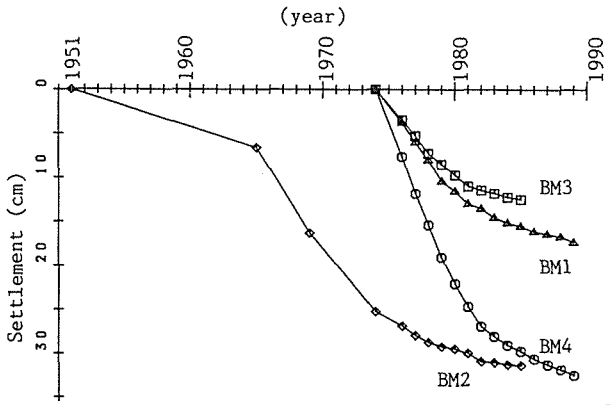

FIG.3 Settlement behavior of bench marks; after Committee for Land Subsidence in Tottori City(1990).

With this system, the magnitude of compression of Um and Uc layers were separately measured.

The results are presented in FIG.5. We can see that the main compressive layer is the Uc layer. The Lc layer does not compress and the Um layer compresses slightly.

GROUNDWATER LEVEL

The level of the groundwater in the Ls layer is gradually rising from the beginning of the measurement (see FIG.9(b)). On the other hand the level of that in Us layer is almost constant, which is not shown in the figure. This fact will be taken into account in the analysis, i.e. only the variation of the groundwater level of the Ls layer will be considered.

Ones say that, when shallow wells were bored in the area, the groundwater, probably, of the Us layer rose above the ground surface. This will not be accounted for in the analysis.

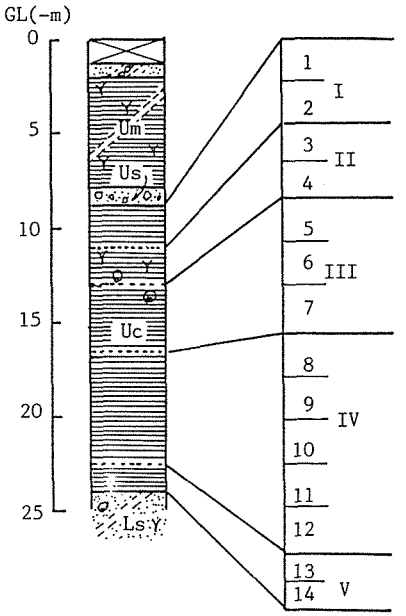

FIG.4 Representative soil profile and the domain and finite elements used in the analysis.

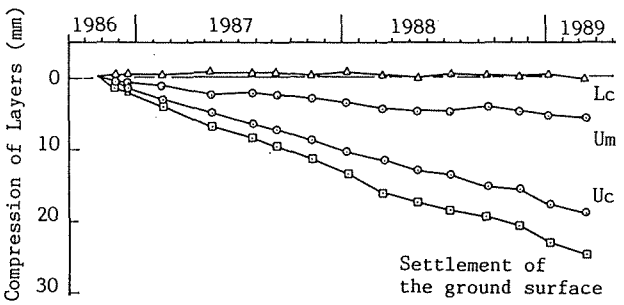

FIG.5 Compressive behavior of layers. (After Tottori Office of the Ministry of Construction (1989)).

METHOD FOR ANALYSIS

Model of the subsoil

The soil profile at the point K was adopted as a representative one for the area and used in the analysis (see FIG.4). The domain occupied by the Uc layer was analyzed. Undisturbed samples were taken from

various depths to be served for oedometer tests of which results were used for the construction of the subsoil model.

In taking into account the difference in mechanical and physical properties between samples, the layer was divided into five soil types: soil types I to V. Mechanical and physical characteristics are listed in TABLE 1. For the finite element analysis the domain was discretized into 14 elements as shown in FIG.4. Each element is about 1 m thick.

Procedures in the analysis

One dimensional consolidation problem was solved under the condition of infinitely small deformation. The weighted residual method was applied to the equilibrium equation of stresses and continuity equation of pore water. They were discretized with finite element technique. Increments of displacement and pore pressure are unknown functions. For the former three noded elements were used, and for the latter two noded elements were used.

The boundary condition is as follows:

(a) On the upper end of the domain, both surface traction and pore pressure were held constant. The constant surface traction means the constant overburden pressure. The condition that the pore pressure is constant corresponds to the assumed condition that the groundwater level in the Us layer does not vary.

(b) On the lower end of the domain, the displacement was held null and pore pressure was specified. The compression of the layers lower than the Uc layer is neglected. The variation of the groundwater level in the Ls layer was accounted for by specifying the value of pore pressure. The method for specifying it will be described in the subsequent paragraph.

Modeling of the variation in groundwater level

We have no record on the variation of the groundwater level in the Ls layer before April 1978. (See FIG.9(b)) Hence, the variation before then have to be estimated in a reasonable way. On estimating it, following assumptions were made:

(a) the subsidence was slight before 1964;

(b) before 1964 the level of the groundwater in the Ls layer was the same as the current level of the groundwater in the Us layer;

(c) since January 1964 till February 1978, the level of groundwater in the Ls layer gradually fell to the level measured in April 1978; and

(d) during the duration above, the variation can be approximated with a function composed of a linear function and a sinusoidal one with the period of 6 months.

The value for the groundwater level in the Ls layer was calculated every one month with these assumptions. (The estimated part is shown in FIG.9.(b).)

For the finite element calculation, the initial distribution of pore water pressure was assumed to be hydrostatic.

The increments of time and corresponding increment of pore pressure at the lowest node were given in the way explained in FIG.6.

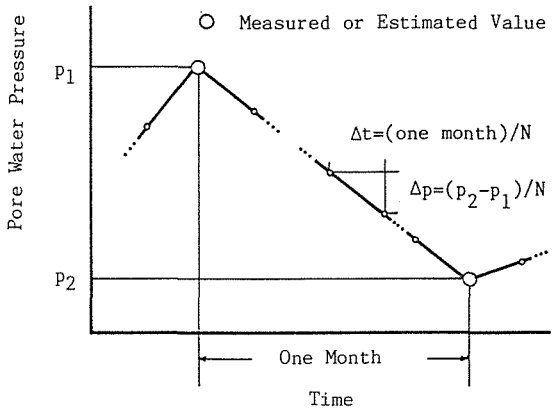

FIG.6 Schematic presentation to explain how to determine the time interval and the corresponding pore water pressure increment at the lowest end of analyzed domain.

The value of groundwater level and therefore the pore water pressure at the node is estimated or measured every one month; the duration of one month were divided into N intervals; and each interval was used as the time increment for the calculation. Corresponding increment of pressure can be determined. The value for N was 100.

Constitutive model for soils

Stress-strain relationship The following relationship between increments of effective stress, $\Delta\sigma'$, and strain, $\Delta\varepsilon$, was assumed:

$$\Delta\sigma' = \frac{1}{m_v}\Delta\varepsilon \tag{1}$$

where m_v is the volume change coefficient. The coefficient m_v was evaluated on the basis of linear relationships between void ratio e and the logarithm of effective stress σ' (see FIG.7). The coefficient m_v can be defined as:

$$m_v = 0.434\ \frac{C}{(1+e)\sigma'} \tag{2}$$

where C is the compression index, i.e. the inclination of e-log p relationships; C=Cc in the normally consolidated state and C=Cr in the overconsolidated state. The normally consolidated state is defined by $\sigma'>=\sigma'_c$ and overconsolidated state by $\sigma'<\sigma'_c$ where σ'_c is the maximum preconsolidation stress. As is clear from Eq.(2), m_v is a function of σ' and e.

Permeability coefficient Permeability coefficient k was evaluated in terms of consolidation coefficient c_v' and m_v, both of which can be determined from results of oedometer tests. In FIG.8, k

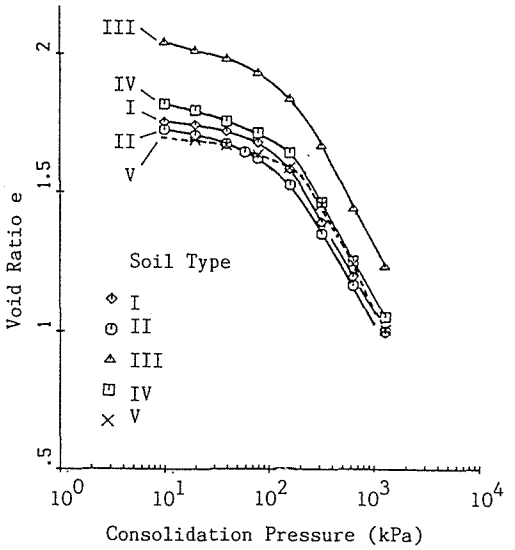

FIG.7 Relationships between void ratio and consolidation pressure. The results from oedometer tests on undisturbed samples.

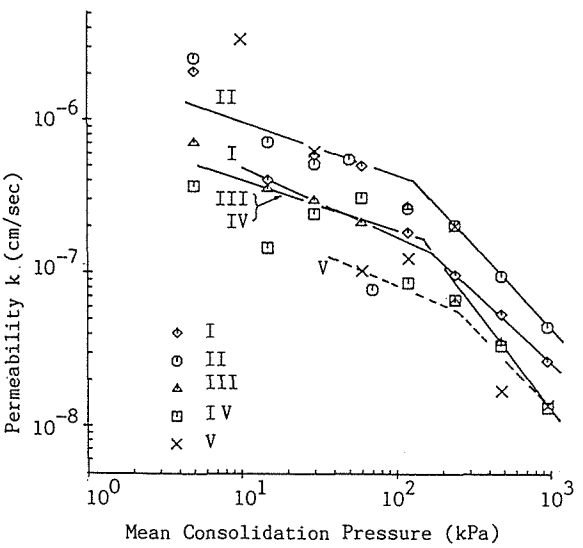

FIG.8 Permeability coefficient vs mean consolidation pressure.

is plotted against consolidation pressure p on the log-log scale. In this figure it is assumed that relationships between log k and log p are bi-linear and that the change of the inclination occurs when $p=p_c$, where p_c is the maximum preconsolidation pressure that undisturbed samples possessed when tested.

These assumptions can be expressed mathematically by:

TABLE 1 Values for parameters used in the finite element analysis.

Soil Type	I	II	III	IV	V
Depth*1 (GL-m)	10.0	12.8	16.8	20.8	22.0
Density ρ (Mg m^{-3})	1.615	1.606	1.523	1.563	1.605
Initial void ratio e_0*2	1.764	1.809	2.090	1.868	1.713
Compression index C_c	0.65	0.60	0.74	0.69	0.77
Recompression index C_r	0.087	0.104	0.075	0.113	0.115
Permeability constants					
ξ_{NC}	1.05	1.075	1.425	1.425	1.075
ξ_{OC}	0.35	0.325	0.325	0.325	0.55
σ'_0 (MPa)	0.48	0.48	0.48	0.48	0.96
k_0 ($\times 10^{-4}$ m day^{-1})	0.458	8.11	3.02	3.02	1.16

Note: *1 The depth from which undisturbed samples were taken.
*2 The value of void ratio that samples possessed before tests.

$$k=k_0\left(\frac{\sigma'}{\sigma'_0}\right)^{\xi} \tag{3}$$

where $\xi=\xi_{NC}$ if $\sigma'>=\sigma'_c$ and $\xi=\xi_{OC}$ if $\sigma'<\sigma'_c$; and σ'_0 is the reference value of σ' and k_0 is the corresponding value of k to $\sigma'=\sigma'_0$.

Values for mechanical parameters used in the analysis are listed in TABLE 1.

RESULTS OF ANALYSIS

The relation between the calculated settlement and time is presented in FIG.9(a). The variation of pore water pressure given at the lowest end of the Uc layer is shown in FIG.9(b) for the convenience of the comparison with the settlement. We find that:

(a) the calculated settlement tends to vary roughly in the similar way to that of the pore water pressure; however,
(b) during two years after the pore water pressure began to rise, the settlement continues slightly.

We can compare the calculated settlement with the observed settlements shown earlier in FIG.3. The magnitude of the calculated settlement is in the order of half the magnitude of observed one; and the calculation can not simulate the tendency for the settlement to continue although the groundwater level has been rising.

The variation of σ' with depth shows that the whole of the subsoil has become overconsolidated since February 1978, when the groundwater level was the lowest.

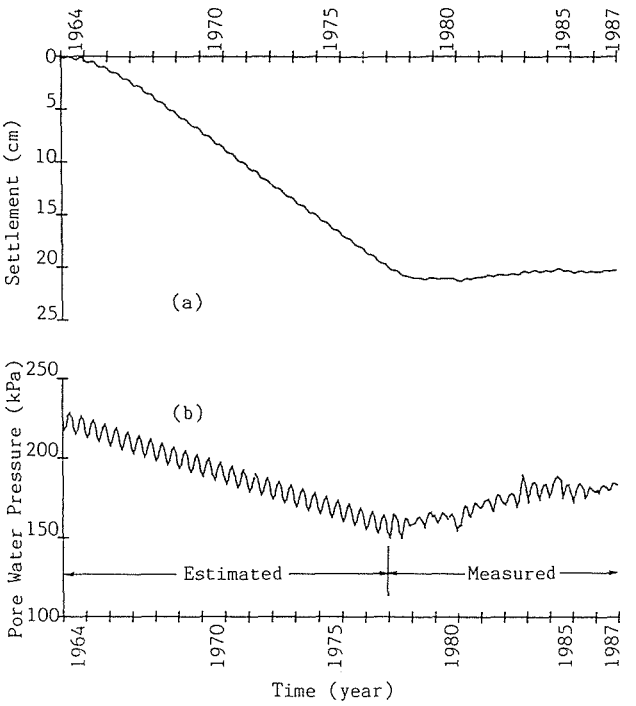

FIG.9(a) Calculated settlement behavior. (b) Variation of the pore water pressure at the lowest end of the analyzed domain.

In FIG.10, pore water pressure distribution is given. At any depth, it has not been recovered to the magnitude assumed at the start of the calculation. We see that the current gradient is steeper, particularly in the lower part of the domain, than the hydrostatic one. The last observation suggests us that the settlement will continue if the rising of the groundwater level stops after January 1988.

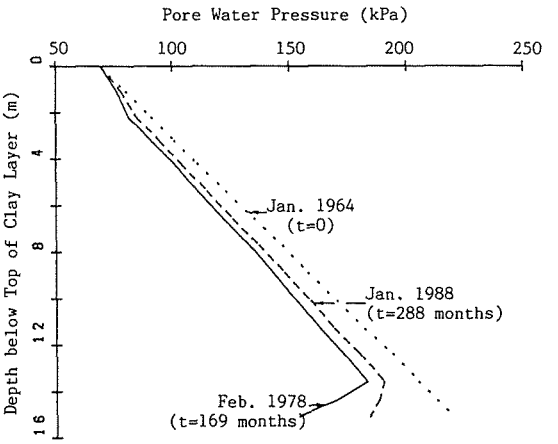

FIG.10 Distribution of the pore water pressure; calculated results.

DISCUSSION

We can cite some reasons why the calculation could not accurately simulate the actual behavior of settlement:

(a) The variation of the groundwater level in the Ls layer was modeled in a assumed manner; this can not be avoided because the data on it before 1978 does not exist.
(b) The viscous or viscid nature of stress-strain behavior of soils was not taken into account because, in this study, data from only practical tests were used; it will not be difficult to incorporate the nature in constitutive models of soils.
(c) In the calculation, the compression of the Um layer was neglected although it was observed as shown in FIG.5.
(d) The fact that the level of groundwater in the Us layer was higher than the current level was not accounted for.

The reasons mentioned above are all for the simplification of the problem and indicate the limitation of the approach taken in this study.

In spite of such a simplification, the results obtained here will be used to predict the future trend of the subsidence in the district: as was pointed out in the preceding section in referring to FIG.10, there is the possibility that the settlement will redevelop even if the groundwater level is held on the current level in future. Of course, for more accurate prediction, the measurement of the pore water pressure in the clay layer would be necessary.

ACKNOWLEDGMENTS

The technical reports issued by the Tottori Local Office of Ministry of Construction and by the Committee for Land Subsidence in Tottori City were referred to. The Author expresses his sincere acknowledgments to them.

REFERENCES

Chugoku Branch of Japanese Society of Architecture (1981) Geological Map of Tottori.
Committee for Land Subsidence in Tottori City (1990) Technical Reports on Results of Leveling.
Tottori Local Office of Ministry of Construction (1988) Technical Reports on Land Subsidence in Tottori City.

Land Subsidence (Proceedings of the Fourth International Symposium on Land Subsidence, May 1991). IAHS Publ. no. 200, 1991.

Analysis of Ground Water Level Fluctuations and Borehole Extensometer Data from the Baytown Area, Houston, Texas

ROLANDO BRAVO, JERRY R. ROGERS & THEODORE G. CLEVELAND
Department of Civil and Environmental Engineering, University of Houston, Houston, Texas 77204, U.S.A.

ABSTRACT Former use of ground water in the Baytown area in Houston, Texas has been about equally divided between public supply and industry. In this area piezometer wells and borehole extensometers have been constructed by the U.S. Geological Survey. The extensometer (LJ 65-16-930) was completed at a depth of 131 meters (431 feet), and another extensometer (LJ 65-16-931) was completed at a depth of 450 meters (1475 feet). A continuous record of the water levels in piezometers exists for different depths. Continuous records of consolidation (compaction) between the land surface and the depth of each extensometer also exist. This data was used to generate stress-strain diagrams. The head decline and the recovery (stress changes) plotted against compaction (strain) generates a series of open loops that represent the elastic and inelastic parts of the consolidation curve. Fourteen years of continuous records were analyzed for each of the clay layers in the Baytown area to compute important properties such as the storage coefficient for either the elastic range or the inelastic range and the vertical hydraulic conductivity.

INTRODUCTION

Use of ground water in the Baytown area, Houston Texas, was equally divided between public supply and industry. The use of ground water in this area slowly increased until 1973 when the industry started using surface water for its needs. Generally speaking, water levels in the Houston region declined from the beginning of development until 1977. Since 1977 no additional withdrawals have been allowed in this area. Nevertheless the piezometric level continues to fluctuate. This is associated with the consolidation of the compressible beds of the subsoil.

To determine small changes in elevation at specific locations, the United States Geological Survey (USGS) has placed borehole extensometers that give precise continuous records for determining the interval of consolidation that causes subsidence. The purpose of this work is to present the methodology for determining some fundamental properties of the compressible layers in the Baytown area using the relationship between the changes in the piezometric level and the recorded consolidation.

BACKGROUND

The Houston-Galveston area has two major aquifers: the Chicot and the deeper Evangeline aquifer, with the Burkeville Confining layer below. Electrical logs in the Baytown area indicate alternating sand and clay layers scattered throughout the vertical aquifer sections

(Figure 1). One log interpretation has 16 layers of compressible material that are present between 131 m (431 feet) and 450 m (1475 feet) below land surface. The total clay thickness in this range is 155 m (510 feet) which represents 49% of the total thickness under study, 318 m (1044 feet).

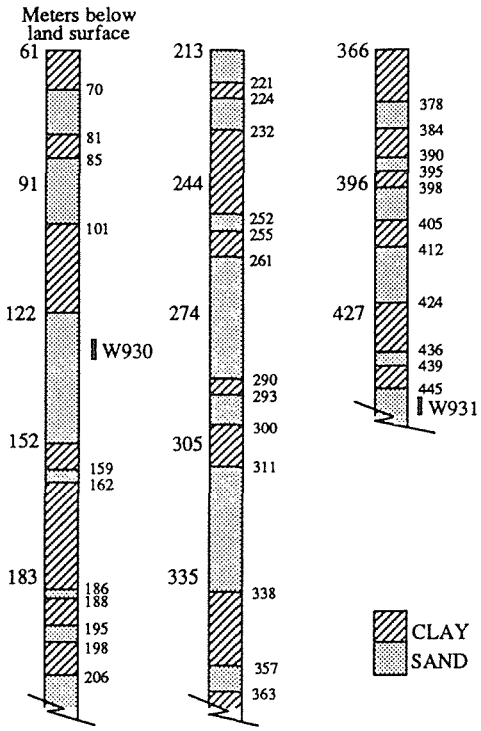

FIG. 1 Soil profile: Baytown area. Solid vertical lines indicate the interval of well perforation.

Ground water pumping in the Baytown area slowly increased until 1973. During 1972, about 1.4 $m^3 s^{-1}$ (32 Mgal/day) was pumped while in 1978 a total of 0.95 $m^3 s^{-1}$ (21.6 Mgal/day) was pumped (Gaybrisch 1984). Since 1972 the ground water pumping has decreased because industry increased its use of surface water. During 1973-1977, water levels rose as much as 6.1 m (20 feet) in wells in the Baytown area. The Baytown site, established in 1972, has two extensometers installed to depths of 131 m (431 feet) and 450 m (1475 feet) to measure the consolidation in two depth intervals. In addition piezometers at different depths were also installed. Data (taken each 28 days from 1976 to 1989) is presented in Figures 2,3,4 and 5. The wells where these devices are placed are numbered as LJ-65-16-930 and LJ-65-16-931 respectively. The plot of the water level changes for both wells was made with the depth increasing downward to emphasize the correlation of this depth to the piezometric head. These graphs show that since 1976 the water has risen almost 37 m (120 feet) in the well LJ-65-16-930 and appears to remain stable since 1987 indicating that the system is reaching equilibrium. The water level in well LJ-65-16-931 has risen more than 24 m (80 feet) and the system also appears to be in equilibrium. The difference in these heads depicts the change in effective stress.

Recording borehole extensometers (that sometimes are called compaction monitors) are holes drilled and cased to selected depths, into which smaller diameter standpipes have

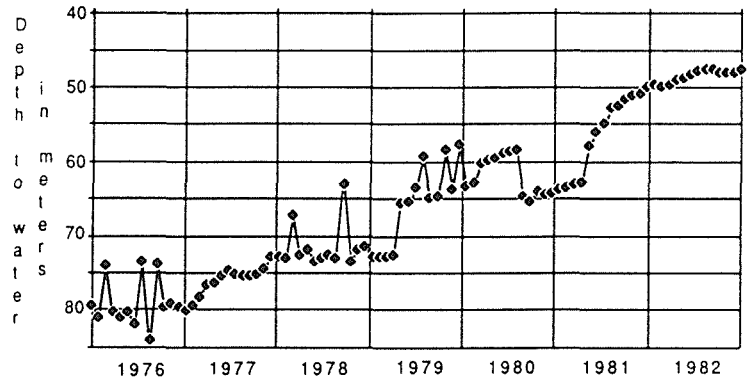

FIG. 2 Water level changes: Baytown area well LJ-65-16-930, 131 m depth (1976–1982).

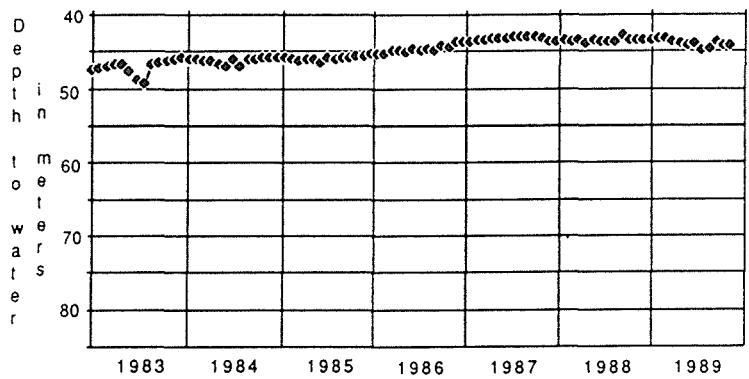

FIG. 3 Water level changes: Baytown area well LJ-65-16-930, 131 m depth (1983–1989).

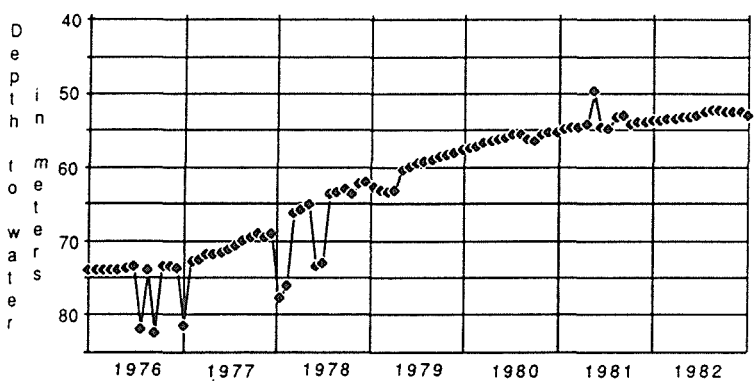

FIG. 4 Water level changes: Baytown area well LJ-65-16-931, 450 m depth (1976–1982).

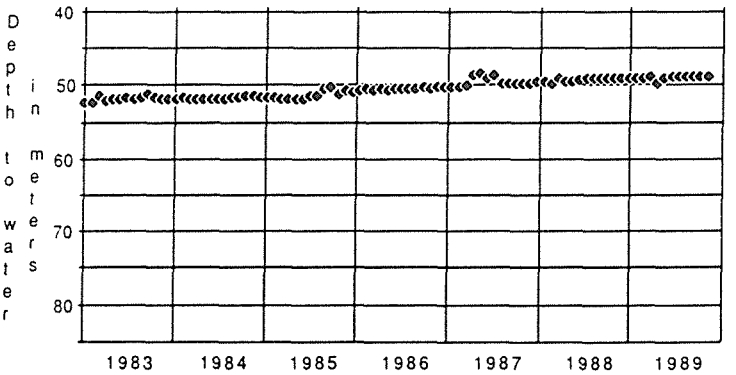

FIG. 5 Water level changes: Baytown area well LJ-65-16-931, 450 m depth (1983–1989).

been installed. The United States Geological Survey (USGS) has 11 borehole extensometers in operation at 11 different sites in the Houston-Galveston region. These borehole extensometers are able to continuously record the consolidation of the interval between the land surface and the bottom of the standpipe. Moreover, in the Houston-Galveston region, the United States Geological Survey (USGS) is collecting data on water level changes in different sands. From these data estimates of pressure change (stress change) at different depths for various time intervals may be made. Electrical logs are available for the places where the borehole extensometers are placed. These electrical logs can be used to identify the compressible and incompressible layers present either in the Chicot or the Evangeline aquifers.

BASIC RELATION BETWEEN SOIL MECHANICS AND GROUND WATER FLOW

The principle of mass conservation applied to one small elemental volume of a porous medium gives the following (Jacob, 1950):

$$-\frac{\partial(\rho_w v_x)}{\partial x} - \frac{\partial(\rho_w v_y)}{\partial y} - \frac{\partial(\rho_w v_z)}{\partial z} = \rho_w n \left(\frac{1}{E_w} + \frac{1}{E_k n}\right) \frac{\partial u}{\partial t} \qquad (1)$$

where E_w = bulk modulus of elasticity of water,

E_k = constrained modulus of elasticity (ratio of of vertical effective stress to laterally confined strain),

n = porosity (ratio of the volume of voids to the total volume).

This differential equation assumes, anisotropy of the density (density of the fluid moving through the porous media is not independent of direction), movement of the solid matrix is in the vertical direction (negligible movement in the x and y directions), the porous medium grains have no flexural strength and the load is transferred downward undiminished, and the change in volume of the soil grains is small in comparison to the change in the volume of water.

Substituting Darcy's law for the velocity terms, assuming isotropic density, and recalling that $h = z + (u/\rho_w g)$ gives the following equation that can be considered as a general differential equation for ground water flow in porous medium (Jacob 1950):

$$K_{xx}\frac{\partial^2 h}{\partial x^2} + K_{yy}\frac{\partial^2 h}{\partial y^2} + K_{zz}\frac{\partial^2 h}{\partial z^2} = n\gamma_w \left(\frac{1}{E_w} + \frac{1}{E_k n}\right) \frac{\partial h}{\partial t} \qquad (2)$$

The storage coefficient is the volume of water that an aquifer releases or takes into storage per unit surface area per unit change in head,i.e.:

$$S = \rho_w g b \left(\frac{n}{E_w} + \frac{1}{E_k} \right) \tag{3}$$

where b is the thickness of the aquifer,

ρ_w is the density of the water,

g is the gravity acceleration.

The specific storage (S_s) is the storage coefficient per unit width (sometimes called specific unit compaction).

In modeling the relationship of subsidence and ground water withdrawal, the aim is to determine how a change in the piezometric head deforms the soil, i.e., one needs to calculate the amount of consolidation of the compressible layers underlain in the area of study.

To achieve this goal, one important aquifer characteristic to determine is the storage coefficient . When water is pumped from confined aquifers, the ground water is removed from three sources: the expansion of water, the compression of the aquifer material, and compression of the clayey beds that are adjacent to and within the aquifer. When the compression does not result in a permanent rearrangement of the skeletal structure, the water can be replaced with an increase in pore pressure. This process is called elastic compression. Sometimes the term elastic compaction is used. However, if the pore pressure decreases beyond the interval where the soil particles compress elastically, additional water is released by rearrangement of the solid skeleton and the aquifer is permanently deformed (consolidated or compacted). This latter process is called permanent or inelastic compression (compaction) and causes the subsidence. Storage lost during the consolidation of the compressible layers is not recoverable.

The resulting compression per unit increase in effective stress in the inelastic range (virgin compression) is considerably greater than in the elastic range.In consolidation tests in soil mechanics this behavior is measured by the Compressibility Index C_c. This value of C_c is not constant and must be determined at the appropriate load. When the effective stress compressing the aquifer in the inelastic range is reduced (unloaded), the soil material again expands. In soil mechanics this behavior is measured by the Swelling Index C_s. The soil will recompact with elastic characteristics until effective stress increases beyond the new maximum effective stress (preconsolidation load).

The Compressibility Index C_c is determined by the slope of the closest straight line fit of a curve defined by a plot of void ratio values versus the logarithm of the effective stress of soil. The range of the effective stress must be in the virgin compression zone (inelastic range) (Das, 1985). Inelastic compaction is more nearly proportional to the increase in log of effective stress. C_c and consequently the corresponding storage coefficient S_{skv} is not a constant but rather is a function of effective stress. The subindex v in the notation corresponds to the virgin range. For modelling subsidence one needs to specify the corresponding value of S_{skv} when the load exceeds the preconsolidation load. Therefore it will be necessary to recalculate the value of S_{skv} for each change in the load.

The error in assuming a linear relationship between the change in the thickness of the compressible layer and the change in the effective stress can be calculated as:

$$\text{error} = \frac{\Delta b^* - \Delta b}{\Delta b} \tag{4}$$

where Δb^* is the inelastic compaction assuming a constant value of S_{skv},

Δb is the actual inelastic compaction.

If the constant value of S_{skv} corresponds to an initial value of effective stress σ_o, then the error can be expressed as (Leake and Prudic, 1988):

$$\text{error} = \frac{0.434\ \Delta\sigma'}{\sigma'_0 \Delta \log_{10}\sigma'} - 1 \tag{5}$$

where $\Delta\sigma'$ is the change in effective stress with respect to the initial value.

From equation 5, one can conclude that the percentage of error in calculating the deformation of the soil assuming a constant value of the specific inelastic storage coefficient is less than one half the percentage increase in the effective stress. Normally in most ground water flow systems, increments in effective stress are a relatively small percentage of the initial state of stress.

The coefficient of consolidation relates the effects of both storage and hydraulic conductivity by the relation:

$$c_v = \frac{KE_k}{\rho_w g} \tag{6}$$

and neglecting the contribution of water elasticity to specific storage:

$$c_v = \frac{K}{S_{sk}} \tag{7}$$

The time factor or dimensionless time T is:

$$T = \frac{Kt}{S_s H_{dr}^2} = \frac{c_v t}{H_{dr}^2} \tag{8}$$

Finally, the specific inelastic storage coefficient was considered with the dimensionless time factor T used in soil mechanics in the solution of the partial differential equation of Terzaghi's consolidation theory. The time factor is defined as (Das, 1985):

$$T_v = \frac{c_v t}{H_{dr}^2} \tag{9}$$

where H_{dr} is the two way drainage thickness of the layer or b/2 for this case. Sometimes the same time factor is defined in terms of a time constant denoted by τ as:

$$T_v = \frac{t}{\tau} \tag{10}$$

which indicates that 100% of consolidation occurs when the time t is equal to the time constant τ. Combining equation (7) with (8) and (9) we have:

$$\tau = \frac{\left(\frac{b}{2}\right)^2 S_{skv}}{K_z} \tag{11}$$

This equation allows one to determine the hydraulic conductivity in the vertical

direction if one knows the consolidation percentage and the specific inelastic storage coefficient.

All of the equations developed in this paper are applicable only for single layers; however, most systems studied in nature consist of many layers of material, each with its own characteristics.

Hantush (1960), studied pumping from an aquifer with scattered pervious and semipervious layers and found that the drawdown can be computed using an effective or equivalent storage coefficient equal to the sum of the storage coefficients of the individual aquifer layers. The specific storage coefficient of the system is the weighted mean of the specific storage of the individual layers:

$$S_{s\ system} = \frac{S_{s1}b_1 + S_{s2}b_2 + \ldots S_{sn}b_n}{B} \tag{12}$$

where S_{sn} is the specific storage coefficient of the n^{th} layer and,

b_n is the thickness of the n^{th} layer,

$B = b_1 + b_2 + \ldots + b_n$.

Similarly, the horizontal hydraulic conductivity of a layered system is the weighted mean:

$$K_{system} = \frac{K_1b_1 + K_2b_2 + \ldots K_nb_n}{B} \tag{13}$$

and equation (13) can be considered to represent the maximum hydraulic conductivity of a layered system.

The vertical hydraulic conductivity of a layered system is given by:

$$K_{z\ system} = \frac{B}{\frac{b_1}{K_{z1}} + \frac{b_2}{K_{z2}} + \cdots \frac{b_n}{K_{zn}}} \tag{14}$$

and can be considered as the minimum vertical hydraulic conductivity of a layered system.

THEORY

Effective stress in the compressible layers of an unconfined aquifer can change because of the change in the buoyant support associated with the water table fluctuation. In a confined aquifer the fluctuation of the piezometric head induces hydraulic gradients and seepage stresses. Roughly, the change in effective stress in a confined aquifer is equal to the change in hydraulic head (Lofgren, 1968, 1970)

The study of regional subsidence can be made by analyzing one dimensional consolidation because the extent of the study area is large enough to neglect the effects of lateral strains.

With the documented data available for the Houston area, it is possible to determine the history of the change in effective stress that will cause the consolidation for every one of the clay layers. The history of the soil deformation is also available from the recorded borehole extensometers. Therefore it is possible to plot stress-deformation graphs for each of the clay layers.

The plot of the consolidation history for the Baytown area (Figure 6 and Figure 7), shows in some periods of time a rebound of the soil and then again a recompression. This indicates an unloading followed by a loading process similar to the consolidation test

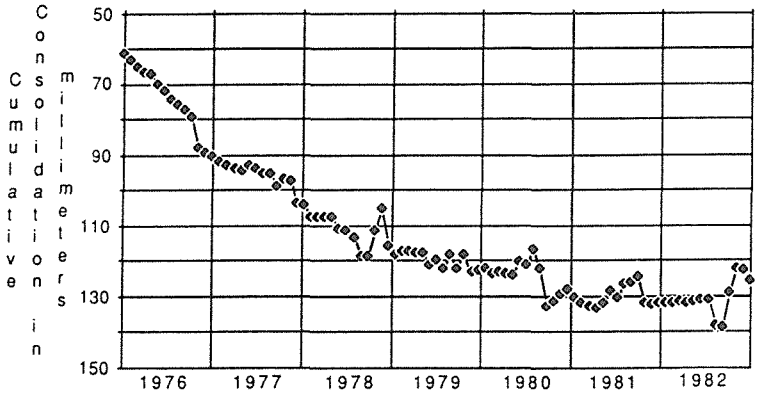

FIG. 6 Consolidation history: Baytown area.

performed in the laboratory where the compressibility and the swelling coefficients are determined by the slopes of the rebound and the virgin compression curves. The stress-deformation plot should show loops clearly indicating the unloading and loading process especially during the rebound periods. Because the process in each one of the clay layers is complicated, the behavior will not be the ideal, and some deviation is expected. Once the loop is found, the slope (of the unloading portion which represents the elastic expansion in response to a decreasing applied stress) will represent the corresponding storage coefficient:

$$S_{ke} = \frac{\Delta b}{\Delta h} \tag{15}$$

where Δb is the change in deformation of the clay layer and,

Δh is the effective stress change for the corresponding change in deformation measured in meters of water.

By constructing a line with a slope equal to S_{ke} from the point of minimal stress in the same loop to an interception with the deformation axis of the plot, it is possible to determine the amount of permanent deformation as the difference between these two points.

Likewise, the distance between the minimum stress and the intersection of the

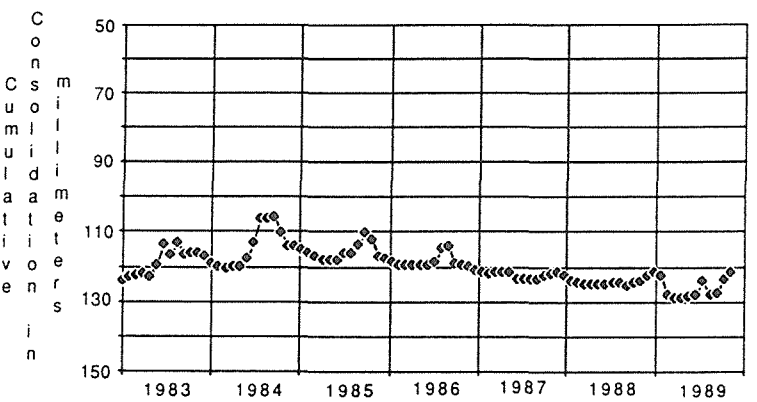

FIG. 7 Consolidation history: Baytown area.

recompression part of the loop determines the preconsolidation load. Once the preconsolidation load is selected the slope of the ascending part of the loop will represent the inelastic storage coefficient S_{kv}.

After the inelastic storage coefficient (which is a measure of the permanent deformation) has been obtained, the proportion of ultimate consolidation can be calculated from the ratio of the change in height at time t and the ultimate change in height. This relation is expressed in terms of the inelastic storage coefficient as:

$$U\% = \frac{\Delta b}{\Delta h\, S_{kv}} 100 \tag{16}$$

where Δb is the permanent deformation measured in the stress-deformation graph,

Δh represents the increase of stress beyond the preconsolidation load level.

The calculation of the consolidation percentage allows the calculation of the time constant τ given the value of the time factor T_v. The time factor T_v is a function of the initial excess pore pressure distribution and the percentage of consolidation. In the present work the pore pressure distribution was simulated as a triangular increase and decrease. Thus the values of T_v can be obtained from tables such as Leonards (1962).

For calculating the time constant τ, one can assume that the consolidation at the end of the loading period is the same as that which would have resulted in half the loading period had all the load been applied at once (Terzaghi, 1950). This procedure also applied by Ryley (1969) requires the definition of the time of the loading period and the time of the maximum load. Both of these times are available from the stress history graph because the loop for the preconsolidation load determines the time of the loading period and the maximum load that corresponds to the time of the maximum stress. Mathematically the time constant using this approximation is given by the expression:

$$\tau = \frac{0.5\,(t_1 - t_0)}{T_v} \tag{17}$$

By combining equation (17) with equation (11), the vertical hydraulic conductivity can be calculated.

Since the change in water level is recorded for the total thickness, one can assume that the water level change or head loss for a clay layer is proportional to the corresponding thickness. If ΔW is the total difference in water level between the piezometers LJ-65-16-930 and LJ-65-16-931, and b is the thickness of the clay layer, the head loss or hydraulic head that is determining the change in effective stress is:

$$\Delta h = \frac{\Delta W}{L} b \tag{18}$$

This change in effective stress could be added or subtracted from the initial depth H of the clay layer under study, depending upon the position of the water level in the piezometers. For instance when the water level measured in the deeper piezometer LJ-65-16-931, (450 m below land surface) is less than the water level measured in the shallower piezometer LJ-65-16-930, (131 m below land surface), the amount calculated by the equation (18) is subtracted from H. The water level in the piezometers was measured with respect to the land surface. This procedure was followed to calculate the effective stress acting on each of the clay layers present in the Baytown area.

The plot of the consolidation history (Figure 6 and Figure 7) shows that even though the pumping in the Baytown area has been stopped since 1976, the soils between 131 m (431 feet) and 450 m (1475 feet) are still consolidating and during the period 1976-1989

have subsided 60.65 mm (0.199 foot). Likewise measurements from the extensometers show consolidation of about 98 mm (0.30 foot) between the land surface and 131 m (431 feet), and about 174 mm (0.53 foot) between the surface and 450 m (1475 feet). Consolidation measured by the extensometers probably does not reflect total subsidence because some additional consolidation may be occurring below the depth of 1475 feet (450 m) where the second extensometer is placed. To analyze each one of the compressible layers, the corresponding deformation is assumed to be also proportional to the thickness of the layer.

Once the effective stress and the consolidation for each one of the layers has been calculated, it is possible to plot these two variables and select one loop to determine the storage coefficients and the other soil parameters discussed above. In the Baytown area data for the year 1985 generates the loop shown in Figure 8 for the layer denoted as I. In this case a proportional variation of the stress and consolidation has been assumed. The rest of the layers generate similar loops.

The results of the calculations are summarized in Tables 1 and 2.

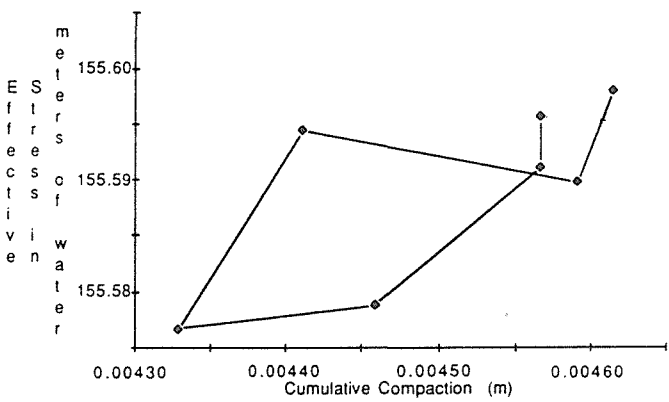

FIG. 8 Stress and deformation: Baytown layer I, 1985.

RESULTS AND CONCLUSIONS

A close relation between the change in piezometric head and soil deformation was observed from actual measurements. This fact was used to determine properties of the deformable soils in the Baytown area. In spite of the simplicity of the analytical procedure, the calculated values are consistent with other published values as shown in Table 2. This fact indicates that this simple methodology can be applied in other subsidence modeling with confidence.

The data presented is valuable since the other method to determine the compressibility of the fine grained material obtaining representative undisturbed cores is difficult and expensive. Where subsidence has been well documented, such as in the Houston-Galveston region, subsidence may be coupled with historic stress changes and the amount of compressible material to determine compressibility to use for regional appraisal (Bravo, 1990; Bravo et.al.,1991).

ACKNOWLEDGEMENTS The authors wish to thank Mr. Robert K. Gabrysch, Chief of the Houston Subdistrict of the United States Geological Survey and his staff for providing much of the background data and reports.

TABLE 1 Baytown storage coefficients and vertical hydraulic conductivities in the compressible layers (61 to 445 m).

Layer	Thickness m	S_{ke}	S_{ske} m^{-1}	S_{kv}	S_{skv} m^{-1}	K_z m day^{-1}
I	6.10	8.50×10^{-3}	1.40×10^{-3}	6.10×10^{-2}	1.00×10^{-2}	2.80×10^{-4}
II	24.40	8.80×10^{-3}	1.90×10^{-3}	5.80×10^{-2}	2.40×10^{-3}	1.80×10^{-5}
III	7.60	9.00×10^{-3}	1.20×10^{-3}	5.50×10^{-2}	7.20×10^{-3}	0.40×10^{-4}
IV	7.60	9.00×10^{-3}	1.20×10^{-3}	5.50×10^{-2}	7.20×10^{-3}	0.40×10^{-4}
V	3.00	9.00×10^{-3}	2.95×10^{-3}	5.50×10^{-2}	1.80×10^{-2}	0.30×10^{-4}
VI	19.80	8.80×10^{-3}	4.40×10^{-4}	5.90×10^{-2}	3.00×10^{-3}	2.40×10^{-4}
VII	6.10	8.50×10^{-3}	1.40×10^{-3}	6.10×10^{-2}	1.00×10^{-2}	3.00×10^{-5}
VIII	3.00	9.00×10^{-3}	2.95×10^{-3}	5.50×10^{-2}	1.80×10^{-2}	0.35×10^{-4}
IX	10.70	8.80×10^{-3}	8.20×10^{-4}	5.80×10^{-2}	5.45×10^{-3}	0.70×10^{-4}
X	18.30	8.80×10^{-3}	4.80×10^{-4}	5.70×10^{-2}	3.10×10^{-3}	1.30×10^{-4}
XI	15.20	8.80×10^{-3}	5.80×10^{-4}	5.90×10^{-2}	3.90×10^{-3}	1.60×10^{-4}
XII	6.10	8.50×10^{-3}	1.40×10^{-3}	6.10×10^{-2}	1.00×10^{-2}	2.90×10^{-5}
XIII	3.00	9.00×10^{-3}	2.95×10^{-3}	5.50×10^{-2}	1.80×10^{-2}	0.30×10^{-4}
XIV	6.10	8.50×10^{-3}	1.40×10^{-3}	6.10×10^{-2}	1.00×10^{-2}	2.70×10^{-5}
XV	12.20	8.90×10^{-3}	2.23×10^{-4}	5.80×10^{-2}	4.75×10^{-3}	0.30×10^{-3}
XVI	6.10	8.50×10^{-3}	1.40×10^{-3}	6.10×10^{-2}	1.00×10^{-2}	2.90×10^{-5}

$K_{z\ system} = 4.36\times10^{-5}$ m day^{-1} $S_{ske\ system} = 9.00\times10^{-4}$ m^{-1}

$S_{skv\ system} = 5.90\times10^{-3}$ m^{-1}

TABLE 2 Comparison of Baytown calculated storage coefficients and vertical hydraulic conductivities with published values.

Source	S_{ke}	S_{ske} m^{-1}	S_{kv}	S_{skv} m^{-1}	K_z m day^{-1}
Bravo, et.al., (1991)	2.90×10^{-1}	9.00×10^{-4}	9.20×10^{-1}	5.90×10^{-3}	4.36×10^{-5}
Gabrysch,R.K. (1984)	4.10×10^{-2} 2.20×10^{-1}	3.95×10^{-5} 2.10×10^{-4}			
Meyer & Carr (1979)		4.90×10^{-5} 2.85×10^{-4}	3.00×10^{-4} 3.50×10^{-2}		3.65×10^{-5} 1.40×10^{-3}
Jorgensen,D.G. (1975)			5.00×10^{-3} 3.00×10^{-2}		
Riley,F.S.* (1969)	1.00×10^{-3}	2.80×10^{-6}	5.70×10^{-2}	1.40×10^{-4}	2.40×10^{-6}

* Values obtained for a cyclical load in Central California.

REFERENCES

Bravo, R. (1990) A new Houston ground water flow and subsidence model utilizing three dimensional finite differences. Ph.D. Dissertation, University of Houston, Houston, Texas.

Bravo, R., Rogers, J. R. & Cleveland, T. G. (1991) On the determination of the compressible soil properties required to model subsidence in the area of Houston, Texas. Proceedings of the Fourth International Symposium on Land Subsidence, Houston, Texas.

Das, Braja M. (1985) Principles of Geotechnical Engineering, PWS Publishers, Boston.

Jacob, C.E. (1950) Flow of ground water in Rouse, Hunter. Engineering Hydraulics; New York, John Wiley, pp 312-386.

Terzaghi, Karl and Peck, R.B.(1948) Soil Mechanics in Engineering Practice, New York, John Wiley.

Riley, Francis, R.(1969) Analysis of borehole extensometer data from central California. Proceedings of the International Symposium on Land Subsidence, Tokyo , v II, pp 423-431, IASH/AIHS-UNESCO.

Leake, S.A. & Prudic, D.E.(1988) Documentation of a computer program to simulate aquifer-system compaction using the Modular Finite-Difference Ground-Water Flow Model. U.S. Geol. Survey, Open File Report 88-482.

Leonards, G.A. (1962) Foundation Engineering. McGraw-Hill Book Co., New York.

Lofgren, Ben E.(1968) Analysis of stresses causing land subsidence. U.S. Geological Survey, professional paper 600, pages B129-B225.

Lofgren, Ben E.(1970) Field measurements of aquifer-system compaction, San Joaquin Valley, California. Proceedings of the International Symposium on Land Subsidence, Tokyo , v I, pp 272-284, IASH/AIHS-UNESCO.

Gabrysch, R.K.(1984) Ground water withdrawals and land-surface subsidence in the Houston-Galveston Region, Texas, 1906-80, U.S. Geological Survey report 287.

Jorgensen, Donald G.(1975) Analog model studies of ground water hydrology in the Houston district, Texas. U.S. Geological Survey, report 190.

Meyer, W.R. and Carr, J.E.(1979) A digital model for simulation of ground water hydrology in the Houston area, Texas. Texas Dept. Water Resources LP-103.

Land Subsidence (Proceedings of the Fourth International Symposium on Land Subsidence, May 1991). IAHS Publ. no. 200, 1991.

On the Determination of the Compressible Soil Properties Required to Model Subsidence in the Area of Houston, Texas

ROLANDO BRAVO, JERRY R. ROGERS & THEODORE G. CLEVELAND
Department of Civil and Environmental Engineering, University of Houston, Houston, Texas 77204, U.S.A.

ABSTRACT One of the most important characteristics used to simulate the consolidation of an aquifer being pumped is the compressibility of the subsurface material. The present work, based on water level fluctuations and borehole extensometer data in the Houston area, determines, analyzes and compares the storage coefficient for either the elastic and inelastic ranges and the vertical hydraulic conductivity. Specifically coastal and inland areas are examined and values are recommended for use in modeling. In the coastal Houston area, data from Baytown, Clear Lake and the Johnson Space Center (NASA) taken each 28 days by the USGS since 1973 is analyzed. Similarly in the inland area, data from gages in the Southwest and Addicks areas are analyzed. The boreholes used for the extensometers at the Clear Lake, and Addicks sites were drilled to the base of the Evangeline aquifer. This is the deepest aquifer being pumped in most of the region. Since little or no water level decline has occurred below the aquifer, these extensometers measure total man-made consolidation (compaction). The extensometer at the Johnson Space Center is designed to measure compaction in the Chicot aquifer. This is the shallowest aquifer in the region; it overlies the Evangeline aquifer. The Clear Lake site was selected so that the information obtained there could be coupled with information from the Johnson Space Center. The results of the present analysis will be used to determine the percentage of subsidence for each of the aquifers being pumped in the region.

INTRODUCTION

Ground water in the Houston area is used for public supply, industry and irrigation. The use of ground water in this area slowly increased until 1973 when the industry started using surface water for its needs. Generally speaking, water levels in the Houston area (regional basis) declined from the beginning of development until 1977. The declines in water levels have caused pronounced regional subsidence of the land surface. The center of regional subsidence is the Pasadena area, where more than 2.7 m (9 feet) of subsidence occurred between 1906 and 1978. Localized centers of subsidence exist throughout in the region, especially in the Baytown-La Porte and Texas City areas (Gabrysch, 1984).

Since late 1976, changes in the pumping distribution resulting from efforts to control subsidence and the introduction of surface water from Lake Livingston have altered the pattern of water level changes.The average daily withdrawals of ground water in Harris County and parts of Fort Bend and Waller Counties between 1975-1984 was 20 m^3/s (464 Mgal/day). The percentage of ground water to total average daily use during 1975-1984 was between 48 to 58% (Williams and Ranzau, 1987). During 1985-1989, the City of Houston's water supply averaged about 55% ground water. During 1985-1989, the City of

Houston's ground water withdrawal decreased from 8.5 m^3/s (194 Mgal/day) in 1985 to 7.7 m^3/s (175.4 Mgal/day). During the decade 1980-1989 the average daily withdrawal of ground water in Harris County and parts of Fort Bend and Waller Counties was 19.26 m^3/s (439.77 Mgal/day).

The purpose of the present work is to present the analysis performed at four different places in the Houston area following the methodology described in Bravo et.al., 1991.

BACKGROUND

The Houston-Galveston area has two major aquifers: the Chicot and the deeper Evangeline aquifer, with the Burkeville Confining layer below.

Recording borehole extensometers, which sometimes are called compaction monitors are holes drilled and cased to selected depths, into which smaller diameter standpipes are installed. Since 1979 the United States Geological Survey (USGS) has 11 boreholes extensometers in operation at 11 different sites in the Houston-Galveston region. These borehole extensometers continuously record the consolidation of the interval between the land surface and the bottom of the standpipe. Moreover, in the Houston-Galveston region, the United States Geological Survey (USGS) is collecting data on water level changes in different sand layers at the aquifers. From these data estimates of pressure change (stress change) at different depths for various time intervals may be made. Electrical logs are available for the places where the borehole extensometers are placed. These electrical logs can be used to identify the compressible and incompressible layers present either in the Chicot or the Evangeline aquifers.

Electrical logs in the area indicate alternating sand and clay layers scattered throughout the vertical aquifer sections. Log interpretation made at Baytown, Clear Lake and Johnson Space Center (NASA), Southwest and Addicks sites indicates that aproximately 50% of the Chicot and Evangeline aquifers is composed of compressible materials.

BAYTOWN

Ground water pumping in the Baytown area slowly increased until 1973. During 1972, about 1.4 m^3/s (32 Mgal/day) was pumped while in 1978 a total of 0.95 m^3/s (21.6 Mgal/day) was pumped (Gabrysch,1984). Since 1972 the ground water pumping has decreased because industry increased its use of surface water. During 1973-1977, water levels rose as much as 6.1 m (20 feet) in wells in the Baytown area. The Baytown site, established in 1972, has two extensometers installed to depths of 131 m (431 feet) and 450 m (1475 feet) to measure the consolidation in two depth intervals. In addition piezometers at different depths were also installed. Data has been taken every 28 days since 1976. The wells where these devices are placed are numbered LJ-65-16-930 and LJ-65-16-931 respectively. The plot of the water level changes for both wells show that since 1976 the water has risen almost 37 m (120 feet) in the well LJ-65-16-930 and appears to remain stable since 1987 indicating that the system is reaching equilibrium. The water level in well LJ-65-16-931 has risen more than 24 m (80 feet) and the system also appears to be in equilibrium. The difference in these heads roughly depicts the change in effective stress.

Electrical logs in the Baytown area indicate alternating sand and clay layers scattered throughout the vertical aquifer sections. Log interpretation has 16 layers of compressible material that are present between 131 m (431 feet) and 450 m (1475 feet). The total clay thickness in this range is 155 m (510 feet) which represents 49% of the total thickness under study: 318 m (1044 feet).

CLEAR LAKE AND JOHNSON SPACE CENTER (NASA)

The Clear Lake and Johnson Space Center areas are located in the southern part of Harris

County. During 1960, 0.05 m^3/s (1.2 Mgal/d) was pumped in the Johnson Space Center area. This pumping increased gradually until 1976, when 0.90 m^3/s (20.6 Mgal/d) was pumped for municipal supply and industrial use. During 1976 both of the mentioned areas began using some surface water from Lake Houston. During 1978, total ground water pumping decreased to 0.22 m^3/s (5.2 Mgal/d), of which 0.18 m^3/s (4.0 Mgal/d) was for municipal use (Gabrysch,1984). The history of the water level changes in the Johnson Space Center shows a decline of 76 m (250 feet) between 1943 and 1970. Later during 1973-1977, water levels rose as much as 20 feet (6.1 m) in the same area.

Alternating sand and clay layers are scattered throughout the vertical aquifer sections in this area. Log interpretation in the Clear Lake and Johnson Space Center, shown in Figure 1, has 21 layers of compressible material that are present between 235 m (770 feet) and 936 m (3072 feet) below land surface. The total clay thickness in this interval is 307 m (1007 feet) which represents 44% of the total thickness under study.

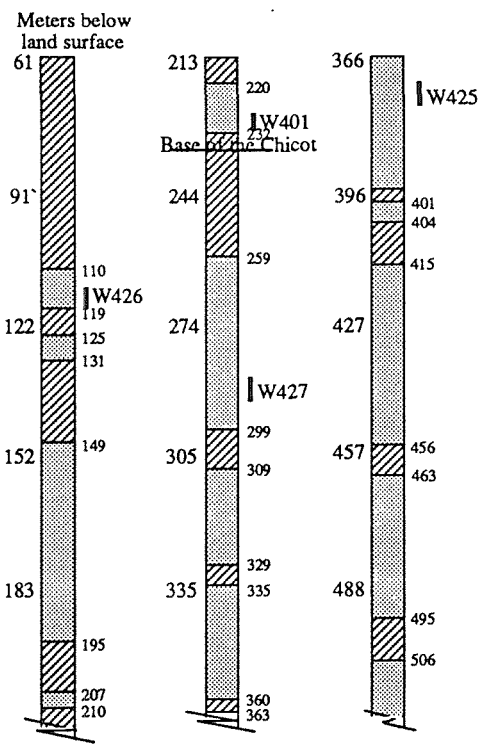

FIG. 1(a) Soil profile: Clear lake area. Solid vertical lines indicate the interval of well perforation.

The extensometer installed at the space center by the United States Geological Survey USGS in 1962 is the second extensometer installed and is the oldest in existence in the Houston Galveston region. This borehole extensometer records the consolidation of the compressible layers between the land surface and 235 m (770 feet). It is designed to measure consolidation of the Chicot aquifer. Because additional information about consolidation and subsidence was required, the Houston Galveston Coastal Subsidence District funded the installation of two extensometers and three separate piezometers at the Clear Lake site in 1976. This site was selected so the information obtained could be coupled with information from the Johnson Space Center site. The deepest extensometer was completed at 936 m (3072 feet) in the Burkeville confining layer at the base of the

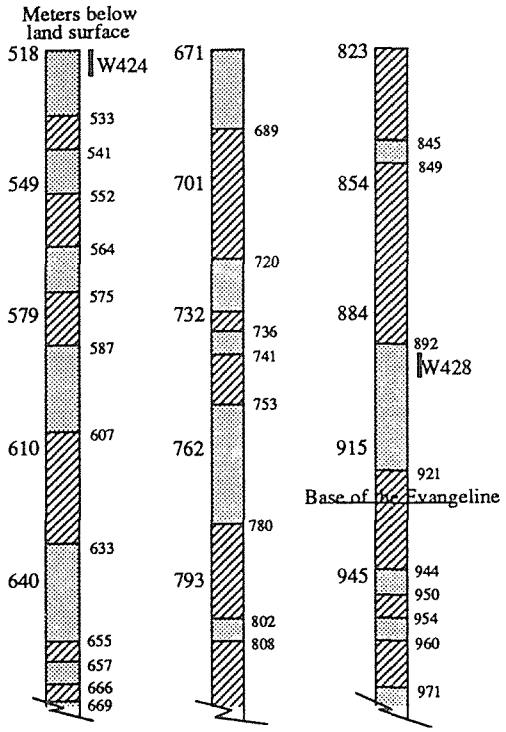

FIG. 1(b) Soil profile: Clear lake area. Solid vertical lines indicate the interval of well perforation.

Evangeline aquifer.

Records of the water level changes from piezometers installed at different depths at the Clear Lake and Johnson Space Center sites are available. These data collected every 28 days since 1977 were used to determine the hydraulic head change or stress change acting on the different clay layers following the procedure described in Bravo et.al., (1991).

The plot of the water level changes for the piezometer well installed at the Johnson Space Center, LJ 65-32-401 (235 m (770 feet) depth from 1977 to 1989) (Bravo, 1990) indicates that the water level during 1977-1979 rose about 8.0 m (25 feet) and only about 3.0 m (10 feet) during 1980-1989. Since 1987 there is a tendency towards an equilibrium.

The plot of the water level changes for the piezometer well installed at Clear Lake, LJ 65-32-428 (937 m (3072 feet) depth from 1977 to 1989) indicates that the water level has dropped 4.0 m (13 feet) between the period 1977-1979, and rose almost 12.0 m (40 feet) from 1980 to 1987. During 1988, the water level did not change. Afterwards, the water level dropped again.

Data from the extensometers installed at the bottom of the Chicot and Evangeline aquifer were also available. The consolidation and difference in consolidation at the Johnson Space Center and Clear Lake sites is shown in Figure 2. The plot shows that during late 1978 and early 1979 the subsurface material expanded. More expansion occurred in the Evangeline and Chicot aquifers than in the Chicot alone. In early 1979 both aquifers resumed consolidating. The consolidation of the Chicot aquifer between 1977 and 1989 has been about 122 mm (0.40 foot) and the consolidation of the clay layers in the same period of time between the land surface and the bottom of the Evangeline aquifer was 178 mm (0.58 foot). Of the 44 mm (0.145 foot) of subsidence that occurred from January 1977 to September 1978, 33 mm (0.109 foot) was the subsidence of the Chicot aquifer so the remaining 11 mm (0.036 foot) of subsidence was in the Evangeline. These numbers

imply that 75% of the total consolidation (between the land surface and the bottom of the Evangeline aquifer) was due to the consolidation of the Chicot aquifer. The other 25% was due to the consolidation of the Evangeline aquifer. Therefore one can conclude that the clay layers present in the Chicot aquifer are more compressible than the clay layers present in the Evangeline aquifer.

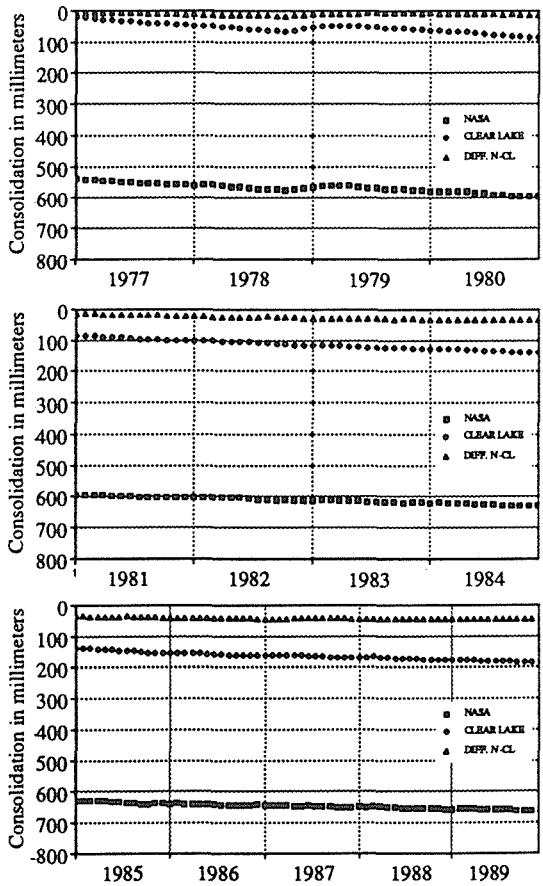

FIG. 2 Cumulative consolidation: Clear Lake and NASA areas.

Further analysis for the period 1978-1989, assuming no significant expansion has occurred since 1978, indicated that 131 mm (0.43 foot) was the total consolidation; 97.5 mm (0.32 foot) was consolidation of the Chicot aquifer, and 33.5 mm (0.11 foot) was the consolidation of the Evangeline aquifer. Again 75% of the total subsidence in this area was due to the clays present in the Chicot aquifer while only 25% was due to clays in the Evangeline aquifer.

The effective stress acting in each of the 21 layers of clay in the Johnson Space Center and Clear Lake areas was determined using water level data changes from the multilevel piezometers. This information was coupled graphically with the corresponding soil deformation which was assumed to be proportional to the thickness of the layer. In Figure 3 the stress versus deformation for the Clear Lake and NASA area layer II, is presented to illustrate the loops used to determine the soil properties by the method described in Bravo et.al.,1991.

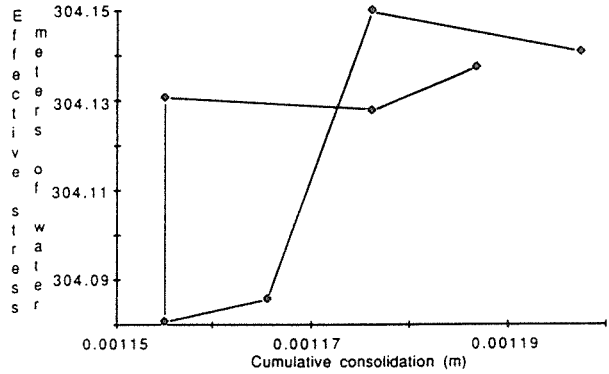

FIG. 3 Stress deformation: Clear Lake and NASA areas, layer II, 1984.

SOUTHWEST

The southwest site is located inside the Houston loop freeway area, where ground water withdrawals increased from 4.3 m^3/s (98 Mgal/d) during 1960 to 9.9 m^3/s (227 Mgal/d) during 1978. About 83% of the water being pumped in this area was used by the City of Houston. The increase in ground water use can be considered as fairly uniform. By 1976 even though the city had periodically increased the use of surface water, the rapidly increasing population required more water. Ground water was the only available supply so that by 1978, water use in the city was 14.6 m^3/s (333 Mgal/d), of which 8.3 m^3/s (189 Mgal/d) was ground water and 6.3 m^3/s (144 Mgal/d) was surface water from Lake Houston. The pumping stress on the aquifer was barely reduced.

In the Houston area, most pumping is from the Evangeline aquifer. In the southwestern part of the Houston area during 1973-1977, water levels declined as much as 6.1 m (20 feet), which reflects an increase in pumping during this period of time (Gabrysch 1984).

During 1980 a borehole extensometer, 710 m (2330 feet) depth was installed in the southwest part of Houston, at the intersection of Newcastle and West Park, South of Highway 59. There are also 5 piezometers installed at the same location.

Alternating sand and clay layers are scattered throughout the vertical aquifer sections in this area as well. Interpretation of electrical logs in the southwest site indicates 17 layers of compressible material are present between 74 m (243 feet) and 710 m (2330 feet) below the land surface. The total clay thickness in this interval is 247 m (810 feet) which is 39% of the total thickness under study.

Water level in the piezometer well installed at the Southwest site (LJ 65-21-226) rose in 1980, dropped 8.0 m (25 feet) until 1983 when the water level rose again, regaining the 8.0 m (25 feet) lost earlier.

The consolidation in the southwest area does not present as much a rebound as in the other two places already analyzed. The subsidence measured from 1980 to 1989 is about 427 mm (1.4 feet).

The effective stress acting in each of the 17 layers of clay in the Southwest area was determined using water level data from the piezometers. This information was coupled graphically with the corresponding soil deformation, which was assumed to be proportional to the thickness of the layer. Stress and deformation loops were used to determine the soil properties following the method described by Bravo,et.al.,1991.

ADDICKS

The Addicks site also belongs to the Houston area or region.

Alternating sand and clay layers are scattered throughout the vertical aquifer sections in this area. Interpretation of electrical logs in the Addicks site indicates 18 layers of compressible material between 15 m (50 feet) (497 m (1630 feet) below the land surface). The total clay thickness in this interval was 287 m (940 feet), which is 59% of the total thickness under study.

Consolidation monitoring at the Addicks site began in 1974 with installation of an extensometer to the top of the Burkeville confining layer at a depth of 549 m (1802 feet). Piezometers also were installed in 1974 and 1978. These piezometers (numbered as LJ-65-12-725, LJ-65-12-728, LJ-65-12-729, LJ-65-12-726) were placed at 15 m (49 feet), 47 m (153 feet), 72 m (237 feet) , and 503 m (1650 feet) respectively.

The water level in the piezometer well, LJ-65-12-729, installed at the Addicks site, was dropping more or less uniformly from 1978 to 1984. A sudden rise occurred in 1985, then the water level continued dropping, which indicates that the aquifer is still under the load process. Between 1978-1989 the water level in this well has dropped about 5.5 m (18 feet).

The water level in the piezometer well LJ-65-12-726, dropped almost 30 m (100 feet) between the period 1978-1979, which again is an indication that the compressible layers in this area are still compacting.

The consolidation history of the Addicks site, is shown in Figure 4. Between the surface and 549 m (1802 feet) it was 518 mm (1.7 feet). The consolidation appears constant with a rate equal to 61 mm/year (0.2 foot per year).

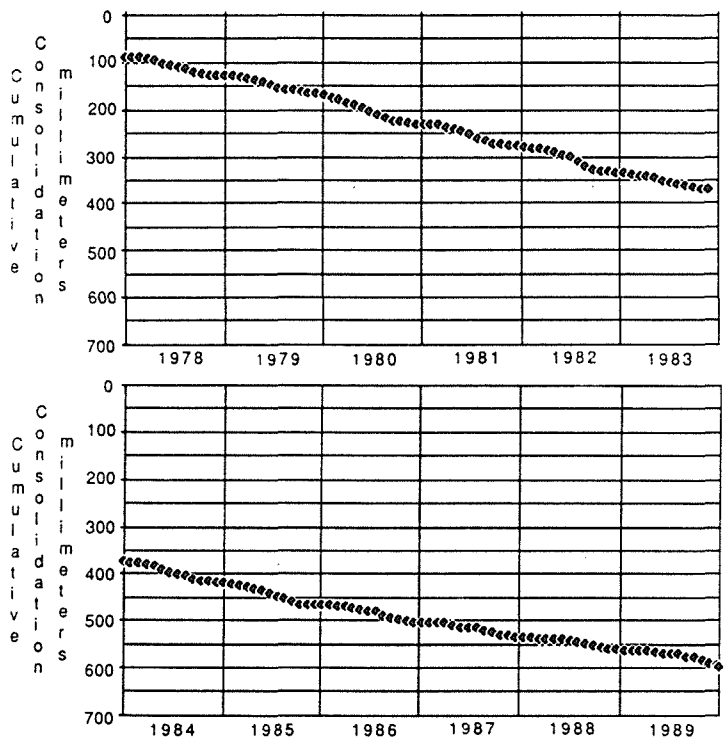

FIG. 4 Consolidation history: Addicks area.

RESULTS AND CONCLUSIONS

The data described here was used to determine the vertical hydraulic conductivity $K_{z\,system}$,

TABLE 1 Calculated parameters for the Houston area.

	Baytown	Clear Lake & NASA	Southwest
$K_{z\ system}$	4.36×10^{-5} m/day	1.10×10^{-5} m/day	0.73×10^{-5} m/day
$S_{ske\ system}$	9.00×10^{-4} m^{-1}	1.70×10^{-3} m^{-1}	2.95×10^{-5} m^{-1}
$S_{skv\ system}$	5.90×10^{-3} m^{-1}	1.30×10^{-3} m^{-1}	2.85×10^{-4} m^{-1}

TABLE 2 Comparison of Clear Lake & NASA calculated storage coefficients and vertical hydraulic conductivities with published values.

Source	S_{ke}	S_{ske} (m^{-1})	S_{kv}	S_{skv} (m^{-1})	K_z (m day^{-1})
Bravo, et.al. (1991)	1.25×10^{-1}	1.70×10^{-3}	4.01×10^{-1}	1.30×10^{-3}	1.10×10^{-5}
Gabrysch, R.K. (1984)	1.86×10^{-2} 4.60×10^{-1}	2.70×10^{-5} 6.60×10^{-4}			
Meyer and Carr. (1979)		4.90×10^{-5} 2.85×10^{-4}	3.00×10^{-4} 3.50×10^{-2}		3.90×10^{-5} 1.40×10^{-3}
Jorgensen, D.G (1975)			5.00×10^{-3} 3.00×10^{-2}		
Riley, F.S.* (1969)	1.0×10^{-3}	9.20×10^{-6}	5.70×10^{-2}	4.60×10^{-4}	2.40×10^{-6}

* Values obtained for a cyclical load in Central California.

TABLE 3 Comparison of Southwest calculated storage coefficients and vertical hydraulic conductivities with published values.

Source	S_{ke}	S_{ske} m^{-1}	S_{kv}	S_{skv} m^{-1}	K_z m day^{-1}
Bravo,et.al. (1991)	1.38×10^{-2}	3.00×10^{-5}	5.06×10^{-2}	2.85×10^{-4}	7.30×10^{-6}
Gabrysch, R.K. (1984)	1.86×10^{-2} 4.60×10^{-1}	2.70×10^{-5} 6.60×10^{-4}			
Meyer and Carr (1979)		5.00×10^{-5} 2.85×10^{-4}	3.00×10^{-4} 3.50×10^{-2}		3.65×10^{-5} 1.40×10^{-3}
Jorgensen, D.G. (1975)			5.00×10^{-3} 3.00×10^{-2}		
Riley, F.S.* (1969)	1.00×10^{-3}	9.20×10^{-6}	5.70×10^{-2}	4.60×10^{-4}	2.40×10^{-6}

* Values obtained for a cyclical load in Central California.

and the elastic and inelastic storage coefficients ($S_{ske\ system}$, $S_{skv\ system}$) using the methodology described by Bravo et.al., (1991).

The calculated values are shown in Table 1. These values are consistent with other published values as shown in Tables 2 and 3.

There are seven other places where one could perform the same kind of analysis. Future work includes the study of these additional sites. These results can improve any regional or local modeling of ground water flow and land surface subsidence.

ACKNOWLEDGEMENTS The authors wish to thank Mr. Robert K. Gabrysch, Chief of the Houston Subdistrict of the United States Geological Survey and his staff for providing much of the background data and reports.

REFERENCES

Bravo, R. (1990) A new Houston ground water flow and subsidence model utilizing three dimensional finite differences. Ph.D. Dissertation, University of Houston, Houston, Texas.

Bravo, R., Rogers, J.R. & Cleveland, T.G. (1991) Analysis of ground water level fluctuations and borehole extensometer data from the Baytown area, Houston, Texas. Proceedings of the Fourth International Symposium on Land Subsidence, Houston, Texas.

Riley, Francis, R. (1969) Analysis of borehole extensometer data from central California. Proceedings of the International Symposium on Land Subsidence, Tokyo , v II 423-431, IASH/AIHS-UNESCO.

Gabrysch, R.K. (1984) Ground water withdrawals and land-surface subsidence in the Houston-Galveston Region, Texas, 1906-80. U.S. Geological Survey report 287.

Jorgensen, Donald G. (1975) Analog model studies of ground water hydrology in the Houston district, Texas. U.S. Geological Survey, report 190.

Meyer, W.R. and Carr, J.E. (1979) A digital model for simulation of ground water hydrology in the Houston area, Texas. Texas Dept. of Water Resources LP-103.

Williams III, James F. and Ranzau, Jr., C.E. (1987) Ground water withdrawals and changes in ground water levels, ground water quality, and land surface subsidence in the Houston District, Texas, 1980-1984. U.S. Geological Survey, Water Resources Investigation Report 87-4153.

Land Subsidence (Proceedings of the Fourth International Symposium on Land Subsidence, May 1991). IAHS Publ. no. 200, 1991.

Subsidence Due to Intensive Pumping from a Layered Soil

CHEO K. LEE, SOPHIE N. FALLOU and CHIANG C. MEI
Parsons Laboratory for Water Resources and Hydrodynamics
Department of Civil Engineering
Massachusetts Institute of Technology
Cambridge, MA 02139, USA

ABSTRACT We describe the results of a theoretical study of pumping of groundwater from a layered soil. The model soil system consists of three horizontal layers where a very soft and highly impervious aquitard is sandwiched by two hard and highly porous aquifers. Water is pumped from the bottom aquifer through a vertical well. This type of problem is usually solved in hydrology by assuming constant total stress in the soil, and that the drawdown can be calculated in advance of the soil stress. By a perturbation theory and the use of Lagrangian coordinates, these common assumptions are found to be inadequate if the aquitard is very soft or thick. Specifically the drawdown should be nonlinearly coupled to the soil deformation and that the total stress is not quite uniform in depth. By a model constitutive law representative of clays, two patterns of cyclic pumping or recharging are compared.

INTRODUCTION

Groundwater is frequently pumped from an aquifer layer at the bottom of a soil stratum consisting of alternating layers of highly porous sand (aquifers) and highly impervious clay (aquitards). Many existing works are based on Biot's linearized equations of poroelasticity. Since fully three-dimensional problems coupling several soil layers are prohibitively complex, a plausible simplification is often added that the total stress, which is the sum of the effective soil stress and the pore pressure, does not vary with depth in a soil layer (see *e.g.*, Verruijt, 1969). As a consequence, the soil dilation rate is then proportional to the pore pressure. This leads to a linear diffusion equation for the incremental pore pressure (or drawdown) which is decoupled from the soil deformation. Thus the drawdown can be calculated ahead of the soil strain. Afterwards the effective stress is found simply by substracting the pore pressure from the total pressure. The soil strain then follows by using a proper constitutive law.

Since natural soils often consist of many layers of different properties, solutions for the drawdown must be constructed for each layer and matched by continuity across interfaces. This is still a numerically demanding task. In a

pioneering study of pumping from a single well, Hantush (1960) introduced a simplification that retains the essential physics. Since the fluid tends to follow the path of the least resistance, the flow should be nearly horizontal in a porous aquifer and nearly vertical in a highly impermeable aquitard. Thus in an aquifer the drawdown is adequately described by its depth-average, which satisfies:

$$b\left(\frac{\partial^2}{\partial x^2}+\frac{\partial^2}{\partial y^2}\right)\bar{s}+\left[\frac{\partial s}{\partial z}\right]_-^+=\frac{\rho g b}{kD}\frac{\partial \bar{s}}{\partial t} \tag{1}$$

where b and $\bar{s}$ are the aquifer thickness and the depth-averaged aquifer drawdown respectively, and:

$$\left[\frac{\partial s}{\partial z}\right]_-^+=\left.\frac{\partial s}{\partial z}\right|_+-\left.\frac{\partial s}{\partial z}\right|_-=\frac{\partial s_+}{\partial z}-\frac{\partial s_-}{\partial z} \tag{2}$$

is proportional to the net flux into the aquifer from the aquitard immediately above and below. In the highly impermeable aquitard, the drawdown is diffused primarily in the vertical direction:

$$\frac{\partial^2 s_+}{\partial z^2}=\frac{\rho g}{k_+ D_+}\frac{\partial s_+}{\partial t} \tag{3}$$

The lower aquitard is governed by a similar equation. Thus the original problem in three dimensions becomes one dimensional (vertical) in the aquitard and two dimensional (horizontal) in the aquifer. This quasi three-dimensional *hydrological approximation* significantly eases the computational task and has been the basis of many later extensions.

The assumption of constant total stress, which is the basis of the hydrological approximation, has been critisized by de Josselin de Jong (1963). Fallou, Mei & Lee(1991) have recently reexamined the classical problem of pumping from a well in a three-layered system, by applying perturbation analysis to Biot's theory of linear poroelasticity. While the quasi-three dimensional picture is indeed confirmed as the first approximation in a power series expansion of the small ratio of aquitard-to-aquifer permeabilities, self weight can nevertheless cause the total stress to be nonuniform in a thick and soft aquitard.

In cases of severe subsidence attributable to soft clay layers the total vertical displacement is small at all as compared to the typical depth of a clay layer. For instance the soil foundation in Mexico City consists of many clay strata of a few to a few tens of meters thick, alternating with sand and gravel layers, the total subsidence is nearly 7 m during the period 1880 to 1970 while the rate of subsidence reached 30 cm/year in 1952 (Zeevaert, 1983). Therefore in addition to accounting for finite soil strain, questions should be raised as to whether the pore pressure is still governed by a linear equation uncoupled to the soil response and can be calculated in advance.

For strictly one dimensional consolidation, large deformation can be most elegantly dealt with by a Lagrangian approach introduced by Cooper (1966, with revisions by Gambolati, 1973 a,b) and Gibson, England & Hussey(1967). This

approach allows one to follow the finite displacement of the soil matrix in the most direct manner. It is therefore desirable to see how this approach can be combined with the three dimensional field of the pore pressure.

In this paper we shall outline a recent study to be more fully reported elsewhere(Lee, Fallou & Mei 1991). The classical example of pumping from an isolated region is treated by asssuming a soil system consisting of three horizontal layers of comparable thickness, with an aquitard sandwiched between two aquifers. All layers are infinite in radial extent. Lagrangian coordinates are used. Rather than invoking the hydrological approximation of Hantush heuristically, we have extended our perturbation theory for small permeability ratio (aquitard to aquifer), in order to deduce a similar simplification for the flow. It can be shown that the one dimensional Lagrangian theory for the soil matrix is still valid to certain degree of accuracy. Compressibility of water and partial saturation will be neglected. The aquifers are assumed to be very much more rigid than the aquitard. The sharp phreatic surface will be found as a part of the nonlinear solution. In addition to ground subsidence, we shall also examine the variations of the soil parameters as functions of the pumping rate. Two types of transient pumping schedules will be discussed.

EXACT GOVERNING EQUATIONS

Consider the saturated region in an aquifer or an aquitard. Let n be the porosity of the soil matrix, ρ_w and $\mathbf{v}_w$ the density and velocity respectively of the pore water. Similarly, we let ρ_s and $\mathbf{v}_s$ denote the density and velocity of the solid matrix. Mass conservation of either phase requires that:

$$\frac{\partial n\rho_w}{\partial t} + \nabla \cdot (n\rho_w \mathbf{v}_w) = 0 \tag{4}$$

and:

$$\frac{\partial (1-n)\rho_s}{\partial t} + \nabla \cdot [(1-n)\rho_s \mathbf{v}_s] = 0 \tag{5}$$

They can be combined to give the so-called *storage equation*:

$$\nabla \cdot [n(\mathbf{v}_w - \mathbf{v}_s)] + \nabla \cdot \mathbf{v}_s = 0 \tag{6}$$

Let p be the pore pressure and k the hydraulic conductivity of the soil matrix. Following a convention in ground water hydraulics, we define the *drawdown* s as the change in piezometric head from the initial state:

$$s = \frac{p}{\rho_w g} + z - H \tag{7}$$

where H is the initial height of the water table in the phreatic aquifer, measured from the bed rock at the bottom of the whole system. Darcy's law can be expressed as:

$$k\nabla s = -n(\mathbf{v}_w - \mathbf{v}_s) \tag{8}$$

Combining (8) with (3), the storage equation may be written:

$$\nabla \cdot (k \nabla s) = \nabla \cdot \mathbf{v}_s \tag{9}$$

If the total stress tensor in the solid matrix is denoted by τ, with components τ_{ij}, the approximate equation of solid momentum conservation is, after ignoring inertia:

$$\nabla \cdot \tau = -((1-n)\rho_s + n\rho_w)\mathbf{g} \tag{10}$$

The convention of positive tension is adopted here. Let the effective stress tensor σ, with components σ_{ij}, be defined by:

$$\sigma = \tau + p\mathbf{I} \tag{11}$$

where I is the identity tensor. Equations (9), (10) and (11), can be combined to give:

$$\nabla \cdot \sigma = \rho_w g \nabla s - (1-n)(\rho_s - \rho_w)\mathbf{g} \tag{12}$$

Let all quantities (except depths) of the initial state before pumping starts be distinguished by the overhead bar, then:

$$\bar{s} = \bar{\mathbf{v}}_s = \bar{\mathbf{v}}_w = 0 \qquad \bar{p} = \rho_w g(H - z) \tag{13}$$

and:

$$\nabla \cdot \bar{\sigma} = \rho_w \mathbf{g} - [(1-\bar{n})\rho_s + \bar{n}\rho_w]\mathbf{g} \tag{14}$$

All pumping-induced departures from the initial state will be distinguished by the overhead tilde, i.e.:

$$\begin{aligned} &n = \bar{n} + \tilde{n} \qquad p = \bar{p} + \tilde{p} \qquad \sigma = \bar{\sigma} + \tilde{\sigma} \\ &k = \bar{k} + \tilde{k} \qquad \mathbf{v}_s = \tilde{\mathbf{v}}_s \qquad \mathbf{v}_w = \tilde{\mathbf{v}}_w \\ &b = B + \tilde{b} \qquad h = H + \tilde{h} \qquad s = \tilde{s} = \tilde{p}/\rho_w g \end{aligned} \tag{15}$$

where h and $\tilde{h}$ are respectively the instantaneous height and the change of height of the water table.

We now introduce the soil constitutive laws for finite strain. It will be shown later that soil deformation in this three dimensional problem is approximately one dimensional to the desired accuracy. Hence empirical relations between stresses and strains well established from one dimensional tests suffice here. One customary form of the empirical relation is:

$$de = -C_c d(\log_{10}(-\sigma_{zz})) \tag{16}$$

where C_c is the compression index (Lambe & Whitman, 1969, p. 155). For virgin compression, the compression index C_c of some materials may be approximated by a constant within certain range of stresses. For cyclic loadings, C_c is often multi-valued as the stress changes quasi-statically through virgin compression, swelling and recompression (see, e.g., Lambe & Whitman, 1969). To explore

possible hysteretic responses caused by this multivaluedness, we shall adopt a schematized relation between e and $\log_{10}(-\sigma)$ in which virgin compression follows a straight line with constant slope C_c, and both swelling and recompression follow another straight line with the same smaller slope C_c'. The rest of theory is however applicable to any nonlinear $\sigma - e$ relation. While typical values of C_c for sand are $0.001 \sim 0.01$ and 0.2 - 0.4 for common clays, the Mexico City clay is exceptionally soft and C_c has been variably estimated to be in the range 4.5 - 8 (Holtz and Kovacs, 1981; Lambe, 1951). Since the consolidation process is usually very slow, these quasi-static relations will be adopted for both the initial and the transient states.

We remark that the void ratio e is related to the porosity n by:

$$e = \frac{n}{1-n} \qquad \text{or} \qquad n = \frac{e}{1+e} \tag{17}$$

and that the constrained modulus:

$$D = \frac{1+e}{a_v(e)} = (1+e)\frac{d\sigma_{zz}}{de} \tag{18}$$

will be taken to be the same as the bulk modulus (see e.g., Lambe & Whitman, 1969, *p.* 157) in Biot's linearized theory of poroelasticity, to be used only for order estimation.

The initial value of $\bar{e}$ will be given at one reference depth within the layer; its variation $\bar{e}(z)$ throughout the layer as well as $\bar{\sigma}_{ij}(z)$, $\bar{k}(z)$, and $\bar{D}(z)$ are calculated by assuming virgin compression. Such computations and results have been made by Fallou, Mei & Lee (1991), and will be cited later.

Now the boundary conditons. Referring to Fig. 1, let the subscript $(.)_1, (.)_3$, and $(.)_2$ signify respectively the lower and upper aquifers and the aquitard between them. On the horizontal bottom $\Gamma_0 : z = 0$, the bed rock is assumed to be rigid and impermeable, hence:

$$u_1 = w_1 = 0 \qquad \text{and} \qquad \frac{\partial s_1}{\partial z} = 0 \tag{19}$$

Across each interface between soil layers $\Gamma_1 : z = b_1(r,t)$ and $\Gamma_2 : z = b_1 + b_2(r,t)$, the solid velocity, water flux and stresses must be continuous:

$$[\mathbf{v}_s]_- = [\mathbf{v}_s]_+ \tag{20}$$

$$[k\nabla\tilde{s}\cdot\mathbf{n}]_- = [k\nabla\tilde{s}\cdot\mathbf{n}]_+ \tag{21}$$

$$[\sigma\cdot\mathbf{n}]_- = [\sigma\cdot\mathbf{n}]_+ \tag{22}$$

where the subscripts $[f]_-$ and $[f]_+$ stand for f measured just below and above the interface respectively. On the water table $\Gamma_H : z = h = H + \tilde{h}(r,t)$, capillarity is ignored so that:

$$s = \tilde{h} \qquad \text{on} \quad \Gamma_H \tag{23}$$

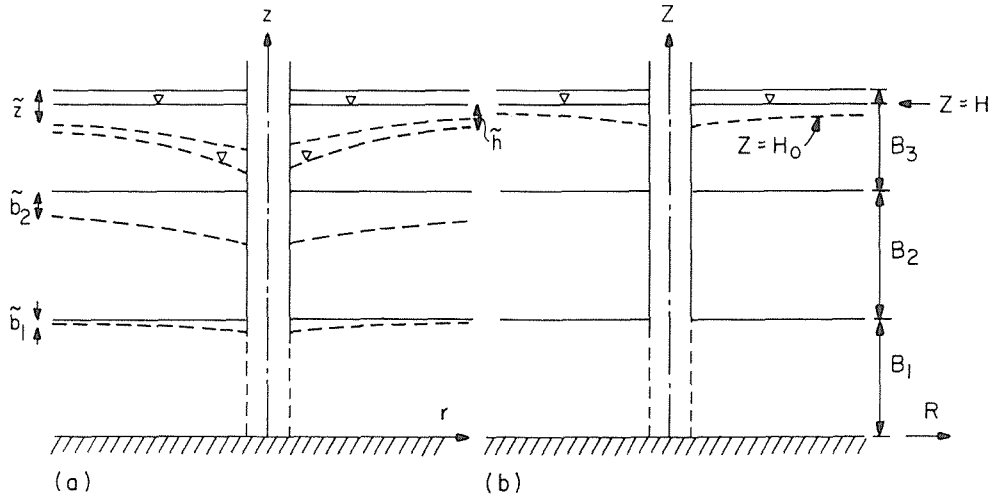

FIG. 1 Definition sketch of three-layer aquifer system in (a) Eulerian coordinate and (b) Lagrangian coordinates.

Since the seepage flow can only be tangential to the water table we have:

$$\left(\frac{\partial}{\partial t} + \mathbf{v}_w \cdot \nabla\right)[z - h(r,t)] = 0 \tag{24}$$

or:

$$\frac{\partial \tilde{h}}{\partial t} + (\mathbf{v}_w - \mathbf{v}_s) \cdot \nabla \tilde{h} + \mathbf{v}_s \cdot \nabla \tilde{h} = \mathbf{v}_w \cdot \nabla z \tag{25}$$

It follows after invoking Darcy's law that:

$$\frac{\partial \tilde{h}}{\partial t} - \frac{k_3}{n_3}\frac{\partial s_3}{\partial r}\frac{\partial \tilde{h}}{\partial r} + u_3 \frac{\partial \tilde{h}}{\partial r} = -\frac{k_3}{n_3}\frac{\partial s_3}{\partial z} + w_3 \quad \text{on} \quad \Gamma_H \tag{26}$$

In addition:

$$[\sigma \cdot \mathbf{n}]_- = [\sigma \cdot \mathbf{n}]_+ \quad \text{on} \quad \Gamma_H \tag{27}$$

The ground surface, $\Gamma_3 : z = b_1 + b_2 + b_3$, is assumed to be stress free:

$$\sigma \cdot \mathbf{n} = 0 \quad \text{on} \quad \Gamma_3 \tag{28}$$

We schematize the pumping region by a vertical well of radius a into which water is extracted only from the bottom aquifer, at the rate of Q per unit height:

$$2\pi a\, b_1\, k_1 \frac{\partial s_1}{\partial r} = Q(t) \qquad r = a \qquad 0 < z < b_1 \tag{29}$$

No water is pumped from the top aquifer:

$$\frac{\partial s_3}{\partial r} = 0 \qquad r = a \qquad b_1 + b_2 < z < h \tag{30}$$

Finally all velocity components must vanish at $r \to \infty$.

ORDER OF MAGNITUDE AND SCALES OF NORMALIZATION

As a basis of approximation it is necessary to estimate the order of magnitude of all physical variables, so as to define the scales for normalization. The generic symbol $\hat{f}$ will be used to denote the scale of any quantity f. While a full acount of the estimation will be given elsewhere (Lee, Fallou and Mei,1991), we summarize the results in Table 1. Results therein are deduced essentially by invoking mass and force balances, under the following two assumptions:

i) The ratio of aquitard permeability and aquifer permeability is very small.

$$\delta \equiv \frac{\hat{k}_2}{\hat{k}_1} = \left(\frac{\hat{b}}{\hat{r}}\right)^2 \ll 1 \tag{31}$$

The principal implication is that the horizontal length scale of flow, $\hat{r}$, i.e., the radius of influence, is much greater than the typical layer thickness $\hat{b}$.

ii) The aquifers are much harder than the aquitard. Therefore compaction takes place mainly in the aquitard. The bottom aquifer, being supported on a hard bed rock, suffers negligible compaction. The top aquifer, on the other hand, sinks or swells by following the interface with the aquitard, without much internal strain.

As may be expected intuitively, the radial movement of the solid matrix is also shown to be much smaller than the vertical movement.

The effect of self weight in the vertical force balance, which is often neglected in the existing literature of hydrology, is represented by the storage coefficient:

TABLE 1 Orders of Magnitude and Normalization Scales.

Variable or parameter	Order of Magnitude	Normalization Scale
Q	$\hat{Q}$	$\hat{Q}$
s_1, s_2, s_3	$\hat{s} = Q/2\pi\hat{b}\hat{k}_1$	$\hat{b}$
$\tilde{h}$	$\hat{s}$	$\hat{b}$
$\tilde{\sigma}_1, \tilde{\sigma}_2, \tilde{\sigma}_3$	$\rho_w g \hat{s}$	$\rho_w g \hat{b}$
$\hat{r}_1, \hat{r}_2, \hat{r}_3$	$\rho_w g \hat{s}$	$\rho_w g \hat{b}$
w_1, w_2, w_3	$\hat{w} = \hat{k}_2 \hat{s}/\hat{b}$	$\hat{k}_2$
u_1, u_2, u_3	$\hat{u} = \delta^{\frac{1}{2}} \hat{w}$	$\delta^{\frac{1}{2}} \hat{k}_2$
$\tilde{b}$	$S_T \tilde{s}$	$\hat{b}$
B_1, B_2, B_3	$\hat{b}$	$\hat{b}$
r, a	$\hat{r} = \hat{b}/\delta^{\frac{1}{2}}$	$\hat{b}/\delta^{\frac{1}{2}}$
z	$\hat{b}$	$\hat{b}$
t	$S_T \hat{b}/\hat{k}_2$	$S_T \hat{b}/\hat{k}_2$
$D_i (i = 1,2,3)$	$\hat{D}_i$	$\hat{D}_i$
$k_i (i = 1,2,3)$	$\hat{k}_i$	$\hat{k}_i$

$$S_T = \frac{\rho_w g \hat{b}}{\hat{D}} \tag{32}$$

For a thick layer of soft clay, S_T is of order unity, hence the body force term cannot always be neglected in the aquitard.

All scales are summarized in the second column of Table 1. An equivalent set of scales is listed in the third column for normalization purposes. (Note that k_i and D_i are normalized by their depth averages in each layer.) They will be used to assess the relative importance of each term in the governing equations and boundary conditions. Mathematically this is done by first normalizing all variables. Various powers of the small parameter δ will multiply each term and indicate its relative importance in the equation. Perturbation expansions in power series of δ are then introduced and each order problem is solved successively.

AQUITARD EQUATIONS IN NORMALIZED FORM

Omitting the details of the asymptotic analysis, we simply state that for efficient description of large deformation, Lagrangian coordinates (R, Z) which represent the initial position of a solid particle, are used to replace the Eulerian coordinates. For the aquitard the one dimensional equaiton of Gibson et al (1967) is recovered as the leading order approximation, at order $O(\delta^0)$. In the aquifers, the drawdowns are shown to be independent of depth at order $O(\delta^0)$. From the next order $O(\delta)$, consideration of the aquifers leads to two boundary conditions for the vertical flux at the lower and upper interfaces. The mathematical problem is finally reduced to one for the aquitard alone. In normalized form the approximate equations are summarized below. To avoid unwieldy notation, we do not use new symbols for dimensionless quantities, which are the only ones used from here on.

The dimensionless equations are:

$$\frac{\partial s_2^{(0)}}{\partial T} = \frac{1+\bar{e}_2}{a_v}\frac{\partial}{\partial Z}\left(k_2 \frac{1+\bar{e}_2}{1+e_2}\frac{\partial s_2^{(0)}}{\partial Z}\right) + S_T\left[k_2\frac{1+\bar{e}_2}{1+e_2}\frac{\partial s_2^{(0)}}{\partial Z}\right]_{\bar{\Gamma}_1}^{\bar{\Gamma}_2}$$

$$+\bar{e}_3\left[\frac{(1+\bar{e}_2)}{a_v}\frac{\partial}{\partial Z}\left(k_2\frac{1+\bar{e}_2}{1+e_2}\frac{\partial s_2^{(0)}}{\partial Z}\right)\right]_{\bar{\Gamma}_2} \qquad B_1 < Z < B_1 + B_2 \tag{33}$$

in the aquitard, with T denoting time and:

$$k_2\frac{\partial s_2^{(0)}}{\partial Z} = -B_1\bar{k}_1\frac{1}{R}\frac{\partial}{\partial R}\left(R\frac{\partial s_2^{(0)}}{\partial R}\right) \qquad \text{on} \quad \bar{\Gamma}_1 \tag{34}$$

on the lower interface $Z = B_1$ and:

$$\frac{1-\bar{n}_3}{\bar{n}_3}\left(k_2\frac{1+\bar{e}_2}{1+e_2}\frac{\partial s_2^{(0)}}{\partial Z}\right)_{\bar{\Gamma}_2} = -\frac{1}{S_T}\frac{\partial s_2^{(0)}}{\partial T} + B_1\bar{k}_1\frac{1}{R}\frac{\partial}{\partial R}\left(R\frac{\partial s_2^{(0)}}{\partial R}\right)_{\bar{\Gamma}_1}$$

$$+(H-B_1-B_2)\frac{\bar{k}_3}{\bar{n}_3}\frac{1}{R}\frac{\partial}{\partial R}\left(R\frac{\partial s_2^{(0)}}{\partial R}\right)_{\bar{\Gamma}_2}$$

$$\frac{\bar{k}_3}{\bar{n}_3(1-\bar{n}_3)}\left[\frac{\partial\tilde{\sigma}_2^{(0)}}{\partial R}\frac{\partial s_2^{(0)}}{\partial R} + \frac{\tilde{\sigma}_2^{(0)}}{R}\frac{\partial}{\partial R}\left(R\frac{\partial s_2^{(0)}}{\partial R}\right)\right]_{\bar{\Gamma}_2} \tag{35}$$

on the upper interface $Z = B_1 + B_2$. The normalized radial boundary conditions on $\bar{\Gamma}_1$ and $\bar{\Gamma}_2$ are:

$$R\frac{\partial s_2^{(0)}}{\partial R} = \nu Q(t) \qquad R = a \quad \text{on} \quad \bar{\Gamma}_1 \tag{36}$$

$$\frac{\partial s_2^{(0)}}{\partial R} = 0 \qquad R = a \quad \text{on} \quad \bar{\Gamma}_2 \tag{37}$$

$$s_2^{(0)} \to 0 \qquad R \sim \infty \tag{38}$$

The dimensionless parameter ν is defined to be:

$$\nu = \frac{\hat{s}}{\hat{b}} = \frac{\hat{Q}}{2\pi\hat{b}^2\hat{k}_1} \tag{39}$$

and is a measure of the maximum rate of pumping.

In dimensionless variables, the water table displacement relative to the moving ground surface is:

$$\tilde{s}_2^{(0)}(\bar{\Gamma}_2) - \tilde{b}_2 = -(H - H_o) = \frac{\sigma_2^{(0)}(\bar{\Gamma}_2)}{(1-\bar{n}_3)} \tag{40}$$

where the vertical subsidence of the ground surface is:

$$\tilde{b}_2 = \int_{B_1}^{B_2}\frac{e_2-\bar{e}_2}{1+e_2}dZ \tag{41}$$

The pumping induced variation of the total stress in the aquitard is:

$$\tilde{\tau}_2^{(0)} = \tilde{\tau}_2^{(0)}(\bar{\Gamma}_2) - \int_Z^{B_2}\frac{e_2-\bar{e}_2}{1+e_2}dZ \tag{42}$$

The pumping induced variation of the effecitve stress in the aquitard is:

$$\tilde{\sigma}_2^{(0)} + \bar{e}_3\tilde{\sigma}_2^{(0)}(\bar{\Gamma}_2) = s_2^{(0)} - \int_{B_1}^{B_2}\frac{e_2-\bar{e}_2}{1+\bar{e}_2}dZ = s_2^{(0)} - \int_{X_1}^{X_2}(e_2-\bar{e}_2)dX \tag{43}$$

where X is related to Z by $(1+\bar{e}_2)dX = dZ$. Note that (33) to (39) must be solved together with (43) and (16) for $\tilde{\sigma}_2^{(0)}$ and e_2; the responses in the pore fluid and soil are nonlinearly coupled.

SAMPLE NUMERICAL RESULTS

The governing equations are solved by an alternating direction scheme. Euler forward scheme is used in the vertical direction and Crank-Nicholeson scheme in the radial direction. In our numerical examples it is assumed that all three layers are of equal thickness, and that the two aquifers have the same permeability and the compression index. The dimensionless well radius a is taken to be $a = 0.05$ whose precise value is important only very near the well. At $T = 0$, the water table is at the mid-height of the top aquifer.

The initial state of static equilibrium is a one-dimensional problem. It can be reduced to a nonlinear first order differential equation for $\bar{e}$ which can be numerically integrated for a prescribed $\bar{e}$ at the top of the layer. After $\bar{e}(Z)$ is calculated $\bar{k}(Z), \bar{\sigma}(Z)$ and $\bar{D}(Z)$ follow from the constitutive laws. Details can be found in Fallou, Mei & Lee (1991) for the same three layered system. In this paper the following inputs, typical of the Mexico City clay which is exceptionally soft and porous (Zeevart, 1983, Holz & Kovacs, 1981, Marsal, 1959), are chosen for the aquitard:

$$B_1 = B_2 = B_3 = 1, \qquad \hat{k}_1 = \hat{k}_3$$

$$\bar{e}_1(\bar{\Gamma}_1) = 2.0 \qquad \bar{e}_2(\bar{\Gamma}_2) = 8.0 \qquad \bar{e}_3(\bar{\Gamma}_3) = 2.5 \qquad C_c = 6.0$$

The storage coefficient S_T is calculated to be S_T =0.45. The vertical variations of the normalized $\bar{e}_2$ and $\bar{k}_2$ are then calculated.

We have considered steady pumping at different rates, and four different patterns of transient pumping. Only two transient patterns are discussed here with a view to examining their possible hysteretic effect on subsidence. In the aquitard we have chosen $C_c = 6.0$ for virgin compression and $C_c' = 0.2C_c = 1.2$ for swelling and recompression. All time histories are shown for $R = 0.2$ which is representative of the neigborhood of the well.

(i) Steady vs Intemittent Pumping

As shown in Fig. 2 (a), the two pumping rates share the same average. In the intermittent case $Q(T)$ is cyclic, being a constant $Q(T) = 1.0$ for the first half of a cycle $0 < T < 0.5$ and zero for the second half $0.5 < T < 1$, etc. The curve of stress vs. void ratio necessarily branches off from virgin compression to swelling and recompression, etc. In the steady case water is drawn steadily at the average rate of $Q(T) = 0.5$. The soil undergoes virgin compression monotonically. Time variations of $s_2^{(0)}$, $\tilde{\sigma}_2^{(0)}$ and $\tilde{\tau}_2^{(0)}$ at $R = 0.2$ and three depths $X = X_1, X = X_m = \frac{1}{2}(X_1 + X_2)$ and X_2 are shown in Figs. 3 (a) and (b). The mid-level X_m is slightly below the initial mid level of the aquitard because the initial void ratio distribution is not uniform, but is representative of the center portion of the aquitard. Except for the change in total stress all quantities behave

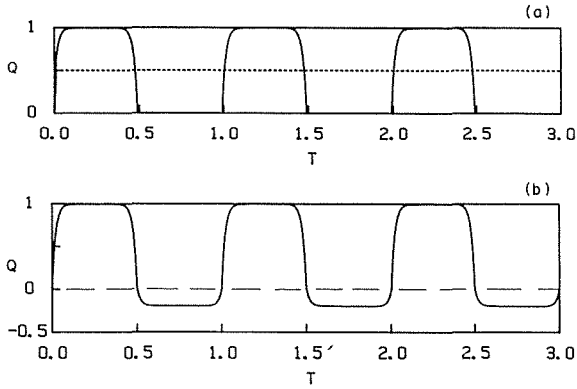

FIG. 2 **Two patterns of transient pumping.**

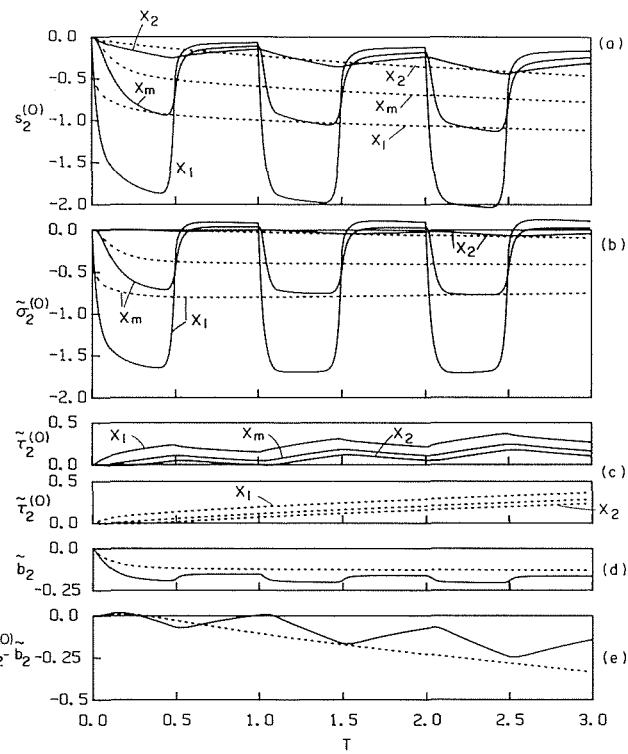

FIG. 3 **Time variations of (a)$s_2^{(0)}$, (b) $\tilde{\sigma}_2^{(0)}$, (c)$\tilde{\tau}_2^{(0)}$, (d)$\tilde{b}_2$ and (e) $H_0 - H$ for $R = 0.2$ induced by steady (solid) and intermittent (dashed) pumping depicted in Fig. 2 (a).**

drastically differently in the two cases. In particular the ground subsidence by cyclic pumping is considerably greater than that by uniform pumping at all T as shown in Fig. 3 (d). In order to lessen subsidence, it is therefore better to pump steadily rather than intermittently over a long time.

The history of the water table level just outside the well region at $R = a = 0.05$ is shown in Fig. 3 (e). Notice again the initial rise in both cases (Mandel-Cryer effect). For large T, the water table drops more rapidly and steadily when pumping is steady. Therefore for preserving the water table near the ground surface, intermittent pumping appears more preferable.

Results for other pumping patterns including pumping and recharging will be reported elsewhere.

(ii) Cyclic Pumping and Recharging

Water is pumped at the rate $Q = 1$ during the first half of each cycle and recharged at the rate $Q = -0.2$ during the second half. The low rate of recharge is chosen so as to avoid liquefaction anywhere in the soil in the entire computation, i.e., to keep the sign of $\sigma = \bar{\sigma} + \tilde{\sigma}$ negative (compression) throughout the computation so that (16) remains valid.

The aquitard drawdowns at three levels $X_1, X_m, (X_1 + X_2)$ and X_2 for $R = 0.2$ are shown in Fig. 4 (a). During the recharging phase of the first cycle, the vertical distribution of $s_2^{(0)}$ is reversed and the flow direction in the aquitard becomes upward. In the second $(1.0 < t < 2.0)$ and third $(2.0 < t < 3.0)$ cycles

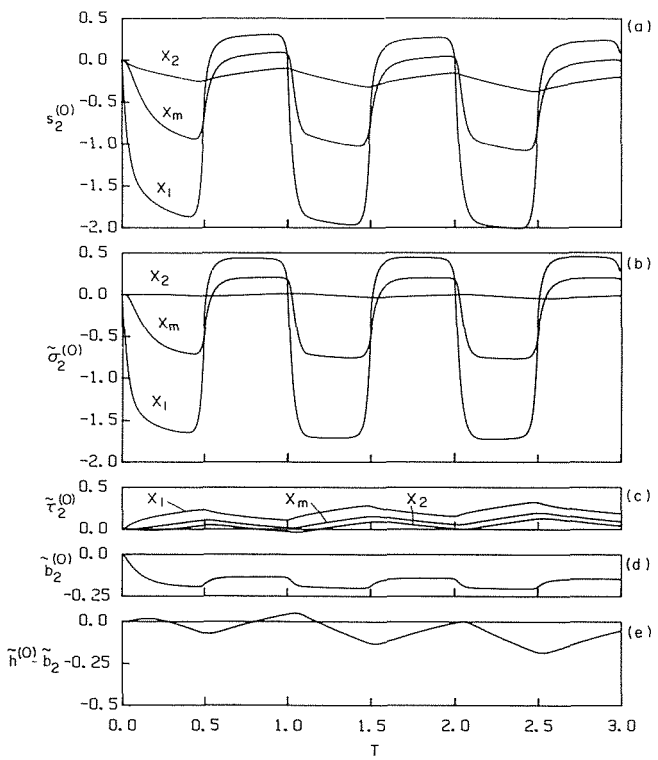

FIG. 4 Time variations of (a) $s_2^{(0)}$, (b) $\tilde{\sigma}_2^{(0)}$, (c) $\tilde{\tau}_2^{(0)}$, (d) $\tilde{b}_2$ and (e) $H_0 - H$ for $R = 0.2$ induced by pumping and recharging depicted in Fig. 2(b).

the same kind of variation of $s_2^{(0)}$ is repeated. The amplitude of $s_2^{(0)}$ is quite large. In Fig. 4 (b), the effective stress variation is shown for the same settings. During injections, most of the vertical cross-section is in compression as compared to the initial state, since $\tilde{\sigma}_2^{(0)} > 0$. The vertical settlement is shown in Fig. 4 (d). Hysteresis is obvious after the first pumping period. While $\tilde{\sigma}_2^{(0)}$ fluctuates greatly, the ground level recovers only slightly. The water table recovers significantly after each cycle, as shown in Fig. 4 (e).

CONCLUDING REMARKS

In this paper we have outlined the results obtained by using a perturbation analysis and Lagrangian coordinates. The key points are that for soft and thick aquitards the fluid drawdown and effective soil stress are in general coupled nonlinearly, and the total stress is no longer constant in depth. With a constitutive model representing the well known nonlinear and hysteretic behavior of soft soils we have examined the effects of pumping from an isolated well on the finite displacement of the ground surface and the water table, as well as the transient evolution of the drawdown in various parts of the soil. Examples for transient pumpings (intermittent or cyclic pumping and recharging) show that the ground surface and the water table can respond in interesting manners which are relevant to the planning or operation of wells. Although not shown here, in all examples the common approximation of constant total stress is found to be not quite accurate.

Extension of the present theory to allow finite compressibilities in all layers is straightforward and worthwhile. Since for a single well the physics is already highly nonlinear, the interaction between two or more adjacent wells or concentrated zones of pumping, separated by distances comparable to the typical radius of influence, cannot be treated by superposition, neither is the combined effect of pumping and surface loading. For these more complex problems the present theory can be modified by changing the boundary conditions, and by expanding the numerical task.

ACKNOWLEDGEMENT

We thank the Solid and Geomechanics Program, U.S. National Science Foundation, for supporting this research through Grant MSM 8616693.

REFERENCES

Cooper, H.H. (1966) The equation of groundwater flow in fixed and deforming coordinates. *J. Geophy. Res.* 71(20),4785-4790.

DeJosselin de Jong, G. (1963) Considatie in drie dimensies, LGM, Mededelingen, 7,57-73.

Fallou, S.N., C.C. Mei and C.K. Lee (1991) Subsidence due to pumping

from a layered soil - a perturbation theory. (to appear in *Int. J. Num. Analy. Meth. Geomech.*)

Gambolati (1973 a) Equation for one-dimensional vertical flow of groundwater 1. The rigorous theory. *Wat. Resourc. Res.* 9(4) 1022-1028.

Gambolati (1973 b) Equation for one-dimensional vertical flow of groundwater. 2. Validity range of the diffusion equation. *Wat. Resourc. Res.* 9 (5) 1385-1395.

Gibson, R.E., G.L. England and M.J.L. Hussey (1967) The theory of one-dimensional consolidation of saturated clays I: Finite nonlinear consolidation of thin homogeneous layers. *Geotechnique* 17,261-273.

Hantush, M.S. (1960) Modification of the theory of leaky aquifers. *Jour. of Geophy. Res.* 65(11),3713-3725.

Holtz, R.D. and W.D. Kovacs (1981) *An Introduction To Geotechnical Engineering.* Prentice Hall, Inc., New Jersey.

Lambe, T.W. (1951) *Soil Testing for Engineers.* John Wiley and Sons, Inc., New York, *p.* 84.

Lambe, T.W. and R.V. Whitman (1969) *Soil Mechanics.* John Wiley and Sons, New York.

Lee, C. K. ,Fallou, S. N. & Mei, C. C. (1991) Ground subsidence due to intensive pumping from a layered soil. submitted.

Marsal, R.J. (1959) Unconfined compression and vane shear tests in volcanic lacustrine clays. *ASTM Spec. Tech. Pub.* No. 232, 229-241.

Verruijt, A. (1969) Elastic Storage of Aquifers in *Flow through porous media.* edited by Roger M. deWiest, Academic Press.

Zeevaert, L. (1983) *Foundation Engineering for Difficult Subsoil Conditions.* Van Nostrand Reinhold.